# A Revision of the Evolutionary Relationships of Crocodylia

---

**Jonathan Paul Rio**

**August, 2020**

*A thesis submitted in fulfilment of the degree of Doctor of Philosophy,*
*Department of Earth Science and Engineering, Imperial College London*

# Copyright Declaration

The copyright of this thesis rests with the author. Unless otherwise indicated, its contents are licensed under a Creative Commons Attribution-Non Commercial 4.0 International Licence (CC BY-NC). Under this licence, you may copy and redistribute the material in any medium or format. You may also create and distribute modified versions of the work. This is on the condition that: you credit the author and do not use it, or any derivative works, for a commercial purpose. When reusing or sharing this work, ensure you make the licence terms clear to others by naming the licence and linking to the licence text. Where a work has been adapted, you should indicate that the work has been changed and describe those changes. Please seek permission from the copyright holder for uses of this work that are not included in this licence or permitted under UK Copyright Law.

# Declaration of Originality

I declare that this work is original research undertaken by me, apart from where indicated in the text, for which full references are provided. No part of this thesis has been submitted for consideration towards another degree at this or any other institution.

Jonathan Rio

August, 2020



Figure 1: The Chinese alligator, *Alligator sinensis*, photographed in Xuancheng, Anhui Province, China. July, 2017.

# Acknowledgements

First and foremost, I must extend my gratitude to my supervisors Phil Mannion, Mark Sutton, and Samuel Turvey for their help throughout the whole PhD process. Furthermore, this work could not have been accomplished without funding from the NERC Science and Solutions for a Changing Planet doctoral training programme, as well as funding from the Palaeontological Association's Small Grants Scheme.

This work would also not have been possible without the generosity of many museum curators and collection managers. Carl Mehling, Lauren Vonhame, David Kizirian, David Dickey (AMNH); Matt Riley (CAMSM); Alan Resetar, Bill Simpson, Adrienne Stroup (FMNH); Torsten Wappler (HLMD); Annelise Folie (IRScNB); Zheng Fang, Xu Xing (IVPP); Martin Ezcurra (MACN); Jessica Cundiff (MCZ); Paula Bona (MLP); Ronan Allain (MNHN); Diego Pol (MPEF); Paul Barrett; Patrick Campbell, Susie Maidment, Lorna Steel (NHMUK); Andrew Amey, Scott Hocknull, Andrew Rozefelds, Kristen Spring (QM); Krister Smith (SMF); Eberhard Frey (SMNK); Rainer Schoch (SMNS); Patricia Holroyd (UCMP); Matt Lowe (UCMZ); Edson Guiherme, Jonas Pereira de Souza-Filho (UFAC); Amanda Millhouse, Addison Wynn (USNM); Daniel Brinkman (YPM); and Zheng Wenjie (ZMNH).

Finally, I would like to thank my family, friends, and especially Aaron for support over the last 4 years.

# Abstract

First appearing in the latest Cretaceous, Crocodylia is a clade of mostly semi-aquatic, predatory reptiles, defined as all of the descendants of the last common ancestor of the extant alligators, caimans, crocodiles, and gharials. Crocodylian phylogeny has been extensively studied using molecular and morphological datasets; however, numerous systematic problems exist, notably the disagreement between these datasets over the affinities of the extant gharials, *Gavialis gangeticus* and *Tomistoma schlegelii*. I constructed a new morphological dataset for Crocodylia, through (1) an anatomical reappraisal of a 'basal' crocodylian taxon, *Diplocynodon hantoniensis*; (2) a critical reappraisal of published character data matrices; and (3) extensive, first-hand observations of a global sample of crocodylians. This comprises the most taxonomically comprehensive crocodylian dataset to date (144 OTUs and 330 characters) including a new, illustrated character list, modifications to the construction and scoring of most characters, and 45 novel characters. Nine phylogenetic analyses under maximum parsimony compared the effects of weighting strategies and the treatment of quantitative characters. In agreement with the molecular hypothesis, and for the first time based on morphology alone, *Gavialis* is recovered as more closely related to *Tomistoma* than to any other extant crocodylian. This result is recovered in all analyses; however, those using continuous characters and extended implied weighting (with a high *k*-value) produce the most reliable and stratigraphically congruent topologies. Nevertheless, temporal incongruence between morphological and molecular datasets exists, indicating that several putative gavialids require reappraisal. New interrelationships are discussed along with a comprehensive review of their evolutionary and biogeographic implications, including: (1) support for a North American origin of Caimaninae in the latest Cretaceous; (2) recovery of the early Paleogene South American taxon *Eocaiman* as a 'basal' alligatoroid; and (3) modifications to the taxonomic content of Mekosuchinae, suggesting biogeographic affinities of this Australasian clade with latest Cretaceous–early Paleogene Asian crocodyloids.

# Contents


**1 Introduction** **21**

1.1 Overview . . . 22

1.2 Background . . . 25

1.2.1 Previous studies of crocodylian interrelationships . . . 25

1.2.2 Taxonomic terms . . . 29

1.3 Research Motivation . . . 32

1.3.1 Problems in crocodylian systematics . . . 32

1.3.2 Methodological approaches in crocodylian systematics . . . 38

1.3.3 Critically assessing characters used in crocodylian systematics . . . 41

1.4 Thesis Aims . . . 43

1.5 Thesis Outline and Structure . . . 43

1.6 Institutional Abbreviations . . . 44

1.7 Author Contributions . . . 45

**2 Reappraisal of the Morphology of the Alligatoroid Crocodylian *Diplocynodon hantoniensis* from the Late Eocene of the United Kingdom** **47**

2.1 Introduction . . . 48

2.2 Systematic Palaeontology . . . 50

2.3 Description . . . 51

2.3.1 Skull . . . 51

2.3.2 Mandible . . . 67

2.3.3 Dentition . . . 74

2.3.4 Axial column . . . 75

2.3.5 Osteoderms . . . 81

2.3.6 Appendicular skeleton . . . 83

2.4 Taxonomic Status of Previously Referred Material . . . 95

2.4.1 Early Eocene of the USA . . . 95

2.4.2 Late Eocene of Switzerland . . . 95
2.4.3 Early Oligocene of Germany . . . 97
2.4.4 Early Oligocene of France . . . 97
2.5 Discussion . . . 98
2.5.1 Comparisons of *D. hantoniensis* with other crocodylian species . . . 98
2.6 Summary . . . 106

**3 A New Morphological Character List for Crocodylia 107**
3.1 Introduction . . . 108
3.2 Methods . . . 108
3.2.1 Character list construction . . . 108
3.2.2 Character construction . . . 109
3.3 Continuous characters . . . 111
3.3.1 Skull . . . 111
3.3.2 Mandible . . . 118
3.3.3 Postcrania . . . 119
3.4 Discrete characters . . . 125
3.4.1 Skull . . . 125
3.4.2 Mandible . . . 252
3.4.3 Axial column . . . 287
3.4.4 Hyoid and interclavicle . . . 302
3.4.5 Appendicular skeleton . . . 304
3.4.6 Soft tissue . . . 311
3.4.7 Osteoderms . . . 315
3.5 Summary . . . 324

**4 Exploring the Evolutionary Relationships of Crocodylia 327**
4.1 Introduction . . . 328
4.2 Methods . . . 328
4.2.1 Taxon sampling . . . 328
4.2.2 Phylogenetic analyses . . . 328
4.2.3 Measures of phylogenetic accuracy . . . 330
4.2.4 Stratigraphic congruence . . . 330
4.2.5 Constrained searches . . . 331
4.2.6 Categorisation of synapomorphies . . . 331
4.3 Results . . . 332

4.3.1 Overall topological results . . . 332
4.3.2 Phylogenetic accuracy . . . 333
4.3.3 Stratigraphic congruence . . . 335
4.3.4 Detailed topological results . . . 335
4.4 Discussion . . . 341
4.4.1 The impact of quantitative character treatment . . . 341
4.4.2 The use of extended implied weighting . . . 341
4.4.3 Implications for the systematics and taxonomy of non-crocodylian eusuchians . . . 343
4.4.4 Diagnosis of Crocodylia . . . 346
4.4.5 Implications for the systematics and taxonomy of Alligatoroidea . . . 347
4.4.6 The affinities of Planocraniidae . . . 370
4.4.7 Implications for the systematics and taxonomy of Gavialoidea . . . 370
4.4.8 Implications for the systematics and taxonomy of Crocodyloidea . . . 407
4.5 Summary . . . 417

**5 A Review of the Evolutionary and Biogeographic History of Crocodylia 419**
5.1 Introduction . . . 420
5.2 Eusuchia and the Origin of Crocodylia . . . 420
5.3 Alligatoroidea . . . 422
5.4 Planocraniidae . . . 433
5.5 Crocodyloidea . . . 433
5.6 Gavialoidea . . . 442
5.7 Summary . . . 450

**6 Conclusions and Future Work 453**
6.1 Conclusions . . . 454
6.1.1 Summary of research outcomes . . . 454
6.1.2 Thesis summary . . . 456
6.2 Future Directions of Research . . . 457
6.2.1 Reappraisals of problematic taxa . . . 457
6.2.2 Targets for improved taxon sampling . . . 462
6.2.3 Future directions for character sampling . . . 464
6.2.4 Methodological considerations . . . 465
6.2.5 Additional directions of research . . . 466

**Bibliography** **467**

**Appendix A Referred material of *Diplocynodon hantoniensis*** **509**

**Appendix B List of Specimens Examined** **511**

**Appendix C Rejected Characters** **523**

**Appendix D Measurements for Continuous Characters 1–26** **529**

**Appendix E Taxon Stratigraphic Ranges** **535**

**Appendix F Constrained Analyses** **541**

**Appendix G Strict Consensus Trees from All Analyses** **557**

**Appendix H Comparisons between Strict Consensus Trees** **567**

**Appendix I Character Consistency Index (CI) Values from Analysis 1.3** **571**

**Appendix J Character score changes** **575**

# List of Figures


1.1 A sample of extant crocodylians . . . 23
1.2 A sample of extinct crocodylians . . . 24
1.3 Interrelationships of Crocodylomorpha . . . 26
1.4 Early interrelationships of crocodylians . . . 26
1.5 Phenetic cladogram of Densmore (1983) . . . 27
1.6 Traditional morphological interrelationships of extant crocodylians . . . 29
1.7 Temporal incongruence between morphological and molecular phylogenies . . . 33
1.8 Stratigraphic distribution of "gavialoids" and "tomistomines" . . . 34
1.9 Summary of problems in crocodylian phylogeny . . . 39

2.1 Skull of *Diplocynodon hantoniensis* NHMUK 25166 . . . 52
2.2 Skull of *Diplocynodon hantoniensis* NHMUK 30392, dorsal and ventral views . . . 54
2.3 Skull of *Diplocynodon hantoniensis* NHMUK 30392, lateral and occipital views . . . 55
2.4 Skull of *Diplocynodon hantoniensis* NHMUK 30393, dorsal and lateral views . . . 58
2.5 Juvenile skull of *Diplocynodon hantoniensis* NHMUK 25170.a . . . 59
2.6 Juvenile skull of *Diplocynodon hantoniensis* NHMUK OR 25167 . . . 60
2.7 Isolated cranial elements of *Diplocynodon hantoniensis* . . . 62
2.8 Ectopterygoid-pterygoid flexure in *Diplocynodon hantoniensis* . . . 67
2.9 Left mandible of *Diplocynodon hantoniensis* NHMUK 25188 . . . 69
2.10 Right mandible of *Diplocynodon hantoniensis* (NHMUK 30394) . . . 70
2.11 Surangular morphology of *Diplocynodon hantoniensis* NHMUK 30381 . . . 73
2.12 Dentition of *Diplocynodon hantoniensis* . . . 75
2.13 Atlas-axis complex of *Diplocynodon hantoniensis* . . . 77
2.14 Cervical vertebrae of *Diplocynodon hantoniensis* . . . 78
2.15 Dorsal vertebrae of *Diplocynodon hantoniensis* NHMUK 30402, lateral view . . . 79
2.16 Dorsal vertebrae of *Diplocynodon hantoniensis* NHMUK 30402, anterior view . . . 80
2.17 Sacral vertebrae of *Diplocynodon hantoniensis* NHMUK 30402 . . . 81

2.18 Caudal vertebrae of *Diplocynodon hantoniensis* NHMUK R.1052 . . . . . 82
2.19 Osteoderms of *Diplocynodon hantoniensis* . . . . . 82
2.20 Explanation of anatomical orientations . . . . . 83
2.21 Pectoral girldle of *Diplocynodon hantoniensis* . . . . . 85
2.22 The humerus of *Diplocynodon hantoniensis* . . . . . 87
2.23 The ulna and radius of *Diplocynodon hantoniensis* . . . . . 88
2.24 The ilium of *Diplocynodon hantoniensis* . . . . . 91
2.25 The ischium of *Diplocynodon hantoniensis* . . . . . 92
2.26 The femur of *Diplocynodon hantoniensis* . . . . . 93
2.27 The tibia and fibula of *Diplocynodon hantoniensis* . . . . . 96
2.28 Comparison of *Diplocynodon* skull proportions . . . . . 98
2.29 Comparison of preorbital step morphology . . . . . 99
2.30 Comparison of narial morphology in *Diplocynodon hantoniensis* . . . . . 100
2.31 Comparison of sutural relationships of the orbitotemporal canal . . . . . 101
2.32 Comparison of choanal morphology . . . . . 103
2.33 Comparison of angular morphology . . . . . 104
2.34 Comparison of humeral morphology . . . . . 105

3.1 Characters 1–8, cranium part 1 . . . . . 114
3.2 Characters 9–16, cranium part 2 . . . . . 123
3.3 Characters 18–26, mandible and postcrania . . . . . 124
3.4 Characters 27–30, rostral ornamentation . . . . . 128
3.5 Characters 31–32, development of an antorbital spectacle . . . . . 129
3.6 Character 33, position of the antorbital spectacle . . . . . 130
3.7 Character 34, enlargement of the naris and narial fossa . . . . . 131
3.8 Character 35, prefrontal protuberances . . . . . 132
3.9 Character 36, cranial table ornamentation . . . . . 133
3.10 Character 37, cranial table slope . . . . . 134
3.11 Characters 38–40, squamosal horn morphology . . . . . 136
3.12 Character 41, direction of the naris . . . . . 137
3.13 Character 42, ghara . . . . . 138
3.14 Characters 43–44, development of a narial crest and posterolateral notch . . . . . 139
3.15 Character 45, lateral narial fossa . . . . . 140
3.16 Characters 46–48, sutural relationships of the premaxillae and nasals . . . . . 142
3.17 Characters 49–50, narial position and premaxillary processes . . . . . 143
3.18 Character 51, development of cecal recesses . . . . . 144

3.19 Character 52, posterior extent of the maxilla . . . . . 145
3.20 Characters 53–57, sutural relationships of the lacrimal, prefrontal and nasal . . . . . 147
3.21 Characters 58–63, sutural relationships of the prefrtonal, lacrimal and frontal . . . . . 150
3.22 Character 64, morphology of the prefrontal sulcus . . . . . 151
3.23 Character 65, variation in jugal, lacrimal contact . . . . . 152
3.24 Characters 66–69, prefrontal pillar morphology . . . . . 154
3.25 Characters 70–71, morphology of the frontal . . . . . 155
3.26 Character 72, upturning of orbital margins . . . . . 157
3.27 Characters 73–74, relative position of the orbit . . . . . 158
3.28 Characters 75–81, Variation in cranial table morphology . . . . . 162
3.29 Character 82, morphology of the supraoccipital . . . . . 163
3.30 Characters 83–85, morphology of the parietal . . . . . 165
3.31 Character 86, morphology of the parietal recess . . . . . 166
3.32 Character 87, sutural relationships surrounding the orbitotemporal canal . . . . . 167
3.33 Character 88, variation in morphology of the orbitotemporal canal . . . . . 169
3.34 Characters 89–91, morphology of the postorbital bar . . . . . 171
3.35 Characters 92–93, postorbital-jugal morphology . . . . . 172
3.36 Characters 94–95, morphology of the jugal arch . . . . . 174
3.37 Characters 96–97, jugal recess and foramina . . . . . 175
3.38 Characters 98–101, sutural relationships and morphology of the infratemporal fenestra . 177
3.39 Characters 102–104, quadratojugal morphology . . . . . 179
3.40 Characters 105–106, sutural relationships of the postorbital, quadrate, and quadratojugal 181
3.41 Characters 107–109, morphology of the lateral cranial table margin . . . . . 183
3.42 Character 110, squamosal prong length . . . . . 184
3.43 Character 111, position of the infratemporal fenestra . . . . . 185
3.44 Characters 112–115, sutural relationships around the external auditory meatus . . . . . 189
3.45 Characters 116–119, morphology of the quadrate condyle . . . . . 190
3.46 Character 120, lateral exposure of the quadrate . . . . . 191
3.47 Characters 121–123, morphology of the exoccipital and quadrate . . . . . 192
3.48 Character 124, morphology of the exoccipital and quadrate . . . . . 193
3.49 Character 125, exoccipital-squamosal suture . . . . . 194
3.50 Character 126, position of the lateral carotid foramen . . . . . 195
3.51 Character 127, ventral extent of the exoccipital . . . . . 196
3.52 Character 128, exoccipital inclination . . . . . 197
3.53 Characters 129–132, morphology of the basioccipital . . . . . 198

3.54 Character 133, basioccipital concavity . . . 199
3.55 Character 134, position of the lateral eustachian foramina . . . 200
3.56 Characters 135–136, basisphenoid height and pterygoid processes . . . 201
3.57 Characters 137–139, morphology of the incisive foramen . . . 204
3.58 Characters 140–141, premaxillary alveoli number and size . . . 206
3.59 Characters 142–145, premaxillary alveoli arrangement . . . 208
3.60 Character 146, ventral premaxilla-maxilla suture . . . 209
3.61 Characters 147–150, maxillary alveoli . . . 212
3.62 Characters 151–153, occlusal pattern . . . 215
3.63 Character 155, maxillary alveoli shape . . . 216
3.64 Character 156, posterior maxillary and dentary teeth . . . 217
3.65 Character 157, dental serrations . . . 218
3.66 Character 158, elevation of the maxillary toothrow . . . 219
3.67 Character 159, foramen for palatine ramus of cranial nerve V . . . 219
3.68 Characters 160–164, morphology of the palatines and suborbital fenestrae . . . 222
3.69 Character 165, ventrolateral palatine processes . . . 223
3.70 Characters 166–174, sutural relationships and morphology of the suborbital fenestra . . . 228
3.71 Character 175, morphology of the ectopterygoid-maxilla suture . . . 229
3.72 Character 176, morphology of the ectopterygoid tip . . . 230
3.73 Character 177, ectopterygoid contact with suborbital fenestra . . . 231
3.74 Character 178, ectopterygoid contribution to maxillary alveolar walls . . . 232
3.75 Character 179, non-dentigerous posterior process of the maxilla . . . 232
3.76 Characters 180–181, ectopterygoid morphology viewed medially . . . 233
3.77 Characters 182–183, medial sutural relationships of the jugal . . . 234
3.78 Character 184, medial jugal foramen . . . 235
3.79 Character 185, ectopterygoid-pterygoid flexure . . . 236
3.80 Character 186, posterior extent of the ectopterygoid . . . 236
3.81 Characters 187–194, morphology and sutural relationships of the pterygoid . . . 240
3.82 Characters 195–197, morphology of the choanae . . . 243
3.83 Character 198, pterygoid ridges . . . 244
3.84 Character 199, pterygoid bullae . . . 244
3.85 Character 200, quadrate ventral scars . . . 245
3.86 Characters 201–202, basisphenoid exposure and jugal posterior extent . . . 246
3.87 Characters 203–204, basisphenoid rostrum . . . 247
3.88 Character 205, sulcus on the basisphenoid rostrum . . . 248

3.89 Character 206, orientation of the laterosphenoid capitate process . . . . . 249
3.90 Characters 207–210, caudal and lateral laterosphenoid bridges . . . . . 251
3.91 Characters 211–214, laterosphenoid bridge morphology and prootic exposure . . . . . 253
3.92 Character 215, laterosphenoid bridge continued and prootic exposure . . . . . 254
3.93 Characters 216–218, anterior dentary alveoli . . . . . 255
3.94 Character 219, dentary alveoli size . . . . . 256
3.95 Character 220, dentary curvature . . . . . 256
3.96 Character 221, mandibular symphysis length . . . . . 257
3.97 Characters 222–223, splenial symphysis rostral tip . . . . . 260
3.98 Characters 224–225, splenial symphysis length and constriction . . . . . 261
3.99 Character 226, dentary symphysis shape . . . . . 262
3.100 Character 227, posterior dentary alveoli orientation . . . . . 263
3.101 Character 228, ventral dentary process in the angular and splenial . . . . . 264
3.102 Characters 229–232, splenial perforations and shape . . . . . 265
3.103 Character 233, splenial-dentary suture inflection . . . . . 266
3.104 Characters 234–238, external mandibular fenestra . . . . . 268
3.105 Character 239, surangular and angular flanges . . . . . 269
3.106 Character 240, angular fossa . . . . . 271
3.107 Character 241, surangular processes . . . . . 272
3.108 Characters 242–243, morphology of the surangular spur . . . . . 274
3.109 Characters 244–245, dorsal and posterior extent of the surangular . . . . . 275
3.110 Character 246, sulcus on the dorsolateral margin of the surangular . . . . . 276
3.111 Characters 247–248, morphology of the articular . . . . . 277
3.112 Character 249, lamina on the articular foramen aerum . . . . . 278
3.113 Characters 250–251, morphology of the retroarticular process . . . . . 280
3.114 Character 252, crest on the retroarticular process . . . . . 281
3.115 Characters 253–256, sutural relationships of the posterior mandibular adductor chamber 283
3.116 Characters 257–262, sutural relationships on the posteromedial mandible surface . . . . 286
3.117 Characters 264–265, morphology of the proatlas . . . . . 288
3.118 Characters 266–271, morphology of the atlas-axis complex . . . . . 291
3.119 Characters 272–278, morphology of the axis . . . . . 294
3.120 Characters 279–282, morphology of the cervical vertebrae . . . . . 299
3.121 Character 283, cervical rib morphology . . . . . 300
3.122 Characters 289–290, sacral rib morphology . . . . . 301
3.123 Characters 295–296, morphology of the hyoid . . . . . 303

3.124 Characters 297–298, morphology of the interclavicle . . . . . 304
3.125 Characters 299–301, morphology of the scapulocoracoid . . . . . 306
3.126 Characters 302–304, morphology of the humerus . . . . . 310
3.127 Characters 305–306, morphology of the ulna . . . . . 311
3.128 Characters 307–310, morphology of the ilium . . . . . 313
3.129 Character 314, distribution of integumentary sense organs . . . . . 314
3.130 Character 317, tail scalation . . . . . 316
3.131 Characters 318–319, morphology of the palpebral . . . . . 317
3.132 Characters 321–323, postoccipital and nuchal osteoderm arrangement . . . . . 319
3.133 Character 324, dorsal osteoderm arrangement . . . . . 320
3.134 Characters 325–328, osteoderm morphology . . . . . 322
3.135 Character 329, osteoderm coverage on the tail . . . . . 324
3.136 Character 330, osteoderm coverage on the limbs . . . . . 325

4.1 Categorisation of synapomorphies . . . . . 332
4.2 Summary of phylogenetic results . . . . . 334
4.3 Phylogenetic results of Analysis 1.3 . . . . . 342
4.4 Time-calibrated stem crocodylian interrelationships . . . . . 345
4.5 Time-calibrated phylogeny of Alligatoroidea . . . . . 348
4.6 The anatomy of *Eocaiman* . . . . . 361
4.7 *Caiman lutescens* MACN PV 13551 . . . . . 363
4.8 Comparison of occiput curvature in selected caimanines . . . . . 365
4.9 Comparison of spectacle morphology in selected caimanines . . . . . 366
4.10 UCMP 39978 (‘*Caiman* cf. *lutescens*’) . . . . . 368
4.11 Time-calibrated phylogeny of Gavialoidea . . . . . 371
4.12 Illustration of an atavistic character . . . . . 374
4.13 Simplified crocodylian phylogeny based on Narváez et al. (2016) . . . . . 375
4.14 Summary of changes in atavistic character optimisations . . . . . 384
4.15 Synapomorphies of Gavialoidea and less inclusive clades . . . . . 388
4.16 Examples of ‘thoracosaurs’ . . . . . 397
4.17 Constraining ‘thoracosaurs’ outside of Crocodylia . . . . . 404
4.18 Constraining ‘thoracosaurs’ outside of Gavialidae . . . . . 405
4.19 Constraining traditional ‘thoracosaurs’ outside of Crocodylia . . . . . 406
4.20 Time-calibrated phylogeny of Crocodyloidea . . . . . 409

5.1 Spatiotemporal distribution of Hylaeochampsidae . . . . . 421

5.2 Spatiotemporal distribution of Allodaposuchidae and *Borealosuchus* . . . . . 422
5.3 Spatiotemporal distribution of Alligatoroidea, Paleocene . . . . . 425
5.4 Spatiotemporal distribution of Alligatoroidea, Eocene . . . . . 426
5.5 Latest Cretaceous–early Paleogene biogeographic routes . . . . . 428
5.6 Spatiotemporal distribution of *Alligator* . . . . . 429
5.7 Spatiotemporal distribution of Caimaninae, Neogene–Quaternary . . . . . 432
5.8 Spatiotemporal distribution of Planocraniidae . . . . . 433
5.9 Spatiotemporal distribution of Crocodyloidea, latest Cretaceous–Paleogene . . . . . 435
5.10 Mekosuchine dispersal routes . . . . . 437
5.11 Spatiotemporal distribution of Osteolaeminae . . . . . 439
5.12 Spatiotemporal distribution of *Crocodylus* . . . . . 441
5.13 Spatiotemporal distribution of Gavialoidea, Cretaceous to Eocene . . . . . 443
5.14 Spatiotemporal distribution of Gavialoidea, Oligocene to Recent . . . . . 445
5.15 The origin of Neotropical gavialoids . . . . . 447
5.16 Biogeography of *Gavialis* . . . . . 448

D.1 Continuous measurement plots 1–15 . . . . . 530
D.2 Continuous measurement plots 16–26 . . . . . 531
D.3 Histograms for characters 1–15 . . . . . 532
D.4 Histograms for characters 16–26 . . . . . 533

F.1 Constrained tree: monophyletic *Diplocynodon* . . . . . 545
F.2 Constrained tree: *Eocaiman* in Caimaninae . . . . . 546
F.3 Constrained tree: *Eocaiman* in South American caimaninine clade . . . . . 547
F.4 Constrained tree: Jacarea sensu Brochu (1999) . . . . . 548
F.5 Constrained tree: traditional morphological hypothesis . . . . . 549
F.6 Constrained tree: *Portugalosuchus* excluded from Crocodylia . . . . . 550
F.7 Constrained tree: ‘basal’ crocodyloids forced to stem Longirostres . . . . . 551
F.8 Constrained tree: Mekosuchinae to stem Longirostres . . . . . 552
F.9 Constrained tree: *Asiatosuchus nanlingensis* excluded from Mekosuchinae . . . . . 553
F.10 Constrained tree: *Australosuchus* and *Quinkana* forced into Mekosuchinae . . . . . 554
F.11 Constrained tree: *Mecistops* forced into Osteolaeminae . . . . . 555

G.1 Strict consensus tree: Analysis 1.1 . . . . . 558
G.2 Strict consensus tree: Analysis 1.2 . . . . . 559
G.3 Strict consensus tree: Analysis 2.1 . . . . . 560
G.4 Strict consensus tree: Analysis 2.2 . . . . . 561

G.5 Strict consensus tree: Analysis 2.3 . . . . . 562
G.6 Strict consensus tree: Analysis 3.1 . . . . . 563
G.7 Strict consensus tree: Analysis 3.2 . . . . . 564
G.8 Strict consensus tree: Analysis 3.3 . . . . . 565
G.9 Strict consensus tree: longirostrine characters excluded . . . . . 566

H.1 Strict consensus tree: analyses 1.1, 1.2, and 1.3 . . . . . 568
H.2 Strict consensus tree: analyses 1.3, 2.3, and 3.3 . . . . . 569

# List of Tables


1.1 Taxon definitions . . . . . 30
1.2 Sources of characters in eusuchian datasets . . . . . 42

2.1 Cranial measurements for *Diplocynodon hantoniensis* . . . . . 53
2.2 Mandibular measurements for *Diplocynodon hantoniensis* . . . . . 68

3.1 Summary of major modifications to character list . . . . . 326

4.1 Summary of phylogenetic analyses performed . . . . . 329
4.2 Summary of measures of internal tree support . . . . . 335
4.3 Average Bremer support values by clade . . . . . 337
4.4 Summary of indices of stratigraphic congruence . . . . . 338
4.5 Agreement subtree comparisons . . . . . 343
4.6 Synapomorphies of *Diplocynodon* and *Diplocynodon* + *Leidyosuchus* . . . . . 350
4.7 Synapomorphies of *Diplocynodon* recovered by Brochu (1999) . . . . . 352
4.8 Caimanine cranial measurements . . . . . 364
4.9 Comparisons of UCMP 39978 with other caimanines . . . . . 369
4.10 Morphological characters associated with longirostry . . . . . 373
4.11 Changes to characters that supported the traditional morphological topology. . . . . 382
4.12 Synapomorphies of Gavialoidea . . . . . 394
4.13 Characters supporting gavialoid affinities of ‘thoracosaurs’ . . . . . 399
4.14 Characters distinguishing ‘thoracosaurs’ from gavialoids . . . . . 401

5.1 Minimum divergence estimates and earliest fossil occurrences of eusuchian clades . . . . 423

6.1 Taxa targeted for future anatomical reappraisal . . . . . 457
6.2 Targets for improved taxon sampling . . . . . 462

B.1 Sources of data for specimens included in the phylogenetic analysis. . . . . 511

C.1 Rejected characters . . . . . 523

D.1 Results of the Shapiro-Wilk test . . . . . 534

E.1 First and last appearance dates used in measures of stratigraphic congruence . . . . . 535

F.1 Summary of constrained analyses . . . . . 542

J.1 Key character score changes in Gavialoidea . . . . . 576

# Chapter 1

# Introduction

## 1.1 Overview

Extant crocodylians are semi-aquatic ambush predators and piscivores that are globally distributed across the tropics and subtropics, inhabiting freshwater and estuarine environments (Grigg & Kirshner, 2015). They currently number 25 species, comprising alligators, caimans, crocodiles, and gharials (Fig. 1.1); however, this number is most likely an underestimate, given that several established species continue to be recognised as cryptic species complexes (e.g. Eaton et al., 2009; Hekkala et al., 2011; Shirley et al., 2018; Brochu & Sumrall, 2020). The last common ancestor of living crocodylians defines the crown group Crocodylia (Benton & Clark, 1988; Brochu et al., 2009). This group currently comprises approximately 140 species, the earliest unambiguous members of which appear in the Campanian (latest Cretaceous), ∼80 million years ago (Ma) (Brochu, 2003). Crocodylians have been described as 'living fossils' because of their apparently conservative body plan (e.g. Meyer, 1984) and, over the course of the evolutionary history of their ancestors and extinct relatives (Crocodyliformes), have repeatedly converged on similar skull shapes (e.g. Brochu, 2001; Wilberg, 2017; Groh et al., 2020). Nevertheless, crocodylians have a rich evolutionary history (Brochu, 2003; Mannion et al., 2015). They achieved a global distribution, including dispersals into high palaeolatitudes (e.g. Estes & Hutchison, 1980; Willis & Stilwell, 2000) and across large oceanic barriers (Vélez-Juarbe et al., 2007; Meredith et al., 2011; Oaks, 2011; Nicolaï & Matzke, 2019). They exhibited dramatic differences in body size (Godoy et al., 2019), ranging from dwarf forms such as *Osteolaemus* to the giant *Purussaurus* (Scheyer et al., 2019). Additionally, the fossil record of crocodylians reveals a greater disparity in skull morphology than in extant taxa, including 'surfboard'-snouted forms such as *Mourasuchus* (Price, 1964) and the saw-snouted longirostrine *Euthecodon* (Ginsburg & Buffetaut, 1978) (Fig. 1.2). The fossil record of Crocodylia also provides evidence of a broader ecological diversity than that of their extant representatives. Crocodylians transitioned from fully aquatic to terrestrial habitats at least twice (Wilberg et al., 2019), and evolved feeding strategies beyond the carnivorous and piscivorous habits of extant taxa (Melstrom & Irmis, 2019). This includes durophagy (Salas-Gismondi et al., 2015) and possibly filter- or 'gulp'- feeding (Langston, 1965; Cidade et al., 2017; Cidade et al., 2019d). Furthermore, these diverse forms sometimes occupied the same habitat, greatly exceeding the number of sympatric occurrences in today's crocodylian diversity hotspots (Scheyer et al., 2013; Salas-Gismondi et al., 2015). Additionally, Crocodylia underwent a series of radiations and extinctions throughout its evolutionary history, including the survival of the clade across the Cretaceous/Paleogene (K/Pg) mass extinction, 66 Ma. Although likely constrained by a combination of abiotic and biotic factors (Solórzano et al., 2020), crocodylian diversification dynamics appear to show close ties to environmental and climatic fluctuations (Markwick, 1998; Brochu, 2003; Bronzati et al., 2015; Mannion et al., 2015; De Celis et al., 2020; Pan et al., 2020).

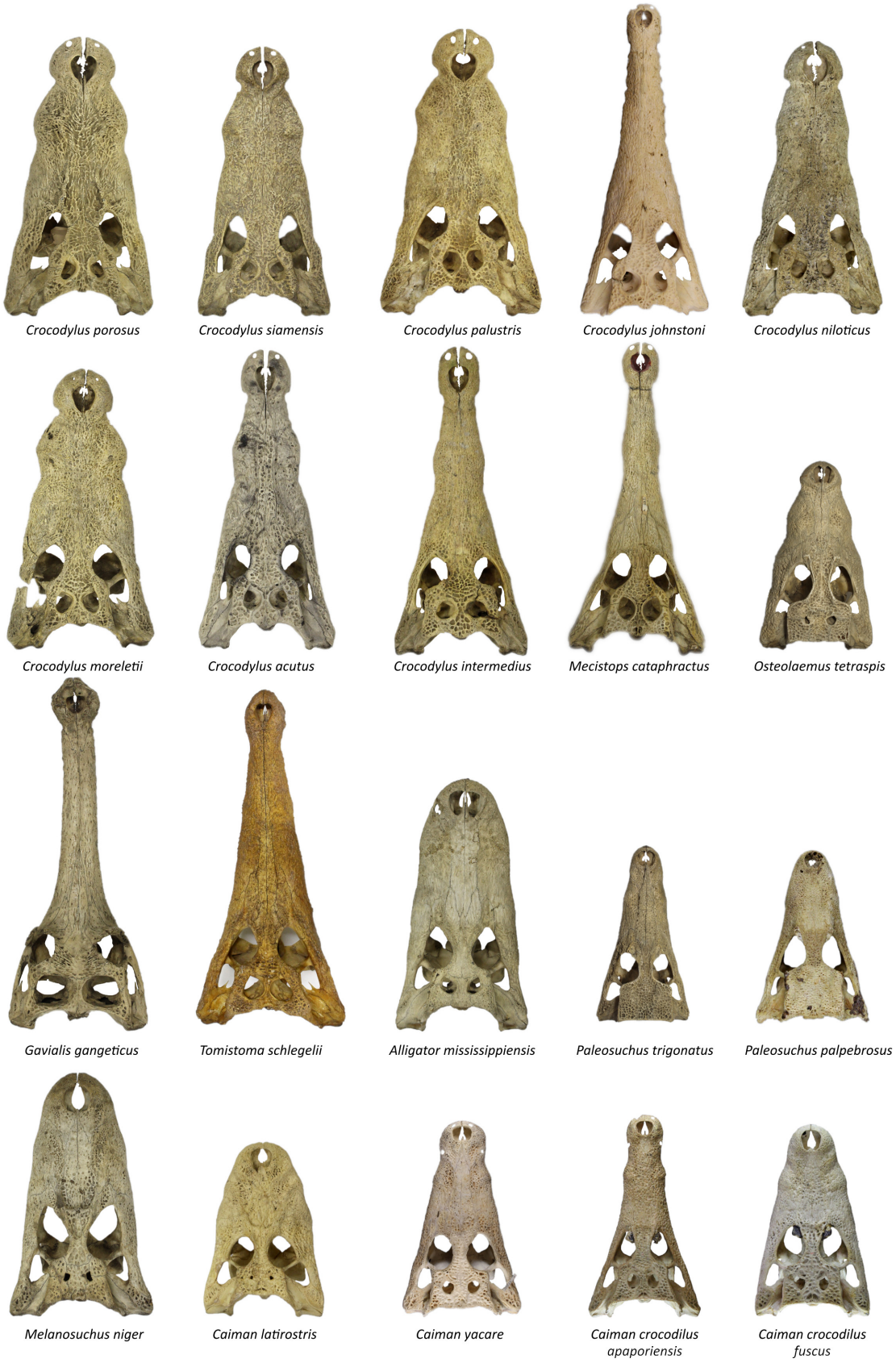



Figure 1.1: An assortment of skulls of extant crocodylians. Scaled to width across quadrates.

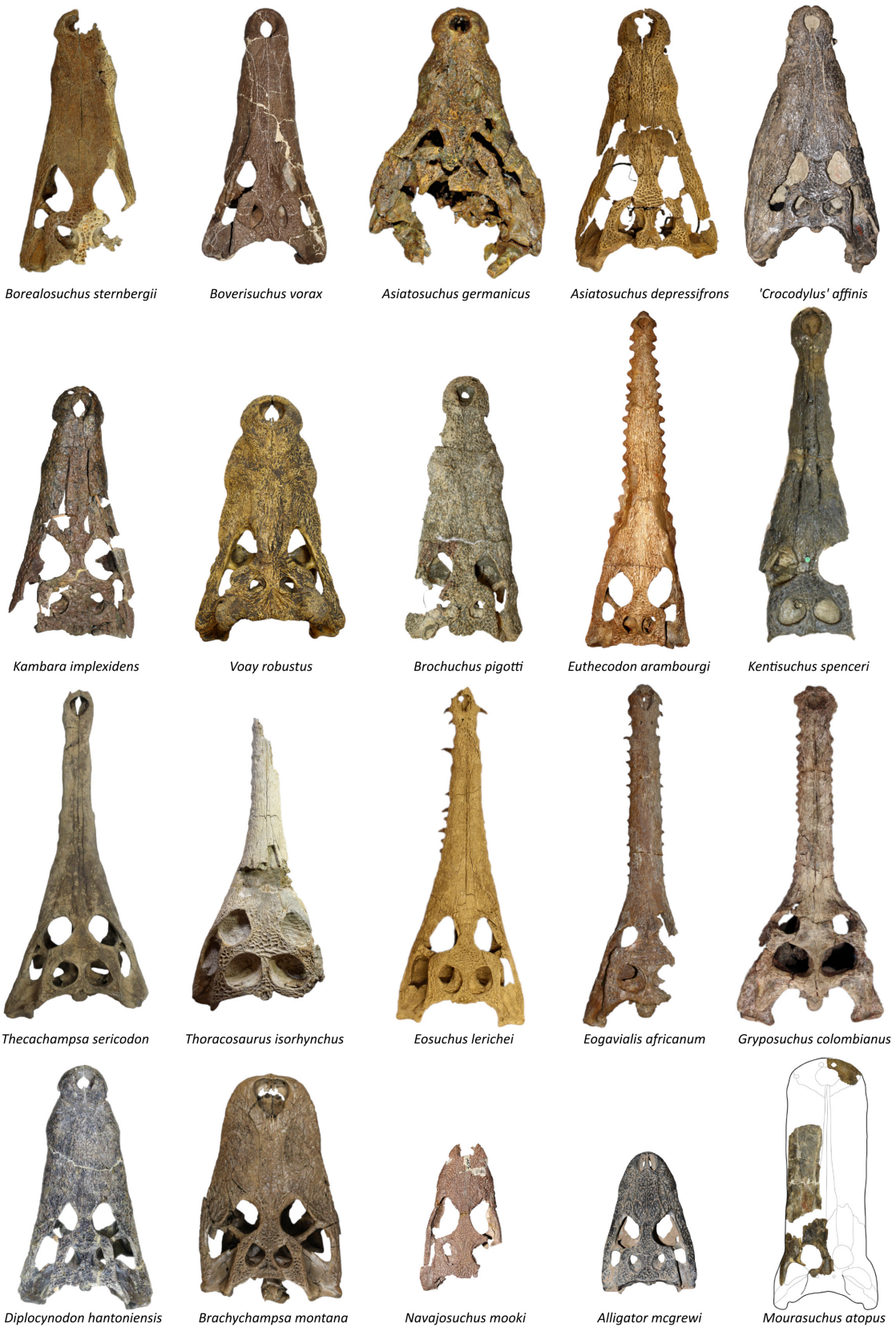



Figure 1.2: An assortment of skulls of fossil crocodylians. Scaled to width across quadrates.

It is not surprising then that crocodylians and their close relatives have attracted a considerable amount of scientific interest. Indeed, attempts at determining the evolutionary interrelationships of Crocodylia have a long history of study, dating back to the work of the earliest comparative anatomists on specimens of extant species (e.g. Duméril, 1806; Cuvier, 1807; Duméril & Bibron, 1835). However, the largest strides in resolving crocodylian phylogeny have occurred in the last four decades, from new morphological (e.g. Brochu, 1999) and molecular data (e.g. Green et al., 2014), as well as methodological advances in data analysis (e.g. Yang & Rannala, 2012). Nevertheless, there are still substantial gaps in our knowledge, as well as discrepancies between datasets that stand in the way of a robust phylogeny of Crocodylia. Most notably, this includes the conflicting phylogenetic affinities of the gharial, *Gavialis gangeticus*, based on molecular and morphological datasets, but also includes a plethora of additional systematic problems. As well as hindering our understanding of the groups' evolutionary and biogeographic history, these problems also limit our ability to use phylogenetic trees to evaluate extinction risk and determine conservation priorities in extant species (e.g. Isaac et al., 2007; Gumbs et al., 2018).

In this thesis I will revise the evolutionary relationships of Crocodylia. I will outline, illustrate, and discuss a new morphological character list, based on a comprehensive literature review and first-hand observations of a global sample of extant and fossil crocodylians, including a detailed anatomical reappraisal of an early diverging crocodylian. Based on this new character list, which also incorporates quantitative characters, I will conduct a series of phylogenetic analyses that explore the effects of alternative treatments of quantitative characters (i.e. continuously or discretely coded) and weighting strategies. I will test new hypotheses of crocodylian interrelationships and explore the biogeographic consequences of the new evolutionary relationships that are recovered.

## 1.2 Background

### 1.2.1 Previous studies of crocodylian interrelationships

The definition of Crocodylia as the crown-group of extant crocodylians is relatively recent (Benton & Clark, 1988). Previously, 'Crocodilia' comprised a far more inclusive and imprecisely defined group, including taxa from the Triassic, $>$ 200 Ma (e.g. Hay, 1930; Mook, 1934; Sill, 1968). Indeed, the taxonomic content of 'Crocodilia' outlined by Mook (1934) approximately corresponds to Crocodyliformes in today's phylogenetic nomenclature, i.e. Protosuchia + Mesoeucrocodylia (Benton & Clark, 1988; Sereno et al., 2001) (Fig. 1.3). Nevertheless, extant crocodylians have consistently been placed within Eusuchia, which was originally defined by Huxley (1875) as an apomorphy-based group for taxa with pterygoid-bound choanae and procoelous vertebrae. Eusuchia is now phylogenetically defined, and more exclusive, comprising the last common ancestor of *Hylaeochampsa vectiana* and Crocodylia, and all of its descen-

dants (Brochu, 1999). In turn, Eusuchia is a clade within a larger grouping, Neosuchia (Fig. 1.3), that is defined as all crocodyliforms more closely related to *Crocodylus niloticus* than to *Notosuchus terrestris* (Sereno et al., 2001).

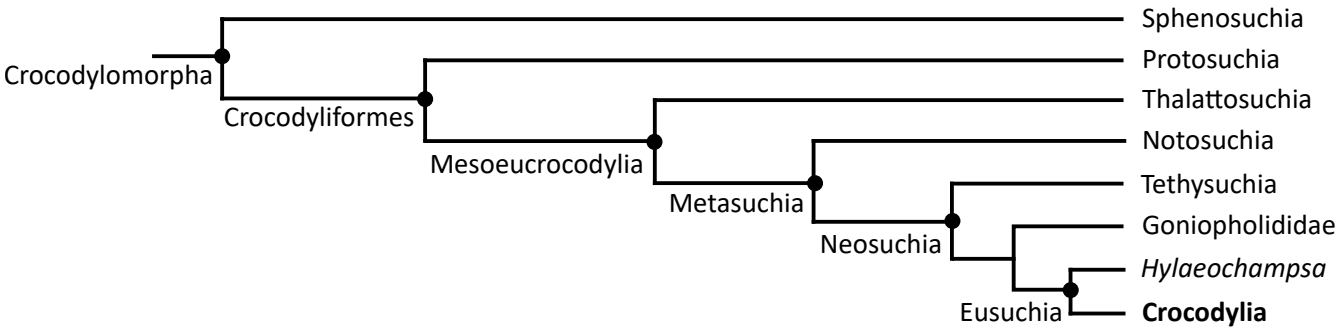



Figure 1.3: Simplified cladogram of Crocodylomorpha, after Wilberg et al. (2019).

Over the last century, multiple pre-cladistic classification schemes of extant crocodylians have emerged based on traditional comparative anatomical data (Fig. 1.4). These classification schemes agree in several respects, for example in considering *Crocodylus* to be closely related to *Osteolaemus*, and recognising *Alligator* to group with caimanines (*Caiman*, *Melanosuchus*, and *Paleosuchus*) (e.g. Mook, 1934; Kälin, 1955; Romer, 1956; Sill, 1968; Steel, 1973). However, there has historically been disagreement over the affinities of the extant gharials (*Gavialis* and *Tomistoma*) to other living crocodylians. Whereas Romer (1956) and Steel (1973) placed all living crocodylians within the same family ('Crocodylidae'), Mook (1934), Kälin (1955) and Sill (1968) positioned *Gavialis* within a separate family, indicating that it is more distantly related to all other extant crocodylians. Although some pre-cladistic classifications suggested a closer relationship between *Gavialis* and *Tomistoma* (e.g. Hay, 1930), the prevailing morphological hypothesis has been that *Gavialis* is distantly related to all other extant crocodylians.

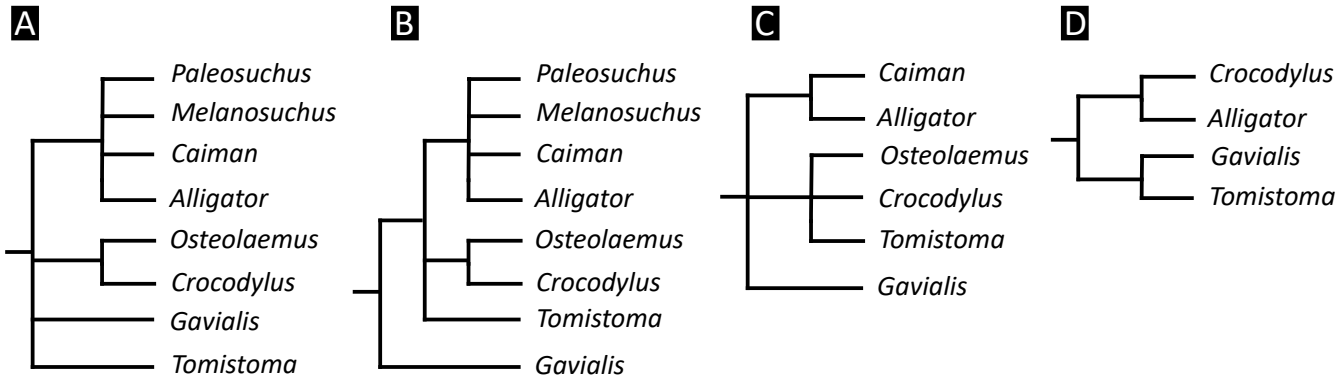



Figure 1.4: Cladograms outlining the interrelationships of extant crocodylians implied from the taxonomic classification schemes of earlier studies. **A**, after Romer (1956) and Steel (1973); **B**, after Kälin (1955) and Sill (1970); **C**, after Mook (1934); and **D**, after Hay (1930).

Crocodylian systematics received a surge of interest in the 1980s. This was stimulated by the introduction of phylogenetic systematics (Hennig, 1965), technological advancements such as amino acid and DNA sequencing, new morphological character datasets, as well as computational advances in analysing morphological and molecular datasets. Another important driver of investigations into crocodylian interrelationships was continued debate over the affinities of the two extant gharials. Disagreement between traditional morphological hypotheses and new, molecular hypotheses would propel and shape the course of investigations. The earliest crocodylian cladogram based on biomolecular data was generated by Densmore (1983), who conducted a series of distance-based analyses on blood proteins. By contrast to the morphological hypothesis, these analyses suggested a sister relationship between *Tomistoma schlegelii* and *Gavialis gangeticus*, with this clade (Gavialidae) more closely related to crocodylids (*Crocodylus* and *Osteolaemus*) than to alligatorids (Fig. 1.5). The crocodylian clade excluding Alligatoridae was later named Longirostres (Harshman et al., 2003). Densmore (1983) also found evidence for a relatively recent divergence of *Crocodylus* in the Miocene, which until then had been considered an ancient taxon with representatives extending back to the Cretaceous (e.g. Marsh, 1872; Cope, 1882; Lydekker, 1886; Etheridge, 1917).

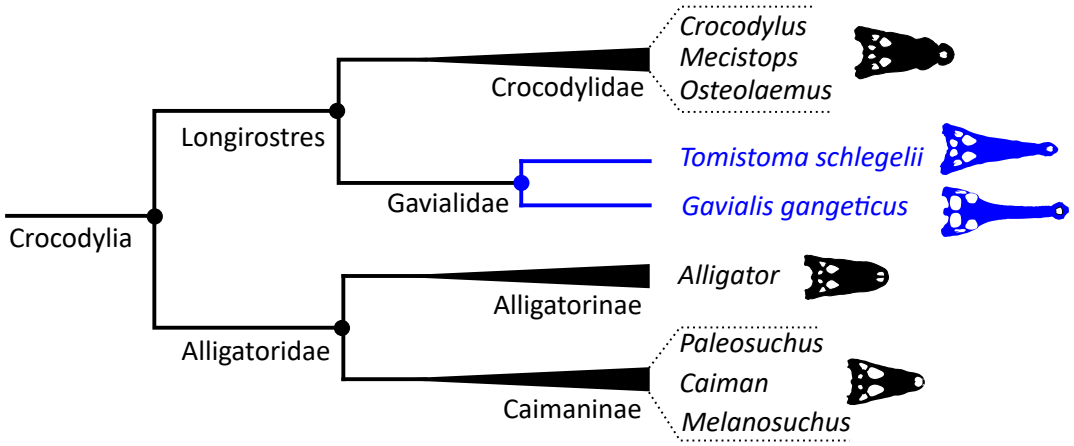



Figure 1.5: Simplified interrelationships of Crocodylia based on the phenogram generated by Densmore (1983).

The emergence of a new hypothesis for crocodylian interrelationships prompted some to attempt to reconcile the morphological and molecular data. Buffetaut (1985) outlined morphological similarities between *Gavialis*, *Crocodylus*, and *Tomistoma*. Furthermore, he asserted that the fossil record was compatible with the molecular hypothesis, and that suitable candidates for a common ancestor of *Tomistoma* and *Gavialis* could be found in the Eocene of North Africa, such as '*Tomistoma*' (=*Eogavialis*) *africanum*. By contrast, traditional comparative anatomical studies continued to support the early divergence of *Gavialis* from all other extant crocodylians, with evidence from osteoderm arrangement, braincase and appendicular anatomy, as well as differences in tail musculature (e.g. Ross & Mayer, 1983; Tarsitano, 1985; Frey et al., 1989; Tarsitano et al., 1989). Furthermore, in parallel, new morphological character datasets were

published that would further support the early divergence of *Gavialis* (e.g. Norell, 1988, 1989; Norell & Clark, 1990; Willis, 1993; Clark, 1994; Salisbury & Willis, 1996). Based on the morphology of outgroups such as the Early Cretaceous neosuchian *Bernissartia fagesii*, Norell (1989) argued that many of the proposed anatomical similarities between *Gavialis*, *Crocodylus*, and *Tomistoma* were plesiomorphic for Crocodylia, and simply lost in Alligatoridae.

Not all comparative anatomical evidence distinguishes *Gavialis* from other crocodylians. All extant *Crocodylus* species, *Osteolaemus*, *Tomistoma*, and *Gavialis* share adaptations for tolerating saltwater, to the exclusion of alligatorids. These include a keritanised buccal cavity and lingual osmoregulatory pores (Taplin et al., 1985; Taplin & Grigg, 1989). Although the latter are greatly reduced in *Gavialis* (which can be interpreted as secondary adaptation to inhabiting freshwater environments), the presence of these pores suggests a closer affinity of *Gavialis* with *Tomistoma* and crocodylids, than to alligatorids (Taplin & Grigg, 1989). Reconsiderations of the biomolecular evidence, using more refined techniques continued to support the sister relationship of *Gavialis* and *Tomistoma* (Hass et al., 1992). Furthermore, in the late 1980s to 1990s, new support for Longirostres emerged from the analyses of DNA sequences and restriction fragment length polymorphism matrices (Densmore & Owen, 1989; Densmore & White, 1991; Gatesy & Amato, 1992; Gatesy et al., 1993; Aggarwal et al., 1994). As such, morphological and molecular datasets continued to support contrasting hypotheses for crocodylian interrelationships.

Poe (1997) presented the first combined phylogenetic analysis of extant crocodylians, incorporating 64 morphological characters (osteological, external morphological, chromosomal, and behavioural), restriction fragment characters, and mtDNA sequences. The resulting strict consensus tree was congruent with the typical molecular topology. Brochu (1997b) conducted a similar combined analysis. Using the same biomolecular data as Poe (1997), Brochu (1997b) included 164 morphological characters, which constituted the largest morphological character dataset applied in crocodylian systematics at the time. Approximately two-thirds of these characters were new, with the remainder drawn from a synthesis of earlier studies (Benton & Clark, 1988; Norell, 1988, 1989; Norell & Clark, 1990; Buscalioni et al., 1992; Willis, 1993; Clark, 1994; Poe, 1997). Brochu (1997b) conducted a series of analyses that used different combinations of extant and fossil taxa, as well as morphological and molecular data. *Gavialis* was consistently recovered as the sister taxon to all other extant crocodylians, in agreement with the traditional morphological hypothesis (Fig. 1.6); however the position of *Tomistoma* depended on whether fossil ingroup taxa were included or excluded (Brochu, 1997b). Brochu's (1997b) dataset has formed the basis of essentially all morphological phylogenetic analyses of Crocodylia over the last two decades. Numerous studies have augmented it with newly described taxa and novel characters, resulting in revised phylogenetic hypotheses (e.g. Brochu, 1999, 2004a, 2004b; Hua & Jouve, 2004; Salisbury et al., 2006; Brochu, 2010, 2011; Brochu & Storrs, 2012; Jouve et al., 2015; Salas-Gismondi et al., 2015; Jouve, 2016; Narváez et al., 2016; Salas-Gismondi et al., 2016; Cidade et al., 2017; Lee & Yates, 2018; Iijima

& Kobayashi, 2019; Massonne et al., 2019; Salas-Gismondi et al., 2019; Groh et al., 2020). Similarly, there has been a synchronous burst of molecular studies of Crocodylia, with phylogenetic analyses of several mitochondrial and nuclear genes (e.g. Harshman et al., 2003; Janke et al., 2005; Ji et al., 2006; McAliley et al., 2006; Roos et al., 2007; Willis et al., 2007; Meganathan et al., 2010; Yan et al., 2010; Man et al., 2011; Meredith et al., 2011; Oaks, 2011; Pan et al., 2020), as well as a whole genome analysis (Green et al., 2014). Despite these developments, the topologies produced from morphological and molecular datasets have remained unchanged, such that the *Gavialis-Tomistoma* morphology versus molecular dichotomy remains unresolved.

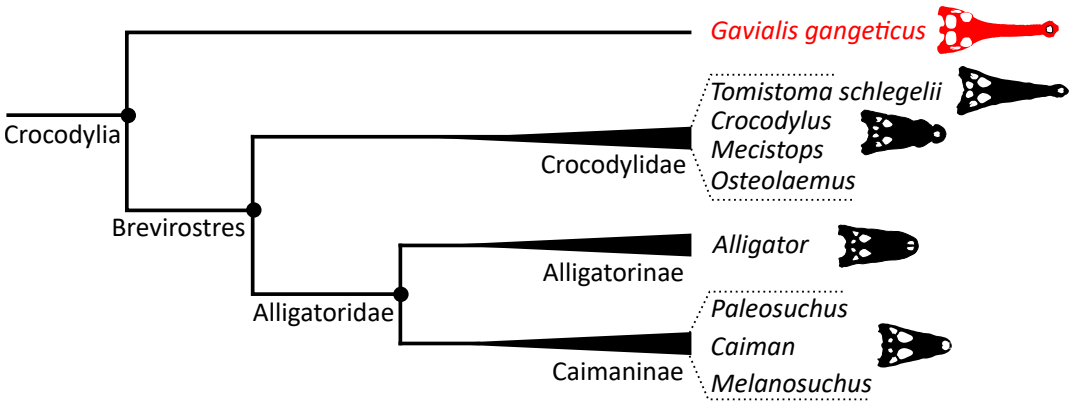



Figure 1.6: Simplified cladogram, illustrating the traditional morphological hypothesis of extant crocodylian interrelationships (e.g. Brochu, 1997b, fig.3a).

### 1.2.2 Taxonomic terms

The definitions of the principal crocodylian clades are listed in Table 1.1. The above mentioned differences between morphological and molecular hypotheses result in differences in the taxonomic content of the principal crocodylian clades, depending on whether a morphological or molecular topology is considered. As such, whenever the constituents of morphological only clades are discussed, quotations marks are used. As an example, Norell et al. (1994) defined Crocodyloidea as *Crocodylus niloticus* and all crocodylians more closely related to it than to *Alligator mississippiensis* or *Gavialis gangeticus*. Among extant species, "Crocodyloidea" refers herein to *Crocodylus*, *Osteolaemus*, *Mecistops*, and *Tomistoma*, in accordance with the morphological hypothesis (Fig. 1.6). By contrast, Crocodyloidea excludes *Tomistoma*, which is more closely related to *Gavialis* than *Crocodylus* in molecular topologies (Fig. 1.5).

Table 1.1: Explanation of clade names, ordered systematically.

| Taxon name | Taxon definition | Definition |
|---|---|---|
| Eusuchia Huxley, 1875 | Brochu (1999) | The last common ancestor of *Hylaeochampsa vectiana*, *Alligator mississippiensis*, *Crocodylus niloticus*, *Gavialis gangeticus* and all of its descendants. |
| Hylaeochampsidae Andrews, 1913 | Buscalioni et al. (2011) | The last common ancestor of *Hylaeochampsa vectiana*, *Iharkutosuchus makadii*, *Pachycheilosuchus trinquei*, *Pietraroiasuchus ormezzanoi* and all of its descendants. |
| Allodaposuchidae Narváez et al., 2015 | Narváez et al. (2015) | *Allodaposuchus precedens* and all crocodyliforms more closely related to it than to *Hylaeochampsa vectiana*, *Shamosuchus djadochtaensis*, *Borealosuchus sternbergii*, *Planocrania datangensis*, *Alligator mississippiensis*, *Crocodylus niloticus*, or *Gavialis gangeticus*. |
| Crocodylia Gmelin, 1789 | Benton and Clark (1988) | The last common ancestor of *Alligator mississippiensis*, *Crocodylus niloticus* and *Gavialis gangeticus*, and all of its descendants. |
| Alligatoroidea Gray, 1844 | Norell et al. (1994) | *Alligator mississippiensis* and all crocodylians more closely related to it than to *Crocodylus niloticus* and *Gavialis gangeticus*. |
| Diplocynodontinae Brochu, 1999 | Brochu (1999) | *Diplocynodon ratelii* and all crocodylians more closely related to it than to *Alligator mississippiensis*. |
| Globidonta Brochu, 1999 | Brochu (1999) | *Alligator mississippiensis* and all crocodylians more closely related to it than to *Diplocynodon ratelii*. |
| Alligatoridae Cuvier, 1807 | Norell et al. (1994) | The last common ancestor of *Alligator mississippiensis*, *Caiman crocodilus* and all of its descendants. |
| Alligatorinae Kälin, 1939 | Brochu (1999) | *Alligator mississippiensis* and all crocodylians more closely related to it than to *Caiman crocodilus*. |
| Caimaninae Norell, 1988 | Brochu (1999) | *Caiman crocodilus* and all crocodylians more closely related to it than to *Alligator mississippiensis* |
| Jacarea Norell, 1988 | Brochu (1999) | The last common ancestor of *Caiman latirostris*, *Caiman crocodilus*, *Caiman yacare*, *Melanosuchus niger*, and all of its descendants. |

**Table 1.1 continued from previous page**

| Taxon name | Taxon definition | Definition |
|---|---|---|
| Planocraniidae Li, 1976 | Brochu (2012) | The last common ancestor of *Planocrania hengdongensis*, *Planocrania datangensis*, *Boverisuchus vorax*, *Boverisuchus magnifrons*, and all of its descendants. |
| Longirostres Cuvier, 1807 | Harshman et al. (2003) | The last common ancestor of *Crocodylus niloticus*, *Gavialis gangeticus*, and all of its descendants. |
| Crocodyloidea Fitzinger, 1826 | Norell et al. (1994) | *Crocodylus niloticus*, and all crocodylians more closely related to it than to *Alligator mississippiensis* or *Gavialis gangeticus*. |
| Crocodylidae Cuvier, 1807 | Norell et al. (1994); Brochu (2003) | The last common ancestor of *Crocodylus niloticus*, *Osteolaemus tetraspis* and all of its descendants. |
| Osteolaeminae Brochu, 2003 | Brochu (2003) | *Osteolaemus tetraspis* and all crocodylians more closely related to it than to *Crocodylus niloticus*. |
| Crocodylinae Cuvier, 1807 | Modified from Brochu (1999) | *Crocodylus niloticus*, and all crocodylians more closely related to it than to *Osteolaemus tetraspis*. |
| Mekosuchinae Balouet and Buffetaut, 1987 | Modified from Salisbury and Willis (1996) and Brochu (2003) | The last common ancestor of *Kambara implexidens* and *Mekosuchus inexpectatus*, and all of its descendants. |
| Gavialoidea Hay, 1930 | Norell et al. (1994) | *Gavialis gangeticus*, and all crocodylians more closely related to it than to *Alligator mississippiensis* and *Crocodylus niloticus*. |
| Gavialidae Adams et al., 1854 | Norell et al. (1994) | The last common ancestor of *Gavialis gangeticus*, *Tomistoma schlegelii*, and all of its descendants. |
| Tomistominae Kälin, 1955 | Brochu (2003) | *Tomistoma schlegelii* and all crocodylians more closely related to it than to *Gavialis gangeticus*. |
| Gavialinae Nopcsa, 1923 | Brochu (2003) | *Gavialis gangeticus* and all crocodylians more closely related to it than to *Tomistoma schlegelii*. |
| Gryposuchinae Vélez-Juarbe et al., 2007 | Vélez-Juarbe et al. (2007) | *Gryposuchus jessei* and all crocodylians more closely related to it than to *Gavialis gangeticus* and *Tomistoma schlegelii*. |

**Table 1.1 continued from previous page**

| Taxon name | Taxon definition | Definition |
|---|---|---|
| Brevirostres Zittel, 1890 | Brochu (1999) | The last common ancestor of Alligatoroidea, Crocodyloidea, and all of its descendants. |

## 1.3 Research Motivation

The research in this thesis is primarily driven by a series of systematic problems and discrepancies between morphological and molecular datasets, which have been partly alluded to in Section 1.2. It is also motivated by the need to consolidate and critically assess the body of published character lists for crocodylian systematics, which may provide a tractable approach to resolving these problems. Furthermore, the research is motivated by the desire to implement and test the efficacy of some methodological approaches in phylogenetic inference that are infrequently applied to crocodylian datasets.

### 1.3.1 Problems in crocodylian systematics

#### The gharial problem

As outlined in Section 1.2.1, the phylogenetic position of *Gavialis gangeticus* in relation to other crocodylians is one of the most persistent problems in crocodylian systematics. It is also the most significant problem, given that the contrasting hypotheses indicate fundamentally different rearrangements of the crocodylian tree. Thus far, the discussion of the gharial problem has centred on topological differences; however, the incongruence has implications for the estimated divergence time of the extant gharials too (Fig. 1.7). Molecular data indicate that *Tomistoma schlegelii* and *Gavialis gangeticus* last shared a common ancestor 31–18 Ma (Oaks, 2011). This estimate is at odds with fossil data, which indicate that taxa ("gavialoids") more closely related to *Gavialis* than to *Tomistoma* first appeared by the latest Cretaceous (ca 70 Ma) (Brochu, 2004a). Harshman et al. (2003) commented that if some of these early appearing "gavialoids" are incorrectly assigned to this clade, then the temporal incongruence would become narrower. In particular, those authors referred to the early diverging taxon, *Thoracosaurus*, remains of which are present in the latest Cretaceous–early Paleogene of Europe and North America (Brochu, 2004a). However, in the subsequent years, several new "gavialoid" taxa have been described, such that it is not only one or two taxa that result in this incongruence. Indeed, there is now a relatively continuous fossil record of morphologically intermediate forms, bridging the gap between the earliest appearing fossil gavialoids and extant *Gavialis* (Fig. 1.8A), including *Eothoracosaurus* from the latest Cretaceous of North America (Brochu, 2004a), *Ocepesuchus* from the latest Cretaceous of North Africa (Jouve et al., 2008), *Eosuchus*

from the early Paleogene of Europe and North America (Delfino et al., 2005; Brochu, 2006b), *Eogavialis* from the late Paleogene to Neogene of Africa (Andrews, 1906; Hecht & Malone, 1972; Storrs, 2003), and *Aktiogavialis* from the late Paleogene to early Neogene of the Caribbean (Vélez-Juarbe et al., 2007; Salas-Gismondi et al., 2019). Similarly, there is an extensive, near-global fossil record of "tomistomines" spanning the early Eocene (~50 Ma) to the Pleistocene (Kobayashi et al., 2006; Brochu, 2007b; Piras et al., 2007; Jouve et al., 2015; Jouve, 2016) (Fig. 1.8B). As such, the morphological hypothesis for an early diverging "Gavialoidea" is highly congruent stratigraphically. Although this hypothesis could of course be incorrect, it would require a large rearrangement of evolutionary relationships among fossil crocodylians, which have been largely stable over the last two decades (e.g. Brochu, 2004a; Brochu et al., 2012; Jouve et al., 2015; Narváez et al., 2016; Salas-Gismondi et al., 2019).

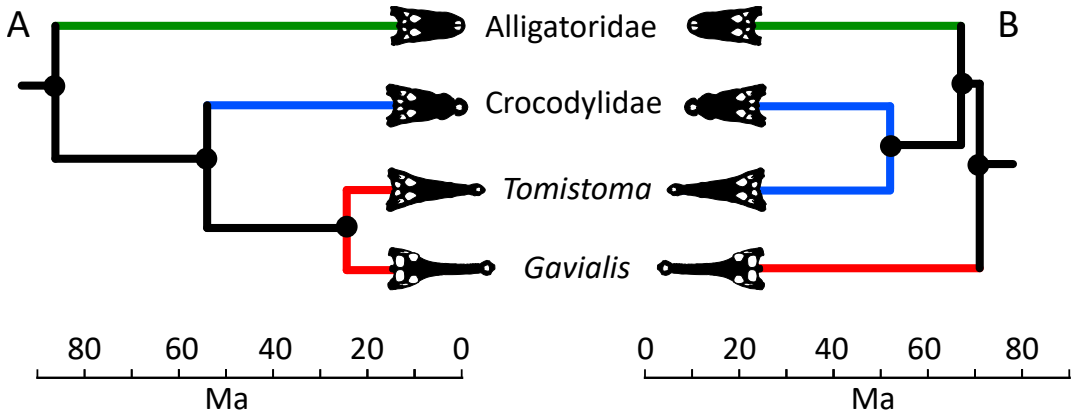



Figure 1.7: Contrasting topologies of molecular (**A**) and morphological (**B**) phylogenies illustrating differences in the divergence timing of principal crocodylian clades. Divergence estimates in A based on Oaks (2011), B based on fossil first appearances.

With the wealth of new morphological character data (Brochu, 1997b), early investigations of the gharial problem explored whether there might be hidden support for the molecular hypothesis in the morphological data, i.e. a 'secondary signal' that supports a grouping of *Tomistoma* + *Gavialis* (Trueman, 1998; Gatesy et al., 2003; Harshman et al., 2003). Trueman (1998) used reverse successive weighting of morphological characters, i.e. down-weighting non-homoplastic characters, in order to allow the secondary signal (if present) to influence the topology. As a result, Trueman (1998) recovered the molecular topology and identified 12 morphological characters that supported this grouping. Using a simpler approach, Harshman et al. (2003) optimised Brochu's (1997b) morphological characters on both the molecular and morphological trees. Harshman et al. (2003) characterised the secondary signal as those characters that had fewer steps on the molecular than the morphological tree, resulting in 17 characters that supported the molecular topology. Furthermore, Harshman et al. (2003) recognised that the construction of several morphological characters precluded "tomistomines" and "gavialoids" from sharing the same character states. Using alternative criteria and based on a slightly different set of characters,

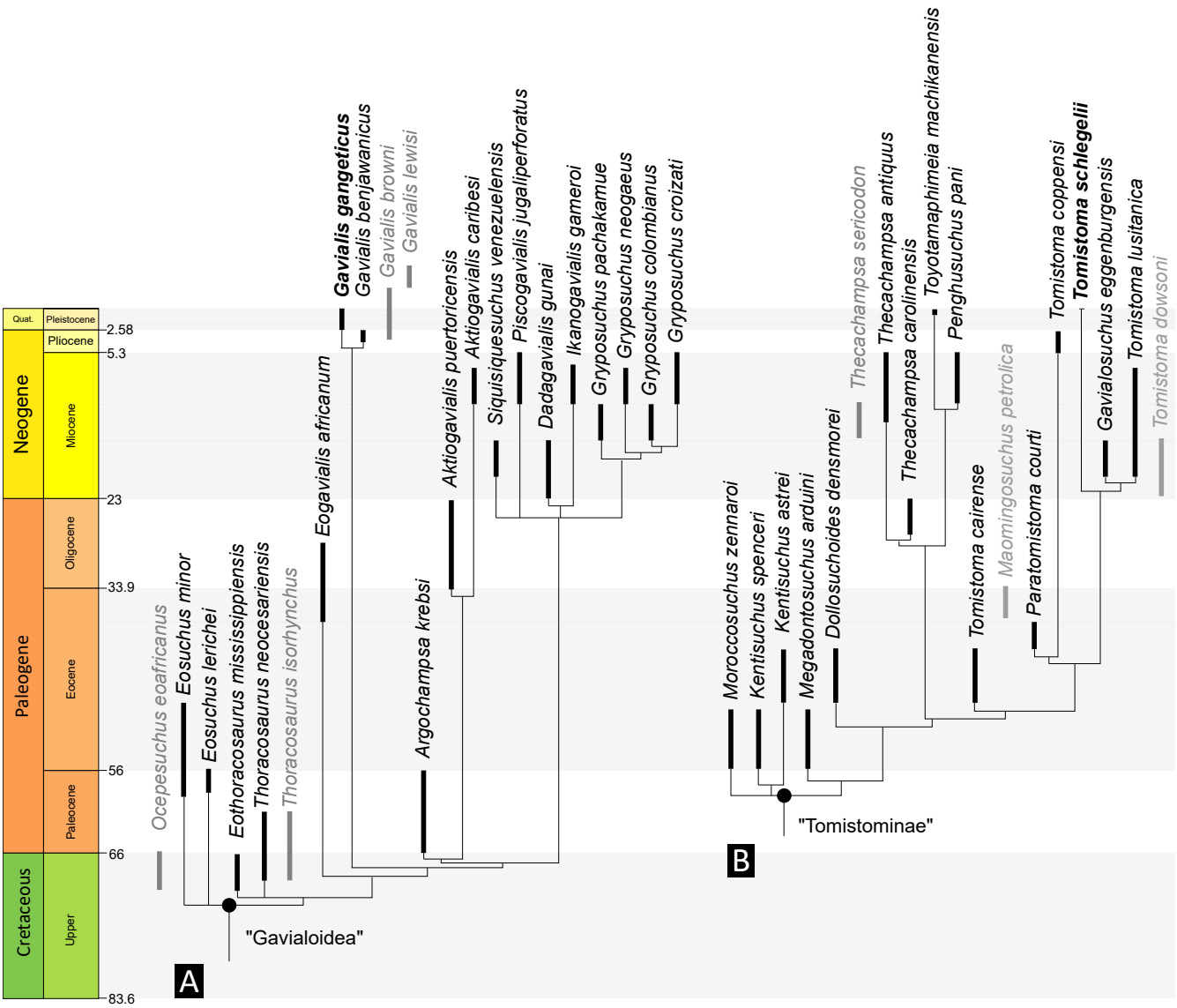



Figure 1.8: Time calibrated phylogenies illustrating the stratigraphic distribution of **A**, "Gavialoidea" after Salas-Gismondi et al. (2019), and **B**, "Tomistominae" after Jouve (2016). Taxa in grey not included in aforementioned analyses. Ages = Ma.

Gatesy et al. (2003) also recovered a secondary signal. As such, it has been demonstrated that there is support for the molecular hypothesis 'hidden' in the morphological data.

Several studies have also turned to combined morphological and molecular analyses to resolve the gharial problem, and these typically recover the molecular topology (Poe, 1997; Gatesy et al., 2003; Gold et al., 2014; Lee & Yates, 2018; Iijima & Kobayashi, 2019). However, the results of combined analyses depend strongly on the proportions of different data types (e.g. Brochu, 1997b; Poe, 1997), and might simply reflect the data with the strongest signal (Brochu, 2003). Furthermore, combined analyses including fossil taxa continue to face the issue of temporal incongruence, given that the earliest appearing, latest Cretaceous "gavialoids" are still recovered within the crown gharial clade (Gatesy et al., 2003; Gold

et al., 2014; Iijima & Kobayashi, 2019). Lee and Yates (2018) introduced stratigraphic data (Bayesian tip-dating) into combined analyses, which resolved both the topological and temporal incongruence. Unlike previous combined analyses, all pre-Neogene "gavialoids" in their analysis were recovered outside of Crocodylia. Furthermore, they recovered several "tomistomines" in the stem of the crown gharial group, resulting in a topology largely consistent with the molecular divergence time of Gavialidae presented by Oaks (2011). Although the use of stratigraphic data in phylogenetic analyses is controversial (e.g. Smith, 2000; Alroy, 2002; Fisher, 2008), Lee and Yates' (2018) study demonstrates that the fossil record can be stratigraphically congruent with the molecular hypothesis.

There are several arguments that support the acceptance of the molecular over the morphological topology. The molecular topology has withstood numerous independent analyses, including the use of multiple gene loci in mitochondrial and nuclear DNA (e.g. Harshman et al., 2003; Man et al., 2011; Oaks, 2011). By contrast, although morphological character datasets have been augmented with new characters, morphological characters are typically reused in subsequent iterations of a dataset, meaning that there is little real independence between analyses. The molecular hypothesis might also be considered correct *a priori* for several reasons. Whereas recent morphological character lists applied to crocodylian systematics contain 200–600 characters (e.g. Brochu et al., 2012; Lee & Yates, 2018; Groh et al., 2020), molecular phylogenies employing multiple gene loci can consider over 7000 base-pair sequences (e.g. Oaks, 2011), and considerably more in whole genome analyses (Green et al., 2014). It might also be argued that DNA sequence data have an advantage over morphological character data, since the delimitation between the four nucleotide bases is unequivocal. Although binary presence/absence characters might be simple to delimit in morphological datasets, the appropriate approach for complex, multistate characters is the subject of much debate (e.g. Wilkinson, 1995; Sereno, 2007; Brazeau, 2011).

Nevertheless, it is prudent to consider ways in which the molecular data could be misleading. A criticism of early biomolecular studies (e.g. Densmore, 1983) was that these were based on phenetic analyses and they lacked outgroup rooting (Norell, 1989). Additionally, in molecular phylogenetic analyses, the issue emerges that the closest living relatives of Crocodylia, Aves, is separated by extremely long branches of approximately 250 million years (Harshman et al., 2003). Using outgroups that are so distantly separated could result in spurious relationships (e.g. Wilberg, 2015). A common argument against the morphological datasets has been that they are strongly affected by convergence (Hass et al., 1992; Brochu, 1997b). However, molecular data can be just as prone to convergence as morphological data, and could be misled by long-branch attraction, i.e. distantly related taxa with many convergently acquired genetic features can be incorrectly grouped together. It is possible then that *Tomistoma* and *Gavialis* truly belong to distantly related lineages as suggested by morphological data, but that their evolutionary (genetic) ancestry has essentially been erased by the accumulation of apomorphies. However, these criticisms have been addressed through: (1) the construction of molecular phylogenies rather than

phenetics; and (2) the use of less convergence-prone, non-coding gene loci to ameliorate issues of long-branch attraction (Harshman et al., 2003). As such, it appears difficult to reject the molecular topology, and thus it is likely that the morphological data is problematic. Indeed, several authors have suggested that the scrutiny of morphological characters might be critical in resolving the incongruence (e.g. Hass et al., 1992; Brochu, 1997b; Harshman et al., 2003). Accordingly, a few studies have begun to reassess the morphological character data. Sookias (2020) conducted a review of morphological characters applied in crocodylian systematics. Based on a sample of extant crocodylians, he found that the removal or revision of characters lacking a 'robust' construction resulted in a topology that is more concordant with the molecular hypothesis. Also, recent studies have demonstrated that a review of certain 'important' taxa could also be formative in the debate. Iijima and Kobayashi (2019) re-evaluated the anatomy of two "tomistomines" from East Asia. They recognised several characteristic "gavialoid" features in these taxa, as well as new characters that begin to bridge the morphological gap between the extant gharials. As such, it appears that the gharial problem might be tractable through improved character and taxon sampling, as well as improved character construction.

**The interrelationships of early diverging crocodylians**

Determining the interrelationships of 'basal' crocodylian taxa with similar plesiomorphic morphologies is challenging. Further complicating this is the fact that crocodylians are generally morphologically conservative (Figs 1.1, 1.2), and their evolutionary history appears to be replete with convergence (Brochu, 2001; Wilberg, 2017). A consequence of this is that early appearing, presumptive 'basal' taxa might be drawn into nested positions within the crocodylian tree (e.g. Cossette & Brochu, 2018; Cossette, 2020). Indeed, this has historically been a problem, with the recovery of several non-crocodylian eusuchians within Alligatoroidea, because of shared cranial features that are now understood to be independently derived (e.g. Wu et al., 1996; Martin, 2007; Delfino et al., 2008b; Martin, 2010b). As such, it is increasingly important to study and improve character sampling from basal members of the principal crocodylian clades: Alligatoroidea, Crocodyloidea, and Gavialoidea. Ultimately this will help us determine ancestral character states in early diverging taxa and distinguish these from highly nested members of a clade. This task is a long-term endeavour, that involves the targeted reappraisal of multiple taxa in each of the principal crocodylian clades.

A relevant issue regarding morphological character sampling is the proportional sampling of different components of the skeleton. The contribution of postcranial characters to morphological character lists used in crocodylian systematics is generally low, as is the case for all of Crocodylomorpha (Godoy et al., 2016). For example, in the data matrix of Brochu and Storrs (2012), 46 out of 187 characters are postcranial ($\sim$25%). The small proportion of postcranial characters may reflect that they are truly less phylogenetically informative than other skeletal components. For example, unlike the cranium,

postcranial elements typically do not comprise many separate osteological elements to create complex sutural relationships amenable to discretisation. However, recent studies of axial and appendicular skeletal components in extant crocodylians have demonstrated that there are broad differences in crocodylian postcrania, which have yet to be incorporated into phylogenetic studies (Chamero et al., 2014; Iijima et al., 2018a). Furthermore, recent studies of notosuchian (Pol et al., 2012; Godoy et al., 2016), basal neosuchian (Martin et al., 2016b), and crocodylian (Iijima & Kobayashi, 2019) anatomy have started to demonstrate that there is a potentially richer suite of postcranial characters, and that these might impact upon crocodylomorph phylogenetic relationships. Nevertheless, few anatomical descriptions of crocodylian taxa include detailed consideration of the postcranial anatomy, which limits our ability to make comparisons and ultimately recognise discerete morphological differences.

*Diplocynodon* is an example of an early diverging alligatoroid crocodylian, whose fossil record extends from the late Paleocene until the middle Miocene (Martin & Gross, 2011; Martin et al., 2014). One of the the most completely preserved species of *Diplocynodon* is *D. hantoniensis* from the late Eocene of the United Kingdom. This species was last described over 150 years ago (Owen, 1850). In addition to extensive cranial and mandibular remains, the postcranial skeleton is exceptionally preserved in this species, which provides an opportunity to explore this typically neglected portion of the skeleton. The revision of early diverging taxa such as *Diplocynodon* may be an important source for character sampling, which could improve our understanding of the interrelationships of early diverging crocodylians, and address suspected instances of convergence.

### The phylogenetic affinities of *Mecistops cataphractus*

Molecular and morphological incongruence is not restricted to the *Tomistoma-Gavialis* debate; the phylogenetic affinities of the African slender snouted crocodile, *Mecistops cataphractus*, also differ between these datasets. Most morphological, and several molecular phylogenies (usually based on single genes), recover *Osteolaemus* and *Mecistops* as successive sister groups to *Crocodylus* (e.g. Poe, 1997; Brochu, 2000; McAliley et al., 2006; Brochu, 2007a; Li et al., 2007; Brochu et al., 2010). By contrast, molecular studies based on multiple gene loci and combined analyses recover *Mecistops* as the sister taxon of *Osteolaemus* (Gatesy et al., 2003; Schmitz et al., 2003; Willis, 2009; Man et al., 2011; Oaks, 2011; Lee & Yates, 2018). The relationship of *Mecistops* to recent *Crocodylus* species and *Osteolaemus* is particularly significant because of its implications on the biogeographic origin of *Crocodylus* (McAliley et al., 2006). *Osteolaemus* and *Mecistops* are endemic to Africa and Madagascar; as such, recovering them as successive outgroups to *Crocodylus* supports an African origin of *Crocodylus* (McAliley et al., 2006). By contrast, if *Mecistops* is more closely related to *Osteolaemus* than to *Crocodylus*, then the geographic origin of *Crocodylus* depends on the interrelationships within *Crocodylus* (Oaks, 2011).

#### Other taxonomic problems

In addition to these broader systematic problems, there are a number of other issues in crocodylian systematics (Fig. 1.9), including: (1) the affinities of the non-crocodylian eusuchian clade Allodaposuchidae, which has been recovered as either the sister clade to Crocodylia (e.g. Narváez et al., 2016) or forming a grouping with Hylaeochampsidae (e.g. Brochu et al., 2012; Narváez et al., 2015); (2) the phylogenetic affinities of *Borealosuchus* (Brochu, 1997a), which has been recovered in the stem of Alligatoroidea and Crocodyloidea (e.g. Brochu, 1997a), as the sister taxon to Gavialoidea (e.g. Puértolas-Pascual et al., 2011), or in a polytomy with Gavialoidea and Brevirostres (e.g. Brochu et al., 2012); (3) the biogeographic origin and phylogenetic affinities of the endemic Australasian clade Mekosuchinae (e.g. Salisbury & Willis, 1996; Brochu & Storrs, 2012; Yates & Pledge, 2017; Lee & Yates, 2018); (4) the taxonomic content and biogeographic origin of Caimaninae, with several recent studies (e.g. Salas-Gismondi et al., 2015; Bona et al., 2018) recovering latest Cretaceous North American taxa as the earliest members of what is typically considered a South American clade (e.g. Brochu, 1999; Bona, 2007); and (5) the species interrelationships of the crown group *Crocodylus* (e.g. Brochu, 2000, 2003; Meganathan et al., 2010; Meredith et al., 2011; Oaks, 2011), as well as the resulting biogeographic implications.

### 1.3.2 Methodological approaches in crocodylian systematics

Morphological phylogenetic analyses of Crocodylia have been relatively methodologically conservative. Only a handful of studies have deviated from exclusively using discrete morphological characters. For example, only two studies have implemented geometric morphometric characters (Gold et al., 2014; Bona et al., 2018) and only one study has used continuous characters (Groh et al., 2020). Similarly, few studies have ordered multistate characters (e.g. Iijima & Kobayashi, 2019), explored the effects of alternative weighting strategies, and considered the optimal method of constructing morphological characters, i.e. whether or not to reductively code characters (Groh et al., 2020). The background for two principal methodological approaches used and later discussed in this study are outlined below.

#### Extended Implied Weighting

It has been argued that characters that are highly homoplastic are less useful in determining phylogenetic relationships than characters exhibiting little homoplasy (Farris, 1969; Goloboff, 1993). Indeed, down-weighting homoplastic characters has been shown to increase phylogenetic accuracy in both simulations and with morphological and molecular datasets (Chippindale & Wiens, 1994; Goloboff et al., 2008a; Goloboff, 2014; Goloboff et al., 2018; Groh et al., 2020). Goloboff (1993) introduced a novel approach to weighting homoplastic characters, 'implied weights', which weights characters during a tree search.

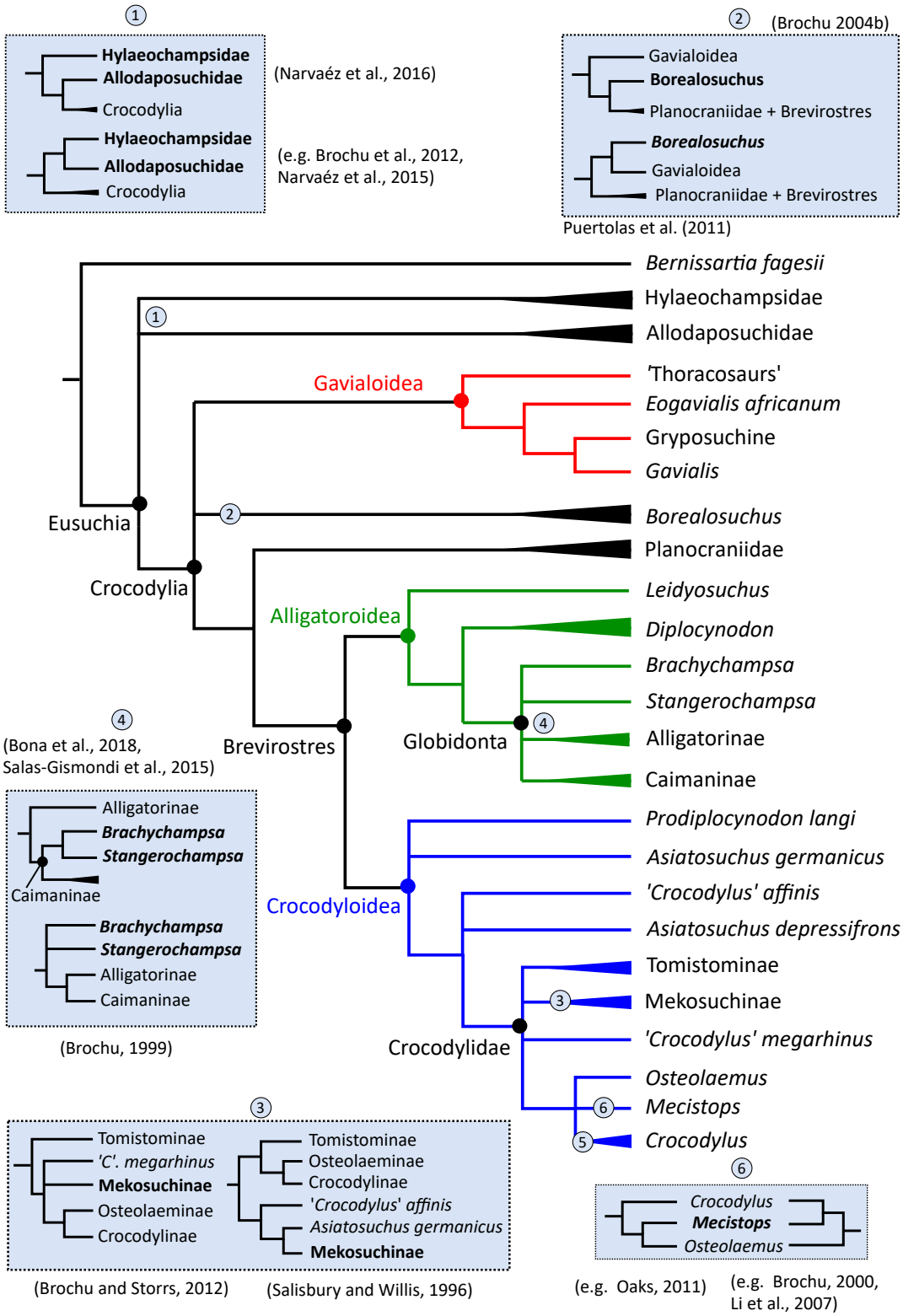



Figure 1.9: Simplified morphological phylogeny of Crocodylia based on Brochu et al. (2012), summarising some of the taxonomic problems discussed in Section 1.3.1.

A weight is calculated for each character depending on its fit to a given tree using the following formula:

$$weight = \frac{k}{h + k} \tag{1.1}$$

where '*k*' is a constant defined in advance that controls the severity of the weighting function (lower *k* values resulting in more severe down weighting), and '*h*' is a measure of a character's homoplasy. The sum of weighted character scores is calculated for each tree recovered during the tree search and tree searches attempt to find trees that maximise these scores (Goloboff, 2014). Missing data can negatively influence traditional implied weighting. This occurs because homoplastic characters that are only scored in a few taxa are not down-weighted when convergent taxa are grouped together. As such, a modification to the algorithm was introduced by Goloboff (2014) – 'extended implied weighting' (EIW) – which is better able to cope with missing data. Since the choice of *k* value has a strong impact on results, multiple *k* values should be tested (higher values especially for larger datasets) (Goloboff et al., 2008a; O'Reilly et al., 2016; Goloboff et al., 2018; Tschopp & Upchurch, 2019; Groh et al., 2020).

**Continuous Morphological Characters**

Morphological characters used in phylogenetic analyses often describe variation that is quantitative, for example describing the relative sizes of processes and lengths of sutural contacts (Rae, 1998; Wiens, 2001). Commonly, such quantitative features are discretely delimited using terminology such as 'large', 'small', and 'poorly developed'. This kind of terminology is very common in crocodylian systematics; for example (italics added by author of present study):

- Brochu (1997b), character 110: "Palatine process extends (0) or does not extend (1) *significantly* beyond the anterior end of the suborbital fenestra."
- Brochu (1997b), character 83: "Quadratojugal sends long anterior process along lower temporal bar (0) or sends *modest* process, or none at all, along lower temporal bar (1)."
- Brochu (1997b), character 111: "Maxillary foramen for palatine ramus of CN-V *small* or not present (0) or *very large* (1)."

Such terminology is problematic, given the subjective nature of determining whether a feature is 'large' or 'small', etc. This has ramifications for repeatability and consistency, particularly when other authors add taxa to a matrix, who might have a very different concept of what connotes a 'large' or 'small' feature. A partial remedy to this problem is through the delimitation of quantitative character states by threshold values. In theory, these thresholds should represent discontinuities in measured values of all the taxa included in an analysis; however, since such data are seldom presented, it might be assumed that previous character delimitations are arbitrarily drawn. Examples in crocodylian systematics include:

- Jouve et al. (2015), character 237: Pterygoid at least 50% wider than its minimal length (0) or nearly as wide as its minimal length (1).
- Lee and Yates (2018), character 217: Elongation of the retroarticular process: length at least 1.5 times the maximum width (0), or less than 1.5 times the maximum width (1).

A number of methods have been developed to delimit quantitative variation into discrete character states, such as gap-coding (Mickevich & Johnson, 1976), gap weighting (Thiele, 1993), and step-matrix gap weighting (Wiens, 2001). These methods use different statistical criteria for delimiting continuous variation; however, a common concern is that taxa with significantly different values may be assigned to the same state, whereas taxa with non-significant differences can be assigned to different states (Farris, 1990; Goloboff et al., 2006). Additionally, Garcia-Cruz and Sosa (2006) demonstrated that alternative methods of character discretisation applied to the same dataset can result in significant differences in phylogenetic results.

Goloboff et al. (2006) introduced a procedure that allows continuous data to be included directly in a phylogenetic analysis, eliminating the need for prior discretisation. Nevertheless, the use of continuous characters is controversial. Arguments against the use of continuous characters include the potential for greater homoplasy, the artificial grouping of taxa based on phenetic data, the arbitrary choices of measurements, and character redundancy (Cox & Urbatsch, 1990; Stevens, 1991; Brocklehurst et al., 2016). Despite these criticisms, many of which are also applicable to discrete morphological characters and can be mitigated, continuous characters have been found to contain useful phylogenetic information in numerous studies across a broad suite of taxonomic groups (e.g. Goloboff et al., 2006; Hornung-Leoni & Sosa, 2008; Mannion et al., 2013; Parins-Fukuchi, 2017; Randle & Sansom, 2017; Jones & Butler, 2018; Groh et al., 2020). An important consideration when using continuous characters is how extensively they should be applied. For example, Wiens (2001) implied that all morphological characters are best treated continuously. However, as commented upon by Goloboff et al. (2006), this is not practical, and characters showing well-defined, discrete variation should be coded as such.

### 1.3.3 Critically assessing characters used in crocodylian systematics

Transparency in morphological phylogenetic datasets is critical, especially considering the strong scientific interest that results from new phylogenetic hypotheses (e.g. Baron et al., 2017; Langer et al., 2017). In morphological phylogenetics, this includes the need for explanations of new and modified characters, justifications for modifications to character scores, as well as the inclusion of reference images to facilitate future reuse of a character list (e.g. Nesbitt, 2011; Tschopp et al., 2015; Groh et al., 2020; Sookias, 2020).

The morphological character lists used in studies of crocodylian phylogeny over the last two decades were partly adapted from earlier studies of more inclusive clades, such as Crocodylomorpha and Crocodyliformes from the 1980s–1990s (e.g. Clark, 1986; Benton & Clark, 1988; Clark, 1994) (Table 1.2). A number of characters used in modern crocodylian datasets also originate from studies in the 1990s; however, these studies still used relatively few morphological characters (typically $< 50$), as they were addressing questions of higher level relationships of Neosuchia and Eusuchia (e.g. Buscalioni & Sanz, 1990; Norell & Clark, 1990), crocodylians (e.g. Norell, 1989), or the interrelationships within crocodylian clades, e.g. Crocodyloidea (Willis, 1993; Salisbury & Willis, 1996) and Alligatoroidea (Buscalioni et al., 1992).

Table 1.2: Summary of previous studies of eusuchian and crocodylian interrelationships. * Note that earlier more inclusive datasets are listed as they were the source of characters for later crocodylian datasets. The dataset of Poe (1997) includes 240 characters but only 64 are osteological morphological characters.

| Study | Clade | Number of characters | Number of taxa |
|---|---|---|---|
| Benton and Clark, 1988 | Crocodylomorpha* | 150 | 33 |
| Norell, 1989 | Crocodylia | 12 | 6 |
| Buscalioni and Sanz, 1990 | Neosuchia* | 52 | 8 |
| Norell and Clark, 1990 | Neosuchia* | 16 | 6 |
| Buscalioni et al., 1992 | Alligatoroidea | 23 | 7 |
| Willis, 1993 | Crocodyloidea | 13 | 11 |
| Clark, 1994 | Crocodyliformes* | 101 | 39 |
| Salisbury and Willis, 1996 | Crocodyloidea | 44 | 23 |
| Poe, 1996 | Crocodylia (extant only) | 64* | 17 |
| Wu et al., 1996 | Eusuchia | 44 | 20 |
| Brochu, 1997b | Crocodylia | 164 | 89 |
| Salisbury et al., 2006 | Eusuchia | 176 | 46 |
| Jouve et al., 2008 | Crocodylia | 201 | 69 |
| Brochu et al., 2012 | Crocodylia | 179 | 95 |
| Brochu and Storrs, 2012 | Crocodylia | 189 | 51 |
| Jouve et al., 2015 | Crocodylia | 238 | 65 |
| Salas-Gismondi et al., 2015 | Crocodylia | 201 | 86 |
| Jouve, 2016 | Crocodylia | 243 | 62 |
| Lee and Yates 2018 | Crocodylia | 278 | 114 |
| Salas-Gismondi et al., 2019 | Crocodylia | 209 | 64 |
| Iijima and Kobayashi, 2019 | Crocodylia | 254 | 69 |
| Groh et al., 2020 | Neosuchia* | 569 | 112 |

Some of the earliest studies to synthesise and adapt characters from these earlier works, and include a large sample of fossil crocodylian taxa were Wu et al. (1996) and Brochu (1997a, 1997b) (Table 1.2). The dataset of Brochu (1997a, 1997b) constituted one of the largest increases in character and taxon sampling (102 new characters, 89 taxa). This dataset and later modifications of it (Brochu, 1999, 2004b) have generally formed the basis of most datasets addressing crocodylian interrelationships over the last

two decades. However, there are few studies that have both synthesised and critically evaluated the body of morphological characters that have been published since the works of Brochu (1997a, 1997b) (e.g. Groh et al., 2020; Sookias, 2020). Although Groh et al. (2020) included a large number of crocodylian taxa, their study focused on the evolutionary relationships of Neosuchia, and did not sample a number of crocodylians (e.g. Mekosuchinae) and non-crocodylian eusuchians (e.g. Allodaposuchidae). Furthermore, whereas their study provides the most comprehensive synthesis of characters used in studies of Crocodylomorpha, it does not provide justifications for modifications of individual characters. Conversely, whereas Sookias (2020) provided an in-depth evaluation of Brochu's (1997a, 1997b) morphological characters (applied in the dataset of Narváez et al., 2016), his study assessed the robustness of characters based only on extant taxa and disregarded characters that did not show variation in that sample. Furthermore, although a commonly used character list was used in the study of Sookias (2020), a large number of additional characters from other studies were not considered. As such, and considering that significant discrepancies still exist in crocodylian systematics (most notably the gharial problem), further scrutiny of morphological characters is warranted.

## 1.4 Thesis Aims

In light of the motivation outlined in Section 1.3, the aims of this thesis are:

1. To reassess the anatomy of the basal alligatoroid crocodylian, *Diplocynodon hantoniensis*.
2. To construct a new, illustrated, consistently and clearly defined character list for phylogenetic analyses of Crocodylia, including justifications for new and modified characters.
3. To assess the phylogenetic interrelationsips of Crocodylia, exploring systematic problems in the clade, as well as the effects of different treatments of quantitative data and weighting strategies.
4. To review the evolutionary and biogeographic history of Crocodylia.

## 1.5 Thesis Outline and Structure

This thesis is organised into four research chapters (Chapters 2–5). In Chapter 2, I provide a comprehensive reappraisal of the anatomy of the 'basal' alligatoroid *Diplocynodon hantoniensis*. Based on this description and comparisons with other crocodylians, I begin to outline several potential new characters that bear on crocodylian phylogenetics, including new data from the postcranial skeleton (**Aim 1**). In Chapter 3, I present a new, illustrated character list for Crocodylia, based on a synthesis of existing character lists and first hand observations of a global sample of crocodylian specimens. Here I justify

the extensive modifications made to the delimitation of most characters, and explain notable changes to character scores (**Aim 2**). In Chapter 4 I present the results of several phylogenetic analyses based on the new character list in Chapter 3. Herein I discuss the effects of different weighting strategies, treatments of quantitative characters and test new topological relationships (**Aim 3**). Furthermore, I provide new diagnoses for the principal crocodylian clades and address some specimen level problems. In Chapter 5 I present a synthesis of crocodylian evolutionary history and historical biogeography based on the phylogenetic results in Chapter 4, and a comprehensive literature review (**Aim 4**). I summarise the main research findings of this thesis in Chapter 6, and in light of these findings I outline several avenues for future research.

## 1.6 Institutional Abbreviations

**AMNH**, American Museum of Natural History, New York, USA; **CAMSM**, Sedgwick Museum of Earth Sciences, University of Cambridge, UK; **FMNH**, Field Museum of Natural History, Chicago, Illinois, USA; **HLMD**, Hessisches Landesmuseum Darmstadt, Germany; **IGM**, Instituto Nacional de Investigaciones en Geociencias, Minería y Quimica, Bogotá, Colombia; **IRScNB**, Institut Royal des Sciences Naturelles de Belgique, Brussels, Belgium; **IVPP**, Institute of Vertebrate Paleontology and Paleoanthropology, Beijing, China; **MACN**, Museo Argentino de Ciencias Naturales, Buenos Aires, Argentina; **MCZ**, Museum of Comparative Zoology, Harvard University, Cambridge, Massachusetts, USA; **MLP**, Museo de la Plata, Buenos Aires Province, Argentina; **MMS/VBN**, Musée du Moulin seigneurial/Velaux-La Bastide Neuve; **MNHN**, Museum national d'Histoire naturelle, Paris, France; **MPEF**, Museo Paleontológico Egidio Feruglio, Trelew, Argentina; **NHMUK**, Natural History Museum, London, UK; **NMC**, Canadian Museum of Nature, Ottawa, Ontario, Canada; **QM**, Queensland Museum, Brisbane, Australia; **SMF**, Senckenberg Museum, Frankfurt, Germany; **SMNK**, Staatliches Museum für Naturkunde, Karlsruhe, Germany; **SMNS**, Staatliches Museum für Naturkunde, Stuttgart, Germany; **UCMP**, University of California Museum of Paleontology, Berkeley, California, USA; **UCMZ**, University of Cambridge Museum of Zoology, Cambridge, UK; **UFAC**, Universidade Federal do Estado de Acre, Rio Branco, Brazil; **USNM**, United States National Museum, Smithsonian Institution, Washington DC, USA; **YPM**, Yale Peabody Museum of Natural History, Yale University, New Haven, Connecticut, USA; **ZMNH**, Zhejiang Museum of Natural History, Zhejiang Province, China.

## 1.7 Author Contributions

Chapter 2 forms the basis of the following publication:

Rio, J. P., Mannion, P. D., Tschopp, E., Martin, J. E., and Delfino, M. 2020. Reappraisal of the morphology and phylogenetic relationships of the alligatoroid crocodylian *Diplocynodon hantoniensis* from the late Eocene of the United Kingdom. *Zoological Journal of the Linnean Society*, 188(2), 579–629.

M. Delfino, P. D. Mannion, and I conceived this project. I carried out the research, writing all sections included here, as well as producing all photographs and illustrations. All authors contributed comments on earlier drafts. E. Tschopp wrote the methodology and performed phylogenetic analyses in the publication, which are excluded here, given that I incorporate the findings of this chapter in a new dataset for phylogenetic analysis (see Chapter 4). All remaining chapters were conceived by myself and P. D. Mannion, with comments from P. D. Mannion in earlier drafts of each chapter.

# Chapter 2

# Reappraisal of the Morphology of the Alligatoroid Crocodylian *Diplocynodon hantoniensis* from the Late Eocene of the United Kingdom

---

## 2.1 Introduction

Alligatoroidea is one of the three principal lineages in Crocodylia, whose fossil record begins in the Campanian of North America (Brochu, 2003). Among the earliest diverging members of Alligatoroidea is *Diplocynodon*. The fossil record of this 'basal' alligatoroid genus extends from the late Paleocene to middle Miocene of western Europe (Martin, 2010a; Martin & Gross, 2011; Delfino & Smith, 2012; Martin et al., 2014; Aráez et al., 2017). Nine species are currently considered valid, comprising: (1) *D. remensis* from the late Paleocene of France (Martin et al., 2014); (2) the middle Eocene species *D. darwini* (Ludwig, 1877; Hastings & Hellmund, 2015) and *D.* (*Baryphracta*) *deponiae* (Frey et al., 1987; Delfino & Smith, 2012) from Germany, and *D. tormis* from Spain (Buscalioni et al., 1992); (3) *D. elavericus* (Martin, 2010a) and *D. hantoniensis* (Wood, 1844) from the late Eocene of France and the UK, respectively; (4) *D.* (*Hispanochampsa*) *muelleri* from the early Oligocene of Spain (Kälin, 1936; Piras & Buscalioni, 2006); (5) the type species *D. ratelii* from the early Miocene of France (Pomel, 1847; Vaillant, 1872) and Spain (Aráez et al., 2017), and possibly from the early Oligocene of France (Brinkmann & Rauhe, 1998) and Italy (Kotsakis et al., 2004) too; and (6) *D. ungeri* from the middle Miocene of Austria (Pragner, 1845; Martin & Gross, 2011) and France (Ginsburg & Bulot, 1997). Whereas remains of nearly all of these species of *Diplocynodon* have been described or revised recently, one of the earliest named, *Diplocynodon hantoniensis*, has not been re-described for over 150 years.

The Headon Hill Formation is a late Eocene (Priabonian) freshwater unit within the Hampshire Basin that crops out in southern England and the Isle of Wight (Edwards & Daley, 1997; Daley, 1999). One mainland locality, Hordle (=Hordwell) Cliff, near the town of Lymington, in Hampshire, has yielded abundant fossil remains from several beds of the lowermost unit of the Headon Hill Formation: the Totland Bay Member (formerly the 'Lower Headon Beds') (Edwards & Daley, 1997).

The first report of crocodylian remains from the beds at Hordle Cliff was presented by Edward Charlesworth on behalf of Searles Wood in the Annals and Magazine of Natural History in 1844. This short account reported the discovery of: "A great portion of the head of an alligator, having nearly all the upper range of teeth (42 in number) remaining, along with the humerus, dermal scutæ and other parts of the skeleton" and that "Mr. Wood proposes to call the Hordwell alligator *A. Hantoniensis*" (Wood, 1844, p. 351). A second account of Hordle Cliff was published by Wood (1846, p. 6), in which he reported, under the genus *Alligator*, that: "A considerable portion of the skeleton of a crocodile, resembling the New World type, for which I propose the specific name *Hantoniensis*". Wood (1846, pls 1, 6, 7) also figured some cranial remains, a femur, and a cervical vertebra, under the name '*Alligator Hantoniensis*'. As the 1844 publication lacked either an accession number or figures to identify the material, Wood (1846) should be considered the authority for the name *Alligator hantoniensis*.

Both the Marchioness of Hastings and Owen presented new crocodylian remains from Hordle Cliff

at the Seventeenth Meeting of the British Association for the Advancement of Science held at Oxford in June 1847, which were published as reports the following year (Hastings, 1848; Owen, 1848). According to these reports, Lady Hastings exhibited two crocodylian skulls from Hordle Cliff, that Owen (1848, p. 66) argued more closely resembled modern crocodiles than alligators or gavials, based on "the festooned contour of the alveolar border of the upper jaw" and that "the inferior canines rest in grooves or notches upon the outer margin of the upper jaw when the mouth is closed, and their entire crowns are exposed". Consequently, "Owen proposed to call the extinct species from Hordle *Crocodilus Hastingsiae*, in honour of the accomplished lady by whom the singularly perfect examples of the species had been recovered and restored" (Owen, 1848, p. 66). This report also notes that Mantell, who was in the audience, mentioned the presence of "a fossil species of *Alligator* (*Alligator Hantoniensis*) described by Mr. Searles Wood, from a specimen of the lower jaw and teeth found in the freshwater beds at Hordwell Cliff", but that Owen "had not seen this specimen" (Owen, 1848, p. 66).

Owen (1850) subsequently described and figured this material as *Crocodilus Hastingsiae*. He also commented upon a suite of similarities with the type specimen of *Alligator hantoniensis*, noting that the skulls of these two taxa were almost indistinguishable. However, the one notable difference pertained to the nature of the occlusion of the jaws. Whereas the fourth dentary tooth in the skulls of *Crocodilus hastingsiae* occludes into a notch (i.e. it remains visible with the jaws closed), that of *Alligator hantoniensis* occludes into a pit (i.e. it is obscured with the jaws closed). Although Owen (1850) suggested that this difference might merely reflect individual variation, he was also wary that this was a feature consistently used to distinguish modern crocodiles from alligators. As such, he maintained that *Crocodilus hastingsiae* represents a crocodile, rather than an alligator, and tentatively retained *Alligator hantoniensis* as a distinct taxon. The crocodylian-bearing bed was subsequently informally named the 'Crocodile Bed' by Wright (1851), and this fine white sandstone unit is one of the most fossiliferous layers at Hordle Cliff (Wright, 1851).

Pomel (1853, p. 124) referred *Alligator hantoniensis* to *Diplocynodon* on the basis of shared features with the French species *Diplocynodon ratelii*, which he had named several years earlier (Pomel, 1847). However, this new combination, *Diplocynodon hantoniensis*, seems to have gone unnoticed for the next three decades. Meyer (1857, p. 538) also noticed close affinities between the French and UK remains, but did not make any taxonomic referral. Subsequently, Huxley (1859) described the dermal armour of the Hordle Cliff crocodylian. He contended that only one crocodylian was present at this locality, and that this taxon should be referred to as *Crocodilus hastingsiae*. Woodward (1885) also only recognized one taxon, and argued that the differences in occlusion were likely individual variation. Although Woodward (1885, p. 509) commented that the Hordle Cliff crocodylian "combines the characters both of Crocodiles and Alligators to a remarkable extent; and it also possesses some features that would quite entitle it to rank as a distinct genus", he also made no mention of Pomel's (1853) referral to *Diplocynodon*, continuing

to refer to the material as *Crocodilus hastingsiae*. Finally, following Pomel (1853), Lydekker (1887) argued that this material should be referred to *Diplocynodon hantoniensis* (see also Lydekker, 1888). The latter assignment has since been followed in the literature, and supported in later phylogenetic analyses (e.g. Buscalioni et al., 1992; Brochu, 1999), with the differences in occlusal morphology likely to reflect ontogenetic variation (Norell et al., 1994; Brochu, 1999).

Here, I provide the first revision of *Diplocynodon hantoniensis* since Owen (1850), presenting a comprehensive description of all cranial and postcranial remains from Hordle Cliff accessioned in the NHMUK and the CAMSM. I provide a new diagnosis for the species, and comment on referrals to *Diplocynodon hantoniensis* from approximately contemporaneous deposits in Switzerland (Pictet et al., 1857), Germany (Gramann, 1958), France (Vignaud et al., 1996), and the USA (Weems & Grimsley, 1999). Based on comparison with other species of *Diplocynodon* and a description of the usually neglected postcranial skeleton, I outline several anatomical features that will form the basis of morphological phylogenetic characters.

## 2.2 Systematic Palaeontology

EUSUCHIA Huxley, 1875
CROCODYLIA Gmelin, 1789
ALLIGATOROIDEA Gray, 1844
*DIPLOCYNODON* Pomel, 1847
*Diplocynodon hantoniensis* Wood, 1846
*Alligator hantoniensis* Wood, 1846
*Crocodilus hastingsiae* Owen, 1848
*Crocodilus hastingsiae* Owen, 1850
*Diplocynodon hantoniensis* Pomel, 1853
*Crocodilus hastingsiae* Huxley, 1859
*Crocodilus hastingsiae* Woodward, 1885
*Diplocynodon hantoniensis* Lydekker, 1887
*Diplocynodon hantoniensis* Buscalioni et al., 1992
*Diplocynodon hantoniensis* Brochu, 1999

Holotype: NHMUK OR 25166 (holotype of '*Alligator hantoniensis*'), anterior portion of a skull (Fig. 2.1).

Referred material : see Appendix A.

Type locality: Hordwell Cliff, near Lymington, Hampshire, United Kingdom.

Type horizon: Totland Bay Member, Headon Hill Formation; Priabonian (late Eocene) (Edwards & Daley, 1997; Daley, 1999).

Revised diagnosis: *Diplocynodon hantoniensis* can be diagnosed by the following unique combination of characters (autapomorphies marked by an asterisk): (1) premaxillary surface posterolateral to naris with a deep notch; (2) short anterior ectopterygoid process, which forms the medial wall of the posteriormost maxillary alveolus, before veering medially to the suborbital fenestra*; (3) ectopterygoid-pterygoid flexure retained throughout ontogeny*; (4) surangular-angular suture meets the articular dorsal to its ventral tip in the mandibular adductor chamber*; (5) broad preorbital ridge on the lacrimal; (6) prominent laminae and sulci either side of the choana.

## 2.3 Description

### 2.3.1 Skull

#### General proportions, preservation and ornamentation

Several remains represent portions of the skull, including three nearly complete skulls: NHMUK OR 30392, NHMUK OR 30393 (Figs 2.1–2.4), and CAMSM TN 907. All three of these skulls are large: NHMUK OR 30392 is 375 mm long from the anterior tip of the premaxillae to the posterior margin of the skull table (measured along the midline on the skull surface), with NHMUK OR 30393 and CAMSM TN 907 comparable in size (Table 2.1). The preserved portion of NHMUK OR 25166 also indicates a similarly sized individual. At the other end of the spectrum, NHMUK OR 25170.a is a partial juvenile skull that is about 60 mm long from the anterior tip of the maxillae (the premaxillae are not preserved) to the posterior edge of the skull table. Preservation varies significantly from specimen to specimen, with different degrees of completeness, but deformation is generally very minor. For example, the nasals of NHMUK OR 30393 are slightly lowered in respect to the maxillae. Some partial skulls, including NHMUK R 1042, OR 25170a and OR 29694, are still partly embedded in matrix, whereas others have been internally reinforced with plaster or a cement-like material, including NHMUK OR 30392. The surfaces of the two best-preserved skulls have been partly covered by plaster in order to provide the impression of completeness (Fig. 2.2–2.4). The overall appearance of the skull is that of a generalized crocodylian, with the rostrum (the region anterior to the orbits) representing about 65% of the entire length of the skull. There is no medial dorsal boss on the rostrum. Canthi rostrali are clearly absent, but preorbital ridges are prominent in adult individuals (see description of the lacrimal). In posterior view, the skull table is approximately planar, except for a modest depression in mature specimens (e.g. NHMUK OR 30392 and 30393) (Fig. 2.3D), at the dorsal exposure of the supraoccipital. The lateral sides of the skull table are convex in juvenile specimens (NHMUK OR 25167 and OR 25170.a), and the paroccipital

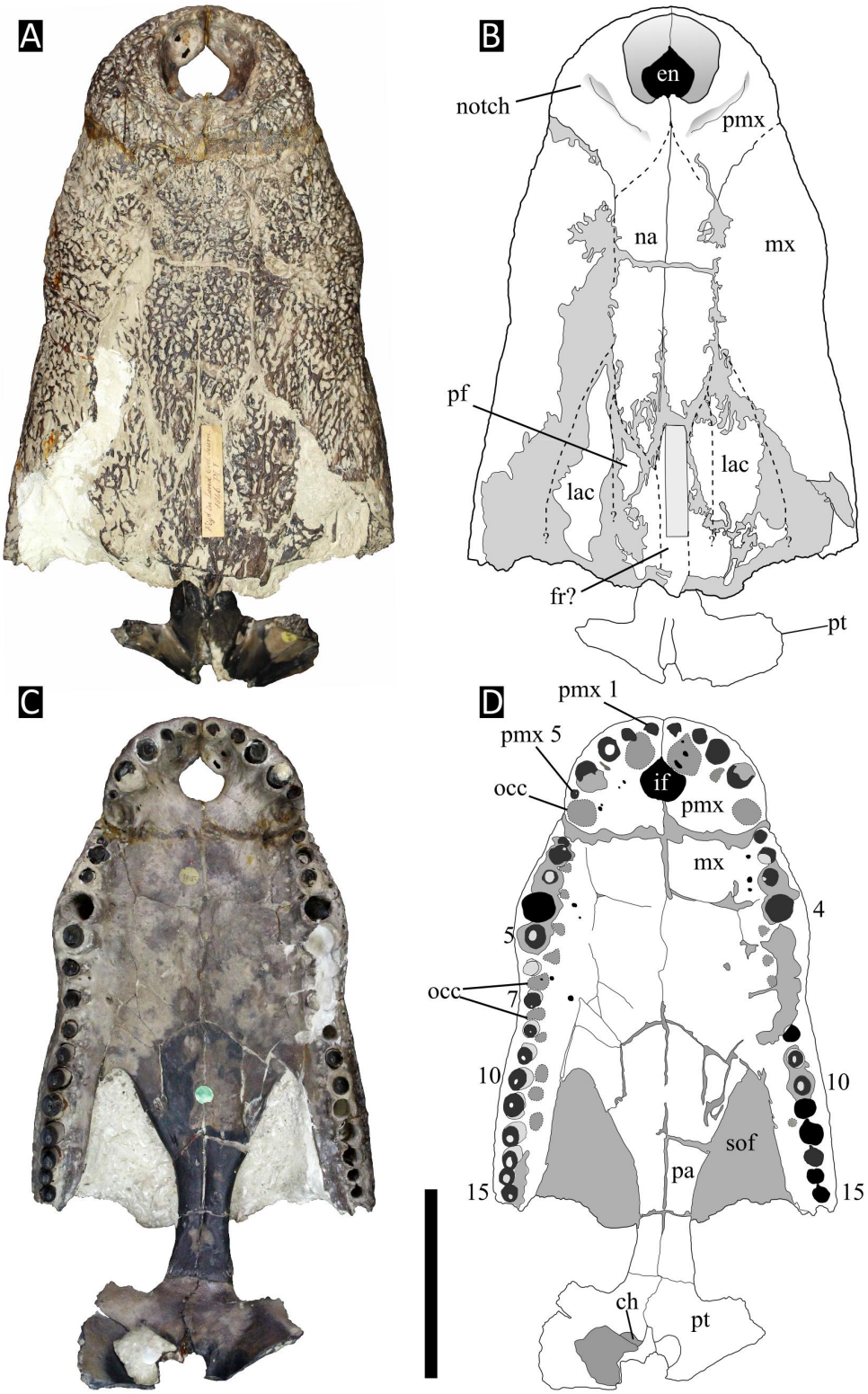



Figure 2.1: The skull of *Diplocynodon hantoniensis*, holotype of '*Alligator hantoniensis*' (NHMUK 25166) in dorsal (**A**, **B**) and ventral (**C**, **D**) views. Abbreviations: **en**, external naris; **ch**, choana; **fr**, frontal; **if**, incisive foramen; **lac**, lacrimal; **mx**, maxilla; **na**, nasal; **occ**, occlusal pit; **pa**, palatine; **pmx**, premaxilla; **pmx 1**, premaxillary tooth 1; **pt**, pterygoid; **sof**, sub-orbital fenestra. Scale bar = 10 cm.

Table 2.1: Cranial measurements of *Diplocynodon hantoniensis* (mm).

| Feature | NHMUK OR 30393 | NHMUK OR 25166 | NHMUK OR 30392 | CAMSM TN 907 |
|---|---|---|---|---|
| Dorsal skull length | 375 | NA | 375 | 344 |
| Narial length | 37 | 40 | 33 | 41 |
| Narial width | 29 | 40 | 35 | 42 |
| Snout length along medial axis | 255 | 240 | 240 | 213 |
| Rostrum width at notch/pit for fourth dentary tooth | 97 | 102 | 84 | 82 |
| Orbit length | 60 | NA | 59 | 58 |
| Interorbital width | 25 | NA | 23 | 25 |
| Supratemporal fenestra length | 46 | NA | 44 | 41 |
| Supratemporal fenestra width | 25 | NA | 26 | 28 |
| Skull table anterior width | 86 | NA | 79 | 77 |
| Maximum skull width across quadrates | 227 | NA | 220 | 215 |

processes have short squamosal rami (Figs 2.5, 2.6). However, the lateral sides are straight or slightly concave in adult specimens (NHMUK OR 30392 and 30393), in which the squamosal rami are long.

### Cranial fenestrae and openings

The anterodorsally facing naris is entirely hosted within the premaxillae (Figs 2.1, 2.2). It is approximately circular and has a rounded, convex anterior rim, nearly straight lateral rims (especially in NHMUK OR 25166), and a concave posterior rim (as a result of an anterior projection of the medial edge of each premaxilla). The rim of the external naris is flush with the dorsal surface of the surrounding premaxillae, which is posterolaterally marked by a depression that is nearly as developed as the one that characterizes *Alligator* (Figs. 2.1B, 2.2B). Whereas the lateral walls of the naris are nearly vertical, the anterior walls are very shallowly inclined posteroventrally. The dorsal margin of each orbit is composed of the frontal, the posterior margin by the postorbital, the posterolateral and lateral margins by the jugal, and the anterior margin is formed by the lacrimal and prefrontal. The orbits are deeply concave medially, but straight or slightly convex laterally, and are truncated by the postorbital bars posteriorly. The orbital rim is flush with the jugal surface (a hint of a crest is present in NHMUK OR 30392), but raised into a crest along the prefrontal edge. In the juvenile partial skull NHMUK OR 25170a (Fig. 2.5), the posterolateral edge of the prefrontal is extremely high and forms a vertical laminar ridge delimiting the anteromedial surface of the orbit. It is not clear if palpebral bones were originally absent or are simply not preserved in any available specimen. The supratemporal fenestrae are oval-shaped, with their long-axes oriented anteroposteriorly. They are much smaller than either the orbits or infratemporal fenestrae in adult specimens, but comparatively large in the juvenile individual NHMUK OR 25170.a, which has a very broad supratemporal fossa.

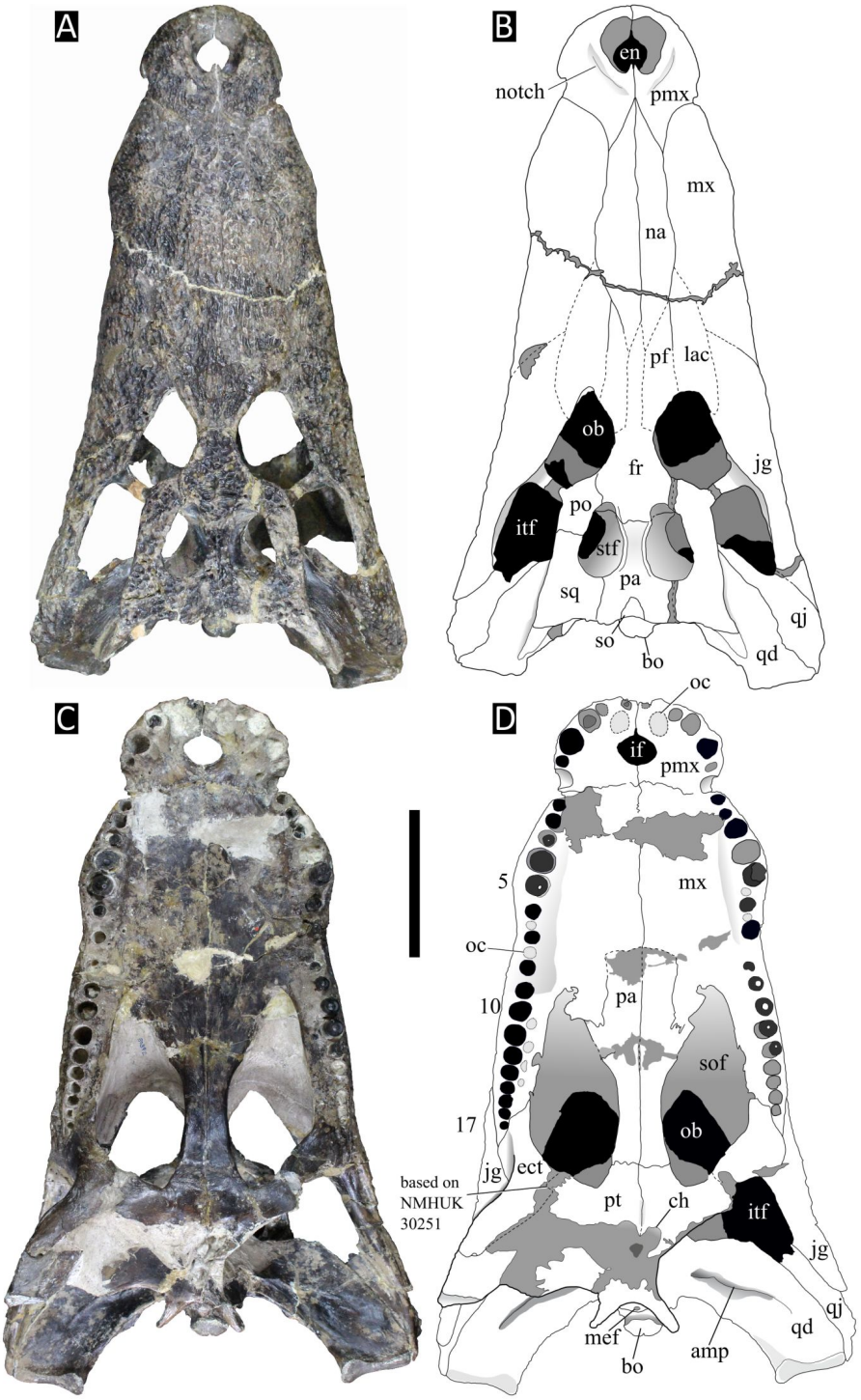



Figure 2.2: The skull of *Diplocynodon hantoniensis* (NHMUK 30392) in dorsal (**A**, **B**) and (**C**, **D**) ventral view. Abbreviations: **amp**, scar for musculus adductor mandibulae posterior; **bo**, basioccipital; **ch**, choana; **en**, external naris; **fr**, frontal; **itf**, infratemporal fenestra; **jg**, jugal; **lac**, lacrimal; **mef**, median eustacian foramen; **mx**, maxilla; **na**, nasal; **ob**, orbit; **oc**, occlusal pit; **pmx**, premaxilla; **pf**, prefrontal; **po**, postorbital; **qd**, quadrate; **qj**, quadratojugal; **so**, supraoccipital; **sq**, squamosal; **stf**, supratemporal fenestra. Scale bar = 10 cm.

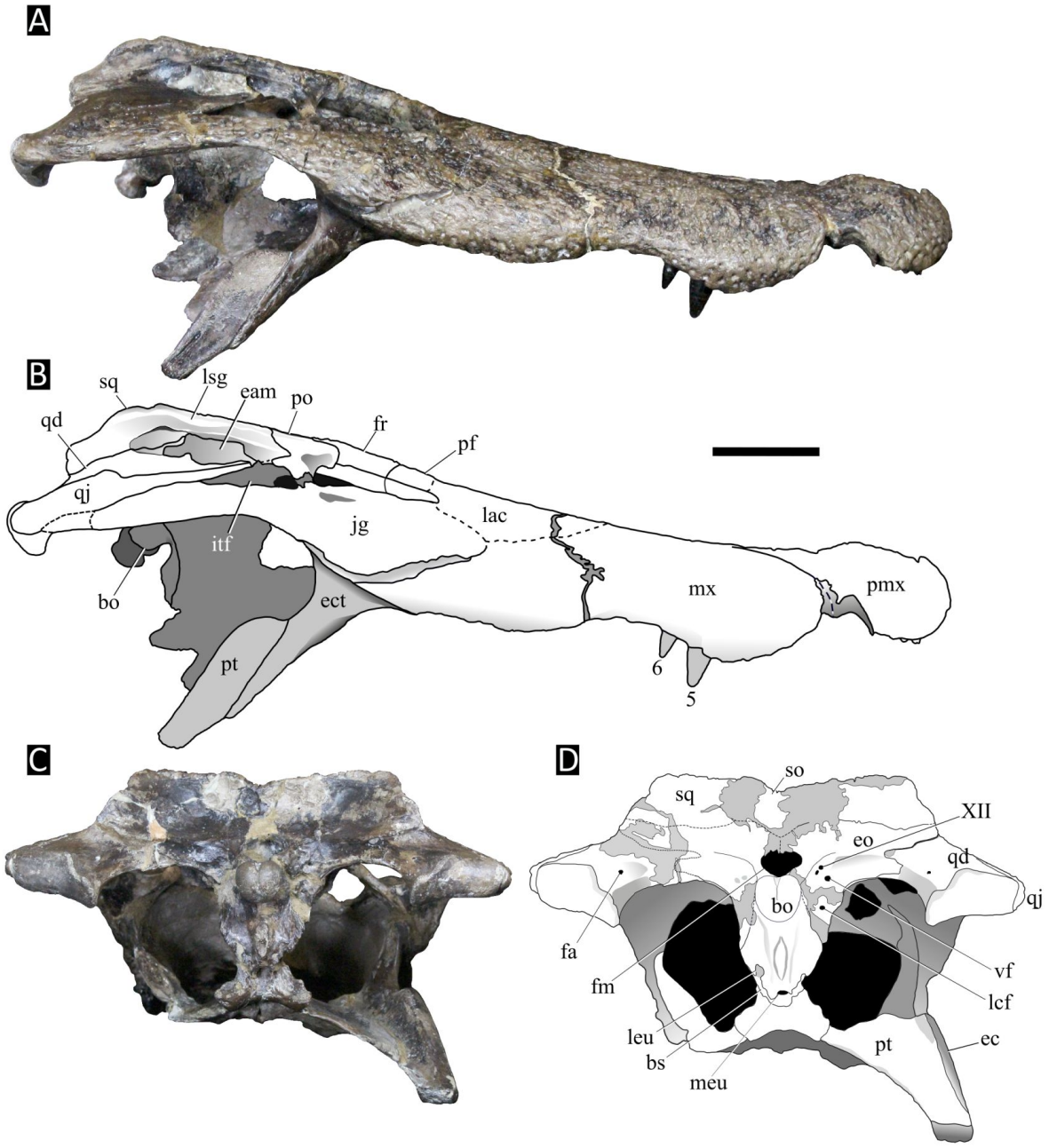



Figure 2.3: The skull of *Diplocynodon hantoniensis* (NHMUK 30392) in lateral (**A**, **B**) and occipital (**C**, **D**) views. Abbreviations: **5**, **6**, maxillary tooth numbers; **bo**, basioccipital; **bs**, basisphenoid; **eam**, external auditory meatus; **ect**, ectopterygoid; **eo**, exoccipitals; **fm**, foramen magnum; **fr**, frontal; **itf**, infratemporal fenestra; **jg**, jugal; **lac**, lacrimal; **leu**, lateral eustachian foramen **lsg**, lateral squamosal groove; **meu**, median eustachian foramen; **mx**, maxilla; **pf**, prefrontal; **pmx**, premaxilla; **po**, postorbital; **pt**, pterygoid; **qd**, quadrate; **qj**, quadratojugal; **so**, supraoccipital; **sq**, squamosal; **vf**, vagus foramen; **XII**, foramen for cranial nerve 12. Scale bar = 5cm.

The medial rim of each supratemporal fenestra is slightly raised into a ridge in the largest specimens, with a depressed interfenestral bar (Figs 2.2B, 2.4B). However, in smaller specimens (e.g. NHMUK OR 25167 and 25170a) the rim of the supratemporal fenestrae is nearly flush with the parietal surface (Figs 2.5, 2.6). Whereas the posterior and medial fenestral margins are curved, the anterolateral margins are straight, and the fenestrae taper in width anteriorly to form an acute corner (Fig. 2B). The rim of each supratemporal fenestra does not significantly overhang the supratemporal fossa. The medial parietal wall of the supratemporal fenestra is imperforate. The infratemporal fenestrae are triangular in shape and are approximately as long as the orbits, although their surface area is smaller overall than that of the orbits. The most completely preserved infratemporal fenestra is the right opening of NHMUK OR 30392, which is missing only a very small portion of the quadratojugal, close to the postorbital (Fig. 2.3B). The jugal forms the ventral margin and anterior angle of the infratemporal fenestra, and the dorsal angle appears to be formed by the quadratojugal (CAMSM TN 918). From the juvenile specimen NHMUK OR 25167 (Fig. 2.6), it is clear that the quadratojugal formed the entire posterior corner of the infratemporal fenestra. The external auditory meatus is clearly visible in NHMUK OR 30392 and 30393 (Figs 2.3B, 2.4D) and has a clover leaf shape. Whereas the dorsal margin of the external auditory meatus is composed of the squamosal, the quadrate forms the bowed posterior rim, as well as the ventral and anterior margins. The quadrate–squamosal suture extends dorsally along the posterior margin of this opening. The quadrate forms a narrow ridge on the floor of the external auditory meatus, extending medially into the ear canal. A large preotic foramen pierces the quadrate anterior to the external auditory meatus (Fig. 2.4D). The elliptical foramen magnum, delimited by the exoccipitals and the basioccipital, is equal in width to the occipital condyle (Fig. 2.3D). Post-temporal fenestrae are rather small: they are delimited by the parietal and squamosal dorsally, and by the supraoccipital and exoccipital ventrally. The lateral carotid foramen opens lateral to the basisphenoid, and the small lateral Eustachian canals open dorsally to the large, medial canal. The suborbital fenestrae are fully visible in NHMUK OR 30392 (Fig. 2.2D) and CAMSM TN 907. Anteriorly, they reach the level of the ninth maxillary alveolus, but reach the tenth alveolus in NHMUK OR 25166 (Fig. 2.1D). The lateral edge of the suborbital fenestra is straight, not bowed medially at the ectopterygoid-maxilla suture. Each suborbital fenestra has a posterior notch (best observed on the right opening of NHMUK OR 30392). The posterior corner of the suborbital fenestra is formed by the pterygoid, with the pterygoid–ectopterygoid suture situated on the posterolateral margin of the fenestra. Anteriorly, the suborbital fenestra tapers to an acute tip. The anterolateral margin of the fenestra is longer than the posterolateral margin. The incisive foramen is relatively large and is located far from the toothrow, with the anterior rim corresponding to the third alveolus, and the posterior margin corresponding to the fourth or fifth alveolus. Whereas this foramen is circular in NHMUK OR 30392 and CAMSM TN 907 it is tear-drop-shaped in NHMUK OR 25166, with an acute anterior margin, resulting from the intrusion of the occlusal pits for the first dentary teeth. The internal choana is best preserved

in CAMSM TN 907, and the juvenile specimen NHMUK OR 25167 (Fig. 2.6D). The posteroventrally oriented choana is heart-shaped, and situated entirely within the posterior region of the pterygoids, with its posterior rim close to the posterior edge of the pterygoids. The anterior rim of the choana is flush with the pterygoid surface, whereas the lateral rim develops a large lamina that separates the choana from a slightly depressed area. In addition, the midline of the anterior margin of the choana is interrupted by a posteriorly directed process of the pterygoid. This is observed in all specimens where preserved. In NHMUK OR 30392, this process extends quite far posteriorly into the choana, although it does not fully bisect it. The posterior rim of the choana, preserved in NHMUK OR 25167 and CAMSM TN 907, is smooth lacking the sharp notch which characterises *Caiman*, but there is a small concavity on the posterior edge. Although slightly incomplete in its median sector, these specimens shows the presence of a sagittal bony septum recessed within the choana.

**Premaxilla**

The premaxillae completely encircle the external naris. They are characterized by five alveoli, even in adult specimens. Palatal laminae are flat, with no obvious ornamentation except for a slightly rugose texture leading up to the alveolar necks (e.g. NHMUK OR 25166). Numerous small foramina pierce the premaxillary palate, adjacent to the alveoli. The dorsal process of the premaxilla is relatively short and wide, posteriorly reaching the level of the second or third maxillary alveolus. The premaxilla-maxilla suture is slightly irregular, rather than straight. One large reception pit for the first dentary tooth occurs lingually, in between the first and second premaxillary alveoli. Posteriorly, the premaxillae are separated along their midline by the anterior process of the nasal.

**Maxilla**

The well-preserved maxillary toothrows of NHMUK OR 30392 host 17 alveoli on each side (Fig. 2.2C, D). In ventral view, the toothrow has a slight lateral concavity at the level of the sixth and seventh alveoli, but it is nearly straight posteriorly. The fourth and fifth alveoli are about the same size. They are not fully confluent in any of the three best-preserved skulls, and are separated by a thin (but complete) bony septum. Confluent alveoli, in which the septum is not complete, having a V-shaped fenestration, is observed in one small, isolated maxilla NHMUK OR 25168-9. In dorsal view, at the level of the fifth maxillary alveolus, and slightly medially inset, there are two protuberances. On the ventral surface of the skull, the maxilla terminates a significant distance anterior to the postorbital bar, forming a short edentulous process that is as long as the distance between the last two maxillary alveoli (Fig. 2.2D). The penultimate alveolus is slightly less than twice the diameter of the last alveolus. The medial walls of the last two maxillary alveoli are formed by the ectopterygoid.

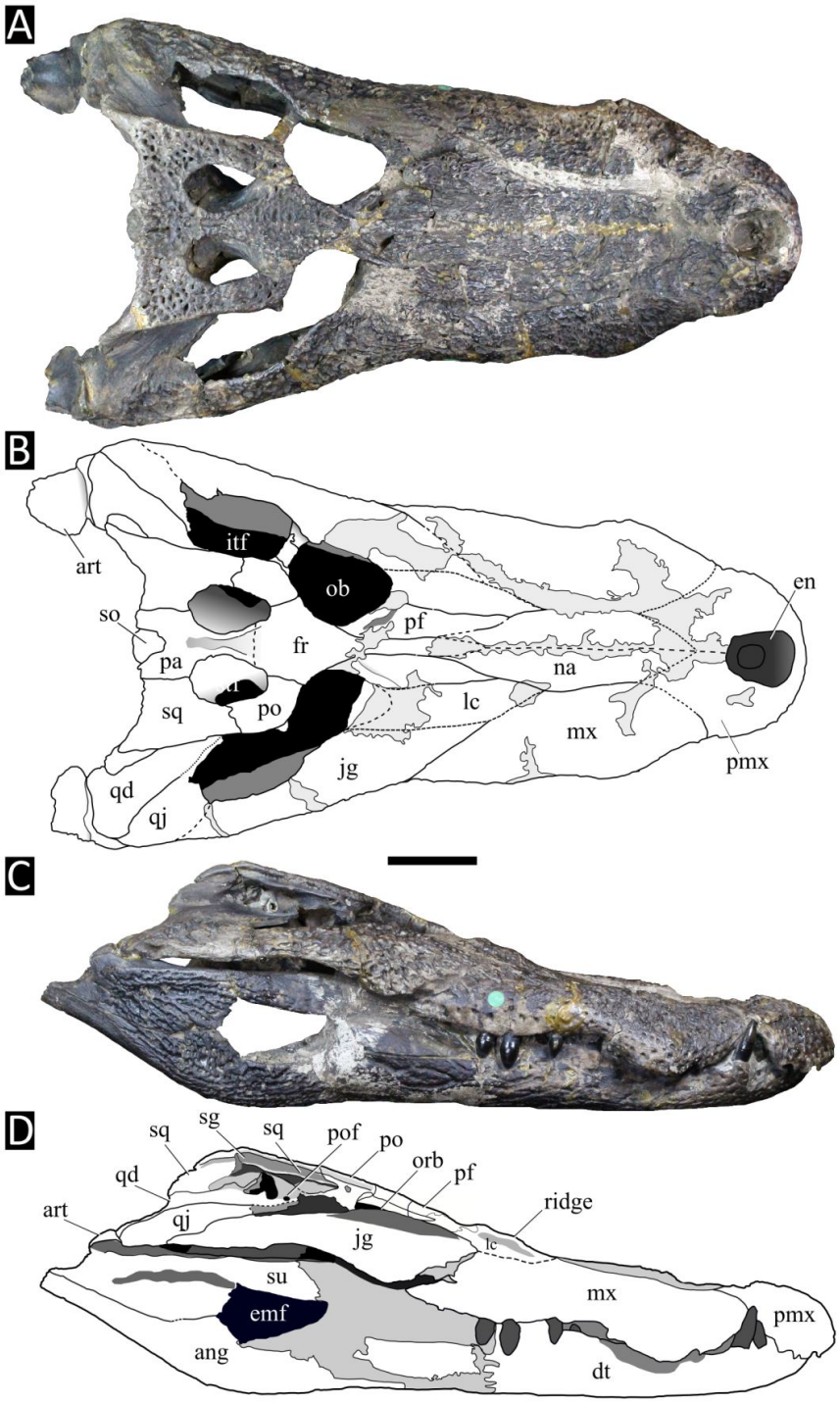



Figure 2.4: Articulated skull and mandibles of *Diplocynodon hantoniensis* (NHMUK 30393) in dorsal (**A**, **B**) and lateral (**C**, **D**) view. Abbreviations: **art**, articular; **dt**, dentary; **emf**, external mandibular fenestra; **en**, external naris; **fr**, frontal; **itf**, infratemporal fenestra; **jg**, jugal; **lac**, lacrimal; **mx**, maxilla; **na**, nasal; **ob**, orbit; **pmx**, premaxilla; **pf**, prefrontal; **pof**, preotic foramen; **po**, postorbital; **qd**, quadrate; **qj**, quadratojugal; **so**, supraoccipital; **sq**, squamosal; **stf**, supratemporal fenestra; **su**, surangular. Scale bar = 5 cm.

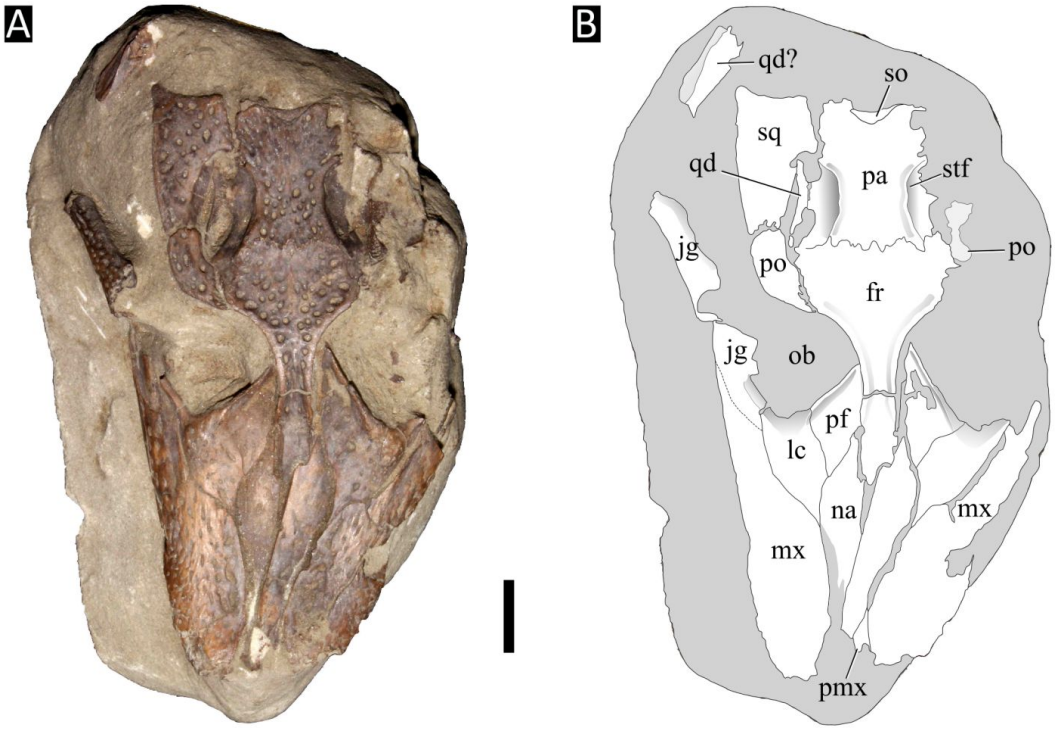



Figure 2.5: Juvenile skull of *Diplocynodon hantoniensis* (NHMUK 25170.a) in dorsal view. Abbreviations: **fr**, frontal; **jg**, jugal; **lac**, lacrimal; **mx**, maxilla; **na**, nasal; **ob**, orbit; **pmx**, premaxilla; pf, prefrontal; po, postorbital; qd, quadrate; **so**, supraoccipital; **sq**, squamosal; **stf**, supratemporal fenestra. Scale bar = 1 cm.

### Nasal

An acute process of the nasal protrudes anteriorly between the premaxillae, but does not reach the external naris. In NHMUK OR 30392 (Fig. 2.2), this nasal process terminates about 20 mm posterior to the external naris. The nasals broaden posteriorly along the maxilla–nasal suture, reaching a maximum width at their mid-length. Whereas the nasal–prefrontal suture is concave, the nasal–lacrimal suture is linear.

### Lacrimal

The lacrimal forms the anterolateral rim of the orbit. It is longer than the prefrontal (Fig. 2.7A). NHMUK OR 30381 preserves the right lacrimal duct, which is large and opens immediately lateral to the lacrimal–prefrontal suture. The lacrimal and the nasal appear to be in broad contact, lacking any posterior process from the maxilla (Fig. 2.7A), although the poor demarcation of sutures makes this morphology difficult to establish conclusively in the four largest skulls. Preorbital ridges are present in all three of the adult skulls preserving the lacrimals: they are more prominently developed in NHMUK OR 30393 and CAMSM TN 907 than in NHMUK OR 30392. A low ridge is present in the smaller specimen NHMUK OR 30381, and a clear boss is present in the juvenile skull NHMUK OR 25170.a, immediately anterior to the anterior

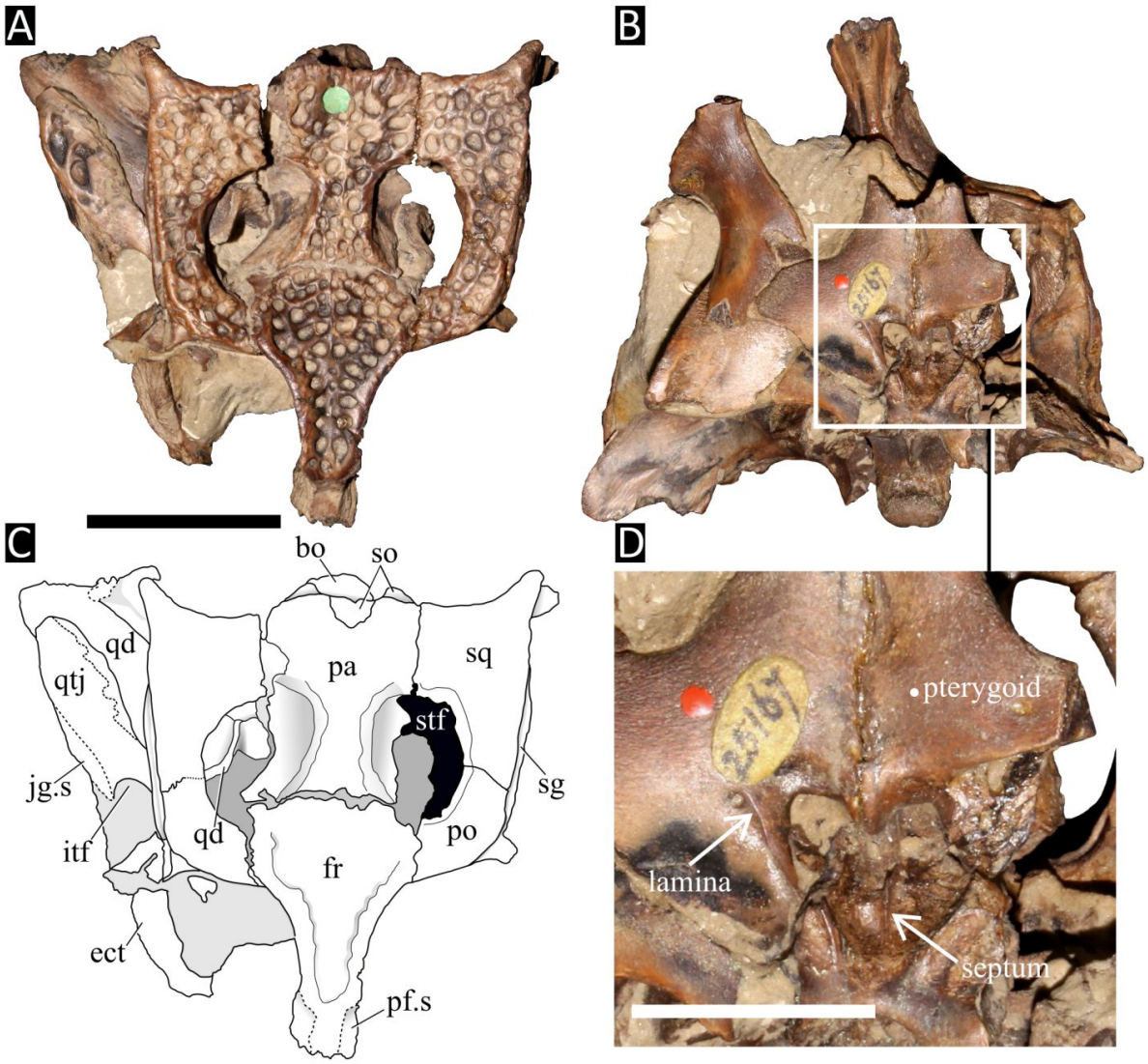



Figure 2.6: Juvenile skull of *Diplocynodon hantoniensis* (NHMUK OR 25617) in dorsal view (**A**, **C**). **B**, ventral view; **D**, enlargement of the choana in **B**. Abbreviations: **bo**, basioccipital; **ect**, ectopterygoid; **fr**, frontal; **itf**, infratemporal fenestra; **jg.s**, jugal suture; **pa**, parietal; **po**, postorbital; **qd**, quadrate; **qtj**, quadratojugal; **sg**, squamosal groove; **so**, supraoccipital; **sq**, squamosal; **stf**, supratemporal fenestra. Scale bar A–C = 5 cm, D = 1 cm.

orbital corner (Fig. 2.5A).

### Jugal

The jugal forms the ventral margin of the orbit and extends posteriorly past the level of the infratemporal fenestra (Fig. 2.4D). The lateral and ventral margins of the jugal are heavily ornamented with pits, whereas the medial side is smooth. A very large medial jugal foramen is visible in the isolated juvenile jugal NHMUK 20219, the juvenile partial skull NHMUK R 1041, and in NHMUK OR 30393. Three of the four isolated jugals catalogued as NHMUK OR 30289 have large medial foramina, but the fourth one shows a foramen of moderate size. Two medial jugal foramina are visible in the isolated jugal arch NHMUK OR 25188 (Fig. 2.7B) and in the left jugal of NHMUK OR 30392, although there is only one foramen on the right jugal. The ectopterygoid is sutured onto the anteromedial side of the jugal, ventral to the postorbital bar. The ventral portion of the postorbital bar that is formed by the jugal is inset from the dorsal edge of the jugal, with a moderately developed sulcus. At the level of the postorbital bar there is a small step in the dorsal outline of the jugal, reminiscent of the condition in *Alligator* and *Caiman*, and differing from the straight dorsal outline of *Crocodylus*. Posteriorly, the jugal terminates in an acute process that is sutured ventrolaterally to the quadratojugal. This process extends slightly further posteriorly than the level of the basioccipital tubera.

### Prefrontal

The prefrontals are separated from one another along the midline by the frontal process and by the posterior tip of the nasals (Fig. 2.4B). Around the orbit, the prefrontal surface is raised into a ridge (Figs 2.4, 2.5). The prefrontal pillars are poorly preserved and/or partially obscured in all specimens, limiting anatomical observations. Ventrally, they form a suture with the dorsolateral margin of the palatines, forming two walls.

### Frontal

There is a distinct step at the base of the frontal process in two of the largest skulls, NHMUK OR 30392 and NHMUK OR 30393, and it is also weakly developed in CAMSM TN 907. A slight step is present in both the juvenile skull NHMUK OR 25167 (Fig. 2.6) and the much larger, though not fully grown, individual represented by NHMUK OR 30381 (Fig. 2.7A). A very steep slope is visible in the very small individual represented by NHMUK OR 25170.a (Fig. 2.5). The step in both NHMUK OR 25167 and 30381 is highlighted by the ornamentation of the frontal: it is pitted posterior to the step (similar to that of the skull table), but smooth along the frontal process. The dorsal surface of the frontal is gently concave, and its dorsolateral (orbital) margin is slightly upturned. The anterior process of the frontal

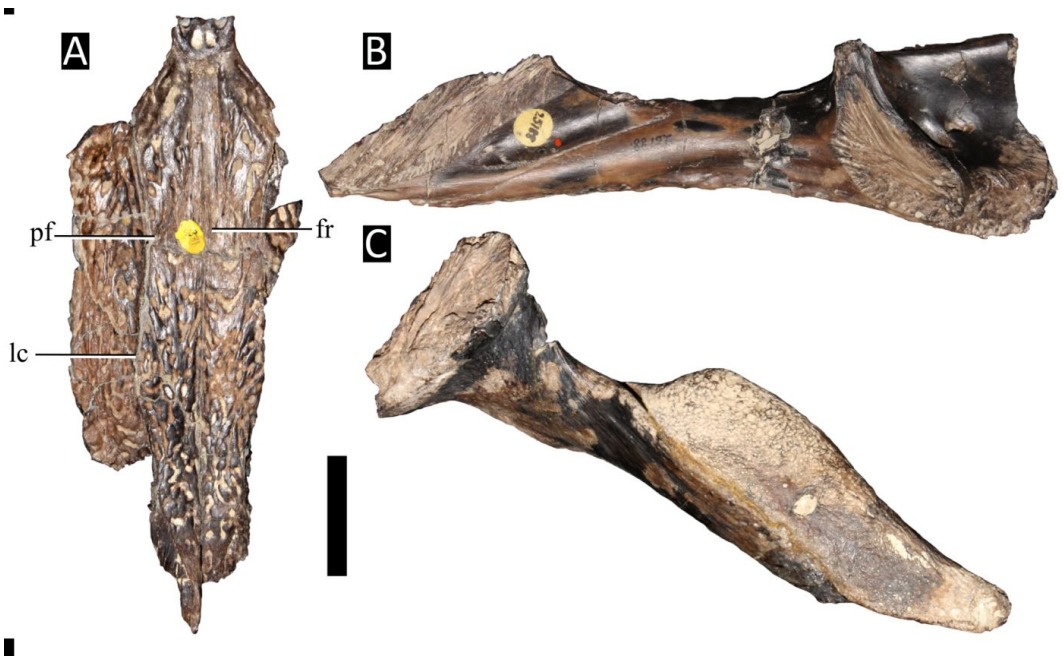



Figure 2.7: Selected skull details of *Diplocynodon hantoniensis*. **A**, NHMUK 30381, fragment of the rostrum showing the anterior extent of the prefrontal, frontal and lacrimal; **B**, NHMUK 25188, left jugal and quadratojugal in medial view; **C**, NHMUK 30251 isolated pterygoids and ectopterygoids in left lateral view. Abbreviations: **fr**, frontal; **lc**, lacrimal; **pf**, prefrontal. Scale bar = 4 cm.

extends beyond the orbital margin, to the level of the anterior tip of the prefrontal and the mid-length of the lacrimal. It is difficult to discern the anterior extent of the frontal relative to the jugal in NHMUK OR 30392 and 30393 as a result of poorly defined sutures, as well as the plaster that covers the dorsal surface. However, based on NHMUK R 1042 and OR 29694, the anterodorsal tip of the jugal lies just posterior to the anterior extent of the frontal process. In the juvenile specimen NHMUK OR 25170.a, the anterior extent of the frontal and jugal appear to be approximately equal; however, the frontal process is not well preserved in this specimen. On the skull table, the linear frontoparietal suture enters so deeply into the supratemporal fenestrae that the parietal and postorbital are not in contact. Often in crocodylians, the anterior frontal process bisects the nasals for a short distance. The morphology in this area is extremely difficult to discern in the largest specimens of *Diplocynodon hantoniensis*(i.e. NHMUK OR 30392, 30393 and 25166). In NHMUK OR 30381 (Fig. 2.7A) (and possibly also NHMUK OR 29694), the frontal appears to invade the nasals anteriorly via two separate processes, between which the nares project posteriorly. However, in the juvenile NHMUK OR 25170.a the usual condition is observed. In NHMUK OR 30381 and 29694, the elements may have been pulled apart at their sutures and filled with matrix. Consequently, this unusual morphology might merely be an artefact of preservation.

### Postorbital

The postorbital bar is incomplete in most specimens and often reconstructed with plaster. However, it appears strongly inclined laterally, and inset from the lateral surface of the skull based on NHMUK OR 30392 and CAMSM TN 918. The bar is slender and circular in cross section, with a short and low process. A deep fossa excavates the lateral surface of the dorsal portion of the postorbital bar, pierced by a large foramen. The postorbital is in contact with a thin dorsal projection from the quadratojugal, but not with the quadrate (see NHMUK OR 30392, CAMSM TN 918) (Fig. 2.3B).

### Squamosal

The squamosals form the posterolateral corners of the cranial table and the posterolateral margins of the supratemporal fenestrae. Their dorsal surfaces are flat in both juvenile (NHMUK OR 25167 and 25170.a) and fully grown individuals (NHMUK OR 30392, 30393, CAMSM TN 907). A prominent squamosal groove is delimited by sub-parallel rims. A linear series of foramina pierce the groove, as well as the dorsal margin of the groove. Dorsal to the external auditory meatus, there is a slight ventral deflection along the ventral margin of the squamosal. The squamosal–quadrate suture is visible on the right side of NHMUK OR 30393 (Fig. 2.4D), extending along the posterior margin of the external auditory meatus. The squamosal rami do not reach the tip of the paroccipital processes.

### Parietal

The parietal forms the medial margin of the supratemporal fossa and fenestra, a large portion of the post-temporal fossa, and the roof of the braincase. Posterior to the supratemporal fenestra, the dorsal surface of the parietal is concave, and the interfenestral bar has a sagittal sulcus (Fig. 2.4). The medial wall of the supratemporal fossa is steeply inclined, facing laterally and slightly dorsally, and the parietal rim of the supratemporal fenestra only slightly overhangs the supratemporal fossa. On the medial wall of the supratemporal fenestra, the laterosphenoid–parietal suture is horizontal. The post-temporal fossa is prominent, forming a shelf that is principally composed of the parietal, leading into the orbitotemporal canal. The parietal approaches, but does not contact, the squamosal on the posterior wall of the supratemporal fenestra, ventral to the orbitotemporal canal.

### Quadrate

The quadrate condyle is characterized by a small, ventrally deflected medial hemicondyle, and by a prominent dorsal, medially positioned notch that hosts the foramen aerum (Fig. 2.3D). The latter opening is relatively small and placed on the dorsal surface of the quadrate, far from the mediodorsal edge. Whereas the articular surface of the medial hemicondyle faces posteriorly and ventrolaterally, the lateral

hemicondyle faces posteroventrally. On the midline of the ventral surface of the quadrate ramus, there is a well-developed attachment scar for *M. adductor mandibulae posterior* (Holliday et al., 2013) (scar 'B' of Iorndansky [1973]) (Fig. 2.2D). This scar develops into a large sharp lamina, projecting approximately 10 mm from the ventral surface of the quadrate in NHMUK OR 30392 and NHMUK OR 30393. The scar continues ventrally along the posterolateral braincase wall, although it becomes less pronounced.

### Quadratojugal

The quadratojugal is well preserved on the right side of NHMUK OR 30392 and CAMSM TN 918 (Fig. 2.2B). As can be observed on NHMUK OR 25188 (Fig. 2.7B), a moderately developed process extends along the medial surface of the lower temporal bar. The quadratojugal has a long, apically very thin process that reaches the dorsal corner of the infratemporal fenestra. Posteriorly, the quadratojugal extends to the level of the quadratic condyles, forming the lateral margin of the lateral hemicondyle. The ventral suture with the jugal is approximately parallel with the quadrate–quadratojugal suture.

### Supraoccipital

The supraoccipital is well exposed on the posterior surface of the skull, and delimits the ventromedial rim of the post-temporal fenestra. The dorsal exposure of the supraoccipital is clearly visible in juvenile specimens (Figs 2.5, 2.6), in which it forms a small, triangular-shaped exposure. The exposure appears larger in mature specimens (e.g. Fig. 2.4B); however, it never blocks the parietal from the posterior edge of the cranial table. The posterior surface of the supraoccipital is excavated by two circular sulci that are separated by a vertical, sagittal crest. Two processes project posteriorly from the supraoccipital, immediately ventral to the slit-like post-temporal fenestrae, and are most clearly observable in NHMUK OR 30393 and NHMUK OR 25167 (Fig. 2.6). These processes are not large enough to exceed the level of the posterior margin of the cranial table in the adult specimen NHMUK OR 30392, but they are clearly visible in dorsal view of the juvenile specimen NHMUK OR 25167.

### Exoccipital

The exoccipitals have a smooth paroccipital surface devoid of any boss. They extend considerably lateral to the posterior opening of the cranioquadrate passage, but do not reach the basioccipital tubera ventrally (Fig. 2.3D). Lateral to the post-temporal fenestra, the surface of the exoccipital is strongly concave. Overall, the occipital surface formed by the exoccipitals faces posterodorsally. The paroccipital process extends posterolaterally, sitting above the posterior quadrate rami. The ventral margin of the paroccipital process above the cranioquadrate canal is marked by a ventrally directed lamina. This lamina terminates immediately medial to the cranioquadrate canal, continuing towards the foramen magnum as a faint

horizontal ridge. Neurovascular foramina pierce the exoccipitals and are well preserved in NHMUK OR 30392, 30393 and 25166. Four foramina are present on the right exoccipital of NHMUK OR 30392 (Fig. 2.3D). Two foramina occur close together at the level of the foramen magnum for the hypoglossal (XII) nerve. Slightly ventral and lateral to these foramina is the vagus (X) foramen. Further ventrally, approximately at the dorsoventral midpoint of the occipital condyle, is the much larger lateral carotid foramen. This foramen sits within a fossa and is orientated posteroventrally and slightly laterally.

**Basisphenoid and basioccipital**

The basisphenoid forms the anterior margin of the median eustachian foramen and extends ventrally on to the posterior pterygoid processes. Ventral to the basioccipital, the basisphenoid is anteroposteriorly very thin, but dorsoventrally tall (Fig. 2.3D). The median eustachian foramen opens between the basioccipital and the basisphenoid. The lateral eustachian foramina are positioned dorsal to the level of the median eustachian foramen (Fig. 2.3D). The external surface of the basioccipital faces posteriorly, ventral to the spherical occipital condyle. A small vertical, sagittal crest extends along the basioccipital plate.

**Braincase and orbitotemporal region**

One unnumbered juvenile specimen in the CAMSM preserves some of the braincase anatomy. The epipterygoid appears to be absent in this specimen. There is little to no exposure of the prootic on the external braincase wall ventral to the foramen ovale. The anterior margins of the laterosphenoid capitate processes are oriented obliquely relative to the midline. The well-formed lateral laterosphenoid bridge is anteroposteriorly thick, fully enclosing the ophthalmic foramen medially. The lateral surface of the laterosphenoid bridge is excavated by a broad groove for the maxillary ramus of cranial nerve 5, and there is no development of a caudal laterosphenoid bridge dorsal to the foramen ovale. The supraorbital foramen, which usually pierces the laterosphenoid-quadrate suture at this level, cannot be discerned. The pterygoid is broken away ventrally, but it is unlikely that any ascending process of the pterygoid contributed to the laterosphenoid bridge sensu *Alligator*. Although missing, the suture scar for the pterygoid can be traced on the quadrate, and this was most likely linear from the large, posterior, semi-lunate basisphenoid exposure to the foramen ovale. Only the posteriormost portion of the basisphenoid rostrum is preserved, which lacks a large lateral fossa, and is poorly exposed on the lateral braincase wall anterior to the foramen ovale. The foramina for the palatine ramus of cranial nerve VII are not preserved.

**Palatine**

The palatines flare anteriorly, developing a lateral process projecting into the suborbital fenestra. The palatine–maxilla suture enters the suborbital fenestra at its anteromedial margin. The broad anterior

margin of the palatine reaches beyond the anterior margin of the suborbital fenestra, to the level of the seventh maxillary interalveolar space. The palatines do not significantly flare posteriorly, and thus do not form a palatine shelf, such as the one seen in *Alligator*; instead, the lateral margins of the palatines are roughly parallel posteriorly. The palatine–pterygoid suture is well preserved in NHMUK OR 25166, 30392 (Figs 2.1, 2.2) and CAMSM TN 907; in all specimens it is situated far anterior to the posterior corner of the suborbital fenestra, but varies in shape from being straight to prominently 'W' shaped.

**Ectopterygoid**

The relationship between the ectopterygoid and the maxilla was evaluated on the basis of NHMUK OR 30392, the only specimen preserving the posterior region of the maxillary toothrow. The anterior process of the ectopterygoid is pointed, reaching the level of the anterior margin of the $15^{th}$ maxillary alveolus (Fig. 2.2D). The ectopterygoid forms the medial wall of the last maxillary alveolus only. Anterior to this alveolus, the maxilla is so prominently developed medially that the ectopterygoid does not abut the maxillary toothrow. This condition appears to be rare, otherwise only recognised in some *Caiman crocodilus* specimens (e.g. FMNH 73694, 73701, 73721). However, as commented upon by Brochu (1997a), who also observed this morphology, the condition is closer to other alligatoroids than to the plesiomorphic crocodylian condition, in which the ectopterygoid fully abuts the maxillary toothrow. The posteroventral process is approximately twice the length of the anterior process. This posteroventral process does not reach the tip of the pterygoid at maturity; instead it terminates beyond mid-length of the pterygoid wing. The ectopterygoid–pterygoid flexure is clearly visible in the juvenile skull NHMUK OR 25167, as well as the pterygoids and associated ectopterygoids (NHMUK OR 30251) (Fig. 2.8A) of a fully-grown individual that might belong with NHMUK OR 30393. Based on NHMUK OR 30251, the ventrolateral surface of the ectopterygoid, near the margin of the suborbital fenestra, is pierced by two foramina on the right side and three on the left. The ectopterygoid has a blunt posterior process on the medial surface of the jugal arch (Fig. 2.7B), and sends an ascending branch along the medial surface of the postorbital bar. Immediately anterior to the sutural surface for the jugal, on the anterior branch of the left ectopterygoid, there is a large foramen.

**Pterygoid**

The pterygoid forms the posterior margin of the suborbital fenestra. The pterygoid wings are large and robust. Their lateral margins are thickened and expanded dorsoventrally, with a rugose texture. A distinct sulcus runs parallel and dorsal to the suture with the ectopterygoid along the lateral surface of the pterygoid (Fig. 2.7C). Two foramina are present within the fossa on the left side of NHMUK OR 30251: a large posterior foramen, filled with matrix, and a much smaller anterior foramen. An equivalent small anterior foramen is also present on the right side. Anteriorly, the pterygoid is sutured to the palatine.

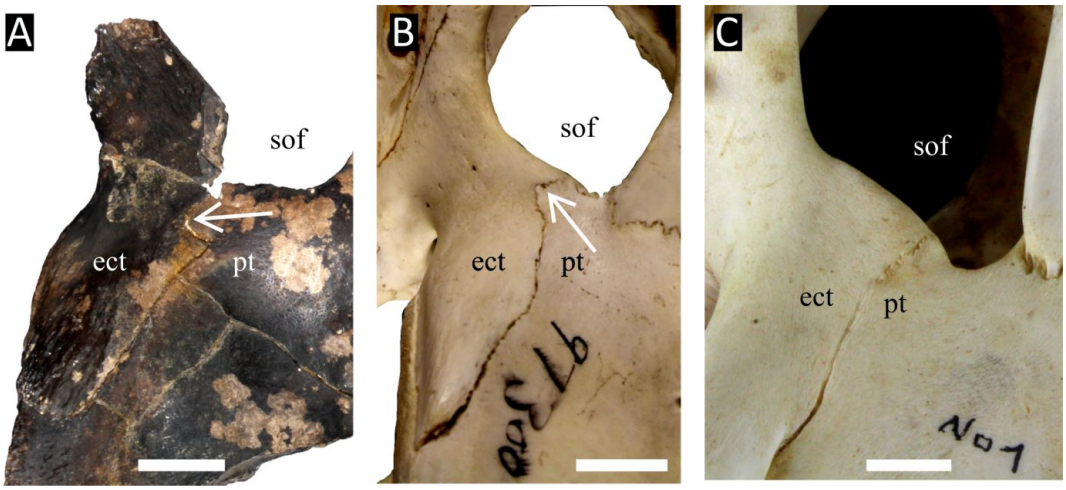



Figure 2.8: Comparisons of the ectopterygoid-pterygoid suture in *Diplocynodon hantoniensis* and other crocodylians: **A**, *D. hantoniensis* (NHMUK 30251); **B**, *Caiman yacare* (AMNH 97300); **C**, *Crocodylus acutus* (FMNH 69884). White arrows indicate the position of the ectopterygoid-pterygoid flexure. Scale bars = 2 cm in all specimens.

Dorsally, they form the dorsolateral walls of the nasopharyngeal passage. The two halves of the pterygoids rise dorsomedially, meeting at the midline to surround the airways, forming a dorsoventrally tall and transversely very thin wall, immediately below the level of the frontal. The dorsoventrally tall posterior pterygoid processes project posteriorly and slightly laterally (Fig. 2.3D). The choanae open centrally within the pterygoids. In posterior view, the pterygoid wings extend posteroventrally at around 30° from the horizontal.

### 2.3.2 Mandible

#### Preservation

As with the crania, some lower jaws are completely isolated (NHMUK OR 25188 [Fig. 2.9], NHMUK OR 30394 [Fig. 2.10], NHMUK OR 30397, NHMUK OR 30396; CAMSM TN 904) whereas others are preserved on a slab along with vertebrae, e.g. NHMUK R 1045. NHMUK OR 30396 is a fused pair of mandibles braced with a metal rod. Only one pair of mandibles is associated with a cranium – NHMUK OR 30393 (Fig. 2.4); however, very few mandibular features can be discerned from this specimen. Across these specimens, nearly all elements of the mandible are preserved, with the exception of the coronoid. A list of mandibular measurements is presented in Table 2.2.

#### Mandibular fenestrae and major openings

The laterally opening external mandibular fenestra is moderately large and oval shaped, but the medially opening foramen intermandibularis caudalis is barely visible through it. The presence of the foramen

Table 2.2: Mandibular measurements for *Diplocynodon hantoniensis* (mm).

| Feature | NHMUK OR 30394 | NHMUK OR 25188 |
|---|---|---|
| Mandible length | 480 | 469 |
| Toothrow length | 265 | 259 |
| External mandibular fenestra length | 62 | 60 |
| External mandibular fenestra height | 29 | 32 |
| Width across glenoid fossa | 42 | 42 |
| Retroarticular process length | 61 | 62 |
| Mandible height at fourth tooth | 39 | 37 |
| Symphysis length | 54 | 52 |

intermandibularis medius cannot be determined due to the absence of the coronoid in all specimens. The dentary–surangular suture intersects the external mandibular fenestra slightly anterior to its posterodorsal angle (very close to the angle in NHMUK OR 25178) (Fig. 2.9C, D), whereas the dentary–angular suture reaches about the midlength of the ventral rim of the fenestra. The angular–surangular suture intersects the fenestra ventral to the posterodorsal angle (Fig. 2.9D).

**Dentary**

The best preserved dentaries (i.e. NHMUK OR 30396, 30397) each host 20 alveoli. The dentaries are gently curved between the $4^{th}$ and $11^{th}$ alveoli. There is some variation in the posterior extent of the dentary symphysis: it extends to the middle of the fourth alveolus in NHMUK OR 25178 and 30394 (Figs 2.18A, 2.10A), to the posterior rim of the fourth alveolus in NHMUK OR 30397, and to the middle of the fifth alveolus in NHMUK OR 30396 and R 1043). In lateral view, the dorsal edge of the dentary undulates: the concavities correspond to the $2^{nd}$, $7^{th}$, and $14^{th}$ alveoli, whereas the convexities correspond to the $1^{st}$, $3^{rd}$ and $4^{th}$, as well as the $12^{th}$ alveoli. The jaw is also slightly festooned in dorsal view, with a main lateral convexity corresponding to the confluent third and fourth alveoli. Posteriorly, between the fourth and tenth alveoli, the jaw is slightly concave laterally. The third and fourth alveoli are the largest, with the latter slightly the larger of the two, and are confluent with one another. Posteriorly, alveoli 5 to 9 are smaller and approximately equal in anteroposterior length. The next largest dentary alveolus is the twelfth. The seventh interalveolar space is at least a little larger than the surrounding ones in all specimens (for very clear examples, see NHMUK OR 30287 and 30321). The Meckelian groove begins at the posterior end of the dentary symphysis, at approximately mid-height. In NHMUK OR 30397, a foramen perforates the dentary along the Meckelian groove, at the level of the ninth dentary alveolus.

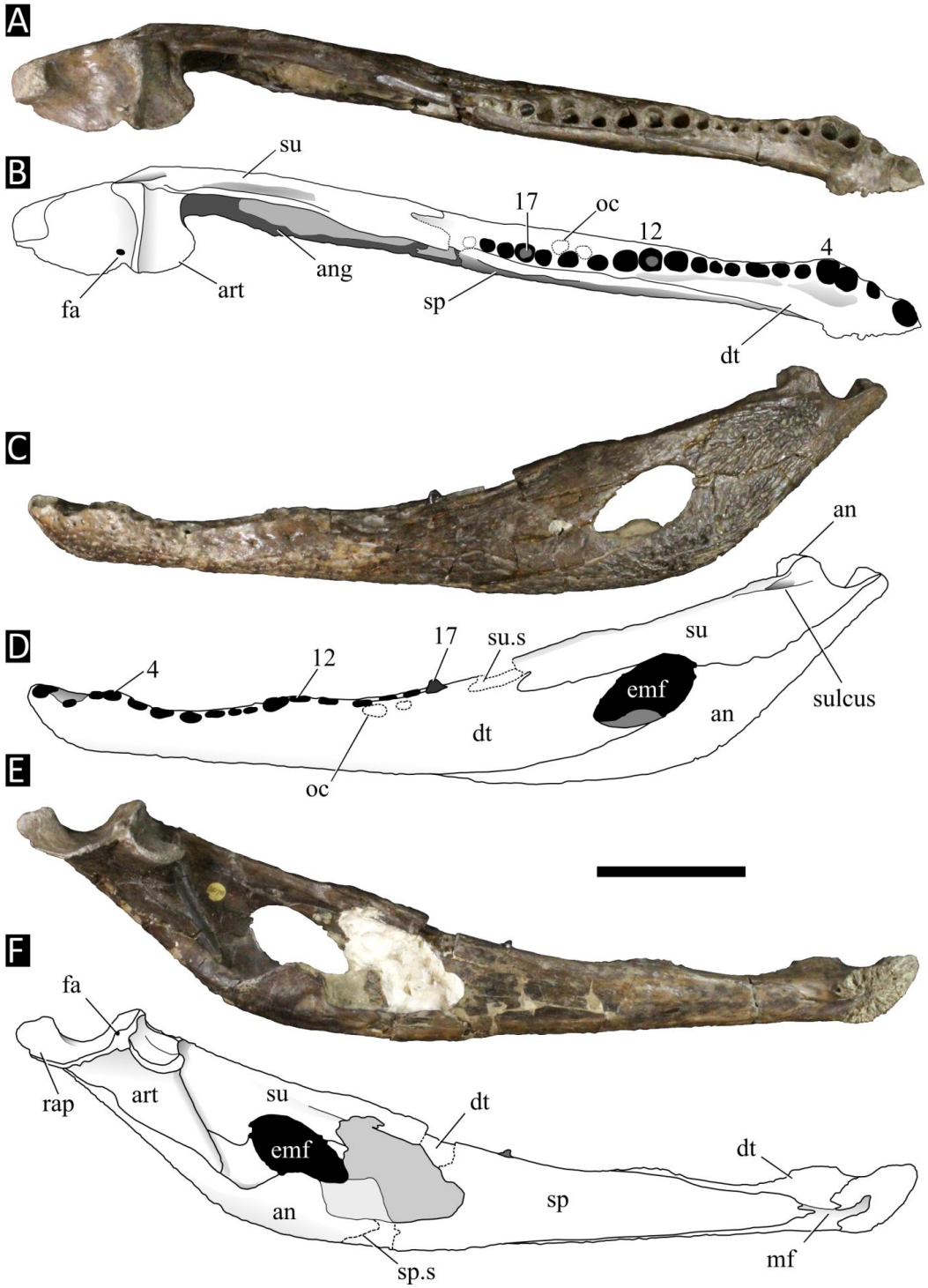



Figure 2.9: Left mandibular ramus of *Diplocynodon hantoniensis* (NHMUK 25188) in dorsal (**A**, **B**); lateral (**C**, **D**); and medial (**E**, **F**) views. Abbreviations: **4**, **12**, **17**, alveolus positions in the dentary; **an**, angular; **art**, articular; **dt**, dentary; **emf**, external mandibular fenestra; **fa**, foramen aerum; **fo**, foramen; **mf**, Meckelian fossa; **oc**, occlusal pit; **sp**, splenial; **sp.s**, suture scar for the splenial; **su**, surangular. Scale bar = 10 cm.

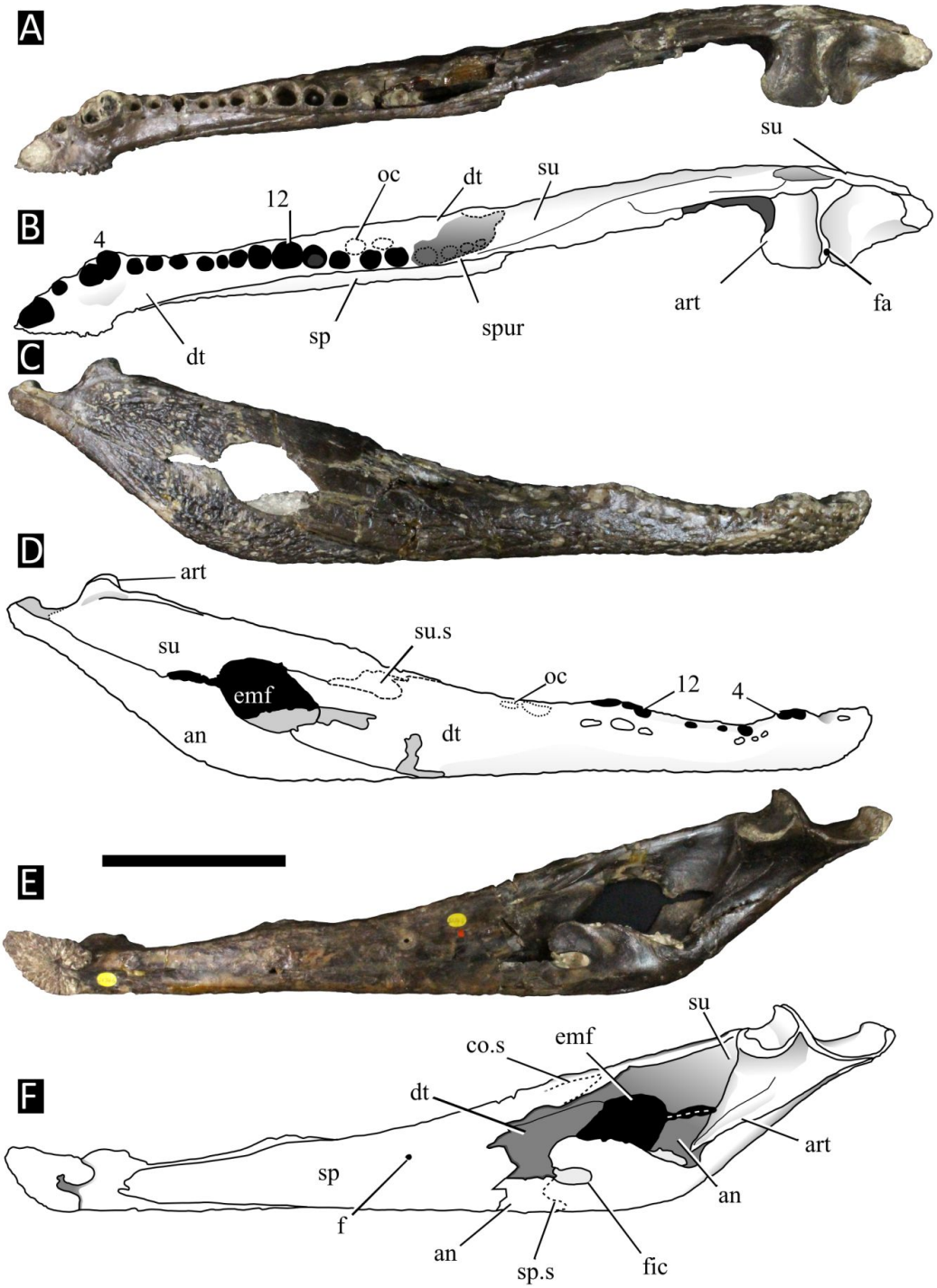



Figure 2.10: Right mandibular ramus of *Diplocynodon hantoniensis* (NHMUK 30394) in dorsal (**A**, **B**); lateral (**C**, **D**); and medial (**E**, **F**) views. Abbreviations: **4**, **12**, alveolus positions in the dentary; **an**, angular; **art**, articular; **co.s**, suture scar for coronoid; **dt**, dentary; **emf**, external mandibular fenestra; **fa**, foramen aerum; **fic**, foramen intermandibularis caudalis; **fo**, foramen; **mf**, Meckelian fossa; **oc**, occlusal pit; **sp**, splenial; **sp.s**, suture scar for the splenial; **su**, surangular. Scale bar = 10 cm.

### Splenial

The splenials are well preserved in at least NHMUK OR 25178 (Fig. 2.9, 30394 (Fig. 2.10) and 30396. They are not involved in the symphysis of the lower jaw and their anterior tip is located ventral to the Meckelian groove (Fig. 2.9E, F). Given the lack of foramina in this region, the mandibular ramus of cranial nerve V can be inferred to have left the Meckelian groove at the anterior end of the splenial. There is a foramen at mid-height of the splenial, at the level of the $16^{th}$ dentary alveolus in NHMUK OR 30394 (Fig. 2.10F), and possibly in NHMUK OR 25178 too. In NHMUK OR 30396, the splenial does not form the dorsomedial wall of the posteriormost dentary alveoli; however, in NHMUK OR 25178, the splenial approaches the medial wall of the final three alveoli, and formed the wall at least in the last two. The anterodorsal margin of the foramen intermandibularis caudalis is open in all specimens where preserved, indicating that the splenial formed the anterior margin of this foramen.

### Angular

The angular of NHMUK OR 30394 (Fig. 2.10) is well preserved. Towards its anterior end, the angular extends dorsally to the foramen intermandibularis caudalis, with a tip that is rather rounded and dorsoventrally tall (Fig. 2.10F). The lateral surface of the angular is strongly ornamented with pits and furrows (Figs 2.9C, 2.10C). However, they do not continue onto the ventral surface, nor do they extend onto the lateral surface of the retroarticular process. A longitudinal ridge occurs on the ventral margin of the angular, extending onto the lateral surface, and defines the boundary between the anterior ornamented surface of the angular from the posteriorly smooth surface, beneath the retroarticular process (Fig. 2.10D). This ridge is very prominent in NHMUK OR 30396, NHMUK OR 30397 and CAMSM TN 904 but less well-developed in NHMUK OR 30394 and 25178. This feature probably marks the anterior limit of the insertion of *M. pterygoideus ventralis* (Bona & Desojo, 2011). There is a large longitudinal sulcus along the ventromedial surface of the angular. This sulcus begins posterior to the foramen intermandibularis caudalis, and terminates approximately at its anterior margin. A series of large foramina occur posterior to this sulcus in all specimens except for NHMUK OR 30397, which is poorly preserved in this region. Whereas there are two foramina in NHMUK OR 30394, there are three in NHMUK OR 25178 and NHMUK OR 30396. The anterior extent of the angular is difficult to fully discern; however, it appears to reach the level of the $17^{th}$ alveolus based on the articulated mandible NHMUK OR 30396 and the isolated left ramus NHMUK OR 25178. Posteriorly, the angular extends to the posterior end of the retroarticular process, along the ventrolateral margin, terminating in an acute process.

### Surangular

The anterior processes of the surangular are best preserved in NHMUK OR 30381 (Fig. 2.11) and NHMUK OR 30396. They are subequal in length, with the dorsal process extending slightly further anteriorly than the ventral one. This morphology is confirmed by NHMUK OR 25178 (Fig. 2.9D), in which the dorsal process, despite being slightly incomplete anteriorly, is so thick and robust at its preserved anterior end that it had to be longer than the completely preserved ventral process. NHMUK OR 30394 preserves a broken ventral process of the surangular (whose development is implied by the scar it left on the accompanying dentary) and a very long, tapering, laminar dorsal process (Fig. 2.10D). The surangular spur between the dentary and splenial is not completely preserved in any one specimen. In NHMUK OR 30394, the spur is mostly preserved and visible sutured to the medial surface of the splenial (Fig. 2.10B). The posteriormost alveoli are not preserved in this specimen; however, the process most likely reached at least the $17^{th}$ interalveolar space. This can be confirmed in NHMUK OR 25178 and CAMSM TN 904. In both specimens, the surangular spur is not completely preserved. However, the scar for the spur on the splenial is adjacent to the last three alveoli. Just above the external mandibular fenestra, the dorsal edge of the surangular forms a flat laterally inclined surface (Fig. 2.9A, B). Posteriorly, the surangular approaches the dorsal tip of the lateral wall of the glenoid fossa, though does not completely cover it in lateral view. A very prominent sulcus occurs on the dorsolateral margin of the surangular, at the level of the glenoid fossa (Fig. 2.9D). Posteriorly, the tip of the surangular does not reach the posterior tip of the retroarticular process in either of the mandibular rami of NHMUK OR 30396, but it is much more posteriorly developed in NHMUK OR 25178 (Fig. 2.9D). The surangular–angular suture intersects the articular close, but dorsal to its ventral tip on the posterior wall of the mandibular adductor chamber (Fig. 2.9F). The surangular-articular suture is very straight in the posterior wall of the adductor chamber, lacking laminae and not recessed in a sulcus. A lingual foramen for the articular artery, infilled with matrix, can be discerned in all specimens. In NHMUK OR 30396 and CAMSM TN 904, the lingual foramen is situated on the surangular–articular suture, whereas it is located solely on the articular in remaining specimens (i.e. NHMUK OR 25178, 30394, and 30397). Posteriorly, the surangular–articular suture is situated on the lateral edge of the glenoid fossa, and is not bowed within the fossa.

### Articular

The retroarticular process is short and oriented posterodorsally. The foramen aerum is large, and clearly inset from the margin of the retroarticular process. A sharp, vertical lamina occurs for a short distance posterior to the foramen aerum. On the medial surface, there is a prominent, wedge shaped sulcus, dorsally defined by a ridge. This runs approximately parallel to the articular–angular suture, and is perpendicular to the anteromedial corner of the articular. This ridge was probably associated with the attach-

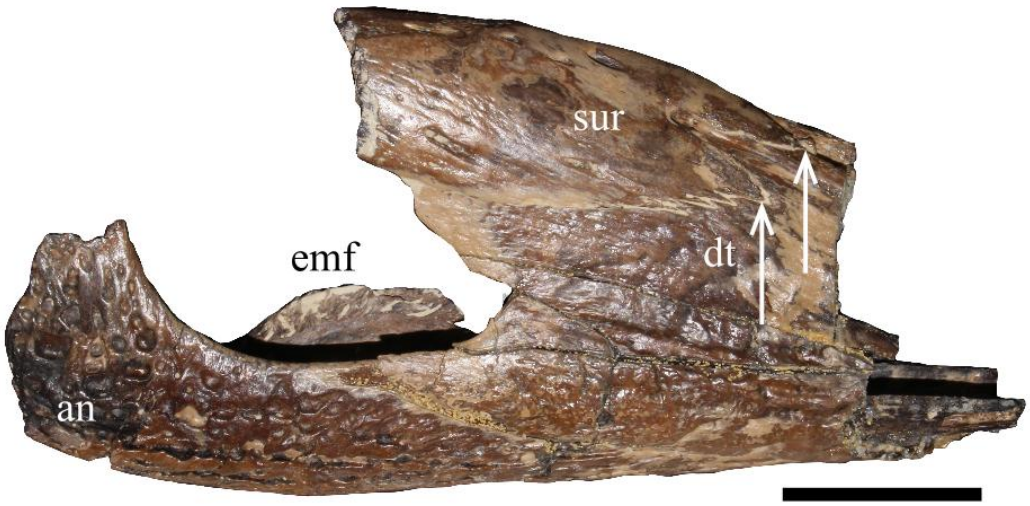



Figure 2.11: Posterior ramus of the right mandible of *Diplocynodon hantoniensis* (NHMUK 30381), lateral view. Arrows indicate the anterior extent of the dorsal and ventral surangular processes. Abbreviations: **an**, angular; **dt**, dentary; **emf**, external mandibular fenestra; **sur**, surangular. Scale bar = 4 cm.

ment of *M. pterygoideus dorsalis*, which is known to attach to the medial surface of the articular in living crocodylians, e.g. *Alligator mississippiensis* (Holliday et al., 2013). The medial edge of the retroarticular process is sharp, and overhangs the medial surface of the articular as a shelf, as does the medial edge of the hemifossa. At the level of the transverse ridge, there is a large medial notch dividing the retroarticular process from the glenoid fossa.

**Pattern of occlusion**

There are five alveoli in each premaxilla, 17 in each maxilla, and 20 in each dentary. All of the alveoli are approximately circular in cross-section. None of the juvenile specimens preserve the premaxilla, meaning that it is not possible to directly assess the changes through ontogeny of the relationships between the fourth dentary tooth and the region corresponding to the premaxillo-maxillary suture. However, the four fully grown specimens show significant variation, suggesting that ontogenetically the primitive condition was the one with the tooth hosted in a pit, and that in some cases the outer wall of the pit could be progressively eroded, giving origin to a notch. In particular, NHMUK OR 25166 has a deep pit on the premaxilla between the last alveolus and the suture with the maxilla (Fig. 2.1C, D). NHMUK OR 30392, 30393 and CAMSM TN 907 all clearly show a notch corresponding to the premaxillo-maxillary suture (Figs 2.2D, 2.3B). Such variability is also shown in the isolated premaxillae, NHMUK OR 30369 and 30370, with a pit in the former and a lateral notch in the latter. The left premaxilla of NHMUK OR 25166 (the type of *Diplocynodon hantoniensis*) shows a very deep and large occlusal pit located lingual to the toothrow, close to the suture with the maxilla; a second pit, much smaller but as deep, is placed

lingual to the first maxillary alveolus. The preservation on the right side of the same skull hinders the detection of the latter pit, but the one on the premaxilla is placed more in-line with the alveoli than the corresponding pit on the left premaxilla. The disposition of the occlusal pits on the maxillae indicates that the dentary teeth occluded lingual to the maxillary teeth, except for those occluding in-line after the sixth and seventh maxillary teeth. This is clearly shown in the maxillae of NHMUK OR 25166 (Fig. 2.1D), 25168-9, and 30392 (Fig. 2.2D), and is confirmed by the dentaries of NHMUK R1043, 25178, 30394, and 30397, all of which have occlusal pits labial to interalveolar spaces 14 and 15 (Figs 2.9B, 2.10B). In the premaxilla, the third and fourth alveoli are the largest, with the latter slightly larger. The fifth alveolus is the smallest, and the first and second alveoli are equally intermediate in size. Two large occlusal pits (one on each side) occur within the premaxillary palate, between the first and second premaxillary alveoli, and are separated posteromedially from the incisive foramen by a thin straight wall. Only the left occlusal pit is visible in NHMUK OR 30392, as the right is infilled with matrix. In NHMUK OR 25166, the walls of the pit are very thin and worn. In the maxilla, alveoli 4 and 5 are the largest, and subequal in size, corresponding to the first lateral and ventral convexity of the maxilla. Alveoli 6–8 are smaller and subequal in size. Alveolus size increases posteriorly from alveolus 8, reaching a second maximum at position 10 and 11, which are subequal. Posteriorly from alveolus 11, the alveoli gradually decrease in size and remain circular. In the dentary, the first alveolus is largest and the second alveolus is considerably smaller. Alveoli 3 and 4 are subequal and confluent; they are larger than alveolus 2, and slightly smaller than alveolus 1. Alveoli 5–10 are smaller than alveoli 3 and 4. Alveoli 11 and 12 are larger than the preceding six alveoli. In some specimens, alveolus 13 is as large as 11 and 12, e.g. NHMUK OR 30396. Posteriorly from alveolus 13, the alveoli are subequal and smaller.

### 2.3.3 Dentition

NHMUK OR 25166 preserves a nearly continuous series of premaxillary and maxillary teeth in place. All premaxillary and anterior maxillary teeth are conical and lingually curved, with smooth carinae, and commonly preserve faint longitudinal striations (Fig. 2.12A, B). Carinae occur on the medial and lateral edges of the anteriormost premaxillary teeth, but on the anterior and posterior edges of all other premaxillary and maxillary teeth (Fig. 2.12 D). Posteriorly, the maxillary teeth become shorter, more globular and less lingually curved, though never becoming blunt as they retain modest carinae and pointed tips (Fig. 2.12C). A small constriction separates the tooth crown from the root, as in *D. remensis* (Martin et al., 2014) (Fig. 2.12E, F). Fewer dentary teeth are preserved in place (e.g. NHMUK OR 30396). However, the same pattern is observed, with anteriorly very conical teeth, with smooth carinae, becoming shorter and more globular posteriorly.

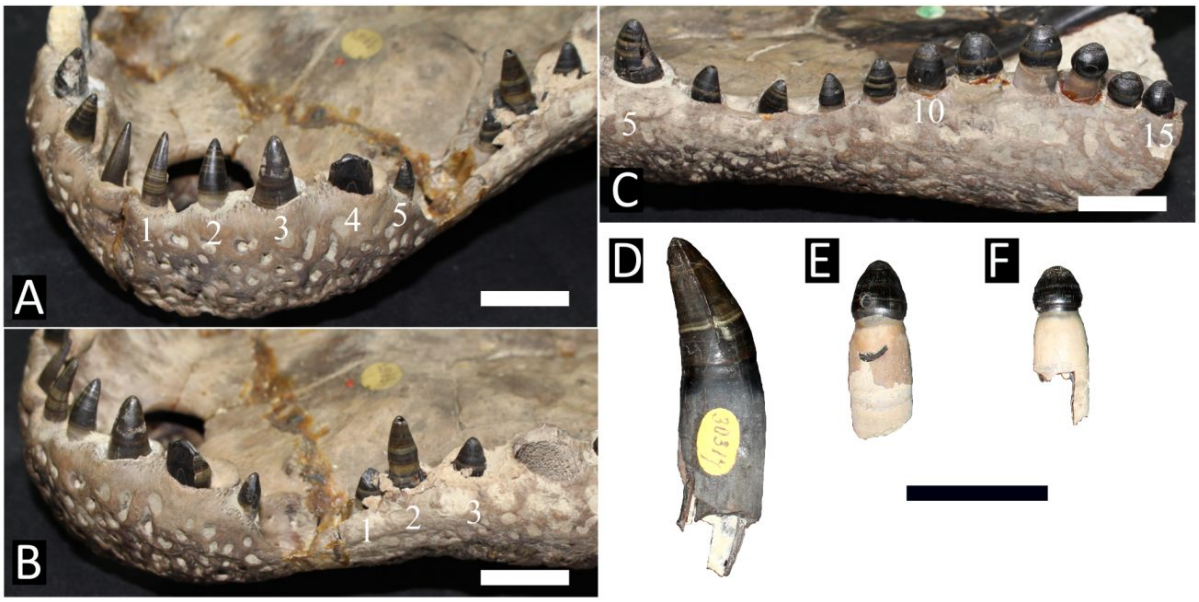



Figure 2.12: The dentition of *Diplocynodon hantoniensis*. **A**–**C**, NHMUK 25166 in anteroventral view (**A**), anterolateral view, showing the premaxilla-maxilla transition (**B**) and lateral view showing the posterior maxillary dentiton (**C**). **D**, NHMUK 30317, isolated tooth from the anterior region of the dentition in mesial view; E–F, unregistered isolated teeth from the posterior region of the dentition in labial view. All scale bars = 2 cm.

### 2.3.4 Axial column

Cervical, dorsal, lumbar, sacral and caudal vertebrae are all preserved, as are postaxial ribs from these regions (excluding gastralia). Most vertebrae in the NHM collections are isolated, except for a continuous series of cervical to sacral vertebrae (NHMUK OR 30402), which have been manually assembled. It is unknown whether these associated vertebrae belong to one or multiple individuals. However, the preservation of the vertebrae is similar, and there is serial variation in size and morphology, indicating that they might belong to one individual. This specimen is used as a basis for a description of the axial column. *Diplocynodon hantoniensis* appears to have had 9 cervical, 15 dorsal, and 2 sacral vertebrae, as in extant crocodylians (Hoffstetter & Gasc, 1969). The number of caudal vertebrae cannot be determined. None of the associated cervical to sacral vertebrae of NHMUK OR 30402 show any hint of neurocentral suture, suggesting that they belong to an adult individual (Brochu, 1996). All of the vertebral centra are fully procoelous, with the exception of the first sacral centrum, which is concave anteriorly and flat to slightly convex posteriorly, and the second sacral centrum, which is nearly flat anteriorly and slightly concave posteriorly.

#### Atlas–axis complex

The proatlas, NHMUK OR 30289, is incomplete (Fig. 2.13G–I): the right posteroventral tip is missing and the long anterior process is partially damaged. When compared to the dorsal crest, the ventral tubercle

is rather short in lateral view. The height of the dorsal keel cannot be fully determined because it is partly damaged. No atlantal intercentrum is preserved. The odontoid process and the axis are preserved in connection only in NHMUK R 1045 (a block hosting a fragmentary lower jaw, several cervical vertebrae, ribs, and osteoderms), but the large odontoid process NHMUK OR 25186 (Fig. 2.13E, F) fits well in size, shape and colour with an unnumbered axis (Fig. 2.13A). The anterior surface of the axial centrum is flat for reception of the odontoid process, whereas the posterior end forms a condyle. Two deep grooves, pierced by foramina, excavate the lateral surface of the centrum, delimiting a prominent ridge (Fig. 2.13A). The ventral surface of the centrum is defined by a sharp midline keel. The unforked axial hypapophysis does not approach the anterior end of the centrum. In lateral view, the neurocentral suture is clearly visible. The neural canal is taller than wide. Whereas the circular prezygapophyses are very small, postzygapophyses are much larger and oval shaped. In axial view, both sets of zygapophyses are inclined at an angle of approximately 45° to the horizontal. The axial neural arch bears an anteroventrally-facing, sub-rounded facet directly ventral to the prezygapophyses, which contacts the odontoid process. The lateral margins of the neural arches are sculpted with fossae and ridges, and there is no trace of a diapophysis on their lateral surfaces. The axial neural spine is tall, with a consistent thickness along its length. Its dorsal margin is near-horizontal (although the anterior sector of the neural spine is broken off in NHMUK R 1045), and does not develop any posterior crest. The posterior-most tip of the axial neural spine extends beyond the posterior margins of the condyle and postzygapophyses. A fossa excavates the lateral surface of the axial neural spine at mid-length.

**Cervical vertebrae**

The ventral surfaces of the cervical centra lack deep pits (these are also absent from the first dorsal vertebra [Dv1]). Posterior to the hypapophyses, the ventral margin of the centrum is very sharp in most cervical vertebrae, except in cervical vertebrae (Cv) 4 and 5, in which the ventral margin is flat and wide. Assuming that the sequence of the associated series of vertebrae NHMUK OR 30402 is correct, the posteriormost hypapophysis is represented by a small elongated knob on the twelfth vertebrae posterior to the atlas. The hypapophyses are not preserved in Cv3–5 of NHMUK OR 30402 (Fig. 2.14), but a raised broken surface indicates that they were still present. Relatively short hypapophyses are consistently positioned towards the anterior margin of the centrum, and are closely flanked either side by parapophyses. In Cv7, 8, and Dv3 and 4 of NHMUK OR 30402, hypapophyses are swept slightly anteriorly. This can also be observed in several well preserved isolated cervical vertebrae (NHMUK R 1046, NHMUK OR 25177 and NHMUK OR 25210). However, Cv9 and Dv1 of NHMUK OR 30402, although slightly worn, have hypapophyses which are directed almost directly ventrally. The parapophyses in the first postaxial cervical vertebra (Cv3) are poorly preserved, but are situated very close to the hypapophyses. Moving posteriorly through the cervical vertebrae, the parapophyses remain approximately at the same level on

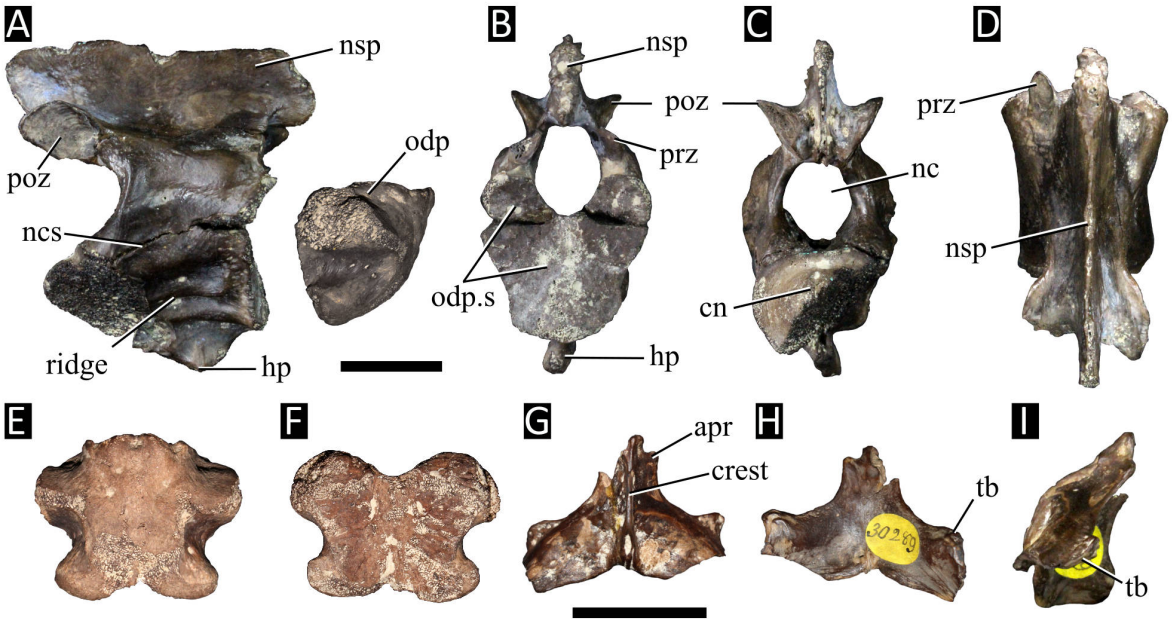



Figure 2.13: Atlas-axis complex of *Diplocynodon hantoniensis*. **A**–**D**, axis in lateral (**A**), anterior (**B**), posterior (**C**) and dorsal (**D**) views. **E**–**F**, unregistered odontoid process in anterior (**E**) and posterior (**F**) views. **G**–**H**, proatlas NHMUK 30289 in dorsal (**G**), ventral (**H**), and ventrolateral (**I**) views. Abbreviations: **apr**, anterior process; **cn**, condyle; **hp**, hypapophysis; **nc**, neural canal; **ncs**, neurocentral suture; **nsp**, neural spine; **odp**, odontoid process; **odp.s**, sutural surface for the odontoid process; **poz**, postzygapophysis; **prz**, prezygapophysis; **tb**, ventral tubercle. All scale bars = 3 cm.

the centrum. Parapophyses are preserved and articulated with cervical ribs in Cv4–7. Here, the parapophyseal articular facets are elliptical, with the long-axis oriented anteroposteriorly. The parapophyseal facets are directed ventrolaterally, slightly more laterally than the diapophyses. In the 10th postaxial vertebra (Dv3), the parapophyses move dorsally to the base of the transverse process. In between the parapophyses and diapophyses, the lateral surface of the centrum has a prominent sulcus in Cv3–7. A lateral fossa is still present in Cv8 to Dv2, although it is much shallower and located posterior to the parapophysis on the lateral surface of the centrum. Diapophyses have small circular facets on Cv3, which are directed ventrally and slightly laterally. In subsequent cervical vertebrae, the diapophyseal facets become more elliptical, with the long-axis oriented anteroposteriorly, although they still project ventrolaterally. The width across the prezygapophyses is smaller than that of the postzygapophyses in Cv3–4. Further along the cervical series, the zygapophyseal widths are subequal. The prezygapophyseal facets are elliptical, inclined approximately at 45° to the horizontal in axial view. The size of the prezygapophyseal facets increase posteriorly from Cv3 to Cv5 as vertebral size increases. The anteriormost cervical vertebrae have anterolaterally orientated prezygapophyses, but these become more laterally elongated in subsequent cervical vertebrae. The postzygapophyses have the same inclination as the prezygapophyses, with elliptical facets. Cervical neural spines are positioned at the posterior end of the neural arch. The dorsally incomplete neural spine of Cv3 is anteroposteriorly long, greater than half the anteroposterior

length of the non-condylar centrum. An isolated, but better preserved, Cv3 (NHMUK R 1046) preserves the same shape, but the neural spine is anteriorly hooked at its dorsal tip (Fig. 2.14A). Cv4 has a similarly wide neural spine, but the neural spines become anteroposteriorly shorter in Cv5–7. In Cv4, the neural spine is oriented primarily dorsally, with a slight anterior deflection. In lateral view, it has a concave anterior margin. The neural spines of Cv5–6 have a similar orientation, but lack the concave anterior margin. The neural spines become anteroposteriorly longer in Cv8 and Cv9.

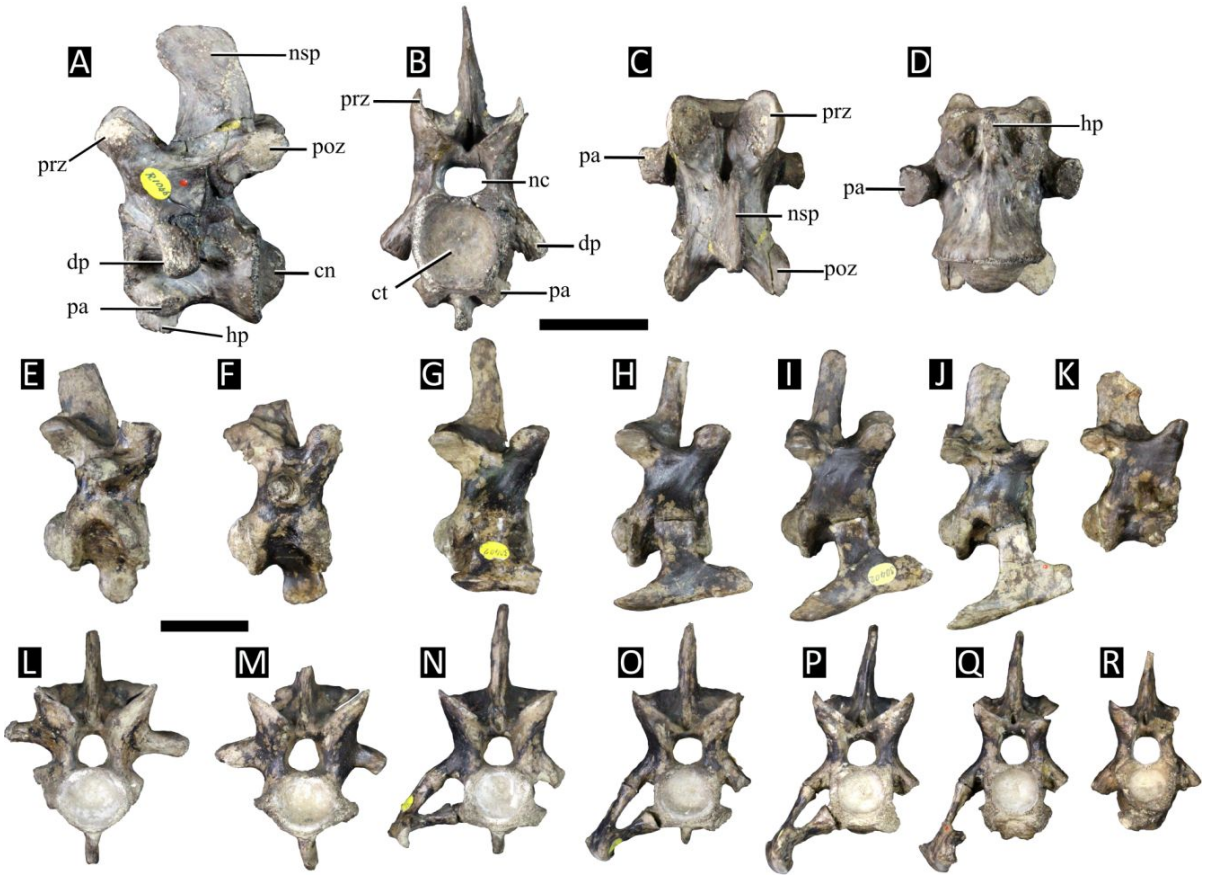



Figure 2.14: Cervical vertebrae of *Diplocynodon hantoniensis*. **A**–**D**, cervical vertebra 3, NHMUK R.1046 in left lateral (**A**), anterior (**B**), dorsal (**C**), and ventral (**D**) views. **E**–**K**, NHMUK 30402, cervical vertebra 9 (**E**), 8 (**F**), 7 (**G**), 6 (**H**), 5 (**I**), 4 (**J**) and 3 (**K**) in right lateral view. Abbreviations: **cn**, condyle; **ct**, cotyle; **dp**, diapophyses; **hp**, hypapophysis; **nc**, neural canal; **nsp**, neural spine; **pa**, parapophysis; **poz**, postzygapophysis; **prz**, prezygapophysis. All scale bars = 3 cm.

### Dorsal vertebrae

The lateral and ventral surfaces of the dorsal vertebral centra are featureless, lacking the lateral fossa seen in cervical vertebrae, as well as a hypapophysis after Dv3 (Fig. 2.15). Dorsal vertebrae have prominent transverse processes and their zygapophyses are more shallowly inclined than those of the cervical vertebrae (Fig. 2.16). The width across the prezygapophyses is consistently greater than that across the

postzygapophyses, but the long axes of both are laterally directed. Neural spines are anteroposteriorly long, with an inclined dorsal edge (i.e. higher at the anterior end, and sloping posteriorly) and laterally flared dorsal tips (Fig. 2.16). Neural spine height decreases across the first four dorsal vertebrae, stabilising at a consistent height from Dv4.

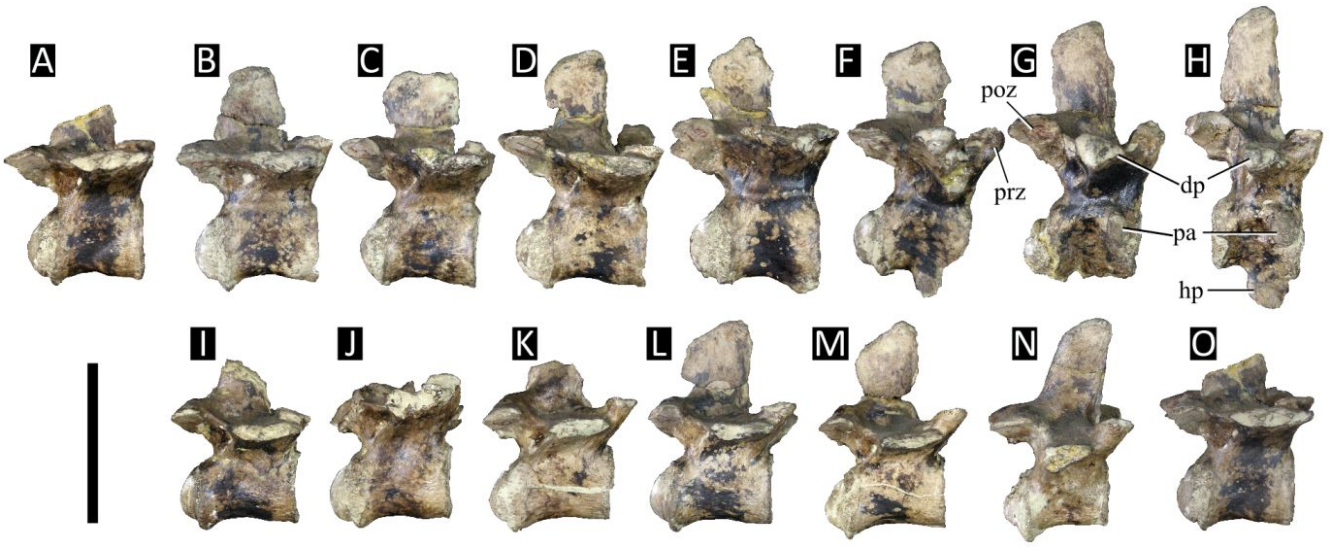



Figure 2.15: Dorsal vertebrae of *Diplocynodon hantoniensis* (NHMUK 30402). **A**–**O**, dorsal vertebrae 15–1 respectively in right lateral view. Abbreviations: **dp**, diapophysis; **hp**, hypapophysis; **pa**, parapophysis; **poz**, postzygapophysis; **prz**, prezygapophyis. Scale bar = 5 cm.

### Sacral vertebrae

The tuberculum and capitulum of the sacral vertebrae (Fig. 2.17) are approximately equally well-developed in most specimens, such that it is not possible to see the latter in dorsal view (e.g. NHMUK OR 25179). This is also the case in three anterior sacral vertebrae accessioned under NHMUK R 1050. However, the tuberculum is slightly shorter than the capitulum (meaning that the latter is visible) in a fourth anterior sacral vertebra, bearing the same collection number, and in NHMUK OR 30402 (Fig. 2.17D).

### Caudal vertebrae

Relatively few caudal vertebrae are preserved, and they are disarticulated (NHMUK R 1052 and several unnumbered specimens) (Fig. 2.18). The vertebral centrum is very elongated, with tuberosities on the ventral surface, immediately anterior to the posterior condyle, for articulation with chevrons (which are not preserved). A longitudinal sulcus occurs on the ventral surface of the centrum, defined on each side by a ridge. Where preserved, the anteroposteriorly narrow neural spine is directed vertically and positioned towards the level of the mid-length of the centrum. Transverse processes are short and the width across the prezygapophyses is significantly greater than the postzygapophyseal width.

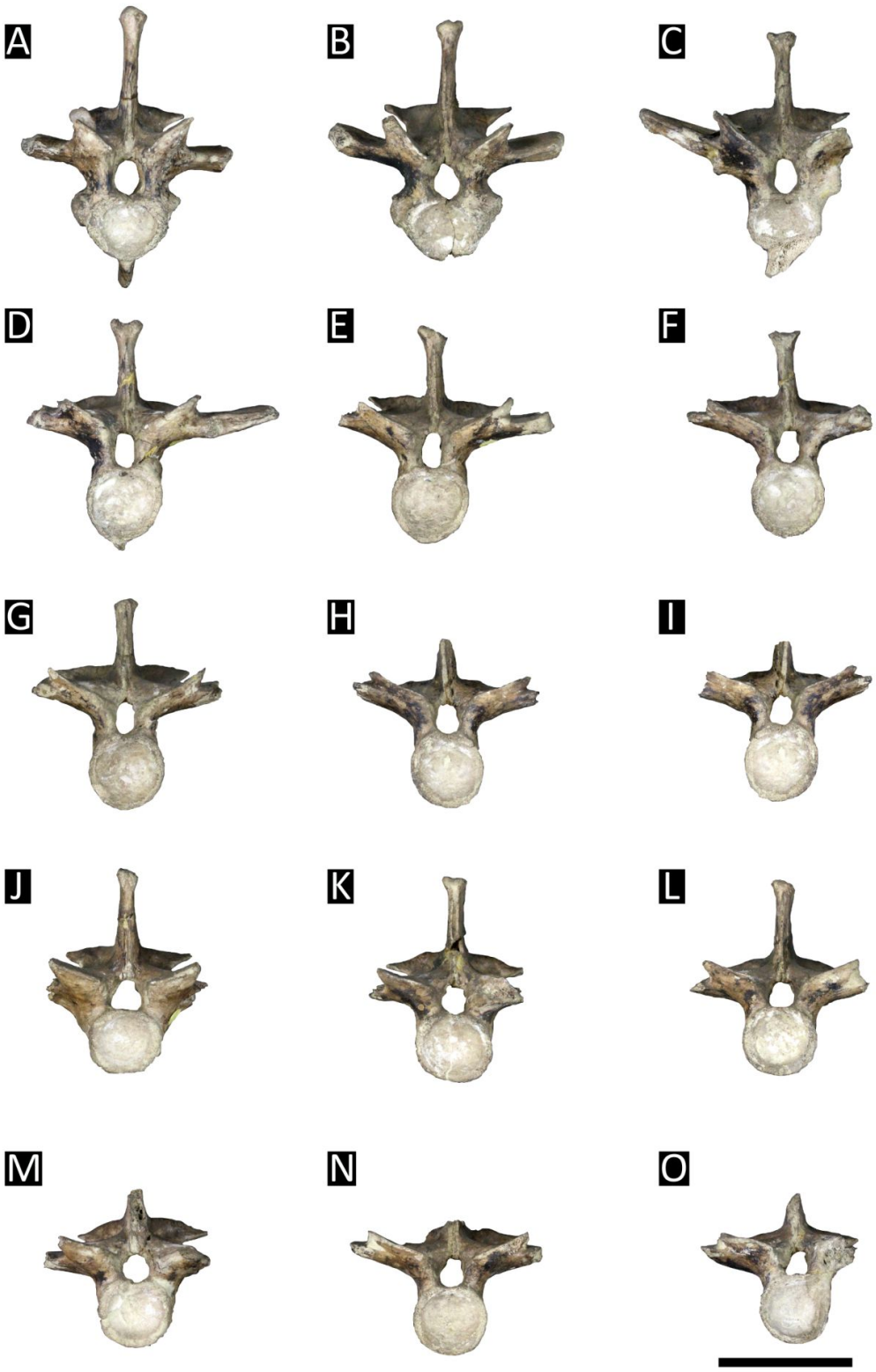



Figure 2.16: Dorsal vertebrae of *Diplocynodon hantoniensis* (NHMUK 30402). **A**–**O**, dorsal vertebrae 1–15 respectively, in anterior view. Scale bar = 5 cm.

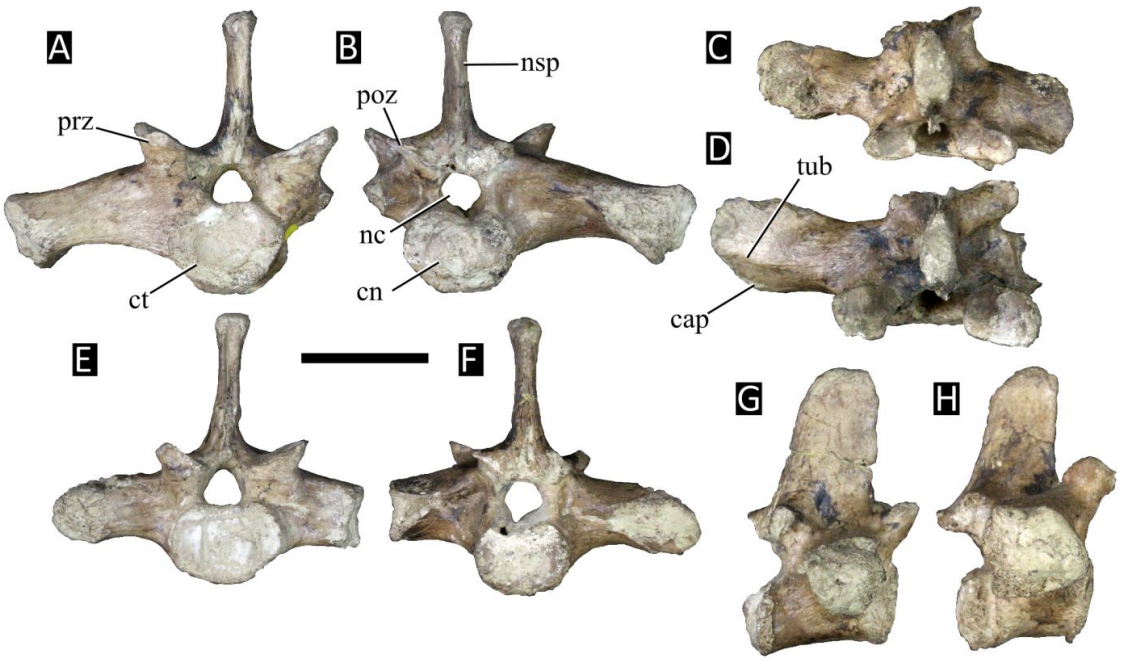



Figure 2.17: Sacral vertebrae of *Diplocynodon hantoniensis* (NHMUK 30402). The first sacral vertebra in anterior (**A**), posterior (**B**), dorsal (**D**), right lateral (**H**) views; and the second sacral vertebra in anterior (**E**), posterior (**F**), dorsal (**C**), and right lateral (**G**) views. Abbreviations: **cap**, capitulum; **cn**, condyle; **cot**, cotyle; **nc**, nueral canal; **nsp**, neural spine; **poz**, postzygapophysis; **prz**, prezygapophysis. Scale bar = 5 cm.

### 2.3.5 Osteoderms

Osteoderms are preserved both as isolated elements, and embedded in blocks of matrix along with other skeletal elements (Fig. 2.19). The rectangular dorsal osteoderms are characterized by a smooth and narrow anterior strip, followed by a broad and pitted area that hosts a medial keel (Fig. 2.19A). In most of the dorsal osteoderms, the anterior margin is straight, but at least three specimens (NHMUK R 5267 partim, R 5214 partim, and 46434) show an undulating anterior profile that can be defined as an anterior process (sensu Norell & Clark, 1990) (Fig. 2.19A, B, and D). The ventral osteoderms are represented by two units that are sutured together: the anterior one is anteroposteriorly narrow, with a smooth anterior half and a pitted posterior one (Fig. 2.19C); the posterior unit is entirely pitted and devoid of any keel (Fig. 2.19E, F).

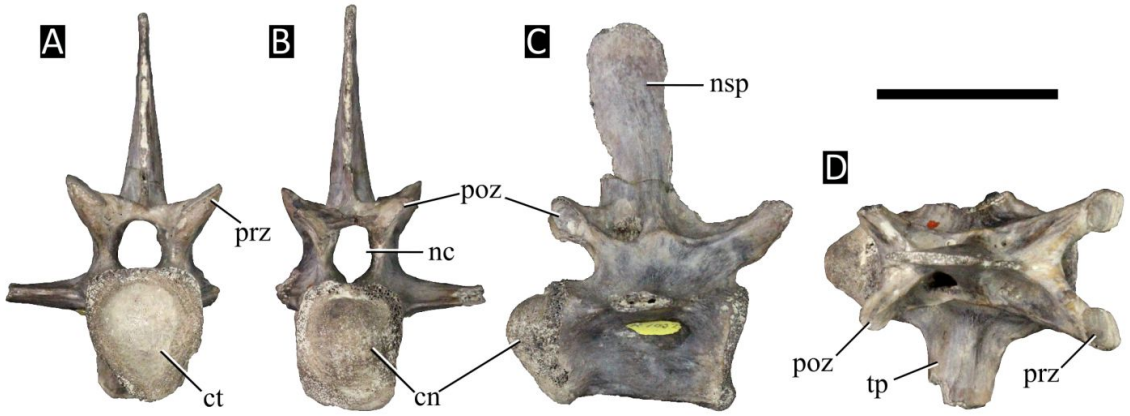



Figure 2.18: Caudal vertebrae of *Diplocynodon hantoniensis*. **A**–**D**, NHMUK R.1052 in anterior (**A**), posterior (**B**), right lateral (**C**), and dorsal (**D**) views. Abbreviations: **cn**, condyle; **ct**, cotyle; **nc**, neural canal; **nsp**, neural spine; **poz**, postzygapophysis; **prz**, prezygapophysis; **tp**, transverse process. Scale bar = 3 cm.

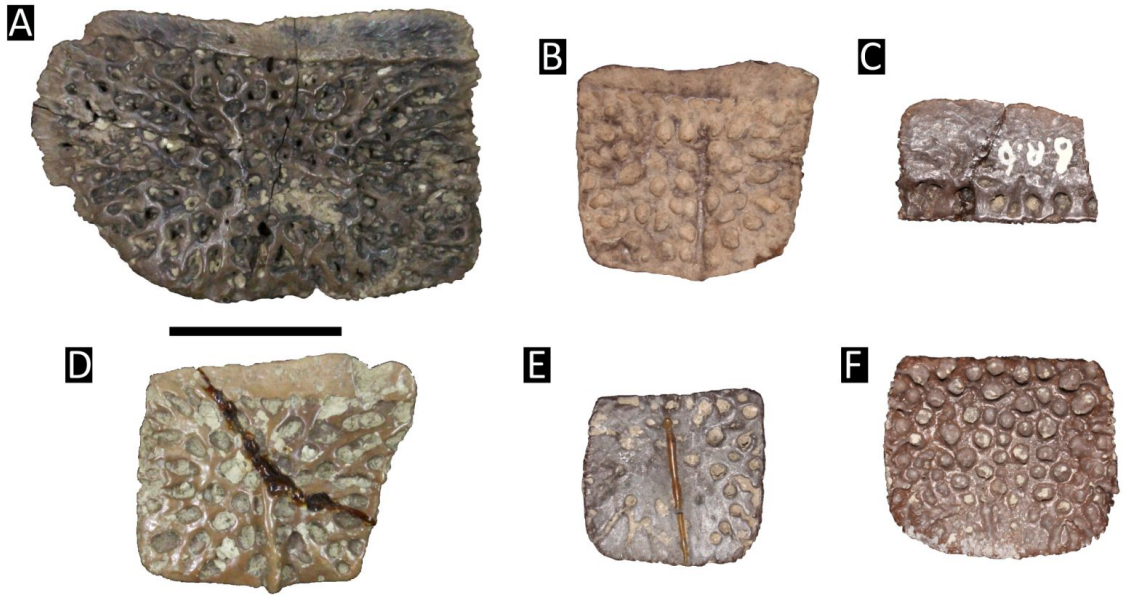



Figure 2.19: Osteoderms of *Diplocynodon hantoniensis*. **A**, unregistered dorsal midline osteoderm. Accessory osteoderms: **B**, NHMUK 46434; **D**, NHMUK R.5214. **C**, unregistered, anterior half of bipartite ventral osteoderm; **E**–**F**, unregistered posterior halves of bipartite ventral osteoderms. Scale bar = 2 cm.

### 2.3.6 Appendicular skeleton

Appendicular remains comprise most of the pectoral and pelvic girdles, as well as the proximal (upper) elements of the limbs. The limb bones are represented by robust elements, exemplified by large-sized remains, including a humerus (NHMUK OR 30206), an ulna (NHMUK OR 30236), femora (NHMUK OR 25244, 30210, 30211, 30213, 30399), tibiae (NHMUK OR 25236, 30215, 30216, 30217), and fibulae (NHMUK OR 30333, 30335). Although no associated limb bones are available, it seems likely that the forelimb was shorter than the hindlimb, as all the preserved femora are longer than the largest preserved humerus (NHMUK OR 30206). The relative anatomical orientations (i.e. medial, lateral, dorsal, ventral, etc.) reflect the sprawling posture (Fig. 2.20) following Meers (2003, fig. 1), and Klinkhamer et al. (2017, fig. 2).

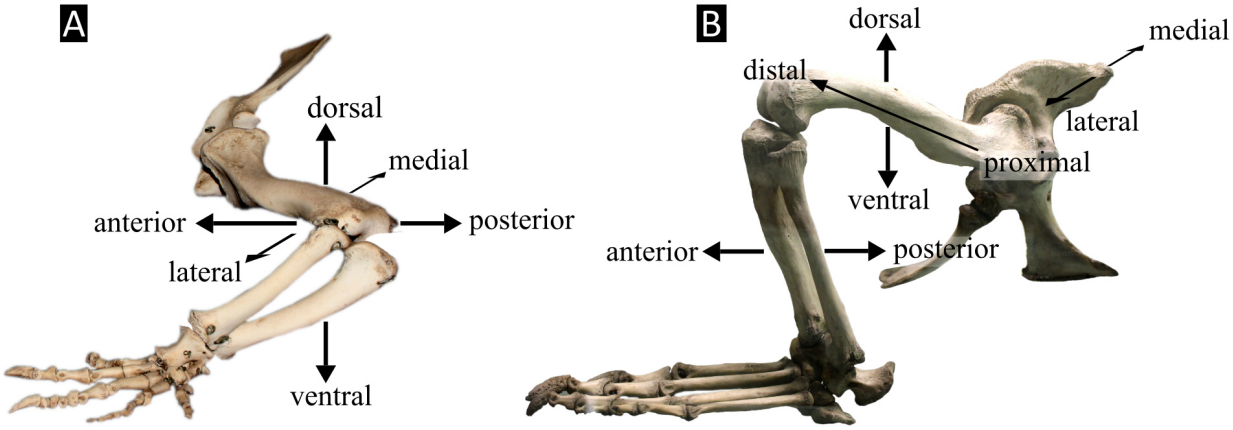



Figure 2.20: Explanation of relative anatomical orientations, projected on the forelimb (**A**) and hindlimb (**B**) of *Crocodylus porosus*. A: (NHMUK specimen on exhibit), B: (QM unnumbered mounted skeleton). Not to scale.

#### Scapula

The horizontal articular surface for the coracoid is poorly preserved in all scapulae, but is teardrop-shaped, with a narrow anterior tip and a much larger posterior area, close to the glenoid surface. The fact that the largest scapula (NHMUK OR 30247) is quite large, but not fused to the coracoid, implies that their fusion must have occurred very late in ontogeny (Brochu, 1995). The glenoid surface of the scapula faces posterolaterally (Fig. 2.21A). It is large and ovoid, with a rounded dorsal margin, and a modest constriction at its anterior margin. This constriction is related to a prominent fossa anterior to the glenoid surface that is pierced by a small foramen (see NHMUK OR 30247 and 30414) (Fig. 2.21E, F). In all specimens, regardless of size, the deltoid crest is thin. The posterior edge of the scapular blade is straight to slightly convex, and the anterior edge is concave. There is a large constriction between the ventral corpus of the scapula and the distal blade, which flares. In dorsal view, the blade is sharp and

straight. The lateral surface of the scapula blade is smooth and slightly convex proximally, becoming flatter distally. Attachment sites for several muscles can be recognised on the lateral surface of the largest scapula NHMUK OR 30247 (Fig. 2.21F). Two distinct, broad depressions extend over the greater part of the blade. The anterior of these two depressions is the larger origin site for *M. deltoideus scapularis*. A low ridge separates this scar from a posterior depression, which is inferred to be the smaller origin site of *M. teres major* (Meers, 2003). Anterior to the attachment for *M. deltoideus scapularis* is a depression which occupies the anteriormost edge of the scapula and adjacent to the deltoid crest. This is the origin of *M. deltoideus clavicularis*. The posteriromost edge of the scapula blade also has a depression, which is inferred to be the area of insertion of *M. serratus ventralis thoracis* dorsally, and the site of origin for *M. scapulohumeralis caudalis* ventrally (Fig. 2.21F). The medial surface of the blade is less sculpted than the lateral surface, with one broad depression situated slightly posterior to the blade at mid-length: this likely marks the origin of *M. subscapularis*. Dorsal to the glenoid surface, on the glenoid buttress, is a large tubercle. This scar is prominent even in the smallest scapulae (e.g. NHMUK OR 30414), and is the attachment site for *M. triceps longus lateralis* (Meers, 2003).

### Coracoid

Two left coracoids are preserved (NHMUK OR 30359 and 25245), although the distal ends of both are missing (Fig. 2.21G). The sub-circular glenoid surface faces posterolaterally. A small projection of the glenoid surface overhangs the recess ventral to the glenoid surface. A large coracoid foramen is situated anterior to the glenoid surface. The coracoid blade is directed ventrally and medially. Although incomplete, it expands distally, but the shape and width of the distal end cannot be determined.

### Humerus

Two right humeri (NHMUK OR 30219 and 30206) are preserved, along with a partial left humerus (NHMUK OR 30206a) (Fig. 2.22). The proximal extremity is poorly preserved in the largest humerus (NHMUK OR 30206). In NHMUK OR 30219, the dorsal border of the articular surface is significantly raised relative to the proximal extremity of the humeral shaft. The medial condyle of the proximal end is larger than its lateral counterpart. Although slightly eroded, the deltopectoral crests of NHMUK OR 30219 and 30206a clearly emerge abruptly from the humerus. The straight deltopectoral crest is aligned with the lateral margin of the humerus (Fig. 2.22D, H). The apex of the deltopectoral crest projects ventrally, perpendicular to the humeral shaft, with no medial deflection. Dorsal to the deltopectoral crest, on the lateral margin of the humeral shaft, there is a single scar for the insertion of *M. teres major* and *M. latissimus dorsi*, which is especially prominent in NHMUK OR 30206 (Fig. 2.22G). In lateral view, a longitudinal ridge can be traced, extending from the proximal articular border, through the scar for *M. latissimus dorsi*, then running diagonally across the lateral side of the diaphysis (Fig. 2.22F).

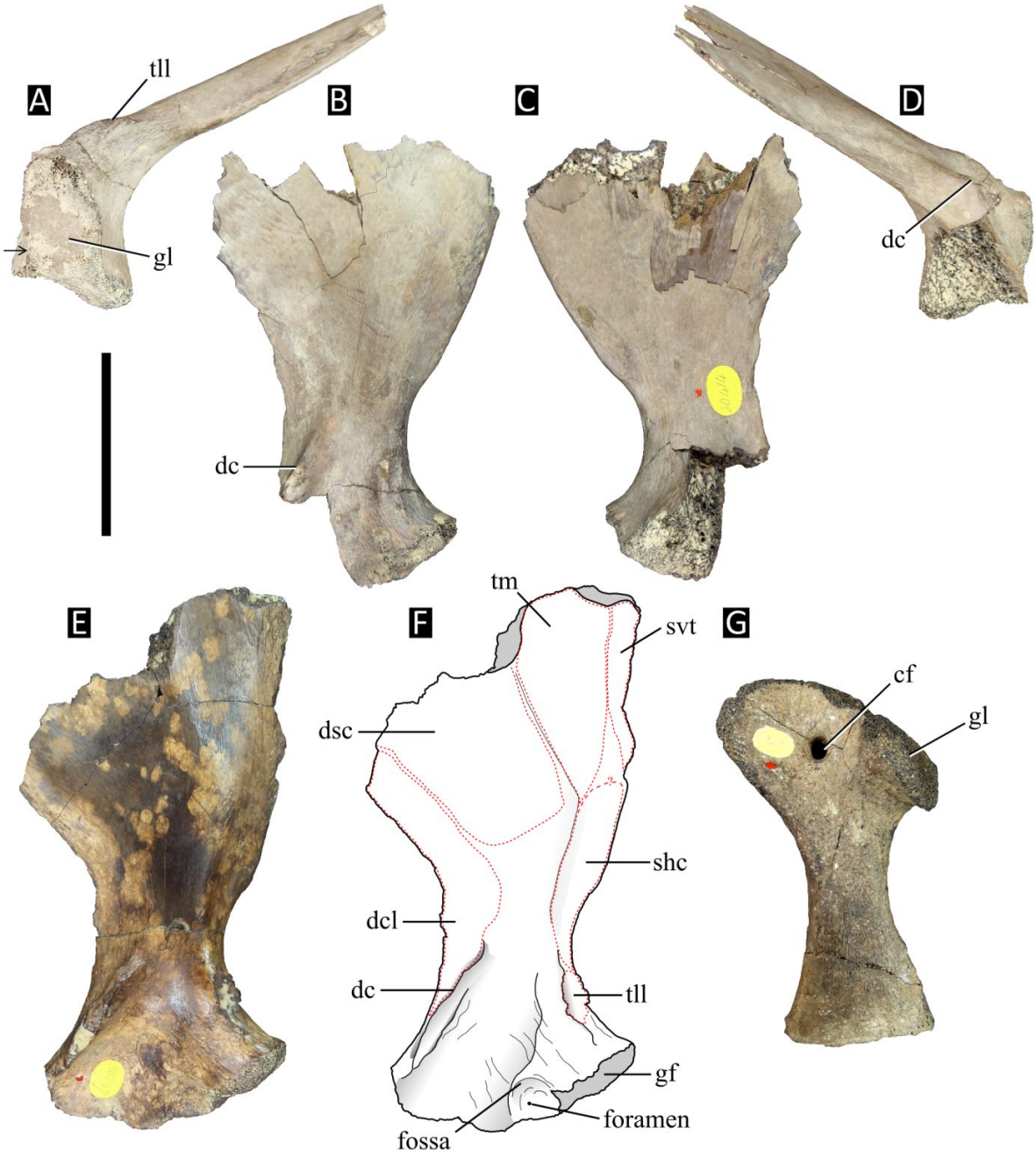



Figure 2.21: The pectoral girdle of *Diplocynodon hantoniensis*. **A**–**D**, left scapula (NHMUK 30414) in anterior (**A**), lateral (**B**), medial (**C**), and posterior (**D**) views, arrow indicates the position of a constriction in the glenoid fossa. Photograph and interpretive drawing of the left scapula (NHMUK 30247) in lateral view (**E**, **F**). **G**, left coracoid (NHMUK 30359) in lateral view. Abbreviations: **cf**, coracoid foramen; **dc**, deltoid crest; **dcl**, *M. deltoideus clavicularis*; **dsc**, *M. deltoideus scapularis*; **gl**, glenoid surface; **shc**, *M. scapulohumeralis caudalis*; **svt**, *M. serratus ventralis thoracis*; **tm**, *M. teres major*; **tll**, *M. triceps longus lateralis*. Scale bar = 4 cm.

This ridge probably defines the boundary between *M. humeroradialis* and *M. triceps brevis cranialis* from the extensive dorsal origin of *M. triceps brevis intermedius* (Meers, 2003). Medial to the *M. teres major* scar, there is a broad depression on the dorsal surface of the proximal metaphysis. Based on a comparison with extant crocodylians this might be the insertion of *M. scapulohumeralis caudalis* (Meers, 2003) (Fig. 2.22G). The proximal and distal epiphyses are offset, with the former extending further dorsally and resulting in a sigmoidal outline to the humerus in medial view. The medial margin of the proximal extremity extends dorsally and medially away from the humeral shaft, forming a tuberosity which would have articulated with the glenoid surface of the scapula and coracoid. The medial edge of this tuberosity is scarred, possibly marking the origin of *M. triceps brevis* as in extant crocodylians (Meers, 2003; Klinkhamer et al., 2017). The medial margin of the humeral shaft is strongly concave. Posteriorly, the humeral shaft widens towards the distal extremity. Scarring on the medial side of the distal metaphysis may mark the origins of *M. pronator teres* and *M. flexor digitorum longus* (Meers, 2003). The medial and lateral condyles of the distal extremity are not equidimensional. The medial condyle is mediolaterally compressed and has an acute posterior termination, whereas the lateral condyle is wider and rounded. In dorsal view, the lateral margins of the distal and proximal extremities are approximately in line, and the humeral shaft has a distinct lateral bow between these extremities. The medial distal extremities are more offset, with the proximal medial margin directed more medially than the distal margin. A prominent trochlea divides the lateral and medial hemicondyles of the humerus. A broad depression occurs on the ventral surface of the distal extremity, at the midline, immediately anterior to the condyles.

**Ulna**

Three right ulnae (NHMUK OR 30326, 30327, 30389) and one left ulna (NHMUK OR 30242) are preserved. The proximal epiphysis of the ulna is much larger than the distal epiphysis (Fig. 2.23). There is a large, rounded olecranon process (Fig. 2.23D). The proximal articular surface has a sub-quadrangular shape (Fig. 2.23B), with its straight dorsal and lateral margins perpendicular to one another. The dorsal half of the medial margin of the proximal articular surface is parallel to the lateral margin, whereas the ventral half has a prominent notch (Fig. 2.23B). This notch might mark the posterior extent of the attachment of *M. pronator quadratus* on the medial surface (Meers, 2003). The diaphysis is mediolaterally compressed across its entire length, with a modest medial bowing. It is narrowest anterior to the mid-length of the shaft. In lateral view, the ventral edge of the ulna is convex and the dorsal margin is concave. On the dorsolateral surface of the diaphysis, immediately anterior to the proximal epiphysis, is a circular scar (Fig. 2.23E). A very prominent, straight ridge runs parallel to the long-axis of the ulna along the dorsal surface (best seen in NHMUK OR 30242 and 30389). A very small sulcus extends longitudinally along the lateral surface of the diaphysis, and probably marks the insertion of *M. flexor ulnaris* (Meers,

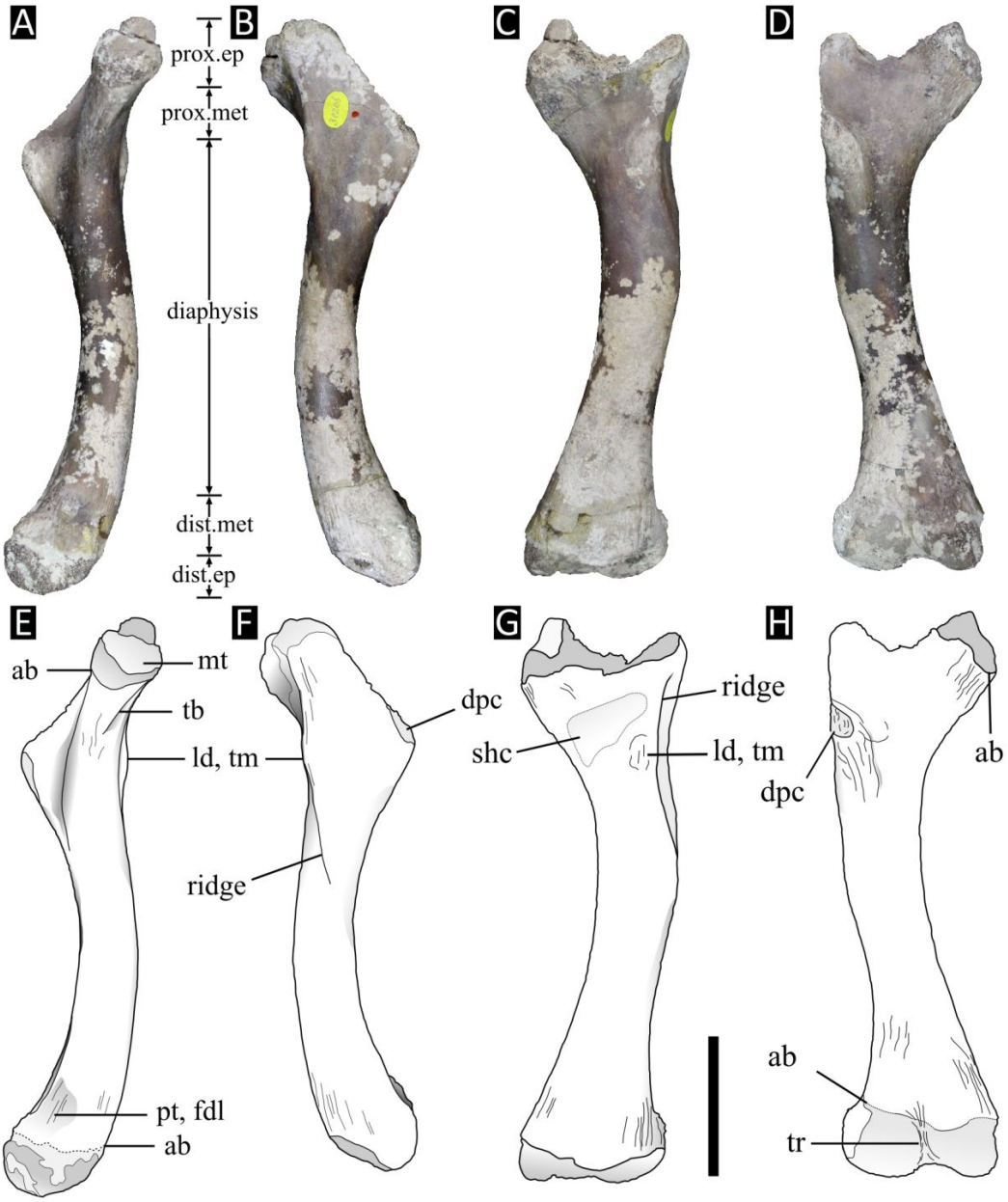



Figure 2.22: Humeral morphology of *Diplocynodon hantoniensis*. Right humerus (NHMUK 30206) in medial (**A**, **E**), lateral (**B**, **F**), dorsal (**C**, **G**), and ventral (**D**, **H**) views. Abbreviations: **ab**, articular border; **di**. diaphysis; **dist.ep**, distal epiphysis; **dist.met**, distal metaphysis; **dpc**, deltopectoral crest; **fdl**, *M. flexor digitorum longus*; **ld**, *M. latissimus dorsi*; mt, medial tuberosity; **prox.ep**, proximal epiphysis; **prox.met**, proximal metaphysis; **pt**, *M. pronator teres*; **shc**, *M. scapulohumeralis caudalis*; **tb**, *M. triceps brevis*; **tm**, *M. teres major*; **tr**, trochlea. Scale bar = 4 cm.

2003) (Fig. 2.23C, E). On the dorsal surface at the distal end, posterior to the epiphysis, is a modestly developed ridge that extends posteriorly, slightly onto the medial surface. The distal epiphysis is strongly compressed mediolaterally. Its articular surface is elliptical, facing anteromedially and slightly ventrally. In anterior view, its lateral margin is crescentic, and the medial margin has a small notch around the dorsoventral midpoint. There is also a prominent ventromedial projection on the articular surface, from which a small lamina extends onto the diaphysis (see NHMUK OR 30389).

### Radius

The proximal epiphysis of the radius is quadrangular, with perpendicular ventral, medial and lateral margins, and a rounded dorsal margin. This proximal articular surface is bevelled, such that the dorsolateral margin projects further dorsally than the dorsomedial margin. The mediolateral widths of the proximal and distal epiphyses are subequal. Whereas the diaphysis widens abruptly towards the proximal epiphysis, there is a much more gradual increase in mediolateral width towards the distal epiphysis. Proximally, the diaphysis has a rounded cross-section, becoming dorsoventrally compressed distally. The diaphysis is straight, and sculptured with ridges that mark muscle attachment sites. On the ventromedial side, there is a longitudinal ridge, which terminates above the mid-length of the diaphysis. In proximal view, the distal epiphysis has a semi-circular outline, with a flat ventral margin and rounded dorsal margin. The medial half of the distal epiphysis projects further anteriorly than the lateral half.

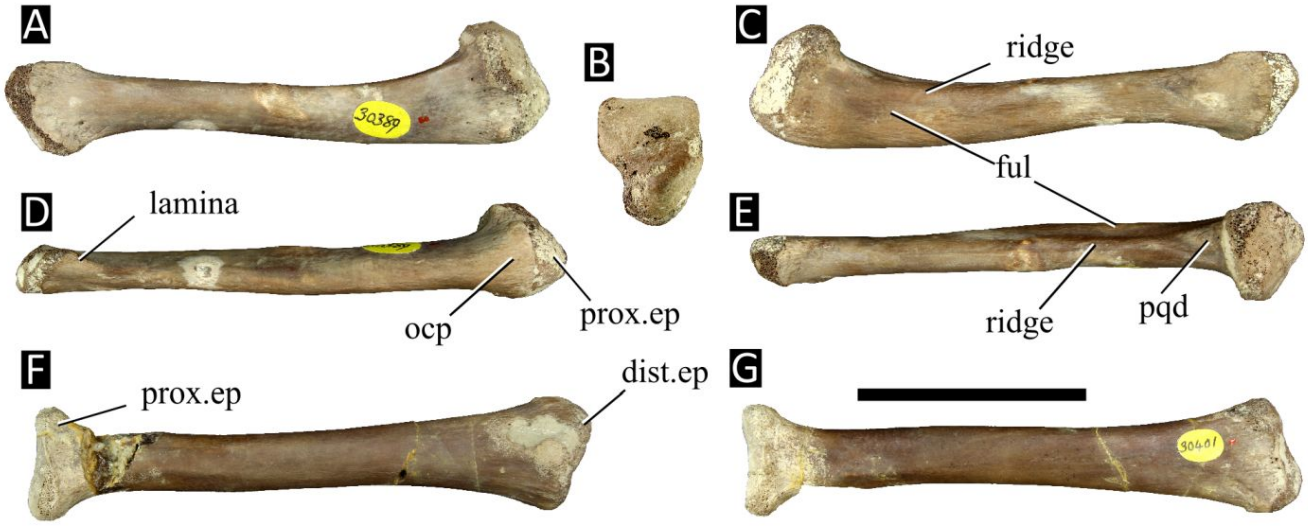



Figure 2.23: The ulna and radius of *Diplocynodon hantoniensis*. **A**–**E**, right ulna (NHMUK 30389) in medial (**A**), proximal (**B**), lateral (**C**), ventral (**D**), and dorsal (**E**) views. **F**–**G**, right radius (NHMUK 30401) in dorsal (**F**), and ventral (**G**) views. Abbreviations: **dist.ep**, distal epiphysis; **ful**, *M. flexor ulnaris*; **ocp**, olecranon process; **pqd**, *M. pronator quadratus*; **prox.ep**, proximal epiphysis. Scale bar = 4 cm.

### Ilium

Four right (NHMUK OR 30362, 25252a, 25253, 30414a) and two left (NHMUK OR 25252b, 30414b) ilia are preserved (Fig. 2.24). The anterior process of the ilium is not well-developed and the dorsal margin is rounded, with a smooth border, and with a very deep posterior tip. The postacetabular process is approximately equivalent to the height of the acetabulum. On the posterior margin of the postacetabular process, the attachment site for *M. ilioischio caudalis* is situated dorsomedially (Fig. 2.24A). The acetabulum occupies approximately half of the lateral surface of the ilium. The supracetabular crest is narrow, with a rugose texture, ornamented with a series of small parallel vertical ridges. The inclination of the iliac crest relative to the sagittal plane varies anteroposteriorly: it rises to a sub-vertical orientation anteriorly, whereas the inclination of the crest becomes shallower (at approximately 45° to the sagittal plane) towards the posterior end of the postacetabular process (Fig. 2.24D). In dorsal view, the iliac crest is not linear, but curves laterally (Fig. 2.24C). The articular surface of the pubic peduncle faces ventrally. The condyles of the pubic peduncle are asymmetric, with a large anterior condyle and small posterior condyle (Fig. 2.24E). Between the pubic peduncle and the preacetabular process, the anterior edge of the ilium is concave. The ischial peduncle forms the posterior wall of the acetabulum. It projects further laterally than the pubic peduncle, but they reach the same level ventrally. Although worn in all specimens, the ventral surface of the ischial peduncle appears to be horizontal and triangular. The iliac margin of the acetabular perforation is well defined. Its dorsal margin is broadly curved, and the acetabulum is deeply concave, especially around its ventral margin. Attachment sites for the transverse processes of the sacral vertebrae are centrally positioned on the medial surface of the ilium (Fig. 2.24B). The attachment for the posterior transverse process extends posteriorly along the ventral margin of the postacetabular process, leading slightly on to its ventromedial side. As such, the postacetabular process would not have extended much further than the posterior sacral vertebra. The attachment site for the anterior sacral vertebrae is sub-triangular and adjacent to the posterior scar. An anteroposteriorly thin, vertical strut (or 'bridge') of bone separates these two attachment sites.

### Ischium

Two partial ischia are preserved (both NHMUK OR 30354) (Fig. 2.25): a left ischium, and a smaller right element. In both specimens, the tip of the distal blade is broken off and the posterior peduncle is worn. Although worn, the posterior peduncle is larger than the anterior peduncle. The posterior peduncle would have articulated with the ilium to enclose the posterior and ventral margins of the acetabulum. A laterally directed articular surface is preserved on the posterior peduncle of the right ischium, for articulation with the proximal head of the femur. The head of the anterior peduncle is anteroposteriorly compressed, and its articular surface is flat and orientated ventromedially. This peduncle encloses the

anterior margin of the acetabulum, which probably had a dorsoventrally elongated elliptical outline. The large, rounded ventral margin of the acetabular perforation is formed by the peduncle bridge of the ischium. The peduncle bridge is mediolaterally constricted at the level of the acetabular perforation. Towards the head of the anterior peduncle, the margins of the bridge flare outwards. A prominent scar occurs ventral to the peduncle bridge, on the anterolateral surface of the ischium. This probably marks the attachment site for one of the '*flexor tibialis internus* group' muscles, as in *C. porosus* (Klinkhamer et al., 2017). In the larger left ischium, this scar is significantly bigger and more rugose, extending further onto the anterior margin of the ischial blade. A prominent ridge is also associated with this scar, extending along the long axis of the ischial blade. A series of muscle attachment scars occur on the posterior margin of the ischium, ventrolateral to the posterior peduncle. The dorsal most scar probably marks the attachment of *M. pubo-ischio-tibialis*, whereas the more ventral scars are for the remaining *flexor tibialis internus* muscles (Klinkhamer et al., 2017). Again, this scar is much more prominent and rugose in the larger left ischium. The ischial blade is directed medially and slightly posteriorly. Whereas the anterior edge of the blade is sharp, the posterior margin is more rounded. Although incomplete in both ischia, the distal blade expands towards its distal end: this expansion occurs along an anteromedial-to-posterolateral axis. However, it is not possible to determine whether the distal end of the blade reached a greater width than the proximal head.

**Femur**

There are several well preserved femora. Among the more complete are two right (NHMUK OR 30211, 25244) and three left (NHMUK OR 30210, 30399 and R.5215) elements. Although it is not possible to determine which elements belong to which individuals, all femora are longer than the preserved humeri. The proximal epiphysis of the femur is mediolaterally compressed (Fig. 2.26). The dorsal surface of the proximal metaphysis is broadly concave. Scarring towards the posterior end of the proximo-dorsal metaphysis is regarded as evidence for the tendinous insertion of *M. pubo-ischio-femoralis internus* (Fig. 2.26C). On the ventral surface of the proximal metaphysis, two broad fossae occur either side of a discrete knob that projects from the proximal head (Fig. 2.26B, D). On the proximo-anterior edge of the femur there is a prominent notch covered in striations, which extend towards the articular border of the proximal epiphysis. This is interpreted as the site for the tendinous insertion of *M. pubo-ischio-femoralis externus*, as in *C. porosus* (Klinkhamer et al., 2017) (Fig. 2.26 C). In dorsal view, the femur is strongly sigmoidal in outline. This results from curvature along the diaphysis, and torsion between the proximal and distal epiphyses. The dorsal surface of the diaphysis is characterised by a centrally positioned, raised surface, which is defined by two longitudinal ridges (Fig. 2.26A, C) The posteriormost of these ridges intersects the posterior margin of the diaphysis at the femoral mid-length, converging with the anteriormost ridge centrally on the femoral shaft. A fossa, pierced by a foramen, occurs anterior to the raised flat ridge.

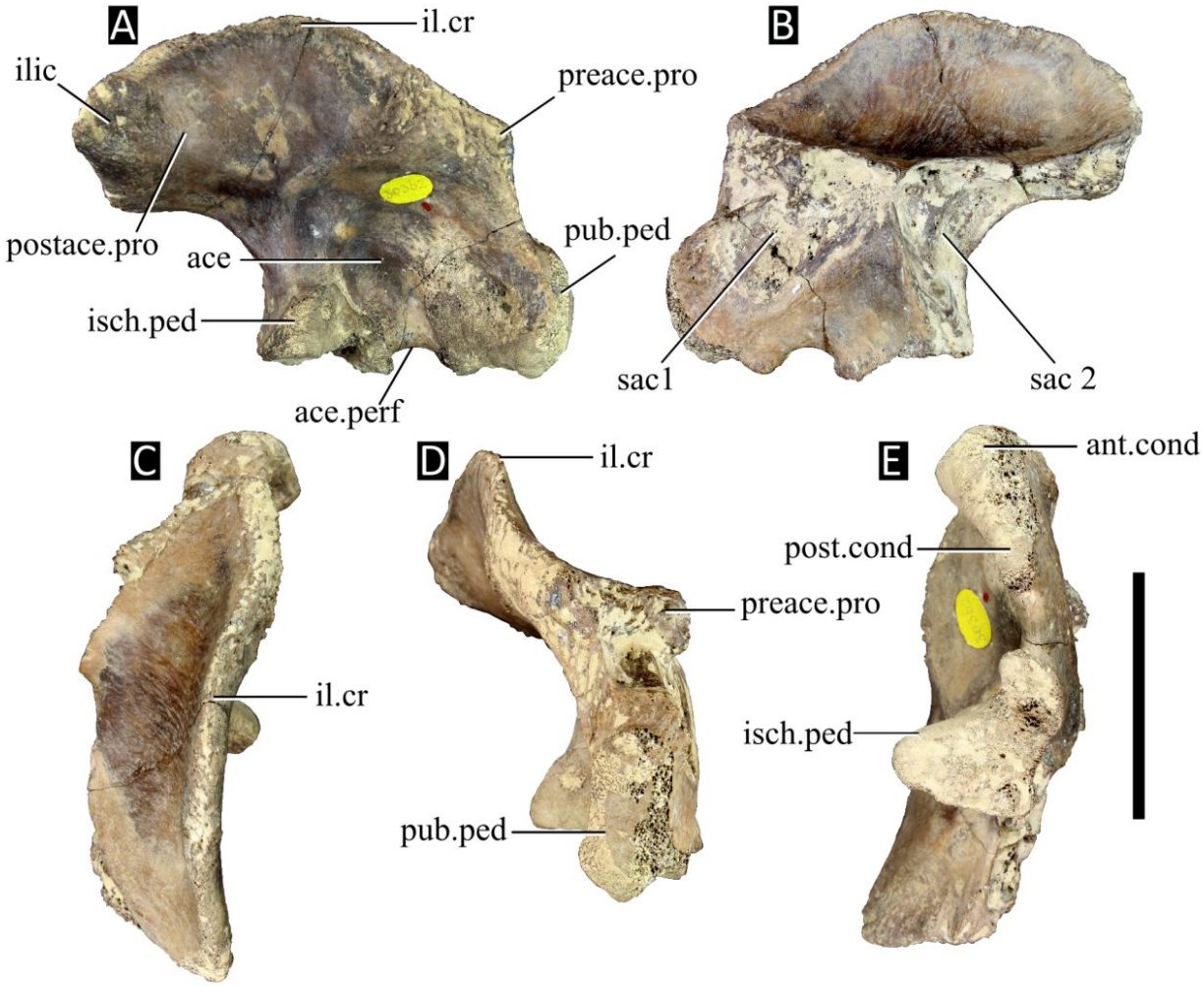



Figure 2.24: Right ilium (NHMUK 30362) of *Diplocynodon hantoniensis* in lateral (**A**), medial (**B**), dorsal (**C**), anterior (**D**) and ventral (**E**) views. Abbreviations: **ace**, acetabulum; **ace.perf**, acetabular perforation; **ant.cond**, anterior condyle; **ilic**, M. ilioischio caudalis; **il.cr**, iliac crest; **isch.ped**, ischial peduncle of the ilium; **post.cond**, posterior condyle; **postace.pro**, postacetabular process; **prace.pro**, preacetabular process; **pub.ped**, pubic peduncle. Scale bar = 4 cm.

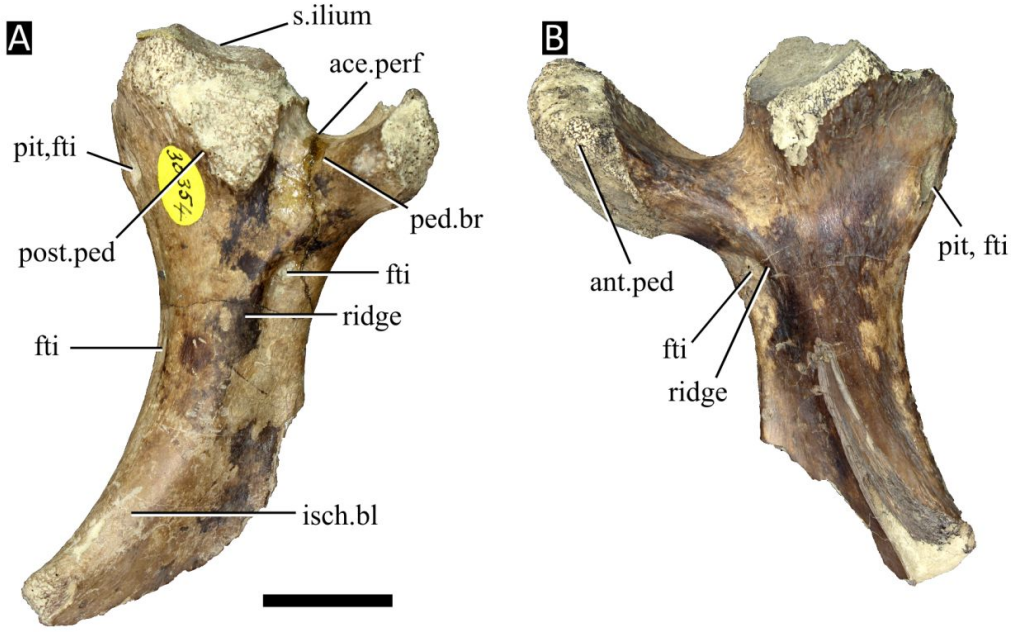



Figure 2.25: Ischia of *Diplocynodon hantoniensis* (NHMUK 30354). **A**, right ischium in lateral view; **B**, left ischium in lateral view. Abbreviations: **ace.perf**, acetabular perforation; **ant.ped**, anterior peduncle; **fti**, *M. flexor tibialis internus*; **isch.bl**, ischial blade; **ped.br**, peduncle bridge; **pit**, *M. puboischio tibialis*. Scale bar = 2 cm.

These ridges correspond with the insertions of three muscles in living crocodylians: (1) *M. iliofemoralis*; (2) *M. femorotibialis internus*; and (3) *M. femorotibialis externus*. *M. iliofemoralis* has a fleshy insertion along the distal third of the dorsolateral surface of the femur in living crocodylians (Tumarkin-Deratzian et al., 2007; Klinkhamer et al., 2017), and it probably formed the raised flat surface that is so prominent in *D. hantoniensis*. *M. femorotibialis internus* and *M. femorotibialis externus* surround *M. iliofemoralis* anteriorly and posteriorly, respectively. The ventral side of the femur is dominated by scarring associated with muscle attachments around the $4^{th}$ trochanter (Fig. 2.26D). The $4^{th}$ trochanter comprises a short, longitudinal ridge. Immediately anterior to the $4^{th}$ trochanter ridge is a depression that corresponds to the area of insertion for *M. pubo-ischio-femoralis internus* (Klinkhamer et al., 2017). The prominent ridge that defines the $4^{th}$ trochanter, as well as a large scarred depression following on from the ridge, are interpreted as the sites for tendinous insertions of *M. caudofemoralis longus* and *M. caudofemoralis brevis*. Distally, there is a depression on the ventromedial edge of the diaphysis, which is interpreted as the area of insertion for *M. adductor*, as in *C. porosus* (Klinkhamer et al., 2017). The distal epiphysis is poorly preserved in the largest femora, but well preserved in NHMUK R 5215. A very prominent constriction occurs at the midpoint of the distal epiphysis, dividing the lateral and medial condyles. The lateral half of the distal articular surface is dorsoventrally taller than the medial half. The ventral margin of the lateral half is very acute, extending further ventrally than the medial half.

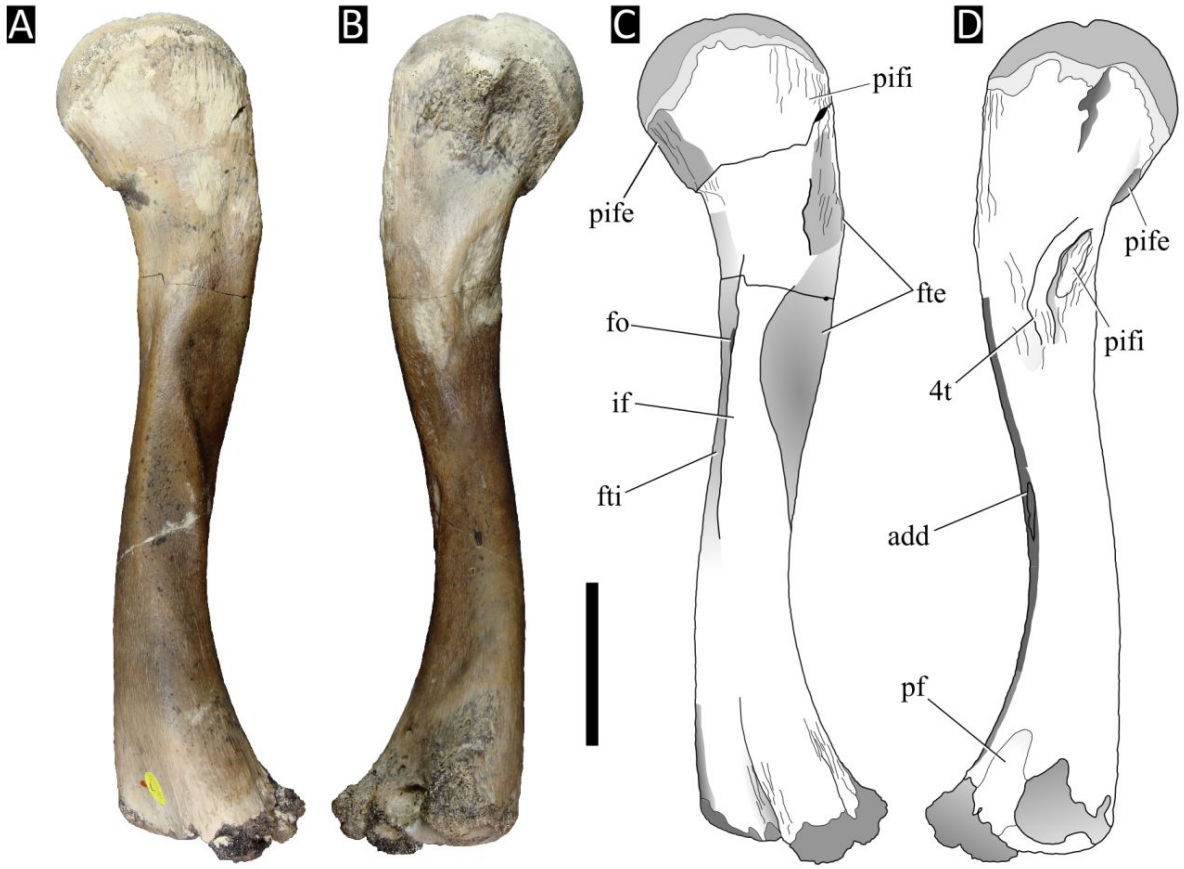



Figure 2.26: Photographs and line drawings of the left femur of *Diplocynodon hantoniensis* (NHMUK 30210) in dorsal (**A**, **C**), and ventral (**B**, **D**) views. Abbreviations: **4t**, $4^{th}$ trochanter; **add**, *M. adductor*; **fo**, foramen; **fte**, *M. femorotibialis externus*; **fti**, *M. femorotibialis internus*; **if**, *M. iliofemoralis*; **pf**, popliteal fossa; **pife**, *M. pubo-ischio-femoralis externus*; **pifi**, *M. pubo-ischio-femoralis internus*. Scale bar = 5 cm.

### Tibia

Several tibiae are preserved, with two right (NHMUK OR 30215, 30217) and two left (NHMUK OR 30216 and 25236) elements amongst the best preserved. The proximal epiphysis is broader than the distal epiphysis, facing dorsally and slightly posteriorly (Fig. 2.27A–D). A large sulcus occurs towards the medial edge of the facet, for the tibial condyle of the femur. The posterior margin of the proximal articular facet forms an overhanging triangular lip. The proximal metaphysis of the tibia is circumscribed by a striated surface indicating the attachment of numerous muscles, but it is not possible to distinguish between them in detail. The proximo-medial edge is particularly scarred, and in *C. porosus* this area corresponds with multiple tendinous insertions including: *M. flexor tibialis internus*, *M. pubo-ischio-tibialis*, *M. ambiens*, and *M. iliotibialis* (Klinkhamer et al., 2017). A pale discoloured tuberosity occurs on the proximal anterior surface, and probably marks the origin of *M. tibialis anterior*. This tuberosity leads onto a longitudinal ridge where *M. tibialis anterior* attaches in *C. porosus* (Klinkhamer et al., 2017). Whereas the medial edge of the tibial diaphysis is concave, the lateral edge is slightly convex. On the posterior surface of the diaphysis, there is a prominent longitudinal ridge (Fig. 2.27C). This ridge begins proximally, on the centre of the diaphysis, and moves to the medial edge distally. A second ridge occurs in NHMUK OR 30215, at a slight angle to the first ridge, merging with its distal end. These ridges probably correspond to the sites of insertion of *M. interosseous cruris*, as in living crocodylians (Klinkhamer et al., 2017). The distal epiphysis is anteroposteriorly compressed, with a notch on the posterior side, producing an arcuate articular facet for the astragalus (Fig. 2.27C). This facet faces posteroventrally. The medial portion of the facet projects slightly further distally than the lateral counterpart.

### Fibula

Two right (NHMUK OR 30233 [Fig. 2.27E–H], 30235) and two broken and fragmentary left (NHMUK OR 30241, 30234) fibulae are preserved. The proximal end is mediolaterally compressed, with a dorsomedially orientated, elliptical, articular facet. The proximal epiphysis is strongly expanded posteriorly for the long external lateral ligament (Fig. 2.27L). It has a notch at its midpoint, which results in a dorsally concave outline in medial and lateral views. The proximomedial surface of the fibula has a triangular crest, which has a rough, striated texture. This texture extends proximally until the border of the articular surface. This surface probably marks the tendinous insertion of *M. interosseous cruris* and another tendinous attachment for *M. fibularis longus* (Fig. 2.27H). The trochanter for the insertion of *M. iliofibularis* occurs on the proximolateral surface of the fibula, near the anterior edge, as in extant crocodylians (Fig. 2.27G). Above the iliofibularis trochanter, on the proximolateral metaphysis, there is more scarring, although less prominent than on the medial side. In extant crocodylians, this is the location of origin for *M. extensor digitorum longus* and *M. fibularis brevis*. The distal half of the lateral fibular surface has a

centrally positioned, longitudinal ridge, which likely marks the origin of *M. extensor digitorum brevis* (Klinkhamer et al., 2017). The distal epiphysis is compressed in a posteromedial-to-anterolateral direction. This generates a small amount of torsion between the proximal and distal epiphyses. The articular facet of the distal epiphysis faces anteroventrally for articulation with the astragalus. In distal view, the facet is sub-triangular. Its lateral edge is straight, whereas the medial edge is slightly concave, forming a distinct notch at the anteroposterior mid-point. The posterior edge of the distal metaphysis is defined by a thin ridge, possibly marking the origin of *M. pronator profundus*.

## 2.4 Taxonomic Status of Previously Referred Material

Several specimens have been referred to *Diplocynodon hantoniensis* from Paleogene deposits in western Europe and the USA. If correctly attributed, these remains would demonstrate that this species had a much greater spatiotemporal distribution.

### 2.4.1 Early Eocene of the USA

Weems and Grimsley (1999) referred a single tooth (USNM 496207) and a keeled dorsal osteoderm (unnumbered specimen) to *D. hantoniensis* from the early Eocene Nanjemoy Formation, which crops out in the Fisher/Sullivan site in Stafford County, Virginia. The referral was based partly on the purported presence of '*Diplocynodon stuckeri*' from the middle Eocene of Wyoming (Mook, 1960). However, this latter material has since been referred to *Borealosuchus wilsoni* (Brochu, 1997a). The tooth described by Weems and Grimsley (1999) is conical, with carinae on the anterior and distal edges, and the osteoderm is approximately rectangular with a modest keel. The morphology of these elements is insufficient for specific or even generic identification. This material from Virginia is considered to represent an indeterminate crocodylian, pending the discovery of diagnostic material from this locality.

### 2.4.2 Late Eocene of Switzerland

Pictet et al. (1857) described fragmentary remains of a crocodylian from the late Eocene of Mormont (=Mauremont), in the canton of Vaud, western Switzerland. The material consists of five unnumbered cranial fragments, a fragment of the retroarticular process, and two isolated teeth. Pictet et al. (1857) referred the material to *D.* cf. *hantoniensis* based on the presence of a large occlusal pit (for dentary tooth 1) on the ventral surface of the premaxilla (described but not figured). The shapes of both the squamosal and supratemporal fenestra were also regarded as identical to *D. hantoniensis*, along with two isolated teeth that display similar carinae. Similarities are found in the material with *D. hantoniensis*, such as the long squamosal prongs and elongate supratemporal fenestra. However, none of the diagnostic features of

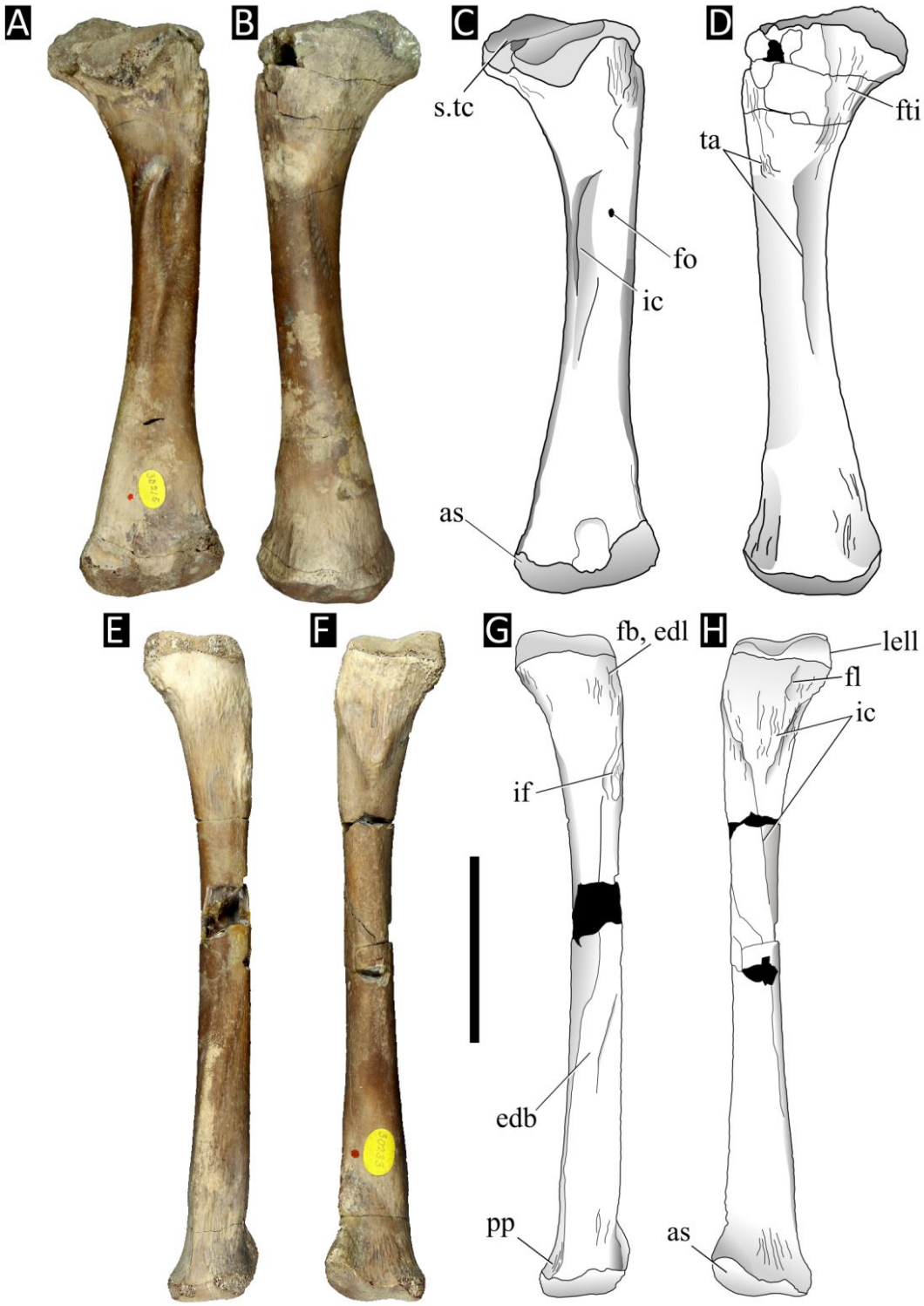



Figure 2.27: The tibia and fibula of *Diplocynodon hantoniensis*. **A**–**D**, right tibia (NHMUK 30215) in posterior (**A**, **C**), and anterior (**B**, **D**) views. **E**–**H**, right fibula (NHMUK 30233) in lateral (**E**, **G**), and medial (**F**, **H**) views. Abbreviations: **as**, astragalar articular surface; **edb**, *M. extensor digitorum brevis*; **edl**, *M. extensor digitorum longus*; **fb**, *M. fibularis brevis*; **fl**, *M. fibularis longus*; **fo**, foramen; **fti**, *M. flexor tibialis internus*; **ic**, *M. interosseous cruris*; **if**, *M. iliofibularis*; **lell**, long external lateral ligament; **pp**, *M. pronator profundus*; **s.tc**, surface for the tibial condyle of the femur; **ta**, *M. tibialis anterior*. Scale bar = 5 cm.

*D. hantoniensis* recognised in this study can be identified in the Swiss material. Furthermore, large occlusal pits for the dentary teeth are not unique to *D. hantoniensis*: they occur in all other alligatoroids and crocodyloids. Carinae on the anterior and posterior edges of teeth are equally undiagnostic, being present in essentially all non-longirostrine crocodylians. Additionally, two potential differences are recognised: the rim of the premaxilla is very sharp in the Swiss material, unlike *D. hantoniensis*, and the size of the external naris in proportion to the surface area of the premaxilla is larger than that of *D. hantoniensis*. Given that none of the diagnostic features of *Diplocynodon* (Martin et al., 2014) can be identified in the Swiss material, I regard it as Alligatoroidea indet.

### 2.4.3 Early Oligocene of Germany

Gramann (1958), and later Karl and Müller (2008), described crocodylian remains from the early Oligocene 'Melanian clay' (=Melanienton), which crops out around the Altenburg IV quarry at Borken, in Hesse, central Germany. Gramann (1958) noted the presence of an anterior dentary fragment (lacking the splenial), a lacrimal, fragments of a left and right angular, teeth, portions of two femora, and numerous osteodermal and vertebral fragments, which he referred to *D. hantoniensis*. No specimen numbers were assigned to the material; however, they are reposited in the Institute for Geology and Paleontology at the University of Marburg, Germany. Additional osteoderms were later referred to *D.* cf. *hantoniensis* by Karl and Müller (2008) (PMLU HS 389-A10.02.05). Of the figured and described material, only the dentary is taxonomically informative. Three character states can be determined: (1) confluence of the $3^{rd}$ and $4^{th}$ dentary alveoli; (2) a gently curved dentary between alveoli 4 and 10; and (3) dentary symphysis extending to the $3^{rd}$/$4^{th}$ dentary alveolus. One further character, the position of the anterior splenial tip relative to the Meckelian groove, is indiscernible from figures in Gramann (1958). Confluence of the $3^{rd}$ and $4^{th}$ alveoli, and the gently curved dentary, are features that are common to all *Diplocynodon* species. The presence of a short dentary symphysis can restrict the referral to one of four species, as it is only present in *D. ratelii*, *D. hantoniensis*, *D. muelleri* and *D. remensis*; however, in *D. remensis* the splenial participates in the symphysis, unlike any other *Diplocynodon* species (Martin et al., 2014). If the rostral tip of the splenial was preserved in the German specimen, this would allow us to distinguish between *D. muelleri* (where it passes dorsal to the Meckelian groove) and *D. hantoniensis* and *D. ratelii* (in which it passes ventral to the groove). No further diagnostic characters can be retrieved from the dentary, and other remains are non-diagnostic; therefore, this German occurrence is assigned to *Diplocynodon* sp.

### 2.4.4 Early Oligocene of France

A relatively complete skull of an adult crocodylian was referred to *Diplocynodon* cf. *hantoniensis* by Vignaud et al. (1996) from early Oligocene sediments in the Razac-d'Eymet commune in Dordogne, south-

western France. The specimen is unnumbered but described as part of the 'Guevel collection', which may be housed in the University of Poitiers, France. The proportions of the skull match *D. hantoniensis*, in particular the relatively wide rostrum and lack of a prominent constriction at the premaxillary-maxillary suture. Unfortunately, the figures are not detailed enough to comment on the sutural relationships of the skull. However, there are important differences based on the description, which suggest the material might not be referable to *D. hantoniensis*. Vignaud et al. (1996, fig. 1b) described and figured a narrow ectopterygoid which runs beside the border of the maxillary alveoli, as in *D. ratelii*. This condition contrasts with *D. hantoniensis*, which has a unique condition of the ectopterygoid (see Section 2.3.1). The presence of other diagnostic features of *D. hantoniensis* cannot be discerned from either the description or figures, such as the presence of ectopterygoid-pterygoid flexure, or a sulcus posterolateral to the external naris. In summary, until further descriptions of this specimen are made, it can only be referred to *Diplocynodon* sp.

## 2.5 Discussion

### 2.5.1 Comparisons of *D. hantoniensis* with other crocodylian species

#### Skull proportions

*Diplocynodon hantoniensis* has a particularly broad rostrum, which among the known species of *Diplocynodon* is closest in shape to *D. darwini* (Fig. 2.28C), *D. deponiae* (Fig. 2.28D), *D. elavericus*, and *D. muelleri*. By contrast, *D. ratelii* (Fig. 2.28E), *D. ungeri*, and *D. tormis* have notably narrower, more pointed rostra. Furthermore, those taxa with a narrow rostrum appear to have a very modest canthus, which is absent in *D. hantoniensis*.

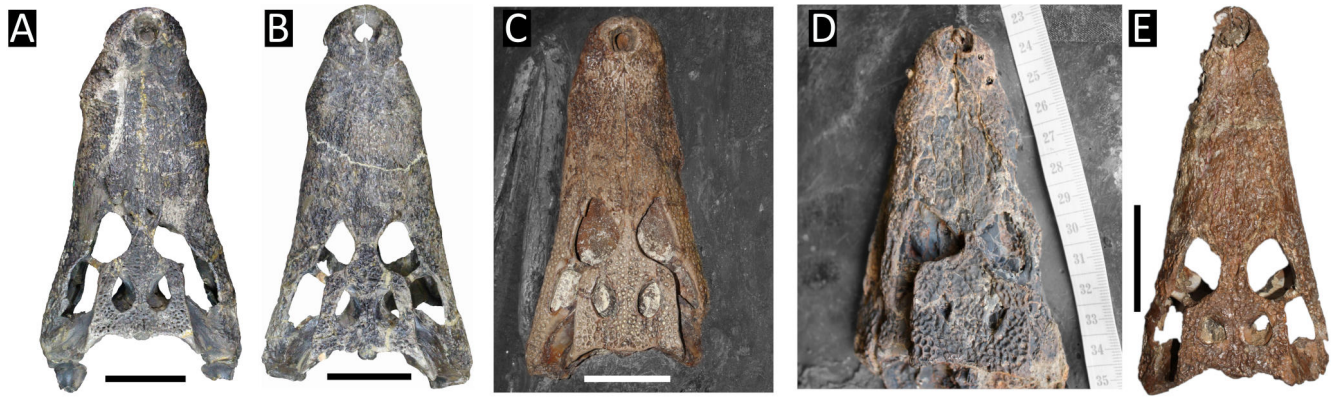



Figure 2.28: Comparison of skull proportions in selected *Diplocynodon* species. **A**–**B**, *Diplocynodon hantoniensis*: NHMUK OR 30393 (**A**) and NHMUK OR 30392 (**B**); **C**, *Diplocynodon darwini* (HLMD Me 7492); **D**, *Diplocynodon deponiae* (SMF Me 2609); and **E**, *Diplocynodon ratelii* (MNHN SG 539). Scale bars A–C, E = 10 cm, D = cm.

### Ornamentation

A small step immediately anterior to the orbits, and crossing the frontals is newly recognised in *D. hantoniensis* (Fig. 2.29A, C), as well as *D. ratelii* (e.g. MNHN SG 539), *D. tormis* (Buscalioni et al., 1992, fig. 2), and *D. muelleri* (Piras & Buscalioni, 2006, figs 2, 3a), but absent in *D. darwini* (e.g. HLMD Me 7500). The holotype of *D. deponiae* does not preserve the dorsal surface of the rostrum, and the best-preserved referred specimens are broken along the frontal (e.g. SMF Me 2609, IRSNB R 261). A juvenile specimen (HLMD-Be-147) apparently lacks a step, and so it is inferred to be absent in adult *D. deponiae* too. A step is also present in *D. remensis*; however, it is much more prominent in this taxon (Martin et al., 2014).

The step in several *Diplocynodon* species appears to be homologous to the spectacle that is characteristic of many extant caimanines (Fig. 2.29B, D), and also some non-crocodylian eusuchians, e.g. *Allodaposuchus precedens* (Delfino et al., 2008a). Whereas the presence or absence of a step has been discretised in some previous studies (Barrios, 2011; Cidade et al., 2017; Lee & Yates, 2018), variation in its size and position have not been considered. Here it is found that many species of *Diplocynodon* exhibit a low spectacle (Fig. 2.29A), contrasting with the tall spectacle of most extant caimanines (Fig. 2.29B). Furthermore, the step is positioned further posteriorly than all extant caimanines (Fig. 2.29B, D), and similar to some other extinct alligatoroids, such as *Purussaurus neivensis* (UCMP 39704) and *Bottosaurus harlani* (Cossette & Brochu, 2018, fig. 12).

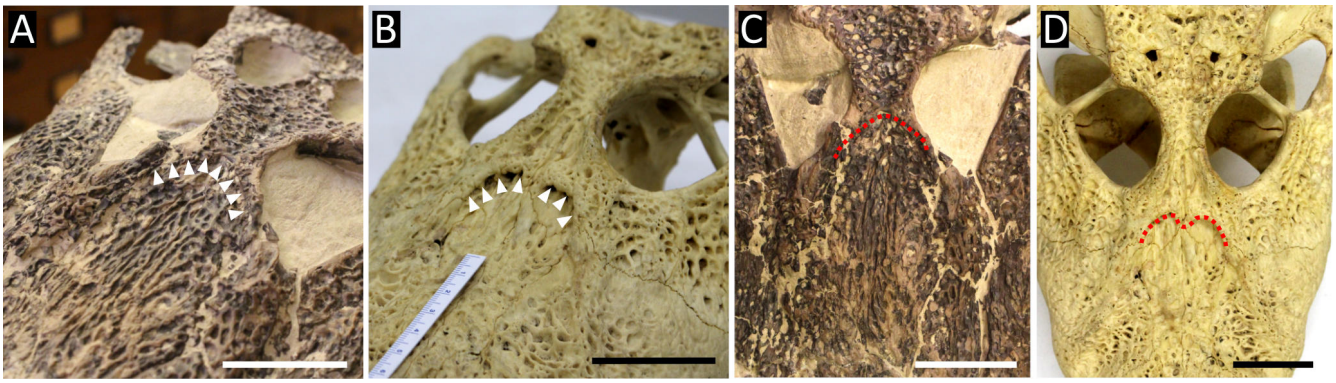



Figure 2.29: Comparison of the morphology of the preorbital step (spectacle) in *Diplocynodon hantoniensis* (CAMSM TN 907) (**A**, **C**) and *Caiman latirostris* (NHMUK 86.10.4.2) (**B**, **D**). All scale bars = 5 cm.

### External naris

The outline of the naris is quite square in *D. hantoniensis* (Fig. 2.30A), with straight, anteriorly diverging lateral margins. This is quite similar to *D. darwini* (Fig. 2.30B) but contrasts with the strongly rounded narial margins seen in *D. ratelii* (Fig. 2.30C), *D. ungeri* (Martin & Gross, 2011, fig. 4), *D. tormis* (Buscalioni et al., 1992, fig. 2) and *D. deponiae* (SMF Me 2609). The presence of a deep notch situated

lateral and slightly posterior to the external nares has typically been considered characteristic of *Alligator* (e.g. Brochu, 1999) (Fig. 2.30D), but a similarly deep notch is observed in *D. hantoniensis* (Fig. 2.30A), *D. muelleri* (Piras & Buscalioni, 2006), *D. tormis* (Buscalioni et al., 1992), and *D. ratelii* (MNHN SG 539). *Diplocynodon hantoniensis* is newly recognised as having an anterodorsally facing naris (Fig. 2.30E). This similarly occurs in *D. deponiae* (SMF Me 2609); but, it faces dorsally in all other species of *Diplocynodon* (e.g. Fig. 2.30B). An anterodorsally facing naris appears to be the plesiomorphic condition in Crocodylia, as it occurs in non-crocodylian eusuchians such as *Allodaposuchus precedens*. They similarly occur in *Borealosuchus*, the 'basal' alligatoroid *Leidyosuchus canadensis* (Wu et al., 2001a), and 'basal' alligatorines, such as *Navajosuchus* (Brochu, 2004b).

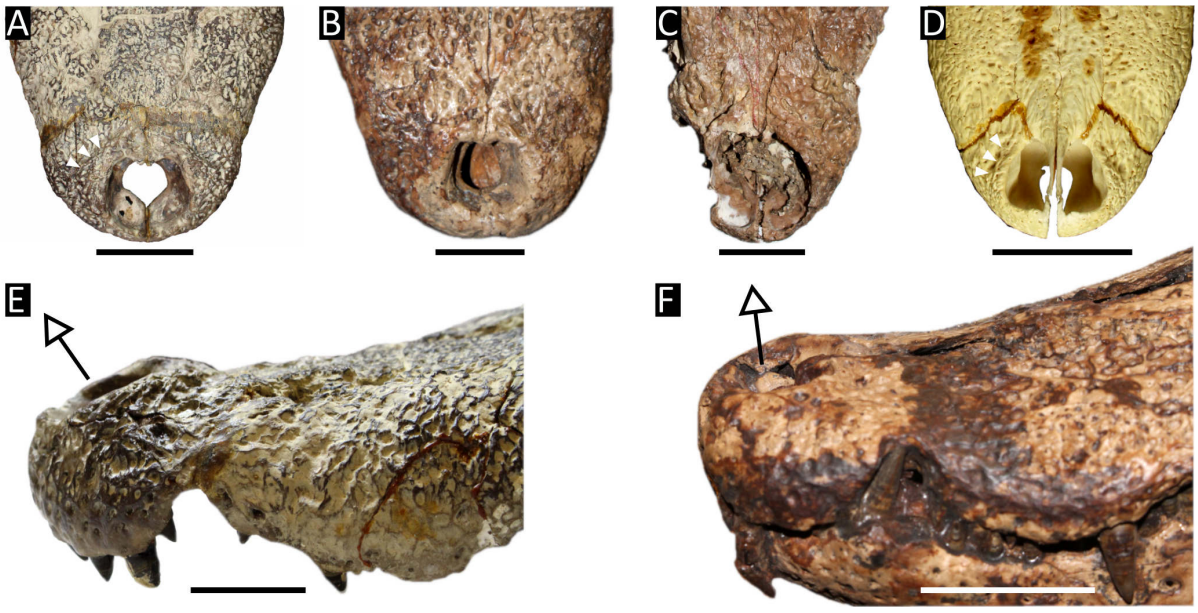



Figure 2.30: Comparison of narial morphology between *Diplocynodon hantoniensis* and selected crocodylians. **A**, **E**, *Diplocynodon hantoniensis* (NHMUK OR 25166); **B**, *Diplocynodon darwini* (HLMD Me 7492); **C**, *Diplocynodon ratelii* (MNHN SG 539); **D**, *Alligator mississippiensis* (AMNH 71621); and **F**, *Diplocynodon darwini* (HLMD Me 7500). White filled arrows indicate position of narial notch. Unfilled arrows indicate direction of naris. All scale bars = 5 cm.

### Supratemporal fenestrae

In all extant alligatorids, the squamosal and parietal have a large sutural contact on the posterior wall of the supratemporal fenestra, anterior to the orbitotemporal canal (Brochu, 1997a) (Fig. 2.31A). By contrast, extant *Crocodylus*, *Tomistoma*, and *Gavialis* express an alternative condition, in which the quadrate widely separates the squamosal and parietal, forming the floor of the orbitotemporal foramen (Fig. 2.31B). *D. ratelii* possesses an intermediate condition, in which the squamosal approaches the parietal, but a narrow wedge of the quadrate separates them (Brochu, 1997a) (Fig. 2.31C). Previously, the condition was considered unknown in *D. hantoniensis* (Brochu et al., 2012; Martin et al., 2014).

However, close inspection of the walls of the supratemporal fenestra in NHMUK 30393 reveals that the intermediate condition is also present in this taxon (Fig. 2.31D). This condition is now recorded in almost all *Diplocynodon* species, except *D. ungeri*, in which it is unknown (Martin & Gross, 2011), and *D. elavericus* (Martin, 2010a), which seems to express the derived alligatorid condition. However, in the latter species, the supratemporal fenestra is poorly preserved. Other than *Diplocynodon*, this condition is known only in *Brachychampsa montana* (Norell et al., 1994).

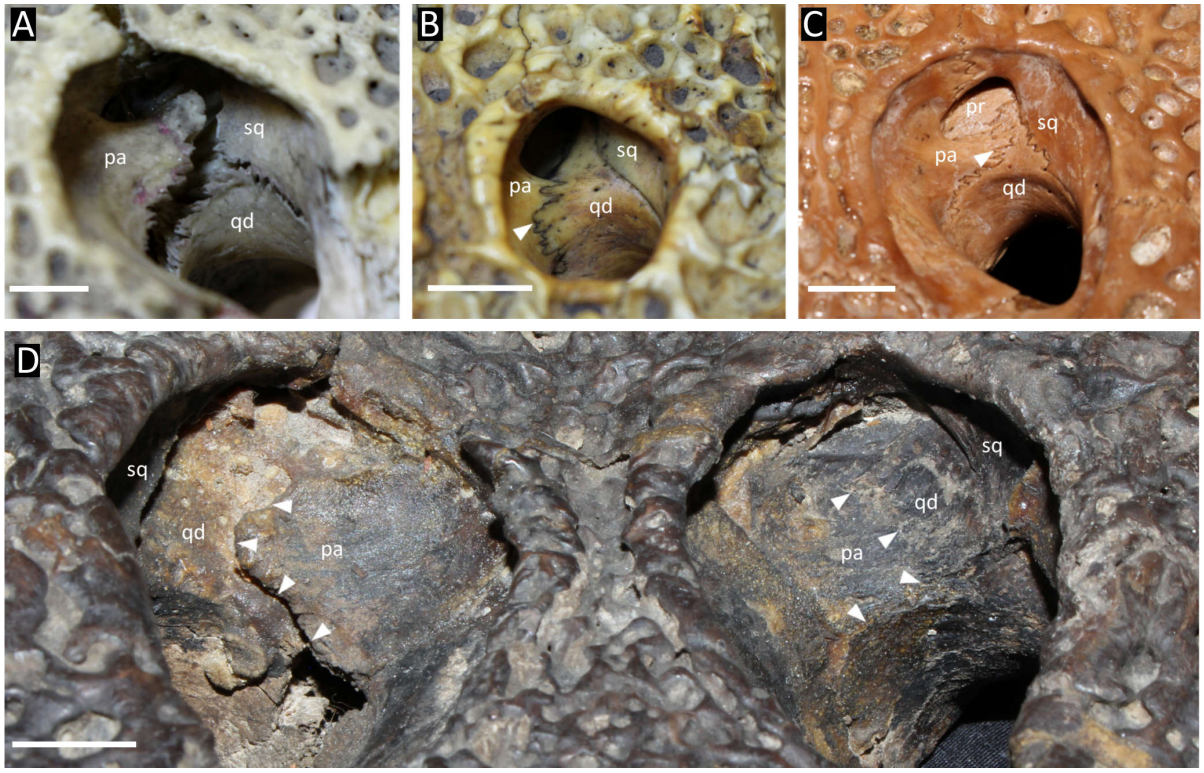



Figure 2.31: Comparison of the sutural relationships in the orbitotemporal canal in *Diplocynodon* and selected crocodylians. **A**, *Alligator mississippiensis* (NHMUK uncatalogued); **B**, *Crocodylus porosus* (NHMUK uncatalogued); **C**, *Diplocynodon ratelii* (MNHN SG 539); and **D**, *Diplocynodon hantoniensis* (NHMUK OR 30393). All scale bars = 1 cm.

### Palate

Flexure of the ectopterygoid-pterygoid suture is retained into adulthood in *D. hantoniensis* (Fig. 2.8A). This feature was previously regarded as an unambiguous synapomorphy of crown caimans (Brochu, 1999) (Fig. 2.8B). However, it appears to occur more widely, as it is present in the stem crocodylian *Allodaposuchus precedens* (Martin et al., 2016a), the "gavialoid" *Thoracosaurus isorhynchus* (Brochu, 1999, character scores therein), and possibly in *D. deponiae* (Delfino & Smith, 2012). In the latter case, Delfino and Smith (2012) expressed some doubt that IRScNB 261, which formed the basis of their description, was a mature individual of *D. deponiae*. As a result, it is not certain whether ectopterygoid-

pteryoid flexure is retained into adulthood in *D. deponiae*. All other species of *Diplocynodon* lack the ectopterygoid-pterygoid flexure.

### Choanae

The choanae of *D. hantoniensis* are heart shaped, resulting from a posterior projection of the pterygoid, which aligns with the recessed choanal septum (Fig. 2.32A). Furthermore, they are ornamented with an anterolaterally directed ridge on each side, which is newly recognised in this taxon here. This ridge is even developed in juvenile specimens, becoming a prominent ventrally directed lamina bound by a sulcus at maturity (e.g. CAMSM TN 917). Heart shaped choanae with anterolaterally developed ridges are also present in *D. remensis* (Martin et al., 2014, fig. 6K), *D. deponiae* (Fig. 2.32B), *D. darwini* (Fig. 2.32C), and tentatively in *D. ratelii* (Fig. 2.32D). The lateral walls of the choanae are broken off in specimens of the latter taxon studied here, but deep sulci similar to *D. hantoniensis* are suggestive of a similar ridge. Wu et al. (2001a) also described ridges lateral to the choana in *Leidyosuchus canadensis*, although restricted to some of the largest individuals. This contrasts with the condition in *D. hantoniensis*, in which they appear throughout ontogeny. The choanal ridges in *Diplocynodon* appear homologous to those of several caimanines, although the morphology is clearly different. In extant *Caiman* (Fig. 2.32E), these ridges are shorter, restricted to the posterolateral choanal margins, and commonly folded medially into the choana. The ridges are also probably homologous to those developed in *Alligator* (Fig. 2.32F), but in that taxon they form a near continuous posterior wall to the choana and do not extend very far anteriorly.

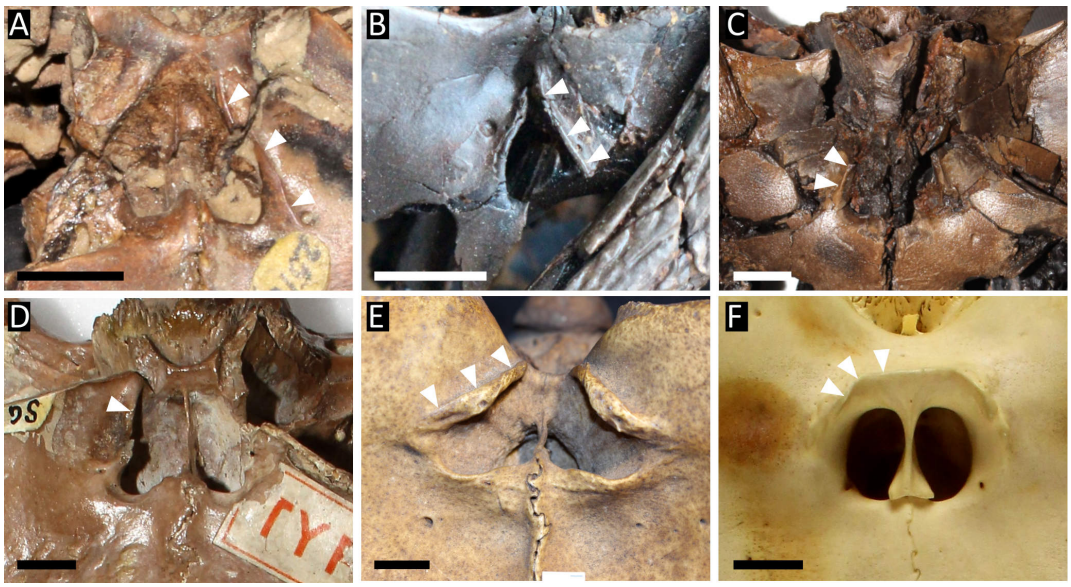



Figure 2.32: Comparison of morphology of the choanae in *Diplocynodon*. **A**, *Diplocynodon hantoniensis* (NHMUK OR 25167); **B**, *Diplocynodon deponiae* (IRScNB R 261); **C**, *Diplocynodon darwini* (HLMD Me 17680a); **D**, *Diplocynodon ratelii* (MNHN SG 539); **E**, *Caiman latirostris* (MACN-PV 1420); and **F**, *Alligator mississippiensis* (AMNH 71621). All scale bars = 5 mm.

**Posterolateral margin of the angular**

In *Diplocynodon hantoniensis*, the unornamented posterolateral surface of the angular is not visible in lateral view (Fig. 2.33A), similar to *Caiman* (Fig. 2.33A). This contrasts with the condition in *Alligator* and *Crocodylus*, in which there is a broad lateral exposure of the unornamented angular surface (Fig. 2.33C). This is absent in *D. remensis* (Martin et al., 2014) and *D. darwini* (HLMD Me 7500), but present in *D. ratelii*. The condition is unknown in all other *Diplocynodon* species.




Figure 2.33: Comparison of the posterior ramus of the mandible in lateral view in **A**, *Diplocynodon hantoniensis* CAMSM TN 904; **B**, *Caiman latirostris* MACN V 1420; and **C**, *Crocodylus siamensis* NHMUK 1921.4.1.168. Black arrow indicates the boundary between the ornamented and unornamented surface. Scale bar = 5 cm.

**Humerus**

Only three humeral characters appear regularly in phylogenetic analyses of Crocodylia. These pertain to the shape of the deltopectoral crest, the presence of a common insertion, or separate insertions for *M. teres major* and *M. dorsalis scapulae*, and the slenderness and relative lengths of the forelimb and hindlimb (Brochu et al., 2012, C27, C28, and C36) (see Chapter 3). However, biomechanichal studies of crocodylians have outlined humeral variation that might be suitable for discretisation, and which can be observed in *Diplocynodon hantoniensis* (Stein et al., 2012). Stein et al. (2012) recognised differences in the degree of rotation of the proximal humeral epiphysis relative to the distal epiphysis between several crocodyloid taxa (*Kambara*, *Crocodylus porosus*, and *Crocodylus johnstoni*. This axial rotation of the proximal epiphysis results in movement of the apex of the deltopectoral crest from the lateral edge, to the centre of the humerus, when viewed ventrally (Fig. 2.34). In lateral view, this rotation results in greater exposure of the ventral surface of the proximal epiphysis (Fig. 2.34). Broad differences can be recognised in crocodylian taxa. For example, whereas the degree of axial rotation is high in *Gavialis* (Fig. 2.34F), it is low in alligatoroids such as *Diplocynodon hantoniensis* (Fig. 32B) and *Alligator* (Fig. 2.34A), as well as the stem-brevirostrine *Borealosuchus sternbergii* (Fig. 2.34D) and the crocodyloid *Asiatosuchus germanicus* (Fig. 2.34C).




Figure 2.34: Comparison of humeral morphology illustrating variation in axial rotation of the proximal epiphysis in crocodylian taxa. All left humeri in lateral (left) and ventral (right) views. Arrows indicate position of apex of deltopectoral crest. **A**, *Alligator mississippiensis* (AMNH 72621); **B**, *Diplocynodon hantoniensis* (NHMUK OR 30206); **C**, *Asiatosuchus depressifrons* (SMF Me 1801); **D**, *Borealosuchus sternbergii* (USNM 6533); **E**, *Crocodylus porosus* (QM J48127); and **F**, *Gavialis gangeticus* (USNM 576261). All scale bars = 2 cm.

## 2.6 Summary

The basal alligatoroid *Diplocynodon hantoniensis* from the late Eocene of southern England, is fully described for the first time in 150 years. This includes a detailed description of the often-neglected postcranial skeleton, including a reconstruction of numerous muscle attachment sites, allowing future comparisons with other crocodylians. After the evaluation of several referrals, *Diplocynodon hantoniensis* is currently restricted to the late Eocene of the UK. Based on this reappraisal, numerous previously unrecognised features are identified in *Diplocynodon hantoniensis* and other *Diplocynodon* species, which will be incorporated into a phylogenetic dataset (see Chapter 4). These include the presence of a posterolateral narial notch, an anterodorsally facing naris, preorbital ridges, and ectopterygoid-pterygoid flexure that is retained until maturity. Additionally, through comparisons with other crocodylian taxa, several anatomical features are recognised that can form the basis of new morphological characters. This includes (1) variation in the height and position of a preorbital step; (2) variation in ornamentation surrounding the choanae; and (3) variation in the posterolateral surface of the angular. Furthermore, based on a comparison of the humeri of several crocodylians, the basis for a new character is outlined: axial rotation of the proximal humeral epiphysis. These new observations are discussed further in Chapter 3, in which they are compared with a broader sample of crocodylians, and delimited as morphological characters. Future reappraisals should target other stemward alligatoroid taxa, including the extensive and exceptionally preserved material that is referred to *Diplocynodon darwini*, which has not been revisited in some 30 years (e.g. Frey et al., 1987).

# Chapter 3

# A New Morphological Character List for Crocodylia

## 3.1 Introduction

In this chapter I explain the approach to character construction, then systematically outline and discuss a new illustrated morphological character list for Crocodylia. This character list is based on a comprehensive synthesis of existing character lists, a literature review, and personal observations of a global sample of crocodylians (Appendix B), including new data from the reappraisal of *Diplocynodon hantoniensis* in Chapter 2.

## 3.2 Methods

### 3.2.1 Character list construction

An initial character list was constructed by assimilating all existing morphological characters from previously published studies of crocodylian systematics. The largest single source of characters was the dataset of Brochu (1997b), which contains a substantial number of novel characters, as well as characters modified from earlier studies (Benton & Clark, 1988; Norell, 1988; Norell & Clark, 1990; Clark, 1994). Significant contributions of new characters were later introduced by Hua and Jouve (2004), Jouve et al. (2015), Salas-Gismondi et al. (2015), Salas-Gismondi et al. (2016), Salas-Gismondi et al. (2019), Lee and Yates (2018), and Iijima and Kobayashi (2019). A large number of additional studies also introduced crocodylian characters in fewer numbers; the origin of these and all other characters is described in detail in the character list.

All characters were sorted anatomically and checked for redundancy. When overlapping characters were found, the original contribution was retained and accepted modifications were cited. All attempts were made to understand existing characters. This includes scoring characters alongside specimens in museum collections, and checking which taxa were scored for particular character states in a large sample of published character taxon matrices (Brochu, 1999; Buscalioni et al., 2001; Salisbury et al., 2006; Brochu, 2007a; Ősi et al., 2007; Brochu, 2011; Brochu et al., 2012; Brochu & Storrs, 2012; Salas-Gismondi et al., 2016; Cidade et al., 2017; Cossette & Brochu, 2018; Lee & Yates, 2018; Iijima & Kobayashi, 2019; Salas-Gismondi et al., 2019; Souza-Filho et al., 2019). Similar to Sookias (2020), these methods provided a means of assessing the "robustness" of characters. Where inconsistencies emerged between character formulations and personal observations of specimens, characters were modified by the addition, removal, and/or modification of character states, as well as the introduction of new characters when necessary. All such changes are described in detail in the character list.

In total, 162 characters from previous studies of crocodylian systematics were omitted from the dataset for one of several reasons: (1) they were autapomorphies, and therefore phylogenetically uninfor-

mative; (2) they were accidental duplicates, being redundant with another morphological character; (3) the morphological variation that was described was ambiguous, and/or not visible in specimens studied first hand; (4) the character varied intraspecifically in most or all taxa studied. All discarded characters, their origin, and reason for removal, are listed in Appendix C.

### 3.2.2 Character construction

All new characters and modifications to existing characters were constructed following the protocols of Sereno (2007) and Brazeau (2011) and as recently used for crocodyliforms by Tennant et al. (2016) and Groh et al. (2020). The most important aspects of character construction are detailed below:

1. Multistate characters that combine an 'absent' state plus two or more 'present but variable' states were reductively coded into two or more characters.

   Example – Brochu (1997b) character 152: Internal choana not septate (0) or with septum that remains recessed within choana (1) or with septum that projects out of choana (2).

   This character was reductively coded into two characters:

   (a) (C193) Choanae, septum: present (0); absent (1).

   (b) (C194) Choanae, external projection of the septum: absent, septum remains recessed within choanae (0); present, septum approaches external margin of choanae (1).

   Reductively coding characters such as this has the benefit of capturing the grouping information in the presence or absence of a feature (Brazeau, 2011). The disadvantage is that parsimony algorithms treat inapplicable data in the same way as missing data. As such, the parsimony algorithm will optimise character (b) in taxa that lack a choanal septum, influencing the parsimony scores of trees and possibly leading to spurious groupings of taxa (Maddison, 1993; Brazeau, 2011). The latter can be alleviated if zero-length branches are set to collapse (as is the default in TNT). Furthermore, in Chapter 4, the phylogenetic results are explored in detail, including the optimisation of several reductively coded characters, allowing the assessment of characters supporting particular nodes.

2. Compound characters, which describe variation in two or more non-homologous morphological features, were separated into two or more characters.

   Example – Jouve et al. (2015), character 43: Splenial participates in mandibular symphysis and splenial symphysis adjacent to no more than one dentary alveolus (0); splenial excluded from mandibular symphysis and anterior tip of splenial passes ventral to Meckelian groove (1); splenial excluded from mandibular symphysis and anterior tip of splenial passes dorsal to Meckelian groove

(2); participates in the mandibular symphysis over the length of two to five teeth (3); deep splenial symphysis, participates in the mandibular symphysis over the length of five to seven teeth, and forms wide "V" within symphysis (4); or deep splenial symphysis participates in the mandibular symphysis over the length of five to seven teeth, and splenial constricted within symphysis and forms narrow "V" (5); or deep splenial symphysis, longer than seven dentary alveoli (6).

This character is split into four separate morphological characters: (i) one that describes the presence or absence of contact of the splenial in the dentary symphysis (C222); (ii) one that describes the position of the anterior splenial tip relative to the Meckelian groove (C223); (iii) one that describes the length of participation of the splenial in the symphysis (C224); and (iv) one that describes the shape of the splenial within the symphysis as either wide or narrow (C225).

### Continuous characters

This dataset implements continuous characters. The measurements for continuous characters were taken first-hand where possible using digital callipers, but also from published tables of measurements, and based on figures of specimens that lacked deformation and were appropriately orientated. For example, the ratio of snout length to skull length (Character 1) can be measured from a skull figured in dorsal view. Multiple measurements where made where possible and based only on adult specimens to ameliorate the influence of intraspecific variation. Ratios of measurements were calculated in Microsoft Excel, and converted into ranges of values where multiple measurements could be taken. These values can be found in Supplementary file 1.

### Character rediscretisation

Rediscretised versions of continuous characters are also outlined in the character list. The threshold values used to delimit the rediscretised character states were based on the original character description, to allow comparisons between this and earlier studies. If no threshold was given, or if the character was new, the state boundaries were determined by plotting the continuous character values from smallest to highest and seeking clear discontinuities in the data (Appendix D.1–D.2). Histograms for all continuous characters were also plotted to identify distribution patterns that might guide the delimitation of the continuous data (Appendix D.3–D.4), using the Shapiro-Wilk test to statistically assess the presence of normally distributed values (calculated in R version 3.5.1 [R Core Team, 2018]). For example, if the continuous values were found to contain multiple modes (e.g. they were biomodal), then these modes might serve as the thresholds for delimiting character states. Difficulty arises when no discontinuity exists in the data. In such cases, the boundary was drawn first using the measured value in the outgroup as a delimiter, and if not possible, using an anatomically 'sensible' and phylogenetically informative value (e.g. C26).

## 3.3 Continuous characters

### 3.3.1 Skull

1. Snout length in dorsal view, ratio of anteroposterior snout length (measured from level of anterior orbital margin, to anteriormost point of rostrum), to total skull length (measured from posteriormost level of quadrate condyle to anteriormost point of rostrum): $\leq 0.5$ (0); $> 0.5$ (1) (after Wu & Sues, 1996 [4]; Groh et al., 2020 [16]).

   Crocodylian taxa with the most elongated snouts are predominantly "gavialoids", e.g. *Gryposuchus neogaeus* (0.79) (MLP 26-413) and "tomistomines", e.g. *Toyotamaphimeia* (0.71) (Kobayashi et al., 2006), but also the giant caimanine *Mourasuchus amazonensis* (0.75) (Price, 1964). On the other end of the spectrum, the shortest snout lengths are observed in alligatorines, such as *Hassiacosuchus haupti* (0.42) (HLMD Be 137) and *Arambourgia gaudryi* (0.38) (MNHN QU 17155). This character differs to that of Groh et al. (2020) only in the measurement of snout length, which is measured in a straight anteroposterior line rather than diagonally from the anterior orbit corner (Fig. 3.1A). The rediscretised state boundary follows Groh et al. (2020), but snout length is normally distributed (Shapiro-Wilk test $= 0.98$, $p = 0.14$), with no discrete discontinuity in the data (Appendix D.1).

2. Skull proportions, ratio of mediolateral rostrum width at the level of the anterior orbital margin, to mediolateral width across anterior margin of the cranial table: $< 3$ (0); $\geq 3$ (1) (new character, after Jouve, 2004 [170]; Jouve et al., 2008 [170]).

   This character captures the differences in mediolateral width of the cranial table in crocodylians (Fig. 3.1B). At one extreme, some alligatoroids (e.g. *Mourasuchus*) have narrow cranial tables in proportion to their rostral widths. By contrast, several (mostly "gavialoid") crocodylians exhibit a cranial table that is almost equal to the antorbital rostral width. Measured values have a skewed distribution (Shapiro-Wilk test = 0.94, $p < 0.001$). The discrete character boundaries are based on the marked discontinuity between two species of *Mourasuchus* and all other taxa in the dataset (Appendix D.1).

3. External naris, mediolateral width to anteroposterior length ratio: $\leq 1$ (0); $> 1$ (1) (after Brochu, 1997b [161]; Groh et al., 2020 [4]).

   Brochu (1997b [161]) originally delimited the morphology for the external naris as either being "*circular or keyhole-shaped (0) or wider than long (1)*". A keyhole-shaped naris could not be identified in any taxon in this dataset, and therefore this character was simply quantified following Groh et al. (2020) (Fig. 3.1C). The rediscretised thresholds follow earlier studies (Brochu, 1997b; Groh et al., 2020). Measured values are positively skewed (Shapiro-Wilk test = 0.93, $p < 0.001$) and aside from

the morphology in *Mourasuchus amazonensis* (Price, 1964, fig.1), which is the outlier in this dataset (naris width to length >2) (Appendix D.1), there is no other obvious discontinuity in the data.

4. External nares, anterior margin thickness, ratio of distance between anterior margin of nares and anterior margin of rostrum to maximum anteroposterior length of external nares in dorsal view: $< 0.5$ (0); $\geq 0.5$ (1) (after Hastings et al., 2010, [2]; Groh et al., 2020 [3]).

   Variation in thickness of the anterior margin of the external naris (Fig. 3.1D) is rarely considered in studies of crocodylian phylogeny, yet it exhibits considerable variation between taxa (Appendix D.1) (Groh et al., 2020). The anterior wall of the naris is thickest in a series of longirostrine crocodylians, e.g. *Argochampsa krebsi* (Hua & Jouve, 2004, fig.2) and *Tomistoma schlegelii* (NHMUK 1894.2.21.1). By contrast, the anterior wall is exceptionally thin in several alligatoroids, e.g. *Brachychampsa montana* (UCMP 133901) and *Stangerochampsa mccabei* (Wu et al., 1996, fig.A1). The rediscretised state boundary (0.5) follows Hastings et al. (2010) and Groh et al. (2020), but measured values appear to vary continuously with a positive skew (Shapiro-Wilk test = 0.95, $p < 0.05$).

5. Rostral depth, ratio of maximum dorsoventral height of the maxilla to mediolateral width of the maxilla at the $5^{th}$ maxillary alveolus: <0.5 (0); $\geq 0.5$ (1) (new character, after Wu et al., 1997 [3]; Groh et al., 2020 [8]).

   Rostral depth is measured similarly to that Groh et al. (2020), except that the measurement of depth is made at the tallest point of the rostrum, rather than at the premaxilla-maxilla suture (Fig. 3.1E). One might expect an altirostral crocodylian, such as *Baru wickeni* (QM F16822), to exhibit the highest value for this character; however, since snout width is taken into consideration, higher values of rostral depth correspond with the mediolaterally narrow, tubular snouts of most longirostrine crocodylians, e.g. *Tomistoma schlegelii* (rostral depth = 0.64) and *Gavialis gangeticus* (rostral depth = 0.58). Shallow rostra are exhibited primarily in some alligatoroids, e.g. *Brachychampsa montana* (UCMP 133901, rostral depth = 0.16). A small discontinuity occurs at a cut-off value of 0.5, which was adapted from Wu et al. (1997) (Appendix D.1); however, the data are normally distributed (Shapiro-Wilk test = 0.98, $p = 0.50$), with several small discontinuities that might be considered character state boundaries.

6. Interorbital distance, ratio of minimum mediolateral width between orbits to maximum mediolateral width across anterior cranial table: $< 0.5$ (0); $\geq 0.5$ (1) (after Jouve, 2004 [181]; Jouve et al., 2008 [177]; Salas-Gismondi et al., 2015 [190]; Groh et al., 2020 [26]).

   Characters describing variation in interorbital width have been implemented in several earlier studies, but using different points of comparison, e.g. interorbital width in relation to orbital width (Salas-Gismondi et al., 2015) or minimum rostrum width (Jouve et al., 2008). Comparisons here are made

relative to cranial table width, similar to that of Groh et al. (2020) (Fig. 3.1F). Some of the largest interorbital distances were measured in extant *Crocodylus* species, e.g. *C. acutus* (interorbital distance = 0.53), *C. moreletti* (0.52), and *C. niloticus* (0.50). By contrast, the interorbital distance is extremely narrow in taxa such as *Bernissartia fagesii* (0.17) (IRScNB 1538) and *Borealosuchus formidabilis* (0.20) (Erickson, 1976, fig.4). There is no existing cut-off value, so this is set at 0.5, where a modest discontinuity can be seen (Appendix D.1). Otherwise the data appear entirely continuous, although it is not normally distributed (Shapiro-Wilk test = 0.96, $p < 0.05$).

7. Infratemporal fenestra size, ratio of maximum anteroposterior infratemporal fenestra length, to maximum anteroposterior length of the cranial table: $< 0.8$ (0); $\geq 0.8$ (1) (adapted from Ortega et al., 2000 [74]; Groh et al., 2020 [33]).

   Earlier studies characterised the morphology of the infratemporal fenestra using the ratio of its anteroposterior length to dorsoventral height (Ortega et al., 2000; Groh et al., 2020). A similar character is adapted here, but characterises the maximum anteroposterior length of the infratemporal fenestra relative to the cranial table length instead (Fig. 3.1G). This is based on the observation that several caimanines, e.g. *Mourasuchus* and *Purussaurus*, have extremely enlarged infratemporal fenestrae. Indeed, there is a marked discontinuity between the size of the fenestra in these taxa (infratemporal fenestra size $> 0.8$) and all other taxa in the dataset (Appendix D.1). These few taxa impart a positive skew in the data (Shapiro-Wilk test = 0.91, $p < 0.001$).

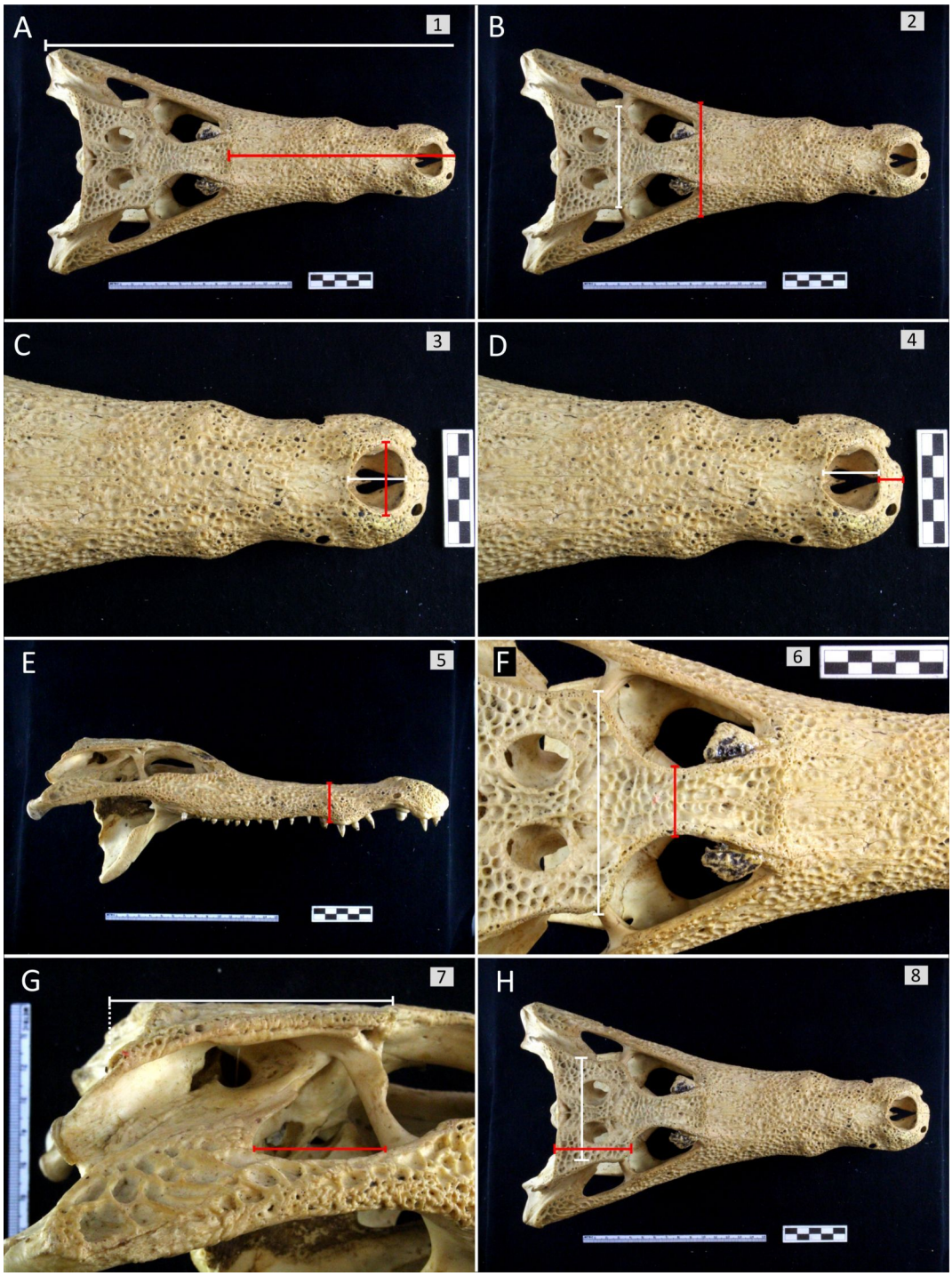



Figure 3.1: Continuous characters 1–8. All characters illustrated using *Caiman crocodilus apaporiensis* (FMNH 69812). Scale bars = cm.

8. Cranial table shape, ratio of maximum anteroposterior cranial table length (measured from the level of the frontal-postorbital suture), to maximum mediolateral width (measured at the level of the anterior table corner): $< 1$ (0); $\geq 1$ (1) (after Wu et al., 2001b [131]; Groh et al., 2020 [41]).

   Cranial table shape was characterised similarly to that of Groh et al. (2020), except that its length is measured as the ratio of the distance between the anteriormost extent of the frontal-postorbital suture, to the posterior margin of the cranial table (Fig. 3.1H) instead of the maximum length including the squamosal prong (Groh et al., 2020, fig.S35). In almost all taxa in this dataset, the cranial table is wider than long, but a few taxa have approximately square-shaped cranial tables, including *Hylaeochampsa vectiana* (length to width = 1.1) *Diplocynodon hantoniensis* (NHMUK OR 30393, 0.97), and *Diplocynodon muelleri* (0.97) (Piras and Buscalioni, 2006). By contrast, the cranial table is approximately twice as wide as long in some *Borealosuchus* species, e.g. *B. formidabilis* (0.51) (Erickson, 1976, fig.4) and *B. wilsoni* (0.55) (FMNH PR 1674), and some gavialoids, e.g. *Gryposuchus neogaeu*s (0.48) (MLP 26-413) and *Ikanogavialis gameroi* (0.52) (Sill, 1970, fig.1). The rediscretised character state boundary follows earlier studies (Wu et al., 2001b; Groh et al., 2020), but the measured values appear completely continuous (Appendix D.1) and are normally distributed (Shapiro-Wilk test = 0.99, $p = 0.26$).

9. Cranial table shape, minimum angle subtended by the posterolateral cranial table margin and sagittal axis of skull: $< 10°$ (0); $\geq 10°$ (1) (new character, after Brochu & Storrs, 2012).

   Brochu and Storrs (2012) described a strongly trapezoidal outline of the cranial table in *Crocodylus thobjarnarsoni* resulting from anteriorly converging lateral margins of the cranial table (Fig. 3.2A). Measurements of taxa in the present study reveal continuous variation in this feature (Fig. D.1). Several paralligatorids exhibit lateral margins of the cranial table that are subparallel with the sagittal plane, e.g. *Shamosuchus djadochtaensis* (Pol et al., 2009) and *Wannachampsus kirpachi* (Adams, 2014). By contrast, some crocodyloids exhibit strongly anteriorly converging margins, e.g. *Asiatosuchus germanicus* (16°) (HLMD Me-7499) and *Voay robustus* (23°) (NHMUK R 36685). Measured values are positively skewed (Shapiro-Wilk test = 0.93, $p < 0.001$). As there is no similar existing character, nor a discontinuity in the data, the cut-off between character states is set at 10°, which is the measured value for the outgroup, *Bernissartia fagesii*.

10. Supratemporal fenestra size, ratio of maximum anteroposterior supratemporal fenestra length to anteroposterior cranial table length (measured from the level of the frontal-postorbital suture): $< 0.5$ (0); $\geq 0.5$ (1) (after Wu et al., 2001b [67]; Groh et al., 2020 [34]).

    Supratemporal fenestra size (Fig. 3.2B) varies considerably in eusuchians. Measurements of fenestra size reveal a continuous range of values (Appendix D.1), which appears normally distributed, but this is not statistically significant (Shapiro-Wilk test = 0.96, $p <$0.001). Some of the largest supratemporal

fenestrae are measured in "gavialoids", e.g. *Gryposuchus neogaeus* (MLP 26-413, supratemporal fenestra size ratio = 0.66) and *Gavialis gangeticus* (0.62) (NHMUK 1974.3009), as well as alligatoroids, e.g. *Stangerochampsa mccabei* (0.68) (Wu et al., 1996). The smallest supratemporal fenestrae are measured almost exclusively in caimanines, which exhibit varying degrees of closure of the fenestrae, e.g. *Melanosuchus niger* (0.18) (NHMUK 45.8.25.125) and *Paleosuchus*, in which they are completely closed (NHMUK 1868.10.8.1). The rediscretised character state boundary follows earlier studies (cut-off = 0.5) (Wu et al., 2001b).

11. Supratemporal fenestra shape, ratio of maximum mediolateral width to maximum anteroposterior length: $\leq 1$ (0); $> 1$ (1) (after Jouve et al., 2008 [199]; Jouve, 2016 [198]; Lee & Yates, 2018 [75]).

    Earlier studies typically characterised the shape of the supratemporal fenestrae as either circular or wider than long (Jouve et al., 2008; Lee & Yates, 2018). However, when measured (Fig. 3.2C), supratemporal fenestra shape varies continuously between these limits (Appendix D.1). Most eusuchians in this dataset exhibit supratemporal fenestrae that are slightly longer than wide (mean = 0.81). The widest supratemporal fenestrae were measured in *Borealosuchus wilsoni* (FMNH PR 1674) (fenestra shape = 1.30) and several longirostrine crocodylians, e.g. *Thecachampsa antiquus* (1.24) (AMNH 5663), *Maroccosuchus zennaroi* (1.19) (IRScNB R408), and *Gavialis gangeticus* (1.20) (NHMUK 1974.3009). By contrast, highly narrow supratemporal fenestrae occur in *Diplocynodon deponiae* (0.33) (SMF Me 2609), *Trilophosuchus rackhami* (0.35) (QM F16856) and *Tsoabichi greenriverensis* (0.39) (FMNH PR 1793). The rediscretised threshold value 1 used here is adapted from Jouve et al. (2008), but there is no discontinuity here, nor at any other value. Indeed, measured values are continuous and normally distributed (Shapiro-Wilk test = 0.99, p = 0.64).

12. Incisive foramen size, ratio of maximum mediolateral width to the mediolateral width of the rostrum at the premaxilla-maxilla suture: $< 0.3$ (0); $\geq 0.3$ (1) (after Brochu, 1997b [124]; Jouve et al., 2008 [124]; Groh et al., 2020 [5]).

    The size of the incisive foramen (Fig. 3.2D) was previously characterised in a multistate character that combined quantitative and more subjectively defined character states, e.g. "*incisive foramen small and less than half the greatest width of the premaxillae*" or "*extremely reduced and thin*" (Jouve et al., 2008, character 124). Measurements of eusuchians in this dataset reveal that the incisive foramen is always less than half the width across the premaxillae (Appendix D.1). Even in taxa with the largest incisive foramina, the foramen does not exceed 40% of the width across the premaxillae e.g. *Brachychampsa montana* (0.33) (UCMP 133901). As in earlier studies, the smallest incisive foramina were predominantly found in "gavialoids", e.g. *Piscogavialis jugaliperforatus* (SMNK 1282 PAL) (foramen size = 0.04), and *Gryposuchus neogaeus* (MLP 26-413) (0.5). A rediscretised threshold of 0.5, as implied in the original character (Brochu, 1997b), would be uninformative, so the threshold is

set at 0.3, where a small discontinuity is observed. Nevertheless, the measured values are normally distributed (Shapiro-Wilk test = 0.97, $p$ = 0.15).

13. Suborbital fenestra shape, ratio of maximum mediolateral width to maximum anteroposterior length: $\leq$ 0.5 (0); $>$ 0.5 (1) (after Buscalioni et al., 2011 [183]; Groh et al., 2020 [30]).

    Despite significant variation in the proportions of the suborbital fenestrae (Fig. 3.2E), this variation is not discretised in most studies of crocodylian phylogeny. The fenestra is longer than wide in all taxa in this dataset (average ratio = 0.40), but a few crocodylians have more equidimensional fenestrae, e.g. *Eocaiman cavernensis* (fenestra shape = 0.63) (AMNH 3158) and *Alligator mcgrewi* (0.53) (AMNH FAM 7905). Taxa with highly elongated suborbital fenestrae tend to be longirostrines, e.g. *Crocodylus johnstoni* (0.28) (QM J45309) and *Piscogavialis jugaliperforatus* (SMNK 1282 PAL) (0.30), but not exclusively, e.g. *Borealosuchus sternbergii* (0.30) (UCMP 126099). The rediscretised threshold value of 0.5 follows Buscalioni et al. (2011); however, the data is almost entirely continuous and normally distributed (Shapiro-Wilk test = 0.98, $p$ = 0.25).

14. Choana shape, ratio of maximum mediolateral choanal width to maximum anteroposterior length: $<$ 2 (0) $\geq$ 2 (1) (after Wu et al., 1997 [42]; Jouve et al., 2006 [18]; Groh et al., 2020 [46]).

    In most eusuchians in this dataset, the choana is approximately equidimensional (Fig. 3.2F). Measured values are positively skewed, with an average value of 1.5 (Shapiro-Wilk test = 0.69, p = $<$0.001). The upper tail end of the distribution corresponds with a highly divergent choanal morphology, which is mediolaterally wide. This condition predominantly occurs in caimanines, such as *Mourasuchus atopus* (choanae width to length = 5.79) (UCMP 38012) and *Purussaurus neivensis* (3.6) (UCMP 39704). Earlier studies did not provide a clear threshold for discrete delimitation, but a small discontinuity in the data supports a cut-off value of 2 (Appendix D.1).

15. Pterygoid, proportions of pterygoid wing: maximum mediolateral width to maximum anteroposterior length ratio: $\geq$ 3 (0); $<$ 3 (1) (after Turner, 2015 [303]; Jouve et al., 2015 [237]).

    The width across both pterygoids (Fig. 3.2G) is more than twice their anteroposterior length in most eusuchians (average = 2.71). The highest values of pterygoid width to length were measured in "tomistomines", e.g. *Toyotamaphimeia* (Kobayashi et al., 2006) (pterygoid width to length = 3.82) and '*Tomistoma*' *cairense* (SMNS 50739) (3.70). By contrast, the pterygoids are more equidimensional in *Osteolaemus tetraspis* (NHMUK 1862.6.30.5) (1.68) and *Mecistops cataphractus* (NHMUK 1924.5.10.1) (1.79). The rediscretised character state boundary is adopted from earlier studies, at which point a small discontinuity can be observed; nevertheless, the data appears normally distributed (Shapiro-Wilk test = 0.96, $p$ = 0.051).

16. Basioccipital tubera, ratio of maximum mediolateral width of basioccipital tubera to maximum mediolateral width of the occipital condyle: $< 2$ (0); $\geq 2$ (1) (new character, based on personal observations).

    Mediolaterally wide basioccipital tubera are known in several taxa, typically "gavialoid" crocodylians, e.g. *Gavialis gangeticus* (NHMUK 1974.3009) and *Gryposuchus* (Riff & Aguilera, 2008; Salas-Gismondi et al., 2016), but variation in tubera width has not been discretised in previous studies. Measured values (Fig. 3.2H) are not normally distributed (Shapiro-Wilk test = 0.90, $p < 0.001$), but positively skewed, with most eusuchians exhibiting basioccipital tubera that are $> 1.5$ times the width of the occipital condyle (average = 1.63). As expected, "gavialoids" exhibit the widest tubera, e.g. *Gavialis lewisi* (YPM VP 3226) (ratio = 2.5), and *Gavialis gangeticus* (1.9) (NHMUK 1974.3009). By contrast, the narrowest basioccipital tubera were measured in *Paleosuchus trigonatus* (1.3) (NHMUK 1868.10.831) and *Crocodylus porosus* (1.2) (NHMUK 1852.12.9.2). A prominent discontinuity in the measured values supports a cut-off value of 2 (Appendix D.2).

17. Number of maxillary alveoli: $< 18$ (0); 18–22 (1); $> 22$ (2) (after Wu & Sues, 1996 [30]; Jouve, 2004 [169]; Jouve et al., 2008 [169]; Groh et al., 2020) (ORDERED).

    Most eusuchians examined in this dataset have 13–14 maxillary alveoli, including all extant alligatorids and crocodylids; however, there is continuous variation in alveolar counts above and below this value (Appendix D.2). Longirostrine crocodylians exhibit the most alveoli, e.g. *Ikanogavialis gameroi* (30 alveoli) (Sill, 1970) and *Piscogavialis jugaliperforatus* (28 alveoli) (SMNK 1282 PAL). By contrast, *Gnatusuchus pebasensis* has only nine maxillary alveoli (Salas-Gismondi et al., 2015), whereas the paralligatorids *Wannchampsus kirpachi* (Adams, 2014) and the 'Glen Rose Form' (USNM 22039) have 11 alveoli. Although counts of maxillary alveoli do not appear to be normally distributed (Shapiro-Wilk test = 0.83, $p < 0.001$), there are no obvious discontinuities that naturally delimit the data. Nevertheless, character state boundaries follow Jouve et al. (2008).

### 3.3.2 Mandible

18. External mandibular fenestra shape, ratio of anteroposterior length (between anterior and posterior limits) to dorsoventral height (between dorsal and ventral limits): $< 2.5$ (0); $\geq 2.5$ (1) (after Montefeltro et al., 2013 [306]; Groh et al., 2020 [56]).

    The proportions of the external mandibular fenestra (EMF) are measured using the maximum length of its axes horizontally and vertically (Fig. 3.3A), not diagonally (i.e. the maximum and minimum axes used by Groh et al., (2020 [fig. 56]). The EMF is approximately two times longer than tall in most eusuchians examined here (average = 1.89). The most elongate fenestrae were measured in *Diplocynodon darwini* (2.82) (HLMD Me 7500) and *Borealosuchus sternbergii* (2.79) (UCMP 133930). By

contrast, several *Crocodylus* species have more equidimensional fenestrae, e.g. *C. palustris* (1.21) (NHMUK 1868.4.9.11) and *C. niloticus* (1.26) (NHMUK 1900.9.22.2). Measured values are normally distributed (Shapiro-Wilk test = 0.97, p = 0.08). The cut-off value used in earlier datasets (3) is uninformative, as all taxa examined here have a lower ratio. A discontinuity at a value of 2.5 was instead used to delimit character states (Appendix D.2).

19. External mandibular fenestra shape, minimum angle subtended by dorsal margin of fenestra and the horizontal: $< 25°$ (0); $\geq 25°$ (1) (after Andrade et al., 2011; Groh et al., 2020 [55]).

    This character essentially describes the orientation of the long axis of the EMF using the inclination of its dorsal margin (Fig. 3.3B). As originally formulated, the character distinguished between a horizontally or anterodorsally orientated long axis, and was applied to a dataset comprising mostly non-crocodylian neosuchians (Andrade et al., 2011; Montefeltro et al., 2013). The original delimitation of the character is uninformative here, as the long axis of the EMF is inclined in all taxa in this dataset. Minimal inclination of the EMF is found in *Alligator mississippiensis* (10°) (NHMUK 68.2.12.6) and is steepest in *Mekosuchus inexpectatus* (55°) (MNHN NCP 06), with a full range of normally distributed values in between (Shapiro-Wilk test = 0.97, $p = 0.16$). The character state boundary is based on a small discontinuity at 25° (Appendix D.2).

20. Articular, retroarticular process, ratio of anteroposterior length (measured from the transverse ridge to the posteriormost tip of articular) to the mediolateral width across the glenoid fossa: $< 1.5$ (0); $\geq 1.5$ (1) (after Lee & Yates, 2018 [217]).

    Lee and Yates (2018) characterised the length of the retroarticular process relative to its 'width'. Here the width is measured across the articular glenoid fossa, since the width of the retroarticular process is variable (narrowing posteriorly) (Fig. 3.3C). A cut-off of 1.5 is retained in the rediscretised character; however, although the data are not normally distributed (Shapiro-Wilk test = 0.93, $p < 0.05$) there does not appear to be any natural discontinuity in this dataset (Appendix D.2). Indeed, retroarticular process length varies continuously from the longest process measured in *Gavialis gangeticus* (1.89 times the width) (NHMUK 1974.3009), to the shortest process measured in *Mekosuchus inexpectatus* (1.0 times the width) (MNHN NCP 06).

### 3.3.3 Postcrania

21. Scapular blade, anteroposterior flare of dorsal end (at maturity): angle subtended by anterior and posterior margins $\geq 35°$ (0); $< 35°$ (1) (after Benton & Clark, 1988; Brochu, 1997b [22]).

    Benton and Clark (1988) considered a narrow, subparallel-sided scapular blade to be diagnostic of Crocodylia, but a dorsally flaring scapula has been recognised in several crocodylians, e.g. *Gavialis*

*gangeticus* and *Paleosuchus* (Brochu, 1999). In earlier datasets, dorsal flare of the scapular blade was essentially described as present or absent (e.g Brochu, 1997b; Brochu et al., 2012; Jouve et al., 2015; Lee & Yates, 2018); however, Brochu (1999) alluded to different degrees of flare that could be further delimited. The angle subtended by the anterior and posterior margins of the scapular blade was measured for this dataset (Fig. 3.3D), revealing a fully continuous and normally distributed range of values (Shapiro-Wilk test = 0.96, $p$ = 0.12). Scapular blade flare ranges from a minimum in *Caiman yacare* (flare = 8°) (AMNH 97300) to a prominent flare in *Hassiacosuchus haupti* (flare = 73°) (HLMD Be-137) (Appendix D.2). A high degree of flare is also observed in *Bernissartia fagesii* (68°) (IRScNB 1538), *Borealosuchus formidabilis* (63°) (Erickson, 1976, fig.24), and *Diplocynodon darwini* (61°) (SMF Me-1289). When plotted, the largest discontinuity in the data occurs between a scapula flare of 32° (*Alligator prenasalis*, YPM PU 13799) and 38° (*Brachychampsa montana*, UCMP 133901), and so the rediscretised boundary was set in between these values at 35°.

22. Scapula-coracoid, ratio of maximum proximodistal coracoid length to maximum proximodistal scapula length: $< 1.0$ (0); $\geq 1$ (1) (after Clark, 1994 [83]; Pol & Norell, 2004 [83]; Groh et al., 2020 [68]).

    As originally formulated (Clark, 1994), this character described a coracoid that is either two-thirds the length of the scapula or equal in length to the scapula (Clark, 1994). This distinction is uninformative in this dataset, as all measurements of the coracoid to scapula length ratio are greater than 0.7 (Appendix D.2). Measured values of the coracoid-scapula ratio are normally distributed (Shapiro-Wilk test = 0.94, $p$ = 0.22), but there is a small discontinuity between a number of taxa with a ratio greater than 1, e.g. *Gavialis gangeticus* (UCMZ R5783) and *Crocodylus johnstoni* (QM J58446), and all other taxa.

23. Coracoid shape, ratio of maximum expansion of distal coracoid, to maximum proximo-distal coracoid length: $< 0.5$ (0); $\geq 0.5$ (1) (new character, based on personal observations).

    The coracoids of several longirostrine crocodylians are proportionally slenderer than those of other crocodylians, exhibiting a small distal expansion relative to the proximo-distal length of the element (Fig. 3.3E). For example, whereas the ratio of distal expansion to coracoid length is $<$0.4 in *Piscogavialis jugaliperforatus* (SMNK 1282 PAL) and *Eogavialis africanum* (NHMUK R 3199), this ratio is $>$ 0.6 in *Voay robustus* (NHMUK R36659) and *Asiatosuchus germanicus* (SMF Me 1801). A range of intermediate, normally distributed values occur between these extremes (Shapiro-Wilk test = 0.99, $p$ = 0.99), with no obvious discontinuities in the data (Appendix D.2), and the condition unknown in the outgroup. As such, a cut-off is set at 0.5 for the rediscretised analysis.

24. Ulna length, ratio of maximum proximodistal ulna length to maximum proximodistal humeral length: $< 0.7$ (0); $\geq 0.7$ (1) (after Jouve, 2009 [330]; Groh et al., 2020 [69]).

There are broad differences in the relative lengths of the ulna and humerus in Crocodylia (Appendix D.2). In line with Iijima et al. (2018a), *Gavialis gangeticus* has the shortest ulna in proportion to the humerus among extant crocodylians (ratio = 0.6) (Fig. 3.3F). This is similar to extinct "tomistomines", e.g. *Toyotamaphimeia* (0.5) (Iijima et al., 2018a) and *Penghusuchus* (0.6) (Shan et al., 2009, fig.14). In general, the proportional length of the ulna to the humerus is lower in crocodyloids than in alligatoroids, in which they are more equidimensional in some taxa, e.g. *Hassiacosuchus haupti* (0.9) (HLMD Be-137) and *Wannanganosuchus brachymanus* (0.8) (Iijima et al., 2018). Measured values are not normally distributed (Shapiro-Wilk test = 0.92, $p < 0.05$) and although the rediscretised threshold follows earlier studies (cut-off = 0.7) (Jouve, 2009; Groh et al., 2020) there is no notable discontinuity in the data.

25. Femur length, ratio of maximum proximodistal femur length to maximum proximodistal humeral length (at maturity): $< 1.2$ (0); $\geq 1.2$ (1) (after Brochu, 1997b [33]; Jouve, 2009 [328]; Groh et al., 2020 [80]).

    Brochu (1997b) originally distinguished taxa with slender limbs, in which the fore- and hindlimb are subequal in length (*Borealosuchus*), from taxa with 'robust' limbs, with a longer hindlimb than forelimb (*Bernissartia fagesii* and all other crocodylians). Whereas the distinction in slenderness between *Borealosuchus* and all other crocodylians is captured in character 306 here, the current character quantifies the proportional differences in forelimb and hindlimb length. Ideally, total limb lengths would be measured; however, this would only allow a few exceptionally preserved fossil crocodylians to be considered, and therefore the relative lengths of the stylopodials are used as a proxy (Fig. 3.3G). Measurements are restricted to mature individuals given that the hindlimb grows with negative allometry relative to the forelimb in most extant crocodylians (Iijima & Kubo, 2019a). Alligatoroids tend to exhibit much longer femora than humeri, e.g. *Hassiacosuchus haupti* (1.5) (HLMD Be 137), *Tsoabichi greenriverensis* (1.3) (FMNH PR 1793), and *Wannaganosuchus brachymanus* (1.3) (Iijima et al., 2018). By contrast, the stylopodials of other crocodylians are subequal in length, e.g. *Gavialis gangeticus* (1.1) (UMZC R5783), *Tomistoma schlegelii* (1.1) (AMNH 113078), and most *Crocodylus* species ($\sim$1.0). Measured values are not normally distributed (Shapiro-Wilk test = 0.90, $p < 0.05$), and a small discontinuity at a value of 1.2 is used to delimit the rediscretised character states (Appendix D.2).

26. Ischial blade shape, ratio of maximum expansion of distal ischial blade to maximum proximodistal length of ischium: $< 0.5$ (0); $\geq 0.5$ (1) (new character, based on personal observations).

    The distal end of the ischial blade in *Gavialis gangeticus* prominently flares (AMNH 110145, UCMZ R5783). Indeed, measurements of the degree of flare (relative to ischium length 3.3G) reveal that *Gavialis gangeticus* exhibits the highest value among taxa in this dataset (0.7). A similar expansion

also characterises *Tomistoma schlegelii* (AMNH 113078) (0.6), contrasting with the narrower ischial blades of *Borealosuchus wilsoni* (FMNH PR 1674) (0.4) and most extant crocodylids, e.g. *Crocodylus johnstoni* (QM J58446) (0.4). A range of intermediate, normally distributed values occurs between these limits (Shapiro-Wilk test = 0.99, $p$ = 0.96). There is no informative discontinuity in the data and the condition in the outgroup could not be assessed; as such, a cut-off value is set at 0.5 based on those aforementioned values (Appendix D.2).

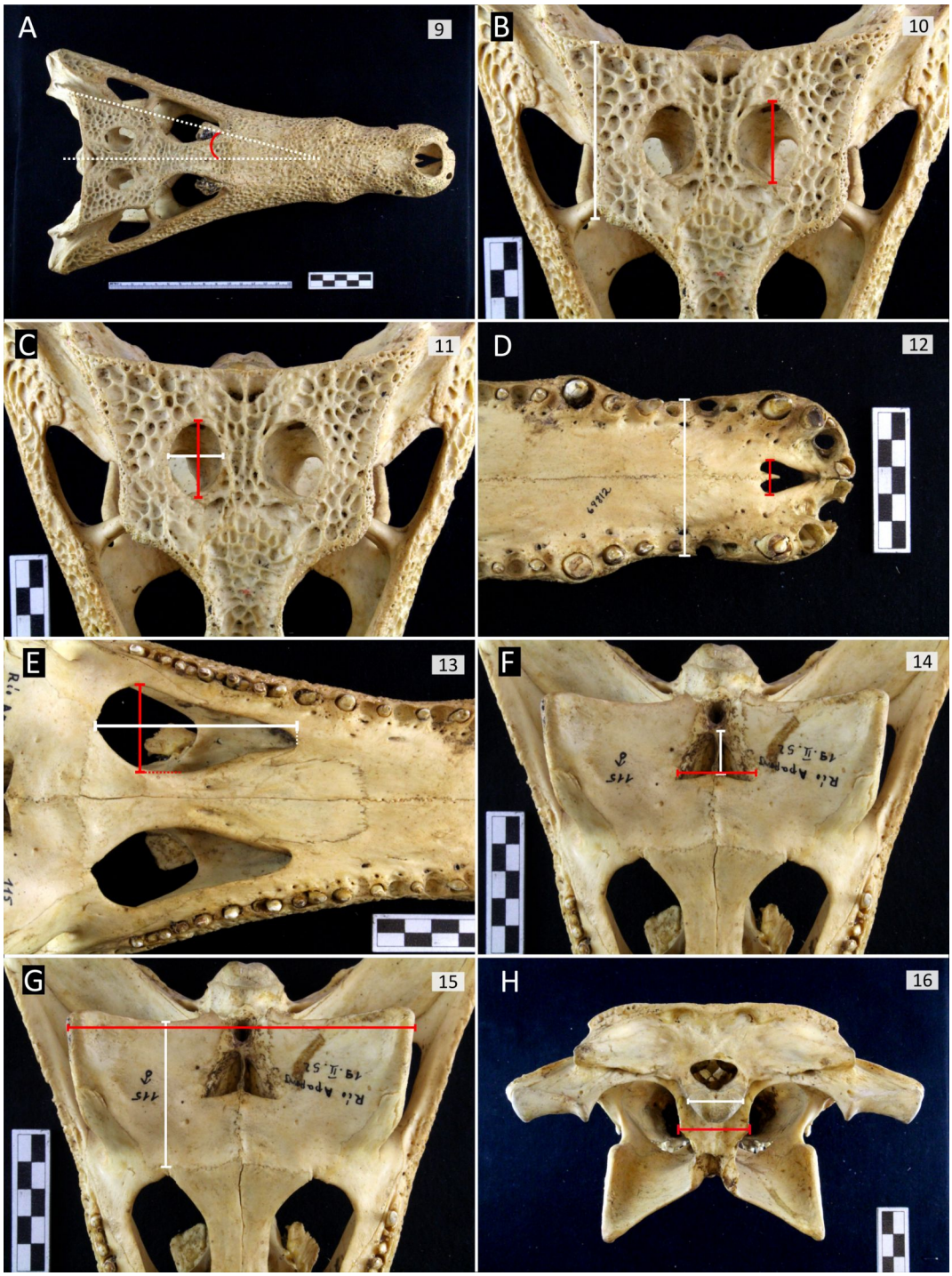



Figure 3.2: Continuous characters 9–16. All characters illustrated using *Caiman crocodilus apaporiensis* (FMNH 69812). Scale bars = cm.

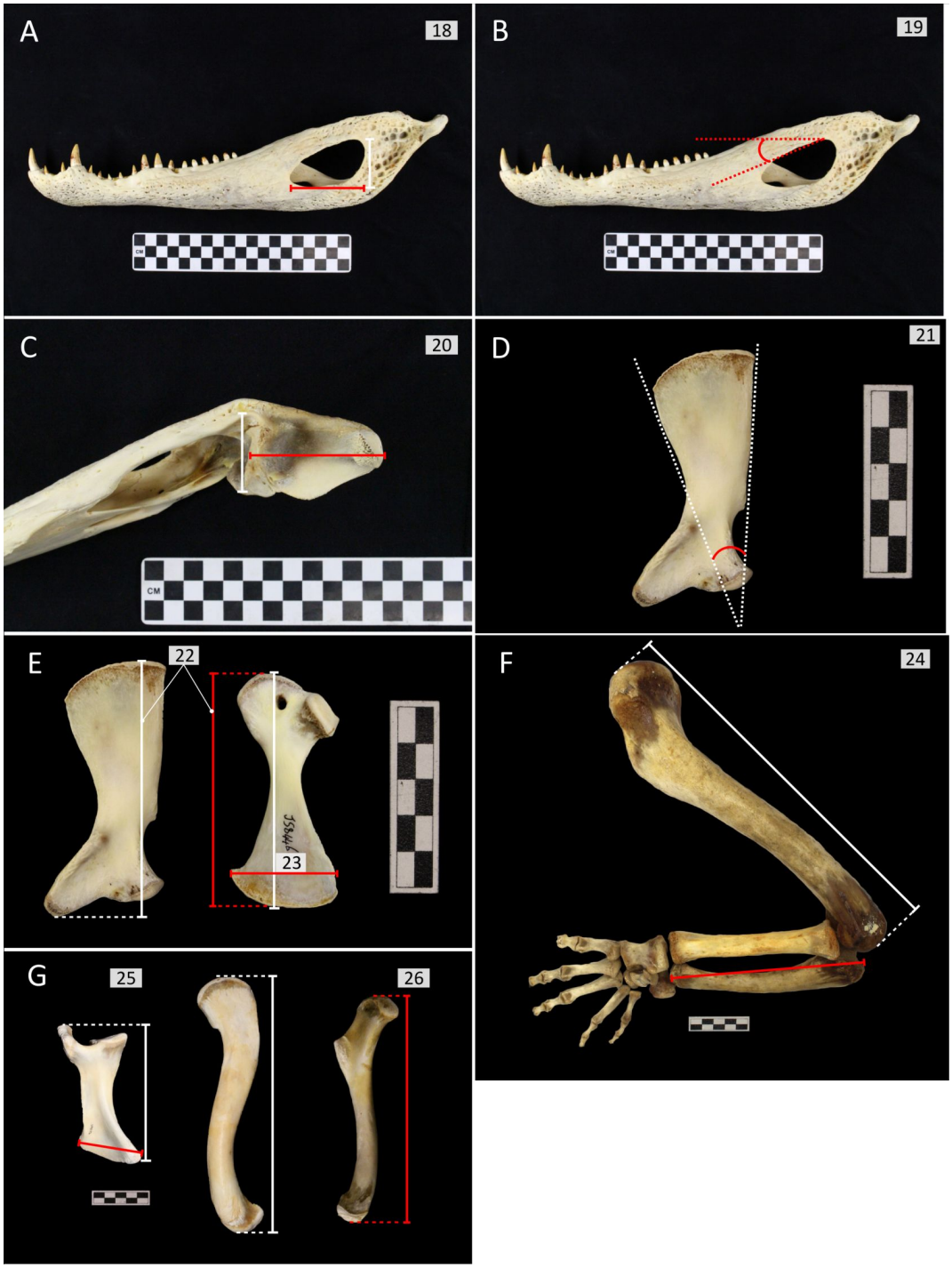



Figure 3.3: Continuous characters 18–26. **A**–**C**, *Caiman yacare* (AMNH 97300): left mandible in lateral view (**A**), (**B**); dorsal view of right mandibular ramus (**C**); **D**–**E**, *Crocodylus johnstoni* (QM J58446): left scapula (**D**), left scapula and coracoid (**E**); **F**, left forelimb of *Gavialis gangeticus* (UMZC R 5783); **G**, (from left to right) left ischium, femur and humerus of *Crocodylus porosus* (QM J 48127). All scale bars = cm.

## 3.4 Discrete characters

### 3.4.1 Skull

27. Rostral ornamentation, canthi rostralii: absent (0); present (1) (new character, after Norell, 1988 [34]; Brochu, 1997b [143]).

    Brochu (1997b) and later studies (e.g. Brochu et al., 2012; Jouve, 2016) used the term 'canthus rostralis' to describe anterolaterally directed rostral ridges that occur prominently in caimanines, e.g. *Melanosuchus niger* and *Caiman latirostris*, which are instead described as 'rostral ridges' here (see Character 28). In this study, canthi rostralii (or canthal ridges) are distinguished from 'rostral ridges', in that they extend anterolaterally from the dorsomedial margin of the orbit to the level of the $4^{th}$ maxillary alveolus, imparting an angle that separates two planar surfaces on the skull (Fig. 3.4B). Taxa with canthi rostralii include *Paleosuchus palpebrosus* (Medem, 1958), *Hassiacosuchus haupti* (Fig. 3.4B), *Arambourgia gaudryii* (MNHN QU 17155), and *Boverisuchus vorax* (UCMP 170767), none of which have rostral ridges.

28. Rostral ornamentation, development of anterolaterally directed ridges on the lateral surface of the rostrum (at maturity): absent (0); present (1) (after Norell, 1988 [34]; Brochu, 1997b [143]).

    Anterolaterally directed rostral ridges typically occur in pairs, and are often associated with a spectacle (see Character 31). The largest ridge originates from the anteromedial margin of the orbit, and extends anterolaterally across the prefrontal, lacrimal and maxilla (Fig. 3.4D). A second, shorter anterior ridge extends anterolaterally over the nasal and maxilla. These ridges are not necessarily associated with a spectacle nor are they always paired, as is the case in *Purussaurus brasiliensis* (UFAC 1403), in which one prominent anterolateral ridge extends from the anteromedial orbital margin to the lateral edge of the maxilla.

29. Rostral ornamentation, dorsal boss on sagittal axis: absent (0); present (1) (after Brochu, 1997b [101]).

    As discussed by Brochu (2000), all extant Neotropical *Crocodylus* species i.e. *C. acutus*, *C. intermedius*, *C. moreletti*, and *C. rhombifer*, are characterised by sulci on the nasal-maxilla sutures. This imparts a median elevation (boss) on the rostrum that is restricted mostly to the nasals, and is present throughout posthatching ontogeny (Brochu, 2000) (Fig. 3.4H). The dorsal boss is also known in two extinct *Crocodylus* species, the Venezuelan *Crocodylus falconensis* (Scheyer et al., 2013), and North African *Crocodylus checchiai* (Delfino et al., 2020).

30. Rostral ornamentation, anteroposteriorly orientated preorbital ridges extending from the anterior corner of the orbit (at maturity): absent (0); present (1) (after Brochu, 1997b [144]).

A pair of anteroposteriorly orientated ridges extend from the anterior corner of the orbit in several crocodylians (Brochu, 2000). These ridges are particularly well-developed in Indopacific *Crocodylus* species such as *Crocodylus porosus* (Fig. 3.4F), *Crocodylus mindorensis*, *Crocodylus novaeguineae*, and *Crocodylus siamensis*. These ridges are always positioned on the medial edge of the lacrimal, adjacent to the lacrimal-prefrontal suture, and are typically straight; however, in some *Crocodylus siamensis* individuals (NHMUK 1924.4.1.168), the ridges are sigmoidal in shape. As discussed by Brochu (2000), juvenile *Crocodylus johnstoni* is also characterised by such ridges, but they are lost at maturity. This is also the case in *Crocodylus palustris* (NHMUK 1845.1.8.204, 1868.4.9.11). Preorbital ridges are not restricted to *Crocodylus*, but occur in several osteolaemines e.g. *Osteolaemus tetraspis* (NHMUK 1862.6.30.5), *Voay robustus* (NHMUK R 36685), and *Euthecodon armabourgi* (MNHN ZEL 001), as well as mekosuchines such as *Baru wickeni* (QM 16822) and *Quinkana* spp. (Molnar, 1981; Megirian, 1994). A number of taxa are newly scored for the derived character state in this study, including several species of *Diplocynodon* where they are modestly developed: *D. hantoniensis* (see Section 2.3.1), *D. ratelii* (MNHN SG 539), and *D. remensis* (Martin et al., 2014).

31. Rostral ornamentation, transverse ridge between the orbits (i.e. spectacle): absent (0); present (1) (after Barrios, 2011 [109]; Cidade et al., 2017 [186]; Lee & Yates, 2018 [56]).

32. Rostral ornamentation, morphology of the transverse orbital ridge (i.e. spectacle): low, lacking a posterior fossa (0); tall, with deep posterior fossa (1) (new character, based on personal observations).

33. Rostral ornamentation: anterior extent of transverse bridge between orbits (i.e. spectacle): posterior to anterior orbital margin (0); level with or anterior to anterior orbital margin (1) (new character, based on personal observations).

    The presence of a step approximately at the level of the anterior orbital margin is widespread among both extant and fossil crocodyliforms (Delfino et al., 2008a). This step is often referred to as a 'spectacle', especially in reference to extant caimanines (e.g. the spectacled caiman – *Caiman crocodilus*) in which this bony interorbital bridge is very prominent. In this study, presence (Character 31), size variation (Character 32), and position (Character 33) of a spectacle are all recognised as characters. The first of these describes the presence or absence of any change in elevation around the anterior orbit margin, and is equivalent to characters 186 in Cidade et al. (2017) and 56 in Lee and Yates (2018). By contrast with the character scores in those studies, here the spectacle is found to be more widely distributed among Crocodylia (Fig. 3.5). For example, in addition to most extant caimanines, the spectacle is found in the putative early caiman *Eocaiman cavernensis* (AMNH 3158), all but one species of *Alligator* (*A. mcgrewi*), *Navajosuchus mooki* (as scored in Lee and Yates [2018], but not Cidade et al. [2017]), *Leidyosuchus canadensis* (Wu et al., 2001a, fig.2.1) and most species of *Diplocynodon*

(except *D. darwini* and *D. deponiae*, see Section 2.5.1). Also noteworthy is the presence of a spectacle in some basal crocodyloids, such as *Asiatosuchus grangeri* (AMNH 6607) and *Jiangxisuchus nankangensis* (Li et al., 2019, fig.2A).

Most of the above listed taxa, such as *Alligator* and *Diplocynodon* have a low spectacle, which lacks a deep fossa on the anterior margin of the step (C32-0, Fig. 3.6). A different condition is expressed in several caimanines such as *Caiman latirostris*, in which the vertical wall of the spectacle is excavated by a deep fossa (C32-1, Fig. 3.5E–F). Further variation occurs in the posteriormost extent of the spectacle relative to the anterior margin of the orbit (Character 33) (Fig. 3.6). The spectacle rarely forms a straight horizontal bridge across the rostrum; instead, the spectacle is anteriorly concave. The apex of the concavity varies in position relative to the orbit. In all extant caimanines, the spectacle does not extend posteriorly beyond the level of the anterior margin of the orbit (C33-1). However, several fossil taxa, including *Purussaurus neivensis*, *Diplocynodon*, and *Bottosaurus harlani* exhibit a strong posterior shift in the spectacle (C33-0). The morphology of the spectacle in *Bottosaurus* was originally described as a "distinct 'U'-shaped depression", and used to diagnose the genus (Cossette & Brochu, 2018, p.4). Here, it is regarded as a posteriorly shifted spectacle, a condition similar to that of the giant Miocene caimanine, *Purussaurus neivensis* (UCMP 39704).

34. Rostral ornamentation, extensive fossa extending anteriorly from the frontal to the posterior margin of the external naris: absent (0); present (1) (new character, based on personal observations).

    The derived character state describes a unique condition of the naris present only in *Purussaurus brasiliensis* and *Purussaurus mirandai* (Aguilera et al., 2006). Unlike all other eusuchians, the naris covers almost the entire anteroposterior length of the rostrum in these two species, and are so enlarged that "*one can literally put one's head in the narial aperture and look around*" (Brochu, 2003) (Fig. 3.7B). Furthermore, the posterior margin of the naris merges continuously into a large fossa on the rostrum.

35. Prefrontal, prominence at anteromedial orbital margin: not thickened (0); hypertrophied, forming rounded protuberances (1) (after Bona et al., 2013b [167]; Cidade et al., 2017 [186]; Souza-Filho et al., 2019 [182]).

    As discussed by Cidade et al. (2017), a protuberance or 'knob' at the anteromedial margin of the orbit is diagnostic of the caimanine *Mourasuchus*, present in all three *Mourasuchus* species studied here (e.g. *Mourasuchus arendsi*, Fig. 3.8B). This thickening occurs on the prefrontal orbital margin, and in all *Mourasuchus* species occurs along with a spectacle (31-1). The spectacle is nonetheless independent of the prefrontal protuberances, since several crocodylians with a spectacle lack a prefrontal protuberance, e.g. *Caiman* (Fig. 3.6G–I).

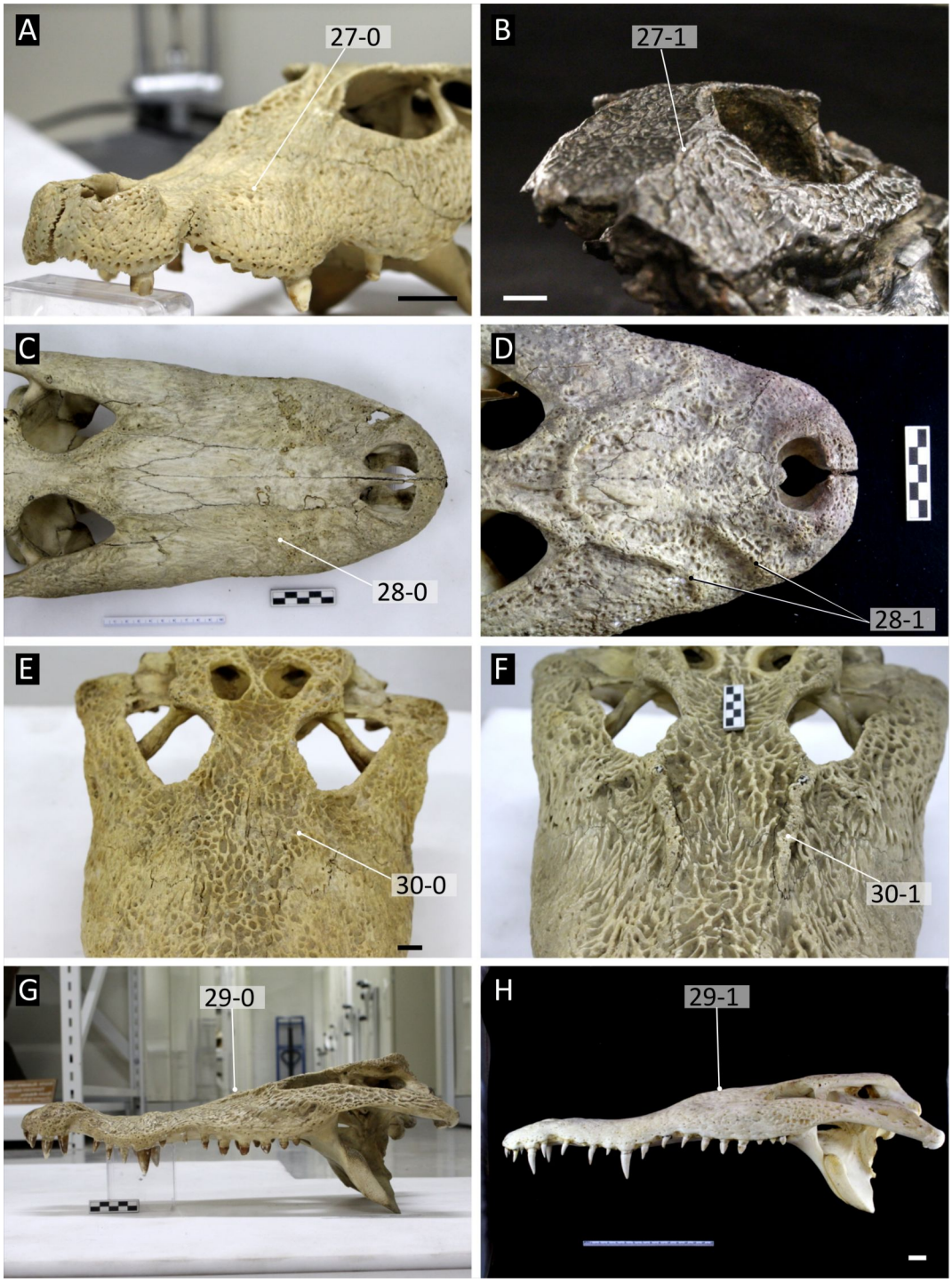



Figure 3.4: Variation in rostral ornamentation in Crocodylia. **A**, *Osteolameus tetraspis* (NHMUK 1862.6.30.5); **B**, *Hassiacosuchus haupti* (HLMD Me-4415); **C**, *Alligator mississippiensis* (NHMUK 1873.2.21.1); **D**, *Caiman latirostris* (FMNH 9713); **E**, *Crocodylus palustris* (1897.12.31.1); **F**, *Crocodylus porosus* (NHMUK 1852.12.9.2); **G**, *Crocodylus siamensis* (NHMUK 1921.4.1.168); **H**, *Crocodylus acutus* (FMNH 69884). Scale bars in A, B, E, and H = 2 cm, all other scale bars = cm.

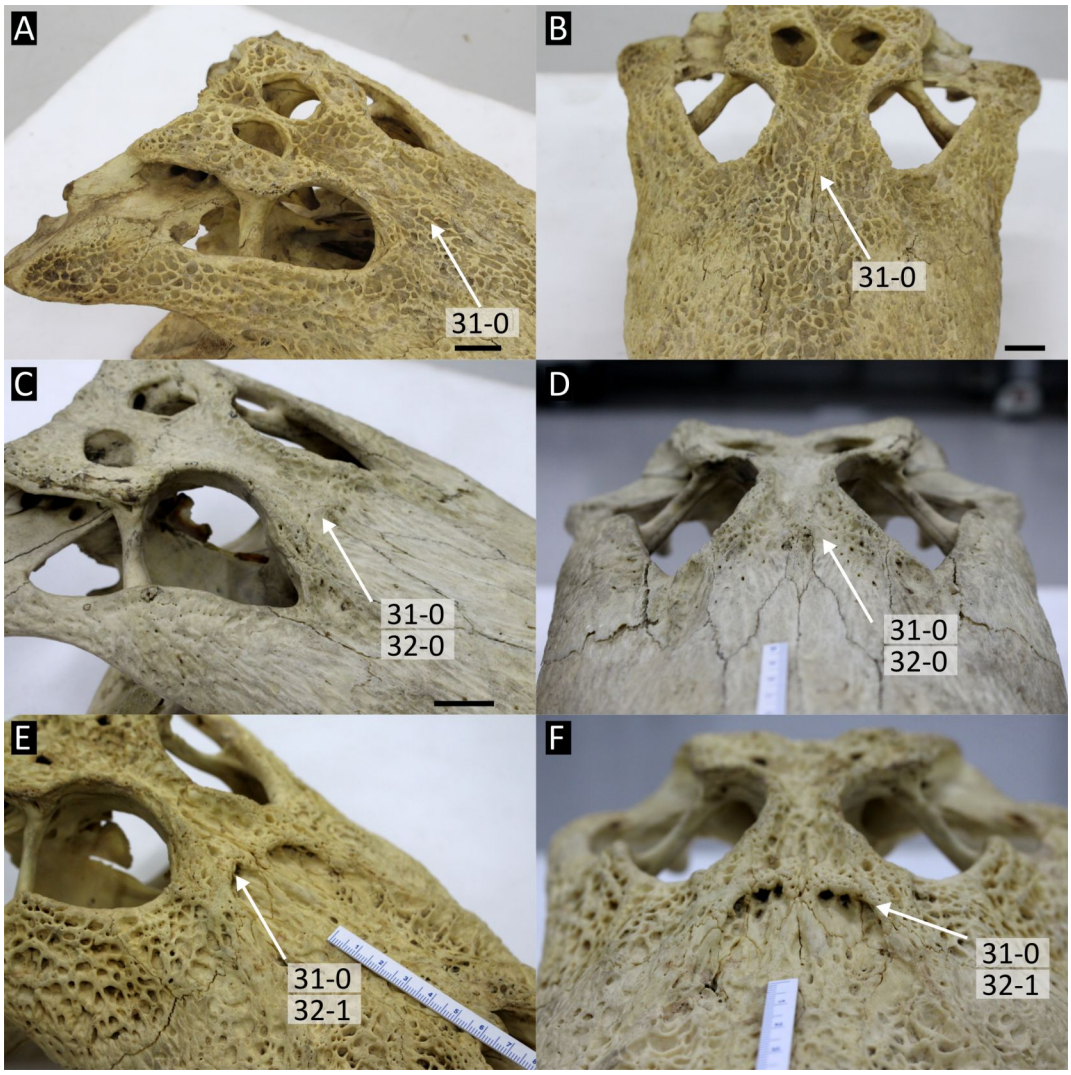



Figure 3.5: Variation in development of a transverse orbital ridge (spectacle). **A–B**, *Crocodylus palustris* (NHMUK 1897.12.31.1); **C–D**, *Alligator mississippiensis* (NHMUK 1873.2.21.1); **E–F**, *Caiman latirostris* (NHMUK 1897.12.31.1). Scale bars A–C = 2 cm, all other scale bars = cm.

36. Cranial table ornamentation, fossa on the sutural intersection of the postorbital, frontal and parietal: absent (0); present (1) (after Lee & Yates, 2018 [71]; adapted from Willis et al., 1993).

    A pit that occurs on each side of the skull at the triple junction of the postorbital, parietal and frontal was first described in *Kambara murgonensis* (Willis et al., 1993), and later observed in all species of *Kambara* that preserve the cranial table (Salisbury & Willis, 1996; Buchanan, 2009). These pits are easily distinguished from the characteristic pitted crocodylian dermatocranium by their large size, as well as their paired nature (Fig. 3.9).

37. Skull table morphology: posterolateral edges directed ventrolaterally from the sagittal axis (0); planar across entire length, or lateral edges directed dorsolaterally $<20°$ across entire length (1); lateral edges directed dorsolaterally $\geq 20°$ along entire length (2) (after Brochu, 1997b [123]; Barrios, 2011 [108];

Jouve, 2016 [123]; Cidade et al., 2017 [185]) (ORDERED).

This character is modified from Brochu (1997b, character 123) by the addition of a third character state

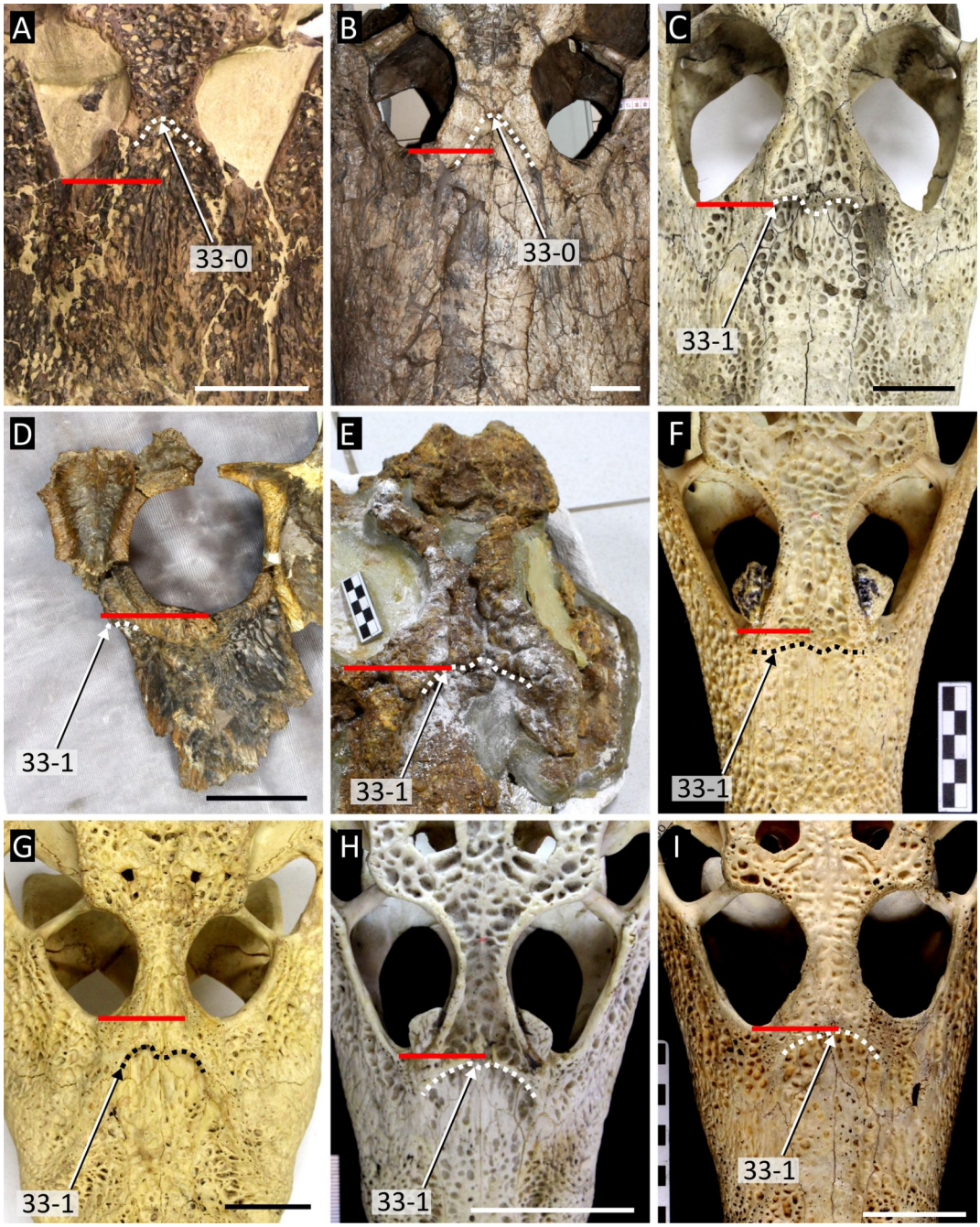



Figure 3.6: Variation in the position of the transverse orbital ridge (spectacle). **A**, *Diplocynodon hantoniensis* (CAMSM TN 907); **B**, *Purussaurus neivensis* (UCMP 39704); **C**, *Melanosuchus niger* (NHMUK 45.8.25.125); **D**, *Mourasuchus atopus* (UCMP 38012); **E**, *Mourasuchus arendsi* (UFAC 5883); **F**, *Caiman crocodilus apaporiensis* (FMNH 69812); **G**, *Caiman latirostris* (NHMUK 1897.12.31.1); **H**, *Caiman crocodilus chiapasius* (FMNH 73701); **I**, *Caiman yacare* (AMNH 97300). Dashed lines mark spectacle position, red line marks anterior margin of orbit. All scale bars = 5 cm.




Figure 3.7: Comparison of the morphology of the naris in **A**, *Alligator mississippiensis* (NHMUK 1873.2.21.1); **B**, *Purussaurus brasiliensis* (UFAC 1403). Scale bar in A = cm, B = 30 cm.

(37-2), and the quantification and ordering of the character states. In occipital view, the skull table of *Bernissartia fagesii* (IRScNB 1538) is approximately planar, with the lateral edges upturned less than 20° (37-1). This condition is common to most eusuchians in this dataset (Fig. 3.10C–F). By contrast, the lateral edges of the cranial table slope ventrally from the sagittal axis in several "gavialoids" (37-0), e.g. *Gavialis gangeticus* (Fig. 3.10A–B) and *Gryposuchus neogaeus* (MLP 26-413), as well as in the non-crocodylian eusuchian *Hylaeochampsa vectiana* (NHMUK R177) (albeit to a lesser degree). Thus far, these observations follow the original scoring of the character as implemented in earlier studies (e.g. Brochu, 1999; Brochu et al., 2012; Salas-Gismondi et al., 2015; Lee & Yates, 2018). However, a third character state is added based on character 185 in Cidade et al. (2017), which appears to describe a continuation of the dorsal upturning of the lateral cranial table edges, which is found in species of *Purussaurus* (37-2, edges orientated $\geq 20°$) (Fig. 3.10G–H). Jouve (2016) also introduced a third state to the same character, which described a skull table that is "medially depressed". This morphology is distinct from the condition in *Purussaurus*; furthermore, it is not considered homologous to the morphology described in this character. As such it is discretised separately as Character 82.

It is possible for Character 37 to be conflated with the presence or absence of squamosal horns (dis-

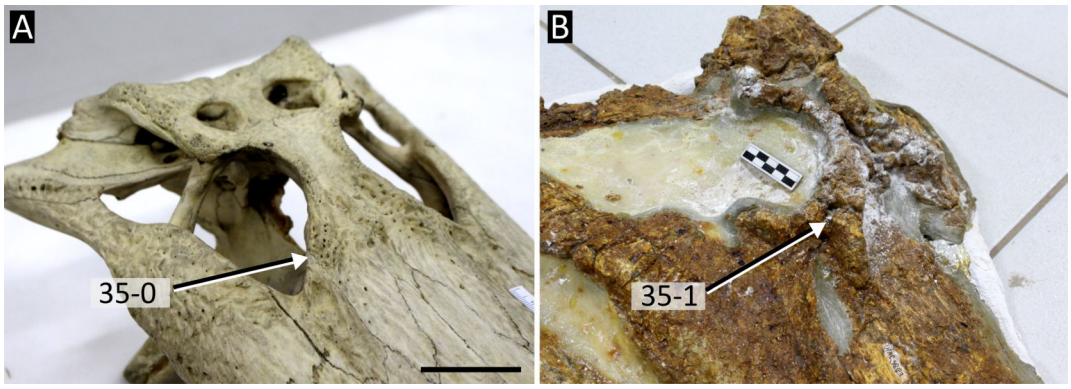



Figure 3.8: Dorsolateral view of the orbit, showing development of a protuberance on the prefrontal in **A**, *Alligator mississippiensis* (NHMUK 1873.2.21.1); **B**, *Mourasuchus arendsi* (UFAC 5883). All scale bars = 5 cm.

crete bony protrusions on the posterior margin of the cranial table, see Characters 38–40). Indeed, in the data matrix of Souza-Filho et al. (2019), *Purussaurus* is scored as having squamosal horns. By contrast, I regard *Purussaurus* as lacking horns, and suggest that Souza-Filho et al. (2019) conflate the broad concavity of the skull table in this taxon (resulting in upturned lateral cranial table margins, Fig. 3.10G–H) with a hypertrophied skull table (true squamosal horns, Fig. 3.11C–H). I regard the curvature of the cranial table and the development of horns as independent. For example, whereas some taxa have squamosal horns and a concave skull table (*Acresuhcus pachytemporalis*, UFAC 2507), others have squamosal horns and a flat skull table (*Certaosuchus burdoschi*, FMNH P 15576) and some species (including *Purussaurus neivensis*, UCMP 39704) lack squamosal horns, but have a concave skull table.

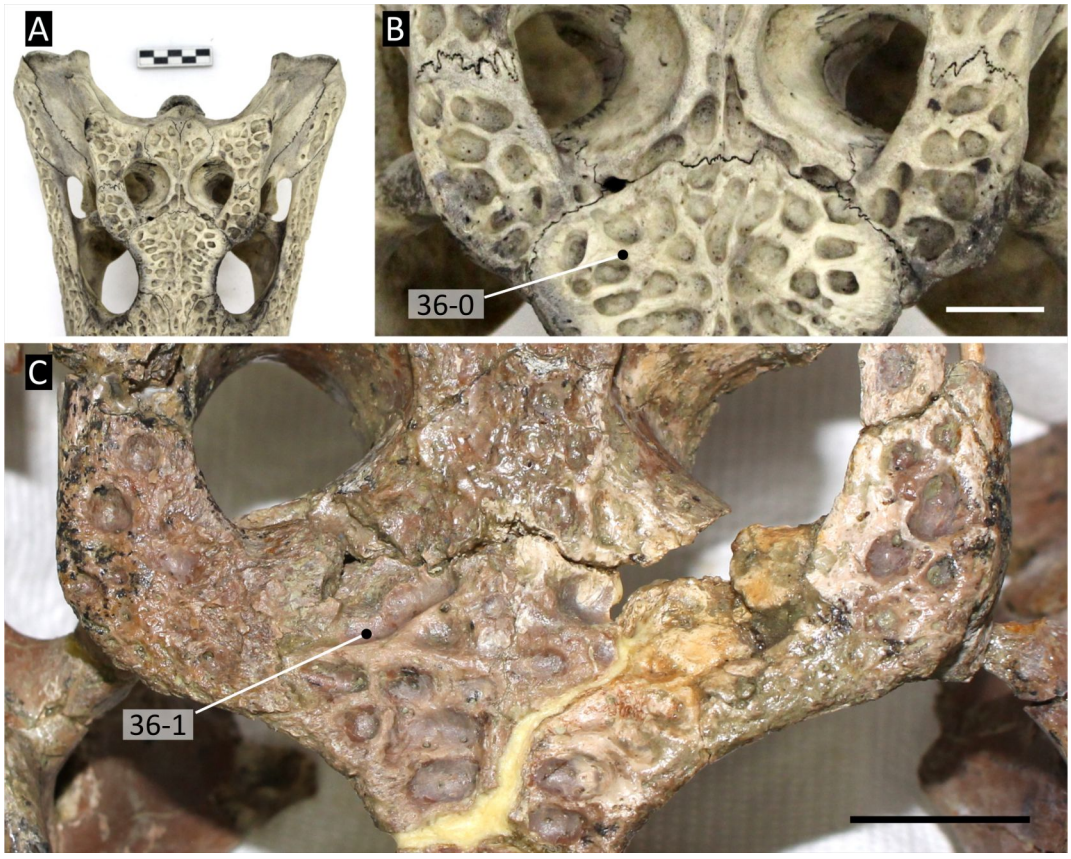



Figure 3.9: Dorsal view of the cranial table in **A**-**B**, *Crocodylus acutus* (NHMUK 1975.997); and **C**, *Kambara implexidens* (QM 29662). Scale bar A = cm, scale bars B, C = 2 cm.

38. Cranial table ornamentation: posterolateral and/or posterior margin of squamosal flat (0); upturned to form a discrete eminence (i.e. a squamosal horn) (1) (after Brochu, 2011 [157]).

39. Cranial table ornamentation, squamosal horn position: restricted to posterior end of skull table (0); extends anteriorly along the whole lateral margin of the skull table (1) (after Salas-Gismondi et al., 2015 [157]; Souza-Filho et al., 2019 [156]).

40. Cranial table ornamentation, direction of squamosal horn expansion from cranial table: dorsally only (0); dorsally and laterally (1) (after Souza-Filho et al., 2019 [156]).

    Squamosal horns are abrupt dorsal/dorsolateral projections of the squamosal (sometimes also including the postorbital) (Fig. 3.11C–H). Among extant crocodylians, squamosal horns are consistently found only in *Crocodylus siamensis* and *Crocodylus rhombifer* (Brochu & Storrs, 2012). Large, overgrown individuals of *Crocodylus* species can also develop a thickening of the lateral margin of the cranial table, which resembles squamosal horns (Brochu et al., 2010). Here these are differentiated from 'true' squamosal horns by having more rounded/ less acute dorsal apices, and by a gradual transition from the anterior end of the skull table to the posterior end. As originally formulated by

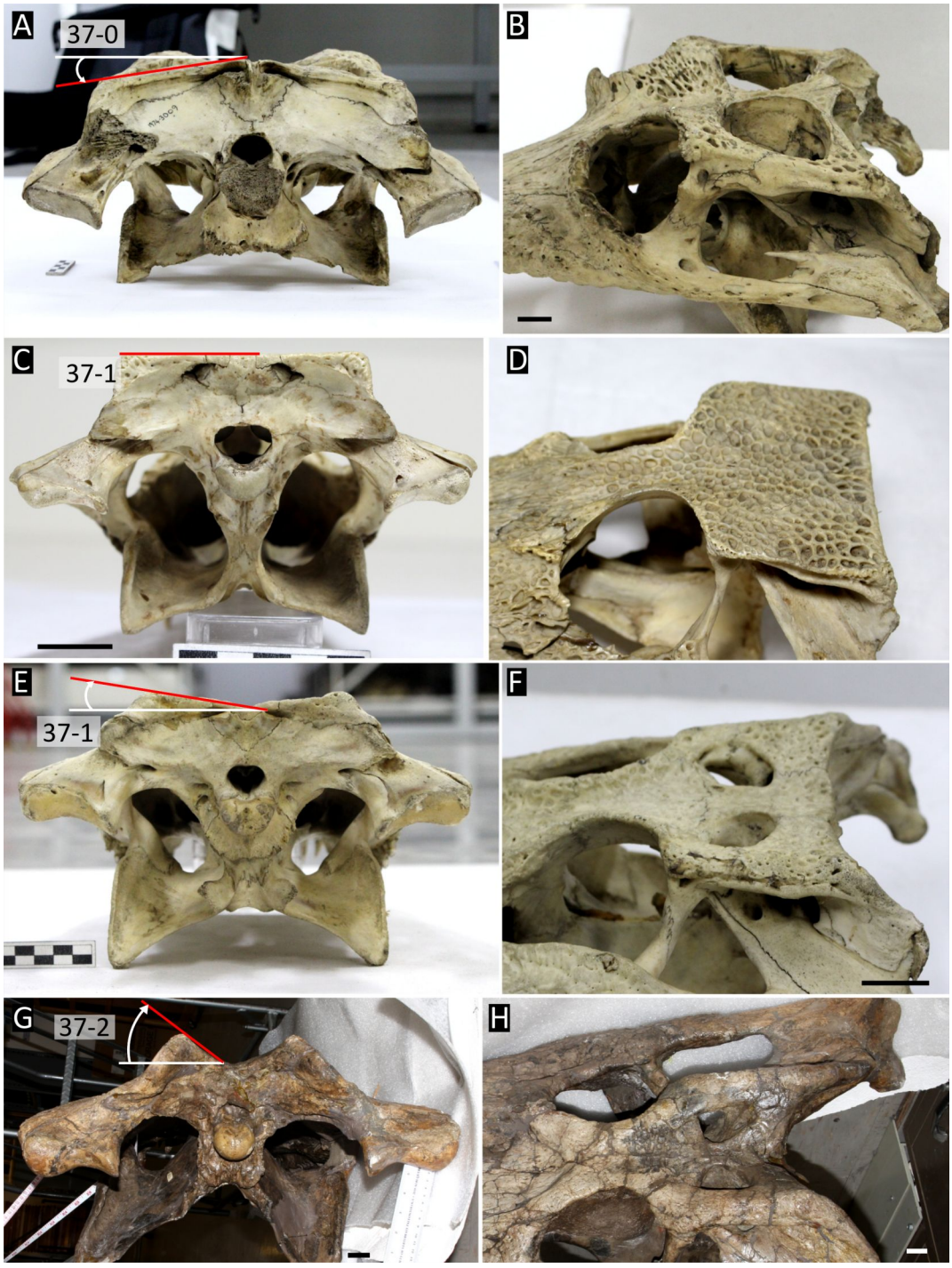



Figure 3.10: Comparisons of cranial table morphology in occipital (left) and dorsolateral (right) views. **A–B**, *Gavialis gangeticus* (NHMUK 1974.3009); **C–D**, *Paleosuchus trigonatus* (NHMUK 1868.10.8.1); **E–F**, *Alligator mississippiensis* (NHMUK 1873.2.21.1); **G–H**, *Purussaurus neivensis* (UCMP 39704). All scale bars = 2 cm.

Brochu (2011), the absence or presence of a squamosal horns is treated as a binary character; however, as illustrated by Souza-Filho et al. (2019, fig.13), squamosal horns can exhibit discrete morphological differences. Characters 38–40 are derived by reductively coding a multistate character (156) in Souza-Filho et al. (2019). Variation in squamosal horn morphology can be broadly divided into: (1) the position of the horn (Character 39); and (2) the direction of the horn's projection (Character 40). In the caimanine *Mourasuchus* the squamosal horns are entirely restricted to the posterior end (39-0) (Fig. 3.11C–D). By contrast, the squamosal horns of *Crocodylus siamensis*, *Crocodylus rhombifer*, *Voay robustus*, *Acresuchus*, and *Ceratosuchus* extend over most of the anteroposterior length of the cranial table, being tallest at the posterior end (39-1) (Fig. 3.11E, G). Whereas *Ceratosuchus* and *Voay* share anteriorly extensive squamosal horns, the horns are dorsally directed in *Ceratosuchus* (40-0) (Fig. 3.11F), but dorsolaterally directed in *Voay* (40-1) (Fig. 3.11H).

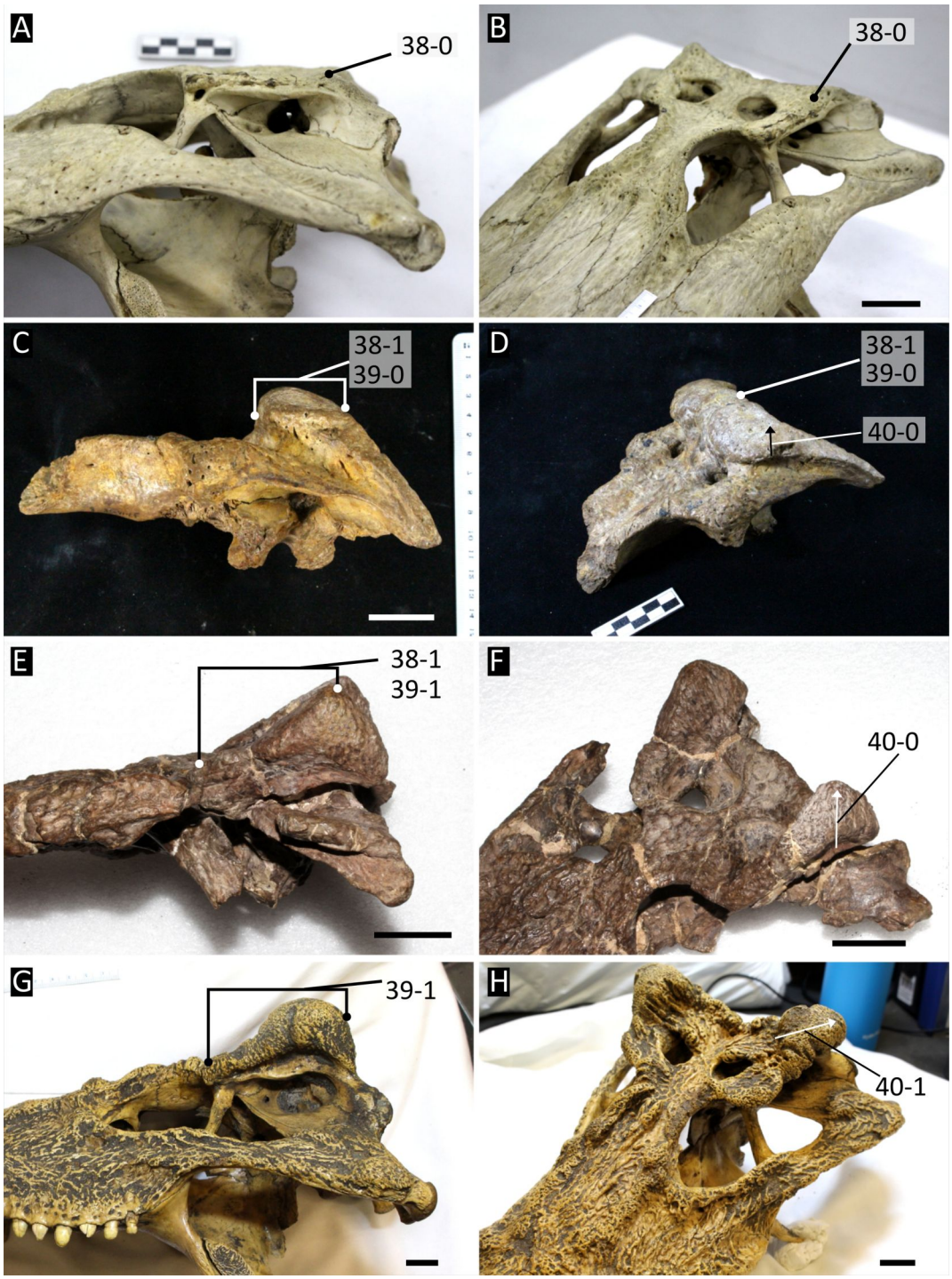



Figure 3.11: Left lateral (left) and dorsolateral (right) views of the cranium showing variation in development of squamosal horns. **A**-**B**, *Alligator mississippiensis* (NHMUK 1873.2.21.1); **C**-**D**, *Mourasuchus arendsi* (MLP 73-IV15-8); **E**-**F**, *Ceratosuchus burdoschi* (FMNH P 15576); **G**-**H**, *Voay robustus* (NHMUK R 366885). All scale bars = 3 cm.

41. External nares, orientation: projects anterodorsally (0); dorsally (1) (after Brochu, 1997b [79]).

    In most crocodylians, the margins of the external naris are approximately in the same plane, resulting in dorsally facing external nares (Fig. 3.12C). By contrast, the anterior and anterolateral margins of the nares in some crocodylians are depressed, resulting in anterodorsally facing nares (Fig. 3.12A–B). Similar to previous studies, anterodorsally facing external nares are herein scored as present in 'basal' alligatorines such as *Navajosuchus* and *Allognathosuchus*, *Borealosuchus* (Fig. 3.12A), and several non-crocodylian taxa (*Bernissartia fagesii*, *Shamosuchus*, *Theriosuchus*, and the 'Glen Rose Form') (Brochu, 1999; Salisbury et al., 2006; Brochu et al., 2012; Jouve, 2016). A number of mekosuchines also exhibit anterodorsally facing nares, such as *Baru wickeni* (QM F16822), *Mekosuchus inexpectatus* (MNHN NCP 06), and *Quinkana* (Megirian, 1994). By contrast with some studies (e.g. Brochu et al., 2012; Jouve, 2016; Lee & Yates, 2018), anterodorsally facing nares are also identified in some species of *Diplocynodon* (e.g. *D. hantoniensis*, Fig. 3.12b, see also Section 2.5.1), and in the osteolaemine, *Voay robustus* (NHMUK R36685).

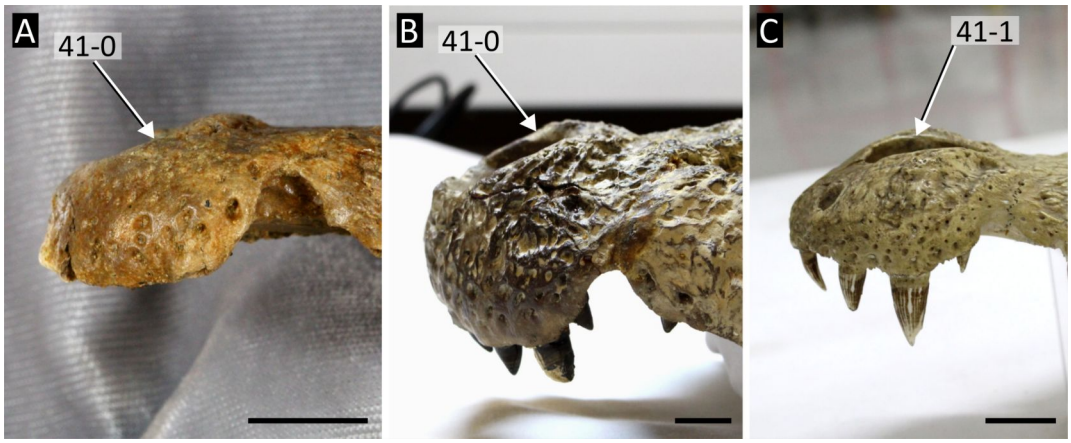



Figure 3.12: Lateral view of the external naris in **A**, *Borelaosuchus sternbergii* (UCMP 126099); **B**, *Diplocynodon hantoniensis* (NHMUK 25166) and **C**, *Crocodylus siamensis* (NHMUK 1921.4.1.168). All scale bars = 2 cm.

42. External nares, development of bony excrescence (ghara) in reproductively mature males: absent (0); present (1) (after Brochu, 2011 [84]).

    The ghara is a bulbous, bony outgrowth on the dorsal margin of the nares. Among extant crocodylians, the ghara is found only in mature, male *Gavialis gangeticus*, where it serves as a resonating chamber (Grigg & Kirshner, 2015) (Fig. 3.13B). It generally occurs in male individuals of at least 3 m total body length; however, smaller individuals (2.4 m) and females in captivity have on occasion exhibited a ghara (Martin & Bellairs, 1977). In osteological specimens, evidence for the ghara occurs as a fossa, delimited by a thin crest anterior to the external nares. In dorsal view, the premaxillae also appear more circular in *Gavialis gangeticus* specimens that have a ghara. This partially obscures the characteristic posteriorly tapering outline of the premaxillae in *Gavialis*. In this study, only taxa known

from at least two large (and therefore mature) crania preserving the nares were scored. The ghara is here recognised only in *Gavialis gangeticus* and *Gryposuchus colombianus*; however, a number of other fossil crocodylians that were not included in this study also possess a ghara including *Gavialis bengawanicus* (Martin et al., 2012) and *Rhamphosuchus crassidens* (Cautley & Falconer, 1840).




Figure 3.13: Dorsal view of the external naris showing development of the ghara in *Gavialis gangeticus*. **A**, NHMUK 61.4.1.2; **B**, NHMUK 1974.3009. Scale bars = cm.

43. External nares, thin crest circumscribing narial margin: absent (0); present (1) (after Brochu, 2011 [85]).

    In most crocodylians the margins of the external nares are flush with the dorsal surface of the premaxilla (Fig. 3.14A). A slightly everted margin of the nares was first described in the 'basal' alligatoroid *Diplocynodon muelleri* (Piras & Buscalioni, 2006), and later recognised in the caimanine *Tsoabichi greenriverensis* (Brochu, 2010) (Fig. 3.14B). A homologous crest is newly recognised in *Diplocynodon tormis* (Buscalioni et al., 1992), *Diplocynodon deponiae* (SMF Me 2609), and occurs variably in *Diplocynodon darwini* (absent in HLMD Me 7500, present in SMNK uncatalogued material). A narial crest was not observed in *Paleosuchus palpebrosus* contrary to character scores in Lee and Yates (2018).

44. Premaxilla, notch posterolateral to naris: absent (0); present (1) (after Brochu, 1997b [142]).

    A sulcus on each side of the rostrum, posterolateral to the external nares, was originally recovered as an unambiguous synapomorphy of *Alligator* (Brochu, 1999) (Fig. 3.14A). This sulcus is often associated with a swelling of the posterolateral margins of the nares. Later analyses identified this sulcus in a larger number of mostly alligatoroid taxa, such as *Arambourgia gaudryi*, *Procaimanoidea utahensis*, and *Brochuchus pigotti* (Brochu, 2011; Brochu et al., 2012). In this study, a posterolateral notch is also recognised in several *Diplocynodon* species, such as *D. hantoniensis* (Section 2.5.1). Furthermore, it

occurs in some *Mourasuchus* species, e.g. *M. atopus* (UCMP 38012) and *M. arendsi* (UFAC 5716). The occurrence of a notch in *Mourasuchus* was also recognised by Cidade et al. (2017), who added a third character state in their analysis to distinguish *Mourasuchus* from all other crocodylians. According to Cidade et al. (2017) *Mourasuchus* has a: "*naris surrounded by a dorsoventrally developed rim*" (Cidade et al., 2017, character 86). However, the morphology of the narial notch in *Mourasuchus* is not notably different to that in *Alligator* (i.e. 44-1), and thus the addition of a third character state is rejected.

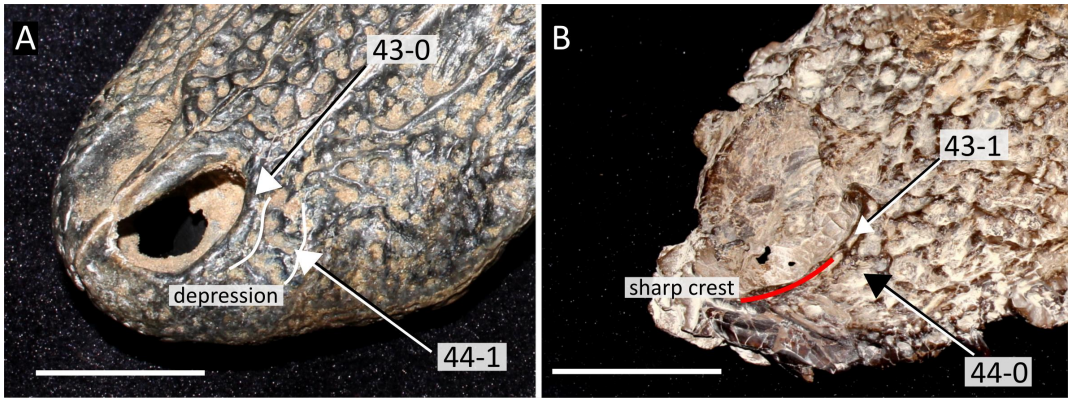



Figure 3.14: Dorsolateral view of the external naris in **A**, *Alligator mcgrewi* (AMNH FAM 7905); and **B**, *Tsoabichi greenriverensis* (AMNH 3666). All scale bars = 2 cm.

45. Premaxilla, fossa on the lateral margin of the naris: absent (0); present (1) (new character, based on personal observations).

    The derived character state applies to three alligatoroid taxa in this analysis: *Brachychampsa montana* (Gilmore, 1911; Norell et al., 1994), *Stangerochampsa mccabei* (Wu et al., 1996), and *Wannaganosuchus brachymanus* (Erickson, 1982). Unlike all other crocodylians, the lateral edges of the nares in these taxa bear a fossa, such that the inner lateral walls of the external nares are bevelled (Fig. 3.15B). The derived condition appears to be incipiently developed in some alligatorids (particularly *Alligator*); however, the condition is not developed strongly enough to be scored for the derived condition.

46. Nasals, external contact with naris: present (0); absent (1) (after Norell, 1988 [3]; Clark, 1994 [13, 14]; Brochu, 1997b [95]).

47. Nasals, bisect nares completely (0); protrude partially into posterior narial margin (1); excluded internally from posterior narial margin (2) (after Norell, 1988 [3]; Clark, 1994 [13, 14]; Brochu, 1997b [95]) (ORDERED).

    Characters 46–48 are derived from reductively coding character 95 in Brochu (1999):

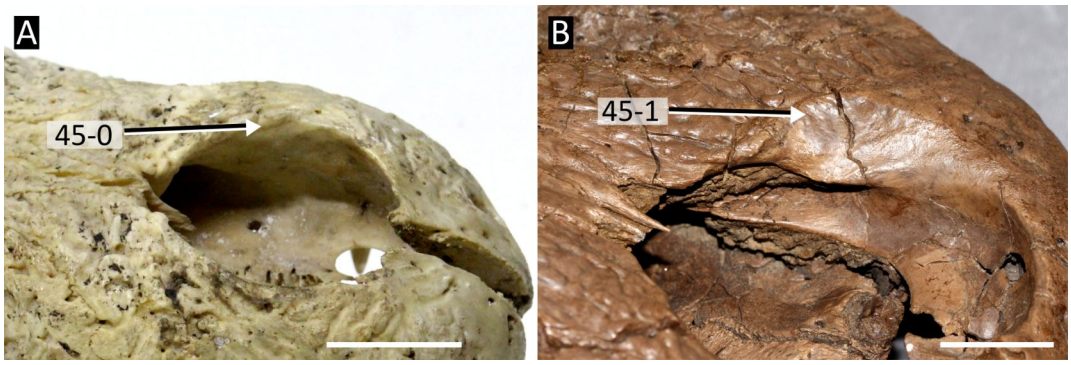



Figure 3.15: Dorsolateral view of the medial wall of the naris in **A**, *Crocodylus niloticus* (NHMUK 1934.6.3.1); **B**, *Brachychampsa montana* (UCMP 133901). All scale bars = 2 cm.

"*External naris bisected by nasals (0) or nasals contact external naris, but do not bisect it (1), or nasals excluded, at least externally, from naris; nasals and premaxillae still in contact (2), or nasals and premaxillae not in contact (3)*"

Whereas Character 46 describes the presence or absence of an external contact between the nares and nasals, Character 47 describes the degree of protrusion of the nasals internally. The distinction between external and internal contact was not accounted for in the original formulation of the character, i.e. some taxa could be scored for both character states 1 and 2 in character 95 of Brochu (1999). For example, *Caiman yacare* (AMNH 97300) and several other *Caiman* species lack an external nasal-naris contact (46-1), but exhibit an internal protrusion on the posterior wall of the naris (47-1). By contrast, *Tomistoma schlegelii* (NHMUK 1894.2.21.1), *Gavialis gangeticus* (NHMUK 1974.3009), and *Diplocynodon hantoniensis* (NHMUK 30392), among other taxa, lack an external (46-1) and internal (47-2) nasal-narial contact.

48. Nasals, contact with premaxillae: overlapping (0); point contact (1); no contact (2) (after Norell, 1988 [3]; Clark, 1994 [13, 14]; Brochu, 1997b [95]; Jouve et al., 2008 [95]) (ORDERED).

The nasals extensively contact the premaxillae on the anterior end of the rostrum in almost all crocodylians, being wedged between the posterodorsal processes of the premaxillae (Fig. 3.16A–F). An exception to this occurs in *Gavialis*, in which the nasals terminate anterior to the mid-length of the rostrum (Fig. 3.16I). An intermediate condition was recognised by Jouve et al. (2008, C95-3) in several longirostrines, who described this as a "weak contact" between the premaxilla and nasals. This condition is incorporated here, but as part of an ordered multistate character describing the progressive separation of the nasals from the premaxillae. The original description as "weak" is replaced with "point contact" here, which is more precise. Taxa scored for character state 48-1 are mostly longirostrines such as *Piscogavialis jugaliperforatus* (Fig. 3.16G), *Ikanogavialis gameroi* (Sill, 1970) and *Gryposuchus neogaeus* (Fig. 3.16H). By contrast to the character scores in Jouve (2016), the condition in

*Thoracosaurus isorhynchus* (MNHN 1902.22; MNHN.F.MTA 61) and *Thoracosaurus neocesariensis* (multiple specimens in AMNH, YPM) is scored as missing, and *Eothoracosaurus mississippiensis* (Brochu, 2004a) is considered to exhibit an extensive premaxilla-nasal contact (48-0). Furthermore, two brevirostrine taxa (*Purussaurus mirandai* [Aguilera et al., 2006] and *Purussaurus brasiliensis* [UFAC 1403]) are scored for the intermediate condition here, which is related to the peculiar development of an extensive narial opening in these taxa (see Character 34).

49. Premaxilla-maxilla suture, anterior limit relative to posterior margin of external naris: posterior to (0); level with or anterior to (1) (after Jouve et al., 2008 [198]).

    The anterior limit of the premaxilla-maxilla suture on the dorsal surface of the rostrum typically coincides with the level of the pit or notch for the $4^{th}$ dentary tooth. The anterior extent of this suture varies with respect to the posterior margin of the external naris. In most crocodylians, the anteriormost extent is posterior to the naris (Fig. 3.17G–I), but a large number of taxa (almost exclusively alligatorids) have an anteriorly positioned suture (Fig. 3.17A). By contrast to previous studies (Jouve, 2016; Iijima & Kobayashi, 2019), the derived condition is also recognised in some crocodylid species (Fig. 3.17D–F), such as *Crocodylus palaeindicus* (NHMUK 39795), *Crocodylus palustris* (NHMUK 1897.12.31.1), and variably in *Crocodylus porosus* (e.g. present in NHMUK 1852.12.9.2, absent in QM J47447).

50. Premaxilla, posterior extent of dorsal process: terminating level with or anterior to the third maxillary alveolus (0); extending posterior to third maxillary alveolus (1) (after Brochu, 1997b [145]).

    The length of each posterodorsal premaxillary process is characterised as originally formulated by Brochu (1997b). Long processes, exceeding the level of the $3^{rd}$ maxillary alveoli, are commonly found in longirostrine crocodylians, including all putative "tomistomines" and "gavialoids" (Fig. 3.17B). By contrast, in *Bernissartia fagesii* (IRScNB 1538), as well as most crocodyloids and alligatoroids, the posterodorsal processes are short, at most reaching the level of the $3^{rd}$ maxillary alveolus (Fig. 3.17A).

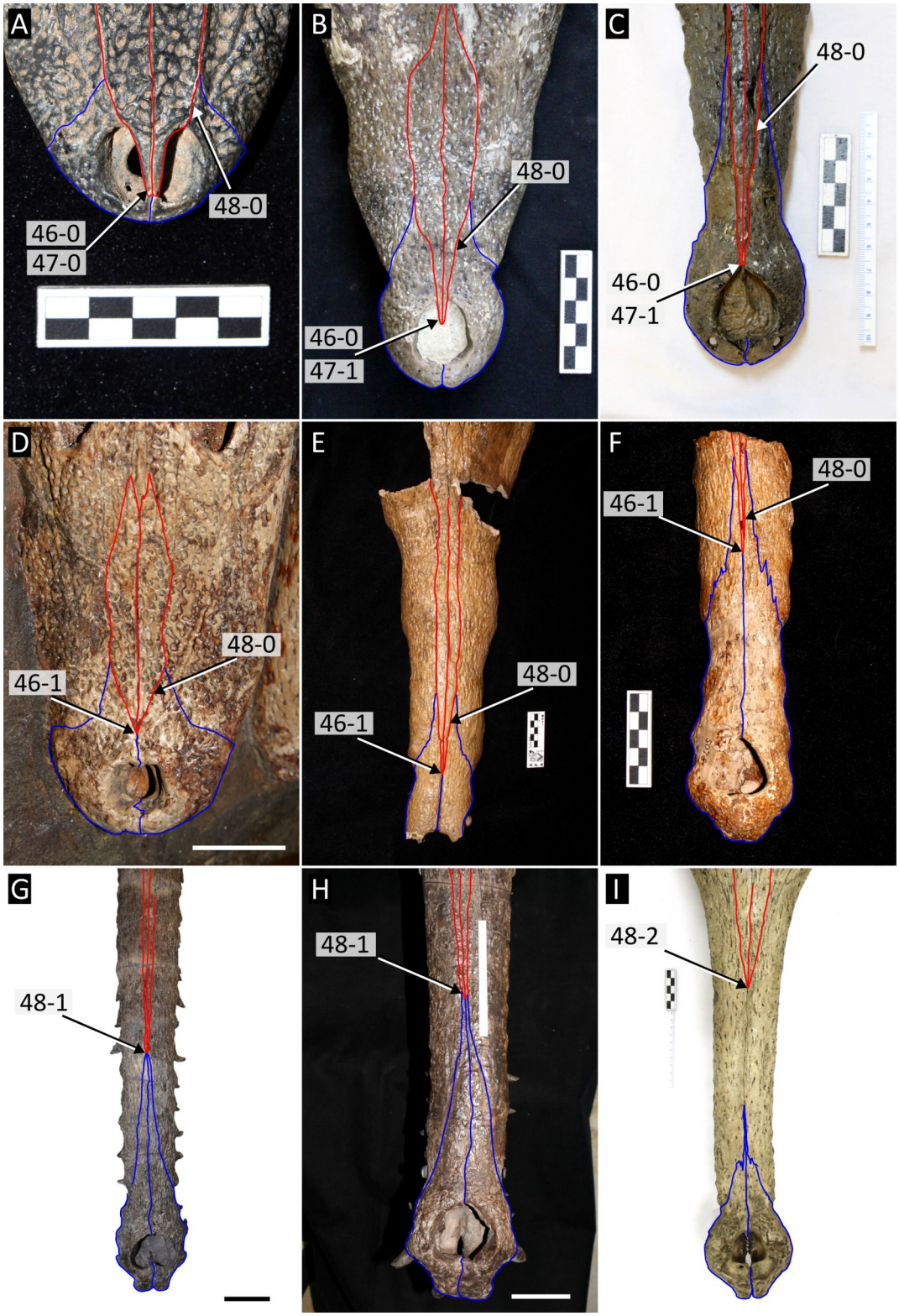



Figure 3.16: Morphology of the nasal-premaxilla suture. **A**, *Alligator mcgrewi* (AMNH FAM 7905); **B**, *'Crocodylus' affinis* (USNM 18171); **C**, *Kentisuchus spenceri* (NHMUK 38975); **D**, *Diplocynodon darwini* (HLMD-Me-7492); **E**, *Thecachampsa antiquus* (AMNH 5663); **F**, *Eogavialis africanum* (AMNH 5075); **G**, *Piscogavialis jugaliperforatus* (SMNK 1282 PAL); **H**, *Gryposuchus neoagaeus* (MLP 26-413); **I**, *Gavialis gangeticus* (NHMUK 1974.3009). Red = nasals, blue = premaxillae. All scale bars = 5 cm.




Figure 3.17: Dorsal view of the rostrum in crocodylian taxa showing variation in position of the premaxilla-maxilla suture (red line) relative to the posterior margin of the naris (blue line). **A**, *Alligator sinensis* (NHMUK X184); **B**, *Tomistoma schlegelii* (NHMUK 1894.2.21.1); **C**, *Crocodylus niloticus* (NHMUK 1934.6.3.1); **D**, *Crocodylus porosus* (NHMUK 1852.12.9.2); **E**, *Crocodylus palustris* (NHMUK 1897.12.31.1); **F**, *Crocodylus palaeindicus* (NHMUK 39795); **G**, *Crocodylus acutus* (NHMUK 1975.997); **H**, *Crocodylus moreletii* (NHMUK 1861.4.1.4); **I**, *Mecistops cataphractus* (NHMUK 1924.5.10.1). All scale bars = 5 cm.

51. Maxilla, linear array of pits (cecal recesses) on lateral margin of narial canal: absent (0); present (1) (after Brochu, 1997b [148]).

    As discussed by Brochu (2000), the lateral walls of the narial canal (caviconchal recess) are lined with a series of pits in all extant species of *Crocodylus* (Fig. 3.18B), but are smooth in all other crocodylians (Fig. 3.18A). The presence or absence of cecal recesses can only be scored in well preserved and disarticulated maxillae or from CT scan data.

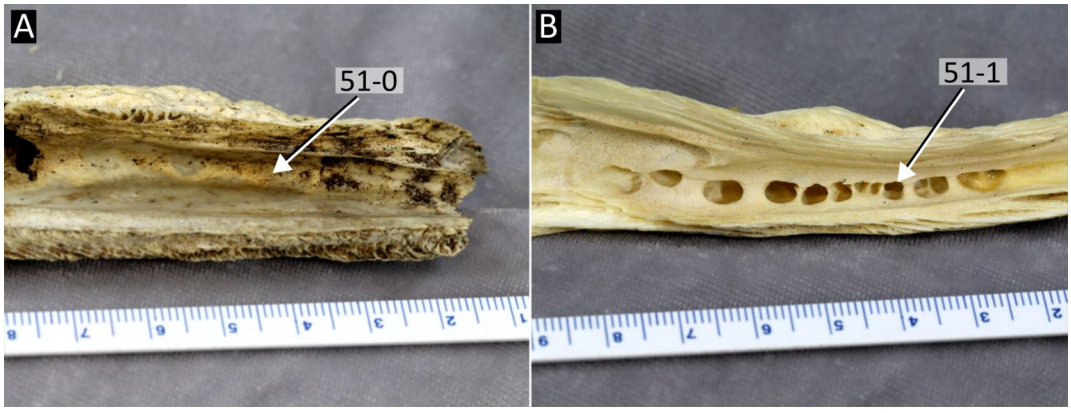



Figure 3.18: Medial view of the narial canal lateral wall in **A**, *Alligator mississippiensis* (UCMP 71672); **B**, *Crocodylus acutus* (UCMP 81699). Scale bars = cm.

52. Maxilla, posterior extent relative to anterior margin of postorbital bar: terminates anterior to the level of the postorbital bar (0); level with or posterior to the postorbital bar (1) (after Brochu, 2011 [105]).

    The anatomical meaning of this character remains unchanged from Brochu (2011); however, the character has been rephrased to use the postorbital bar instead of the lower temporal bar as a more precise landmark for the posterior extent of the maxilla. In earlier studies (e.g. Brochu, 2011; Brochu et al., 2012; Jouve, 2016; Salas-Gismondi et al., 2019) the derived condition was only scored as present in *Hylaeochampsa vectiana* (Clark & Norell, 1992) (Fig. 3.19B), *Iharkutosuchus makadii* (Ősi et al., 2007), *Acynodon iberoccitanus* (Buscalioni et al., 1997), and *Acynodon adriaticus* (Delfino et al., 2008b). A number of additional taxa have been scored for the derived state in this study including *Portugalosuchus azenhae* (Mateus et al., 2019), *Gavialis gangeticus* (NHMUK 1974.3009) (Fig. 3.19D), *Gavialis lewisi* (YPM 3226), *Gavialis browni* (AMNH 6279), and *Trilophosuchus rackhami* (QM F16856). Although *Gavialis* and *Hylaeochampsa* share the derived condition, there are subtle differences in their morphologies. Whereas the maxilla is positioned more on the ventral side of the lower temporal bar in *Gavialis*, the maxilla is more laterally exposed in *Hylaeochampsa*. However, this difference is too small, and not consistently found in enough taxa in the present analysis to warrant the addition of another character state here.

53. Lacrimal, sutural contact with nasal: present (0); absent (1) (after Brochu, 1997b [93]).

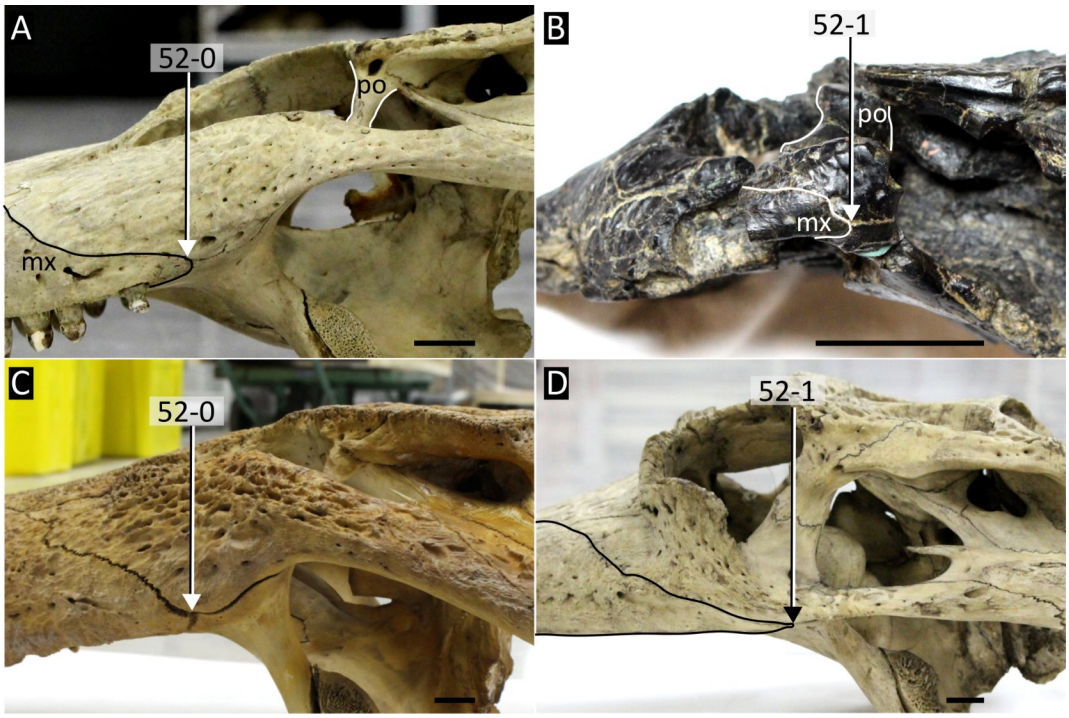



Figure 3.19: Variation in posterior extent of the maxilla. Lateral view of **A**, *Alligator mississippiensis* (NHMUK 1873.2.21.1); **B**, *Hylaeochampsa vectiana* (NHMUK PV R 177); **C**, *Tomistoma schlegelii* (NHMUK 1894.2.21.1); **D**, *Gavialis gangeticus* (NHMUK 1974.3009). Abbreviations: **mx**, maxilla; **po**, postorbital bar. All scale bars = 3 cm.

54. Maxilla, posterior process in the lacrimal: absent (0); present (1) (after Brochu, 1997b [93]).

55. Maxilla, posterior process extends between lacrimal and prefrontal: absent (0); present (1) (after Brochu, 1997b [93]).

56. Maxilla, posterior process extends between nasal and lacrimal: absent (0); present (1) (after Brochu, 1997b [93]; Jouve et al., 2008 [93]; Jouve, 2016 [93]).

    Characters 53–56 are derived from Character 93 in Brochu (1997b) and later modifications to the character (Jouve et al., 2008 [93]; Jouve, 2016 [93]). Brochu (1997b) originally formulated the character as follows:

    "*Lacrimal makes broad contact with nasal; no posterior process of maxilla (0), or maxilla with posterior process within lacrimal (1), or maxilla with posterior process between lacrimal and prefrontal (2)*"

    Jouve (2016) added a fourth character state, which described a process "*between the lacrimal and nasal*".

    As originally worded, this character suggests that contact between the nasal and lacrimal, as well as a posterior process of the maxilla in the lacrimal are mutually exclusive. However, both conditions are

commonly present in crocodylians. For example in all datasets examined here, *Caiman* are characterised as sending a posterior process of the maxilla into the lacrimal (Brochu, 1999; Jouve et al., 2008; Brochu et al., 2012; Jouve, 2016; Cidade et al., 2017; Lee & Yates, 2018; Iijima & Kobayashi, 2019); however, most *Caiman* species also exhibit contact between the lacrimal and nasal (Fig. 3.20C). The choice to include *Caiman* under character state 1 in previous studies is probably based on the short length of the nasal-lacrimal contact; however, the length of the nasal-lacrimal suture in some *Caiman* species can be equal to that of some *Crocodylus* species, which have a broad lacrimal nasal contact (Fig. 3.20A). In addition, there are some taxa which lack a nasal-lacrimal sutural contact, but still retain a posterior maxillary process in the lacrimal (e.g. *Purussaurus neivensis*, UCMP 39704). In this study, the presence of a lacrimal-nasal contact is not considered homologous to the development of any process in or between the lacrimal, prefrontal, or nasal. As such, a new character has been formulated which describes the presence or absence of a lacrimal-nasal sutural contact (Character 53). Additional issues concern the homology of the posterior processes between the lacrimal, prefrontal and nasals that are implied in the original character. Some taxa, such as '*Caiman* cf. *lutescens*' (UCMP 39978) and the 'Glen Rose form' (USNM 22039), possess both a posterior process of the maxilla in the lacrimal and a posterior process between the lacrimal and prefrontal. As a result, these features have been discretised in separate characters here. Furthermore, the posterior maxillary process between the lacrimal and nasal is not homologous to the posterior maxillary process in the lacrimal, because both are present in *Thecachampsa sericodon* (Fig. 3.20F).

57. Lacrimal, mediolateral width in relation to prefrontal: equal to or greater than twice the maximum prefrontal width (0); less than twice the maximum prefrontal width (1) (after Jouve, 2016 [242]).

    This character was rephrased to improve repeatability of scoring from "*lacrimal nearly twice wider (0) or nearly as wide as the prefrontal (1)*" in Jouve (2016). The mediolateral widths of the prefrontal and lacrimal are approximately equidimensional in most crocodylians, e.g. *Crocodylus porosus* (Fig. 3.20A) and *Alligator mississippiensis* (Fig. 3.20B). Extremely widened lacrimals, usually greater than twice the width of the prefrontals, are present in most extant caimanines (Fig. 3.20C), such as *Melanosuchus niger* (NHMUK 45.8.25.125), *Caiman yacare* (AMNH 97300), and *Paleosuchus trigonatus* (NHMUK 1868.10.8.1), as well as some "tomistomines" such as *Thecachampsa sericodon* (USNM 25243). By contrast to previous studies (e.g. Jouve, 2016; Iijima & Kobayashi, 2019), the width of the lacrimals in *Brachychampsa montana* (UCMP 133901, Fig. 3.20D), *Tomistoma schlegelii* (1894.2.21.1), *Tomistoma lusitanica* (Antunes, 1961), and *Maroccosuchus zennaroi* (Jouve et al., 2015), is not found to be significantly greater than that of the prefrontals.

58. Lacrimal, anteroposterior length relative to that of prefrontal: longer (0); equal in length (1); shorter (2) (after Norell, 1988 [7]; Brochu, 1997b [117]) (ORDERED).

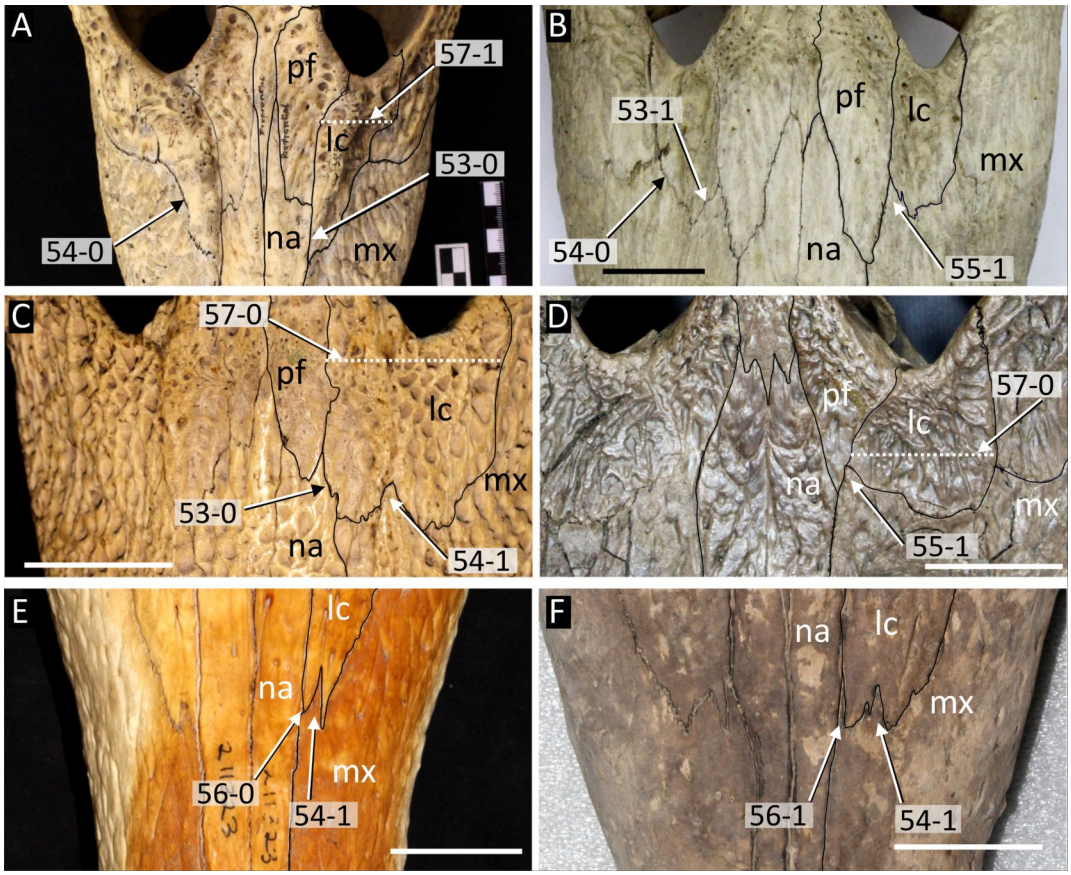



Figure 3.20: Dorsal view showing sutural relationships of the rostrum in selected crocodylian taxa. **A**, *Crocodylus porosus* (QM J47447); **B**, *Alligator mississippiensis* (NHMUK 1873.2.21.1); **C**, *Caiman yacare* (MACN uncatalogued); **D**, *Brachychampsa montana* (UCMP 133901); **E**, *Tomistoma schlegelii* (USNM 211323); **F**, *Thecachampsa sericodon* (USNM 25243). Abbreviations: **lc**, lacrimal; **mx**, maxilla; **na**, nasal; **pf**, prefrontal. All scale bars = 5 cm.

This character has been restructured and rephrased from Brochu (1997b) to enable the character to be ordered. In most crocodylians, the lacrimal is much longer than the prefrontal (Fig. 3.21G), some taxa (mostly alligatorids) exhibit a clearly shorter lacrimal than the prefrontal (Fig. 3.21I), and a small number have a lacrimal and prefrontal that are sub-equal in length (Fig. 3.21H). The latter condition was previously found only in *Borealosuchus* species, such as *B. formidabilis* (Erickson, 1976), *B. acutidentatus* (Sternberg, 1932), and *B. wilsoni* (Mook, 1959b) (Brochu, 1997a; Brochu et al., 2012). This intermediate condition is newly recognised in a number of additional species, such as *Kentisuchus spenceri* (NHMUK 38975), *Baru wickeni* (QM 16822), and *Acresuchus pachytempralis* (UFAC 2507).

59. Prefrontals, sutural contacts (at maturity): separated by frontal and nasals (0); prefrontals meet medially (1) (after Norell, 1988 [27]; Brochu, 1997b [100]).

Whereas the prefrontals are separated by the frontal and nasals in most crocodylians (Fig. 3.21A), they are sutured in some caimanine taxa, blocking the anterior frontal process from the nasals (Fig.

3.21C). For example, *Caiman yacare* exhibits inter-prefrontal contact consistently at maturity (AMNH 97300, MACN uncatalogued, FMNH 9141) (Medem, 1960). By contrast it appears to occur variably in *Caiman latirostris* (present in NHMUK 86.10.4.2, absent in FMNH 9713, MACN V 1420).

60. Frontal, anterior process morphology: forms an acute, 'v' shape that extends anteriorly into posterior margins of nasals (0); forms broad sutural contact with the nasals or prefrontals (1) (after Brochu, 2011 [131]; Salas-Gismondi et al., 2015 [131]).

    The anterior tip of the frontal process forms an acute point in most crocodylians, regardless of whether it contacts the nasals. By contrast, a number of crocodylians exhibit a broader (sometimes undulating) frontal process. The modification to character wording by Salas-Gismondi et al. (2015) is followed here, which recognises that the frontal might or might not contact the prefrontals. The derived condition is present in several alligatoroids, including *Brachychampsa montana* (Fig. 3.21D), *Mourasuchus atopus* (Fig. 3.21E), *Purussaurus neivensis* (Fig. 3.21C), as well as some species of *Mekosuchus*, e.g. *M. sanderi* (QM F31166).

61. Frontal, position of tip of anterior process relative to anterior tip of prefrontal: posterior or at the same level (0); anterior (1) (after Jouve, 2004 [172]; Jouve et al., 2008 [171])

62. Frontal, position of tip of anterior process relative to anterior orbital margin: anterior (0); level with or posterior (1) (after Jouve, 2004 [178]; Jouve et al., 2008 [175]).

63. Jugal, anterior extent relative to anterior tip of frontal: anterior to or level with frontal (0): posterior to frontal (1) (after Jouve, 2004 [177]; Jouve et al., 2008 [174]; Jouve, 2016 [174]).

    Characters 61–63 were introduced by Jouve (2004), and describe variation in the anterior extent of the frontal relative to the prefrontal, orbit, and jugal respectively. Characters 61 and 63 have been modified by the removal of a character state. Character 61 was originally formulated with an additional state in which the frontal reached the same level as the prefrontal (Jouve, 2016). This condition is not practical to score as the frontal rarely lies precisely at the same level as the prefrontal. For example, *Euthecodon arambourgi* (MNHN ZEL 001) was scored for this condition by Jouve (2016) but the frontal extends anterior to the prefrontal in that taxon.

    As originally formulated by Jouve (2004), Character 63 had an additional character state which described a condition whereby the jugal does not extend beyond the anterior margin of the orbit. This condition was only scored in *Iharkutosuchus makadii* and *Hylaeochampsa vectiana* in a more recent iteration of this data matrix (Jouve, 2016). This state has been removed here because the condition is absent in *Hylaeochampsa* (NHMUK R177, Clark & Norell, 1992) rendering it as an uninformative autapomorphy of *Iharkutosuchus*. As such *Iharkutouchus* is scored as 63-1 here along with other crocodylian taxa.

It might appear that these characters describe the same anatomical feature, namely the length of the anterior frontal process, and that taxa with a 'long' frontal process might receive the same scores for each of these characters i.e. 61-1, 62-0, and 63-1. However, these characters are scored with different combinations in several taxa, reflecting their independence. For example many crocodylians have a frontal process that exceeds the anterior margin of the orbits (62-0). This is the case in *Brachychampsa montana* and *Gavialis gangeticus*; however, whereas the frontal process is anterior to the prefrontal tip in *Gavialis* (61-1) (Fig. 3.21F), it is posterior to the prefrontal tip in *Brachychampsa* (61-0) (Fig. 3.21D). Similarly, if the frontal exceeds the anterior margin of the prefrontal, it does not necessarily exceed the jugal anterior tip. This is the case in *Navajosuchus mooki* (AMNH 5186) and *Gavialosuchus eggenburgensis* (NHMUK PV R797), which share an anterior frontal tip that extends beyond the level of the prefrontal (61-1), but not the jugal (63-0).

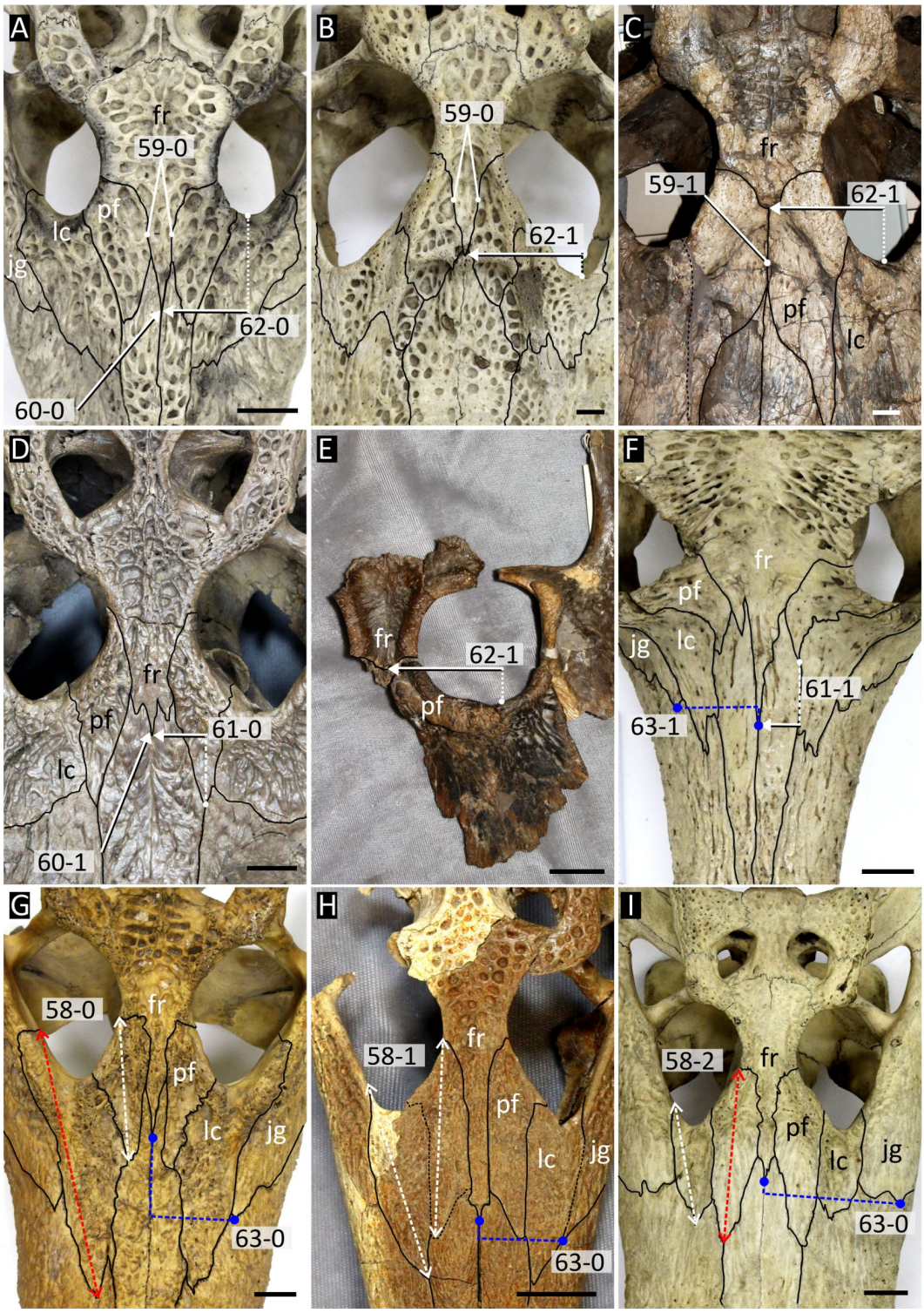



Figure 3.21: Preorbital sutural relationships in selected crocodylian taxa. **A**, *Crocodylus acutus* (NHMUK 1975.997); **B**, *Melanosuchus niger* (NHMUK 45.8.25.125); **C**, *Purussaurus neivensis* (UCMP 39704); **D**, *Brachychampsa montana* (UCMP 133901); **E**, *Mourasuchus atopus* (UCMP 38012); **F**, *Gavialis gangeticus* (NHMUK 1974.3009); **G**, *Tomistoma schlegelii* (NHMUK 1894.2.21.1) **H**, *Borealosuchus sternbergii* (UCMP 126099); **I**, *Alligator mississippiensis* (NHMUK 1873.2.21.1). Abbreviations: **fr**, frontal; **jg**, jugal; **lc**, lacrimal; **pf**, prefrontal. All scale bars = 2 cm.

64. Prefrontal, linear sulcus adjacent to medial orbital margin: absent (0); present (1) (new character, after Delfino et al., 2005)

    Delfino et al. (2005) described a "step-like" structure on the prefrontal, forming the medial margin of the orbit in *Eosuchus lerichei* (Fig. 3.22C). This step is the result of a linear sulcus which runs adjacent to the medial orbital margin, and this feature is newly recognised here in *Eosuchus minor* (USNM 321933) and *Thoracosaurus isorhynchus* (MNHN.F.MTA 61) (Fig. 3.22B).

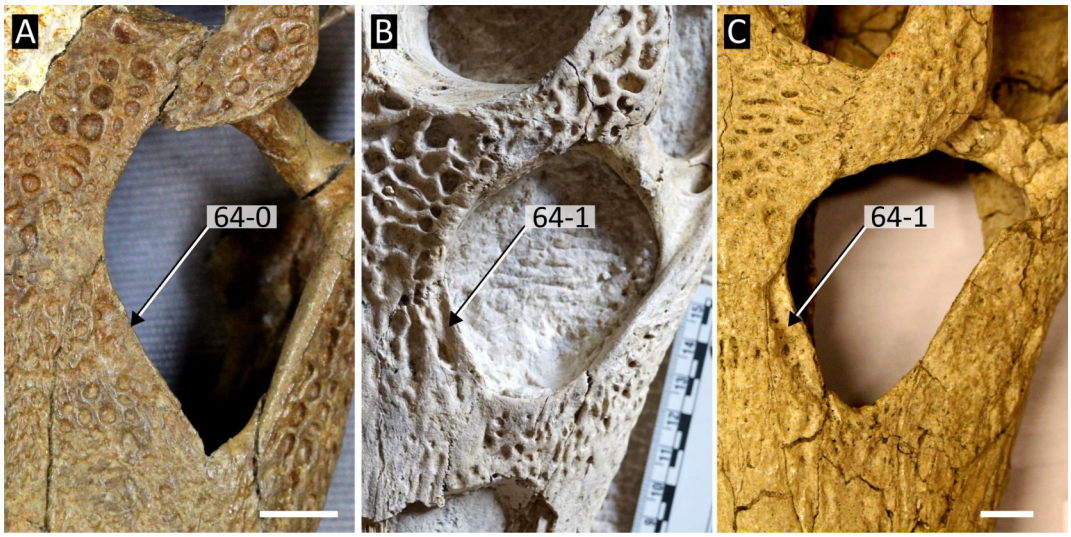



Figure 3.22: Dorsal view of the orbit in **A**, *Borealosuchus sternbergii* (UCMP 126099); **B**, *Thoracosaurus isorhynchus* (MNHN.F.MTA 61); **C**, *Eosuchus lerichei* (IRSNB R 49). Scale bar in A and C = 1 cm, B = cm.

65. Jugal, suture with lacrimal: long, widely separating maxilla from orbital margin (0); point contact, narrowly separating maxilla from orbital margin (1); jugal-lacrimal contact absent, maxilla contributes to orbital margin (2) (after Willis 1997, 2001; Lee & Yates 2018 [38]) (ORDERED).

    In nearly all crocodylians, the maxilla is distantly separated from the orbital margin by the jugal and lacrimal (Fig. 3.23B). By contrast, the maxillae of *Mekosuchus inexpectatus* (MNHN NCP 06), *Mekosuchus sanderi* (QM F31188) (Fig. 3.23D), and *Mekosuchus whitehunterensis* (QM F31051) form a small portion of the lateral orbital margin (Willis, 2001). The orbital contribution of the maxilla can be challenging to recognise in these taxa due to the nature of their preservation as isolated elements; however, the orbital contribution is evidenced by a short, suture-free length of the maxillary dorsal outline (Fig. 3.23D). *Trilophosuchus rackhami* (QM F16856) exhibits an intermediate condition (65-1), in which the jugal and lacrimal have a point contact that narrowly separates the maxilla from the orbit (Willis, 1997a) (Fig. 3.23C). As such, this character is ordered here.

66. Prefrontal pillar morphology: dorsal half of pillar narrow, less than twice minimum anteroposterior length (0); equal to or greater than twice minimum anteroposterior length (1) (after Norell, 1988 [41]; Brochu, 1997b [137]).

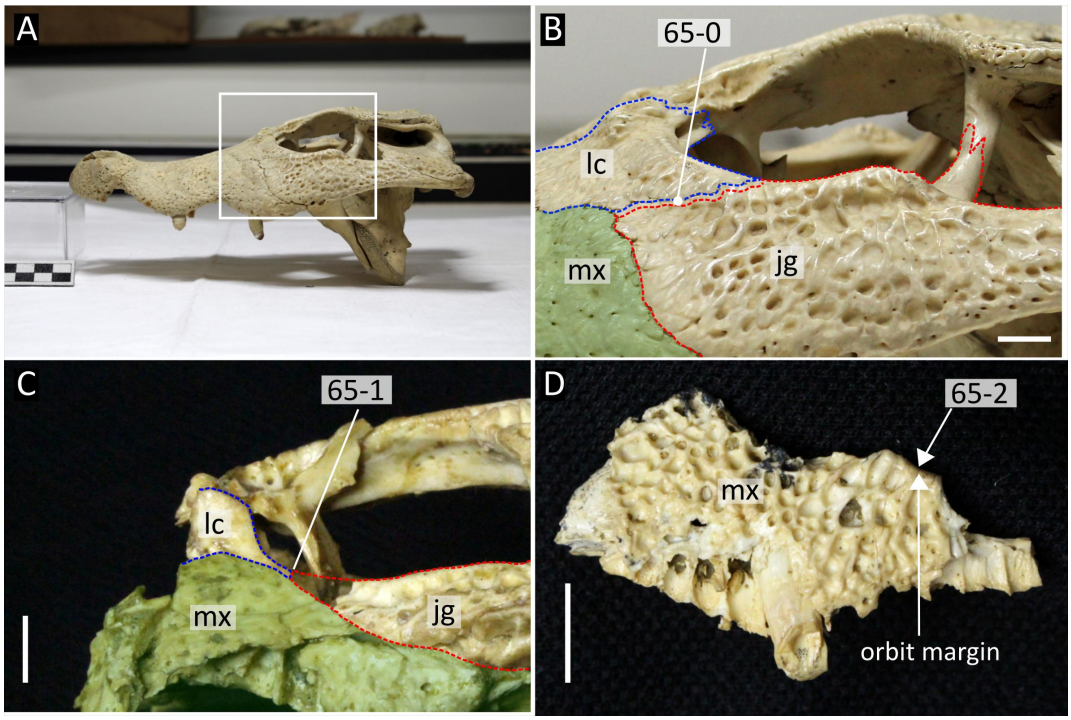



Figure 3.23: Variation in extent of jugal-lacrimal contact in crocodylian taxa. **A–B**, *Osteolaemus tetraspis* (NHMUK 1862.6.30.5); **C**, *Trilophosuchus rackhami* (QM F16856); **D**, *Mekosuchus sanderi* (QMF 31188), left maxilla in lateral view showing maxilla contribution to orbital margin. Blue and red dashed lines outline the lacrimal (**lc**) and jugal (**jg**) bones respectively. Green shading shows position of the maxilla (**mx**). All scale bars = 1 cm.

In most crocodylians, the dorsal half of the prefrontal pillar is anteroposteriorly expanded, such that in transverse section the pillar appears to be flared (66-1). This is visible in CT scan data (Brochu, 1999, fig.53B) and sometimes externally too (Fig. 3.24B). This character has received modification to the original wording of Brochu (1997b) by quantifying the degree of expansion to improve the consistency of scoring. Previous studies have traditionally scored "gavialoids" (e.g. *Gavialis gangeticus*, Fig. 3.24A) as having the narrow condition (i.e. 66-0). Here, the flared condition is newly recognised in several "gavialoids", including *Eogavialis africanum* (YPM 6263), and *Eosuchus lerichei* (IRScNB R49).

67. Prefrontal pillar, morphology of medial processes, long axis orientation: dorsoventrally (0); anteroposteriorly (1) (after Brochu, 1997b [136]).

The medial surface of each prefrontal pillar contacts its counterpart via a distinct ventromedial projection, referred to as a medial process. These processes are seldom preserved and often obscured by matrix. When preserved, the articular facet of the medial process is usually anteroposteriorly expanded (67-1) (Fig. 3.24C, F, I). Less commonly, the medial processes are dorsoventrally expanded (67-0) (Fig. 3.24A, B, G, H). Following previous studies, the anteroposteriorly expanded condition has

been observed in all crocodyloids (where preserved), and extant species of *Alligator*. By contrast to scores in previous studies (e.g. Brochu, 1999; Brochu et al., 2012), *Tomistoma schlegelii* (Fig. 3.24B) and some caimanines (e.g. *Caiman yacare*, Fig. 3.24G) and *Paleosuchus trigonatus*, Fig. 3.24H), are herein found to exhibit the dorsoventrally expanded condition. The condition in *Hylaeochampsa vectiana* is also changed from being dorsoventrally expanded to unknown, as this portion of anatomy is not well enough preserved (NHMUK R177).

68. Prefrontal pillar internal morphology: solid (0); with pneumatic recess (1) (state 1 is synonymous with the prefrontal recess of Witmer, 1997) (after Brochu, 1997b [99]).

    In most crocodylians, the prefrontal pillar is a solid vertical bar that descends from the skull roof to contact the palatines and pterygoids. In *Alligator mississippiensis* the prefrontal pillar is hollow, as evident from CT data (Brochu, 1999, fig.53). However, CT data is not always required to score this character, as the hollow condition is associated with a discernible inflation of the prefrontal pillar that is visible externally (Fig. 3.24I). For example, the fossil alligatorid *Alligator mcgrewi* is scored as having a pneumatic recess (68-1) based on the inflation of the prefrontal pillars in AMNH FAM 8700.

69. Prefrontal pillar, morphology of medial process at base of pillar: wide (0); constricted (1) (after Brochu, 1997b [138]).

    The ventral margin of the prefrontal medial process bears a notch in most crocodyloids, giving a dorsoventrally constricted appearance to the medial process (69-1) (Fig. 3.24F). This constriction is absent in all alligatoroids and gavialoids, where preserved (69-0). Minor changes have been made to character scores here, such as the recognition of the constricted condition in *Borealosuchus formidabilis* (Erickson, 1976, fig.10) ('wide' according to Brochu et al. [2012]), and *Borealosuchus sternbergii* (Fig. 3.24D) (unknown according to Brochu et al. [2012]).

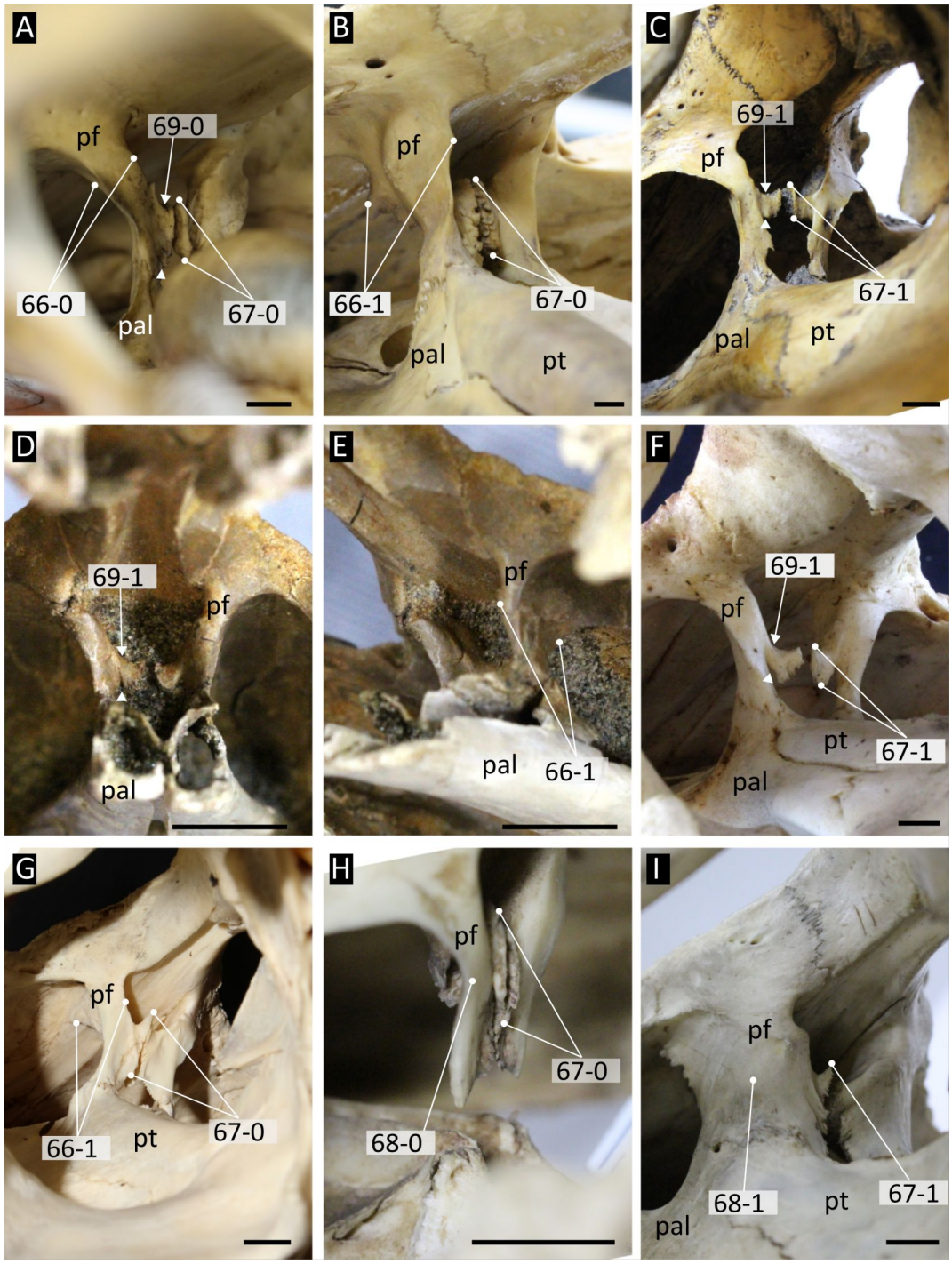



Figure 3.24: Anteromedial view of the prefrontal pillars in selected crocodylians. **A**, *Gavialis gangeticus* (NHMUK 61.4.1.2); **B**, *Tomistoma schlegelii* (NHMUK 1894.2.21.1); **C**, *Voay robustus* (NHMUK R 36685); **D–E**, *Borealosuchus sternbergii* (UCMP 126099) in anterior (D) and anteromedial (E) views; **F**, *Crocodylus acutus* (FMNH 69884); **G**, *Caiman yacare* (AMNH 97300); **H**, *Paleosuchus trigonatus* (NHMUK 1868.10.8.1); **I**, *Alligator mississippiensis* (NHMUK 1873.2.21.1). Abbreviations: **pal**, palatine; **pf**, prefrontal; **pt**, pterygoid. All scale bars = 1 cm.

70. Frontal, ornamentation, midsagittal crest on fused frontals: absent (0); present (1) (after Brochu & Storrs, 2012 [188]).

    In the dataset of Brochu and Storrs (2012) a sagittal interorbital ridge on the frontal is known only in *Crocodylus siamensis* (Fig. 3.25B); however, it is recognised as a relatively common ornament in Eusuchia here. A sagittal frontal ridge is present in several non-crocodylian eusuchians such as *Wannchampsus kirpachi* (Adams, 2014), and *Theriosuchus pusillus* (NHMUK 48270), as well as mekosuchines such as *Trilophosuchus rackhami* (QM F16856), *Mekosuchus sanderi* (QM F31188), and *Mekosuchus inexpectatus* (MNHN NCP 06). A frontal ridge is considered diagnostic of *Crocodylus siamensis* among extant *Crocodylus* species (Delfino & De Vos, 2010). This was observed in all *Crocodylus siamensis* specimens studied here (NHMUK 1921.4.1.168, NHMUK 1921.4.1.172; NHMUK 1931.12.6.6); however, a frontal ridge is also variably present in *Crocodylus niloticus* (present in NHMUK 1934.6.3.1; absent in NHMUK 1864.6.5.53).

71. Orbit, ornamentation, protuberance on the frontal-prefrontal suture intersection with the orbit: absent (0); or present (1) (new character, based on personal observation).

    The medial orbital margins are slightly upturned in almost all crocodylians. In addition to this, some taxa exhibit a rounded protuberance at the intersection of the frontal-prefrontal suture with the orbital margin (Fig. 3.25B). This condition is observed in all *Crocodylus siamensis* specimens examined here (NHMUK 1921.4.1.168, NHMUK 1921.4.1.172; NHMUK 1931.12.6.6) and occurs variably in *Crocodylus palustris* (e.g. absent in NHMUK 1868.4.9.11, present in NHMUK 1861.4.1.5), *Crocodylus porosus* (e.g. absent in NHMUK 1852.12.9.2, present in NHMUK 67.4.2.188), and *Crocodylus palaeindicus* (e.g. absent in NHMUK 39799, present in NHMUK 39795).

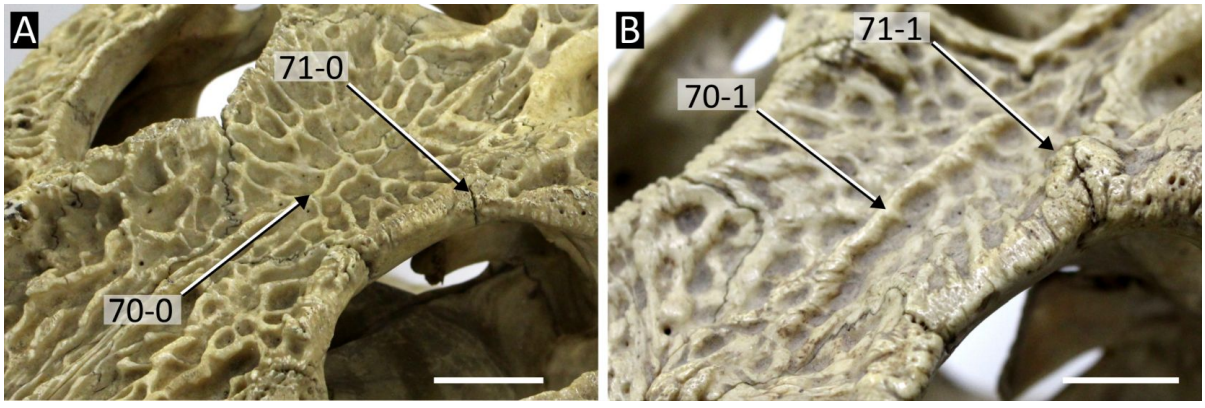



Figure 3.25: Dorsolateral view of the frontal in **A**, *Crocodylus porosus* (NHMUK 1852.12.9.2); **B**, *Crocodylus siamensis* (NHMUK 1921.4.1.168). All scale bars = 2 cm.

72. Orbit, dorsomedial margin: flush with skull surface (0); upturned (1); projecting into orbit (2) (after Brochu, 1997b [103]) (ORDERED).

This character has received no modifications to character states, but is newly ordered and several scores have been changed. The dorsomedial margins of the orbit are slightly upturned (72-1) in most crocodylians (Fig. 3.26C). Among other eusuchians, this condition is here considered intermediate between the flush orbital margins exhibited in *Borealosuchus* (72-0) and the telescoped orbits that characterise *Gavialis gangeticus* (72-2) (Fig. 3.26F). A comparison between the character scores in different datasets suggests that the distinction between upturned (72-1) and telescopic (72-2) orbital margins is ambiguous. For example, according to Brochu et al. (2012), the late Paleogene gavialoid, *Eogavialis africanum*, has telescoped orbits. However, following Salas-Gismondi et al. (2019), the orbital margins of *Eogavialis africanum* are here considered upturned (Fig. 3.26D), reminiscent of the condition in juvenile individuals of *Gavialis* (NHMUK 96.7.7.4, NHMUK 96.7.7.4.2). The upturned condition is shared by some South American Miocene gavialoids, such as *Ikanogavialis gameroi* (Sill, 1970) and *Gryposuchus pachakamue* (Salas-Gismondi et al., 2016) and might represent an incipient telescoped condition, leading to the fully everted orbital margins of *Gavialis* and all other *Gryposuchus* species. Telescoped orbits are newly recognised in several species of the giant caimanine *Mourasuchus*, e.g. *M. atopus* (Fig. 3.26G–H). Previously, these taxa were scored as having upturned orbits (Cidade et al., 2017; Souza-Filho et al., 2019); however, the orbital margins are everted from the cranial surface in a similar style to *Gavialis*, although not to the same degree.

73. Orbit, position of posterior margin (measured at the level of the postorbital-frontal suture) relative to posterior margin of suborbital fenestra: posterior to or at the same level (0); anterior (1) (after Jouve, 2004 [195]; Jouve et al., 2008 [186]; Salas-Gismondi et al., 2015 [195]).

    The anatomical meaning of this character is consistent with earlier studies; however, there are several score changes here relative to earlier studies (e.g. Jouve, 2016). This character was assessed by examining crania in dorsal view and noting the relative positions of the posterior margin of the suborbital fenestra and orbit (at the level of the frontal-postorbital suture). In many "gavialoids", e.g. *Gavialis gangeticus* (Fig. 3.27A), the posterior margin of the suborbital fenestra cannot be observed through the orbits, as it is positioned further posteriorly (73-1). By contrast, in all extant alligatorids and most crocodylids, the posterior margin of the suborbital fenestra is positioned anterior to the posterior margin of the orbits, such that it is visible through the orbits in dorsal view (Fig. 3.27B). By contrast with scores in Jouve (2016), several "tomistomines" share the same condition as *Gavialis*, including *Tomistoma schlegelii* (NHMUK 1894.2.21.1) and *Tomistoma cairense* (SMNS 10575, SMNS 50739).

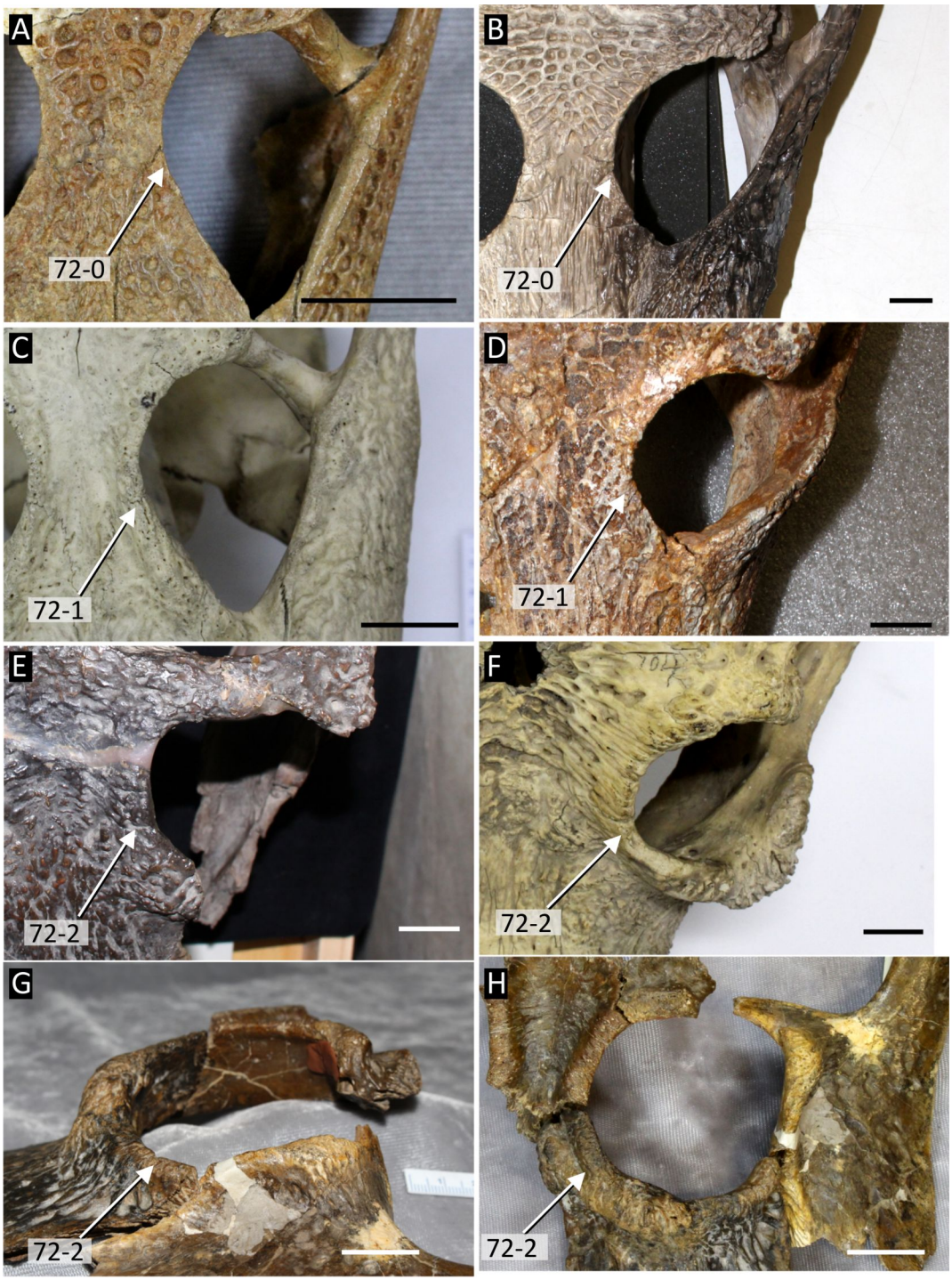



Figure 3.26: Variation in degree of upturning of orbital margins. **A**, *Borealosuchus sternbergii* (UCMP 126099); **B**, *Piscogavialis jugaliperforations* (SMNK 1282 PAL); **C**, *Alligator mississippiensis* (NHMUK 1873.2.21.1); **D**, *Eogavialis africanum* (YPM 6263); **E,** *Gryposuchus neogaeus* (MLP 26-413); **F**, *Gavialis gangeticus* (NHMUK 704); **G**-**H**, *Mourasuchus atopus* (UCMP 38012). All scale bars = 2 cm.

74. Orbit, lateral-most margin relative to the lateral margin of the maxilla at the level of alveoli 3–6: lateral (0); level with or medial (1) (after Jouve, 2004 [206]; Jouve, 2016 [208]).

    Following Jouve (2004), this character essentially describes the width of the rostrum, broadly distinguishing brevirostrine crocodylians from longirostrines. For example, whereas in all "tomistomines" and "gavialoids" the orbit is positioned lateral to the level of maxillary alveoli 3–6 (Fig. 3.27A), it is medial in most alligatoroids and crocodyloids (Fig. 3.27B). Not all taxa exhibiting the plesiomorphic condition are longirostrines, this morphology also occurs in *Caiman crocodilus* (FMNH 69812), *Caiman yacare* (AMNH 97300), *Borealosuchus* (e.g. *B. sternbergii*, USNM 6533), '*Crocodylus*' *affinis* (USNM 18171), and *Asiatosuchus depressifrons* (IRScNB R251).




Figure 3.27: Dorsal view of the cranium of **A**, *Gavialis gangeticus* (NHMUK 1974.3009); **B**, *Alligator mississippiensis* (NHMUK 1873.2.21.1). Scale bars = cm.

75. Frontoparietal suture, intersection with supratemporal fenestra (at maturity): deep intersection, postorbital-parietal suture not exposed on skull table (0); frontoparietal suture incipiently contacts supratemporal fenestra, postorbital-parietal suture slightly visible (1); frontoparietal suture does not intersect supratemporal fenestra, postorbital-parietal contact fully exposed on skull table (2) (after Brochu,

1997b [81]) (ORDERED).

Character state definitions for this character are unchanged from Brochu (1997b). Minor character score changes have been made, and the character is newly ordered. The frontoparietal suture runs transversely across the anterior cranial table in all eusuchians; however, its proximity to the supratemporal fenestrae varies. In most crocodylians, the suture does not enter the supratemporal fenestrae (75-2), and a triple intersection between the postorbital, parietal, and frontal is visible (Fig. 3.28A, D). This condition occurs in most alligatorids and crocodyloids. By contrast, some crocodylians exhibit a deep intersection of the frontoparietal suture with the supratemporal fenestrae (Fig. 3.28H), such that the postorbital-parietal suture is hidden on the inner wall of the supratemporal fenestra. Several "gavialoids" and species of *Borealosuchus* among other taxa exhibit an intermediate condition, in which the frontoparietal suture 'grazes' the anterior edge of the supratemporal fenestrae (Fig. 3.28G). As in character state 2, the postorbital-parietal suture is hidden on the inner wall of the supratemporal fenestra, but the unique nature of the intersection with the supratemporal fenestrae warrants a separate character state. By conrast with the data matrix of Brochu et al. (2012), *Brachychampsa montana* is scored as lacking an intersection of the frontoparietal suture (75-2) (Fig. 3.28C) and *Navajosuchus mooki* (AMNH 6780) and *Hassiacosuchus haupti* (HLMD-Me-4415) are characterised by the intermediate condition (75-1).

76. Frontoparietal suture, shape between supratemporal fenestrae: concavo-convex (0); straight (1) (after Brochu, 1997b [86]).

    The anatomical meaning of this character follows Brochu (1997b). A concavo-convex frontoparietal suture is exemplified by *Alligator mississippiensis*, *Crocodylus*, and *Brachychampsa montana* (Fig. 3.28A–C). By contrast, the straight condition is exhibited clearly in *Gavialis gangeticus* (Fig. 3.28G). Sookias (2019) did not consider this character to be robust based on the sample of extant crocodylians studied therein; however, broad differences can be observed and it is therefore retained herein. There are some differences in character scores between this dataset and that of earlier studies (e.g. Brochu et al., 2012), e.g. *Melanosuchus niger* $1 \rightarrow 0$ (Fig. 3.28D) and *Tomistoma schlegelii* $1 \rightarrow 0$ (NHMUK 1894.2.21.1). This probably represents the subtle difference between concavo-convex and straight in some taxa. Here, any degree of curvature in the suture was taken to be representative of the plesiomorphic condition.

77. Supraoccipital, exposure on dorsal skull table: present (0); absent (1) (after Norell, 1988 [11]; Brochu, 1997b [92]).

78. Supraoccipital, extent of exposure on skull table: small, mediolateral width across dorsal supraoccipital exposure less than half that along the posterior margin of the parietal (0); moderate, mediolateral

width across dorsal supraoccipital exposure more than half to equal that along the posterior margin of the parietal (1); large, such that the parietal is excluded from the posterior edge of skull table (2) (after Norell, 1988 [11]; Brochu, 1997b [82]) (ORDERED).

Characters 77 and 78 were derived by reductively coding Character 92 from Brochu (1997b). These characters describe the degree of dorsal exposure of supraoccipital on the cranial table. Character state definitions are essentially the same as Brochu (1997b), but the supraoccipital exposure is quantified relative to the parietal width to improve repeatability. Furthermore, Character 78 is ordered, as it describes a transformational series. As in previous studies, caimanines exhibit the largest supraoccipital exposure, to the extent that the parietal is excluded from the posterior margin of the cranial table (Fig. 3.28D).

79. Supraoccipital, posterolateral tuberosities in dorsal view: not visible (0); visible (1) (after Jouve, 2004 [193]; in Jouve, 2016 [201]).

As well as being dorsally exposed on the skull table, the supraoccipital can also be visible as two rounded processes extending beyond the level of the posterior margin of the cranial table in some taxa (Fig. 3.28C). This condition occurs in a variety of eusuchians, including *Hylaeochampsa vectiana* (NHMUK R177), most *Alligator* species (e.g. *A. mississippiensis* [NHMUK 68.2.12.16], *A. mcgrewi* [AMNH 7905]), and several gavialoids, e.g. *Gavialis gangeticus* (NHMUK 1974.3009) and *Piscogavialis jugaliperforatus* (SMNK 1282).

80. Supraoccipital, acute process projecting posteriorly from the midline of the cranial table: absent (0); present (1) (new character, after Hua & Jouve, 2004 [82]; Jouve, 2016 [82]).

In a small number of mostly "gavialoids", the supraoccipital forms a mediolaterally narrow, midline posterior projection on the cranial table, e.g. *Gavialis gangeticus* (NHMUK 1974.3009) (Fig. 3.28G) and *Piscogavialis jugaliperforatus* (SMNK 1282) (Fig. 3.28H). This projection is distinct from the paired posterior processes described in Character 79. This feature was recognised by Jouve (2016), who discretised this condition under a character describing supraoccipital size (Character 78 here). Here, this character state has been converted into an independent character, because the posterior projection of the supraoccipital, and degree of dorsal exposure of the supraoccipital, are not considered homologous.

81. Supratemporal fenestra, morphology of fenestral rim (at maturity): with fossa, dermal bones of skull roof do not overhang rim (0); dermal bones overhang rim (1); supratemporal fenestra completely closed (2) (after Norell, 1988 [9]; Brochu, 1997b [87]) (ORDERED).

The supratemporal fenestrae of most crocodylians are surrounded by fossae, such that the fenestral margins do not overhang (Brochu, 1999) (Fig. 3.28A, B). By contrast, bones surrounding the fenestrae

in several crocodylians bear laminae that constrict the fenestra. This condition commonly occurs in caimanines, e.g. *Caiman* and *Melanosuchus niger* (Fig. 3.28D), but also in some crocodyloids, such as *Osteolaemus tetraspis* (NHMUK 1862.6.30.5) and *Voay robustus* (NHMUK R 36685). In rarer cases, the supratemporal fenestrae become completely closed, a condition only observed consistently in *Paleosuchus trigonatus* (Fig. 3.28E), *Paleosuchus palpebrosus* (AMNH 93812), and *Iharkutosuchus makadii* (Ősi et al., 2007), in this dataset. The supratemporal fenestrae may appear incipiently closed in some *Caiman crocodilus* specimens (e.g. FMNH 69859); however, this is disregarded in character scoring due to its rarity. As noted by Brochu (1999), the supratemporal fenestrae of hatchling caimans bear fossa, like all other extant crocodylians, with overhanging fenestral rims developing later in ontogeny. This could potentially distort character scores, as fossil taxa exhibiting supratemporal fossae, and scored as such, might be juveniles in which the overhanging condition has yet to be acquired. Similarly, fossil taxa exhibiting overhanging rims could later develop closed supratemporal fenestrae. There is little data on the precise timing of such ontogenetic changes. Based on illustrations in Blanco et al. (2015), juvenile *Caiman yacare* and *Caiman latirostris* (defined by SVL $<$ 500 mm) exhibit overhanging supratemporal fenestral rims. This suggests that although hatchling caimanines might not yet develop overhanging fenestrae, it is acquired relatively early in ontogeny. This is corroborated by personal observations of *Caiman crocodilus*, in which overhanging fenestral rims are observed in cranial specimens with a skull length $<$ 70 mm (FMNH 73712, FMNH 69837). Similar observations are made for the timing of closure of supratemporal fenestrae in *Paleosuchus*. Supratemporal fenestrae are closed in juvenile *Paleosuchus palpebrosus* (AMNH 93812) as reported by Medem (1958). Although they are open in juvenile *Paleosuchus trigonatus*, these are notably more constricted than the overhanging fenestrae of all other extant caimanines (Medem, 1958, AMNH 66391). Since no specimens included in this analysis could be regarded as hatchlings, and the development of overhanging and closed supratemporal fenestrae appears early in ontogeny, this character could be scored in all taxa where preserved.

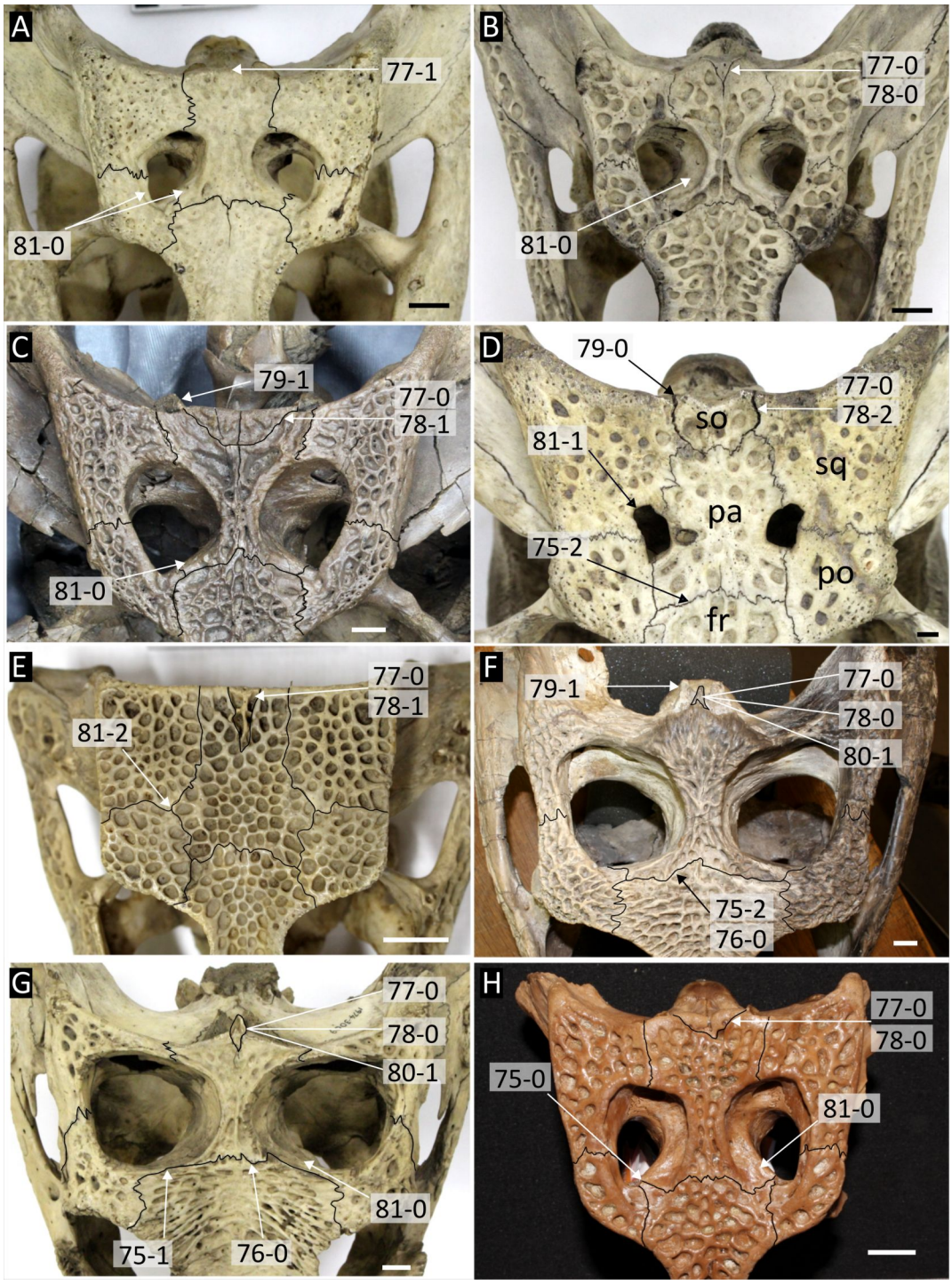



Figure 3.28: Sutural relationships and morphology of the cranial table in selected crocodylians. **A**, *Alligator mississippiensis* (NHMUK 1873.2.21.1); **B**, *Crocodylus acutus* (NHMUK 1975.997); **C**, *Brachychampsa montana* (UCMP 133901); **D**, *Melanosuchus niger* (NHMUK 45.8.25.125), **E**, *Paleosuchus trigonatus* (NHMUK 1868.10.8.1); **F**, *Piscogavialis jugaliperforatus* (SMNK 1282 PAL); **G**, *Gavialis gangeticus* (NHMUK 1974.3009); **H**, *Diplocynodon ratelii* (MNHN SG 539). Abbreviations: **fr**, frontal; **pa**, parietal; **po**, postorbital; **so**, supraoccipital; **sq**, squamosal. All scale bars = 1 cm.

82. Skull table morphology, acute dorsal indentation on the supraoccipital (and sometimes the parietal): absent (0); present (1) (new character, after Brochu 1997b [123]; Jouve, 2016 [123]).

    The cranial table in most crocodylians is flat or weakly concave about its sagittal axis (82-0) (Fig. 3.29A). By contrast, some crocodylians exhibit a prominent indentation on the sagittal axis, which is most apparent in occipital view as a sharp notch on the supraoccipital (82-1). Jouve (2016) recognised this condition and introduced a new character state to Character 123 of Brochu (1997b). However, this morphological feature is considered as an independent, binary character here. In the data matrix of Jouve (2016), this condition only occurs in two taxa: *Tomistoma schlegelii* and *Kentisuchus spenceri*. However, the presence of this indentation is additionally recognised in several caimanines herein (Fig. 3.29C, D), including *Caiman lutescens* (see Section 4.4.5).

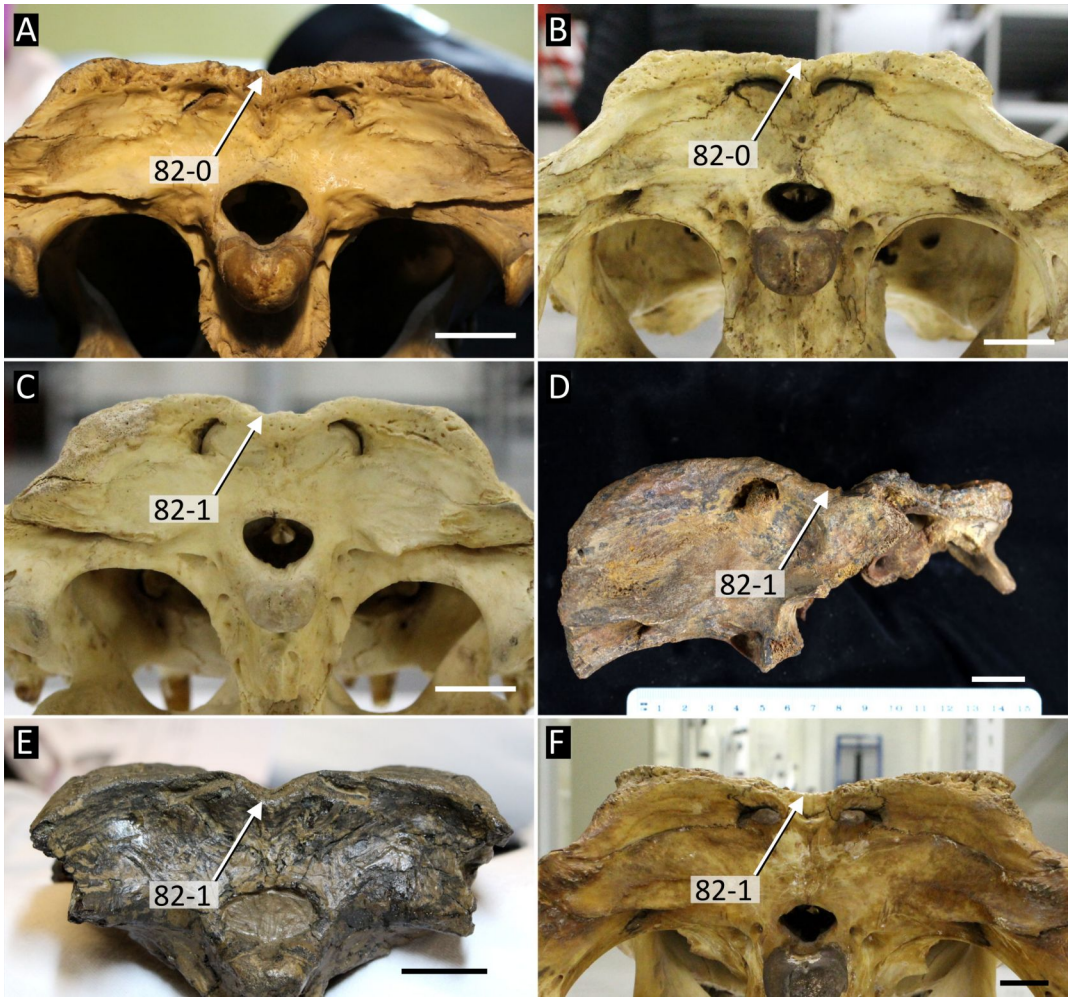



Figure 3.29: Occipital view of the cranium showing presence or absence of a dorsal midline indentation of the cranial table. **A**, *Caiman yacare* (MACN uncatalogued); **B**, *Crocodylus plaustris* (NHMUK 1897.12.31.1); **C**, *Caiman latirostris* (NHMUK 86.10.4.2); **D**, *Caiman gasparinae* (MLP 73-IV-15-1); **E**, *Kentisuchus spenceri* (NHMUK 38974); **F**, *Tomistoma schlegelii* (NHMUK 1894.2.21.1). All scale bars = 2 cm.

83. Parietal, sagittal crest between supratemporal fenestrae: absent (0); present (1) (after Clark, 1994 [33]; Pol et al., 2009 [33]).

    Most eusuchians exhibit ornamentation on the cranial table in the form of regular, equally distributed pits. The Glen Rose Form (MCZ 3484), as well as several taxa commonly assigned to Paralligatoridae (including *Shamosuchus djadochtaensis* [Pol et al., 2009] and *Wannchampsus kirpachi* [Adams, 2014]), also exhibit a sagittal crest between the supratemporal fenestrae. A handful of crocodylian taxa also exhibit this crest, including *Trilophosuchus rackhami* (Fig. 3.30C), *Mourasuchus amazonensis* (UFAC 1424), and *Mourasuchus arendsi* (MLP 73-IV-15-8).

84. Supratemporal fenestra, shallow fossa at anteromedial corner: present (0); absent (1) (after Brochu, 1997b [92]).

    A shallow fossa at the anteromedial corner of the supratemporal fenestra is distinct from the development of fossae described in Character 81. The 'anteromedial fossa' is a discrete shelf that is ventrally inset in the supratemporal fenestrae, and is present in several taxa commonly assigned to the clade Allodaposuchidae, including *Allodaposuchus precedens* (Fig. 3.30C), *Lohuecosuchus megadontos* (Narváez et al., 2015), and *Agaresuchus fontisensis* (Narváez et al., 2016).

85. Parietal, medial wall of the supratemporal fenestra with one or more foramina: absent (0); present (1) (after Norell, 1988 [51]; Brochu, 1997b [104]).

    Unlike most crocodylians, the medial parietal walls of extant *Caiman* species and *Melanosuchus niger* are perforated. This condition has recently been identified in the putative early caimanine *Protocaiman peligrensis* (Bona et al., 2018) (Fig. 3.30G) and herein in *Brachychampsa montana* (Fig. 3.30H). Despite reports of perforations in *Paleosuchus* (Norell, 1988; Brochu, 1999), closure of the supratemporal fenestrae in this taxon precludes observation of the medial parietal wall.

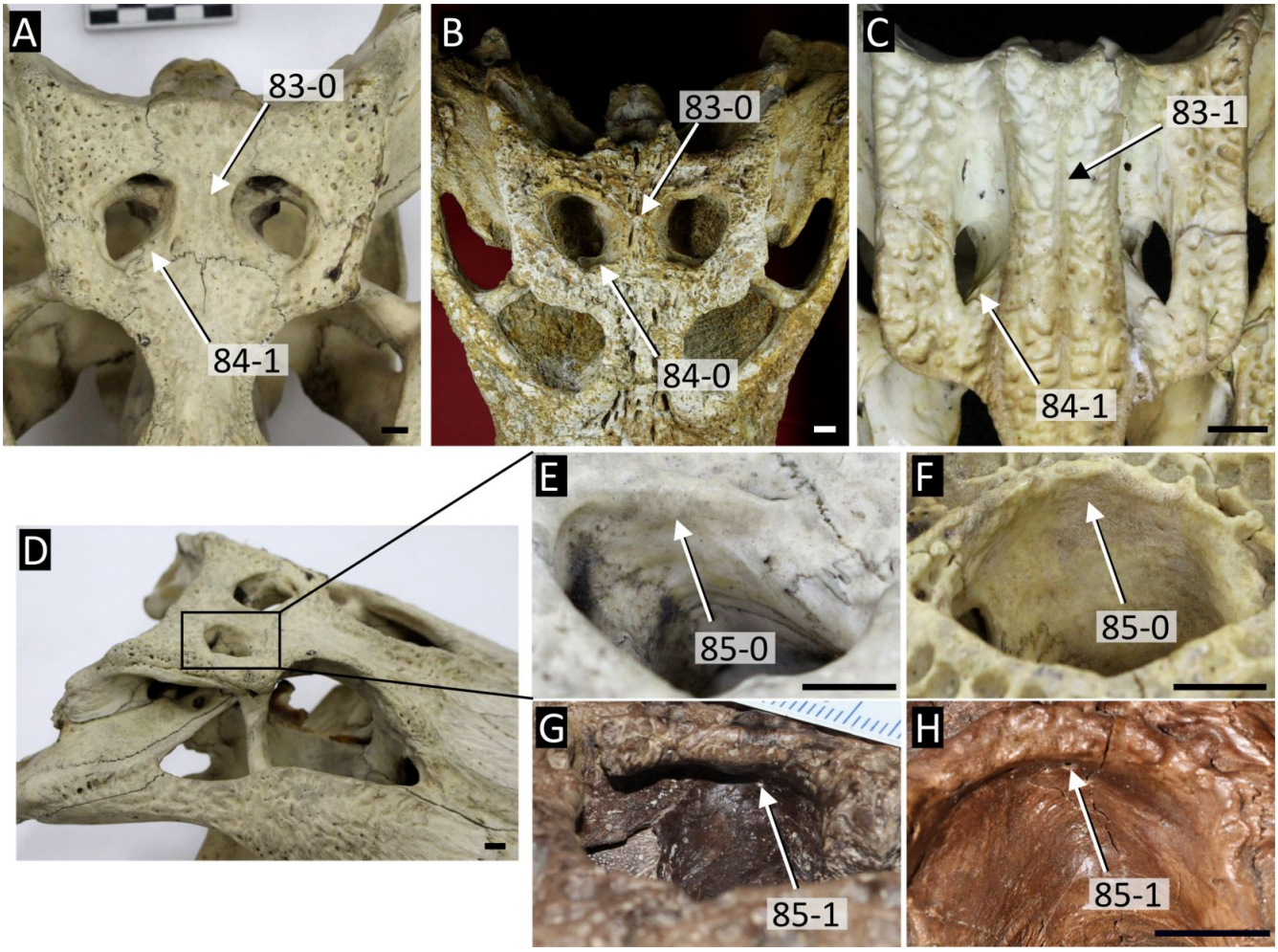



Figure 3.30: Morphology of the parietal in selected crocodylians. **A**, *Alligator mississippiensis* (NHMUK 1873.2.21.1); **B**, *Allodaposuchus precedens* (MMSVBN-12-10A); **C**, *Trilophosuchus rackhami* (QM F16856); **D**, area enlarged in E–F, **E**, *Alligator mississippiensis* (NHMUK 1873.2.21.1); **F**, *Crocodylus palustris* (NHMUK 1897.12.31.1); **G**, *Protocaiman peligrensis* (MLP 80X-10-1); **H**, *Brachychampsa montana* (UCMP 133901). All scale bars = 1 cm.

86. Parietal, recess communicating with pneumatic system: present (0); absent (1) (after Brochu, 1997b [154]).

    As illustrated by Brochu (2004a, fig.17) this character describes an internal cavity (recess) in the parietal, which requires CT scans or a cross section through the skull. In the dataset of Brochu et al. (2012), the character is only scored in extant crocodylians, with a recess occurring in *Gavialis gangeticus*, *Tomistoma schlegelii*, and all extant crocodylids (86-0), but absent in alligatorids (86-1). It was only possible to evaluate the distribution of this feature in a small number of taxa, based on limited (and often low resoluion) CT scans, as well as cross sections through some extant crocodylian skulls (Fig. 3.31). Given the scarcity of data, character scores largely follow those of Brochu et al. (2012), although the recess appears to occur in at least two alligatorids, *Alligator mississippiensis* (Brochu, 2004a, fig.17C) and *Caiman yacare* (Fig. 3.31F).

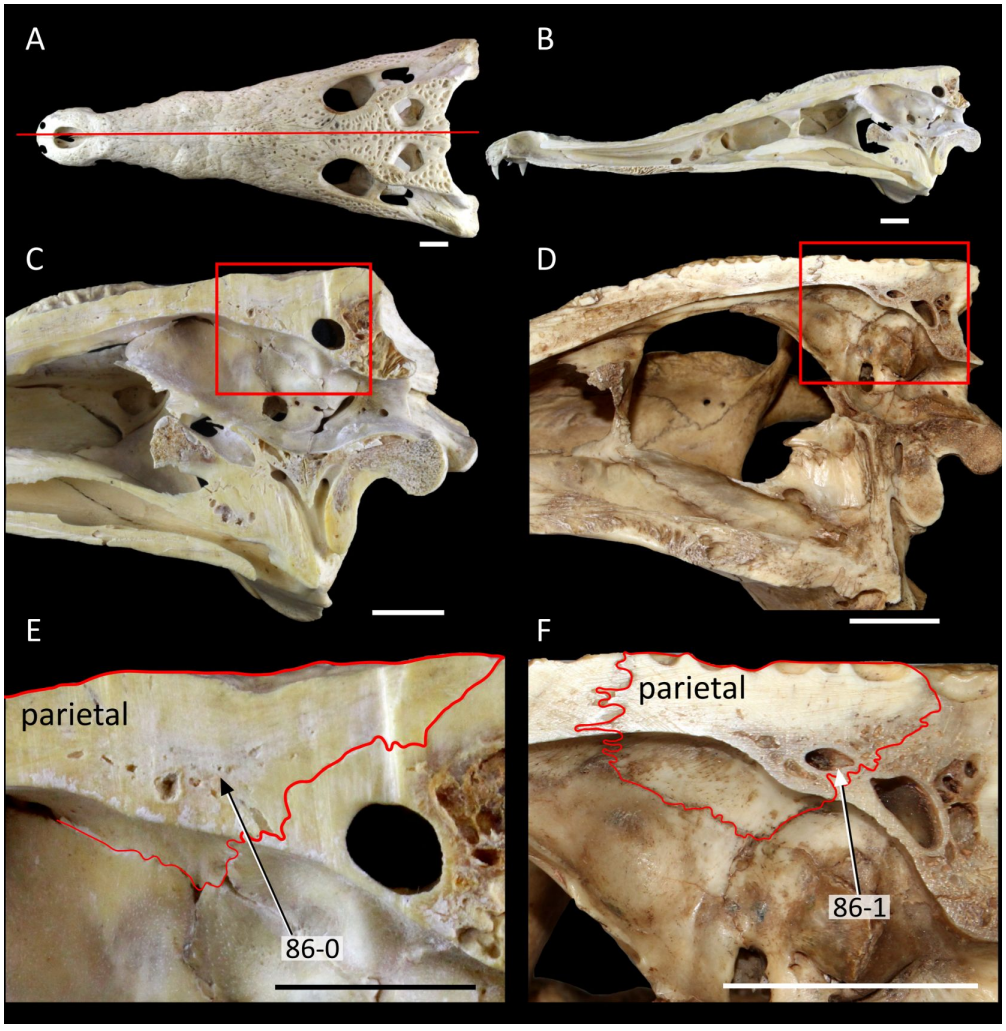



Figure 3.31: Sagittal sections of the skull showing the development of a parietal recess. The line of section in B–F is illustrated in *Crocodylus acutus* (**A**), with cross sections though *Crocodylus porosus* (FMNH 15229) (**B**, **C** and **D**) and *Caiman yacare* (MLP uncatalogued specimen) (**D**, **F**). All scale bars = 2 cm.

87. Supratemporal fenestra, posterior wall: quadrate forms entire ventral margin of orbitotemporal canal (no parietal-squamosal contact) (0); quadrate partially forms ventral margin of orbitotemporal canal (parietal and squamosal narrowly separated) (1); quadrate excluded from ventral margin of orbitotemporal canal (parietal and squamosal in contact) (2) (after Brochu, 1997b [131]) (ORDERED).

    The orbitotemporal canal is a circular passage on the posterior wall of the supratemporal fenestra that is bound by the squamosal, parietal and, to varying degrees, the quadrate (Fig. 3.32). In most crocodylians, the quadrate forms the entire ventral margin of the canal, preventing contact between the parietal and squamosal here (Fig. 3.32A). Among extant crocodylians, this condition is observed in crocodylids, *Gavialis gangeticus* (NHMUK 1974.3009), and *Tomistoma schlegelii* (NHMUK 1894.2.21.1). By contrast, there is no participation of the quadrate to the ventral margin of the orbitotemporal canal in extant alligatorids (Fig. 3.32C). A handful of crocodylian taxa exhibit an intermediate condition, in which the quadrate forms a small portion of the ventrolateral orbitotemporal margin, constricted between the squamosal and parietal. This condition is observed in *Brachychampsa montana* (Fig. 3.32B), and most species of *Diplocynodon* (where preserved), including *D. ratelii* (MNHN SG 539) and *D. hantoniensis* (CAMSM TN 907, see Section 2.5.1).

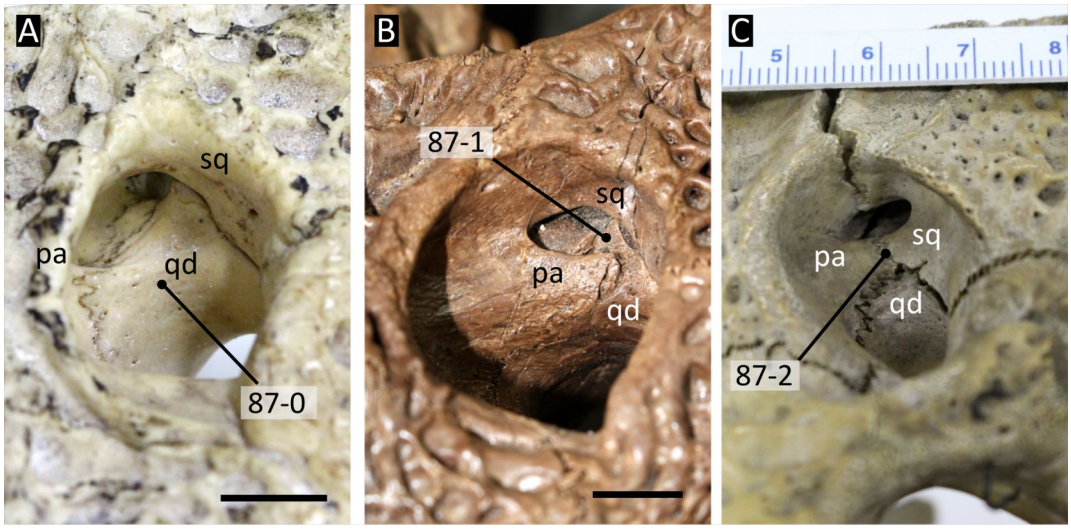



Figure 3.32: Variation in sutural relationships of the orbitotemporal canal in selected crocodylians. **A**, *Crocodylus niloticus* (NHMUK 1934.6.3.1); **B**, *Brachychampsa montana* (UCMP 133901); **C**, *Alligator sinensis* (NHMUK X184). Abbreviations: **pa**, parietal; **qd**, quadrate; **sq**, squamosal. Scale bars = 1 cm.

88. Supratemporal fenestra, posterior wall: squamosal-parietal suture passes medially to the orbitotemporal foramen, little to no development of fossa medial to orbitotemporal foramen (0); squamosal-parietal suture intersects dorsal margin of orbitotemporal foramen, large medial fossa (1); squamosal-parietal suture intersects dorsal margin of orbitotemporal canal, medial fossa extends over entire width of posterior supratemporal fenestra wall (2) (new character, based on personal observations) (ORDERED).

The orbitotemporal canal in most crocodylians is large and circular to elliptical in shape. Within the orbitotemporal canal, there is a discrete fossa which forms the floor of the canal, on which the supraoccipital and prootic are exposed. There is notable variation in the morphology of the canal, which appears to be constrained by its mediolateral extent (Fig. 3.33). *Gavialis gangeticus* and *Thoracosaurus isorhynchus* represent extreme end members of this morphological variation. In *Thoracosaurus isorhynchus* (Fig. 3.33A), the canal is mediolaterally restricted: the parietal forms a large portion of the posterior wall of the supratemporal fenestra, and the parietal-squamosal suture intersects the orbitotemporal canal on the medial or ventromedial edge. This condition is also observed in *Allodaposuchus precedens* (Martin et al., 2016a, fig.7) and *Portugalosuchus azenhae* (Mateus et al., 2019, fig.8). In *Gavialis gangeticus* (Fig. 3.33F), the parietal does not contribute much to the posterior supratemporal fenestra wall, exposing the prootic and supraoccipital on the floor of the canal. Also contrasting with *Thoracosaurus isorhynchus*, the squamosal-parietal suture intersects the dorsal margin of the orbitotemporal canal. The same condition is observed in *Gryposuchus colombianus* (Fig. 3.33E) and *Gryposuchus neogaeus* (MLP 26-413). In between these extremes lie almost all other crocodylians, e.g. *Piscogavialis jugaliperforatus*, *Eogavialis africanum*, and *Tomistoma schlegelii* (Fig. 3.33B–D). In those taxa the orbitotemporal canal is intermediate in size between *Thoracosaurus isorhynchus* and *Gavialis gangeticus*. Whereas the squamosal-parietal suture intersects the dorsal margin of the canal in those taxa, as in *Gavialis*, the parietal still forms a large portion of the posterior wall of the supratemporal fenestra. As these character states appear to belong on a morphological continuum, the character is ordered.

89. Postorbital, morphology of postorbital bar: anteroposteriorly expanded, elliptical in cross section (0); columnar and slender, circular in cross section (1) (after Norell, 1989 [3]; Brochu, 1997b [70]; Groh et al., 2020 [213]).

    The morphology of the postorbital bar can be divided into two morphotypes in Eusuchia. In most eusuchians, the bar is narrow and columnar with an approximately circular cross section (Fig. 3.34D–F). By contrast, some taxa exhibit a postorbital bar that is anteroposteriorly longer than mediolaterally wide (Fig. 3.34A–C). The latter condition occurs in the outgroup, *Bernissartia fagesii* (IRScNB 1538), and several non-crocodylian eusuchians such as *Hylaeochampsa vectiana* (NHMUK R177), indicating that it is the plesiomorphic condition for Eusuchia. The character states have been modified from Brochu (1997b) by describing the shape of the postorbital bar in cross section.

90. Postorbital, protuberance on the dorsolateral margin of the postorbital bar (at maturity): present (0); absent (1) (after Norell, 1989 [2]; Brochu, 1997b [134]; Brochu et al., 2012 [132]).

    This character was modified from its formulation in Brochu et al. (2012): "*Postorbital bar bears process that is prominent, dorsoventrally broad, and divisible into two spines (0) or bears process*

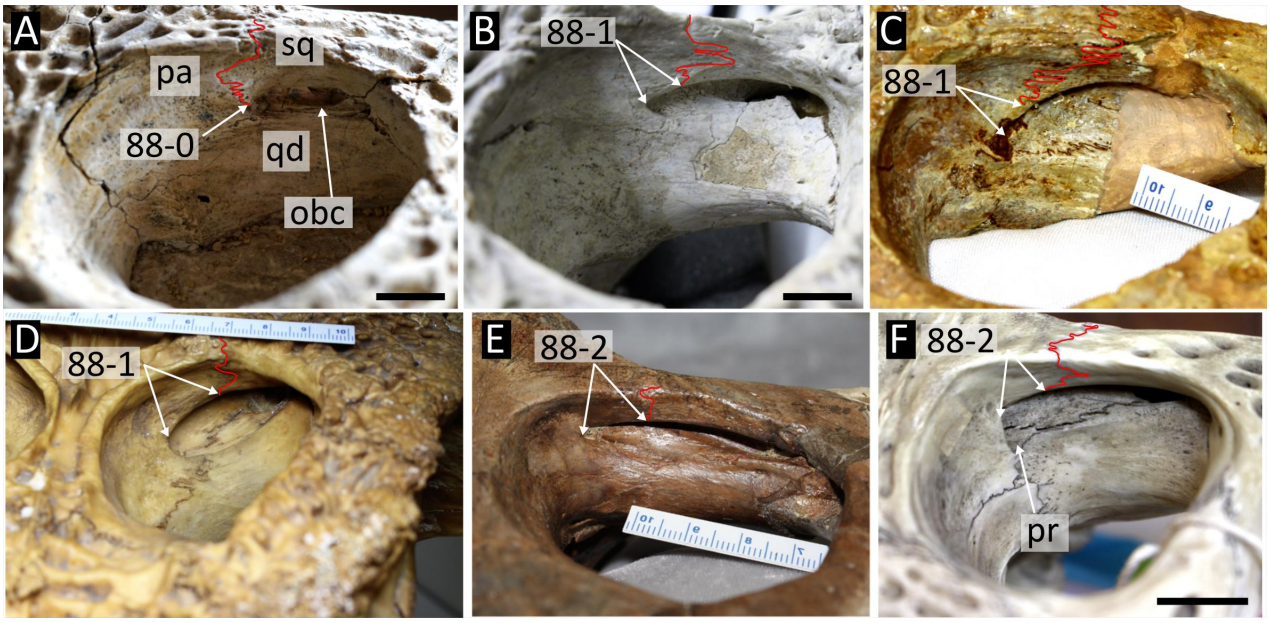



Figure 3.33: Variation in morphology of the orbitotemporal canal in crocodylian taxa. **A**, *Thoracosaurus isorhynchus* (MNHN.F.MTA 61); **B**, *Piscogavialis jugaliperforatus* (SMNK 1282 PAL); **C**, *Eogavialis africanum* (NHMUK PV R3430, digitally reversed); **D**, *Tomistoma schlegelii* (NHMUK 1894.2.21.1); **E**, *Gryposuchus colombianus* (UCMP 38358, digitally reversed); **F**, *Gavialis gangeticus* (NHMUK 61.4.1.2). Abbreviations: **obc**, orbitotemporal canal; **pa**, parietal; **pr**, prootic; **sq**, squamosal. Scale bars in A, B, F = 1 cm, all other scale bars = cm.

*that is short and generally not prominent (1)*". This character has been simplified to describe the presence or absence of a postorbital process at maturity. This modification is based on the variability of the postorbital bar process morphology. It is not always divisible into two spines, nor is it always dorsoventrally tall. Two discrete spines could only be observed in *Gavialis gangeticus* in this study (NHMUK 1974.3009). Where a process is present in other taxa, it can form a single sharp projection (e.g. *Thoracosaurus isorhynchus*, Fig. 3.34C), an anteroposteriorly elongated ridge (e.g. *Eogavialis africanum*, Fig. 3.34B, *Hylaeochampsa vectiana*, NHMUK R177, and *Allodaposuchus precedens*, MMS/VBN-12-10A), or a single and large irregular protuberance (e.g. *Gryposuchus colombianus*, UCMP 41136). The character is also only scored for matrue individuals, since prominent processes occur in juvenile individuals of several extant crocodylians but are lost at maturity, e.g. *Alligator mississippiensis* (Norell, 1989), and *Tomistoma schlegelii* (Aoki, 1976; Buffetaut, 1985).

91. Postorbital bar, orientation: laterally inclined, greater than or equal to 20° (bar visible in dorsal view) (0); slightly inclined to vertical, lateral inclination $< 20°$ (not visible in dorsal view) (1) (after Jouve, 2004 [192]; Jouve et al., 2008 [184]; Hastings et al., 2010 [50]; Jouve, 2016 [184]; Groh et al., 2020 [211]).

    The postorbital bar is subvertical in *Gavialis gangeticus* (Fig. 3.34I), such that it is concealed under-

neath the cranial table in dorsal view. A similar condition is observed in several "gavialoids", such as *Piscogavialis jugaliperforatus* (SMNK 1282 PAL) and *Eogavialis africanum* (NHMUK R3108). Most other eusuchians exhibit a less inclined postorbital bar, such that it is visible in dorsal view (Fig. 3.34G–H).

92. Postorbital bar: flush with dorsolateral margin of jugal (0); dorsolateral margin of jugal raised to form ridge, with sulcus separating it from postorbital bar (1) (after Benton & Clark, 1988; Norell & Clark, 1990 [3]; Brochu, 1997b [146]).

    The wording of this character has received slight modifications from the original but its anatomical meaning is unchanged; however, there have been several character score changes compared to other datasets. In most eusuchians, the ventral margin of the postorbital bar is prominently delimited from the dorsolateral margin of the jugal arch by a sulcus, as in *Tomistoma schlegelii* (Fig. 3.35A). In fewer cases, the demarcation between the ventral margin of the postorbital bar and the dorsolateral edge of the jugal arch is not apparent, such that one merges into the other, e.g. *Gavialis gangeticus* (Fig. 3.35B). By contrast to the scores of existing datasets, the 'flush' condition is no longer recognised in several "gavialoid" taxa such as *Piscogavialis jugaliperforatus* (Fig. 3.35C), *Thoracosaurus isorhynchus* (Fig. 3.35D), and *Eogavialis africanum* (Fig. 3.35E) (Brochu et al., 2012; Narváez et al., 2016). Furthermore, changes have been made to the scores of some non-crocodylian taxa, such as *Bernissartia fagesii* (92: 0→1) and *Hylaeochampsa vectiana* (NHMUK R177). The latter has consistently been scored for the flush condition (e.g. Brochu, 1999; Brochu et al., 2012; Narváez et al., 2016; Lee & Yates, 2018); however, the jugal of the holotype is damaged and the condition cannot be determined (92: 0→?) (Fig. 3.35F).

93. Jugal, posterodorsal jugal foramen, at base of postorbital bar: absent or small, diameter less than half the minimum mediolateral width of the jugal arch (0); large, equal to or greater than half the minimum jugal arch width (1) (after Jouve, 2016 [239]).

    In most crocodylians, one or more foramina are often present at the base of the postorbital bar, on the dorsal surface of the jugal arch. These foramina are typically small (Fig. 3.35A, C), but in several, mostly longirostrine crocodylians they are enlarged, e.g. *Gavialis gangeticus* (Fig. 3.35B), *Thoracosaurus isorhynchus* (Fig. 3.35D), and *Eogavialis africanum* (Fig. 3.35E). Alhough it was considered impractical to measure the diameter of the foramen, it is nevertheless quantified simply in proportion to the mediolateral width of the jugal arch to improve repeatability.

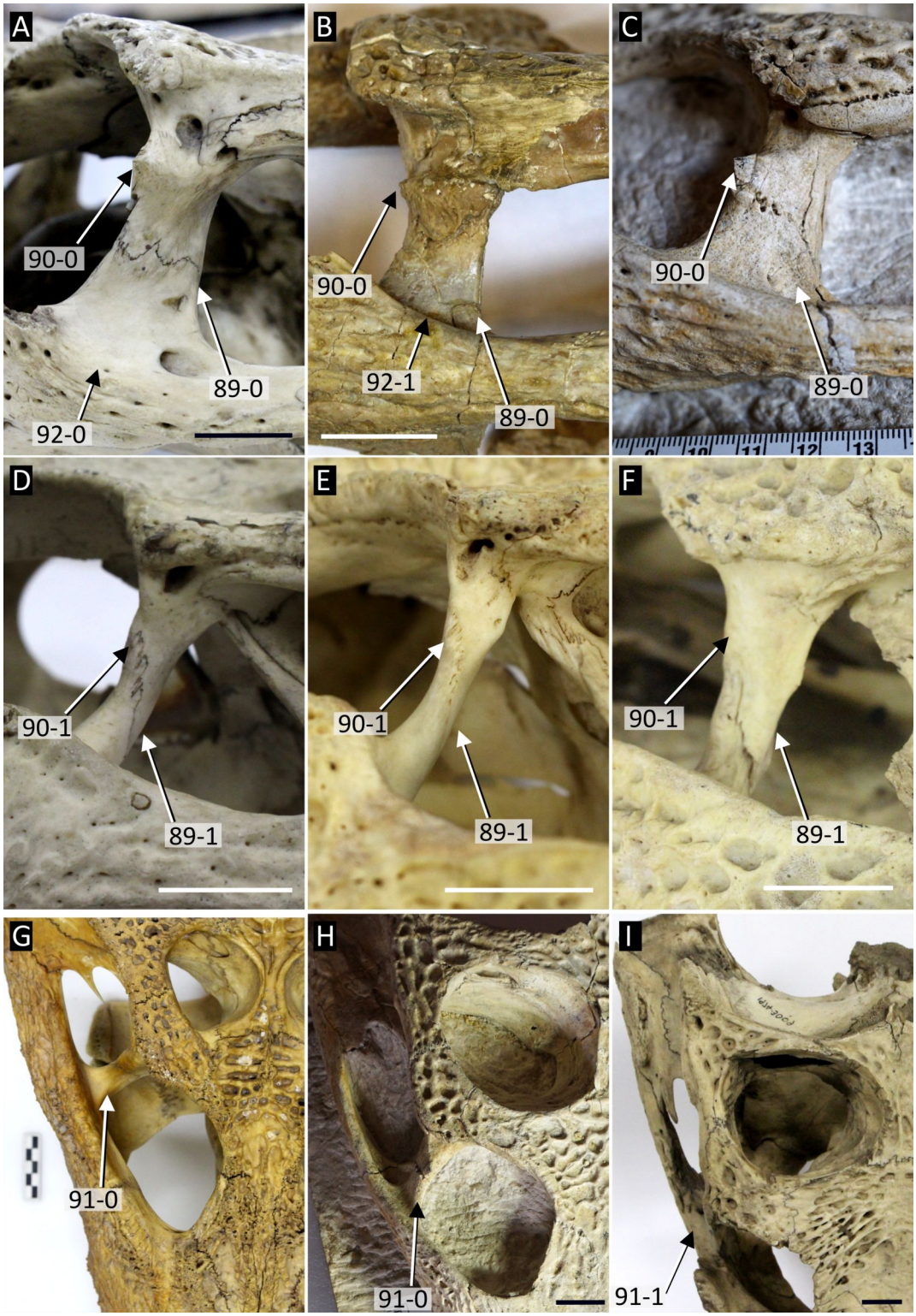



Figure 3.34: Morphology of the postorbital bar in selected crocodylians. **A**, **I**, *Gavialis gangeticus* (NHMUK 1974.3009); **B**, *Eogavialis africanum* (NHMUK PV R3108); **C**, **H**, *Thoracosaurus isorhynchus* (MNHN.F.MTA 61); **D**, *Alligator mississippiensis* (NHMUK 1873.2.21.1); **E**, *Caiman latirostris* (NHMUK 1897.12.31.1); **F**, *Crocodylus palustris* (NHMUK 1897.12.31.1); **G**, *Tomistoma schlegelii* (NHMUK 1894.2.21.1). All scale bars = 2 cm.

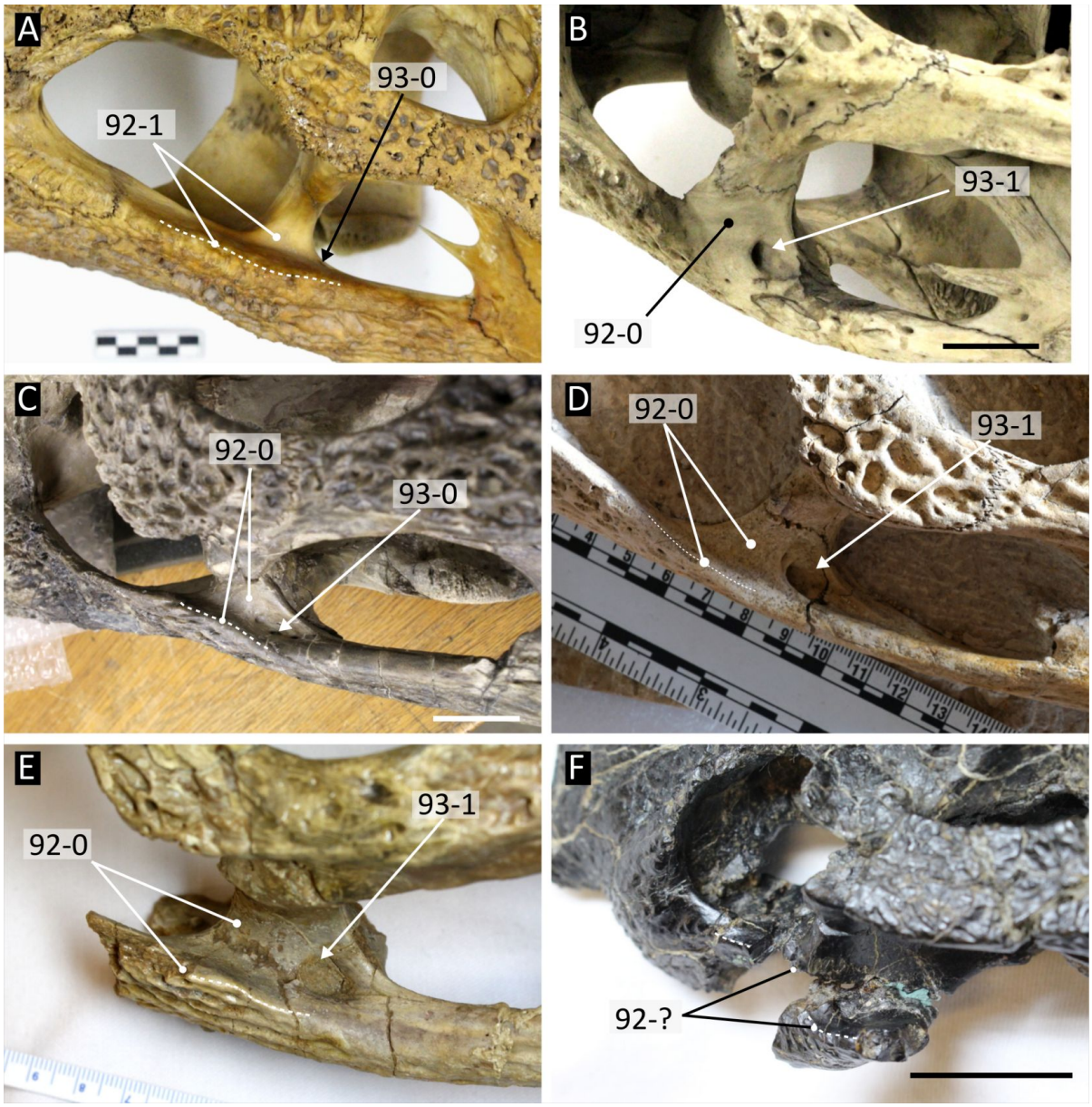



Figure 3.35: Dorsal view of the postorbital bar in selected crocodylians, showing variation in the inset of the postorbital bar. **A**, *Tomistoma schlegelii* (NHMUK 1894.2.21.1); **B**, *Gavialis gangeticus* (NHMUK 1974.3009); **C**, *Piscogavialis jugaliperforatus* (SMNK 1282 PAL); **D**, *Thoracosaurus isorhynchus* (MNHN.F.MTA 61); **E**, *Eogavialis africanum* (NHMUK PV R3108); **F**, *Hylaeochampsa vectiana* (NHMUK PV R 177). All scale bars = 2 cm.

94. Orbit, dorsal profile of jugal forming posteroventral margin: convex or straight, continuous with the dorsal margin of the lower temporal bar (0); posteroventrally sloping, gradually descending into the lower temporal bar (1); strongly convex with a step anterior to the lower temporal bar (2); abruptly angled ventrally, creating a near vertical margin descending toward the postorbital bar (i.e. a notch) (3) (after Brochu, 1997b [139]; Jouve et al., 2006, fig.7; Jouve, 2016 [139]; Lee & Yates, 2018 [61]).

    This character originated in Brochu (1997b) (Character 139), wherein it described the absence or presence of a 'notch' in the orbital margin. The notched condition is typified by *Gavialis gangeticus* (94-3) (Fig. 3.36D), and was scored in several other "gavialoids", e.g. *Gryposuchus*, *Piscogavialis* and *Eogavialis* (Brochu et al., 2012). Later studies modified this character, adding new character states to reflect the greater variation in the dorsal profile of the jugal. Jouve (2016) recognised two additional states: a convex shaped jugal profile that is present in most species of *Crocodylus* and *Tomistoma schlegelii* (Fig. 3.36A), and a step-like condition that is present mainly in caimanines (Fig. 3.36C). Furthermore, Lee and Yates (2018) described a posteroventrally sloping condition in their modification of the character, which can be exemplified by *Piscogavialis* (Fig. 3.36B). Character score changes have also been made, including the recognition of the abruptly angled, 'notched' condition (94-3) in several species of the giant caimanine genus, *Mourasuchus*, e.g. *M. atopus* (UCMP 38012). All species of *Mourasuchus* were formerly scored as lacking a notch (e.g. Brochu et al., 2012; Cidade et al., 2017; Souza-Filho et al., 2019), but the morphology of the jugal is strikingly similar to *Gavialis gangeticus*, which might be a result of similar modifications towards a telescopic orbit (Fig. 3.26H). The decision was made to assimilate the various character states into an unordered multistate character, but it is recognised that some of these character states might belong to a transformational series that could be ordered. In particular, character states 0, 1, and 3 (Fig. 3.36A, B, D) could be considered part of an ordered character describing the progressive deepening of a notch in the jugal. Similar gradational differences in gavialoids were described by Salas-Gismondi et al. (2016). On the other hand, difficulty arises in the placement of the typical caimanine condition (Fig. 3.36C), which does not have an obvious place in this continuum. As such, the character is currently best treated as unordered.

95. Jugal, ventral margin of jugal arch: concave (0); or straight (1) (after Jouve, 2004 [182]).

    The ventral margin of the jugal arch is strongly concave in most crocodylians (Fig. 3.36A). By contrast, some taxa exhibit a straight jugal arch, which is typically dorsoventrally shallow, including *Gavialis gangeticus* (Fig. 3.36D), *Eosuchus lerichei* (IRScNB R 49), *Eosuchus minor* (USNM 299730), and *Piscogavialis jugaliperforatus* (Fig. 3.36B).

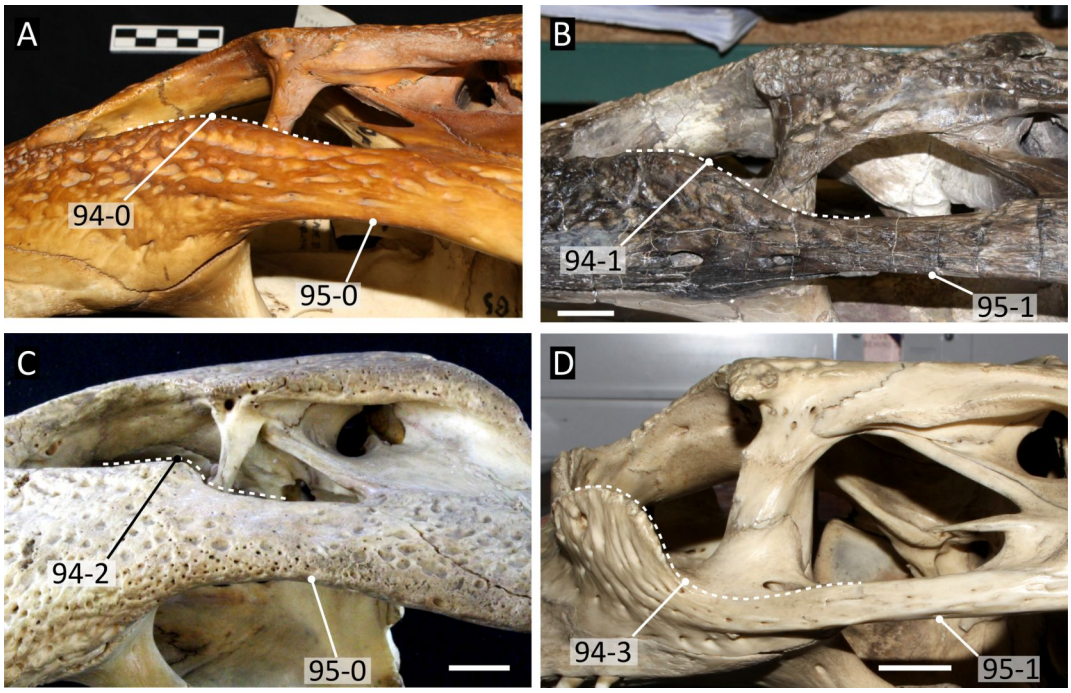



Figure 3.36: Left lateral view of the jugal arch in: **A**, *Tomistoma schlegelii* (NHMUK 1894.2.21.1); **B**, *Piscogavialis jugaliperforatus* (SMNK 1282 PAL); **C**, *Caiman latirostris* (FMNH 9713); **D**, *Gavialis gangeticus* (NHMUK 1974.3009). Scale bar A = cm, all other scale bars = 2 cm.

96. Jugal, ventrolateral sulcus on jugal and maxilla, at level of the jugal-maxilla suture: absent (0); present (1) (new character, adapted from Wu et al., 1996, 2001a; Kraus, 1998).

97. Jugal, ventrolateral foramina adjacent to the jugal-maxilla suture: small, less than half the diameter of the last maxillary alveolus (and usually numerous) (0); large, equal to or greater than half the diameter of the last maxillary alveolus (usually 2–3 foramina) (new character, based on personal observations).

    The specific epithet of *Piscogavialis jugaliperforatus* (Kraus, 1998) arises from the presence of large ventrolateral foramina on the jugal, adjacent to the jugal-maxilla suture. Foramina are present in this position in most crocodylians; however, there is variation in their size, number, and whether or not they are situated in a prominent sulcus. In addition to *Piscogavialis*, enlarged foramina, equal in diameter to the last maxillary alveolus, are present in *Argochampsa krebsi* (Hua & Jouve, 2004) (Fig. 3.37D), *Gryposuchus colombianus* (Fig. 3.37C), and *Dadagavialis gunai* (Salas-Gismondi et al., 2019). This contrasts to the condition in *Gavialis gangeticus*, wherein a linear array of small foramina pierce the jugal in both juvenile and adult specimens (Fig. 3.37B). This appears to be the plesiomorphic eusuchian condition, with small foramina observed in *Bernissartia fagesii* (IRScNB 1538), and *Hylaeochampsa vectiana* (NHMUK R177). The size of the sulcus (if present at all) in which these foramina sit appears to be independent of foramen size. For example, in *Piscogavialis* (SMNK 1282 PAL), there is little to no sulcus, whereas the foramina are equally large in *Gryposuchus colombianus* (Fig.

3.37C), but the sulcus is much deeper. The 'groove-shaped recess' described in *Stangerochampsa* (Wu et al., 1996) and *Leidyosuchus* (Wu et al., 2001a), and a conspicuous depression on the jugal present in *Asiatosuchus depressifrons* (Delfino & Smith, 2009; Delfino et al., 2019) (IRScNB R 0251), are herein considered homologous to this sulcus.

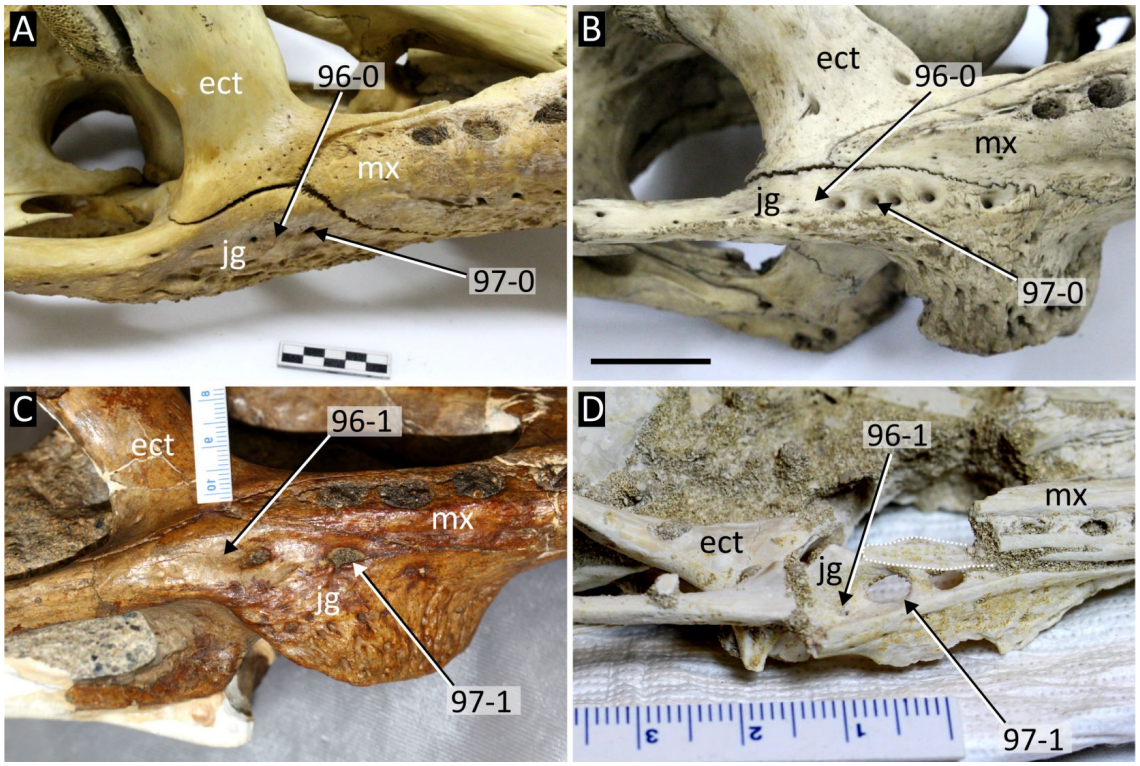



Figure 3.37: Ventrolateral view of the maxilla-jugal-ectopterygoid sutural intersections. **A**, *Tomistoma schlegelii* (NHMUK 1894.2.21.1); **B**, *Gavialis gangeticus* (NHMUK 1974.3009); **C**, *Gryposuchus colombianus* (UCMP 41136) (digitally reversed); **D**, *Argochampsa krebsi* (NHMUK R 36872). Abbreviations: **ect**, ectopterygoid; **jg**, jugal; **mx**, maxilla. Scale bar B = 5 cm, all other scale bars = cm.

98. Infratemporal fenestra, dorsal margin shape: acute, triangular (0); broadly curved, oval-shaped (1) (after Salas-Gismondi et al., 2016 [204]).

    The infratemporal fenestra is triangular in most eusuchians, with an acute dorsal margin (98-0). This includes all extant alligatorids and most crocodylids (Fig. 3.38C–E). By contrast, several "gavialoids" exhibit a rounded dorsal margin, such that the fenestra is more oval-shaped (98-1). In common with this analysis, Salas-Gismondi et al. (2016) scored several taxa for the rounded condition, such as *Eosuchus*, *Gryposuchus colombianus*, and *Eogavialis africanum*. However, by contrast to that study, the derived condition is additionally recognised in *Gavialis gangeticus* (Fig. 3.38A), *Tomistoma schlegelii* (Fig. 3.38B), and several non-gavialoid crocodylians, including *Asiatosuchus depressifrons* (IRScNB R251) and *Crocodylus johnstoni* (e.g. QM J4280).

99. Infratemporal fenestra, dorsal extent of quadratojugal: reaches dorsal angle of fenestra (0); does not

reach dorsal angle of fenestra (1) (after Buscalioni et al., 1992 [6]; Brochu, 1997b [80]).

The quadratojugal forms the posterior margin of the infratemporal fenestra in all crocodylians, but variation occurs in its dorsal extent. In *Bernissartia fagesii* and most eusuchians the quadratojugal reaches the dorsal angle of the fenestra (Fig. 3.38B), preventing the quadrate from participating in its posterior margin (99-0) (Buscalioni et al., 1992, fig.9; Norell et al., 1994, fig.8; Brochu, 1999, fig.25). By contrast, the quadratojugal forms only half the length of the posterior margin of the infratemporal fenestra in extant *Crocodylus* species, with the remainder formed by the quadrate (Fig. 3.38E). Several caimanines exhibit a similar condition, but differ in that the quadratojugal is dorsally truncated by the postorbital, which forms the remainder of the posterior fenestral margin (Fig. 3.38D).

100. Postorbital, posteroventral process in quadratojugal at dorsal corner of the infratemporal fenestra: absent (0); present (1) (after Norell, 1989 [11]; Brochu, 1997b [76]).

101. Postorbital, morphology of posteroventral process in quadratojugal: narrow with acute 'V' shaped tip (0); broad, blunt tip (1) (after Norell, 1989 [11]; Brochu, 1997b [76]).

The dorsal margin of the infratemporal fenestra is a complex region where several bones intersect, including the quadrate, quadratojugal, squamosal and postorbital. Norell (1989) described the presence of a 'postorbital process' in *Bernissartia fagesii*, *Gavialis gangeticus*, and all alligatorids, which descends along the posterior margin of the infratemporal fenestra and is most clearly observed in lateral view (Fig. 3.38A). Brochu (1999) also recognised this 'postorbital process' but suggested that the intersection of the postorbital, quadrate, and quadratojugal was more complex, and best viewed from a ventromedial direction. Accordingly, Brochu (1999) incorporated the presence of a postorbital process into a multistate character that also described various sutural intersections between the postorbital, quadrate, and quadratojugal ventromedially. This version of the character is commonly used in crocodylian phylogenetics; however, examination of several datasets reveals that the state describing the presence of a postorbital process is not scored in any taxon that clearly possesses it (e.g. Brochu, 1999; Brochu et al., 2012; Jouve, 2016; Narváez et al., 2016; Cidade et al., 2017; Iijima & Kobayashi, 2019). Here, the presence of a postorbital process is treated as a binary character following Norell (1989), independent of the ventromedial sutural relationships of the postorbital, quadrate, and quadratojugal (Characters 105 and 106). Furthermore, variation in the morphology of the postorbital process is also recognised (Character 101). Where preserved, all species of *Alligator* exhibit a small, acute postorbital process (101-0, Fig. 3.38C). This contrasts with the condition exhibited by most caimanines, which have a notably broader postorbital process (101-1, Fig. 3.38D).

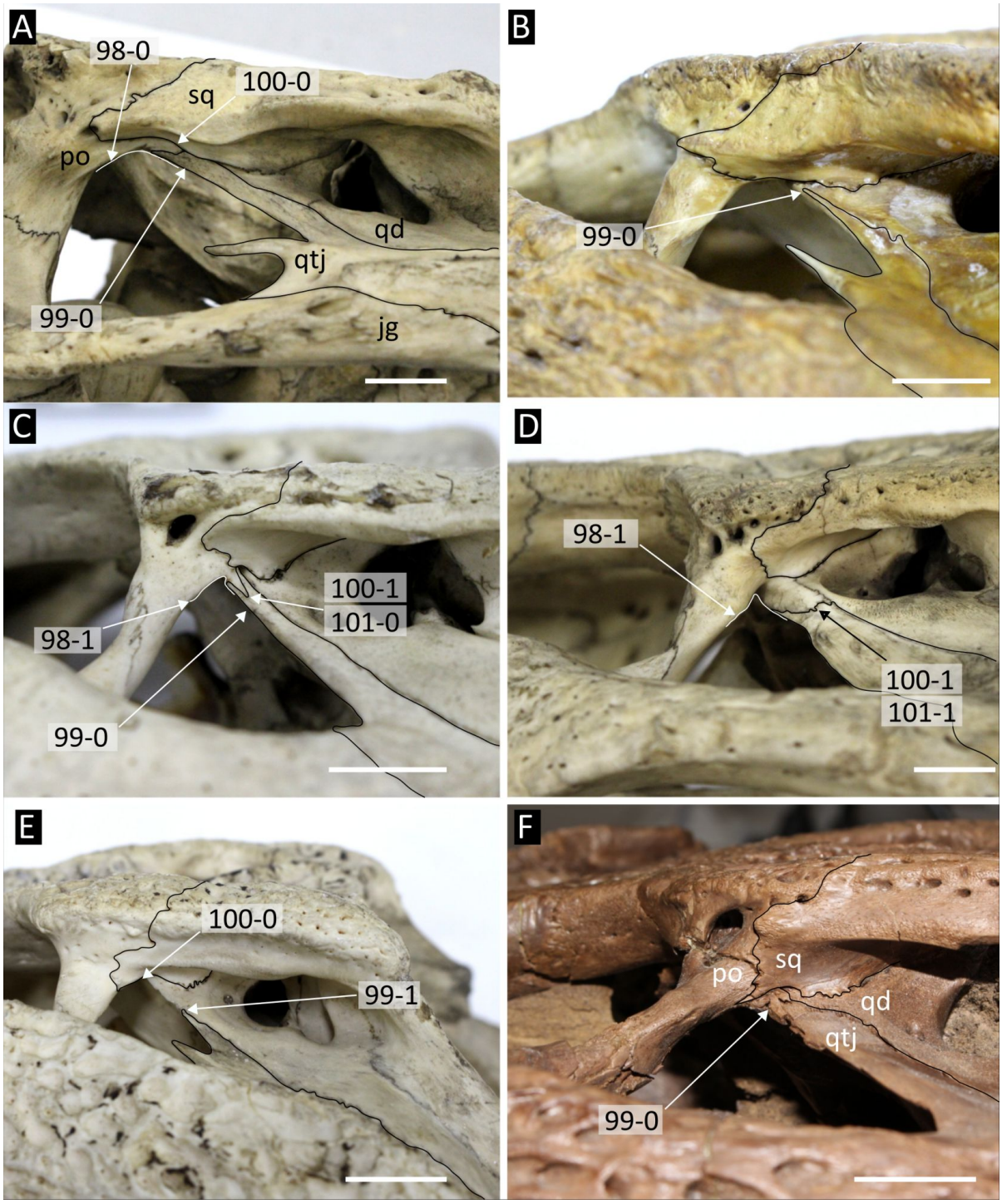



Figure 3.38: Sutural relationships and morphology of the infratemporal fenestra in selected crocodylians. **A** *Gavialis gangeticus* (NHMUK 1974.3009); **B**, *Tomistoma schlegelii* (NHMUK 1894.2.21.1); **C**, *Alligator mississippiensis* (NHMUK 1873.2.21.1); **D**, *Melanosuchus niger* (NHMUK 45.8.25.125); **E**, *Crocodylus niloticus* (NHMUK 1934.6.3.1); **F**, *Brachychampsa montana* (UCMP 133901). Abbreviations: **po**, postorbital; **qd**, quadrate; **qtj**, quadratojugal; **sq**, squamosal. All scale bars = 2 cm.

102. Infratemporal fenestra, posterior angle: quadratojugal forms posterior angle (0); quadratojugal-jugal suture lies at posterior angle (1); jugal forms posterior angle (2) (after Norell, 1989 [5]; Brochu, 1997b [75]) (ORDERED).

    Norell (1989) recognised that the quadratojugal forms the posterior angle of the infratemporal fenestra in *Bernissartia fagesii*, *Gavialis gangeticus*, and all alligatorids (Fig. 3.39A), contrasting with the condition in extant *Crocodylus* species, in which the angle is formed by the jugal (Fig. 3.39D). Brochu (1999) later introduced a condition in which the jugal-quadratojugal suture lies directly on the posterior angle of the infratemporal fenestra (Fig. 3.39C) (102-1), a condition which appears to be restricted to several mekosuchines according to the data matrices of Brochu (2007a) and Brochu et al. (2012). This latter condition is recognised more widely in crocodylids in this analysis, with a polymorphic condition present in several *Crocodylus* species, e.g. *C. porosus* (102-1 in NHMUK 1852.12.9.2, 102-2 in NHMUK 85.2.4.1). Furthermore, the character is ordered, describing the progressive decrease in participation of the quadratojugal in the posterior angle of the infratemporal fenestra.

103. Quadratojugal, development of spina quadratojugalis (at maturity): prominent (0); greatly reduced or absent (1) (after Norell, 1989 [1]; Brochu, 1997b [69]).

    This character has received minor modifications to wording only, and the meaning of the character is as originally described by Norell (1989). A prominent spine (e.g. Fig. 3.39A, C, D) is considered plesiomorphic in Crocodylia as it occurs in *Bernissartia fagesii* as well as taxa such as *Allodaposuchus precedens* (Narváez et al., 2019). All extant crocodylids, as well as *Tomsitoma schlegelii* (NHMUK 1894.2.21.1), and *Gavialis gangeticus* (NHMUK 1974.3009), exhibit the prominent spine, which is absent or restricted to a small protuberance in alligatorids (Fig. 3.39B).

104. Quadratojugal, position of spina quadratojugalis: low, near posterior angle of infratemporal fenestra (0); high, between posterior and dorsal angles of infratemporal fenestra (1) (after Brochu, 1997b [114]).

    This character has received only minor modifications to wording but several character score changes. In most eusuchians that possess a quadratojugal spine, it occurs at a 'low' position, below the dorsoventral mid-height of the infratemporal fenestra (Fig. 3.39A). In all alligatorids that preserve a quadratojugal spine, it occurs beyond the dorsoventral mid-height of the infratemporal fenestra (Fig. 3.39B). Fewer taxa are scored for the derived condition than in previous studies (e.g. Brochu et al., 2012; Salas-Gismondi et al., 2015; Cidade et al., 2017), as the quadratojugal spine is too poorly developed or absent to determine its position in some taxa.

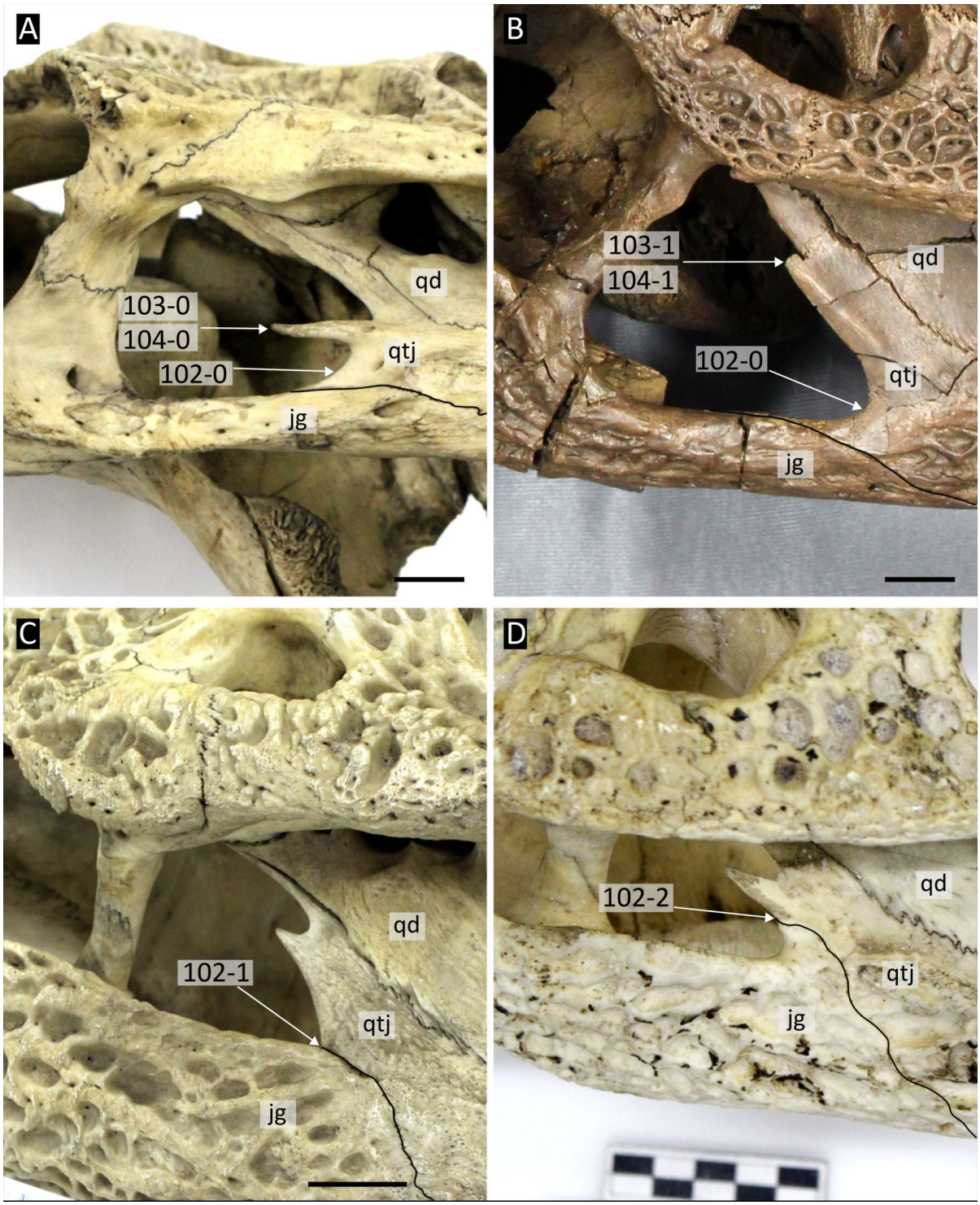



Figure 3.39: Variation in the contribution of the quadratojugal to the infratemporal fenestra in selected crocodylians. **A**, *Gavialis gangeticus* (NHMUK 1974.3009); **B**, *Brachychampsa montana* (UCMP 133901); **C**, *Crocodylus porosus* (NHMUK 1852.12.9.2); **D**, *Crocodylus niloticus* (NHMUK 1934.6.3.1). Abbreviations: **jg**, jugal; **qd**, quadrate; **qtj**, quadratojugal. Scale bars A–C = 2 cm, D = cm.

105. Postorbital, medial contact with quadrate at dorsal corner of the infratemporal fenestra: absent (0); present (1) (after Brochu, 1997b [76]).

106. Postorbital, medial contact with quadratojugal at dorsal angle of infratemporal fenestra: absent (0); present (1) (after Brochu, 1997b [76]).

    Characters 105 and 106 describe variation in sutural relationships between the postorbital, quadratojugal, and quadrate in a ventromedial orientation (Fig. 3.40). This variation was originally discretised as follows: "*Postorbital neither contacts quadrate nor quadratojugal medially (0), or contacts quadratojugal, but not quadrate, medially (1), or contacts quadrate and quadratojugal at dorsal angle of infratemporal fenestra (2), or contacts quadratojugal with significant descending process (3)*" (Brochu, 1997b). The original formulation incorrectly implies that contact between the quadratojugal and postorbital is homologous to contact between the quadrate and postorbital. It also precludes the recognition of evolutionary relationships between taxa that share a postorbital-quadratojugal contact. Furthermore, alternative combinations of postorbital-quadrate-quadratojugal contact cannot be accounted for in the original formulation. For example, Jouve (2016) recognised a contact between the postorbital and quadrate to the exclusion of the quadratojugal in *Maroccosuchus zennaroi*, which is also recognised here in *Tomistoma schlegelii* (Fig. 3.40F). As a result, the original character was converted into two binary presence/absence characters. Generally, crocodylids exhibit no medial contact between the quadrate, quadratojugal, and postorbital (Fig. 3.40A–C). By contrast, alligatorids exhibit contact between the postorbital and both the quadrate and quadratojugal (Fig. 3.40G–I). Other taxa exhibit different combinations of these conditions. For example, whereas *Gavialis gangeticus* exhibits a quadratojugal-postorbital contact (106-1), but no quadrate-postorbital contact (105-0) (Fig. 3.40E), *Tomistoma schlegelii* exhibits the opposite conditions (106-0, 105-1) (Fig. 3.40F).

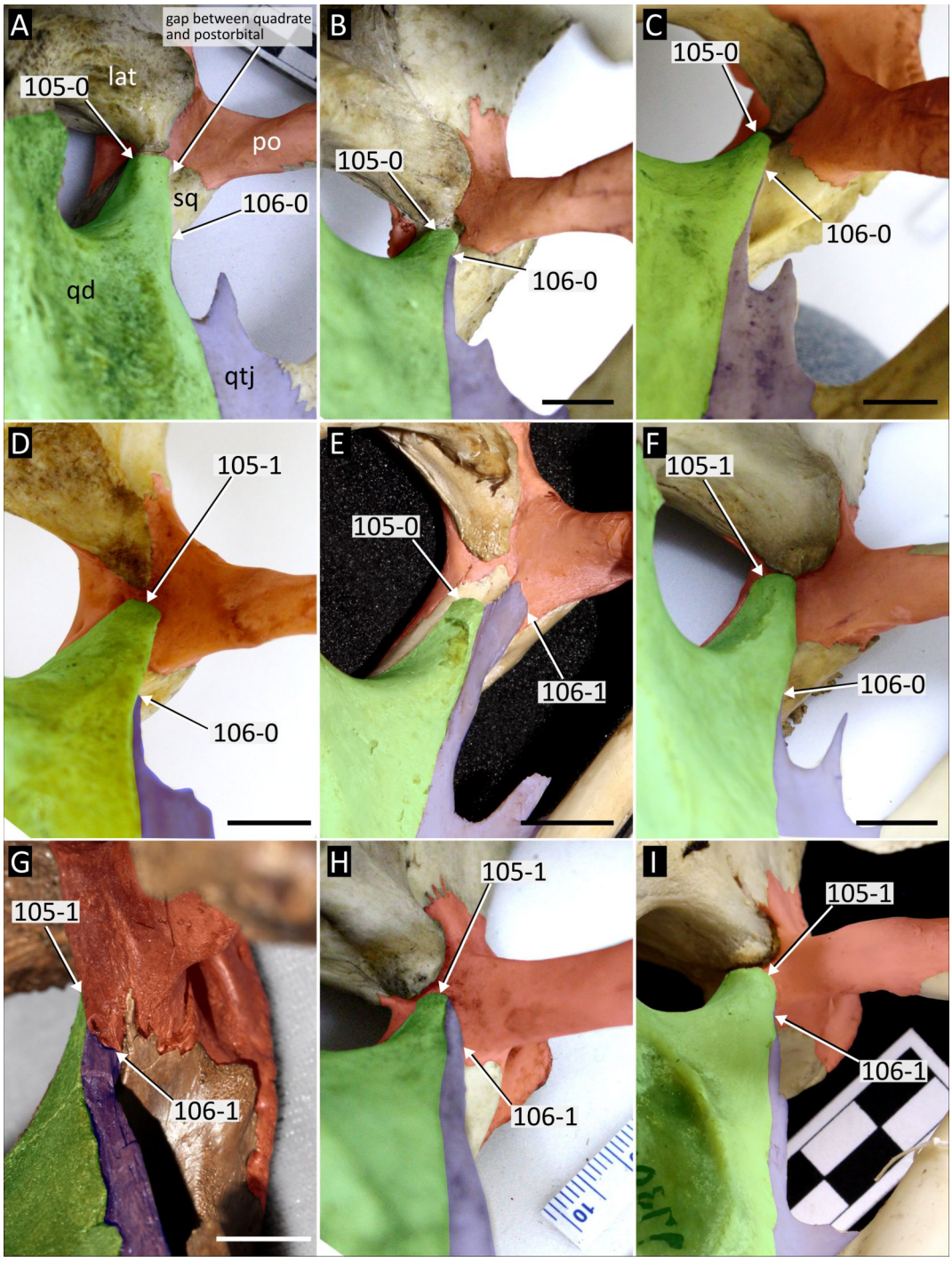



Figure 3.40: Ventromedial view of the dorsal corner of the postorbital showing sutural relationships of the postorbital (red), quadrate (green), and quadratojugal (blue). **A**, *Crocodylus moreletti* (NHMUK 1861.4.1.4); **B**, *Crocodylus siamensis* (NHMUK 1921.4.1.168); **C**, *Crocodylus palustris* (NHMUK 1897.12.31.1); **D**, *Mecistops cataphractus* (NHMUK 1924.5.10.1); **E**, *Gavialis gangeticus* (NHMUK uncatalogued); **F**, *Tomistoma schlegelii* (NHMUK 1894.2.21.1); G, *Brachychampsa montana* (UCMP 133901); **H**, *Alligator mississippiensis* (NHMUK 1873.2.21.1); **I**, *Caiman yacare* (AMNH 97300). Abbreviations: **lat**, laterosphenoid; **po**, postorbital; **qd**, quadrate; **qtj**, quadratojugal. All scale bars = 1 cm.

107. Squamosal, anterior divergence of dorsal and ventral rims of lateral groove: absent (0); present (1) (after Brochu, 1997b [84]).

Only minor modifications have been made to the wording of this character and scores are similar to previous studies (e.g. Brochu et al., 2012). The lateral groove of the squamosal is a narrow sulcus on the lateral cranial table edge that serves as an attachment site for external ear valve musculature (Fig. 3.41). In most crocodylians, the dorsal and ventral margins of the squamosal groove are either sub-parallel (Fig. 3.41A) or slightly taper anteriorly (Fig. 3.41D). By contrast, several (mostly longirostrine) crocodylians exhibit a dorsoventral expansion of the groove anteriorly, including *Thecachampsa sericodon* (Fig. 3.41), *Kentisuchus spenceri* (Fig. 3.41C), and *Piscogavialis jugaliperforatus* (Fig. 3.41E).

108. Squamosal, shape of the lateral cranial table edge, dorsal to the otic aperture: vertical, dorsal and ventral edges equally expanded laterally; (0) bevelled, ventral edge projects further laterally than dorsal edge (1) (after Lee & Yates, 2018 [81]).

The lateral cranial table margins slope prominently (i.e. they are bevelled) in *Hylaeochampsa vectiana* (NHMUK R177) and several (mostly longirostrine) crocodylians, including the "gavialoids" *Gavialis gangeticus* (NHMUK 1974.3009), *Piscogavialis jugaliperforatus* (Fig. 3.41E), and *Gryposuchus neoageus* (MLP 26-413), and the "tomistomines" *Kentisuchus spenceri* (Fig. 3.41C) and '*Tomistoma*' *dowsoni* (NHMUK PV R4769). This contrasts with the more commonly observed vertical lateral edge of the cranial table found in all extant alligatorids (Fig. 3.41A, C), crocodylids, and *Tomistoma schlegelii* (NHMUK 1894.2.21.1).

109. Squamosal, angle between dorsal profile of the paroccipital process and dorsal margin of the cranial table: $< 10°$ (approximately horizontal) (0); 10–50° (1); $> 50°$ (2) (after Lee & Yates, 2018 [88]) (ORDERED).

This character was modified from Lee and Yates (2018) by the addition of a state (109-0) and by ordering of the character. In most eusuchians, the dorsal profile of the paroccipital process is posteroventrally inclined, around 45° (109-1), as in *Hylaeochampsa vectiana* (NHMUK R177), most extant alligatorids (e.g. *Alligator mississippiensis*, Fig. 3.41A), crocodylids (e.g. *Crocodylus*), and "tomistomines" (e.g. *Kentisuchus spenceri*, Fig. 3.41C). In some crocodylians, the paroccipital process curves off abruptly to form a $\sim$90° angle between the dorsal and posterior edges of the squamosal (109-2), e.g. *Paleosuchus trigonatus* (Fig. 3.41D), *Osteolaemus tetraspis* (NHMUK 1862.6.30.5), and *Mekosuchus* (e.g. *M. sanderi*, QM F31166). A small number of crocodylians exhibit a subhorizontal dorsal profile of the paroccipital process (109-0). This condition is principally observed in "gavialoids", such as *Piscogavialis jugaliperforatus* (Fig. 3.41E), *Gryposuchus colombianus* (UCMP 41136), and *Gryposuchus neogaeus* (MLP 26-413).

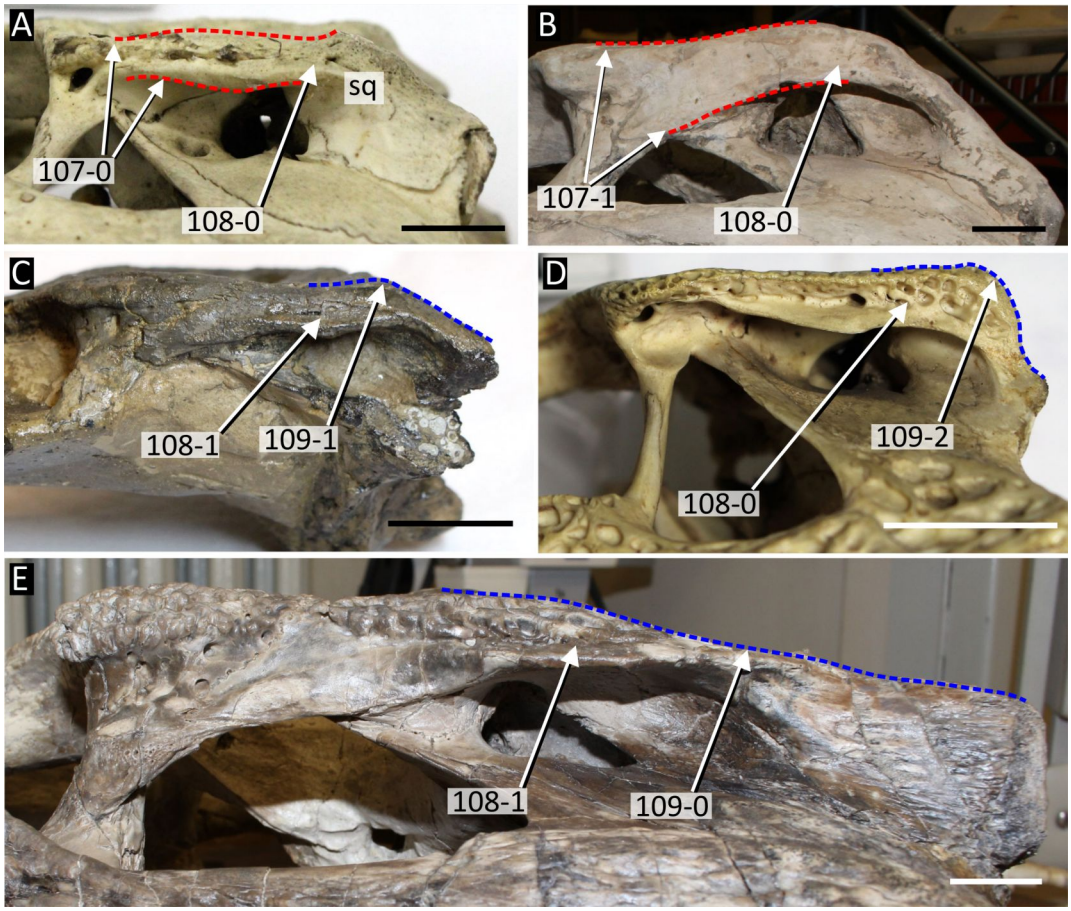



Figure 3.41: Left lateral view of the posterior cranium showing variation in lateral cranial table morphology in **A**, *Alligator mississippiensis* (NHMUK 1873.2.21.1); **B**, *Thecachampsa sericodon* (USNM 25243); **C**, *Kentisuchus spenceri* (NMHUK PV R 38975); **D**, *Paleosuchus trigonatus* (NHMUK 1868.10.8.1, digitally reversed); **E**, *Piscogavialis jugaliperforatus* (SMNK 1282 PAL). Abbreviations: **sq**, squamosal. All scale bars = 2 cm.

110. Squamosal, posterolateral prongs: absent, or very short, barely exceeding the level of the posterior wall of the cranial table behind supratemporal fenestrae (0); long, exceeding the level of the posterior margin of the cranial table, less than half anteroposterior cranial table length (1); long, greater than or equal to half anteroposterior cranial table length (2) (after Brochu, 1997b [140]; Jouve et al., 2008 [140]; Jouve, 2016 [64]) (ORDERED).

Squamosal prongs are posterolateral projections of the squamosal that extend from the cranial table (Fig. 3.42). As originally formulated by Brochu (1997b), this character was binary, describing the presence or absence of squamosal prongs. Jouve (2016) introduced a third character state describing 'very long' squamosal prongs. This modification is followed, but the length of the squamosal prongs is measured in proportion to the anteroposterior cranial table length. Furthermore, the character is now ordered, as it describes the progressive lengthening of the squamosal prongs. *Bernissartia fagesii* (IRScNB 1538) and most crocodylians exhibit the intermediate condition (Fig. 3.42B). *Hylaeochampsa vectiana* (NHMUK R177), *Iharkutosuchus makadii* (Ősi et al., 2007), and *Paleosuchus*

(Fig. 3.42A) exhibit the shortened condition. Highly elongated squamosal prongs occur exclusively in several longirostrine crocodylians (Jouve, 2016), including *Piscogavialis jugaliperforatus* (Fig. 3.42C), *Argochampsa krebsi* (NHMUK R36872), and *Gryposuchus colombianus* (UCMP 41136). Equally elongate prongs are newly recognised here in *Tomistoma cairense* (SMNS 50740) and *Tomistoma lusitanica* (Antunes, 1961).

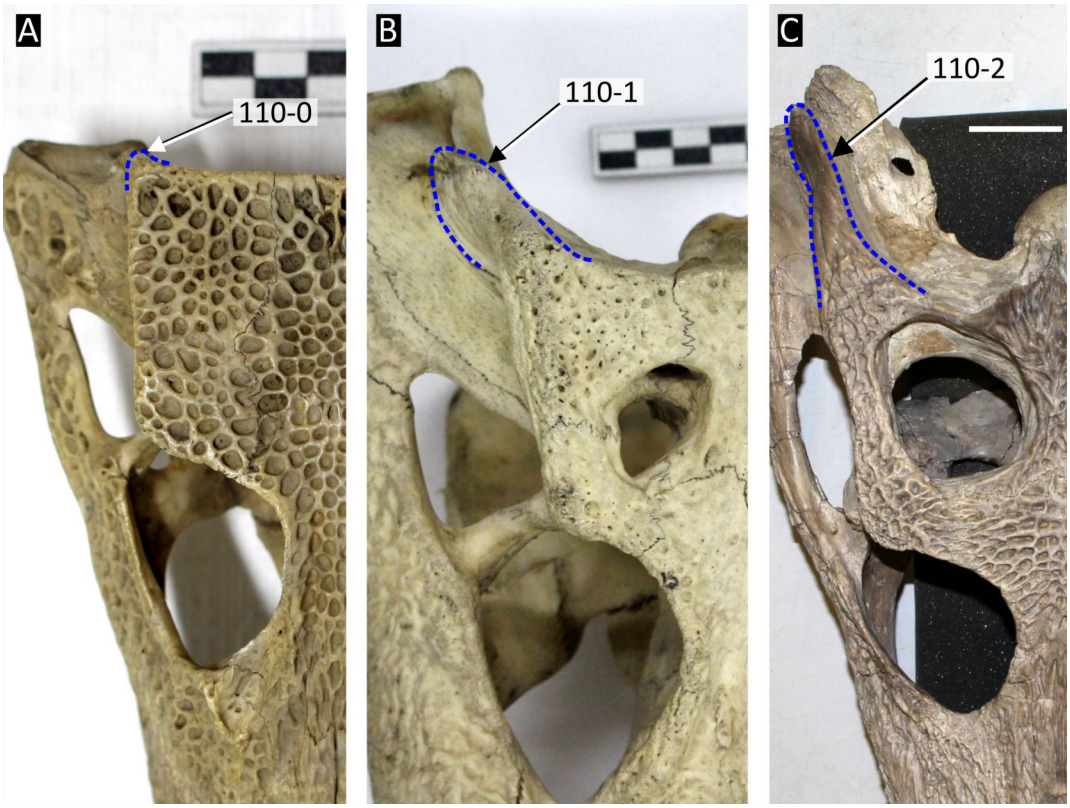



Figure 3.42: Dorsal view of the cranial table showing variation in length of the squamosal prongs (blue). **A**, *Paleosuchus trigonatus* (NHMUK 1868.10.8.1); **B**, *Alligator mississippiensis* (NHMUK 1873.2.21.1); **C**, *Piscogavialis jugaliperforatus* (SMNS 1282 PAL). Scale bar in C = 5 cm, all other scale bars = cm.

111. External auditory meatus, position of ventral margin: ventral to the level of the dorsal margin of infratemporal fenestra (0); level with or dorsal to the dorsal margin of the infratemporal fenestra (1) (new character, based on personal observations).

    The ventral margin of the external auditory meatus is lower than the level of the dorsal apex of the infratemporal fenestra in almost all eusuchians (Fig. 3.43A, C). By contrast, in *Purussaurus neivensis* (Fig. 3.43B), *Purussaurus brasiliensis* (UFAC 1403), and *Acresuchus pachytemporalis* (Fig. 3.43D), the external auditory meatus is positioned in a notably more dorsal position, beyond the dorsal margin of the infratemporal fenestra.

112. Quadrate, sutural contact with squamosal posterior to external auditory meatus: present (0); absent,

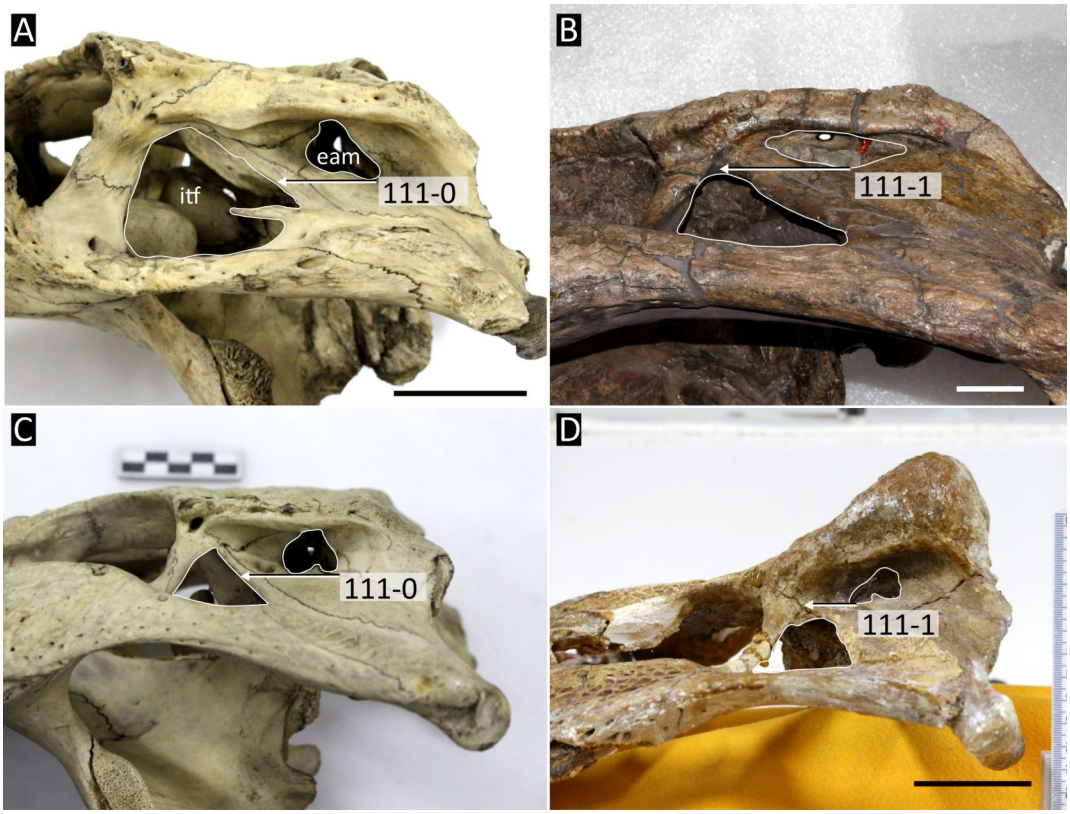



Figure 3.43: Lateral view of the cranium showing variation in dorsoventral height of the external auditory meatus relative to the infratemporal fenestra. **A**, *Gavialis gangeticus* (NHMUK 1974.3009); **B**, *Purussaurus neivensis* (UCMP 39704); **C**, *Alligator mississippiensis* (NHMUK 1873.2.21.1); **D**, *Acresuchus pachytemporalis* (UFAC 2507). Abbreviations: **eam**, external auditory meatus; **itf**, infratemporal fenestra. All scale bars = 5 cm.

exoccipital separates squamosal and quadrate posterior to external auditory meatus (1) (after Brochu, 1997b [132]; Delfino et al., 2008a [132]; Lee & Yates, 2018 [106]).

In all crocodylians, the squamosal and quadrate are in sutural contact posterior to the external auditory meatus (EAM), enclosing the cranioquadrate canal (112-0) (Fig. 3.44C–F). In *Allodaposuchus precedens* (Fig. 3.44A), *Hylaeochampsa vectiana* (Fig. 3.44B), and several other non-crocodylian eusuchians, the squamosal and quadrate are not in contact in this region, laterally exposing the cranioquadrate canal and the exoccipital that floors it (112-1) (Buscalioni et al., 2001; Delfino et al., 2008a). The condition in *Bernissartia fagesii* (IRScNB 1538) is unknown.

Characters 113 to 115 describe variation in the posterior margin of the EAM, which can only be scored if the squamosal and quadrate are in sutural contact (112-1). Several earlier analyses implemented these characters, without consideration for the absence of squamosal-quadrate contact in some taxa (e.g. Brochu, 1999; Brochu et al., 2012; Salas-Gismondi et al., 2015; Cidade et al., 2017). Other analyses included a modification used by Delfino et al. (2008a), in which characters 114 and 115 were each augmented with a character state, which effectively describes the absence of squamosal-quadrate

contact (Delfino et al., 2008a; Narváez et al., 2015; Jouve, 2016; Iijima & Kobayashi, 2019). This modification was not included here following the application of reductive coding, and because the inclusion of an additional state describing the same anatomical feature in two characters would be redundant, resulting in overweighting of this morphological feature.

113. Squamosal, descending lamina extending anteriorly over quadrate ramus from paroccipital process: absent (0); present (1) (after Brochu, 1997b [150]).

In taxa that exhibit contact between the squamosal and quadrate, the squamosal may extend ventrally along the paraoccipital process as a descending lamina. This condition occurs in several osteolaemines, comprising *Osteolaemus tetraspis* (Fig. 3.44F), *Brochuchus pigotti* (NHMUK R7729), *Euthecodon armabourgi* (MNHN ZEL 001), and variably in *Voay robustus* (Brochu, 2007a). In all other crocodylians, there is no descending lamina, and the squamosal-quadrate suture is straight (Fig. 3.44C–E).

114. Quadrate-squamosal suture, intersection with external auditory meatus: extends dorsally along posterior margin of EAM (suture separated from posterior margin) (0); or extends only to posteroventral corner of EAM (suture incipiently contacts posterior margin) (1) (after Brochu, 1997b [132]).

As described by Brochu (1999) and following most earlier studies, the quadrate-squamosal suture intersects the posteroventral corner of the EAM in most alligatoroids (Fig. 3.44E), *Boverisuchus vorax* (FMNH PR 399), and *Trilophosuchus rackhami* (QM F16856), whereas it ascends the posterior margin in most other crocodylians (Fig. 3.44C–D) (Brochu et al., 2012; Salas-Gismondi et al., 2015; Jouve, 2016; Iijima & Kobayashi, 2019). In several caimanines, the suture ascends the posterior EAM margin for a short distance, e.g. *Caiman latirostris* (NHMUK 86.10.4.2, FMNH 9713), *Melanosuchus niger* (NHMUK 45.8.25.125), and *Paleosuchus trigonatus* (NHMUK 1868.10.8.1); however, as with previous authors, I regard the condition in these taxa as closer to the derived condition.

115. External auditory meatus, posterior margin shape: straight (0); invaginated (1) (after Brochu, 1997b [102]; Salisbury et al., 2006 [102]; Delfino et al., 2008a [102]).

In most crocodylians that exhibit contact between the quadrate and squamosal, the posterior wall of the EAM is infolded to form an anterior process (Fig. 3.44F). This condition occurs in most extant crocodylids (Fig. 3.44D), alligatorids (Fig. 3.44E), and *Tomistoma schlegelii*. By contrast, the suture is straight in most "gavialoid" crocodylians, e.g. *Gavialis gangeticus* (Fig. 3.44C), as well as planocraniids, among other crocodylians.

116. Quadrate, foramen aereum size: small, diameter less than half dorsoventral height of medial hemicondyle (0); large, equal to or greater than half dorsoventral height of medial hemicondyle (1) (after Brochu, 2006 [165]; Brochu, 2011 [178]).

The quadratic foramen aerum is a circular opening on the dorsomedial margin of the quadrate condyle. This foramen accommodates an epithelial tube which runs towards a corresponding foramen on the articular (Brochu, 2006b). In most crocodylians, the quadratic foramen aerum is very small (Fig. 3.45R), but it is notably enlarged in *Eosuchus lerichei* (Fig. 3.45S) and *Eosuchus minor* (YPM 282).

117. Quadrate, foramen aereum position on posterior quadrate ramus: on dorsomedial corner (0); or on dorsal surface (1) (after Brochu, 1997b [121]).

The derived character state describes a dorsally positioned foramen aerum that has long been held as an alligatoroid synapomorphy (Brochu, 1999). Indeed, this condition occurs in all extant alligatorids such as *Alligator mississippiensis* (Fig. 3.45H), *Melanosuchus niger* (Fig. 3.45I), and *Caiman yacare* (Fig. 3.45J), as well as 'basal' alligatoroids such as *Diplocynodon hantoniensis* (Fig. 3.45F). The condition has also been recognised in some non-crocodylian eusuchians, such as *Allodaposuchus precedens* (Delfino et al., 2008a; Martin et al., 2016a; Narváez et al., 2019) and *Lohuecosuchus megadontos* (Narváez et al., 2015). *Bernissartia fagesii* (IRScNB 1538) and most non-alligatoroid crocodylians have a medially positioned foramen (Fig. 3.45N, O). Character scores between this study and previous studies (e.g. Brochu et al., 2012; Narváez et al., 2016; Lee & Yates, 2018), are mostly in agreement, except that the dorsally positioned foramen aerum is newly recognised in two *Borealosuchus* species: *B. sternbergii* (Fig. 3.45G) and *B. formidabilis* (Erickson, 1976, fig.6).

118. Quadrate condyle, notch on the dorsal articular border: absent or small, restricted to dorsomedial edge of quadrate articular border (0); large, as an extensive indentation of the dorsal articular border, covering up to a third of the mediolateral width of the quadrate condyle (1); inset from dorsomedial edge of the condyle (2) (adapted from Brochu, 1997b [112]).

119. Quadrate condyle shape, dorsal and ventral margins: subparallel across length (sub-rectangular condyle) (0); medially tapering (1); constricted at mid-length (2); ventrally reflected medial hemicondyle (3) (adapted from Brochu, 1997b [112]).

Characters 118 and 119 attempt to capture the seemingly nebulous variation in the morphology of the quadrate condyle that was originally discretised in one multistate character: "*Quadrate with small, ventrally-reflected medial hemicondyle (0) or with small medial hemicondyle; dorsal notch for foramen aerum (1), or with prominent dorsal projection between hemicondyles (2), or with expanded medial hemicondyle (3)*" (Brochu, 1997b). There are several issues with the previous delimitation of this character, as well as scores in earlier datasets. Firstly, the original character describes morphological features that might not be homologous: the presence of a dorsal notch in state 1; the presence of a dorsal projection between the hemicondyles in state 2; and the shapes of the medial and lateral hemicondyles in states 0, 1, and 3. Furthermore, examination of taxa assigned to each state reveals

differences in morphology. Taxa usually scored for character state 0 in the original character such as *Gavialis gangeticus*, *Eogavialis africanum*, *Eosuchus lerichei*, and *Borealosuchus*, do not share the same morphology of the quadrate condyle. *Gavialis gangeticus* has a rectangular quadrate condyle (Fig. 3.45R), with indistinct medial and lateral hemicondyles, and little to no notch at maturity. By contrast, *Borealosuchus sternbergii* has a large notch on the medial hemicondyle (Fig. 3.45G), similar to the condition in *Alligator* (Fig. 3.45E, H) and *Diplocynodon hantoniensis* (Fig. 3.45F). *Eogavialis africanum* also differs (Fig. 3.45Q), with a dorsoventral constriction in the quadrate condyle similar to *Voay robustus* (Fig. 3.45M), *Crocodylus* (Fig. 3.45N), and *Eosuchus lerichei* (Fig. 3.45S). Taxa scored for character state 112-1 of Brochu (1997b) are almost entirely alligatoroids, including *Diplocynodon*, *Caiman*, *Melanosuchus*, and *Alligator*, as well as some mekosuchines (Brochu et al., 2012). Although it is agreed that the medial hemicondyle in all alligatoroids bears a notch (Fig. 3.45E–F, I–I), the morphology of the notch is variable. In all extant caimanines, there is a small dorsal notch, inset from the medial edge of the quadrate condyle (Fig. 3.45I–J). This contrasts with the condition in *Alligator* (Fig. 3.45E, H), *Diplocynodon hantoniensis* (Fig. 3.45F) and several mekosuchines (Fig. 3.45C–D), in which the notch is wide and deep, reaching up to one third of the quadrate condyle width. Character state 112-2 (Brochu, 1997b) describes "*a prominent dorsal projection between hemicondyles*" that is shared only by *Boverisuchus vorax* and *Boverisuchus magnifrons* in the dataset of Brochu et al. (2012). The quadrate condyles of *Boverisuchus* were figured by Brochu (2012, fig.14), but their morphology is considered more similar to the condition in mekosuchines and alligatoroids here (Fig. 3.45C–D). The morphology described in character state 112-3, and the taxa assigned to this character state, are mostly agreed on here. The dorsoventrally expanded lateral hemicondyle is well expressed in most crocodyloids, resulting in an hour-glass shaped quadrate condyle (Fig. 3.45M–N). These observations have led to the division of the original character into two multistate characters: one describing the morphology of the notch (118) and the other describing the shapes of the medial and lateral hemicondyles (119). Neither character is ordered. The notch on the quadrate condyle is extremely small (118-0) in all *Crocodylus* species (118-0) (Fig. 3.45N), *Gavialis gangeticus* (Fig. 3.45R), and *Tomistoma schlegelii* (Fig. 3.45O). In caimanines, the notch becomes medially inset and remains small (118-2), e.g. *Melanosuchus niger* (Fig. 3.45I). The notch is deep and wide (118-1) in *Alligator olseni* (Fig. 3.45E), *Diplocynodon hantoniensis* (Fig. 3.45F), *Borealosuchus sternbergii* (Fig. 3.45G), *Trilophosuchus rackhami* (Fig. 3.45D), and *Boverisuchus vorax* (Fig. 3.45A). Character 119 describes four morphotypes of the quadrate: sub-rectangular (119-0), e.g. *Boverisuchus vorax* (Fig. 3.45A) and *Alligator* (Fig. 3.45E); medially tapering (119-1), e.g. *Melanosuchus* (Fig. 3.45I), *Caiman yacare* (Fig. 3.45J), *Protocaiman peligrensis* (Fig. 3.45K), and *Procaimanoidea utahensis* (Fig. 3.45L); constricted at the mid-length (119-2), e.g. *Voay robustus* (Fig. 3.45M), *Crocodylus acutus* (Fig. 3.45N), *Tomistoma schlegelii* (Fig. 3.45O), and *Eogavialis africanum* (Fig. 3.45Q); and

ventrally reflected, e.g. *Piscogavialis jugaliperforatus* (Fig. 3.45T).

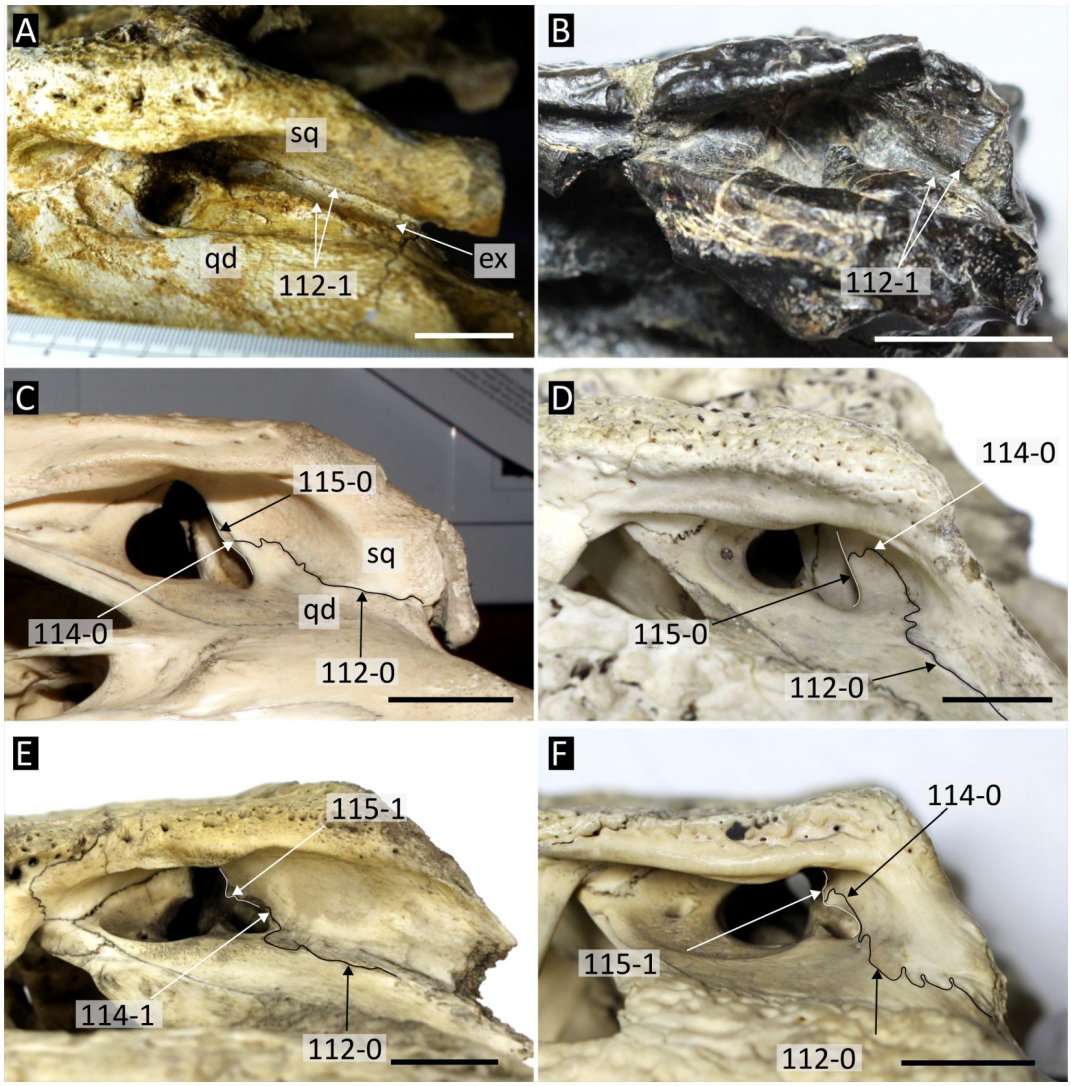



Figure 3.44: Sutural relationships of the external auditory meatus in Eusuchia. **A**, *Allodaposuchus precedens* (MMSVBN-12-10A); **B**, *Hylaeochampsa vectiana* (NHMUK PV R 177); **C**, *Gavialis gangeticus* (NHMUK 1974.3009); **D**, *Crocodylus niloticus* (NHMUK 1934.6.3.1); **E**, *Melanosuchus niger* (NHMUK 45.8.25.125); **F**, *Osteolaemus tetraspis* (NHMUK 1862.6.30.5). All scale bars = 2 cm.

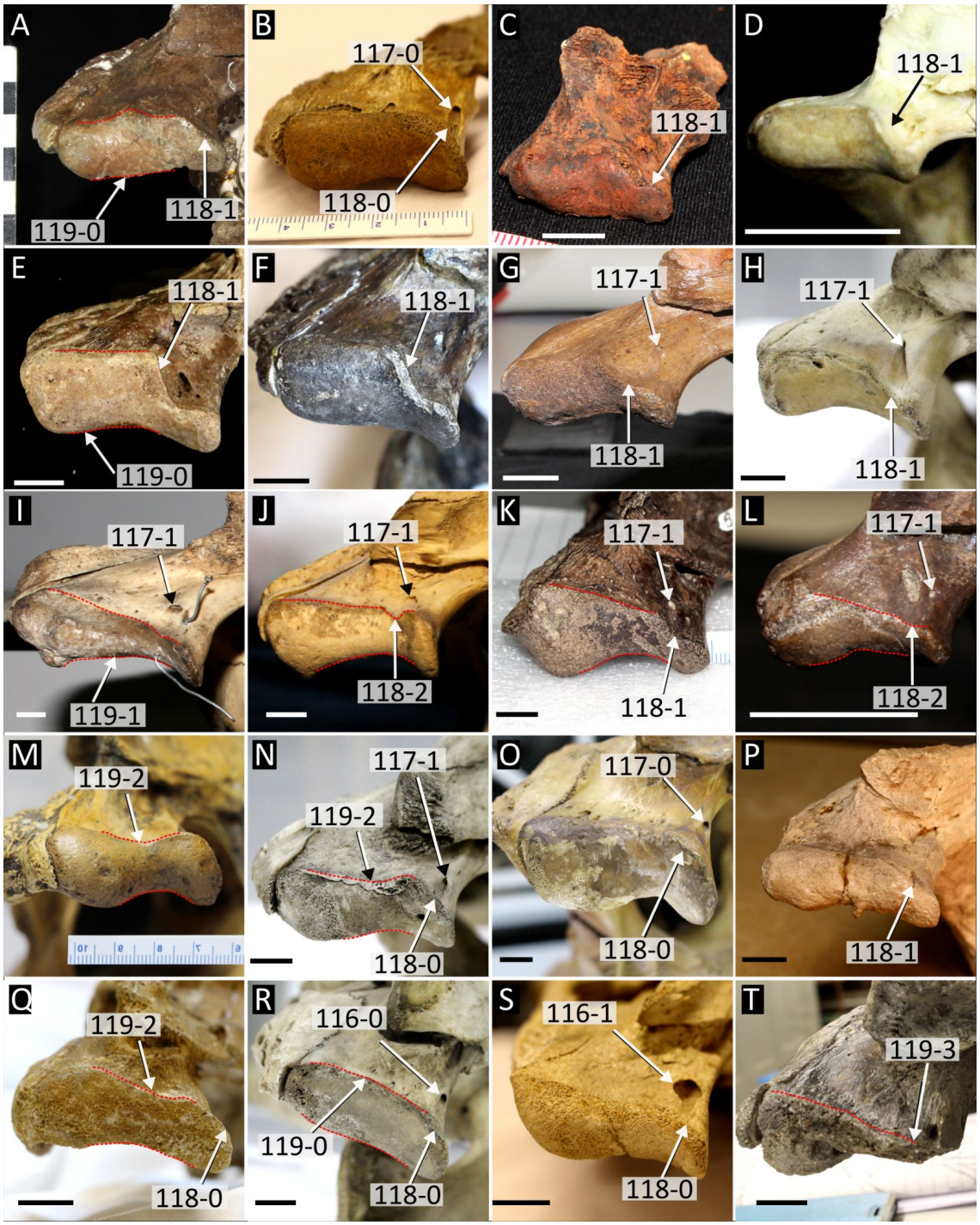



Figure 3.45: Posterior view of the quadrate condyle showing variation in condyle morphology in selected crocodylians. **A**, *Boverisuchus vorax* (FMNH PR 399); **B**, *Asiatosuchus depressifrons* (IRSNB R 0251); **C**, *Mekosuchus inexpectatus* (MNHN NCP 06); **D**, *Trilophosuchus rackhami* (QM F16856); **E**, *Alligator olseni* (MCZ uncatalogued); **F**, *Diplocynodon hantoniensis* (NHMUK 30392); **G**, *Borealosuchus sternbergii* (USNM V6533) **H**, *Alligator mississippiensis* (NHMUK 1873.2.21.1); **I**, *Melanosuchus niger* (NHMUK 45.8.25.125); **J**, *Caiman yacare* (MACN uncatalogued); **K**, *Protocaiman peligrensis* (MLP 80X-10-1), **L**, *Procaimanoidea utahensis* (USNM V 15996); **M**, *Voay robustus* (NHMUK R 36685); **N**, *Crocodylus acutus* (NHMUK 1975.997) **O**, *Tomistoma schlegelii* (NHMUK 1894.2.21.1); **P**, '*Tomistoma*' *cairense* (SMNS 50739); **Q**, *Eogavialis africanum* (NHMUK PV R3108, digitally reversed); **R**, *Gavialis gangeticus* (NHMUK 1974.3009); **S**, *Eosuchus lerichei* (IRSNB R 49); **T**, *Piscogavialis jugaliperforatus* (SMNK 1282 PAL). All scale bars = 1 cm.

120. Quadratojugal, extent over lateral surface of posterior quadrate ramus: covers entire lateral surface (0); notch in quadratojugal, exposing quadrate ventrolaterally (1) (new character, based on personal observations).

In *Bernissartia fagesii* (IRScNB 1538) and most eusuchians, the jugal and quadratojugal extend posteriorly to conceal the lateral surface of the quadrate condyle (Fig. 3.46A, C). By contrast, a small gap is left where the quadrate remains exposed in all extant alligatorids (Fig. 3.46B, D). Several fossil alligatoroids also exhibit exposure of the quadrate here, including *Brachychampsa montana* (UCMP 133901), *Navajosuchus mooki* (MCZ 8381), *Procaimanoidea utahensis* (USNM 15996), and *Protocaiman peligrensis* (MLP 80X-10-1).

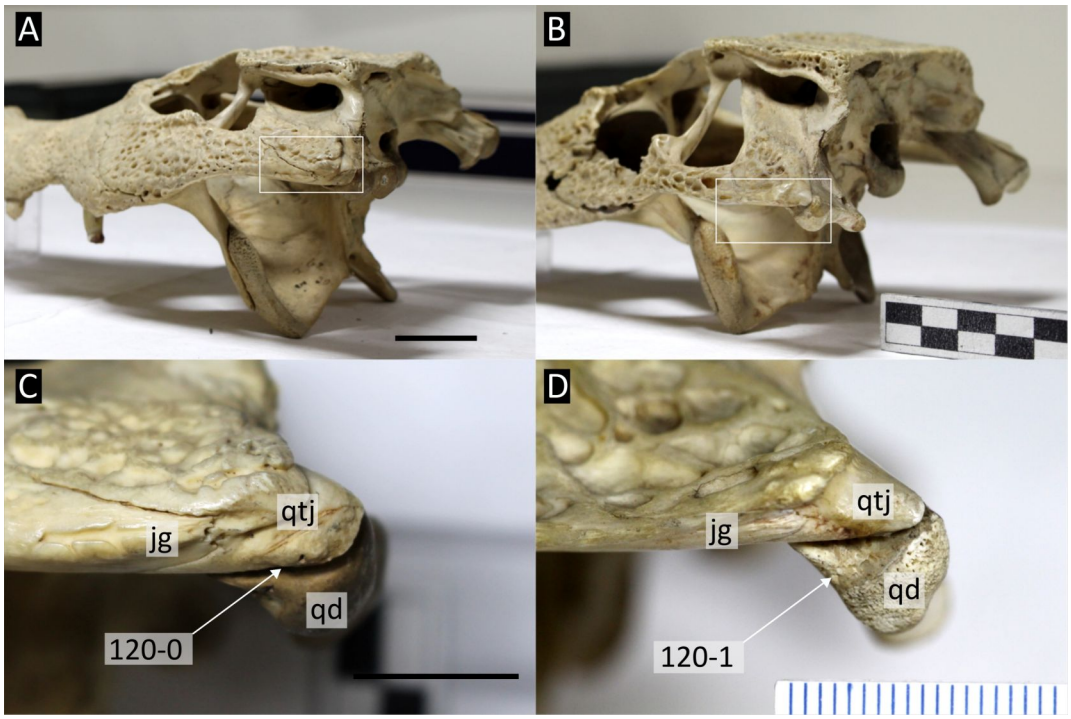



Figure 3.46: Lateral view of the quadrate ramus, showing variation in exposure of the quadrate beneath the quadratojugal. **A** and **C**, *Osteolaemus tetraspis* (NHMUK 1862.6.30.5); **B** and **D**, *Paleosuchus trigonatus* (NHMUK 1868.10.8.1). Abbreviations: **jg**, jugal; **qd**, quadrate; **qtj**, quadratojugal. Scale bars A, C = 2 cm; B = cm; D = mm.

121. Quadrate, posterior ramus length: distance between posterior margin of quadrate condyle and the level of the anterior margin of the occipital condyle, less than quadrate condyle mediolateral width (0); equal to or greater than quadrate condyle mediolateral width (1) (after Buscalioni et al., 2011 [184]).

The posterior ramus of the quadrate is anteroposteriorly long in most eusuchians, exceeding the posterior margin of the cranial table by at least the width of the quadrate condyle (Fig. 3.47A). By contrast, in *Bernissartia fagesii* (IRScNB 1538), *Isisfordia duncani* (QM F44320), and *Hylaeochampsa vectiana* (Fig. 3.47B), the quadrate ramus is short, barely exceeding the posterior edge of the cranial table

at most. The same condition occurs in some crocodylians, including *Alligator mcgrewi* (AMNH FAM 8700) and *Trilophosuchus rackhami* (QM F16856).

122. Exoccipital, extent on dorsal surface of quadrate ramus: small, not reaching articular border of quadrate condyle (0); large, extending to border of quadrate condyle (1) (new character, based on personal observations).

The exoccipital is minimally exposed on the dorsal surface of the posterior quadrate ramus in *Bernissartia fagesii* (IRScNB 1538) and nearly all eusuchians (Fig. 3.47A). However, in *Hylaeochampsa vectiana* (Fig. 3.47B), and *Iharkutosuchus makadii* (Mateus et al., 2019, fig.S14), the quadrate exoccipital suture extends over the dorsal surface of the quadrate ramus, such that the exoccipital reaches the border of the quadrate condyle.

123. Exoccipital, posterior projection of the paroccipital process: absent (0); present (1) (after Brochu, 1997b [141]).

Clark and Norell (1992) described a large protuberance positioned medial to the cranioquadrate canal in *Hylaeochampsa vectiana* (Fig. 3.47B). A similar process was subsequently described in several non-crocodylian eusuchians, such as *Allodaposuchus precedens* (Buscalioni et al., 2001), *Iharkutosuchus makadii* (Ősi, 2008), and *Lohuecosuchus megadontos* (Narváez et al., 2015). Furthermore, scores in existing matrices indicate that it occurs in *Bernissartia fagesii* and *Acynodon iberoccitanus* (e.g. Brochu et al., 2012; Jouve, 2016), which is agreed upon here. A protuberance or lamina occasionally occurs in large individuals of some crocodylians (Clark & Norell, 1992), but it is never as prominent as in *Hylaeochampsa*. Small differences occur in the morphology of the protuberance; for example, it is more of a ridge in *Allodaposuchus precedens* (Buscalioni et al., 2001, fig.10; Delfino et al., 2008a), but a discrete boss in *Hylaeochampsa* (NHMUK R177). These differences are not consistently found in enough taxa to allow further categorisations of the morphology.

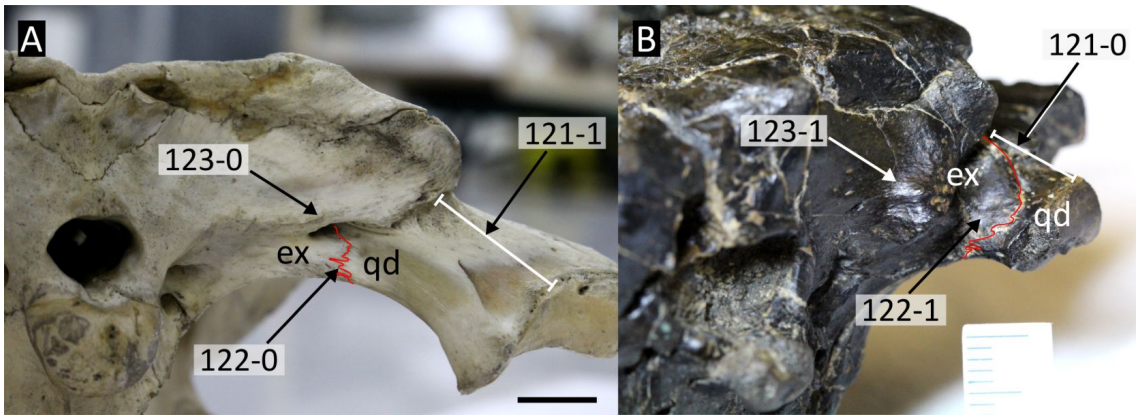



Figure 3.47: Posterolateral view of the occiput in **A**, *Alligator mississippiensis* (NHMUK 1873.2.21.1); and **B**, *Hylaeochampsa vectiana* (NHMUK PV R 177). Abbreviations: **ex**, exoccipital; **qd**, quadrate. Scale bar = 1 cm.

124. Quadrate, paroccipital process, distance between distal tip of paroccipital process and distal end of the quadrate condyle: less than the maximum mediolateral width of the quadrate condyle (0); equal to or greater than the maximum mediolateral width of the quadrate condyle (1) (after Lee & Yates, 2018 [111]).

    In most crocodylians, the paroccipital process extends towards the posterior end of the quadrate ramus, terminating shortly before the quadrate condyle (Fig. 3.48A). As recognised by Lee and Yates (2018), several crocodylians exhibit a notably wider gap between the distal tip of the paroccipital process and the distal tip of the quadrate ramus, e.g. *Australosuchus clarkae* (Fig. 3.48B). Whereas Lee and Yates (2018) scored the derived condition exclusively in a series of mekosuchines (*Palimnarchus gracilis*, *Baru*), here it is recognised in a broader sample of crocodylians, including alligatoroids, such as *Mourasuchus arendsi* (UFAC 2515) and *Alligator mississippiensis* (NHMUK 68.2.12.6), and "tomistomines", e.g. *Thecachampsa sericodon* (USNM 24938).

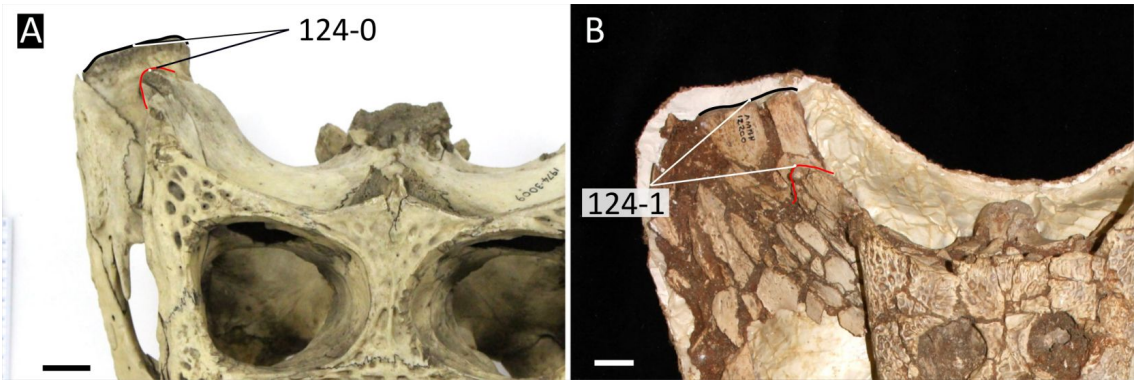



Figure 3.48: Dorsal view of the posterior end of the cranium showing variation in posterior extent of the paroccipital process on the quadrate ramus. **A**, *Gavialis gangeticus* (NHMUK 1974.3009); **B**, *Australosuchus clarkae* (AMNH 12200). Scale bars = 2cm.

125. Exoccipital, paroccipital process dorsal margin: squamosal-exoccipital suture sub-horizontal (0); dorsolaterally directed (1) (new character, adapted from Clark & Norell, 1992).

    Clark and Norell (1992) noted that the dorsolateral margin of the paroccipital process in *Hylaeochampsa vectiana* (NHMUK R177) curves dorsolaterally along the squamosal-exoccipital suture (Fig. 3.49B). A similar condition occurs in *Iharkutosuchus makadii* (Mateus et al., 2019, fig.S14). This differs to the condition in *Bernissartia fagesii* (IRScNB 1538) and all other eusuchians examined here, wherein the squamosal-exoccipital suture is straight and sub-horizontal (Fig. 3.49A).

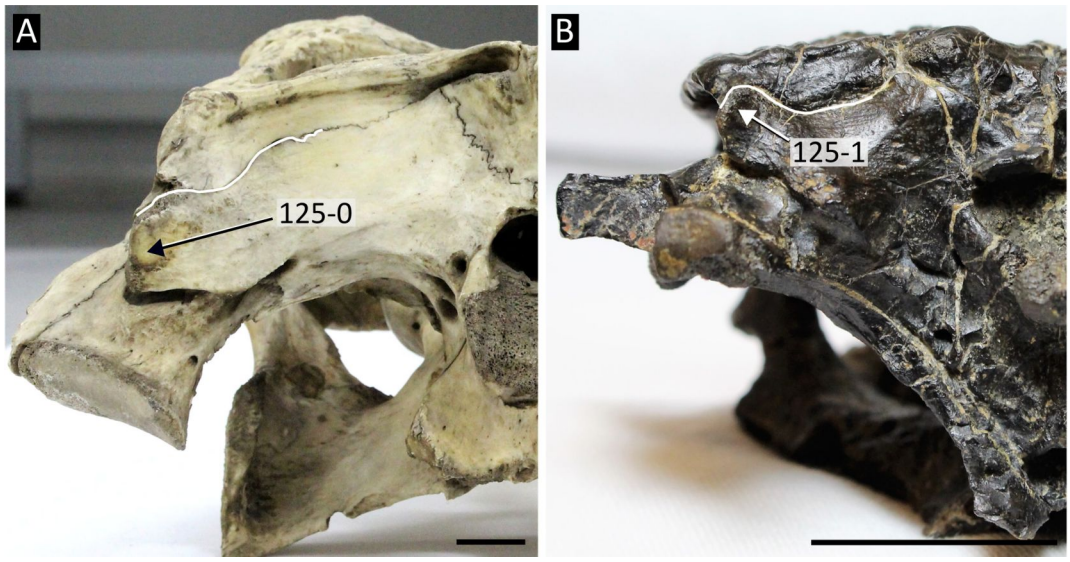



Figure 3.49: Occipital view of the cranium showing variation in orientation of the paroccipital process in **A**, *Gavialis gangeticus* (NHMUK 1974.3009); **B**, *Hylaeochampsa vectiana* (NHMUK PV R 177). Scale bars = 2 cm.

126. Lateral carotid foramen, proximity to metotic foramen: separated (positioned ventral to metotic foramen) (0); adjacent to the metotic foramen (1) (new character, based on personal observations).

    Several foramina pierce the exoccipital lateral to the foramen magnum in crocodylians (Fig. 3.50). Typically, there are two medially positioned openings for the hypoglossal nerves (CN XII), lateral to which is the much larger metotic foramen, which houses CN IX–XI (Iordansky, 1973; Bona & Desojo, 2011). The lateral carotid foramen is distantly separated and ventral to the metotic foramen in most crocodylians (e.g. Fig. 3.50A). By contrast, the lateral carotid foramen in several "gavialoids" is adjacent to the metotic foramen, separated by a thin wall. This latter condition occurs in *Gavialis gangeticus* (Fig. 3.50B), *Gryposuchus neogaeus* (Fig. 3.50C), *Gryposuchus colombianus* (UCMP 38358), *Eogavialis africanum* (YPM 6263), and *Piscogavialis jugaliperforatus* (SMNK 1282 PAL). It is also present in some non-crocodylian taxa such as *Hylaeochampsa vectiana* (NMHUK R177) and the 'Glen Rose Form' (MCZ 4384).

127. Exoccipitals, contact with basioccipital tubera: absent (0); present (1) (after Norell, 1988 [20]; Clark, 1994 [57, 60]; Brochu, 1997b [151]).

    Basioccipital tubera refer to the rugose ventral and ventrolateral surfaces of the basioccipital. In most crocodylians, the exoccipitals suture laterally to the basioccipital and do not extend ventrally to contact the tubera (Fig. 3.51A–B). An alternative condition is exemplified by *Gavialis gangeticus*, in which the exoccipitals have long descending processes that contact the tubera (Fig. 3.51C–D). This condition also occurs in several additional "gavialoids", including *Eogavialis africanum* (YPM 6263) and *Gryposuchus neogaeus* (MLP 68-IX-V-1). Brochu (1997b) included an additional state in his

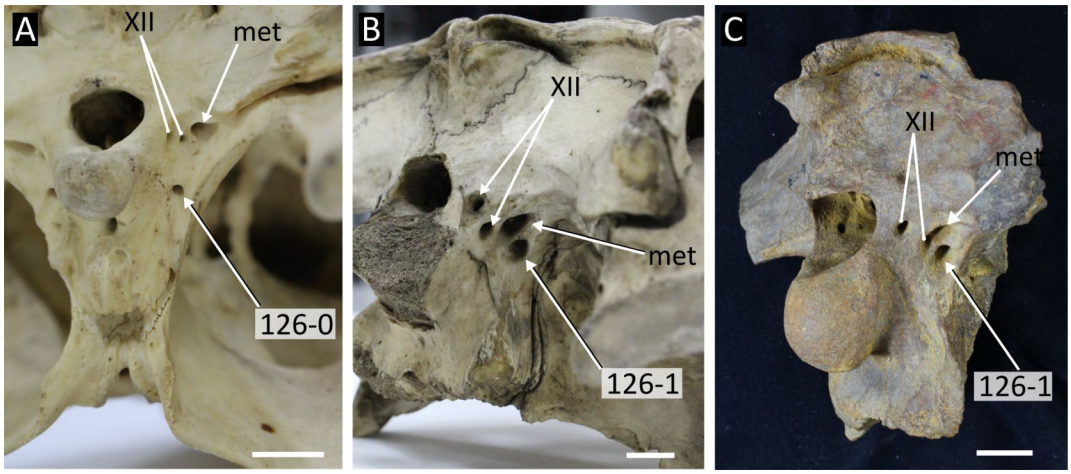



Figure 3.50: Proximity of the lateral carotid foramen relative to the metotic foramen in selected crocodylian taxa. **A**, *Caiman latirostris* (NHMUK 1897.12.31.1); **B**, *Gavialis gangeticus* (NHMUK 1974.3009); and **C**, *Gryposuchus neogaeus* (MLP 68-IX-V-1) (digitally reversed). Abbreviations: **met**, metotic foramen; **XII**, foramen for cranial nerve XII. All scale bars = 2 cm.

original formulation of the character, which described slender ventral processes that "participate in basioccipital tubera", which was scored in most caimanines. However, Brochu (1999) later noted that these processes do not actually contact the tubera in Caimaninae, but only extend slightly further ventrally than most other crocodylians. The description of these processes as slender is considered vague herein. Furthermore, the descending processes of caimanines examined here (e.g. *Caiman latirostris*: NHMUK 86.10.4.2; *Caiman crocodilus*: USNM 69812; *Melanosuchus niger*: NHMUK 1872.6.4.1) do not appear more slender than other taxa which lack an exoccipital-tubera contact. As a result, this character state has been removed and taxa formerly assigned to this state are now scored as lacking contact between the basioccipital tubera and exoccipital.

128. Exoccipitals, posteroventral inclination: absent, occiput vertical and not visible in dorsal view (0); present, occiput inclined posteriorly, visible in dorsal view (1) (after Hua & Jouve, 2004 [167]; Jouve et al., 2008 [167]).

When viewed dorsally, the occipital surface of most crocodylians is concealed, as a result of the vertical orientation of the exoccipitals that form much of the occipital surface (Fig. 3.52A, C). In rare instances, the exoccipitals are steeply inclined posteriorly, such that they are visible in dorsal view. The latter condition is exhibited exclusively in taxa recovered as "gavialoids" in most analyses, such as *Gavialis gangeticus* (Fig. 3.52B, D), *Gryposuchus neogaeus* (MLP 26-413), and *Piscogavialis jugaliperforatus* (SMNK 1282 PAL). By contrast with the scores in Jouve (2016), the condition is considered absent in *Thoracosaurus isorhynchus* (MNHN.F.MTA 61), *Borealosuchsus sternbergii* (USNM 6533, UCMP 126099), and *Borealosuchus formidabilis* (Erickson, 1976, fig.4).

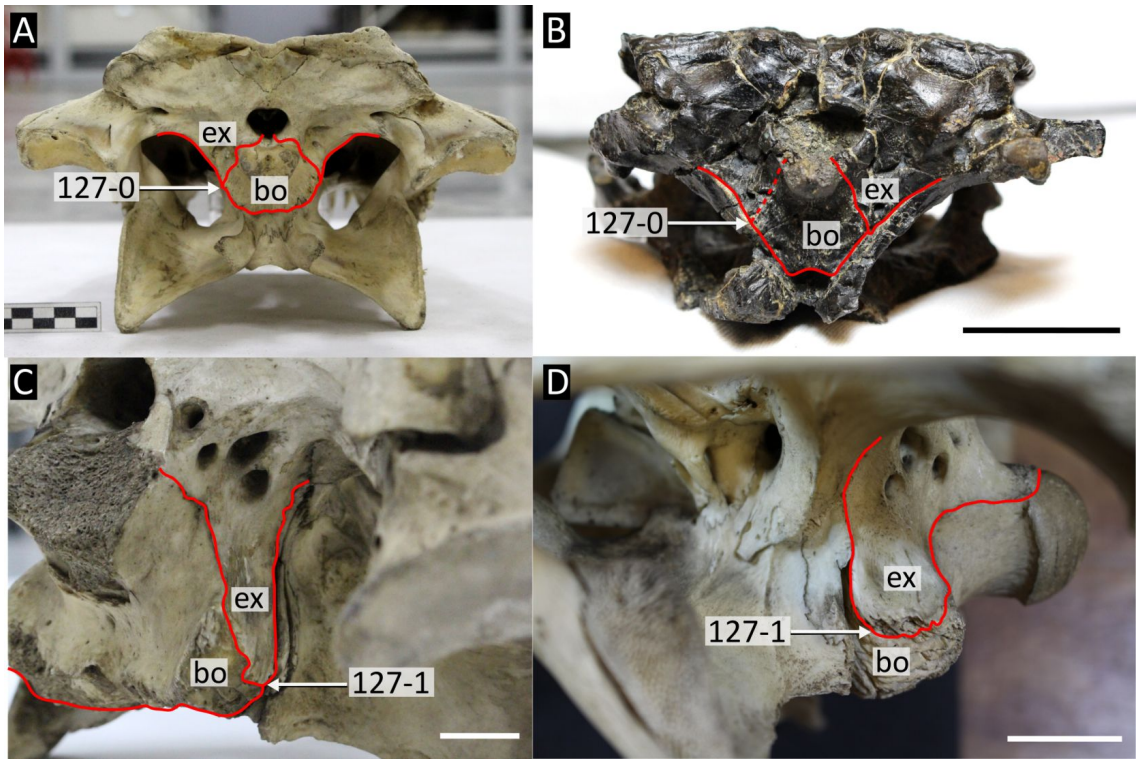



Figure 3.51: Ventral extent of the exoccipitals in selected crocodylian taxa. **A**, *Alligator mississippiensis* (NHMUK 1873.2.21.1); **B**, *Hylaeochampsa vectiana* (NHMUK PV R 177); **C**, *Gavialis gangeticus* (NHMUK 1974.3009) in posterolateral view; **D**, *Gavialis gangeticus* (NHMUK uncatalogued) lateral view of braincase. Abbreviations, **ex**, exoccipital; **bo**, basioccipital. All scale bars = 2 cm.

129. Basioccipital, orientation of lateral margins of ventral basioccipital plate: parallel or ventrally convergent (0); ventrally divergent (1) (after Jouve, 2004 [176]; Jouve et al., 2008 [189]; Salas-Gismondi et al., 2015 [196]).

    The lateral margins of the basioccipital are parallel for a short distance before converging ventrally in most eusuchians (Fig. 3.53A). However, some crocodylians, mainly "gavialoids", exhibit a different condition, in which the lateral margins flare ventrally, e.g. *Gavialis gangeticus* (Fig. 3.53B), *Eogavialis africanum* (NHMUK R3108), and *Piscogavialis jugaliperforatus* (SMNK 1282 PAL). Flaring basioccipital margins are additionally present in some species of the caimanine genus, *Mourasuchus*, including *M. arendsi* (UFAC 2515) and *M. amazonensis* (UFAC 1424).

130. Basioccipital, dorsoventral height of ventral plate exposed below occipital condyle relative to occipital condyle height: greater or equal in height (0); shorter (1) (adapted from Jouve, 2004 [197]; Jouve et al. 2008 [187]).

    Most crocodylians exhibit a basioccipital that is dorsoventrally tall, reflecting the verticalisation of the cranium that is common to most eusuchians (Tarsitano et al., 1989) (Fig. 3.53A). Variation in height of the basioccipital was discretised by previous authors using vague terms such as 'short'

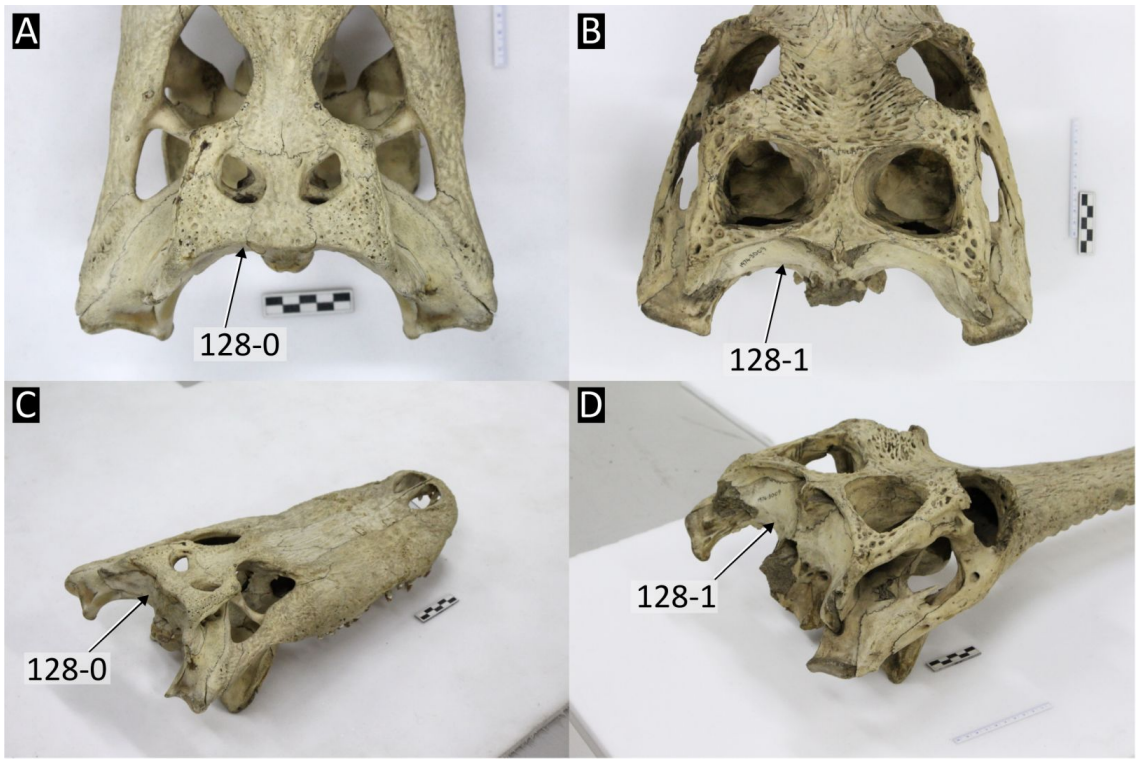



Figure 3.52: Variation in orientation of the occiput in *Alligator mississippiensis* (NHMUK 1873.2.21.1) (**A**, **C**); and *Gavialis gangeticus* (NHMUK 1974.3009) (**B**, **D**).

and 'tall' (Jouve, 2004; Jouve et al., 2008). Here the morphology is quantified using the relative dorsoventral height of the portion of the basioccipital below the occipital condyle (basioccipital plate) to that of the occipital condyle. The basioccipital plate is shorter than the occipital condyle in *Gavialis gangeticus* (Fig. 3.53B), *Gryposuchus* (e.g. *G. neogaeus*, MLP 68-18-5-1), *Eogavialis africanum* (NHMUK R3108), and *Thoracosaurus isorhynchus* (MNHN.F.MTA 61). In addition to these "gavialoids", a shortened basioccipital plate occurs in *Mourasuchus* (e.g. *M. atopus*, UCMP 38012), *Toyotamaphimeia machikanensis* (Kobayashi et al., 2006) and, despite its otherwise verticalised cranium, *Alligator mississippiensis* (e.g. NHMUK 68.2.12.6).

131. Basioccipital and ventral portion of exoccipital (otoccipital), orientation (at maturity): inclined anteriorly (0); vertical (1) (after Gomani, 1997 [32]; Hua & Jouve, 2004 [167]; Salisbury et al., 2006 [174]; Pol et al., 2009 [112]; Brochu et al., 2012 [168]).

In extant hatchling crocodylians, the ventral occipital surface formed by the exoccipitals and basioccipital is strongly inclined anteriorly (Tarsitano et al., 1989). With maturity, the occipital surface becomes vertical, which is common to most eusuchians (Fig. 3.53D). A small number of taxa studied here that are considered ontogenetically mature also exhibit this condition, including *Trilophosuchus rackhami* (QM F16856), *Shamosuchus djadochtaensis* (Pol et al., 2009), the 'Glen Rose Form' (MCZ 4384), and *Isisfordia duncani* (QM F44320).

132. Basioccipital, sagittal crest on ventral plate: present (0); absent (1) (after Jouve, 2004 [185]; Jouve et al., 2008 [180]).

The ventral plate of the basioccipital bears a midline crest in most eusuchians, including alligatorids (e.g. *Alligator mississippiensis*, Fig. 3.53E; *Caiman latirostris*, NHMUK 86.10.4.2; and *Paleosuchus trigonatus*, NHMUK 1868.10.8.1), crocodylids (e.g. *Osteolaemus tetraspis*, NHMUK 1862.6.30.5 and *Crocodylus porosus*, QM J47448), and *Borealosuchus sternbergii* (USNM 6533). Less commonly, the sagittal crest is absent, which mostly occurs in "gavialoids", e.g. *Gavialis gangeticus* (Fig. 3.53F), *Gavialis lewisi* (YPM 3226), *Gryposuchus neogaeus* (MLP 68-18-5-1), but also '*Tomistoma*' *dowsoni* (NHMUK R4769).

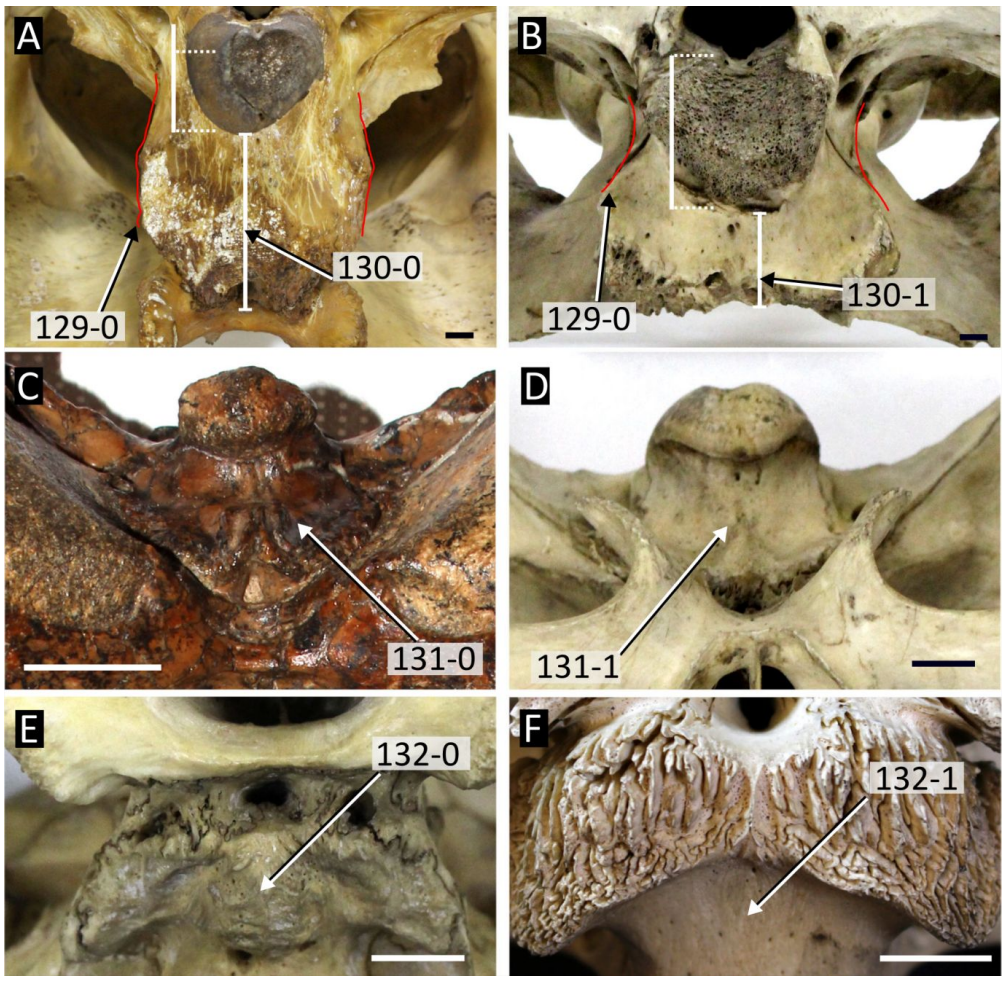



Figure 3.53: Morphology of the basioccipital. Posterior view in *Tomistoma schlegelii* (NHMUK 1894.2.21.1) (**A**) and *Gavialis gangeticus* (NHMUK 1974.3009) (**B**); ventral view in *Isisfordia duncani* (QM F44320) (**C**) and *Alligator mississippiensis* (NHMUK 1873.2.21.1) (**D**); posteroventral view in *Crocodylus porosus* (NHMUK 1852.12.9.2) (**E**) and *Gavialis gangeticus* (NHMUK 61.4.1.2) (**F**). All scale bars = 1 cm.

133. Basioccipital, concavity on ventral margin, posterior to median eustachian foramen: absent (0); present (1) (after Jouve, 2004 [198]; Jouve et al., 2008 [187]).

The profile of the ventral margin of the basioccipital plate is straight or ventrally convex in most crocodylians (Fig. 3.54A–B). Jouve (2004) recognised that in some "gavialoids", the ventral margin has a marked concavity at the midline, e.g. *Piscogavialis jugaliperforatus* (Fig. 3.54C), *Gryposuchus neogaeus* (Fig. 3.54D), and *Ikanogavialis gameroi* (Sill, 1970). This condition is additionally recognised here in two caimanines: *Mourasuchus atopus* (UCMP 38012) and *Mourasuchus arendsi* (UFAC 4925).

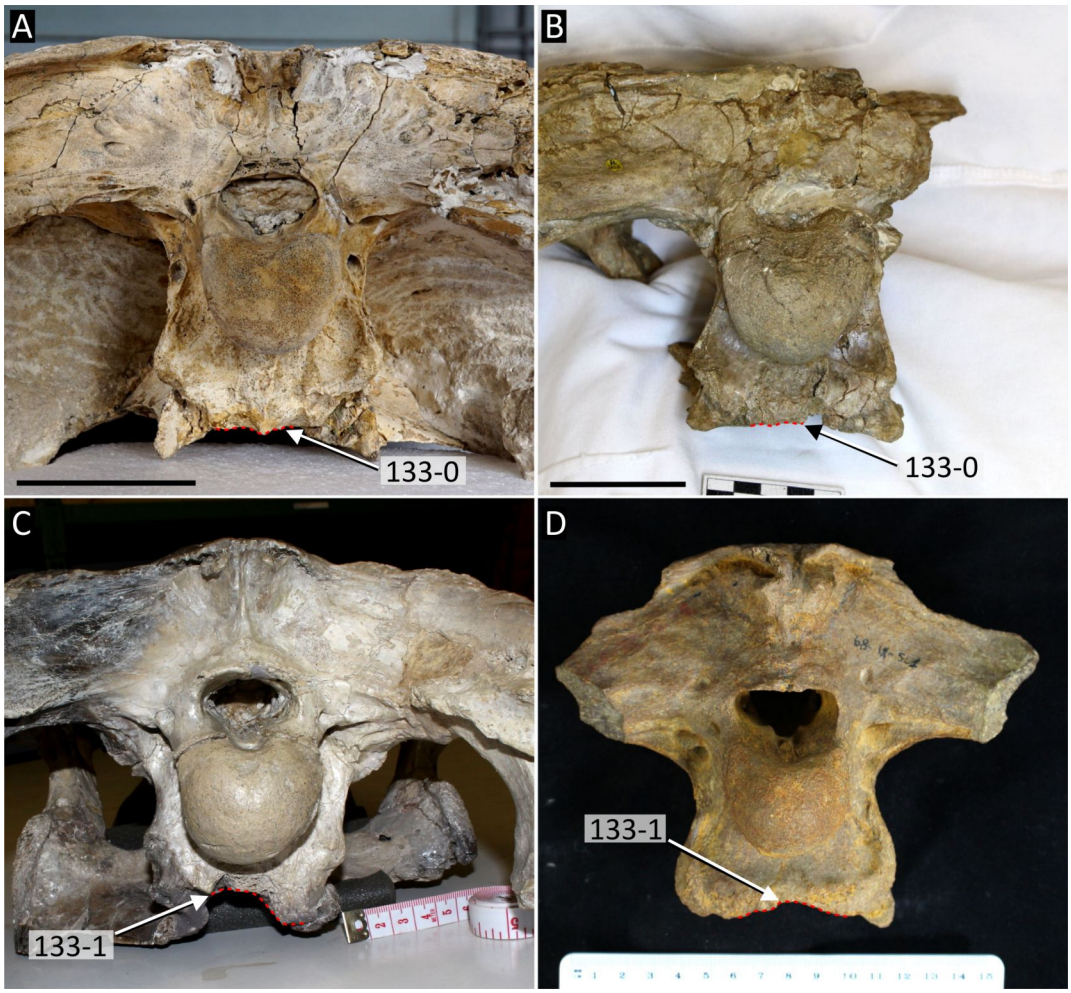



Figure 3.54: Occipital view of the cranium in **A**, *Thoracosaurus isorhynchus* (MNHN.F.MTA 61); **B**, *Eogavialis africanum* (NHMUK R 3108); **C**, *Piscogavialis jugaliperforatus* (SMNK 1282 PAL); **D**, *Gryposuchus neogaeus* (MLP 68-IX-V-1). Scale bars in A and B = 5 cm, all other scale bars = cm.

134. Lateral eustachian foramina, position relative to medial eustachian foramen: dorsal (0); lateral (at the same level) (1) (after Norell, 1988 [46]; Brochu, 1997b [147]).

As explained by Brochu (2000), the three openings of the eustachian tube (one median and two lateral) are in-line in all hatchling crocodylians. By maturity, the lateral eustachian foramina migrate dorsal to the median eustachian foramen in many crocodylians. This condition occurs in *Borealo-*

*suchus* (e.g. *B. sternbergii*, Fig. 3.55A), *Asiatosuchus depressifrons* (Fig. 3.55A), *Gavialis gangeticus* (NHMUK 1974.3009), *Tomistoma schlegelii* (1894.2.21.1), and *Alligator mississippiensis* (NHMUK 1873.2.21.1). By contrast, in all extant *Crocodylus* species, as well as *Crocodylus thorbjarnarsoni* (Brochu & Storrs, 2012) and *Crocodylus anthropophagus* (Brochu et al., 2010), the lateral eustachian foramina remain in line with the median eustachian foramen.

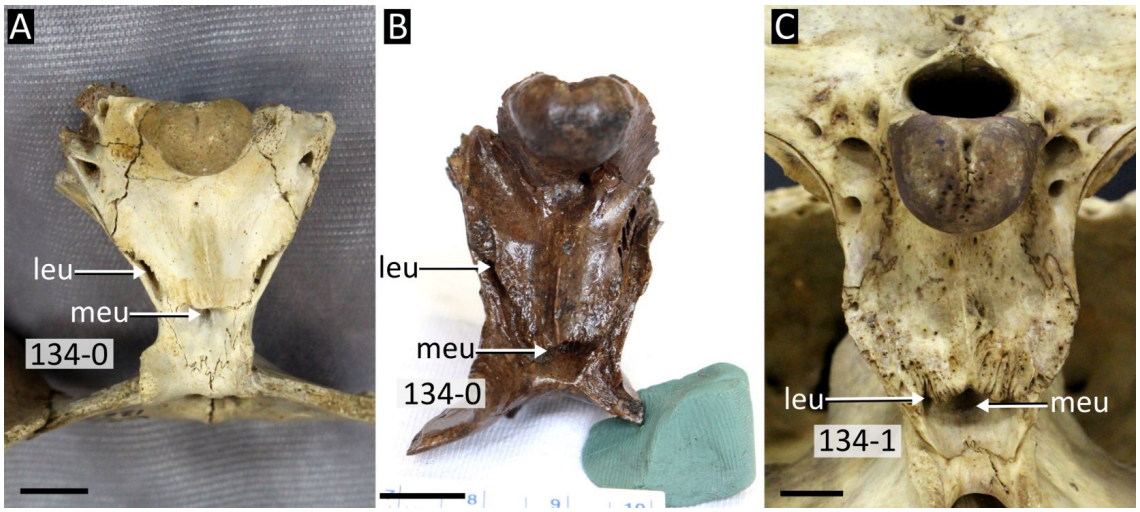



Figure 3.55: Posterior view of the occiput showing position of the lateral and medial eustachian foramina. **A**, *Borealosuchus sternbergii* (UCMP 126099); **B**, *Asiatosuchus depressifrons* (IRSNB R 0253); **C**, *Crocodylus palustris* (NHMUK 1897.12.31.1). Abbreviations: **leu**, lateral eustachian foramen, **meu**, median eustachian foramen. All scale bars = 1 cm.

135. Basisphenoid, dorsoventral exposure ventral to basioccipital, in posterior view (at maturity): little to no exposure (0); large exposure (1) (after Brochu, 1997b [119]).

As noted in Character 131, most crocodylians exhibit a "verticalised" cranium, characterised by a dorsoventrally tall skull, pterygoid wings that extend below the basioccipital, and several discrete morphological changes in the braincase (Tarsitano et al., 1989). Whereas the verticalised condition is considered plesiomorphic for Crocodylia, the flattened cranium of *Gavialis gangeticus* is thought to be secondarily evolved (Brochu, 2006b). Increased dorsoventral exposure of the basisphenoid between the pterygoid and basioccipital is associated with this verticalisation (Fig. 3.56A). This condition occurs in *Hylaeochampsa vectiana* (NHMUK R177), *Allodaposuchus precedens* (Delfino et al., 2008a, fig.3A), *Borealosuchus sternbergii* (UCMP 126099), and most alligatoroids, e.g. *Melanosuchus niger* (Fig. 3.56A), *Paleosuchus palpebrosus* (AMNH 93812), and *Diplocynodon hantoniensis* (NHMUK 30392). By contrast, "gavialoids" such as *Gavialis gangeticus* (Fig. 3.56B), *Piscogavialis jugaliperforatus* (SMNK 1282 PAL), and *Eosuchus lerichei* (IRScNB R49), appear to lack any dorsoventral exposure of the basisphenoid. The basisphenoid is dorsoventrally exposed in many crocodyloids (e.g. *Crocodylus*) and "tomistomines", but this exposure is small, and considered more like the "gavialoid"

condition, following (Brochu, 2006b).

136. Pterygoid, shape of posterior process ventrolateral to basioccipital: tall, long axis orientated dorsoventrally (0); dorsoventrally short, no discernible long axis (1) (after Brochu, 1997b [98]).

Posterior processes of the pterygoid are projections from the pterygoid wings that occur ventral to the basioccipital. Brochu (1997b) recognised that pterygoid processes varied in being tall and prominent in some taxa, but smaller in others. He also subdivided the 'small condition' based on their orientation, from being posteriorly directed (some derived "gavialoids", e.g. *Gavialis gangeticus*) or posteroventrally directed (most crocodyloids and "tomistomines"). This formulation precludes taxa sharing small pterygoid processes from being assigned the same character state. Furthermore, differences in orientation of the pterygoid processes were not discernible during the examination of specimens. Consequently, this character has been simplified to a binary character describing only the size (dorsoventral elongation) of the pterygoid processes. Whereas most crocodylians exhibit dorsoventrally expanded processes, including all alligatoroids (Fig. 3.56A), most crocodyloids, "tomistomines", and "gavialoids" exhibit dorsoventrally short pterygoid processes (Fig. 3.56B).

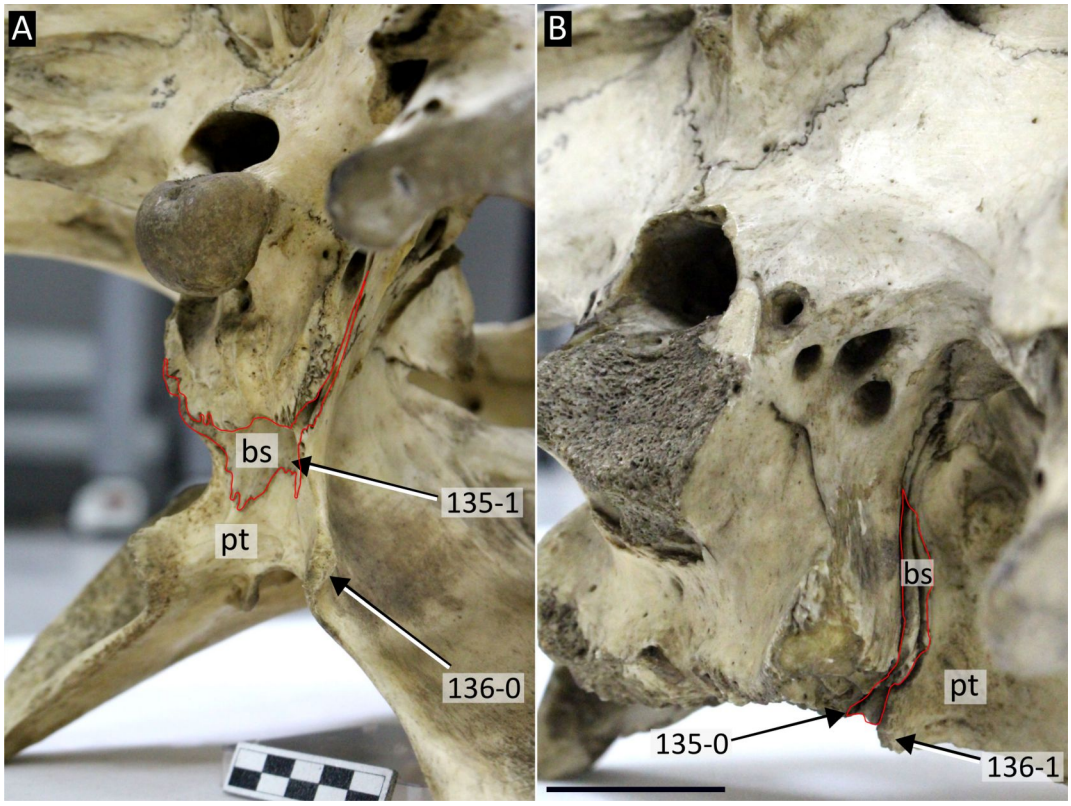



Figure 3.56: Occipital view of the cranium in **A**, *Melanosuchus niger* (NHMUK 45.8.25.125); **B**, *Gavialis gangeticus* (NHMUK 1974.3009). Abbreviations: **bs**, basisphenoid; **pt**, pterygoid. All scale bars = 5 cm.

137. Incisive foramen, intersection of premaxilla-maxilla suture: separated by inter-premaxillary suture

(0); intersecting at posterior margin (1); intersecting at lateral margin (2) (after Brochu, 1997b [124]) (ORDERED).

In palatal view, the premaxilla-maxilla suture is separated from the incisive foramen by the interpremaxillary suture in most crocodylians (Fig. 3.57A–B). Less commonly, the premaxilla-maxilla suture intersects the incisive foramen on its lateral margin e.g. *Brachychampsa montana* (Fig. 3.57E). Brochu (1997b) characterised this morphological variation in terms of the size of the incisive foramen, which was considered either small (less than half the width across premaxillae), large (greater than half the width across the premaxillae), or so large that it intersects the incisive foramen (as in *Brachychampsa*). Here, the size of the incisive foramen is characterised in a continuous character (Character 12) and the intersection of the premaxilla-maxilla suture is treated independently. This is justified because taxa with proportionally similar-sized incisive foramina may or may not exhibit contact with the premaxilla-maxilla suture. Sutural contact with the incisive foramen (137-1) is newly recognised in *Alligator prenasalis* (Fig. 3.57C), *Navajosuchus mooki* (Fig. 3.57D), and *Allognathosuchus wartheni* (YPM PU 16989), all of which have intermediate-sized incisive foramina that are similar to many other crocodylians. In these taxa, the sutural intersection with the incisive foramen is considered intermediate between most crocodylians (Fig. 3.57A) and *Brachychampsa* (Fig. 3.57E), and thus the character is ordered.

138. Incisive foramen, anterior margin intersection with premaxillary toothrow: absent (anterior margin around $2^{nd}$ or $3^{rd}$ alveolus) (0); present (projects between or abuts first premaxillary teeth) (1) (after Brochu, 1997b [153]).

The distance between the anterior margin of the incisive foramen and the premaxillary toothrow varies in Crocodylia (Fig. 3.57E–F). As originally formulated by Brochu (1997b), this variation could be delimited with three character states: "*Incisive foramen . . . at the level of second or third alveolus (0); abuts premaxillary toothrow (1); projects between first premaxillary teeth (2)*" (Brochu, 1997b).

Brochu (1999) scored most caimanines where preserved, with his character state 2, e.g. *Caiman crocodilus* (Fig. 3.57B) and *Melanosuchus niger* (Fig. 3.57F). This is agreed on here; however, the distinction between this condition and character state 1 is not apparent (Brochu, 1999, fig.45A–B). As such, these character states have been combined here. Under the new binary character construction, most crocodylians exhibit a broad separation of the incisive foramen from the toothrow by the premaxilla (Fig. 3.57A, E), whereas several *Alligator* species and caimanines exhibit the derived condition (Fig. 3.57F). In recent datasets that use the character as formulated by Brochu (1997b), character state 2 is absent from scores altogether (e.g. Brochu, 2011; Brochu et al., 2012; Brochu & Storrs, 2012; Narváez et al., 2016). This appears to be an error carried over to subsequent iterations of this dataset, as other authors (e.g. Cidade et al., 2017) follow the scores of Brochu (1999).

139. Incisive foramen, posterior margin: rounded (0); invaginated by anterior process of premaxilla (spade-shaped foramen) (1) (new character, based on personal observations).

    In *Bernissartia fagesii* (IRScNB 1538) and many eusuchians, the incisive foramen is circular to oval. This condition is exhibited by *Allodaposuchus precedens* (MMS/VBN-12-10A), *Borealosuchus sternbergii* (USNM 6533), *Boverisuchus vorax* (FMNH PR 399), and many alligatoroids, e.g. *Alligator mississippiensis* (NHMUK 1873.2.21.1) and *Purussaurus neivensis* (UCMP 39704). A different condition is expressed in several caimanines, "tomistomines", and *Crocodylus* species, which have strongly spade-shaped incisive foramina due to an anterior projection of both premaxillae into the posterior margin, e.g. *Caiman crocodilus* (Fig. 3.57B), *Crocodylus johnstoni* (QM J45309), *Crocodylus moreletti* (NHMUK 1861.4.1.4), *Paleosuchus* (NHMUK 1868.10.8.1, AMNH 93812), and *Tomistoma schlegelii* (NHMUK 1894.2.21.1).

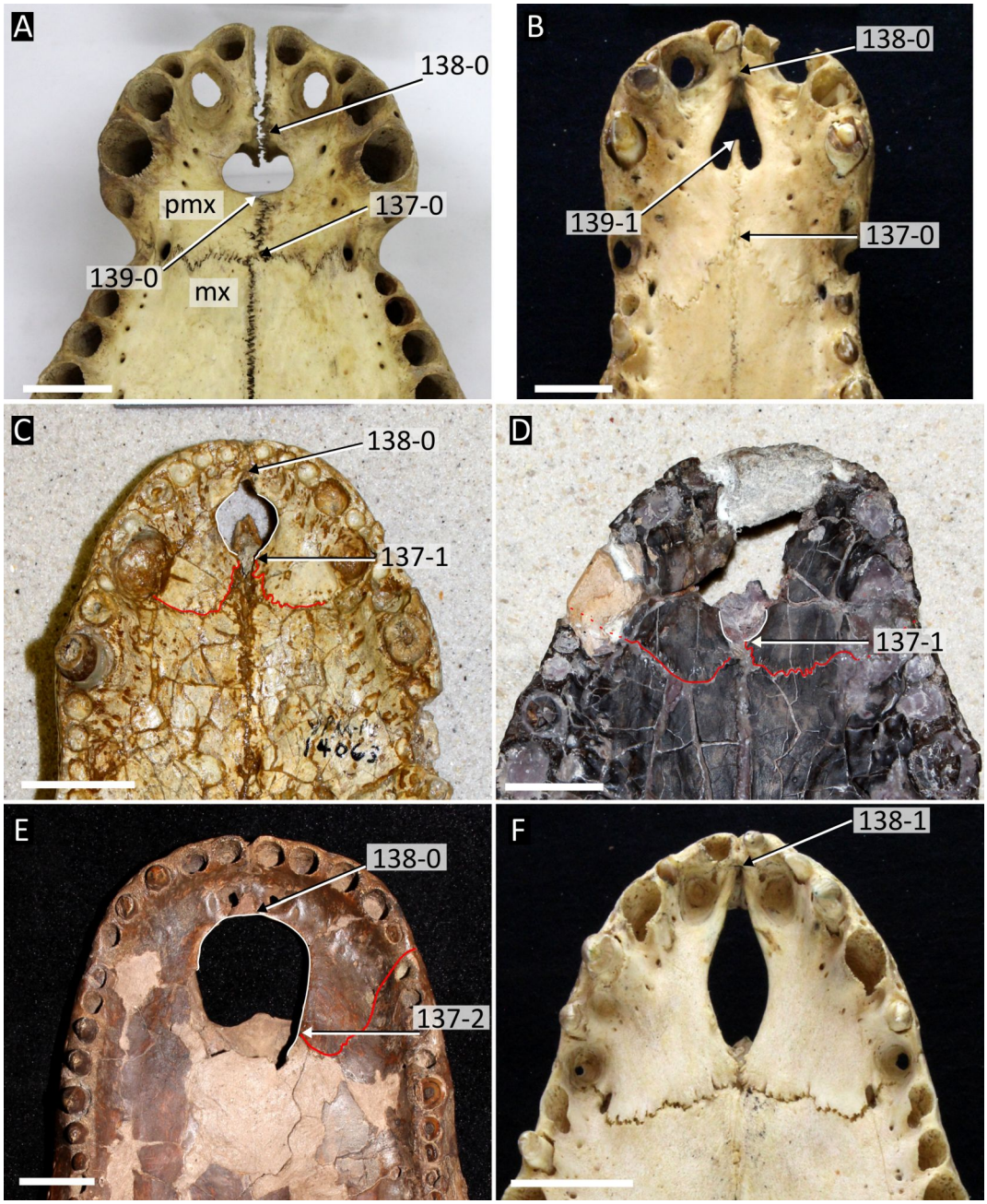



Figure 3.57: Ventral view of the anterior palate showing variation in morphology of the incisive foramen. **A**, *Crocodylus palustris* (NHMUK 1897.12.31.1); **B**, *Caiman crocodilus apaporiensis* (FMNH 69812); **C**, *Alligator prenasalis* (YPM PV 14063); **D**, *Navajosuchus mooki* (AMNH 5186); **E**, *Brachychampsa montana* (AMNH 5032); **F**, *Melanosuchus niger* (FMNH 45653). Red lines trace premaxilla-maxilla suture, white lines mark boundary of incisive foramen. Abbreviations: **mx**, maxilla; **pmx**, premaxilla. All scale bars = 2 cm.

140. Premaxilla, number of teeth early in post-hatching ontogeny: five (0); four (1) (after Norell, 1988 [17]; Brochu, 1997b [97]).

    Where known, most eusuchians have five premaxillary alveoli upon hatching (Brochu, 1999) (Fig. 3.58B–C). By contrast, *Paleosuchus trigonatus* and *Paleosuchus palpebrosus* only have four (Fig. 3.58A) (Norell, 1988). Some longirostrine crocodylians, e.g. *Tomistoma schlegelii* (Fig. 3.58B), appear to only have four alveoli in adulthood (Iordansky, 1973); however, this is a result of reduction and loss of the $2^{nd}$ premaxillary alveolus, which occurs secondarily (Brochu, 1999). Evidence for secondary loss of the $2^{nd}$ alveolus can occasionally be found as a scar for the missing alveolus immediately anterior to the third alveolus (e.g. Fig. 3.58C). In cases where four alveoli are preserved, with no evidence of a scar for the second alveolus, and no information is known of the post hatchling condition, taxa are scored as a "?". This is the case for *Piscogavialis jugaliperforatus* (SMNK 1282 PAL) and *Gryposuchus colombianus* (Fig. 3.58D).

141. Premaxilla, size of the three most posterior alveoli: penultimate alveolus is the largest (0); penultimate and antepenultimate alveoli are largest and similar in size (1); the antepenultimate alveolus is largest (2); alveoli are same size (3) (after Jouve et al., 2014 [225]; Salas-Gismondi et al., 2015 [201]; Salas-Gismondi et al., 2016 [201]).

    Of the three posteriormost premaxillary alveoli, the penultimate is the largest in most eusuchians (141-0), including allodaposuchids (Narváez et al., 2016; Narváez et al., 2019), most crocodylids (e.g. *Crocodylus porosus*, Fig. 3.58B), alligatorids (e.g. *Alligator mcgrewi*, AMNH 7905; *Caiman yacare*, AMNH 97300), and some "tomistomines", e.g. *Maroccosuchus zennaroi* (IRScNB R408). The penultimate and antepenultimate alveoli are equally enlarged (141-1) in all *Borealosuchus* species, where preserved, *Diplocynodon hantoniensis* (NHMUK 25188), *Tomistoma schlegelii* (Fig. 3.58B), and *Gavialis gangeticus* (NHMUK 1974.3009). In a smaller number of taxa, the antepenultimate alveolus is the largest (141-2), e.g. *Gryposuchus neogaeus* (MLP 26-413) and *Gryposuchus pachakamue* (Salas-Gismondi et al., 2016), whereas in others, all premaxillary alveoli are equally enlarged (141-3), e.g. *Mourasuchus atopus* (Fig. 3.58E) and *Gavialosuchus eggenburgensis* (NHMUK R797).

142. Premaxilla, posterior extent on palate, relative to number of maxillary alveoli, in ventral view: 0 (0); 1 (1); 2 (2); 3 (3); 4 (4); 5 or more (5) (after Jouve, 2004 [168]; Jouve et al., 2008 [168]) (ORDERED).

    Variation in the posterior extent of the premaxillae on the palate has been characterised by previous authors by means of a binary character, which described the presence or absence of extension beyond the $3^{rd}$ maxillary alveolus (Jouve, 2004). Finer variation is recognised here with the addition of numerous, ordered character states. In *Toyotamaphimeia machikanensis* (Kobayashi et al., 2006), *Maomingosuchus petrolica* (Shan et al., 2017), and *Diplocynodon* species (e.g. *D. hantoniensis*, NHMUK 25166 and *D. ratelii*, MNHN SG 539), the premaxillae do not reach the level of even

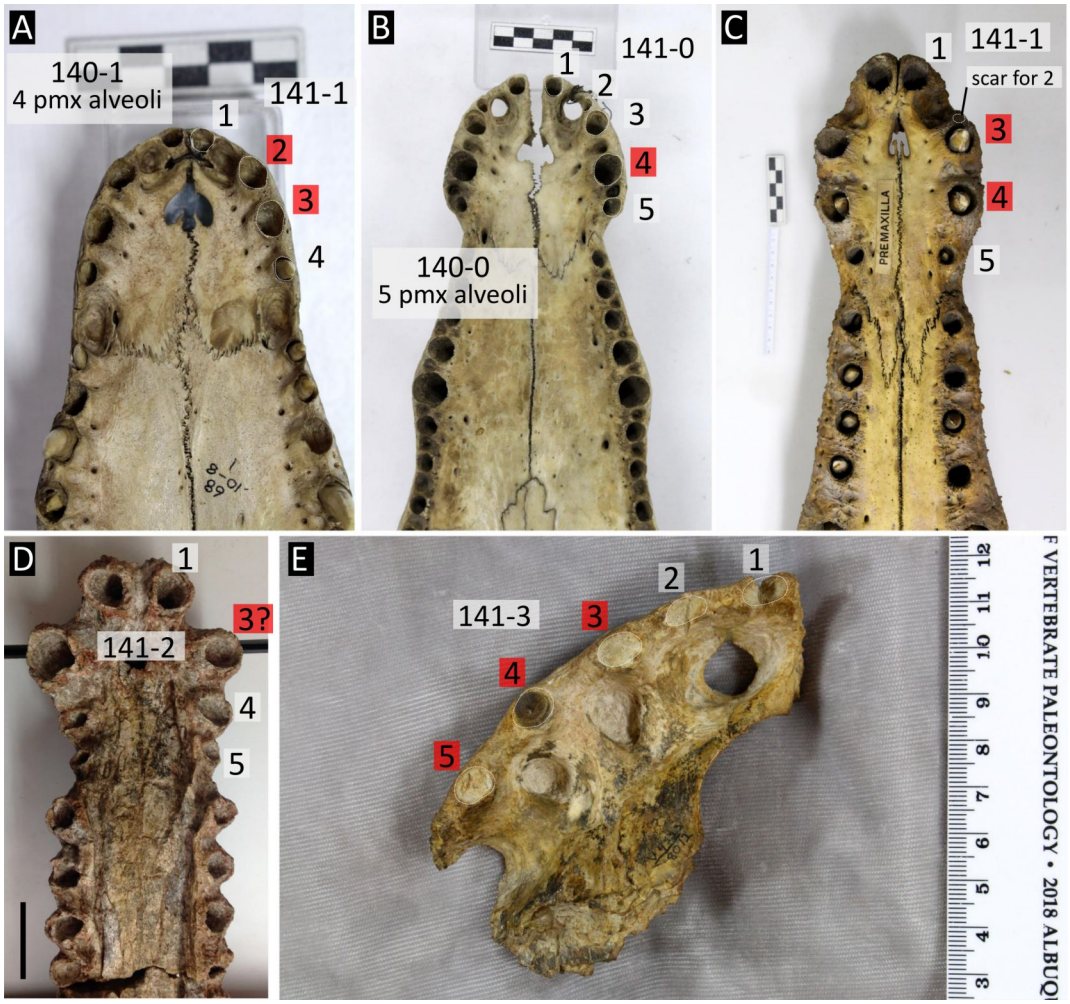



Figure 3.58: Ventral view of premaxilla in selected crocodylians showing variation in alveolar size and number. **A**, *Paleosuchus trigonatus* (NHMUK 1868.10.8.1); **B**, *Crocodylus porosus* (NHMUK 86.2.4.1); **C**, *Tomistoma schlegelii* (NHMUK 1894.2.21.1); **D**, *Gryposuchus colombianus* (IGM 201400011); **E**, *Mourasuchus atopus* (UCMP 38012). Red boxes indicate position of largest alveoli (Character 141). Scale bar in D = 5 cm. All other scale bars = cm.

one maxillary alveolus. In most species of *Crocodylus*, *Alligator*, and *Borealosuchus*, they reach one alveolus (Fig. 3.59A). The premaxillae reach two full maxillary alveoli in *Eosuchus lerichei* (IRScNB R49), *Tomistoma schlegelii* (Fig. 3.59B), and *Gryposuchus colombianus* (Fig. 3.59C). The premaxillae extend to the level of the $3^{rd}$, $4^{th}$, and $5^{th}$ maxillary alveoli in *Eogavialis africanum* (Fig. 3.59D), *Gavialis gangeticus* (Fig. 3.59E), and *Piscogavialis jugaliperforatus* (Fig. 3.59F), respectively.

143. Premaxilla, position of the penultimate premaxillary alveolus relative to the antepenultimate alveolus: posterolateral or in the same line (0); posteromedial (1) (after Jouve et al., 2015 [202]).

144. Premaxilla, position of the last premaxillary alveolus relative to the penultimate alveolus: posterior or posterolateral (0); or posteromedial (1) (after Jouve et al., 2015 [204]).

Characters 143–144 capture variation in the premaxillary alveolar arrangement and are modified from characters 202 and 204 in Jouve et al. (2015). Overlapping statements occurred in the original character descriptions that would result in overweighting. Furthermore, the original characters did not account for the full range of morphological variation observed in crocodylians. In most eusuchians the premaxillary toothrow is arranged in an arched, posterolateral line (Fig. 3.59A). In this condition the antepenultimate, penultimate and last premaxillary alveoli are positioned progressively further laterally (143-0, 144-0). Several longirostrines exhibit the opposite condition, in which the final three alveoli are arranged in a posteromedial line (143-1, 144-1) (Fig. 3.59C). This gives rise to the characteristic widened premaxilla ('Greifapparat') of several "gavialoids" (Kälin, 1933). In other longirostrines, the penultimate alveolus is lateral to, or at the same level as the antepenultimate alveolus (143-0), but the final alveolus is positioned medial to them (144-1) (Fig. 3.59B, F). This morphological variation could alternatively be described in one character describing the three aforementioned conditions; however, this would ignore the shared presence of a medially inset last premaxillary alveolus in *Gavialis gangeticus* (Fig. 3.59E), *Gryposuchus colombianus* (Fig. 3.59C), *Tomistoma schlegelii* (Fig. 3.59B), *Thecachampsa sericodon* (USNM 24938), and *Maroccosuchus zennaroi* (IRScNB R408), among other longirostrines.

145. Premaxilla, alveolar spacing (at maturity): all alveoli equally separated (0); second alveolus separated from the first and close to the third (1) (after Jouve et al., 2015 [224]).

As explained in Character 140, the second premaxillary alveolus may be completely lost in adult forms of some species, but more often it remains small and weakly separated from the third (Fig. 3.59E) (Brochu, 1999). This condition occurs in most *Crocodylus* species (e.g. *C. intermedius*, FMNH 75659), all *Caiman* species, where preserved (e.g. *Caiman crocodilus*, Fig. 3.58B), *Borealosuchus sternbergii* (USNM 6533), some *Diplocynodon* species (e.g. *D. ratelii*, MNHN SG 539), and *Baru huberi* (QM F31060). An almost equal number of taxa exhibit equidistant premaxillary alveoli. This condition occurs in all *Alligator* species (Fig. 3.59A), *Mourasuchus atopus* (Fig. 3.58E), *Thoracosaurus isorhynchus* (MNHN 1902-22), *Eosuchus lerichei* (IRScNB R49), and *Boverisuchus vorax* (FMNH PR 399).

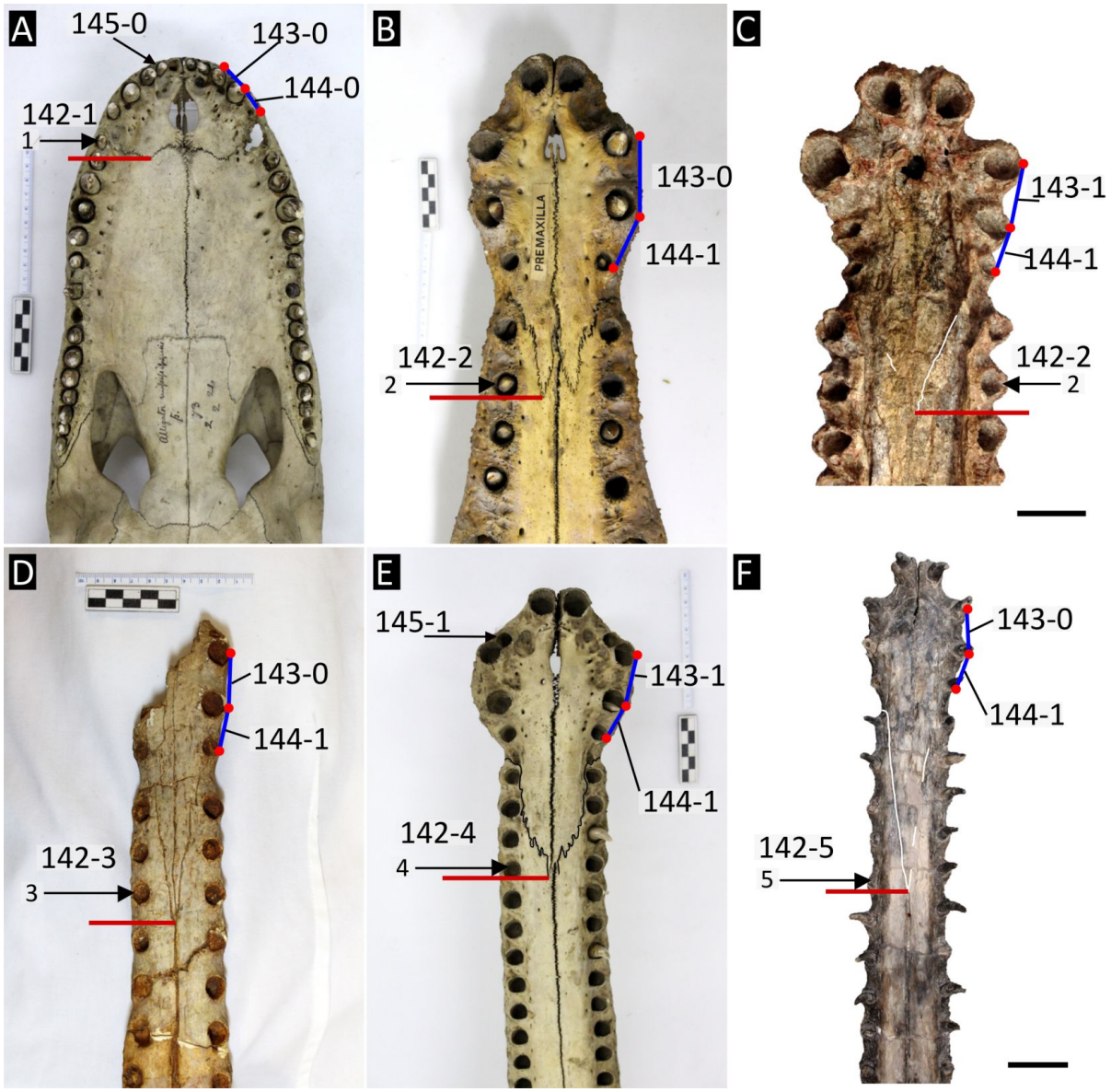



Figure 3.59: Ventral view of the rostrum in selected crocodylians showing posterior extent of the premaxilla and variation in alveolar arrangement. **A**, *Alligator mississippiensis* (NHMUK 1873.2.21.1); **B**, *Tomistoma schlegelii* (NHMUK 1894.2.21.1); **C**, *Gryposuchus colombianus* (IGM 201400011); **D**, *Eogavialis africanum* (NHMUK PV R3329); **E**, *Gavialis gangeticus* (NHMUK 1974.3009); **F**, *Piscogavialis jugaliperforatus* (SMNK 1282 PAL). Red lines indicate posterior extent of premaxillae, black lines indicate alveolus position. Red points mark premaxillary alveolar positions All scale bars = 5 cm.

146. Premaxilla-maxilla suture, shape on palate in ventral view: horizontal (0); posteriorly bowed, with one rounded apex (1); posteriorly bowed, with one acute apex (2); posteriorly bowed with two or more apices (3) (after Groh et al., 2020 [122]).

The ventral premaxilla-maxilla suture undulates in most crocodylians, most commonly with two posterior projections (146-3). This condition occurs in most extant alligatorids (e.g. *Caiman crocodilus*, FMNH 69812), crocodylids (e.g. *Crocodylus niloticus*, Fig. 3.60D), "tomistomines" (e.g. *Tomistoma schlegelii*, NHMUK 1894.2.21.1), and some "gavialoids" (e.g. *Eosuchus lerichei*, IRScNB R49). Alternatively, the suture may be straight (146-0), as in *Bernissartia fagesii* (IRScNB 1538), *Voay robustus* (Fig. 3.60A), *Asiatosuchus germanicus* (HLMD Me 5649), *Baru* (QM F16822, F31060), and *Diplocynodon hantoniensis* (NHMUK 25166). Several taxa exhibit one median posterior projection of the premaxilla-maxilla suture, which might be acute (146-2) (Fig. 3.60C), or as newly introduced here, rounded (146-1) (Fig. 3.60B). Whereas the acute condition commonly occurs in longirostrine crocodylians, e.g. *Crocodylus johnstoni* (QM J4280), *Gavialis gangeticus* (NHMUK 1974.3009), and *Kentisuchus spenceri* (NHMUK 38974), the rounded condition is less common, occurring in some crocodyloids, e.g. *C. moreletti* (Fig. 3.60B), '*C*'. *affinis* (AMNH 16622, UCMP 131090), and '*C*'. megarhinus (YPM 53582).

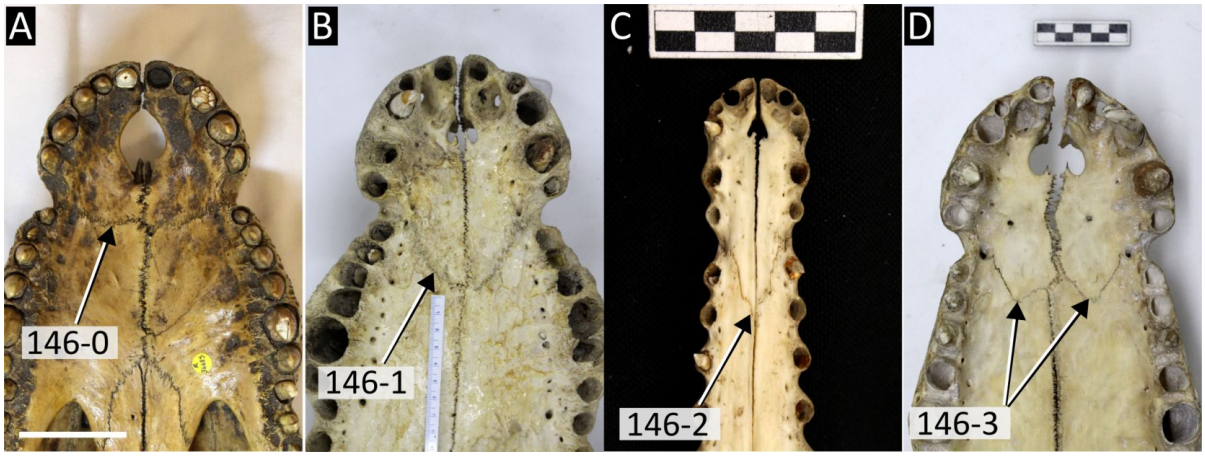



Figure 3.60: Ventral view of the premaxilla-maxilla suture. **A**, *Voay robustus* (NHMUK R 36685); **B**, *Crocodylus moreletti* (NHMUK 1861.4.1.4); **C**, *Crocodylus johnstoni* (QM J4280); **D**, *Crocodylus niloticus* (NHMUK 1934.6.3.1). Scale bar in A = 5 cm, all other scale bars = cm.

147. Maxilla, number of the largest alveolus: 3 (0); 5 (1); 4 (2); 4 and 5 (3); 6 (4); 7 (5); maxillary alveoli gradually increase in diameter posteriorly toward penultimate alveolus (6); homodont (7) (after Norell, 1988 [1]; Brochu, 1997b [89]; Shan et al., 2009 [89]; Brochu, 2010 [73]; Jouve et al., 2015 [89]).

The number of states in this character has steadily grown with the discovery of new size arrangements of maxillary alveoli. The largest maxillary alveolus is the third in paralligatorids (Turner, 2015). This includes the 'Glen Rose Form' (Fig. 3.61A), *Wannchampsus kirpachi* (Adams, 2014), and *Shamo-*

*suchus djadochtaensis* (Pol et al., 2009). The $5^{th}$ maxillary alveolus is enlarged in all crocodyloids (e.g. *Crocodylus porosus*, Fig. 3.61E) and *Asiatosuchus germanicus*, HLMD Me 5652) and most "tomistomines" (e.g. *Tomistoma schlegelii*, Fig. 3.61F and *Thecachampsa sericodon*, Fig. 3.61G). In members of Allodaposuchidae (e.g. *Allodaposuchus precedens*, MMS/VBN-12-10A), as well as most alligatoroids (e.g. *Caiman yacare*, Fig. 3.61B) and *Navajosuchus mooki*, AMNH 5186) the $4^{th}$ maxillary alveolus is largest. The $4^{th}$ and $5^{th}$ maxillary alveoli are equally enlarged in all *Borealosuchus* species (Brochu, 1997a) (Fig. 3.61D), planocraniids (e.g. *Boverisuchus vorax*, FMNH PR 399), and 'basal' alligatoroids, e.g. *Diplocynodon hantoniensis* (Fig. 3.61C) and *Leidyosuchus canadensis* (NHMUK R10904). Enlargement of the $6^{th}$ maxillary alveolus has only been observed in *Gavialosuchus eggenburgensis* (Fig. 3.61H). Similarly, enlargement of the $7^{th}$ alveolus is rare, only observed in *Penghusuchus pani* (Shan et al., 2009, fig.2B) and *Toyotamaphimeia machikanensis* (Kobayashi et al., 2006, fig.8). A progressive enlargement of the posteriormost maxillary alveoli is only recovered in *Hylaeochampsa vectiana* (NHMUK R177), *Iharkutosuchus makadii* (Ősi, 2008, fig.9) and *Acynodon iberoccitanus* (Martin, 2007, fig.3D). Equally sized (homodont) maxillary alveoli are recovered in several longirostrine crocodylians, including *Gavialis gangeticus* (Fig. 3.61K), *Eosuchus lerichei* (Fig. 3.61J), and '*Tomistoma*' *dowsoni* (Fig. 3.61I). Given the great degree of variation that does not form a clear, continuous range of values, this character is unordered.

148. Maxilla, interalveolar distances between alveoli 1–10: less than or equal to diameter of first maxillary alveolus (0); greater than the diameter of the first maxillary alveolus (1) (after Jouve et al. 2015 [235]).

In most brevirostrine crocodylians, the maxillary teeth sit close together such that most of the interalveolar spaces between maxillary alveoli 1–10 are small, being equal to or less than the diameter of the first maxillary alveolus (Fig. 3.61A–E). Although variation occurs depending on how the dentary teeth occlude (see Character 151), the interalveolar distances are never consistent, nor widely spaced, across the maxillary toothrow. Several longirostrine crocodylians exhibit very evenly spaced maxillary alveoli; however, the interalveolar distances are still small, typically less than the diameter of the first maxillary alveolus, e.g. *Eosuchus lerichei* (Fig. 3.61J) and *Gavialis gangeticus* (Fig. 3.61K). By contrast, a small number of longirostrine crocodylians exhibit maxillary alveoli that are both consistently distributed and large, approximately 1.5 times the diameter of the first maxillary alveolus. This occurs in *Gavialosuchus eggenburgensis* (Fig. 3.61H), '*Tomistoma*' *dowsoni* (Fig. 3.61I), *Tomistoma cairense* (SMNS 50739), *Eogavialis africanum* (YPM 6263), and *Piscogavialis jugaliperforatus* (SMNK 1282 PAL), among other longirostrine crocodylians.

149. Maxilla, shape of the lateral profile between alveoli 1 to 5: flaring posteriorly (0); or straight (1) (new character, based on personal observations).

The rostra of all brevirostrine eusuchians widen posteriorly from the level of the first maxillary alve-

olus to either the $3^{rd}$, $4^{th}$, or $5^{th}$, depending on which is the largest (149-0) (Fig. 3.61A–E). This is sometimes described as the first 'wave' of the maxilla (i.e. a convexity in the lateral profile), with a second wave occurring posteriorly. Almost all longirostrine crocodylians with homodont dentition lack such a wave, and the lateral profile of the maxilla is straight between alveoli 1–5 (149-1), being parallel to the sagittal axis (Fig. 3.61I–K). This might suggest that this morphological variation is associated with the presence or absence of homodont dentition, which is described in Character 147-7. Indeed, longirostrines with heterodont dentition tend to exhibit the same widening as all brevirostrines e.g. *Tomistoma schlegelii* (Fig. 3.61F), *Maroccosuchus zennaroi* (IRScNB R408), and *Kentisuchus spenceri* (NHMUK 38974); however, some longirostrines with heterodont dentition have a straight profile between alveoli 1–4, e.g. *Thecachampsa sericodon* (Fig. 3.61G), *Gavialosuchus eggenburgensis* (Fig. 3.61H), and *Maomingosuchus petrolica* (IVPP unnumbered complete skull). This indicates that the shape of the lateral maxillary margin is not always associated with differentiation of the maxillary alveoli, supporting the independence of this character.

150. Maxilla, shape of the toothrow posterior to the first six alveoli: laterally convex or linear (0); laterally concave (1) (after Brochu, 1997b [135]; Clark, 1994 [79]).

In most eusuchians, the posteriormost maxillary alveoli are arranged in a straight line which, although orientated posterolaterally, recurves medially at its distal end (Fig. 3.61A–E). Brochu (1997a) recognised that the posterior end of the toothrow does not medially recurve in *Borealosuchus* species (Fig. 3.61D), a condition which has since been used to diagnose the genus (Brochu et al., 2012). However, this condition is recognised much more widely in crocodylians in this study, particularly in longirostrines e.g. *Tomistoma schlegelii* (Fig. 3.61F), *Thecachampsa sericodon* (Fig. 3.61G), *Eosuchus lerichei* (Fig. 3.61J), and *Gavialis gangeticus* (Fig. 3.61K). Furthermore, the posterior toothrow is considered linear in *Borealosuchus sternbergii* (Fig. 3.61D).

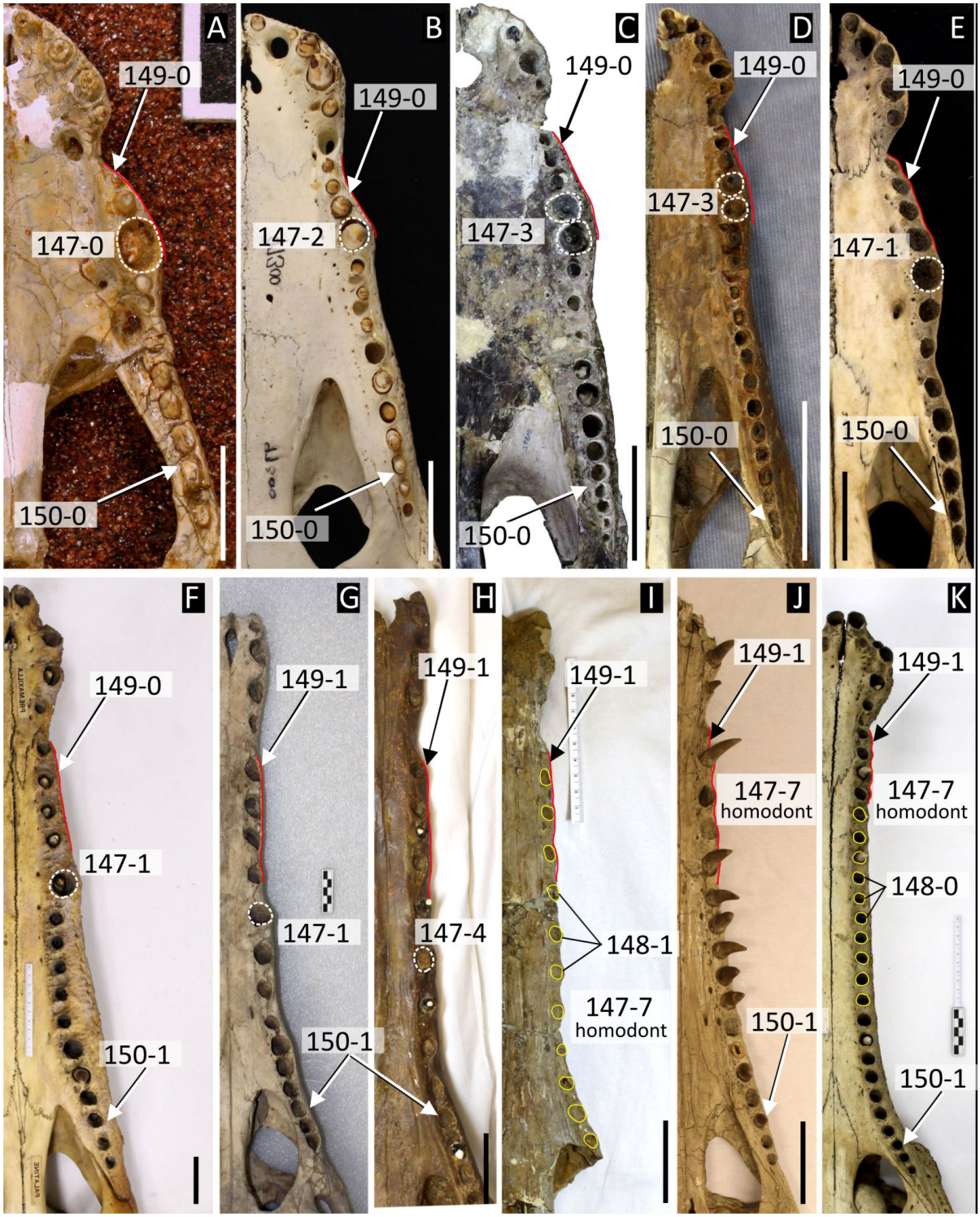



Figure 3.61: Ventral view of the palate in selected crocodylians showing variation in maxillary alveolar morphology. **A**, the Glen Rose Form (USNM 22039); **B**, *Caiman yacare* (AMNH 97300, digitally reversed); **C**, *Diplocynodon hantoniensis* (NHMUK 30392, digitally reversed); **D**, *Borealosuchus sternbergii* (UCMP 126099); **E**, *Crocodylus porosus* (QM J47447); **F**, *Tomistoma schlegelii* (NHMUK); **G**, *Thecachampsa sericodon* (USNM); **H**, *Gavialosuchus eggenburgensis* (NHMUK PV R 797); **I**, '*Tomistoma*' *dowsoni* (NHMUK PV R 4769); **J**, *Eosuchus lerichei* (IRSNB R 49); **K**, *Gavialis gangeticus* (NHMUK 1974.3009). Scale bar A = 1 cm, all other scale bars = 5 cm.

151. Occlusion pattern: all dentary teeth occlude lingual to maxillary teeth (0); partial interlocking occlusion, with at least one pit between maxillary teeth 5–8, all other dentary teeth occlude lingually (1); all dentary teeth occlude in line with maxillary teeth (2) (after Norell, 1988 [5]; Willis, 1993 [1]; Brochu, 1997b [78]; Lee & Yates 2018 [27] (ORDERED).

    In *Bernissartia fagesii* (IRScNB 1538), Hylaeochampsidae, Paralligatoridae and most alligatoroids, the dentary teeth occlude lingual to the maxillary teeth (Fig. 3.62A–B). This also occurs in some 'basal' crocodyloids, such as *Asiatosuchus germanicus* (HLMD Me 5652). By contrast, the dentary teeth occlude in line with the maxillary teeth in most crocodyloids (e.g. *Crocodylus*, Fig. 3.62D), all gavialoids (e.g. *Tomistoma schlegelii*, NHMUK 1894.2.21.1 and *Gavialis gangeticus*, NHMUK 1974.3009), and most *Borealosuchus* species (e.g. *B. acutidentatus*, NMC 8544). In a less common condition that was recognised by Brochu (1997b), occlusal pits can occur between maxillary teeth 5–8, but lingual to all other maxillary teeth (Fig. 3.62C). Previously, only a single pit was recognised between alveoli 7 and 8 (Brochu, 1997b) or 7–9 (Lee & Yates, 2018), but greater variation exists. Whereas occlusal pits are present between alveoli 6 and 7, and 7 and 8 in '*Crocodylus*' *affinis* (USNM 18171) and *Diplocynodon hantoniensis* (Chapter 2, Fig. 2.1), an occlusal pit only occurs between alveoli 7 and 8 in *Asiatosuchus depressifrons* (Fig. 3.62C). In *Caiman crocodilus apaporiensis* (FMNH 69812) an occlusal pit occurs between alveoli 5–8, and in *Caiman yacare* (AMNH 97300) they occur between alveoli 5–7. These conditions are considered intermediate between a full lingual occlusion (151-0) and fully interlocking dentition (151-2), hence the character is ordered.

152. Occlusion pattern, $4^{th}$ dentary tooth occludes in notch between premaxilla and maxilla early in ontogeny (0); occludes in a pit between premaxilla and maxilla; no notch early in ontogeny (1) (after Norell, 1988 [29]; Brochu, 1997b [77]).

    The occlusal position of the $4^{th}$ dentary caniniform tooth has classically been used to distinguish alligatorids from all other crocodylians (Duméril, 1806; Norell et al., 1994; Brochu, 1999, 2003). Whereas alligatoroids exhibit a pit that encloses the $4^{th}$ dentary tooth (Fig. 3.62E), crocodyloids and gavialoids exhibit a notch, such that the $4^{th}$ dentary tooth is laterally exposed (Fig. 3.62F). The character must be qualified with a statement about ontogeny, as it has long been recognised that a pit can become worn to a notch with maturity (Kälin, 1933; Norell et al., 1994; Brochu, 1999). This is exemplified by *Caiman crocodilus*, hatchling specimens of which exhibit a pit (Fig. 3.62G), but the lateral wall of the pit can become worn out and entirely lost with maturity (Fig. 3.62H). Similar intraspecific variation is observed in fossil specimens e.g. *Diplocynodon hantoniensis* (Norell et al., 1994; Brochu, 1999, see also Section 2.1).

153. Maxilla, diastema between alveoli 5 and 6: absent (0); present (1) (new character, based on personal observation).

A prominent diastema occurs between alveoli 5 and 6 in the 'Glen Rose Form' (USNM 22039, Fig. 3.62A), *Wannchampssus kirpachi* (Adams, 2014, fig.8), and *Thoracosaurus isorhynchus* (MNHN 1902-22). All other eusuchians exhibit sub-equally separated maxillary alveoli.

154. Maxilla, diastema between alveoli 6–8: absent (0); present (1) (after Montefeltro et al. 2013 [484]; Jouve et al. 2015 [235]).

The derived character state describes the presence of a diastema between alveoli 6–8. This might appear redundant with Character 151, as taxa with occlusal pits between alveoli 5–8 (151-1) naturally exhibit increased interalveolar spacing similar to that described in 154-1. However, several crocodylians exhibit increased interalveolar spacing between alveoli 6–8 regardless of occlusal pattern. For example, most *Crocodylus* species (which have fully interlocking dentition, 151-2) exhibit increased interalveolar spaces (154-1). By contrast, *Gavialis gangeticus*, which also has interlocking dentary and maxillary teeth, lacks a diastema between alveoli 6–8 (154-0). Furthermore, despite the full lingual occlusion of all *Alligator* species (151-0), some exhibit slightly larger interalveolar spaces between alveoli 6–8, e.g. *A. mississippiensis* (Fig. 3.62B).

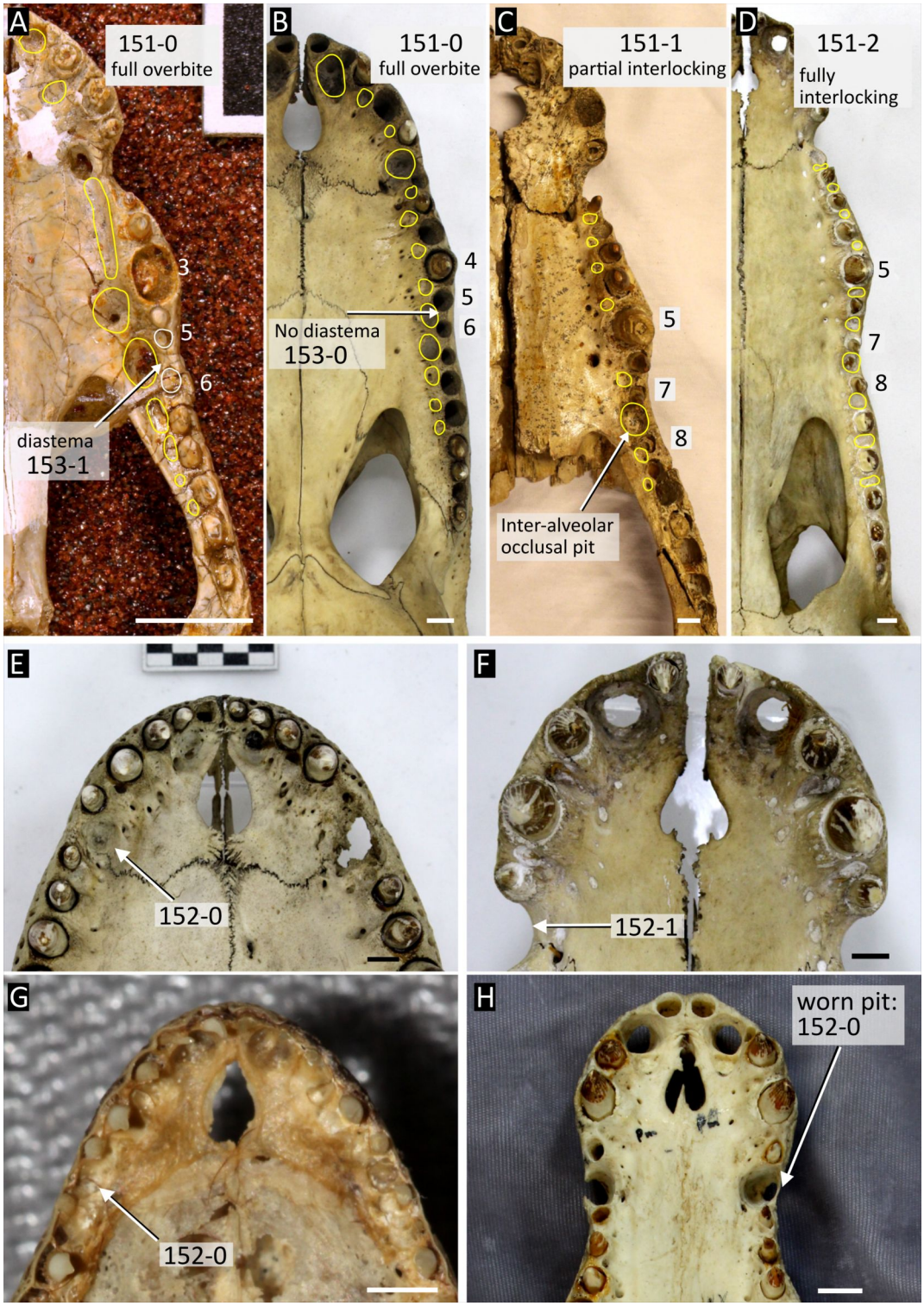



Figure 3.62: Ventral view of the palate showing variation in occlusal pattern in **A**, the Glen Rose Form (USNM 22039); **B**, *Alligator mississippiensis* (NHMUK 1873.2.21.1); **C**, *Asiatosuchus depressifrons* (IRSNB R 0251); **D**, *Crocodylus siamensis* (NHMUK 1921.4.1.171); **E**, *Alligator mississippiensis* (NHMUK 1873.2.21.1); **F**, *Crocodylus siamensis* (NHMUK 1921.4.1.171); **G**, *Caiman crocodilus apaporiensis* (hatchling) (UCMP unnumbered); **H**,*Caiman crocodilus apaporiensis* (adult) (UCMP 42843). Scale bars G = 2 mm, all other scale bars = 1 cm.

155. Maxillary and dentary alveoli, shape: all circular in cross-section (0); posterior alveoli mediolaterally compressed (1); all alveoli mediolaterally compressed (2) (after Brochu, 2004 [165]; Brochu, 2010 [61]).

The maxillary and dentary alveoli of *Bernissartia fagesii* (IRScNB 1538) and most eusuchians are circular throughout the toothrow (Fig. 3.63A). By contrast, the posteriormost alveoli are mediolaterally compressed in *Isisfordia duncani* (QM F44320) and some alligatoroids, e.g. *Paleosuchus* (Fig. 3.63B), *Arambourgia gaudryi* (MNHN QU17155), *Procaimanoidea utahensis* (USNM 15996), and *Bottosaurus harlani* (Cossette & Brochu, 2018). In planocraniids such as *Boverisuchus vorax* (Fig. 3.63D), and the crocodyloid *Quinkana* (Fig. 3.63C), the alveoli are mediolaterally compressed throughout the toothrow (Brochu, 2004b, 2012).

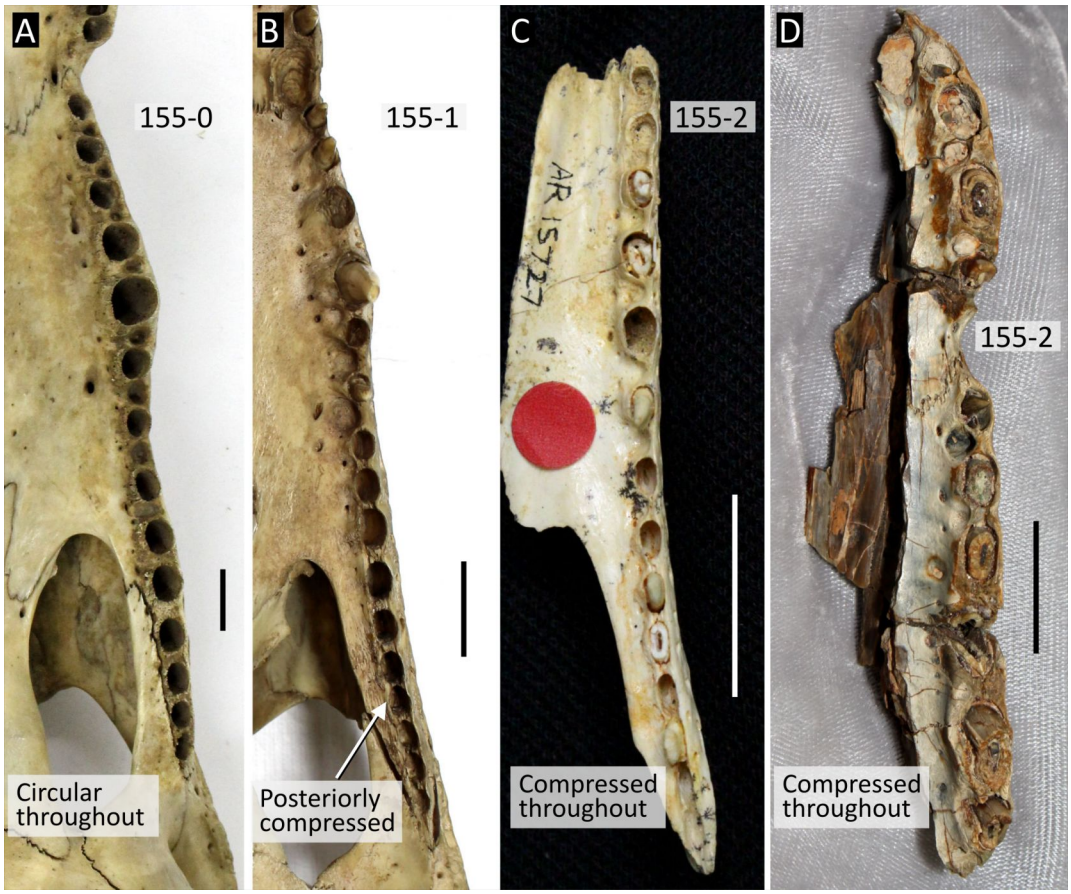



Figure 3.63: Ventral view of the maxillary toothrow showing variation in alveolar compression. **A**, *Crocodylus porosus* (NHMUK 85.2.4.1); **B**, *Paleosuchus trigonatus* (NHMUK 1868.10.8.1); **C**, *Quinkana meboldi* (QM F31056); **D**, *Boverisuchus vorax* (UCMP 170767). All scale bars = 2 cm.

156. Dentary and maxillary teeth, shape behind alveoli 12–13: pointed to slightly blunt (0); globular (1); molariform, multicusped (2) (after Salas-Gismondi et al. 2015 [198]).

Moving posteriorly through the toothrow, the maxillary and dentary teeth of most alligatoroids become

short and stout, sometimes with blunter apices than the anteriormost teeth (Cidade et al., 2019b). Some taxa exhibit a prominent increase in size, becoming bulbous and blunt (156-1) (Brochu, 1999, 2004b). This condition occurs in several alligatoroids including *Brachychampsa montana* (Fig. 3.64C), *Hassiacosuchus haupti* (Fig. 3.64D), *Navajosuchus mooki* (AMNH 6780), *Allognathosuchus wartheni* (YPM PU 16989), and the caimanines *Globidentosuchus brachyrostris* (Scheyer & Delfino, 2016), *Gnatusuchus pebasensis*, and *Caiman wannlangstoni* (Salas-Gismondi et al., 2015). In fewer cases, the posteriormost teeth are not only enlarged and flattened, but develop multiple furrows and ridges (cusps) to give a molariform appearance e.g. *Iharkutosuchus makadii* (Ősi, 2008, fig.7).

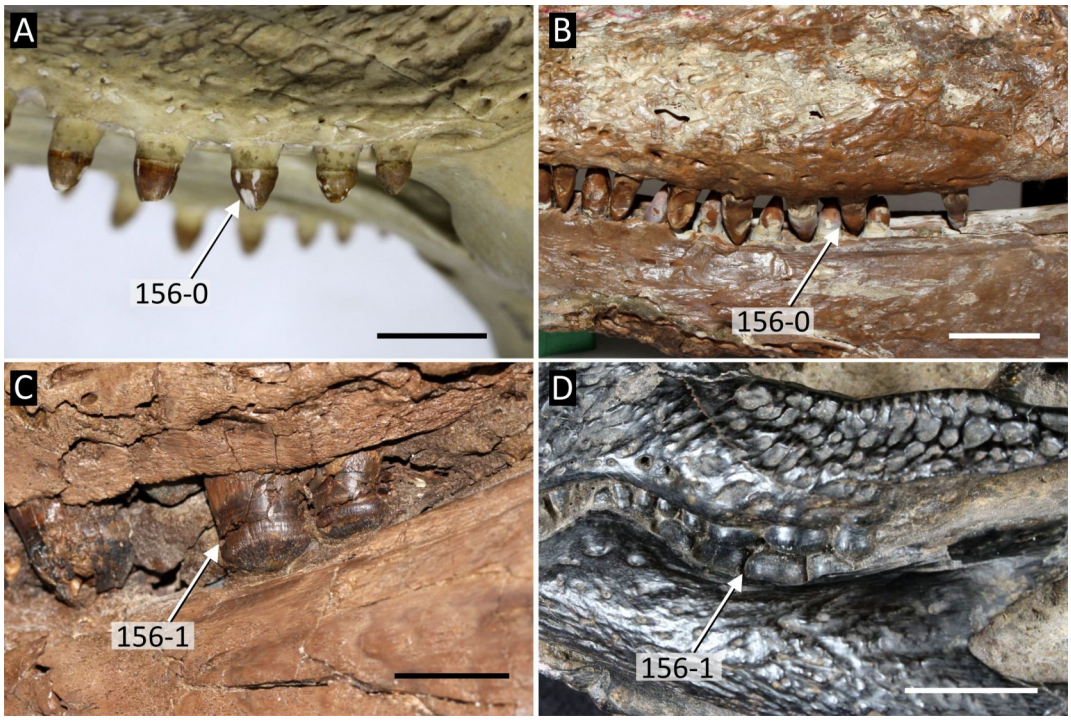



Figure 3.64: Lateral view of the posteriormost maxillary and dentary teeth in selected crocodylians. **A**, *Crocodylus siamensis* (NHMUK 1921.4.1.171); **B**, *Diplocynodon ratelii* (MNHN SG 539); **C**, *Brachychampsa montana* (UCMP 133901); **D**, *Hassiacosuchus haupti* (HLMD-Me-4415). All scale bars = 2 cm.

157. Maxillary and dentary tooth carinae: smooth (0); serrated (1) (after Brochu 2010 [62]).

Whereas the sharp anterior (mesial) and posterior (distal) edges (carinae) of the teeth of most crocodylians are smooth (Fig. 3.65A), those of *Boverisuchus vorax* (Fig. 3.65C, D), *Boverisuchus magnifrons* (Brochu, 2012), and species of *Quinkana* (e.g. *Q. fortirostrum*, QM 32153) bear saw-like serrations. Teeth associated with the giant caimanine crocodylian, *Purussaurus neivensis* (UCMP 38932, Fig. 3.65A, B), have structures that superficially resemble serrations, but lack a saw-like edge. Lee and Yates (2018) modified this character by the addition of a character state: "*weakly crenulated* (i.e. serrated) *with microscopic crenulations*". Of the five taxa scored for this condition in their study (*Planocrania datangensis*, *Baru darrowi*, *Baru* 'Alcoota', *Quinkana timara*, and *Volia athollander-*

*soni*), only *P. datangensis* was examined first hand here, and the condition was not observed; as such, this character state is excluded.

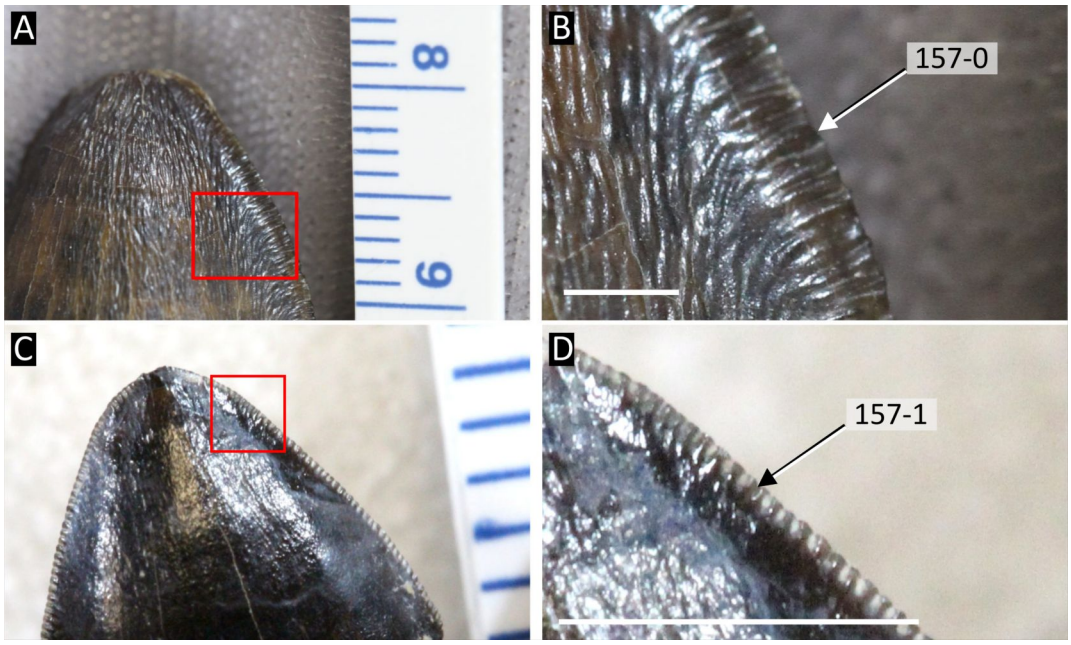



Figure 3.65: Tooth morphology showing variation in development of serrations. **A**, *Purussaurus neivensis* (UCMP 38932); **B**, enlargement of highlighted area in A; **C**, *Boverisuchus vorax* (UCMP 170767). **D**, enlargement of highlighted area in C. Scale bars in B and D = 1 mm, A = cm, C = mm.

158. Maxilla, position of alveoli relative to maxillary palate separating toothrows: ventral or at the same level (0); dorsal (1) (after Hua & Jouve, 2004 [165]; in Jouve 2016 [165]).

In *Bernissartia fagesii* (IRScNB 1538) and most eusuchians, the maxillary alveolar walls are positioned ventral to the remainder of the palatal surface. This occurs is all longirostrines recovered as "tomistomines", e.g. *Tomistoma schlegelii* (Fig. 3.66A), *Maroccosuchus zennaroi* (IRScNB R408), and *Thecachampsa sericodon* (USNM 24938). By contrast, the maxillary toothrow is dorsally inset relative to the remainder of the palate in several exclusively longirostrine crocodylians, most of which have been recovered as "gavialoids", e.g. *Gavialis gangeticus* (Fig. 3.66B), *Piscogavialis jugaliperforatus* (SMNK 1282 PAL), *Eosuchus minor* (USNM 299730), and '*Tomistoma*' *dowsoni* (NHMUK R4769).

159. Maxilla, size of foramen for palatine ramus of cranial nerve V: small or absent, less than half diameter of $6^{th}$ maxillary alveolus (0); large, equal to or greater than half diameter of $6^{th}$ maxillary alveolus (1) (after Brochu, 1997b [111]; Groh, 2020 [136]).

The maxillary foramen for the palatine ramus of cranial nerve V is usually the largest of a linear series of foramina adjacent to the maxillary toothrow, posterior to the level of the $5^{th}$ maxillary alveolus (Fig.

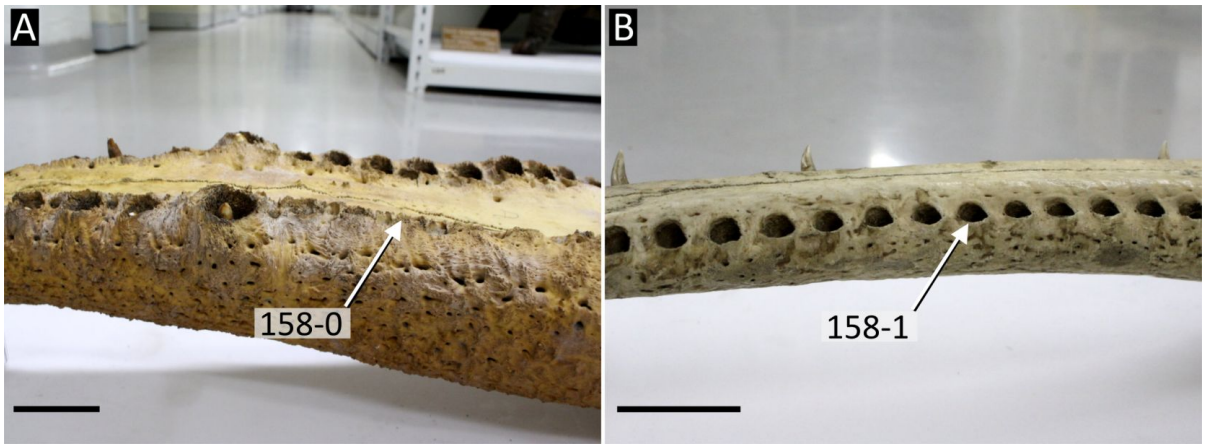



Figure 3.66: Lateral view of the cranial rostrum showing differences in elevation between the alveolar walls of: **A**, *Tomistoma schlegelii* (NHMUK 1894.2.21.1); **B**, *Gavialis gangeticus* (NHMUK 1974.3009). All scale bars = 5 cm.

3.67). In most crocodylians, this foramen is inconspicuously small, e.g. all species of *Crocodylus* (Fig. 3.67A). In several 'basal' crocodyloids, this foramen is notably larger, e.g. '*Crocodylus*' *affinis* (Fig. 3.67B), *Asiatosuchus germanicus* (HLMD Me 5652), and *Asiatosuchus depressifrons* (IRScNB R251). A slit-like, but enlarged foramen is also found in *Thecachampsa sericodon* (USNM 24938). This character is modified from its original formulation by Brochu (1997b) only by the quantification of foramen size by comparison with the adjacent maxillary alveolus, following Groh et al. (2020).

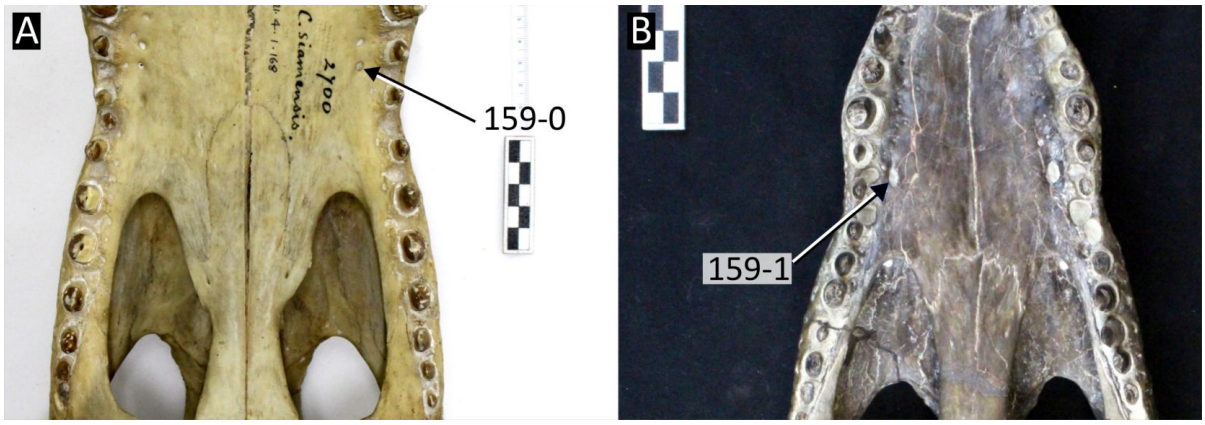



Figure 3.67: Ventral view of the palate showing variation in cranial nerve V in **A**, *Crocodylus siamensis* (NHMUK 1921.4.1.168); and **B**, *'Crocodylus' affinis* (USNM 18171). Scale bars = cm.

160. Palatine, anterior process shape: rounded or quadrangular (0); wedge shaped (i.e. forms a 'V' shape anteriorly) (1) (after Brochu, 1997b [118]).

The anterior palatine process is broadly rounded or squared-off at its anterior end in *Bernissartia fagesii* (IRScNB 1538) and most eusuchians (Fig. 3.68A–C). This condition contrasts with the anteriorly acute, wedge-shaped palatine process that occurs almost exclusively in longirostrine crocodylians,

e.g. *Mecistops cataphractus* (Fig. 3.68D), *Gavialis gangeticus* (Fig. 3.68F), *Tomistoma schlegelii* (NHMUK 1894.2.21.1), *Brochuchus pigotti* (NHMUK R7729), and *Baru darrowi* (Willis et al. 1990, fig.1).

161. Palatine, invagination of anterior process: absent (0); present (1) (after Brochu, 1997b [108]; Brochu, 2010 [84]; Delfino & De Vos, 2010).

The derived character state describes the invagination of a short posterior projection of the maxilla into the palatine anterior process that occurs in several crocodylians. In taxa with a broad palatine process (160-0), this results in a heart-shaped palatine process, e.g. *Paleosuchus* (Fig. 3.68E) and *Caiman latirostris* (NHMUK 86.10.4.2, MACN PV 1420, FMNH 9713). By contrast, taxa with wedge-shaped palatine processes (160-1) exhibit a narrow, bifurcated process (Fig. 3.68F), e.g. *Eosuchus lerichei* (IRScNB R49), *Dollosuchoides densmorei* (Brochu, 2007b, fig.3), and *Maomingosuchus petrolica* (Shan et al., 2017, fig.4C). In both cases the invagination is considered homologous. Delfino and De Vos (2010) recognised a similar invagination in *Gavialis benjawanicus* (not studied here), which was used to distinguish that species from all other *Gavialis* species. However, all specimens of *Gavialis gangeticus* studied here possess a similar (albeit smaller) invagination, e.g. NHMUK 1974.3009 (Fig. 3.68F), NHMUK 704, NHMUK 1846.1.7.3. Whereas the palatines are not bifurcated in *Gavialis browni* (Mook, 1932, fig.2), the condition is unknown in *Gavialis lewisi* (YPM 3226).

162. Palatine, anterior process position relative to anterior margin of suborbital fenestra: anterior to, and at the level of more than two full alveoli; (0) anterior to and at the level of two or fewer full alveoli (1); at the same level or posterior to anterior margin of suborbital fenestra (2) (after Willis, 1993 [2]; Brochu, 1997b [110]) (ORDERED).

Willis et al. (1990) noted similarities in the relative length of the palatine process of the crocodyloids *Baru darrowi* and *Brachyuranochampsa eversolei* (Zangerl, 1944). In both taxa, the palatine processes do not exceed the anterior margin of the palatal fenestrae. Willis (1993) discretised this morphological variation as a binary character (see also Brochu (1997b), distinguishing between a palatine process that exceeds the anterior margin of the suborbital fenestra (common to most eusuchians) (Fig. 3.68A–B), and one that remains posterior to the level of the anterior margin of the suborbital fenestrae (Fig. 3.68C). The latter condition is described here in character state 2 and is found in several 'basal' crocodyloids, e.g. '*Crocodylus*' *affinis* (UCMP 131090, USNM 18171), *Asiatosuchus depressifrons* (IRScNB R251), *Asiatosuchus germanicus* (HLMD Me 5652), and *Quinkana fortirostrum* (Molnar, 1982b, fig.3). The character has been modified here to describe varying lengths of the palatine process beyond the suborbital fenestra. Most eusuchians have an intermediately long palatine process, which reaches the level of less than two maxillary alveoli beyond the anterior margin of the suborbital fenestra (162-1) e.g. *Hylaeochampsa vectiana* (NHMUK R177), *Borealosuchus sternbergii* (USNM

6533), *Alligator mississippiensis* (Fig. 3.68G), and *Crocodylus siamensis* (Fig. 3.68B). By contrast, some crocodylians have a highly elongated palatine process, which reaches the level of two or more alveoli beyond the suborbital fenestra (162-0), e.g. *Melanosuchus niger* (Fig. 3.68A) and *Gavialis gangeticus* (Fig. 3.68F).

163. Palatine, palatal bar, lamina projecting into suborbital fenestrae from anterolateral margin: absent (0); present (1) (after Brochu, 1997b [94]).

    The anatomical meaning of this character is consistent with Brochu (1999, fig.44E), who recognised that some crocodylians exhibit an anterolateral process/flange of the palatine that projects into the suborbital fenestra (Fig. 3.68E). This process probably serves as an attachment site for *M. pterygoideus dorsalis* (Holliday et al., 2013). As previously scored (e.g. Brochu et al., 2012), the derived condition characterises both species of *Paleosuchus* (Fig. 3.68E), some *Alligator* species (e.g. *A. olseni*, MCZ 1887), *Diplocynodon muelleri* (Piras & Buscalioni, 2006, fig.4), and *Borealosuchus sternbergii* (USNM 6533). It is additionally recognised in several further *Diplocynodon* species, e.g. *D. ratelii* (Fig. 3.68H) and *D. hantoniensis* (Fig. 3.68I). Furthermore, the condition in *Leidyosuchus canadensis* is scored here as polymophic, given that specimens variably exhibit the flange (Wu et al., 2001a).

164. Palatine, palatal bar, orientation of posterolateral margin realtive to sagittal axis: sub-parallel (angle $< 40°$) (0); flared ($\geq 40°$) (1) (after Norell, 1988 [2]; Brochu, 1997b [90]).

    The posterolateral margin of the palatal bar is sub-parallel to the sagittal axis in *Bernissartia fagesii* (IRScNB 1538) and most eusuchians, with minimal flare posteriorly (Fig. 3.68B). In several crocodylians, the palatal bar flares abruptly at its posterior end to produce a shelf (Brochu, 1999, fig.44G). This occurs mainly in alligatoroids, e.g. *Melanosuchus niger* (Fig. 3.68A), *Alligator mississippiensis* (Fig. 3.68G), *Paleosuchus trigonatus* (Fig. 3.68E), and *Mourasuchus atopus* (UCMP 38012), but also in the crocodylid *Osteolaemus tetraspis* (Fig. 3.68C). Fewer taxa are scored for the derived condition compared to previous studies, because the character states are quantified here with an angular measurement of flare. For example, the palatines flare $<40°$ in *Diplocynodon ratelii* (Fig. 3.68H) and *Diplocynodon hantoniensis* (Fig. 3.68I), and thus they were scored for the plesiomorphic condition (differing to Brochu et al. [2012]). The development of pterygoid bullae (see Character 199), or the inflation of the palatines and pterygoids can result in the appearance of flared palatines (Fig. 3.68D, F). This is distinguished from truly flared palatines in that the lateral margins of the palatal bar remain sub-parallel, and no shelf is developed.

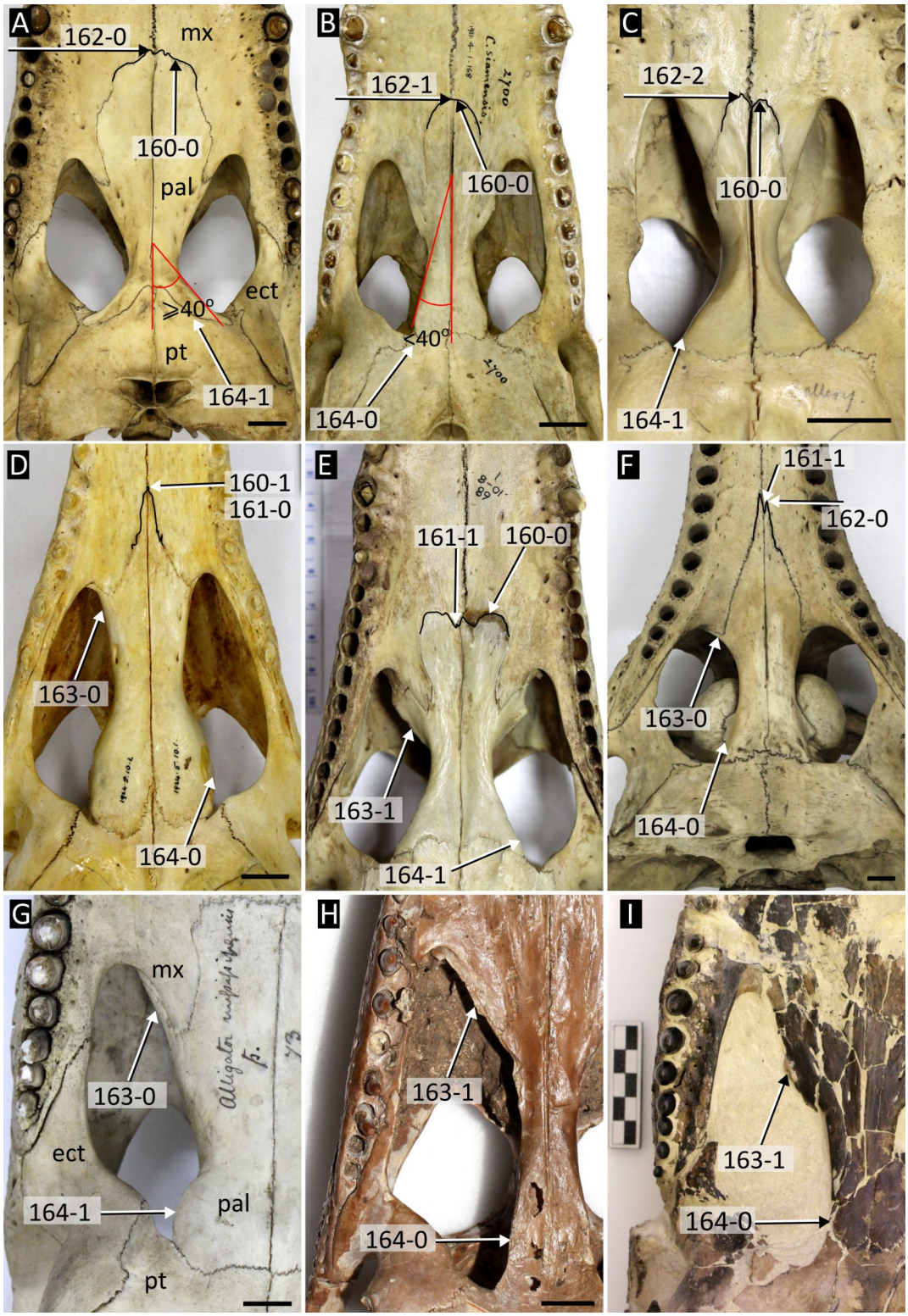



Figure 3.68: Variation in morphology of the palatine in ventral view. **A**, *Melanosuchus niger* (NHMUK 45.8.25.125); **B**, *Crocodylus siamensis* (NHMUK 1921.4.1.168); **C**, *Osteolaemus tetraspis* (NHMUK 1862.6.30.5); **D**, *Mecistops cataphractus* (NHMUK 1924.5.10.1); **E**, *Paleosuchus trigonatus* (NHMUK 1868.10.8.1); **F**, *Gavialis gangeticus* (NHMUK 1974.3009); **G**, *Alligator mississippiensis* (NHMUK 1873.2.21.1); **H**, *Diplocynodon ratelii* (MNHN SG 539); **I**; *Diplocynodon hantoniensis* (CAMSM TN 907). Abbreviations: **ect**, ectopterygoid; **mx**, maxilla; **pal**, palatine, **pt**, pterygoid. Scale bars E, I = cm, all other scale bars = 2 cm.

165. Palatine, ventrolateral 'ear-shaped' process projecting from base of prefrontal pillar: absent (0); present (1) (new character, adapted from Wu et al. 2001).

This process refers to a small, elliptical-shaped projection either side of the palatine bar, first noted in *Leidyosuchus canadensis* (Wu et al., 2001a, fig.14C). In their study, Wu et al. (2001a) noted intraspecific variation in the occurrence of such processes in *Leidyosuchus*, and briefly mentioned their occurrence in some specimens of *Caiman*, *Crocodylus*, and *Alligator*. Most eusuchians studied here lack these features at all stages of ontogeny, where known (Fig. 3.69A), but they occur variably in some crocodylids such as *Crocodylus niloticus* (present in NHMUK 1882.3.7.1 and NHMUK 1934.6.3.1, absent in NHMUK 1894.6.5.33) and *Osteolaemus tetraspis* (present in FMNH 229974, absent in NHMUK 1862.6.30.5). By contrast, they were consistently observed in Neotropical *Crocodylus* species. For example, they occur in *C. intermedius* (FMNH 75658, FMNH 75659, FMNH 75662, NHMUK 1851.8.25.29, NHMUK 62.10.19.1) and most specimens of *C. rhombifer* (AMNH 77595, AMNH R154087), although only some specimens of *C. acutus* (FMNH 69884). Other than *Leidyosuchus canadensis*, the only fossil eusuchian found to exhibit these processes in this study was *Agaresuchus fontisensis* (Narváez et al., 2016, fig.2C). Further study of a larger sample of specimens of extant species is required to explore intraspecific variation and the utility of this character.

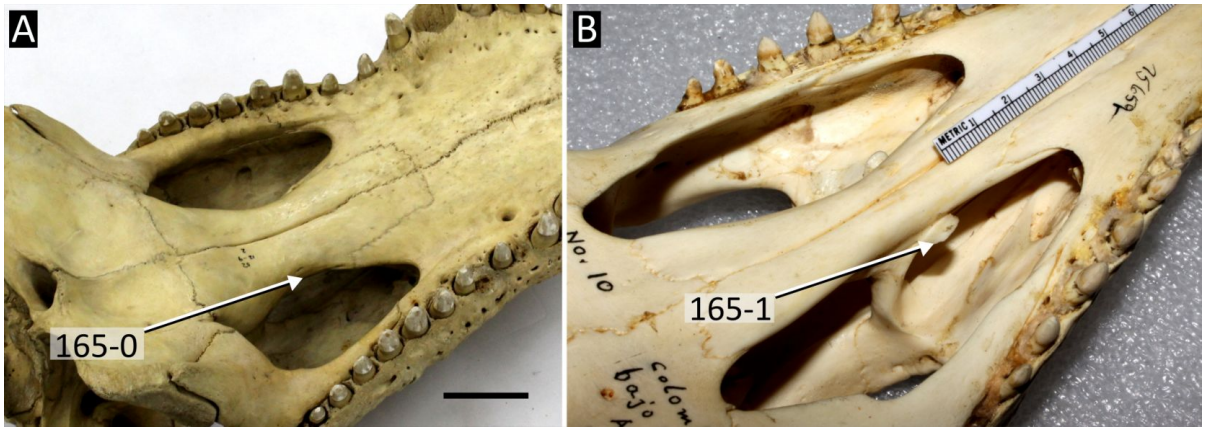



Figure 3.69: Development of ventrolateral processes of the palatines. **A**, *Crocodylus porosus* (NHMUK 1852.12.9.2); **B**, *Crocodylus intermedius* (FMNH 75659). Scale bar A = 5 cm, B = cm.

166. Suborbital fenestra, position of anterior margin relative to anterior orbital margin: anterior to (0); level with, or posterior to (1) (after Jouve et al., 2008 [201]).

In *Bernissartia fagesii* (IRScNB 1538) and most eusuchians, the anterior margin of the suborbital fenestra is positioned substantially anterior to that of the orbital margin. As such, only a portion of the orbit can be viewed through the suborbital fenestrae (Fig. 3.70A, C). Less commonly, the anterior margins of the suborbital fenestra and orbit are approximately level. In this condition, most of the orbit is visible through the suborbital fenestra, e.g. *Gavialis gangeticus* (Fig. 3.70B), *Hylaeochampsa*

*vectiana* (NHMUK R177), and *Procaimanoidea utahensis* (USNM 15996).

167. Suborbital fenestra, anteromedial margin, intersection of maxilla-palatine suture: at the anteromedial margin (0); at the anterior corner (1) (after Brochu & Storrs, 2012 [187]).

In most eusuchians, the maxilla-palatine suture intersects the suborbital fenestra at its anteromedial margin (Fig. 3.70A, C). Brochu and Storrs (2012) recognised a new condition, in which this suture intersects the anterior corner of the suborbital fenestra, but this was only recognised in *Mecistops cataphractus* (Fig. 3.70F). Jouve (2016) scored the condition more widely in crocodylians, noting the same condition in several hylaeochampsids (*Hylaeochampsa vectiana* [Clark & Norell, 1992, fig.5], and *Iharkutuosuchus makadii* [Ősi et al., 2008, fig.1D]) and gavialoids (e.g. *Gavialis gangeticus*, Fig. 3.70B, *Piscogavialis jugaliperforatus*, SMNK 1282 PAL, *Gryposuchus colombianus*, UCMP 41136), which were similarly observed in this study. The condition is recognised in several additional crocodylians, including *Eosuchus lerichei* (IRScNB R 49), *Thecachampsa sericodon* (USNM 24938), *Thoracosaurus isorhynchus* (MNHN 1902-22), and *Maomingosuchus petrolica* (Shan et al., 2017, fig.4C).

168. Suborbital fenestra, anterolateral margin width, distance from medial edge of the toothrow to fenestral margin: narrow, less than or equal to one alveolus width (0); broader than one alveolar width (usually at least twice alveolar width) (1) (after Jouve et al. 2008 [146], adapted from Wu et al. 2001a).

The derived character state describes a broad lateral margin of the suborbital fenestra formed by the maxilla and ectopterygoid. As noted by Wu et al. (2001a), this area is especially broad in *Leidyosuchus canadensis*, a condition that is shared by most alligatoroids, e.g. *Eocaiman cavernensis* (Fig. 3.70H), *Caiman crocodilus* (Fig. 3.70D), and *Alligator mississippiensis* (Fig. 3.70E), as well as some crocodyloids, e.g. *Osteolaemus tetraspis* (Fig. 3.70G) and *Baru wickeni* (QM F16822). By contrast, most crocodyloids as well as gavialoids have narrow lateral margins of the suborbital fenestra, that are typically no more than one alveolar width, e.g. *Gavialis gangeticus* (Fig. 3.70B), *Crocodylus porosus* (Fig. 3.70C), and *Mecistops cataphractus* (Fig. 3.70F).

169. Suborbital fenestra, lateral margin shape: straight (0); projecting medially into fenestra (1) (rephrased from Brochu, 1997b [105]).

170. Suborbital fenestra, contribution of maxilla to medial projection: absent, projection entirely formed by ectopterygoid (0); present (1) (new character, adapted from Brochu, 1997b).

Characters 169 and 170 describe the presence and position of a medial projection into the suborbital fenestra from its lateral wall, and were derived by reductively coding Character 105 in Brochu (1997b). A medial projection (169-1) was recognised in *Bernissartia fagesii* (IRScNB 1538), some alligatoroids, (e.g. *Alligator mcgrewi*, AMNH 7905 and *Eocaiman cavernensis*, Fig. 3.70H), and the

crocodyloids *Osteolaemus tetraspis* (Fig. 3.70G) and *Trilophosuchus rackhami* (QM F16856). Brochu (1999) noted that the degree to which the maxilla participates varies between taxa, which is herein captured in Character 170. Whereas the process is formed entirely by the ectopterygoid (170-0) in the crocodyloids *Osteolaemus tetraspis* (Fig. 3.70G) and *Trilophosuchus*, the maxilla contributes to this process (170-1) in the alligatoroids *Eocaiman cavernensis* (Fig. 3.70H) and *Alligator mcgrewi* (AMNH 7905).

171. Suborbital fenestra, posterolateral margin shape at ectopterygoid-pterygoid suture intersection: straight (0); bowed anteromedially (1) (after Brochu, 1997b [88]; Brochu, 2010 [119]).

    In *Bernissartia fagesii* (IRScNB 1538) and most eusuchians, the posterior margin of the suborbital fenestra is rounded (Brochu, 1999) (Fig. 3.70B, D). By contrast, some eusuchians exhibit a convexity in the fenestral margin around the level of the intersection of the ectopterygoid-pterygoid suture, which produces an embayment near the posterior corner of the suborbital fenestra (Brochu, 1999). Among eusuchians, this condition occurs in some *Alligator* species (e.g. *A. mississippiensis*, Fig. 3.70E and *A. sinensis*, USNM 292078), and most *Crocodylus* species, e.g. *C. porosus* (Fig. 3.70C), *C. acutus* (NHMUK 1975.997), and *C. johnstoni* (QM J39230).

172. Suborbital fenestra, posterior margin, intersection of palatine-pterygoid suture: at the posterior corner (0); on the posteromedial margin (1) (after Brochu, 1997b [85]).

    This character has received minor changes to its wording. Originally, the plesiomorphic condition described the palatine-pterygoid suture being "nearly at" the posterior margin of the suborbital fenestra (Brochu, 1997b, Character 85). In the revised format, taxa scored for the plesiomorphic condition must exhibit a pterygoid-palatine suture which intersects precisely at the posterior corner of the suborbital fenestra (Fig. 3.70E). Consequently, by contrast with previous studies (e.g. Brochu et al., 2012), some taxa are newly scored for the derived condition, e.g. *Paleosuchus trigonatus* (Fig. 3.70I), *Procaimanoidea utahensis* (USNM 15996), and *Allodaposuchus precedens* (MMS/VBN-12-10-A).

173. Ectopterygoid, anterior extent relative to maxillary alveoli: reaches the level of two or fewer alveoli (0); more than two alveoli (1) (after Jouve, 2016 [91], Lee & Yates, 2018 [28]).

    The ectopterygoid extends beyond two maxillary alveoli in most eusuchians, e.g. *Borealosuchus sternbergii* (Fig. 3.70A), *Boverisuchus vorax* (FMNH PR 399), *Crocodylus porosus* (Fig. 3.70C), *Caiman crocodilus* (Fig. 3.70D), and *Alligator mississippiensis* (Fig. 3.70E). By contrast, the ectopterygoid reaches fewer than two maxillary alveoli in *Bernissartia fagesii* (IRScNB 1538), some gavialoids (e.g. *Gavialis gangeticus*, Fig. 3.70B), *Tomistoma schlegelii* (NHMUK 1894.2.21.1), and some alligatoroids, e.g. *Brachychampsa montana* (UCMP 133901) and *Melanosuchus niger* (NHMUK 45.8.25.125).

174. Ectopterygoid, anterior extent relative to anteroposterior length of suborbital fenestra: less than two thirds of fenestra length (0); equal to or greater than two thirds of fenestra length (1) (after Brochu & Storrs, 2012 [185]).

The anterior extent of the ectopterygoid relative to the anteroposterior length of the suborbital fenestra is independent of ectopterygoid extent relative to maxillary alveoli (Character 173). This is evidenced by the occurrence of all possible combinations of characters 173 and 174 in multiple taxa examined here. For example, in *Gavialis gangeticus* (Fig. 3.70B), *Brachychampsa montana* (UCMP 133901), and *Stangerochampsa mccabei* (Wu et al., 1996, fig.1B), the ectopterygoid anteriorly reaches the level of fewer than two alveoli (173-0), but the anterior ectopterygoid ramus still forms more than two thirds the length of the suborbital fenestra (174-1). By contrast, in *Borealosuchus sternbergii* (Fig. 3.70A), *Borealosuchus formidabilis* (Erickson, 1976, fig.5), and *Diplocynodon hantoniensis* (NHMUK 30392), the ectopterygoid is adjacent to two or more maxillary alveoli (173-1), but the anterior ectopterygoid ramus forms around half the anteroposterior length of the suborbital fenestra (174-0).

175. Ectopterygoid, sutural contact with maxilla adjacent to maxillary toothrow: widely separated from medial toothrow margin (0); adjacent to medial toothrow margin (1); fully abutting medial toothrow margin (2) (after Norell, 1988 [19]; Brochu, 1997b [91]; Jouve, 2016 [91]) (ORDERED).

Most studies follow the original formulation of this character by Brochu (1997b) (e.g. Brochu et al., 2012; Salas-Gismondi et al., 2015; Narváez et al., 2016; Salas-Gismondi et al., 2016; Lee & Yates, 2018; Salas-Gismondi et al., 2019): "*Ectopterygoid abuts maxillary toothrow (0); or maxilla broadly separates ectopterygoid from maxillary toothrow (1)*" (Brochu, 1997b, Character 91). The condition in which the maxilla broadly separates the ectopterygoid from the toothrow (e.g. Fig. 3.71H) has long been considered diagnostic of Alligatoroidea, and strongly contrasts with the fully abutting ectopterygoid of crocodylids (e.g. Fig. 3.71R) (Norell et al., 1994, fig.6; Brochu, 1999, fig.24A–B). Accordingly, alligatoroids are scored for character state 1 in most matrices, with gavialoids, "tomistomines", *Borealosuchus*, and *Bernissartia fagesii* all described as having an ectopterygoid which abuts the maxillary toothrow, as in crocodylids. However, this is inaccurate, as the ectopterygoid is separated by the maxilla in many of the aforementioned taxa, e.g. *Bernissartia fagesii* (Fig. 3.71A) (see also Martin et al., 2020, fig.2D), *Borealosuchus sternbergii* (Fig. 3.71B–C), *Tomistoma schlegelii* (Fig. 3.71D), and *Gavialis gangeticus* (Fig. 3.71E). This was alluded to by Delfino et al. (2005), who indicated that it is inappropriate to describe *Gavialis gangeticus* and *Crocodylus niloticus* as sharing the same condition, and that the character should be better defined. Jouve (2016) evidently reached the same conclusion, as he introduced a new character state that distinguished several gavialoids, "tomistomines", 'basal' crocodyloids, and all *Borealosuchus* species, from the alligatoroid and crocodylid

conditions. According to Jouve (2016), these taxa exhibit an "*ectopterygoid* (that) *does not abut the maxillary teeth, and the ectopterygoid-maxillary suture parallels the toothrow*". The difference between the condition in taxa such as *Gavialis*, *Tomistoma*, and *Borealosuchus*, to that of an alligatoroid such as *Alligator mississippiensis* (Fig. 3.71H), is only a matter of degree. The important distinction is between those with an ectopterygoid-toothrow contact, and those without. Furthermore, the difference in degree of separation can be attributed, in part, to differences in the width of the lateral margin of the suborbital fenestra, which, as established earlier in Character 168, tends to be wider in alligatoroids (Wu et al., 2001a) (Fig. 3.71I–J). Consequently, most of the taxa scored for the new condition by Jouve (2016) have been changed to character state 0 here, i.e. the same condition exhibited by alligatoroids. Nevertheless, Jouve's additional character state has been co-opted to describe a distinct condition (175-1) that occurs mainly in crocodyloids (e.g. *Asiatosuchus depressifrons*, Fig. 3.71K, *Kambara implexidens*, Fig. 3.71L and *Australosuchus clarkae*, UCMP 71396), but also *Diplocynodon ratelii* (Fig. 3.71M), *Boverisuchus vorax* (Fig. 3.71N), and *Piscogavialis jugaliperforatus* (Fig. 3.71O). In these taxa, the ectopterygoid incipiently contacts the toothrow, barely separated by a thin slither of the maxilla. The revised character is ordered given that this character state is considered intermediate (175-1) between a widely separated ectopterygoid (175-0) and a fully abutting ectopterygoid (175-2), the latter characterising most crocodylids (Fig. 3.71P–T) as in previous studies.

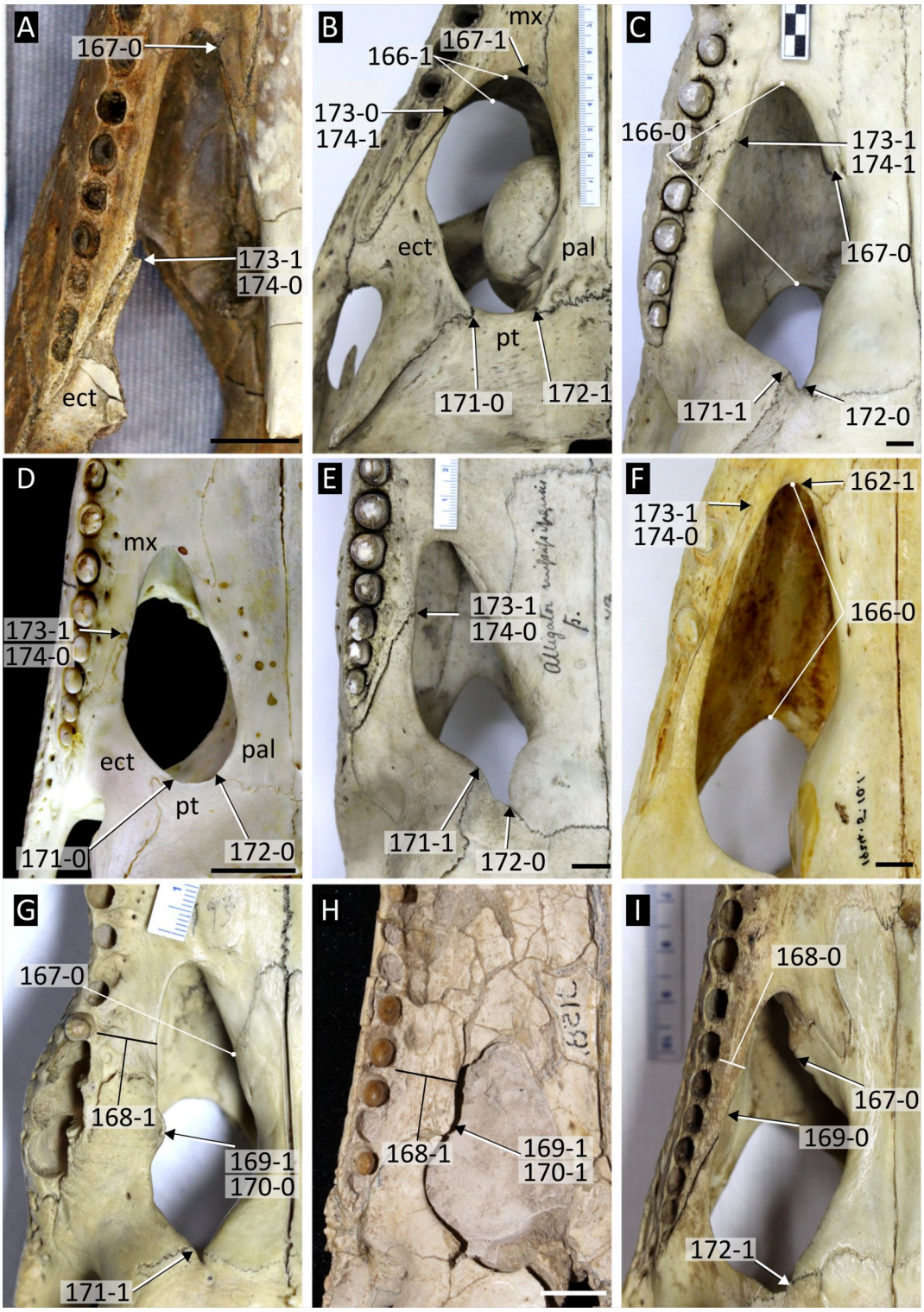



Figure 3.70: Sutural relationships and morphology of the suborbital fenestra in selected crocodylians. **A**, *Borealosuchus sternbergii* (UCMP 126099); **B**, *Gavialis gangeticus* (NHMUK 1974.3009) (digitally reversed); **C**, *Crocodylus porosus* (NHMUK 1852.12.9.2); **D**, *Caiman crocodilus chiapasius* (FMNH 73694); **E**, *Alligator mississippiensis* (NHMUK 1873.2.21.1); **F**, *Mecistops cataphractus* (NHMUK 1924.5.10.1) (digitally reversed); **G**, *Osteolaemus tetraspis* (NHMUK 1862.6.30.5); **H**, *Eocaiman cavernensis* (AMNH 3158) (digitally reversed); **I**, *Paleosuchus trigonatus* (NHMUK 1868.10.8.1). Abbreviations: **ect**, ectopterygoid; **mx**, maxilla; **pal**, palatine; **pt**, pterygoid. All scale bars = 1 cm.

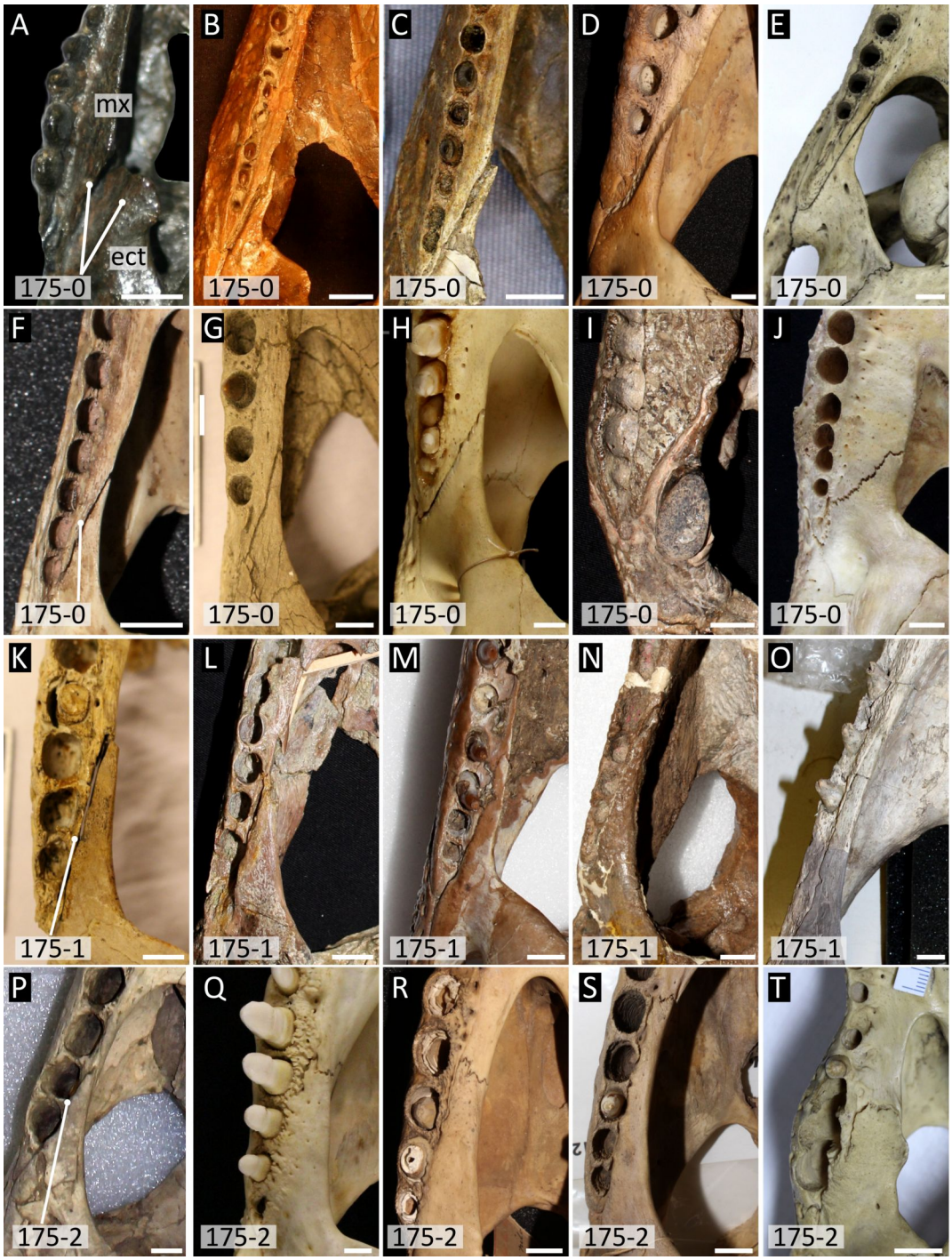



Figure 3.71: Variation in the ectopterygoid-maxilla suture. **A**, *Bernissartia fagesii* (IRSNB 1538); **B**, *Borealosuchus sternbergii* (USNM 6533); **C**, *Borealosuchus sternbergii* (UCMP 126099); **D**, *Tomistoma schlegelii* (USNM 211323); **E**, *Gavialis gangeticus* (NHMUK 1974.3009); **F**, *Paleosuchus trigonatus* (NHMUK 1868.10.8.1); **G**, *Eosuchus lerichei* (IRSNB R 49); **H**, *Alligator mississippiensis* (AMNH 71621); **I**, *Navajosuchus mooki* (AMNH 6780); **J**, *Caiman latirostris* (FMNH 9713); **K**, '*Crocodylus*' *depressifrons* (IRSNB R 251); **L**, *Kambara implexidens* (QM 29662); **M**, *Diplocynodon ratelii* (MNHN SG 539); **N**, *Boverisuchus vorax* (FMNH PR 399); **O**, *Piscogavialis jugaliperforatus* (SMNK 1282 PAL); **P**, *Thecachampsa sericodon* (USNM 25243); **Q**, *Crocodylus rhombifer* (AMNH R 154087); **R**, *Crocodylus porosus* (NHMUK 1852.12.9.2); **S**, *Crocodylus niloticus* (NHMUK 1934.6.3.1); **T**, *Osteolaemus tetraspis* (NHMUK 1862.6.30.5). Abbreviations: **ect**, ectopterygoid; **mx**, maxilla. All scale bars = 1 cm.

176. Ectopterygoid, morphology of anterior maxillary ramus on lateral suborbital fenestra wall: acute, tapering to a single point (0); forked (1) (after Brochu, 1997b [109]).

The anterior tip of the ectopterygoid forms an acute point on the inner lateral wall of the suborbital fenestra in most crocodylians (Fig. 3.72A). In *Mecistops cataphractus* (NHMUK 62.6.30.8), *Brochuchus pigotti* (NHMUK R7729), *Crocodylus palaeindicus* (NHMUK 39795), and some individuals of all extant *Crocodylus* species, the anterior margin bears a cleft (Fig. 3.72B) (Brochu, 2000). Following the observations of Brochu et al. (2010), the condition is scored as polymorphic in extant *Crocodylus* species.

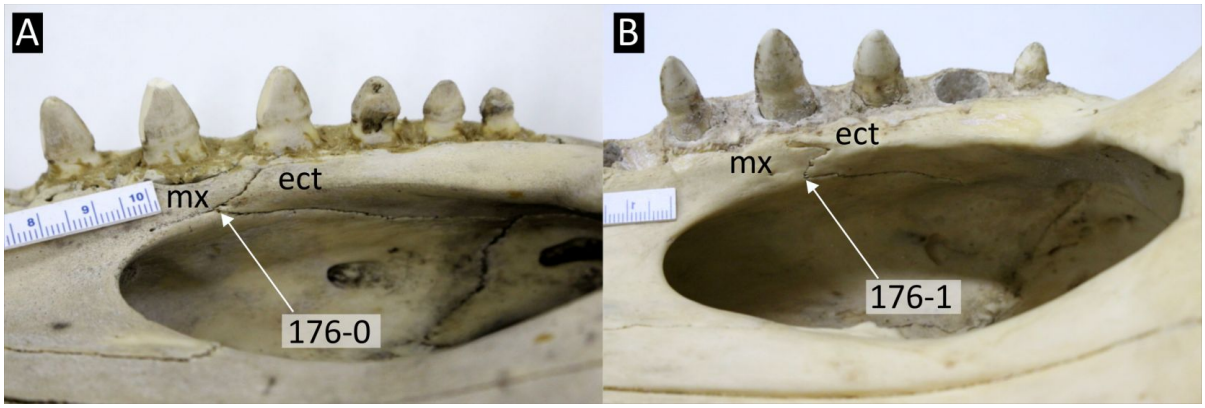



Figure 3.72: Variation in morphology of the ectopterygoid tip in crocodylians. **A**, *Crocodylus acutus* (NHMUK 1975.997); **B**, *Crocodylus niloticus* (NHMUK 1934.6.3.1) (digitally reversed). Abbreviations: **ect**, ectopterygoid; **mx**, maxilla. Scale bars = cm.

177. Ectopterygoid, anterior maxillary ramus: contacts suborbital fenestra (0); separated from the suborbital fenestra by the maxilla (1) (after Brochu & Storrs, 2012 [186]).

In most crocodylians, the anterior tip of the ectopterygoid contributes to the lateral margin of the suborbital fenestra, e.g. *Crocodylus porosus* (Fig. 3.73A). Less commonly, the ectopterygoid may be blocked from the suborbital fenestra at its anterior tip by a thin posterior projection of the maxilla. This condition occurs in *Mecistops cataphractus* (Fig. 3.73B), some mekosuchines (e.g. *Mekosuchus sanderi* [QM F31188], *Kambara implexidens* [QM F29662], *Baru wickeni* [QM F16822], and *Baru huberi* [QM F31063]), and is polymorphic in *Crocodylus johnstoni* (e.g. present in QM J39230, absent in QM J45309).

178. Ectopterygoid, position relative to maxillary alveoli: restricted to medial side (0); forming posterior and lateral margins (1) (new character, adapted from Clark & Norell, 1992).

Clark and Norell (1992) recognised that the putative 'palatal foramen' of *Hylaeochampsa vectiana* is actually a highly enlarged posterior maxillary alveolus (Fig. 3.74B), which can also be found in *Iharkutosuchus makadii* (Ősi, 2008). Furthermore, the ectopterygoid partially roofs this alveolus in

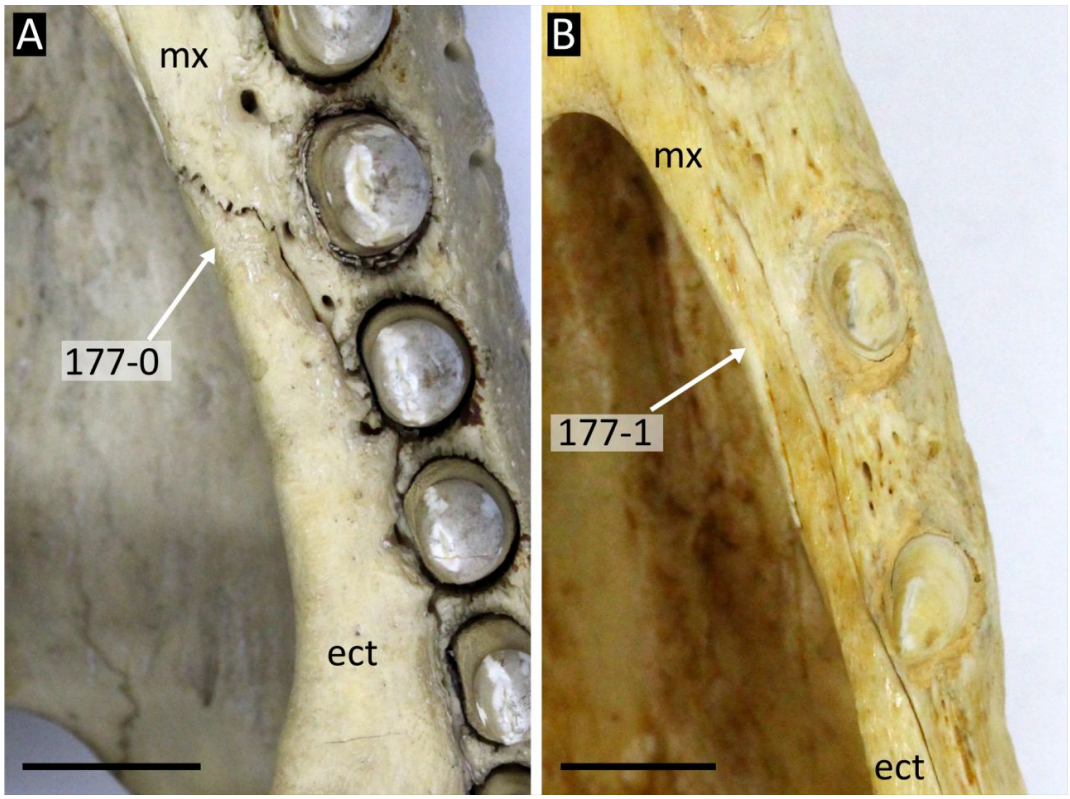



Figure 3.73: Relationship of the ectopterygoid anterior tip and suborbital fenestra. **A**, *Crocodylus porosus* (NHMUK 1852.12.9.2) (digitally reversed); **B**, *Mecistops cataphractus* (NHMUK 1924.5.10.1). Abbreviations: **ect**, ectopterygoid; **mx**, maxilla. All scale bars = 1 cm.

both taxa, forming the posterior and lateral alveolar walls (178-1) (Fig. 3.74B) (Ősi, 2008, fig.1D). In *Bernissartia fagesii* (IRScNB 1538) and all other eusuchians, the ectopterygoid is completely excluded from the posterior and lateral margins of the toothrow (178-0), e.g. *Caiman latirostris* (Fig. 3.74A).

179. Maxilla, non-dentigerous posterior process between jugal and ectopterygoid: short, less than anteroposterior length across last three maxillary alveoli (0); long, equal to or greater than anteroposterior length across last three maxillary alveoli (1) (after Jouve et al., 2008 [172]).

    In all crocodylians the maxilla forms an acute posterior process between the jugal and ectopterygoid (Fig. 3.75). In most species this process is short, approximately the length of one or two maxillary alveoli e.g. *Alligator mississippiensis* (Fig. 3.75A). This process is notably longer in *Mecistops cataphractus* (NHMUK 1924.5.10.1), and several gavialoids, e.g. *Gavialis gangeticus* (Fig. 3.75B), *Piscogavialis jugaliperforatus* (SMNK 1282 PAL), and *Argochampsa krebsi* (NHMUK R36872).

180. Ectopterygoid, dorsal extent along medial surface of postorbital bar: large, extends dorsal to level of ventral orbital margin (0); small, level with or ventral to level of ventral orbital margin (1) (after Brochu, 1997b [133]).

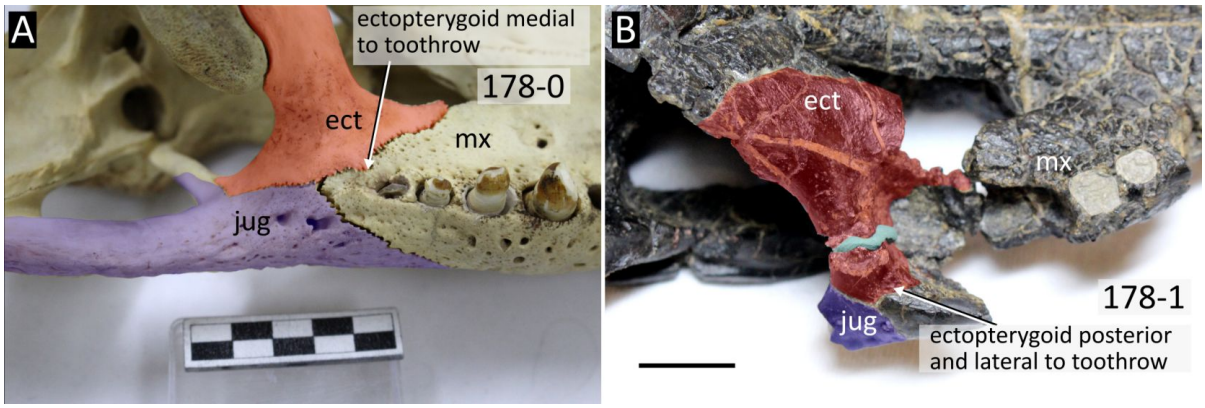



Figure 3.74: Ventrolateral view of the posterior maxillary toothrow showing the relationship of the ectopterygoid to the toothrow. **A**, *Caiman latirostris* (NHMUK 1897.12.31.1); **B**, *Hylaeochampsa vectiana* (NHMUK PV R 177). Abbreviations: **ect**, ectopterygoid; **jug**, jugal; **mx**, maxilla. Scale bar in B = 1 cm.

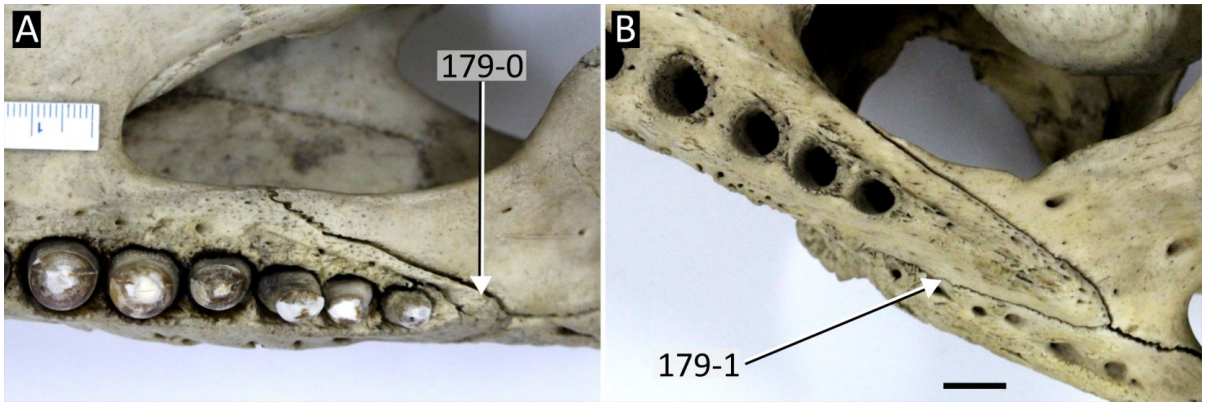



Figure 3.75: Ventral views of the suborbital fenestra showing variation in size of the maxillary non-dentigerous process in **A**, *Alligator mississippiensis* (NHMUK 1873.2.21.1); and **B**, *Gavialis gangeticus* (NHMUK 1974.3009). Scale bar A = cm, B = 1 cm.

The ectopterygoid sutures to the medial surface of the jugal, ascending the postorbital bar in most neosuchians, dorsal to the level of the ventral orbital margin (180-0) (Brochu, 1999). This occurs in *Bernissartia fagesii* (IRScNB 1538), *Hylaeochampsa vectiana* (NHMU R177), planocraniids (e.g. *Boverisuchus vorax*, FMNH PR 399), crocodyloids (e.g. *Crocodylus acutus*, Fig. 3.76A), gavialoids (e.g. *Gavialis gangeticus*, Fig. 3.76C) and *Tomistoma schlegelii* (NHMUK 1894.2.21.1). The dorsal extent of the ectopterygoid is low in all extant alligatorids (180-1) and several fossil alligatoroids (e.g. *Brachychampsa montana*, UCMP 133901), not exceeding the level of the ventral margin of the orbit (Fig. 3.76B). All species of *Borealosuchus* were previously scored for the plesiomorphic condition, where preserved (Brochu et al., 2012), but the derived condition can be observed in *Borealosuchus sternbergii* (UCMP 126099).

181. Ectopterygoid, morphology of posterior process on the medial jugal surface: acute, extends beyond level of posterior margin of postorbital bar (0); acute, terminating before posterior margin of postor-

bital bar (1); rounded (2) (after Norell, 1989 [9]; Jouve, 2004 [146]; Jouve, 2016 [243]) (ORDERED).

In addition to the dorsomedial ascending ramus of the ectopterygoid (Character 180), some taxa exhibit a posteromedial process, which runs along the medial surface of the jugal arch (Fig. 3.76). Norell (1989), and later Jouve (2016) characterised this morphological variation in a binary, presence/absence character. One additional intermediate character state is included here, and the character is ordered. Taxa exhibiting a long posterior process that exceeds the level of the postorbital bar (181-0) include *Bernissartia fagesii* (IRScNB 1538), most "gavialoids" (e.g. *Gavialis gangeticus* [Fig. 3.76C] and *Eogavialis africanum* [YPM 6263]), some crocodyloids (e.g. *Trilophosuchus rackhami* [QM F16856] and *Kambara implexidens* [QM F29662]), and some caimanines (e.g. *Mourasuchus atopus* [UCMP 38012] and *Acresuchus pachytemporalis* [UFAC 2507]). By contrast, the process is absent (182-2) in all extant crocodylids (e.g. *Crocodylus acutus* [Fig. 3.76A] and *Osteolaemus tetraspis* [NHMUK 1862.6.30.5]), and most "tomistomines" (e.g. *Tomistoma schlegelii* [NHMUK 1894.2.21.1] and *Thecachampsa sericodon* [USNM 24938]). In the intermediate condition (181-1), the ectopterygoid forms a posteromedial process, but it does not exceed the posterior margin of the postorbital bar (Fig. 3.76B). This occurs in some *Diplocynodon* species (e.g. *D. ratelii* [MNHN SG 539] and *D. hantoniensis* [NHMUK OR 30392]), *Eosuchus lericheri* (IRScNB R49), and all extant caimanines, e.g. *Caiman latirostris* (Fig. 3.76B).

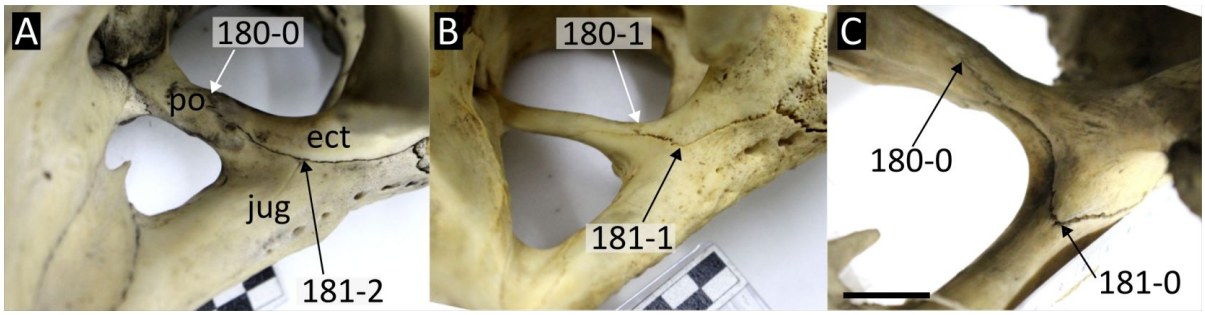



Figure 3.76: Ventromedial view of the temporal bar in selected crocodylians. **A**, *Crocodylus acutus* (NHMUK 1975.997); **B**, *Caiman latirostris* (NHMUK 1897.12.31.1); **C**, *Gavialis gangeticus* (NHMUK 1974.3009) (digitally reversed). Abbreviations: **ect**, ectopterygoid; **jug**, jugal; **po**, postorbital. Scale bar in C = 2 cm, all other scale bars = cm.

182. Jugal, extent of ectopterygoid and maxilla on medial surface, anterior to the postorbital bar: minimal, jugal visible (0); extensive, covering medial surface of jugal (1) (new character, based on personal observations).

In most crocodylians, a large portion of the medial jugal surface is exposed anterior to the postorbital bar in between the sutural contacts of the ectopterygoid and maxilla (Fig. 3.77A). By contrast, the ectopterygoid and maxilla cover most of the medial jugal surface in all *Mekosuchus* species, where

preserved (e.g. *M. inexpectatus* [Fig. 3.77B] and *M. sanderi* [QM F31166]), and also in *Trilophosuchus rackhami* (QM F16856).

183. Quadratojugal, anterior process on medial surface of lower temporal bar: present (0); absent (or very modest) (1) (Brochu, 1997b [83]).

In *Bernissartia fagesii* (IRScNB 1538) and most eusuchians, the medial surface of the jugal forming the lower temporal bar bears an anterior process of the quadratojugal (Fig. 3.77B). This process occurs in all "gavialoids", alligatoroids, and some crocodyloids, e.g. *Mekosuchus inexpectatus* (Fig. 3.77B), '*Crocodylus*' *affinis* (USNM 1811), and *Asiatosuchus depressifrons* (IRScNB IG 9912). By contrast, the process is absent in all extant crocodylids and some "tomistomines", e.g. *Tomistoma schlegelii* (NHMUK 1894.2.21.1).

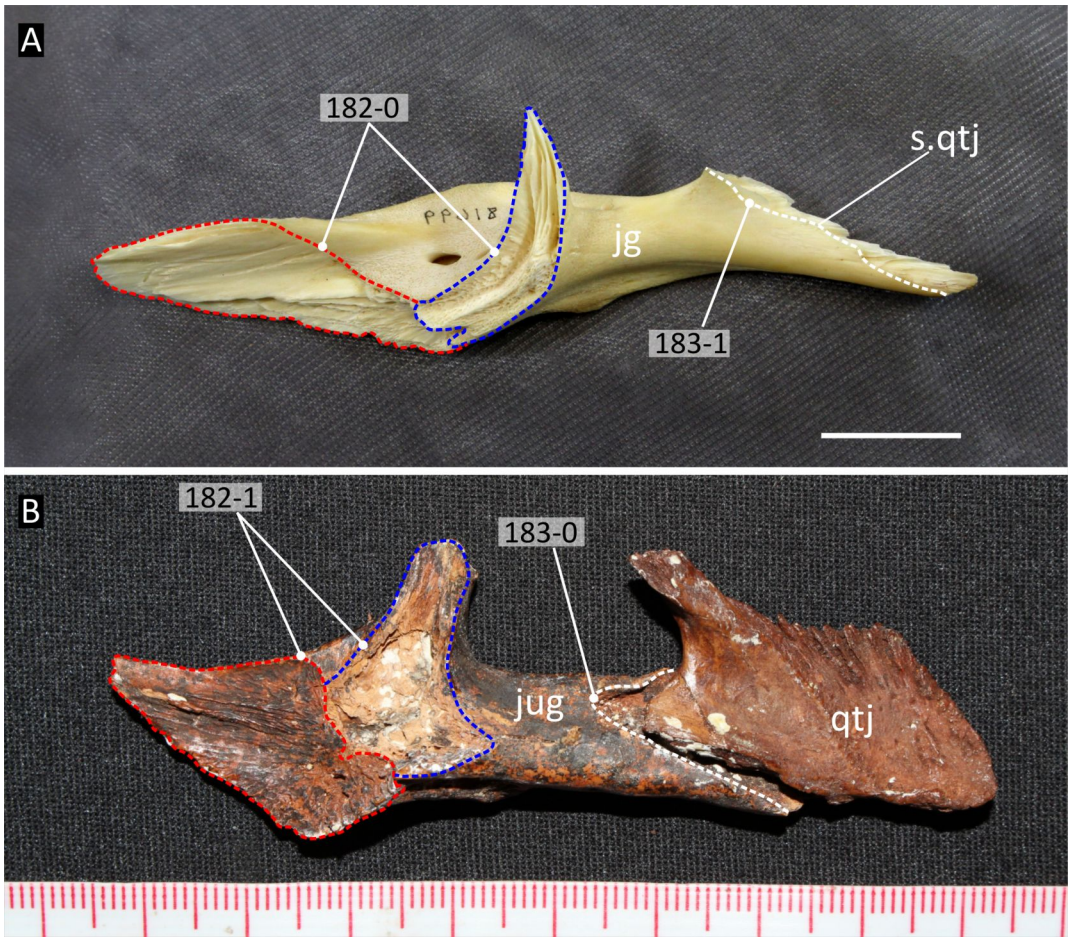



Figure 3.77: Isolated jugals in medial view showing the development of the anterior quadratojugal process (white), and extent of ectopterygoid (blue) and maxilla (red) sutures. **A**, *Crocodylus acutus* (UCMP 81699); **B**, *Mekosuchus inexpectatus* (MNHN NCP 06). Abbreviations: **jug**, jugal; **qtj**, quadratojugal. Scale bar = 1 cm.

184. Jugal, morphology of medial foramen anterior to postorbital bar: small foramen (0); large recess (1) (Brochu, 1997b [120]).

As noted by Brochu (1997a), the medial surface of the jugal is perforated by a foramen in all eusuchians (Fig. 3.78). This foramen usually remains small, as in all alligatoroids (Fig. 3.78A) and "gavialoids". By contrast, the foramen is enlarged to the extent that it forms a deep recess in *Borealosuchus sternbergii* (Brochu, 1997a, fig.5A), all extant crocodylids, and most "tomistomines", e.g. *Tomistoma schlegelii* (Fig. 3.78B) and *Thecachampsa sericodon* (USNM 24938). A measure of foramen size was not used because the distinction between the two character states is clear, and intermediate sized foramina are not present in any of the taxa in this dataset.

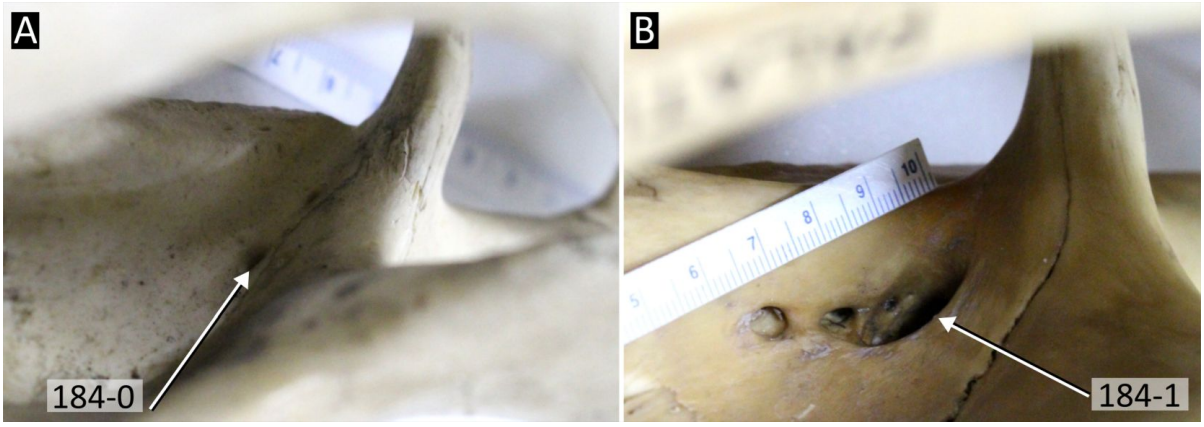



Figure 3.78: Medial view of the right jugal through the orbit in **A**, *Alligator mississippiensis* (NHMUK 1873.2.21.1); **B**, *Tomistoma schlegelii* (NHMUK 1894.2.21.1). Scale bars = cm.

185. Ectopterygoid-pterygoid suture, shape (at maturity): straight (0); kinked (i.e. with 'flexure') (1) (after Brochu, 1997b [116]).

In juvenile individuals of all extant crocodylians, the pterygoid-ectopterygoid suture posterior to the suborbital fenestra is prominently kinked (Brochu, 1999). This results from a process of the pterygoid that projects into the descending process of the ectopterygoid. Brochu (1999) recognised that whereas adult individuals of all extant caimanines paedomorphically retain this feature (e.g. *Caiman latirostris*, Fig. 3.79B), all other crocodylians lose it at maturity (e.g. *Crocodylus acutus*, Fig. 3.79C). Accordingly, Brochu (1999) recovered this feature as a synapomorphy of the crown group of caimanines, also present in some extinct species, e.g. *Purussaurus neivensis* (UCMP 45719). This condition is also present in some species of the 'basal' alligatoroid genus *Diplocynodon*, e.g. *D. deponiae* (Delfino & Smith, 2012) and *D. hantoniensis* (Fig. 3.79A, see also Section 2.3.1).

186. Ectopterygoid, posterior extent on pterygoid flange: reaches posterior tip (0); does not reach posterior tip (1) (after Norell, 1988 [32]; Brochu, 1997b [149]).

The descending process of the ectopterygoid underlies the pterygoid flange (Fig. 3.80). In almost all eusuchians, the ectopterygoid terminates before reaching the posterior tip of the pterygoid flange,

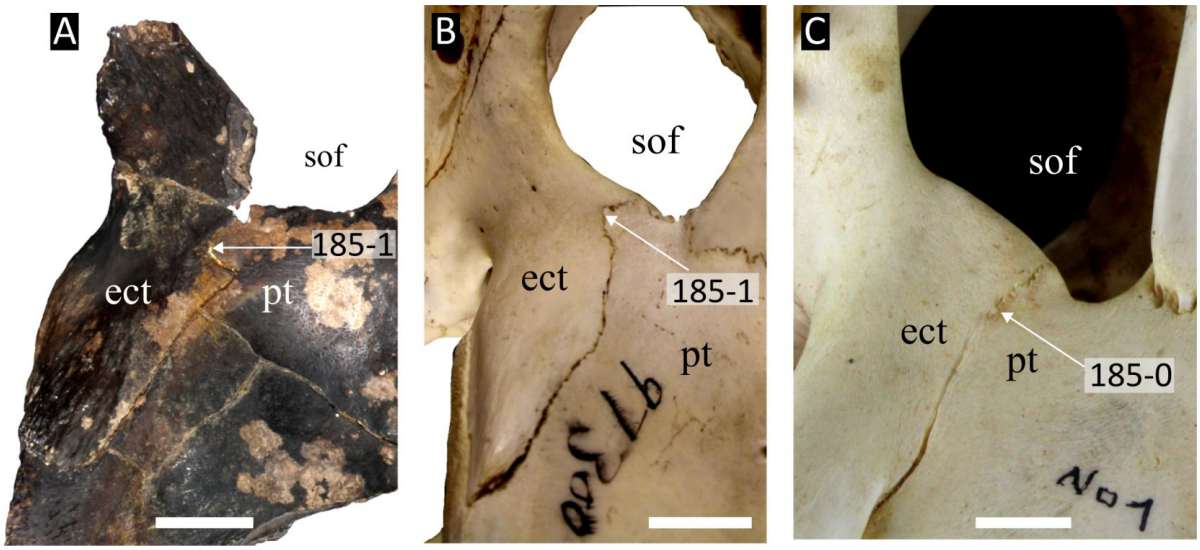



Figure 3.79: Ventral view of the ectopterygoid-pterygoid suture in selected crocodylians. **A**, *Diplocynodon hantoniensis* (NHMUK 30251); **B**, *Caiman yacare* (AMNH 97300); **C**, *Crocodylus acutus* (FMNH 69884). Abbreviations: **ect**, ectopterygoid; **pt**, pterygoid; **sof**, suborbital fenestra. Scale bars = 2 cm.

e.g. *Crocodylus siamensis* (Fig. 3.80C). As in previous datasets, the plesiomorphic condition is rare, occurring only in *Bernissartia fagesii* (Fig. 3.80A) and *Penghusuchus pani* (Shan et al., 2009, fig.3b). This condition was previously considered to be present in the 'Glen Rose Form' (e.g. Brochu, 1999). However, although the ectopterygoid almost reaches the posterior end of the pterygoid in this taxon, it nonetheless terminates shortly before the posterior tip (Fig. 3.80B).

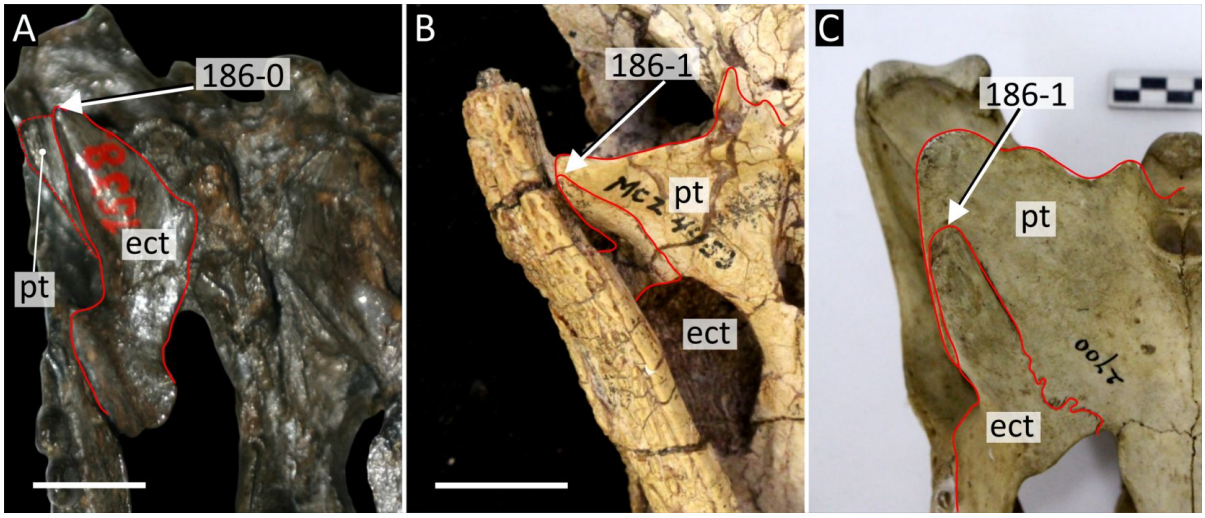



Figure 3.80: Ventral view of the pterygoids showing variation in posterior extent of the ectopterygoid on the pterygoid. **A**, *Bernissartia fagesii* (IRScNB 1538); **B**, the 'Glen Rose Form' (MCZ 4453); **C**, *Crocodylus siamensis* (NHMUK 1921.4.1.168). Abbreviations: **ect**, ectopterygoid; **pt**, pterygoid. Scale bar = 1cm.

187. Choanae, palatine participation: present, forms anterior margin of choanae (0); absent, choanae entirely surrounded by the pterygoids (1) (adapted from Benton & Clark, 1988; Norell & Clark, 1990

[1]; Clark, 1994 [43]; Brochu, 1997b [71]).

The degree of involvement of the palatines in the choanae has long been recognised as an evolutionarily significant morphological feature of crocodyliforms (e.g. Benton & Clark, 1988; Norell & Clark, 1990; Wu & Brinkman, 1993; Clark, 1994). Indeed, Huxley (1875) originally diagnosed Eusuchia by the enclosure of the choanae by the pterygoids (among other features). There are several existing morphological characters that describe the degree of palatine participation in the choanae, with slightly different formulations (e.g. Clark, 1994; Pol et al., 2009; Tennant et al., 2016; Groh et al., 2020). Here the character is binary, describing the presence or absence of palatine contact with the choanae, as variation in the degree of palatine participation was not observed in the taxa in the current dataset. The palatines contribute to the anterior margins of the choanae in *Bernissartia fagesii* (Norell & Clark, 1990) and some non-crocodylian eusuchians e.g. the 'Glen Rose Form' (Fig. 3.81A), *Theriosuchus pusillus* (Tennant et al., 2016, NHMUK 48330), and *Shamosuchus djadochtaensis* (Pol et al., 2009). By contrast, the choanae are fully enclosed by the pterygoids in allodaposuchids (e.g. *Allodaposuchus precedens* [MMS/VBN-12-10A]), hylaeochampsids (e.g. *Hylaeochampsa vectiana* [NHMUK R177]), and all crocodylians (Fig. 3.81C–H).

188. Choanae, position of anterior margin: anterior to posterior margin of suborbital fenestra (0); level with posterior margin of suborbital fenestra (1); posterior to posterior margin of suborbital fenestra (2) (after Clark, 1994 [44]; Pol & Norell, 2004 [44]; Pol et al., 2009 [44]) (ORDERED).

    In all eusuchians with pterygoid-bound choanae, the anterior margins of the choanae lie considerably posterior to the suborbital fenestrae (188-2) (Fig. 3.81C–H). Taxa in which the palatine contributes to the choanae exhibit variation in choanal position relative to the suborbital fenestra. In *Bernissartia fagesii*, the anterior margins of the choanae are at the level of the posterior margin of the suborbital fenestra (188-1) (Pol et al., 2009, fig.40). By contrast, the anterior margins of the choanae are positioned anterior to the posterior margin of the suborbital fenestra (188-0) in Paralligatoridae (e.g. the 'Glen Rose Form', Fig. 3.81A), and in *Isisfordia duncani* (Turner & Pritchard, 2015) (Fig. 3.81B). The character is ordered to capture the anterior to posterior transition of the choanae.

189. Choanae, position of posterior margin relative to posterior edge of pterygoid flange: anterior to or at the same level as the posterior edge of pterygoid flange (0); posterior to posterior edge of pterygoid flange (1) (after Jouve 2016 [209]; Pol et al. 2009 [44]).

    This character describes the relative positions of the posterior margins of the choanae and the pterygoid flange, which is independent of the variation described in Character 188. The derived state in Character 189 occurs exclusively in longirostrine crocodylians, in which the fully pterygoid-bound choanae (187-1) are positioned posterior to the suborbital fenestra (188-2). In taxa with character

state 189-1, the posterior margin of the pterygoid flange tends to be straight, and positioned anterior to the posterior choanal margin across its entire length, e.g. *Gavialis gangeticus* (Fig. 3.81E), *Thecachampsa sericodon* (USNM 24938), *Eogavialis africanum* (YPM 6263), and *Thoracosaurus isorhynchus* (MNHN 1902-22). In *Bernissartia fagesii* (IRScNB 1538) and most eusuchians (Fig. 3.81C, D, G), the posterior margin of the pterygoid flange is concave and its posterolateral tip extends beyond the level of the posterior choanal margin (189-0).

190. Choanae, shape: circular or elliptical (0); sub-triangular, tapering posteriorly (1); sub-rectangular (long-axis orientated mediolaterally) (2); sub-triangular, tapering anteriorly (3) (after Montefeltro et al., 2013 [22]; Jouve et al., 2015 [236]; Groh et al., 2020 [360]).

    Several studies of crocodylian systematics have included a character similar to this, but it usually characterises choanal shape as either circular or triangular (Jouve et al., 2015; Iijima and Kobayashi, 2019). Character states from studies of neosuchian phylogeny have been incorporated here (e.g. Montefeltro et al., 2013; Groh et al., 2020), as they are also recognised in crocodylian taxa. In *Bernissartia fagesii* and most eusuchians the choanae are circular to elliptical (190-0) (Fig. 3.81C, E). Exclusively to some alligatoroids, the choanae are triangular, tapering posteriorly (190-1), e.g. *Diplocynodon ratelii* (Fig. 3.81F), *Caiman latirostris* (Fig. 3.81G), and *Paleosuchus trigonatus* (NHMUK 1868.10.8.1). By contrast, the choanae are triangular and taper anteriorly (190-3) in *Thecachampsa sericodon* (Fig. 3.82C), *Tomistoma lusitanica* (Antunes, 1961, pl.VI, fig.13), and *Penghusuchus pani* (Shan et al., 2009, fig.2b). Rectangular choanae that are strongly mediolaterally elongate (190-2) occur in the giant caimanine taxa *Mourasuchus atopus* (Fig. 3.81H), *Purussaurus neivensis* (UCMP 39704), and *Purussaurus mirandai* (Aguilera et al., 2006), as well as *Gavialis lewisi* (YPM 3226).

191. Choanae, anterior margin shape: linear or curved (0); invaginated (1) (new character, based on personal observations).

    In most eusuchians, the anterior margins of the choanae are straight or slightly curved, e.g. *Crocodylus porosus* (Fig. 3.81C) and *Gavialis gangeticus* (Fig. 3.81D). By contrast, some (almost exclusively alligatoroid) crocodylians exhibit a posterior midline projection of the pterygoids into the choanae (191-1), giving them a heart-shaped outline, e.g. *Caiman latirostris* (Fig. 3.81D), *Diplocynodon ratelii* (Fig. 3.81F) and *Diplocynodon hantoniensis* (NHMUK OR 25167). Several taxa that have this feature are also characterised by a protruding choanal septum (Character state 194-1), potentially calling into question the independence of these characters. Nevertheless, some taxa that lack this protruding choanal septum (194-0), e.g. *Leidyosuchus canadensis*, do have an invaginated anterior choanal margin (191-1) (Wu et al., 2001a, fig.2).

192. Choanae, direction of choanal projection (at maturity): posteroventrally (0); ventrally to anteroventrally (1) (after Clark, 1994 [39]; in Brochu, 1997b [72]).

As discussed by Norell (1989) and Brochu (1999, fig.43), the nasopharyngeal duct terminates in posteriorly-to-posteroventrally opening choanae in extant crocodylids (Fig. 3.81C), *Gavialis gangeticus* (Fig. 3.81E), and *Tomistoma schlegelii* (e.g. NHMUK 1894.2.21.1). This condition appears to be plesiomorphic for Crocodylia, given that it occurs in *Bernissartia* and most non-crocodylian eusuchians e.g. *Hylaeochampsa vectiana* (NHMUK R177). By contrast, the choanae of extant alligatorids face ventrally to anteroventrally, e.g. *Caiman latirostris* (Fig. 3.81D). Several 'basal' alligatoroids exhibit the posteroventrally-opening condition (192-0), e.g. *Diplocynodon ratelii* (Fig. 3.81F).

193. Choanae, septum: present (0); absent (1) (after Brochu, 1997b [152]; Groh et al., 2020 [353]).

194. Choanae, external projection of septum: absent, septum remains recessed within choanae (0); present, septum approaches external margin of choanae (1) (after Brochu, 1997b [152]).

Characters 193 and 194 were derived by reductively coding character 152 in Brochu (1997b). A choanal septum occurs in *Bernissartia fagesii* (IRScNB 1538), all alligatoroids, where preserved (e.g. *Caiman yacare* [Fig. 3.81D] and *Diplocynodon ratelii* [Fig. 3.81F], all extant crocodylids (e.g. *Crocodylus porosus* [Fig. 3.81C]), and most "tomistomines", e.g. *Tomistoma schlegelii* (NHMUK 1894.2.21.1) and *Thecachampsa sericodon* (USNM 24938). By contrast, most "gavialoids" lack a choanal septum; for example, it is absent in *Gavialis gangeticus* (Fig. 3.81E) and *Piscogavialis jugaliperforatus* (SMNK 1282 PAL), but present in *Eosuchus lerichei* (IRScNB R49). A choanal septum is also absent in several paralligatorids (e.g. the 'Glen Rose Form', Fig. 3.81A) and some allodaposuchids (e.g. *Lohuecosuchus megadontos* [Narváez et al., 2015]). Among taxa that possess a choanal septum, it is rarely so prominent that it approaches the external surface of the choanae (194-1). This condition occurs in some *Alligator* species (e.g. *A. mississippiensis*, Fig. 3.82D), all extant species of *Caiman* (e.g. *C. latirostris*, Fig. 3.82E), and *Melanosuchus niger* (NHMUK 45.8.25.125). A prominent choanal septum was very likely present in *Diplocynodon ratelii* (194-1) but subsequently worn down (Fig. 3.82H).

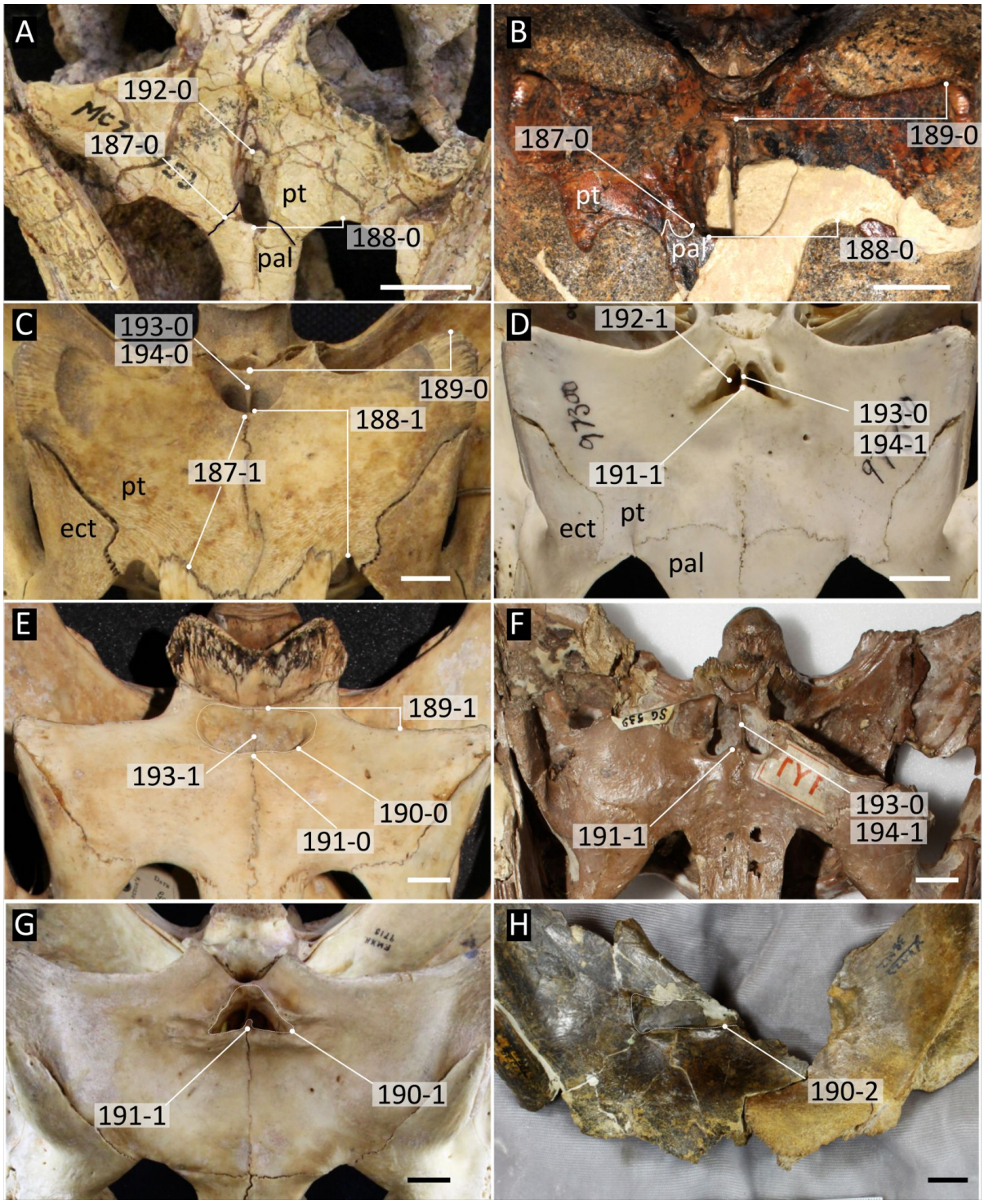



Figure 3.81: Position and morphology of choanae in selected crocodylian taxa. **A**, the 'Glen Rose Form' (MCZ 4453); **B**, *Isisfordia duncani* (QM F44320); **C**, *Crocodylus porosus* (QM J47448); **D**, *Caiman yacare* (AMNH 97300); **E**, *Gavialis gangeticus* (NHMUK 1935.6.4.1); **F**, *Diplocynodon ratelii* (MNHN SG 539); **G**, *Caiman latirostris* FMNH 9713; **H**, *Mourasuchus atopus* (UCMP 38012). Abbreviations: **ect**, ectopterygoid; **pal**, palatine; **pt**, pterygoid. Scale bars = 1 cm.

195. Choanae, ornamentation of margins: unornamented, margins (usually) flush with pterygoid surface (0); elevated, forming a wall restricted to the posterior and posterolateral margins (1); elevated forming a wall which extends to the anterolateral (but not anterior) margins of the choanae (2); elevated, forming a wall which completely circumscribes the choanae (3) (after Brochu, 1997b [73]; Pol & Norell, 2004 [183]).

    In *Bernissartia fagesii* (IRScNB 1538) and most eusuchians, the choanal margins are unornamented (195-0) and essentially flush with the pterygoids. Some species variably develop a thin lip surrounding the choanae (Fig. 3.82B), or a slight thickening of the margins, which might be ontogenetic (Fig. 3.82C), but this is still considered unornamented. Furthermore, in taxa wherein the choanae faces posteroventrally (e.g. *Crocodylus porosus*, Fig. 3.82A), they cannot strictly be described as flush (hence "usually"). Nevertheless, the margins are all equally developed and considered unornamented (195-0). Character state 1 describes a condition that occurs in all extant alligatorids, in which the posterior and posterolateral margins form a ventrally projecting lamina. This was noted by Brochu (1999), although he only discretised the presence or absence of a notch in this posterior wall, a feature that occurs in caimanines (see Character 196). This posterior wall also occurs in *Brachychampsa montana* (UCMP 133901), *Stangerochampsa maccabei* (Wu et al., 1996, fig.1B), and *Eocaiman cavernensis* (AMNH 3158, see also Chapter 4, Fig. 4.6). Similarly upturned walls were recognised in *Diplocynodon hantoniensis* (Fig. 3.82G, see Section 2.5.1), but in a slightly different arrangement. In that taxon, the lateral to anterolateral margins of the choanae are prominently upturned, but not the posterior margins (195-2). This condition is observed in all other *Diplocynodon* species, where preserved (Chapter 2, Fig. 2.32), e.g. *D. darwini* (HLMD Me 17680a), *D. deponiae* (IRScNB R 261), and (although worn) *D. ratelii* (Fig. 3.82H). It is also tentatively recognised in *Leidyosuchus canadensis*, based on the description and figures of Wu et al. (2001a). Character state 3 describes the choanal morphology exhibited by *Voay robustus* (Fig. 3.82L), in which the choanae is completely circumscribed by ventrally projecting lamina. This condition also occurs in both species of *Osteolaemus* (Fig. 3.82J), *Brochuchus pigotti* (Fig. 3.82K), and *Maomingosuchus petrolica* (Shan et al., 2017, fig.3C). Given that there is not a clear transition from the flush (195-0) to the fully-walled states, this character is not ordered.

196. Choanae, morphology of posterior wall: not notched, or with broadly rounded notch (0); acutely notched (1) (after Brochu, 1997b [107]).

    This character describes the presence or absence of an acute midline incision of the posterior choanal wall described in Character state 195-1. As recognised by Brochu (1999), the acutely notched condition occurs in all extant caimanines and several fossil species (Fig. 3.82N). The derived condition is newly recognised in *Alligator mcgrewi* (Fig. 3.82O). The distinction between 'broadly rounded' (196-0) and 'acutely notched' (196-1) is important, as several alligatorids have a notch in the posterior

choanal margin (e.g. *Alligator mississippiensis*, Fig. 3.82A), but it is notably different to the condition in caimanines (e.g. *Paleosuchus trigonatus*, Fig. 3.82N).

197. Pterygoid, surface lateral and anterior to choanae flush (0); depressed to form 'neck' (1) (after Brochu, 1997b [73]).

The presence of a choanal 'neck' was recovered as diagnostic of Osteolaeminae (Brochu, 2007a). This condition arises from a depression anteriorly and anterolateral to the choanae, and was indeed observed in *Osteolaemus tetraspis* (Fig. 3.82J), *Brochuchus pigotti* (Fig. 3.82K), and *Voay robustus*. A 'neck' is additionally observed in several other crocodyloids, including most extant *Crocodylus* species as well as *Gavialis lewisi* (YPM 3226).

198. Pterygoid, ornamentation lateral to choanae, anteriorly directed ridges on the pterygoid extending from the lateral margins of the choanae: absent (0); present (1) (after Lee & Yates, 2018 [161]).

Ridges on the pterygoid, lateral to the choanae, were first identified in *Kambara implexidens* (Salisbury & Willis, 1996) (Fig. 3.83B), and later found in several additional mekosuchines, e.g. *Kambara taraina* (Buchanan, 2009) and *Baru wickeni* (Yates, 2017). Here they are still exclusively recognised in mekosuchines. These ridges are distinguished from the upturned lateral margins of the choanae described in Character state 195-2: they are much lower and extend anteriorly on the pterygoid beyond the choanae.

199. Pterygoid, bulbous differentiated bullae (at maturity): absent (0); present (1) (after Lee & Yates, 2018 [158]; Salas-Gismondi et al., 2019 [206]).

The pterygoids and palatines forming the walls of the nasopharyngeal duct can become inflated through ontogeny in several species of *Crocodylus*, e.g. *C. porosus* (Fig. 3.84A). However, this condition is distinguished from the condition exhibited by all species of *Gavialis* examined here (e.g. *G. gangeticus* [Fig. 3.84B] and *Gavialis lewisi* [YPM 3226]), which develop bulbous, differentiated 'bullae' that are formed entirely by the pterygoids at maturity (199-1).

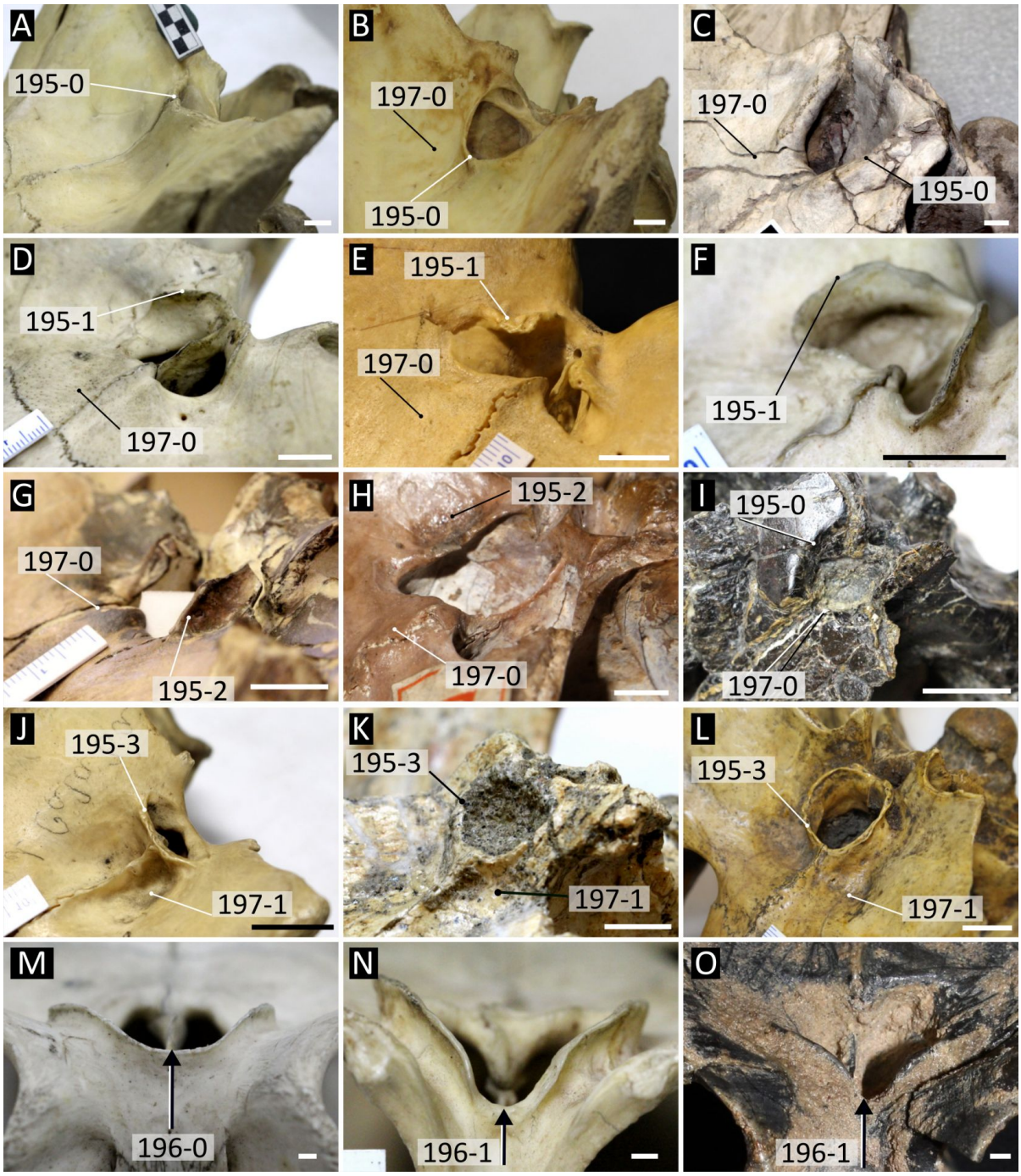



Figure 3.82: Morphology of the choanal rim in selected crocodylians. **A**, *Crocodylus porosus* (NHMUK 1852.12.9.2); **B**, *Mecistops cataphractus* (NHMUK 1924.5.10.1); **C**, *Thecachampsa sericodon* (USNM 24938); **D**, *Alligator mississippiensis* (NHMUK 1873.2.21.1); **E**, *Caiman yacare* (MACN uncatalogued specimen); **F**, *Paleosuchus trigonatus* (NHMUK 1868.10.8.1); **G**, *Diplocynodon hantoniensis* (CAMSM TN 907) ; **H**, *Diplocynodon ratelii* (MNHN SG 539); **I**, *Hylaeochampsa vectiana* (NHMUK R 177); **J**, *Osteolaemus tetraspis* (NHMUK 1862.6.30.5); **K**, *Brochuchus pigotti* (NHMUK R 7729); **L**, *Voay robustus* (NHMUK R 36685); **A**, *Alligator mississippiensis* (NHMUK 1873.2.21.1); **B**, *Paleosuchus trigonatus* (NHMUK 1868.10.8.1); **D**, *Alligator mcgrewi* (AMNH FAM 7905). Scale bars A–L = 1 cm, M–O = 2 mm.

200. Quadrate, ventral surface, attachment scar for posterior mandibular adductor muscle, morphology: linear crests (0); ventrally directed knob (1) (after Brochu, 2011 [180]; Ősi et al., 2007 [165]).

The ventral surface of the quadrate is ornamented with several low, linear crests (200-0) that form the attachment sites for the mandibular adductor muscles in *Bernissartia fagesii* and most eusuchians (Fig. 3.85A) (Iordansky, 1973, fig.10). By contrast, in *Hylaeochampsa vectiana* (Fig. 3.85B), and *Iharkutosuchus makadii* (Ősi, 2008), the ventral surface of the quadrate bears a discrete knob-like protuberance (200-1).

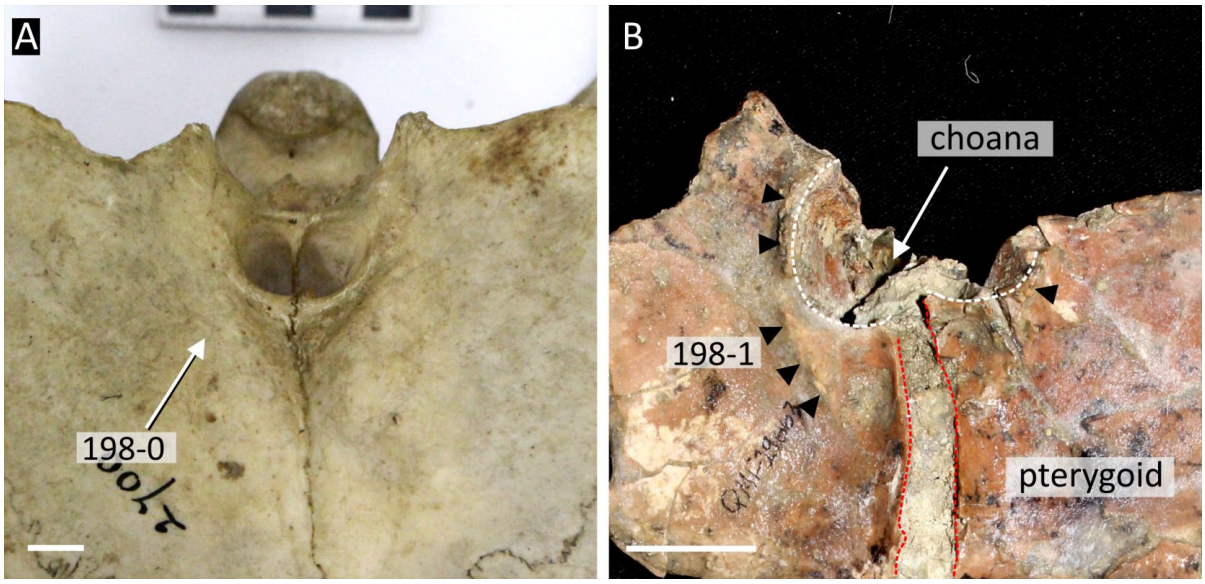



Figure 3.83: Ventral view of the choanae showing variation in development of ridges anterolateral to the choanae in: **A**, *Crocodylus siamensis* (NHMUK 1921.4.1.168); **B**, *Kambara implexidens* (QM 29663). Black arrows mark position of ridge. All scale bars = 1 cm.

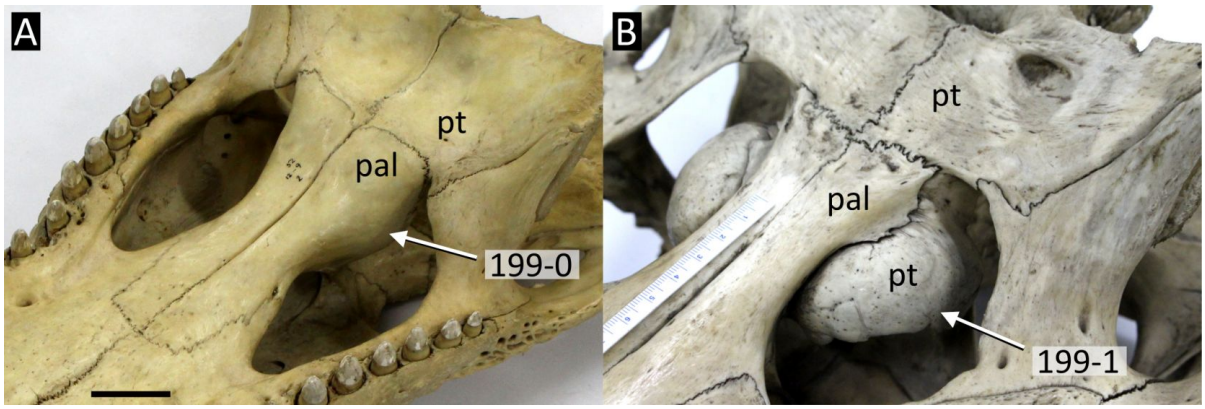



Figure 3.84: Ventrolateral view of the palatine bar showing the development of pterygoid bullae. **A**, *Crocodylus porosus* (NHMUK 1852.12.9.2); **B**, *Gavialis gangeticus* (NHMUK 1974.3009). Abbreviations: **pal**, palatine; **pt**, pterygoid. Scale bar in A = 3cm, B = cm.

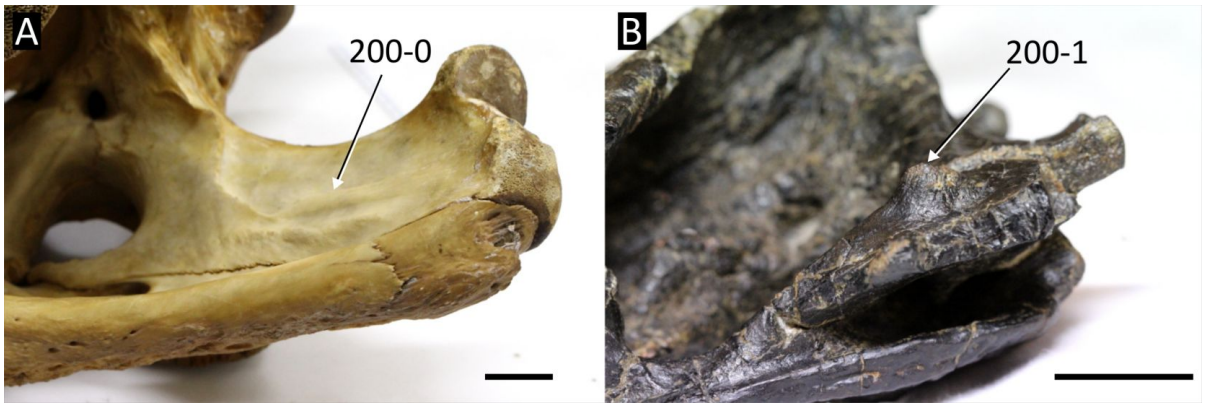



Figure 3.85: Ventromedial view of the quadrate ramus in **A**, *Tomistoma schlegelii* (NHMUK 1894.2.21.1); and **B**, *Hylaeochampsa vectiana* (NHMUK PV R 177). All scale bars = 2 cm.

201. Basisphenoid, exposure between basioccipital and pterygoids in ventral view: not or poorly exposed, basisphenoid anteroposteriorly short (0); largely exposed, basisphenoid anteroposteriorly long (1) (after Brochu, 1997b [113]; Jouve, 2016 [113]).

    The derived character state describes the anteroposteriorly long basisphenoid exposure that is unique to *Gavialis gangeticus* (Fig. 3.86C) among extant crocodylians (Fig. 3.86A–B) (Brochu, 2006b). The derived condition also occurs in most fossil "gavialoids", e.g. *Eogavialis africanum* (YPM 6263) and *Eosuchus minor* (Brochu, 2006b).

202. Jugal, posterior extent relative to basioccipital tubera: extends beyond level of posterior margin of basioccipital tubera (0); level with or anterior to posterior margin of basioccipital tubera (1) (after Jouve, 2004 [186]; Jouve et al., 2008 [181]; Jouve, 2016 [181]).

    In most eusuchians, the jugal extends beyond the level of the posterior margin of the basioccipital tubera (Fig. 3.86A–B). By contrast, in some "gavialoids", e.g. *Gavialis gangeticus* (Fig. 3.86C) and *Argochampsa krebsi* (NHMUK R36872), the jugals do not extend beyond this margin, usually terminating anterior to the level of the basioccipital tubera. This feature is best observed in ventral view.

203. Basisphenoid rostrum, posteroventrally directed ridge on lateral margins: absent (0); present (1) (new character, based on personal observations).

    Few taxa preserve the basisphenoid rostrum sufficiently to score this character; however, in all extant alligatorids examined here, an arcuate ridge occurs on the posterolateral surface of the basisphenoid rostrum, e.g. *Alligator mississippiensis* (Fig. 3.87A). This ridge is absent in *Gavialis gangeticus* (NHMUK 96.7.7.4.2), *Tomistoma schlegelii* (NHMUK 1894.2.21.1) and all extant *Crocodylus* species, e.g. *C. siamensis* (Fig. 3.87B).

204. Basisphenoid, exposure on the lateral braincase wall, anteroventral to the trigeminal foramen: absent

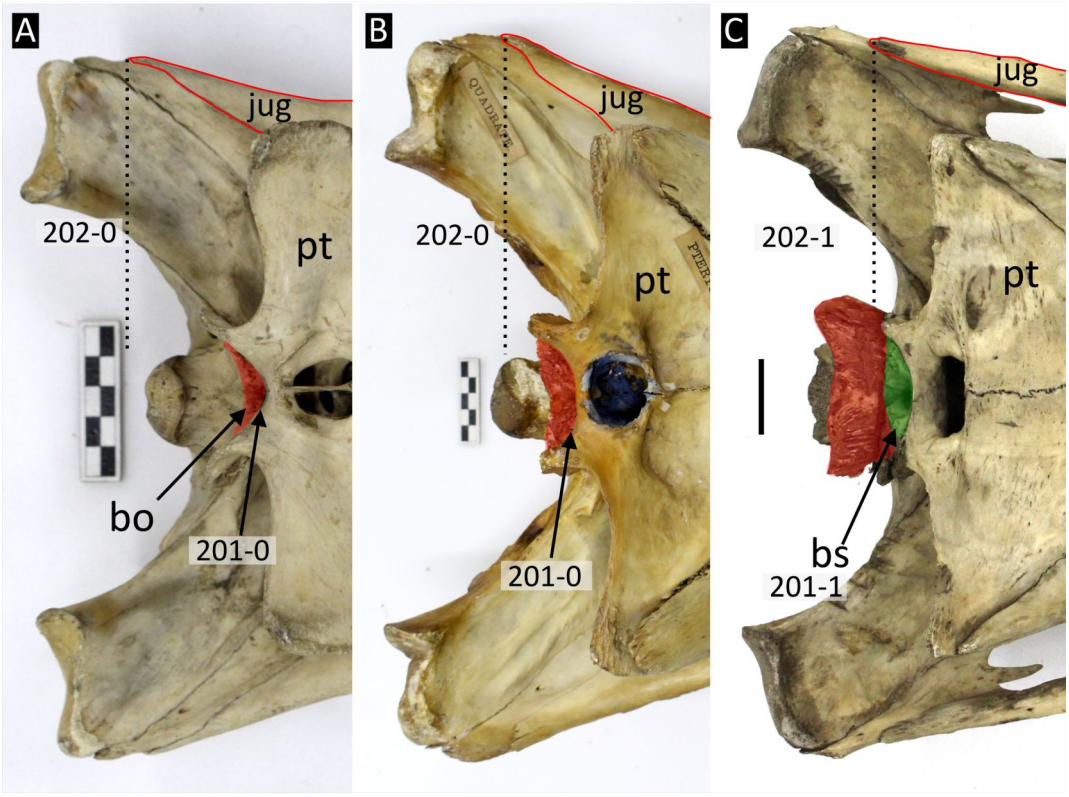



Figure 3.86: Variation in the posterior extent of the jugal relative to the basioccipital tubera. **A**, *Alligator mississippiensis* (NHMUK 1873.2.21.1); **B**, *Tomistoma schlegelii* (NHMUK 1894.2.21.1); **C**, *Gavialis gangeticus* (NHMUK 1974.3009). Basioccipital tubera highlighted in red, basisphenoid in green, dotted line marks posterior extent of jugal. Abbreviations: **bo**, basioccipital; **bs**, basisphenoid; **jug**, jugal; **pt**, pterygoid. All scale bars = 5 cm.

(0); present (1) (after Brochu, 1997b [129]).

The derived character state describes a posterior extension of the basisphenoid onto the lateral braincase wall. This typically reaches the level of the laterosphenoid bridge in all extant crocodylids, e.g. *Crocodylus* (Fig. 3.87B), *Osteolaemus tetraspis* (NHMUK 1862.6.30.5), and *Mecistops cataphractus* (NHMUK 1924.5.10.1), as well as *Tomistoma schlegelii* (Fig. 3.87F). By contrast, the basisphenoid is not visible on the lateral braincase wall, or extends posteriorly by only a small amount, in *Gavialis gangeticus* (NHMUK 1974.3009) and all extant alligatorids, e.g. *Alligator mississippiensis* (Fig. 3.87A), *Caiman crocodilus* (Fig. 3.87E), and *Melanosuchus niger* (Fig. 3.87C).

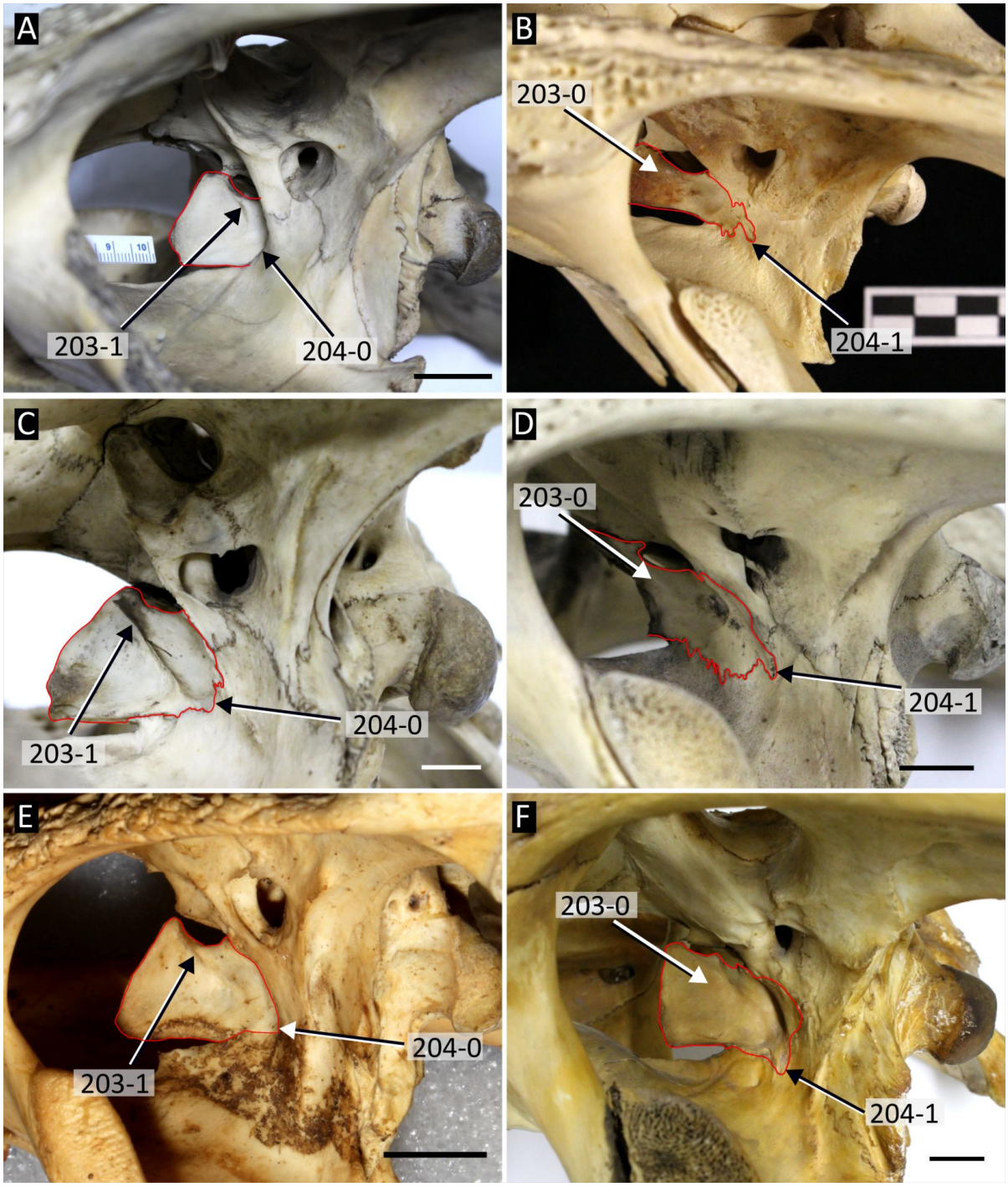



Figure 3.87: Variation in morphology of the basisphenoid rostrum. Left lateral view of the braincase in **A**, *Alligator mississippiensis* (NHMUK 1873.2.21.1); **B**, *Crocodylus rhombifer* (AMNH 77595); **C**, *Melanosuchus niger* (NHMUK 45.8.25.125); **D**, *Crocodylus acutus* (NHMUK 1975.997); **E**, *Caiman crocodilus* (FMNH 69812); **F**, *Tomistoma schlegelii* (NHMUK 1894.2.21.1). Basisphenoid outlined in red. All scale bars = 2 cm.

205. Basisphenoid, sulcus on anterior braincase wall, lateral to basisphenoid rostrum: present (0); absent (1) (after Brochu, 1997b [122]).

    In anteromedial view of the braincase, a sulcus can be observed on the posterolateral surface of the basisphenoid in some crocodylians (205-1), e.g. *Gavialis gangeticus* (Fig. 3.88A). This condition is recognised here in almost all extant crocodylians, except for some species of *Crocodylus* (*C. intermedius*, *C. johnstoni*, *C. mindorensis*, and *C. novaeguineae*); this contrasts with previous datasets, which scored all extant crocodylids and *Tomistoma schlegelii* as lacking this fossa (e.g. Jouve, 2016). These differences may be a result of interspecific variation in the degree of development of the fossa, which could lead some authors to score the condition as absent when it is here considered 'weakly' developed.

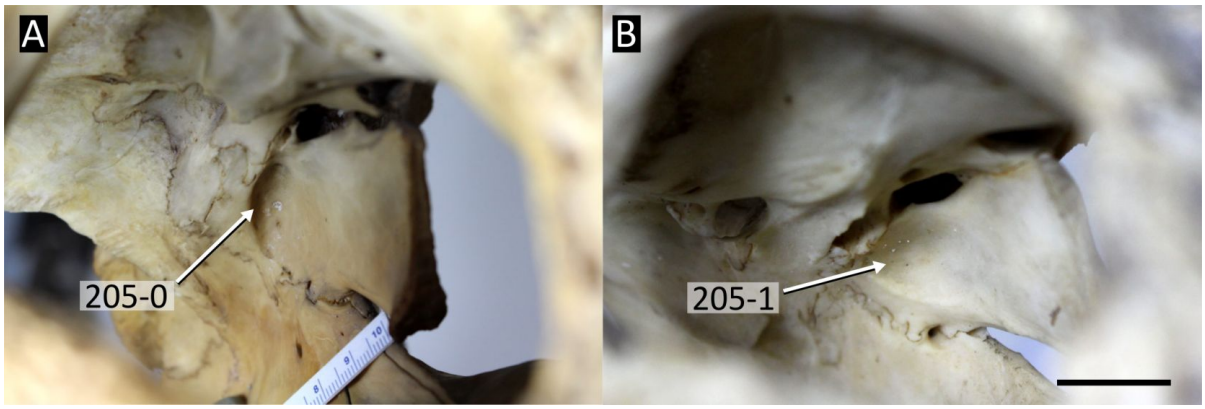



Figure 3.88: Anteromedial view of the basisphenoid rostrum through the orbit in **A**, *Gavialis gangeticus* (NHMUK 1935.6.4.1); and **B**, *Crocodylus niloticus* (NHMUK 1934.6.3.1). Scale bar = 2 cm.

206. Laterosphenoid, orientation of capitate process anterior margin: perpendicular to the sagittal plane (0); directed anterolaterally from the sagittal plane (1) (after Brochu, 1997b [130]).

    The capitate process is a dorsolateral extension of the laterosphenoid, that contacts the ventral margins of the postorbital and frontal at the anterolateral corner of the cranial table (Fig. 3.89). In most crocodylians, the anterior margin of the capitate process is orientated anterolaterally relative to the sagittal plane (Fig. 3.89A). By contrast, the anterior margin is orientated almost perpendicular to the sagittal plane in some longirostrine crocodylians, e.g. *Gavialis gangeticus* (Fig. 3.89B), *Eogavialis africanum* (NHMUK R 3325), *Piscogavialis jugaliperforatus* (SMNK 1282 PAL), *Thecachampsa sericodon* (USNM 24938), and *Thoracosaurus neocesariensis* (AMNH 2542).

207. Laterosphenoid, lateral laterosphenoid bridge over cavum epiptericum: absent (0); present (1) (after Lee & Yates, 2018 [122]; Brochu, 1999; Holliday & Witmer, 2009).

208. Laterosphenoid, lateral laterosphenoid bridge morphology: short process, which does not suture to

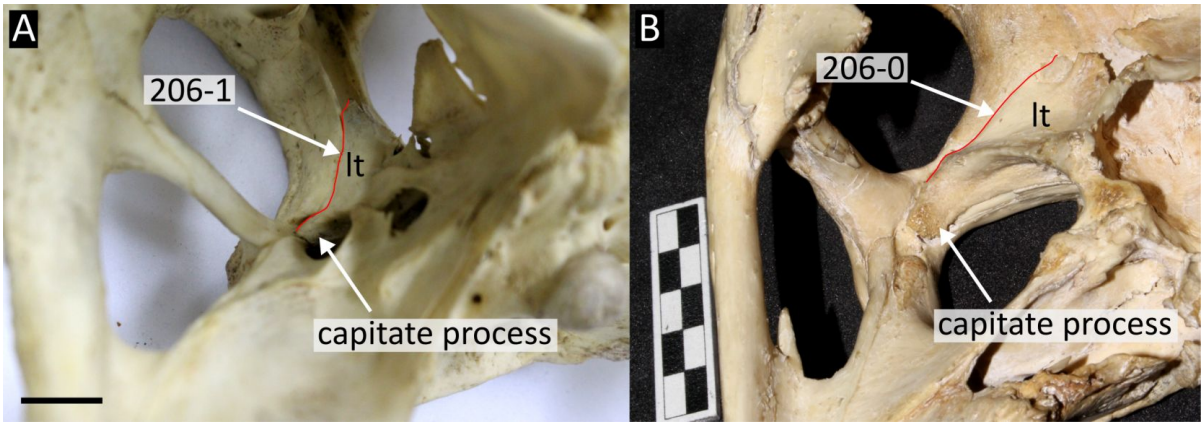



Figure 3.89: Ventromedial view of the braincase in **A**, *Caiman latirostris* (NHMUK 86.10.4.2); **B**, *Gavialis gangeticus* (NHMUK uncatalogued). Abbreviations: **lt**, laterosphenoid. Scale bar in A = 2 cm, B = cm.

the pterygoid ventrally (0); robust process, which sutures to the pterygoid ventrally (1) (adapted from Holliday & Witmer, 2009; Lee & Yates, 2018 [122]).

The lateral laterosphenoid bridge is a dorsoventrally orientated strut of bone formed predominantly by a descending process of the laterosphenoid anterior to the foramen ovale (Fig. 3.90). This bridge encloses the ophthalmic branch of cranial nerve V (Iordansky, 1973; Brochu, 1999; Holliday et al., 2013). Where preserved, all extant and most fossil crocodylians possess a lateral laterosphenoid bridge (207-1) (Fig. 3.90B–F). By contrast, the bridge is absent (207-0) in *Hylaeochampsa vectiana* (NHMUK R177), *Portugalosuchus azenhae* (Mateus et al., 2019, fig.9B), *Shamosuchus djadochtaensis* (Pol et al., 2009) and several "gavialoids" including *Piscogavialis jugaliperforatus* (Fig. 3.90A), *Eogavialis africanum* (NHMUK R3325), and *Gryposuchus colombianus* (UCMP 38358) (Holliday & Witmer, 2009, fig.12A). Brochu and Gingerich (2000) commented that the laterosphenoid bridge of most "crocodylids" is incomplete, such that it does not contact the pterygoid to fully enclose the ophthalmic branch of CN V. By contrast, the bridge was found to contact the pterygoid in all extant "crocodylids" examined here (208-1), with the exception of *Tomistoma schlegelii*, in which it forms a small discontinuous process (Fig. 3.90B) (208-0), similar to that described in the "tomistomine" *Paratomistoma courti* (Brochu & Gingerich, 2000).

209. Laterosphenoid, caudal laterosphenoid bridge over cavum epiptericum: absent (0); present (1) (after Lee & Yates, 2018 [124]; adapted from Holliday & Witmer, 2009).

210. Laterosphenoid, caudal laterosphenoid bridge morphology: short ventrally directed strut (0); long ventral process joining with extra process of the quadrate (1); hypertrophied wall, which bisects the foramen ovale (2) (after Lee and Yates, 2018 [124]; adapted from Holliday and Witmer, 2009) (ORDERED).

Characters 209 and 210 were derived by reductively coding Character 124 from Lee and Yates (2018),

and by the addition of a character state. The caudal (=posterior) bridge of the laterosphenoid (sensu Holliday & Witmer, 2009) is a ventral process positioned at the dorsal margin of the foramen ovale, at the level of the laterosphenoid-quadrate suture (Fig. 3.90). This bridge is absent in most fossil crocodylians in which the braincase is preserved (e.g. *Piscogavialis jugaliperforatus*, Fig. 3.90A), but occurs in some form in most extant crocodylians. For example, the bridge forms a short, discontinuous strut (210-0) in *Tomistoma schlegelii* (Fig. 3.90B) and several species of *Crocodylus* (e.g. *Crocodylus novaeguineae*, Fig. 3.90D). As noted by Holliday and Witmer (2009), the bridge is elongate in some extant *Crocodylus* species, with extra bony processes that form a continuous bridge e.g. *Crocodylus siamensis* (Fig. 3.90E). The new character state (210-2) included here is based on observations of *Mourasuchus arendsi* (Cidade et al., 2019e) (Fig. 3.90F), and describes a single robust caudal bridge, which is not known in any other eusuchian studied here. The character is also ordered.

211. Laterosphenoid, ascending process of the pterygoid forming ventral portion of lateral laterosphenoid bridge: absent (0); present (1) (after Brochu, 1997b [115]).

    Most crocodylian character lists describe an ascending process of the palatine that contributes to the base of the laterosphenoid bridge, which appears to be an error carried forward from the character list of Brochu (1997b). As described and clearly figured by Brochu (1999, fig.52C), the derived character state refers in fact to an ascending pterygoid process, which forms a robust ventral portion of the lateral laterosphenoid bridge in some crocodylians, e.g. *Alligator mississippiensis* (Fig. 3.91B) and *Diplocynodon ratelii* (Fig. 3.91A). By contrast, the lateral bridge receives little to no contribution from the pterygoid in most crocodylians, where known (Fig. 3.91C–F).

212. Epipterygoid: present (0); absent (1) (after Lee & Yates, 2018 [121]; adapted from Holliday & Witmer, 2009).

213. Epipterygoid, retraction from the cavum epitericum: epipterygoid overhangs cavum epitericum (0); or epipterygoid isolated from cavum epitericum (1) (after Lee & Yates, 2018 [121]; adapted from Holliday & Witmer, 2009).

    Characters 212 and 213 were derived by reductively coding Character 121 in Lee and Yates (2018). The epipterygoid links the palate with the braincase plesiomorphically in Crocodylomorpha, forming the lateral wall of the cavum epitericum (Holliday & Witmer, 2009). The epipterygoid appears to be absent in nearly all crocodylians (212-0), where the laterosphenoid bridge forms an analogous structure; however, Holliday and Witmer (2009) identified the epipterygoid in *Leidyosuchus canadensis*, *Eosuchus minor*, and *Borealosuchus sternbergii* (212-1). The morphology of the epipterygoid is variable. For example, in *Eosuchus minor* the epipterygoid is small and triangular, and does not overhang the cavum epitericum (213-1) (Holliday & Witmer, 2009, fig.11H). By contrast, the epipterygoid

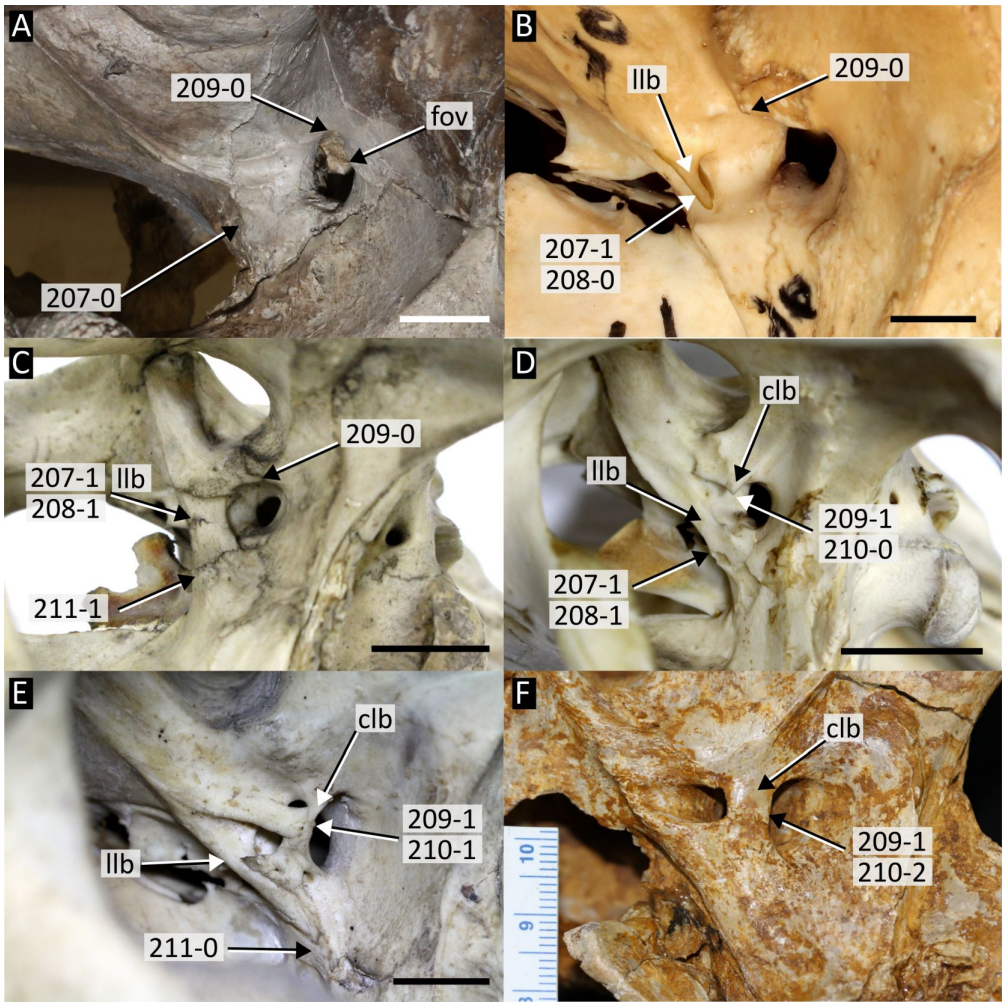



Figure 3.90: Left lateral view of the braincase showing variation in morphology of the laterosphenoid in **A**, *Piscogavialis jugaliperforatus* (SMNK 1282 PAL); **B**, *Tomistoma schlegelii* (USNM 211323); **C**, *Alligator mississippiensis* (NHMUK 1873.2.21.1); **D**, *Crocodylus novaeguineae* (NHMUK 1886.5.20.1); **E**, *Crocodylus siamensis* (NHMUK 1897.12.31.1); **F**, *Mourasuchus arendsi* (UFAC 2515). Abbreviations: **clb**, caudal laterosphenoid bridge; **fov**, foramen ovale; **llb**, lateral laterosphenoid bridge. All scale bars = 2 cm.

is larger and more ventrally developed in *Leidyosuchus* and *Borealosuchus sternbergii*, such that it overhangs the cavum epitericum (213-0) (Holliday & Witmer, 2009, fig.11D).

214. Prootic, exposure on external braincase wall: small, little to no exposure dorsal and ventral to the trigeminal foramen (0); large exposure ventral to trigeminal foramen only (1); extensive exposure dorsal and ventral to trigeminal foramen (2) (after Norell, 1989 [5]; Brochu, 1997b [74]) (ORDERED).

The prootic is a poorly exposed bone that is partially visible in the walls of the foramen ovale in most eusuchians (Fig. 3.91). As originally formulated, this character was binary, distinguishing between a small or extensive exposure of the prootic. Here, an intermediate state is added and the character is ordered. In previous datasets (e.g. Brochu et al., 2012), the extensive prootic exposure was recognised in *Gavialis gangeticus*, "tomistomines" (e.g. *Tomistoma schlegelli*, *Paratomistoma courti*,

*Thecachamapsa antiquus*), some *Borealosuchus* (e.g. *B. sternbergii*), and *Diplocynodon* species (e.g. *D. ratelii* and *D. hantoniensis*). Here, the extensive exposure (214-2) is only considered present in *Gavialis gangeticus* and *Tomistoma schlegelii*. The condition in these two taxa is remarkably similar, with prominent, anteroposteriorly narrow dorsal and ventral extensions of the prootic on the braincase wall (Fig. 3.91C, E). By contrast, *Diplocynodon ratelii* has a modest ventral exposure of the prootic, but it is hidden dorsally in the walls of the foramen ovale (Fig. 3.91A). This condition is similar to that of a number of additional crocodylians, including *Borealosuchus sternbergii* (USNM 6533), *Paratomistoma courti* (Brochu & Gingerich, 2000, fig.3D), *Alligator mississippiensis* (Fig. 3.91B) and some *Crocodylus* species (Fig. 3.91D). These taxa have been assigned to a new character state (214-1), which is considered intermediate between the very small prootic exposure of most crocodylians (214-0) (Fig. 3.91F), and the extensive exposure of *Gavialis gangeticus* and *Tomistoma schlegelii*.

215. Quadrate-pterygoid suture, path on lateral braincase wall between basisphenoid exposure and foramen ovale: ventrally deflected (0); straight (1) (after Brochu, 1997b [127]).

In extant alligatorids, the quadrate-pterygoid suture runs diagonally along the lateral braincase wall, from the basisphenoid exposure to the foramen ovale, with a prominent ventral deflection (215-0), e.g. *Alligator mississippiensis* (Fig. 3.92A). The same condition occurs in *Gavialis gangeticus* (NHMUK 1935.6.4.1), *Tomistoma schlegelii* (USNM 211323), and several fossil crocodylians, including *Brachychampsa montana* (UCMP 133901) and *Gryposuchus colombianus* (UCMP 38358). By contrast, the quadrate-pterygoid suture is approximately straight in *Diplocynodon* (e.g. *D. ratelii*, Fig. 3.92B), and all extant crocodylids. The condition is unknown in the outgroup *Bernissartia fagesii*, and the only non-crocodylian eusuchian scored for this character (*Iharkutosuchus makadii*) exhibits the ventrally deflected condition (215-0) (Mateus et al., 2019, fig.S13).

### 3.4.2 Mandible

216. Dentary, anteriormost teeth: strongly procumbent, approaching sub-horizontal (0); project dorsally or steeply anterodorsally (1) (after Brochu, 1997b [53]).

Strongly procumbent anterior dentary teeth occur in the outgroup *Bernissartia fagesii* (IRScNB 1538) and some paralligatorids, e.g. the 'Glen Rose Form' (Fig. 3.93A) and *Wannchampsus kirpachi* (Adams, 2014). Among crocodylians, procumbent dentary teeth also characterise *Arambourgia gaudryi* (MNHN QU17155), and *Mekosuchus*, e.g. *M. inexpectatus* (MNHN NCP 06). All other eusuchians exhibit dorsally or steeply anterodorsally-projecting anterior dentary teeth (Fig. 3.93B).

217. Dentary, alveoli 3 and 4: confluent (0); separate (1) (after Brochu, 1997b [52]).

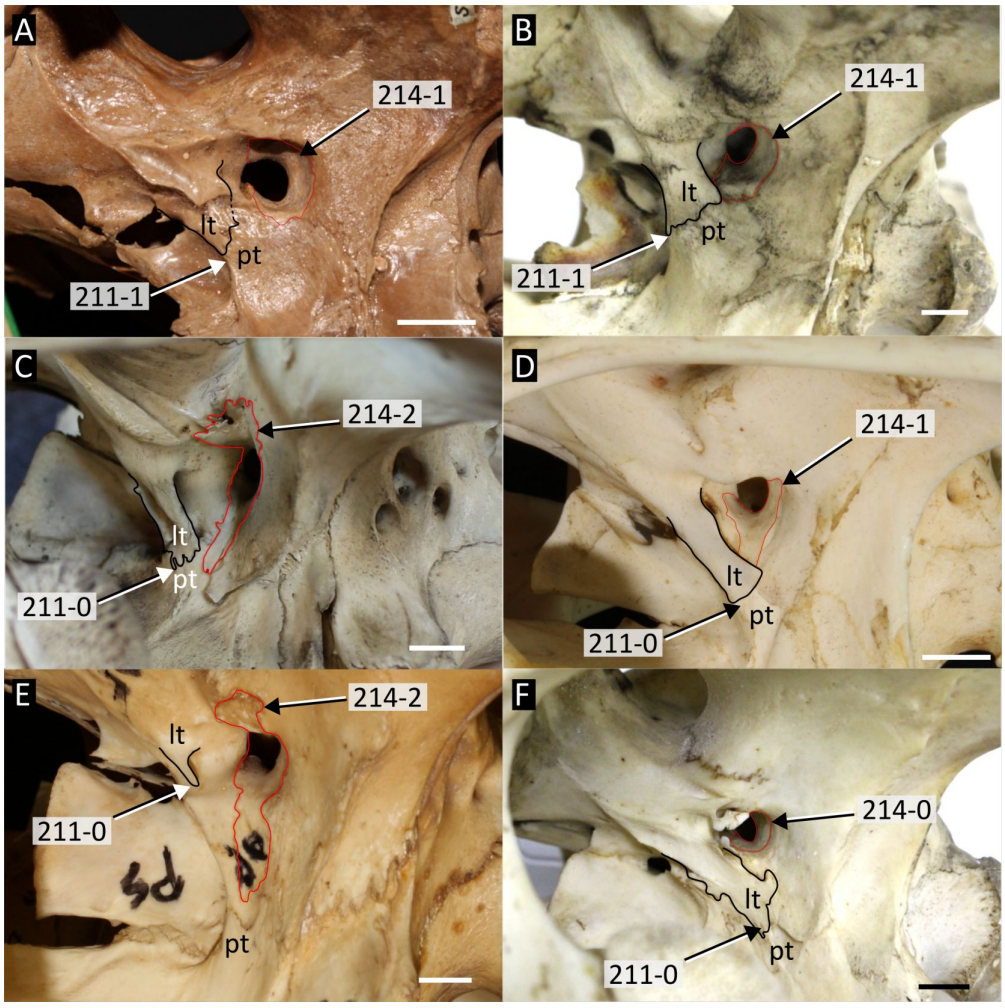



Figure 3.91: Left lateral view of the braincase showing variation in prootic exposure (red outline). **A**, *Diplocynodon ratelii* (MNHN SG 557); **B**, *Alligator mississippiensis* (NHMUK 1873.2.21.1); **C**, *Gavialis gangeticus* (NHMUK uncatalogued); **D**, *Crocodylus intermedius* (FMNH 75659); **E**, *Tomistoma schlegelii* (USNM 211323); **F**, *Crocodylus niloticus* (NHMUK 1934.6.3.1). Abbreviations: **lt**, laterosphenoid, **pt**, pterygoid. All scale bars = 1 cm.

Most eusuchians have an enlarged $4^{th}$ dentary caniniform tooth. Equal enlargement of the $3^{rd}$ and $4^{th}$ dentary alveoli, such that they are weakly separated and share the same interalveolar wall, occurs in *Bernissartia fagesii* (IRScNB 1538), *Diplocynodon* (e.g. *D. ratelii*, Fig. 3.93C), *Leidyosuchus canadensis* (YPM 284), *Borealosuchus* (e.g. *B. sternbergii*, USNM 6533), and *Eothoracosaurus mississippiensis* (Brochu, 2004a). In all other crocodylians, the $3^{rd}$ and $4^{th}$ dentary alveoli are separated (Fig. 3.93D), with the $4^{th}$ alveolus being notably larger than the third.

218. Dentary, dorsoventral height at the level of alveoli 1–4 relative to alveoli 11–12: at the same level or higher (0); lower (1) (adapted from Bona, 2007; Pinheiro et al., 2013 [124]; Cidade et al., 2017 [183]).

In most crocodylians, the dorsal margins of the alveolar walls of dentary alveoli 1–4 are approximately in line with alveoli 11–12 (Fig. 3.93E). Bona (2007) recognised an alternative condition in *Eocaiman*,

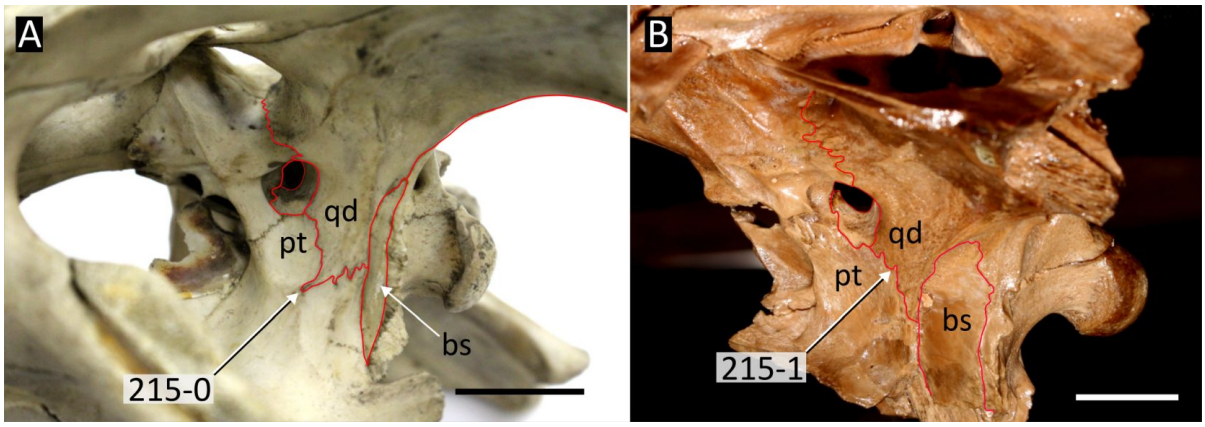



Figure 3.92: Lateral view of the braincase showing variation in the quadrate-pterygoid suture. **A**, *Alligator mississippiensis* (NHMUK 1873.2.21.1); and **B**, *Diplocynodon ratelii* (MNHN SG 557). Abbreviations: **bs**, basisphenoid; **pt**, pterygoid; **qd**, quadrate. All scale bars = 2 cm.

in which the anteriormost dentary alveoli are more ventrally positioned than the posterior dentary alveoli (Fig. 3.93F). Whereas this condition has only been recognised in *Eocaiman* in previous studies (e.g. Cidade et al., 2017), it also occurs in several non-caimanine alligatoroids, e.g. *Alligator mcgrewi* (AMNH FAM 8700), *Navajosuchus mooki* (AMNH 6780), and *Allognathosuchus wartheni* (YPM PU 16989).

219. Dentary, numerical position of largest alveolus posterior to $4^{th}$ dentary alveolus: 13 and/or 14 (0); 13 and/or 14 and a posterior series (1); 10, 11 and/or 12 (2); no differentiation posterior to $4^{th}$ alveolus (3); posterior to 14 (4) (after Brochu, 2004a [167]; Brochu, 2010 [37]; Brochu, 2011 [51]).

Most crocodylians have two areas of enlarged alveoli in the dentary (Brochu, 2004b). Whereas the first consistently occurs at the $4^{th}$ alveolus, the second is variable and can extend over a series of alveoli. In most eusuchians the second region of enlargement occurs between alveoli 10–12 (219-2), e.g. all extant caimanines (Fig. 3.94C), extant crocodylids, *Diplocynodon*, and *Borealosuchus*. In many alligatorines (including *Alligator*), this enlargement occurs at the level of alveoli 13 and 14 (219-0) (Fig. 3.94A), but other alligatorines show enlargement of the $13^{th}$, $14^{th}$, and a posterior series of dentary alveoli (219-1) e.g. *Allognathosuchus wartheni* (Fig. 3.94B). Several longirostrine crocodylians, e.g. *Gavialis gangeticus* (Fig. 3.94D) and *Mourasuchus atopus* (UCMP 38012), have homodont dentition. In the case of *Gavialis*, enlargement of the $4^{th}$ dentary alveolus is not apparent; however, it is dorsally raised compared to all other dentary alveoli (219-3) (Fig. 3.95A). Character state 4 describes the enlargement of alveoli posterior to the $14^{th}$ alveolus (Fig. 3.94E), which occurs in some non-crocodylian eusuchians, e.g. *Iharkutosuchus makadii* (Mateus et al., 2019, fig.S11).

220. Dentary, shape of dorsal profile between $4^{th}$ and $10^{th}$ alveoli in lateral view: linear (0); curved (1); deeply curved (2) (after Brochu, 1997b [68]) (ORDERED).

The dentary is broadly curved between alveoli 4 and 10 in *Bernissartia fagesii* (IRScNB 1538) and most eusuchians (Fig. 3.95B). As noted by Brochu (1999), the depth of this curvature is notably

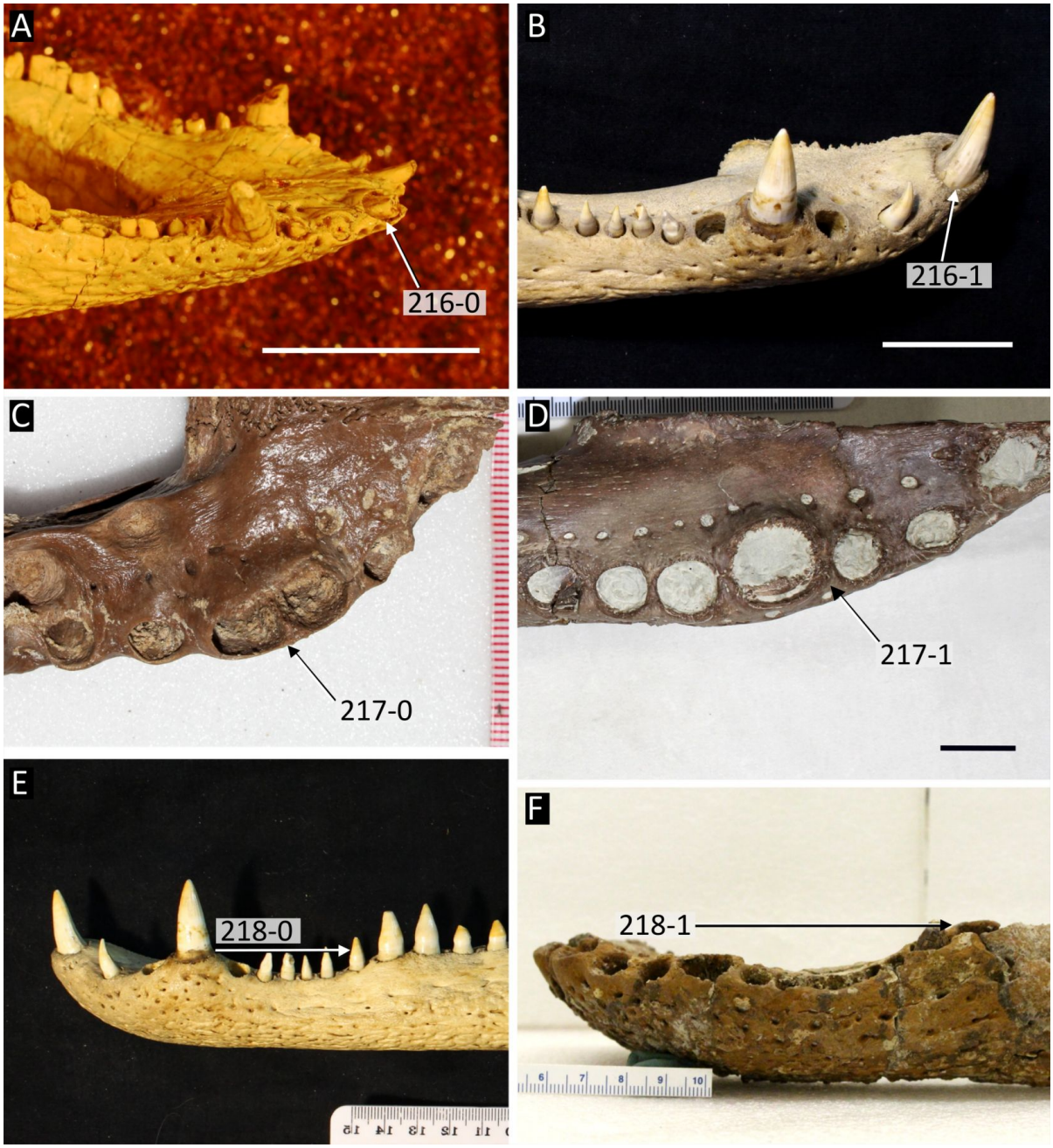



Figure 3.93: Morphology of the anterior dentary toothrow. **A**, the 'Glen Rose Form' (USNM 22039); **B**, *Caiman yacare* (MACN uncatalogued); **C**, *Diplocyndon ratelii* (MNHN G 660); **D**, '*Crocodylus*' *affinis* (UCMP 154341); **E**, *Caiman yacare* (MACN uncatalogued); **F**, *Eocaiman palaeocenicus* (MPEF PV 1933a). Scale bars in A, B, and D = 2 cm; C = mm; E, F = cm.

greater in some *Alligator* species (e.g. *A. mcgrewi*, AMNH FAM 8700), as well as some putative alligatorines, e.g. *Allognathosuchus* (Fig. 3.95C), *Hassicaosuchus haupti* (HLMD Me 4415), and *Navajosuchus mooki* (AMNH 6780). By contrast, the dentary is completely linear in this region in most longirostrine crocodylians, e.g. *Gavialis gangeticus* (Fig. 3.95A).

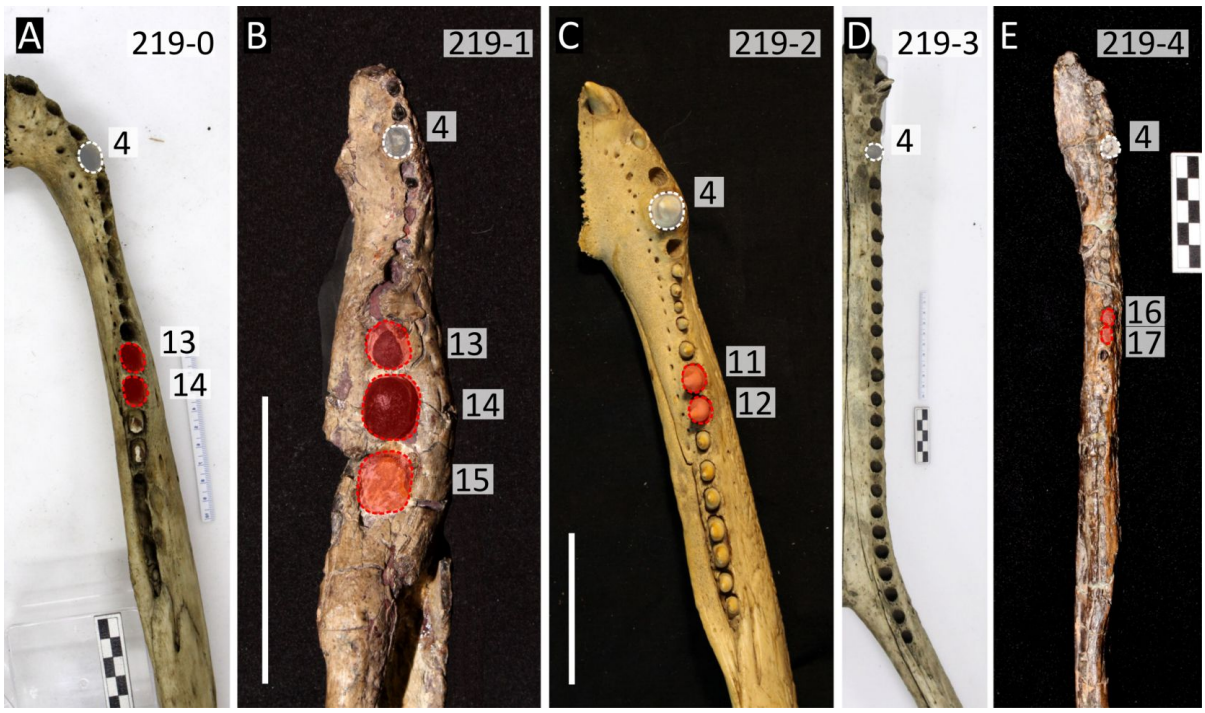



Figure 3.94: Dorsal view of the right mandibular ramus showing variation in alveolar size in: **A**, *Alligator mississippiensis* (NHMUK 68.2.12.6); **B**, *Allognathosuchus wartheni* (YPM PU 16989); **C**, *Caiman yacare* (MACN uncatalogued); **D**, *Gavialis gangeticus* (NHMUK 1974.3009); **E**, *Listrognathosuchus multidentatus* (AMNH 5179). Largest alveoli posterior to the $4^{th}$ are shaded in red. Scale bars in B and C = 5 cm, all other scale bars = cm.

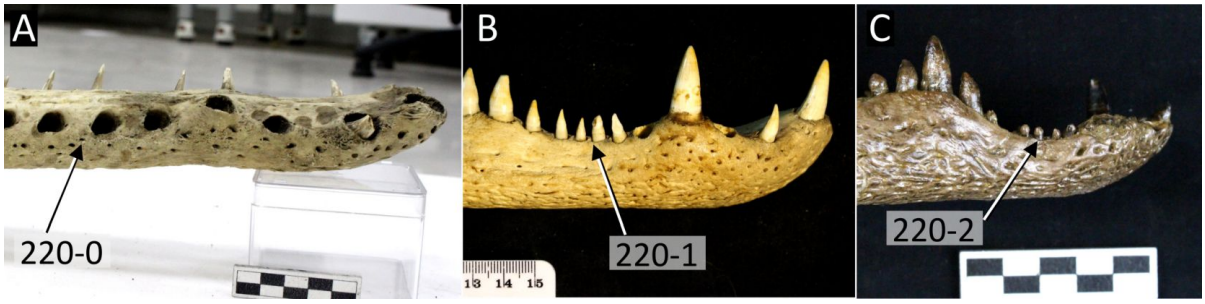



Figure 3.95: Variation in degree of curvature of the dentary toothrow between alveoli 4 and 10 in selected crocodylians. **A**, *Gavialis gangeticus* (NHMUK 1974.3009); **B**, *Caiman yacare* (MACN uncatalogued); **C**, *Allognathosuchus* sp. (USNM 25807). All scale bars = cm.

221. Mandibular symphysis, posterior extent, adjacent to number of full dentary alveoli: <6 (0); 6–8 (1); 9–12 (2): 13–20 (3); >20 (4) (after Jouve, 2004 [180]; Brochu, 2004a [166]; Salas-Gismondi et al., 2016 [49]) (ORDERED).

This character refers to the full length of the mandibular symphysis, i.e. formed by the dentary and splenial (where present) (Fig. 3.96). In *Bernissartia fagesii* (IRScNB 1538) and most eusuchians, the dentary symphysis only reaches the level of the $4^{th}$ dentary tooth (221-0) (Fig. 3.96A). Most taxa exhibit intraspecific variation by one alveolus at most. For example, in *Alligator mississippiensis* the symphysis might reach five alveoli lengths (Brochu, 2004b), but never six. The plesiomorphic character state also occurs in most extant *Crocodylus* species and *Diplocynodon*. The symphysis is adjacent to 6–8 alveoli (221-1) in several alligatorines (e.g. *Navajosuchus mooki* [AMNH 6780] and *Allognathosuchus wartheni* [YPM PU 16989]), 'basal' crocodyloids (e.g. '*Crocodylus*' *affinis*, UCMP 154341), and some extant longirostrine crocodylids, e.g. *Crocodylus johnstoni* (QM J45309) and *Mecistops cataphractus* (Fig. 3.96B). Fewer taxa are scored for the remaining character states, which are mostly present in longirostrine crocodylians. Whereas the mandibular symphysis reaches 9–12 alveoli (221-2) in some "tomistomines" (e.g. *Thecachampsa antiquus* [Fig. 3.96C] and *Maroccosuchus zennaroi* [MNHN APH 18]), it is longer (221-3) in all *Gryposuchus* species (e.g. *G. colombianus* [Fig. 3.96D]), and longer still (221-4) in *Gavialis gangeticus* (Fig. 3.96E) and *Piscogavialis jugaliperforatus* (SMNK 1282 PAL). Given this continuous spectrum of values, this character is ordered.

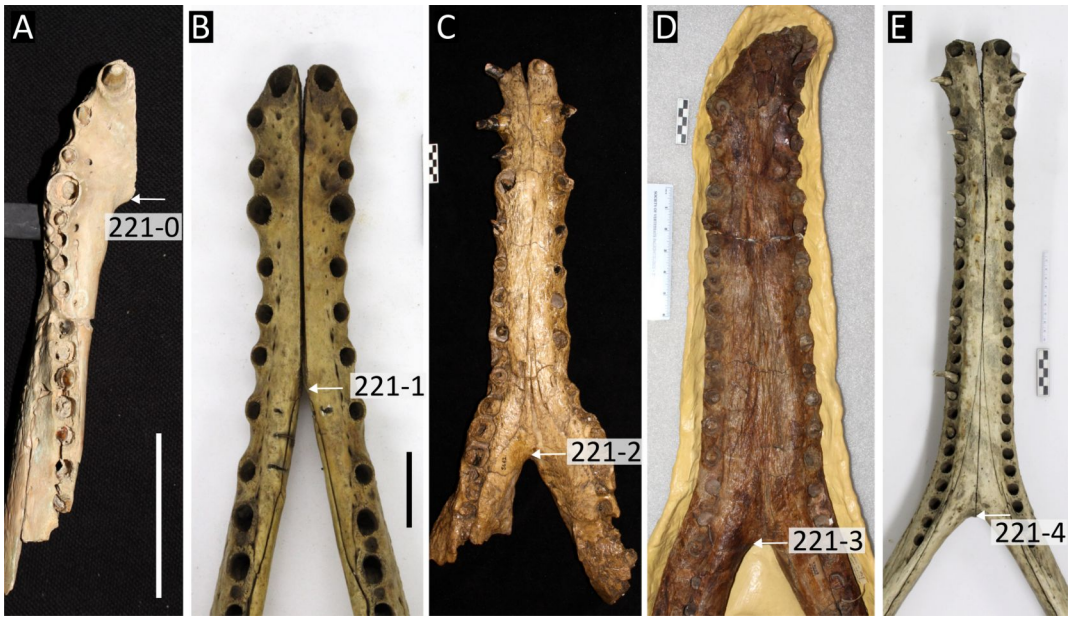



Figure 3.96: Dorsal view of the dentary symphysis in **A**, *Australosuchus clarkae* (QM F18151); **B**, *Mecistops cataphractus* (NHMUK 1865.4.6.1); **C**, *Thecachampsa antiquus* (AMNH 5662); **D**, *Gryposuchus colombianus* (UCMP 40062); **E**, *Gavialis gangeticus* (NHMUK 1974.3009). Scale bars in A and B = 5 cm, all other scale bars = cm.

222. Splenial, participation in symphysis: full participation, dorsal and ventral to Meckelian fossa (0); partial participation by splenial rostral tip (1); no participation (2) (after Clark, 1994 [77]; Brochu,

1997b [43]; Jouve, 2016 [43]) (ORDERED).

223. Splenial, position of anteriormost tip relative to Meckelian fossa: ventral (0); dorsal (1) (after Clark, 1994 [77]; Brochu, 1997b [43]).

224. Splenial, anterior extent in dentary symphysis: adjacent to 1 full alveolus (0); 2 to 3 alveoli (1); 4 to 7 alveoli (2); more than 7 alveoli (3) (after Clark, 1994 [77]; Jouve, 2016 [43]) (ORDERED).

225. Splenial, shape of splenial-dentary suture adjacent to dentary toothrow (in dorsal view): constricted, laterally concave (narrow 'V'-shape) (0); straight (wide 'V'-shape) (1) (after Brochu, 1997b [43]).

Characters 222–225 were derived by reductively coding Character 43 from Jouve (2016), which was adapted from Brochu (1997b, Character 43). As originally formulated, the character combined descriptions of the splenial length and morphology. For example: "*... deep splenial symphysis, participates in the mandibular symphysis over the length of five to seven teeth, and forms wide "V" within symphysis (4); or deep splenial symphysis participates in the mandibular symphysis over the length of five to seven teeth, and splenial constricted within symphysis and forms narrow "V" (5) ...*" (Jouve, 2016). As noted by Harshman et al. (2003), this precludes the grouping of taxa with an elongate symphysis, such as *Tomistoma schlegelii* and *Gavialis gangeticus*. Similarly, character states 1 and 2 in the same character preclude the grouping of taxa that lack a splenial symphysis, based on differences in splenial morphology: "*... splenial excluded from mandibular symphysis and anterior tip of splenial passes ventral to Meckelian groove (1); splenial excluded from mandibular symphysis and anterior tip of splenial passes dorsal to Meckelian groove (2) ...*". Character 222 describes the presence (Fig. 3.97A–B) or absence (Fig. 3.97C–D) of a splenial symphysis, but is augmented by a new intermediate character state, describing a ventral contribution to the symphysis observed in '*Crocodylus*' *affinis* (Fig. 3.97E) and *Asiatosuchus depressifrons* (Fig. 3.97F). This is considered distinct from the condition of some caimanines, in which the splenial approaches the symphysis but does not participate in it (Fig. 3.97G–H) (222-2). Character 223 describes the morphology of the anterior splenial tip in taxa that lack a splenial symphysis. As recognised by Brochu (1999), the anterior splenial tip is positioned dorsal to the Meckelian fossa in all extant alligatorids (e.g. *Melanosuchus niger*, Fig. 3.97D), but ventral in some 'basal' alligatoroids (e.g. *Diplocynodon*) and all extant crocodylids, e.g. *Crocodylus moreletii* (Fig. 3.97C). Taxa with a splenial symphysis must be scored as a "?". Where present, the splenial symphysis length is variable. For example, it is adjacent to only one alveolus (224-0) in *Asiatosuchus germanicus* (Fig. 3.98A), and *Boverisuchus vorax* (UCMP 170767). The splenial symphysis reaches 2–3 alveoli (224-1) in *Borealosuchus sternbergii* (Fig. 3.98B), *Borealosuchus formidabilis* (YPM PU 16241), and *Maroccosuchus zennaroi* (Jouve et al., 2015, fig.4B). In most longirostrine crocodylians, the symphysis is adjacent to 4–7 alveoli (224-2), e.g. *Thecachampsa*

(Fig. 3.98C), *Eosuchus* (Fig. 3.98D), and *Tomistoma schlegelii* (Fig. 3.98E). Some "gavialoids" exhibit a highly elongated splenial symphysis that extends beyond seven alveoli (224-3), e.g. *Gavialis gangeticus* (Fig. 3.98F), *Eogavialis africanum* (YPM 6263), and *Ikanogavialis gameroi* (Sill, 1970). Character 225 describes the morphology of the splenial symphysis strictly in taxa with a long splenial symphysis, i.e. taxa scored for character state 224-2 or 224-3. The constricted condition has traditionally been recognised only in "tomistomines", e.g. *Thecachampsa* (Fig. 3.98C) and *Tomistoma schlegelii* (Fig. 3.98E). This contrasts with the unconstricted splenials of most "gavialoids", e.g. *Eosuchus* (Fig. 3.98D) and *Gavialis gangeticus* (Fig. 3.98F), but not *Gryposuchus colombianus* (UCMP 40293), which exhibits the constricted condition (Fig. 3.98G).

226. Dentary symphysis, shape of posterior margin of symphyseal surface in medial view: dorsal lobe extends further posterior than ventral lobe (0); dorsal and ventral lobes subequal in extent, or ventral lobe projects further posterior than dorsal lobe (1) (after Lee & Yates, 2018 [176]).

    In taxa that lack a splenial symphysis, the posterior margin of the symphyseal surface of the dentary exhibits dorsal and ventral lobes that are separated by the Meckelian fossa (Fig. 3.99). In taxa with a full splenial symphysis (222-0), these lobes are poorly delimited, such that this character is considered inapplicable (Fig. 3.99C). In extant species of *Alligator*, *Crocodylus*, *Caiman*, and *Melanosuchus* the ventral lobe is anteriorly recessed such that the dorsal lobe clearly extends further posteriorly (Fig. 3.99A). By contrast, the lobes are subequally developed in some mekosuchines (e.g. *Baru wickeni* [Fig. 3.99B] and *Australosuchus clarkae* [QM F18151]), *Asiatosuchus depressifrons* (IRScNB R 253), and some *Diplocynodon* species, e.g. *D. hantoniensis* (NHMUK OR 30394).

227. Dentary, orientation of posteriormost alveoli: in a straight line (0); in a laterally curved line (1) (new character, based on personal observations).

    In *Bernissartia fagesii* (IRScNB 1538) and most eusuchians, the posteriormost dentary alveoli are arranged in a straight line, e.g. *Alligator mississippiensis* (Fig. 3.100A). By contrast, the posteriormost dentary alveoli of some crocodylians are arranged in a laterally curved line. This latter condition is most prominent in the putative basal alligatorines, *Allognathosuchus* (Fig. 3.100F) and *Navajosuchus mooki* (Fig. 3.100E). Indeed, in *Allognathosuchus*, the whole posterior ramus of the mandible appears to be laterally deflected (Fig. 3.100F). A posteriorly curved toothrow also occurs in some species of *Alligator*, e.g. *A. mcgrewi* (Fig. 3.100D) and *A. prenasalis* (Fig. 3.100C), but not *A. mefferdi* (Fig. 3.100B).

228. Dentary, posterior process between angular and splenial on ventral side of the mandible: absent (0); present (1) (after Jouve, 2004 [187]; in Jouve, 2016 [182]).

    A posterior process of the dentary between the angular and splenial, on the ventral side of the mandible

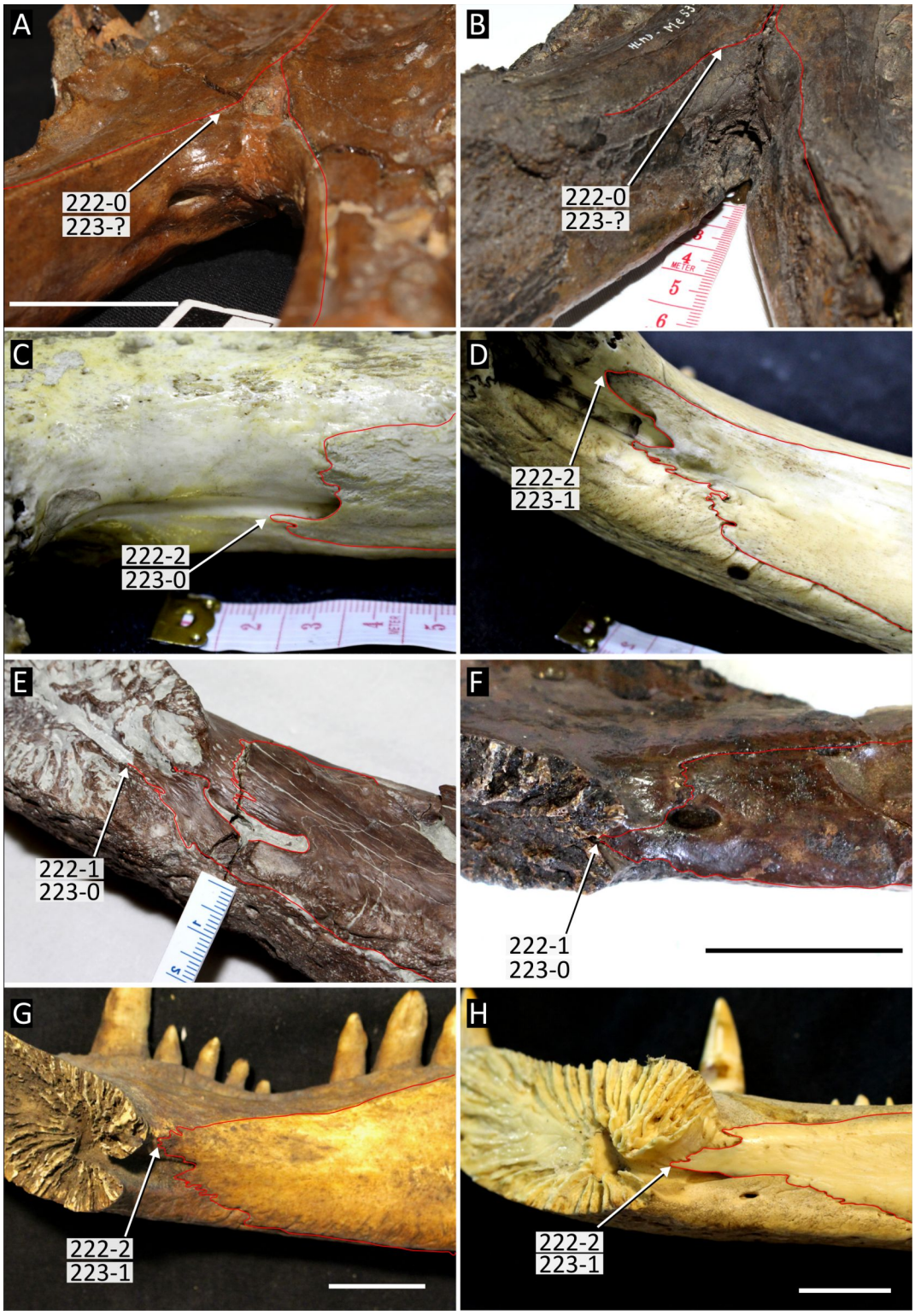



Figure 3.97: Medial view of the dentary symphysis in selected crocodylians showing variation in participation of the splenial (outlined in red). **A**, *Borealosuchus sternbergii* (USNM V 6533); **B**, *Asiatosuchus germanicus* (HLMD Me 5344); **C**, *Crocodylus moreletti* (NHMUK 1861.4.1.4); **D**, *Melanosuchus niger* (NHMUK 45.8.25.125); **E**, *'Crocodylus' affinis* (UCMP 154341); **F**, *Asiatosuchus depressifrons* (IRSNB R 253); **G**, *Caiman latirostris* (MACN V 1420); **H**, *Caiman yacare* (MACN uncatalogued). Scale bars in A, F–H = 2 cm, all other scale bars = cm.

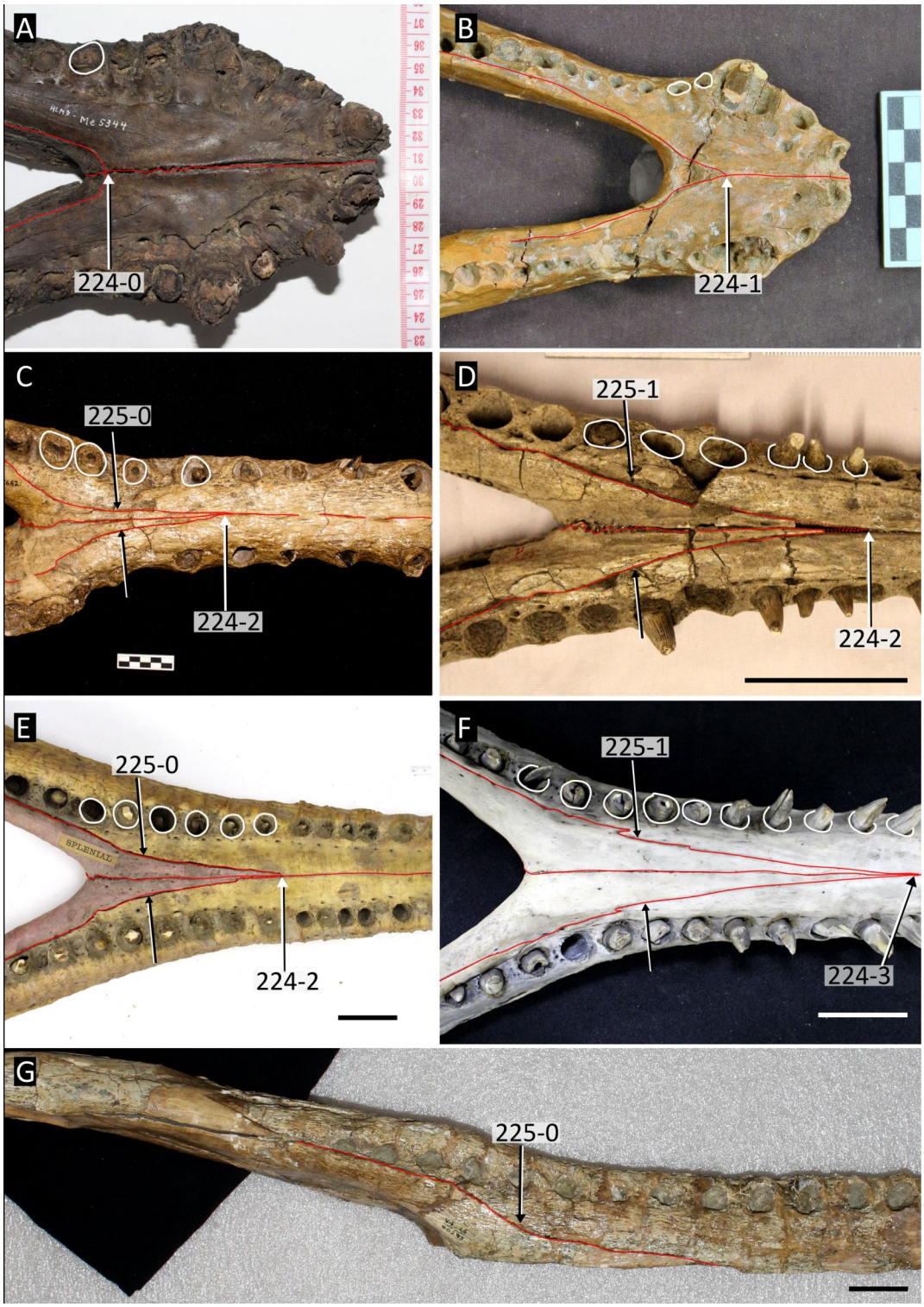



Figure 3.98: Dorsal view of the mandible showing variation in the splenial symphysis (outlined in red). **A**, *Asiatosuchus germanicus* (HLMD Me 5344); **B**, *Borealosuchus sternbergii* (USNM V 6533); **C**, *Thecachampsa antiquus* (AMNH 5662); **D**, *Eosuchus lerichei* (IRSNB R 49); **E**, *Tomistoma schlegelii* (NHMUK 1894.2.21.1); **F**, *Gavialis gangeticus* (NHMUK uncatalogued); **G**, *Gryposuchus colombianus* (UCMP 40293). All scale bars = 5 cm.

was scored in *Gavialis gangeticus* by Jouve (2016) (Fig. 3.101B). A comparable process is present in some fossil specimens (e.g. NHMUK R36727) of this species (Martin, 2019), as well as in *Gavialis lewisi* (YPM 3226). Given its apparent absence in all other taxa considered, it might be diagnostic of *Gavialis*. *Gavialis browni* (AMNH 6279) does not preserve a mandible (Mook, 1932) and, although the mandible is preserved in *Gaviali benjawanicus* (not studied here), the presence or absence of this feature was not described, nor can it clearly be ascertained from the figures (Martin et al., 2012).

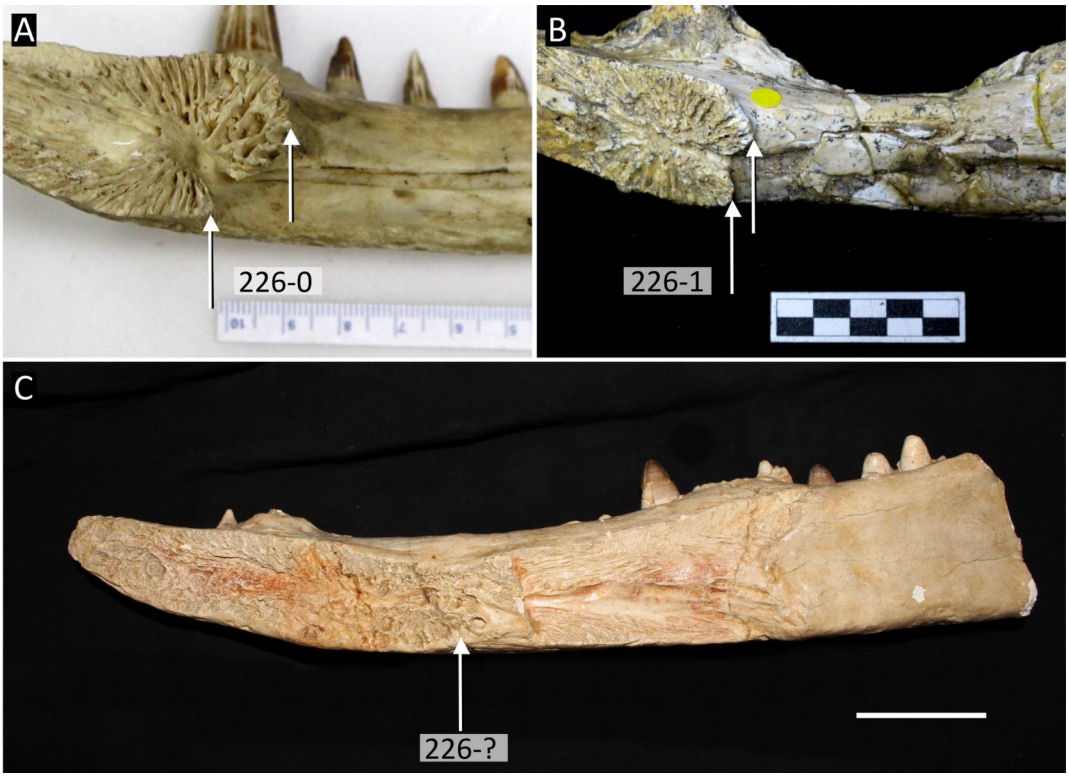



Figure 3.99: Medial view of the dentary symphysis in: **A**, *Crocodylus siamensis* (NHMUK 1921.4.1.171); **B**, *Baru wickeni* (QM 31070); **C**, *Maroccosuchus zennaroi* (MNHN APH 18). Scale bar in C = 5 cm, all other scale bars = cm.

229. Splenial, anterior perforation for mandibular ramus of cranial nerve V (i.e. foramen intermandibularis oralis): present (0); absent (1) (after Norell, 1988 [15]; Norell, 1989 [8]; Brochu, 1997b [41]).

The mandibular branch of cranial nerve V exists the splenial anteriorly through the opening of the Meckelian fossa in crocodylians (Schumacher, 1973, fig.30). In some crocodylians, cranial nerve V also exits through the anteriorly positioned foramen intermandibularis oralis (229-0) (Norell, 1989) (Fig. 3.102B). Among extant crocodylians, this foramen only occurs in *Alligator sinensis* (Brochu, 1999) and *Gavialis gangeticus*, where it is obscured from view by the mandibular symphysis (Norell, 1989, fig.5). Among fossil taxa, the foramen is present in *Bernissartia fagesii* (IRScNB 1538), *Borealosuchus*, alligatorines (e.g. *Allognathosuchus wartheni*, YPM PU 16989), and all species of *Alligator*, except *A. mississippiensis*.




Figure 3.100: Dorsal view of the mandible in selected alligatorid taxa. **A**, *Alligator mississippiensis* (NHMUK 68.2.12.6); **B**, *Alligator mefferdi* (AMNH 7016); **C**, *Alligator prenasalis* (YPM-PV-14063); **D**, *Alligator mcgrewi* (AMNH FAM 8700); **E**, *Navajosuchus mooki* (AMNH 6780); **F**, *Allognathosuchus* sp. (USNM 25807). All scale bars = 5 cm.

230. Splenial, posterior perforation(s) for mandibular ramus of cranial nerve V: absent (0); present (1) (after Norell, 1988 [15]; Norell, 1989 [8]; Brochu, 1997b [42]).

231. Splenial, number of posterior perforations for mandibular ramus of cranial nerve V: one (0); two (1) (after Norell, 1988 [15]; Norell 1989 [8]; Brochu, 1997b [42]).

    Characters 230 and 231 were derived by reductively coding character 42 in Brochu (1997b). Cranial nerve V always exits the splenial anteriorly through the Meckelian fossa and/or the foramen intermandibularis oralis (Character 229). Some taxa also have a posterior perforation (Fig. 3.102A), or two posterior perforations (Fig. 3.102D). The latter condition has traditionally only been recognised in *Paleosuchus* (e.g. Brochu, 1999), but some *Caiman* species (e.g. *Caiman yacare*, Fig. 3.102D) are polymorphic in terms of the number of posterior perforations.

232. Splenial, shape of dorsal profile: straight (anterodorsally inclined) (0); concave (abruptly dorsally inclined at posterior end) (1) (after Lee & Yates, 2018 [191]).

    This character was adapted from Lee and Yates (2018); however, different taxa are scored for the derived character state here, suggesting the anatomical meaning is different between our studies. Character state 1 here captures the distinctive morphology of the mandible in *Mekosuchus* (Balouet & Buffetaut, 1987) and *Iharkutosuchus makadii* (Ősi et al., 2007), in which the splenial is abruptly dorsally inclined at its posterior end (Fig. 3.102E–F). This contrasts with all other eusuchians where known, in which the dorsal margin of the splenial is largely straight and only modestly inclined, with

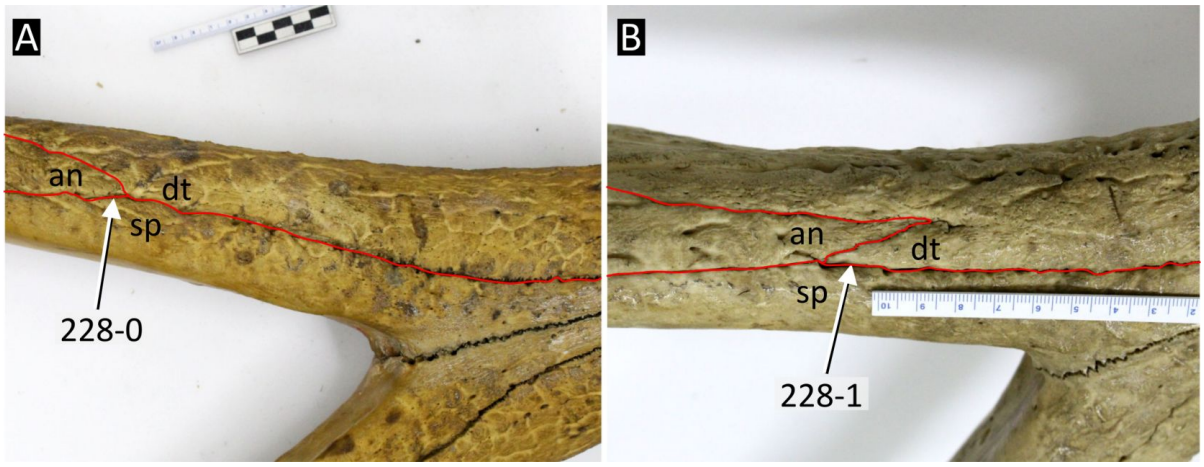



Figure 3.101: Ventral view of the mandible showing the suture between the dentary, angular and splenial. **A**, *Tomistoma schlegelii* (NHMUK 1894.2.21.1); **B**, *Gavialis gangeticus* (NHMUK 1974.3009). Abbreviations: **an**, angular; **dt**, dentary; **sp**, splenial. All scale bars = cm.

no distinct change of slope posteriorly (Fig. 3.102C–D).

233. Splenial, anterior process within the dentary, medial to the posterior toothrow: absent (0); present (1) (new character, based on personal observations).

The derived character state describes an acute inflection of the splenial-dentary suture, lingual to the posteriormost dentary alveoli. Where preserved, this process occurs in all *Gavialis* species. This comprises *G. gangeticus* (Fig. 3.103A), *G. lewisi* (YPM 3226), and *G. benjawanicus* (Delfino & De Vos, 2010, fig.3; Martin et al., 2012, fig.4), as well as some indeterminate fossil *Gavialis* specimens (Fig. 3.103C) . The condition is unknown in *G. browni* (AMNH 6279), for which the mandible is not preserved.

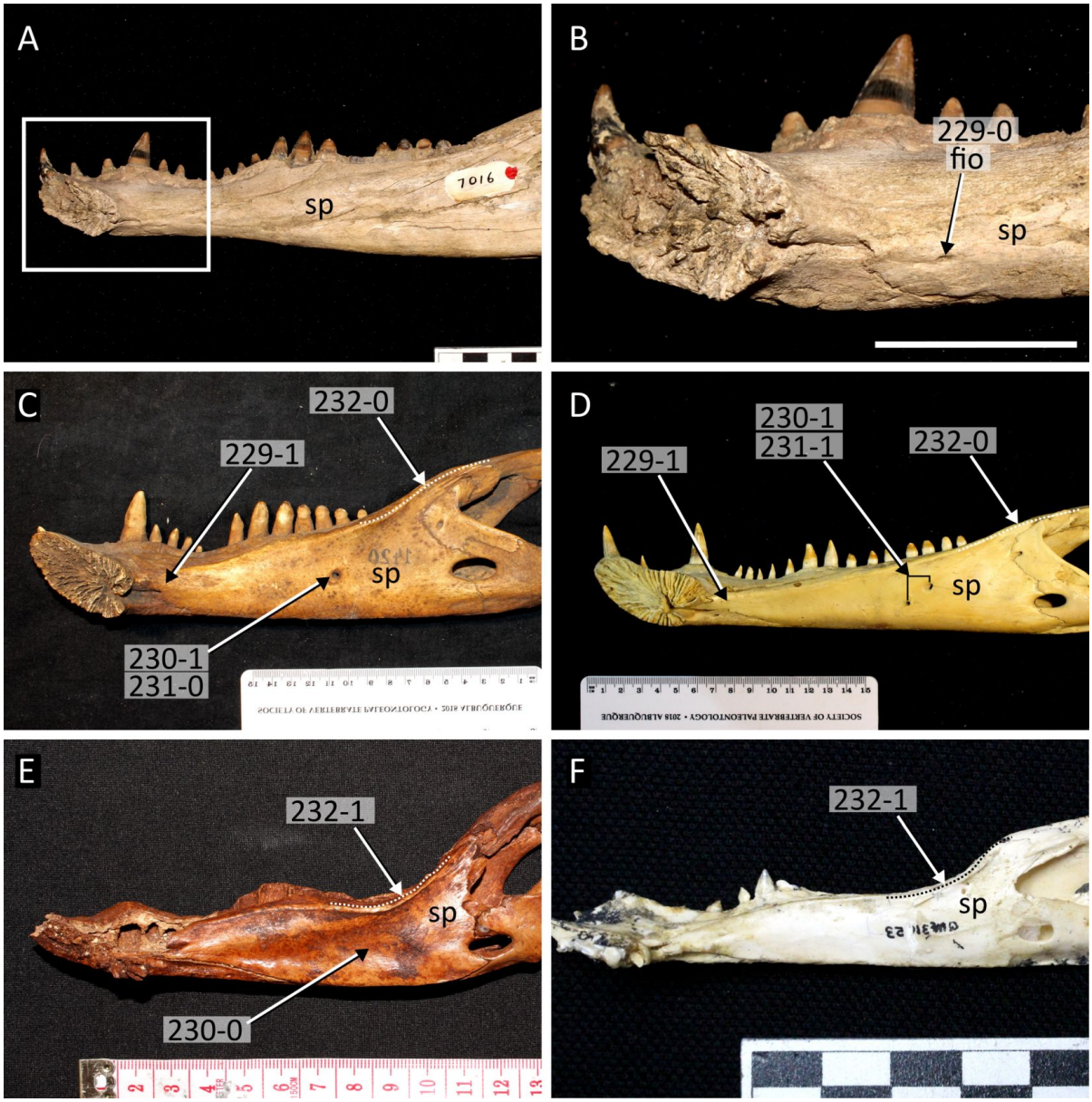



Figure 3.102: Medial view of the splenial. **A**–**B**, *Alligator mefferdi* (AMNH 7016); **C**, *Caiman latirostris* (MACN V 1420); **D**, *Caiman yacare* (MACN uncatalogued); **E**, *Mekosuchus inexpectatus* (MNHN NCP 06) (digitally reversed); **F**, *Mekosuchus whitehunterensis* (QM 31053). Abbreviations: **fio**, foramen intermandibularis oralis; **sp**, splenial. Scale bar in **B** = 4 cm, all other scale bars = cm.




Figure 3.103: Dorsal view of the splenial symphysis in **A**, *Gavialis gangeticus* (NHMUK 1974.3009); **B**, *Tomistoma schlegelii* (NHMUK 1848.10.31.19); **C**, fossil *Gavialis* sp. (NHMUK R 3095); **D**, *Gryposuchus colombianus* (UCMP 40293). All scale bars = cm.

234. External mandibular fenestra: absent (0); present (1) (Clark, 1994 [75]; Brochu, 1997b [62]).

235. External mandibular fenestra, size: narrow slit, no discrete fenestral concavity on angular dorsal margin, foramen intermandibularis caudalis not visible (0); moderate discrete concavity on angular dorsal margin, foramen intermandibularis caudalis not visible (1); large, most of foramen intermandibularis caudalis visible (2) (after Norell, 1988 [14]; Brochu, 1999 [62]; Brochu, 2011 [63]; Brochu & Storrs, 2012 [63]) (ORDERED).

    Characters 234 and 235 were derived by reductively coding Character 63 in Brochu and Storrs (2012). The external mandibular fenestra is absent in *Bernissartia fagesii* (Fig. 3.104A), and several non-crocodylian eusuchians, e.g. *Theriosuchus pusillus* (NHMUK 48304), *Iharkutosuchus makadii* (Ősi et al., 2007), and *Lohuecosuchus megadontos* (Narváez et al., 2015). Where present, variation occurs in the size of the fenestra. A small, slit-like fenestra (235-0) occurs in *Mekosuchus* (Fig. 3.104B), some *Borealosuchus* species (e.g. *B. threeensis* and *B. wilsoni* [Brochu et al., 2012]), and *Portugalosuchus azenhae* (Mateus et al., 2019). All other crocodylians exhibit notably larger fenestra, which can be divided into those in which the foramen intermandibularis caudalis is poorly visible through the fenestra (235-1) (Fig. 3.104G–I), and those with a largely exposed foramen intermandibularis caudalis (235-2) (Fig. 3.104D–E).

236. Surangular-dentary suture, intersection with external mandibular fenestra: anterior to posterodorsal corner (0); at posterodorsal corner (1) (Brochu, 1997b [65]).

    This character is inapplicable to taxa without an external mandibular fenestra (234-0). In most crocodylians the surangular-dentary suture intersects the external mandibular fenestra at a shallow angle, anterior to the posterodorsal corner, e.g. *Alligator mississippiensis* (Fig. 3.104D), *Tomistoma schlegelii* (Fig. 3.104G), *Gavialis gangeticus* (Fig. 3.104H) and *Crocodylus* (Fig. 3.104J–K). By contrast, the surangular-dentary suture is posterodorsally shifted in some taxa, e.g. *Mekosuchus* (Fig. 3.104B), *Alligator mcgrewi* (Fig. 3.104C), *Caiman latirostris* (Fig. 3.104E), and *Procaimanoidea utahensis* (USNM 15996).

237. Surangular-angular suture, intersection with external mandibular fenestra (at maturity): at posterodorsal angle (0); at posterior margin (1); passes broadly along ventral margin (2) (after Norell, 1988 [40]; Brochu, 1997b [47]).

    In most eusuchians with an external mandibular fenestra, the surangular-angular suture is horizontal up to the point where it intersects the posterior margin of the fenestra (237-1), e.g. *Alligator mississippiensis* (Fig. 3.104D), most *Crocodylus* species (Fig. 3.104J), and '*Crocodylus*' *affinis* (Fig. 3.104L). Less commonly, the suture intersects the external mandibular fenestra at a shallow angle, running down the posterior edge of the fenestra (237-2), e.g. *Caiman* (Fig. 3.104E–F), *Tomistoma schlegelii* (Fig. 3.104G), and *Gavialis gangeticus* (Fig. 3.104H). The plesiomorphic state is newly included to capture an uncommon condition wherein the suture intersects the external mandibular fenestra at its posterodorsal corner. Among taxa included in this study, this condition is only observed in *Alligator mcgrewi* (Fig. 3.104C), *Navajosuchus mooki* (AMNH 6780), *Mekosuchus* (Fig. 3.104B), and *Penghusuchus pani* (Shan et al., 2009, fig.4D). As the states do not capture a clearly continuous series, this character is not ordered.

238. Dentary, acute posterior process in the angular ventral to the external mandibular fenestra: present (0); absent (1) (after Jouve 2016 [240]).

    In most eusuchians with an external mandibular fenestra, the dentary-angular suture approaches the ventral margin of the fenestra in a posterodorsal direction, before recurving sharply anteriorly to form an acute process (238-0) (Fig. 3.104C–G). By contrast, the suture simply intersects the ventral margin of the fenestra (238-1) in *Gavialis gangeticus* (Fig. 3.104H), *Gavialis lewisi* (YPM 3226), *Mekosuchus* (Fig. 3.104B), and *Ultrastenos willisi* (Stein et al., 2016, fig.4C). Based on character scores therein, Jouve (2016) considered *Gryposuchus colombianus* and *Toyotamaphimeia machikanensis* to also share this latter condition. However, this portion of the mandible is obscured in all specimens of *Gryposuchus colombianus* examined here (UCMP 40062, UCMP 40293), and albeit small, *Toyotamaphimeia* appears to possess a ventral process (238-0) (Kobayashi et al., 2006, fig.11B).

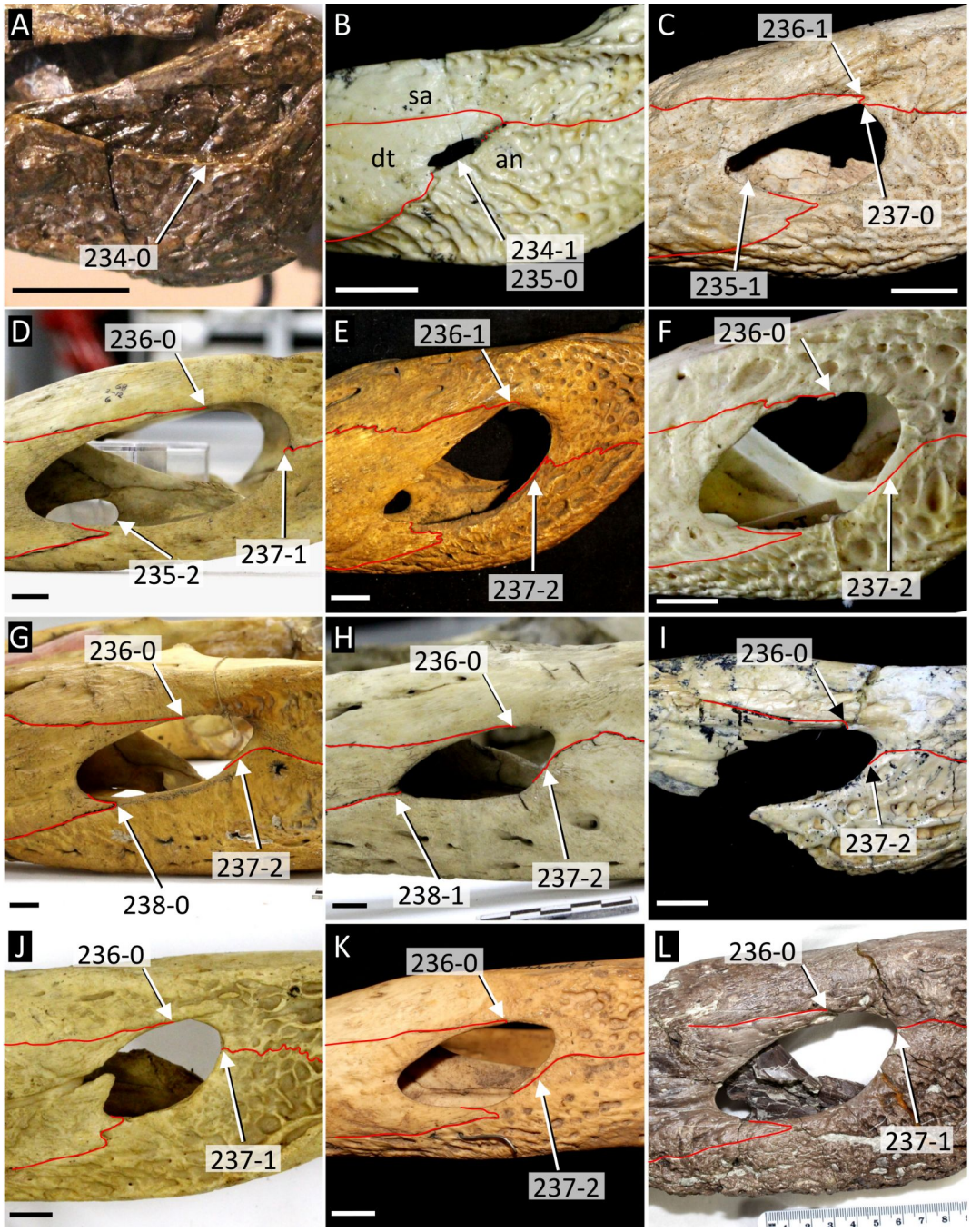



Figure 3.104: Left lateral view of the external mandibular fenestra in selected crocodylians, showing variation in size and sutural relationships. **A**, *Bernissartia fagesii* (IRSNB 1538); **B**, *Mekosuchus whitehunterensis* (QM 31053); **C**, *Alligator mcgrewi* (AMNH FAM 8700); **D**, *Alligator mississippiensis* (NHMUK 68.2.12.6); **E**, *Caiman latirostris* (MACN V 1420); **F**, *Caiman crocodilus chiapasius* (FMNH 73701); **G**, *Tomistoma schlegelii* (NHMUK 1894.2.21.1); **H**, *Gavialis gangeticus* (NHMUK uncatalogued); **I**, *Baru wickeni* (QM 31072); **J**, *Crocodylus palustris* (NHMUK 1897.12.31.1); **K**, *Crocodylus johnstoni* (QM J39230); **L**, *'Crocodylus' affinis* (UCMP 154341). Abbreviations: **an**, angular; **dt**, dentary; **sa**, surangular. Scale bar L = cm, all other scale bars = 1 cm.

239. Angular and surangular, margins flush with lateral surface of mandible (0); margins everted forming flange (1) (after Lee & Yates, 2018 [199]).

The surangular and angular form the dorsal and ventral margins of the posterior mandibular ramus, respectively, and are flush with the remainder of the lateral mandibular surface in *Bernissartia fagesii* (IRScNB 1538) and most eusuchians (Fig. 3.105A). By contrast, some eusuchians exhibit prominent ridges in this region, notably *Mekosuchus inexpectatus* (Fig. 3.105B), *Mekosuchus whitehunterensis* (Fig. 3.105C), and *Voay robustus* (Fig. 3.105D). Although less prominent, homologous ridges are considered present in *Paleosuchus* (AMNH 66391, AMNH 93812), *Boverisuchus vorax* (USNM 12957), and some paralligatorids, e.g. *Theriosuchus pusillus* (NHMUK 48304) and *Shamosuchus djadochtaensis* (Pol et al., 2009). These ridges might serve as sites for muscle attachment on the mandible, and could potentially vary ontogenetically; however, they appear to occur at an early stage of ontogeny where known. For example, the material known for *Mekosuchus whitehunterensis* probabaly represents a juvenile based on its size, and yet this exhibits the dervied state (Fig. 3.105C). Similar ridges are also present at an early ontogenetic stage in *Paleosuchus* specimens studied here (e.g. AMNH 66391, AMNH 93812). Finally, these ridges were not observed in the largest extant crocodylian specimens studied here, e.g. *Tomistoma schlegelii* (NHMUK 1894.2.21.1), *Crocodylus palustris* (NHMUK 97.12.31.1), and *Crocodylus porosus* (NHMUK 1864.9.11.1).

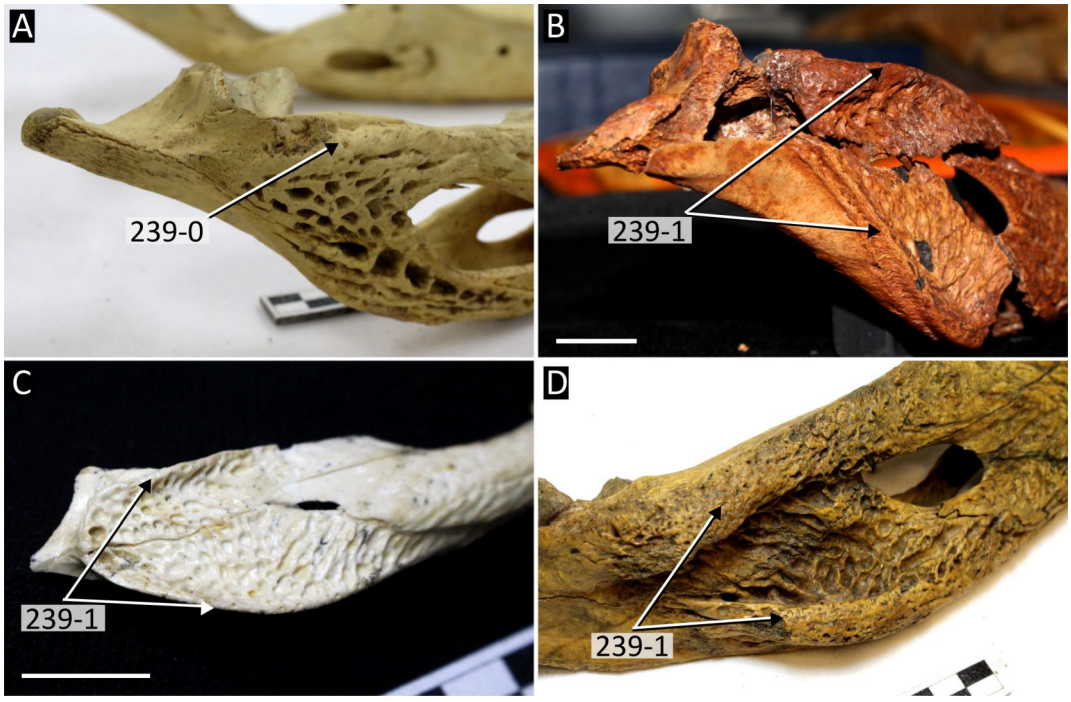



Figure 3.105: Posterolateral view of the mandible showing variation in development of a flange on the surangular. **A**, *Caiman latirostris* (NHMUK 1897.12.31.1); **B**, *Mekosuchus inexpectatus* (MNHN NCP 06); **C**, *Mekosuchus whitehunterensis* (QM 31053); **D**, *Voay robustus* (NHMUK R 36686). Scale bars B and C = 2 cm, A and D = cm.

240. Angular, fossa for *M. pterygoideus ventralis* visible on posterolateral surface of the mandible (0); not visible on posterolateral surface (1) (new character, based on personal observations).

In most eusuchians, the angular is broadly exposed ventral to the retroarticular process, as a smooth and unpitted surface (240-0). This surface is separated from the remainder of the sculpted lateral mandibular surface by a shallow 'step'. This boundary might mark the anterior extent of insertion for *M. pterygoideus ventralis* (Bona & Desojo, 2011), and occurs in all extant *Crocodylus* species (Fig. 3.106A), *Alligator* (Fig. 3.106C), *Allognathosuchus* (Fig. 3.106E), *Eocaiman palaeocenicus* (Fig. 3.106G), and *Brachychampsa montana* (Fig. 3.106H). By contrast, the unornamented angular is minimally exposed ventral to the retroarticular process in all extant caimanines (Fig. 3.106D, F), *Diplocynodon hantoniensis* (Fig. 3.106B, Section 2.5.1), and several non-crocodylian taxa including *Bernissartia fagesii* (IRScNB 1538), *Theriosuchus pusillus* (NHMUK 48304) and *Agaresuchus fontisensis* (Narváez et al., 2016, fig.4A).

241. Surangular, relative length of the anterior processes: unequal, ventral process $<$75% anteroposterior length of dorsal process (measured from surangular foramen) (0); sub-equal, ventral process $\geq$75% length of dorsal process (1) (after Brochu, 1997b [48]).

The presence of sub-equal anterior processes of the surangular (241-1) (Fig. 3.107C–D) is considered to be an unambiguous synapomorphy of Alligatoroidea (Brochu, 1999), contrasting with the unequal processes of *Tomistoma schlegelii* (Fig. 3.107A), *Gavialis gangeticus*, and all extant crocodylids (Fig. 3.107B). The qualifier 'sub-equal' is necessary, since the surangular processes are seldom equal in length, with the dorsal process extending further anteriorly than the ventral process in most eusuchians. For example, in *Alligator mississippiensis* (Fig. 3.107C), the dorsal process is slightly longer than the ventral process; however, the ventral process is consistently greater than 75% of the length of the dorsal process (measured from the surangular foramen) in all specimens. This contrasts with most other eusuchians, in which the ventral process is usually less than 50% the anteroposterior length of its dorsal counterpart. However, sub-equal surangular processes are not restricted to Alligatoroidea, occuring in a small number of other taxa, including *Eothoracosaurus mississippiensis* (Brochu, 2004a) and *Borealosuchus formidabilis* (Fig. 3.107D).




Figure 3.106: Lateral view of the posterior right mandible in selected crocodylians. **A**, *Crocodylus siamensis* (NHMUK 1921.4.1.168); **B**, *Diplocynodon hantoniensis* (CAMSM TN 904); **C**, *Alligator mississippiensis* (NHMUK 68.2.12.6, digitally reversed); **D**, *Caiman latirostris* (MACN V 1420); **E**, *Allognathosuchus* sp. (USNM 25807, digitally reversed); **F**, *Melanosuchus niger* (NHMUK 45.8.25.125); **G**, *Eocaiman palaeocenicus* (MACN 1914, digitally reversed); **H**, *Brachychampsa montana* (UCMP 133901, digitally reversed). Abbreviations: **an**, angular; **emf**, external mandibular fenestra; **sa**, surangular. All scale bars = 2 cm.

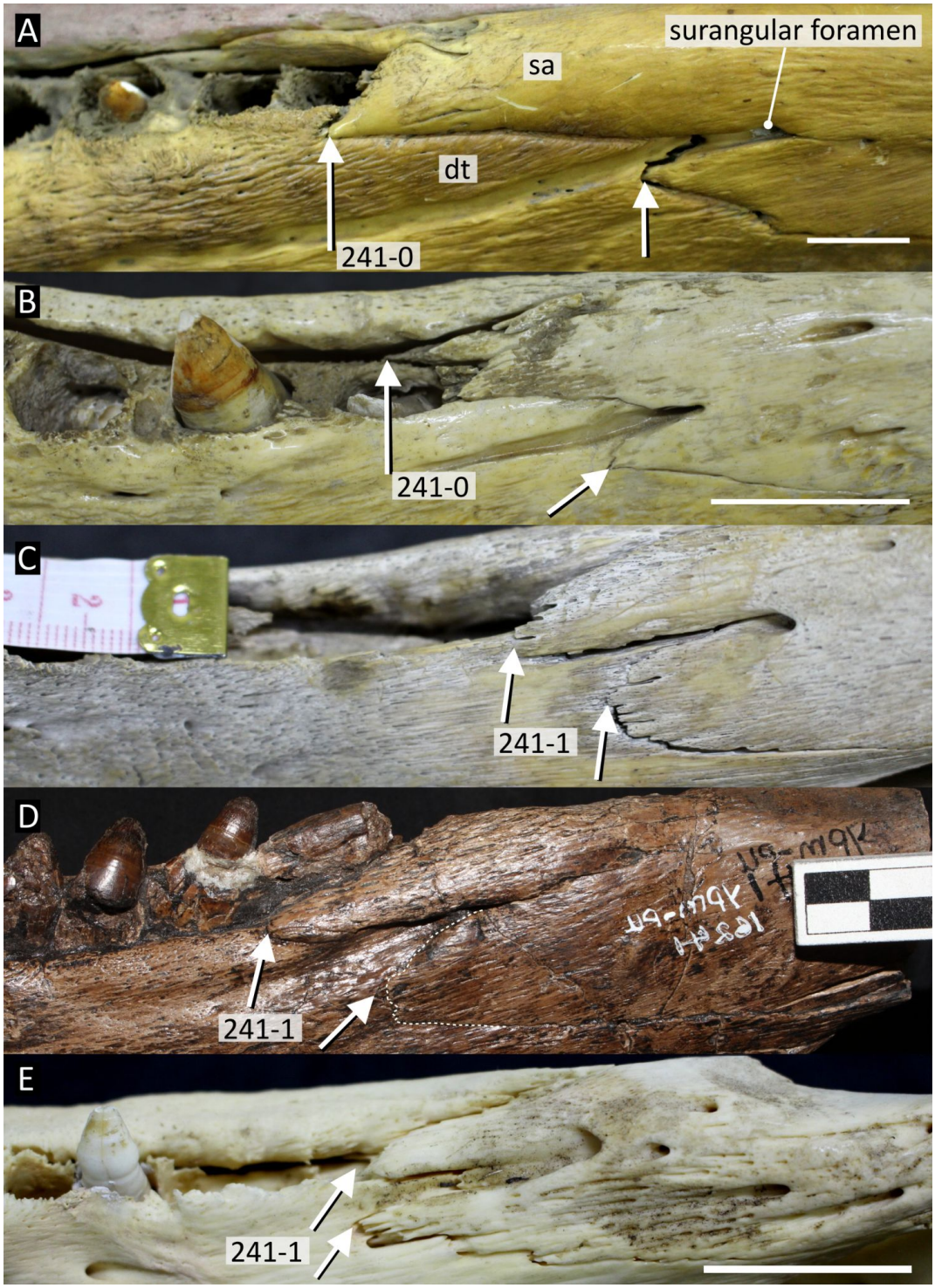



Figure 3.107: Dorsolateral view of the surangular showing relative lengths of the anterior processes in **A**, *Tomistoma schlegelii* (NHMUK 1894.2.21.1); **B**, *Crocodylus moreletii* (NHMUK 1861.4.1.4); **C**, *Alligator sinensis* (NHMUK X184); **D**, *Borealosuchus formidabilis* (YPM PU 16241, digitally reversed) **E**, *Caiman latirostris* (NHMUK 1897.12.31.1). Abbreviations: **dt**, dentary, **sa**, surangular. Scale bars in A, B and E = 2 cm, all other scale bars = cm.

242. Surangular, anterodorsal process (spur) lingual to posterior most dentary alveoli, between splenial and dentary: present (0); absent (1) (after Brochu, 1997b [61]).

243. Surangular, anterodorsal process (spur), anterior extent: not reaching 1 full alveolus (0); reaching 1–2 alveoli (1); reaching 3 or more alveoli (2) (new character, adapted from Brochu, 1997b [61]) (ORDERED).

    The surangular 'spur' is an anterodorsal process of the surangular, which projects between the dentary and the splenial, lingual to the posteriormost dentary alveoli (Fig. 3.108). The original character was binary, describing the presence or absence of a spur adjacent to one alveolus length, as originally formulated by Brochu (1997b). In most previous datasets, this spur has been recognised in *Bernissartia fagesii*, "tomistomines", and "gavialoids" (e.g. Brochu et al., 2012; Jouve, 2016; Salas-Gismondi et al., 2016; Iijima & Kobayashi, 2019); indeed Brochu (1999) noted that very few non-longirostrine crocodylians possess it. Here, this character has been reductively coded, with a new character capturing variation in spur length (Character 243). The surangular spur is recognised much more widely than previous studies, including in many non-longirostrine crocodylians. For example, all extant *Crocodylus* species exhibit a spur, which can extend either less than one alveolus length (243-0) (e.g. *C. siamensis*, Fig. 3.108C), or between 1–2 alveoli (243-1) (e.g. *C. palustris*, Fig. 3.108D). An elongated spur extending the length of 3 alveoli (243-2) is restricted to a few longirostrine crocodylians, including *Tomistoma schlegelii* (Fig. 3.108E) and *Gavialis gangeticus* (Fig. 3.108F). Taxa which lack a spur altogether include all extant alligatorids (Fig. 3.108A–B), for which Character 243 is inapplicable.

244. Surangular, ascending process on lateral wall of glenoid fossa: present (0); absent (1) (Brochu, 1997b [106]).

    As originally formulated, the plesiomorphic character state described an ascending process of the surangular that reaches the "*dorsal tip of* [the] *lateral wall of* [the] *glenoid fossa*" (Brochu, 1997b). The character wording has been modified here, because even in taxa with an ascending process, it never fully reaches the tip of the glenoid fossa lateral wall, and a small portion of the articular is always exposed. An ascending process occurs in *Bernissartia fagesii* (IRScNB 1538), several non-crocodylian eusuchians (e.g. *Iharkutosuchus makadii* [Ősi et al., 2007] and *Theriosuchus pusillus* [NHMUK 48304]), and many crocodylians, e.g. *Gavialis gangeticus* (Fig. 3.109A), all extant caimanines (Fig. 3.109C), *Diplocynodon* (Fig. 3.109D), and *Borealosuchus*, e.g. *B. sternbergii* (USNM 6533).

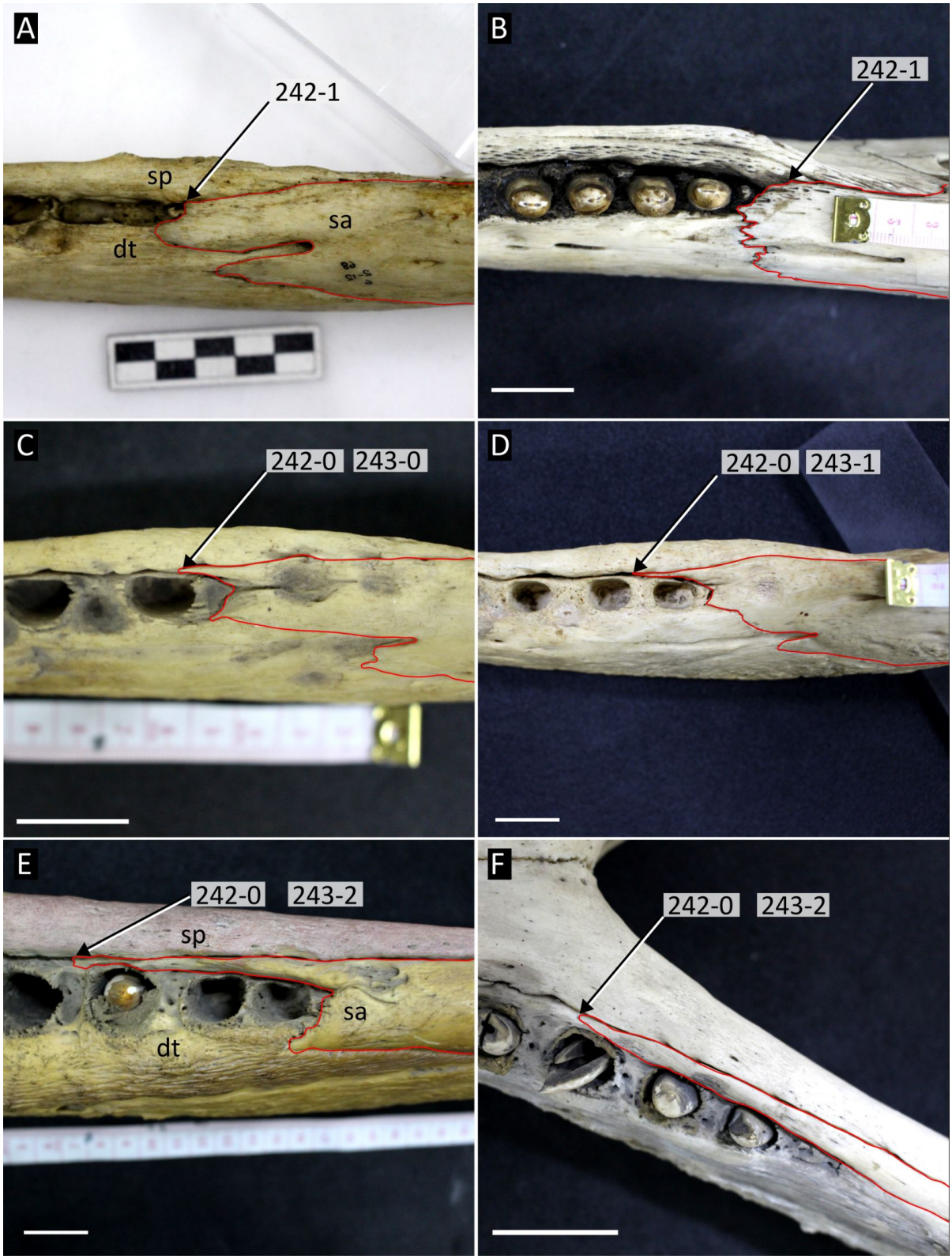



Figure 3.108: Dorsal view of the left posterior mandibular toothrow showing variation in development of the surangular spur. **A**, *Alligator mississippiensis* (NHMUK 68.2.12.6); **B**, *Melanosuchus niger* (NHMUK 45.8.25.125); **C**, *Crocodylus siamensis* (NHMUK 1921.4.1.171); **D**, *Crocodylus palustris* (NHMUK 1897.12.31.1); **E**, *Tomistoma schlegelii* (NHMUK 1894.2.21.1); **F**, *Gavialis gangeticus* (NHMUK uncatalogued). Abbreviations: **dt**, dentary; **sa**, surangular; **sp**, splenial. Scale bar A = cm, all other scale bars = 2 cm.

245. Surangular, posterior extent on lateral margin of retroarticular process: reaches posterior tip (0); pinches out anterior to posterior tip (1) (after Norell, 1988 [42]; Brochu, 1997b [51]).

The anatomical meaning of this character is identical to Brochu (1997b). The surangular extends to the posterior tip of the retroarticular process in *Borealosuchus* (e.g. *B. sternbergii*, USNM 6533), *Tomistoma schlegelii* (NHMUK 1894.2.21.1), all extant caimanines (Fig. 3.109C), and all extant species of *Crocodylus*. By contrast, *Bernissartia fagesii* (IRScNB 1538), *Gavialis gangeticus* (Fig. 3.109A), *Alligator* (Fig. 3.109B), and some *Diplocynodon* species (Fig. 3.109D) exhibit a posteriorly truncated surangular.

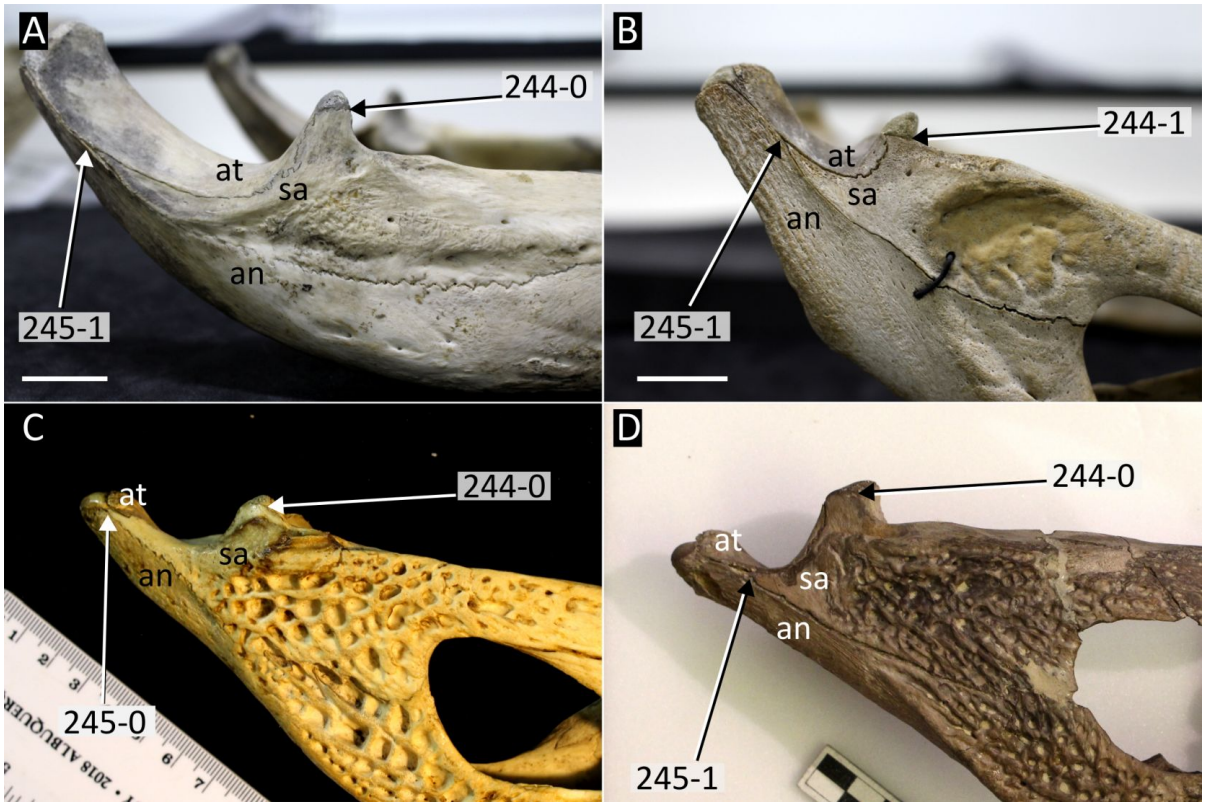



Figure 3.109: Variation in dorsal and posterior extent of the surangular. **A**, *Gavialis gangeticus* (NHMUK uncatalogued specimen); **B**, *Alligator sinensis* (NHMUK X 184); **C**, *Caiman yacare* (MACN uncatalogued specimen); **D**, *Diplocynodon hantoniensis* (CAMSM TN 904). Abbreviations: **an**, angular; **at**, articular; **sa**, surangular. Scale bars A and B = 2 cm, C and D = cm.

246. Surangular, sulcus on dorsal margin lateral to glenoid fossa: absent (0); present (1) (after Wang et al. 2016; Lee & Yates, 2018 [204]).

Wang et al. (2016) described a pit on the dorsolateral margin of the surangular, adjacent to the glenoid fossa, which they considered diagnostic of *Asiatosuchus nanlingensis*. Lee and Yates (2018 [character scores therein]) recognised that this fossa is more common within Crocodylia, occurring in some mekosuchines e.g. *Kambara* (Fig. 3.110B). Here, a pit is also recognised in *Bernissartia fagesii*

(IRScNB 1538), *Kentisuchus spenceri* (Fig. 3.110C), some *Borealosuchus* species (e.g. *B. sternbergii* [USNM 6533] and *B. formidabilis* [YPM PU 16241]) and some 'basal' crocodyloids, e.g. *Asiatosuchus depressifrons* (Fig. 3.110D) and '*Crocodylus*' *affinis* (UCMP 154341).

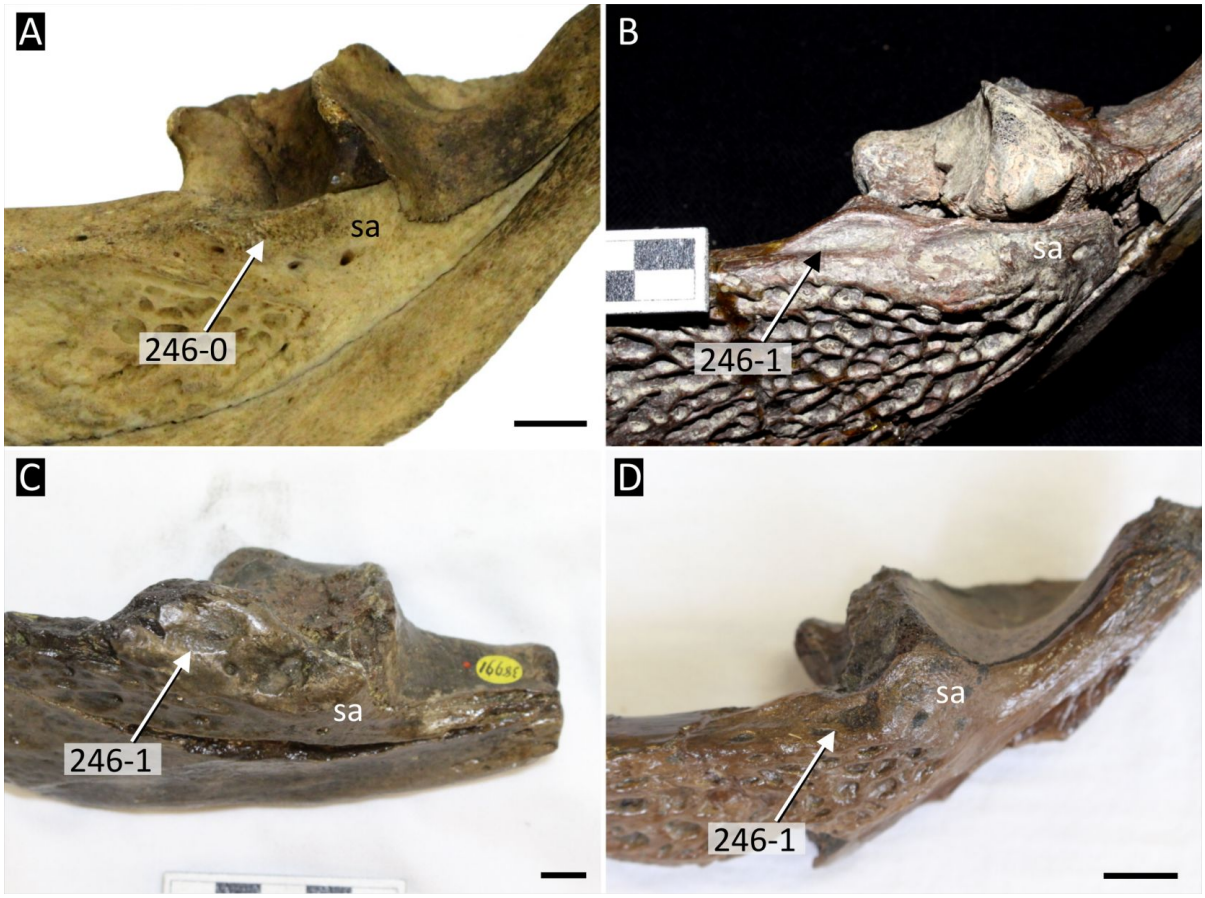



Figure 3.110: Lateral view of the surangular showing variation in development of a pit on the dorsolateral margin. **A**, *Alligator mississippiensis* (NHMUK); **B**, *Kambara molnari* (QM F12364); **C**, *Kentisuchus spenceri* (NHMUK 38991); **D**, *Asiatosuchus depressifrons* (IRScNB IG 9912). Abbreviations: **sa**, surangular. Scale bar C = cm, all other scale bars = 1 cm.

247. Surangular-articular suture, shape in glenoid fossa: straight, oriented anteroposteriorly (0); bowed laterally (1) (after Brochu, 1997b [162]).

In *Bernissartia fagesii* (IRScNB 1538) and most eusuchians, the surangular-articular suture is orientated in a straight, anteroposterior line in the floor of the glenoid fossa. This condition occurs in all extant alligatorids (e.g. *Alligator mississippiensis*, Fig. 3.111A), most "gavialoids" (e.g. *Gavialis gangeticus*), *Diplocynodon* (e.g. *D. hantoniensis*, NHMUK OR 25188), and *Borealosuchus* (e.g. *B. sternbergii*, USNM 6533). By contrast, all extant crocodylids as well as "tomistomines" exhibit an acute 'kink' in the suture (Fig. 3.111B–C). This condition also occurs in the 'basal' crocodyloids, *Asiatosuchus depressifrons* (IRScNB R253) and '*Crocodylus*' *affinis* (UCMP 154341).

248. Articular, position of foramen aerum: at medial margin of retroarticular process (0); inset from medial margin of retroarticular process (1) (after Norell, 1988 [16]; Brochu, 1997b [49]).

The foramen aerum, which is positioned on the transverse ridge of the articular, is inset from the medial edge (248-1) in all extant alligatorids (Fig. 3.111A), as well as *Diplocynodon* (Fig. 3.111B) and *Leidyosuchus canadensis*. Brochu (1999) noted the potential linkage of this character with that describing the position of the foramen aerum on the quadrate (Character 117 here). Indeed, most taxa with a dorsally positioned quadratic foramen aerum (117-1) also possess a medially inset articular foramen aerum (248-1). Nevertheless, several taxa exhibit different combinations of these characters. For example, in *Mekosuchus inexpectatus* (MNHN NCP 06), *Borealosuchus sternbergii* (USNM 6533), and *Borealosuchus formidabilis* (Erickson, 1976), the quadratic foramen aerum is dorsally positioned (117-1), but the articular foramen aerum is medially positioned (248-0).

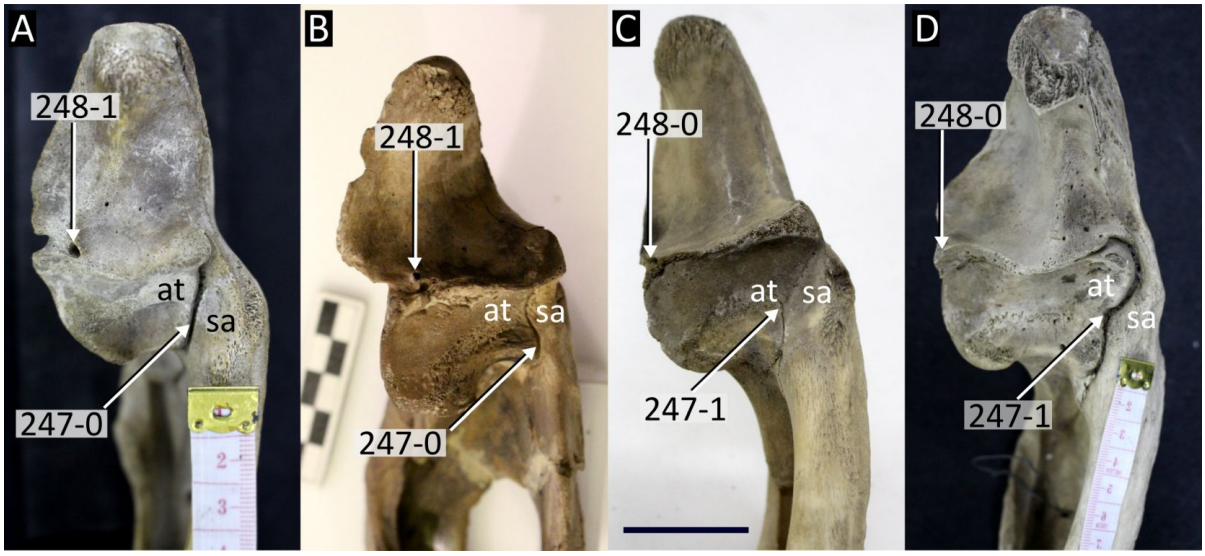



Figure 3.111: Dorsal view of the left glenoid fossa in **A**, *Alligator sinensis* (NHMUK X184); **B**, *Diplocynodon hantoniensis* (CAMSM TN 904, digitally reversed); **C**, *Crocodylus siamensis* (NHMUK 1921.4.1.171); **D**, *Crocodylus porosus* (NHMUK 1864.9.11.1). Abbreviations: **at**, articular; **sa**, surangular. Scale bar C = 2 cm, all other scale bars = cm.

249. Articular, lamina extending from posterior edge of foramen aerum: absent (0); present (1) (new character, based on personal observations).

In *Bernissartia fagesii* (IRScNB 1538) and most eusuchians, the articular foramen aerum is a simple perforation, the margins of which are flush with the surface of the articular (Fig. 3.112A). By contrast, the foramen aerum of some crocodylians is posteriorly bound by a large, anteroposteriorly orientated lamina, which in some cases overhangs the foramen. This condition is mainly observed in caimanines, such as *Caiman latirostris* (Fig. 3.112B), *Mourasuchus atopus* (Fig. 3.112C), and *Eocaiman palaeocenicus* (Fig. 3.112E). A similar condition occurs in *Diplocynodon hantoniensis* (Fig. 3.112D),

*Brachychampsa montana* (Fig. 3.112F), and the "gavialoid" *Eosuchus minor* (Brochu, 2006a, fig.18).

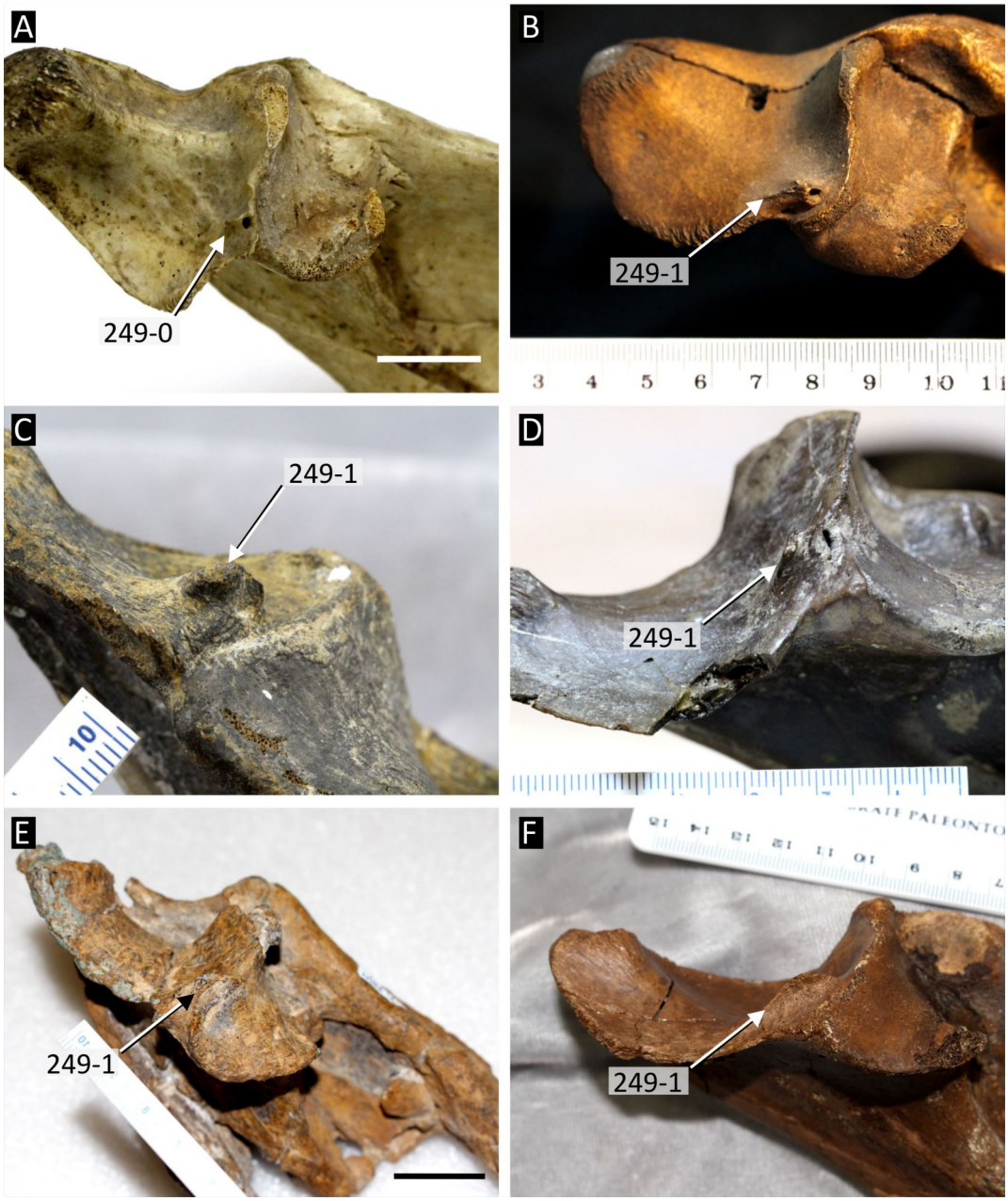



Figure 3.112: Dorsomedial view of the articular showing variation in development of a lamina trailing from the posterior margin of the foramen aerum. **A**, *Crocodylus siamensis* (NHMUK 1921.4.1.171); **B**, *Caiman latirostris* (MACN V 1420); **C**, *Mourasuchus atopus* (UCMP 38012); **D**, *Diplocynodon hantoniensis* (NHMUK 30397); **E**, *Eocaiman palaeocenicus* (MPEF 1933a); **F**, *Brachychampsa montana* (UCMP 133901). Scale bars in A and E = 2 cm, all other scale bars = cm.

250. Articular, orientation of retroarticular process: projects posteriorly (0); projects posterodorsally (1) (after Benton & Clark, 1988; Norell & Clark, 1990 [7]; Clark, 1994 [71]; Brochu, 1997b [50]).

251. Articular, dorsal extent of retroarticular process: at the same level or ventral to posterior edge of articular fossa (0); dorsal to posterior edge of articular fossa (1) (after Jouve, 2004 [190]; Jouve et al., 2008 [190]; Salas-Gismondi et al., 2015 [71]).

    The retroarticular process is directed posteriorly (250-0) in *Bernissartia fagesii* (IRScNB 1538) and several non-crocodylian eusuchians, including *Theriosuchus pusillus* (Fig. 3.113A), and *Shamosuchus djadochtaensis* (Pol et al., 2009). The only crocodylian found to exhibit this condition is *Mekosuchus inexpectatus* (Fig. 3.113B). All other crocodylians exhibit a posterodorsally directed retroarticular process (250-1) (Fig. 3.113C–F). The retroarticular process also varies in its dorsal extent relative to the glenoid fossa of the articular. This would appear to be linked to the orientation of the retroarticular process; indeed, in all taxa with a posteriorly directed retroarticular process (250-0), it does not surpass the glenoid fossa dorsally (251-0) (Fig. 3.113A–B). However, taxa scored for character state 250-1 can exhibit either a low retroarticular process (251-0) (e.g. *Diplocynodon hantoniensis* and *Caiman latirostris* [Fig. 3.113C–D]) or a dorsally positioned process (251-1) (e.g. *Alligator mississippiensis* and *Gavialis gangeticus* [Fig. 3.113E–F]).

252. Articular, sharp longitudinal crest on dorsal surface of retroarticular process: absent (0); present (1) (after Salas-Gismondi et al. 2016 [203]).

    The dorsal surface of the retroarticular process is slightly convex in all crocodylians, with a low antero-posterior ridge running along the midline (Fig. 3.114A). In a few, mostly "gavialoid" crocodylians, a tall crest is present instead, e.g. *Gryposuchus colombianus* (Fig. 3.114B) and *Argochampsa krebsi* (Fig. 3.114C). The development of this crest does not appear to be ontogenetic. For example, it does not occur in any specimen of *Gavialis gangeticus* studied here, including the largest individuals (e.g. NHMUK 1974.3009, UMZC R5783). Conversely, it does occur in a very small, and potentially juvenile specimen of *Argochampsa krebsi* (Fig. 3.114C).

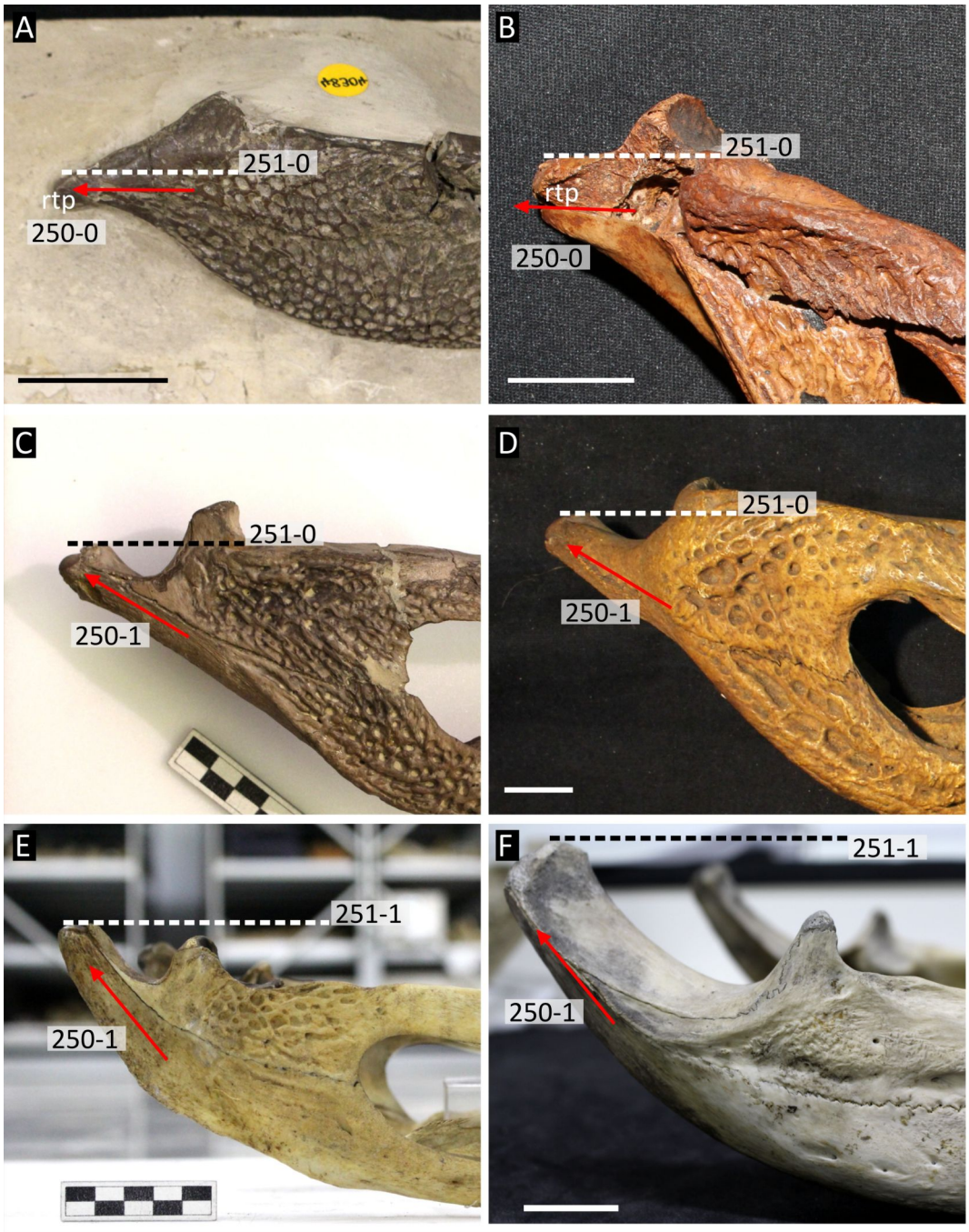



Figure 3.113: Lateral view of the right posterior mandibular ramus showing variation in height and orientation of the retroarticular process. **A**, *Theriosuchus pusillus* (NHMUK 40384) (digitally reversed); **B**, *Mekosuchus inexpectatus* (MNHN NCP 06); **C**, *Diplocynodon hantoniensis* (CAM TN 904); **D**, *Caiman latirostris* (MACN V 1420) (digitally reversed); **E**, *Alligator mississippiensis* (NHMUK 68.2.12.6); **F**, *Gavialis gangeticus* (NHMUK uncatalogued). Abbreviations: **rtp**, retroarticular process. Scale bars C and E = cm, all other scale bars = 2 cm.




Figure 3.114: Dorsal view of the mandibular retroarticular process showing development of a crest in **A**, *Gavialis gangeticus* (NHMUK uncatalogued, left articular); **B**, *Gryposuchus colombianus* (UCMP 40293, left articular); **C**, *Argochampsa krebsi* (NHMUK R36872, right articular). Scale bar in A = 2 cm, all other scale bars = cm.

253. Articular, lingual foramen for articular and alveolar nerve perforates surangular only (0); perforates surangular-articular suture (1) (after Brochu, 1997b [45]; Brochu, 2011 [69]).

    This character is described and illustrated by Brochu (1999, fig.33). Here it is unmodified, except for the description of the lingual foramen as perforating the surangular-*articular* suture, rather than the surangular-*angular* suture, which appears to be a typographical error. As in earlier studies, a surangular-articular perforation (253-1) is observed in all extant species of *Crocodylus* (Fig. 3.115G–I) and *Alligator* (Fig. 3.115B), in addition to *Kambara* (e.g. QM F30077), and *Mekosuchus* (e.g. MNHN NCP 06). The condition also occurs in *Diplocynodon* (all species, where preserved), although it is polymorphic in *D. hantoniensis* (see Chapter 2). A surangular-only perforation (253-0) occurs in all extant caimanines (Fig. 3.115D–F), *Gavialis gangeticus* (Fig. 3.115C), *Tomistoma schlegelii* (NHMUK 1894.2.21.1), and some *Borealosuchus* species, e.g. *B. sternbergii* (USNM 6533).

254. Articular, anterior process on posterior wall of adductor chamber: absent (0); present (1) (after Brochu, 1997b [44]; Brochu, 2011 [68]).

255. Articular, position of anterior process on posterior wall of adductor chamber: dorsal to lingual foramen (0); ventral to lingual foramen (after Brochu, 1997b [44]; Brochu, 2011 [68]).

    Characters 254 and 255 were derived by reductively coding Character 68 in Brochu (2011). In *Bernissartia fagesii* and most eusuchians, the surangular-articular suture forms a straight line in the posterior wall of the mandibular adductor chamber (254-0) (Fig. 3.115A–C). By contrast, all extant crocodylids, *Melanosuchus*, and *Caiman* exhibit an anterior process of the articular (254-1) (Fig. 3.115D–I). Whereas in crocodylids this process is dorsal to the lingual foramen (255-0) (Fig. 3.115G–I), it occurs ventral to the lingual foramen in *Melanosuchus* and *Caiman* (255-1) (Fig. 3.115D–F). An additional character state introduced by Brochu (2011) (68-3): "*bears laminae* (= processes) *above and below foramen*", appears to occur in some species of *Thecachampsa*, based on character scores in

Brochu (2011) and Iijima and Kobayashi (2019). However, the relevant portion of the mandible could not be examined in any specimen of *Thecachampsa*, nor has it been clearly figured before, and so this state was excluded.

256. Surangular-angular suture, lingual intersection with articular in the floor of the adductor chamber: at ventral tip (0); dorsal to ventral tip (1) (after Brochu, 1997b [67]).

In postero-medial view of the mandibular adductor chamber, the surangular-angular suture can be seen extending from the external mandibular fenestra to the ventral tip of the articular in most eusuchians (Fig. 3.115A–C). This suture is more or less straight, but can exhibit a kink (commonly in *Crocodylus* species [Fig. 3.115G]). By contrast, the suture intersects the articular dorsal to its ventral tip in all extant caimanines (Fig. 3.115D–F) (Brochu, 1999). Among fossil crocodylians, this condition occurs in *Acresuchus pachytemporalis* (UFAC 2507), *Diplocynodon hantoniensis* (Section 2.3.2), and *Voay robustus* (NHMUK R36686). Commonly in taxa exhibiting this condition, the surangular forms a narrow, 'finger'-like descending process on the posterior wall of the adductor chamber, e.g. *Melanosuchus niger* (Fig. 3.115D) and *Caiman yacare* (Fig. 3.115E); however, this does not occur in *Caiman latirostris* (Fig. 3.115F), *Caiman crocodilus* (FMNH 69812), *Voay robustus* (NHMUK R36686), or *Diplocynodon hantoniensis* (CAM TN 904).

257. Angular, anterior extent relative to foramen intermandibularis caudalis (FIC) (in medial view): extends anteriorly beyond half the anteroposterior length of the FIC (0); terminates at, or posterior to the anteroposterior mid-length of the FIC (1) (after Brochu, 1997b [66]).

The anatomical meaning of this character follows the description and figures in Brochu (1999, fig.47), who noted that all extant caimanines exhibit an angular that does not extend far anteriorly relative to the FIC. Here, the anterior extent of the angular is measured relative to the anteroposterior midpoint of the FIC, and the derived condition is recognised in a few additional taxa. Following (Brochu, 1999), all extant caimanines exhibit the derived condition, and it is newly recognised in *Mecistops cataphractus* (Fig. 3.116) and *Alligator mcgrewi* (Fig. 3.116C).

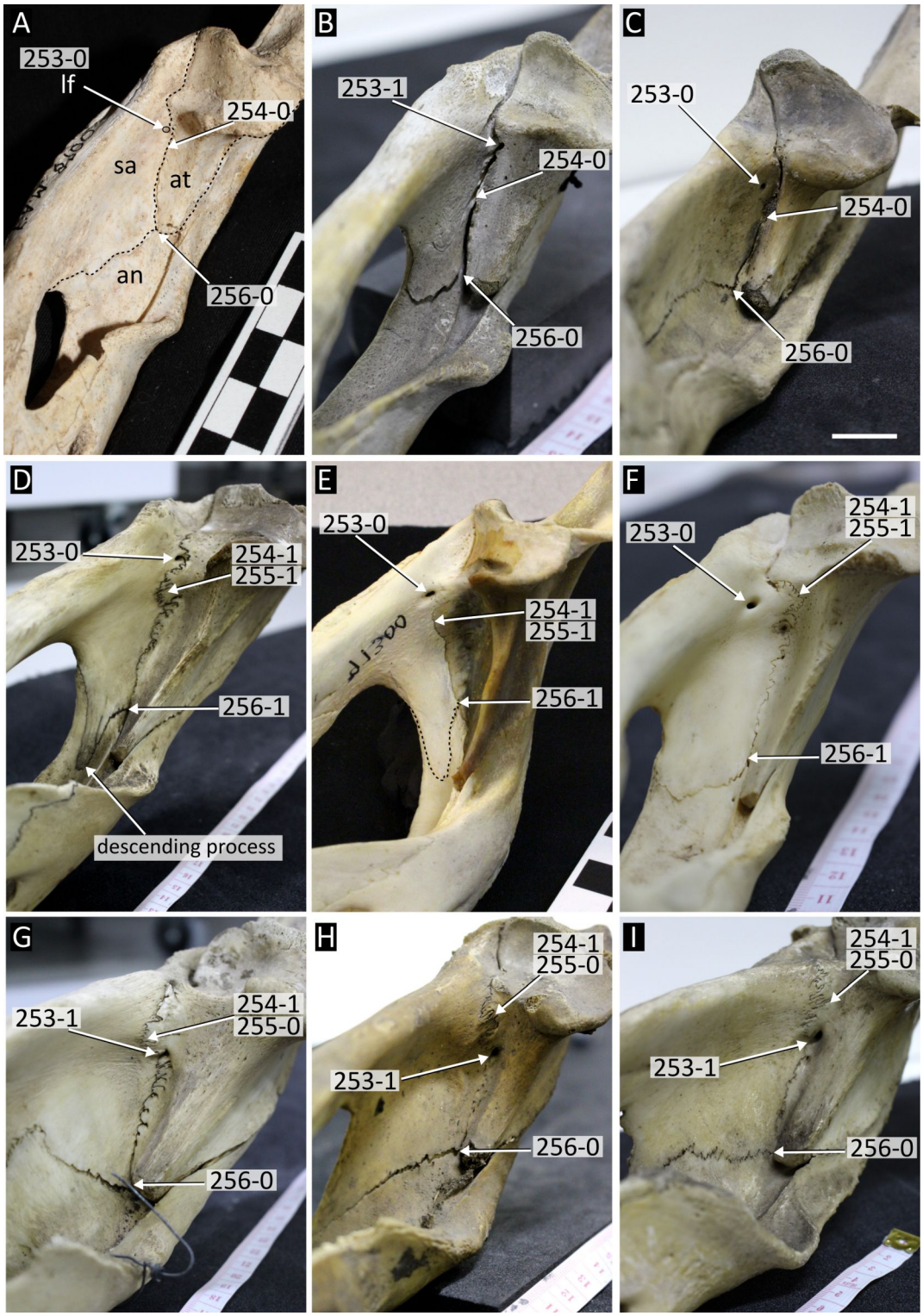



Figure 3.115: Posteromedial view of the right mandibular adductor chamber. **A**, *Alligator mcgrewi* (AMNH FAM 8700) (digitally reversed); **B**, *Alligator sinensis* (NHMUK X184); **C**, *Gavialis gangeticus* (NHMUK uncatalogued); **D**, *Melanosuchus niger* (NHMUK 45.8.25.125); **E**, *Caiman yacare* (AMNH 97300) (digitally reversed); **F**, *Caiman latirostris* (NHMUK 86.10.4.2); **G**, *Crocodylus porosus* (NHMUK 1864.9.11.1); **H**, *Crocodylus siamensis* (NHMUK 1921.4.1.171); **I**, *Crocodylus moreletii* (NHMUK 1861.4.1.4). Abbreviations: **an**, angular; **at**, articular; **lf**, lingual foramen; **sa**, surangular. Scale bar in C = 2 cm, all other scale bars = cm.

258. Splenial, acute posterior process separating angular and coronoid: present (0); absent (1) (after Brochu, 1997b [59]).

Brochu (1999) recognised the presence of a 'V' shaped process of the splenial between the angular and coronoid, which is present in extant crocodylids, *Gavialis gangeticus*, and *Tomistoma schlegelii* (Fig. 3.116A–B), but absent in most alligatorines, (e.g. *Alligator mississippiensis* [Fig. 3.116F] and *Alligator mcgrewi* [Fig. 3.116C]), and all extant caimanines, e.g. *Caiman latirostris* (Fig. 3.116G). Here this process is recognised in a few alligatorines, including *Alligator sinensis* (USNM 292078; Cong et al., 1998, fig.47C) and *Alligator prenasalis* (YPM PU 14063), which were previously scored as absent and unknown for this feature, respectively. The condition is unknown in the outgroup, but at least one non-crocodylian eusuchian, *Agaresuchus fontisensis*, appears to exhibit the process (Narváez et al., 2016, fig.4C), suggesting this is the plesiomorphic condition in Crocodylia.

259. Foramen intermandibularis medius (FIM), anteroposterior length relative to foramen intermandibularis caudalis (FIC): short, less than 25% FIC length (0); long, equal to or greater than 25% FIC length (1) (new character, based on personal observations).

In most eusuchians, the FIM is very small, perforating the coronoid or the splenial-coronoid suture (see Character 260). Uniquely in *Crocodylus acutus* and *Crocodylus intermedius*, this foramen is highly enlarged, such that it is greater than 25% the anteroposterior length of the FIC (Fig. 3.116D). The same condition is also present (and scored as such) in *Stangerochampsa mccabei*, although in this species this appears to be a result of reduction in size of the FIC, rather than enlargement of the FIM (Wu et al., 1996, fig.2B).

260. Coronoid, position of foramen intermandibularis medius (FIM) (at maturity): on coronoid-splenial suture (0); entirely within coronoid (1) (after Norell, 1988 [12]; Brochu, 1997b [46]).

Where preserved, the FIM is positioned on the anterior sutural contact between the coronoid and splenial in most eusuchians (Fig. 3.116A–B, D–F). By contrast, this foramen is completely situated within the coronoid in extant *Caiman*, *Melanosuchus* (Fig. 3.116G–H) and *Purussaurus neivensis* (USNM 10889). Brochu (1999) considered the FIM to be lost at maturity in both *Paleosuchus* species, which was captured in an additional character state (46-2 therein). Nevertheless, he noted that a foramen does occur on the coronoid, but because its position and form were considered different to the FIM, it was tentatively treated as an independent structure. Accordingly, the presence or absence of this foramen was characterised in a separate character (Brochu, 1999: [56]). If the coronoid foramen of *Paleosuchus* is not the FIM, one would expect to see two foramina at some point in ontogeny. Hatchling *Paleosuchus* specimens were not available for study here, but in two juvenile specimens (AMNH 93812, 66391) only one foramen occurs on the coronoid. Furthermore, the position of the foramen in these specimens (and indeed that figured in a more mature specimen by Brochu [1999, fig.59]) does

not appear notably different to the FIM of other caimanines (Fig. 3.116I). These observations do not disprove the independence of these foramina; however, this could be tested by comparing a series of *Paleosuchus* specimens of different ontogenetic stages. Until then, the simplest explanation is that the perforation of the coronoid in *Paleosuchus* is the FIM at all ontogenetic stages, and it is treated as such here. As a result, I do not include Character 56 of Brochu (1999).

261. Coronoid, anterior extent relative to level of anterior margin of foramen intermandibularis caudalis (FIC): anterior (0); at the same level or posterior (1) (after Jouve et al., 2015 [228]; Lee & Yates, 2018 [194]).

    This condition is difficult to assess in most fossil taxa because of poor preservation of the coronoid. The coronoid is positioned posterior to the level of the FIC (261-1) in all extant crocodylids, *Voay* (NHMUK R36686)*, Mekosuchus* (QM F31053, MNHN NCP 06), and *Melanosuchus niger* (Fig. 3.116H). By contrast, the coronoid is at the same level or anterior to the FIC in *Lohuecosuchus* (Narváez et al., 2015, fig.4D), *Agaresuchus* (Narváez et al., 2016, fig.4D), most extant alligatorids (Fig. 3.116C, F, G), *Gavialis gangeticus* (Fig. 3.116A), *Maomingosuchus petrolica* (Shan et al., 2017, fig.7C), and *Tomistoma schlegelii* (Fig. 3.116B).

262. Coronoid, orientation of dorsal profile: inclined anteriorly across entire length (0); horizontal towards posterior end (1) (after Brochu, 1997b [54]).

    The coronoid has two posteriorly directed processes, one dorsal and one ventral (Brochu, 1999). In all eusuchians (where known), the anterodorsal edge of the dorsal process is inclined anteriorly (Fig. 3.116). However, differences occur in the posterior extent of the dorsal process, as well as its orientation. Commonly, the dorsal process has a long posterior extension, which tends to level off to become horizontal (262-1). In this case, the dorsal process almost reaches the level of the posterior extent of the ventral process. This condition occurs in all extant crocodylids and *Alligator* (Fig. 3.116C–F). By contrast, the dorsal process is anteroposteriorly shorter in some caimanines, and the dorsal profile is inclined across its entire length (262-0) (Fig. 3.116G). Both *Gavialis gangeticus* and *Tomistoma schlegelii* have distinct morphologies that do not fit easily into either state. In *Gavialis gangeticus*, the dorsal process is strongly truncated posteriorly, such that it can appear absent altogether (Fig. 3.116A). In *Tomistoma schlegelii* there is some truncation of the dorsal process, but it levels off at its posteriormost extent (Fig. 3.116B) similar to crocodylids. No other taxa in this dataset share these conditions, rendering a new character or character states uninformative. Since the condition in these taxa is more reminiscent of caimanines, they are provisionally scored with the plesiomorphic condition, following previous authors (e.g. Brochu, 1999).

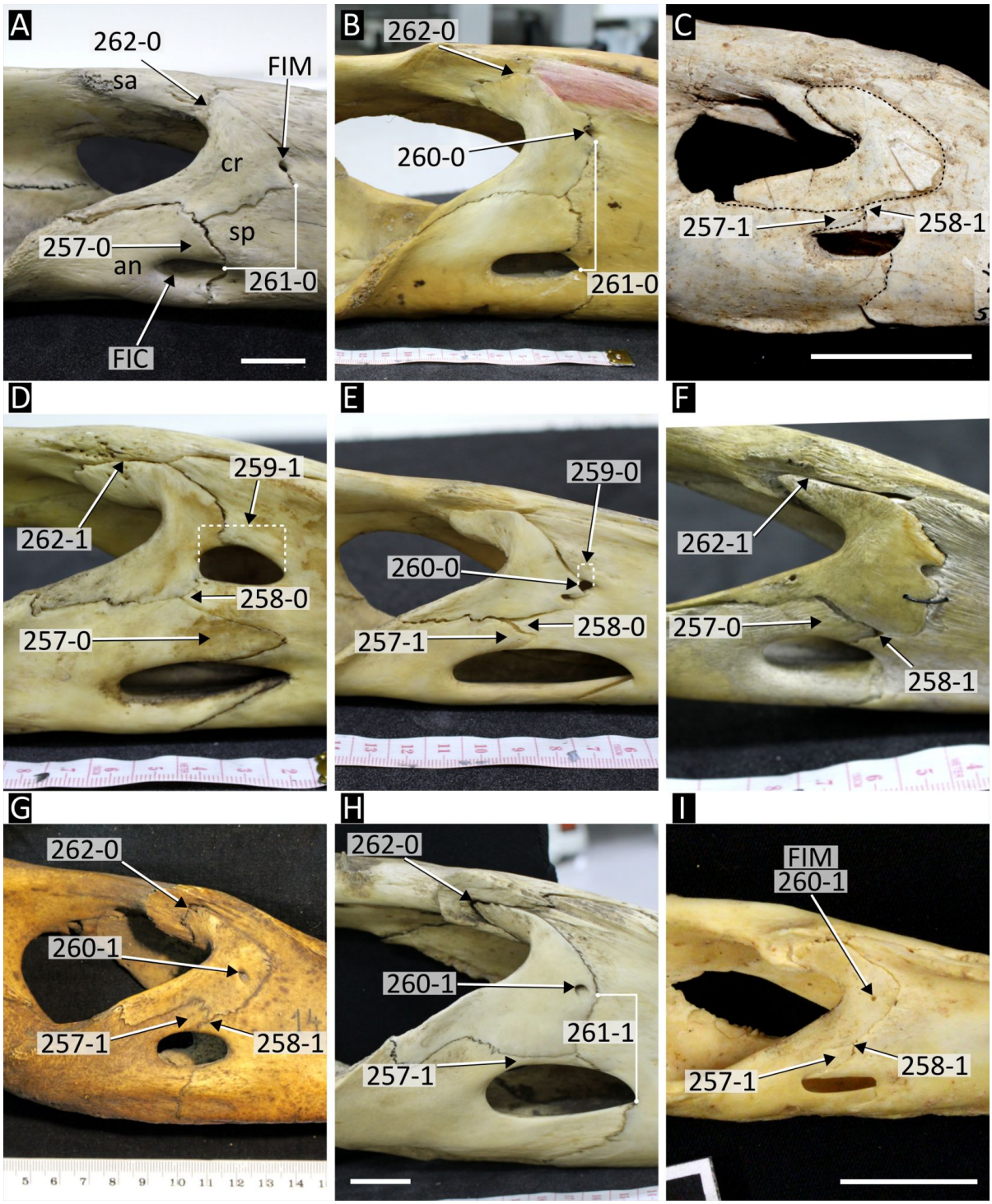



Figure 3.116: Medial view of the left posterior mandibular ramus. **A**, *Gavialis gangeticus* (NHMUK uncatalogued); **B**, *Tomistoma schlegelii* (NHMUK 1894.2.21.1); **C**, *Alligator mcgrewi* (AMNH FAM 8700), **D**, *Crocodylus intermedius* (NHMUK 1851.8.25.29); **E**, *Mecistops cataphractus* (62.6.30.8); **F**, *Alligator sinensis* (NHMUK X184); **G**, *Caiman latirostris* (MACN V 1420); **H**, *Melanosuchus niger* (45.8.25.125); **I**, *Paleosuchus palpebrosus* (AMNH 93812). Abbreviations: **an**, angular; **cr**, coronoid; **FIC**, foramen intermandibularis caudalis; **FIM**, foramen intermandibularis medius; **sp**, splenial; **sa**, surangular. Scale bars A, C, H, I = 2 cm, all other scale bars = cm.

263. Coronoid, prominent medioventral lamina extending over inner (medial) surface of Meckelian fossa: present (0); absent (1) (after Brochu, 1997b [55]).

The anatomical meaning of this character follows that described and illustrated by Brochu (1999, fig.47D–F). In most eusuchians (where known), the coronoid has a ventral process that laps over the inner surface of the Meckelian fossa (63-0). Among extant crocodylians, this occurs in crocodylids and *Alligator*, but not in caimanines (263-1).

### 3.4.3 Axial column

264. Proatlas, acute anterior process: present, anterolateral margin of proatlas prominently concave (0); absent, anterior margin of proatlas straight or convex (1) (after Brochu, 1997b [10]).

The proatlas is one of the most poorly preserved elements of the skeleton in Eusuchia; indeed, it was not even possible to examine it in all extant crocodylians for this study. Nevertheless, based on the sample of crocodylians examined, inconsistencies were observed in exisitng characters delimiting the proatlas morphology. Brochu (1999) and all subsequent iterations of this dataset have discretised the morphology of the proatlas into two characters. The first (Brochu, 1997b:[C2]) describes the overall morphology as either 'boomerang'-shaped (0), 'strap'-shaped (1), or massive and 'block'-shaped (2). The second (Brochu, 1997b:[C10]) described the presence or absence of an anterior process, which was argued as being independent of the first character. The distinction between taxa scored for each of the states of the first of these characters in earlier studies is not always apparent, nor was the proatlas morphology consistent within taxa scored for the same state, as also noted by Sookias (2020). For example, whereas *Crocodylus rhombifer* (Fig. 3.117G) and *Crocodylus acutus* (Fig. 3.117H) are scored as having boomerang-shaped proatlases, *Crocodylus porosus* (Fig. 3.117D) is scored as having a strap-shaped proatlas (Brochu, 2007). However, these taxa do not appear notably different. By contrast, the proatlases of taxa such as *Alligator* (Fig. 3.117B–C) and *Diplocynodon* (Fig. 3.117A), which are also scored for the boomerang-shaped condition, appear completely different to those *Crocodylus* species. This is principally due to a prominent anterior process in these taxa. Furthermore, although the proatlases of *Tomistoma schlegelii* (Fig. 3.117E) and *Gavialis gangeticus* (Fig. 3.117F) match their description of being "massive and block-shaped" (Brochu, 1997b), the distinction between this and the condition of several *Crocodylus* species is very subtle. Based on these observations, Character 2 of Brochu (1997b) is excluded here, and the morphology of the proatlas is characterised only by the presence or absence of a prominent anterior process. The definition of a process can be subjective, as all proatlases taper anteriorly to a degree. Here, an anterior process is considered present when the anterolateral margins of the proatlas are concave. This is most prominently expressed in *Diplocynodon* (Fig. 3.117A) and *Paleosuchus*, but it also occurs in *Alligator mississippiensis* (Fig. 3.117C). By

contrast, *Gavialis* (Fig. 3.118F), *Tomistoma* (Fig. 3.117E), and all *Crocodylus* species (Fig. 3.117G–H) examined here, are considered to lack this process. Among fossil crocodylians, *Borealosuchus formidabilis* (Erickson, 1976, fig.14) and *Asiatosuchus germanicus* (HLMD Me 3092) also lack the anterior process.

265. Proatlas, dorsal keel: present (0); absent (1) (after Brochu, 1997b [17]).

Brochu (1999) noted that the proatlas of most crocodylians exhibits either a low dorsal midline keel, or lack a keel altogether. By contrast, the keel is very prominent in some crocodylians, e.g. *Gavialis gangeticus* (Fig. 3.117F), *Diplocynodon* (Fig. 3.117A), and *Brachychampsa* (UCMP 133901). Brochu (1997b) used a binary state character in which only a prominent keel was considered as 'present'. Here, the presence of a midline keel is recognised regardless of size. Consequently, many more taxa are scored for the plesiomorphic state than in the dataset of Brochu (1999), including several *Crocodylus* species. An examination of later iterations of that dataset (e.g. Brochu, 2007a) reveal a similar basis for character state delimitation was used, with most *Crocodylus* species scored as possessing a dorsal keel.

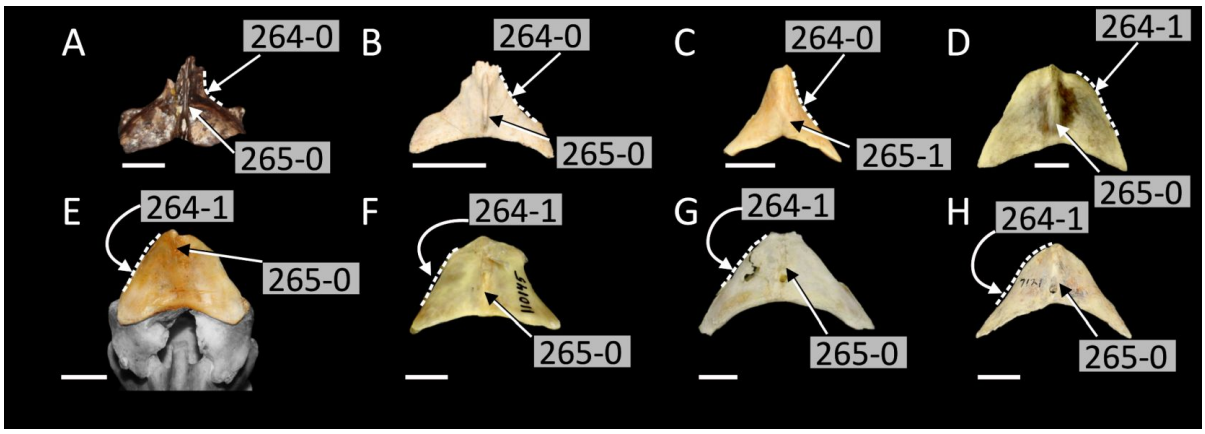



Figure 3.117: Morphology of the proatlas. **A**, *Diplocynodon hantoniensis* (NHMUK OR 30289); **B**, *Alligator mcgrewi* (AMNH FAM 8700); **C**, *Alligator mississippiensis* (AMNH 71621); **D**, *Crocodylus porosus* (NHMUK uncatalogued); **E**, *Tomistoma schlegelii* (AMNH 113078); **F**, *Gavialis gangeticus* (AMNH 110145); **G**, *Crocodylus rhombifer* (AMNH R154087); **H**, *Crocodylus acutus* (AMNH 7121). All scale bars = 1 cm.

266. Atlas intercentrum, shape in lateral view: wedge-shaped (0); plate-shaped (1) (after Clark, 1994 [89]; Brochu, 1997b [5]).

The presence of a flattened, plate-shaped atlantal intercentrum (Fig. 3.118A–B) has consistently been recovered as an unambiguous synapomorphy of Globidonta (e.g. Brochu, 1999), i.e. crown group Alligatoridae and a few stemward alligatoroid taxa, e.g. *Brachychampsa montana* (UCMP 133901). By contrast, 'basal' alligatoroids such as *Diplocynodon* (all species, where known) have a distinctive, wedge-shaped atlantal intercentrum (Fig. 3.118D–E) as is the case in most non-alligatoroid

crocodylians. This includes *Gavialis gangeticus* (Fig. 3.118E), *Tomistoma schlegelii* (AMNH 113078), and all extant crocodylids (Fig. 3.118A). The same condition has been noted in all members of *Borealosuchus* (Brochu et al. 2012), e.g. *B. formidabilis* (Erickson, 1976, fig.13B) (Erickson, 1976, fig.13B). By contrast, the alligatorid condition is newly recognised in *Borealosuchus sternbergii* (UCMP 134470, Fig. 3.118C).

267. Atlantal rib, process on dorsal margin: absent (0); present (1) (Brochu, 1997b [14]).

    Brochu (1999) identified a prominent dorsal process on the atlantal ribs of most extant alligatorids, *Brachychampsa*, and *Toyotamaphimeia* (Fig. 3.118H), contrasting with *Gavialis gangeticus*, *Tomistoma schlegelii*, most extant crocodylids and *Borealosuchus* (Fig. 3.118F). The anatomical meaning and distribution of this feature is consistent with earlier studies (e.g. Brochu et al., 2012; Cidade et al., 2017).

268. Atlantal rib, thin medial lamina at proximal end: absent (0); present (1) (after Brochu, 1997b [16]).

269. Atlantal rib, proximal articular facet for opposing atlantal rib: absent (0); present (1) (Brochu, 1997b [15]).

    Characters 268 and 269 describe two similar, but independent processes that occur on the anteromedial end of the atlantal rib. Character 268 describes a medial lamina that serves as the attachment point of the atlantodental ligament, which connects the paired atlantal ribs (Fig. 3.118H) (Brochu, 1999). According to Brochu (1999), and as scored therein, among extant crocodylians this process only occurs in caimanines. Indeed, this process is observed in *Caiman* (e.g. *Caiman yacare*, AMNH 97300), *Paleosuchus* (e.g. AMNH 66391) and *Melanosuchus niger* (AMNH 97325). Nevertheless, the only caimanine scored for this condition in all subsequent iterations of the dataset of Brochu (1999) is *Paleosuchus* (e.g. Brochu, 2011; Brochu et al. 2012; Salas-Gismondi et al., 2015; Cidade et al., 2017). This seems likely to be a typographical error that has been carried forward, since the figures in Brochu (1999, fig.28C), clearly show that these medial laminae are present in all extant caimanines. Scores are further modified here, as this process is also recognised on the atlantal ribs of *Alligator mississippiensis* (Fig. 3.118H), *Brachychampsa montana* (UCMP 133901), and *Borealosuchus sternbergii* (UCMP 134470). Character 269 describes the development of anteroposteriorly long atlantal articular facets, a condition exclusively known in *Paleosuchus* (Brochu, 1999) (Fig. 3.118I).

270. Odontoid process: mediolateral width across axial rib facets, relative to mediolateral width across axial tubercula facets: narrower (0); subequal (1) (after Ijima & Kobayashi, 2019 [244]).

    Iijima and Kobayashi (2019, fig.S1) illustrated differences in morphology of the odontoid process among crocodylians, noting that the mediolateral width across the ventral facets for the axial rib capitula is notably narrower than that across the dorsal facets for the axial rib tubercula in *Bernissartia*

*fagesii* and all extant alligatorids (Fig. 3.118J). By contrast, the facets are subequal in width in all extant crocodylids (except *Osteolaemus*), *Gavialis gangeticus*, and *Tomistoma schlegelii* (Fig. 3.118K). The plesiomorphic condition is recognised in some additional alligatorids including *Alligator mcgrewi* and *Purussaurus neivensis*. By contrast, the 'basal' alligatoroid *Diplocynodon* exhibits the derived condition, e.g. *D. hantoniensis* (Chapter 2, Fig. 2.13), and *D. darwini* (Ludwig, 1877, plate 3, 13d).

271. Axial rib, tuberculum shape: short and broad, equal in size to capitulum (0); long and acute, narrower than capitulum (1) (after Brochu, 1997b [20]).

Following Brochu (1997b), two distinctive morphologies of the axial rib tuberculum can be observed in crocodylians (Fig. 3.118L–R); however, the taxa assigned to each state in this study contrasts with scores in earlier studies (e.g. Brochu, 1999; Brochu et al., 2012; Salas-Gismondi et al., 2015). Whereas the scores herein concur for *Gavialis gangeticus*, in which the axial rib tuberculum is short and broad, approximately equal in dimensions to the capitulum (Fig. 3.118M), they differ in that I also regard this condition as characterising *Crocodylus* (e.g. *C. acutus* [Fig. 3.118O], *C. rhombifer* [Fig. 3.118L], *C. porosus* [Fig. 3.118Q]), *Tomistoma schlegelii* (AMNH 113078), and *Osteolaemus tetraspis* (AMNH 69057). In the derived character state, the proximal end of the axial rib forms a broad capitulum and a long, narrower tuberculum. This condition is found in all extant alligatorids (e.g. *Alligator mississippiensis* [Fig. 3.118N] and *Caiman yacare* [Fig. 3.118P]) as also scored in previous analyses.

272. Axial rib, tuberculum, contact with axial diapophysis: absent, or occurs late in ontogeny (0); present early in ontogeny (1) (Brochu, 1997b [21]).

The definition and scoring of this character is consistent with earlier studies. As described and illustrated by Brochu (1999, fig.30), contact between the axial rib tuberculum and the axial diapophysis can be observed in all extant alligatorids at an early ontogenetic stage (Fig. 3.119C), but is absent in crocodylids, *Gavialis gangeticus* (AMNH 110145), *Tomistoma schlegelii* (AMNH 113078), *Borealosuchus formidabilis* (Erickson, 1976) and *Brachychampsa montana* (Fig. 3.119B). For a taxon to be scored for the derived character state, a juvenile specimen is ideally required. However, contact between the axial rib and diapophysis was observed in (probably) mature specimens of two fossil taxa: *Mourasuchus arendsi* (Cidade et al., 2020b, fig.8A) and *Purussaurus neivensis* (UCMP 39657). These taxa are scored for the derived condition here pending new data on juvenile individuals that demonstrates such contact was absent early in ontogeny.

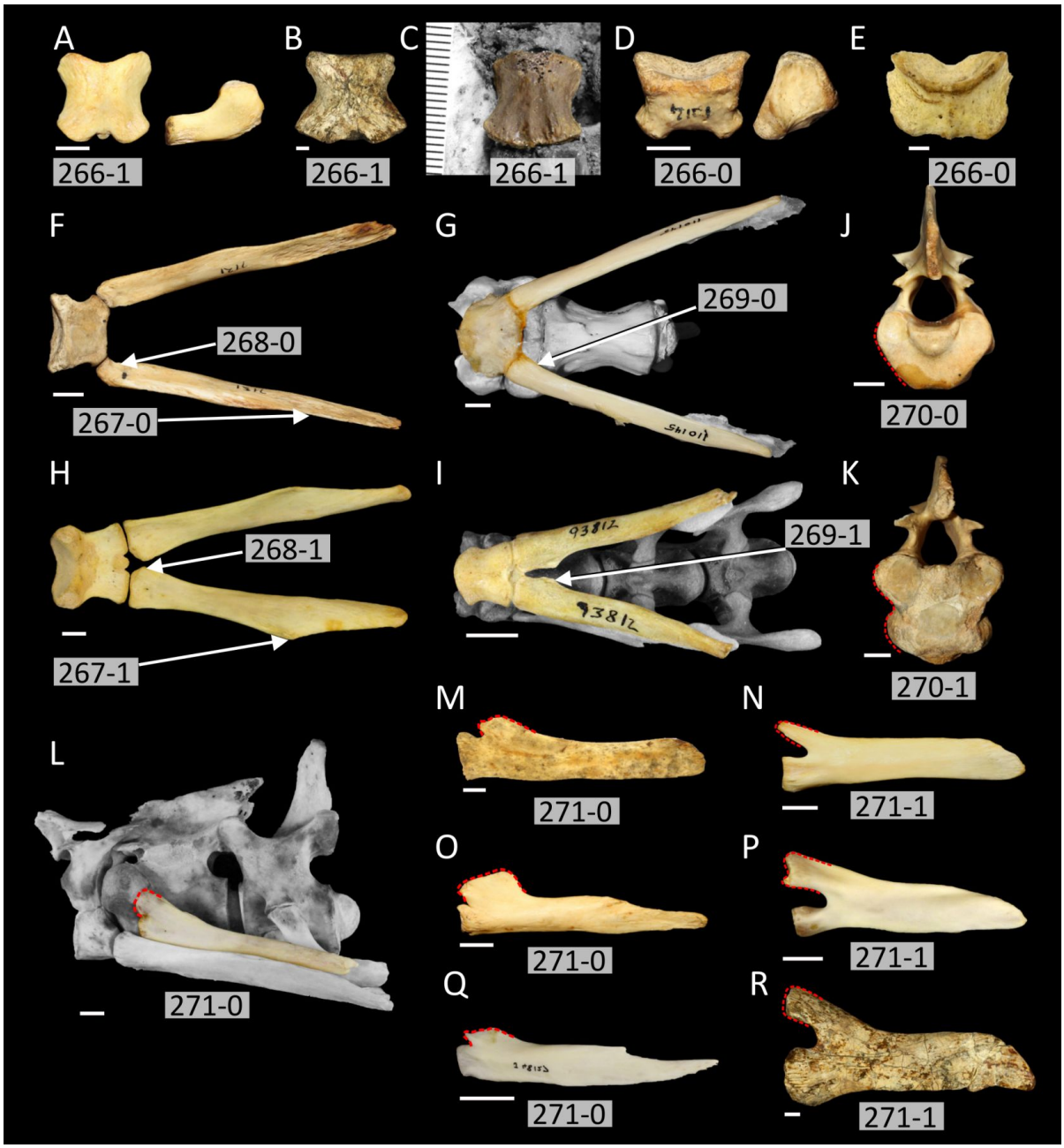



Figure 3.118: Morphology of the atlas-axis complex. **A**–**E**, atlantal intercentrum (all in ventral view except A and D, which include right lateral views): **A**, *Alligator mississippiensis* (AMNH 71621); **B**, *Purussaurus neivensis* (UCMP 39657); **C**, *Borealosuchus sternbergii* (UCMP 134470); **D**, *Crocodylus acutus* (AMNH 7121); **E**, *Gavialis gangeticus* (UMZC R 5783); **F**–**I**, atlantal ribs of: **G**, *Crocodylus acutus* (AMNH 7121, dorsal view); **G**, *Gavialis gangeticus* (AMNH 110145, ventral view); **H**, *Alligator mississippiensis* (AMNH 71621, dorsal view); **I**, *Paleosuchus palpebrosus* (AMNH 93812, ventral view); **J**–**K**, odontoid process in anterior view: **J**, *Caiman yacare* (AMNH 97300); **K**, *Crocodylus acutus* (AMNH 7121); **L**, atlas-axis complex of *Crocodylus rhombifer*, left lateral view highlighting the axial rib (AMNH R154087); **M**–**R**, lateral view of the left axial rib: **M**, *Gavialis gangeticus* (UMZC R 5783); **N**, *Alligator mississippiensis* (AMNH 71621); **O**, *Crocodylus acutus* (AMNH 7121); **P**, *Caiman yacare* (AMNH 97300); **Q**, *Crocodylus porosus* (QM J48127, digitally reversed); **R**, *Purussaurus neivensis* (UCMP 39657). All scale bars = 1 cm.

273. Axis, neural spine, anterior half of dorsal margin in lateral view (at maturity): horizontal (0); slopes such that it faces anterodorsally (1) (after Brochu, 1997b [11]).

274. Axis, neural spine, posterior half: dorsally inflected to form crest (0); continuous with anterior half, not crested (1) (after Brochu, 1997b [12]).

275. Axis, neural spine, shape of distal end: dorsoventrally thick (0); dorsoventrally thin, rod-like (1) (after Brochu, 1997b [3]).

Characters 273–275 describe subtle differences across regions of the axial neural spine. These characters are respectively based on characters 11, 12, and 3 in Brochu (1997b), all of which were not considered robust by Sookias (2020). Inconsistencies in the character scores of some taxa were similarly observed here; however, these characters are retained, with modifications to wording and character scores. Character 273 describes the orientation of the anterior half of the dorsal margin of the the axial neural spine. According to Brochu (1999), the anterior half is horizontal early in ontogeny in all extant crocodylians, but becomes anteriorly inclined at maturity in some taxa, e.g. *Caiman* and *Melanosuchus* (Fig. 3.119C). This broadly matches observations made in this study. A sloping anterior half of the neural spine characterises all extant jacareans, *Borealosuchus*, *Boverisuchus vorax*, and *Alligator mcgrewi* (AMNH FAM 8700). This condition contrasts with that exhibited by *Diplocynodon* (Fig. 3.119A) and *Gavialis gangeticus* (Fig. 3.119F), in which the anterior half of the spine is horizontal. The distinction between anterior and posterior portions of the axial neural spine appears to be significant, as regardless of the orientation of the anterior half, the posterior half can take on a range of morphologies. These are captured in characters 274 and 275. Character 274 was originally described in terms of the presence or absence of a posterior 'crest'. Based on character scores in Brochu et al. (2012), a crest occurs in all extant *Caiman* species, extant crocodylids, *Tomistoma schlegelii*, and *Gavialis gangeticus*. The wording of the original character is ambiguous since the posterior tip of the axial neural spine could be considered crest-like in most crocodylians. Herein, the crested condition only applies to taxa with a concavity in the dorsal outline of the neural spine, such that spine is dorsally inflected posteriorly. This condition is exemplified by *Purussaurus neivensis* (Fig. 3.119C), *Brachychampsa montana* (Fig. 3.119B), contrasting with the uncrested neural spines of *Diplocynodon hantoniensis* (Fig. 3.119A) and *Caiman* (contra Brochu, 1999) (Fig. 3.119C). Character 275 originally described the posterior half of the axial neural spine as either "wide" or "narrow" (Brochu, 1997b, character 3). This wording was considered ambiguous, as it is not clear whether this neural spine dimension should be considered as mediolateral or dorsoventral. Here, the derived character state applies to taxa in which the distal end of the neural spine forms a dorsoventrally narrow, rod-like process. This is distinct from the dorsally inflected (crested) condition described in Character 274. The rod-like condition (275-1) is exemplified by *Gavialis gangeticus* (Fig. 3.119F), *Eosuchus*

*minor* (Fig. 3.119G) and most extant crocodylids, e.g. *C. rhombifer* (Fig. 3.118T).

276. Axis, lateral process (diapophysis) on neural arch lateral margin: absent (0); present (1) (after Norell, 1989 [7]; Brochu, 1997b [4]).

    Among extant crocodylians, *Gavialis gangeticus* is the only species with an axial diapophysis (Baur, 1886; Norell, 1989) (Fig. 3.119F, J). The co-occurrence of this diapophysis in the non-crocodylian neosuchian, *Bernissartia fagesii*, was considered as evidence of the sister relationship of *Gavialis gangeticus* to all other crocodylians (Norell, 1989; Norell & Clark, 1990). Where observed in *Gavialis gangeticus*, this process tends to be a very low, anteroposteriorly orientated crest, positioned dorsal to the neurocentral suture (Fig. 3.119J). Among fossil crocodylians, an axial diapophysis has traditionally only been recognised in "gavialoids", e.g. *Eosuchus* (Fig. 3.119K–L) and *Thoracosaurus* (Brochu et al., 2012, character scores therein). However, the diapophysis is also present in at least two "tomistomines": *Toyotamaphimeia* and *Penghusuchus* (Iijima & Kobayashi, 2019).

277. Axis, hypapophysis position: located towards centre of centrum (0); toward anterior end of centrum (1) (Brochu, 1997b [6]).

    In most crocodylians, the axial hypapophysis is located towards the anterior end of the centrum (Fig. 3.119E). Brochu (1999) recognised a posteriorly shifted hypapophysis exclusively in *Diplocynodon*, such that it occurs around the anteroposterior mid-length of the centrum (Fig. 3.119A). This is similarly recognised here, but several additional crocodylians exhibit the derived condition, e.g. *Caiman yacare* (AMNH 97300), *Alligator sinensis* (USNM 292078), *Alligator mcgrewi* (AMNH FAM 8700), and *Borealosuchus formidabilis* (Erickson, 1976, fig.13B).

278. Axis, hypapophysis shape: un-forked (0); forked (1) (after Brochu, 1997b [19]).

    Uniquely among extant crocodylians, *Gavialis gangeticus* exhibits a forked axial hypapophysis (Fig. 3.119N), a condition shared by several fossil "gavialoids", e.g. *Thoracosaurus* (Brochu, 2004a) and *Eosochus minor* (USNM 181577) (but not *Eosuchus lerichei* [IRScNB R49]) and some "tomistomines", e.g. *Toyotamaphimeia* and *Penghusuchus* (Iijima & Kobayashi, 2019). By contrast, *Bernissartia fagesii* and all other crocodylians exhibit a single, un-forked hypapophysis (Fig. 3.119M).

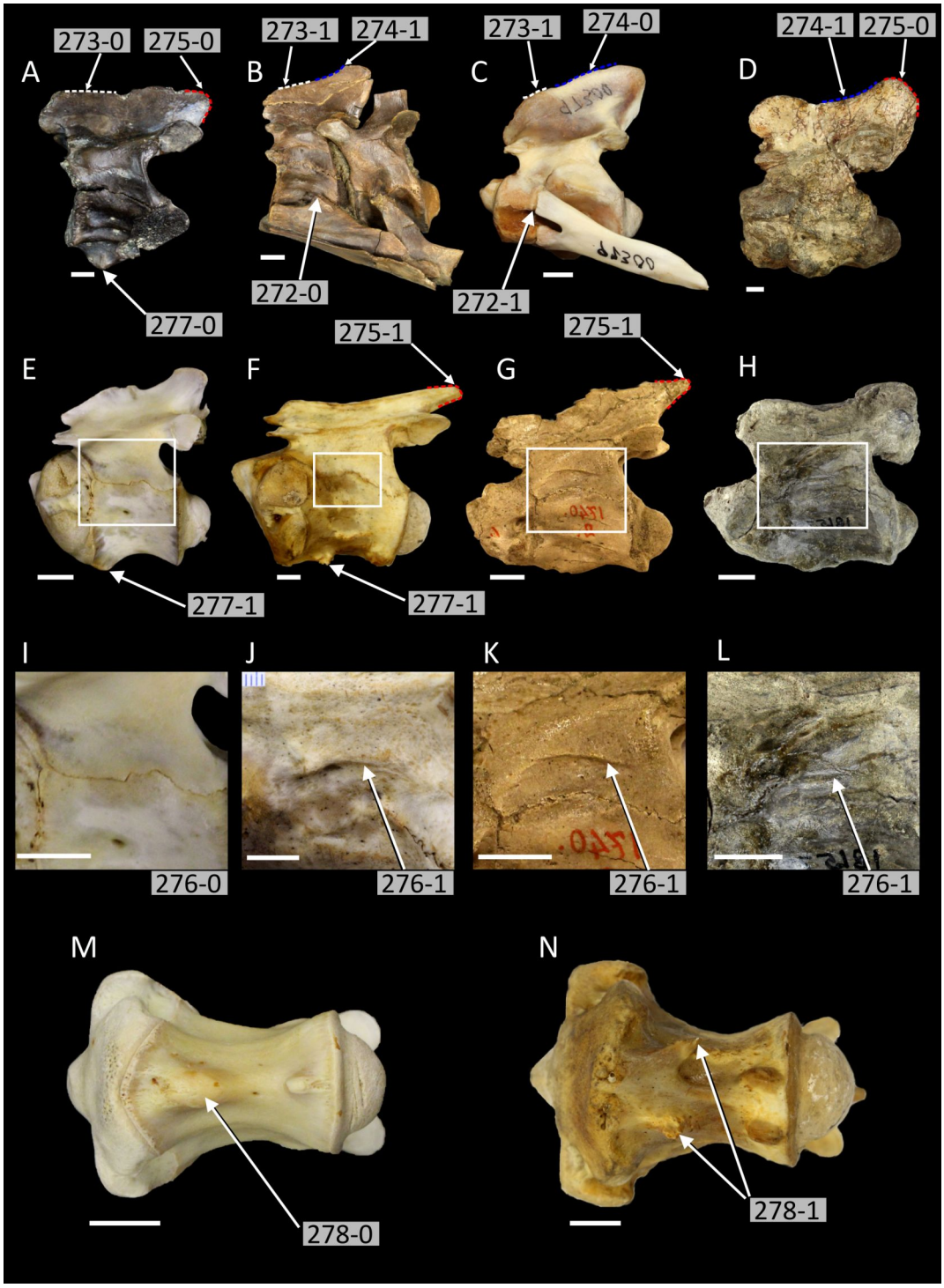



Figure 3.119: Morphology of the axis in selected crocodylian taxa. **A**–**H**, left lateral view of the axis in: **A**, *Diplocynodon hantoniensis* (NHMUK uncatalogued, digitally reversed); **B**, *Brachychampsa montana* (UCMP 133901); **C**, *Caiman yacare* (AMNH 97300, digitally reversed); **D**, *Purussaurus neivensis* (UCMP 39657, digitally reversed); **E**, *Crocodylus porosus* (QM J48127); **F**, *Gavialis gangeticus* (UMZC R 5783); **G**, *Eosuchus lerichei* (IRScNB R 1740, digitally reversed); **H**, *Eosuchus minor* (USNM 181577, digitally reversed); **I**–**L** enlargement of the regions highlighted in **E**–**H** respectively; **M**, *Crocodylus johnstoni*, ventral view (QM J58446); **N**, *Gavialis gangeticus*, ventral view (UMZC R 5783). All scale bars = 1 cm.

279. Prominent cervical hypapophyses: present (0); absent (1) (after Norell, 1989 [12]; Norell & Clark, 1990 [11]; Clark, 1994 [92]; Brochu, 1997b [8]).

    Norell (1989) noted that *Gavialis gangeticus* lacks hypapophyses on its cervical vertebrae, unlike all other extant crocodylians, which have prominent cervical hypapophyses. The absence of prominent cervical hypapophyses is recognised in *Bernissartia fagesii* (Norell & Clark, 1990), *Borealosuchus* (Brochu et al., 2012), some "gavialoids" (e.g. *Eosuchus minor* [Fig. 3.120B] and *Thoracosaurus*), and also in the "tomistomine" *Toyotamaphimeia machikanensis* (Iijima & Kobayashi, 2019).

280. First postaxial vertebra (Cv3), anteroposterior length at the distal end of the neural spine: long, greater than or equal to half the length of the non-condylar centrum (0); short, dorsal tip acute and less than half the length of the non-condylar centrum (1) (after Brochu, 1997b [9]).

    The neural spine of the first postaxial vertebra (third cervical vertebrae) in *Bernissartia fagesii* (IRScNB 1538), *Borealosuchus*, and some caimanines is anteroposteriorly long and often square shaped (280-0) (Fig. 3.120C). By contrast the neural spine is anteroposteriorly short (280-1) and often acute in most extant crocodylids (Fig. 3.120A), *Gavialis gangeticus* (Fig. 3.120G), and "tomistomines" (e.g. *Tomistoma schlegelii* [AMNH 113078], *Toyotamaphimeia*, and *Penghusuchus* [Iijima and Kobayashi, 2019]).

281. Cervical centra: amphicoelous (both articular surfaces concave) (0); procoelous (anterior articular surface concave, posterior articular surface convex) (1) (after Norell & Clark, 1990 [8]; Clark, 1994 [92]; Brochu, 1997 [18]; Brochu et al., 2012 [21]).

    As noted by Norell and Clark (1990), the cervical centra are plesiomorphically amphicoelous in neosuchians (Fig. 3.120D), e.g. *Bernissartia fagesii* (IRScNB 1538), contrasting with the procoelous cervical centra of eusuchians (Fig. 3.120C). The morphology of the dorsal and caudal centra is discretised separately (Characters 285 and 292) as both can vary independently of that of the cervical vertebrae.

282. Posterior cervical vertebrae (C7–C9), anterior extent of hypapophyses (C7–C9): level with, or anterior to the level of anterior margin of the prezygapophyses (0); posterior to the level of anterior margin of prezygapophyses (1) (after Iijima & Kobayashi, 2019 [246]).

    Iijima and Kobayashi (2019, character 246) note that the posterior cervical hypapophyses of all extant alligatorids project anteroventrally "well beyond" the level of the centrum (Fig. 3.120F). In all eusuchians examined here, the posterior cervical hypapophyses are anteriorly hooked to a degree, and can still extend towards and slightly beyond the centrum margin, e.g. *Crocodylus acutus* (Fig. 3.120E), *Gavialis gangeticus* (Fig. 3.120G); nevertheless, they never reach the same anterior extent

as in alligatorids. To capture this difference, here the anterior hypapophyseal extent is measured relative to the anterior extent of the prezygapophyseal facets. These provide a more anteriorly positioned landmark for measuring hypapophyseal extent, removing the need for subjective terminology such as "well-beyond". In addition to extant alligatorids, strongly anteroventrally directed hypapophyses are newly recognised in *Alligator mcgrewi* (Fig. 3.120H) and *Purussaurus neivensis* (UCMP 39657).

283. Cervical rib 8, length in proportion to cervical rib 9: long, greater than half the length of cervical rib 9 (0); short, equal to or less than half the length of cervical rib 9 (1) (after Iijima & Kobayashi, 2019 [247]).

Mook (1921c) noted that the $8^{th}$ cervical rib of extant *Crocodylus* and *Tomistoma schlegelii* is elongate, being similar in morphology to the $9^{th}$ cervical rib (described as the first dorsal rib therein) (Fig. 3.121A–B). By contrast, he noted that the $8^{th}$ cervical rib is shorter in *Alligator* (Fig. 3.121E) and *Caiman* (Fig. 3.121F). As later demonstrated by Iijima and Kobayashi (2019, fig.S2), *Gavialis gangeticus* also exhibits an elongated $8^{th}$ cervical rib, like crocodylids (Fig. 3.121C), whereas all extant alligatorids exhibit a shortened rib. This character does not necessarily require the preservation of the $9^{th}$ rib, as in both plesiomorphic and derived conditions, the morphology of the $8^{th}$ rib is distinct from any other rib. The shortened $8^{th}$ cervical rib of alligatorids can be distinguished from any of the preceding cervical ribs, in that the capitular and tubercular processes are parallel to the shaft of the rib (rather than perpendicular). Furthermore, the shaft is only slightly longer than the proximal articular processes, unlike any subsequent presacral ribs. Isolated $8^{th}$ cervical ribs in crocodylids, *Tomistoma* and *Gavialis* are very similar in appearance to the $9^{th}$ and subsequent dorsal ribs, yet they lack the prominent medial curvature of the shaft. The morphology of the $8^{th}$ cervical rib is poorly known in fossil crocodylians. For example in the dataset of Iijima and Kobayashi (2019) the condition was scored only in *Borealosuchus formidabilis* and *Toyotamaphimeia* (283-0 in both). The derived, short condition is additionally recognised in several fossil alligatoroids including *Alligator mcgrewi* (Fig. 3.121H), *Purussaurus neivensis* (Fig. 3.121I), and *Diplocynodon darwini* (Fig. 3.121J). By contrast, *Borealosuchus sternbergii* (UCMP 134470) and '*Crocodylus*' *affinis* (Fig. 3.121D) exhibit an elongate rib.

284. Hypapophyseal keels, posterior retention: until tenth postatlantal vertebra (Dv2) (0); eleventh postatlantal vertebra (Dv3) (1); twelfth postatlantal vertebra (Dv4) (2) (after Brochu, 1997b [7]) (ORDERED).

This character requires the consecutive preservation of the anteriormost dorsal vertebrae, and so is poorly known in fossil crocodylians. In *Bernissartia fagesii* (IRScNB 1538) (and no other taxon in this dataset), hypapophyses occur up to and including the $10^{th}$ postatlantal vertebra (dorsal vertebra 2) (284-0). In most extant crocodylians, hypapophyses occur up to the $11^{th}$ postatlantal vertebra (dorsal

vertebra 3) (284-1), e.g. *Alligator mississippiensis* (AMNH 71621), *Gavialis gangeticus* (UCMZ R5783), and *Tomistoma schlegelii* (AMNH 113078). In fewer taxa, the hypapophyses occur further posteriorly, up to the $12^{th}$ postatlantal vertebra (284-2), e.g. *Paleosuchus* (AMNH 97326), *Alligator sinensis* (USNM 292078) and *Diplocynodon hantoniensis* (Chapter 2, Fig. 2.15). Character states are re-organised relative to earlier studies as the character is newly ordered.

285. Dorsal centra: amphicoelous (0); procoelous (1) (after Norell & Clark, 1990 [10]; Clark, 1994 [93]).

    Where preserved procoelous dorsal centra occur in all taxa in this dataset, except *Bernissartia fagesii* (IRScNB 1538) and *Theriosuchus pusillus* (e.g. NHMUK 48216; see also Tennant et al., 2016:p.914), which exhibit amphicoelous dorsal centra.

286. Dorsal vertebrae, maximum mediolateral width across both transverse processes at vertebrae 7–10: equal to or greater than twice the equivalent width on DV1 (0); less than twice the equivalent width on DV1 (1) (after Iijima & Kobayashi, 2019 [248]).

287. Dorsal vertebrae, fusion of the diapophysis and parapophysis, occurrence: anterior to or on the $12^{th}$ dorsal vertebra (0); on the $13^{th}$ dorsal vertebra (1) (after Iijima & Kobayashi, 2019 [249]).

    Characters 286–287 were based on the observations of Iijima and Kubo (2019b) who recognised two currently autapomorphic features of *Gavialis gangeticus*. The first is that the maximum width across the transverse processes (usually around dorsal vertebrae 7–10) is approximately twice the width of that of the first dorsal vertebrae, contrasting with all other extant crocodylians (286-0). This requires serial measurements of dorsal vertebrae 1–10. Secondly, whereas the fusion of the parapophysis and diapophysis occurs anterior to or on the $12^{th}$ dorsal vertebra in most crocodylians, it occurs at the $13^{th}$ dorsal vertebra in *Gavialis gangeticus*. Given ongoing work revising *Gavialis* and closely related forms (e.g. Martin, 2019), these characters have been included here to aid future studies that might be able to incorporate more *Gavialis* OTUs, and that might demonstrate their wider distribution within the genus.

288. Presacral vertebrae, maximum mediolateral width across prezygapophyses: sub-equal throughout (0); increases posteriorly throughout presacral vertebrae (1) (after Iijima & Kobayashi, 2019 [250]).

    This character requires measurements of width across the prezygapophyses in all presacral vertebrae, and character scores were based on the observations of Iijima and Kobayashi (2019, fig.3b) and Iijima and Kubo (2019b). The width across the prezygapophyses appears very consistent across presacral vertebrae in *Gavialis gangeticus* and *Toyotamaphimeia*. By contrast, in all other extant crocodylians, as well as *Penghusuchus pani*, the width across the prezygapophyses increases posteriorly along the presacral vertebrae.

289. Sacral vertebra 1, anterior extent of sacral rib capitulum: anterior to tuberculum (visible in dorsal view) (0); at the same level as tuberculum (obscured in dorsal view) (after Brochu, 1997b [13]).

    In dorsal view, the anterior surface of the first sacral rib is visible in *Gavialis gangeticus* (Fig. 3.122C) and all extant alligatorids, e.g. *Alligator mississippiensis* (Fig. 3.122A) (289-0). This results from the more anterior position of the capitulum relative to the tuberculum. By contrast, the capitulum is obscured in dorsal view by the tuberculum in all extant crocodylids (289-1) (Fig. 3.122B). *Tomistoma schlegelii* was scored with the 'crocodylid' condition in most earlier datasets (e.g. Brochu et al., 2012; Narváez et al., 2016) but, as noted by Sookias (2020), it exhibits a dorsally exposed capitulum (Fig. 3.122D). Other "tomistomines" show variation in this feature. For example, whereas the sacral rib capitulum is dorsally exposed in *Penghusuchus* (Shan et al., 2009, fig.10a), it is concealed in *Toyotamaphimeia* (Kobayashi et al., 2006, fig.43B).

290. Sacral vertebra 2, posterior extent of ribs: extend beyond level of posterior extent of postzygapophyses (0); terminate level with or anterior to level of postzygapophyses (after Iijima & Kobayashi, 2019 [251]).

    Where known, in most eusuchians, the posterolateral tip of the second sacral rib extends posteriorly beyond the level of the postzygapophyses (Fig. 3.122A, B, D). By contrast, in *Gavialis gangeticus* (Fig. 3.122C) and *Bernissartia fagesii* (IRScNB 1538), the second sacral rib terminates notably further anteriorly, such that it does not exceed the posterior extent of the postzygapophyses. This character was modified from Iijima and Kobayashi (2019, character 251), who used the posterior end of the centrum as a marker point for the posterior extent of the sacral ribs; however, the sacral ribs extend beyond the posterior end of the centrum in all taxa in this dataset.

291. Caudal vertebra 1, centrum: opisthocoelous or procoelous (0); biconvex (1) (after Salisbury et al., 2006 [171]; Norell & Clark, 1990 [9]; Clark, 1994 [94]).

    In *Bernissartia fagesii* (IRScNB 1538) and most eusuchians, the centrum of the first caudal vertebra is biconvex. This contrasts with *Isisfordia duncanii*, which exhibits a procoelous first caudal centrum (Salisbury et al., 2006), and *Theriosuchus pusillus* (NHMUK 48216), in which the anteriormost caudal centra are opisthocoelous.

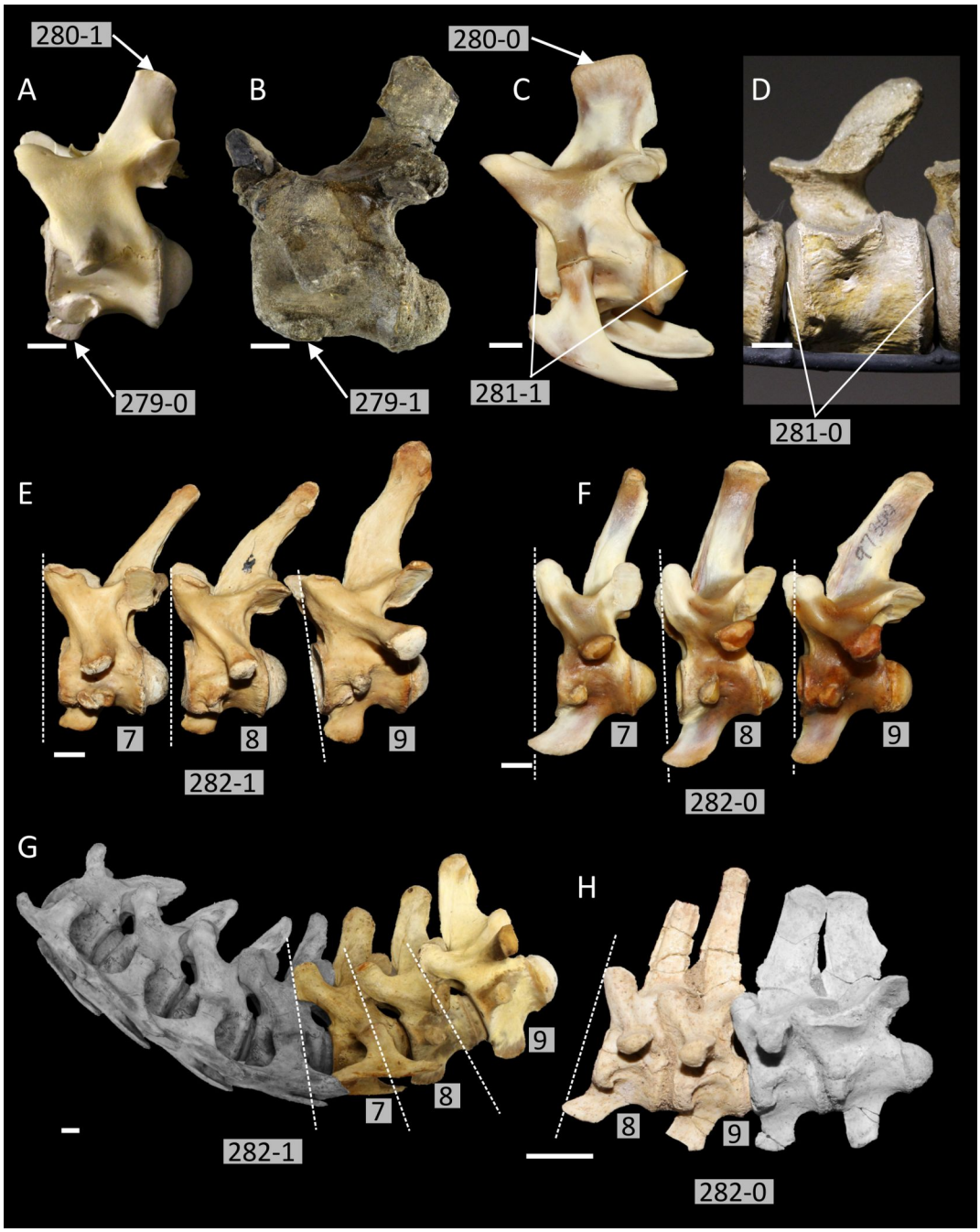



Figure 3.120: Morphology of the cervical vertebrae. **A–C**, $3^{rd}$ cervical vertebra (i.e. $1^{st}$ postaxial vertebra) in: **A**, *Crocodylus porosus* (QM J48127); **B**, *Eosuchus minor* (USNM 181577); **C**, *Caiman yacare* (AMNH 97300); **D**, *Champsosaurus lemoinei* (IRScNB 1582); **E–H**, posteriormost cervical vertebrae (7–9) of **E**, *Crocodylus acutus* (AMNH 7121); **F**, *Caiman yacare* (AMNH 97300); **G**, *Gavialis gangeticus* (UMCZ R5783); **H**, *Alligator mcgrewi* (AMNH FAM 8700). Numbers indicate position in cervical series. All scale bars = 1 cm.




Figure 3.121: Morphology of the cervical and dorsal ribs in selected crocodylians. All left ribs in anterior view except J (right rib). **A**, *Crocodylus acutus* (AMNH 7121); **B**, *Tomistoma schlegelii* (USNM 52972); **C**, *Gavialis gangeticus* (AMNH 110145); **D**, *'Crocodylus' affinis* (USNM 18171); **E**, *Alligator mississippiensis* (AMNH 71621); **F**, *Caiman yacare* (AMNH 97300); **G**, *Melanosuchus niger* (AMNH 97325); **H**, *Alligator mcgrewi* (AMNH FAM 8700, D1 and D2 digitally reversed); **I**, *Purussaurus neivensis* (UCMP 39657); **J**, *Diplocynodon darwini* (Ludwig, 1877: Plate 12, fig.1). All scale bars = 2 cm.

292. Caudal centra, posterior to first caudal vertebra: procoelous (0); amphicoelous or opisthocoelous (1) (after Norell & Clark, 1990 [9]; Clark, 1994 [94]; Salisbury et al., 2006 [171]; Pol et al., 2009 [94]).

In *Bernissartia fagesii* (IRScNB 1538) and most eusuchians, the caudal centra posterior to the first caudal vertebra are procoelous. By contrast, in *Shamosuchus djadochtaensis* (Pol et al., 2009) and *Theriosuchus pusillus* (NHMUK 48216), they are amphicoelous.

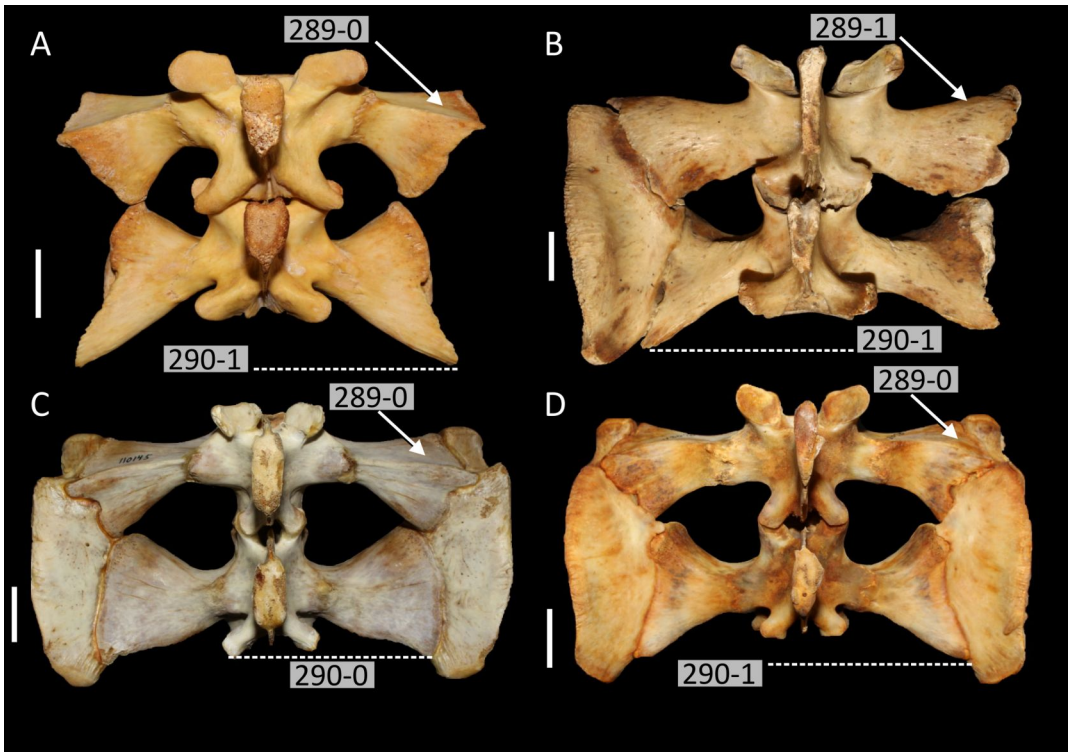



Figure 3.122: Dorsal view of the sacral vertebrae 1 (top) and 2 (bottom). **A**, *Alligator mississippiensis* (AMNH 71621); **B**, *Crocodylus acutus* (AMNH 7121); **C**, *Gavialis gangeticus* (AMNH 110145); **D**, *Tomistoma schlegelii* (AMNH 113078). All scale bars = 2 cm.

293. Caudal vertebrae, number with transverse processes: first 15 or fewer (0); 16 to 20 (1); 21 or more (2) (after Iijima & Kobayashi, 2019 [253]) (ORDERED).

In all extant crocodylians, the width across the vertebral transverse processes increases posteriorly through the vertebral column, reaching a maximum around dorsal vertebrae 7–9 (Iijima & Kubo, 2019b, fig.4). The width across the transverse processes then decreases through the remaining dorsal vertebrae, continuing through the anteriormost caudal vertebrae, until becoming lost in the posteriormost caudal vertebrae. Iijima and Kobayashi (2019) noted differences in the number of caudal vertebrae with transverse processes in extant crocodylians. In general, the transverse processes extend further posteriorly in extant alligatorids (293-1, 293-2) than in crocodylids, *Gavialis gangeticus*, and *Tomistoma schlegelii* (293-0). Three exceptionally preserved fossil taxa are newly scored in this dataset: *Bernissartia fagesii* (IRScNB 1538), *Diplocynodon darwini* (HLMD Me 10262), and *Asiato-*

*suchus germanicus* (SMNK 1801), all of which exhibit transverse processes on 15 or fewer caudal vertebrae (293-0). The character is also ordered.

294. Caudal vertebrae, articular surfaces of chevrons posterior to the first: open, or partially fused (0); completely fused (1) (after Iijima & Kobayashi, 2019 [254]).

This character was illustrated by Iijima and Kobayashi (2019, fig.S5), which shows that the articular surfaces of the haemal arches (connecting the chevrons with the ventral surface of the caudal vertebrae) are fused (294-1) in all extant alligatorids, with the exception of *Alligator mississippiensis*. By contrast, in all extant crocodylids, *Gavialis gangeticus*, and *Tomistoma schlegelii* the articular surfaces are incipiently or completely fused (294-1). Among fossil crocodylians, *Borealosuchus* (Erickson, 1976, fig.20) and *Piscogavialis jugaliperforatus* (SMNK 1282 PAL) exhibit incipiently or unfused chevrons, whereas *Diplocynodon darwini* (SMF Me 1137) exhibits the fully fused condition, like most extant alligatorids. The first chevron is excluded from the character, as its articular surfaces are always fused.

### 3.4.4 Hyoid and interclavicle

295. Hyoid, shape of dorsal projection (cornu): plate-shaped (0); rod-shaped (1) (after Brochu, 1997b [57]).

296. Hyoid, flare of dorsal projection (cornu): absent (0); present (1) (after Brochu, 1997b [58]).

Characters 295 and 296 describe two independent features in the morphology of the proximal end of the hyoid (cornu), as outlined by Brochu (1999, fig.56). The hyoids flare anteriorly in all extant caimanines (Wermuth, 1953, fig.11a), as well as *Gavialis gangeticus* (Fig. 3.123A) and *Borealosuchus formidabilis* (Erickson, 1976, fig.12). This contrasts with the parallel-sided proximal end of the hyoid in all extant crocodylids, *Tomistoma schlegelii*, and *Alligator* (Fig. 3.123C, D). The hyoid of extant crocodylids can be distinguished further from all other crocodylians by the presence of a cylindrical, rod-shaped proximal end (295-1) (Fig. 3.123B). This contrasts with the mediolaterally narrow, plate-shaped proximal end of the hyoid in all other crocodylians (where known). Sookias (2020) did not consider the character describing the presence or absence of hyoid flare to be robust, stating that *Tomistoma* and *Gavialis* share the same flared condition. However, the observations in this study re-affirm earlier character scores (Fig. 3.123).

297. Interclavicle flexure: minimal dorsoventral flexure, minimum angle between anterior and posterior ends $<15°$ (0); moderate dorsoventral flexure, minimum angle 15–25° (1); severe dorsoventral flexure, minimum angle $> 25°$ (2) (after Brochu, 1997b [30]) (ORDERED).

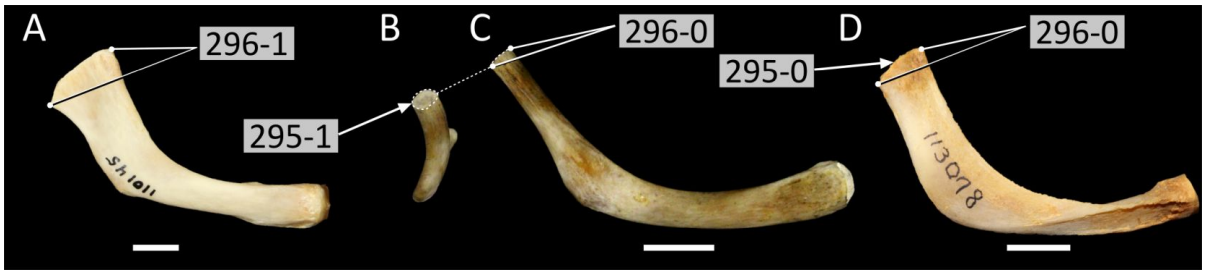



Figure 3.123: Variation in hyoid morphology (all left hyoids in lateral view except B, which is in anterior view). **A**, *Gavialis gangeticus* (AMNH 110145), **B–C**, *Crocodylus porosus* (AMNH 7115); **D**, *Tomistoma schlegelii* (AMNH 113078). All scale bars = 1 cm.

The interclavicle is an ossified median process that projects from the anterior end of the sternum. Brochu (1999) described variation in the dorsoventral curvature (flexure) of the interclavicle, which was discretised into three, subjectively-defined character states describing increasing degrees of flexure. Sookias (2020) recognised inconsistencies between character scores in earlier datasets and observations of actual specimens, as is also found here. As described by Brochu (1999), and later scored by Brochu et al. (2012), *Paleosuchus* exhibits the most extreme dorsoventral flexure (297-2), which is also shared by *Osteolaemus* (AMNH 69057). This condition is newly recognised in *Alligator mcgrewi* (Fig. 3.124D). By contrast with Brochu et al. (2012), severe flexure of the interclavicle was not observed in any *Crocodylus* species, which instead show little to no flexure, e.g. *Crocodylus johnstoni* (Fig. 3.124B). Minimal dorsoventral flexure (297-0) was also observed in extant *Caiman* and *Melanosuchus*, as well as extant *Alligator* and *Brachychampsa montana* (Fig. 3.124A). An intermediate degree of flexure (297-1) is exemplified by *Gavialis gangeticus* (Fig. 3.124C) and *Tomistoma schlegelii* (AMNH 113078). This character is ordered given the clear, continuous nature of increasing flexure.

298. Interclavicle, shape of anterior end (at maturity): plate-shaped (0); rod-shaped (1) (after Brochu, 1997b [31]).

A rod-like anterior tip of the interclavicle (298-1) has been recovered as an unambiguous autapomorphy of *Paleosuchus* (Brochu, 1999). Furthermore, in all datasets examined here, *Paleosuchus* is the only taxon to exhibit this condition (e.g. Brochu et al., 2012; Narváez et al., 2016; Cidade et al., 2017). Sookias (2020) noted that there was no marked difference between the condition of the interclavicle in *Paleosuchus* and other crocodylians. However, based on specimens photographed in his supplementary material, this could be a result of the study of juvenile specimens. Indeed, Brochu (1999) stated that 'mature' *Paleosuchus* specimens exhibit this condition, implying that it is absent in juveniles. Accordingly, larger *Paleosuchus* interclavicles studied here do exhibit a rod-like condition (Fig. 3.124F), which is distinct from the plate-shaped condition of all other crocodylians (Fig. 3.124E).

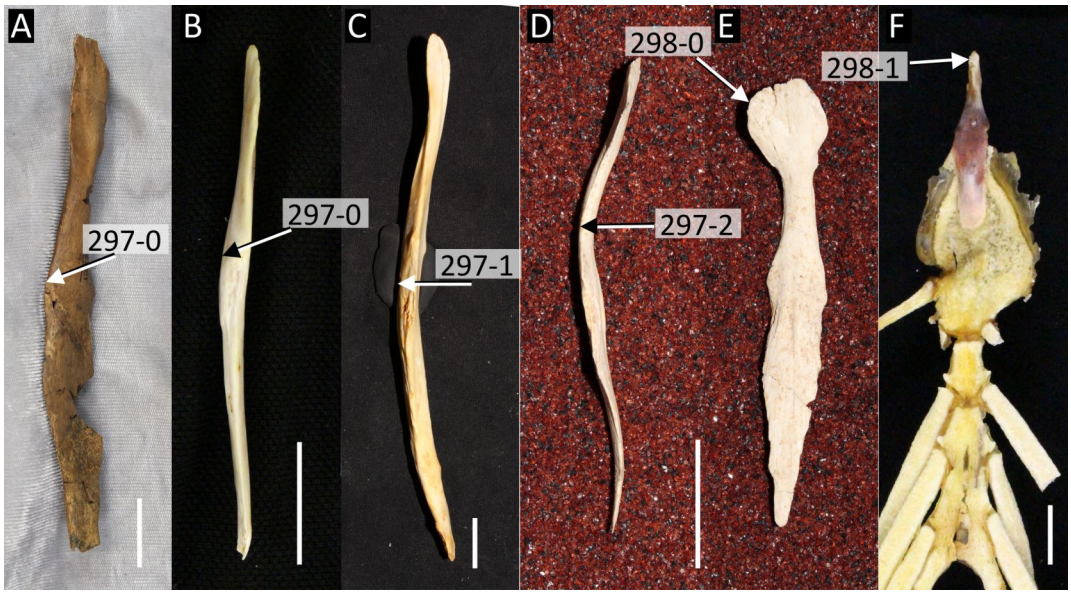



Figure 3.124: Morphology of the interclavicle. **A**–**C**, left lateral view of the interclavicle in **A**, *Brachychampsa montana* (UCMP 133901); **B**, *Crocodylus johnstoni* (QM J58446) **C**, *Gavialis gangeticus* (USNM 576261, digitally reversed); **D**–**E**, *Alligator mcgrewi* (AMNH FAM 8700) in left lateral (**D**) and dorsal views (**E**); **F**, *Paleosuchus palpebrosus* (AMNH 97326, dorsal view attached to sternum). All scale bars = 2 cm.

### 3.4.5 Appendicular skeleton

299. Scapula, deltoid crest shape: thin, with sharp margin (0); wide, with broad margin (1) (after Brochu, 1997b [23]).

The deltoid crest (acromion process) of the scapula serves as the point of origin of *M. coracobrachialis brevis dorsalis* and *M. deltoideus clavicularis* (Meers, 2003). The derived character state applies principally to species of *Alligator*, e.g. *A. mississippiensis*, and *A. sinensis*, which at maturity exhibit a broad crest (Brochu, 1999, fig.51) (Fig. 3.125A). One might expect that this character will be influenced by ontogeny, i.e. juvenile individuals of a species will exhibit a narrow crest (299-0), which broadens with maturity (299-1). However, at maturity, the scapulae of taxa with the derived character state, e.g. *A. mississippiensis*, consistently exhibit a broader deltoid crest than those of equally sized or even larger crocodylians (Fig. 3.125B, D, F).

300. Scapulocoracoid synchondrosis: closes very late in ontogeny (0); closes early in ontogeny (1) (after Brochu, 1997b [24]).

In all extant caimanines, the scapulocoracoid synchondrosis closes relatively early in ontogeny (300-0), before that of the neurocentral sutures (Brochu, 1995) (Fig. 3.125H). By contrast, the suture remains open in all but the most mature individuals of other extant crocodylians (300-1) (Brochu, 1999) (Fig. 3.125G). In this study, all crocodylians known from mature individuals, with disarticu-

lated scapulocoracoids, are scored with the plesiomorphic character state, given that had the scapulocoracoid been fused early in ontogeny, these elements should presumably still be in articulation. Very few fossil crocodylians are scored for character state (1). The material known for *Necrosuchus* represents an immature individual, since the dorsal and sacral neurocentral sutures are still visible (Brochu, 1996). Based on this, and the incipient closure of the scapulocoracoid synchondrosis, it can be scored for the derived character state. A specimen of *Mourasuchus arendsi* preserving the scapulocoracoid (Cidade et al., 2020b) was close to maturity, based on partial closure of the cervical neruocentral sutures. Since it exhibits incipient closure of the scapulocoracoid synchondrosis, it too can be scored for the derived condition.

301. Scapulocoracoid facet, shape anterior to glenoid fossa (at maturity): uniformly narrow (0); broad immediately anterior to glenoid fossa, tapering anteriorly (1) (after Brochu, 1997b [25]).

The morphology of the scapulocoracoid facet can be determined by viewing either the scapula or coracoid in proximal view (Fig. 3.125I–M). Brochu (1999) noted that the facet is tear-drop-shaped in all species, but some (mostly 'brevirostrine') crocodylians exhibit a prominent difference in facet width between the anterior and posterior ends, which is accentuated at maturity (301-1). Sookias (2020) rejected this character as it was unobservable in the sample of crocodylians in his study. However, this sample appears to be entirely juvenile, and all the relevant images are in lateral view, from which point the morphology cannot be determined. The observations of Brochu (1999) are supported here, albeit with some character score changes. A uniformly narrow facet is exhibited in *Bernissartia fagesii* (IRScNB 1538), some *Borealosuchus* species (e.g. *B. sternbergii*), *Brachychampsa montana* (Fig. 3.125M), and some "gavialoids" e.g. *Eogavialis africanum* (Fig. 3.125K) and *Eosuchus minor* (USNM 355967). However, the condition in *Gavialis gangeticus* (Fig. 3.125L) is considered closer to that of extant crocodylids (Fig. 3.125I), *Tomistoma schlegelii*, alligatorids, and the gavialoid *Piscogavialis jugaliperforatus* (Fig. 3.125J).




Figure 3.125: Morphology of the scapulocoracoid. A–F, lateral view of the left scapula in: **A**, *Alligator mississippiensis* (AMNH 71621); **B**, *Brachychampsa montana* (UCMP 133901); **C**, *Caiman yacare* (AMNH 97300); **D**, *Asiatosuchus germanicus* (SMF Me 1801); **E**, *Voay robustus* (NHMUK R 36661); **F**, *Gavialis gangeticus* (UMZC R 5783); G–H, medial view of the left scapulocoracoid in: **G**, *Alligator sinensis* (USNM 292078, digitally reversed) and **H**, *Caiman crocodilus* (FMNH 13062); I–K, proximal view of the articular facet of the left coracoid in: **I**, *Crocodylus acutus* (AMNH 7121); **J**, *Piscogavialis jugaliperforatus* (SMNK 1282 PAL); **K**, *Eogavialis africanum* (SMNS 11225, digitally reversed); L–M, proximal view of the articular facet of the right scapula in **L**, *Gavialis gangeticus* (UMZC R 5783); **M**, *Brachychampsa montana* (UCMP 133901, digitally reversed). All scale bars = 2 cm.

302. Humerus, proximal margin of deltopectoral crest: straight, emerging smoothly from proximal end of the humerus (0); concave, emerging abruptly from proximal end of humerus (1) (after Brochu, 1997b [26]).

The morphology of the deltopectoral crest of the humerus appears to vary continuously in eusuchians. For example, in *Gavialis gangeticus* (Fig. 3.126A), the crest is very low, lacking a prominent apex. This condition is broadly similar to several *Borealosuchus* species (Fig. 3.126B), *Leidyosuchus canadensis* (Fig. 3.126C), and the outgroup, *Bernissartia fagesii* (IRScNB 1538). By contrast, the deltopectoral crest is more prominent in extant crocodylids, *Alligator* (Fig. 3.126F) and *Diplocynodon* (Fig. 3.126D). In extant caimanines and some fossil representatives, the apex of the crest appears even sharper (Fig. 3.126G–H). It was not considered practical to characterise this morphology as a continuous character. As such, following earlier studies, the morphology is discretised as a binary character describing either a low, smoothly emerging crest (302-0), or an abruptly emerging crest (302-1).

303. Humerus, axial rotation of the proximal epiphysis relative to the distal epiphysis: small, ventral surface of the proximal epiphysis not visible in medial view (0); large, ventral surface exposed in medial view (1) (new character, after Stein et al., 2012).

This character describes the degree of torsion between the proximal and distal ends of the humerus. Uniquely among extant crocodylians, the proximal epiphysis of the humerus is highly rotated relative to the distal epiphysis in *Gavialis gangeticus* (Fig. 3.126A). Consequently, when viewed medially, the ventral surface of the proximal epiphysis is visible. This can also be described in terms of the orientation of the long axes of the distal and proximal epiphyses, which are offset in *Gavialis*. By contrast, other extant crocodylians exhibit a minimal degree of torsion, such that the long axes of the epiphyses are aligned, and the ventral surface of the proximal epiphysis is not visible e.g. *Alligator mississippiensis* (Fig. 3.126F). Other than *Gavialis gangeticus*, the derived condition is only tentatively found in the "tomistomine" *Penghusuchus pani* (Shan et al., 2009, fig.14).

304. Humerus, scarring on proximodorsal surface for *M. teres major* and *M. dorsalis scapulae* (at maturity): two muscle scars (0); single muscle scar (*M. teres major* and *M. dorsalis scapulae* insert on common tendon) (1) (after Brochu, 1997b [29]).

This character was introduced by Brochu (1997b), and has never been illustrated and only briefly described (Brochu, 1997a). According to earlier datasets (Brochu et al., 2012), *Bernissartia fagesii*, and some "gavialoids", (e.g. *Gavialis gangeticus*, *Eosuchus minor*, and *Thoracosaurus*) exhibit two muscle scars on the dorsal surface of the humerus (304-0), approximately level with the location of the deltopectoral crest on the ventral surface. By contrast, all other eusuchians exhibit one prominent scar (304-1), which serves as the insertion point for *M. teres major* and *M. latissimus dorsi* (Meers, 2003). The latter was commonly found in most crocodylians in this dataset (Fig. 3.126L). Two scars

matching the description of the plesiomorphic character state were observed in a mature specimen of *G. gangeticus* (UMZC R 5783) (Fig. 3.126K); however, these are not apparent in slightly smaller specimens, which appeared to have only one prominent scar (AMNH 110145, USNM 576261). As such the character must be scored in mature specimens. Two scars are also present in *Eosuchus minor* (USNM 355967 Brochu, 2006b), and *Thoracosaurus*. The condition in the latter is based on character scores in a previous dataset (Brochu et al., 2012), since appendicular remains of *Thoracosaurus* were not studied herein.

305. Ulna, shape of olecranon process: narrow and sub-angular (0); wide and rounded (1) (after Brochu, 1997b [27]).

The olecranon process is narrow (mediolaterally compressed) in *Bernissartia fagesii* and all species of *Borealosuchus* (Fig. 3.127A). This contrasts with the broadly rounded olecranon process of all other crocodylians (Fig. 3.127B), where known.

306. Ulna, proximal diaphysis curved (0); straight (1) (new character, based on personal observations).

In most eusuchians, the ulna is almost entirely straight and robust, with a slight dorsal curvature at its proximal end (Fig. 3.127B). By contrast, in *Bernissartia fagesii* (IRScNB 1538), *Isisfordia duncani* (QM F36211), and at least two *Borealosuchus* species (*B. sternbergii* [Fig. 3.127A] and *B. formidabilis* [Erickson, 1976, fig.26]), the ulna is slender, and prominently curved at its proximal end.

307. Ilium, preacetabular process shape: acute, pointed anteriorly (0); broad, rounded anteriorly (1) (after Benton & Clark, 1988; Clark, 1994 [84]; Brochu, 1997b [34]).

All earlier studies characterised the preacetabular process of the ilium as either “prominent” or “virtually absent” (Brochu, 1997b; Brochu et al., 2012). However, examination of a large sample of crocodylian ilia reveals a significant amount of variation in the development of this process (Fig. 3.128). A convexity on the anterodorsal margin of the ilium, which could be interpreted as a preacetabular process, occurs in most eusuchians, but differs in its size. Although, this justifies the use of the terms “prominent” or “virtually absent”, it introduces subjectivity. Here, a distinction is made between the morphology of the preacetabular process, from those with an acute tip (307-0) to those with a rounded tip (307-1). As a result, the plesiomorphic condition is more widespread. Whereas *Bernissartia fagesii* (IRScNB 1538), *Borealosuchus* (Fig. 3.128A), and *Gavialis gangeticus* (Fig. 3.128D) exhibit a prominent, acute preacetabular process (307-0), all extant alligatorids and most crocodylids exhibit a smaller, rounded process (307-1). By contrast to earlier studies (e.g. Brochu et al., 2012), the morphology of the preacetabular process in *Diplocynodon darwini* (Fig. 3.128C), *Crocodylus acutus* (Fig. 3.128H), and *Alligator prenasalis* (Fig. 3.128Q), is scored with the plesiomorphic condition, whereas that of *Eogavialis africanum* (Fig. 3.128E) more closely resembles the derived state.

308. Ilium, dorsal outline of postacetabular process: convex, no dorsal indentation (0); broadly concave with a small indentation (1);strongly concave, with an acute indentation ("wasp-waisted") (2) (after Brochu, 1997b [28]) (ORDERED).

309. Ilium, posterior margin of the postacetabular process: deep, anteroposterior length to dorsoventral height ratio $<1$ (0); shallow, length to height $\geq 1$ (1) (after Brochu, 1997b [28]; Groh et al., 2020 [523]).

    Characters 308 and 309 were derived by reductively coding character 28 in Brochu (1997b), which originally combined descriptions of the dorsoventral height (Character 309) and dorsal outline (Character 308) of the postacetabular process. Under the original format, some combinations of morphological features could not be accounted for in several crocodylians. For example, all *Diplocynodon* species were described as exhibiting a postacetabular process that was deep, lacking a dorsal indentation (Brochu, 1997b, character 28-4). Although this applies to *D. hantoniensis* (NHMUK OR 30362) and *D. darwini* (Fig. 3.128C), *D. ratelii* exhibits a deep postacetabular process (309-0) with an acute indentation (308-2) (Fig. 3.128B).

310. Ilium, postacetabular process: projects posteriorly (0); posterodorsally (1) (after Wu and Suez, 1996 [41]; Pol & Norell, 2004 [110]; Groh et al., 2020 [530]).

    This character is not usually applied to datasets consisting primarily of crocodylian taxa (e.g. Brochu, 1999; Brochu et al., 2012; Jouve et al., 2015; Lee & Yates, 2018); however, a posterodorsally directed postacetabular process is present in *Borealosuchus formidabilis* (Fig. 3.128A) and *Borealosuchus wilsoni* (FMNH PR 1674) in this dataset. In *Bernissartia*, and all other eusuchians (Fig. 3.128B–R), the process is primarily posteriorly directed.




Figure 3.126: Variation in humeral morphology in Crocodylia. **A**–**H**, medial view of the left humerus in: **A**, *Gavialis gangeticus* (AMNH 110145); **B**, *Borealosuchus sternbergii* (USNM 6533); **C**, *Leidyosuchus canadensis* (UCMP 131696, digitally reversed); **D**, *Diplocynodon hantoniensis* (NHMUK OR 30206, digitally reversed); **E**, *Brachychampsa montana* (UCMP 133901); **F**, *Alligator mississippiensis* (AMNH 71621); **G**, *Caiman yacare* (AMNH 97300); **H**, *Mourasuchus atopus* (UCMP 38012). **I**–**J**, dorsal view of the humerus in **I**, *Gavialis gangeticus* (UMZC R 5783); **J** *Crocodylus acutus* (AMNH 7121); **K**–**L**, enlargement of muscle attachments highlighted in I and J respectively. Scale bars in A–H = 2 cm, I–J = 5 cm, K–L = 1 cm.

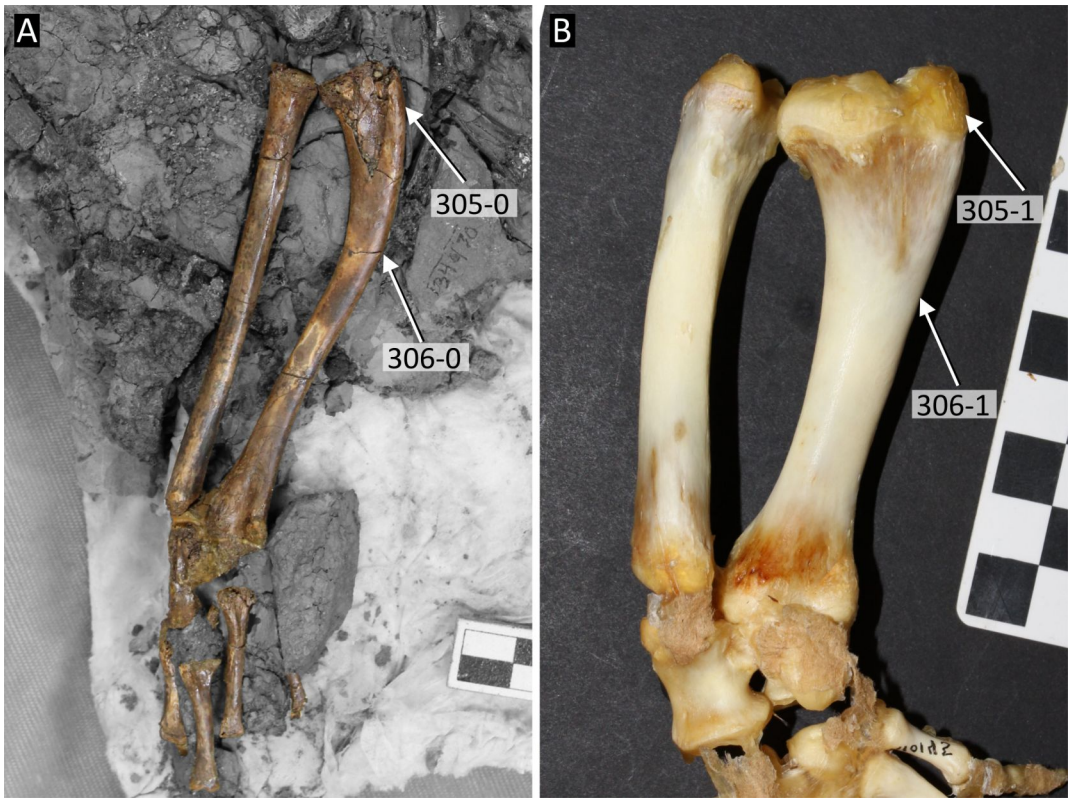



Figure 3.127: Medial view of the right ulna and radius of **A**, *Borealosuchus sternbergii* (UCMP 134430); **B**, *Gavialis gangeticus* (AMNH 110145, digitally reversed). Scale bars = cm.

### 3.4.6 Soft tissue

311. Cerebrum, posterodorsal outline anterior to optic lobe: flat (0); with sharp step (1) (new character, after Serrano-Martinez et al., 2019b).

In extant alligatorids (where known), there is a pronounced step on the dorsal margin of the cerebrum, anterior to the region of the optic lobes (311-1) (Serrano-Martínez et al., 2019b). This condition also appears in some extant crocodylids, e.g. *Osteolaemus tetraspis* and *Crocodylus niloticus*, but not *Crocodylus johnstoni*, which has a broadly rounded posterodorsal outline (311-0) (Serrano-Martínez et al., 2019b). The broadly rounded condition also characterises the non-crocodylian eusuchian *Lohuecosuchus megadontos* (Serrano-Martínez et al., 2019a), 'basal' alligatoroids (e.g. *Diplocynodon tormis* and *Leidyosuchus canadensis*), *Tomistoma schlegelii*, *Gavialis gangeticus*, and *Gryposuchus neogaeus*) (Storrs et al., 1983; Bona et al., 2017b; Serrano-Martínez et al., 2019b).

312. Medial pharyngeal sinus, ratio of ventral length (measured from ventral tip to junction with basisphenoid diverticulum) to dorsal length (measured from basisphenoid diverticulum to dorsal tip): $\geq 2$ (0); $< 2$ (1) (new character, after Serrano-Martinez et al. 2019b).

Serrano-Martínez et al. (2019b) described differences in length of the medial pharyngeal sinus in Crocodylia. In their sample of extant crocodylids (*Osteolaemus tetraspis*, *Crocodylus johnstoni*, and *Crocodylus niloticus*), the length of the ventral portion of the medial pharyngeal sinus (i.e. below the intersection with the basisphenoid diverticulum) is twice the length of the dorsal portion (312-0) (Serrano-Martínez et al., 2019b, fig.5). This condition is otherwise only known in *Lohuecosuchus megadontos* (Serrano-Martínez et al., 2019a). By contrast, the ventral portion of the medial pharyngeal sinus is shorter (312-1) in alligatoroids (*Alligator mississippiensis*, *Caiman crocodilus*, *Diplocynodon tormis*, and *Mourasuchus arendsi*), *Tomistoma schlegelii*, and *Gavialis gangeticus* (Bona et al., 2013a; Serrano-Martínez et al., 2019b).

313. Keratinised buccal cavity: present (0); absent (1) (after Brochu, 1997b [159], adapted from Taplin & Grigg, 1989).

Taplin and Grigg (1989) noted that all extant crocodylids, as well as *Tomistoma schlegelii* and *Gavialis gangeticus*, share a similar morphology of the tongue and buccal cavity, which has a yellow/ orange tint, and is keratinised (Grigg & Kirshner, 2015, fig.11.23). This keratinisation reduces the permeability of the buccal cavity, which is interpreted as an adaptation for inhabiting saltwater environments (Taplin & Grigg, 1989). By contrast, all extant alligatorids lack keratinisation of the tongue and buccal cavity, in which it is smooth, with a glutinous sheen (Grigg & Kirshner, 2015, fig.11.30).

314. Integumentary sensory organs, distribution on body: cranial only (0); cranial and postcranial (1) (after Lee & Yates, 2018 [275], adapted from Grigg & Kirshner, 2015).

Integumentary sense organs (ISOs) (Brazaitis, 1987) are small, millimetre-sized black pits that occur on the cranial scales of all extant crocodylians (Fig. 3.129A). These serve a diverse number of functions, including the detection of water-borne disturbances (Grigg & Kirshner, 2015). Whereas in extant alligatorids ISOs are restricted to the skull and mandible, they occur all over the body and limbs of extant crocodylids, *Tomistoma schlegelii*, and *Gavialis gangeticus* (Fig. 3.129C) (Grigg and Kirshner, 2015).

315. Ventral scales, follicle gland pore: present (0); absent (1) (after Poe, 1996 [113]; Brochu, 1997b [155]; adapted from Brazaitis, 1973).

Brazaitis (1973) described the presence of 'follicle gland pores' on the ventral scales of all extant crocodylids, *Tomistoma schlegelii* and *Gavialis gangeticus*, whereas these are absent in extant alligatorids (Brazaitis, 1973, fig.2C). The difference in structure between these pores and ISOs has not been explored, but they are tentatively treated independently pending examination of additional crocodylian skins.

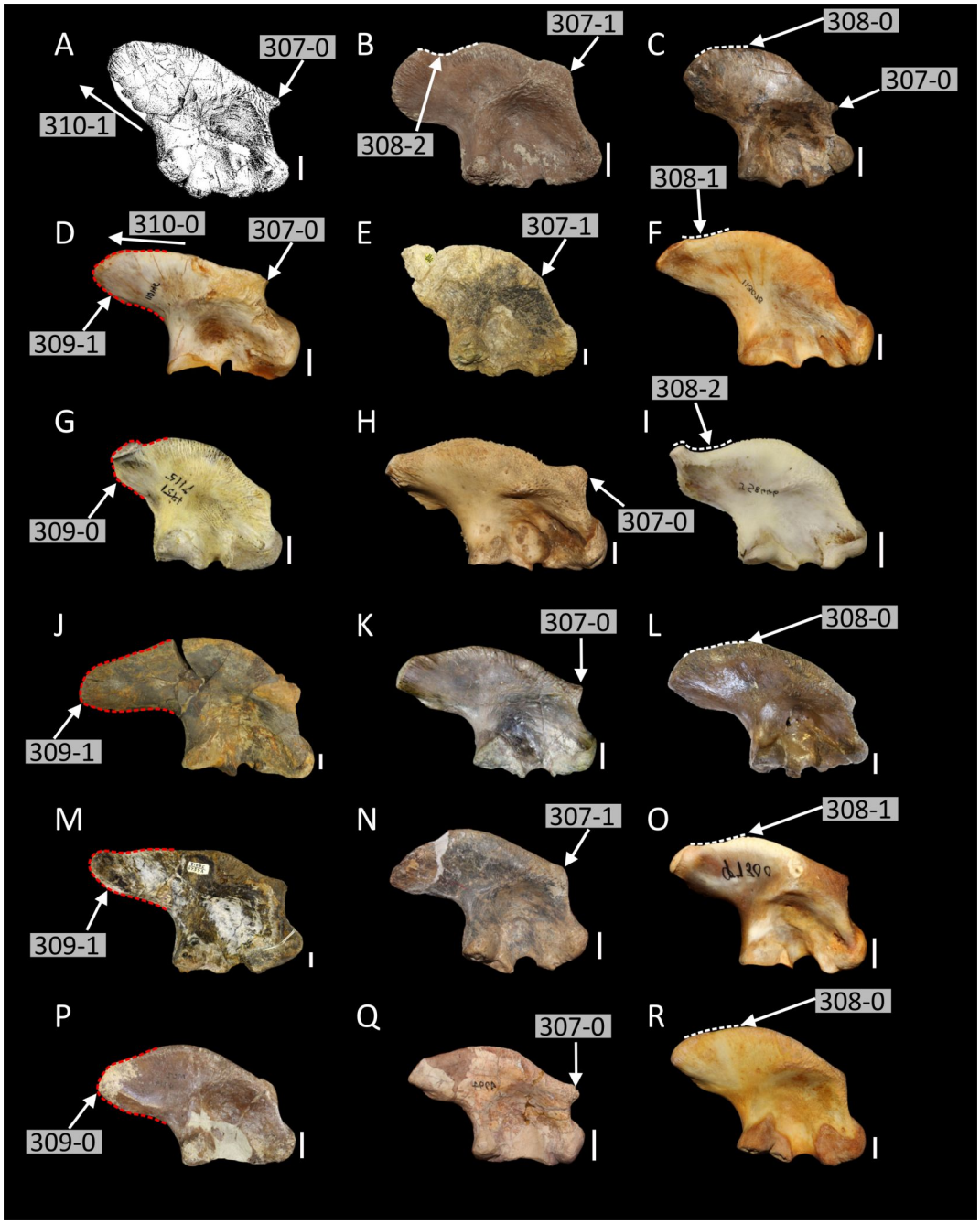



Figure 3.128: Variation in morphology of the ilium in Crocodylia (right ilium, lateral view). **A**, *Borealosuchus formidabilis* (Erickson, 1976, fig.27A, digitally reversed); **B**, *Diplocynodon ratelii* (MNHN uncatalogued, digitally reversed); **C**, *Diplocynodon darwini* (SMF Me-3784); **D**, *Gavialis gangeticus* (AMNH 110145, digitally reversed); **E**, *Eogavialis africanum* (NHMUK R 6199); **F**, *Tomistoma schlegelii* (AMNH 113078, digitally reversed); **G**, *Crocodylus porosus* (AMNH 7115); **H**, *Crocodylus acutus* (AMNH 7121); **I**, *Crocodylus johnstoni* (QM J 58446, digitally reversed); **J**, *Asiatosuchus germanicus* (SMF Me-1801); **K**, '*Crocodylus*' *affinis* (USNM 18171); **L**, *Asiatosuchus depressifrons* (IRSNB 9912); **M**, *Mourasuchus atopus* (UCMP 38012); **N**, *Necrosuchus ionensis* (AMNH 3219); **O**, *Caiman yacare* (AMNH 97300); **P**, *Alligator olseni* (MCZ 4719, digitally reversed); **Q**, *Alligator prenasalis* (AMNH 4994, digitally reversed); **R**, *Alligator mississippiensis* (AMNH 71621). All scale bars = 1 cm.

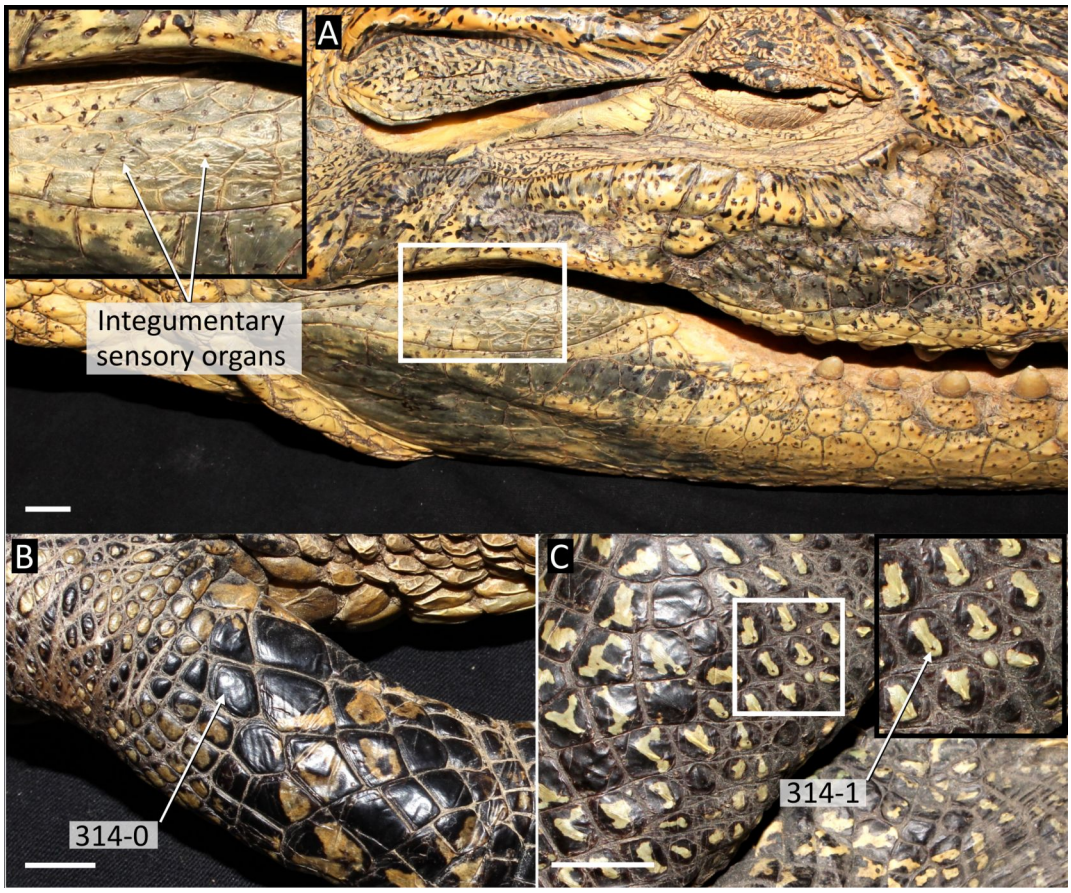



Figure 3.129: Variation in distribution of integumentary sensory organs (ISOs) in crocodylian skin. **A**, lateral view of the skull in *Crocodylus niloticus* (USNM 63592); **B**, right forelimb of *Alligator mississippiensis* (USNM 25148); **C**, right forelimb of *Crocodylus porosus* (USNM 72730). All scale bars = 2 cm.

316. Ventral collar scales: not enlarged relative to other ventral scales (0); in 1–2 enlarged rows (1) (after Poe, 1996 [115]; Brochu, 1997b [156]; adapted from Brazaitis, 1973 and Fuchs, 2006 [13]).

'Ventral collar scales' refer to ventral scales at the level of the forelimbs (Fuchs, 2006, fig.4). Brazaitis (1973) described different degrees of enlargement of the ventral collar scales in extant crocodylians, which were later discretised into three character states by Poe (1997, character 115): not enlarged (0); one enlarged row (1); or two enlarged rows (2). According to earlier datasets (e.g. Brochu, 1997b; Brochu et al., 2012), all extant crocodylids, *Tomistoma schlegelii*, and *Gavialis gangeticus* lack enlargement of the ventral collar scales, most alligatorids exhibit two enlarged rows, and *Paleosuchus* exhibits one enlarged row. However, these scores do not match the descriptions and illustrations in Fuchs (2006), which provides the most comprehensive account of crocodylian skins. For example, some *Crocodylus* species e.g. (*C. palustris*, *C. rhombifer*, and *C. novaeguineae*), *Osteolaemus tetraspis*, and *Tomistoma schlegelli* exhibit 1–2 enlarged rows (Fuchs, 2006). Additionally, although *Paleosuchus* exhibits one single enlarged row, so does *Caiman crocodilus* (Fuchs, 2006, fig.37). Furthermore, the distinction between 1 or 2 enlarged rows is challenging, as scale size varies

gradationally in this region. Based on these observations, the character has been simplified to distinguish between taxa that lack enlargement of the ventral collar scales (316-0) (*Gavialis gangeticus* and some *Crocodylus* species), from those with any degree of enlargement in this region (316-1) (all alligatorids, *Tomistoma schlegelii*, and most crocodylids).

317. Tail dorsal scalation, number of transverse scale rows from the level of the cloacal vent to the point of convergence of paired mid-dorsal crests into a single longitudinal crest: $>13$ (0); $\leq 13$ (1) (after Wermuth, 1953; Poe, 1996 [116]; Brochu, 1997b [157]; Fuchs, 2006 [17]).

    In all extant crocodylians, the dorsal scutes of the tail form paired longitudinal crests, which become more prominent posteriorly. These occur as two parallel rows on the lateral edges of the tail and converge posteriorly (Fig. 3.130). The point at which they converge into a single, midline longitudinal crest varies between species (Wermuth, 1953, fig.4). The number of transverse rows between the level of the cloacal vent and the point of convergence of the paired midline osteoderms, was counted in all extant crocodylians based on data in Fuchs (2006). There is a discontinuity in the data at 13 transverse rows, and thus this was used to define the character states. In general, the crests converge further anteriorly in caimanines (Fig. 3.130B) and *Osteolaemus* (317-1) than in all other extant crocodylians (317-0) (Fig. 3.130A).

### 3.4.7 Osteoderms

318. Palpebral, number of ossifications: one (0); two or more (1) (after Norell, 1988 [8]; Clark, 1994 [65]; Brochu, 1997b [96]).

319. Palpebral, size in relation to orbit: small, covering no more than half the area of the orbit (0); large, covering more than half the orbit (usually completely concealing it) (1) (new character, based on personal observations).

    The crocodylian palpebral is essentially an orbital osteoderm (Vickaryous & Hall, 2008). In most extant crocodylians, this is a small, anteromedially positioned element comprising one ossification (318-0, 319-0) (Nesbitt et al., 2012). This is the case in *Alligator* (Fig. 3.131A), Jacarea (Fig. 3.131B), *Crocodylus*, *Mecistops*, *Tomistoma schlegelii*, and *Gavialis gangeticus* (Nesbitt et al., 2012). By contrast, the palpebral is composed of multiple ossifications in *Osteolaemus* (two ossifications) and *Paleosuchus* (three ossifications) (Fig. 3.131E) (318-1) (Brochu, 1999). Among extant crocodylians, *Paleosuchus* exhibits the largest palpebral, which almost entirely conceals the orbit (319-1), a condition also found in the 'Glen Rose Form' (MCZ 4384) and *Theriosuchus pusillus* (NHMUK 48270). Although enlarged in *Osteolaemus*, the palpebral does not conceal the orbit (319-0).

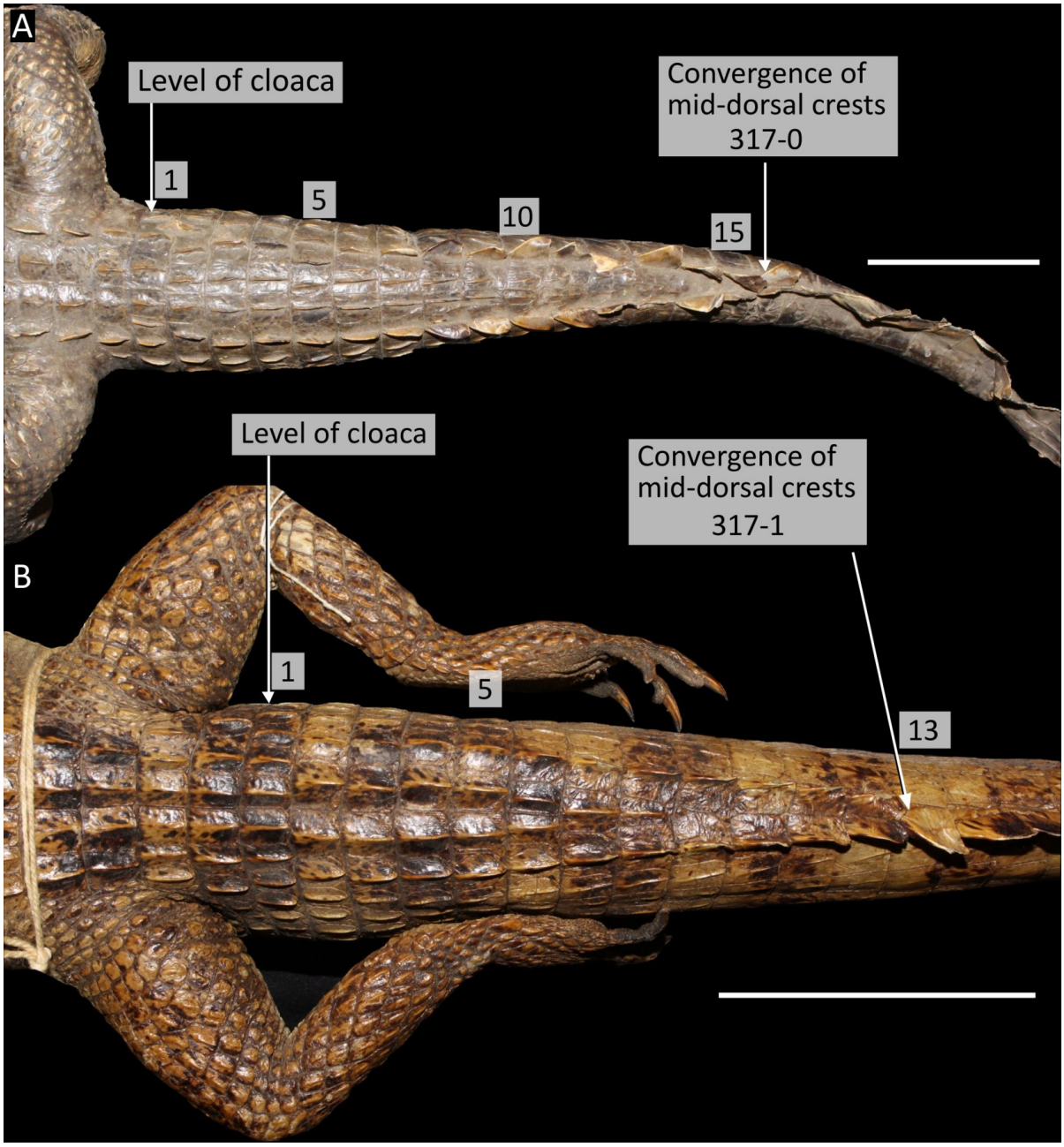



Figure 3.130: Dorsal view of the tail showing variation in scale crests between: **A**, *Crocodylus acutus* (USNM 52491); **B**, *Caiman crocodilus* (USNM 54094). Numbers refer to counts of the transverse scale row beginning from the level of the cloaca. All scale bars = 5 cm.

320. Tongue, lingual osmoregulatory pores: large, 1–2 mm (0); small, < 1 mm (1) (after Brochu, 1997b [158]; adapted from Taplin & Grigg, 1989).

As is the case in extant crocodylids and *Tomistoma schlegelii*, *Gavialis gangeticus* exhibits some specialisations for saltwater tolerance, e.g. a keritanised buccal cavity. *Tomistoma schlegelii* and all extant crocodylids also exhibit large osmoregulatory pores on the tongue, which secrete excess sodium chloride (Grigg & Kirshner, 2015, fig.11.23). While *Gavialis gangeticus* exhibits these pores, they are highly reduced, similar to the condition in all extant alligatorids that principally inhabit freshwater environments (320-0) (Taplin & Grigg, 1989).

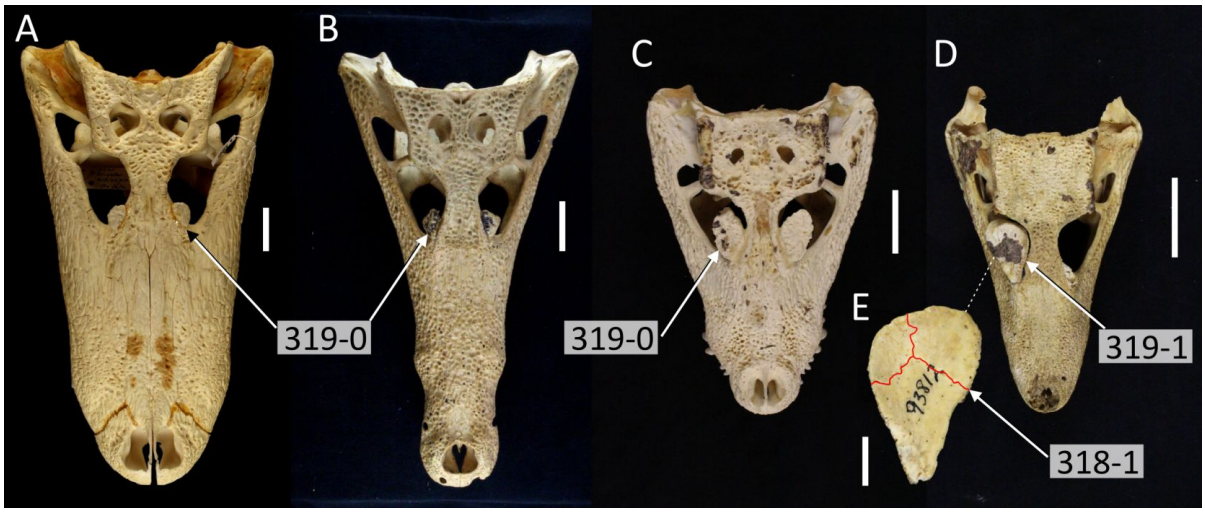



Figure 3.131: Variation in the morphology of the palpebral in **A**, *Alligator mississippiensis* (AMNH 71621); **B**, *Caiman crocodilus apaporiensis* (FMNH 69812); **C**, *Osteolaemus tetraspis* (AMNH 117801); **D**, *Paleosuchus palpebrosus* (AMNH 93812), **E**, enlargement of the palpebral in D in ventral view showing multiple ossifications. Scale bars A–D = 5 cm, E = 1 cm.

321. Postoccipital osteoderms, number of rows: two or more (0); one (1) (after Brochu & Storrs, 2012 [183]).

Postoccipital osteoderms are the small, anteriormost osteoderms of the nape (Fig. 3.132). As with the arrangement of the nuchal osteoderms (discussed below), their precise arrangement, number, and size is considerably variable in extant crocodylians (Ross & Mayer, 1983). Nevertheless, broad differences are discernible. In extant *Crocodylus*, *Gavialis gangeticus*, and *Paleosuchus palpebrosus*, there is one enlarged, transverse row of postoccipital osteoderms (321-1) (Fig. 3.132D–E). This differs from most caimanines, *Alligator*, *Tomistoma schlegelii* (contra Brochu & Storrs, 2012) and osteolaemines, which exhibit multiple rows of tightly packed osteoderms in this region (Fig. 3.132F–H). This character cannot be scored for any fossil crocodylian in this dataset.

322. Nuchal osteoderms, grade continuously into dorsal shield (0); differentiated from dorsal shield (1) (after Brochu, 1997b [38]).

323. Number of nuchal osteoderms: four (0); six (1); eight or more (2) (after Brochu, 1997b [38]) (ORDERED).

Characters 322 and 323 were derived by reductively coding character 38 in Brochu (1997b). As originally formatted, the character does not allow the consideration of the number of nuchal osteoderms in taxa with a continuous nuchal-dorsal transition (322-0), e.g. *Mecistops cataphractus* (USNM 60578), *Gavialis gangeticus* (Fig. 3.132I), and *Tomistoma schlegelii* (Fig. 3.132F). This might be considered a reasonable distinction, as determining at which point the nuchal osteoderms 'end' and the dorsal osteoderms 'start' is challenging in taxa with a continuous nuchal-dorsal transition. However, this can be achieved given that there is a one-to-one relationship between transverse osteoderm rows and vertebrae (Ross & Mayer, 1983). Following the illustrations in Ross and Mayer (1983), nuchal osteoderms were considered to be those in between the postoccipital osteoderms, and the $18^{th}$ precaudal row of osteoderms (measured from the sacro-caudal junction). Accordingly, *Tomistoma schlegelii* and *Gavialis gangeticus* share the same number of osteoderms (323-2), in common with all extant caimanines (Fig. 3.132G–H) and *Brachychampsa montana* (UCMP 133901). All extant *Crocodylus* species, *Mecistops*, and *Alligator*, exhibit 6 nuchal osteoderms (323-1) (Fig. 3.132B–E), whereas *Osteolaemus* exhibits only 4 (323-0) (Fig. 3.132A).

324. Dorsal osteoderms, maximum number in the middle transverse row (at maturity): two (0); four (1); six (2); eight (3); ten (4) (after Norell & Clark, 1990 [12]; Clark, 1994 [97]; Brochu, 1997b [37] (ORDERED).

This character has been modified by the addition of a character state (324-0), which is observed in *Theriosuchus pusillus* (Fig. 3.133A), and by ordering the character. The wording is also modified such that the number of osteoderms is counted in the transverse row with the most osteoderms (usually at the anteroposterior mid-point). This difference accounts for the fact that the number of osteoderms per row decreases towards the anterior and posterior ends of the dorsal shield. For example, whereas there are ten osteoderms in the middle transverse row in *Brachychampsa montana* (324-4) (Fig. 3.133E), there are only four in the anteriormost row. A maximum of four dorsal osteoderms per row (324-1) occurs in *Bernissartia fagesii* (Fig. 3.133D), and some "gavialoids" (e.g. *Gavialis gangeticus* [Fig. 3.132I] and *Eosuchus minor* [USNM 321933]), as well as the "tomistomine" *Maomingosuchus petrolica* (ZMNH uncatalogued specimens on display). Most commonly there are six (324-2), as found in most extant *Crocodylus*, osteolaemines, *Alligator*, *Paleosuchus*, *Tomistoma schlegelii* (Ross & Mayer, 1983) and the 'basal' alligatoroid *Diplocynodon darwini* (Fig. 3.133B). Extant *Caiman*, *Melanosuchus*, and *Hassiacosuchus haupti* exhibit eight osteoderms (324-3) (Fig. 3.133C).

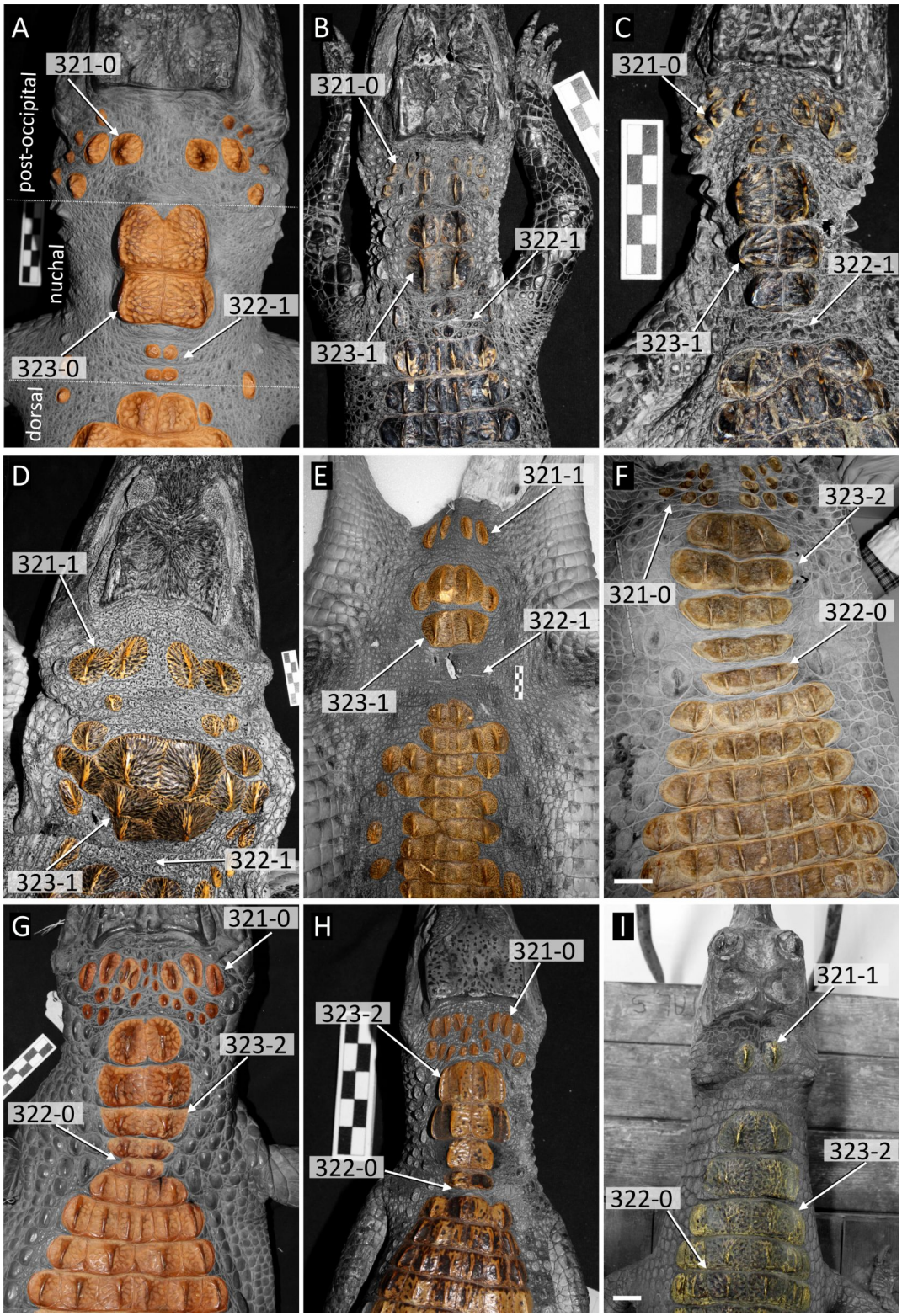



Figure 3.132: Morphological variation of the postoccipital and nuchal osteoderms in extant crocodylians. **A**, *Osteolaemus tetraspis* (USNM 233978); **B**, *Alligator mississippiensis* (USNM 25148); **C**, *Alligator sinensis* (USNM 67712); **D**, *Crocodylus niloticus* (USNM 63592); **E**, *Crocodylus acutus* (USNM 243433); **F**, *Tomistoma schlegelii* (FMNH uncatalogued); **G**, *Caiman latirostris* (USNM 98780); **H**, *Caiman crocodilus* (USNM 142089); **I**, *Gavialis gangeticus* (NHMUK). Scale bars in F and I = 5 cm, all other scale bars = cm.

325. Dorsal osteoderms, longitudinal midline keel: absent (0); present (1) (after Buscalioni et al., 1992 [22]; Brochu, 1997b [35]).

The anatomical meaning of this character follows that outlined by Buscalioni et al. (1992). A sagittal keel occurs on the dorsal osteoderms of *Bernissartia fagesii* (IRScNB 1538) and most eusuchians in this dataset (325-1) (Fig. 3.134I). By contrast, the keel is absent entirely in *Borealosuchus* and most longirostrine crocodylians, including "gavialoids" (e.g. *Eogavialis africanum* [Fig. 3.134], *Eosuchus lerichei* [IRScNB R 49]) and "tomistomines", e.g. *Toyotamaphimeia* (Iijima & Kobayashi, 2019).

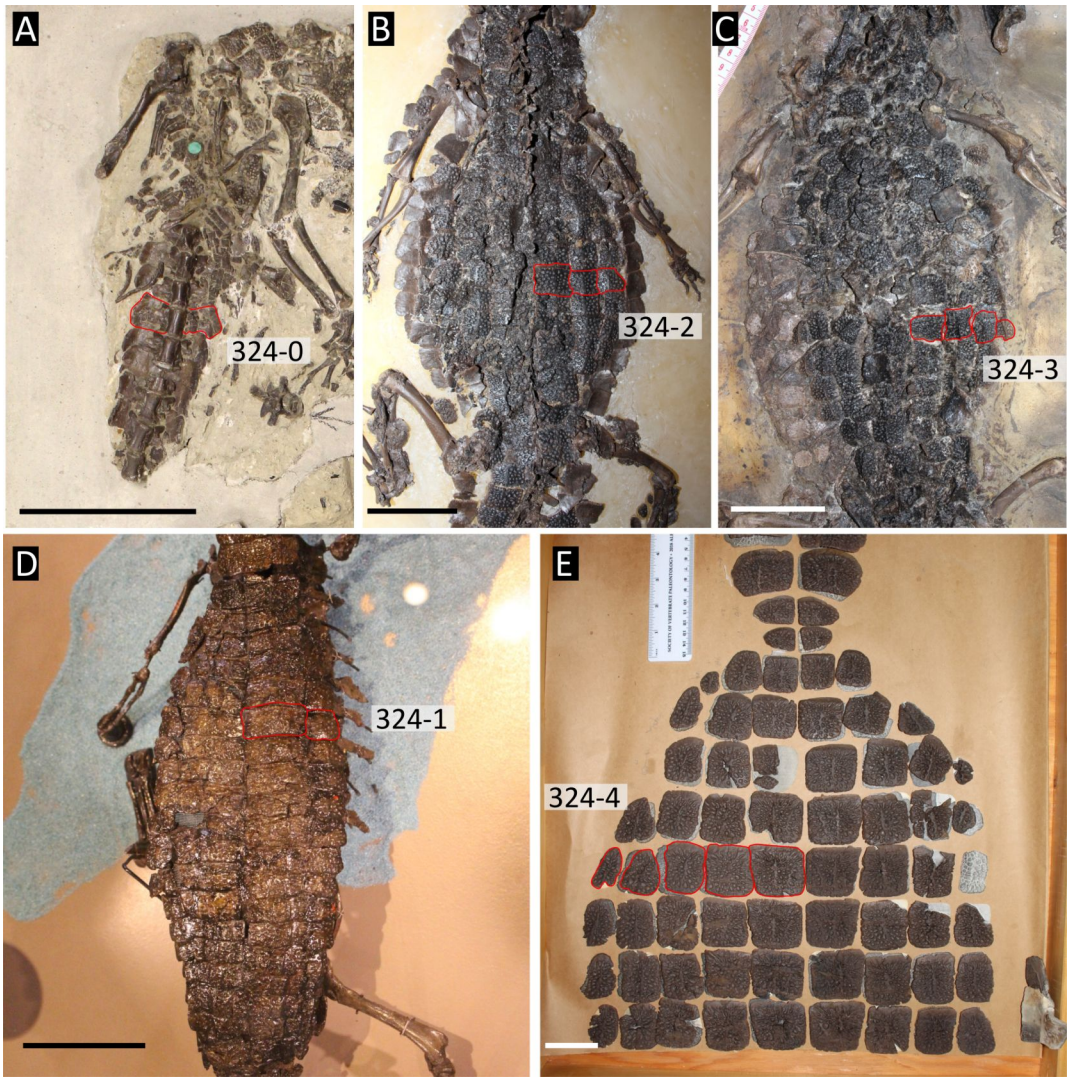



Figure 3.133: Variation in number of contiguous osteoderm rows. (All specimens in dorsal view except A, which is in ventral view). **A**, *Theriosuchus pusillus* (NHMUK 48216); **B**, *Diplocynodon darwini* (HLMD Me-10262); **C**, *Hassiacosuchus haupti* (HLMD Be-137); **D**, *Bernissartia fagesii* (IRSNB 1538); **E**, *Brachychampsa montana* (UCMP 133901). All scale bars = 5 cm.

326. Dorsal midline osteoderm shape: rectangular, width to length ratio $>$ 1 (0); approximately square, width to length ratio $\leq$ 1 (1) (after Norell & Clark, 1990 [16]; Clark, 1994 [95]; Brochu, 1997b [36]).

327. Dorsal midline osteoderms, anterolateral process: present (0); absent (1) (after Norell and Clark, 1990 [31]; Clark, 1994 [96]; Brochu, 1997b [40]).

    Characters 326 and 327 refer to the morphology of dorsal osteoderms in the first paravertebral (longitudinal) row, i.e. either side of the sagittal plane. This is a salient point as the shape of the osteoderms can vary along a single transverse row. These osteoderms are notably wider than long in *Bernissartia* (IRScNB 1538), *Borealosuchus* (Erickson, 1976, fig.30), and most longirostrine crocodylians, including *Gavialis gangeticus* and *Tomistoma schlegelii*. The decision was made not to treat this character continuously since osteoderm shape varies across transverse rows of the same individual, and there is uncertainty in the position of isolated fossil osteoderms.

    Where present the anterolateral process of the dorsal midline osteoderms varies in morphology between taxa. In *Theriosuchus pusillus* (NHMUK 48216), this process is extremely acute, forming a peg-like process. A homologous rounded swelling at the anterolateral margin of the osteoderm also occurs in *Bernissartia* (IRScNB 1538), *Borealosuchus* (e.g. *B. sternbergii*, UCMP 134470), "gavialoids" (e.g. *Eogavialis africanum*, NHMUK R 3343), and some *Diplocynodon* species (Fig. 3.134D). This condition differs to the approximately straight anterior margin of the osteoderm in all other eusuchians where known (Fig. 3.134F–H).

328. Ventral osteoderms: absent (or poorly developed) (0); present, single ossification (1); present, paired ossification (2) (after Buscalioni et al., 1992 [21]; Brochu, 1997b [39]).

    Uniquely among extant crocodylians, caimanines exhibit paired (bipartite) ventral osteoderms. These typically comprise a short anterior element, with an unornamented gliding surface at its anterior end, and a sutural margin on its posterior end for a larger posterior element (Fig. 3.134C, J). Paired ventral osteoderms occur in a few fossil crocodylians, including all *Diplocynodon* (Fig. 3.134E, see also Section 2.3.5) and *Borealosuchus* species where known (Brochu, 1997a; Brochu et al., 2012). By contrast, *Bernissartia fagesii* (IRScNB 1538) exhibits single, well-formed osteoderms, as is the case in the 'basal' alligatoroids *Leidyosuchus* (Brochu, 1997a) and *Brachychampsa montana* (UCMP 133901), as well as *Alligator sinensis* (Fig. 3.134B) and *Crocodylus johnstoni* (Grigg & Kirshner, 2015, fig.3.15) among extant crocodylians. The remaining extant crocodylids (all further species of *Crocodylus* and *Mecistops*), *Tomistoma schlegelii*, and *Gavialis gangeticus*, exhibit poorly formed ventral osteoderms, or they are absent altogether. The poorly formed condition (328-0) is distinguished from 328-1 by the small, irregular shape of the osteoderms (Fig. 3.134A).

329. Tail armour: partial covering (usually $\leq$ 10 transverse rows of contiguous osteoderms posteriorly from the level of caudal vertebra one) (0); tail completely encased in osteoderms (1) (new character, adapted from Frey et al. 1987).

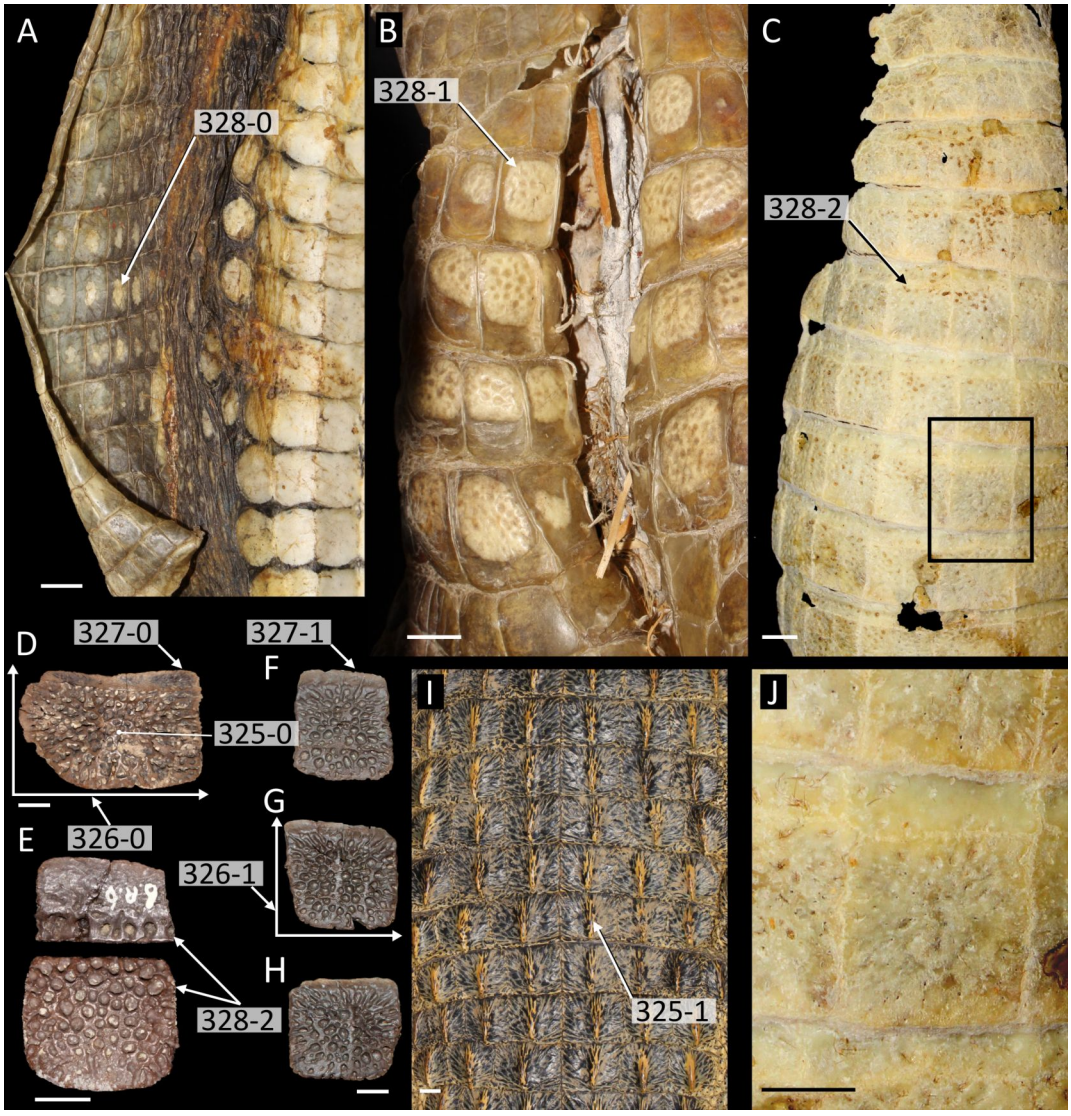



Figure 3.134: Morphology of the dorsal and ventral osteoderms. **A**–**B**, ventral view of the skin showing ventral osteoderms in **A**, *Mecistops cataphractus* (USNM 60578); **B**, *Alligator sinensis* (USNM 52557); **C**, ventral view of the ventral osteoderms in *Paleosuchus trigonatus* (USNM 302052); **D**, dorsal midline osteoderm of *Diplocynodon hantoniensis* (NHMUK uncatalogued); **E**, paired ventral osteoderm in *Diplocynodon hantoniensis* (NHMUK uncatalogued); **F**–**H**, dorsal midline osteoderms of *Brachychampsa montana* (UCMP 133901); **I**, dorsal osteoderms of *Crocodylus niloticus* (USNM 63592); **J**, enlargement of paired ventral osteoderms in **C**. All scale bars = 1 cm.

330. Limb armour: forelimbs and hindlimbs lack osteoderms, or weakly armoured with patches of poorly developed osteoderms (0); densely covered in well-formed osteoderms (1) (new character, adapted from Frey et al. 1987).

Frey et al. (1987) compared the distribution of osteoderms in two co-occurring alligatoroids from the Eocene age Messel Lagerstätte, *Diplocynodon* ('*Baryphracta*') *deponiae* and *Diplocynodon darwini*. They noted differences in osteoderm extent on the tail (Character 329) and limbs (Character 330) in these taxa. In particular, *Diplocynodon deponiae* exhibits a tail that is completely encased in osteoderms (329-1) (Fig. 3.135C). This condition is found in a few other taxa in this dataset, including extant caimanines (e.g. *Paleosuchus*, Fig. 3.135B), *Hassiacosuchus haupti* (Fig. 3.135D), *Tsoabichi greenriverensis* (FMNH PR 1793), and *Theriosuchus pusillus* (NHMUK 48216). By contrast, multiple exceptionally preserved specimens of *Diplocynodon darwini* consistently lack an osteoderm-encased tail. Indeed, most specimens of this species exhibit less than ten transverse rows of contiguous osteoderms on the tail (beginning from the first caudal vertebra). Osteoderms on the remainder of the tail of this species comprise two linear arrays of pin-shaped ossifications on the dorsolateral edges (329-0) (Fig. 3.135A). All other extant crocodylians similarly lack a tail encased in osteoderms, along with *Bernissartia* fagesii (IRScNB 1538), *Alligator prenasalis* (YPM 13799), and *Borealosuchus wilsoni* (FMNH PR 1674).

The distribution of osteoderms on the limbs follows a very similar pattern to that described for the tail. Indeed, almost all taxa with an osteoderm-encased tail (329-1) also exhibit a dense covering of osteoderms on the limbs (330-1). *Diplocynodon darwini* proves the exception to this rule, since it lacks an osteoderm encased tail (329-0) (Fig. 3.135A), but exhibits a dense covering of osteoderms on the fore- and hindlimbs (330-1) (Fig. 3.136C–D), as in *Diplocynodon deponiae* (Fig. 3.136E–G).

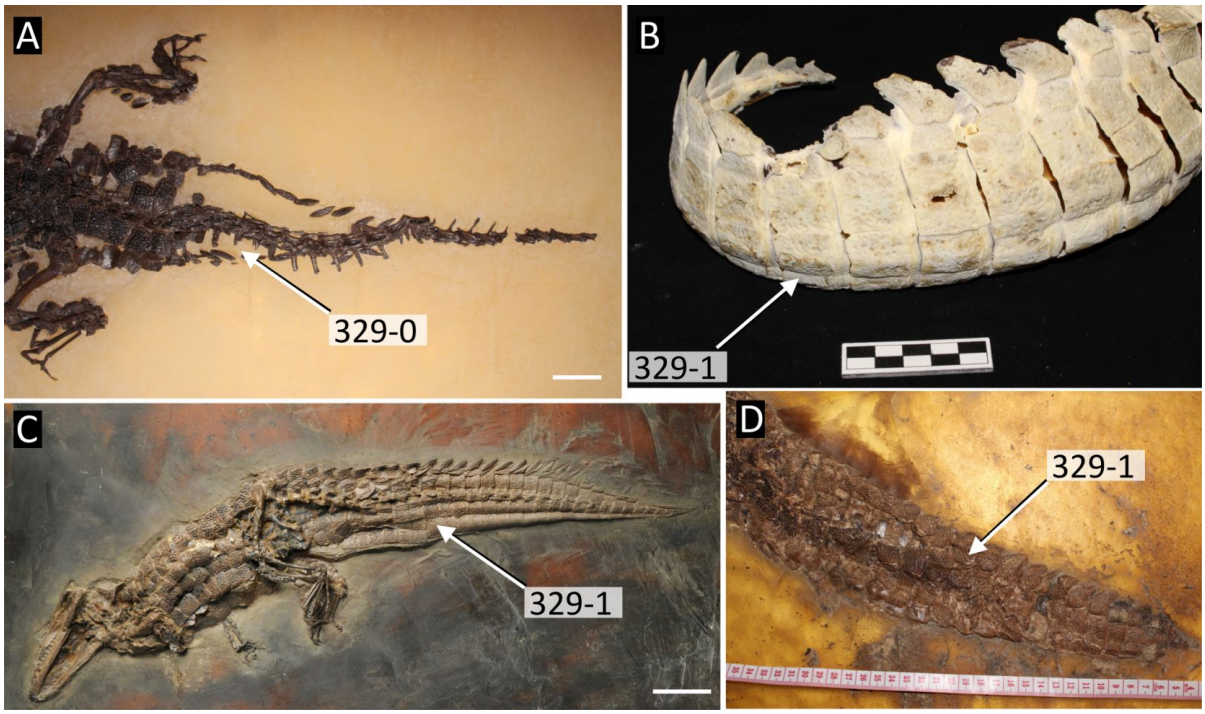



Figure 3.135: Variation in osteoderm arrangement in the tail of selected crocodylians: **A**, *Diplocynodon darwini* (HLMD Me-10262); **B**, *Paleosuchus trigonatus* (USNM 302052); **C**, *Diplocynodon deponiae* (SMF Me-899); **D**, *Hassiacosuchus haupti* (HLMD-Me-9119). Scale bars in A and C = 5 cm, B and D = cm.

## 3.5 Summary

This new character list constitutes the largest character list presented for a phylogenetic analysis of Crocodylia (330 characters). 45 characters are new, of which 27 are based on personal observations and 18 are adapted from a review of the literature (Table 3.1). 41 characters are derived by atomising complex multistate characters that either (1) combine non-homologous features, or (2) combine 'absent' and 'present but variable' states. A further 26 characters received major modifications by the addition or removal of character states, and 36 multistate characters are identified that can be ordered (Table 3.1). All characters received rephrasing to improve clarity, and 312 characters ($\sim$ 95%) are illustrated. Characters lacking illustration are either self-explanatory (e.g. tooth counts, Character 17) or with references to relevant sources for further guidance. 26 characters are continuous and include rediscretised state boundaries based on measured values. The rediscretisation of continuous characters demonstrated that existing character state boundaries for some characters appear arbitrarily drawn. Furthermore, in characters where new character state boundaries had to be erected, discontinuities in the data marking obvious threshold values were sometimes absent or challenging to interpret (Appendix D). 50% of the continuous characters had normally distributed values (indicated by the Shapiro-Wilk test) and the remainder exhibited skewed distributions. Multimodal distribution patterns, which might serve as a basis for delimiting quan-

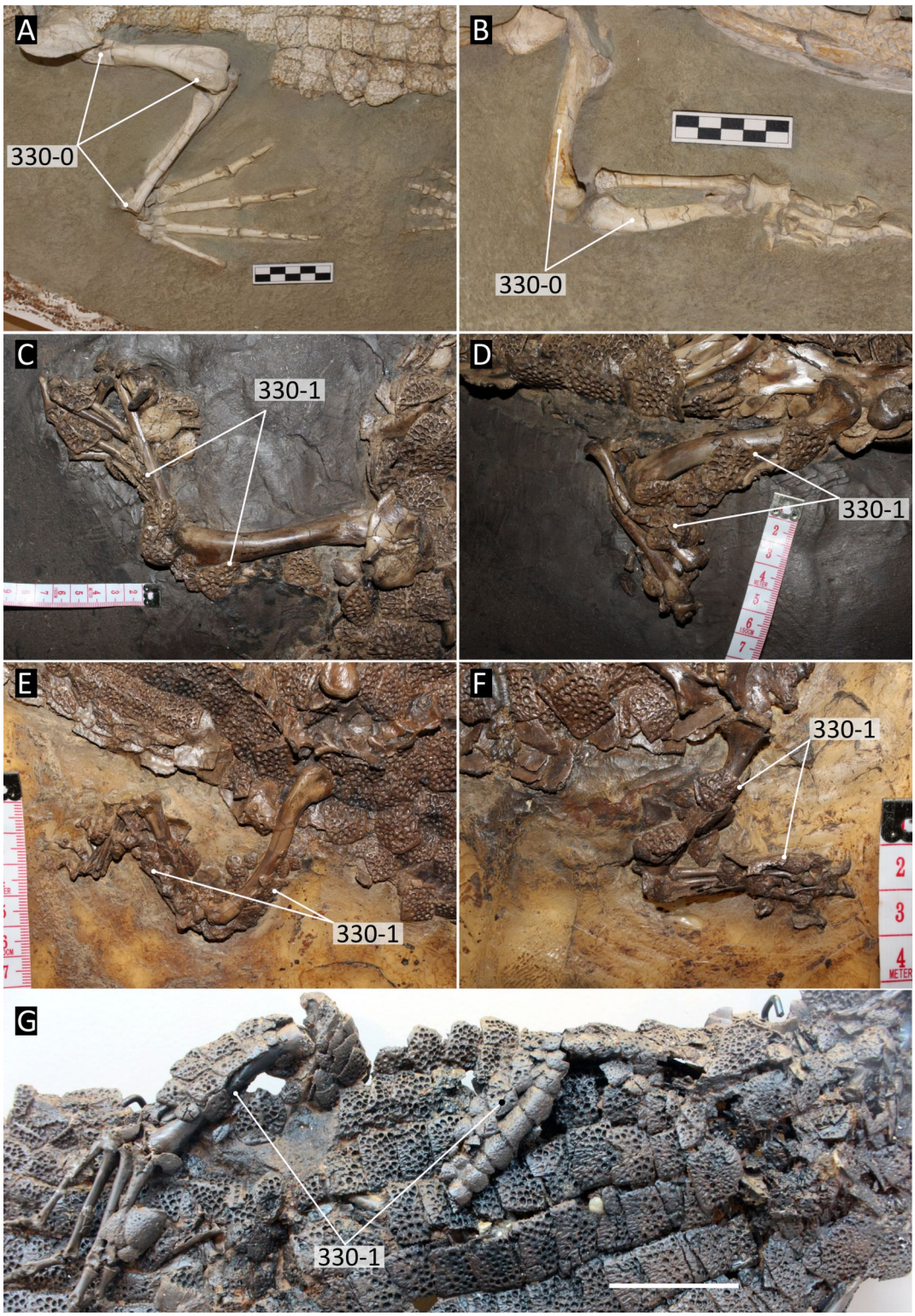



Figure 3.136: Variation in osteoderm cover on the hindlimb (left) and forelimb (right) (all right hand side): **A**–**B**, *Alligator prenasalis*, dorsal view (YPM 13799, digitally reversed in B); **C**–**D**, *Diplocynodon darwini*, dorsal view (HLMD Me-236); **E**–**F**, *Diplocynodon deponiae*, dorsal view (HLMD-Be-147); **G**, *Diplocynodon deponiae*, ventral view (IRScNB R261). Scale bars A–F = cm, G = 5cm.

titative characters, were not identified. Altogether, this provisionally demonstrates the efficacy of treating quantitative data continuously, rather than imposing arbitrary values to delimit discrete character states. Nevertheless, the role of these alternative coding strategies are explored in Chapter 4.

Table 3.1: Summary of major modifications to the character list. Emboldened new characters are based on personal observations. *Atomised characters include reductively coded characters and atomised complex multistate characters.

| | Number | Characters |
|---|---|---|
| New characters | 45 | 2, 5, 9, **16**, **23**, **26**, 27, **32**, **33**, **34**, **45**, 64, **71**, 80, 82, **88**, 96, **97**, **111**, **120**, **122**, 125, **126**, **139**, **149**, **153**, 165, 170, 178, **182**, **191**, **203**, **227**, **233**, **240**, **243**, **249**, **259**, 303, **306**, 311, 312, **319**, 329, 330 |
| Atomised characters* | 41 | 38–40, 46–48, 53–56, 77–78, 100–101, 105–106, 112–115, 118–119, 169–170, 193–194, 207–208, 209–210, 212–213, 222–225, 230–231, 234–235, 254–255, 308–309, 322–323 |
| Characters ± states | 26 | 37, 61, 63, 94, 109, 118–119, 127, 136–138, 142, 146, 157, 162, 181, 195, 210, 214, 222, 237, 255, 260, 316–317, 324 |
| Ordered multistate characters | 36 | 17, 37, 47, 48, 58, 65, 72, 75, 78, 81, 87, 88, 102, 109, 110, 137, 142, 151, 162, 175, 181, 188, 210, 214, 220, 221, 222, 224, 235, 243, 284, 293, 297, 308, 323, 324 |

# Chapter 4

# Exploring the Evolutionary Relationships of Crocodylia

# 4.1 Introduction

The primary aim of this chapter is to discuss the results of phylogenetic analyses based on the new morphological character list discussed in Chapter 3. After outlining the analytical protocols, I compare the results of several analyses that use alternative character weighting strategies and different treatments of quantitative characters. I present a new hypothesis for crocodylian interrelationships, then systematically outline and discuss new diagnoses for principal crocodylian clades, critically assess major topological differences with previous studies using constrained searches, and address several specimen level problems.

# 4.2 Methods

## 4.2.1 Taxon sampling

The complete dataset consists of 144 operational taxonomic units (OTUs), 119 of which were studied first-hand. Character scoring for the remaining 25 OTUs was based on descriptions and figures in the literature, supplemented by photographs from colleagues. The choice of outgroup can have a significant effect on topology, as demonstrated previously for crocodyliforms (Wilberg, 2015; Sookias, 2020). As such, 12 of the OTUs consist of taxa that lie outside of the crocodylian radiation, comprising: *Bernissartia fagesii* (the designated outgroup taxon), *Isisfordia duncani*, *Theriosuchus pusillus*, three paralligatorids (the 'Glen Rose Form', *Wannchampsus kirpachi*, and *Shamosuchus djadochtaensis*), three hylaeochampsids (*Hylaeochampsa vectiana*, *Iharkutosuchus makadii*, and *Acynodon iberoccitanus*), and three allodaposuchids (*Allodaposuchus precedens*, *Agaresuchus fontisensis*, and *Lohuecosuchus megadontos*). A full list of OTUs, including which specimens and publications were used for scoring is provided in Appendix B.

## 4.2.2 Phylogenetic analyses

Three sets of analyses were performed, each with a different treatment of quantitative data (Table 4.1): (1) quantitative characters treated continuously; (2) quantitative characters treated discretely; and (3) quantitative characters omitted. Within each set, parsimony analyses were conducted under: (i) equal weighting; (ii) EIW with a $k$ value of 3 (EIW3), and (iii) EIW with a $k$ value of 12 (EIW12).

Table 4.1: Summary of phylogenetic analyses performed.

| Analysis | Characters | Weighting | No. characters |
|---|---|---|---|
| 1.1 | Continuous and discrete | Equal weights | 330 |
| 1.2 | Continuous and discrete | EIW, *k*=3 | 330 |
| 1.3 | Continuous and discrete | EIW, *k*=12 | 304 |
| 2.1 | Rediscretised | Equal weights | 330 |
| 2.2 | Rediscretised | EIW, *k*=3 | 330 |
| 2.3 | Rediscretised | EIW, *k*=12 | 304 |
| 3.1 | Quantitative excluded | Equal weights | 330 |
| 3.2 | Quantitative excluded | EIW, *k*=3 | 330 |
| 3.3 | Quantitative excluded | EIW, *k*=12 | 304 |

### Scaling continuous characters

When characters are treated continuously in software such as TNT (Goloboff et al., 2008b), the absolute difference between one character value and another is used to calculate the cost of character state transformations, with up to 3 decimal places considered (Brocklehurst et al., 2016). As such, the cost of a transformation between a condition in one species to the condition in another is proportional to the magnitude of that difference. Difficulty arises, however, when trying to determine the relative cost of transformations between characters that vary on different orders of magnitude (Goloboff et al., 2006; Koch et al., 2015). This occurs in continuous character datasets because it is possible to combine meristic characters, ratios of measurements, and characters measured using different units. This raises the need to scale continuous characters, i.e. to adjust the cost of transformations between characters (Goloboff et al., 2006). In particular, characters varying on larger orders of magnitude need to be scaled down relative to characters that vary on smaller orders of magnitude.

Implied weighting was proposed as a way to decrease the problem of scaling. Measures of homoplasy will be greater in characters that vary on a larger scale, and those characters would be down-weighted when implied weighting is implemented (Goloboff et al., 2006). Other authors have re-scaled continuous characters to unity, i.e. making the total range of a continuous character equal to one step of a discretely coded character (Escapa & Catalano, 2013; Koch et al., 2015; Groh et al., 2020). Empirical evidence demonstrates that while both methods diminish the issue of scaling, implied weights only does so partially, and higher values of group support result from first re-scaling continuous characters (Koch et al., 2015). As such, continuous characters were re-scaled by taking the reciprocal of the total range of the continuous character ($x$) (Equation 4.1). Since character weights must be integers in TNT, this value was multiplied by 100. Rescaled character transformation costs for continuous characters 1–26 can be found in Supplementary file 1.

$$\frac{1}{x} \times 100 \tag{4.1}$$

**Analytical protocols**

All analyses were performed using the New Technology Search in TNT (Goloboff et al., 2008b; Goloboff & Catalano, 2016), with all algorithms enabled and the consensus tree stabilized five times with a factor of 75. Trees recovered from the first iteration were used as starting trees for a traditional search using tree bisection and reconnection (TBR). 36 multistate characters were treated as ordered as they represent a clear transformational series (Brazeau, 2011) (Table 3.1).

### 4.2.3 Measures of phylogenetic accuracy

The consensus of optimal trees from analyses using continuous characters and extended implied weighting tends to be more resolved than trees obtained from discrete characters and equal weighted analyses. This is because taxa seldom share identical scores for continuous characters (values of which can have up to three decimal places), resulting in fewer ties in tree lengths. Similarly, fewer ties between most parsimonious trees (MPTs) are recovered under extended implied weighting, because the differential weighting of characters based on their homoplasy results in tree lengths with non-integer values. Consequently, very well resolved, but poorly supported, clades can be encountered, such that measures of internal accuracy become even more important. A total of nine phylogenetic analyses were conducted in this study, each producing a series of MPTs. After each analysis, support was assessed by resampling using the Jackknife and Bootstrap scripts provided in TNT, each with 100 replicates to reduce computational time across the nine analyses. Support was also assessed using the Bremer decay index. Differences in the relative step-length of characters after rescaling and extended implied weighting can obscure Bremer support values. These become non-integers, and their order of magnitude changes between analyses using a different $k$ value. This makes the practice of collapsing nodes with a Bremer support value of less than 1 step difficult. To account for this, the average step length of a character after weighting was calculated for each analysis similar to the approach of Jones and Butler (2018). This was achieved by dividing tree length by the sum of all character transformations. Nodes with a Bremer support below the weighting-adjusted average step length were collapsed, and the remaining nodes were counted for each analysis. The consistency index (CI) and retention index (RI) were also calculated using the Stats.run script provided in TNT. Individual character CI and RI values were calculated using the Charstats.run script made available by Martin Ramírez (https://sites.google.com/site/teosiste/tp/archivos).

### 4.2.4 Stratigraphic congruence

Bremer support, Jackknife, and Bootstrap each provide a measure of a tree's internal accuracy, which does not necessarily mean the topology is correct. As such, stratigraphic congruence was used as an independent measure of validity following previous studies (e.g. Jones & Butler, 2018; Groh et al., 2020).

Stratigraphic congruence was calculated for each set of MPTs in R version 3.5.1 (R Core Team, 2018) using the 'StratPhyloCongruence' command in the package strap (Bell & Lloyd, 2015). Taxon age ranges were extracted from Mannion et al. (2019) and a review of the literature (Appendix E). The strap package implements four measures of stratigraphic congruence. Firstly, the Stratigraphic Consistency Index (SCI) is the ratio of the stratigraphically 'consistent' internal nodes to the total number of nodes (Huelsenbeck, 1994). To be considered 'consistent', the first appearance datum of a node's descendants must be equal to or younger than its sister node. Secondly, the Relative Completeness Index (RCI) is defined by the ratio of the minimum implied ghost ranges of a time calibrated tree, to the sum of the stratigraphic ranges of all taxa (Benton & Storrs, 1994). Thus, it effectively describes the proportion of time in a phylogenetic tree that is occupied by known taxon ranges. Thirdly, the Manhattan Stratigraphic Measure (MSM*) works by optimising the differences in first appearance ages of taxa as a Sankoff character in a target tree, and calculating its total length (Siddall, 1998; Pol & Norell, 2001). The ratio of target tree length is taken to the minimum possible tree length (a tree in which the youngest appearing taxa are deeply nested, and older taxa are successively nested towards the root). Fourthly, the Gap Excess Ratio (GER) operates by defining optimal and suboptimal hypothetical trees based on the maximum and minimum possible sum of ghost ranges, respectively (Wills, 1999). Stratigraphic congruence is then based on the proportion of ghost ranges in a target tree compared to the suboptimal and optimal trees. The significance of each congruence measure was tested using the 'StratPhyloCongruence' command, using 1000 permutations each for randomly generated and resampled trees.

### 4.2.5 Constrained searches

Constrained searches were performed using the 'Force' command in TNT to compare the topologies of each analysis with existing hypotheses. The significance of tree length increase was assessed using the Templeton test with the TNT script 'templetontest.run' provided by Alexander Schimdt-Lebuhn (http://phylo.wikidot.com/tntwiki). A full list of constraints applied in this study can be found in Appendix F.

### 4.2.6 Categorisation of synapomorphies

Where synapomorphies are discussed, they are categorised following the protocol in Tschopp et al. (2015). Unambiguous synapomorphies are present in all ingroup taxa, but no taxa (in this dataset) outside of the ingroup (Fig. 4.1A). Exclusive synapomorphies occur in some though not all ingroup taxa, but not in any taxon (in this dataset) outside of the ingroup (Fig. 4.1B). Shared synapomorphies are present in all ingroup taxa and occur in some taxa outside of the ingroup (Fig. 4.1C). Ambiguous synapomorphies occur in some but not all ingroup taxa, and also occur outside of the ingroup (Fig. 4.1D). 'Potential

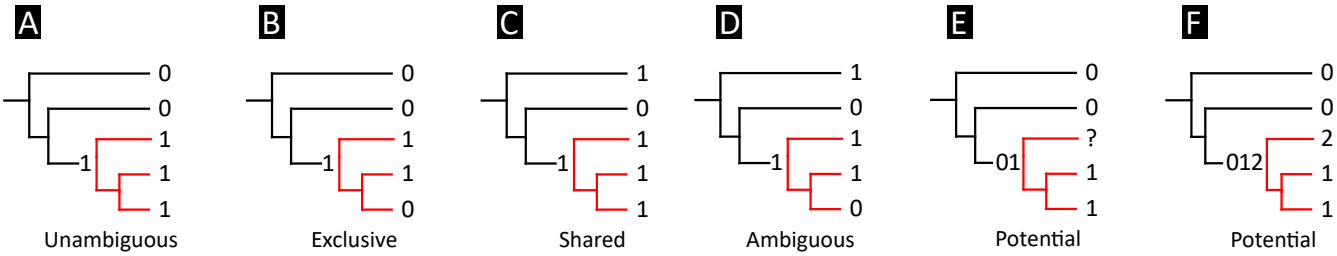



Figure 4.1: Summary of terms used to categorise synapomorphies. Red branches highlight the ingroup.

synapomorphies' is a new category added here, describing character states which could be diagnostic of the ingroup. When optimising synapomorphies in TNT, these potential synapomorphies are not listed because of uncertainty in the condition of taxa immediately in the stem of the ingroup (Fig. 4.1E), or because closely related taxa and immediate outgroups exhibit different conditions (Fig. 4.1F). These definitions differ to previous studies of crocodylian systematics, e.g. Brochu (1999). Although no definitions of 'unambiguous' and 'ambiguous' were outlined by Brochu (1999), the use of the term 'unambiguous' appears to be more conservatively applied here. An examination of the data matrix of Brochu (1999) reveals that some characters described therein as unambiguous would be described as shared or ambiguous here. For example, his character state 41-1 was recovered as an 'unambiguous' synapomorphy of *Diplocynodon hantoniensis* + *Diplocynodon ratelii*. Here it would be described as 'shared', as it also occurs outside of this clade. Similarly, his character state 93-1 was unambiguously diagnostic of Alligatoridae (Brochu, 1999), but here it would be considered 'ambiguous' due to the absence of the feature in some ingroup taxa, and occurrence of the feature in some outgroup taxa.

## 4.3 Results

### 4.3.1 Overall topological results

All analyses produced informative results (Fig. 4.2, Appendix G), with the exception of Analysis 3.1 (quantitative characters excluded, equal weights), which resulted in >400,000 MPTs, recovering a large polytomy between most in-group taxa (Fig. 4.2C, Appendix G.6). Nevertheless, in all analyses (including Analysis 3.1), *Gavialis gangeticus* is recovered as the closest living relative of *Tomistoma schlegelii*, together defining the crown gharial clade Gavialidae. Results of the eight informative analyses can be divided into two topological categories that tend to correlate with weighting strategy. The first set comprises all equal weighted analyses (1.1 and 2.1, but not the unresolved 3.1) (Fig. 4.2A, 4.2B) and all analyses using EIW12 (analyses 1.3, 2.3, and 3.3) (Fig. 4.2D). In the resultant topologies from these analyses, Crocodylia comprises three lineages: (Alligatoroidea + (Crocodyloidea + Gavialoidea)). Crocodyloidea is shorn of morphological "tomistomines" that are now recovered within Gavialoidea. To-

gether, Gavialoidea and Crocodyloidea comprise Longirostres, which is the sister clade to Alligatoroidea (Harshman et al., 2003). The second category comprises all analyses under EIW3 (1.2, 2.2, and 3.2). These analyses recover an unconventional relationship, in which Crocodylia comprises: (Crocodyloidea + (Alligatoroidea + Gavialoidea)) (Fig. 4.2E). The compositions of Alligatoroidea and Crocodyloidea are very similar between all analyses and identical in Gavialoidea. Principle differences in topology mostly pertain to three labile taxa: *Borealosuchus*, *Diplocynodon*, and Planocraniidae (Fig. 4.2). *Borealosuchus* is recovered as a stem crocodylian in all analyses except 2.1 (in which it is recovered as a stem longirostrine) (Fig. 4.2B) and 3.1 (unresolved). *Diplocynodon* is recovered as a 'basal' alligatoroid in all analyses except 2.1 (in which it is recovered as a stem longirostrine) and 3.1 (unresolved). Whereas Planocraniidae is recovered as a 'basal' alligatoroid in analyses 1.2, 2.2, and 3.2 (EIW3), it occurs in the stem to Longirostres in analyses 1.3, 2.3, 3.3 (EIW12) and analysis 2.1. In Analysis 1.1, Planocraniidae is polyphyletic; whereas *Planocrania hengdongensis* is recovered in the stem to Crocodylia, the clade (*Planocrania datangensis* + (*Boverisuchus vorax* + *Boverisuchus magnifrons*)) is recovered as a 'basal' member of Alligatoroidea. Otherwise, the taxonomic content of the principal crocodylian clades is relatively consistent between analyses.

### 4.3.2 Phylogenetic accuracy

Table 4.2 summarises three measures of internal phylogenetic accuracy for each analysis: Bremer support (as number of nodes retained after collapsing branches with a support value less than one average step length), average Jackknife, and average Bootstrap. Furthermore, these values are mapped on to the topology resulting from Analysis 1.3 (Fig. 4.3). Overall, these measures are low across the trees of all analyses, which is most likely the result of the high degree of taxon sampling in this study, which includes a large number of incompletely preserved specimens. In Analysis 1 (quantitative characters treated continuously), the highest Bremer support, Jackknife, and Bootstrap values are consistently recovered under EIW12 (Analysis 1.3). The lowest support values are consistently obtained under EIW3 (Analysis 1.2). In the rediscretised dataset, average Bootstrap and Jackknife values are highest in the analysis employing EIW12, but lowest in the equal weighted analysis (Analysis 2.1). However, Analysis 2.1 retains the greatest number of nodes (84) above one step length and Analysis 2.2 retains the fewest (30). Among the analyses that excluded quantitative characters, Analysis 3.2 has the lowest Bremer support and Bootstrap values on average, whereas Analysis 3.3 has the highest Bremer support and Jackknife values on average.

A comparison of average Bremer Support values in different parts of the tree (Alligatoroidea, Crocodyloidea and Gavialoidea) in each analysis, reveal that internal support within Crocodyloidea is typically lower than in Alligatoroidea and Gavialoidea (Table 4.3). The exceptions are in Analysis 3.1, in which Alligatoroidea could not be resolved at all, and in Analysis 2.1, in which average Bremer support values were equally low in Crocodyloidea and Alligatoroidea. By contrast, average internal support was higher

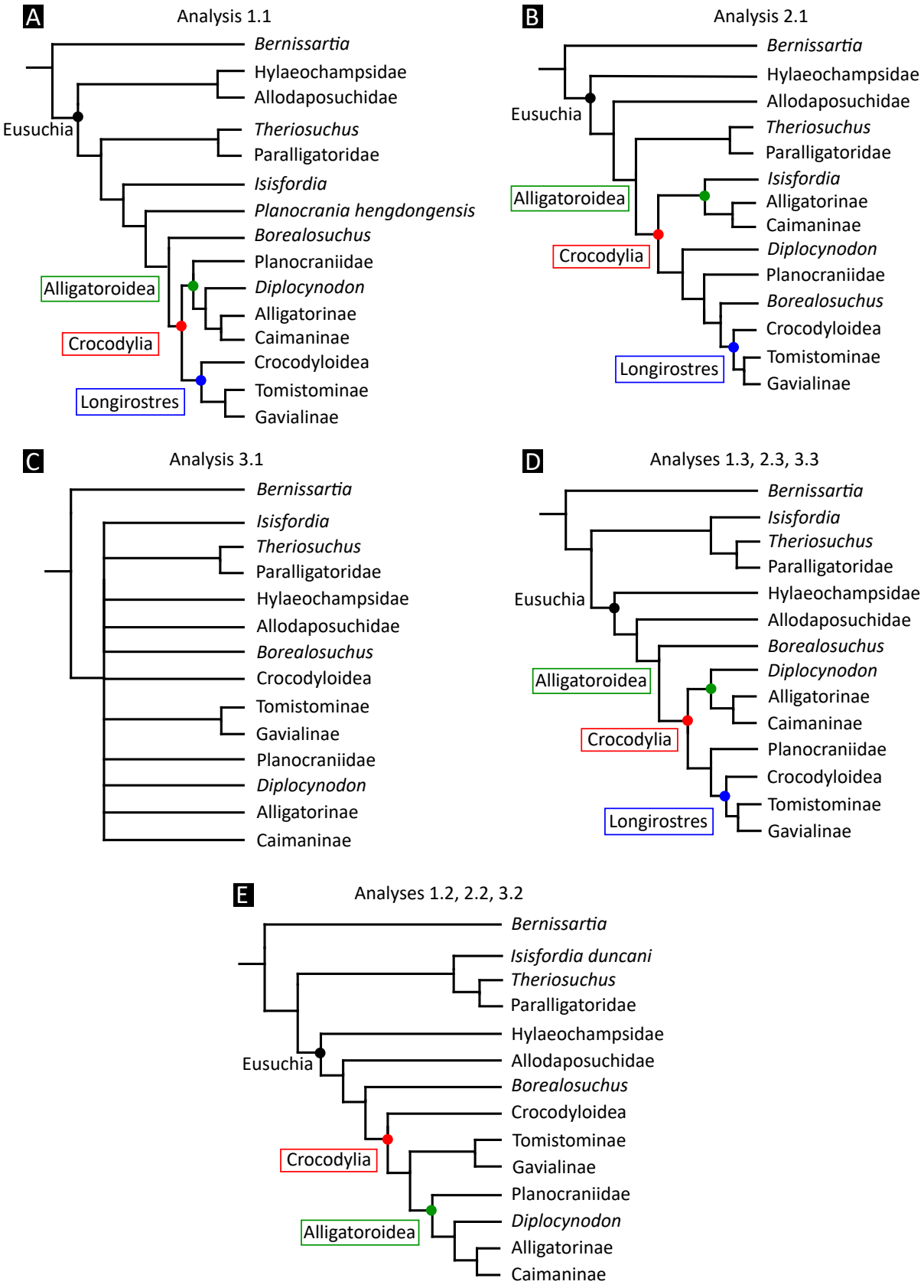



Figure 4.2: Summary of phylogenetic results from all nine analyses. The strict consensus trees from all analyses are produced in full in Apendix G.

Table 4.2: Summary of measures of internal tree support.

| Analysis | MPTs | Tree length | CI | RI | Step length | Nodes retained | Average Bootstrap | Average Jackknife |
|---|---|---|---|---|---|---|---|---|
| 1.1 | 6 | 225142.3 | 0.182 | 0.665 | 101.600 | 52 | 16.7 | 20.6 |
| 1.2 | 9 | 15852.4 | 0.175 | 0.649 | 6.880 | 20 | 15.5 | 14.1 |
| 1.3 | 3 | 8181.9 | 0.178 | 0.657 | 3.620 | 54 | 18.0 | 23.8 |
| 2.1 | >400000 | 2279 | 0.182 | 0.644 | 1.000 | 84 | 7.5 | 7.9 |
| 2.2 | 3 | 158.0 | 0.170 | 0.645 | 0.067 | 30 | 13.9 | 19.2 |
| 2.3 | 3 | 83.2 | 0.174 | 0.654 | 0.037 | 49 | 17.5 | 22.3 |
| 3.1 | >400000 | 2042 | 0.191 | 0.661 | 1.000 | 46 | 20.5 | 16.6 |
| 3.2 | 69 | 144.6 | 0.178 | 0.663 | 0.068 | 25 | 15.7 | 19.5 |
| 3.3 | 3 | 75.3 | 0.182 | 0.672 | 0.036 | 48 | 18.0 | 22.9 |

in Gavialoidea than Crocdyloidea and Alligatoroidea in all analyses except Analysis 3.2.

### 4.3.3 Stratigraphic congruence

The topologies recovered under all analyses are more stratigraphically congruent than would be expected of random data. Three of the four indicies (RCI, GER, and MSM*) show overall consistent trends. These indicate that Analysis 1.3 (continuous and discrete data with EIW12) recovered the most stratigraphically congruent topology, and Analysis 2.1 recovered the most incongruent topology (equal weighting and quantitative characters rediscretised) (Table 4.4). However, the SCI values do not follow this trend, instead indicating that the most stratigraphically congruent topology is recovered under Analysis 3.1, followed by analyses 2.1, 1.1, and 1.3, respectively. It is noteworthy that analyses 3.1 and 2.1 produced the largest number of MPTs. As such, the ranges of values of stratigraphic congruence between the best and worst trees in these analyses are the largest of all other analyses. Indeed, although analyses 3.1 and 2.1 recover the highest SCI values, Analysis 3.1 also recovers the lowest, and the worst tree in Analysis 2.1 is less stratigraphically congruent than the worst tree recovered in analyses 1.1, 1.3, and 2.3. Across all analyses, values for RCI, GER, and MSM* were consistently higher in analyses under EIW12 and usually lowest under EIW3 (Table 4.4).

### 4.3.4 Detailed topological results

In order to facilitate the presentation of topological results in more detail, the results of one analysis are chosen to avoid lengthy and unwieldy comparisons between multiple alternative topologies. The results of analyses 1.2, 2.2, and 3.2 are considered the least probable, because the sister relationship between Alligatoroidea and Gavialoidea contradicts the consensus of all morphological and molecular analyses to date. Furthermore, the trees produced from these analyses are among the least stratigraphically congruent and had the lowest Bremer support values of all analyses (Table 4.2). These results likely reflect the

severe weighting factor ($k$=3) implemented in these analyses, which has been advised against in large datasets (Goloboff et al., 2018). Analyses 3.1 and 2.1 recovered large numbers of MPTs (>400,000 in each case), such that the resultant strict consensus trees are the least informative of all other analyses, and are also characterised by low values of stratigraphic congruence. Analyses 1.1, 1.3, 2.3, and 3.3 recover similar topologies (Fig. 4.2), with Analysis 1.3 producing the most stratigraphically congruent result. Consequently, further discussion is centred on Analysis 1.3, although comparisons are made with analyses 1.1, 2.3, and 3.3, where relevant.

### Overall topology

The stem of Crocodylia comprises a series of successively nested, early diverging non-crocodylian eusuchians (Fig. 4.3). A division occurs at the crown node Crocodylia, which separates Alligatoroidea from Planocraniidae + Longirostres. Within Longirostres, a further branching occurs between Gavialoidea and Crocodyloidea.

### Non-crocodylian eusuchians

*Isisfordia duncani* + (*Theriosuchus pusillus* + Paralligatoriidae) are recovered as the earliest diverging non-crocodylian eusuchians in this dataset. The clade comprising *Theriosuchus pusillus* + (*Shamosuchus djadochtaensis* + (*Wannchampsus kirpachi* + the 'Glen Rose Form')) is similar to previous studies (e.g. Turner, 2015; Tennant et al., 2016). Hylaeochampsidae (*Acynodon iberoccitanus* + (*Iharkutosuchus makadii* + *Hylaeochampsa vectiana*)) and Allodaposuchidae (*Lohuecosuchus megadontos* + (*Allodaposuchus precedens* + *Agaresuchus fontisensis*) are recovered as successively branching lineages. This is consistent with Narváez et al. (2016), but differs from many earlier studies, which support a sister relationship between Hylaeochampsidae and Allodaposuchidae (e.g. Brochu et al., 2012; Narváez et al., 2015; Turner, 2015). Moving crownward, the multispecific *Borealosuchus* is recovered as the sister clade to Crocodylia. The monophyly of *Borealosuchus* is well supported (recovered in 50% of Jacknife replicates, Bremer support 4.7). Relationships within the genus are weakly supported, but *Borealosuchus sternbergii* is recovered as the earliest diverging member of the group, outside of two pairs of nested sister taxa: (*Borealosuchus wilsoni* + *Borealosuchus threeensis*) + (*Borealosuchus formidabilis* + *Borealosuchus acutidentatus*).

### Alligatoroidea

Similar to most previous studies, *Leidyosuchus canadensis* and *Diplocynodon* are recovered as the earliest diverging members of Alligatoroidea (Fig. 4.3) (Brochu, 1999; Brochu et al., 2012). However, by contrast to nearly all previous analyses, the multispecific genus *Diplocynodon* is paraphyletic. This paraphyly

Table 4.3: Average Bremer support values by clade. *Calculated by dividing average Bremer support by average step length (see Table 4.2).

| Analysis | Clade | Average Bremer Suppport | *Standardised Bremer Support |
|---|---|---|---|
| A1.1 | Alligatoroidea | 136.3 | 1.3 |
| | Gavialoidea | 175.65 | 1.7 |
| | Crocodyloidea | 73.95 | 0.7 |
| A1.2 | Alligatoroidea | 4.17 | 0.6 |
| | Gavialoidea | 5.36 | 0.8 |
| | Crocodyloidea | 1.21 | 0.2 |
| A1.3 | Alligatoroidea | 3.52 | 1.0 |
| | Gavialoidea | 4.4 | 1.2 |
| | Crocodyloidea | 1.98 | 0.5 |
| A2.1 | Alligatoroidea | 1.22 | 1.2 |
| | Gavialoidea | 1.71 | 1.7 |
| | Crocodyloidea | 1.24 | 1.2 |
| A2.2 | Alligatoroidea | 0.044 | 0.7 |
| | Gavialoidea | 0.048 | 0.7 |
| | Crocodyloidea | 0.014 | 0.2 |
| A2.3 | Alligatoroidea | 0.03 | 0.8 |
| | Gavialoidea | 0.042 | 1.1 |
| | Crocodyloidea | 0.022 | 0.6 |
| A3.1 | Alligatoroidea | 0 | 0.0 |
| | Gavialoidea | 1.77 | 1.8 |
| | Crocodyloidea | 1.14 | 1.1 |
| A3.2 | Alligatoroidea | 0.049 | 0.7 |
| | Gavialoidea | 0.037 | 0.5 |
| | Crocodyloidea | 0.014 | 0.2 |
| A3.3 | Alligatoroidea | 0.032 | 0.9 |
| | Gavialoidea | 0.043 | 1.2 |
| | Crocodyloidea | 0.019 | 0.5 |

Table 4.4: Summary of indices of stratigraphic congruence. The *p*-values for all stratigraphic congruence values (not shown) were all $< 0.0001$.

| Analysis | SCI | | RCI | | GER | | MSM* | |
|---|---|---|---|---|---|---|---|---|
| | Best tree | Worst tree | Best tree | Worst tree | Best tree | Worst tree | Best tree | Worst tree |
| 1.1 | 0.493 | 0.479 | -219.177 | -219.703 | 0.837 | 0.836 | 0.054 | 0.054 |
| 1.2 | 0.451 | 0.430 | -236.654 | -247.555 | 0.828 | 0.822 | 0.052 | 0.050 |
| 1.3 | 0.472 | 0.456 | -204.232 | -206.205 | 0.845 | 0.844 | 0.057 | 0.057 |
| 2.1 | 0.507 | 0.437 | -252.765 | -314.393 | 0.819 | 0.786 | 0.05 | 0.042 |
| 2.2 | 0.437 | 0.415 | -248.362 | -254.279 | 0.821 | 0.818 | 0.050 | 0.049 |
| 2.3 | 0.458 | 0.444 | -218.074 | -219.269 | 0.838 | 0.837 | 0.055 | 0.055 |
| 3.1 | 0.542 | 0.415 | -238.322 | -307.601 | 0.827 | 0.789 | 0.051 | 0.043 |
| 3.2 | 0.458 | 0.430 | -252.106 | -277.419 | 0.819 | 0.806 | 0.049 | 0.046 |
| 3.3 | 0.451 | 0.437 | -217.368 | -220.034 | 0.838 | 0.837 | 0.055 | 0.054 |

results in the replacement of a conventional divergence between 'Diplocynodontinae' and 'Globidonta' (i.e. all other alligatoroids) (Brochu, 1999) with successive branching lineages in the stem leading to the crown group Alligatoridae. Whereas *Diplocynodon hantoniensis* is most closely related to *Diplocynodon ratelii* + *Diplocynodon darwini*, *Diplocynodon deponiae* + (*Diplocynodon tormis* + *Diplocynodon muelleri*) are recovered further crownward. *Diplocynodon remensis* is recovered most crownward of all putative *Diplocynodon* species.

Crown group Alligatoridae is divided into Alligatorinae and Caimaninae; however, the taxonomic content and arrangement of both subclades is very different to previous studies. Firstly, the putative early caimanines, *Eocaiman cavernensis* and *Eocaiman palaeocenicus*, are placed outside of Alligatoridae, as is also the case for a series of taxa usually recovered as alligatorines (*Hassiacosuchus haupti*, *Procaimanoidea utahensis*, and *Arambourgia gaudryi*). Alligatorinae comprises the early diverging *Allognathosuchus wartheni*, which lies outside of the clade formed by (*Allognathosuchus polyodon* + *Navajosuchus mooki*) + *Alligator*. Except for the recovery of *Alligator mcgrewi* as the earliest diverging member of *Alligator*, the topology within *Alligator* is congruent with most previous studies (e.g. Brochu, 1999). *Alligator mississippiensis* and *Alligator mefferdi* are recovered as deeply nested sister taxa, with *Alligator mcgrewi*, *Alligator prenasalis*, *Alligator olseni*, and *Alligator sinensis*, as successively branching stemward taxa. The composition and topology of Caimaninae also differs from most previous findings. Firstly, two taxa traditionally recovered as alligatorines, *Ceratosuchus burdoschi* and *Wannaganosuchus brachymanus*, and two traditionally 'basal globidontans', *Brachychampsa montana* and *Stangerochampsa mccabei*, form an early diverging stem caimanine clade. The latter two species were also recovered in a similar position in the analyses of Salas-Gismondi et al. (2015) and Bona et al. (2018). In line with other recent studies, *Gnatusuchus pebasensis*, *Kuttanacaiman iquitosensis*, and

*Globidentosuchus brachyrostris* are also recovered among the earliest diverging caimanines (e.g. Salas-Gismondi et al., 2015; Salas-Gismondi et al., 2019; Cidade et al., 2020a); however, moving crownward from this point, support values for Caimaninae are very low.

A divergence occurs between Jacarea and the clade comprising: *Caiman lutescens* + (*Caiman gasparinae* + *Mourasuchus*) (Fig. 4.3). The composition of Jacarea is considerably expanded from its traditional meaning, but support for internal nodes is very low. *Caiman yacare* is the earliest diverging member of Jacarea, 'basal' to a clade comprising (*Acresuchus pachytemporalis* + (*Purussaurus neivensis* + (*Purussaurus mirandai* + *Purussaurus brasiliensis*))) and a complex series of successively branching clades (Fig. 4.3). Notably, the clade consisting of *Caiman crocodilus* + (*Tsoabichi greenriverensis* + (*Paleosuchus trigonatus* + *Paleosuchus palpebrosus*)) is deeply nested within Jacarea, and sister to a polytomous clade of stratigraphically early caimanines comprising *Protocaiman peligrensis*, *Necrosuchus ionensis*, and *Bottosaurus harlani*. The placement of this latter trio of taxa within Caimaninae is consistent with recent analyses, including evidence for a deeply nested position for both *Bottosaurus* and *Necrosuchus* (Brochu, 2011; Bona et al., 2018; Cossette & Brochu, 2018; Cidade et al., 2020a).

### Crocodyloidea

Crocodyloidea is recovered as the sister lineage to Gavialoidea, forming the clade Longirostres. The earliest diverging crocodyloids are *Asiatosuchus germanicus*, ('*Crocodylus*' *affinis* + *Asiatosuchus depressifrons*), and *Jiangxisuchus nankangensis*. These taxa form the stem of a large clade marked by a basal division broadly separating Mekosuchinae and the crown group Crocodylidae. The composition of Mekosuchinae is slightly different to previous analyses (e.g. Lee & Yates, 2018). Most notably, *Asiatosuchus nanlingensis* is deeply nested in Mekosuchinae, as the sister taxon to *Kambara murgonensis*. Furthermore, two putative mekosuchines are recovered outside of Mekosuchinae, with *Australosuchus clarkae* recovered in the stem to Crocodylidae, and *Quinkana* recovered as the sister taxon of '*Crocodylus*' *megarhinus*, within Crocodylinae. Mekosuchinae is composed of two sister lineages, which separate (*Kambara implexidens* + (*Kambara taraina* + (*Kambara murgonensis* + *Asiatosuchus nanlingensis*))) from (*Baru wickeni* + *Baru huberi* + (*Baru darrowi* + (*Trilophosuchus rackhami* + (*Ultrasetoni willisi* + *Mekosuchus* spp.)))). Crocodylidae is divided into two clades: Osteolaeminae and Crocodylinae. Within Osteolaeminae, *Euthecodon arambourgi* and *Brochuchus pigotti* are successively nested taxa to a clade consisting of *Voay robustus* + *Osteolaemus tetraspis*. The clade ('*Crocodylus*' *megarhinus* + *Quinkana*) is recovered in the stem of Crocodylinae, outside of the crown genus *Crocodylus*. *Crocodylus thorbjarnarsoni* and the African slender snouted crocodile, *Mecistops cataphractus*, are similarly recovered as stem crocodylines.

The relationships within the crown genus *Crocodylus* are weakly supported (Fig. 4.3), but show broad similarities to the results of molecular and existing morphological phylogenies (e.g. Brochu, 2000; Oaks,

2011). Three extant Indo-Pacific *Crocodylus* species (*Crocodylus johnstoni*, *Crocodylus novaeguineae*, and *Crocodylus mindorensis*) are the earliest diverging members of the genus (Fig. 4.3). These species are successively nested in the stem of the crown genus *Crocodylus*, which broadly separates extant Neotropical *Crocodylus* species from the remaining Indo-Pacific and African *Crocodylus*. Within the Neotropical clade, *Crocodylus morelettii* and *Crocodylus rhombifer* are successively nested species stemward to *Crocodylus intermedius* + *Crocodylus acutus*. On the opposite branch of the clade, (*Crocodylus niloticus* + (*Crocodylus palaeindicus* + *Crocodylus palustris*)) and (*Crocodylus porosus* + (*Crocodylus siamensis* + *Crocodylus anthropophagus*)) are sister clades.

**Gavialoidea**

By contrast to the results of most morphological phylogenies, I do not recover "Tomistominae" and "Gavialoidea" as separate lineages. In line with molecular analyses, as well as many combined morphological and molecular analyses, I recover *Tomistoma schlegelii* as the closest living relative of *Gavialis gangeticus*, defining the crown clade Gavialidae. Here, "Tomistominae" in the traditional sense (e.g. Brochu, 2007b; Piras et al., 2007; Jouve, 2016) is paraphyletic, recovered as a series of successively nested, early diverging lineages in Gavialoidea. This topology is most similar to that recovered in combined morphological and molecular analyses (Lee & Yates, 2018; Iijima & Kobayashi, 2019). The earliest diverging gavialoids recovered here are: (*Maroccosuchus zennaro*i + (*Kentisuchus spenceri* + *Dollosuchoides densmorei*)). Support is found for a second early diverging clade of traditional "tomistomines" at the base of Gavialoidea, composed of (*Maomingosuchus petrolica* + (*Gavialosuchus eggenburgensis* + ('*Tomistoma*' *lusitanica* + (*Thecachampsa sericodon* + *Thecachampsa antiquus*)))) (Fig. 4.3). This lineage is the sister group of the crown clade Gavialidae. The earliest diverging gavialids are: (*Tomistoma schlegelii* + *Paratomistoma courti*), *Toyotamaphimeia machikanensis*, and *Penghusuchus pani*. Taxa commonly referred to as 'thoracosaurs', such as *Thoracosaurus* spp., *Eosuchus* spp., and *Eothoracosaurus mississippiensis*, are nested within Gavialidae, but comprise a polyphyletic assemblage. Whereas the clade consisting of *Thoracosaurus macrorhynchus* + (*Eosuchus minor* + *Eosuchus lerichei*) is recovered as the sister clade to '*Tomistoma*' *cairense*, *Thoracosaurus neocesariensis* and *Eothoracosaurus mississippiensis* form a separate clade with *Portugalosuchus azenhae* (Mateus et al., 2019).

Moving crownward, '*Tomistoma*' *dowsoni*, *Eogavialis africanum*, *Aktiogavialis caribesi*, and *Argochampsa krebsi* are successively nested taxa, 'basal' to a clade of Neotropical and Indian gavialids. This clade divides (*Picogavialis jugaliperforatus* + (*Siquisiquesuchus venezuelensis* + *Ikanogavialis gameroi*)) from *Dadagavialis gunai* and all species of *Gryposuchus* and *Gavialis*. *Gryposuchus* is paraphyletic, with *Gryposuchus neogaeus* and *Gryposuchus croizati* more closely related to *Gavialis* than to the remaining two species usually included within *Gryposuchus* (*Gryposuchus pachakamue* + *Gryposuchus colombianus*). Consequently, 'Gryposuchinae' sensu Vélez-Juarbe et al. (2007) is not recovered .

*Gavialis* is monophyletic, with a sister relationship between *Gavialis gangeticus* and *Gavialis browni*, to the exclusion of *Gavialis lewisi*.

## 4.4 Discussion

### 4.4.1 The impact of quantitative character treatment

The impact of different treatments of quantitative characters is most apparent between equal weighted analyses. The strict consensus trees of analyses 2.1 and 3.1 were increasingly less well-resolved than analysis 1.1. This result was anticipated, given that equal step lengths resulting from the use of discrete-only characters in these analyses allows for numerous ties in optimal tree length. Furthermore, Analysis 3.1 was also expected to have the poorest resolution given that fewer characters were utilised (304) than in the other two analyses (330). The treatment of quantitative characters appears to be relatively insignificant under extended implied weighting. There were fewer topological differences between the three analyses using a k-value of 3, and those applying a value of 12, compared to the three equal weighted analyses. This is illustrated by the number of taxa retained in the agreement subtrees of analyses under different weighting strategies (Table 4.5). Furthermore, the differences in topology are restricted to the interrelationships of nested taxa, rather than the overall topology of the tree. This is exemplified in the strict consensus of the 9 trees resulting from analyses 1.3, 2.3 and 3.3 (Appendix H.2). By contrast, there are considerably fewer taxa retained in the agreement subtrees of analyses that treat quantitative data the same, but use different weighting strategies (Table 4.5). Furthermore, the differences in topology are widespread. For example, a strict consensus of analyses 1.1, 1.2, and 1.3 results in a large polytomy between the principal crocodylian lineages, with little to no resolution in any major clade (Appendix H.1). This indicates that weighting strategy has more control on tree topology than how quantitative data is treated in this dataset, a result similarly found in a study of sauropod phylogeny (Mannion et al., 2013), and neosuchian phylogeny (Groh et al., 2020).

### 4.4.2 The use of extended implied weighting

The use of extended implied weighting with k=3 results in trees that consistently score more poorly for measures of phylogenetic accuracy, internal consistency, and stratigraphic congruence, than those produced with a *k*-value of 12, and (in most cases) those under equal weights (Table 4.2). All analyses using EIW3 recovered a topology in which Gavialoidea is more closely related to Alligatoroidea than to Crocodyloidea, a hypothesis that contrasts with all previous results based on morphological, molecular, and combined analyses. Fewer internal nodes are supported in Jackknife and Bootstrap replicates, and those retained have lower support values compared to analyses under EIW12. Furthermore, analyses

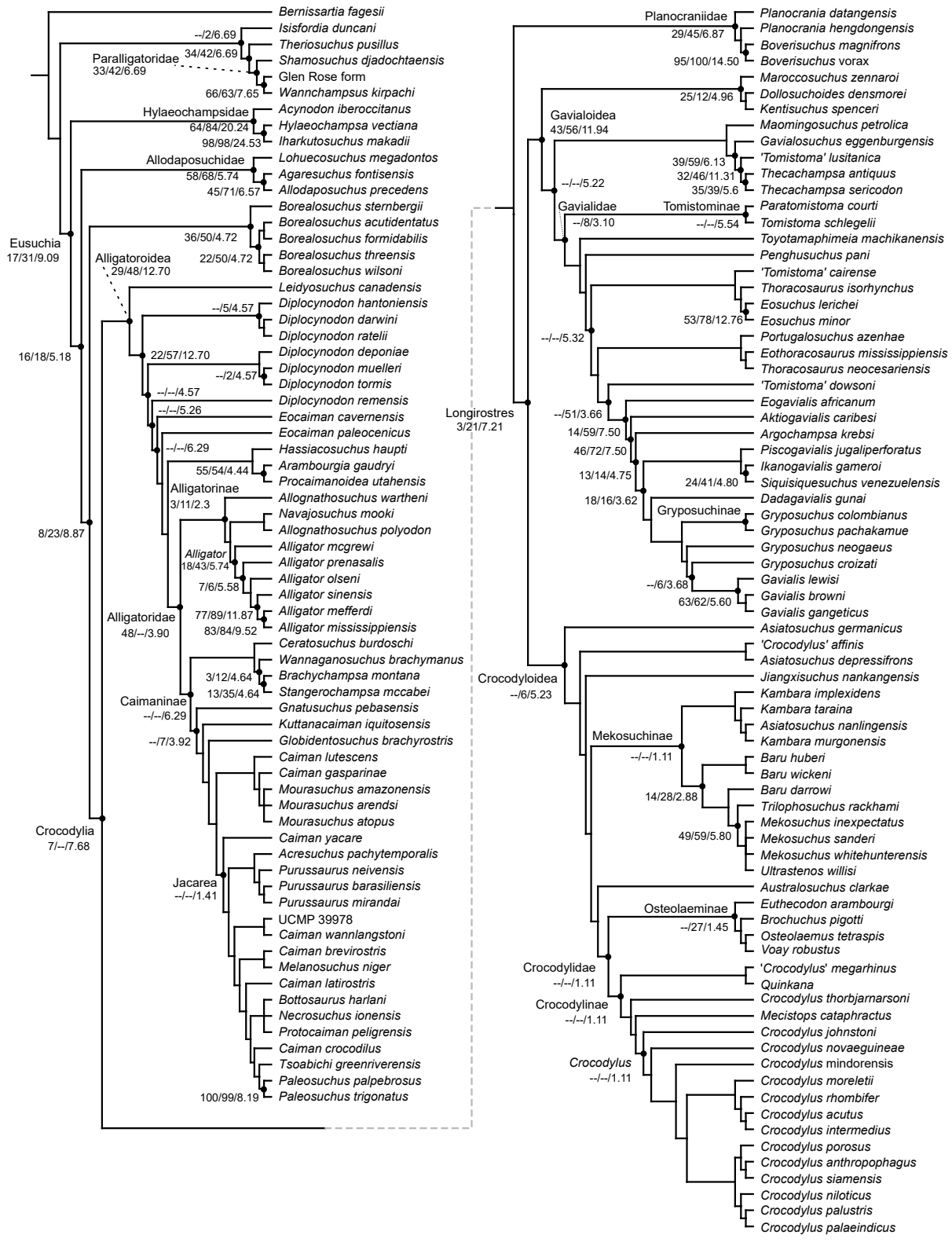



Figure 4.3: The strict consensus of the three most parsimonious trees obtained from Analysis 1.3 (discrete and continuous characters, EIW12). Values adjacent to nodes are measures of internal consistency (Bootstrap/Jacknife/Bremer) and are shown only for named nodes, and those with Bremer support over 1 average step length (see Section 4.2.3).

Table 4.5: Maximum number of taxa retained out of 144 OTUs in agreement subtrees from pairwsie comparisons of each analysis. Colours indicate the level of similarity (red = few similarities, green = many similarities).

| Analysis | 1.1 | 1.2 | 1.3 | 2.1 | 2.2 | 2.3 | 3.1 | 3.2 | 3.3 |
|---|---|---|---|---|---|---|---|---|---|
| 1.1 | | 53 | 83 | 69 | 53 | 87 | 65 | 54 | 89 |
| 1.2 | | | 72 | 34 | 119 | 74 | 22 | 117 | 71 |
| 1.3 | | | | 53 | 68 | 114 | 20 | 74 | 126 |
| 2.1 | | | | | 34 | 66 | 41 | 48 | 68 |
| 2.2 | | | | | | 74 | 23 | 117 | 74 |
| 2.3 | | | | | | | 23 | 72 | 126 |
| 3.1 | | | | | | | | 23 | 23 |
| 3.2 | | | | | | | | | 73 |
| 3.3 | | | | | | | | | |

implementing EIW3 consistently achieved lower values for stratigraphic congruence than analyses using EIW12, and were often lower than equal weighted analyses. Following Goloboff et al. (2018) these results argue in favour of the use of higher *k*-values. This contrasts with the crocodyliform-focused dataset of Groh et al. (2020), who consistently found greater values of stratigraphic congruence with *k*=3. Several factors might have contributed to this, including differences in character sampling, numbers of continuous characters, ingroup composition, and number of OTUs.

### 4.4.3 Implications for the systematics and taxonomy of non-crocodylian eusuchians

#### The phylogenetic affinities of *Isisfordia*

There are conflicting hypotheses for the phylogenetic affinities of *Isisfordia duncani*, from the mid-Cretaceous of Australia (Salisbury et al., 2006; Turner, 2015; Turner & Pritchard, 2015; Groh et al., 2020). Originally *Isisfordia* was recovered as the earliest diverging member of Eusuchia, sister to the clade formed by *Allodaposuchus precedens* + Crocodylia (Salisbury et al., 2006). This placement was based on the combination of plesiomorphic and derived eusuchian character states, such as the presence of incipiently procoelous vertebrae and the apparently pterygoid-bound choanae. However, Turner and Pritchard (2015) reassessed this morphology, and demonstrated the participation of the palatine in the choanae. In an analysis incorporating this re-interpretation, Turner and Pritchard (2015) recovered *Isisfordia* in the stem of Neosuchia. By contrast, a recent study of neosuchian relationships recovered *Isisfordia* within the crown group Crocodylia (Groh et al., 2020). However, that analysis produced a relatively unconventional topology, in which Hylaeochampsidae was also recovered in the crown group, closely related to *Isisfordia*. This might reflect the absence of members of Allodaposuchidae from that dataset. *Isisifordia* is here recovered outside of Eusuchia, as the sister to Paralligatoridae (Fig. 4.4).

Given that *Isisfordia* might represent an early diverging neosuchian, its relationships may be more thoroughly tested in a larger sample of non-eusuchian neosuchians. Rerunning Analysis 1.3 with *Isisfordia* excluded *a priori* results only in the movement of *Theriosuchus* from the stem of Paralligatoridae to the earliest diverging ingroup taxon.

**Hylaeochampsidae and Allodaposuchidae**

Hylaeochampsidae is relatively well supported (Jackknife = 84, Bootstrap = 64), in particular the sister relationship between *Hylaeochampsa vectiana* + *Iharkutosuchus makadii* (Jackknife = 98, Bootstrap = 98), which is commonly recovered (e.g. Ősi et al., 2007; Brochu et al., 2012; Narváez et al., 2015; Narváez et al., 2016; Mateus et al., 2019). Hylaeochampsidae is supported by ten synapomorphies: (1) premaxilla-maxilla suture at the same level or anterior to the posterior margin of the nares (C49-1, shared); (2) lacrimal nasal contact absent (C53-1, shared); (3) spina quadratojugalis greatly reduced or absent (C103-1, shared); (4) premaxilla extend posteriorly on the palate to the level of 3 maxillary alveoli (C142-3, ambiguous); (5) premaxilla-maxilla suture bowed with one rounded apex (C146-1, shared); (6) maxillary alveoli gradually increase in diameter posteriorly toward penultimate alveolus (C147-6, unambiguous); (7) diastema between maxillary alveoli 5 and 6 (C152-1, shared); (8) posterior dentary and maxillary teeth molariform and multicusped (C156-2, unambiguous); (9) anterior margin of the suborbital fenestra at the same level or posterior to the anterior margin of the orbit (C166-1, shared); and (10) ectopterygoid extends to the level of or anterior to two thirds the suborbital fenestra length (C174-1, shared). There is lower support for Allodaposuchidae (Jackknife = 68, Bootstrap = 58) but, in common with other recent analyses, this clade is more closely related to Crocodylia than to Hylaeochampsidae (Narváez et al., 2016; Mateus et al., 2019). Allodaposuchidae is supported by seven synapomorphies: (1) ratio of interorbital distance to width across the anterior cranial table margin = 0.3–0.4 (C6); (2) ratio of incisive foramen width to rostrum width at premaxilla-maxilla suture = 0.17–0.19 (C12); (3) presence of a transverse interorbital bridge (C31-1, shared); (4) largest maxillary alveolus is number 4 (C147-2, shared); (5) dentary symphysis adjacent to 9–12 alveoli (C222-2, shared); (6) anterior perforation of splenial for cranial nerve V absent (C229-1, shared); and (7) surangular-articular suture bowed laterally in glenoid fossa (C247-1, shared).

***Borealosuchus***

*Borealosuchus* is a speciose eusuchian genus known from the latest Cretaceous–Eocene of North America (Brochu, 1997a, 2003). Whereas most previous analyses have recovered *Borealosuchus* in the stem of "Brevirostres" (Alligatoroidea + Crocodyloidea) (Brochu, 1997a, 2004a; Hua & Jouve, 2004; Brochu, 2006b; Jouve et al., 2015; Narváez et al., 2015; Narváez et al., 2016; Salas-Gismondi et al., 2016; Groh et al., 2020), others recover *Borealosuchus* as either the sister taxon to "Gavialoidea" (Salisbury et al., 2006;

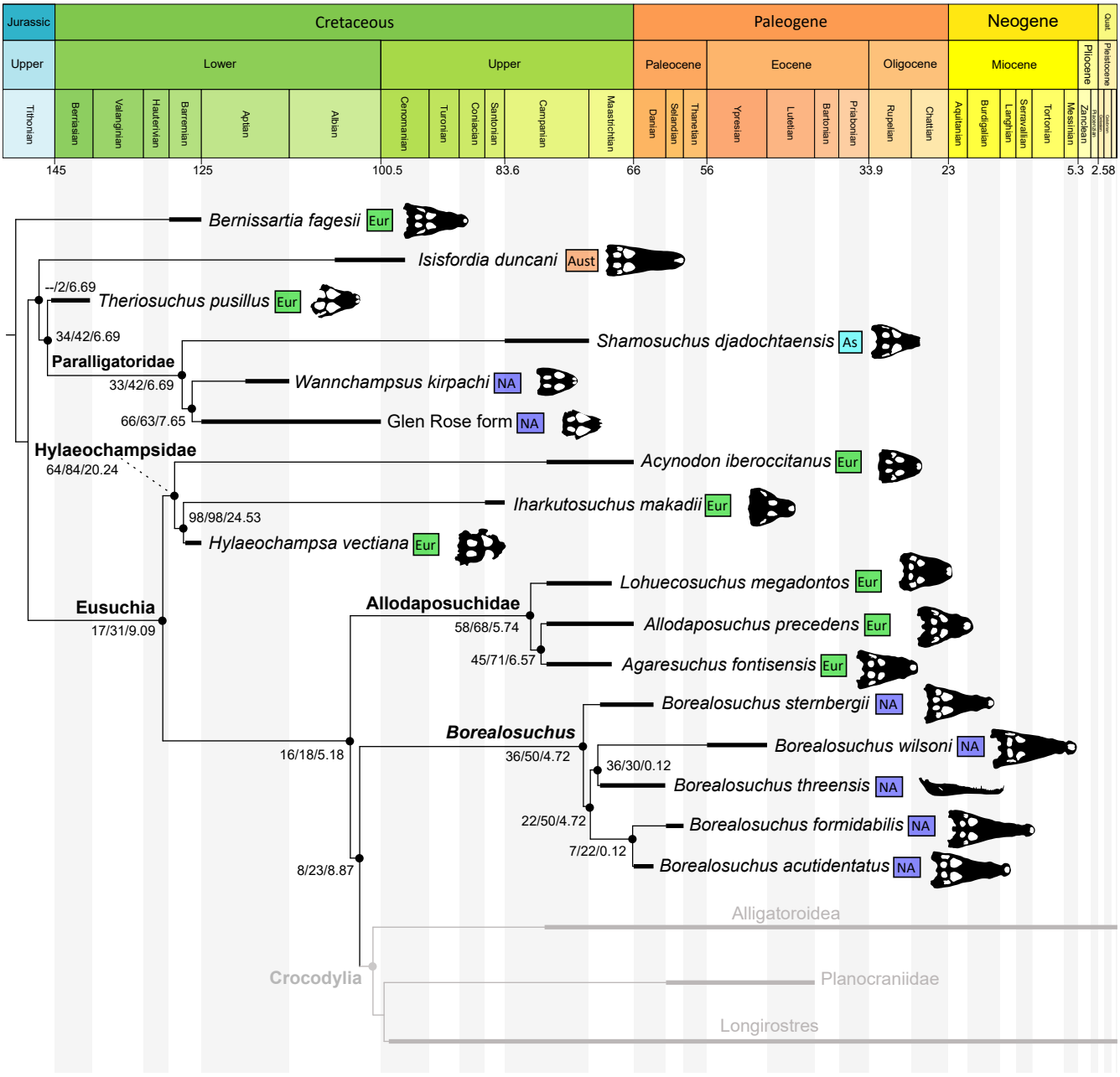



Figure 4.4: Time calibrated phylogeny of stem crocodylian taxa from Analysis 1.3. Ages = Ma. Support values: Bootstrap/Jackknife/Bremer. Abbreviations: **As**, Asia; **Aust**, Australasia; **Eur**, Europe; **NA**, North America.

Pol et al., 2009; Martin, 2010a; Puértolas-Pascual et al., 2011), or in a polytomy with "Gavialoidea" and "Brevirostres" (Brochu, 2012; Brochu et al., 2012; Hastings et al., 2016). In Analysis 1.3 (and indeed all analyses except 2.1 and 3.1), *Borealosuchus* is the sister taxon to Crocodylia, similar to Gatesy et al. (2003) and Gold et al. (2014). This result is weakly supported in Jackknife (23) and Bootstrap (8) replicates, but with Bremer support of 8.9. *Borealosuchus* + Crocodylia is supported by three continuous and three discrete synapomorphies: (1) ratio of snout length to skull length = 0.58–0.60 (C1); (2) cranial table length to width = 0.69 (C8); (3) number of maxillary alveoli = 17 (C17); (4) absence of fossa on anteromedial corner of supratemporal fenestra (C84-1, shared); (5) indentation of the mediolateral margin of quadrate condyle (C118-1. ambiguous); and (6) presence of an external mandibular fenestra (C234-1, shared). Outside of this clade, the absence of an anteromedial fossa of the supratemporal fenestra is known only in *Iisisfordia duncani* and *Shamosuchus djatochtaensis*. Similarly, where preserved, the only non-crocodylian eusuchian to exhibit an external mandibular fenestra is *Isisfordia duncani*. The morphology of the quadrate condyle (118-1) provides additional ambiguous support for *Borealosuchus* + Crocodylia, given that the condition is shared by the outgroup. Furthermore, the morphology of the condyle changes multiple times in crownward nodes of Crocodylia. For example, whereas most alligatoroids share the condition with *Borealosuchus*, it is lost in longirostrines (C118-0) and re-acquired in Mekosuchinae (C118-1) (see also Section 3.3.1, Fig. 3.45).

### 4.4.4 Diagnosis of Crocodylia

Crocodylia is supported by one continuous and nine discrete synapomorphies: (1) width to length ratio of the external naris = 1.0–1.2 (C3); (2) lacrimal anteroposteriorly longer than the prefrontal (C58-0, ambiguous); (3) absence of a protuberance on the dorsolateral margin of the postorbital bar (C90-1, ambiguous); (4) presence of a surangular spur lingual to posteriormost dentary alveoli (C242-0, ambiguous); (5) first postaxial vertebra with a prominent hypapophysis (C279-0, exclusive); (6) scapulocoracoid facet broad immediately anterior to glenoid fossa, and tapering anteriorly (C301-1, exclusive); (7) olecranon process of ulna wide and rounded (C305-1, shared); (8) proximal diaphysis of ulna straight (C306-1, shared); (9) six dorsal osteoderms per transverse row at maturity (C324-2, ambiguous); (10) absence of an anterolateral process on the dorsal midline osteoderms (C327-1, ambiguous).

The diagnostic utility of most of these synapomorphies appears weak, given that many also appear in some non-crocodylian eusuchians and are not present in all crocodylians (e.g. 58-0, 90-1, 242-0, 324-2, 327-1). The presence of a hypopophysis on the first postaxial vertebra (279-0), and a tapering scapulocoracoid facet (301-1) do not characterise any non-crocodylian eusuchians studied herein, where preserved; however, not all crocodylians share these features. Additionally, there is a considerable amount of missing data for both of these characters. Two morphological features of the ulna are shared synapomorphies of Crocodylia: (1) a rounded olecranon process (305-1); and (2) a straight (rather than bowed) proximal

end of the diaphysis (306-1). Both of these features appear independently in some paralligatorids. However, as with other postcranial synapomorphies discussed, there is a large proportion of missing data for these characters.

### 4.4.5 Implications for the systematics and taxonomy of Alligatoroidea

Alligatoroidea has been one of the most stable clades in Crocodylia in terms of taxonomic content and internal phylogenetic relationships, with strong concordance between molecular and morphological topologies (e.g. Brochu, 1999; Oaks, 2011; Jouve et al., 2015). This owes to extensive study of this group. Here I recover a consistent taxonomic content of Alligatoroidea, but with several new interrelationships and support for internal clades (Fig. 4.5).

#### Modifications to the diagnosis of Alligatoroidea

**Emended diagnosis** Alligatoroidea is supported by two continuous and eight discrete synapomorphies: (1) ratio of antorbital rostrum width to cranial table width = 1.7 (C2); (2) supratemporal fenestra width to length = 0.63–0.67 (C11); (3) transverse ridge between orbits (C31-1, ambiguous); (4) quadratojugal spine positioned high between the posterior and dorsal angles of the infratemporal fenestra (C104-1, shared); (5) posterior extent of premaxillae on palate not reaching one maxillary alveolus (C142-0, ambiguous); (6) posterior and anterolateral margins of choanae elevated (C195-2, ambiguous); (7) dorsal surangular processes subequal (C241-1, ambiguous); (8) surangular does not extend to posterior tip of retroarticular process (C245-1, ambiguous); (9) foramen aerum inset from medial margin of retroarticular process (C248-1, shared); and (10) dorsal extent of the retroarticular process at the same level or ventral to articular fossa (C251-0, ambiguous).

**Discussion** This differs to earlier diagnoses of Alligatoroidea (Norell et al., 1994; Brochu, 1999) in several respects. Not only are there differences in the characters considered diagnostic of Alligatoroidea, but many more synapomorphies appear to be shared and ambiguous, and therefore seem ‘weaker’. The latter is usually because of the stricter definition of synapomorphies used here (see Section 4.2.6). A dorsally positioned foramen aerum on the quadrate condyle, and a broad separation of the ectopterygoid from the maxillary toothrow, have long since been regarded as unambiguous synapomorphies of Alligatoroidea (Norell & Clark, 1990; Norell et al., 1994; Brochu, 1999). These characters are still employed in this study, but no longer diagnose the clade. The foramen aerum is dorsally positioned in all alligatoroids where preserved (C117-1), but I consider the same condition to occur in some non-alligatoroid taxa such as *Borealosuchus sternbergii* (USNM 6533, Fig. 3.45) and *Borealosuchus formidabilis* (Erickson, 1976, fig.6). A dorsally positioned foramen aerum has also previously been recognised in Allodaposuchidae,

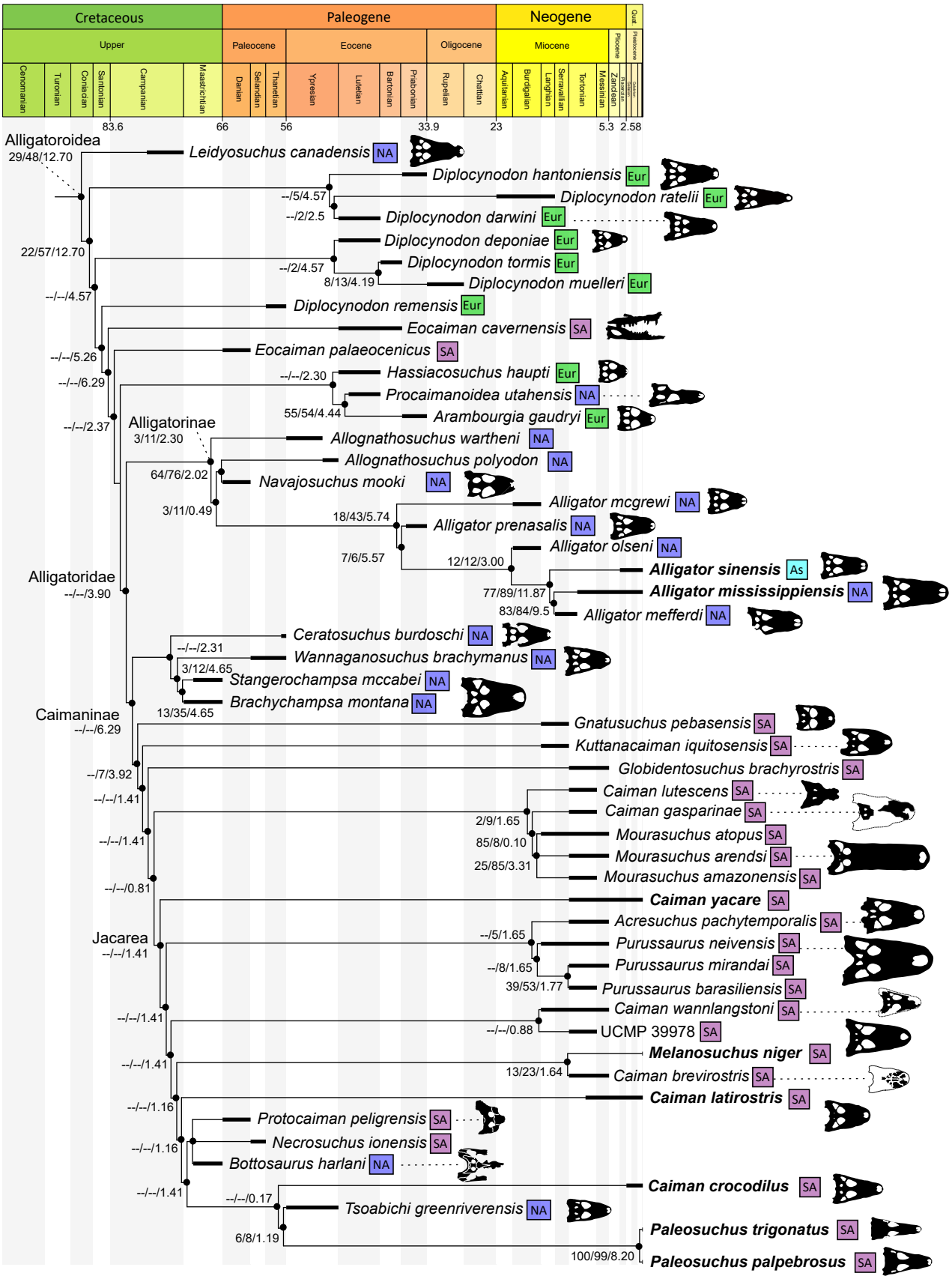



Figure 4.5: Time calibrated phylogeny of Alligatoroidea from Analysis 1.3. Ages = Ma. Support values: Bootstrap/Jackknife/Bremer. Abbreviations: **As**, Asia; **Eur**, Europe; **NA**, North America; **SA**, South America.

e.g. *Allodaposuchus precedens* (MMS/VBN-12-10A) and *Agaresuchus fontisensis* (Narváez et al., 2016, fig.3B), and recently in the hylaeochampsid *Iharkutosuchus makadii* (Mateus et al., 2019, fig.S14B). As such, a dorsally positioned foramen aerum is recovered as a synapomorphy of Eusuchia, which is lost at the node comprising Planocraniidae + Longirostres. Similarly, a broad separation of the ectopterygoid and maxilla (C175-0) is recognised far more widely within Neosuchia. This character has received significant score changes, (see Section 3.4.1, Fig. 3.71) with the 'alligatoroid condition' newly recognised in *Bernissartia fagesii* (Fig. 3.15A), several *Borealosuchus* species (Fig. 3.71B–C), and most gavialoids (Fig. 3.71E, G). Following Brochu (1999), subequal surangular processes (C241-1) and a medially inset foramen aerum on the retroarticular process (C248-1) are still recovered as synapomorphies of Alligatoroidea; however, these are no longer unambiguous. For example, both *Borealosuchus formidabilis* (Erickson, 1976, Fig. 3.107), and the paralligatorid *Shamosuchus djadochtaensis* (Pol et al., 2009) are also characterised by the presence of subequal surangular processes, whereas they are unequal in the alligatoroid, *Procaimanoidea utahensis* (USNM 15996). Similarly, a medially inset foramen aerum is also present in the paralligatorid, *Wannchampsus kirpachi* (Adams, 2014), as well as the crocodyloid, *Mekosuchus inexpectatus* (MNHN NCP 06).

Five synapomorphies of Alligatoroidea are newly recognised in this study, all of which are ambiguous. A transverse interorbital bridge (C31-1) is present in the earliest diverging alligatoroids, but seemingly lost and reacquired independently in some alligatorines and most caimanines. Outside of Alligatoroidea, an interorbital bridge is present in *Acynodon iberoccitanus*, Allodaposuchidae, and the 'basal' crocodyloid *Jiangxisuchus nankangensis*. Within Alligatoroidea, a short posterior extension of the premaxillae on the palate (C142-0) only occurs in *Leidyosuchus canadensis*, *Diplocynodon*, and *Paleosuchus trigonatus*. All other alligatoroids exhibit longer posterior extensions of the premaxillae. The highly shortened condition also occurs multiple times independently in other eusuchians. Everted anterolateral margins of the choanae (C195-2) are a newly recognised condition, exhibited by all species of *Diplocynodon* where preserved and *Leidyosuchus canadensis*. This condition is absent in all alligatoroids crownward of *Diplocynodon remensis*; although they still possess everted lateral margins, these are morphologically distinct. A surangular that is truncated before reaching the posterior tip of the retroarticular process (C245-1) was not listed as a synapomorphy of Alligatoroidea by Brochu (1999), but was optimised as such in a recent dataset (Narváez et al., 2016). This synapomorphy is ambiguous because this condition is lost in most caimanines and is also shared by many gavialoids. Variation in the dorsoventral height of the retroarticular process was not discretised by Brochu (1999). In the current study, a ventrally positioned retroarticular process (C251-0) characterises most alligatoroids, but is also present in several non-crocodylian eusuchians, including Paralligatoridae.

### The phylogenetic relationships and monophyly of *Diplocynodon*

The phylogenetic relationships of *Diplocynodon* have been tested by a number of authors (Brochu, 1997a, 1999; Martin, 2010a; Martin & Gross, 2011; Brochu et al., 2012; Delfino & Smith, 2012; Martin et al., 2014; Groh et al., 2020). *Diplocynodon* has consistently been recovered as a monophyletic group, almost always as an early diverging alligatoroid genus (but see Groh et al., 2020); however, there is surprisingly little consensus over the interrelationships of *Diplocynodon* species. Adding to this lack of previous consensus, the preferred topology of this study recovers a paraphyletic *Diplocynodon* (Fig. 4.5).

**Character support for the monophyly of *Diplocynodon*** In all equal weighted analyses, *Diplocynodon* is recovered as monophyletic. Furthermore, *Diplocynodon* forms the sister taxon to *Leidyosuchus canadensis* in analyses 1.1 and 2.1. The monophyly of both *Diplocynodon* and the clade *Leidysosuchus* + *Diplocynodon* are relatively well supported in those analyses (e.g. Bremer support = 2 in Analysis 2.1). The only other analysis recovering a monophyletic *Diplocynodon* is Analysis 3.1; however, this clade lacked any internal resolution and is itself part of a large polytomy with all other eusuchians.

Constraining Analysis 1.3 to recover a monophyletic *Diplocynodon* results in an insignificant tree length increase of 8.7 steps (templeton test: $p > 0.05$, Appendix F.1). The topology within *Diplocynodon* differs to analyses 1.1 and 2.1, except that in all cases *D. remensis* is now the earliest diverging species, and a sister relationship between *D. darwini* and *D. deponiae* is consistently recovered. In the constrained and equal weighted analyses, nine synapomorphies diagnose *Diplocynodon*, and eight synapomorphies support *Leidyosuchus* + *Diplocynodon* (Table 4.6).

Table 4.6: Synapomorphies of *Diplocynodon* and *Diplocynodon* + *Leidyosuchus* in constrained Analysis 1.3.

| Character state | Type | Description | % scored | CI |
|---|---|---|---|---|
| | | ***Diplocynodon*** | | |
| 41-0 | ambiguous | Dorsally facing external nares. | 80 | 0.06 |
| 63-1 | ambiguous | Jugal anterior extent posterior to anterior frontal process. | 75 | 0.05 |
| 145-1 | ambiguous | Second premaxillary alveolus separated from $1^{st}$ and close to $3^{rd}$. | 90 | 0.05 |
| 151-1 | shared | Partial interlocking occlusion of dentary and maxillary teeth. | 87 | 0.17 |
| 190-1 | ambiguous | Choanae shape sub-triangular, tapering posteriorly. | 60 | 0.27 |

| Character state | Type | Description | % scored | CI |
|---|---|---|---|---|
| 229-1 | shared | Splenial anterior perforation for cranial nerve V absent. | 49 | 0.08 |
| 253-1 | shared | Lingual foramen perforates surangular-articular suture. | 48 | 0.08 |
| 327-0 | ambiguous | Anterolateral process present on dorsal midline osteoderms. | 43 | 0.25 |
| 328-2 | shared | Ventral osteoderms paired. | 28 | 0.25 |
| | | ***Leidyosuchus + Diplocynodon*** | | |
| 31-1 | ambiguous | Absence of transverse ridge between the orbits. | 91 | 0.08 |
| 46-1 | shared | External contact between the nasals and naris absent. | 80 | 0.09 |
| 74-1 | ambiguous | Lateral margin of the orbit is at the same level or medial to the lateral margin of the maxilla at the level of alveoli 3–6 | 78 | 0.04. |
| 76-1 | ambiguous | Frontoparietal suture linear. | 85 | 0.03 |
| 105-0 | shared | Absence of a medial contact between the postorbital and quadratojugal at the dorsal corner of the infratemporal fenestra. | 42 | 0.14 |
| 142-0 | shared | Posterior extent of premaxillae on palate not reaching the level of 1 maxillary alveolus. | 63 | 0.13 |
| 217-0 | shared | Dentary alveoli 3 and 4 confluent. | 75 | 0.20 |
| 221-0 | shared | Dentary symphysis adjacent to fewer than 6 full dentary alveoli. | 73 | 0.14 |

Brochu (1999) recovered eight synapomorphies of *Diplocynodon* in his analysis. All of those characters are implemented here, but only two are still recovered as synapomorphies of *Diplocynodon* (Table 4.7). The first, the presence of paired ventral osteoderms (C328-2), is present in all *Diplocynodon* species in which the relevant region is preserved, but is also shared by Caimaninae and *Borealosuchus*. The second, perforation of the surangular-articular suture by the lingual foramen (C253-1), is also present (where

preserved) in all *Diplocynodon* species but shared by most species of *Alligator* and most crocodyloids. The remaining six synapomorphies of *Diplocynodon* recovered by Brochu (1999) have been variably modified such that they are no longer recovered (Table 4.7).

Table 4.7: Synapomorphies of *Diplocynodon* recovered by Brochu (1999).

| Brochu (1999) | This dataset | Description | Modification | % scored | CI |
|---|---|---|---|---|---|
| 39-2 | 328-2 | Paired ventral osteoderms. | Also recovered. | 28 | 0.25 |
| 45-1 | 253-1 | Perforation of lingual foramen on surangular-articular suture. | Also recovered. | 48 | 0.08 |
| 6-0 | 277-0 | Centrally positioned axial hypopophysis. | Recognised more widely in Alligatoroidea. | 24 | 0.14 |
| 28-4 | 308-0, 309-0 | Rounded (308-0) and deep (309-0) iliac blade. | Character atomised, both conditions more widely recognised in Crocodylia. | C308 (29), C309 (26) | 0.10 |
| 95-2 | 46-1 | Nasals excluded dorsally from naris. | Character atomised, synapomorphy of *Leidyosuchus* + *Dipocynodon*. | 79 | 0.09 |
| 86-1 | 76-1 | Linear frontoparietal suture. | Becomes synapomorphy of *Leidyosuchus* + *Diplocynodon*. | 85 | 0.03 |
| 127-1 | 215-1 | Pterygoid-quadrate suture straight. | Missing data in *Leidyosuchus*, becomes potential synapomorphy of *Leidyosuchus* + *Diplocynodon*. | 29 | 0.14 |

| Brochu (1999) | This dataset | Description | Modification | % scored | CI |
|---|---|---|---|---|---|
| 10-0 | 264-0 | Prominent proatlas process. | Missing data in *Leidyosuchus* and some *Diplocynodon*, becomes potential synapomorphy of *Leidyosuchus* + *Diplocynodon*. | 18 | 0.20 |

Seven synapomorphies of *Diplocynodon* recovered in the constrained and unweighted analyses are new (Table 4.6); however, five are ambiguous, occurring multiple times within Alligatoroidea, or non-crocodylian eusuchians, and are not present in all members of *Diplocynodon* (C41-0, C63-1, C145-1, C190-1, C327-0). The remaining two are shared synapomorphies. The first of these shared synapomorphies, the presence of partial interlocking dentary and maxillary teeth (C151-1), is relatively uncommon in Crocodylia. This otherwise occurs in some 'basal' crocodyloids, *Borealosuchus sternbergii*, *Allodaposuchus precedens*, and one alligatoroid – *Caiman crocodilus*. The second, absence of an anterior perforation on the splenial (C229-1), occurs in most caimanines, where preserved, and almost all crocodyloids.

**Summary** The paraphyly of *Diplocynodon* appears to result from decreased support in previously recovered synapomorphies. As shown in Table 4.7, only two of the eight characters previously recovered as diagnostic of *Diplocynodon* are recovered in unweighted and constrained analyses. The remainder are found more widely in Crocodylia or are recovered as ambiguous or potential synapomorphies of *Leidyosuchus* + *Diplocynodon*. Despite the number of new synapomorphies that support the monophyly of *Diplocynodon*, as well as *Leidyosuchus* + *Diplocynodon*, in unweighted and constrained analyses, these relationships are not supported under extended implied weighting. This suggests that characters capable of supporting a monophyletic *Diplocynodon* are downweighted as a result of missing data or homoplasy. Indeed, characters supporting both the monophyly of *Diplocynodon* and a sister relationship with *Leidyosuchus* in equal weighted and constrained analyses are among the most homoplastic of all characters. For example, characters 41, 63, 145, 229, and 253 all fall within the 20 most homoplastic characters of this data matrix (Table 4.6, Appendix I). Furthermore, more than 50% of all taxa in this dataset cannot be scored for characters 229, 253, 327, and 328. Although characters supporting *Leidyosuchus* + *Diplocynodon* are scored for a greater number of taxa, they are also highly homoplastic.

**The taxonomic content of Caimaninae**

In most phylogenies, the earliest diverging caimanines are known from South America, and all North American members of the clade can be most parsimoniously explained as later dispersals from South America (e.g. Brochu, 2010). By contrast, several recent studies have recovered a series of latest Cretaceous North American crocodylians within an early diverging 'basal' caimanine clade (Salas-Gismondi et al., 2015; Bona et al., 2018; Cossette, 2020). The taxa in question (*Brachychampsa montana*, *Brachychampsa sealyi*, *Albertochampsa langstoni*, and *Stangrochampsa mccabei*) have typically been recovered as 'basal' alligatorids, i.e. outside of Alligatorinae and Caimaninae (e.g. Brochu, 1999; Salisbury et al., 2006; Hastings et al., 2013; Fortier et al., 2014; Jouve et al., 2015; Lee & Yates, 2018; Iijima & Kobayashi, 2019; Salas-Gismondi et al., 2019); however, their relationship to these alligatorid clades has often been unresolved (e.g. Brochu, 2011; Brochu et al., 2012; Hastings et al., 2016; Cossette & Brochu, 2018). The caimanine affinities of these taxa is supported here (note that *Albertochampsa* and *Brachychampsa sealyi* were not included herein). Furthermore, two Paleocene North American taxa usually recovered as alligatorines (*Wannaganosuchus brachymanus* and *Ceratosuchus burdoshi*) are also positioned as members of this early diverging caimanine clade in my analysis. This relationship was recovered in Analysis 1.1 and all EIW12 analyses. If correct, the inclusion of latest Cretaceous–Paleocene North American taxa in Caimaninae would have a significant impact on the timing and biogeographic origin of Caimaninae (Brochu, 2010, 2011; Bona et al., 2018), and therefore warrant a close evaluation of characters supporting this relationship.

Seven synapomorphies diagnose Caimaninae here: (1) ratio of distal ischial blade expansion to ischium length = 0.54 (C26); (2) anterior frontal process at the same level or posterior to anterior orbit margin (C62-1, ambiguous); (3) width across dorsal supraoccipital exposure equal to or greater than half posterior parietal width (C78-1, ambiguous); (4) medial wall of the parietal bears foramina (C85-1, exclusive); (5) dentary alveoli 1–4 at the same level or higher than alveoli 11–12 (C218-0, shared); (6) anterior extent of the angular does not exceed the anteroposterior mid-length of the foramen intermandibularis caudalis (C257-1, ambiguous); and (7) eight nuchal osteoderms (C323-2, ambiguous).

Monophyly of the North American clade is supported by five synapomorphies: (1) ratio of interorbital distance to anterior cranial table width = 0.27 (C6); (2) ratio of supratemporal fenestra length to cranial table length = 0.6 (C10); (3) supratemporal fenestra lateromedial width to anteroposterior length = 0.7–0.8 (C11); (4) anterior margin of the suborbital fenestra at the same level or posterior to the anterior orbit margin (C166-1, ambiguous); and (5) anterior extent of the ectopterygoid greater than or equal to two-thirds of suborbital fenestra length (C174-1, shared). The clade (*Wannaganosuchus* + (*Stangerochampsa* + *Brachychampsa*)) is supported by two synapomorphies: (1) the presence of a fossa on the lateral margin of the naris (C45-1, unambiguous); and (2) a sutural contact between the lacrimal and nasal (C53-0, shared). Finally, the sister relationship between *Stangerochampsa* and *Brachychampsa* is supported by

four synapomorphies: (1) ratio of antorbital rostrum width to anterior cranial table width = 1.8 (C2); (2) anterior frontal process anterior to anterior orbital margin (C62-0, shared); (3) premaxilla-maxilla suture intersects lateral margin of incisive foramen (C137-2, shared); and (4) dentary profile shape between alveoli 4 and 10 curved (C220-1, shared).

**Character support for Caimaninae including the North American Clade** Caimaninae is poorly recovered in Bootstrap and Jackknife replicates, but rather well supported by the Bremer decay index (6.3) (Fig. 4.5). The most compelling morphological support for the inclusion of a latest Cretaceous–Paleocene North American clade in Caimaninae is the presence of foramina on the medial parietal wall in *Brachychampsa montana* (C85-1) (Fig. 3.30H). Medial parietal perforations have hitherto supported the monophyly of South American caimanines (albeit ambiguously, due to non-preservation in some taxa) (Norell, 1988; Brochu, 1999). Although the presence of these perforations can only be determined in *Brachychampsa* amongst these North American taxa, they are otherwise exclusively found in Caimaninae.

The angular does not exceed the anteroposterior mid-length of the foramen intermandibularis caudalis in *Stangerochampsa mccabei* and all South American caimanines where preserved (C257-1), with the exception of *Mourasuchus arendsi*. This condition was also recovered as a synapomorphy of these North American taxa in Caimaninae by Bona et al. (2018). Outside of Caimaniane, this condition is otherwise only present in *Alligator mcgrewi* and *Mecistops cataphractus*; however, there is a considerable amount of missing data across the tree (64% of taxa), including all remaining members of this putative North American caimanine clade.

A short anterior frontal process that does not exceed the anterior margin of the orbits (C62-1), is almost exclusively known in Caimaninae, including two North American taxa, *Ceratosuchus burdoshi* and *Wannaganosuchus brachymanus*. Otherwise, this condition only occurs in *Theriosuchus pusillus*, *Hylaeochampsa vectiana*, *Hassiacosuchus haupti*, and *Mekosuchus inexpectatus*. This character was introduced by Jouve (2004), and has otherwise only been utilised in subsequent iterations of this data matrix (Jouve et al., 2008; Jouve et al., 2015; Jouve, 2016). Jouve (2016) also scored this character state as characterising *Brachychampsa montana* and *Stangerochampsa mccabei*, which would add further support for this inclusion of the North American clade in Caimaninae; however, in both taxa the frontal is actually positioned slightly further anterior than the orbits (Wu et al., 1996, fig.1A).

Unlike all other crocodylians, most caimanines are characterised by a large supraoccipital exposure, which excludes the parietal from the posterior margin of the cranial table (C78-2) (Chapter 3, fig. 3.28). By contrast, most other alligatoroids have a small supraoccipital exposure (C78-0). As previously recognised, *Brachychampsa montana* and *Stangerochampsa* lie between these extremes, with a large supraoccipital exposure that does not exclude the parietal from the posterior cranial table margin

(C78-1) (Brochu, 2010). Ordering of this character such that the condition in *Brachychampsa* and *Stangerochampsa* is intermediate (C78-1) supports a close relationship between these taxa and Caimaninae.

An elevated dentary toothrow at the level of alveoli 1–4 that exceeds the height of the posteriormost dentary alveoli (C218-0) occurs in all members of Caimaninae where preserved, including all members of the North American clade. However, this condition is not unique to Caimaninae, occurring in almost all alligatoroids except for some 'basal' alligatorids and alligatorines, as well as all other crocodylians.

Knowledge of the number of nuchal osteoderms (C323) is restricted to extant and a few exceptionally preserved fossil taxa, and thus this character is only scored in 26 species. Nevertheless, all extant caimanines have eight nuchal osteoderms (323-2), a feature shared by *Brachychampsa montana* (UCMP 133901) and convergently acquired in Gavialoidea (e.g. *Tomistoma schlegelii*, Fig. 3.132F). The condition in all other members of the North American clade is unknown. Extant alligators have six nuchal osteoderms (Fig. 3.132B–C), which appears to be the plesiomorphic condition in Alligatoroidea as exhibited by *Diplocynodon darwini* (e.g. HLMD-Me-10262).

A relatively wide distal expansion of the ischium (C26: 0.54) provides weak support for this clade. Although this character cannot be scored in most taxa, measurements in this dataset reveal that caimanines, including *Wanaganosuchus brachymanus*, have a relatively wider distal expansion than all other alligatoroids where preserved.

Two additional characters should be considered that supported the caimanine affinities of a similar North American clade in the analysis of Bona et al. (2018): (1) a dorsally facing naris (C41-1); and (2) absence of a prominent anterior process of the proatlas (C264-1). Here, the ancestral morphology of the naris in Caimaninae is ambiguous, given that it could be dorsally or anterodorsally facing. The absence of a prominent anterior process of the proatlas is similarly not recovered here as a synapomorphy of Caimaninae. As a result of modifications to character scores, the absence of an anterior process of the proatlas is plesiomorphic in Alligatoroidea, although appearing in some basal alligatoroids such as *Diplocynodon*. Furthermore, the only taxon preserving the proatlas among the North American clade, *Brachychampsa montana*, exhibits a prominent process (C264-0). Thus, this character actually differentiates the North American clade from most members of the South American caimanines.

In summary, character support for Caimaninae including an early diverging North American clade is rather weak. Only one of the synapomorphies uniting a North American clade with South American caimanines is exclusive (C85-1), and it can only be scored in one of the North American taxa. Other synapomorphies follow a similar pattern. Although they are almost exclusively known in the South American caimanines, they are typically scored in two or fewer North American taxa (C62, C78, C257). Other characters are significantly more ambiguous (C218) or exhibit a significant amount of missing data (C26, C323), undermining the support for this clade.

### The Phylogenetic affinities of *Eocaiman*

*Eocaiman* is an alligatoroid genus based on fragmentary remains from the Paleocene–Eocene of South America. Three species have been described: *Eocaiman cavernensis* (Simpson, 1933) and *Eocaiman palaeocenicus* (Bona, 2007) are included here, whereas *Eocaiman itaboraiensis* was not included, as the holotype and referred material comprise phylogenetically uninformative fragments (Pinheiro et al., 2013). By strong contrast to its typical placement as one of the earliest diverging members of traditional (i.e. South American) caimanines, "Caimaninae" hereafter (Brochu, 1999; Bona, 2007; Brochu, 2010, 2011; Brochu et al., 2012; Fortier et al., 2014; Salas-Gismondi et al., 2015; Bona et al., 2018; Cossette & Brochu, 2018; Souza-Filho et al., 2019; Cidade et al., 2020a), this study recovers *Eocaiman* in the stem of Alligatoridae instead. This placement is controversial, as the spatiotemporal distribution of *Eocaiman* fits well with its usual placement as a basal member of "Caimaninae". Nevertheless, the reasons for the exclusion of *Eocaiman* from "Caimaninae" can be recognised by comparing character support between this and previous studies.

**Character support for the placement of *Eocaiman* in Caimaninae** Analyses based on the datasets of Brochu (1999) and Brochu et al. (2012) tend only to include the type species of *Eocaiman cavernensis*. These studies recover many of the following traditional synapomorphies of "Caimaninae" in *Eocaiman cavernensis* (character numbers from Brochu et al. [2012]): (1) a splenial excluded from the dentary symphysis with the anterior tip passing dorsal to the Meckelian fossa (C54-2); (2) surangular-angular suture passing broadly along the ventral margin of the external mandibular fenestra (C60-1); (3) a large supraoccipital exposure blocking the parietal from the posterior margin of the skull table (C158-3); and (4) exoccipitals with slender ventral processes that contact the basioccipital tubera (C174-2). By contrast, most of these are not recovered as synapomorphies supporting a placement of *Eocaiman* in Caimaninae here, as discussed below.

*Eocaiman cavernensis* is known only from the holotype (AMNH 3158) (Fig. 4.6A–D), which preserves portions of both mandibular rami, as well as a fragmentary skull missing the cranial table. The supraoccipital is not preserved, therefore any description of its size in *Eocaiman cavernensis* must instead be based on an undescribed specimen (AMNH 19170) catalogued as *Eocaiman* sp. This specimen was recovered from an unspecified late Eocene locality in Mendoza Province, Argentina, some 500 km from the type locality of *Eocaiman cavernensis*. Furthermore, if anything, the exposure of the supraoccipital is most likely small in AMNH 19170, meaning that C158 in Brochu et al. (2012) is incorrectly scored regardless.

A surangular-angular suture that passes broadly along the ventral margin of the external mandibular fenestra was recovered as an unambiguous synapomorphy of "Caimaninae", including *Eocaiman cavernensis* by previous authors (Brochu, 1999; Brochu et al., 2012; Narváez et al., 2016). Here, this condition

is no longer recovered in many caimanines, including *Eocaiman*, which instead share a posterodorsal intersection of the suture (Fig. 4.6C, E) that is recovered as plesiomorphic in Crocodylia.

Slender, descending processes of the exoccipitals that reach the basioccipital tubera have been recovered as an unambiguous synapomorphy of "Caimaninae" (Brochu, 1999). According to Brochu (1999), these processes do not actually contact the tubera in "Caimaninae", but extend slightly further ventrally than most other crocodylians. The distinction between this condition, and that exhibited by most crocodylians lacking contact between the exoccipitals and basioccipital tubera, was considered too vague in this study. Instead, the character has been simplified to describe absence or presence of contact between the exoccipitals and basioccipital tubera (C127). However, irrespective of whether this distinction is valid, neither the holotype nor AMNH 19170 appear to preserve this portion of the occiput.

I concur with previous studies (e.g. Salas-Gismondi et al., 2015; Souza-Filho et al., 2019) that *Eocaiman palaeocenicus*, *Eocaiman cavernensis*, and members of "Caimaninae" share a rostral tip of the splenial that is positioned dorsal to the meckelian fossa (Fig. 3.97). In such studies, this condition united *Eocaiman* with other caimanines. Here, the original character has been reductively coded, and resultantly this character no longer diagnoses the clade. Furthermore, the same condition is present in all species of *Alligator* that lack a splenial symphysis, and so this condition does not unambiguously diagnose "Caimaninae".

An examination of the character scores in the recently published dataset of Cidade et al. (2020a) supports all of the aforementioned observations. The only exception is character 54 of Brochu et al. (2012), which was not reductively coded, by contrast with my study. Despite these changes, Cidade et al. (2020a) still recovered *Eocaiman* as an early diverging member of "Caimaninae". This rests on two synapomorphies in their study. The first, as expected, pertains to the rostral tip of the splenial, which was delimited as originally described by Brochu (1999). The second is the intersection of the surangular-angular suture dorsal to the ventral tip of the articular, which was scored as present in *Eocaiman palaeocenicus*. This condition is recovered almost exclusively in South American caimanines here, constituting an informative synapomorphy of the clade; however, this region of the mandible is too poorly preserved in *Eocaiman palaeocenicus* to determine what character state it should be scored (MPEF 1933a, and all referred material [Appendix B]).

**Which characters 'pull' *Eocaiman* outside of Caimaninae?** In this study, only two of the characters comprising synapomorphies of Caimaninae could be scored in *Eocaiman*. In both cases, *Eocaiman* exhibits the other condition. In both species of *Eocaiman* included, the height of the dentary at the level of alveoli 1–4 is dorsoventrally lower than alveoli 11–12 (C218-1, Fig. 4.6C, E). Where preserved, all species of Caimaninae exhibit the opposite condition, in which the anterior dentary alveoli are approximately at the same level as the posterior alveoli (C218-0). This character has been included in relatively

few phylogenetic analyses, within which this feature is always recovered as an autapomorphy of *Eocaiman* within "Caimaninae" (Bona, 2007; Pinheiro et al., 2013; Cidade et al., 2017; Souza-Filho et al., 2019; Cidade et al., 2020a). By contrast to these studies, the derived condition is here also found in several alligatorines (see Chapter 3), contributing to the exclusion of *Eocaiman* from Caimaninae.

Only two of the characters diagnostic of "Caimaninae" can be scored in at least one species of *Eocaiman* studied here. Members of "Caimaninae" are diagnosed as having 13 maxillary alveoli, but *Eocaiman cavernensis* has 14. Since the number of maxillary alveoli can vary intraspecifically within crocodylians by 1–2 alveoli (Iordansky, 1973), and several "caimanines" have 14 maxillary alveoli, this character does not strongly support the exclusion of *Eocaiman* from the South American caimanine clade.

The morphology of the posterolateral surface of the mandible was newly characterised in this study (C240), and provides stronger support for the exclusion of *Eocaiman* from "Caimaninae". In *Eocaiman paleocencius*, there is a broad, unornamented exposure of the angular ventral to the retroarticular process for attachment of *M. pterygoideus ventralis* (C240-0) (Fig. 4.6E). This condition is shared by all alligatorines, several 'basal' alligatoroids and the North American caimanine clade (Chapter 3: Fig. 3.106). By contrast, all members of "Caimaninae" lack this unornamented exposed surface (C240-1) where preserved.

**What characters support the inclusion of *Eocaiman* in Caimaninae?** Two morphological features of *Eocaiman cavernensis* support a position within Caimaninae. These features are shared almost exclusively by caimanines, but are most parsimoniously optimised as being convergent in the optimal topology. Firstly, a feature previously unrecognised in *Eocaiman cavernensis* is a prominent spectacle (C32-1) (Fig. 4.6A). Although the presence of a low spectacle was recovered as an ambiguous synapomorphy of Alligatoroidea here, a tall spectacle is almost exclusively known in "Caimaninae". Despite the inclusion of this anatomical feature as a character in several studies (Barrios, 2011; Cidade et al., 2017; Souza-Filho et al., 2019; Cidade et al., 2020a), these did not recognise its presence in *Eocaiman cavernensis*. Secondly, the dorsal jugal margin has a characteristic sharp, orthogonal step (C94-2) in those "caimanines" in which the relevant region is preserved, which is otherwise only known in *Eocaiman cavernensis* (Fig. 4.6A, see also Chapter 3: Fig. 3.36).

**Constrained analyses** Two constrained analyses were performed to test the newly recovered position of *Eocaiman* (Appendix F). In the first, both species of *Eocaiman* were forcibly recovered in Caimaninae, as defined in Analysis 1.3. In the second, they were forcibly recovered in the South American caimanine clade ("Caimaninae"). Both constrained searches resulted in small and insignificant tree length increases. When constrained to be recovered in Caimaninae, *Eocaiman* becomes the earliest diverging caimanine lineage (Appendix F.2). By contrast, forcing *Eocaiman* into the South American clade results

in major topological differences (Appendix F.3). Most notably, the North American caimans are instead recovered in the stem of Alligatoridae. A more traditional Caimaninae is recovered, in which the stem consists of a paraphyletic *Eocaiman*, as well as two taxa otherwise recovered in the stem of Alligatoridae: *Procaimanoidea utahensis* and *Aramburgia gaudryi*.

**Summary** *Eocaiman paleocencius* and *Eocaiman cavernensis* are most parsimoniously recovered outside of Caimaninae here. This is surprising given that all alligatoroid taxa described from South America to date have been phylogenetically recovered within Caimaninae (Cidade et al., 2019a). This novel position is partly the result of modifications to character scores that until now supported its position in Caimaninae. Furthermore, there are a number of morphological features that indicate that *Eocaiman* lies outside of Caimaninae (i.e. dentary height, and morphology of the angular). On the other hand, all three species of *Eocaiman* are known from extremely limited material, such that most of the character states diagnostic of Caimaninae and less inclusive clades cannot be scored. Some of the character states that appear to draw *Eocaiman* outside of the South American caimanine clade (e.g. exposure of the fossa for *M. pterygoideus ventralis* on the angular) are plesiomorphic for Alligatoridae, also occurring in the North American caimanines. As such, these might be expected to occur in the earliest South American caimanines too. Constrained searches that force *Eocaiman* into the South American caimanine clade result in statistically insignificant tree length increases, as a result of the shared presence of some morphological features that are otherwise almost exclusively known in South American caimanines. The position of *Eocaiman* outside of Caimaninae is therefore only tentatively accepted, and this hypothesis will need to be re-tested once more complete material becomes available.

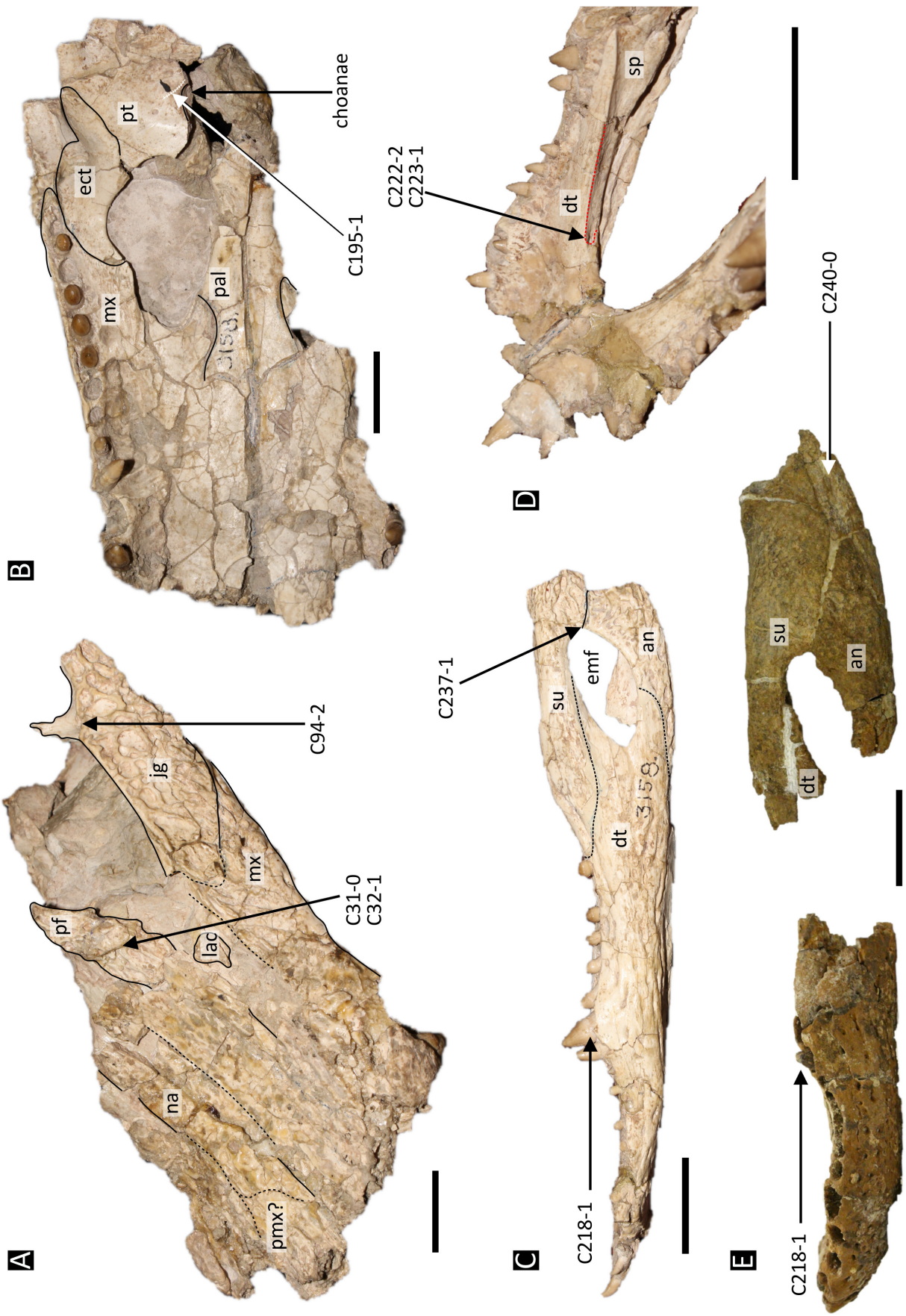



Figure 4.6: Key morphological features of *Eocaiman* described in the text. **A–D**, *Eocaiman cavernensis* (AMNH 3158): skull in anterodorsal (**A**) and ventral (**B**) views; mandible in lateral (**C**) and anteromedial (**D**) views. **E**, left mandibular ramus of *Eocaiman palaeocenicus* (MPEF PV 1933a). Abbreviations: **an**, angular; **dt**, dentary; **ect**, ectopterygoid; **emf**, external mandibular fenestra; **lac**, lacrimal; **max**, maxilla; **na**, nasal; **pal**, palatine; **pf**, prefrontal; **pmx**, premaxilla; **pt**, pterygoid; **jg**, jugal; **su**, surangular. All scale bars = 2 cm.

### The taxonomic content of Jacarea

Jacarea was first applied by Norell (1988) to include the three extant species of *Caiman* (*C. latirostris*, *C. crocodilus*, and *C. yacare*) and *Melanosuchus niger*, as distinguished from the two species of the dwarf caiman genus *Paleosuchus*. Later, Brochu (1999) formally defined this taxon as the last common ancestor of *Caiman* and *Melanosuchus*, and all their descendants. Among fossil taxa, Jacarea has typically included South American caimanines with a general caiman-like morphology, such as *Caiman brevirostris* and *Caiman wannlangstoni* (Brochu, 2011; Salas-Gismondi et al., 2015; Bona et al., 2018; Cossette & Brochu, 2018; Souza-Filho et al., 2019). Although poorly supported, the traditional composition of Jacarea is lost in this study as a result of the deeply nested position of *Paleosuchus*, the polyphyly of the genus *Caiman*, and the general pattern of successive branching found across the South American caimanine clade (Fig. 4.5). Cidade et al. (2020a) also recovered a topology in which *Necrosuchus* was deeply nested within Caimaninae, with possible affinities to Jacarea, although they were unable to determine whether it belonged in the latter clade.

Analysis 1.3 was constrained to recover Jacarea as traditionally defined, allowing several taxa that have been recovered in the group in previous analyses to float (*Caiman brevirostris*, *Caiman wannlangstoni*, UCMP 39978, *Purussaurus*, *Acresuchus*, and *Necrosuchus*). The resultant three MPTs were insignificantly longer by 19.3 steps, and their consensus reveals major topological differences to the unconstrained tree (Appendix F.4). All floating taxa are recovered in Jacarea, except *Necrosuchus*, which along with *Protocaiman* forms a polytomy outside of the crown group of caimanines. Considering only extant taxa, *Paleosuchus* is the sister taxon to Jacarea, consistent with the topology from molecular analyses. Also different to the unconstrained analysis is the exclusion of the North American clade from Caimaninae, which instead is nested in Alligatorinae. *Eocaiman* remains outside of Caimaninae, but is paraphyletic along the stem of Alligatorinae.

### The phylogenetic affinities of *Caiman lutescens* (MACN PV 13551)

*Caiman lutescens* was erected based on fragmentary remains from late Miocene deposits in northeastern Argentina (Rovereto, 1912; Bona & Barrios, 2015). The type material, which consists of a skull table (MACN PV 13551), a large fragment of the rostrum (MACN PV 5416), and numerous vertebrae and dentary fragments, is no longer considered to represent a single individual or even species (Langston, 1965; Brochu, 1999; Bona et al., 2012; Bona & Barrios, 2015). The rostral fragment (MACN PV 5416) is now referred to *Caiman latirostris* (Bona et al., 2012), whereas the mandibular and postcranial elements belong to an indeterminate crocodylian. As such, *Caiman lutescens* is represented only by a skull table (MACN PV 13551) (Fig. 4.7). Nevertheless, despite its incomplete nature, MACN PV 13551 preserves numerous features diagnostic of South American caimanines: (1) a large supraoccipital exposure,

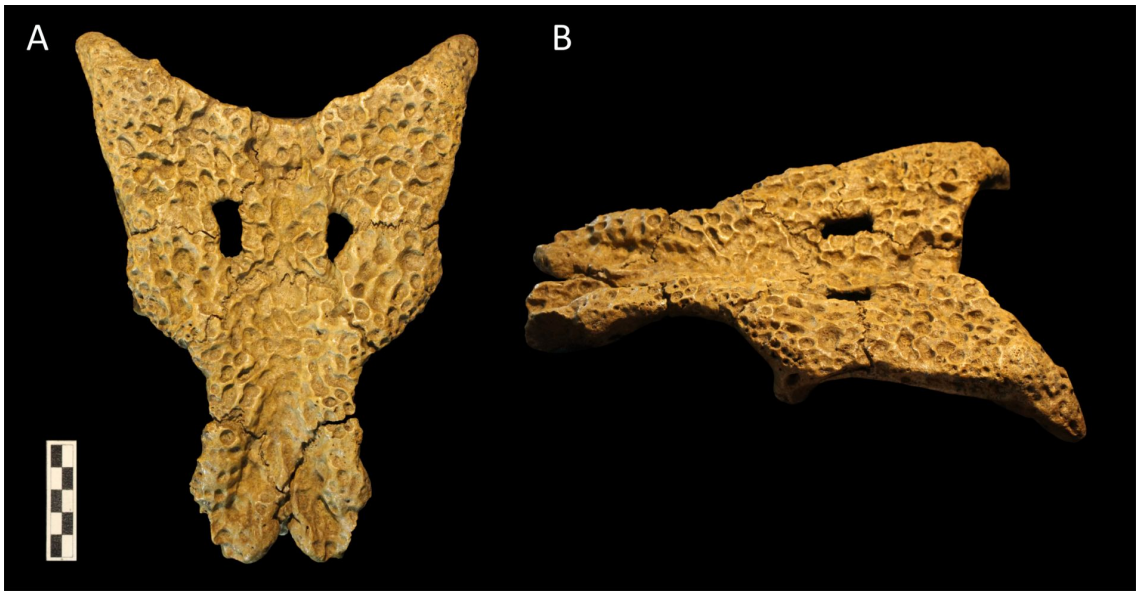



Figure 4.7: *Caiman lutescens* MACN PV 13551 in **A**, dorsal view; **B**, dorsolateral view. Scale bar = 5 cm

.

blocking the parietal from the posterior margin of the cranial table (C78-2); (2) overhanging rims of the supratemporal fenestrae (C81-1); (3) a reduced anterior extent of the frontal process (C62-1); (4) interconnected prefrontals (C59-1); and (5) a tall interorbital spectacle (C32-1). In my analysis, *Caiman lutescens* is recovered as the sister taxon to *Caiman gasparinae* + *Mourasuchus*. This relationship is supported by two synapomorphies: (1) ratio of the interorbital distance to anterior cranial table width = 0.4–0.5 (C6); and (2) presence of an acute dorsal indentation on the supraoccipital (C82-1, shared). The sister relationship between *Caiman gasparinae* and *Mourasuchus* is supported only by ratio of antero-posterior supratemporal fenestra length to cranial table length = 0.3 (C10).

Brochu (1999) suggested close affinities between *Caiman lutescens* and *Purussaurus* or *Mourasuchus*, which are among the largest and most unusual appearing crocodylians known (Price, 1964; Langston, 1966; Gasparini, 1985). The skull table of *Caiman lutescens* indeed belonged to a large animal: its dimensions are greater than all extant *Caiman* species examined here; however, they are approximately equivalent to *Acresuchus* (UFAC 2507), *Mourasuchus amazonensis* (UFAC 1424), adult *Melanosuchus niger* (NHMUK 45.8.25.125), and *Caiman gasparinae* (MLP IV-15-1), and smaller than the largest specimens of *Purussaurus* (e.g. UFAC 2507, UCMP 39704) (Table 4.8), although we cannot be sure of the ontogenetic stage of *Caiman lutescens*. Further similarities between *Caiman lutescens*, *Purussaurus*, and *Mourasuchus* include a wide interorbital distance, and a thickening of the medial orbital margin. The interorbital width is continuously scored in this study, and recovered as a synapomorphy supporting the clade (*C. lutescens* + (*C. gasparinae* + *Mourasuchus*)), but *Purussaurus* exhibits a nearly equivalent interorbital distance. Most alligatoroids exhibit upturned orbital margins; however, in *Caiman lutescens* the upturned margins are thick and rugose, again similar to *Purussaurus* and *Mourasuchus*. Several authors

Table 4.8: Comparison of cranial measurements (mm) in selected caimanine taxa. Abbreviations: **ST**, Skull table; **IO**, Inter-orbital.

| Taxon | Specimen | Skull length | ST anterior width | ST posterior width | ST length | IO width |
|---|---|---|---|---|---|---|
| *Caiman lutescens* | MACN -PV 13551 | ? | 132 | 158 | 79 | 61 |
| *Acresuchus pachytemporalis* | UFAC 2507 | 550 | 104 | 122 | 83 | 35 |
| *Caiman gasparinae* | MLP 73-IV-15-1 | ? | 114 | 73 | 88 | 51 |
| *Caiman latirostris* | MACN 1420 | 320 | 82 | 99 | 54 | 28 |
| *Caiman yacare* | MACN uncat. | 321 | 80 | 91 | 53 | 26 |
| *Melanosuchus niger* | NHMUK 45.8.25.125 | 630 | 122 | 156 | 100 | 39 |
| *Mourasuchus arendsi* | MLP 73-IV-15-8 | ? | 114 | 125 | 65 | 55 |
| *Mourasuchus* cf. *amazonensis* | UFAC 1424 | ∼1220 | ? | ? | 90 | ? |
| *Purussaurus barasiliensis* | UFAC 1403 | 1420 | 315 | 330 | 165 | 170 |
| *Purussaurus neivensis* | UCMP | 990 | 206 | 188 | 156 | 83 |

have recognised that the posterior cranial table margin of *Caiman lutescens* is broadly 'U' shaped across its length (Langston, 1965; Brochu, 1999; Bona et al., 2012) (Fig. 4.7), a condition otherwise known only in *Purussaurus* and *Acresuchus*. Bona et al. (2012) also considered the skull table to be deeply concave about the sagittal line in *Caiman lutescens* (Fig. 4.8B), another feature known only in *Purussaurus* and *Acresuchus*. By contrast with Bona et al. (2012), I regard the morphology of the skull table of *Caiman lutescens* as distinct from that of *Purussaurus* (Fig. 4.8C). *Caiman lutescens* exhibits a deep indentation on the skull table that is restricted to the sagittal line (82-1) (Figs. 4.7B, 4.8B). By contrast, in both *Purussaurus* and *Acresuchus*, the remainder of the skull table is relatively flat. This indentation is also found in *Caiman gasparinae* (Fig. 4.8D), *Mourasuchus* (Fig. 4.8F), and *Caiman latirostris*, although it does not extend as far anteriorly in these taxa as in *Caiman lutescens*. Strongly overhanging rims of the supratemporal fenestrae, and a tall spectacle with a deep posterior fossa (Fig. 4.9), also distinguish *Caiman lutescens* (Fig. 4.9A) from *Acresuchus* and *Purussaurus* (Fig. 4.9B), but unite it with *Mourasuchus* and *Caiman gasparinae*.

Despite these similarities, several features of the cranial table clearly distinguish *Caiman lutescens* from *Mourasuchus*. Most notably, *Caiman lutescens* lacks the squamosal horns characteristic of all

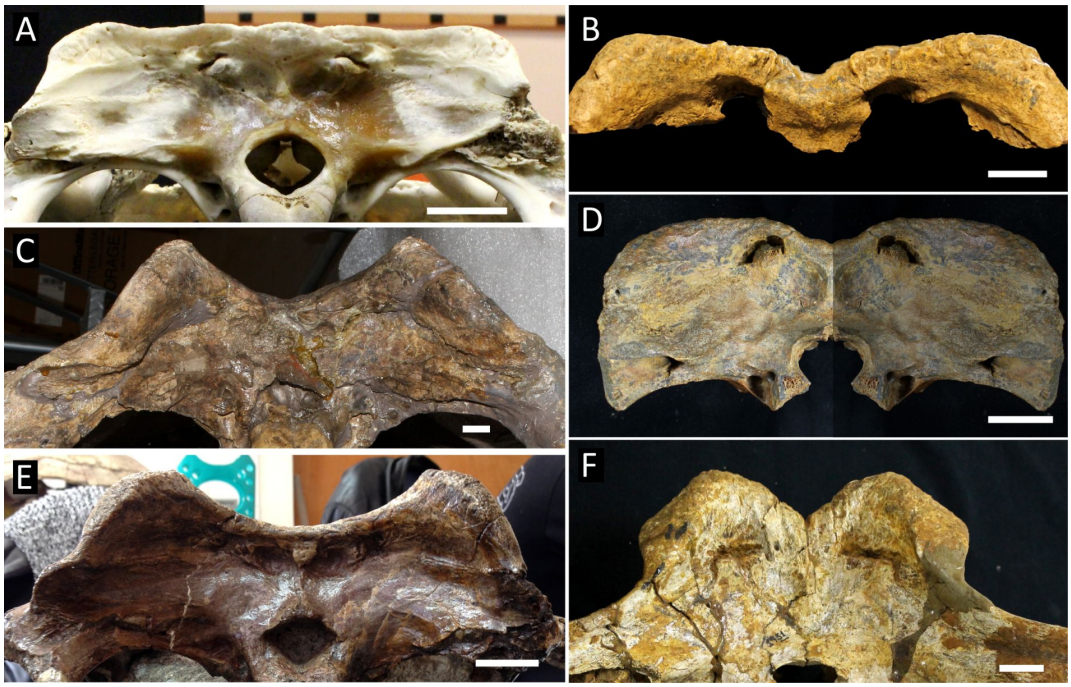



Figure 4.8: Occipital view of the cranium showing variation in morphology of the posterior cranial table margin. **A**, *Caiman yacare* (AMNH 97300); **B**, *Caiman lutescens* (MACN PV 13551); **C**, *Purussaurus neivensis* (UCMP 39704); **D**, *Caiman gasparinae* (right hand side mirrored for clarity) (MLP-IV-15-1); **E**, *Purussaurus neivensis* juvenile (IGM DHL-45); **F**, *Mourasuchus arendsi* (UFAC 1431). All scale bars = 2 cm.

*Mourasuchus* species, where preserved (Cidade et al., 2019c) (Chapter 3, Fig. 3.11C,D). *Mourasuchus arendsi* and *Mourasuchus amazonensis* also exhibit subparallel lateral cranial table margins, unlike the posteriorly divergent margins of *Caiman lutescens*. The anterior corners of the cranial table formed by the postorbitals are sharp in *Mourasuchus arendsi* and *Mourasuchus amazonensis*, but they are smoothly curved and crescentic in *Caiman lutescens*. Finally, *Mourasuchus arendsi* and *Mourasuchus amazonensis* exhibit a sagittal ridge on the parietal, which is absent in *Caiman lutescens*.

In summary, *Caiman lutescens* shares features in common with *Mourasuchus* and *Purussaurus*, but lacks apomorphic features of both taxa. Morphological characters supporting a sister relationship between *Caiman lutescens* and *Caiman gasparinae* + *Mourasuchus* are few, but diagnostic. Among alligatoroids, the indentation of the supraoccipital (C82-1) is otherwise only known in *Caiman latirostris*; however, the anterior extent of the indentation is unique to *Caiman lutescens*. *Caiman lutescens* represents a distinct species, but the discovery of more complete material is needed to further test its phylogenetic affinities with Caimaninae.

### The phylogenetic affinities of UCMP 39978

UCMP 39978 is a skull missing the cranial table, from the middle Miocene Honda Group of Colombia (Fig. 4.10). Langston (1965) identified this specimen as *Caiman* cf. *lutescens* based on similarities

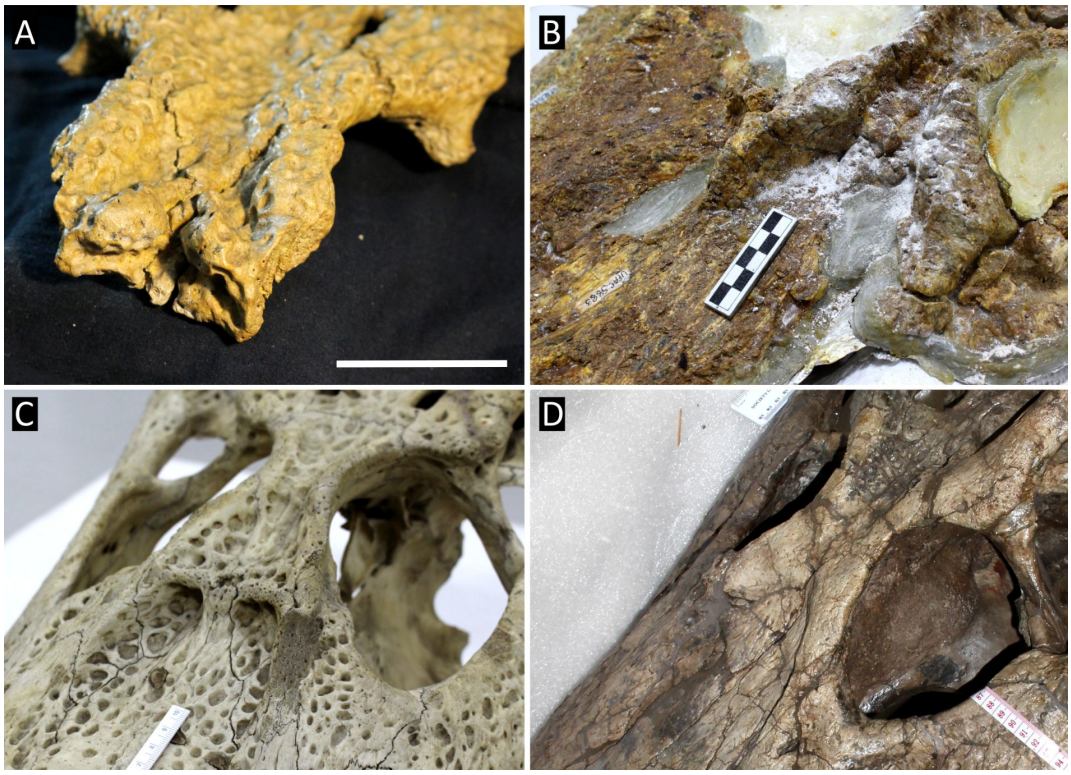



Figure 4.9: Anterolateral view of the rostrum showing morphology of the interorbital bridge (spectacle) in **A**, *Caiman lutescens* (MACN PV 13551); **B**, *Mourasuchus arendsi* (UFAC 5883); **C**, *Melanosuchus niger* (NHMUK 45.8.25.125); **D**, *Purussaurus neivensis* (UCMP 39704). Scale bar in A = 5 cm, all other scale bars = cm.

with MACN PV 5416, which was assigned to *Caiman lutescens* at the time (see above). Now only one overlapping bone (the supraoccipital) exists between UCMP 39978 and *Caiman lutescens*, and by itself does not preserve any diagnostic features. Nevertheless, these taxa are most likely not synonymous. In addition to their geographic and temporal separation, *Caiman lutescens* exhibits highly divergent features reminiscent of *Mourasuchus* or *Purussaurus*, but UCMP 39978 exhibits a generalised *Caiman* morphology (Fig. 4.10). Despite referring the material to *Caiman* cf. *lutescens*, Langston (1965) recognised similarities between UCMP 39978 and the extant species *Caiman latirostris*, suggesting the latter might be descended from UCMP 39978, with only a few evolutionary changes. Among the similarities he noted were the presence of rostral ridges, the overall proportions of the skull, and the large palatine exposure. Brochu (1999) was the first to test the affinities of UCMP 39978 phylogenetically and recovered it in a polytomy with *Caiman latirostris* and *Melanosuchus*. Later, Bona et al. (2012) recovered the specimen in a similar polytomy, also including *Caiman crocodilus*, *Caiman yacare*, and *Caiman gasparinae*. Nevertheless, they referred UCMP 39978 to *Caiman latirostris* based on several of the features listed by Langston (1965), in addition to the wide nasals and maxillae, and a large opening of the external naris. After the discovery of several new caimanines from the middle Miocene of Peru, Salas-Gismondi et al. (2015) noted similarities between UCMP 39978 and *Caiman wannlangstoni*, and Scheyer and Delfino

(2016) listed UCMP 39978 as aff. *Caiman wannlangstoni*. Nevertheless, the most recent phylogenetic analyses of Caimaninae continue to recover UCMP 39978 in a polytomy with most species of *Caiman* and *Melanosuchus* (Souza-Filho et al., 2019; Cidade et al., 2020a). In the present analysis, a weakly supported sister relationship is recovered between UCMP 39978 and *Caiman wannlangstoni* based on one shared synapomorphy: the lateral margin of the orbit is situated further laterally than that of the maxilla at the level of alveoli 3–6 (C74-0). UCMP 39978 is recovered more distantly related to *Caiman latirostris*, and several morphological features argue against its referral to that taxon. For example, by contrast with *Caiman latirostris*, UCMP 39978 lacks an anterior invagination of the palatine process as well as a nasal-lacrimal contact, and exhibits a highly enlarged external naris. Salas-Gismondi et al. (2015) diagnosed *Caiman wannlangstoni* based on a combination of 11 characters. All but one (sinuosity of maxilla lateral margin) were discretised as morphological characters in this analysis, and are listed along with other characters pertinent to caimanine interrelationships in Table 4.9. UCMP 39978 exhibits four of these diagnostic features: (1) sinuous lateral margins of the maxilla; (2) prominent rostral ridges (C27-1); (3) a fossa on the anterior margin of the choanae (C197-1); and (4) a broad maxillary shelf at the anterolateral margin of the suborbital fenestra (C168-1). However, these features provide only weak support for the referral of UCMP 39978 to *Caiman wannlangstoni*, given that they are found in other South American caimanines too. The 'strongly sinuous' lateral rostral margins of *Caiman wannlangstoni* do not appear significantly more sinuous than most South American caimanines. Furthermore, prominent rostral ridges are also present in *Caiman brevirostris*, *Caiman latirostris*, *Melanosuchus niger*, and *Purussaurus neivensis*. Although UCMP 39978 and *Caiman wannlangstoni* do share a deep fossa excavating the anterior margin of the choanae, this appears to be of limited diagnostic use, given that such a fossa appears in several large, mature crocodylians. It commonly occurs in mature *Crocodylus* species, but the condition has also been observed in large individuals of *Caiman latirostris* (MACN V 1420) and *Melanosuchus niger* (NHMUK 45.8.25.125). Furthermore, a broad maxillary shelf on the anterolateral margin of the suborbital fenestra is present in all alligatorids where preserved. Although this condition is accentuated in *Caiman wannlangstoni* and UCMP 39978, it is not discernible from *Caiman latirostris* or *Melanosuchus niger*.

Several anatomical features directly refute the referral of UCMP 39978 to *Caiman wannlangstoni* (Salas-Gismondi et al., 2015). Unlike *Caiman wannlangstoni*, UCMP 39978 lacks globular posterior dentition (otherwise only known in *Caiman brevirostris*) and anterodorsally facing nares (absent in all other caimanines). Furthermore, whereas the rostrum is vaulted in *Caiman wannlangstoni*, in UCMP 39978 the rostrum has a height to width ratio comparable to most other caimanines. An additional feature that distinguishes UCMP 39978 from *Caiman wannlangstoni* is the absence of a nasal-lacrimal contact and the absence of a maxillary process in the lacrimal in UCMP 39978. Finally, although the size of the external naris was not discretised, it is much larger in proportion to the premaxillae in UCMP

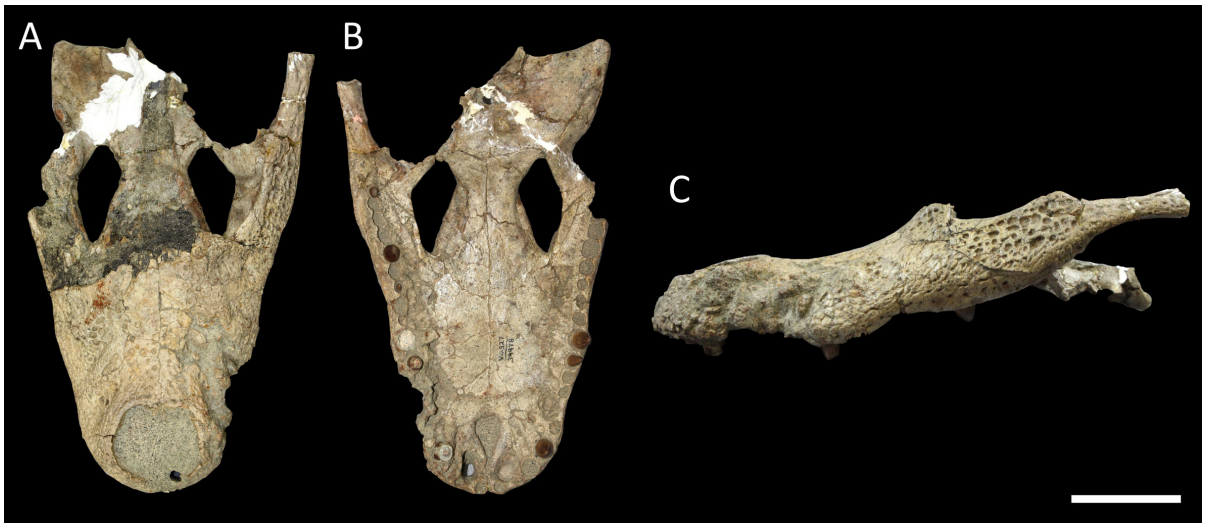



Figure 4.10: UCMP 39978 ('*Caiman* cf. *lutescens*') in **A**, dorsal; **B**, ventral; and **C**, left lateral views. Scale bar = 5 cm.

39978 than all other South American caimanines (except *Purussaurus brasiliensis* [UFAC 1403]).

In summary, I support previous rejections of the referral of UCMP 39978 to *Caiman lutescens*. Whereas UCMP 39978 exhibits a generalised caimanine morphology, the skull table of *Caiman lutescens* indicates that it was a close relative of *Purussaurus* or *Mourasuchus*. Furthermore, the referral to *Caiman latirostris* is rejected based on the presence of several autapomorphies in UCMP 39978, pertaining to the absence of a nasal-lacrimal contact and invagination of the palatine process, as well as the extreme enlargement of the naris. Finally, although UCMP 39978 might be closely related to *Caiman wannlangstoni* (Scheyer & Delfino, 2016), I do not consider them to be conspecific given the absence of several autapomorphies, namely the globular posterior dentition and anterodorsally facing nares that characterise *Caiman wannlangstoni* (Salas-Gismondi et al., 2015). As such, UCMP 39978 likely warrants a new species name, although that is beyond the scope of this study.

Table 4.9: Comparisons between UCMP 39978 and potential closely related taxa. Characters used to diagnose *Caiman wannlangstoni* by Salas-Gismondi et al. (2015) are emboldened. Green cells show features shared with UCMP 39978.

| Feature | UCMP 39978 | *Caiman wannlangstoni* | *Caiman crocodilus* | *Caiman yacare* | *Melanosuchus niger* | *Caiman latirostris* | *Caiman gasparinae* | *Caiman brevirostris* |
|---|---|---|---|---|---|---|---|---|
| **Lateral margins of maxilla** | sinuous | sinuous | sinuous | sinuous | sinuous | sinuous | sinuous | sinuous |
| **Naris direction** | dorsal | anterodorsal | dorsal | dorsal | dorsal | dorsal | dorsal | dorsal |
| **Rostral ridges** | present | present | absent | absent | present | present | absent | present |
| **Globular posterior dentition** | absent | present | absent | absent | absent | absent | ? | present |
| Pmx-mx suture realtive to naris | posterior | anterior | posterior | posterior | anterior | anterior | posterior | anterior |
| External nasal naris contact | absent | present | variable | variable | present | present | absent | present |
| **Choanal fossa** | present | present | absent | absent | present (v) | present (v) | ? | ? |
| **Maxillary shelf** | very wide | very wide | moderate | moderate | very wide | very wide | ? | ? |
| Palatine process invagination | absent | ? | absent | absent | absent | present | ? | ? |
| Orbit position to maxilla | lateral | lateral | lateral | lateral | medial | medial | ? | ? |
| lacrimal: prefrontal width | equal | equal | wide | wide | wide | wide | ? | ? |
| Nasal-lacrimal contact | absent | present | present | present | present | present | present | present |
| maxillary process in lacrimal | absent | present | present | present | present | present | ? | present |
| Naris size | Very large | moderate | moderate | moderate | moderate | moderate | moderate | moderate |
| **Rostral depth** | 0.3 | ? | 0.3 | 0.4 | 0.3 | 0.3 | 0.5 | 0.3 |

### 4.4.6 The affinities of Planocraniidae

Like *Borealosuchus*, Planocraniidae (comprising *Boverisuchus* and *Planocrania*) is typically recovered as a stem "brevirostrine", commonly as the sister clade of Alligatoroidea + Crocodyloidea (e.g. Puértolas-Pascual et al., 2011; Brochu, 2012; Brochu et al., 2012; Salas-Gismondi et al., 2016; Mateus et al., 2019). However, this clade has also been recovered in a 'basal' crocodyloid position (Jouve et al., 2015), as well as in a polytomy with Alligatoroidea and Crocodyloidea (Jouve, 2016). Furthermore, Groh et al. (2020) recovered Planocraniidae as a polyphyletic group, with *Boverisuchus vorax* recovered as a stem "brevirostrine" and *Planocrania* as a crocodyloid. By contrast, some combined analyses suggest that Planocraniidae is the sister clade to Crocodylia (e.g. Gatesy et al., 2003; Lee & Yates, 2018). The sister relationship between Planocraniidae and Longirostres recovered here is weakly supported (Jackknife = 14, Bootstrap = 4, Bremer = 3.4), but is similar to the results of the combined analysis of Iijima and Kobayashi (2019). Only three synapomorphies support Planocraniidae + Longirostres: (1) degree of flare in the scapula blade = 23°–31° (C21); (2) foramen aerum on the dorsomedial corner of the quadrate condyle (C117-0, shared); and (3) ectopterygoid-maxilla suture parallel and adjacent to posterior maxillary alveoli (C175-1, ambiguous). There is little consensus over the position of Planocraniidae between my analyses, with variation principally between those using extended implied weighting with different weighting factors. Whereas all analyses using EIW12 recover Planocraniidae in the stem of Longirostres (Fig. 4.2), those using the more severe weighting factor ($k$=3) position Planocraniidae in the stem of Alligatoroidea (Fig. 4.2). Analyses implementing such a severe weighting factor also recover the highly anomalous topology in which Alligatoroidea was the sister clade to Gavialoidea. The position of Planocraniidae is also different in Analysis 1.1, in which it is polyphyletic, with *Planocrania hengdongensis* recovered as a stem crocodylian, and the remaining planocraniids forming a 'basal' alligatoroid clade (Fig. 4.2).

### 4.4.7 Implications for the systematics and taxonomy of Gavialoidea

Modifications to the taxonomic content of Gavialoidea constitute the most significant changes to the crocodylian tree in this study. Perhaps most notably, and in contrast to all previous morphology-only analyses, *Gavialis gangeticus* and *Tomistoma schlegelii* are found to be closely related, defining the crown gharial clade Gavialidae (Fig. 4.11). Furthermore, Gavialoidea (Bremer support = 11.9) is the sister clade of Crocodyloidea, together defining Longirostres. The latter is moderately well-supported, with Bremer support = 7.2, but poorly recovered in Bootstrap and Jackknife replicates.

Analysis 1.3 was constrained to recover the traditional morphological topology, i.e. Alligatoroidea + Crocodyloidea (=Brevirostres). Under this constraint, Gavialoidea is the sister to all other crocodylians, and Crocodyloidea comprises Tomistominae and Crocodylinae (Appendix F.5). Forcing this topology

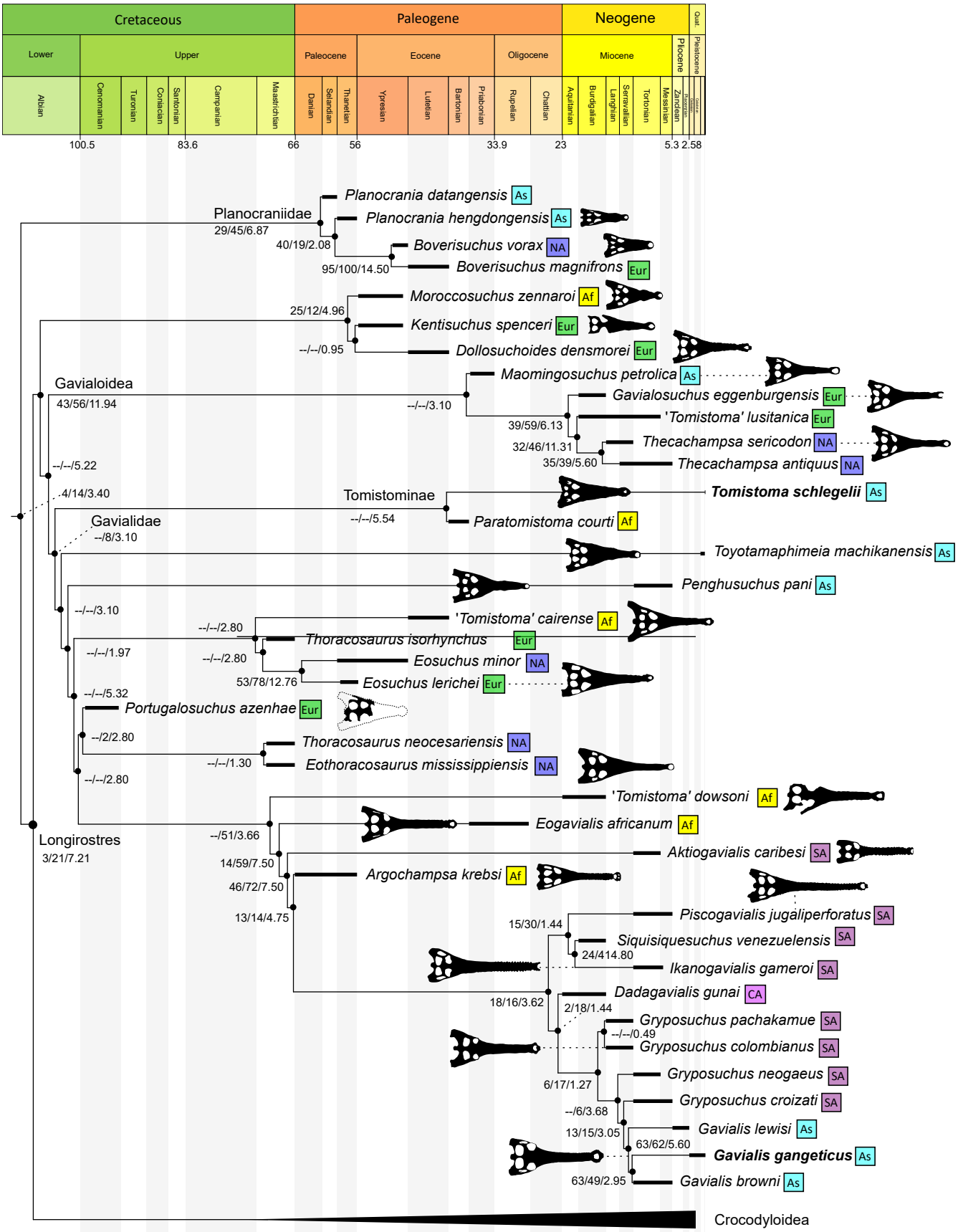



Figure 4.11: Time-calibrated phylogeny of Gavialoidea. Ages = Ma. Support values: Bootstrap/Jackknife/Bremer. Abbreviations: **Af**, Africa; **As**, Asia; **CA**, Central America; **Eur**, Europe; **NA**, North America.

results in a significantly less parsimonious tree than the unconstrained analysis (72.3 extra steps, Templeton test $p < 0.025$). The results of this study are based on a new dataset that includes taxa that have not previously been incorporated, new and revised morphological characters and scores, and the use of continuous characters. To determine why the traditional morphological topology is not recovered, a detailed assessment of all of these factors is provided.

**Is the recovery of Gavialidae due to convergence in long-snouted taxa?**

The gharial problem is unique in the usual narrative of morphology versus molecules in phylogenetics, i.e. groups that are well supported by morphological data are often recovered as polyphyletic in molecular analyses, which indicate that the morphology is the result of convergence. The opposite is the case for Crocodylia. Whereas morphological data indicate that the elongate snouts of *Tomistoma schlegelii* and *Gavialis gangeticus* were convergently acquired, it is explained as true homology by molecular data. The results from this analysis support the molecular hypothesis for the first time based on morphology alone; however, the recovery of Gavialidae raises the question of whether this result is due to an overwhelming number of new characters pertaining to longirostry. Indeed, this analysis has introduced new morphological characters that explicitly factor in snout length and associated characters in phylogenetic reconstruction, e.g. continuous characters 1, 5, 10, 11, and 17. In addition, studies of neosuchian phylogeny have identified multiple morphological characters associated with longirostry (Jouve, 2009; Groh et al., 2020), several of which are included in this study. The role of longirostrine characters in driving these results was tested by repeating analysis 1.3, and excluding 22 characters that have previously been identified as correlates of longirostry (Jouve, 2009; Groh et al., 2020) (Table 4.10). The resultant topology (Appendix G.9) is almost identical to analyses implementing the full dataset. Both Gavialidae and Longirostres are still recovered, but now the crown clade Gavialidae is expanded to include *Maroccosuchus zennaroi*, *Kentisuchus spenceri*, and *Dollosuchoides densmorei*. Further evidence that the result is not a product of convergence is demonstrated by character support for Gavialoidea and Gavialidae that is unrelated to longirostry (see below). Finally, several unequivocally non-gavialoid, longirostrine taxa, such as *Crocodylus johnstoni*, *Crocodylus intermedius*, *Euthecodon arambourgi*, and *Mecistops cataphractus*, do not cluster together, nor with Gavialoidea, suggesting that longirostrine characters have not 'overwhelmed' this analysis.

Table 4.10: Characters employed in this study identified as correlated with longirostry.

| Character | State | Character description |
|---|---|---|
| 1 | NA | Snout length in dorsal view, ratio of anteroposterior snout length to total skull length |
| 5 | NA | Rostral depth, ratio of maximum dorsoventral height of the maxilla to mediolateral width of the maxilla at the 5th maxillary alveolus |
| 10 | NA | Supratemporal fenestra size, ratio of anteroposterior supratemporal fenestra length to maximum anteroposterior cranial table length |
| 11 | NA | Supratemporal fenestra shape, ratio of lateromedial width to anteroposterior length |
| 17 | NA | Number of maxillary alveoli |
| 30 | 0 | Rostral ornamentation, anteroposteriorly orientated preorbital ridges extending from the anterior corner of the orbit: absent or very modest |
| 37 | 0 | Skull table morphology: posterolateral edges directed ventrolaterally from the sagittal axis |
| 46 | 1 | Nasals, external contact with naris: absent |
| 47 | 2 | Nasals, excluded internally from posterior narial margin |
| 48 | 2 | Nasals, contact with premaxillae: absent |
| 76 | 0 | Frontoparietal suture, shape between supratemporal fenestrae: concavoconvex |
| 90 | 0 | Postorbital, protuberance on the dorsolateral margin of the postorbital bar at maturity: present |
| 107 | 1 | Squamosal, anterior divergence of dorsal and ventral rims of lateral groove: present |
| 146 | 2 | Premaxilla-maxilla suture, shape on palate in ventral view: posteriorly bowed, with 1 acute apex |
| 147 | 7 | Maxillary alveoli homodont |
| 158 | 1 | Maxilla, position of alveoli relative to maxillary palate separating toothrows: or dorsal |
| 160 | 1 | Palatines, anterior process shape: wedge shaped |
| 219 | 3 | Dentary alveoli: no differentiation posterior to $4^{th}$ alveolus |
| 220 | 0 | Dentary, shape of dorsal profile in lateral view between $4^{th}$ and $10^{th}$ alveoli: linear |
| 221 | 3, 4 | Dentary symphysis, adjacent to: 13–20 (3) or >20 (4) |
| 224 | 2, 3 | Splenial, anterior extent in dentary symphysis: adjacent to: 4–7 alveoli (2); $>$ 7 alveoli (3) |
| 278 | 1 | Axis, hypapophysis shape: forked (1) |

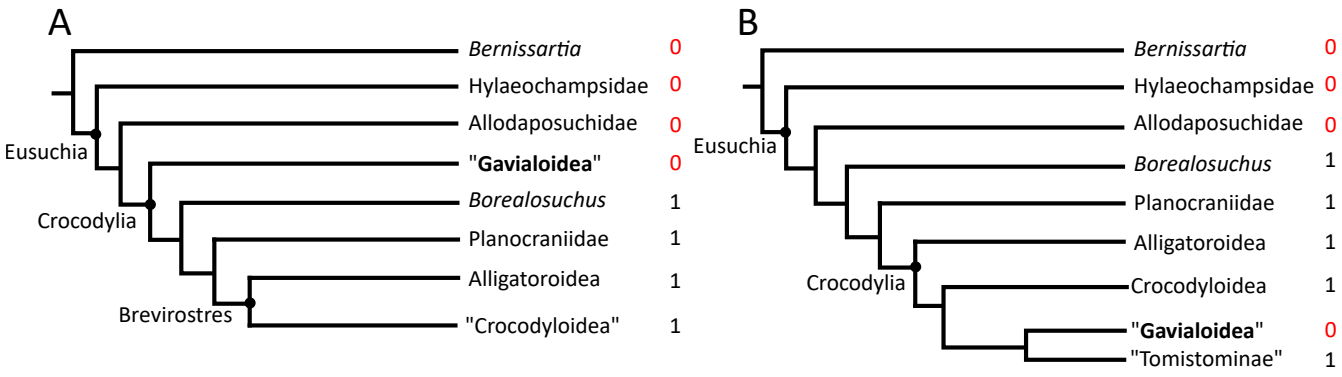



Figure 4.12: Simplified cladograms illustrating alternative optimaisations of a hypothetical character in a morphological (**A**) and molecular (**B**) tree.

### What are the reasons for the recovery of Gavialidae?

In essentially all previous morphological phylogenies, "Gavialoidea" is recovered as the earliest branching crocodylian clade, sister to all other crocodylians. The reason for this can be uncovered by optimising synapomorphies in traditional morphological datasets. "Gavialoids" appear to possess a suite of plesiomorphic morphological features (i.e. typically shared with non-crocodylian neosuchians) that are mostly absent in "Brevirostres" and stem-brevirostrines (Fig. 4.12A). As such, if the molecular topology is to be supported, then these features must be explained as reversals to 'primitive' states (atavisms), which is less parsimonious (Gatesy et al., 2003; Harshman et al., 2003; Iijima & Kobayashi, 2019) (Fig. 4.12B). Modifications to the construction and coding of these atavistic characters might have played a decisive role in the recovery of Gavialidae here. Indeed, Iijima and Kobayashi (2019) recognised several gavialine atavistic character states in the East Asian fossil "tomistomines" *Penghusuchus pani* and *Toyotamaphimeia machikanensis*. Although a phylogenetic analysis implementing the new character state distributions still recovered the traditional morphological topology in that study, searches constrained to recover the molecular topology were non-significantly longer by only five steps (Iijima & Kobayashi, 2019). This demonstrates the importance of these atavistic gavialine characters, as discussed below.

The second question to answer is which synapomorphies unite Gavialoidea, and other less inclusive clades that group morphological "tomistomines" and "gavialoids" together, in this study? Furthermore, does the novel topology reflect changes to character scores, character delimitation, and/or taxon sampling?

### Atavistic characters

Characters supporting a close relationship between Alligatoroidea and "Crocodyloidea", to the exclusion of "Gavialoidea" (and usually most non-crocodylian taxa), were identified by optimising synapomorphies in the stem to "Brevirostres" in the supplementary dataset of Narváez et al. (2016) (Fig. 4.13). That

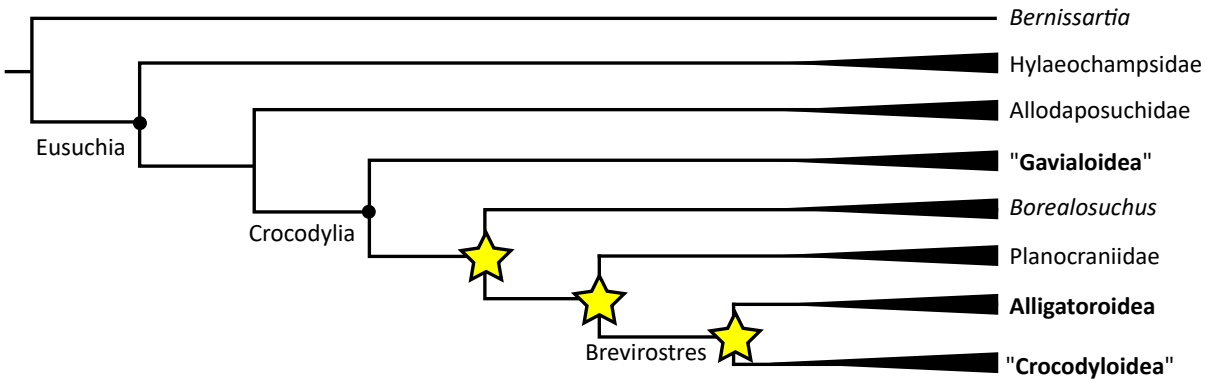



Figure 4.13: Simplified phylogeny illustrating the topology recovered by Narváez et al. (2016). Golden stars indicate the nodes for which synapomorphies were optimised (see text).

dataset is based on the character matrix of Brochu and Storrs (2012), supplemented with a number of non-crocodylian taxa (mostly allodaposuchids) that are also present in my analysis. Narváez et al. (2016) recovered the traditional morphological topology and this is used here as a proxy for most previous morphological phylogenies. Despite differences in taxon sampling between that study and this one, all major crocodylian clades are sampled in both.

Sixteen morphological characters in the dataset of Narváez et al. (2016) were identified that support the exclusion of "Gavialoidea" from the clade comprising (*Borealosuchus* + (Planocraniidae + "Brevirostres")): 9-0, 12-0, 14-1, 18-1, 27-0, 28-0, 33-0, 34-0, 38-0, 40-0, 43-0, 108-0, 134-0, 135-0, 149-1, 181-0 (character numbers and states from Narvaéz et al. [2016]). All of these characters are used in the present study, albeit with varying degrees of modification. The optimisation pattern of these characters was compared between this study and the dataset of Narváez et al. (2016). Modifications to most of these characters appears to be formative in the recovery of Gavialidae herein. The characters, score changes, and changes to character delimitations are discussed below and summarised in Table 4.11.

**Postorbital bar flush with the dorsal margin of the jugal (135-0)** In Narváez et al. (2016) all "gavialoids" were scored for the plesiomorphic condition, in which the postorbital is flush against the jugal (C135-0). By contrast, *Borealosuchus*, Planocraniidae, and "Brevirostres" were scored with the alternative condition, in which the postorbital is separated from the jugal arch by a sulcus (C135-1). Consequently, this character supported the sister relationship of Gavialoidea to all other crocodylians. In this study, all "gavialoids", except *Gavialis*, are shown to share the same condition as all other crocodylians (C92-1) (see Chapter 3, Fig. 3.35) thus weakening the case to separate "Gavialoidea" from *Borealosuchus*, Planocraniidae, and Brevirostres. The flush condition in *Gavialis* is now recovered as a local autapomorphy in Gavialidae (C92-0).

**Medial hemicondyle of the quadrate, small and ventrally reflected (181-0)** In the dataset of Narváez et al. (2016), essentially all "gavialoids" were scored as possessing a ventrally reflected medial hemicondyle (C181-0), which was shared with all non-crocodylian taxa and *Borealosuchus*. By contrast, Planocraniidae, Crocodyloidea, and Alligatoroidea each exhibited a different condition. This character has received significant modification here, including separation into two characters, which describe differences in the morphology of a notch on the quadrate condyle (C118) and the overall shape of the quadrate condyle (C119) (see Chapter 3, Fig. 3.45 and discussion therein). The result is that the presence of a small notch on the dorsomedial corner of the quadrate condyle (C118-0) is recovered as a synapomorphy of Longirostres. The second character (C119) has a more complicated pattern when optimised. Whereas some "gavialoids" are still shown to share a ventrally reflected medial hemicondyle in common with non-crocodylian taxa (C119-3), other "gavialoids" exhibit a rectangular quadrate condyle (C119-0), which is different to non-crocodylian taxa, but also unlike most members of Longirostres.

**Axis neural spine crested (12-0)** According to the dataset of Narváez et al. (2016), a posteriorly crested axial neural spine is the plesiomorphic condition for Eusuchia and Crocodylia (C12-0). The presence of a crested neural spine in "Gavialoidea" (C12-1) appears to draw this clade stemwards. Furthermore, according to their dataset, the crested neural spine is lost at the node comprising ((*Borealosuchus* + (Planocraniidae + Brevirostres)), but then regained in Crocodyloidea. There have been some important changes to character scores and taxon sampling here. For example, the small preserved portion of the axis of *Shamosuchus* is considered uncrested (Pol et al., 2009, fig.21D) (previously "?"). Additionally, *Isisfordia* has been included here, which also has an uncrested axial neural spine (Salisbury et al., 2006, fig.3a). The result of these changes is that an uncrested axial neural spine is the plesiomorphic condition at the nodes of both Eusuchia and Crocodylia (C274-1). This polarity change has been facilitated by the large amount of missing data in non-crocodylian taxa (e.g. all hylaeochampsids and allodaposuchids). The presence of a crested axial neural spine is now recovered as a potential synapomorphy of Gavialidae (C274-0).

**Two scars for *M. teres major* and *M. dorsalis scapulae* dorsal to deltopectoral crest (28-0)** In the dataset of Narváez et al. (2016), where preserved, all non-crocodylian taxa and "Gavialoidea" are scored as having two muscle insertion scars on the humerus. In their study, this condition is optimised as the plesiomorphic condition in Eusuchia and Crocodylia, lost at the node comprising (*Borealosuchus* + (Planocraniidae + "Brevirostres")). Herein, *Bernissartia* is the only non-crocodylian taxon to exhibit the double muscle insertion (C304-0). The plesiomorphic condition for Eusuchia and Crocodylia has thus changed to a single muscle insertion (C304-1), and the double muscle insertion of several "gavialoids" is now an atavism. The change in character optimisation appears to be a result of minor differences

in taxon sampling, a few character score changes in non-crocodylian taxa, coupled with missing data. For example, whereas Narváez et al. (2016) included the hylaeochampsid *Pietraroiasuchus ormezzanoi* (which appears to have the condition of a double insertion scar), it was not incorporated here. Additionally, *Isisfordia* is included in this study (which lacks the condition of a double insertion scar), but was not included in the dataset of Narváez et al. (2016). Furthermore, the condition in *Shamosuchus* has been changed from '?' to '1' (Pol et al., 2009, fig. 25). Coupled with the lack of data in all other non-crocodylian taxa, these minor differences facilitate the change in character optimisation.

**Absence of longitudinal crest on dorsal midline osteoderms (38-0)** In the dataset of Narváez et al. (2016), the absence of a midline keel on dorsal osteoderms is recovered as the plesiomorphic condition in Eusuchia. The shared absence of keeled osteoderms in "Gavialoidea" supports its placement as an early branching crocodylian clade, along with *Borealosuchus*. Unkeeled osteoderms are also present in some "tomistomines", but this is explained by convergence under the traditional topology. In the dataset presented here, the plesiomorphic condition in Eusuchia has changed to the possession of keeled osteoderms (C325-1)). This change in polarity is due in part to the recognition of keeled osteoderms in *Theriosuchus pusillus*, the inclusion of *Isisifordia* (which has keeled osteoderms), and the high proportion of missing data in non-crocodylian taxa such as Allodaposuchidae and Hylaeochampsidae, which are now optimised as having keeled osteoderms. Furthermore, the presence of unkeeled osteoderms is recovered as a synapomorphy of the least inclusive clade comprising *Toyotamaphimeia* and *Gavialis gangeticus*.

**Dorsal half of the prefrontal pillar narrow (108-0)** Based on the dataset of Narváez et al. (2016), the dorsal half of the prefrontal pillar is 'primitively' narrow in Eusuchia, which is shared by "gavialoids", supporting their early divergence in Crocodylia. By contrast, the node comprising (*Borealosuchus* + (Planocraniidae + "Brevirostres")) is characterised by having a dorsally broad prefrontal pillar. As with the preceding characters, the optimisation of the narrow pillar morphology as being plesiomorphic is based on very few taxa that preserve this portion of the anatomy. In the present study, changes to taxon sampling, coupled with minor changes to character scores and missing data, have resulted in a reversal of the plesiomorphic eusuchian condition to dorsally broad prefrontal pillars (C66-1). Furthermore, several gavialoids are found to have a wide pillar (e.g. *Eogavialis*, *Piscogavialis*, *Eosuchus lerichei*), in common with all other crocodylians, whereas others do not preserve this portion of the anatomy (e.g. *Thoracosaurus*, *Tomistoma lusitanica*).

**Posterior margin of the otic aperture linear (149-1)** According to the dataset of Narváez et al. (2016), the posterior margin of the otic aperture is plesiomorphically linear in Eusuchia. This condition is shared by "Gavialoidea", *Borealosuchus*, and Planocraniidae, but absent in "Brevirostres", which exhibit an invaginated posterior margin of the otic aperture. In the present study, it is agreed that most alligatoroids,

crocodyloids, and "tomistomines" exhibit the invaginated condition, and that traditional "gavialoids" exhibit the linear condition. However, by contrast to Narváez et al. (2016), the condition in all non-crocodylian eusuchians, except *Borealosuchus* and *Shamosuchus* is considered unknown. Although the condition in allodaposuchids and hylaeochampsids is scored as a "?", this actually represents inapplicable data. These taxa exhibit an entirely different morphology, in which the squamosal and quadrate do not contact eachother posterior to the otic aperture (C112-1) (Chapter 3, Fig. 3.44). This ambiguity in the stem to Crocodylia reduces the stemward pull on "Gavialoidea", and the linear otic aperture is recovered as a synapomorphy of the least inclusive clade containing *Eothoracosaurus mississippiensis* and *Gavialis gangeticus*.

**Presence of a diapophysis on the axial neural arch (14-1)** The pattern of character optimisation for the presence of an axial diapophysis is essentially the same in this study as that in Narváez et al. (2016). Among non-crocodylian taxa preserving the axis, a diapophysis is only scored as present in *Bernissartia* (C276-1). As in Narváez et al. (2016), the axial diapophysis is lost in subsequent nodes but independently evolves in some gavialoids. An important difference to their study, and most previous morphological analyses is the recognition of an axial diapophysis in the "tomistomines" *Toyotamaphimeia* and *Penghusuchus* (Iijima & Kobayashi, 2019). Incorporating this information means that this condition is now recovered as a synapomorphy of the least inclusive clade comprising *Toyotamaphimeia machikanensis* and *Gavialis gangeticus*.

**Proximal edge of the deltopectoral crest emerges smoothly from proximal end of humerus (27-0)** There are no changes to character scores of non-crocodylian taxa from the dataset of Narváez et al. (2016), and only minor changes to scores in some gavialoids. As in previous analyses, the presence of a low, smoothly emerging deltopectoral crest is optimised as the plesiomorphic condition in Eusuchia (C302-0). Where preserved, this condition is present in *Bernissartia*, *Theriosuchus*, and all *Borealosuchus* species. However, unlike the dataset of Narváez et al. (2016), the "tomistomine" *Penghusuchus pani* is included here, which has recently been shown to exhibit the plesiomorphic condition (Iijima & Kobayashi, 2019). Now the presence of a low deltopectoral crest is recovered as an atavistic synapomorphy of the least inclusive clade comprising *Penghusuchus pani* and *Gavialis gangeticus*.

**Prominent preacetabular process on the ilium (33-0)** As in previous analyses, the presence of a prominent preacetabular process of the ilium is recovered as the plesiomorphic condition in Eusuchia and Crocodylia, present in *Bernissartia*, *Theriosuchus*, and *Allodaposuchus precedens* (C307-0), but unknown in most other non-crocodylian taxa. In the dataset of Narváez et al. (2016), the presence of a prominent preacetabular process in "Gavialoidea" was optimised as providing support for the early divergence of this group. Although the condition is still recovered here in most "gavialoids", it is more

parsimoniously optimised as a re-acquisition of the primitive condition. Score changes to traditional "gavialoid" taxa have probably made little contribution to this result, e.g. *Thoracosaurus isorhynchus* and *Thoracosaurus neocesariensis* are both scored with a "?" for this character, but these taxa are still optimised as possessing a prominent preacetabular process. A prominent preacetabular process has also been recognised in the "tomistomines" *Toyotamaphimeia* and *Penghusuchus* (Iijima & Kobayashi, 2019). As a result, this feature is optimised as a synapomorphy of the least inclusive clade comprising *Toyotamaphimeia machikanensis* and *Gavialis gangeticus*.

**Dorsal margin of the iliac blade rounded with a smooth border (34-0)** In previous studies, the plesiomorphic condition for Eusuchia is for the dorsal outline of the postacetabular process of the ilium to lack an indentation. This condition was scored present in "Gavialoidea" and some 'basal' alligatorines, but not in crocodylines, "tomistomines", or most other alligatoroids. This equivocally supports the early divergence of "Gavialoidea" from all other crocodylians in traditional morphological datasets. In the present study, the plesiomorphic condition remains unchanged; however, multiple character score changes have been made. Furthermore, the inclusion of *Toyotamaphimeia* and *Penghusuchus* in this dataset which, unlike other "tomistomines", retain the plesiomorphic condition, allies them with "gavialoids". The high proportion of missing data in "Tomistominae", which is usually optimised as sharing the same condition as "crocodylines", facilitates a change in the optimised character state to the plesiomorphic condition. This character was listed as a potential atavism by Iijima and Kobayashi (2019), but it is not recovered as such here because the plesiomorphic condition is retained at the base of Longirostres.

**Anterolateral process on dorsal midline osteoderms (43-0)** As in previous analyses, the presence of an anterolateral process on the dorsal midline osteoderms is plesiomorphic for Eusuchia and remains so in the immediate stem to Crocodylia (C327-0). No significant changes are made to scores of non-crocodylian eusuchians, except the presence of the plesiomorphic condition in *Shamosuchus* (previously missing data), but this further supports the 'primitive' nature of this feature. In addition to *Shamosuchus*, the plesiomorphic condition is present in *Bernissartia*, *Theriosuchus*, and *Borealosuchus* (although *Isisfordia* shows the derived condition [C327-1]). Where preserved, the plesiomorphic condition is also present in most traditional "gavialoids", e.g. *Gavialis gangeticus*, *Eogavialis africanum*, *Eosuchus minor*, and *Eothoracosaurus*. However, by contrast to traditional topologies, the anterolateral process is optimised as being an atavism in gavialoids, rather than retention of the plesiomorphic condition. Within Gavialoidea, notable changes to character scores include the recognition of the plesiomorphic feature in *Penghusuchus* and *Toyotamaphimeia* (Iijima & Kobayashi, 2019). Indeed, the presence of an anterolateral process on the dorsal midline osteoderms is recovered as a synapomorphy of the least inclusive clade

comprising *Toyotamaphimeia* and *Gavialis gangeticus*. The plesiomorphic condition is also newly recognised in several other crocodylian taxa, such as some *Diplocynodon* species, but these changes appear to be inconsequential to the placement of Gavialoidea recovered here.

**Broad axial rib tuberculum equal in size to tuberculum (9-0)** In previous studies, the presence of a broad axial rib tuberculum was recovered as the plesiomorphic condition in Eusuchia and Crocodylia. Where preserved, the same condition is recovered in most "gavialoids", as well as *Borealosuchus*. By contrast, a narrow axial rib tuberculum was recovered as a synapomorphy of "Brevirostres". That "gavialoids" possess a broad axial rib tuberculum (C271-0) is agreed upon here; however, major character score changes have been made to Crocodyloidea and some "tomistomines" (*Tomistoma schlegelii* and *Maomingosuchus petrolica*), such that they are also recognised as having a broad axial rib tuberculum. After these modifications, a broad axial rib tuberculum is optimised as a retained plesiomorphic feature in Longirostres that is only lost in Alligatoridae, members which exhibit a narrow axial rib tuberculum (C271-1).

**First postaxial vertebra lacking a prominent hypapophysis (18-1)** As in previous analyses, the absence of a hypapophysis on the third cervical vertebra (C279-1) is recovered as the plesiomorphic condition in Eusuchia and remains so in the immediate stem to Crocodylia. The absence of a hypapophysis in "Gavialoidea" was optimised as the retention of the plesiomorphic condition in previous studies, whereas here it is identified as convergently acquired instead. A number of character score changes have been made to traditional gavialoid taxa, but these do not appear to have significantly altered the topology. For example, both species of *Thoracosaurus* are now scored as "?", but these are still optimised as possessing the feature. Furthermore, *Eosuchus lerichei* is found to share the "gavialoid" condition, strengthening its position within Gavialoidea. One putative "tomistomine", *Toyotamaphimeia*, is scored for the derived condition, but this is recovered as an autapomorphy of the species.

**Four contiguous dorsal osteoderms per row at maturity (40-0)** As in Narváez et al. (2016), "Gavialoidea" is found to have the same number of dorsal osteoderms (four) as occurs plesiomorphically in Eusuchia (C324-1), and unlike all other crocodylians which have between six (C324-2) to eight (C324-3) dorsal osteoderms. Although all non-crocodylian taxa are optimised as having the same condition as Gavialoidea in my analysis, the plesiomorphic condition is somewhat ambiguous. Whereas *Bernissartia* has four dorsal osteoderms, *Theriosuchus* only has two, for which a new character state (C324-0) has been added. *Isisifordia* differs again in having six dorsal osteoderms. Determining the plesiomorphic condition for Crocodylia is further complicated by the lack of data for all allodaposuchid and hylaeochampsid species, which are optimised as having four dorsal osteoderms. Furthermore, the condition in most gavialoids is

unknown: although 22 taxa are optimised as having four osteoderms, in this study the condition is definitively known only in *Gavialis gangeticus* and *Eosuchus minor*. The condition is also extremely poorly known in "tomistomines", for which the character is only scored in *Tomistoma schlegelii*, which has six dorsal osteoderms.

**Process on the dorsolateral surface of the postorbital bar (134-0)** A spine on the dorsolateral surface of the postorbital bar is present in *Bernissartia* and several non-crocodylian eusuchians (C90-0), and has long been recognised as a 'primitive' feature in Eusuchia (e.g Norell, 1989). In most morphological phylogenies, the shared presence of this spine in "Gavialoidea" and its absence in essentially all "brevirostrines" supports the position of "Gavialoidea" as an early diverging crocodylian clade. Here, the presence of a postorbital spine is still recovered as the plesiomorphic condition in Eusuchia and Crocodylia, but the condition in "gavialoids" is homoplastic. The plesiomorphic condition is newly recognised in *Kentisuchus spenceri* and *Maroccosuchus zennaroi*; however, this is recovered as another instance of convergence.

**Summary** In summary, two morphological characters (C135, C181) received significant character score changes in "gavialoid" taxa, such that they now share the condition present in alligatoroids and "crocodyloids" (character numbers refer to Narvaez et al., [2016]) (Fig. 4.14A). Five characters received modifications to scores particularly in non-crocodylian taxa, such that they no longer share the same condition as "gavialoids". This results either in a reversal in character polarity at the nodes of Eusuchia and Crocodylia (C12, C28, C38, C108), or the condition becomes ambiguous at these nodes (C149) (Fig. 4.14B). In six characters, the plesiomorphic condition in Eusuchia and Crocodylia was unchanged, as were scores within "Gavialoidea"; however, the "gavialoid" condition is recognised in putative "tomistomines" (Fig. 4.14C) or in all "crocodyloids" (Fig. 4.14D), supporting an expanded Gavialoidea and Longirostres, respectively (C9, C14, C27, C33, C34, and C43). A further three characters received essentially no character score changes in "gavialoids" and non-crocodylian taxa but are now more parsimoniously optimised as atavisms within Gavialoidea (C18, C40, C134) (Fig. 4.12B).

Table 4.11: Changes to characters that supported the traditional morphological topology.

| Narvaéz et al. (2016) | This study | Character states supporting the traditional morphological topology | Modification to character | Difference in optimisation pattern |
|---|---|---|---|---|
| 135-0 | 92-0 | Postorbital bar, flush with dorsolateral margin of the jugal | Unmodified | “Gavialoid” condition changed |
| 181-0 | 118, 119 | 118: Quadrate condyle, notch on the dorsal articular border: absent or small; 119: quadrate condyle shape, dorsal and ventral margins subparallel across length | Reductively coded, new states added | “Gavialoid” condition changed |
| 12-0 | 274-0 | Axis neural spine, posterior half of spine dorsally inflected to form crest | Unmodified | Change in plesiomorphic condition for Eusuchia and Crocodylia |
| 28-0 | 304-0 | Humerus , scarring on proximodorsal surface: two muscle scars discernible (for M. teres major and M. dorsalis scapulae) | Unmodified | Change in plesiomorphic condition for Eusuchia and Crocodylia |
| 38-0 | 325-0 | Dorsal osteoderms, longitudinal midline keel: absent | Unmodified | Change in plesiomorphic condition for Eusuchia and Crocodylia |
| 108-0 | 66-0 | Prefrontal pillar morphology: dorsal half of pillar narrow, less than twice minimum anteroposteriorly length | Unmodified | Change in plesiomorphic condition for Eusuchia and Crocodylia |
| 149-1 | 115-0 | External auditory meatus, posterior margin shape: straight | Reductively coded | Plesiomorphic condition ambiguous |
| 14-1 | 276-1 | Axis, lateral process (diapophysis) on neural arch lateral margin: present | Unmodified | “Gavialoid” condition found in “tomistomines” |

**Table 4.11 continued from previous page**

| Narvaéz et al. (2016) | This study | Character states supporting the traditional morphological topology | Modification to character | Difference in optimisation pattern |
|---|---|---|---|---|
| 27-0 | 302-0 | Humerus , proximal edge of deltopectoral crest: straight, emerging smoothly from proximal end of the humerus | Unmodified | “Gavialoid” condition found in “tomistomines” |
| 33-0 | 307-0 | Ilium , preacetabular process shape: acute, pointed anteriorly | Unmodified | “Gavialoid” condition found in “tomistomines” |
| 34-0 | 309-0 | Ilium, dorsal outline of the postacetabular process: convex, no dorsal indentation | Reductively coded, ordered | “Gavialoid” condition found in “tomistomines” |
| 43-0 | 327-0 | Dorsal midline osteoderms, anterolateral process: present | Unmodified | “Gavialoid” condition found in “tomistomines” |
| 9-0 | 271-0 | Axial rib, tuberculum shape: broad, equal in size to capitulum | Unmodified | “Gavialoid” condition found in “crocodyloids” |
| 18-1 | 279-1 | First postaxial vertebra, prominent hypapophysis: absent | Unmodified | Atavism |
| 40-0 | 324-1 | Dorsal osteoderms, number in each transverse row at maturity: four | New state added, ordered | Atavism |
| 134-0 | 90-0 | Postorbital, protuberance on the dorsolateral margin of the postorbital bar at maturity: present | Unmodified | Atavism |

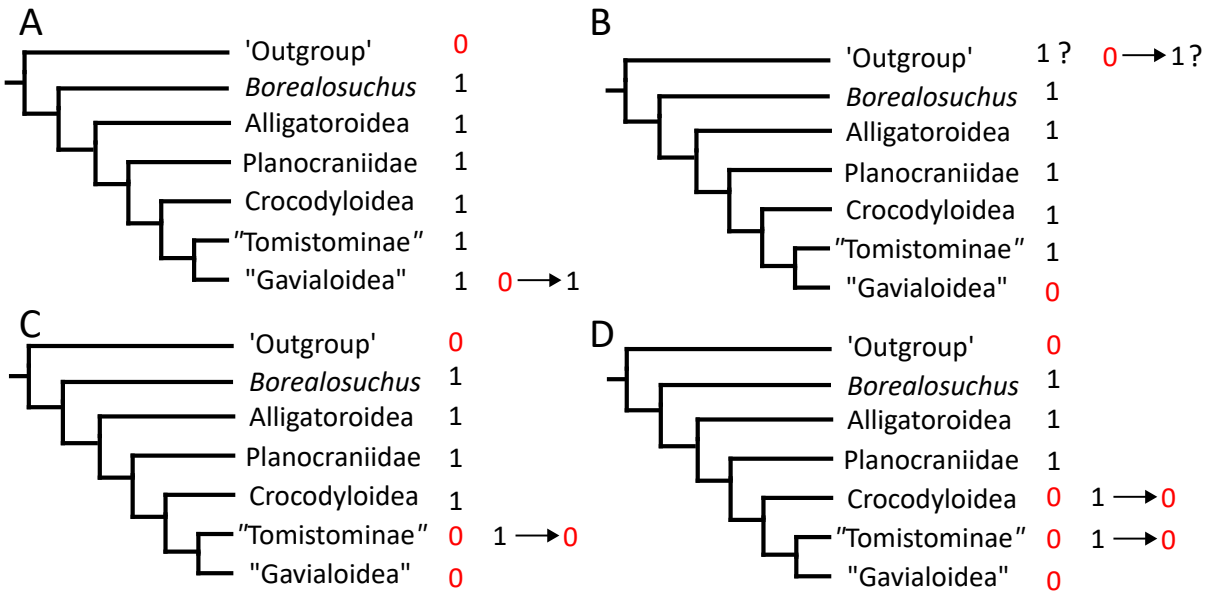



Figure 4.14: Principal changes in character optimisation of synapomorphies of "Brevirostres" and stemwards nodes recovered in Narváez et al. (2016). 'Outgroup' refers to all taxa stemward of *Borealosuchus* recovered here.

### Character support for Gavialoidea and less inclusive clades

In addition to modifications to some characters that previously pulled "gavialoids" towards the stem of Crocodylia, there are also a number of additional characters supporting clades containing traditional "tomistomines" and "gavialoids" (Fig. 4.15). Synapomorphies of all nodes containing morphological "gavialoids" and "tomistomines" are discussed below and summarised in Table 4.12. Score changes relative to earlier studies in gavialoid taxa are listed in Appendix J.

**Gavialoidea** Gavialoidea is supported by 16 synapomorphies: (1) ratio of rostrum length to skull length = 0.67 (C1); (2) ratio of rostral depth to rostrum width = 0.43 (C5); (3) ratio of supratemporal fenestra width to length = 0.98 (C11); (4) inclination of dorsal margin of external mandibular fenestra = 22° (C19); (5) dorsally projecting naris (C41-1, ambiguous); (6) posterodorsal processes of the premaxillae extending beyond the level of the $3^{rd}$ maxillary alveolus (C50-1, ambiguous); (7) frontoparietal suture does not intersect the supratemporal fenestrae (C75-2, ambiguous); (8) lateral grooves of the squamosal flare anteriorly (C107-1, exclusive); (9) rounded posterior pterygoid processes (C136-1, ambiguous); (10) last premaxillary alveolus positioned medially to the penultimate alveolus (C144-1, ambiguous); (11) inline occlusion of the dentary and maxillary teeth (C151-2, ambiguous); (12) absence of a diastema between maxillary alveoli 6 and 7 (C154-0, ambiguous); (13) absence of anterior process of the quadratojugal on medial jugal surface (C183-1, ambiguous); (14) anterior margin of the choanae not invaginated (C191-0, ambiguous); (15) capitate process of the laterosphenoid orientated laterally (C206-0, exclusive); and (16) dentary symphysis adjacent to the level of 9–12 alveoli (C221-2, ambiguous).

Most "tomistomines" and "gavialoids" have previously been scored as sharing an anteriorly flaring lateral squamosal groove (**C107-1**), which has been interpreted as homoplasy (Brochu, 1997b; Harshman et al., 2003; Brochu et al., 2012; Jouve, 2016; Narváez et al., 2016). Potentially significant character score changes have been made here, resulting in the more widespread occurrence of the derived condition in "tomistomines". This derived condition is newly recognised in *Kentisuchus spenceri* (formerly absent in all other studies) and *Maroccosuchus zennaroi* (absent according to Jouve, 2016). This feature is recognised as an exclusive synapomorphy of Gavialoidea here, given that it is absent in *Tomistoma schlegelii*, *Maomingosuchus petrolica*, *Tomistoma cairense*, *Eosuchus lerichei*, and *Portugalosuchus azenhae*.

Traditionally, a laterally directed capitate process of the laterosphenoid (**C206-0**) has been recovered in all "gavialoids", where preserved. This condition has previously been considered present in some, but not all "tomistomines", and has been interpreted as another example of convergence. For example, based on existing datasets (e.g. Jouve, 2016) and corroborated here, *Maroccosuchus*, *Paratomistoma*, and *Thecachampsa* each exhibit a laterally directed process. By contrast, *Tomistoma schlegelii* and *Penghusuchus* exhibit an anterolaterally directed capitate process (C206-1), as in all other crocodylians. Character scores for several other "tomistomines" have been changed from the derived condition (as scored by Jouve, 2016) to missing data (*Kentisuchus* and *Gavialosuchus eggenburgensis*) (see also Narváez et al., 2016). Additionally, the plesiomorphic condition is recognised in '*Tomistoma*' *dowsoni*, which has rarely been included in phylogenetic analyses.

A dorsally facing external naris (**C41-1**) is recovered as a synapomorphy of Gavialoidea here; however, this condition evolved independently multiple times within Crocodylia, including in Caimaninae, some alligatorines, crocodylines, and mekosuchines. As in previous analyses, the plesiomorphic condition in Crocodylia, and indeed in Eusuchia, is for the naris to face anterodorsally. Whereas in the traditional topology the dorsally facing condition was considered to have evolved independently in "Gavialoidea" and "Crocodyloidea", here it is recovered as a shared derived feature of "tomistomines" and "gavialoids" that is convergent in "crocodylines". There have been no significant changes to character scores of gavialoid taxa that have influenced this result.

Posterodorsal processes of the premaxillae which extend posteriorly beyond the level of the $3^{rd}$ maxillary alveolus (**C50-1**) have been recognised in "tomistomines" and "gavialoids" in previous studies (Brochu et al., 2012; Jouve, 2016; Narváez et al., 2016; Salas-Gismondi et al., 2019). Whereas this was formerly explained as convergence, it is recovered as a shared derived feature here. There have been no significant changes to gavialoid character scores, except the recognition of the derived condition in *Maomingosuchus petrolica* (formerly unknown).

A frontoparietal suture that sits entirely on the skull table (**C75-2**) is recovered as a shared synapomorphy of Gavialoidea. This condition evolved independently within Alligatoroidea and Crocodyloidea, and it is also ambiguous because the condition varies within Gavialoidea. Whereas "tomistomine" taxa

forming the stem of Gavialoidea exhibit a frontoparietal suture entirely exposed on the skull table (C75-2), the suture incipiently contacts the supratemporal fenestrae in crownward taxa (C75-1), which mostly correspond to traditional "gavialoids". Furthermore, several taxa (mostly 'thoracosaurs') exhibit a deep intersection of the frontopareital suture with the supratemporal fenestrae (C75-0). Several score changes have been made to gavialoid taxa and the character is newly ordered, but these modifications do not appear to be the reason for uniting "tomistomines" and "gavialoids".

The last premaxillary alveolus is medially inset relative to the penultimate alveolus (**C144-1**) in all "tomistomines" and most "gavialoids", where preserved. This character was first introduced in the analysis of (Jouve et al., 2015), in which this feature was recovered as convergently acquired by "Tomistominae" and "Gavialoidea". By contrast, it is recovered as a shared synapomorphy of Gavialoidea here, also occurring in *Mecistops cataphractus*. This character is slightly ambiguous within Gavialoidea, as the last alveolus is posterior or posterolateral to the penultimate alveolus in *Thecachampsa antiqua*, *Eosuchus*, and *Eothoracosaurus*.

A dentary symphysis adjacent to 9–12 alveoli (**C221-2**) is a shared synapomorphy of Gavialoidea, which evolved convergently in *Borealosuchus formidabilis*, some paralligatorids, and a small number of alligatoroids. This synapomorphy is not shared by all gavialoids as the dentary symphysis elongates stepwise (>20 alveoli, [C221-4]) in crownward nodes, especially in the clade comprising (*Piscogavialis* + (*Siquisiquesuchus* + *Ikanogavialis*)), as well as independently in *Gavialis*. Nevertheless, no non-gavialoid taxon exhibits a dentary symphysis exceeding 12 alveoli. Comparisons of character score changes with previous studies are challenging, as the delimitation of this character differs between datasets (e.g. Brochu et al., 2012; Narváez et al., 2016; Salas-Gismondi et al., 2016). Most datasets delimited this character with only three character states (Brochu et al., 2012; Jouve, 2016; Lee & Yates, 2018; Iijima & Kobayashi, 2019), in which "tomistomines and "gavialoids" have the same score, to the exclusion of all other crocodylians; however, this has always previously been interpreted as homoplasy. Salas-Gismondi et al. (2016, 2019) added a fourth character state to capture the even longer dentary symphysis that distinguishes "gavialoids" from "tomistomines". Whereas the modification by Salas-Gismondi et al. (2016) is accepted here, and is further augmented by an additional character state describing a symphysis adjacent to >20 alveoli, the character is ordered in this study, contrasting with previous analyses. Consequently, although "tomistomines" and "gavialoids" are still scored as having broadly different symphysis lengths, they are recognised as being more similar to eachother than to most other crocodylians.

In previous studies, the presence of interlocking maxillary and dentary teeth (**C151-2**) was recovered as a shared derived feature of "tomistomines" and "crocodylines", which independently evolved in "Gavialoidea". Here, there are few significant changes to character scores in any of these clades, but the interlocking dentition of "gavialoids" and "tomistomines" is now a shared derived feature that convergently evolved within Crocodyloidea. Although the interlocking condition is present in many crocody-

loids, it is not recovered as a synapomorphy of Longirostres, as some basal crocodyloids (e.g. *Asiatosuchus germanicus*) exhibit an overbite (C151-0), and many have an intermediate interlocking condition (C151-1), including several mekosuchines, '*Crocodylus*' *affinis*, and *Asiatosuchus depressifrons*.

Here, as in previous analyses (Brochu et al., 2012; Jouve, 2016; Narváez et al., 2016), the presence of a long anterior quadratojugal process on the medial surface of the lower temporal bar is recovered as the plesiomorphic condition in Eusuchia and in Crocodylia (C183-0). Whereas the absence of an anterior process (**C183-1**) has previously been recovered as an ambiguous synapomorphy of "Crocodylidae" (Narváez et al., 2016), it is here recovered as an ambiguous synapomorphy of Gavialoidea, which convergently evolved in crocodylines, osteolaemines, and some 'basal' crocodyloids. Since traditional "gavialoids" are scored with the plesiomorphic condition (C183-0), this indicates a reversal occurred within crownward nodes of Gavialoidea.

The presence of a linear or curved anterior choanal margin (**C191-0**) provides new support for Gavialoidea. This condition is plesiomorphic in Eusuchia, with the 'derived' invaginated condition (C191-1) evolving in Allodaposuchidae, *Borealosuchus*, and most alligatoroids. The condition in Gavialoidea is recovered as an atavism, which convergently evolved within Crocodylidae (present in all crocodylines, some osteolaemines, and mekosuchines).

The absence of a diastema between maxillary alveoli 6 and 7 also provides new, but ambiguous, support for Gavialoidea (**C154-0**). This is a shared synapomorphy that is highly labile in Crocodylia. The diastema is plesiomorphically absent in Eusuchia, but is gained at the node uniting *Borealosuchus* + Crocodylia. Some alligatoroids secondarily lost the diastema, as also occurred in Gavialoidea. The diastema is 'primitively' present in Crocodyloidea, but independently lost again in several taxa.

The presence of short posterior pterygoid processes (**C136-1**) that are not dorsoventrally expanded, is a shared synapomorphy of Gavialoidea. Formerly, this character had three states, which described: (0) tall posterior processes, optimised as the plesiomorphic condition in Eusuchia and Crocodylia; (1) small processes that are directed posteroventrally, optimised as an ambiguous synapomorphy of "Crocodylidae"; and (2) small processes that are directed posteriorly, optimised as a synapomorphy of derived "gavialoids". Despite the presence of small posterior pterygoid processes in some "gavialoids" and in most "tomistomines", these taxa must be scored for different character states. In the revised format, the direction of the pterygoid processes is disregarded, and character 136 distinguishes between dorsoventrally tall (C136-0) or short (C136-1) processes. The presence of short posterior processes in "gavialoids" and "tomistomines" is recovered as a shared derived feature, convergently evolved in crocodylines. Small posterior processes are not present in all gavialoids. As recognised in previous studies, 'thoracosaurs', such as *Thoracosaurus*, *Eosuchus*, and *Eothoracosaurus*, possess dorsoventrally expanded posterior pterygoid processes.

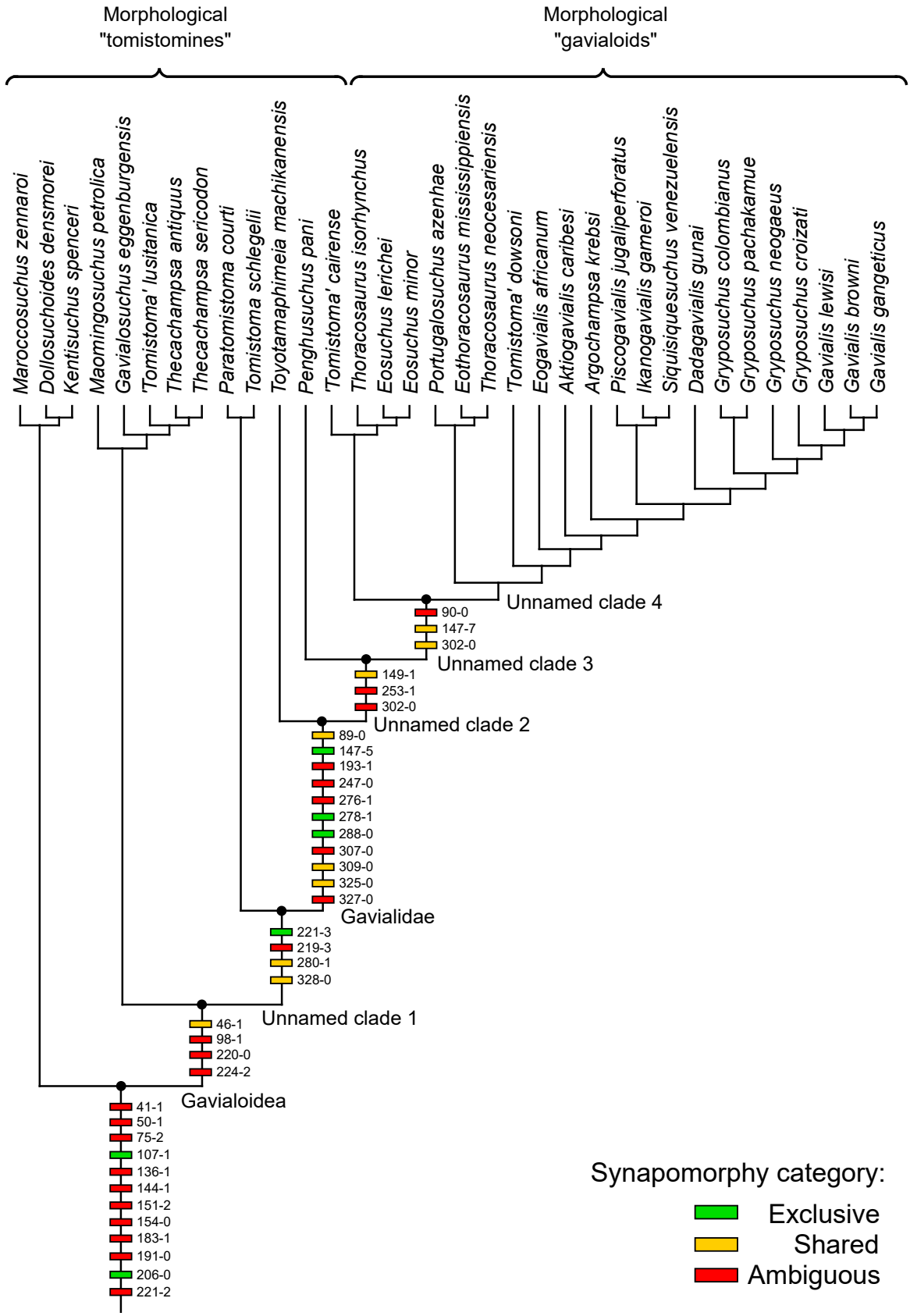



Figure 4.15: Synapomorphies of Gavialoidea and less inclusive clades that unite morpholoigcal “tomistomines” and “gavialoids”.

**Unnamed clade 1–*Maomingosuchus petrolica* + *Gavialosuchus eggenburgensis* + '*Tomistoma*' *lusitanica* + *Thecachampsa sericodon* + *Thecachampsa antiquus* + Gavialidae** This clade is diagnosed by six synapomorphies: (1) ratio of rostrum length to skull length = 0.67–0.68 (C1); (2) ratio of rostral depth to rostral width = 0.46–0.58 (C5); (3) absence of external contact between the nasals and naris (C46-1, shared); (4) dorsal margin of the infratemporal fenestra oval shaped (C98-1, ambiguous); (5) dorsal profile of the dentary linear (C220-0, ambiguous); (6) splenial symphysis adjacent to 4–7 alveoli (C224-2, ambiguous).

This clade is supported by a splenial symphysis whose anterior extent is adjacent to 4–7 teeth (**C224-2**). This synapomorphy is not shared by any other crocodylian taxon, but occurs independently in *Theriosuchus pusillus* and some paralligatorids (*Wannchampsus kirpachi* and the 'Glen Rose Form'). As with the dentary symphysis, the splenial symphysis in Gavialoidea lengthens even further in crownward nodes to more than seven alveoli (C224-3). The reductive coding of this character has clearly factored into the recovery of an expanded Gavialoidea. As delimited in most studies, this character describes separate conditions for "tomistomines" and "gavialoids" (see Chapter 3). Although both share a long splenial symphysis, in "tomistomines" it is described as 'constricted', but in "gavialoids" it is described as 'wide'. These character states are optimised as unambiguous synapomorphies of "Tomistominae" and "Gavialoidea", respectively, in all previous morphological phylogenies. By reductively coding this character, the difference in morphology of the splenial symphysis is still recognised (C225), but the elongated symphyses of "tomistomines" and "gavialoids" are recovered as homologous.

All members of this unnamed clade share a linear dorsal profile of the dentary, where preserved (**C220-0**), except for *Eosuchus minor* and *Penghusuchus pani*. Within Crocodylia , this condition otherwise only occurs in *Mourasuchus*. Previous studies recognised the presence of a linear dorsal profile of the dentary in several "tomistomines" and all "gavialoids", but this was recovered as convergence. Minor character score changes are made here, but this feature is now optimised as a shared derived feature in these taxa.

A broadly rounded dorsal margin of the infratemporal fenestra (**98-1**) supports this clade, but this morphology is absent in some gavialoids (*Eosuchus lerichei*), and independently evolved in some crocodyloids (*Crocodylus johnstoni*, *Brochuchus pigotti*, and *Asiatosuchus depressifrons*). This feature has been recognised in both "tomistomines" and "gavialoids" in previous studies (Salas-Gismondi et al., 2019), and minor character score changes have been made here.

Finally, this unnamed clade is supported by the absence of an external contact between the nasals and naris (**46-1**). The absence of a nasal-narial contact convergently evolved in *Borealosuchus*, several 'basal' alligatoroids (most *Diplocynodon* species and *Leidyosuchus*), and rarely in Crocodyloidea (*Mecistops cataphractus*, *Crocodylus johnstoni*, and *Mekosuchus inexpectatus*). Previous studies discretised the presence or absence of a nasal-narial contact using an unordered multistate character that also

described the degree of contact with the premaxilla. Although, as in this study, most "tomistomines" and "gavialoids" were scored as lacking nasal-narial contact, this was previously optimised as convergence.

**Gavialidae** Gavialidae is diagnosed by seven synapomorphies: (1) infratemporal fenestra size relative to cranial table length = 0.49–0.55 (C7); (2) number of maxillary alveoli = 16 (C17); (3) scapula blade flare = 40 (C21); (4) dentary symphysis adjacent to 13–20 teeth (C221-3, exclusive); (5) no differentiation in dentary alveolus size posterior to $4^{th}$ tooth (C219-3, ambiguous); (6) neural spine of first postaxial vertebra less than half centrum length (C280-1, shared); and (7) ventral osteoderms absent or poorly developed (C328-0, shared).

A dentary symphysis adjacent to 13–20 alveoli (**221-3**) is an exclusive synapomorphy of Gavialidae, lengthening further in crownward nodes. As discussed under the synapomorphies for Gavialoidea above, few studies have increased the number of character states to delimit dentary symphysis length (Salas-Gismondi et al., 2015; Salas-Gismondi et al., 2016; Salas-Gismondi et al., 2019). Fewer still have ordered this character (Iijima & Kobayashi, 2019). Character scores in previous studies reveal that only "gavialoids" possess symphyses elongated beyond the $12^{th}$ dentary alveolus (Salas-Gismondi et al., 2019). In the present study, the elongated condition is also recognised as occurring in *Tomistoma schegelii* and *Penghusuchus pani*.

The absence of differentiation in size of dentary alveoli posterior to the $4^{th}$ dentary tooth (**219-3**) also characterises Gavialidae, but this occurs convergently in *Mourasuchus* and the non-crocodylian *Isisfordia duncani*. This feature tends to be correlated with lengthening of the rostrum, as seen in all gavialids, *Mourasuchus*, and to a degree in *Isisfordia*; however, it is not present in all longirostrines. For example, several of the earliest diverging gavialoids recovered here, such as *Maroccosuchus*, *Dollosuchoides*, *Thecachampsa*, and '*Tomistoma*' *lusitanica*, exhibit a modest enlargement around the $10^{th}$, $11^{th}$, or $12^{th}$ alveolus. Whereas the delimitation of this character is essentially identical to previous studies that employ it (Brochu et al., 2012; Jouve, 2016; Narváez et al., 2016), the character scores of a number of taxa have been modified. Notably, a number of longirostrine taxa were scored as missing data in previous studies (Brochu et al., 2012; Narváez et al., 2016), including taxa for which the anatomy is definitely preserved, such as the extant *Tomistoma schlegelii*, as well as numerous fossil taxa (e.g. *Eosuchus lerichei*, *Eosuchus minor*, *Eothoracosaurus mississippiensis*, *Piscogavialis jugaliperforatus*, and *Thecachampsa antiqua*). Although the large amount of missing data in previous analyses does not support the exclusion of "tomistomines" from Gavialoidea, it results in the optimisation of all "tomistomines" sharing the condition of all other crocodyloids (219-2), whereas several putative "tomistomines" actually have undifferentiated posterior dentary alveoli, similar to *Gavialis*.

The absence or extremely poor development of ventral osteoderms (**C328-0**) is recovered as a shared synapomorphy of Gavialidae. Ventral osteoderms are otherwise only absent in Crocodylinae (all species

except *Crocodylus johnstoni*). The preservation of ventral osteoderms is rare, and within Gavialidae the condition is only known in the extant members *Tomistoma schlegelii* and *Gavialis gangeticus*. The delimitation of this character is the same as expressed in previous studies, and character scores are almost identical; however, whereas the absence of ventral osteoderms was previously recovered as an ambiguous synapomorphy of "Crocodyloidea", and convergent in "Gavialoidea", it is here optimised as a shared derived feature of Gavialidae.

An anteroposteriorly short first postaxial neural spine (**C280-1**) is recovered as a synapomorphy of Gavialidae. This synapomorphy is ambiguous as a result of the large amount of missing data within Gavialidae: only four gavialids can be scored for this feature, whereas the remaining taxa are optimised as having the condition. The distribution of character scores is the same as previous studies. In previous analyses, the lengthened neural spine in traditional "gavialoids" and "tomistomines" was most parsimoniously optimised as two independent acquisitions of the character state. Here the condition is optimised as a truly homologous feature of Gavialidae.

**Unnamed clade 2–Least inclusive clade containing *Toyotamaphimeia machikanensis* and *Gavialis gangeticus*** This unnamed clade is diagnosed by fifteen synapomorphies: (1) rostrum length to skull length = 0.68–0.70 (C1); (2) cranial table length to width ratio = 0.64–0.66 (C8); (3) inclination of dorsal margin of external mandibular fenestra = 23° (C19); (4) ratio of ulna to humeral length = 0.61 (C24); (5) postorbital bar anteroposteriorly expanded, elliptical cross section (C89-0, shared); (6) largest maxillary alveolus is number 7 (C147-5, exclusive); (7) absence of a choanal septum (C193-1, ambiguous); (8) surangular-articular suture straight in glenoid fossa (C247-0, ambiguous); (9) presence of diapophysis on axial neural arch (C276-1, ambiguous); (10) axial hypapophysis forked (C278-1, exclusive); (11) width across prezygapophyses constant throughout presacral vertebrae (C288-0, exclusive); (12) presence of preacetabular process of the ilium (C307-0, ambiguous); (13) dorsal outline of iliac blade lacks indentation (309-0, shared); (14) dorsal midline osteoderms unkeeled (C325-0, shared); (15) dorsal midline osteoderms with anterolateral process (C327-0, ambiguous).

In previous studies, a forked axial hypapophysis (**C278-1)** was recovered as an ambiguous synapomorphy of "Gavialoidea" (Narváez et al., 2016) that was not present in any "tomistomines" or any other crocodylian. Recently, the forked condition has been identified in *Penghusuchus pani* and *Toyotamaphimeia machikanensis* (Iijima & Kobayashi, 2019), supporting a closer relationship between "tomistomines" and "gavialoids" than previously recognised.

An anteroposteriorly expanded postorbital bar (**C89-0**) is a shared synapomorphy of this unnamed clade, present in several non-crocodylians, including *Bernissartia* and *Hylaeochampsa*. Previously, the shared presence of an expanded postorbital bar was optimised as being a reacquired 'primitive' feature in both "Gavialoidea" and "Tomistominae". Here the shared condition unites some "tomistomines" with

"gavialoids". The presence of an expanded postorbital bar in '*Tomistoma*' *lusitanica* and *Thecachampsa* is recovered as an independent reacquisition of the condition.

The largest maxillary alveolus is the seventh in *Toyotamaphimeia* and *Penghusuchus* (**C147-5**). This is recovered as a synapomorphy of this unnamed clade; however, all other crownward members of this clade have homodont dentition (see unnamed clade 4 below).

This clade is also supported by the absence of a choanal septum (**C193-1**). This character is new, derived by contingently coding character 152 in (Brochu, 1997b), but comparisons between character scores are still possible. There have been minor changes to character scores but, as recovered in previous studies, most "tomistomines" have a choanal septum and most "gavialoids" do not. Previously, this supported the exclusion of "Gavialoidea" from the clade (*Borealosuchus* + (Planocraniidae + "Brevirostres")), members of which have choanal septa. Some "tomistomines" are recognised as lacking a choanal septum, e.g. *Maroccosuchus*, *Toyotamaphimeia*, and *Penghusuchus*. Whereas the absence of a choanal septum is recovered as an autapomorphy of *Maroccosuchus*, its absence in *Toyotamaphimeia* and *Penghusuchus* supports a closer relationship of these taxa with traditional "gavialoids" than to "tomistomines".

The presence of a bowed surangular-articular suture in the mandibular glenoid fossa (**C247-1**) is typically recovered as a synapomorphy of "Crocodyloidea", supporting the traditional distinction between "tomistomines" and "gavialoids". Here it is recovered as a synapomorphy of Longirostres, but reverses to the plesiomorphic, straight condition (C247-0) at the node comprising *Toyotamaphimeia* and all taxa more closely related to *Gavialis gangeticus*. Changes to character scores here have increased the uncertainty of the condition in several "tomistomines", and one "gavialoid" exhibits the bowed condition (*Argochampsa krebsi*, NHMUK R 36872).

This clade is also supported by a constant width across the prezygapophyses in presacral vertebrae (**C288-0**), a condition not shared by any other taxa in this study. Nevertheless, this synapomorphy is ambiguous due to the high proportion of missing data. As such, the plesiomorphic condition is only scored in *Gavialis gangeticus* and *Toyotamaphimeia machikanensis* (Iijima & Kobayashi, 2019) amongst gavialoids. Characters 276, 307, 309, 325, and 327 are discussed above under atavistic characters.

**Unnamed clade 3–The least inclusive clade containing *Penghusuchus pani* and *Gavialis gangeticus***

This unnamed clade is diagnosed by five synapomorphies: (1) ratio of supratemporal fenestra length to cranial table length = 0.54 (C10); (2) ratio of basioccipital tubera width to occipital condyle width = 1.52-1.60 (C15); (3) maxillary toothrow linear between alveoli 1–4 (C149-1, shared); (4) lingual foramen perforates surangular-articular suture (C253-1, ambiguous); and (5) deltopectoral crest emerges smoothly from proximal end of humerus (C302-0, ambiguous).

In *Penghusuchus pani* and all taxa more closely related to *Gavialis gangeticus*, the maxillary toothrow between alveoli 1–4 is anteroposteriorly orientated (**149-1**). This contrasts with the laterally flaring con-

dition of essentially all other eusuchians. This derived feature independently evolved in the clade comprising *Gavialosuchus eggenburgensis*, *Tomistoma lusitanica* and *Thecachampsa*. Otherwise, all other gavialoids share the plesiomorphic condition. This character is new, therefore score comparisons with previous studies are not possible.

This unnamed clade is further supported by the position of the lingual foramen, perforating the surangular-articular suture (**C253-1**). Previously, this character was recovered as a shared synapomorphy within "Crocodyloidea", present in Crocodylinae, Osteolaeminae, Mekosuchinae, and some "tomistomines" (not in *Tomistoma schlegelii*, *Toyotamaphimeia*, and *Paratomistoma*). There have been some significant changes to character scores in "tomistomine" taxa. *Maroccosuchus* and *Kentisuchus* are found to exhibit a perforation on the surangular entirely, and the condition in *Thecachampsa antiqua* is considered unknown. As a result, this character has a complicated optimisation pattern. The plesiomorphic condition in Gavialoidea is for the lingual foramen to perforate the surangular only (C253-0). The character state changes at the node comprising Penghusuchus and all taxa more closely related to *Gavialis gangeticus* (C253-1), and then reverses to the plesiomorphic condition in crownward nodes. Character 302 is discussed above under atavistic characters.

**Unnamed clade 4–The least inclusive clade containing *Tomistoma cairense* and *Gavialis gangeticus***
This unnamed clade is diagnosed by five synapomorphies: (1) ratio of rostrum width to cranial table width = 1.1–1.2 (C2); (2) number of maxillary alveoli = 17–20 (C17); (3) protuberance on the dorsolateral margin of the postorbital bar (C90-0, ambiguous); (4) maxillary alveoli homodont (C147-7, shared); (5) two scars discernible on proximodorsal surface of humerus for *M. teres major* and *M. dorsalis scapulae* (C304-0, shared).

This clade is unambiguously supported by the presence of homodont maxillary dentition (**147-7**), with the condition unknown only in *Thoracosaurus neocesariensis* and *Portugalosuchus azenhae*. Previous studies have recovered homodont dentition as a synapomorphy of "Gavialoidea", with homodonty convergently evolving in isolated cases in Crocodylia, e.g. in *Mourasuchus*, *Euthecodon*, and one "tomistomine", *Tomistoma cairense*. Previous studies have recovered *Tomistoma cairense* nested within "Tomistominae", but here this taxon is more closely related to traditional "gavialoids" than any other putative "tomistomine". Characters 90 and 304 are discussed above under atavistic characters.

**Summary of character support** Table 4.12 summarises the synapomorphies of Gavialoidea and less inclusive clades that support the grouping of "tomsitomines" and "gavialoids". Character support uniting "tomistomines" and "gavialoids" has been identified in previous morphological character datasets (Trueman, 1998; Gatesy et al., 2003; Harshman et al., 2003). Whereas these similarities were most parsimoniously optimised as being convergently acquired, here they diagnose Gavialoidea, or less inclu-

sive clades. Four of these characters are exclusively found in “tomistomines” and “gavialoids”: C107-1 and C206-0, which are synapomorphies of Gavialoidea, and C278-1 and C288-0, which are synapomorphies of the least inclusive clade comprising *Toyotamaphimeia* and *Gavialis gangeticus*. The remainder are variably present in other crocodylian lineages and therefore provide more ambiguous support for Gavialoidea.

Four characters supporting Gavialoidea or less inclusive clades are new (C149-1, C191-0), recently introduced (C288-9 Iijima & Kobayashi, 2019), or have not previously been applied to crocodylian datasets (C154-0). These characters provide new support that unites some or all “gavialoids” and “tomistomines”. Five morphological characters used in previous studies of crocodylian phylogeny did not support a close relationship between “Tomistominae” and “Gavialoidea”; however, modifications to character scores, as well as character construction and/or taxon sampling, generates new support uniting “tomistomines” and “gavialoids” (C98-1, C136-1, C193-1, C219-3, C224-2). The remaining 18 character states that are newly recovered as synapomorphies of Gavialoidea, or less inclusive clades, were recognised in morphological “tomistomines” and “gavialoids” in previous datasets, but were optimised as being convergently acquired in these clades. The large amount of missing data in character scores for gavialoid taxa should also be considered. Some of the synapomorphies of Gavialoidea or less inclusive clades identified here are based on poorly preserved elements of the skeleton (e.g. C278 and C328), or which require the comparison of serial variation of interconnected elements that are typically displaced in burial and fossilisation (C288). In such cases, the condition is often only known in two members of a clade, and optimised as present in all others, although the implementation of extended implied weighting partially remedies this problem by down-weighting characters with a high proportion of missing data.

Table 4.12: Synapomorphies of clades uniting morphological “gavialoids” and “tomistomines”.

| Character | Node | Synapomorphy type | Previously in "tomistomines" + "gavialoids" | Character modifications | Score changes |
|---|---|---|---|---|---|
| 41-1 | Gavialoidea | Ambiguous | Yes | None | Minor |
| 50-1 | Gavialoidea | Ambiguous | Yes | None | Minor |
| 75-2 | Gavialoidea | Ambiguous | No | Ordered | Minor |
| 107-1 | Gavialoidea | Exclusive | Yes | None | Major |
| 136-1 | Gavialoidea | Ambiguous | No | State removed | Major |
| 144-1 | Gavialoidea | Ambiguous | Yes | None | Minor |
| 151-2 | Gavialoidea | Ambiguous | Yes | Ordered | Minor |
| 154-0 | Gavialoidea | Ambiguous | New character | NA | NA |
| 183-1 | Gavialoidea | Ambiguous | No | None | Minor |

| Character | Node | Synapomorphy type | Previously in "tomistomines" + "gavialoids" | Character modifications | Score changes |
|---|---|---|---|---|---|
| 191-0 | Gavialoidea | Ambiguous | New character | NA | NA |
| 206-0 | Gavialoidea | Exclusive | Yes | None | Minor |
| 221-2 | Gavialoidea | Ambiguous | Yes | State added, ordered | NA |
| 46-1 | Unnamed clade 1 | Shared | Yes | Reductively coded | NA |
| 98-1 | Unnamed clade 1 | Ambiguous | No | None | Major |
| 220-0 | Unnamed clade 1 | Ambiguous | Yes | None | Minor |
| 224-2 | Unnamed clade 1 | Ambiguous | No | Reductively coded | NA |
| 219-3 | Gavialidae | Ambiguous | No | None | Major |
| 221-3 | Gavialidae | Exclusive | Yes | State added, ordered | NA |
| 280-1 | Gavialidae | Shared | Yes | None | Minor |
| 328-0 | Gavialidae | Shared | Yes | None | Minor |
| 89-0 | Unnamed clade 2 | Shared | Yes | None | Major |
| 193-1 | Unnamed clade 2 | Ambiguous | No | Reductively coded | Minor |
| 247-0 | Unnamed clade 2 | Ambiguous | Yes | None | Minor |
| 278-1 | Unnamed clade 2 | Exclusive | Yes | None | Minor |
| 288-0 | Unnamed clade 2 | Exclusive | Yes | None | Minor |
| 149-1 | Unnamed clade3 | Shared | New character | NA | NA |
| 253-1 | Unnamed clade3 | Shared | Yes | None | Major |
| 147-7 | Unnamed clade4 | Shared | Yes | None | NA |

**Summary of the recovery of Gavialidae?**

There has always been morphological character support uniting “Tomistominae” and “Gavialoidea”; however, the similarities between these taxa appear to have been overwhelmed by the similarities between “Gavialoidea” and many non-crocodylian neosuchians. Modifications to characters that formerly supported the exclusion of “Gavialoidea” from “Brevirostres” have reduced the stemward ‘pull’ on “Gavialoidea”. Additionally, more widespread similarities have been recognised between “tomistomines”

and "gavialoids" through new observations (e.g. Iijima & Kobayashi, 2019), as well as via subtle changes to character delimitation (e.g. C136 and C224) and treatment (e.g. ordering C224).

### Are 'thoracosaurs' gavialoids?

This study is topologically concordant with molecular datasets in recovering *Gavialis gangeticus* as more closely related to *Tomistoma schlegelii* than to any other extant crocodylian. However, the recovery of several latest Cretaceous and early Paleogene species in Gavialidae is temporally incongruent with molecular estimates for divergence times between *Tomistoma schlegelii* and *Gavialis gangeticus*, which place the timing of this split at ∼30–16 Ma (Oaks, 2011; Pan et al., 2020). Most of the taxa resulting in this incongruence are informally known as 'thoracosaurs' (e.g. Brochu, 2004a). Previously, 'thoracosaurs' have been regarded as a paraphyletic group that includes the most stemward morphological "gavialoids" that are typically from the latest Cretaceous and early Paleogene (Brochu, 2004a, 2006b) (Fig. 4.16). The consideration of stratigraphic data in combined Bayesian analyses of morphology and molecules provided the first empirical evidence that 'thoracosaurs' do not belong in Gavialoidea, nor indeed in Crocodylia (Lee & Yates, 2018). Based on the results of Lee and Yates (2018), 'thoracosaurs' comprise a monophyletic group, consisting of *Eothoracosaurus*, *Thoracosaurus* (*T. isorhynchus* + *T. neocesariensis*), *Argochampsa krebsi*, *Eogavialis africanum*, and *Eosuchus* (*E. minor* + *E. lerichei*). In particular, the recovery of *Eogavialis africanum* and *Argochampsa krebsi* as 'thoracosaurs' and outside of Crocodylia is surprising. Although these taxa are often recovered as 'intermediate' forms between 'thoracosaurs' and crownward gavialoids, several analyses have recovered them as more closely related to *Gryposuchus* and *Gavialis* than to 'thoracosaurs' (Brochu, 2004a; Hua & Jouve, 2004; Jouve et al., 2015; Iijima & Kobayashi, 2019). Nevertheless, the dataset of Lee and Yates (2018) incorporated stratigraphic data in their phylogenetic reconstruction, and the older ages of *Argochampsa* (early Paleocene) and *Eogavialis* (Eocene) must factor into this reconstruction.

In the present study, 'thoracosaurs' form a polyphyletic assemblage nested in Gavialidae. Furthermore, a putative early crocodylian taxon, *Portugalosuchus azenhae* (Mateus et al., 2019) from the Cenomanian (early Late Cretaceous) of Portugal, is recovered as being closely related to *Eothoracosaurus* and *Thoracosaurus neocesariensis*. As such, below I evaluate the contrasting placements of 'thoracosaurs'.

**Character support for the inclusion of 'thoracosaurs' in Gavialoidea** There are 40 synapomorphies of Gavialoidea or less inclusive clades that potentially unite 'thoracosaurs' with other gavialoids (Table 4.13). Only six of these synapomorphies are known exclusively in Gavialoidea or less inclusive clades: (1) anteriorly flaring lateral squamosal grooves (C107-1); (2) maxillary alveoli dorsal to maxillary palate (C158-1); (3) laterally directed capitate process of the laterosphenoid (C206-0); (4) dentary symphysis adjacent to 13–20 teeth (C221-3); (5) forked axial hypapophysis (C278-1); and (6) width across prezy-

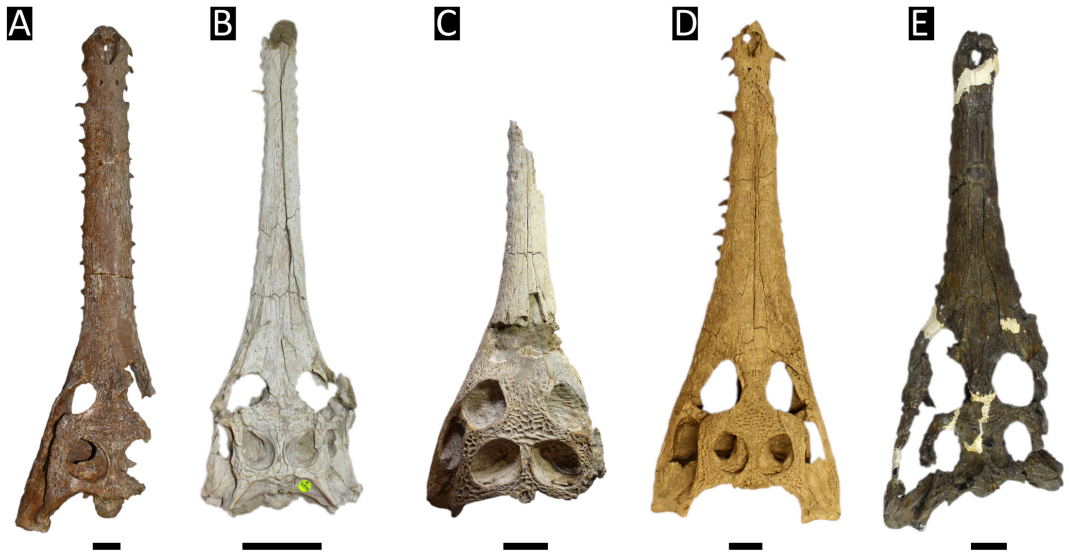



Figure 4.16: Examples of 'thoracosaurs'. **A**, *Eogavialis africanum* (YPM 6263); **B**, *Argochampsa krebsi* (NHMUK R 36872); **C**, *Thoracosaurus isorhynchus* (MNHN.F.MTA 61); **D**, *Eosuchus lerichei* (IRScNB R 49); **E**, *Eosuchus minor* (USNM 299730). All scale bars = 5 cm.

gapophyses constant through presacral vertebrae (C288-0).

| Character | Node/Clade | Longirostrine character? | Synapomorphy type | *Thoracosaurus isorhynchus* | *Thoracosaurus neocesariensis* | *Eothoracosaurus mississippiensis* | *Eosuchus minor* | *Eosuchus lerichei* | *Portugalosuchus azenhae* | *Eogavialis africanum* | *Argochampsa krebsi* |
|---|---|---|---|---|---|---|---|---|---|---|---|
| 107-1 | Gavialoidea | No | Exclusive | 1 | 1 | 1 | 1 | 0 | 0 | 1 | ? |
| 136-1 | Gavialoidea | No | Ambiguous | 0 | ? | 0 | 0 | 0 | 0 | 1 | 1 |
| 144-1 | Gavialoidea | Yes | Ambiguous | 1 | ? | 0 | 0 | 0 | ? | 1 | 1 |
| 151-2 | Gavialoidea | Yes | Ambiguous | 2 | ? | 2 | 2 | 2 | ? | 2 | 2 |
| 154-0 | Gavialoidea | No | Ambiguous | 0 | ? | 0 | 0 | 0 | ? | 0 | 0 |
| 183-1 | Gavialoidea | No | Ambiguous | ? | ? | ? | 0 | 0 | ? | 0 | ? |
| 191-0 | Gavialoidea | No | Ambiguous | 0 | ? | ? | 0 | 0 | ? | 0 | 0 |
| 206-0 | Gavialoidea | No | Exclusive | ? | 0 | 0 | 1 | 0 | ? | 0 | 0 |
| 41-1 | Gavialoidea | No | Ambiguous | 1 | 1 | 1 | 1 | 1 | ? | 1 | 1 |
| 50-1 | Gavialoidea | Yes | Ambiguous | 1 | 1 | 1 | 1 | 1 | ? | 1 | 1 |
| 75-2 | Gavialoidea | No | Ambiguous | 0 | 0 | 0 | 1 | 0 | 0 | 2 | 1 |

| Character | Node/Clade | Longirostrine character? | Synapomorphy type | *Thoracosaurus isorhynchus* | *Thoracosaurus neocesariensis* | *Eothoracosaurus mississippiensis* | *Eosuchus minor* | *Eosuchus lerichei* | *Portugalosuchus azenhae* | *Eogavialis africanum* | *Argochampsa krebsi* |
|---|---|---|---|---|---|---|---|---|---|---|---|
| 46-1 | *Maomingosuchus* + *Gavialis* | Yes | Shared | 1 | ? | 1 | 1 | 1 | ? | 1 | 1 |
| 98-1 | *Maomingosuchus* + *Gavialis* | No | Ambiguous | 1 | ? | ? | ? | 0 | 1 | 1 | ? |
| 220-0 | *Maomingosuchus* + *Gavialis* | Yes | Ambiguous | ? | ? | 0 | 1 | 0 | ? | 0 | 0 |
| 224-2 | *Maomingosuchus* + *Gavialis* | Yes | Ambiguous | ? | ? | 2 | 2 | 2 | ? | 3 | ? |
| 219-3 | Gavialidae | Yes | Ambiguous | ? | ? | 3 | 3 | 3 | ? | 3 | ? |
| 221-3 | Gavialidae | Yes | Exclusive | ? | ? | 3 | 2 | ? | ? | 3 | ? |
| 280-1 | Gavialidae | No | Shared | ? | ? | ? | ? | ? | ? | ? | ? |
| 328-0 | Gavialidae | No | Shared | ? | ? | ? | ? | ? | ? | ? | ? |
| 278-1 | *Toyotamaphimeia* + *Gavialis* | No | Exclusive | 1 | 1 | ? | 1 | 0 | ? | 1 | ? |
| 193-1 | *Toyotamaphimeia* + *Gavialis* | No | Ambiguous | 1 | 1 | 1 | ? | 0 | 1 | 0 | 1 |
| 247-0 | *Toyotamaphimeia* + *Gavialis* | No | Ambiguous | ? | ? | 0 | 0 | ? | ? | 0 | 1 |
| 276-1 | *Toyotamaphimeia* + *Gavialis* | No | Ambiguous | 1 | 1 | ? | 1 | 1 | ? | ? | 0 |
| 288-0 | *Toyotamaphimeia* + *Gavialis* | No | Exclusive | ? | ? | ? | ? | ? | ? | ? | ? |
| 307-0 | *Toyotamaphimeia* + *Gavialis* | No | Ambiguous | ? | ? | ? | 0 | ? | ? | 1 | ? |
| 309-0 | *Toyotamaphimeia* + *Gavialis* | No | Ambiguous | ? | ? | ? | ? | ? | ? | ? | ? |
| 325-0 | *Toyotamaphimeia* + *Gavialis* | No | Shared | 0 | ? | ? | 0 | 0 | ? | 0 | 0 |
| 327-0 | *Toyotamaphimeia* + *Gavialis* | No | Ambiguous | ? | ? | 0 | 0 | 1 | ? | 0 | 1 |
| 89-0 | *Toyotamaphimeia* + *Gavialis* | No | Shared | 0 | ? | 0 | 0 | 0 | 0 | 0 | 0 |
| 149-1 | Penghusuchus + *Gavialis* | Yes | Shared | 1 | 1 | 1 | 1 | 1 | ? | 1 | 1 |
| 253-1 | Penghusuchus + *Gavialis* | No | Ambiguous | ? | ? | 1 | 1 | ? | ? | ? | ? |
| 302-0 | Penghusuchus + *Gavialis* | No | Shared | 0 | 0 | ? | 1 | ? | ? | ? | 0 |
| 90-0 | '*T*'. *cairense* + *Gavialis* | No | Shared | 0 | ? | ? | 0 | 0 | 0 | 0 | 1 |
| 147-7 | '*T*'. *cairense* + *Gavialis* | Yes | Shared | 7 | ? | 7 | 7 | 7 | ? | 7 | 7 |
| 304-0 | '*T*'. *cairense* + *Gavialis* | No | Shared | 0 | 0 | ? | ? | ? | ? | ? | ? |
| 63-1 | *Portugalosuchus* + *Gavialis* | No | Shared | 0 | ? | 1 | 0 | 0 | 1 | ? | 0 |
| 91-1 | *Portugalosuchus* + *Gavialis* | No | Shared | 0 | ? | ? | ? | ? | 1 | 1 | 1 |
| 94-1 | *Portugalosuchus* + *Gavialis* | No | Ambiguous | 1 | ? | 1 | 0 | 0 | 1 | 1 | 1 |

| Character | Node/Clade | Longirostrine character? | Synapomorphy type | *Thoracosaurus isorhynchus* | *Thoracosaurus neocesariensis* | *Eothoracosaurus mississippiensis* | *Eosuchus minor* | *Eosuchus lerichei* | *Portugalosuchus azenhae* | *Eogavialis africanum* | *Argochampsa krebsi* |
|---|---|---|---|---|---|---|---|---|---|---|---|
| 115-0 | *Portugalosuchus* + *Gavialis* | No | Shared | ? | ? | 0 | ? | 1 | ? | 0 | 0 |
| 158-1 | *Portugalosuchus* + *Gavialis* | Yes | Exclusive | 0 | ? | 1 | 1 | 0 | ? | 1 | 1 |

Table 4.13: List of all synapomorphies for Gavialoidea and less inclusive clades that group 'thoracosaurs' and *Portugalosuchus* with other gavialoids. Red cells highlight character states that contrast with most or all other members of the respective node. Grey cells highlight missing data. Nodes described as *taxon x* + *taxon y*, indicate the least inclusive clade defined by those taxa. Underlined rows highlight exclusive synapomorphies.

Two of these characters are certainly associated with longirostry (C158-1 C221-3), and thus their presence in 'thoracosaurs' and other gavialoids could be explained by convergence in snout length. A further two characters (C107-1, C206-0) are more ambiguously associated with longirostry. It has been suggested that a flaring squamosal groove (C107-1) is also associated with longirostry (Brochu, 2004a; Groh et al., 2020); however, this feature is known only in "Tomistominae" and "Gavialoidea", and not in any other neosuchian longirostrine (e.g. Tethysuchia) (Groh et al., 2020). Similarly, it has been suggested that a laterally directed capitate process of the laterosphenoid (C206-0) might be correlated with longirostry (Brochu, 2004a); however, this again has not been identified in other longirostrine neosuchians (Groh et al., 2020). As such, there are four exclusive synapomorphies of Gavialoidea that are not associated with snout length (C107-1, C206-0, C278-1, C288-0), although one of these characters (C288) cannot be assessed in any of the putative 'thoracosaurs'.

An anteriorly flaring squamosal groove (C107-1) is a synapomorphy of Gavialoidea. Among the putative 'thoracosaurs' recovered by Lee and Yates (2018), this condition is present in *Thoracosaurus isorhynchus*, *Thoracosaurus neocesariensis*, *Eothoracosaurus*, *Eogavialis*, and *Eosuchus minor*. The condition is absent in *Eosuchus lerichei* and *Portugalosuchus*, and the condition is unknown in *Argochampsa krebsi*. Some other gavialoids also lack the flaring condition (e.g. *Maomingosuchus petrolica*, *Tomistoma cairense*, and *Tomistoma schlegelii*).

A laterally directed capitate process of the laterosphenoid (C206-0) is another exclusive synapomorphy of Gavialoidea. This condition is exhibited in *Thoracosaurus neocesariensis*, *Eothoracosaurus*, *Eosuchus lerichei*, *Eogavialis africanum* and *Argochampsa krebsi*, but absent in *Eosuchus* minor. The

condition is unknown in *Thoracosaurus isorhynchus* and *Portugalosuchus*. Where preserved, the condition is present in all other gavialoids, with the exception of *Tomistoma schlegelii* and *Maomingosuchus petrolica*.

A forked axial hypophysis (278-1) is a synapomorphy of the least inclusive clade containing *Toyotamaphimeia machikanensis* and *Gavialis gangeticus*. This condition occurs in all members of this gavialid clade, where preserved, including *Thoracosaurus isorhynchus*, *Thoracosaurus neocesariensis*, *Eosuchus minor* and *Eogavialis africanum*, but not *Eosuchus lerichei*, which has an unforked axial hypapophysis. The condition in *Argochampsa krebsi*, *Eothoracosaurus*, and *Portugalosuchus* is unknown.

An elongated dentary symphysis adjacent to 13–20 teeth (221-3) is a synapomorphy of Gavialidae. Among 'thoracosaurs', it is present in *Eogavialis* and *Eothoracosaurus*. *Eosuchus minor* has a slightly shorter dentary symphysis (221-2), and the condition is unknown in all other 'thoracosaurs'. The maxillary alveoli are dorsal to the maxillary palate (158-1) in four 'thoracosaurs': *Eothoracosaurus*, *Eosuchus minor*, *Eogavialis*, and *Argochampsa*. Whereas the condition is unknown in *Thoracosaurus neocesariensis* and *Portugalosuchus*, both *Eosuchus lerichei* and *Thoracosaurus isorhynchus* exhibit the plesiomorphic condition in which the maxillary alveoli are ventral to the palate.

There are a further 32 morphological features which ambiguously support the position of 'thoracosaurs' in Gavialoidea (Table 4.13). These features are present in some but not all 'thoracosaurs', and also occur outside of Gavialoidea (in both other crocodylians and taxa outside of Crocodylia) and thus might be considered less diagnostic.

**Character support for the exclusion of 'thoracosaurs' from Gavialoidea** Despite the character support suggesting that 'thoracosaurs' are gavialoids, there are several morphological features in some 'thoracosaurs' that are typically absent in other gavialoids (Table 4.14). The margins of the orbit are flush against the skull surface (C72-0) in *Eothoracosaurus*, *Eosuchus minor*, *Eosuchus lerichei*, and *Portugalosuchus*. In all other gavialoids they are either upturned (C72-1), or telescoped (C72-2). In *Eothoracosaurus*, *Thoracosaurus neocesariensis*, *Thoracosaurus isorhynchus*, *Eosuchus lerichei*, and *Portugalosuchus* the frontoparietal suture intersects deeply in the supratemporal fenestra, such that the postorbital-parietal suture is not exposed on the skull table (C75-0). This condition is discretised as the end member of an ordered character. In most traditional "tomistomines", the frontoparietal suture is entirely on the skull table (C75-2), whereas all other gavialoids have an intermediate condition where the frontoparietal suture incipiently contacts the supratemporal fenestra (C75-1).

The posteroventral processes of the pterygoids are dorsoventrally expanded (C136-0) in *Eothoracosaurus*, *Thoracosaurus isorhynchus*, *Eosuchus minor*, *Eosuchus lerichei*, and *Portugalosuchus*. This is unlike all other gavialoids, which have dorsoventrally short pterygoid processes.

A medially inset ultimate premaxillary alveolus is recovered as a synapomorphy of Gavialoidea. This

| Character | Character state description | *T. macrorhynchus* | *T. neocesariensis* | *Eoth.mississippiensis* | *Eos. minor* | *Eos. lerichei* | *P. azenhae* | *Eog. africanum* | *A. krebsi* |
|---|---|---|---|---|---|---|---|---|---|
| 72-0 | Dorsomedial margin of the orbit flush with skull surface | 1 | ? | 0 | 0 | 0 | 0 | 1 | 1 |
| 75-0 | Frontopareital suture deeply intersects supratemporal fenestra | 0 | 0 | 0 | 1 | 0 | 0 | 2 | 1 |
| 88-0 | Postorbital-parietal suture passes medially to the orbitotemporal canal | 0 | 0 | ? | ? | 1 | 0 | 1 | 1 |
| 136-0 | Posteroventral process of the pterygoid dorsoventrally exapnded | 0 | ? | 0 | 0 | 0 | 0 | 1 | 1 |
| 144-0 | Last premaxillary alveolus is posterior or posterolateral to penultimate alveolus | 1 | ? | 0 | 0 | 0 | ? | 1 | 1 |
| 217-0 | Dentary alveoli 3 and 4 confluent | 1 | ? | 0 | 1 | 1 | ? | 1 | ? |
| 235-0 | Slit sized external mandibular fenestra | ? | ? | ? | 1 | ? | 0 | 1 | ? |

Table 4.14: Characters distinguishing 'thoracosaurs' from other gavialoids. Red cells highlight character states that are absent in most other gavialoids.

condition is absent in several 'thoracosaurs', including *Eothoracosaurus*, *Eosuchus minor*, and *Eosuchus lerichei*; however, it is also absent in a few other gavialoids, including *Thecachampsa antiquus* and *Aktiogavialis caribesi*.

Dentary alveoli 3 and 4 are essentially confluent in *Eothoracosaurus* (C217-0) (Brochu, 2004a). This is recovered here as an autapomorphy within Gavialoidea, as all other gavialoids have equally separated dentary alveoli. Otherwise, confluent alveoli are found in *Bernissartia fagesii*, *Borealosuchus*, *Leidyosuchus canadensis*, and *Diplocynodon*. A slit-like external mandibular fenestra, lacking a concavity on the angular dorsal margin, is present in *Portugalosuchus* (C235-0). All other gavialoids have a large external mandibular fenestra, producing a concavity on the angular, usually with the foramen intermandibularis caudalis obscured from view (C235-1). The condition in *Eothoracosaurus* was discussed in detail by (Brochu, 2004a). Here it is scored as missing data; however, it is likely that the external mandibular fenestra was either slit-like, or entirely absent, in *Eothoracosaurus*. Slit-like external mandibular fenestrae are otherwise rare in Crocodylia, known only in *Mekosuchus*; however, outside of Crocodylia, this condition also occurs in some *Borealosuchus* species. Furthermore, the external mandibular fenestra is plesiomorphically absent in Eusuchia, as can be observed in *Bernissartia*, *Theriosuchus*, and, where preserved, all hylaeochampsids and allodaposuchids.

In several 'thoracosaurs', the postorbital-parietal suture passes medial to the orbitotemporal canal, and there is little to no development of a fossa medial to this canal (C88-0) (Chapter 3, Fig. 3.33). This condition is present in *Thoracosaurus isorhynchus*, *Thoracosaurus neocesariensis*, *Eosuchus minor*, and *Portugalosuchus*. Unlike all the previous characters discussed, this condition is otherwise known solely outside of Crocodylia, in *Allodaposuchus precedens*, and *Shamosuchus*.

**Constrained Searches** To test the significance of the phylogenetic position of 'thoracosaurs' and *Portugalosuchus*, four constrained searches were performed on Analysis 1.3 (Appendix F). The analysis of

Mateus et al. (2019) recovered the traditional morphological topology, with *Portugalosuchus* as the sister taxon to all non-gavialoid crocodylians; however, those authors noted that support for this relationship was low, and that *Portugalosuchus* might not belong within Crocodylia. As such, the first constraint excludes *Portugalosuchus* from Crocodylia, and 'thoracosaurs' as recovered by Lee and Yates (2018, fig.2) (i.e. *Argochampsa*, *Eothoracosaurus*, *Thoracosaurus*, *Eogavialis*, and *Eosuchus*) are set as floating taxa such that they could be included within Crocodylia, but were not forced to do so. The second constraint excludes 'thoracosaurs' from Crocodylia, while *Portugalosuchus* floats. Due to the labile position of planocraniids and *Borealosuchus* in other analyses, these were also set as floating taxa in both constraints.

Another hypothesis to be explored is whether 'thoracosaurs' are indeed gavialoids, but outside of the crown group Gavialidae. Such a relationship might reconcile the strong gavialoid affinities of 'thoracosaurs' with the stratigraphically young age of Gavialidae inferred from molecular analyses ($\leq$ 30 Ma) (Oaks, 2011; Pan et al., 2020). In fact, we should expect to find 'basal' gavialoids of approximately the same age as some 'thoracosaurs', since the earliest crocodyloids, such as *Jiangxisuchus nankangensis* (Li et al., 2019) and *Prodiplocynodon langi* (Mook, 1941a), are also known from the latest Cretaceous. This hypothesis was tested using a third positive constraint, which forced *Tomistoma schlegelii* and *Gavialis gangeticus* to form a clade (i.e. Gavialidae). All non-'thoracosaur' gavialoids recovered in the original unconstrained Analysis 1.3 (including *Portugalosuchus*) were set as floating taxa, which could be recovered within Gavialidae, but were not forced to do so.

A fourth constrained analysis was conducted to test the affinities of *Argochampsa* and *Eogavialis* with other morphological "gavialoids". As under Constraint 2, *Thoracosaurus*, *Eosuchus*, and *Eothoracosaurus* were forced outside of Crocodylia, but *Eogavialis* and *Argochampsa* were set as floating taxa, along with *Portugalosuchus Borealosuchus*, and Planocraniidae.

Constraint 1 results in an insignificant tree length increase of 47.6 step (Templeton test $p > 0.05$). *Portugalosuchus* is nested in *Borealosuchus*, in the stem of Crocodylia, whereas 'thoracosaurs' remain nested in the crown group Gavialidae (Appendix F.6). Constraint 2 results in a significant tree length increase of 192.1 steps ($p < 0.01$) (Fig. 4.17). 'Thoracosaurs' are recovered as deeply nested in a clade of non-crocodylian eusuchians, comprising Hylaeochampsidae, Allodaposuchidae, and a paraphyletic *Borealosuchus*. Within the 'thoracosaur' clade, *Eosuchus lerichei, Thoracosaurus isorhynchus*, *Thoracosaurus neocesariensis*, and *Eosuchus minor* are successively nested taxa that lie outside of two sister clades: ((*Eothoracosaurus mississippiensis* + *Portugalosuchus azenhae*) + (*Eogavialis africanum* + *Argochampsa krebsi*)). The principal difference to Gavialidae is the inclusion of the clade comprising (*Gavialosuchus eggenburgensis* + (*Tomistoma lusitanica* + (*Thecachampsa antiquus* + *Thecachampsa sericodon*)) as an early diverging gavialid sister taxon to *Penghusuchus pani*. In the unconstrained analysis, this clade was recovered outside of the crown group. *Moroccosuchus zennaroi* + (*Kentisuchus*

*spenceri* + *Dollosuchoides densmorei*) is recovered as the earliest diverging gavialoid clade, as in the unconstrained analysis. A number of additional minor topological changes also occur (Fig. 4.17).

Under the third constraint, tree length increases by a statistically insignificant 100.6 steps ($p > 0.05$). The topology of Gavialoidea and composition of Gavialidae changes dramatically from both the unconstrained topology, and the topology under Constraint 2 (Fig. 4.18). The taxonomic content of Gavialidae is significantly reduced to eight taxa. All species of *Gryposuchus*, except for *Gryposuchus croizati*, are excluded from Gavialidae. *Piscogavialis jugaliperforatus*, *Siquisiquesuchus venezuelensis* and *Ikanogavialis gamerois* are similarly recovered outside of the crown group. 'Thoracosaurs' comprise a polyphyletic group within Gavialoidea, resulting in several ghost lineages, similar to the unconstrained analysis. Both species of *Eosuchus* and *Thoracosaurus* form a clade stemward of Gavialidae and its unnamed sister clade. The latter includes all other putative 'thoracosaurs', although these form a paraphyletic array. *Maroccosuchus*, *Kentisuchus*, and *Dollosuchoides* are once again recovered as the earliest diverging clade of gavialoids.

Under the fourth constraint (Fig. 4.19), *Argochampsa* and *Eogavialis* are recovered within Gavialidae. All remaining 'thoracosaurs' and *Portugalosuchus* are recovered in a clade of early diverging non-crocodylian eusuchians, including hylaeochampsids, allodaposuchids, and *Borealosuchus*, as under Constraint 1. Gavialoidea is now shorn of 'thoracosaurs', and the relationships of *Eogavialis* and *Argochampsa* are identical to the unconstrained Analysis 1.3. A Templeton test indicates that the differences in character state distributions between this tree and that of the unconstrained analysis (1.3) are insignificant ($p > 0.05$).

**Summary** In summary, whereas the exclusion of *Portugalosuchus* from Crocodylia results in an insignificant tree length increase, constraining the exclusion of 'thoracosaurs' produces significantly less parsimonious trees.'Thoracosaurs' are still recovered as nested within Gavialoidea when forced outside of Gavialidae, resulting in a small, insignificant increase in tree length but resulting in numerous additional ghost lineages. *Eogavialis* and *Argochampsa* share a number of derived gavialid features, suggesting a closer relationship with later appearing Neogene taxa, such as *Gryposuchus* and *Gavialis*, than to the 'early thoracosaurs'. The discovery of new non-crocodylian eusuchians may be the key to determining the phylogenetic affinities of 'thoracosaurs'. Although 'thoracosaurs' share a number of features with gavialoids, very few of these are exclusive synapomorphies of the clade: they generally occur more widely in Crocodylia, are often also present in non-crocodylian eusuchians, and many of them are associated with longirostry. 'Thoracosaurs' may ultimately be shown to form a distinct non-crocodylian longirostrine clade. Indeed, this study has started to find character support uniting some 'thoracosaurs' with non-crocodylian eusuchians (e.g. the morphology of the orbitotemporal canal, [C88]); however, these similarities are overwhelmed by shared features with gavialoids.

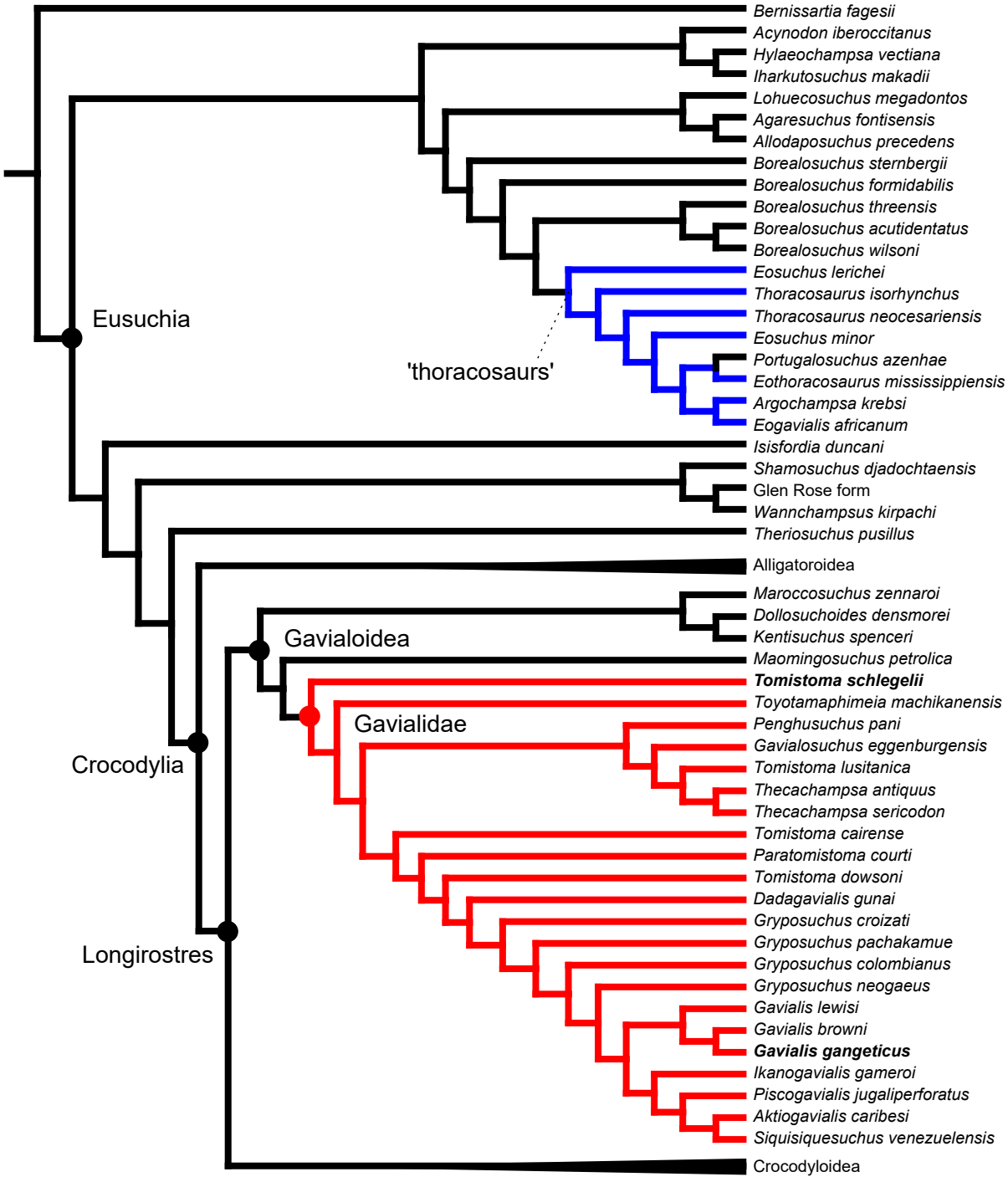



Figure 4.17: Strict consensus of three MPTs resulting from Analysis 1.3 with ‘thoracosaurs’ constrained to be excluded from Crocodylia. Crown gavialids highlighted in red, ‘thoracosaurs’ highlighted in blue.

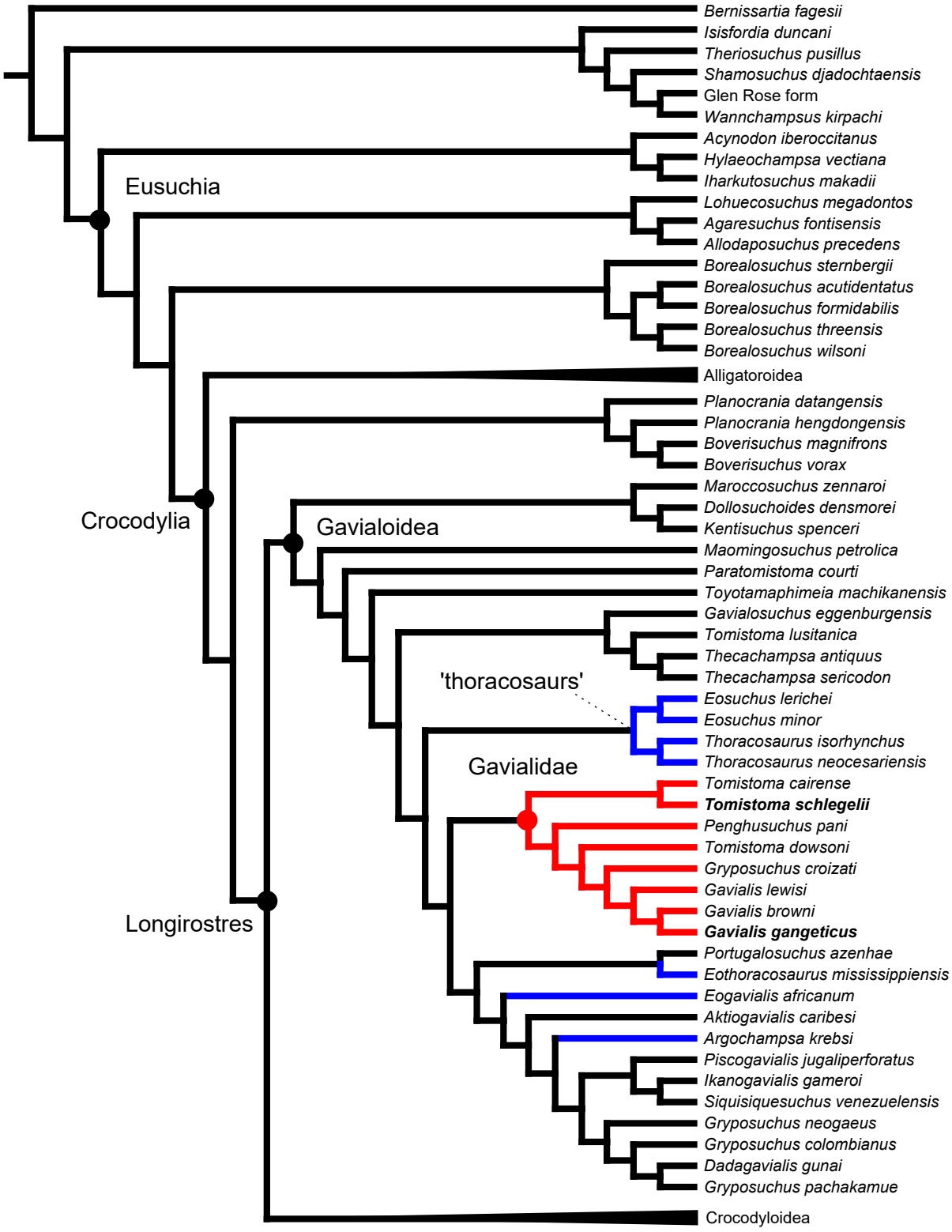



Figure 4.18: Strict consensus of three MPTs resulting from Analysis 1.3 with 'thoracosaurs' constrained to be excluded from Gavialidae. Crown gavialids highlighted in red, 'thoracosaurs' highlighted in blue.

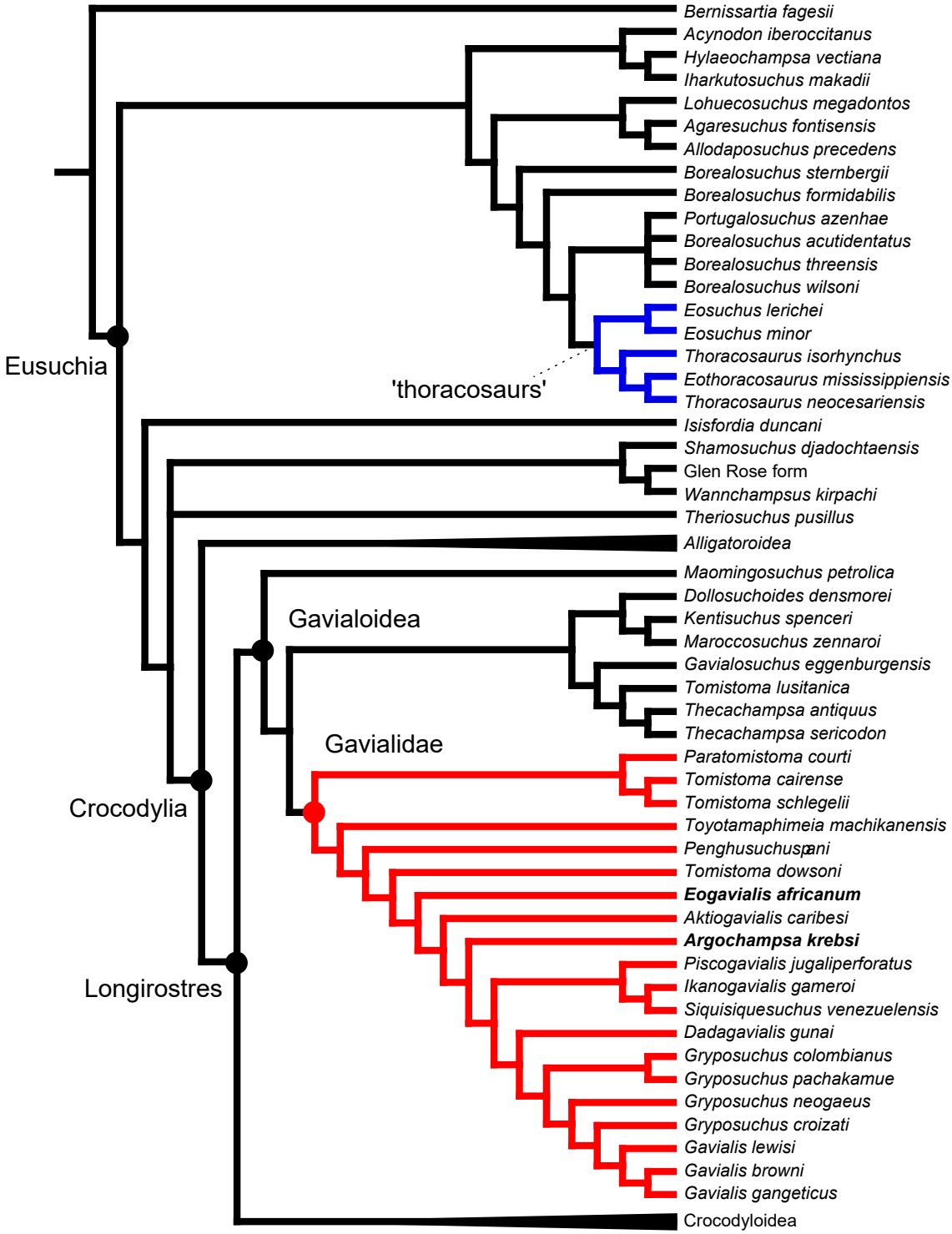



Figure 4.19: Strict consensus of three MPTs resulting from Analysis 1.3 with ‘thoracosaurs’ constrained to be excluded from Crocodylia, but allowing *Eogavialis* and *Argochampsa* to float. Crown gavialids highlighted in red, ‘thoracosaurs’ highlighted in blue.

### 4.4.8 Implications for the systematics and taxonomy of Crocodyloidea

The interrelationships of Crocodyloidea are among the most poorly supported in this phylogeny (average Bremer support = 1.98) (Table 4.3, Fig. 4.20); however, a number of the interrelationships are very stratigraphically congruent and highly concordant with existing molecular and morphological hypotheses, as is discussed.

Crocodyloidea is supported by seven synapomorphies: (1) ratio of snout length to cranium length = 0.55–0.56 (C1); (2) ratio of posterior rostrum width to cranial table width = 1.47–1.52 (C2); (3) infratemporal fenestra length relative to cranial table length = 0.53–0.55 (C7); (4) dorsomedial margin of the orbit flush with skull surface (C72-0, ambiguous); (5) width of the supraoccipital on the skull table greater than half the parietal width (C78-1, ambiguous); (6) palatine ramus of cranial nerve V greater than or equal to half the diameter of the $6^{th}$ maxillary alveolus (C159-1, exclusive); and (7) anterior palatine process at the same level or posterior to the anterior margin of the suborbital fenestra (C162-2, ambiguous).

Only C159-1 is exclusively known in Crocodyloidea; however, this condition reverses in *Australosuchus clarkae* and more crownward taxa. Outside of Crocodyloidea, an extremely shortened anterior palatine process (C162-2) is known only in *Lohuecosuchus megadontos*. Within Crocodyloidea, this condition is lost at the node comprising Mekosuchinae + Crocodylidae, and is independently reacquired in some crocodyloids.

The most significant difference in Crocodyloidea to previous morphological studies is the exclusion of "Tomistominae", which is usually recovered as the sister clade to Mekosuchinae and (Crocodylinae + Osteolaeminae) (Brochu, 2000; Brochu et al., 2012). With the exclusion of "Tomistominae", new interrelationships emerge between the other crocodyloid clades: Crocodylinae, Osteolaeminae, and Mekosuchinae. Furthermore, the taxonomic content and interrelationships of these clades show differences to previous studies.

#### *Asiatosuchus germanicus*, '*Crocodylus*' *affinis* and *Asiatosuchus depressifrons*–basal crocodyloids or stem longirostrines?

Compared to combined morphological and molecular analyses (which also recover Longirostres), the topology of Crocodyloidea differs in the affinities of *Asiatosuchus germanicus*, '*Crocodylus*' *affinis*, and *Asiatosuchus depressifrons* (Fig. 4.20). Here, these taxa are consistently recovered as the earliest diverging crocodyloids, outside of the group including Mekosuchinae and Crocodylidae. By contrast, all combined analyses recover these taxa in the stem of Longirostres, i.e. outside of the clade uniting Gavialoidea and Crocodyloidea (Gatesy et al., 2003; Gold et al., 2014; Lee & Yates, 2018; Iijima & Kobayashi, 2019). This hypothesis was tested by constraining Analysis 1.3 to recover these taxa in the stem of Longirostres, which resulted in an insignificant tree length increase of 2.2 steps (Templeton test, $p > 0.05$, Fig. F.7).

As originally proposed (Li et al., 2019), the latest Cretaceous Asian taxon, *Jiangxisuchus nankangensis*, is recovered as one of the earliest diverging crocodyloids, instead of a 'basal' alligatoroid as recently found by Massonne et al. (2019). However, it is important to note that several taxa belonging to their newly described alligatoroid clade, Orientalosuchinae, were not included in this dataset, meaning that the position of *Jiangxisuchus* will require further testing.

**Phylogenetic affinities and taxonomic content of Mekosuchinae**

Mekosuchinae is weakly supported (Bremer support = 1.11) by five synapomorphies: (1) ratio of infratemporal fenestra length to cranial table length = 0.33–0.40 (C7); (2) ratio of supratemporal fenestra width to length = 0.72–0.77 (C11); (3) quadrate condyle with prominent notch covering 1/3 of mediolateral width (C118-1, ambiguous); (4) anterior maxillary ramus of the ectopterygoid separated from the suborbital fenestra by the maxilla (C177-1, ambiguous); and (5) anteroposteriorly orientated ridges lateral to the choanae (C198-1, exclusive).

Mekosuchinae is recovered as the sister clade to *Australosuchus clarkae* + Crocodylidae in Analysis 1.3, but as the sister clade of Crocodylinae in analyses 1.1 and 2.3. Analysis 3.3 was unable to resolve the interrelationships of Osteolaeminae, Crocodylinae, and Mekosuchinae. The position of Mekosuchinae within Crocodylia is not well resolved in previous studies. The earliest phylogenetic analyses of the clade included a good sample of mekosuchines, but few members of Crocodylinae and Osteolaeminae, and a limited number of morphological characters (Willis, 1993; Salisbury & Willis, 1996). Furthermore, even in recent analyses, few studies have included more than three mekosuchines. Morphology-only analyses that recover the traditional topology (i.e. Crocodyloidea including "Tomistominae") have placed Mekosuchinae as: (1) the sister clade to "Tomistominae" + (Crocodylinae + Osteolaeminae) (Salisbury & Willis, 1996); (2) in a polytomy with "Tomistominae", Osteolaeminae and Crocodylinae (Yates & Pledge, 2017); or most commonly (3) in a polytomy with '*Crocodylus*' *megarhinus* + (Osteolaeminae + Crocodylinae) (e.g. Brochu, 2000; Brochu et al., 2010; Brochu et al., 2012; Brochu & Storrs, 2012; Jouve et al., 2015; Massonne et al., 2019). With the recovery of Longirostres in combined morphological and molecular analyses, different topologies are recovered still. Whereas Lee and Yates (2018) recovered Mekosuchinae as the sister clade to Longirostres, the analyses of Gatesy et al. (2003) and Gold et al. (2014) positioned Mekosuchinae as the sister clade to Crocodylidae, similar to the results presented here. Constraining Mekosuchinae to be recovered in the stem of Longirostres results in an insignificant tree length increase of 6.7 steps (Templeton test, $p > 0.05$, Appendix F.8).

**Phylogenetic intrarelationships of Mekosuchinae**

Comparisons of the internal relationships of Mekosuchinae are limited to a handful of studies, given that few include more than three representatives (Salisbury & Willis, 1996; Stein et al., 2016; Yates &

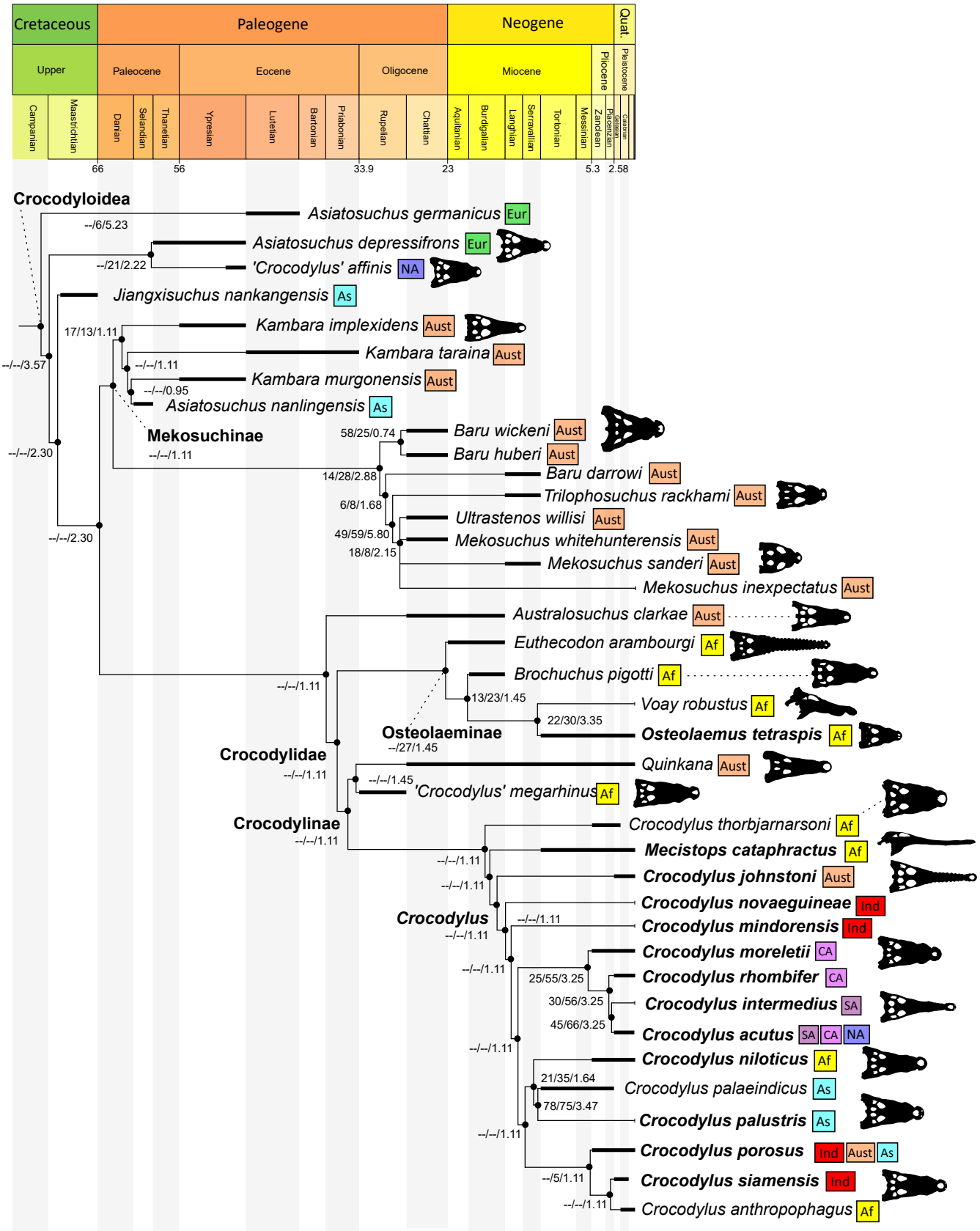



Figure 4.20: Time calibrated phylogeny of Crocodyoidea from Analysis 1.3. Ages = Ma. Support values: Bootstrap/Jackknife/Bremer. Abbreviations: **As**, Asia; **Aust**, Australasia; **CA**, Central America; **Eur**, Europe; **Ind**, Indo-Pacific (Malay Archipelago); **NA**, North America; **SA**, South America.

Pledge, 2017; Lee & Yates, 2018). The internal relationships of Mekosuchinae are highly congruent between analyses 1.1, 1.3, 2.3, and 3.3. Furthermore, they broadly align with existing hypotheses and are highly stratigraphically congruent. All species of the early appearing generalist form, *Kambara*, form a clade that is sister to the later-appearing altirostral and blunt snouted taxa *Baru*, *Mekosuchus*, *Ultrastenos*, and *Trilophosuchus* (Salisbury & Willis, 1996; Brochu, 2003; Lee & Yates, 2018) (Fig. 4.20). Furthermore, as in Lee and Yates (2018), *Trilophosuchus* and *Mekosuchus* are more closely related to each other than to *Baru*, which is paraphyletic. Despite these similarities, two principal differences in the taxonomic content are found. Whereas two putative mekosuchines, *Australosuchus clarkae* and *Quinkana*, are recovered outside of Mekosuchinae here, the Paleocene East Asian crocodyloid, *Asiatosuchus nanlingensis*, is recovered within Mekosuchinae.

**Is *Asiatosuchus nanlingensis* a mekosuchine?** *Asiatosuchus nanlingensis* is known from mostly fragmentary mandibular remains, and its phylogenetic affinities have rarely been studied. When included in phylogenetic analyses, its relationships are usually unresolved within Crocodyloidea (Wang et al., 2016; Wu et al., 2018) and it has even been recovered as a 'basal' alligatoroid by some authors (Li et al., 2019; Massonne et al., 2019). Analyses 1.1, 1.3, 2.3 and 3.3 recover *Asiatosuchus nanlingensis* in Mekosuchinae. This relationship has significant implications for the biogeography of the clade, which has until now been recognised as an endemic Australasian radiation.

Support for the inclusion of *Asiatosuchus nanlingensis* in Mekosuchinae is relatively weak. None of the synapomorphies of Mekosuchinae can be scored in this taxon. Furthermore, of the eight synapomorphies that support the least inclusive clade comprising *Asiatosuchus nanlingensis* + *Kambara implexidens*, only two can be scored in *Asiatosuchus nanlingensis*: (1) dorsal lobe of the dentary symphysis extends further posteriorly than the ventral lobe (C226-0); and (2) the surangular-articular suture is straight within the glenoid fossa (C247-0). The first of these is ambiguous, unknown in *Kambara taraina* and *Kambara murgonensis*, and shared with most crocodylines, '*Crocodylus*' *affinis*, and most caimanines. A straight surangular-articular suture (C247-0) is also ambiguous. Within Crocodyloidea, this condition is otherwise only known in *Mecistops cataphractus*; however, it is the plesiomorphic condition in Eusuchia, occurring in all alligatoroids and most gavialoids. A sulcus excavating the dorsolateral surface of the surangular (C246-1) unites *Kambara taraina*, *Kambara murgonensis*, and *Asiatosuchus nanlingensis*. This synapomorphy is again ambiguous, occurring in *Crocodylus anthropophagus*, '*Crocodylus*' *megarhinus*, and *Asiatosuchus depressifrons*. No alligatoroids exhibit this sulcus, and the only non-crocodyloid taxa to exhibit it are *Bernissartia fagesii*, *Borealosuchus sternbergii*, and *Kentisuchus spenceri*. The sister relationship between *Asiatosuchus nanlingensis* and *Kambara murgonensis* is supported by one ambiguous synapomorphy: dentary symphysis adjacent to 6–8 alveoli (C221-1). Elongation of the dentary symphysis to 6–8 alveoli is very common in Crocodylia, present in *Asiato-*

*suchus germanicus*, '*Crocodylus*' *affinis*, *Asiatosuchus depressifrons*, several crocodylines and alligatorines, as well as some non-crocodylian eusuchians.

Due to poor preservation, only three synapomorphies of Alligatoroidea can be compared with *Asiatosuchus nanlingensis*, all of which are absent. *Asiatosuchus nanlingensis* lacks subequal anterior processes of the surangular (C240-0) (present in almost all alligatoroids), and exhibits a surangular that extends to the posterior tip of the retroarticular process (C245-0) (truncated in most alligatoroids). Finally, the retroarticular process exceeds the dorsal margin of the articular glenoid fossa in *A. nanlingensis* (C251-1), contrasting with the low retroarticular processes of most alligatoroids (C251-0).

Constraining Analysis 1.3 to recover *Asiatosuchus nanlingensis* outside of Mekosuchinae results in a statistically insignificant tree length increase of 0.8 steps (Templeton test $p > 0.05$, Appendix F.9). Under this constraint, *Asiatosuchus nanlingensis* is recovered within Crocodylinae as the sister species of *Mecistops cataphractus*, immediately in the stem of the crown genus *Crocodylus*. This constraint results in significant changes to the topology of Crocodyloidea. Mekosuchinae is now recovered in crown group Crocodylidae as the sister clade to Crocodylinae. Constraining the search to recover *Asiatosuchus nanlingensis* within Alligatoroidea also results in an insignificant tree length increase of 33.65 steps (Templeton test, $p > 0.05$). Under this constraint, *Asiatosuchus nanlingensis* is recovered as an early diverging alligatoroid. The removal of this taxon from Crocodyloidea has a significant impact on topology within Crocodyloidea and Longirostres. *Asiatosuchus germanicus*, *Asiatosuchus depressifrons*, '*Crocodylus*' *affinis*, *Jiangxisuchus*, and *Australosuchus* all become stem longirostrines. Furthermore, Mekosuchinae is again recovered within the crown group Crocodylidae, as the sister clade of Crocodylinae.

In summary, *Asiatosuchus nanlingensis* is most parsimoniously recovered within Mekosuchinae based on several ambiguous synapomorphies shared with *Kambara*. Forcing its inclusion into other crocodylian clades, including Alligatoroidea, results in insignificant tree length increases, but major differences in the topology of Longirostres.

**Are *Australosuchus clarkae* and *Quinkana* mekosuchines?** *Australosuchus clarkae* has consistently been recovered within Mekosuchinae, either as the earliest diverging member (Lee & Yates, 2018), or closely related to *Kambara* (Salisbury & Willis, 1996). There are a number of characters which support the exclusion of *Australosuchus* from Mekosuchinae, as recovered here (Fig. 4.20). All members of Mekosuchinae exhibit a prominent notch on the quadrate condyle, where preserved, which covers approximately a third of the quadrate width (C118-1) (Chapter 3, Fig. 3.45). This condition is an ambiguous synapomorphy of Mekosuchinae, given that it occurs convergently in most alligatoroids and *Borealosuchus*. However, this condition is not present in any other crocodyloid, including *Australosuchus clarkae*. Separation of the anterior process of the ectopterygoid from the suborbital fenestra (C176-1) is also recovered as a synapomorphy of Mekosuchinae, that is absent in *Australosuchus clarkae*. This is

ambiguous, as it can only be scored in *Kambara implexidens*, *Mekosuchus sanderi*, *Baru wickeni*, and *Baru huberi*. Furthermore, *Trilophosuchus rackhami* exhibits the plesiomorphic condition. Outside of Mekosuchinae, this condition only occurs in *Mecistops cataphractus*. The presence of anteriorly directed ridges lateral to the choanae (C198-1) is the most robust synapomorphy of Mekosuchinae; although the presence of this feature cannot be scored for seven putative mekosuchines, it is absent in all other eusuchians. No specimens of *Australosuchus* preserve the palate sufficiently, and so the condition is unknown in this taxon. Finally, *Australosuchus* shares a small opening for the palatine ramus of cranial nerve V (C159-0) with Osteolaeminae and Crocodylinae. Mekosuchinae and all other stemward crocodyloids exhibit an enlarged foramen (C159-1).

Despite being represented by four species (Molnar, 1982d; Megirian, 1994; Willis & Mackness, 1996; Willis, 1997a) *Quinkana*, is scored as an exemplifier due to the extremely limited material that comprises the genus. Furthermore, there has not been a revision of any of the species of *Quinkana* since their initial descriptions. The sister relationship of *Quinkana* and '*Crocodylus*' *megarhinus* recovered here is supported by two ambiguous synapomorphies: (1) sulcus on the ventrolateral margin of the jugal and/or maxilla (C96-1); and (2) anterior palatine process at the same level or posterior to the anterior margin of the suborbital fenestra (C162-2). A ventrolateral sulcus appears multiple times in crocodyloid species, as well as convergently within Gavialoidea. Within Mekosuchinae, only *Baru wickeni* exhibits this sulcus. A reduced anterior process of the palatine has previously been identified as a common feature of several Australasian fossil crocodylians, and is the plesiomorphic condition in Crocodyloidea (Willis et al., 1990; Willis, 1993). A reduced anterior palatine process also characterises some mekosuchines, but here this is optimised as multiple acquisitions of this condition. This character was previously binary, lacking a precise delimitation between character states. Here, a further character state has been added which further subdivides the length of the anterior process. Consequently, fewer taxa are scored for the highly shortened condition (C162-2). Furthermore, of the three characters providing support for Mekosuchinae, *Quinkana* can only be scored for one (C177), for which it has the opposite condition (C177-0) to all other mekosuchines (C177-1).

Constraining Analysis 1.3 to recover *Australosuchus clarkae* and *Quinkana* within Mekosuchinae results in a significant tree length increase of 5.5 steps (Templeton test: $p < 0.05$, Fig. F.10). Under this constraint, *Quinkana* and *Australosuchus* are recovered as the earliest successively branching taxa in Mekosuchinae. The remaining topology is almost identical to the unconstrained analysis, except that *Asiatosuchus germanicus* is recovered as the sister species of '*Crocodylus*' *affinis* + *Asiatosuchus depressifrons*.

**Osteolaeminae**

The sister taxon relationship of Osteolaeminae with Crocodylinae (Fig. 4.20), as well as the relationships among osteolaemines, is largely congruent with previous studies (Brochu, 2007a). Principal differences relate to the synapomorphies supporting Osteolaeminae and its internal nodes. Osteolaeminae is supported by five synapomorphies: (1) ratio of infratemporal fenestra maximum length to anteroposterior cranial table length = 0.49 (C7) (2); minimum angle subtended by lateral cranial table edge and sagittal axis of skull = 6 (C9); (3) anteroposteriorly orientated preorbital ridges (C30-1); (4) descending lamina of the squamosal on the quadrate ramus of the paroccipital process (C113-1); and (5) ectopterygoid forming medial wall of posterior maxillary alveoli (C175-2). Preorbital ridges (C30-1) and a descending squamosal lamina (C113-1) were previously recovered as ambiguous synapomorphies of Osteolaeminae (Brochu, 2007a); however, characters 7, 9, and 175 are newly recognised synapomorphies. All five synapomorphies are ambiguous; for example, the size of the infratemporal fenestrae in Osteolaeminae is approximately equal to most crocodylines, and varies considerably in Osteolaeminae (e.g. ∼30% of cranial table length in *Osteolaemus tetraspis* and 50% in *Voay robustus*). The angular difference between the lateral edge of the cranial table and the sagittal plane is low in most osteolaemines, resulting in square cranial tables. This contrasts with the trapezoidal shape of most crocodylines. Although this is true of *Euthecodon*, *Brochuchus*, and *Osteolaemus*, *Voay* exhibits a strongly trapezoidal skull table (angular difference ∼23°). Contact between the ectopterygoid and the posterior maxillary alveoli (C175-2) is also ambiguous. This character has received considerable changes to delimitation and scoring from previous analyses. Here it is optimised as a synapomorphy of Osteolaeminae, but it also occurs in almost all crocodylines.

Within Osteolaeminae, *Euthecodon arambourgii* and *Brochuchus pigotti* are successively nested taxa that are 'basal' to the clade comprising (*Osteolaemus tetraspis* + *Voay robustus*). This contrasts with the results of Brochu (2007a), who recovered a sister relationship between *Brochuchus* and *Euthecodon arambourgii*. The clade comprising *Brochuchus* + (*Osteolaemus tetraspis* + *Voay robustus*) is supported by a posteroventrally sloping ventral orbital margin (C94-1).

As recovered in previous studies (Brochu, 2007a; Brochu et al., 2012), *Osteolaemus tetraspis* and *Voay robustus* are sister taxa. This relationship is supported six continuous and four discrete synapomorphies: (1) rostrum length = 0.54–0.56 (C1); (2) width to length ratio of the external naris = 1.0 (C3); (3) cranial table length to width ratio = 0.68–0.75 (C8); (4) supratemporal fenestra size relative to cranial table length = 0.30 (C10); (5) ratio of width across the basioccipital tubera to occipital condyle width = 1.56 (C16); (6) number of maxillary alveoli = 13 (C17); (7) frontoparietal suture concavo-convex (C76-0, shared); (8) supratemporal fenestrae with overhanging rims (C81-1, shared); (9) premaxillary alveoli equally separated (C145-0, shared); and (10) margins of the angular and surangular everted to form a flange (C239-1, shared).

Three of these discrete synapomorphies are newly recognised, although they are all shared. A concavo-convex frontoparietal suture (C76-0) is also present in all crocodylines, some mekosuchines, *Asiatosuchus depressifrons*, and '*Crocodylus*' *affinis*; however, it is absent in *Euthecodon arambourgi* and *Brochuchus*. The equal separation of premaxillary alveoli (C145-0) is the plesiomorphic condition in Crocodylia, but is lost in most crocodyloids. The presence of everted margins of the surangular and angular (C239-1) occurs in three other members of Longirostres, although all are mekosuchines (*Mekosuchus inexpectatus*, *Mekosuchus whitehunterensis*, and *Ultrastenos*). Two additional synapomorphies were considered to unite *Voay* and *Osteolaemus* in previous analyses: overhanging rims of the supratemporal fenestrae, and a short anterior palatine process (Brochu, 2007a). The former is also recovered here (C81-1); however, the palatine process is significantly longer in *Voay* (C162-1) than in *Osteolaemus tetraspis* (C162-2), and similar to the condition in most crocodylines.

**Crocodylinae**

Although its placement outside of the genus *Crocodylus* is consistent with previous studies, the position of '*Crocodylus*' *megarhinus* within Crocodyloidea differs. This species is typically recovered in a polytomy with Mekosuchinae and Crocodylidae (e.g. Brochu, 2000; Delfino et al., 2005; Brochu & Storrs, 2012; Lee & Yates, 2018). Here, '*Crocodylus*' *megarhinus* is recovered as an early diverging member of Crocodylinae. This relationship is supported by three synapomorphies: (1) an ectopterygoid which extends anteriorly more than two-thirds the length of the suborbital fenestra (C174-1); (2) dorsoventrally short posteroventral processes of the pterygoid (C136-1); and (3) a concavo-convex frontoparietal suture (C76-0). However, none of these features unambiguously unite '*Crocodylus*' *megarhinus* with Crocodylinae. The frontoparietal suture is also concavo-convex in some osteolaemines, mekosuchines, and 'basal' crocodyloids. Although the elongated ectopterygoid (C174-1) is absent in all osteolaemines, it occurs in several mekosuchines, such as *Baru*, *Kambara taraina*, and *Trilophosuchus rackhami*. Dorsoventrally short posteroventral pterygoid processes are absent in all other crocodyloids, except *Ultrastenos*, but they are present in almost all members of Gavialoidea.

**Intrarelationships of the crown genus *Crocodylus*** Although weakly supported, the interrelationships of crown *Crocodylus* species recovered here show a number of similarities to molecular studies. As in Oaks (2011), the three Australasian species, *Crocodylus johnstoni*, *Crocodylus novaeguineae*, and *Crocodylus mindorensis*, are the earliest diverging members of the crown genus (Fig. 4.20). However, whereas they formed a clade in Oaks (2011) and Pan et al. (2020), they are recovered as successively nested species in this study. Like most morphological and all molecular studies, Neotropical *Crocodylus* forms a monophyletic group, within which *Crocodylus acutus* and *Crocodylus intermedius* are sister species. Also in agreement with molecular studies is the close relationship found between *Crocodylus*

*porosus* and *Crocodylus siamensis* (Meganathan et al., 2010; Oaks, 2011; Pan et al., 2020). The principal difference to molecular studies is that *Crocodylus niloticus* is here more closely related to the remaining Australasian (*C. porosus*) and Indo-Pacific *Crocodylus* species as well as *Crocodylus anthropophagus* from the Plio-Plesitocene of East Africa, than to Neotropical *Crocodylus*.

This study is the first to recover a sister relationship between *Crocodylus palaeindicus* (Miocene–Pliocene of Indo-Pakistan) and the extant mugger crocodile, *Crocodylus palustris*, of the Indian subcontinent and Iran. This relationship is moderately supported (Jackknife: 75, Bremer 3.5). Direct ancestry between these species has long been suggested based on their overlapping geographic range and similar morphology (Lydekker, 1886; Mook, 1933). *Crocodylus palaeindicus* and *Crocodylus palustris* are united by three synapomorphies: (1) premaxilla-maxilla suture at the level or anterior to the posterior margin of the naris (C49-1, shared); (2) posterior margin of the incisive foramen rounded (C139-0, shared); and (3) anterior extent of the ectopterygoid less than two-thirds the length of the suborbital fenestra (C174-0, shared).

**The phylogenetic affinities of *Mecistops cataphractus*** The phylogenetic affinities of the African slender-snouted crocodile, *Mecistops cataphractus*, is a source of ongoing debate (see Chapter 1). Here, I recover *Mecistops* as more closely related to *Crocodylus* following earlier morphological studies (e.g. Brochu, 2000), but contrasting with most molecular studies that suggest that it is instead an Osteolaemine (e.g. Man et al., 2011; Oaks, 2011). Furthermore, the giant Plio-Pleistocene African species, *Crocodylus thorbjarnarsoni*, is recovered as the sister taxon of *Mecistops* + *Crocodylus*. Previously, *Crocodylus thorbjarnarsoni* was recovered as the sister taxon of *Crocodylus anthropophagus*, but in a large polytomy with all Neotropical *Crocodylus* species, *C. niloticus*, *C. palustris*, *C. siamensis*, and *C. palaeindicus* (Brochu & Storrs, 2012).

The close relationship of *Mecistops* to *Crocodylus* is supported by several synapomorphies in common with earlier studies (Brochu, 2000; McAliley et al., 2006). These include a deep dorsal indentation of the ilium (C308-2, shared), caviconchal recesses (C51-1, exclusive), a surangular-angular suture that passes broadly along the ventral margin of the external mandibular fenestra (C237-2, shared), and a forked anterior ectopterygoid process (C176-1, shared). In addition to these synapomorphies five continuous characters and five discrete characters are newly recovered as synapomorphies of *Mecistops* + *Crocodylus*; however, all of these are ambiguous, as they are lost in crownward nodes and/or appear outside of this clade: (1) ratio of antorbital skull width to cranial table with = 1.5 (C2); (2) naris width to length ratio = 0.94 (C3); (3) thickness of the anterior narial wall realtive to naris length = 0.5 (C4); (4) ratio of supratemporal fenestra size to cranial table length = 0.45 (C10); (5) ratio of retroarticular process length to width = 1.3–1.7 (C20); (6) dorsally facing nares (C41-1, ambiguous); (7) orbit positioned lateral to maxillary alveoli 3–6 (C74-0, ambiguous); (8) anterior process of the palatine wedge shaped (C160-1,

ambiguous); (9) maxilla-palatine suture intersects the suborbital fenestra at the anterior corner (C167-1, ambiguous); (10) pterygoid surface lateral and anterior to choanae flush (C197-0, ambiguous).

**Constrained searches** These results should be treated as tentative as the sister relationship between *Mecistops* and *Crocodylus* is weakly supported (Bremer support = 1.1). Furthermore, constraining analysis 1.3 to recover *Mecistops* within Osteolaeminae results in an insignificant tree length increase of 16.2 steps (Templeton test, p>0.05). Under this constraint, the topology within Crocodyloidea changes dramatically (Appendix F.11). Several former basal crocodyloid species such as *Asiatosuchus germanicus*, '*Crocodylus*' *affinis*, *Asiatosuchus depressifrons*, and *Jiangxisuchus* move to the stem of Longirostres. Similarly, *Quinkana* and *Australosuchus* are recovered in the stem of Longirostres. Mekosuchinae is still recovered as the sister clade to Crocodylidae. The relationships among *Crocodylus* change significantly. Notably, *Crocodylus throbjarnarsoni* and *Crocodylus anthropophagus* are sister species. *Crocodylus mindorensis* and *Crocodylus novaeguineae* are recovered further crownward as the sister clade to Neotropical *Crocodylus*.

## 4.5 Summary

- For the first time based on a morphology-only dataset, *Gavialis gangeticus* is recovered as the closest living relative of *Tomistoma schlegelii*. This result is consistent across all analyses, regardless of treatment of quantitative characters or weighting strategies, and measures of internal consistency for Gavialoidea are the highest amongst crocodylian clades.

- Constraining analyses to recover the traditional morphological topology results in significantly less parsimonious trees. The recovery of Gavialidae (*Gavialis* + *Tomistoma*) does not appear to be an artefact of convergence in long-snouted taxa. Indeed, an evaluation of characters supporting this hypothesis indicates that it is a result of changes to both character scores and to character construction. These changes reveal that (1) several species recovered in Gavialoidea lack plesiomorphic features that formerly drew them towards to 'base' of Crocodylia; and (2) more widespread similarities occur between taxa usually classified within Tomistominae and Gavialoidea, which are here interpreted as homology rather than homoplasy.

- Significant temporal incongruence exists between molecular estimates for the divergence between the extant gharials, and minimum divergence times inferred from the first appearances of crown group gavialoids (Gavialidae). This principally results from the inclusion of a polyphyletic array of taxa ('thoracosaurs' and *Portugalosuchus azenhae*) within Gavialidae. *Portugalosuchus* might represent a non-crocodylian eusuchian given its early stratigraphic age (early Late Cretaceous), and the insignificant tree length increase when constrained to lie outside of Crocodylia. By contrast, the constrained exclusion of 'thoracosaurs' from Crocodylia is significantly less parsimonious. 'Thoracosaurs' share some synapomorphies exclusively found in Gavialoidea; however, many of these are ambiguous and/or are associated with longirostry. Furthermore, some new anatomical data (morphology of the orbitotemporal canal) supports the exclusion of *Portugalosuchus* and some 'thoracosaurs' from Crocodylia. It is possible that these taxa belong to a currently unrecognised clade of non-crocodylian eusuchians, and are drawn into Gavialoidea as a result of convergence in snout length.

- The taxonomic content of Alligatoroidea is largely consistent with previous studies, although new interrelationships and support for internal clades are recovered, most notably: (1) the paraphyly of *Diplocynodon*; (2), the recovery of an early diverging North American clade in Caimaninae; and (3) the recovery of the early Paleogene South American taxon, *Eocaiman*, outside of Caimaninae.

- Morphological evidence suggests that *Caiman lutescens* is closely related to *Caiman gasparinae* + *Mourasuchus*, whereas the indeterminate remains belonging to UCMP 39978 are recovered as

closely related to *Caiman wannlangstoni*.

- The recovery of *Tomistoma schlegelii* and species traditionally recovered as tomistomines within Gavialoidea, rather than Crocodyloidea, introduces several changes to the interrelationships of the latter clade. The early Paleogene European taxa *Asiatosuchus depressifrons* and *Asiatosuchus germanicus*, as well as the North American species '*Crocodylus*' *affinis*, are recovered as 'basal' crocodyloids. Similarly, the primarily Australasian clade, Mekosuchinae, belongs outside of the crown group Crocodylidae. The taxonomic composition of Mekosuchinae differs to previous studies by: (1) the inclusion of *Asiatosuchus nanlingensis* from Asia; and (2) the exclusion of the Australian taxa *Australosuchus clarkae* and *Quinkana*.

- The interrelationships of Crocodylinae are consistent to molecular studies in several respects, including (1) the recovery of Indo-Pacific *Crocodylus* as the earliest diverging members of the crown genus and (2) the monophyly of Neotropical *Crocodylus*. By contrast, *Mecistops* is recovered as more closely related to *Crocodylus* than to *Osteolaemus*, as traditioanlly recovered in morphological datasets. However, constrained searches indicate that the molecular hypothesis for *Mecistops* cannot be out-ruled.

- The use of continuous characters in conjunction with extended implied with higher $k$-values produced optimal phylogenetic results with regards to stratigraphic congruence and internal accuracy. Conversely, lower $k$-values produced topologies with lower stratigraphic congruence and a highly anomalous topology in which Alligatoroidea and Gavialoidea were sister taxa. Extended implied weighting tends to override any differences in the treatment of quantitative data, i.e. whether continuously coded, discretised, or excluded. Nevertheless, the main result of this Chapter (i.e. the close relationship of the extant gharials) is consistent across analyses, regardless of treatment of quantitative characters or weighting strategies.

# Chapter 5

# A Review of the Evolutionary and Biogeographic History of Crocodylia

## 5.1 Introduction

In the previous chapter, I described and evaluated a series of new phylogenetic hypotheses for Crocodylia. In this chapter I synthesise these results in the context of a review of the evolutionary and biogeographic history of the clade. In addition to taxa included in the phylogenetic analysis, I discuss the implications of the spatiotemporal distributions of additional named species and indeterminate occurrences.

## 5.2 Eusuchia and the Origin of Crocodylia

There has been some recent disagreement in the taxonomic content of Eusuchia, resulting in differences in the proposed timing of origin of this clade. By contrast with some recent hypotheses (Turner, 2015; Turner & Pritchard, 2015; Narváez et al., 2016; Schwarz et al., 2017), *Theriosuchus* and Paralligatoridae are not recovered in Eusuchia (see also Groh et al., 2020), removing evidence for a Late Jurassic origin of the latter group. Other putative early eusuchian occurrences tend to be extremely fragmentary (e.g. Yi et al., 2017). As such, the earliest unambiguous appearances of Eusuchia come from representatives of Hylaeochampsidae in the Barremian of western Eurasia, comprising *Hylaeochampsa vectiana* from the United Kingdom (Clark & Norell, 1992), *Turcosuchus okani* from Turkey (Jouve et al., 2019), and *Unasuchus reginae* from Spain (Brinkmann, 1992; Jouve et al., 2019) (Fig. 5.1). The nested position of *Hylaeochampsa* implies long ghost lineages ($\sim$40 myr) for other members of Hylaeochampsidae that appear in the Late Cretaceous, i.e. *Iharkutosuchus makadii* from the Santonian of Hungary (Ősi et al., 2007), and the multispecific *Acynodon* from the Campanian–Maastrichtian of southern Europe (Buscalioni et al., 1997; Delfino et al., 2008b). Although Albian occurrences from Italy (*Pietrarosuchus ormezzanoi*; Buscalioni et al., 2011) and the USA (*Pachycheilosuchus trinquei*; Rogers, 2003) might partly fill this gap, these species tend to be recovered in a more 'basal' position within Hylaeochampsidae (e.g. Jouve et al., 2019), or outside of Eusuchia altogether (e.g. Narváez et al., 2015). However, these long ghost lineages may be an artefact of sampling bias: non-marine crocodyliform fossils are almost unknown from the early Late Cretaceous (i.e. Cenomanian–Coniacian) of Europe and North America (Martin & Delfino, 2010; Puértolas-Pascual et al., 2016; Mannion et al., 2019). This interval coincides with a marine transgression and a substantial decline in the preservation of terrestrial deposits on these two continents (see also Puértolas-Pascual et al., 2016), with this sampling gap mirrored in other terrestrial groups (Mannion & Upchurch, 2011).

Allodaposuchidae represents an endemic European clade of stem crocodylians that first appeared in the Campanian (or possibly the Santonian; Ősi et al., 2016), and went extinct at the K/Pg boundary (Buscalioni et al., 2001; Delfino et al., 2008a; Narváez et al., 2015; Martin et al., 2016a; Narváez et al., 2016) (Fig. 5.2). Recent studies have placed Allodaposuchidae as the sister clade to Hylaeochampsidae (e.g.

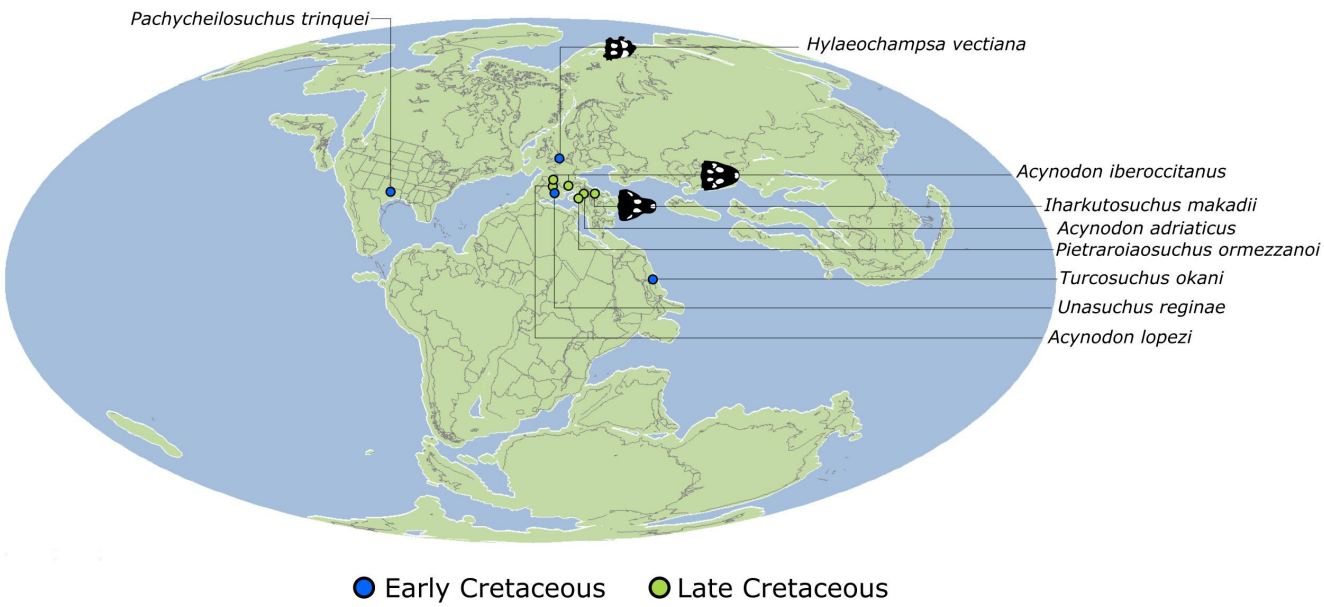



Figure 5.1: The distribution of named species referred to Hylaeochampsidae. Global palaeogeographical reconstruction at 125 Ma from Fossilworks (http://fossilworks.org/) (Alroy, 2013) based on data in the Paleobiology Database (https://paleobiodb.org/).

Narváez et al., 2015), whereas my analyses recover the former in a position closer to Crocodylia (see Section 4.4.3). Although a long ghost lineage remains regardless, the topology presented herein is more stratigraphically congruent, as it necessitates only a single unsampled lineage leading to Allodaposuchidae + Crocodylia.

Remains unambiguously referable to the North American eusuchian *Borealosuchus*, the sister taxon to Crocodylia herein, first appear in Maastrichtian deposits, with the genus passing through the K/Pg boundary until its disappearance in the early Eocene (Brochu, 1997a; Brochu et al., 2012) (Fig. 5.2). Unequivocal members of crown group Crocodylia are first recorded in the Campanian, ∼80 Ma (Table 5.1) (Brochu, 2003, see below for discussion). Given that these occurrences are approximately contemporaneous with the stratigraphically oldest known members of Allodaposuchidae, this might be regarded as robust evidence that these clades originated in the latest Cretaceous and that some of their earliest representatives have been sampled. However, the evolutionary history of these clades might still be obscured by sampling biases. In particular, if the Portuguese neosuchian *Portugalosuchus azenhae* is a member of Crocodylia (see Section 4.4.7), then this would push the origin of Crocodylia (as well as *Borealosuchus* and Allodaposuchidae) back to the Cenomanian, ∼100 Ma (Mateus et al., 2019) (Table 5.1). Nevertheless, both scenarios are concordant with the timing of the split between Alligatoroidea and other crocodylians ∼100–80 Ma (Roos et al., 2007; Oaks, 2011; Green et al., 2014; Pan et al., 2020).

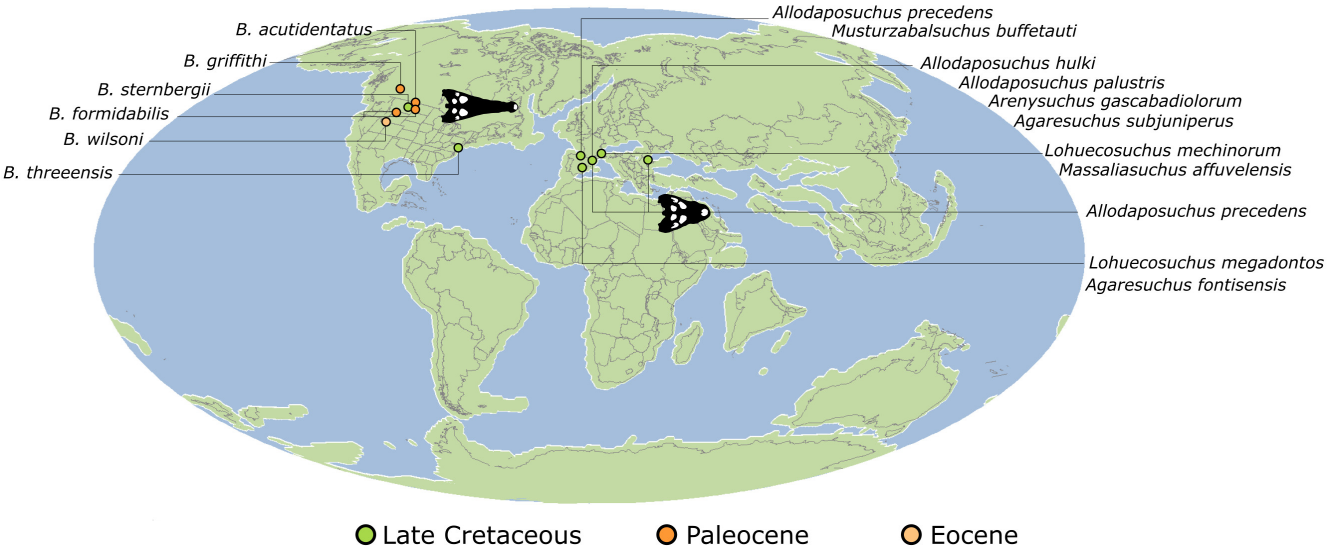



Figure 5.2: The distribution of named species referred to Allodaposuchidae and *Borealosuchus*. Global palaeogeographical reconstruction at 66 Ma from Fossilworks (http://fossilworks.org/ (Alroy, 2013) based on data in the Paleobiology Database (https://paleobiodb.org/).

## 5.3 Alligatoroidea

As traditionally reconstructed, Alligatoroidea seems to have originated in North America, with the earliest appearing representatives known from the Campanian, including the 'basal' members *Leidyosuchus canadensis* and *Deinosuchus hatcheri* (Lambe, 1907; Holland, 1909; Brochu, 1997a; Schwimmer, 2002). Several additional latest Cretaceous alligatoroids are known from North America, comprising taxa (*Albertosuchus langstoni*, *Bottosaurus*, *Brachychampsa*, and *Stangerochampsa mccabei*) usually regarded as non-alligatorid alligatoroids (e.g. Brochu, 1999, 2011; Hastings et al., 2013). However, consistent with a small number of recent analyses (Bona et al., 2018; Cossette & Brochu, 2018; Cossette, 2020), these taxa are recovered as caimanines (Section 4.4.5). This suggests that the initial diversification of Alligatoroidea occurred prior to the K/Pg mass extinction, 66 Ma, rather than in its aftermath.

Although Caimaninae is today restricted to Central and South America (Grigg & Kirshner, 2015), it increasingly appears likely that the clade originated in North America, especially given the total absence of crocodylians currently known from South America during the Cretaceous (e.g. Cidade et al., 2019a). Whereas most of these taxa form an endemic North American clade that comprises the earliest diverging caimanine lineage, *Bottosaurus* is deeply nested within Caimaninae (see also Cossette & Brochu, 2018; Cossette, 2020). This indicates the presence of a second caimanine lineage in the latest Cretaceous of North America and, potentially, a much more complicated and unsampled evolutionary and biogeographic history for this clade that might have involved multiple early dispersals between the Americas. However, it is noteworthy that *Bottosaurus* is known from fragmentary materials and its phy-

logenetic position is weakly supported; it remains possible that characters diagnosing crownward clades in Caimaninae are homoplastic in presumptive basal alligatoroids (e.g. *Bottosaurus*) (Cossette, 2020).

Table 5.1: Minimum divergence estimates and earliest fossil occurrences of eusuchian clades compared with molecular divergence estimates. *Alternative estimate based on differneces in taxonomic content of the clade.

| Clade | Age (Ma) | | Earliest appearing member of respective clades |
|---|---|---|---|
| | This study | Oaks (2011) | |
| Eusuchia | 130–122 | – | *Hylaeochampsa vectiana* |
| Allodaposuchidae | 78–66 | – | *Allodaposuchus precedens* |
| *Borealosuchus* | 70–62 | – | *Borealosuchus sternbergii* and *Borealosuchus threeensis* |
| Crocodylia | 100–95 | 100–81 | *Portugalosuchus* (earliest appearing gavialoid) |
| Alligatoroidea | 78–72 | 100–81 | *Leidyosuchus canadensis* |
| Crocodyloidea | 70–66 | 100–81 | *Jiangxisuchus nankangensis* |
| Alligatoridae | 72–66 | 69–61 | *Brachychampsa montana* (earliest appearing caimanine) |
| Alligatorinae | 66–62 | 69–61 | *Navajosuchus mooki* |
| Crown *Alligator* | 13–10 | 59–30 | *Alligator mefferdi* |
| *Alligator* | 37.2–33.9 | – | *Alligator prenasalis* |
| Crown caimanines | 70–66 | 42–20 | *Bottosaurus harlani* |
| Planocraniidae | 61–59 | – | *Planocrania datangensis* |
| Longirostres | 100–95 | 70–40 | *Portugalosuchus* |
| Mekosuchinae | 62–59 *56–48 | – | *Asiatosuchus nanlingensis* or **Kambara murgonensis* |
| Crocodylidae | 34–28 | 32–19 | '*Crocodylus*' *megarhinus* (earliest appearing crocodyline) |
| Osteolaeminae | 23–20 | 32–19 | *Euthecodon arambourgi* |
| Crown *Crocodylus* | ∼12 | 17–8 | *Crocodylus palaeindicus* |
| Gavialidae | 100–95 | 31–16 | *Portugalosuchus* (earliest appearing gavialine) |
| Tomistominae | 41–38 | 31–16 | *Paratomistoma courti* |
| *Gavialis* | 11.6–5.3 | – | *Gavialis browni* |

Earlier studies also suggested the presence of alligatoroids in the latest Cretaceous of Europe, repre-

sented by *Acynodon* and *Allodaposuchus* (Martin, 2007; Delfino et al., 2008b; Martin, 2010b). However, these taxa have since been universally recovered outside of Crocodylia (e.g. Narváez et al., 2015, this study), and there is no longer any unambiguous evidence of Alligatoroidea on this continent before the K/Pg boundary (Puértolas-Pascual et al., 2016). Massonne et al. (2019) recently erected Orientalosuchina for a newly recovered clade of early-diverging East Asian alligatoroids. In addition to several early Paleogene species that were not included in the present study (*Eoalligator chunyii*, *Krabisuchus siamogallicus*, *Oreintalosuchus naduongensis*, and *Protoalligator huiningensis*), Massonne et al. (2019) also recovered *Jiangxisuchus nankangensis*, from the Maastrichtian of China (Li et al., 2019), in Orientalosuchina. If correct, this would suggest that Alligatoroidea dispersed out of North America earlier than previously thought. However, my analyses recover *Jiangxisuchus* as an early-diverging crocodyloid, in agreement with Li et al. (2019). There is no unequivocal fossil record of Alligatoroidea from Gondwanan continents during the Cretaceous. Referrals of teeth from the Maastrichtian of India to various crocodylian taxa (e.g. *Brachychampsa* and *Allognathosuchus;* Rana & Sati, 2000) are not supported herein: these elements can only be assigned to Crocodyliformes.

In the early Paleocene of North America, the first alligatorines appear in the fossil record, represented by *Navajosuchus mooki* (Simpson, 1930; Brochu, 2004b) (Fig. 5.3). As such, the Paleocene of North America was characterised by the presence of: (1) alligatorines; (2) at least two caimanine lineages that survived the K/Pg mass extinction, as evidenced by *Bottosaurus* (Erickson, 1998; Cossette & Brochu, 2018; Cossette, 2020) and late Paleocene representatives (*Ceratosuchus burdoschi* [Schmidt, 1938] and *Wannaganosuchus brachymanus* [Erickson, 1982]) of the early-diverging North American clade; and possibly (3) some additional non-alligatorid alligatoroids, represented by the incomplete and poorly studied remains of *Listrognathosuchus multidentatus* (Mook, 1930; Brochu, 1997a) (Fig. 5.3). Meanwhile, the first South American caimanines appeared in the early Paleocene, with *Necrosuchus ionensis* and *Protocaiman peligrensis* in Argentina (Simpson, 1937; Brochu, 2011; Bona & Barrios, 2015; Bona et al., 2018; Cidade et al., 2020a). Additional caimanine remains are also known from slightly younger Argentinean deposits (middle Paleocene), including *Notocaiman stromeri* (Rusconi, 1937). Despite their early stratigraphic appearance, *Necrosuchus* and *Protocaiman* are deeply nested in Caimaninae, resulting in long ghost lineages leading to several Neogene South American caimanines (Fig. 4.5). *Eocaiman* also first appears in the early Paleocene of South America, represented by *E. paleocenicus* in Argentina (Bona, 2007), with additional *Eocaiman* species (Simpson, 1930; Pinheiro et al., 2013) present in the early-middle Eocene of Argentina and Brazil.

Uniquely to my study, *Eocaiman* is not recovered within Caimaninae, but is instead part of a paraphyletic array of alligatoroids that lie outside of Alligatoridae. If correct, this would have a significant impact on our understanding of the biogeographic history of Alligatoroidea, given that all South American alligatoroids have previously been universally recovered as caimanines (e.g. Brochu, 1999, 2003,

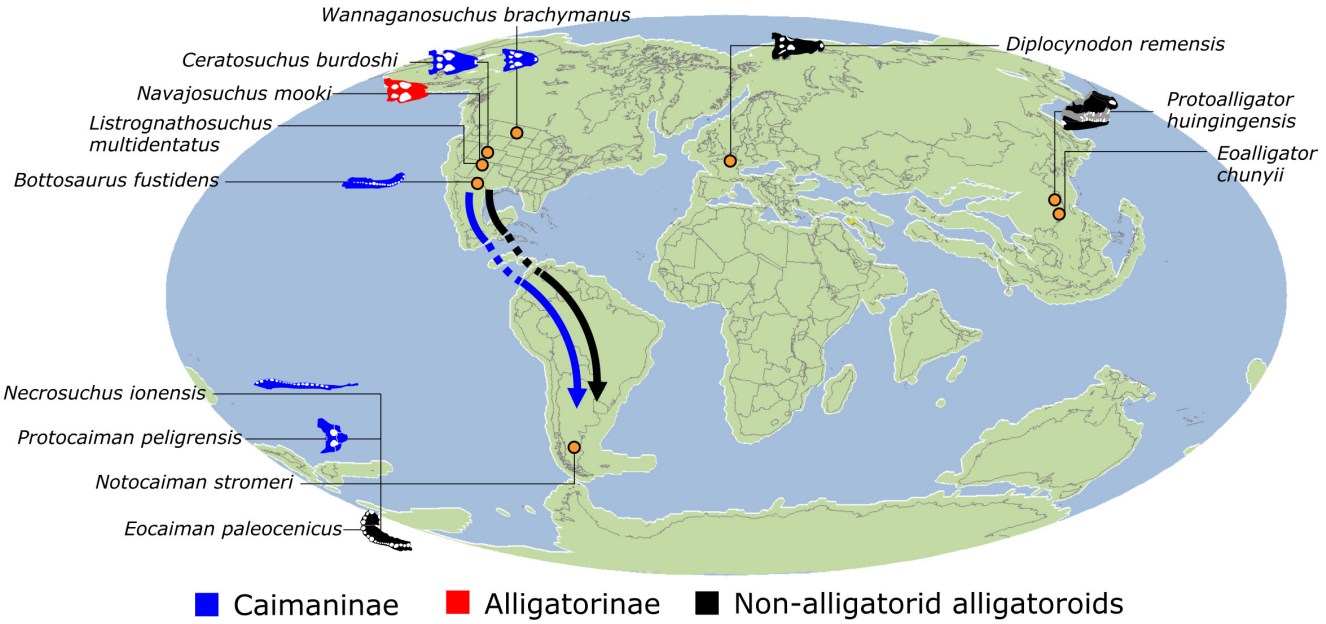



Figure 5.3: The distribution of named alligatoroids in the Paleocene. Global palaeogeographical reconstruction at 60 Ma from Fossilworks (http://fossilworks.org/ (Alroy, 2013) based on data in the Paleobiology Database (https://paleobiodb.org/).

2011; Bona et al., 2018; Cidade et al., 2019a). As such, in addition to at least one caimanine lineage dispersing into South America close to the K/Pg boundary (Brochu, 1999, 2011; Hastings et al., 2013; Bona et al., 2018; Cossette & Brochu, 2018), my results indicate that a non-caimanine alligatoroid lineage also reached South America around this time (Fig. 5.3). However, these stratigraphically early South American alligatoroids are all known from highly fragmentary specimens. As such, this surprising position of *Eocaiman*, and the deeply nested placement of the other taxa, awaits further testing following the discovery of more complete remains. Although it is clear that multiple terrestrial groups dispersed between the Americas during the latest Cretaceous (e.g. Gayet et al., 1992), the geological evidence for this route is less apparent (e.g. Ezcurra & Agnolín, 2012). Most authors suggest that the likely dispersal route was via the proto-Greater Antillean Arc, which has been hypothesised to have formed a landbridge during the late Campanian-Maastrichtian (Iturralde-Vinent & MacPhee, 1999; Hedges, 2006; Iturralde-Vinent, 2006). If this connection was only present in the Cretaceous, this would imply that these alligatoroid lineages most likely arrived in South America prior to the K/Pg mass extinction (Hastings et al., 2013) and that their apparent absence is a sampling artefact.

A presumed reinvasion of North America by South American caimanines occurred by the early Eocene (Fig. 5.4), evidenced by the appearance of *Tsoabichi greenriverensis* (Brochu, 2010), which does not appear to be closely related to *Bottosaurus* (see also Cossette & Brochu, 2018). Indeed, more than one alligatoroid lineage has been suggested to have reinvaded North America during this interval,

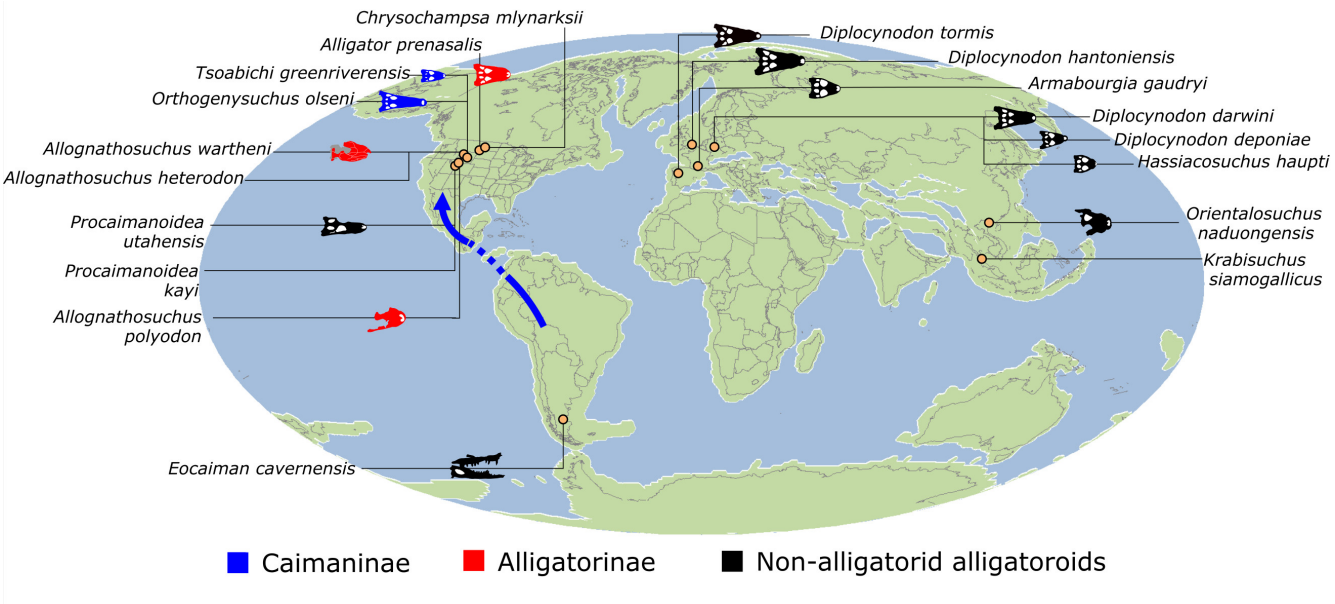



Figure 5.4: The distribution of named and valid alligatoroid species in the Eocene. Global palaeogeographical reconstruction at 40 Ma from Fossilworks (http://fossilworks.org/ (Alroy, 2013) based on data in the Paleobiology Database (https://paleobiodb.org/).

given that the contemporaneous species *Orthogenysuchus olseni* (Mook, 1924) is also recovered as a distantly related caimanine (Brochu, 1999, 2010; Hastings et al., 2013). However, the means of any such dispersal into North America is uncertain, given that there was no clear continuous terrestrial connection between the Americas during the Paleogene (Iturralde-Vinent, 2006), and an island chain only probably became emergent in the late Eocene (Montes et al., 2012). As such, either the ancestors of *Orthogenysuchus* and *Tsoabichi* were present, but unsampled, in the latest Cretaceous-Paleocene of North America, or these lineages dispersed across a marine barrier (Brochu, 2010; Hastings et al., 2013). The former is difficult to reconcile given the nested position of both species within Caimaninae and the high quality of the North American fossil record, whereas the latter is problematic because of the saltwater intolerance that characterises extant alligatoroids (Taplin et al., 1982). However, given that some extant alligatorids are known to periodically inhabit saltwater environments (e.g. Grigg et al., 1998; see also Brochu & Carbot-Chanona, 2015), the crossing of a small marine barrier might be the most likely scenario.

North American alligatorines are represented by several species that have been referred to *Allognathosuchus* during the early Eocene (Brochu, 2004b), but then there is a subsequent gap in that continent's fossil record, prior to the first appearance of *Alligator* (*A. prenasalis*) in the late Eocene (Loomis, 1904; Brochu, 1999; Whiting & Hastings, 2015). This gap was previously partly filled by the middle Eocene taxon *Procaimanoidea* (Mook, 1941b; Gilmore, 1946; Wassersug & Hecht, 1985), which has consistently been recovered as an alligatorine in previous studies (e.g. Brochu, 1999, 2004b; Massonne et al., 2019). However, here I recover *Procaimanoidea* outside of Alligatoridae, forming a clade with the middle–late

Eocene European species *Arambourgia gaudryi* (de Stefano, 1905; Kälin, 1939) and *Hassiacosuchus haupti* (Weitzel, 1935) (Chapter 4, Fig. 4.5). Although its position as the sister taxon to Alligatoridae is novel to my analyses, some previous studies have also indicated a close relationship between the three species forming this clade (Mook, 1941b; Brochu, 2004b). This clade appears to have a long unsampled history that extends into the latest Cretaceous. A similar ghost lineage is implied for the endemic European non-alligatorid alligatoroid *Diplocynodon* (Fig. 5.4), which first appears either in the late Paleocene (if *D. remensis* belongs to this genus [Martin et al., 2014]) or the middle Eocene (Delfino & Smith, 2012). These gaps might partly be explained by the limited availability of suitable Paleocene European deposits (Martin et al., 2014; Mannion et al., 2019), and there are rare, indeterminate occurrences from Paleocene of Europe that have been attributed to alligatoroids (e.g. Smith et al., 2014) and could conceivably belong to these ghost lineages.

Combined with the presence of non-alligatorid alligatoroids (Orientalosuchina) in East Asia (Fig. 5.4), at least by the early–middle Paleocene (*Eoalligator chunyii* and *Protoalligator huiningensis*) (Martin & Lauprasert, 2010; Skutschas et al., 2014; Wang et al., 2016; Massonne et al., 2019), these clades imply biotic exchange between North America and Eurasia. The most likely route to explain the affinities of North American and East Asian taxa was via the Bering landbridge (Beringia) (Brochu, 1999; Wang et al., 2016; Massonne et al., 2019) (Fig. 5.5). This connected northwestern North America with northeastern Asia during intervals of the latest Cretaceous and Paleocene (Brikiatis, 2014). European taxa could conceivably then have dispersed via Asia, although the apparent close relationship of European taxa with North American taxa (e.g. Brochu, 1999, 2004b; Martin & Lauprasert, 2010; Massonne et al., 2019, this study) suggests that this explanation is less likely. Instead, the De Geer route might have provided a high latitude connection between Greenland and Fennoscandia during the Maastrichtian–early Paleocene (Fig. 5.5), with a more southerly (Thulean) route between Greenland and western Europe possible in the late Paleocene (Brikiatis, 2014) (Fig. 5.5). Although the subtropical distribution of crocodylians today argues against such high latitude dispersal routes, the occurrence of alligatorid remains in early Eocene deposits on Ellesmere Island in the Canadian Arctic (Estes & Hutchison, 1980), demonstrates not only their polar presence (paleolatitude of $\sim 76^{o}$), but also their existence along at least the De Geer route (Fig. 5.5).

The alligatoroid fossil record is sparse in the Oligocene, represented almost entirely by occurrences of *Diplocynodon* (*D. muelleri*) in western Europe (e.g. Piras & Buscalioni, 2006; Macaluso et al., 2019). Otherwise, there are rare North American occurrences of *Alligator* that might be earliest Oligocene, in addition to reports of late Oligocene specimens (Whiting & Hastings, 2015), and some fragmentary remains have been attributed to caimanines from the late Oligocene of Peru (Antoine et al., 2016). This dearth of Oligocene occurrences characterises much of the global record of Crocodylia in general (Markwick, 1998; Mannion et al., 2019; De Celis et al., 2020; Solórzano et al., 2020). Although sampling bias almost certainly plays a role in this apparent decline, it also likely reflects genuine latitudinal range re-

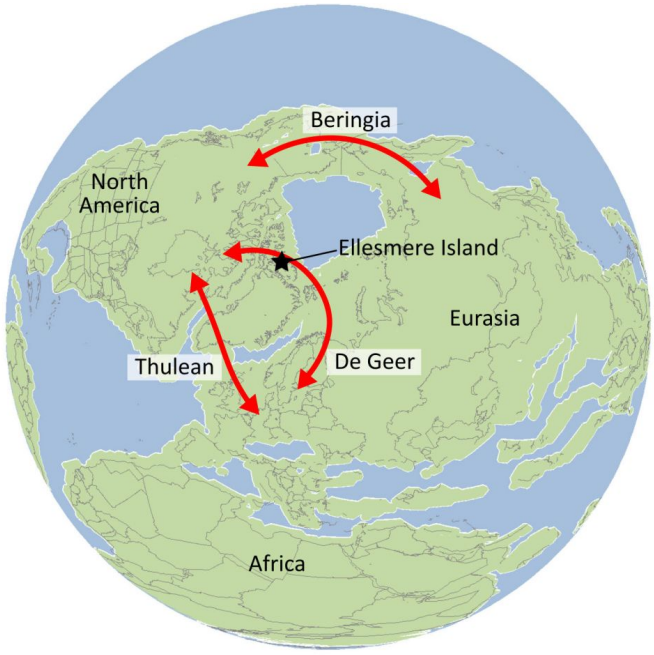



Figure 5.5: Summary of possible palaeobiogeographic routes available from the latest Cretaceous–early Paleogene, after Brikiatis (2014). Global palaeogeographical reconstruction centered on the North Pole at 66 Ma from Fossilworks (http://fossilworks.org/) (Alroy, 2013). Star indicates the location of an indeterminate alligatorid from the early Eocene, based on data in the Paleobiology Database (https://paleobiodb.org/).

traction during the Eocene–Oligocene transition (Markwick, 1998; Martin, 2010a; Mannion et al., 2015; Whiting & Hastings, 2015), which was characterised by global cooling and increased aridity (e.g. Zachos et al., 2001; Zanazzi et al., 2007; Hren et al., 2013). *Diplocynodon* remained abundant in western Europe until its last appearance in the middle Miocene, after which no further alligatoroids are known from Europe (Martin, 2010a; Martin & Gross, 2011; Aráez et al., 2017).

Most species of *Alligator* made their first appearance in the Miocene. These are predominantly North American (Mook, 1923; Schmidt, 1941; White, 1942; Mook, 1946; Brochu, 1999; Snyder, 2007), and include the earliest occurrences of the American alligator, *A. mississippiensis*, in the late Miocene, ∼8 Ma (Whiting et al., 2016b; see also Whiting & Head, 2020) (Fig. 5.6). This extant species was the only North American member of *Alligator* to survive into the Pliocene (Brochu, 1999; Whiting et al., 2016b). A small number of Miocene Asian occurrences have also been assigned to *Alligator*. As well as an isolated tooth (Chow & Wang, 1964), the most notable occurrence is *Alligator luicus* from the middle Miocene of China, which was erected based on a skull and partial postcranial skeleton (Li & Wang, 1987) (Fig. 5.6). A skull from either the late Miocene or Pleistocene of Thailand was also briefly described and figured by (Claude et al., 2011, fig. 3), who assigned it to *Alligator* cf. *sinensis*; however, the proportions of the cranium in this specimen do not resemble *A. sinensis* and this could be a new species. The earliest unequivocal occurrence of the Chinese alligator, *Alligator sinensis*, comes from the late Pliocene of Japan (Iijima et al., 2016), with Pleistocene remains known from mainland China and Taiwan (Shan et al., 2013;

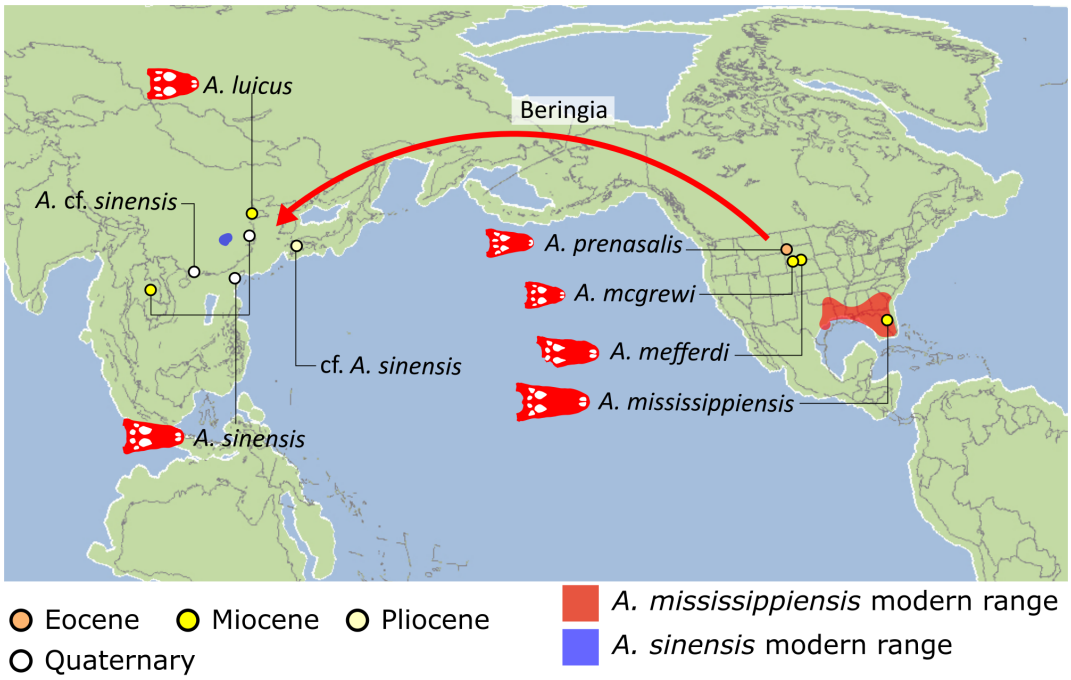



Figure 5.6: The distribution of *Alligator*. Global palaeogeographical reconstruction at 6 Ma from Fossilworks (http://fossilworks.org/) (Alroy, 2013) based on data in the Paleobiology Database (https://paleobiodb.org/). Note that only the oldest occurrence of *A. mississippiensis* is shown, because numerous specimens can be assigned to this species from the Quaternary, all of which approximately fall within its modern range.

Iijima et al., 2016) (Fig. 5.6). No other alligatoroid genus is currently recognised from the Neogene of Asia or North America. There is substantial discordance between the fossil record of *Alligator* and molecular estimates for the divergence of *A. mississippiensis* and *A. sinensis*, which has been placed at 59–30 Ma (Oaks, 2011) (Table 5.1). By contrast, my results indicate that divergence between the crown *Alligator* species occurred ∼13–10 Ma, but possibly ∼20 Ma if *Alligator thompsoni* (Mook, 1923, not studied here) belongs within the crown group (Massonne et al., 2019). As commented upon by Massonne et al. (2019), this incongruence might be the result of overestimations in the divergence of shallow nodes, which can result from using old calibration points (van Tuinen & Torres, 2015), such as the commonly used alligatorine–caimanine split (71–64 Ma) (e.g. Oaks, 2011). However, the affinities of fossil *Alligator* species in Asia are generally poorly understood, with some specimens yet to be fully described (Claude et al., 2011) and included in phylogenetic analyses (i.e. *A. luicus*). Future studies including these taxa might recover alternative alligatorine interrelationships, in which *A. sinensis* is more distantly related to *A. mississippiensis* than currently thought. Depending on the interrelationships of the genus, the presence of these Asian species indicates one or more dispersals from North America to Asia during the Neogene, probably via Beringia (Brochu, 1999, 2003; Snyder, 2007; Iijima et al., 2016; Massonne et al., 2019) (Fig. 5.6).

Caimanines also appear to have diversified both in terms of numbers of species and ecomorphological

disparity in South America during the middle–late Miocene (Scheyer et al., 2013; Salas-Gismondi et al., 2015; Scheyer & Delfino, 2016; Cidade et al., 2019a; Souza-Filho et al., 2019) (Fig. 5.7). This included the giant (∼12.5 m long) generalist predator *Purussaurus* (Aureliano et al., 2015), the indiscriminate 'gulp-feeder' *Mourasuchus* (Cidade et al., 2019d), as well as the durophagous taxa, *Gnatusuchus pebasensis*, *Kuttanacaiman iquitosensis*, and *Caiman wannlangstoni* (Salas-Gismondi et al., 2015). The analyses of Solórzano et al. (2020) suggest that this diversification might have occurred in the early Miocene, with long ghost lineages indicating that the early evolutionary history of much of this diversity might not be sampled (see also Hastings et al., 2013; Hastings et al., 2016; Solórzano et al., 2019), although many of these ghost lineages would be removed if the positions of *Bottosaurus*, *Necrosuchus*, *Protocaiman*, and *Tsoabichi* were resolved as early-diverging caimanines. Most extant caimanine species also make their first appearance in the Miocene fossil record (Cidade et al., 2019a) (Fig. 5.7). This includes the first putative occurrences of *Paleosuchus* in the middle Miocene (Salas-Gismondi et al., 2007; Salas-Gismondi et al., 2015), as well as late Miocene specimens of *Melanosuchus* (Bona et al., 2017a; Foth et al., 2017), *Caiman latirostris* (Bona et al., 2013b; Scheyer & Delfino, 2016), and *Caiman yacare* (Bona et al., 2013b).

Although absent from the USA post-Eocene, caimanines were present in Central America in the Miocene, with three species currently identified in the early Miocene of Panama (Hastings et al., 2013; Hastings et al., 2016) (Fig. 5.7), and an isolated occurrence described from the late Miocene of southern Mexico (Brochu & Carbot-Chanona, 2015). These occurrences all predate the main phase of the Great American Biotic Interchange (GABI), 2.6 Ma (Woodburne, 2010), as well as the full emergence of the Isthmus of Panama between 3.5–2.8 Ma (O'Dea et al., 2016). This could be taken to support the view that these Central American caimanines were descended from unsampled North-Central American species, as appears to be the case for early Miocene Panamanian terrestrial mammals, which nearly all show clear affinities with contemporaneous North American faunas (MacFadden et al., 2014). This might explain the ancestry of at least one Panamanian species (*Culebrasuchus mesoamericanus*), which has been recovered as one of the earliest diverging caimanines (excluding the early North American clade) in recent studies (Hastings et al., 2013; Hastings et al., 2016; Cidade et al., 2017, although see Salas-Gismondi et al. 2019 who recovered it as a species of *Alligator*). However, a number of species from the middle–late Miocene of northern South America (*Globidentosuchus brachyrostris*, *Gnatusuchus pebasensis*, and *Kuttanacaiman iquitosensis*) also occupy early diverging positions within Caimaninae (e.g. Scheyer et al., 2013; Salas-Gismondi et al., 2015; Hastings et al., 2016, this study), and the remaining Central American Miocene caimanine occurrences appear to be most closely related to South American taxa, including specimens that are similar to *Purussaurus* (Hastings et al., 2013; Brochu & Carbot-Chanona, 2015; Hastings et al., 2016). As such, it seems most likely that an earlier wave of caimanine dispersal between South and Central America occurred well before the main phase of the GABI. At face value, this would imply

dispersal across the Central American Seaway (Hastings et al., 2013), which might still have separated Central and South America by ∼200 km in the early Miocene (Montes et al., 2012) (Fig. 5.7), prior to its closure ∼10 Ma (Montes et al., 2015) and the emergence of a permanent landbridge 3.5–2.8 Ma (O'Dea et al., 2016). However, both molecular divergence times and the fossil records of plants, turtles, snakes, and non-volant birds and mammals, all provide evidence for much earlier dispersals of non-marine species, some initiating ∼20 Ma (Bacon et al., 2015; Jaramillo, 2018). Although this does not rule out the possibility that these species might have had to cross marine barriers, and rafting was likely a distinct possibility even for salt-intolerant species (O'Dea et al., 2016), it remains possible that ephemeral terrains might have facilitated these dispersals (Bacon et al., 2015). Today, *Caiman crocodilus* is the only caimanine species present naturally in Central America, extending from Brazil to as far north as Mexico (Fig. 5.7); molecular divergence estimates between subspecies and populations support a recent range extension coincident with the timing of the formation of the Isthmus of Panama and the main phase of the GABI (Venegas-Anaya et al., 2008). The fossil record of *Caiman crocodilus* is currently restricted to a single occurrence from the Plio-Pleistocene of Venezuela (Fortier & Rincón, 2013; Cidade et al., 2019b); if the late Miocene Mexican occurrence also belongs to this species, then *Caiman crocodilus* would represent an additional early dispersal of Caimaninae (Brochu & Carbot-Chanona, 2015).

As noted above, the Laurasian distribution of Alligatoroidea was restricted to the two extant species of *Alligator* by the Pliocene. A substantial diversity decline also characterises post-Miocene Alligatoroidea in South America (Fortier & Rincón, 2013; Scheyer et al., 2013; Mannion et al., 2015; Moreno-Bernal et al., 2016; De Celis et al., 2020), including the extinction of the giant taxa *Purussaurus* and *Mourasuchus*, with only extant genera remaining (Cidade et al., 2019a). This extinction has been attributed to hydrographic changes and the disappearance of the proto-Amazonian mega-wetlands (Scheyer et al., 2013; Salas-Gismondi et al., 2015), driven by Andean uplift (Hoorn et al., 2010; Rohrmann et al., 2016).

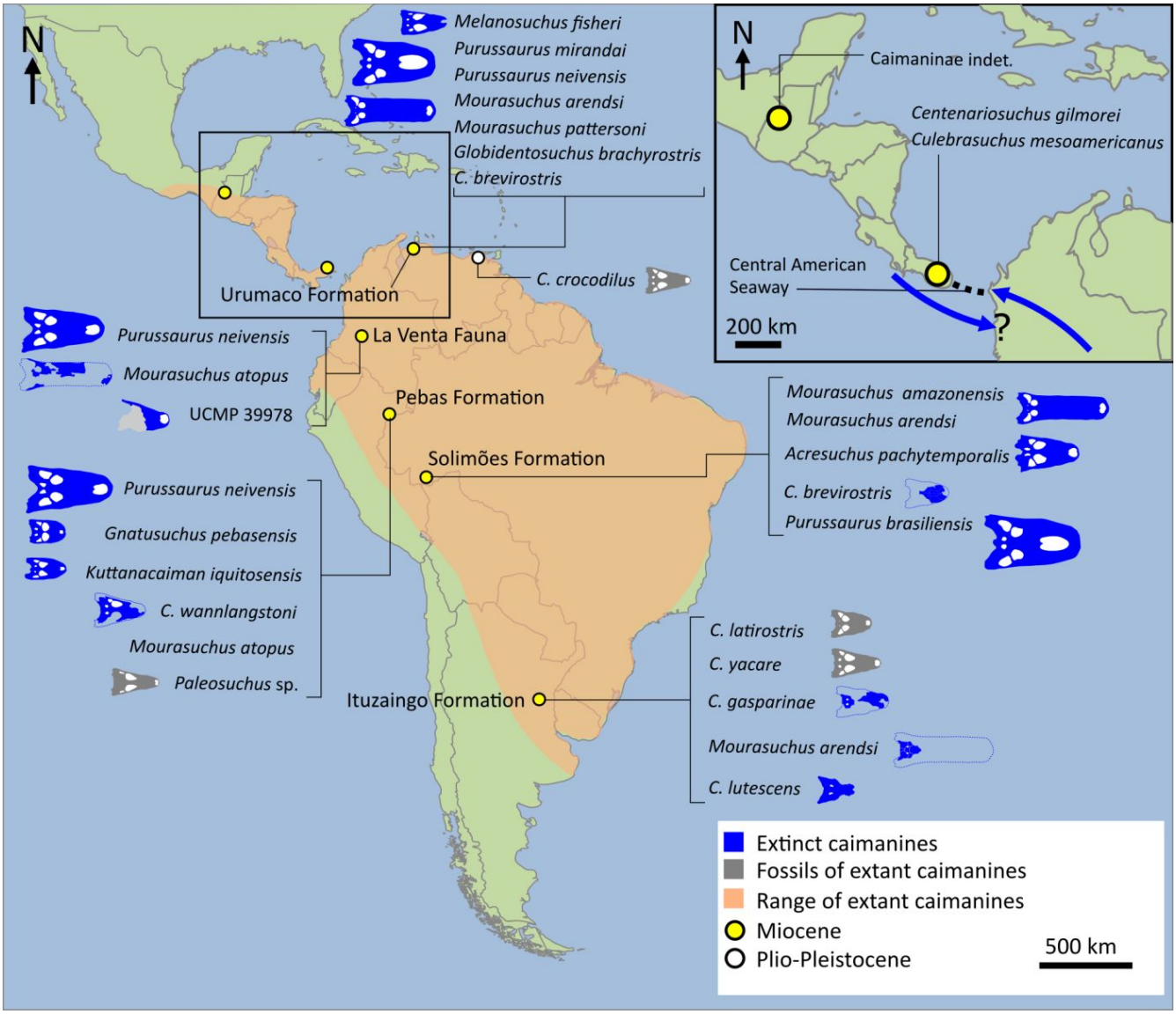



Figure 5.7: Principal South American fossil localities showing caimanine distribution from the Neogene to the Quaternary, based on data in the Paleobiology Database (https://paleobiodb.org/). Extant caimanine range taken from https://www.iucnredlist.org/. Modern map from https://en.wikipedia.org/wiki/Wikipedia:Blankmaps.

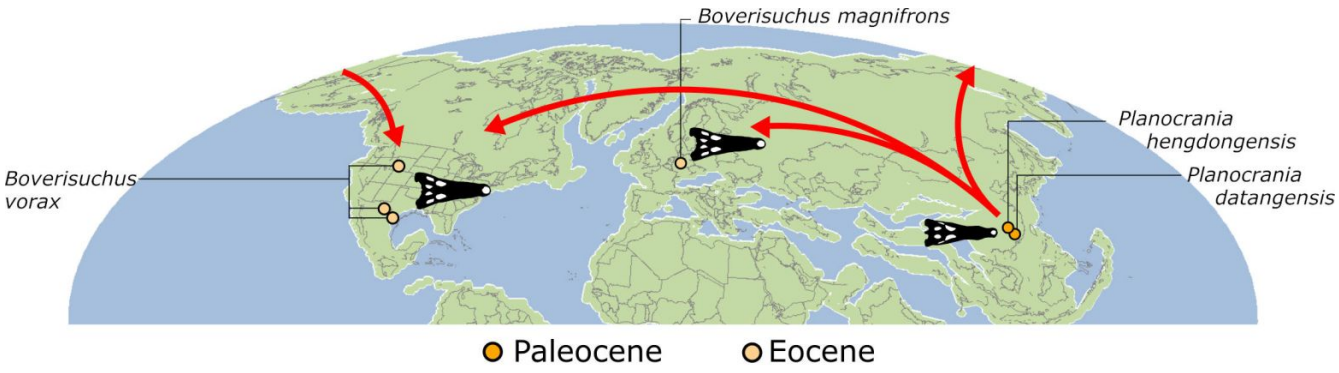



Figure 5.8: The distribution of Planocraniidae. Arrows indicate possible dispersal routes. Global palaeogeographical reconstruction at 50 Ma from Fossilworks (http://fossilworks.org/) (Alroy, 2013) based on data in the Paleobiology Database (https://paleobiodb.org/).

## 5.4 Planocraniidae

Although Planocraniidae is recovered in different positions to most previous studies (e.g. Brochu, 2012), my results still indicate that it was a short-lived Paleogene radiation of early-diverging terrestrial Laurasian crocodylians. The earliest known members of Planocraniidae appear in the middle–late Paleocene of Asia, with *Planocrania datangensis* and *Planocrania hengdongensis* (Li, 1976, 1984; Brochu, 2012) (Fig. 5.8). Following this, planocraniids most likely dispersed to North America and Europe (Kotsakis et al., 2004), where the earliest known non-Asian remains (*Boverisuchus*) unequivocally referred to the clade come from the early and middle Eocene, respectively (Kuhn, 1938; Langston, 1975; Rossmann, 2000; Brochu, 2012; Hastings & Hellmund, 2015). Regardless of the contrasting positions recovered for Planocraniidae within Crocodylia, there is a ghost lineage extending at least into the latest Cretaceous. Fragmentary remains from the Paleocene of Europe and North America might be referable to Planocraniidae (Brochu, 2012), which would both shorten this gap and question a necessarily Asian origin for the clade. Planocraniidae appears to have gone extinct by the late Eocene (Brochu, 2012; Hastings & Hellmund, 2015).

## 5.5 Crocodyloidea

As with alligatoroids, the earliest known crocodyloids are from the latest Cretaceous of Laurasia. They first appear in the fossil record later than alligatoroids, in the Maastrichtian, represented by *Albertosuchus knudsenii* (Wu & Brinkman, 2015) and *Prodiplocynodon langi* (Mook, 1941a) in North America, and possibly by *Jiangxisuchus nankangensis* in Asia (Fig. 5.9) (Li et al., 2019, although see Section 5.3 regarding the possibility of alligatoroid affinities of this species). The late Maastrichtian Spanish species *Arenysuchus gascabadilorum* was originally described as a crocodyloid (Puértolas-Pascual et al., 2011),

but is now regarded as an allodaposuchid (Narváez et al., 2015). As such, the first European appearance of Crocodyloidea is not until the late Paleocene, represented by *Asiatosuchus depressifrons* (Delfino et al., 2019) (Fig. 5.9), with several authors suggesting that crocodyloids only dispersed to Europe after the K/Pg mass extinction (Martin et al., 2014; Puértolas-Pascual et al., 2016). *Asiatosuchus depressifrons* continued into the early Eocene of Europe (Delfino & Smith, 2009), with a second European species of *Asiatosuchus* known from the middle Eocene (*A. germanicus*; Berg, 1966). Although species of *Asiatosuchus* are restricted to the early Paleogene of Eurasia (Vasse, 1992; Delfino et al., 2019), with the earliest known remains from the middle Paleocene of China (*A. nanlingensis*; Young, 1964) and Russia (*A. volgensis*; Efimov & Yarkov, 1993), it is not clear whether they form a clade (Angielczyk & Gingerich, 1998; Jouve et al., 2008; Delfino & Smith, 2009; Wang et al., 2016; Wu et al., 2018; Delfino et al., 2019; Groh et al., 2020). My analyses recover *Asiatosuchus depressifrons* and the early–middle Eocene North American species '*Crocodylus*' *affinis* (Marsh, 1871) as sister taxa, with *Asiatosuchus germanicus* and *Asiatosuchus nanlingensis* as distant lineages (Chapter 4, Fig. 4.20). Most authors consider *Asiatosuchus*-like taxa to have an Asian origin (e.g. Jouve, 2016; Wang et al., 2016), and for the European species to have dispersed from there. Pending a revision of the systematics of *Asiatosuchus*, it remains unclear which species belong to this genus, limiting our ability to determine the biogeographic history of early crocodyloids (Delfino et al., 2019). This also includes determining the affinities of a partial skeleton with similarities to *Asiatosuchus* from the middle Eocene of Pakistan (Angielczyk & Gingerich, 1998), which by then was part of Asia (Hu et al., 2016). Finally, the position of these species as some of the earliest diverging members of Crocodyloidea implies unsampled histories extending into the latest Cretaceous.

No unambiguous occurrences of crocodyloids are known from the Paleocene of North America (Fig. 5.9). However, their presence in the Maastrichtian and Eocene of that continent (Brochu, 2000) suggests that this Paleocene dearth is most likely a sampling artefact, rather than a genuine absence. Given that they were a rare component of latest Cretaceous ecosystems (Brochu, 2000), they might have remained low in abundance and diversity during the Paleocene. However, it is possible that Crocodyloidea became regionally extinct in North America at the K/Pg boundary, with their Eocene representatives (*Brachyuranochampsa eversolei*, '*Crocodylus*' *acer*, and '*Crocodylus*' *affinis* [Marsh, 1871; Cope, 1882; Mook, 1921; Zangerl, 1944]) descended from Eurasian immigrants (see also Planocraniidae). Crocodyloidea appears to have gone extinct in North America in the late Eocene, with no unambiguous occurrences until the appearance of *Crocodylus* in the late Pliocene (Miller, 1980), although the clade might have returned as early as the late Miocene (Carbot-Chanona, 2017). A similar pattern characterises Europe, with crocodyloids absent from the late Eocene until the appearance of *Crocodylus* (or close relatives) in the late Miocene (Delfino et al., 2007; Delfino & Rook, 2008; Delfino & Rossi, 2013). By contrast, at least one crocodyloid (*Astorgosuchus bugtiensis*) has been recognised from the Oligocene of Asia (Martin et

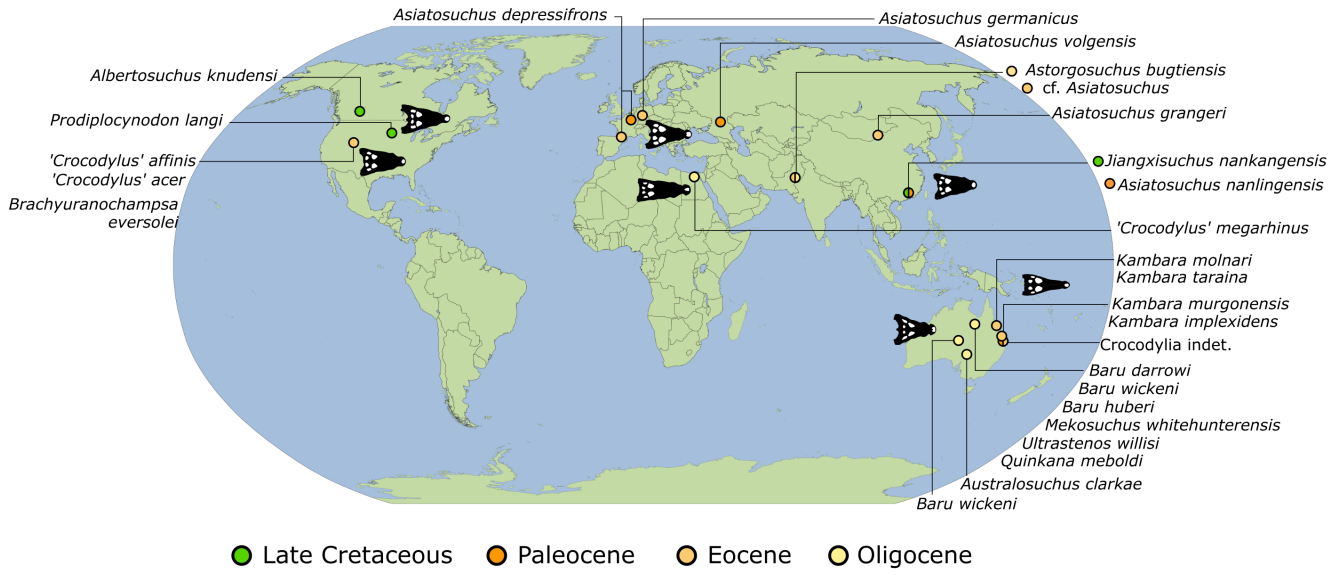



Figure 5.9: The distribution of named/distinct crocodyloids in the latest Cretaceous and Paleogene. Indeterminate remains discussed in text. Based on data in the Paleobiology Database (https://paleobiodb.org/). Modern map from https://en.wikipedia.org/wiki/Wikipedia:Blankmaps. Note than *Australosuchus* and *Baru darrowi* are known from late Oligocene–early Miocene sites.

al., 2019a).

The first record of crocodylians in Australasia occurs in the early Eocene, with mekosuchine crocodyloids *Kambara implexidens* and *Kambara murgonensis* from Australia (Willis et al., 1993; Salisbury & Willis, 1996) (Fig. 5.9). However, an indeterminate occurrence from either the late Paleocene or early Eocene of Australia could predate this (Willis & Molnar, 1991a; Willis, 1997b). Mekosuchinae has been universally regarded as endemic to Australasia; however, its origin has remained enigmatic given its labile position in relation to other members of Longirostres (e.g. Salisbury & Willis, 1996; Brochu & Storrs, 2012; Lee & Yates, 2018). Here, *Asiatosuchus nanlingensis* is recovered as a mekosuchine, within the *Kambara* clade. Combined with the recovery of *Jiangxisuchus nankangensis* as the sister taxon of Mekosuchinae + Crocodylidae in my analyses (Chapter 4: Fig. 4.20), these results provide support for an Asian origin of the clade. An early, cosmopolitan distribution of Crocodyloidea, prior to Gondwanan fragmentation, is extremely unlikely. A terrestrial dispersal route from Asia to Australasia (Fig. 5.10A) would require dispersal through North and South America, as well as Antarctica. Australasia and Antarctica likely retained a connection with South America until the late early Eocene (Wilf et al., 2013), which would fit well with the timing of the earliest appearance of Mekosuchinae in Australasia. Dispersal between Asia and North America in the early Paleogene appears to have been possible, and the presence of 'basal' crocodyloids (e.g. '*Crocodylus*' *affinis*) on the latter continent accords with this scenario. However, this implies that there is an unsampled latest Cretaceous–early Paleogene crocodyloid fossil record in South America. The earliest unambiguous crocodyloid occurrence in South America is

*Crocodylus falconensis* from the early Pliocene of Venezuela (Scheyer et al., 2013). *Brasilosuchus* and *Charactosuchus*, from the middle–late Miocene of Brazil, Colombia, and Venezuela (Langston, 1965; Souza-Filho & Bocquentin, 1989; Souza-Filho, 1991; Scheyer et al., 2013), have been tentatively assigned to "Crocodylidae" or "Tomistominae" by several authors (Langston, 1965; Piras et al., 2007), but even if this is correct these occurrences substantially postdate the possible window for South America to Australasia dispersal. An additional species, "*Charactosuchus*" *kugleri*, from the middle Eocene of Jamaica (Berg, 1969), could provide support that southward dispersal of crocodyloids from North America did occur around this time, but this species is generally thought to be most closely related to "Tomistominae" (e.g. Brochu, 2007b). Furthermore, as noted in Section 5.3, it is not clear that a continuous terrestrial dispersal route between North and South America existed during the Paleogene.

Although we cannot rule out the possibility that crocodyloids might have been present in the latest Cretaceous–early Paleogene of South America, especially given that paleogeographic constraints suggest caimanines might also be unsampled in the latest Cretaceous, the remaining alternative is that mekosuchines colonised Australasia from Asia via oceanic dispersal (Fig. 5.10A). Today, the Indo-Australian (=Malay/Malesia) Archipelago comprises a chain of more than 20,000 islands extending between southeast Asia and Australia (Lohman et al., 2011), and has probably facilitated the distribution of extant *Crocodylus porosus* (Webb et al., 2010). However, this archipelago did not exist in the early Cenozoic, with the eastern Tethys forming a large oceanic barrier between Asia and Australasia, which only began to reduce in the middle Eocene with the northward movement of the Australian plate (Lohman et al., 2011). Although most mekosuchines are known from freshwater environments (Salisbury & Willis, 1996), saltwater tolerance was probably plesiomorphic for Longirostres, based on adaptations in all extant members of the clade such as a keritanised buccal cavity and osmoregulatory pores on the tongue (Taplin & Grigg, 1989). Furthermore, mekosuchines reached several islands in the South Pacific, with their remains known from late Pleistocene–Holocene deposits in Fiji, New Caledonia, and Vanuatu (Balouet & Buffetaut, 1987; Mead et al., 2002; Molnar et al., 2002) (Fig. 5.10B), and possibly from the early Miocene of New Zealand (Molnar & Pole, 1997; Molnar et al., 2002). At face value, these remains would support the notion that Mekosuchinae was capable of oceanic dispersal, although the distances involved would have been dwarfed by that posed by an early Paleogene dispersal from Asia to Australia. Lower sea levels during the Pleistocene glaciations might have facilitated some of these shorter dispersals (Mead et al., 2002), but given that there are potentially long ghost lineages (>20 Myr) leading to some of these Quaternary species (e.g. Lee & Yates, 2018, see also Chapter 4, Fig. 4.20), it remains possible that the ancestors of these island occurrences were present in the South Pacific much earlier, with the early Miocene New Zealand occurrence providing tentative additional support for this scenario (Molnar et al., 2002). Zealandia (including New Zealand and New Caledonia) started to separate from Gondwana in the latest Cretaceous, with continental connections severed in the early Paleogene, and its

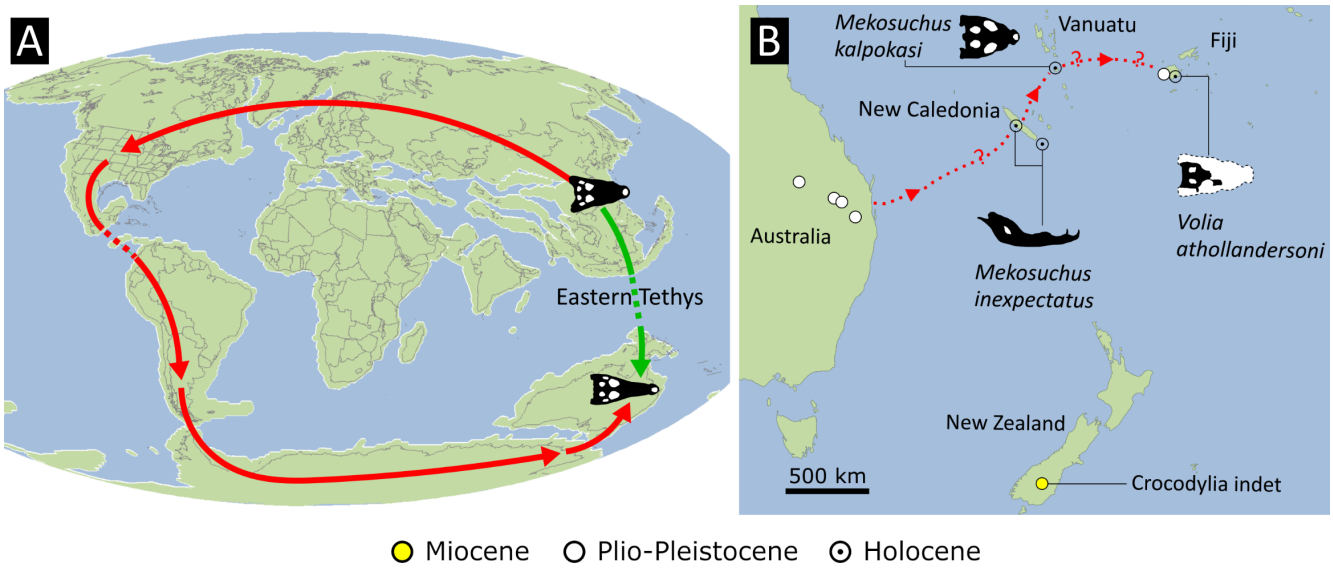



Figure 5.10: Mekosuchine dispersal routes. **A**: Global palaeogeographical reconstruction at 50 Ma from Fossilworks (http://fossilworks.org/) (Alroy, 2013) with arrows showing alternative dispersal routes for an Asian origin of Mekosuchinae. **B**: the distribution of named mekosuchines in eastern Australia and South Pacific islands from the Neogene and Quaternary. Based on data in the Paleobiology Database (https://paleobiodb.org/). Modern map from https://en.wikipedia.org/wiki/Wikipedia:Blankmaps.

approximate present-day distance from Australia established during the middle Eocene (Schellart et al., 2006; Mortimer et al., 2017). Seamounts might have provided stepping-stones to Zealandia, but these were submerged from approximately the early Miocene, which could provide some constraints on when these crocodylians (and other terrestrial groups) dispersed (Worthy et al., 2017). Vanuatu and Fiji lie northeast of New Caledonia (Fig. 5.10B); they likely formed in the late Eocene (Neall & Trewick, 2008), and probably never had a direct continental connection (Mead et al., 2002). As such, it seems difficult to reconcile the distribution of mekosuchines in the South Pacific without some degree of oceanic dispersal. Interestingly, this study is not the first time that a close affinity between *Asiatosuchus* and Mekosuchinae has been proposed. Salisbury and Willis (1996) recovered a sister taxon relationship between the Australasian clade and *Asiatosuchus germanicus*, although they regarded this as probably convergence, especially given their geographic separation. Whilst I also remain sceptical of these results, it is noteworthy that at least two occurrences of an *Asiatosuchus*-like taxon have been discovered in marine deposits (Efimov & Yarkov, 1993; Angielczyk & Gingerich, 1998), indicating the possibility that these early crocodyloids might have possessed adaptions for saltwater tolerance (see also Berg, 1969).

Whereas the Oligocene appears to represent a global nadir in crocodylian diversity (Mannion et al., 2015), crocodyloids are the exception (De Celis et al., 2020). This is almost entirely a result of the apparent diversification of mekosuchines in the late Oligocene–early Miocene of Australia, including the appearance of platyrostral taxa such as *Baru* (Willis et al., 1990; Yates, 2017), as well as the dwarf forms *Mekosuchus whitehunterensis* (Willis, 1997a) and *Ultrastenos willisi* (Stein et al., 2016). Mekosuchines

remained diverse throughout the Miocene, including *Baru darrowi* (Willis et al., 1990), *Trilophosuchus rackhami* (Willis, 1993), and *Mekosuchus sanderi* (Willis, 2001). A number of mekosuchines are also known from the Plio-Pleistocene of Australia, including *Kalthfirons* (Yates & Pledge, 2017) and *Pallimnarchus* (Willis & Molnar, 1997). Mekosuchinae appears to have gone extinct on the Australian mainland as part of the late Pleistocene megafaunal extinction (e.g. Hocknull et al., 2020), with the South Pacific island species of *Mekosuchus* (*M. inexpectatus* and *M. kalpokasi*) and *Volia athollandersoni* the last remnants of this clade (Balouet & Buffetaut, 1987; Mead et al., 2002; Molnar et al., 2002). My analyses place two Australian taxa that are usually recovered as mekosuchines on the crocodylid line instead (Fig. 4.20). *Australosuchus clarkae* and *Quinkana* both first appear in the late Oligocene–early Miocene (Willis & Molnar, 1991b; Megirian, 1994; Willis, 1997a), with the latter taxon present until the Pleistocene (Molnar, 1982d). Whereas *Quinkana* was deeply nested within Mekosuchinae in the analyses of Yates and Pledge (2017) and Lee and Yates (2018), *Australosuchus clarkae* was recovered as the earliest diverging mekosuchine, and thus its placement as the sister taxon to Crocodylidae in my study does not have much overall effect on the crocodyloid topology. Furthermore, the position of both taxa in my study is a better stratigraphic fit, reducing the length of ghost lineages. However, my results would mean that crocodylids reached Australasia at least twice, with Pliocene remains assigned to *Crocodylus* the stratigraphically oldest unequivocal occurrences of the clade on this continent (Molnar, 1982c; Yates & Pledge, 2017). The decline and eventual extinction of mekosuchines might have been driven by increasing aridification of Australia (e.g. Martin, 2006; Hocknull et al., 2020), exacerbated by competition from the arrival of *Crocodylus* (Willis, 1997b; Yates & Pledge, 2017).

The early Oligocene records the first appearance of Crocodyloidea in Africa, represented by the crocodyline '*Crocodylus*' *megarhinus* in Egypt (Andrews, 1905; Mook, 1927; Brochu, 2000). It is here recovered as the sister taxon of *Quinkana*, forming the earliest diverging crocodyline clade. The Egyptian species also indicates that the divergence between Crocodylinae and Osteolaeminae had occurred at least by the Oligocene, in accordance with molecular divergence estimates, which place this between 32–19 Ma (Oaks, 2011) (Table 5.1). Whereas the consensus of recent molecular phylogenies places *Mecistops* as the sister taxon to Osteolaeminae (Schmitz et al., 2003; McAliley et al., 2006; Man et al., 2011; Oaks, 2011; Shirley et al., 2014), my topology is consistent with previous morphological analyses (e.g. Brochu et al., 2010; Conrad et al., 2013; Brochu, 2020) that recover *Mecistops* as closer to *Crocodylus*, and thus part of Crocodylinae.

Osteolaemines first appear in the fossil record later than Crocodylinae, with the stratigraphically oldest occurrences known from the early Miocene of north and east Africa (Brochu, 2000, 2007a; Conrad et al., 2013) (Fig. 5.11), represented by the earliest diverging taxa *Euthecodon arambourgi* (Ginsburg & Buffetaut, 1978) and *Brochuchus pigotti* (Tchernov & Van Couvering, 1978; Conrad et al., 2013). The clade remained endemic to Africa (Brochu, 2007a), including the early–middle Miocene taxon *Rima-*

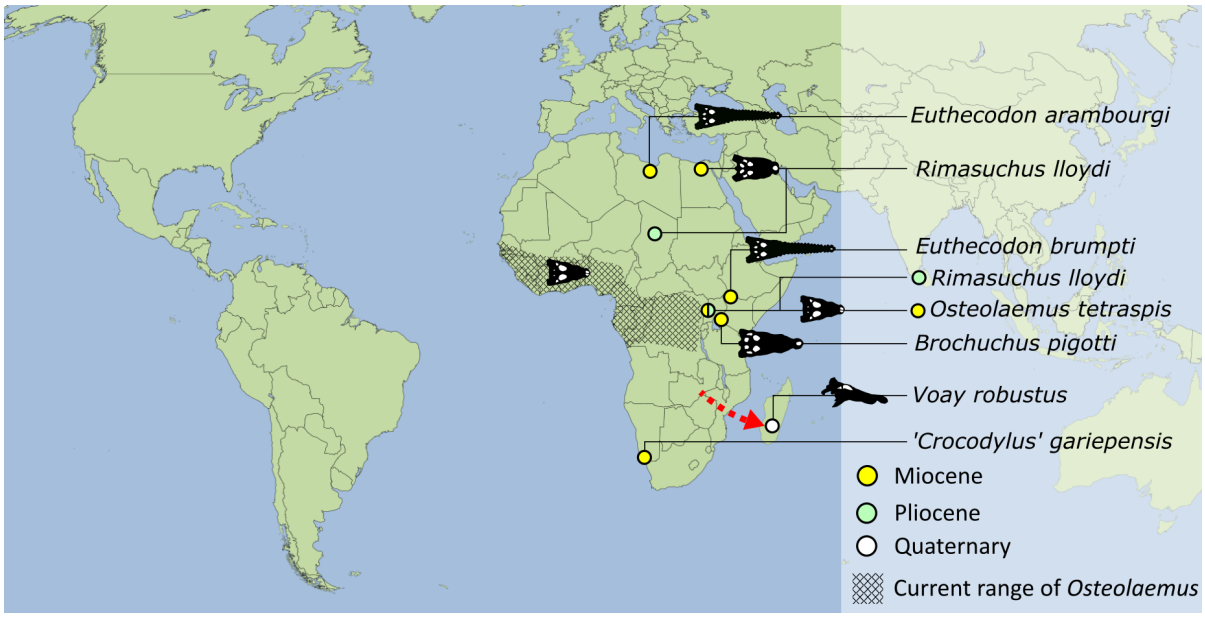



Figure 5.11: The distribution of named osteolaemines. Fossil occurrences based on data in the Paleobiology Database (https://paleobiodb.org/), modern range of *Osteolaemus* based on Shirley et al. (2015). Modern map from https://en.wikipedia.org/wiki/Wikipedia:Blankmaps.

*suchus lloydi* (Fourtau, 1920; Joleaud, 1920; Storrs, 2003; Brochu, 2020). The early Miocene Namibian species '*Crocodylus*' *gariepensis* (Pickford, 2003) might represent an additional osteolaemine based on its position in the topology of Brochu and Storrs (2012), although the analysis of Conrad et al. (2013) recovered it (and *Euthecodon*) in a clade with *Mecistops*. Remains attributed to the extant genus *Osteolaemus* first appear in the late Miocene (Aoki, 1976; Pickford, 1994). One species consistently recovered in Osteolaeminae, *Voay robustus*, is known from outside mainland Africa, with numerous remains present in late Pleistocene–Holocene deposits on Madagascar (Brochu, 2007a; Bickelmann & Klein, 2009). Given Madagascar's geologically long history of isolation, the *Voay* lineage must have undergone oceanic dispersal to have reached the island (Brochu, 2007a) (Fig. 5.11). However, its sister taxon relationship with *Osteolaemus* means that there is at least a 10 myr ghost lineage leading to *Voay*, and thus this dispersal could potentially have occurred at any point in that unsampled window. Osteolaeminae appears to have been a relatively depauperate clade, but many Neogene specimens previously attributed to *Rimasuchus* and other taxa likely represent a richer diversity than currently recognised (e.g. Brochu, 2007a; Brochu & Storrs, 2012, see also Brochu and Sumrall, 2020).

Crocodylinae seems to have diversified in the Miocene (Densmore, 1983; Brochu, 2000; Oaks, 2011), with the first appearances of both the sub-Saharan African taxon *Mecistops* (Tchernov, 1986; Pickford, 1994; Storrs, 2003; Brochu, 2020) and species of the crown genus *Crocodylus* (Brochu, 2000; Brochu & Storrs, 2012), which corresponds well with molecular divergence estimates for the origins of these genera (Oaks, 2011). Late Miocene *Crocodylus* comprises *C. palaeindicus* in Indo-Pakistan (Lydekker, 1886;

Mook, 1933), *C. checchiai* from north and east Africa (Maccagno, 1947; Delfino, 2008; Brochu & Storrs, 2012), *C. niloticus* in sub-Saharan Africa (Storrs, 2003; Brochu & Storrs, 2012), and indeterminate occurrences that extend the distribution of the genus into southern Europe (Kotsakis et al., 2004; Delfino et al., 2007; Delfino & Rook, 2008; Delfino & Rossi, 2013) and possibly even Central America (Carbot-Chanona, 2017) (Fig. 5.12). By the Pliocene, *Crocodylus* had achieved a circumtropical distribution (Brochu, 2000; Meredith et al., 2011; Oaks, 2011), as exemplified by the earliest remains referable to *C. porosus* in Australia (Molnar, 1982b) and the extinct species *C. falconensis* in Venezuela (Scheyer et al., 2013) (Fig. 5.12).

Biogeographic implications based on the intrarelationships of Crocodylinae recovered here are tentative given their low support in my topology, and the notable difference in the placement of *Croodylus niloticus* compared to most previous studies. Determining the biogeographic origin of *Crocodylus* has proven difficult (Brochu, 2000), partly because of disagreements and poor resolution in phylogenetic relationships, but also because the genus appears in the late Miocene fossil record of Africa, Asia, and Europe approximately simultaneously. The recovery of *Mecistops* as the sister taxon to the crown genus *Crocodylus*, the 'basal' positions of '*Crocodylus*' *megarhinus* and the Plio-Pleistocene East African species *Crocodylus thorbjarnarsoni* (Brochu & Storrs, 2012) within Crocodylinae, and the geographic distribution of the crocodyline sister taxon Osteolaeminae, all potentially support an African origin of *Crocodylus*, which is the long-held 'traditional' view (e.g. Brochu, 2000). This contrasts with recent studies based only on extant crocodylian species, which recover an Indo-Pacific origin for *Crocodylus*, either in Australasia (Oaks, 2011) or Asia (Nicolaï & Matzke, 2019). Excluding species outside of crown *Crocodylus*, my topology is generally biogeographically congruent with those two studies. Although I recover them as a paraphyletic array, rather than a 'basal' clade, the Australasian species *C. johnstoni* and the two Indo-Pacific island species, *C. novaeguineae* and *C. mindorensis*, are the earliest-diverging species of *Crocodylus* in my study (though note that the latter two species have no fossil record, and the earliest occurrence of *C. johnstoni* is from the Pleistocene [Willis and Archer, 1990]). I also recover a division between a clade of primarily Indo-Pacific species (including *C. porosus*) and an entirely Neotropical clade, in which the main difference with that of previous studies is that *C. niloticus* is recovered in the former, rather than the latter clade. Even here, this difference only places *C. niloticus* at the 'base' of one clade rather than the other. This means that my topology is still concordant with a trans-Atlantic oceanic dispersal from Africa for the Neotropical radiation of *Crocodylus* (Densmore & White, 1991; Brochu, 2000; Brochu et al., 2007; Meredith et al., 2011; Oaks, 2011; Nicolaï & Matzke, 2019) (Fig. 5.12), prior to its first unambiguous appearance in the Pliocene of northern South America (Scheyer et al., 2013). None of the extant Neotropical *Crocodylus* species appear in the fossil record until the Pleistocene (e.g. Mook, 1959a; Varona, 1984; Morgan et al., 1993; Morgan & Albury, 2013), which supports the view that this clade diversified in the Americas. My results indicate at least two dispersal events of *Crocody-*

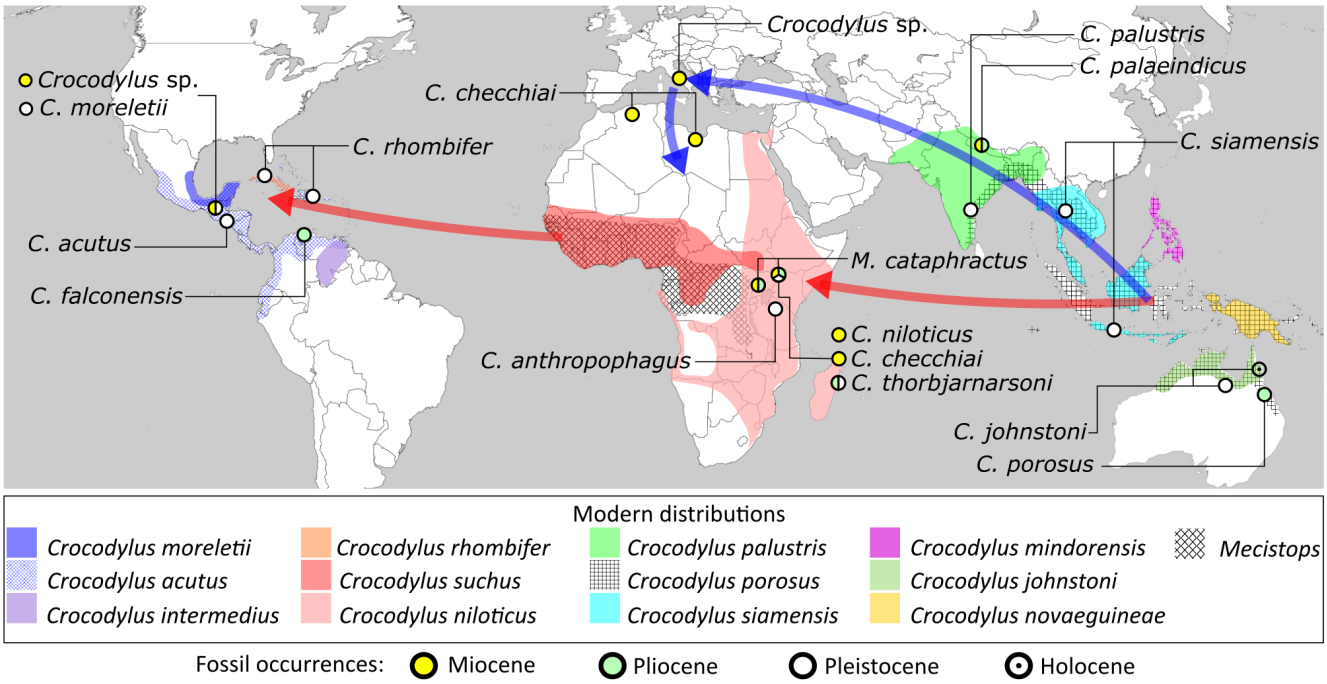



Figure 5.12: The distribution of *Crocodylus*, Neogene to Recent. Fossil occurrences based on data in the Paleobiology Database (https://paleobiodb.org/), modern ranges taken from https://www.iucnredlist.org/. Modern map taken from https://en.wikipedia.org/wiki/Wikipedia:Blankmaps.

*lus* from the Indo-Pacific to Africa. The first of these took place by the late Miocene, giving rise to *C. niloticus* (e.g. Oaks, 2011), with a more recent, second dispersal leading to *C. anthropophagus*, known from the Plio-Pleistocene of East Africa (Brochu et al., 2010). The earlier dispersal has generally been presumed to have been trans-oceanic (e.g. Oaks, 2011), but it remains possible that dispersal from Asia to Africa occurred via Europe (Fig. 5.12), and that the southern European occurrences of *Crocodylus* do not necessarily represent African immigrants (Nicolaï & Matzke, 2019), as is usually proposed (e.g. Delfino et al., 2007; Delfino & Rook, 2008). However, less fragmentary European specimens are required to test this hypothesis. A European route for the second dispersal event is harder to envisage given the complete absence of crocodylian fossils from Europe from the earliest Pliocene, which likely reflects a regional extinction (Kotsakis et al., 2004; Delfino et al., 2007; Delfino & Rossi, 2013).

*Crocodylus palaeindicus* remained present in Indo-Pakistan during the Pliocene, and it has been suggested that the extant species in that region, *C. palustris*, might be its descendent (e.g. Lydekker, 1886; Mook, 1933). My analysis recovers them as sister taxa, providing tentative support for an ancestor-descendent relationship. Currently, the published Quaternary record of *Crocodylus* from Indo-Pakistan comprises largely fragmentary materials, and much of this is probably attributed to *C. palustris* based on geography rather than autapomorphies (Brochu & Sumrall, 2020). The most complete remains referred are still highly fragmentary and latest Pleistocene in age (Shankar & Rao, 1994); as such, better preserved material that bridges the temporal gap between the last occurrences of *C. palaeindicus* and ear-

liest appearance of *C. palustris* are needed to further test this hypothesis, as well as to determine whether there was a greater species richness of *Crocodylus* present in Indo-Pakistan during the Plio-Pleistocene. This is also important with regards to understanding the evolutionary and biogeographic history of the Critically Endangered Indo-Pacific species *C. siamensis* (Bezuijen et al., 2012). Based on its Pleistocene fossil record (Delfino & De Vos, 2010; Lauprasert et al., 2019), it has been suggested that this species dispersed to Java from Indo-Pakistan, via Thailand (the Siva-Malayan route). However, my analysis positions *C. porosus* as its closest living relative, which is supported by some molecular analyses (e.g. Meganathan et al., 2010; Meredith et al., 2011), but not others, which recover it as the sister taxon of *C. palustris* (e.g. Li et al., 2007; Oaks, 2011). New molecular and morphological data might be needed to reconcile these differences.

## 5.6 Gavialoidea

Until now, the biogeographic histories of "Tomistominae" and "Gavialoidea" could be discussed independently, and when treated as such the interrelationships of the two groups were relatively stratigraphically congruent (e.g. Piras et al., 2007; Jouve et al., 2015; Jouve, 2016; Salas-Gismondi et al., 2016; Salas-Gismondi et al., 2019, see also Chapter 1, Fig. 1.8). Here, taxa usually included within "Tomistominae" comprise a paraphyletic array, primarily forming successive outgroups to Gavialidae (*Gavialis* + *Tomistoma*), which is similar to the topologies recovered in combined (morphology + molecular) analyses (Gold et al., 2014; Lee & Yates, 2018; Iijima & Kobayashi, 2019). This also fills the 'gavialoid gap' that has been noted in the Eocene (Brochu, 2006b). However, although I reconcile the placement of *Gavialis* as more closely related to *Tomistoma* than to any other extant crocodylian for the first time solely from morphology, my topology still results in a number of conspicuously long ghost lineages for many taxa, including most "tomistomines". This partly stems from a much earlier divergence between *Gavialis* and *Tomistoma* than estimated from molecular analyses, with the most recent studies placing this split at 30–16 Ma (Oaks, 2011; Pan et al., 2020). My topology places this split no later than ∼100 Ma if *Portugalosuchus* is a gavialid, as recovered here (Table 5.1). Even excluding *Portugalosuchus*, the placement of two clades of 'thoracosaurs' within Gavialidae would still extend the latter clade back into the latest Cretaceous, ∼80–70 Ma, given the Campanian age of the earliest putative specimens of *Thoracosaurus neocesariensis*, and the Maastrichtian age of unequivocal remains of this and additional species (Brochu, 2004a). The forced exclusion of *Portugalosuchus* and 'thoracosaurs' (except *Argochampsa krebsi* and *Eogavialis*) from Gavialoidea in one of my constrained analyses (Section 4.4.7) only goes some way to resolving these issues, with Gavialidae appearing in the Paleocene in my topology and long ghost lineages still present within the clade. Even without considering the Paleocene Moroccan taxon *Argochampsa krebsi* (Hua & Jouve, 2004; Jouve et al., 2006b) or the earliest known *Eogavialis*

(*E. africanum* from the late Eocene of Egypt [Andrews, 1906]), there are still two gavialids in the topology that appear in the fossil record earlier than 30 Ma: *Paratomistoma courti* and '*Tomistoma*' *cairense* from the middle Eocene of Egypt (Müller, 1927; Brochu & Gingerich, 2000). In addition to *Portugalosuchus* and 'thoracosaurs' this might indicate that the recovery of these taxa within Gavialidae is also a misleading phylogenetic signal.

Two gavialoid clades are recovered outside of Gavialidae. The earliest diverging of these consists of the early Eocene Moroccan species *Maroccosuchus zennaroi* (Jonet & Wouters, 1977; Jouve et al., 2015) as the sister taxon to an early–middle Eocene western European clade comprising *Dollosuchoides densmorei* and *Kentisuchus* (Brochu, 2007b; Jouve, 2016) (Chapter 4, Fig. 4.11). Previous analyses have recovered these taxa as a paraphyletic array leading to more nested "tomistomines" (Brochu, 2007b; Jouve, 2016; Iijima & Kobayashi, 2019). The recovery of this Afro-European clade supports previous suggestions that western Tethys was important in the early evolutionary history of the group (Jouve et al., 2015; Jouve, 2016) (Fig. 5.13). Other contemporaneous species in this region might also belong to this clade, including the middle Eocene European taxon *Megadontosuchus arduini* (Zigno, 1880; Piras et al., 2007), as well as several poorly known and neglected Eocene–Oligocene Central Asian taxa ('*Dollosuchus zajsanicus*', *Ferganosuchus planus*, and '*Tomistoma borisovi*' Efimov, 1982, 1988, 1993), whose affinities remain uncertain (Brochu, 2007b; Piras et al., 2007; Jouve et al., 2015) (Fig. 5.13).

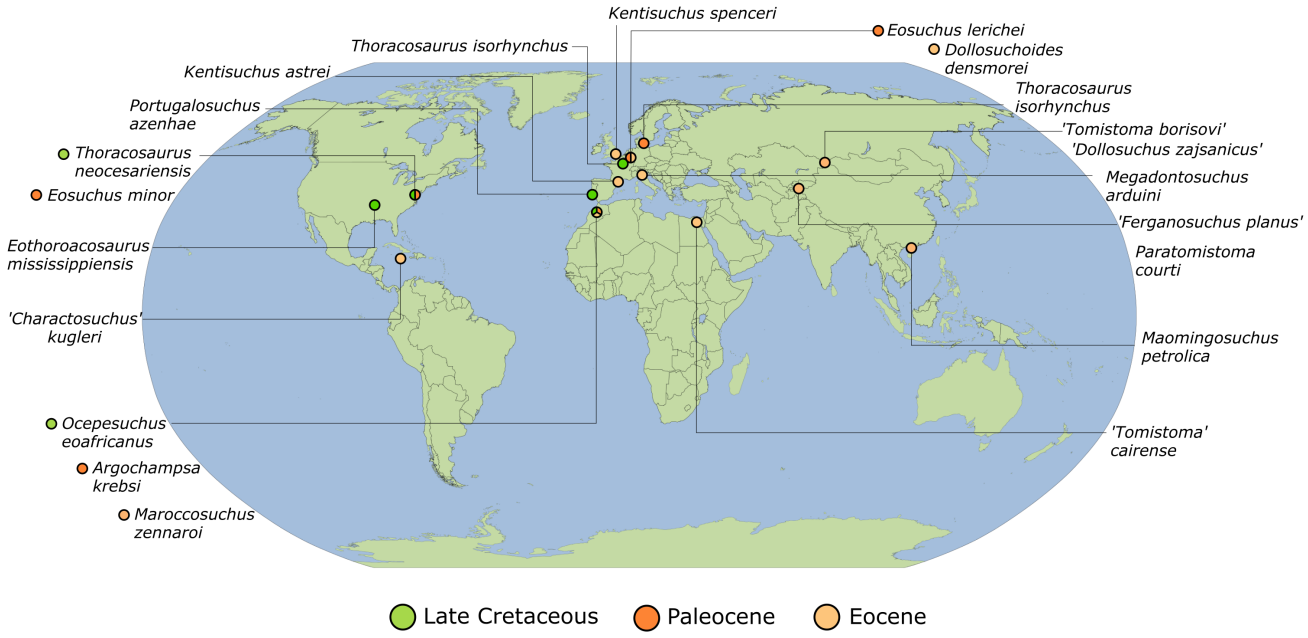



Figure 5.13: The distribution of named gavialoid species from the Cretaceous to Eocene. Fossil occurrences based on data in the Paleobiology Database (https://paleobiodb.org/). Modern ranges taken from https://www.iucnredlist.org/. Modern map taken from https://en.wikipedia.org/wiki/Wikipedia:Blankmaps.

The second of the non-gavialid gavialoid clades places the late Eocene East Asian species *Maomingosuchus petrolica* (Yeh, 1958; Shan et al., 2017; Martin et al., 2019b) as the sister taxon to a clade of

late Oligocene–Miocene western European (*Gavialosuchus eggenburgensis* and '*Tomistoma*' *lusitanica*) and North American (*Thecachampsa*) taxa (Fig. 4.11). A close relationship between *Maomingosuchus petrolica* and these European species was also recovered by Shan et al. (2017). There is a rich fossil record of gavialoids in the Mediterranean region of Europe during the middle–late Miocene (Piras et al., 2007) (Fig. 5.14), comprising *Gavialosuchus eggenburgensis* (Toula & Kail, 1885) and '*Tomistoma*' *lusitanica* (Vianna & Moraes, 1945; Antunes, 1961), as well as fragmentary remains that form the basis of four taxa named in the $19^{th}$ century: *Melitosaurus champsoides* (Owen, 1850), '*Tomistoma*' *gaudense* (Hulke, 1871), '*Tomistoma*' *calaritanum* (Capellini, 1890a, 1890b), and '*Tomistoma*' *lyceense* (Costa, 1848). A recent revision suggests that these fragmentary remains belong to the same lineage as *Gavialosuchus eggenburgensis* and '*Tomistoma*' *lusitanica*, but that they might represent one or two additional contemporaneous species (Nicholl et al., in prep). The multispecific *Thecachampsa* is known from abundant remains from the late Oligocene–Miocene of North America (Sellards, 1915; Auffenberg, 1954; Erickson & Sawyer, 1996; Myrick, 2001; Laurito & Valerio, 2008; Whiting et al., 2016a; Weems, 2018). The recovery of *Thecachampsa* within this clade differs from the results of nearly all previous phylogenetic analyses, which have recovered *Gavialosuchus* and *Thecachampsa* as more distantly related members of "Tomistominae" (e.g. Brochu, 2007b; Jouve, 2016, though see Lee & Yates, 2018 for a sister taxon relationship). This relationship partly accords with earlier workers who referred the North American remains to *Gavialosuchus* (e.g. Sellards, 1915; Auffenberg, 1954; Erickson & Sawyer, 1996). The close relationship with European forms suggests biotic exchange between North America and Europe around this time, in addition to an earlier connection with Asia (Jouve, 2016). These late Miocene occurrences mark the last appearances of gavialoids in both Europe and North America. Only one fossil species is recognised as belonging to Tomistominae sensu stricto here, and this is the aforementioned *Paratomistoma courti*. Similarly, combined analyses have also recovered a depauperate Tomistominae, with '*Tomistoma*' *lusitanica* the only fossil species in Lee and Yates (2018), and the clade monospecific in Iijima and Kobayashi (2019). All of these scenarios result in a long ghost lineage leading to the extant species, *Tomistoma schlegelii*, which currently lacks a fossil record (Piras et al., 2007). The earliest diverging members of non-tomistomine Gavialidae are two species that we might predict should be close relatives of *Tomistoma schlegelii*, given their spatiotemporal distribution. These are *Penghusuchus pani* from the late Miocene of Taiwan (Shan et al., 2009) and *Toyotamaphimeia machikanensis* from the Pleistocene (and possibly Pliocene too) of Japan (Kobatake et al., 1965; Kobayashi et al., 2006; Iijima et al., 2018b). Yet, previous analyses have also failed to recover a close relationship between these taxa and *Tomistoma schlegelii* (Shan et al., 2009; Jouve, 2016; Lee & Yates, 2018; Iijima & Kobayashi, 2019), and thus might indicate the presence of several gavialid lineages in the late Neogene–Quaternary of east and southeast Asia.

Although not included in my analysis, Lee and Yates (2018) recovered *Harpacochampsa camfielden-*

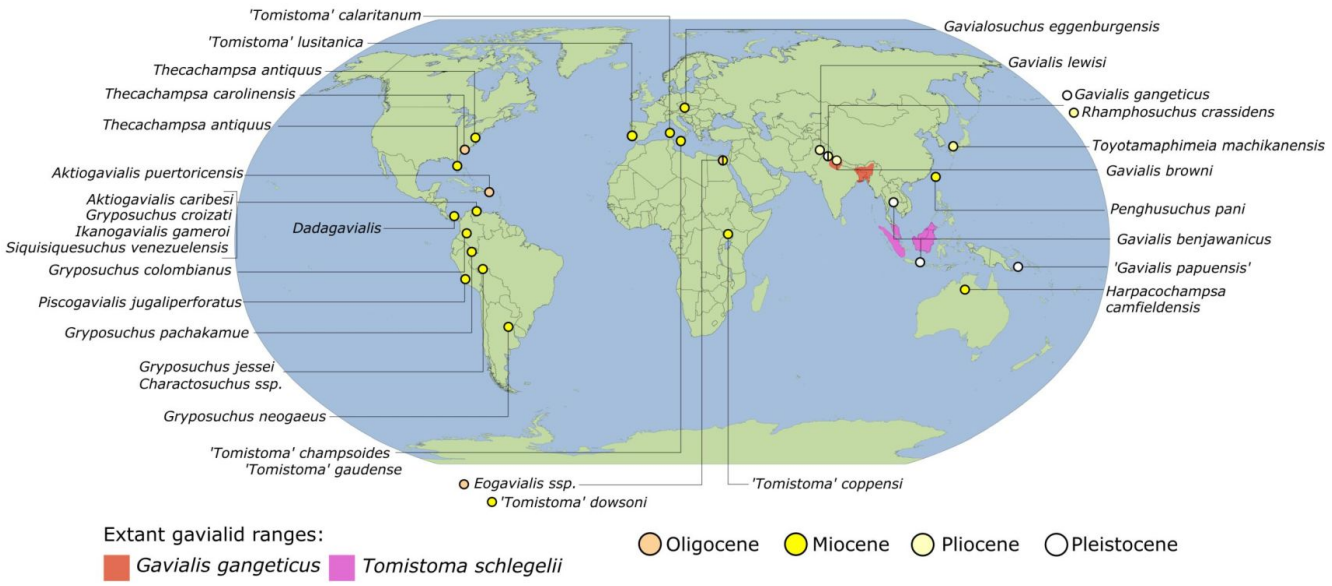



Figure 5.14: The distribution of named gavialoid species from the Oligocene to present day. Fossil occurrences based on data in the Paleobiology Database (https://paleobiodb.org/). Modern ranges taken from https://www.iucnredlist.org/. Modern map taken from https://en.wikipedia.org/wiki/Wikipedia:Blankmaps.

*sis*, from the middle Miocene of Australia (Megirian et al., 1991), as a gavialid (see also Yates & Pledge, 2017). Usually considered a mekosuchine (e.g. Salisbury & Willis, 1996; Willis, 1997b; Brochu, 2001; Jouve et al., 2008), its slender snout is unusual for the clade, as has been previously discussed (e.g. Megirian et al., 1991). Given the otherwise complete absence of Gavialoidea from the Australasian fossil record (e.g. Willis, 1997b), including "Tomistominae" (Piras et al., 2007), this might indicate that the position of *Harpacochampsa camfieldensis* reflects long branch attraction as a result of convergence of longirostrine features (e.g. Brochu, 2003; Ballell et al., 2019; Groh et al., 2020).

As noted, two 'thoracosaur' clades are recovered within Gavialidae. One of these comprises the middle Eocene north African species '*Tomistoma*' *cairense* as the sister taxon of a clade consisting of *Thoracosaurus isorhynchus* + *Eosuchus*. The taxonomy of the various Eurasian species and remains referred to *Thoracosaurus* remains problematic and in need of revision, but *T. isorhynchus* appears to be the appropriate senior synonym for at least some of these remains (Martin & Delfino, 2010). Regardless, at least one species of *Thoracosaurus* appears to be present from the Maastrichtian–early Paleogene in Europe (Brochu, 2004a; Martin & Delfino, 2010; Puértolas-Pascual et al., 2016). *Eosuchus* is currently known from the late Paleocene of Europe (*E. lerichei*, Dollo, 1907; Delfino et al., 2005) and late Paleocene-early Eocene of North America (*E. minor*, Marsh, 1870; Brochu, 2006b). The second of the 'thoracosaur' clades comprises two latest Cretaceous North American species, *Thoracosaurus neocesariensis* and *Eothoracosaurus mississippiensis* (Carpenter, 1983; Brochu, 2004a), which together form a sister taxon relationship with the early Late Cretaceous European species *Portugalosuchus azenhae* (Mateus et al., 2019). My topology is consistent with previous analyses in that 'thoracosaurs' do not appear to be

a monophyletic group (e.g. Brochu, 2004a), and provides further evidence that oceanic dispersal between Europe and North America occurred in multiple coastal to marine eusuchian lineages.

Two north African taxa form successive outgroups to a clade consisting primarily of South American gavialoids and *Gavialis*, comprising the early Miocene species '*Tomistoma*' *dowsoni* (Fourtau, 1920; Agrasar, 2004), as well as the aforementioned *Eogavialis*. As well as the late Eocene species, *Eogavialis africanum*, an additional species (*E. andrewsi*) appears to extend this lineage into the Miocene of Africa (Storrs, 2003). '*Tomistoma*' *coppensi*, from the late Miocene–Pliocene of East Africa (Pickford, 1994), seems to represent the stratigraphically youngest gavialoid known from Africa.

Since the description of *Aktiogavialis puertoricensis* from the late Oligocene of Puerto Rico, several studies have recovered this species as the stratigraphically earliest member of the Neotropical gavialoid radiation, Gryposuchinae (e.g. Vélez-Juarbe et al., 2007; Salas-Gismondi et al., 2019). The analyses of Salas-Gismondi et al. (2016; 2019) also recovered the Paleocene north African species, *Argochampsa krebsi*, as the sister taxon to *Aktiogavialis*. In my topology, these taxa are successively nested, with *Argochampsa* in a more crownward position than *Aktiogavialis*. Either scenario results in long ghost lineages and supports the hypothesis of a trans-Atlantic dispersal of gavialoids in the Paleogene (Buffetaut, 1982; Langston & Gasparini, 1997; Brochu & Rincón, 2004; Delfino et al., 2005; Vélez-Juarbe et al., 2007; Salas-Gismondi et al., 2016). Furthermore, my topology might indicate two independent transoceanic dispersal events, one giving rise to *Aktiogavialis*, and another giving rise to all other South American and Asian gavialids (see also Salas-Gismondi et al., 2016) (Fig. 5.15). Alternatively, this topology could be interpreted as indicating bidirectional dispersals between Africa and the Neotropics, i.e. the common ancestor of *Aktiogavialis* and *Gavialis* dispersed to the Neotropics from Africa, and *Argochampsa* represents a backdispersal (Fig. 5.15). By contrast to some studies that recover a diverse Gryposuchinae (e.g. Salas-Gismondi et al., 2016; Salas-Gismondi et al., 2019), here this clade is restricted to *Gryposuchus colombianus* + *Gryposuchus pachakamue*. This is partly a result of the nested position of *Gavialis*, as well as its sister taxon relationship to a paraphyletic array of *Gryposuchus* species. Nevertheless, a similar topology has been recovered in previous studies (e.g. Jouve et al., 2008; Lee & Yates, 2018; Iijima & Kobayashi, 2019).

Gavialoids reached an apparent peak in diversity during the middle to late Miocene (De Celis et al., 2020), with a near global distribution. Much of this diversity comes from South America (Fig. 5.14), although the relatively limited early Miocene record on this continent indicates that diversity was probably also high during that interval too (e.g. Solórzano et al., 2018). Gavialoids were particularly speciose in the Caribbean (Salas-Gismondi et al., 2019) and northern South America during the Miocene (e.g. Langston, 1965; Brochu & Rincón, 2004; Riff & Aguilera, 2008; Scheyer et al., 2013; Salas-Gismondi et al., 2016) (comprising *Aktiogavialis caribesi*, *Dadagvialis gunai*, *Gryposuchus* spp., *Ikanogavialis gameroi*, *Piscogavialis jugaliperforatus*, and *Siquisiquesuchus venezuelensis*), with fewer occurrences in the remainder

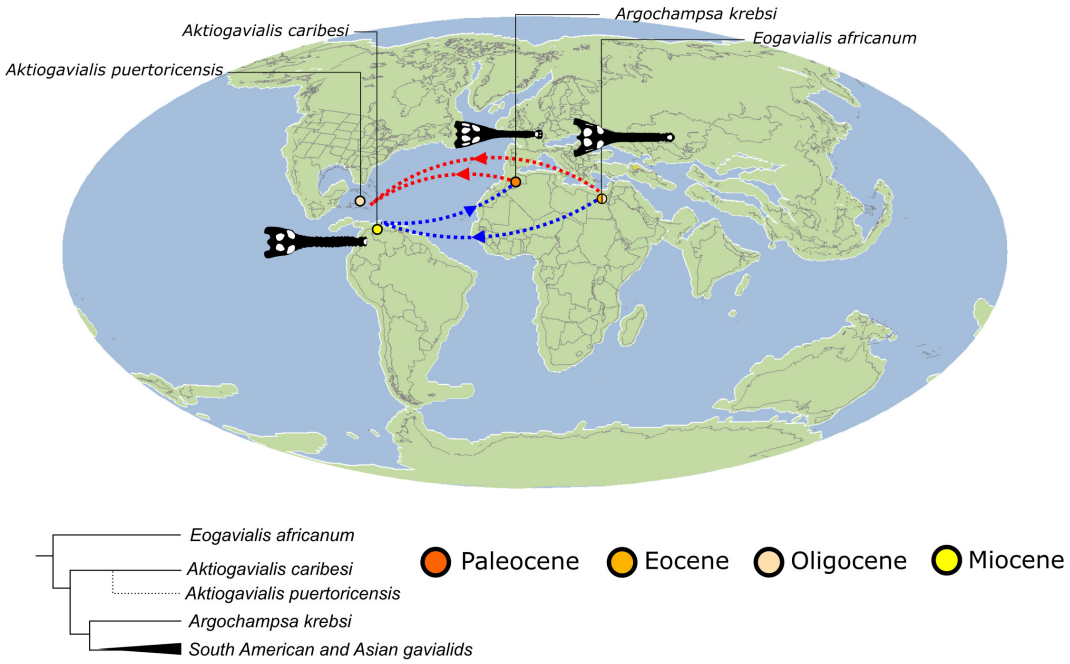



Figure 5.15: Alternative biogeographic scenarios for the origin of Neotropical gavialoids. Global palaeogeographical reconstruction at 50 Ma from Fossilworks (http://fossilworks.org/ (Alroy, 2013) based on data in the Paleobiology Database (https://paleobiodb.org/).

of South America (e.g. Gasparini, 1968; Bona et al., 2013b). The concentration of gavialoids in northern South America probably corresponds to the global pattern of latitudinal contraction of crocodylian diversity (Mannion et al., 2015), as well as the presence of extensive proto-Amazonian wetlands (Scheyer et al., 2013; Salas-Gismondi et al., 2015), with several Miocene species showing clear preferences for estuarine and freshwater environments over coastal to marine settings (e.g. Salas-Gismondi et al., 2016; Solórzano et al., 2018). It remains to be seen whether the putative "tomistomine" *Charactosuchus* might be closely related to these gavialoids, or if this represents a distinct Neotropical lineage. In particular, an understanding of the phylogenetic affinities of the middle Eocene Caribbean species, '*Charactosuchus*' *kugleri* (Berg, 1969), will be important in this regard. Nearly all South American and Caribbean gavialoids were extinct by the end of the Miocene, with *Piscogavialis* possibly surviving later into the Pliocene (Salas-Gismondi et al., 2019). The timing of this extinction likely corresponds to the same orographic and drainage impacts that led to the demise of many other South American crocodylians at the Miocene/Pliocene boundary (e.g. Scheyer et al., 2013; Salas-Gismondi et al., 2015, see also Section 5.3).

*Gavialis* first appears in the Pliocene of the Indian sub-continent, represented by the extinct species *G. browni* and *G. lewisi* (Lydekker, 1886; Mook, 1932; Lull, 1944; Martin, 2019) (Fig. 5.14). Stratigraphically earlier referrals cannot unequivocally be referred to *Gavialis* and might represent occurrences of the poorly known species *Rhamphosuchus crassidens* (Cautley & Falconer, 1840; Head, 2001), or an additional gavialoid taxon (Martin, 2019). The earliest occurrences of the extant species, *Gavialis gangeticus*,

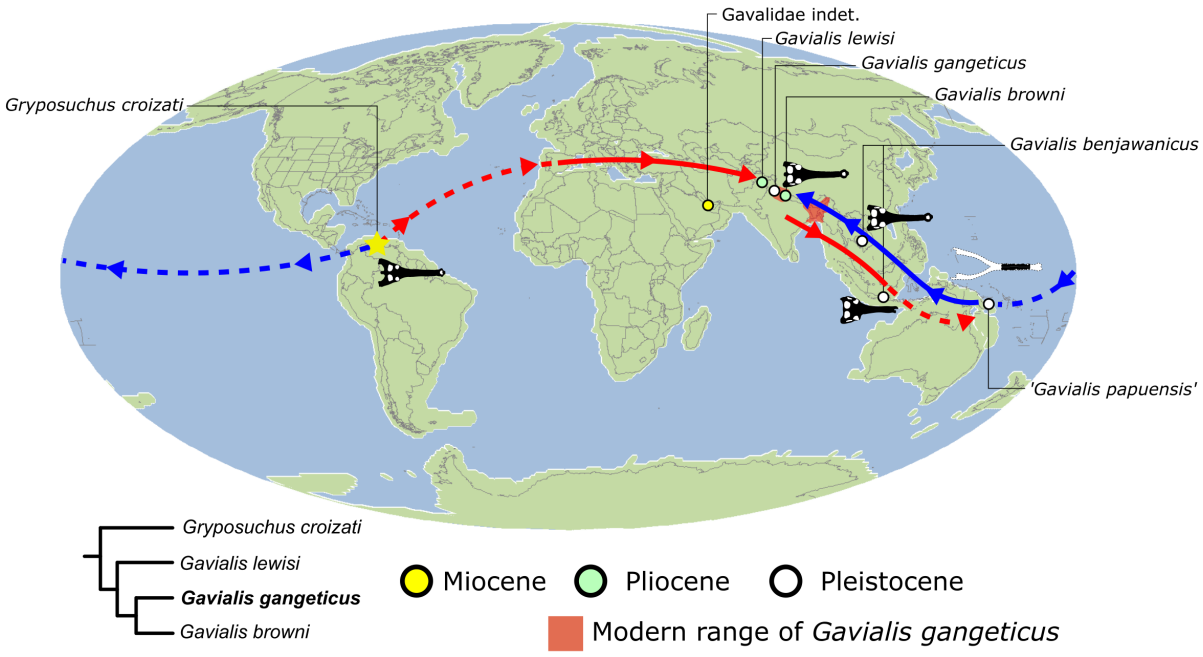



Figure 5.16: The distribution of named *Gavialis* species, illustrating alternative biogeographic routes suggested from a close relationship between South American and Asian gavialids. Global palaeogeographical reconstruction at 2 Ma from Fossilworks (http://fossilworks.org/ (Alroy, 2013) based on data in the Paleobiology Database (https://paleobiodb.org/).

are from the Pleistocene of India (Martin, 2019). By the Pleistocene, *Gavialis* is represented in Thailand and Indonesia by *G. benjawanicus* (Delfino & De Vos, 2010; Martin et al., 2012) (Fig. 5.16); it appears to have dispersed via river drainage systems, potentially reaching Indonesia during an interval of lower sea level (Martin et al., 2012, see also *Crocodylus siamensis* above). '*Gavialis papuensis*' represents additional gavialid material from the Quaternary of Oceania (De Vis, 1905; Molnar, 1982a). Previously likened to the South American gavialoid *Ikanogavialis* (Molnar, 1982a; Martin et al., 2012), the preserved material is undiagnostic at species level, but might be referable to *Gavialis* (personal observations of syntypes, QM F.340, 341, 406), extending the distribution of the genus further eastwards and probably requiring the crossing of some small oceanic barriers (Fig. 5.16).

*Gavialis* is often recovered as the sister taxon to Gryposuchinae, with several African taxa (e.g. *Eogavialis*) immediately outside of this clade (e.g. Brochu & Rincón, 2004; Delfino et al., 2005; Brochu, 2006b; Salas-Gismondi et al., 2016; Salas-Gismondi et al., 2019). This scenario supports the hypothesis for an 'Old World' (i.e. African) origin of gavialids in both the Neotropics and Indo-Pakistan (Buffetaut, 1982; Langston & Gasparini, 1997; Brochu & Rincón, 2004; Delfino et al., 2005; Vélez-Juarbe et al., 2007). By contrast, my results indicate a 'New World' origin of *Gavialis*, given its nested position in a clade of South American gavialids (see also Jouve et al., 2008). This implies a relatively recent oceanic dispersal to Asia by the late Miocene or early Pliocene, via either the Atlantic or Pacific oceans (Fig. 5.16). Given the shorter length of the former route, it is considered the most likely route here. Furthermore, frag-

mentary occurrences from the late Miocene of the Arabian Peninsula provide some possible evidence to support an Atlantic, rather than Pacific route. Rauhe et al. (1999) described a partial dentary and occiput, which they tentatively identified as '*Ikanogavialis*?' and Gavialidae, respectively, noting similarities with *Gavialis* in the latter specimen. If these specimens do belong to members of the South American-Asian clade, then they would partly fill the current spatial gap and provide tentative support for a trans-Atlantic dispersal (Fig. 5.16). *Gavialis gangeticus* is known exclusively from freshwater environments, and unequivocal fossil *Gavialis* specimens are known only from fluvio-lacustrine and fluvio-deltaic environments (Delfino et al., 2005; Delfino & De Vos, 2010; Martin et al., 2012). However, *G. gangeticus* exhibits vestigial adaptations for saltwater tolerance, including a keratinised buccal cavity and (reduced) osmoregulatory pores (see Chapter 3, characters 313, 320) (Taplin & Grigg, 1989; Brochu & Rincón, 2004; Vélez-Juarbe et al., 2007). As noted by previous authors (e.g. Taplin & Grigg, 1989; Vélez-Juarbe et al., 2007), this indicates that the ancestors of *Gavialis* passed through a marine phase, which is also evident from numerous gavialoids discovered in coastal and marine deposits; however, my results indicate that this occurred very recently. Our knowledge of the saltwater tolerance of the closest South American relatives of *Gavialis* is limited, as physiological adaptations for saltwater tolerance leave no trace on the skeleton and must be inferred from the depositional environment (Vélez-Juarbe et al., 2007). That several early diverging Neotropical taxa are known from coastal environments (e.g. *Piscogavialis*, *Siquisiquesuchus*, *Aktiogavialis*, *Dadagavialis*) hints towards saltwater tolerance early in the evolutionary history of neotropical gavialids. This might be expected since they are inferred to have colonised the Neotropics from Africa via the Atlantic Ocean (Vélez-Juarbe et al., 2007; Salas-Gismondi et al., 2019). However, saltwater tolerance is more ambiguous in the taxa most closely related to *Gavialis*. *Gryposuchus croizati* from the Urumaco Formation in Venezuela and *Gryposuchus pachakamue*, from the Pebas Formation of Peru, are known from depositional environments with varying marine influence (Vélez-Juarbe et al., 2007; Riff & Aguilera, 2008; Salas-Gismondi et al., 2016). By contrast, *Gryposuchus colombinaus* and *Gryposuchus neogaeus* are known from freshwater environments (Gasparini, 1968; Vélez-Juarbe et al., 2007), but this does not necessarily mean that these species were saltwater intolerant. The late Neogene transoceanic dispersal implied by my topology indicates that gavialids closely related to *Gavialis* (i.e. *Gryposuchus*) might have been salt-water tolerant, and supports the view that the current restriction of *Gavialis* to freshwater environments is a recent environmental shift (Vélez-Juarbe et al., 2007).

## 5.7 Summary

### Non-crocodylian Eusuchians

- The earliest unambiguous occurrence of Eusuchia is marked by the appearance of *Hylaeochampsa vectiana* in the Barremian of the United Kingdom. The new relationships of Allodaposuchidae and *Borealosuchus* to Crocodylia herein are very stratigraphically congruent given the approximately contemporaneous age (latest Cretaceous) of the earliest unambiguous members of these clades.

### Alligatoroidea

- The inclusion of latest Cretaceous North American taxa in Caimaninae is both consistent with some earlier studies (Salas-Gismondi et al., 2015; Bona et al., 2018) and congruent with the molecular divergence estimate of Caimaninae and Alligatorinae (Table 5.1). Furthermore, it indicates that Caimaninae originated in North America rather than South America, and that Alligatoroidea began to diversify before the K-Pg mass extinction, rather than in its wake.
- There is evidence for two southern dispersal events of alligatoroids around the K/Pg boundary, including a southern dispersal of caimanines and non-caimanine alligatoroids. Furthermore, North American taxa nested within Caimaninae indicate at least two northward dispersals in the latest Cretaceous and Eocene. Additional northward dispersals in the Miocene are likely, evidenced by Panamanian caimanines (Hastings et al., 2010; Hastings et al., 2013).
- Alligatoroids dispersed across Laurasia, reaching Europe and Asia in the early Paleogene (Martin & Lauprasert, 2010; Massonne et al., 2019). Several terrestrial biogeographic pathways existed around this time to allow these dispersals, with the De Geer and Thulean routes providing the most likely connection between North America with Europe, and Beringia connecting North America with Asia (Brikiatis, 2014).

### Crocodyloidea

- Crocodyloids first appear in the Maastrichtian of North America and Asia. Their absence from the Paleocene of North America probably represents a sampling artefact; however, crocodyloids may have become regionally extinct here at this time. Similarly, the absence of crocodyloids from the late Eocene of North America and Europe, until the Miocene appearance of *Crocodylus*, might also represent regional extinctions.
- An Asian origin for Mekosuchinae is proposed, with the ancestors of Mekosuchinae reaching the continent via oceanic dispersal across Eastern Tethys in the early Paleogene. The ability of crocody-

loids to make such an oceanic dispersal is testified by adaptations for saltwater tolerance in extant crocodyloids, and several insular mekosuchine occurrences in the Quaternary.

- An African origin of *Crocodylus* is supported (e.g. Brochu, 2000; Delfino et al., 2007). However, in considering only members of the crown genus, *Crocodylus* appears to originate in the Indo-Pacific region (e.g. Oaks, 2011). The dispersal of *Crocodylus* from the Indo-Pacific region to Africa may have occurred via Europe, which could explain Miocene *Crocodylus* remains here (Delfino et al., 2007; Nicolaï & Matzke, 2019).

**Gavialoidea**

- The interrelationship of several Afro-European gavialoids from the early Paleogene are congruent with previous morphological hypotheses. However, the close relationship of North American *Thecachampsa* and European *Gavialosuchus* contradicts most earlier studies. Nevertheless, along with the interrelationships of Asian *Maomingosuchus*, they continue to support similar biogeographic scenarios that involved dispersals between Europe, North America and Asia (e.g. Jouve et al., 2015; Jouve, 2016). Such frequent dispersals might be expected given the inferred marine lifestyle of most of these taxa.

- Tomistominae appears to be a very depauperate clade, in strong contrast with most earlier morphological hypotheses. Neogene Asian "tomistomines", that might be expected to cluster with the extant *Tomistoma schlegelii*, instead form several separate gavialid lineages; however, this has similarly been recovered in earlier combined analyses (e.g. Lee & Yates, 2018; Iijima & Kobayashi, 2019).

- An African origin of South American gavialids via trans-Atlantic dispersal is supported as in earlier studies (e.g. Langston & Gasparini, 1997; Brochu & Rincón, 2004; Delfino et al., 2005; Salas-Gismondi et al., 2019). Furthermore, the interrelationships recovered here suggest either multiple unidirectional trans-Atlantic dispersals or bi-directional dispersals during the Paleogene, which is also congruent with earlier hypotheses (Salas-Gismondi et al., 2016; Salas-Gismondi et al., 2019).

- *Gavialis* appears to be descended from a Neotropical, rather than an African ancestor, implying an oceanic dispersal in the late Miocene (most likely trans-Atlantic). This supports the view that the restriction of extant *Gavialis* to freshwater environments was a relatively recent environmental shift, acquired no earlier than this oceanic dispersal.

# Chapter 6

# Conclusions and Future Work

## 6.1 Conclusions

The research in this thesis was primarily driven by a series of outstanding problems in crocodylian systematics, most notably the gharial problem. These problems were considered tractable through a synthesis and evaluation of morphological characters applied in crocodylian systematics, which was also overdue. Additionally, the research was driven by the desire to implement different analytical protocols and treatments of quantitative data in parsimony analyses, to compare what impact they have and to assess their efficacy.

### 6.1.1 Summary of research outcomes

**Aim 1: To reassess the anatomy of the basal alligatoroid crocodylian *Diplocynodon hantoniensis*.**

In Chapter 2, I addressed the first aim of this thesis, to reassess the anatomy of *Diplocynodon hantoniensis*. The motivation for this aim was two-fold. Firstly, this taxon had not received an anatomical reappraisal in over 150 years. Secondly, the targeted reappraisal of 'basal' crocodylian taxa, was considered a useful approach to sample morphological characters for crocodylian phylogeny. This reappraisal revealed several new anatomical features in *Diplocynodon hantoniensis*, several of which formed the basis of new characters in the phylogenetic analysis (Characters 44, 185, 195, 240). Additionally, I provided the most comprehensive description of postcranial anatomy in a fossil crocodylian, constituting a valuable tool for comparisons in future studies that may result in greater postcranial character sampling. Overall, this study demonstrates that the reappraisal of previously described species can be fruitful for morphological character sampling.

**Aim 2: To construct a new, illustrated, consistently and clearly defined character list for phylogenetic analyses of Crocodylia, including justifications for new and modified characters.**

Chapter 3 addressed the aim of constructing a new morphological character list for Crocodylia. This was achieved though first-hand study of a global sample of crocodylian specimens, a review of described species, and a synthesis of existing character lists. In this chapter, I produce the largest and most comprehensively illustrated character list aimed at exploring the interrelationships of Crocodylia (330 characters, 95% illustrated). 45 new characters were outlined and discussed. Furthermore, all characters were systematically revised such that they were consistently formatted. This included the reductive coding of complex multistate characters combining either (1) non-homologous states, or (2) "absent" and "present, but variable" states.

**Aim 3: To assess the phylogenetic interrelationsips of Crocodylia, exploring systematic problems in the clade, as well as the effects of different treatments of quantitative data and weighting strategies.**

The results of the phylogenetic analyses based on the new character list were discussed in Chapter 4. Numerous new crocodylian interrelationships have been recovered, which address several problems in crocodylian systematics that motivated this research. This includes: (1) non-crocodylian affinities of *Borealosuchus*; (2) the paraphyly of *Diplocynodon*; (3) recovery of an early diverging North American clade in Caimaninae; (4) new interrelationships of *Eocaiman*; and (5) changes in the taxonomic content of Mekosuchinae. However, by far the most significant result is that *Gavialis gangeticus* is recovered as the closest living relative of *Tomistoma schlegelii*, and together are closely related to crocodylids (Section 4.4.7). This marks the first morphology-only phylogeny to concur with the molecular hypothesis for crocodylian interrelationships. It was found that this resulted from a series of modifications to character construction and character scores, which revealed: (1) that several gavialoids lack plesiomorphic features that formerly drew them into the stem of "Brevirostres", and (2) that more widespread similarities occur between "tomistomines" and "gavialoids", a notion for which evidence has recently been growing (e.g. Iijima & Kobayashi, 2019; Sookias, 2020). Despite resolving this long-held topological incongruence, large discrepancies remain in the timing of divergence of the extant gharials, principally resulting from early Late Cretaceous to early Paleogene taxa (*Portugalosuchus* and 'thoracosaurs') nested within the crown gharial clade. This result is most parsimoniously supported, but the temporal incongruence warrants future systematic reappraisals of these taxa (see Section 6.2.1).

Alternative weighting strategies and treatments of quantitative characters were explored, revealing that more reliable and stratigraphically congruent topologies were recovered under extended implied weighting with higher *k*-values and using continuous characters (Section 4.3). Pragmatically, the latter is also considered the optimal treatment of quantitative data, given the ease of implementation and lack of arbitrary character state delimitation when discretising quantitative data (Chapter 3, Section 3.5). Indeed, in constructing this dataset, there was little to no basis for drawing discrete boundaries between measured values. On the other hand, continuous characters present additional challenges, such as difficulty in measuring deformed specimens. Furthermore, although transformations of values, or ranges of values from continuous characters can be expressed as synapomorphies, their diagnostic utility should be treated carefully. The optimisation of continuous characters often revealed small, step-wise changes in values in successive nodes, which although are considered phylogenetically informative, may not be pragmatic in the diagnosis of a particular taxon.

**Aim 4: To review the evolutionary and biogeographic history of Crocodylia, based on new hypotheses that might be recovered.**

Chapter 5 considered the new topologies of each of the principal crocodylian clades in a temporal and paleogeographic context. These clades have different evolutionary and biogeographic histories, which reflects a combination of their unique physiological constraints and paleogeographic variables. One of the most important appears to be the presence of adaptations for saltwater tolerance in members of Longirostres, that are absent in alligatorids. As such, whereas crocodylids and gavialids achieved cosmopolitan distributions, alligatorids have been restricted to the Americas and Eurasia, and indeed today almost exclusively inhabit the Western Hemisphere. Nevertheless, Alligatoroidea is characterised by recurrent dispersals between North and South America during the latest Cretaceous and Neogene. Although differing to the accepted view of caimanines originating in South America, the recovery of an early diverging North American caimanine clade is consistent with a latest Cretaceous dispersal of alligatoroids into South America. New evidence is also recovered for an additional North to South American dispersal based on the interrelations of *Eocaiman*.

The interrelationships of Crocodyloidea also revealed some new biogeographic and evolutionary implications. Notably, a new hypothesis for the origin of Mekosuchinae in Australasia is outlined (Section 5.5), which involves an early Paleogene, trans-Tethyan dispersal from East Asia.

Neotropical gavialids are descended from African ancestors and their interrelationships imply more than one instance of trans-Atlantic dispersal. *Gavialis* is more closely related to South American than African taxa, implying that the ancestors of *Gavialis* originated in the Neotropics and crossed a large marine barrier (most likely the Atlantic) in the late Miocene, before acquiring specialisations for inhabiting freshwater environments.

### 6.1.2 Thesis summary

The disagreement between morphological and molecular datasets over the affinities of *Gavialis gangeticus* has essentially been the single largest problem in crocodylian systematics, and has had an important role in shaping the course of investigations of Crocodylia. The molecular hypothesis is almost certainly correct given the strong, and consistent support for this topology. Indeed, we have long-since recognised morphological features in common with the extant gharials (e.g. Buffetaut, 1985; Brochu, 1997b; Trueman, 1998); however, these similarities have been most parsimoniously recovered as convergence. Several authors have alluded to a means of addressing this incongruence. Hass et al. (1992) commented "*that a careful re-examination of both the extant and the fossil morphological data is warranted*", which was similarly echoed by Brochu (1997b) who hoped "*that the morphological characters . . . will be closely scrutinized*" and yet still by Harshman et al. (2003), who added that such scrutiny should include "*an eye*

*toward the effects of character coding and ordering on phylogenetic analyses*". Indeed, the reappraisal of morphological data, both in the construction of characters and observations of taxa, has resolved this incongruence. In addition, this thesis has presented several tools to advance the field of crocodylian systematics. This includes a new, illustrated character list, and the first detailed description of the postcranial skeleton of a 'basal' alligatoroid crocodylian. I have also provided updated diagnoses, estimates of divergence times, and new biogeographic insights into several crocodylian clades. Nevertheless, this work highlights numerous problematic taxa and avenues for future investigation, such that crocodylian systematics remains to be a fruitful area for continued research.

## 6.2 Future Directions of Research

### 6.2.1 Reappraisals of problematic taxa

Several taxa can be identified that might be targets for future reappraisals because: (1) their interrelationships here contrast with previous studies; (2) they result in temporal incongruence relative to molecular datasets; or (3) they may clarify particular aspects of crocodylian phylogeny (Table 6.1).

Table 6.1: Taxa targeted for future anatomical reappraisal.

| Taxon | Relevance |
|---|---|
| Allodaposuchidae and Hylaeochampsidae | Changes to the scores of some non-crocodylian eusuchians appears to have contributed in part to the recovery of the molecular topology herein (Section 4.4.7). Taxa such as Allodaposuchidae and Hylaeochampsidae were not the focus of this study, and few new characters were introduced based on direct observations of these taxa. Although several recent phylogenetic studies (e.g. Narváez et al., 2015; Narváez et al., 2016) have explored their interrelationships, this has been based on a dataset essentially designed for delimiting alligatoroid interrelationships. These taxa should be the targets for future character sampling, and must be studied in more inclusive neosuchian phylogenies. |

**Table 6.1 continued from previous page**

| Taxon | Relevance |
|---|---|
| *Thoracosaurus isorhynchus*<br>*Thoracosaurus neocesariensis*<br>*Eothoracosaurus mississippiensis*<br>*Eosuchus* | 'Thoracosaurs' are recovered within Gavialidae, contradicting the molecular divergence estimate for the extant gharials and resulting in problematic ghost lineages for most members of the clade. Although some 'thoracosaurs' are relatively recently described, e.g. *Eothoracosaurus* (Brochu, 2004a) and *Eosuchus* (Delfino et al., 2005; Brochu, 2006b), their recovery in Gavialidae deserves further scrutiny. By contrast, a revision of European *Thoracosaurus* specimens (*Thoracosaurus isorhynchus*) is overdue (Martin & Delfino, 2010), with the most recent anatomical appraisal conducted by Piveteau (1927). Similarly, there are numerous North American remains referred to *Thoracosaurus neocesariensis* from the Hornerstown Formation of New Jersey, which lack a recent revision (Brochu, 2004a). Future studies exploring the affinities of 'thoracosaurs' should also assess the degree to which their gavialoid affinities are a result of convergences in snout length. |
| *Portugalosuchus* | As with 'thoracosaurs', *Portugalosuchus* is a primary cause of temporal incongruence in this dataset, suggesting its gavialoid (and perhaps even crocodylian) affinities are misleading. In their original description, Mateus et al. (2019) included this taxon in a more inclusive crocodyliform dataset, which still supported its placement in Crocodylia. Nevertheless, this taxon deserves further scrutiny and perhaps its inclusion in other large crocodyliform datasets may be better suited to determining its affinities (e.g. Groh et al., 2020). |

**Table 6.1 continued from previous page**

| Taxon | Relevance |
|---|---|
| *Eogavialis africanus* | *Eogavialis* has not received a reappraisal in approximately 50 years (Hecht & Malone, 1972). It has long been considered a potential ancestor of the extant gharials (Buffetaut, 1985) and its age is congruent with this hypothesis, given that it falls within the range for the molecular divergence estimate for Gavialidae (31–18 Ma) (Oaks, 2011). |
| '*Tomistoma*' *cairense*<br>*Paratomistoma courti* | Tomistominae is now an extremely depauperate clade in comparison to earlier studies. Morphological "tomistomines" appear to represent a polyphyletic assemblage, with some grouping together as early diverging gavialoids, and others more closely related to morphological "gavialoids". Several "tomistomines" deserve reappraisal; however, '*Tomistoma*' *cairense* and *Paratomistoma* are notably problematic given that they are nested in Gavialidae, but appear before the proposed divergence between the extant gharials. |

**Table 6.1 continued from previous page**

| Taxon | Relevance |
|---|---|
| *Charactosuchus* | The phylogenetic affinities of *Charactosuchus* have not been explored. This taxon is known from multiple species based on fragmentary mandibular remains from the Miocene of South America and Eocene of Jamaica. Traditionally, this taxon has been viewed as a "tomistomine", which had biogeographic significance given that there is no "tomistomine" currently described from the Neotropics. This is complicated by the new topology here, in which "Tomistominae" is polyphyletic. Furthermore, the material for this taxon is so fragmentary that even a referral to Crocodylia may be tentative. A poorly known cranium from the Miocene, Solimões Formation (Souza-Filho & Maciente, 2009), as well as several undescribed specimens (personal observations of UFAC collections) might represent the cranial components of this longisrostrine taxon. This lacks a full description and phylogenetic consideration, which could elucidate the affinities of this enigmatic taxon. |
| *Jiangxisuchus nankangensis* | The results herein conflict with a recent study that suggests *Jiangxisuchus* is an alligatoroid rather than a crocodyloid (Massonne et al., 2019) (Section 4.4.8). This also has implications on the affinities of other Paleogene crocodylians from East Asia, such as *Orientalosuchus* and *Krabisuchus*. These taxa were not included in this study, but increased sampling of East Asian taxa will be necessary to resolve their affinities. |

**Table 6.1 continued from previous page**

| Taxon | Relevance |
|---|---|
| *Asiatosuchus* | It is not clear that taxa assigned to the 'basal' crocodyloid genus, *Asiatosuchus*, form a clade. Also, some referrals to this genus may be informative in the origin of Australasian crocodyloids (Section 5.5). This genus has come to be a wastebin for Eurasian Paleogene crocodyloids, and despite recent reappraisals of some species (Wang et al., 2016; Delfino et al., 2019), several named species require revision. This includes *Asiatosuchus germanicus* from Germany and the type species, *Asiatosuchus grangeri* from Mongolia. Additionally, several indeterminate and dubious referrals to the genus exist from Asia and Russia (Efimov & Yarkov, 1993; Angielczyk & Gingerich, 1998), which require re-assessment. |
| *Eocaiman cavernensis* | The new interrelationships of *Eocaiman* recovered here have signficiant biogeographic implications, which warrants a review of this taxon (Sections 4.4.5 and 5.3). Indeed, Simpson (1933) provided the last detailed study of *Eocaiman cavernensis*, yet even the relatively brief examination of this specimen conducted in this study has revealed some new anatomical data. |
| *Brachychampsa montana*<br>*Wannaganosuchus brachymanus*<br>*Ceratosuchus burdoschi*<br>*Stangerochampsa mccabei* | In accordance with some earlier studies, *Brachychampsa montana* and *Stangerochampsa mccabei* are recovered as caimanines, rather than 'basal' alligatoroids (Salas-Gismondi et al., 2015; Bona et al., 2018) (Section 4.4.5); however, these studies did not recover *Wannaganosuchus* and *Ceratosuchus* within this clade. Furthermore, they recovered an additional taxon, *Albertochampsa langstoni*, within the clade that was not studied here. These results contrast with most previous studies and warrant a reappraisal of all of these taxa. |

**Table 6.1 continued from previous page**

| Taxon | Relevance |
|---|---|
| *Alligator luicus* | Considerable temporal incongruence exists between morphological and molecular estimates of divergence between the two extant alligators (Table 5.1). Although this could be a result of erroneous molecular divergence estimates of shallow nodes, it alternatively might suggest that the close relationship between extant alligators is misleading. Some Asian *Alligator* species remain to be phylogenetically analysed (*Alligator luicus*), or described in detail (Claude et al., 2011), which could ultimately alter the interrelationships of Alligatorinae and possibly resolve this temporal incongruence. |

### 6.2.2 Targets for improved taxon sampling

Taxa that could not be studied for logistical reasons are listed in Table 6.2 that may have significance in aspects of crocodylian phylogeny.

Table 6.2: Targets for improved taxon sampling.

| Taxon | Relevance |
|---|---|
| *Prodiplocynodon langi* | *Prodiplocynodon* has been recovered as a 'basal' crocodyloid (e.g. Brochu et al., 2012) and a stem longirostrine (Lee & Yates, 2018). |
| *Harpacochampsa camfieldensis* | *Harpacochampsa* may represent a mekosuchine, a 'basal' crocodyloid (e.g. Salisbury & Willis, 1996), or gavialoid (Lee & Yates, 2018). |

**Table 6.2 continued from previous page**

| Taxon | Relevance |
|---|---|
| *Crocodylus falconensis*<br>*Crocodylus checchiai* | *Crocodylus falconensis* from the Pliocene of Venezuela appears to be closely related to Neotropical *Crocodylus* (Scheyer et al., 2013). Similarly, Delfino et al. (2020) demonstrated close affinities of *C. checchiai* from the Miocene of North Africa with Neotropical *Crocodylus*. Inclusion of these taxa in future iterations of this dataset will be important in understanding the Neotropical radiation of *Crocodylus*. Additionally, there are numerous indeterminate contemporary *Crocodylus* remains from Europe (Delfino et al., 2007), with potentially significant biogeographic implications. |
| *Megadontosuchus arduini*<br>*Melitosaurus champsoides*<br>'*Tomistoma*' *gaudense*<br>'*Tomistoma*' *calaritanum*<br>'*Tomistoma*' *lyceense* | *Megadontosuchus* is contemporaneous with early diverging Afro-European gavialoids, and so could be closely related to these forms. The remaining taxa listed are fragmentary, middle to late Miocene European species, that are currently under revision (Nicholl et al., in prep) but likely represent one or two species, whose affinities must be explored in future versions of this dataset. |
| *Deinosuchus*<br>*Deinosuchoides* | Remains of a notable, giant basal alligatoroid taxon, *Deinosuchus*, were not available to study in this analysis, and should be included for completeness in future studies. This taxon is known from the Campanian of North America, and a recent review has concluded that material assigned to the genus represents two basal alligatoroid genera (Cossette & Brochu, 2020). |

**Table 6.2 continued from previous page**

| Taxon | Relevance |
|---|---|
| *Listrognathosuchus multidentatus* | This taxon from the Paleocene of New Mexico was originally referred to *Leidyosuchus* (Mook, 1930), but noting obvious morphological differences, Brochu (1997a) erected a new genus in its place. Later, Brochu (1999) noted that it possess a 'plate-shaped' atlantal intercentrum, which has qualitatively supported its inclusion in Alligatoridae, in which the condition was only known. However, the phylogenetic affinities of *Listrognathosuchus* are poorly explored. |
| *Notocaiman stromeri*<br>*Orthogenysuchus*<br>*Centenariosuchus gilmorei*<br>*Culebrasuchus meoamericanus* | Several caimanine taxa remain to be studied, which could prove useful in testing hypotheses of: (1) the biogeography of Panamanian caimanines (*Culebrasuchus* and *Centenariosuchus*); (2) additional biotic interchange between North and South America in the Paleogene (*Orthogenysuchus*); and (3) the interrelationships of South American Paleocene caimanines (*Notocaiman*). |
| *Krabisuchus siamogallicus*<br>*Orientalosuchus nankangensis*<br>*Eoallgator chunyii*<br>*Protoalligator huiningensis* | According to Massonne et al. (2019), these taxa (along with *Jinagxisuchus*) constitute an early diverging Asian alligatoroid clade, 'Orientalosuchinae'. By contrast, *Jiangxisuchus* has been recovered as a crocodyloid here. Future analyses require a greater sampling of these Asian crocodylians, which may elucidate their interrelationships. |

### 6.2.3 Future directions for character sampling

There are several avenues that may be fruitful for future character sampling. CT scan data may be a valuable source of new morphological characters. In particular, it could be used to target anatomically conserved and potentially phylogenetically informative regions of the skull. Recent studies have described morphological variation in the inner skull cavities of living and fossil eusuchians (Serrano-Martínez et al., 2019a; Serrano-Martínez et al., 2019b). These have already formed the basis of morphological characters here (C311, C312); however, these studies have thus far targeted relatively few fossil eusuchian taxa, e.g. *Allodaposuchus precedens* and *Diplocynodon tormis*. There are numerous exceptionally preserved

crania of fossil taxa amenable to CT scanning, which may reveal informative data for several problematic taxa identified here, as well as taxa lacking extant representatives. This includes the the planocraniid *Boverisuchus vorax* (FMNH PR 399), the gavialoids *Thoracosaurus isorhynchus* (MNHN.F.MTA.61), *Eosuchus lerichei* (IRScNB R 49), and *Kentisuchus spenceri*, as well as the caimanine *Brachychampsa montana* (UCMP 133901).

Variation in postcranial anatomy is still probably underrepresented in morphological character lists. Future studies must make direct and detailed comparisons of postcranial anatomy in fossil as well as extant crocodylians. This will be aided by further neontological studies of extant crocodylian postcranial anatomy (e.g. Meers, 2003; Klinkhamer et al., 2017). The redescription of *Diplocynodon hantoniensis* here provides a basis to begin such comparisons. Additionally, the nature of the morphological variation examined appears to be significant. For example, some recent studies have identified significant serial variation in vertebral anatomy (Iijima & Kubo, 2019b). Although comparisons might be limited to some exceptionally preserved fossil taxa, these may nonetheless be informative. Crocodylian teeth also represent an anatomical region that may benefit from studies of serial morphological variation. Aside from some rare taxa with apomophic dental features (e.g. serrations in *Quinkana* and *Boversichus*), crocodylian teeth are typically regarded as being undiagnostic. However, there are few quantitative studies of serial variation in crocodylian teeth to test this further (e.g. D'Amore et al., 2019). This may also provide a useful tool in making taxonomic determinations from commonly found isolated teeth.

In this study continuous characters formed a relatively small proportion of the total character list, used to characterise morphological features such as cranial, mandibular, and postcranial proportions. By contrast, a recent study applied continuous characters in greater numbers (Groh et al., 2020), and it is recognised that several discretely coded characters here could potentially be treated continuously. As such, future iterations of this datasets could explore the effects of a more extensive use of continuous characters.

### 6.2.4 Methodological considerations

For practical reasons, a model-based method of phylogenetic inference (i.e. Bayesian) was not implemented in this study. It is recognised that there is debate over which methods of phylogenetic inference perform the best, especially pertaining to morphological characters (e.g. Wright & Hillis, 2014; O'Reilly et al., 2016; Goloboff et al., 2018). A recent study of Neosuchia found that analyses using maximum parsimony with extended implied weighting performed better in terms of stratigraphic congruence and addressing issues of homoplasy than analyses using Bayesian methods (Groh et al., 2020). Nevertheless, a future study should compare the optimal results of maximum parsimony with Bayesian methods for this new crocodylian dataset.

The effect of inapplicable data should be explored in future studies (De Laet, 2005). Recently, a mod-

ified parsimony algorithm has been devised to distinguish inapplicable from missing data, which results from reductively coding characters (Brazeau et al., 2019). That study found that significant differences in optimal trees can result depending on the treatment of inapplicable data. Relatively few characters contained inapplicable data here; however, a future study should compare the optimal trees resulting from alternative treatments of inapplicable data.

### 6.2.5 Additional directions of research

A natural progression from this study would be to conduct a more inclusive phylogeny of Neosuchia. Although recently reviewed by Groh et al. (2020), their analysis recovers some inconsistent relationships among eusuchians, including the morphological hypothesis for the affinities of *Gavialis*.

One of the most exciting avenues of future research in crocodylian systematics is the potential to collect and analyse ancient DNA (aDNA), which could be studied in a combined molecular and morphological dataset. This could provide independent evidence for the affinities of fossil crocodylians. The recovery of aDNA from fossil crocodylians is limited given their preference for subtropical and tropical climates that accelerate the degredation of the molecule (Willerslev & Cooper, 2005). Nevertheless, aDNA has been recovered from certain microenvironments in tropical species (e.g. Kehlmaier et al., 2017). There are a few fossil crocodylian taxa that became extinct in the Holocene that could be suitable candidates for aDNA studies. This includes the putative osteolaemine *Voay robustus* from Madagascar, as well as the mekosuchines *Volia athollandersoni* and *Mekosuchus inexpectatus*. The latter two species could be particularly informative given that they are representatives of an extinct crocodyloid lineage.

# Bibliography


Adams, A. J. (2016). *A reassessment of the late Eocene–early Oligocene crocodylids Crocodylus megarhinus Andrews 1905 and Crocodylus articeps Andrews 1905 from the Fayúm Province, Egypt* (Thesis).

Adams, A., Baikie, W. B., & Barron, C. (1854). *A manual of natural history, for the use of travellers; being a description of the families of the animal and vegetable kingdoms: with remarks on the practical study of geology and meteorology. To which are appended directions for collecting and preserving*. J. Van Voorst.

Adams, T. L. (2014). Small crocodyliform from the Lower Cretaceous (Late Aptian) of Central Texas and its systematic relationship to the evolution of Eusuchia. *Journal of Paleontology*, *88*(5), 1031–1049.

Aggarwal, R. K., Majumdar, K. C., Lang, J. W., & Singh, L. (1994). Generic affinities among crocodilians as revealed by DNA fingerprinting with a Bkm-derived probe. *Proceedings of the National Academy of Sciences*, *91*(22), 10601–10605.

Agrasar, E. L. (2004). Crocodile remains from the Burdigalian (lower Miocene) of Gebel Zelten (Libya). *Geodiversitas*, *26*(2), 309–321.

Aguilera, O. A., Riff, D., & Bocquentin-Villanueva, J. (2006). A new giant *Purussaurus* (Crocodyliformes, Alligatoridae) from the upper Miocene Urumaco formation, Venezuela. *Journal of Systematic Palaeontology*, *4*(3), 221–232.

Alroy, J. (2002). Stratigraphy in phylogeny reconstruction–reply to Smith (2000). *Journal of Paleontology*, *76*(4), 587–589.

Alroy, J. (2013). Online paleogeographic map generator. *http://paleodb.org/?a=mapForm*.

Andrade, M. B., Edmonds, R., Benton, M. J., & Schouten, R. (2011). A new Berriasian species of *Goniopholis* (Mesoeucrocodylia, Neosuchia) from England, and a review of the genus. *Zoological Journal of the Linnean Society*, *163*(suppl 1), S66–S108.

Andrews, C. W. (1905). Notes on some new Crocodilia from the Eocene of Egypt. *Geological Magazine*, *2*(11), 481–484.

Andrews, C. W. (1913). On the skull and part of the skeleton of a crocodile from the Middle Purbeck of Swanage, with a description of a new species (*Pholidosaurus lævis*), and a note on the skull of *Hylæochampsa*. *Annals and Magazine of Natural History*, *11*(65), 485–494.

Andrews, C. W. (1906). *A descriptive catalogue of the Tertiary Vertebrata of the Fayum, Egypt*. British Museum, London.

Angielczyk, K. D., & Gingerich, P. D. (1998). New specimen of cf. *Asiatosuchus* (Crocodyloidea) from the middle Eocene Drazinda formation of the Sulaiman range, Punjab (Pakistan). *Contributions from the Museum of Paleontology, University of Michigan*, *30*, 163–189.

Antoine, P.-O., Abello, M. A., Adnet, S., Sierra, A. J. A., Baby, P., Billet, G., Boivin, M., Calderón, Y., Candela, A., & Chabain, J. (2016). A 60-million-year Cenozoic history of western Amazonian ecosystems in Contamana, eastern Peru. *Gondwana Research*, *31*, 30–59.

Antunes, M. T. (1961). *Tomistoma lusitanica, crocodilien du Miocéne du Portugal*. Revista da Faculdade de Ciencias de Lisboa.

Aoki, R. (1976). On the generic status of *Mecistops* (Crocodylidae), and the origin of *Tomistoma* and *Gavialis*. *Bulletin Atagawa Institute*, *6*(7), 23–30.

Aráez, J. L. D., Delfino, M., Luján, À. H., Fortuny, J., Bernardini, F., & Alba, D. M. (2017). New remains of *Diplocynodon* (Crocodylia: Diplocynodontidae) from the early Miocene of the Iberian Peninsula. *Comptes Rendus Palevol*, *16*(1), 12–26.

Auffenberg, W. (1954). Additional specimens of *Gavialosuchus americanus* (Sellards) from a new locality in Florida. *Quarterly Journal of the Florida Academy of Sciences*, *17*(4), 185–209.

Aureliano, T., Ghilardi, A. M., Guilherme, E., Souza-Filho, J. P., Cavalcanti, M., & Riff, D. (2015). Morphometry, bite-force, and paleobiology of the Late Miocene caiman *Purussaurus brasiliensis*. *PloS one*, *10*(2), e0117944.

Bacon, C. D., Silvestro, D., Jaramillo, C., Smith, B. T., Chakrabarty, P., & Antonelli, A. (2015). Biological evidence supports an early and complex emergence of the Isthmus of Panama. *Proceedings of the National Academy of Sciences*, *112*(19), 6110–6115.

Ballell, A., Moon, B. C., Porro, L. B., Benton, M. J., & Rayfield, E. J. (2019). Convergence and functional evolution of longirostry in crocodylomorphs. *Palaeontology*, *62*(6), 867–887.

Balouet, J.-C., & Buffetaut, E. (1987). *Mekosuchus inexpectatus*, ng, n. sp., crocodilien nouveau de l'Holocene de Nouvelle Calédonie. *Comptes rendus de l'Académie des sciences. Série 2, Mécanique, Physique, Chimie, Sciences de l'univers, Sciences de la Terre*, *304*(14), 853–856.

Baron, M. G., Norman, D. B., & Barrett, P. M. (2017). A new hypothesis of dinosaur relationships and early dinosaur evolution. *Nature*, *543*(7646), 501–506.

Barrios, F. (2011). *Nuevos restos de Alligatoridae Cuvier, 1807 (Eusuchia, Crocodylia) del Neógeno del Sur de la província de Salta. Implicancias sistemáticas* (Thesis).

Baur, G. (1886). The proatlas, atlas, and axis of the Crocodilia. *American Naturalist*, *20*(3), 288–293.

Bell, M. A., & Lloyd, G. T. (2015). strap: an R package for plotting phylogenies against stratigraphy and assessing their stratigraphic congruence. *Palaeontology*, *58*(2), 379–389.

Benton, M. J., & Clark, J. M. (1988). Archosaur phylogeny and the relationships of the Crocodylia. In M. J. Benton (Ed.), *The phylogeny and classification of the tetrapods* (pp. 295–338). Clarendon Press, Oxford.

Benton, M. J., & Storrs, G. W. (1994). Testing the quality of the fossil record: paleontological knowledge is improving. *Geology*, *22*(2), 111–114.

Berg, D. E. (1966). *Die Krokodile, insbesondere "Asiatosuchus" und aff. "Sebecus?", aus dem Eozaen von Messel bei Darmstadt/Hessen* (Vol. 52). Hessisches Landesamt für Bodenforschung.

Berg, D. E. (1969). *Charactosuchus kugleri*, eine neue Krokodilart aus dem Eozän von Jamaica. *Eclogae Geologicae Helvetiae*, *62*, 731–735.

Bezuijen, M., Simpson, B., Behler, N., Daltry, J., & Tempsiripong, Y. (2012). *Crocodylus siamensis*. *The IUCN Red List of Threatened Species. Version 2014.3*.

Bickelmann, C., & Klein, N. (2009). The late Pleistocene horned crocodile *Voay robustus* (Grandidier & Vaillant, 1872) from Madagascar in the Museum für Naturkunde Berlin. *Fossil Record*, *12*(1), 13–21.

Blanco, M. V., Bona, P., Olivares, A. I., & Desojo, J. B. (2015). Ontogenetic variation in the skulls of *Caiman*: the case of *Caiman latirostris* and *Caiman yacare* (Alligatoridae, Caimaninae). *The Herpetological Journal*, *25*(2), 65–73.

Bocquentin-Villanueva, J., Souza-Filho, J. P., Buffetaut, E., & Negri, F. R. (1989). Nova interpretação do gênero *Purussaurus* (Crocodylia, Alligatoridae). *Anais do XI Congresso Brasileiro de Paleontologia. Curitiba: Sociedade Brasileira de Paleontologia*, *1*, 427–438.

Bona, P. (2007). Una nueva especie de *Eocaiman* Simpson (Crocodylia, Alligatoridae) del Paleoceno Inferior de Patagonia. *Ameghiniana*, *44*(2), 435–445.

Bona, P., & Barrios, F. (2015). The Alligatoroidea of Argentina: an update of its fossil record. *Publicación Electrónica de la Asociación Paleontológica Argentina*, *15*(1), 143–158.

Bona, P., Blanco, M. V. F., Schever, T. M., & Both, C. (2017a). Shedding light on the taxonomic diversity of the South American Miocene caimans: the status of *Melanosuchus fisheri* (Crocodylia, Alligatoroidea). *Ameghiniana*, *54*(6), 681–687.

Bona, P., & Carabajal, A. P. (2013). *Caiman gasparinae* sp. nov., a huge alligatorid (Caimaninae) from the late Miocene of Paraná, Argentina. *Alcheringa: An Australasian Journal of Palaeontology*, *37*(4), 462–473.

Bona, P., Carabajal, A. P., & Gasparini, Z. (2017b). Neuroanatomy of *Gryposuchus neogaeus* (Crocodylia, Gavialoidea): a first integral description of the braincase and endocranial morphological variation

in extinct and extant gavialoids. *Earth and Environmental Science Transactions of the Royal Society of Edinburgh*, *106*(4), 235–246.

Bona, P., Degrange, F. J., & Fernández, M. S. (2013a). Skull anatomy of the bizarre crocodylian *Mourasuchus nativus* (Alligatoridae, Caimaninae). *The Anatomical Record*, *296*(2), 227–239.

Bona, P., & Desojo, J. B. (2011). Osteology and cranial musculature of *Caiman latirostris* (Crocodylia: Alligatoridae). *Journal of Morphology*, *272*(7), 780–795.

Bona, P., Ezcurra, M. D., Barrios, F., & Fernandez Blanco, M. V. (2018). A new Palaeocene crocodylian from southern Argentina sheds light on the early history of caimanines. *Proceedings of the Royal Society B: Biological Sciences*, *285*(1885), 20180843.

Bona, P., Riff, D., & de Gasparini, Z. B. (2012). Late Miocene crocodylians from northeast Argentina: new approaches about the austral components of the Neogene South American crocodylian fauna. *Earth and Environmental Science Transactions of the Royal Society of Edinburgh*, *103*(3-4), 551–570.

Bona, P., Riff, D., & de Gasparini, Z. B. (2013b). Late Miocene crocodylians from northeast Argentina: new approaches about the austral components of the Neogene South American crocodylian fauna. *Earth and Environmental Science Transactions of the Royal Society of Edinburgh*, *103*(3-4), 551–570.

Brazaitis, P. (1973). The identification of living crocodilians. *Zoologica*, *58*(4), 59–101.

Brazaitis, P. (1987). Identification of crocodilian skins and products. In G. J. Webb, S. C. Manolis, & P. J. Whitehead (Eds.), *Wildlife management: Crocodiles and alligators* (pp. 373–386). Surrey Beatty; Sons, Sydney.

Brazeau, M. D. (2011). Problematic character coding methods in morphology and their effects. *Biological Journal of the Linnean Society*, *104*(3), 489–498.

Brazeau, M. D., Guillerme, T., & Smith, M. R. (2019). An algorithm for morphological phylogenetic analysis with inapplicable data. *Systematic Biology*, *68*(4), 619–631.

Brikiatis, L. (2014). The De Geer, Thulean and Beringia routes: key concepts for understanding early Cenozoic biogeography. *Journal of Biogeography*, *41*(6), 1036–1054.

Brinkmann, W. (1992). Die Krokodilier-Fauna aus der Unter-Kreide (Ober-Barremium) von Una (Provinz Cuenca, Spanien). *Geowissenshaftliche Abhandlungen*, *5*, 1–143.

Brinkmann, W., & Rauhe, M. (1998). *Diplocynodon ratelii* Pomel, 1847 (Crocodylia, Leidyosuchidae) aus dem unter-Oligozän von Céreste (Südfrankreich). *Neues Jahrbuch für Geologie und Paläontologie, Abhandlungen*, *209*(3), 295–322.

Brochu, C. A., & Rincón, A. D. (2004). A gavialoid crocodylian from the Lower Miocene of Venezuela. *Special Papers in Palaeontology*, *71*(71), 61–79.

Brochu, C. A. (1995). Heterochrony in the crocodylian scapulocoracoid. *Journal of Herpetology*, *29*(3), 464–468.

Brochu, C. A. (1996). Closure of neurocentral sutures during crocodilian ontogeny: implications for maturity assessment in fossil archosaurs. *Journal of Vertebrate Paleontology*, *16*(1), 49–62.

Brochu, C. A. (1997a). A review of "*Leidyosuchus*" (Crocodyliformes, Eusuchia) from the Cretaceous through Eocene of North America. *Journal of Vertebrate Paleontology*, *17*(4), 679–697.

Brochu, C. A. (1997b). Morphology, fossils, divergence timing, and the phylogenetic relationships of *Gavialis*. *Systematic Biology*, *46*(3), 479–522.

Brochu, C. A. (1999). Phylogenetics, taxonomy, and historical biogeography of Alligatoroidea. *Journal of Vertebrate Paleontology*, *19 (Supplement to No. 2)*, 9–100.

Brochu, C. A. (2000). Phylogenetic relationships and divergence timing of *Crocodylus* based on morphology and the fossil record. *Copeia*, *2000*(3), 657–673.

Brochu, C. A. (2001). Crocodylian snouts in space and time: phylogenetic approaches toward adaptive radiation. *American Zoologist*, *41*(3), 564–585.

Brochu, C. A. (2003). Phylogenetic approaches toward crocodylian history. *Annual Review of Earth and Planetary Sciences*, *31*(1), 357–397.

Brochu, C. A. (2004a). A new Late Cretaceous gavialoid crocodylian from eastern North America and the phylogenetic relationships of thoracosaurs. *Journal of Vertebrate Paleontology*, *24*(3), 610–633.

Brochu, C. A. (2004b). Alligatorine phylogeny and the status of *Allognathosuchus* Mook, 1921. *Journal of Vertebrate Paleontology*, *24*(4), 857–873.

Brochu, C. A. (2006a). *Eosuchus* (Crocodylia, Gavialoidea) from the Lower Eocene of the Isle of Sheppey, England. *Journal of Vertebrate Paleontology*, *26*(2), 466–470.

Brochu, C. A. (2006b). Osteology and phylogenetic significance of *Eosuchus minor* (Marsh, 1870) new combination, a longirostrine crocodylian from the late Paleocene of North America. *Journal of Paleontology*, *80*(1), 162–186.

Brochu, C. A. (2007a). Morphology, relationships, and biogeographical significance of an extinct horned crocodile (Crocodylia, Crocodylidae) from the Quaternary of Madagascar. *Zoological Journal of the Linnean Society*, *150*(4), 835–863.

Brochu, C. A. (2007b). Systematics and taxonomy of Eocene tomistomine crocodylians from Britain and Northern Europe. *Palaeontology*, *50*(4), 917–928.

Brochu, C. A. (2010). A new alligatorid from the lower Eocene Green River Formation of Wyoming and the origin of caimans. *Journal of Vertebrate Paleontology*, *30*(4), 1109–1126.

Brochu, C. A. (2011). Phylogenetic relationships of *Necrosuchus ionensis* Simpson, 1937 and the early history of caimanines. *Zoological Journal of the Linnean Society*, *163*, S228–S256.

Brochu, C. A. (2012). Phylogenetic relationships of Palaeogene ziphodont eusuchians and the status of *Pristichampsus* Gervais, 1853. *Earth and Environmental Science Transactions of the Royal Society of Edinburgh*, *103*(3-4), 521–550.

Brochu, C. A. (2020). Pliocene crocodiles from Kanapoi, Turkana Basin, Kenya. *Journal of Human Evolution*, *140*, 102410.

Brochu, C. A., & Carbot-Chanona, G. (2015). Biogeographic and systematic implications of a Caimanine from the Late Miocene of Southern Mexico. *Journal of Herpetology*, *49*(1), 138–142.

Brochu, C. A., & Gingerich, P. D. (2000). New tomistomine crocodylian from the middle Eocene (Bartonian) of Wadi Hitan, Fayum Province, Egypt. *Contributions from the Mueum of Paleontology, The University of Michigan*, *30*(10), 251–268.

Brochu, C. A., Nieves-Rivera, A. M., Vélez-Juarbe, J., Daza-Vaca, J. D., & Santos, H. (2007). Tertiary crocodylians from Puerto Rico: evidence for Late Tertiary endemic crocodylians in the West Indies? *Geobios*, *40*(1), 51–59.

Brochu, C. A., Njau, J., Blumenschine, R. J., & Densmore, L. D. (2010). A new horned crocodile from the Plio-Pleistocene hominid sites at Olduvai Gorge, Tanzania. *PLoS One*, *5*(2), e9333.

Brochu, C. A., Parris, D. C., Grandstaff, B. S., Denton Jr, R. K., & Gallagher, W. B. (2012). A new species of *Borealosuchus* (Crocodyliformes, Eusuchia) from the Late Cretaceous–early Paleogene of New Jersey. *Journal of Vertebrate Paleontology*, *32*(1), 105–116.

Brochu, C. A., & Storrs, G. W. (2012). A giant crocodile from the Plio-Pleistocene of Kenya, the phylogenetic relationships of Neogene African crocodylines, and the antiquity of *Crocodylus* in Africa. *Journal of Vertebrate Paleontology*, *32*(3), 587–602.

Brochu, C. A., & Sumrall, C. D. (2020). Modern cryptic species and crocodylian diversity in the fossil record. *Zoological Journal of the Linnean Society*.

Brochu, C. A., Wagner, J. R., Jouve, S., Sumrall, C. D., & Densmore, L. D. (2009). A correction corrected: consensus over the meaning of Crocodylia and why it matters. *Systematic Biology*, *58*(5), 537–543.

Brocklehurst, N., Romano, M., & Fröbisch, J. (2016). Principal component analysis as an alternative treatment for morphometric characters: phylogeny of caseids as a case study. *Palaeontology*, *59*(6), 877–886.

Bronzati, M., Montefeltro, F. C., & Langer, M. C. (2015). Diversification events and the effects of mass extinctions on Crocodyliformes evolutionary history. *Royal Society open science*, *2*(5), 140385.

Buchanan, L. A. (2009). *Kambara taraina* sp. nov. (Crocodylia, Crocodyloidea), a new Eocene mekosuchine from Queensland, Australia, and a revision of the genus. *Journal of Vertebrate Paleontology*, *29*(2), 473–486.

Buffetaut, E. (1982). Systematique, origine et évolution des Gavialidae Sud-Américains. *Geobios*, *15*, 127–140.

Buffetaut, E. (1985). The place of *Gavialis* and *Tomistoma* in Eusuchian evolution: a reconciliation of palaeontological and biochemical data. *Neues Jahrbuch für Geologie und Paläontologie. Monatshefte*, (12), 707–716.

Buffetaut, E., & Ford, R. L. E. (1979). The crocodilian *Bernissartia* in the Wealden of the Isle of Wight. *Palaeontology*, *22*(4), 905–912.

Buscalioni, A. D., Ortega, F., Weishampel, D. B., & Jianu, C. M. (2001). A revision of the crocodyliform *Allodaposuchus precedens* from the Upper Cretaceous of the Hateg Basin, Romania. Its relevance in the phylogeny of Eusuchia. *Journal of Vertebrate Paleontology*, *21*(1), 74–86.

Buscalioni, A. D., Ortega, F., & Vasse, D. (1997). New crocodiles (Eusuchia: Alligatoroidea) from the Upper Cretaceous of southern Europe. *Comptes Rendus de l'Académie des Sciences. Series IIA, Earth and Planetary Science*, *325*(7), 525–530.

Buscalioni, A. D., Piras, P., Vullo, R., Signore, M., & Barbera, C. (2011). Early Eusuchia Crocodylomorpha from the vertebrate-rich Plattenkalk of Pietraroia (Lower Albian, southern Apennines, Italy). *Zoological Journal of the Linnean Society*, *163*, S199–S227.

Buscalioni, A. D., Sanz, J. L., & Casanovas, M. L. (1992). A new species of the eusuchian crocodile *Diplocynodon* from the Eocene of Spain. *Neues Jahrbuch für Geologie und Paläontologie Abhandlungen*, *187*, 1–29.

Buscalioni, A. D., & Sanz, J. L. (1990). The small crocodile *Bernissartia fagesii* from the Lower Cretaceous of Galve (Teruel, Spain). *Bulletin de l'Institut Royal des Sciences Naturelles de Belgique, Sciences de la Terre*, *60*, 129–150.

Capellini, G. (1890a). Sul coccodrilliano garialoide (*Tomistoma calaritanus*) scoperto nella collina di Cagliari nel 1868. *Rendiconti della Reale Accademia dei Lincei, serie 4*, *6 (I Semestre)*, 149–151.

Capellini, G. (1890b). Sul coccodrilliano garialoide (*Tomistoma calaritanus*) scoperto nella collina di Cagliari nel MDCCCLXVIII. *Atti della Reale Accademia Lincei, Memorie della Classe di Scienze Fisiche, Matematiche e Naturali, serie 4*, *6*, 507–533.

Carbot-Chanona, G. (2017). Restos de cf. *Crocodylus* sp. en el Mioceno tardío de Chiapas, México: importancia paleobiogeográfica y paleoambiental. *Quehacer Científico en Chiapas*, *12*(2).

Carpenter, K. (1983). *Thoracosaurus neocesariensis* (De Kay, 1842) (Crocodylia: Crocodylidae) from the Late Cretaceous Ripley Formation of Mississippi. *Mississippi Geology*, *4*, 1–10.

Case, E. C. (1925). Note on a new species of the Eocene crocodilian *Allognathosuchus*, *A. wartheni*. *Contributions from the Mueum of Geology, University of Michigan*, *2*, 93–97.

Cautley, P. T., & Falconer, H. (1840). XXXIV.–Notice on the Remains of a Fossil Monkey from the Tertiary Strata of the Sewalik Hills in the North of Hindoostan. *Transactions of the Geological Society of London*, *2*(3), 499–504.

Chamero, B., Buscalioni, Á. D., Marugán-Lobón, J., & Sarris, I. (2014). 3D geometry and quantitative variation of the cervico-thoracic region in Crocodylia. *The Anatomical Record*, *297*(7), 1278–1291.

Chippindale, P. T., & Wiens, J. J. (1994). Weighting, partitioning, and combining characters in phylogenetic analysis. *Systematic Biology*, *43*(2), 278–287.

Chow, M. C., & Wang, B. Y. (1964). Fossil vertebrates from the Miocene of northern Kiangsu. *Vertebrata PalAsiatica*, *8*(4), 341–351.

Cidade, G. M., Fortier, D., & Hsiou, A. S. (2020a). Taxonomic and phylogenetic review of *Necrosuchus ionensis* (Alligatoroidea: Caimaninae) and the early evolution and radiation of caimanines. *Zoological Journal of the Linnean Society*, *189*(2), 657–669.

Cidade, G. M., Fortier, D., & Hsiou, A. S. (2019a). The crocodylomorph fauna of the Cenozoic of South America and its evolutionary history: a review. *Journal of South American Earth Sciences*, *90*, 392–411.

Cidade, G. M., Fortier, D., Rincon, A. D., & Hsiou, A. S. (2019b). Taxonomic review of two fossil crocodylians from the Cenozoic of South America and its implications for the crocodylian fauna of the continent. *Zootaxa*, *4656*(3), 475–486.

Cidade, G. M., Riff, D., De Souza-Filho, J. P., & Hsiou, A. S. (2019c). A reassessment of the osteology of *Mourasuchus amazonensis* Price, 1964 with comments on the taxonomy of the species. *Palaeontologia Electronica*, *22*(2), 1–23.

Cidade, G. M., Riff, D., & Hsiou, A. S. (2019d). The feeding habits of the strange crocodylian *Mourasuchus* (Alligatoroidea, Caimaninae): A review, new hypotheses and perspectives. *Revista Brasileira de Paleontologia*, *22*(2), 106–119.

Cidade, G. M., Solórzano, A., Rincón, A. D., Riff, D., & Hsiou, A. S. (2017). A new *Mourasuchus* (Alligatoroidea, Caimaninae) from the late Miocene of Venezuela, the phylogeny of Caimaninae and considerations on the feeding habits of *Mourasuchus*. *PeerJ*, *5*, e3056.

Cidade, G. M., Solórzano, A., Rincón, A. D., Riff, D., & Hsiou, A. S. (2020b). Redescription of the holotype of the Miocene crocodylian *Mourasuchus arendsi* (Alligatoroidea, Caimaninae) and perspectives on the taxonomy of the species. *Historical Biology*, *32*(6), 733–749.

Cidade, G. M., Souza-Filho, J. P., Hsiou, A. S., Brochu, C. A., & Riff, D. (2019e). New specimens of *Mourasuchus* (Alligatoroidea, Caimaninae) from the Miocene of Brazil and Bolivia and their taxonomic and morphological implications. *Alcheringa: An Australasian Journal of Palaeontology*, *43*(2), 261–278.

Clark, J. M. (1994). Patterns of evolution in Mesozoic Crocodyliformes. In N. Fraser & H.-D. Sues (Eds.), *In the shadow of the dinosaurs: Early mesozoic tetrapods* (pp. 84–97). Cambridge University Press.

Clark, J. M. (1986). *Phylogenetic relationships of the crocodylomorph archosaurs* (Doctoral dissertation). University of Chicago, Department of Anatomy.

Clark, J. M., & Norell, M. (1992). The Early Cretaceous crocodylomorph *Hylaeochampsa vectiana* from the Wealden of the Isle of Wight. *American Museum Novitates*, *3032*, 1–19.

Claude, J., Naksri, W., Boonchai, N., Buffetaut, E., Duangkrayom, J., Laojumpon, C., Jintasakul, P., Lauprasert, K., Martin, J., Suteethorn, V., & Tong, H. (2011). Neogene reptiles of northeastern Thailand and their paleogeographical significance. *Annales de Paléontologie*, *97*, 113–131.

Cong, L., Hou, L., Wu, X., & Hou, J. (1998). *The gross anatomy of Alligator sinensis Fauvel [in Chinese].* China Forestry Publishing House, Beijing.

Conrad, J. L., Jenkins, K., Lehmann, T., Manthi, F. K., Peppe, D. J., Nightingale, S., Cossette, A., Dunsworth, H. M., Harcourt-Smith, W. E., & Mcnulty, K. P. (2013). New specimens of '*Crocodylus*' *pigotti* (Crocodylidae) from Rusinga Island, Kenya, and generic reallocation of the species. *Journal of Vertebrate Paleontology*, *33*(3), 629–646.

Cope, E. D. (1882). The reptiles of the American Eocene. *The American Naturalist*, *16*(12), 979–993.

Cossette, A. P. (2020). A new species of *Bottosaurus* (Alligatoroidea: Caimaninae) from the Black Peaks Formation (Palaeocene) of Texas indicates an early radiation of North American caimanines. *Zoological Journal of the Linnean Society*. https://doi.org/https://doi.org/10.1093/zoolinnean/zlz178

Cossette, A. P., & Brochu, C. A. (2018). A new specimen of the alligatoroid *Bottosaurus harlani* and the early history of character evolution in alligatorids. *Journal of Vertebrate Paleontology*, *38*(4), 1–22.

Cossette, A. P., & Brochu, C. A. (2020). A systematic review of the giant alligatoroid *Deinosuchus* from the Campanian of North America and its implications for the relationships at the root of Crocodylia. *Journal of Vertebrate Paleontology*, e1767638.

Costa, O. G. (1848). *Paleontologia del regno di Napoli. Parte I. Stable Tip*. Tramater, Napoli.

Cox, P. B., & Urbatsch, L. E. (1990). A phylogenetic analysis of the coneflower genera (Asteraceae: Heliantheae). *Systematic Botany*, 394–402.

Cuvier, G. (1807). Sur les diffèrentes espèces de crocodiles vivans et sur leurs caractères distinctifs. *Annales du Muséum d'Histoire Naturelle*, *10*, 8–66.

Daley, B. (1999). Palaeogene sections in the Isle of Wight. A revision of their description and significance in the light of research undertaken over recent decades. *Tertiary Research*, *19*, 1–69.

D'Amore, D. C., Harmon, M., Drumheller, S. K., & Testin, J. J. (2019). Quantitative heterodonty in Crocodylia: assessing size and shape across modern and extinct taxa. *PeerJ*, *7*, e6485.

De Celis, A., Narváez, I., & Ortega, F. (2020). Spatiotemporal palaeodiversity patterns of modern crocodiles (Crocodyliformes: Eusuchia). *Zoological Journal of the Linnean Society*, *189*(2), 635–656.

De Laet, J. (2005). Parsimony and the problem of inapplicables in sequence data. In A. V. A (Ed.), *Parsimony, phylogeny and genomics* (pp. 81–116). Oxford University Press.

De Vis, C. W. (1905). Fossil vertebrates from New Guinea. *Annals of the Queensland Museum*, *6*, 26–31.

Delfino, M. (2008). New remains of *Crocodylus checchiai* Maccagno 1947 (Crocodylia, Crocodylidae) from the Late Miocene of As Sahabi, Libya. *Garyounis Scientific Bulletin*, *5*, 111–118.

Delfino, M., Böhme, M., & Rook, L. (2007). First European evidence for transcontinental dispersal of *Crocodylus* (late Neogene of southern Italy). *Zoological Journal of the Linnean Society*, *149*(3), 293–307.

Delfino, M., Codrea, V., Folie, A., Dica, P., Godefroit, P., & Smith, T. (2008a). A complete skull of *Allodaposuchus precedens* Nopcsa, 1928 (Eusuchia) and a reassessment of the morphology of the taxon based on the Romanian remains. *Journal of Vertebrate Paleontology*, *28*(1), 111–122.

Delfino, M., & De Vos, J. (2010). A revision of the Dubois crocodylians, *Gavialis bengawanicus* and *Crocodylus ossifragus*, from the Pleistocene *Homo erectus* beds of Java. *Journal of Vertebrate Paleontology*, *30*(2), 427–441.

Delfino, M., Iurino, D. A., Mercurio, B., Piras, P., Rook, L., & Sardella, R. (2020). Old African fossils provide new evidence for the origin of the American crocodiles. *Scientific Reports*, *10*(1), 1–11.

Delfino, M., Martin, J. E., & Buffetaut, E. (2008b). A new species of *Acynodon* (Crocodylia) from the upper cretaceous (Santonian–Campanian) of Villaggio del Pescatore, Italy. *Palaeontology*, *51*(5), 1091–1106.

Delfino, M., Martin, J. E., de Lapparent de Broin, F., & Smith, T. (2019). Evidence for a pre-PETM dispersal of the earliest European crocodyloids. *Historical Biology*, *31*(7), 845–852.

Delfino, M., Piras, P., & Smith, T. (2005). Anatomy and phylogeny of the gavialoid crocodylian *Eosuchus lerichei* from the Paleogene of Europe. *Acta Palaeontologica Polonica*, *50*(3), 565–580.

Delfino, M., & Rook, L. (2008). African crocodylians in the Late Neogene of Europe: a revision of *Crocodylus bambolii* Ristori, 1890. *Journal of Paleontology*, *82*(2), 336–343.

Delfino, M., & Rossi, M. A. (2013). Fossil crocodylid remains from Scontrone (Tortonian, Southern Italy) and the late Neogene Mediterranean biogeography of crocodylians. *Geobios*, *46*(1-2), 25–31.

Delfino, M., & Smith, T. (2009). A reassessment of the morphology and taxonomic status of '*Crocodylus*' *depressifrons* (Crocodylia, Crocodyloidea) based on the Early Eocene remains from Belgium. *Zoological Journal of the Linnean Society*, *156*(1), 140–167.

Delfino, M., & Smith, T. (2012). Reappraisal of the morphology and phylogenetic relationships of the middle Eocene alligatoroid *Diplocynodon deponiae* (Frey, Laemmert, and Riess, 1987) based on a three-dimensional specimen. *Journal of Vertebrate Paleontology*, *32*(6), 1358–1369.

Densmore, L. D., & Owen, R. D. (1989). Molecular systematics of the order Crocodilia. *American Zoologist*, *29*(3), 831–841.

Densmore, L. D. (1983). Biochemical and immunological systematics of the order Crocodilia. In M. K. Hecht, B. Wallace, & G. T. Prance (Eds.), *Evolutionary biology* (pp. 397–465). Springer.

Densmore, L. D., & White, P. S. (1991). The systematics and evolution of the Crocodilia as suggested by restriction endonuclease analysis of mitochondrial and nuclear ribosomal DNA. *Copeia*, 602–615.

de Stefano, G. (1905). Appunti sui Batraci e sui Rettili del Quercy appartenenti alla collezione Rossignol. *Bolletino della Societa Geologia Italiana*, *24*, 17–67.

Dollo, L. (1907). Nouvelle note sur les reptiles de l'Eocène inférieur de la Belgique et des régions voisines (*Eosuchus lerichei* et *Eosphargis gigas*). *Bulletin de la Société belge de Géologie, Paleontologie e Hydrologie*, *21*, 81–85.

Duméril, C. (1806). *Zoologie analytique, ou Méthode naturelle de classification des animaux: rendue plus facile à l'aide de tableaux synoptiques*. Allais.

Duméril, C., & Bibron, G. (1835). *Erpétologie general ou histoire naturelle compléte des reptiles, Vol III*.

Eaton, M. J., Martin, A., Thorbjarnarson, J., & Amato, G. (2009). Species-level diversification of African dwarf crocodiles (Genus *Osteolaemus*): a geographic and phylogenetic perspective. *Molecular Phylogenetics and Evolution*, *50*(3), 496–506.

Edwards, N., & Daley, B. (1997). Stratigraphy of the Totland Bay Member (Headon Hill Formation, Late Eocene) at Hordle Cliff, Hampshire, Southern England. *Tertiary Research*, *18*, 35–50.

Efimov, M. B. (1982). New fossil crocodiles from the USSR [in Russian]. *Paleontologiceskij zurnal*, *2*, 146–150.

Efimov, M. B. (1988). The fossil crocodiles and champsosaurids of Mongolia and USSR [in Russian]. *Trudy, Sovmestnaâ Sovetcko–Mongol'skaâ Paleontologiceskaâ Ékspediciâ*, *36*, 1–108.

Efimov, M. B. (1993). The Eocene crocodiles of the GUS–a history of development. *Kaupia*, *3*, 23–25.

Efimov, M. B., & Yarkov, A. A. (1993). A Paleocene crocodile from the lower Volga Basin. *Paleontologiceskij zurnal*, *27*(11).

Erickson, B. R. (1976). *Osteology of the early eusuchian crocodile Leidyosuchus formidabilis, sp. nov* (Vol. 2). Monographs of the Science Museum of Minnesota (Paleontology).

Erickson, B. R. (1982). *Wannaganosuchus*, a new alligator from the Paleocene of North America. *Journal of Paleontology*, 492–506.

Erickson, B. R. (1998). Crocodilians of the Black Mingo Group (Paleocene) of the South Carolina Coastal Plain. *Transactions of the American Philosophical Society*, 196–214.

Erickson, B. R., & Sawyer, G. T. (1996). *The estuarine crocodile Gavialosuchus carolinensis n. sp. (Crocodylia: Eusuchia) from the late Oligocene of South Carolina, North America* (Vol. 3). Science Museum of Minnesota.

Escapa, I. H., & Catalano, S. A. (2013). Phylogenetic analysis of Araucariaceae: integrating molecules, morphology, and fossils. *International Journal of Plant Sciences*, *174*(8), 1153–1170.

Estes, R., & Hutchison, J. H. (1980). Eocene lower vertebrates from Ellesmere Island, Canadian arctic archipelago. *Palaeogeography, Palaeoclimatology, Palaeoecology*, *30*, 325–347.

Etheridge, R. (1917). Reptilian Notes: *Megalania prisca*, Owen, and *Notiosaurus dentatus*, Owen; Lacertiiian dermal armour; Opalized remains from Lightning Ridge. *Proceedings of the Royal Society of Victoria*, *29*, 127–133.

Ezcurra, M. D., & Agnolín, F. L. (2012). A new global palaeobiogeographical model for the late Mesozoic and early Tertiary. *Systematic Biology*, *61*(4), 553–566.

Farris, J. S. (1969). A successive approximations approach to character weighting. *Systematic Biology*, *18*(4), 374–385.

Farris, J. S. (1990). Phenetics in camouflage. *Cladistics*, *6*(1), 91–100.

Fisher, D. C. (2008). Stratocladistics: integrating temporal data and character data in phylogenetic inference. *Annual Review of Ecology, Evolution, and Systematics*, *39*, 365–385.

Fitzinger, L. J. (1826). *Neue classification der Reptilien nach ihren natürlichen verwandtschaften nebst einer verwandschafts - tafel und einem verzeichnisse der Reptilien-sammlung des zoologischen museum's zu Wien*. J. G. Heubner.

Fortier, D. C., De Souza-Filho, J. P., Guilherme, E., Maciente, A. A., & Schultz, C. L. (2014). A new specimen of *Caiman brevirostris* (Crocodylia, Alligatoridae) from the Late Miocene of Brazil. *Journal of Vertebrate Paleontology*, *34*(4), 820–834.

Fortier, D. C., & Rincón, A. D. (2013). Pleistocene crocodylians from Venezuela, and the description of a new species of *Caiman*. *Quaternary International*, *305*, 141–148.

Foth, C., Fernandez Blanco, M. V., Bona, P., & Scheyer, T. M. (2017). Cranial shape variation in jacarean caimanines (Crocodylia, Alligatoroidea) and its implications in the taxonomic status of extinct species: the case of *Melanosuchus fisheri*. *Journal of Morphology*, *279*(2), 259–273.

Fourtau, R. (1920). *Contribution à l'étude des vertébrés miocènes de l'Egypte*. Cairo Government Press.

Frey, E., Laemmert, A., & Riess, J. (1987). *Baryphracta deponiae* n. g. n. sp. (Reptilia, Crocodylia), ein neues Krokodil aus der Grube Messel bey Darmstadt (Hessen, Bundesrepublik Deutschland). *Neues Jahrbuch für Geologie und Paläontologie, Monatschefte*, *1987*, 15–26.

Frey, E., Riess, J., & Tarsitano, S. F. (1989). The axial tail musculature of recent crocodiles and its phyletic implications. *American Zoologist*, *29*(3), 857–862.

Fuchs, K. (2006). *The crocodile skin: important characteristics in identifying crocodilian species*. Andreas S. Brahm.

Garcia-Cruz, J., & Sosa, V. (2006). Coding quantitative character data for phylogenetic analysis: a comparison of five methods. *Systematic Botany*, *31*(2), 302–309.

Gasparini, Z. (1985). Un nuevo crocodilo (Eusuchia) Cenozoico de America de Sur. *MME-DNPM Série Geologia Paleontologia*, *2*, 51–53.

Gasparini, Z. B. (1968). Nuevos restos de *Rhamphostomopsis neogaeus* (Burm.) Rusconi 1933, (Reptilia, Crocodilia) del "Mesopotamiense" (Plioceno medio-superior) de Argentina. *Ameghiniana*, *5*(8), 299–311.

Gatesy, J., Amato, G., Norell, M., DeSalle, R., & Hayashi, C. (2003). Combined support for wholesale taxic atavism in gavialine crocodylians. *Systematic Biology*, *52*(3), 403–422.

Gatesy, J., & Amato, G. D. (1992). Sequence similarity of 12S ribosomal segment of mitochondrial DNAs of gharial and false gharial. *Copeia*, *1992*(1), 241–243.

Gatesy, J., DeSalle, R., & Wheeler, W. (1993). Alignment-ambiguous nucleotide sites and the exclusion of systematic data. *Molecular phylogenetics and evolution*, *2*(2), 152–157.

Gayet, M., Rage, J.-C., Sempere, T., & Gagnier, P.-Y. (1992). Modalités des échanges de vertébrés continentaux entre l'Amérique du Nord et l'Amérique du Sud au Crétacé supérieur et au Paléocène. *Bulletin de la Société géologique de France*, *163*, 761–791.

Gilmore, C. W. (1910). *Leidyosuchus sternbergii*, a new species of crocodile from the Ceratops Beds of Wyoming. *Proceedings of the United States National Museum*, *38*(1762), 485–502.

Gilmore, C. W. (1911). A new fossil alligator from the Hell Creek beds of Montana. *Proceedings of the United States National Museum*, *41*(1860), 297–302.

Gilmore, C. W. (1946). A new crocodilian from the Eocene of Utah. *Journal of Paleontology*, *20*, 62–67.

Ginsburg, L., & Buffetaut, E. (1978). *Euthecodon arambourgi* n. sp., et l'évolution du genre *Euthecodon*, Crocodilien du Néogène d'Afrique. *Géologie méditerranéenne*, *5*(2), 291–301.

Ginsburg, L., & Bulot, C. (1997). Les *Diplocynodon* (Reptilia, Crocodylia) de l'Orléanien (Miocène inférieur à moyen) de France. *Geodiversitas*, *19*(1), 107–128.

Gmelin, J. F. (1789). *Caroli a Linné. Systema naturae per regna tria naturae, secundum classes, ordines, genera, speciescum characteribus, differentiis, synonymis, locis: 1.3* (Vol. 1). Lipsiae: impensis Georg Emanuel Beer.

Godoy, P. L., Benson, R. B. J., Bronzati, M., & Butler, R. J. (2019). The multi-peak adaptive landscape of crocodylomorph body size evolution. *BMC evolutionary biology*, *19*(1), 167.

Godoy, P. L., Bronzati, M., Eltink, E., Júlio, C. d. A., Cidade, G. M., Langer, M. C., & Montefeltro, F. C. (2016). Postcranial anatomy of *Pissarrachampsa sera* (Crocodyliformes, Baurusuchidae) from the Late Cretaceous of Brazil: insights on lifestyle and phylogenetic significance. *PeerJ*, *4*, e2075.

Godoy, P. L. (2014). *Osteologia e filogenia de dois Crocodyliformes fósseis: Aplestosuchus sordidus do Cretáceo do Brasil e Eocaiman cavernensis do Eoceno da Argentina* (Thesis).

Gold, M. E. L., Brochu, C. A., & Norell, M. A. (2014). An expanded combined evidence approach to the *Gavialis* problem using geometric morphometric data from crocodylian braincases and Eustachian systems. *PloS one*, *9*(9), e105793.

Goloboff, P. A. (1993). Estimating character weights during tree search. *Cladistics*, *9*(1), 83–91.

Goloboff, P. A. (2014). Extended implied weighting. *Cladistics*, *30*(3), 260–272.

Goloboff, P. A., Carpenter, J. M., Arias, J. S., & Esquivel, D. R. M. (2008a). Weighting against homoplasy improves phylogenetic analysis of morphological data sets. *Cladistics*, *24*(5), 758–773.

Goloboff, P. A., & Catalano, S. A. (2016). TNT version 1.5, including a full implementation of phylogenetic morphometrics. *Cladistics*, *32*(3), 221–238.

Goloboff, P. A., Farris, J. S., & Nixon, K. C. (2008b). TNT, a free program for phylogenetic analysis. *Cladistics*, *24*(5), 774–786.

Goloboff, P. A., Mattoni, C. I., & Quinteros, A. S. (2006). Continuous characters analyzed as such. *Cladistics*, *22*(6), 589–601.

Goloboff, P. A., Torres, A., & Arias, J. S. (2018). Weighted parsimony outperforms other methods of phylogenetic inference under models appropriate for morphology. *Cladistics*, *34*(4), 407–437.

Gomani, E. M. (1997). A crocodyliform from the Early Cretaceous dinosaur beds, northern Malawi. *Journal of Vertebrate Paleontology*, *17*(2), 280–294.

Gramann, E. (1958). Der Crocodilide *Diplocynodon hantoniensis* (Wood) aus dem unteroligozanen Melanienton Niederhessens. *Notizblatt der Hessischen Landes-Amte Bodenforschung*, *86*, 77–78.

Gray, J. E. (1844). *Catalogue of the Tortoises, Crocodiles, and Amphisbaenians, in the Collection of the British Museum*. Edward Newman, Devonshire Street, Bishopsgate Street.

Green, R. E., Braun, E. L., Armstrong, J., Earl, D., Nguyen, N., Hickey, G., Vandewege, M. W., John, J. A. S., Capella-Gutiérrez, S., Castoe, T. A., & Kern, C. (2014). Three crocodilian genomes reveal ancestral patterns of evolution among archosaurs. *Science*, *346*(6215), 1254449.

Grigg, G. C., Beard, L. A., Moulton, T., Melo, M. T. Q., & Taplin, L. E. (1998). Osmoregulation by the broad-snouted caiman, *Caiman latirostris*, in estuarine habitat in southern Brazil. *Journal of Comparative Physiology B*, *168*(6), 445–452.

Grigg, G., & Kirshner, D. (2015). *Biology and evolution of crocodylians*. Cornell University Press.

Groh, S. S., Upchurch, P., Barrett, P. M., & Day, J. J. (2020). The phylogenetic relationships of neosuchian crocodiles and their implications for the convergent evolution of the longirostrine condition. *Zoological Journal of the Linnean Society*, *188*(2), 473–506.

Gumbs, R., Gray, C. L., Wearn, O. R., & Owen, N. R. (2018). Tetrapods on the EDGE: Overcoming data limitations to identify phylogenetic conservation priorities. *PloS one*, *13*(4).

Harshman, J., Huddleston, C. J., Bollback, J. P., Parsons, T. J., & Braun, M. J. (2003). True and false gharials: a nuclear gene phylogeny of Crocodylia. *Systematic Biology*, *52*(3), 386–402.

Hass, C. A., Hoffman, M. A., Densmore III, L. D., & Maxson, L. R. (1992). Crocodilian evolution: insights from immunological data. *Molecular Phylogenetics and Evolution*, *1*(3), 193–201.

Hastings, A. K., Bloch, J. I., Cadena, E. A., & Jaramillo, C. A. (2010). A new small short-snouted dyrosaurid (Crocodylomorpha, Mesoeucrocodylia) from the Paleocene of Northeastern Colombia. *Journal of Vertebrate Paleontology*, *30*(1), 139–162.

Hastings, A. K., Bloch, J. I., Jaramillo, C. A., Rincon, A. F., & MacFadden, B. J. (2013). Systematics and biogeography of crocodylians from the Miocene of Panama. *Journal of Vertebrate Paleontology*, *33*(2), 239–263.

Hastings, A. K., & Hellmund, M. (2015). Rare in situ preservation of adult crocodylian with eggs from the Middle Eocene of Geiseltal, Germany. *Palaios*, *30*(6), 446–461.

Hastings, A. K., Reisser, M., & Scheyer, T. M. (2016). Character evolution and the origin of Caimaninae (Crocodylia) in the New World Tropics: new evidence from the Miocene of Panama and Venezuela. *Journal of Paleontology*, *90*(2), 317–332.

Hastings, M. (1848). On the freshwater Eocene beds of the Hordle Cliff, Hants. *Report of the British Association for the Advancement of Science*, *17*, 63–64.

Hay, O. P. (1930). *Second bibliography and catalogue of fossil Vertebrata of North America. Vol. 2* (Vol. 2). Carnegie Institution of Washington.

Head, J. J. (2001). Systematics and body size of the gigantic, enigmatic crocodyloid *Rhamphosuchus crassidens*, and the faunal history of Siwalik Group (Miocene) crocodylians. *Journal of Vertebrate Paleontology*, *21, Supplement to No.3*(59A).

Hecht, M. K., & Malone, B. (1972). On the early history of the gavialid crocodilians. *Herpetologica*, 281–284.

Hedges, S. B. (2006). Paleogeography of the Antilles and the origin of West Indian amphibians and reptiles. *Applied Herpetology*, *3*, 281–292.

Hekkala, E., Shirley, M. H., Amato, G., Austin, J. D., Charter, S., Thorbjarnarson, J., Vliet, K. A., Houck, M. L., Desalle, R., & Blum, M. J. (2011). An ancient icon reveals new mysteries: mummy DNA resurrects a cryptic species within the Nile crocodile. *Molecular ecology*, *20*(20), 4199–4215.

Hennig, W. (1965). Phylogenetic systematics. *Annual review of entomology*, *10*(1), 97–116.

Hocknull, S. A., Lewis, R., Arnold, L. J., Pietsch, T., Joannes-Boyau, R., Price, G. J., Moss, P., Wood, R., Dosseto, A., Louys, J., Olley, J., & Lawrence, R. A. (2020). Extinction of eastern Sahul megafauna coincides with sustained environmental deterioration. *Nature Communications*, *11*(1), 1–14.

Hoffstetter, R., & Gasc, J. P. (1969). Vertebrae and ribs of modern reptiles. In C. Gans, A.-d. Bellairs, & P. T. S (Eds.), *Biology of the Reptilia, Vol. 1. Morphology A* (pp. 201–310). London; New York: Academic Press.

Holland, W. J. (1909). *Deinosuchus hatcheri*, a new genus and species of crocodile from the Judith River beds of Montana. *Annals of the Cernegie Museum*, *6*, 281–294.

Holliday, C. M., Tsai, H. P., Skiljan, R. J., George, I. D., & Pathan, S. (2013). A 3D interactive model and atlas of the jaw musculature of *Alligator mississippiensis*. *PLoS One*, *8*(6), e62806.

Holliday, C. M., & Witmer, L. M. (2009). The epipterygoid of crocodyliforms and its significance for the evolution of the orbitotemporal region of eusuchians. *Journal of Vertebrate Paleontology*, *29*(3), 715–733.

Hoorn, C., Wesselingh, F. P., Ter Steege, H., Bermudez, M. A., Mora, A., Sevink, J., Sanmartín, I., Sanchez-Meseguer, A., Anderson, C. L., Figueiredo, J. P., & Jaramillo, C. (2010). Amazonia through time: Andean uplift, climate change, landscape evolution, and biodiversity. *Science*, *330*(6006), 927–931.

Hornung-Leoni, C. T., & Sosa, V. (2008). Morphological phylogenetics of *Puya* subgenus *Puya* (Bromeliaceae). *Botanical Journal of the Linnean Society*, *156*(1), 93–110.

Hren, M. T., Sheldon, N. D., Grimes, S. T., Collinson, M. E., Hooker, J. J., Bugler, M., & Lohmann, K. C. (2013). Terrestrial cooling in Northern Europe during the Eocene-Oligocene transition. *Proceedings of the National Academy of Sciences*, *110*(19), 7562–7567.

Hu, X., Garzanti, E., Wang, J., Huang, W., An, W., & Webb, A. (2016). The timing of India-Asia collision onset–facts, theories, controversies. *Earth-Science Reviews*, *160*, 264–299.

Hua, S., & Jouve, S. (2004). A primitive marine gavialoid from the Paleocene of Morocco. *Journal of Vertebrate Paleontology*, *24*(2), 341–350.

Huelsenbeck, J. P. (1994). Comparing the stratigraphic record to estimates of phylogeny. *Paleobiology*, *20*(4), 470–483.

Hulke, J. W. (1871). Note on some Reptillian Fossils from Gozo. *Quarterly Journal of the Geological Society*, *27*(1-2), 29–33.

Huxley, T. H. (1859). On the dermal armor of *Crocodilus hastingsiae*. *Quarterly Journal of the Geological Society*, *15*, 678–680.

Huxley, T. H. (1875). On *Stagonolepis robertsoni*, and on the evolution of the Crocodilia. *Quarterly Journal of the Geological Society*, *31*(1-4), 423–438.

Iijima, M., & Kubo, T. (2019a). Allometric growth of limb and body proportions in crocodylians. *Journal of Zoology*, *309*(3), 200–211.

Iijima, M., & Kobayashi, Y. (2019). Mosaic nature in the skeleton of East Asian crocodylians fills the morphological gap between "Tomistominae" and Gavialinae. *Cladistics*, *35*(6), 623–632.

Iijima, M., & Kubo, T. (2019b). Comparative morphology of presacral vertebrae in extant crocodylians: taxonomic, functional and ecological implications. *Zoological Journal of the Linnean Society*, *186*(4), 1006–1025.

Iijima, M., Kubo, T., & Kobayashi, Y. (2018a). Comparative limb proportions reveal differential locomotor morphofunctions of alligatoroids and crocodyloids. *Royal Society Open Science*, *5*(3), 171774.

Iijima, M., Momohara, A., Kobayashi, Y., Hayashi, S., Ikeda, T., Taruno, H., Watanabe, K., Tanimoto, M., & Furui, S. (2018b). *Toyotamaphimeia* cf. *machikanensis* (Crocodylia, Tomistominae) from the Middle Pleistocene of Osaka, Japan, and crocodylian survivorship through the Pliocene-Pleistocene climatic oscillations. *Palaeogeography, Palaeoclimatology, Palaeoecology*, *496*, 346–360.

Iijima, M., Takahashi, K., & Kobayashi, Y. (2016). The oldest record of *Alligator sinensis* from the Late Pliocene of Western Japan, and its biogeographic implication. *Journal of Asian Earth Sciences*, *124*, 94–101.

Iordansky, N. N. (1973). The skull of the Crocodilia. In C. Gans & T. S. Parsons (Eds.), *Biology of the Reptilia* (pp. 201–262). Academic Press, London.

Isaac, N. J. B., Turvey, S. T., Collen, B., Waterman, C., & Baillie, J. E. M. (2007). Mammals on the EDGE: conservation priorities based on threat and phylogeny. *PloS one*, *2*(3).

Iturralde-Vinent, M., & MacPhee, R. D. E. (1999). Paleogeography of the Caribbean region: implications for Cenozoic biogeography. *Bulletin of the American Museum of Natural History*, *238*, 1–95.

Iturralde-Vinent, M. A. (2006). Meso-Cenozoic Caribbean paleogeography: implications for the historical biogeography of the region. *International Geology Review*, *48*(9), 791–827.

Janke, A., Gullberg, A., Hughes, S., Aggarwal, R. K., & Arnason, U. (2005). Mitogenomic analyses place the gharial (*Gavialis gangeticus*) on the crocodile tree and provide pre-K/T divergence times for most crocodilians. *Journal of Molecular Evolution*, *61*(5), 620–626.

Jaramillo, C. (2018). Evolution of the Isthmus of Panama: biological, paleoceanographic and paleoclimatological implications. In C. Hoorn, A. Perrigo, & A. Antonelli (Eds.), *Mountains, climate and biodiversity* (pp. 323–338). Wiley Blackwell.

Ji, X., Wu, X., Li, Y., Yan, P., & Amato, G. (2006). The mitochondrial genome of *Crocodylus niloticus* with implications for phylogenetic relationships among crocodilian species. *Dong wu xue bao.[Acta zoologica Sinica]*, *52*(4), 810–818.

Joleaud, M. L. (1920). Sur la présence d'un Gavialidé du genre *Tomistoma* dans le Pliocene d'eau douce del Éthiopie. *Comptes Rendus de l'Academie des Sciences de Paris*, *170*, 816–818.

Jones, A. S., & Butler, R. J. (2018). A new phylogenetic analysis of Phytosauria (Archosauria: Pseudosuchia) with the application of continuous and geometric morphometric character coding. *PeerJ*, *6*, e5901.

Jonet, S., & Wouters, G. (1977). *Maroccosuchus zennaroi*, crocodilien eusuchien nouveau des phosphates du Maroc. *Notes et Mémoires du Service Géologique du Maroc*, *38*, 177–202.

Jouve, S. (2004). *Etude des Crocodyliformes fini Crétacé-Paléogène du Bassin des Oulad Abdoun (Maroc) et comparaison avec les faunes africaines contemporaines: systématique, phylogénie et paléobiogéographie* (Thesis).

Jouve, S. (2009). The skull of *Teleosaurus cadomensis* (Crocodylomorpha; Thalattosuchia), and phylogenetic analysis of Thalattosuchia. *Journal of Vertebrate Paleontology*, *29*(1), 88–102.

Jouve, S. (2016). A new basal tomistomine (Crocodylia, Crocodyloidea) from Issel (Middle Eocene; France): palaeobiogeography of basal tomistomines and palaeogeographic consequences. *Zoological Journal of the Linnean Society*, *177*(1), 165–182.

Jouve, S., Bardet, N., Jalil, N.-E., Suberbiola, X. P., Bouya, B., & Amaghzaz, M. (2008). The oldest African crocodylian: phylogeny, paleobiogeography, and differential survivorship of marine reptiles through the Cretaceous-Tertiary boundary. *Journal of Vertebrate Paleontology*, *28*(2), 409–421.

Jouve, S., Bouya, B., Amaghzaz, M., & Meslouh, S. (2015). *Maroccosuchus zennaroi* (Crocodylia: Tomistominae) from the Eocene of Morocco: Phylogenetic and palaeobiogeographical implications of the basalmost tomistomine. *Journal of Systematic Palaeontology*, *13*(5), 421–445.

Jouve, S., Iarochene, M., Bouya, B., & Amaghzaz, M. (2006a). A new species of *Dyrosaurus* (Crocodylomorpha, Dyrosauridae) from the early Eocene of Morocco: phylogenetic implications. *Zoological Journal of the Linnean Society*, *148*(4), 603–656.

Jouve, S., Iarochene, M., Bouya, B., & Amaghzaz, M. (2006b). New material of *Argochampsa krebsi* (Crocodylia: Gavialoidea) from the Lower Paleocene of the Oulad Abdoun Basin (Morocco): phylogenetic implications. *Geobios*, *39*(6), 817–832.

Jouve, S., Sarıgül, V., Steyer, J.-S., & Sen, S. (2019). The first crocodylomorph from the Mesozoic of Turkey (Barremian of Zonguldak) and the dispersal of the eusuchians during the Cretaceous. *Journal of Systematic Palaeontology*, *17*(2), 111–128.

Kälin, J. A. (1933). Beiträge zur vergleichenden Osteologie des Crocodiliden schädels. *Zoologische Jahrbücher*, *57*, 535–714.

Kälin, J. A. (1936). *Hispanochampsa mülleri* nov. gen. nov. spec., ein neuer Crocodilide aus dem unteren Oligocaen von Tárrega (Catalonien). *Abhandlungen der Schweizerischen paläontologischen Gesellschaft*, *58*, 1–40.

Kälin, J. A. (1939). Ein extrem kurzschnauziger Crocodilide aus den Phosphoriten des Quercy *Arambourgia* (nov. gen.) *gaudryi* de Stefano. *Abhandlungen der Schweizerischen paläontologischen Gesellschaft*, *62*, 1–18.

Kälin, J. A. (1955). Zur Stammesgeschichte der Crocodilia. *Revue Suisse de Zoologie*, *62*, 347–356.

Karl, H.-V., & Müller, A. (2008). New fossil reptile material (Reptilia: Chelonii, Crocodylia) from the Lower Oligocene of Borken (Central Germany: Hesse). *Studia Geologica Salmanticensia*, *44*(1), 41–58.

Kehlmaier, C., Barlow, A., Hastings, A. K., Vamberger, M., Paijmans, J. L., Steadman, D. W., Albury, N. A., Franz, R., Hofreiter, M., & Fritz, U. (2017). Tropical ancient DNA reveals relationships of the extinct Bahamian giant tortoise *Chelonoidis alburyorum*. *Proceedings of the Royal Society B: Biological Sciences*, *284*(1846), 20162235.

Klinkhamer, A. J., Wilhite, D. R., White, M. A., & Wroe, S. (2017). Digital dissection and three-dimensional interactive models of limb musculature in the Australian estuarine crocodile (*Crocodylus porosus*). *PLoS One*, *12*(4), e0175079.

Kobatake, N., Chiji, M., Ikebe, N., Ishida, S., Kamei, T., Nakaseko, K., & Matsumoto, E. (1965). Discovery of crocodile fossil from the Osaka Group. *The Quaternary Research (Daiyonki-Kenkyu)*, *4*(2), 49–58.

Kobayashi, Y., Tomida, Y., Kamei, T., & Eguchi, T. (2006). Anatomy of a Japanese tomistomine crocodylian, *Toyotamaphimeia machikanensis* (Kamei et Matsumoto, 1965), from the middle Pleistocene of Osaka Prefecture: the reassessment of its phylogenetic status within Crocodylia. *National Science Museum Monographs*, *35*, 1–121.

Koch, N. M., Soto, I. M., & Ramírez, M. J. (2015). First phylogenetic analysis of the family Neriidae (Diptera), with a study on the issue of scaling continuous characters. *Cladistics*, *31*(2), 142–165.

Kotsakis, T., Delfino, M., & Piras, P. (2004). Italian Cenozoic crocodilians: taxa, timing and palaeobiogeographic implications. *Palaeogeography, Palaeoclimatology, Palaeoecology*, *210*(1), 67–87.

Kraus, R. (1998). The cranium of *Piscogavialis jugaliperforatus* n. gen., n. sp. (Gavialidae, Crocodylia) from the Miocene of Peru. *Paläontologische Zeitschrift*, *72*(3-4), 389–405.

Kuhn, O. (1938). Die Crocodilier aus dem mittlerern Eozän des Geiseltales bei Halle. *Nova Acta Leopoldina*, *39*, 313–328.

Lambe, L. M. (1907). On a new crocodilian genus and species from the Judith River Formation of Alberta. *Transactions of the Royal Society of Canada*, *4*, 219–244.

Langer, M. C., Ezcurra, M. D., Rauhut, O. W., Benton, M. J., Knoll, F., McPhee, B. W., Novas, F. E., Pol, D., & Brusatte, S. L. (2017). Untangling the dinosaur family tree. *Nature*, *551*(7678), E1–E3.

Langston, W. (1965). Fossil crocodilians from Colombia and the Cenozoic history of the Crocodilia in South America. *University of California Publications in Geological Sciences*, *52*.

Langston, W. (1966). *Mourasuchus* Price, *Nettosuchus* Langston, and the family Nettosuchidae (Reptilia: Crocodilia). *Copeia*, *1966*(4), 882–885.

Langston, W. (1975). *Pristichampsus vorax* (Troxell), new combination, from the Eocene of North America. *Fieldiana Geology*, *33*, 291–314.

Langston, W., & Gasparini, Z. (1997). Crocodilians, *Gryposuchus*, and the South Americans gavials. In R. V. Kay, R. H. Madden, R. L. Cifelli, & J. J. Flynn (Eds.), *Vertebrate paleontology in the neotropics - the Miocene fauna of La Venta, Colombia* (pp. 113–154). Washington, DC (Smithsonian Institution Press).

Lauprasert, K., Watchajittaphan, P., Juanngam, S., & Bhuttarach, S. (2019). Freshwater crocodile, *Crocodylus siamensis* Schneider, 1801, from the Middle Pleistocene deposits in Chaloem Phrakiat District, Nakhon Ratchasima, Thailand. *Annales de Paléontologie*, *105*(4), 269–274.

Laurito, C. A., & Valerio, A. L. (2008). The first record of *Gavialosuchus americanus* Sellards (1915) (Eusuchia: Crocodylidae, Tomistominae) for the Late Tertiary of Costa Rica and Central America. *Revista Geológica de América Central*, (39), 107–115.

Lee, M. S. Y., & Yates, A. M. (2018). Tip-dating and homoplasy: reconciling the shallow molecular divergences of modern gharials with their long fossil record. *Proceedings of the Royal Society B: Biological Sciences*, *285*(1881), 20181071.

Li, C., Wu, X.-C., & Rufolo, S. J. (2019). A new crocodyloid (Eusuchia: Crocodylia) from the Upper Cretaceous of China. *Cretaceous Research*, *94*, 25–39.

Li, J., & Wang, B. (1987). A new species of *Alligator* from Shanwang, Shandong. *Vertebrata PalAsiatica*, *7*, 199–207.

Li, J. (1976). Fossils of Sebecosuchia discovered from Nanxiong, Guangdong. *Vertebrata PalAsiatica*, *14*(3), 169–174.

Li, J. (1984). A new species of *Planocrania* from Hengdong, Hunan. *Vertebrata PalAsiatica*, *22*(2), 123–133.

Li, Y., Wu, X., Ji, X., Yan, P., & Amato, G. (2007). The complete mitochondrial genome of salt-water crocodile (*Crocodylus porosus*) and phylogeny of crocodilians. *Journal of Genetics and Genomics*, *34*(2), 119–128.

Lohman, D. J., de Bruyn, M., Page, T., von Rintelen, K., Hall, R., Ng, P. K., Shih, H.-T., Carvalho, G. R., & von Rintelen, T. (2011). Biogeography of the Indo-Australian archipelago. *Annual Review of Ecology, Evolution, and Systematics*, *42*.

Loomis, F. B. (1904). Two New River Reptiles from the Titanothere Beds. *American Journal of Science (ser. 4)*, *18*, 427–432.

Ludwig, R. (1877). *Fossile Crocodiliden aus der Tertiärformation des mainzer Beckens* (Vol. 3). Paleontographica Supplement.

Lull, R. S. (1944). Fossil gavials from north India. *American Journal of Science*, *242*(8), 417–430.

Lydekker, R. (1886). Indian Tertiary and Post-tertiary Vertebrata: Siwalik Crocodilia, Lacertilia, & Ophidia. *Palaeontologia Indica Ser. 10*, (3), 209–240.

Lydekker, R. (1887). Note on the Hordwell and other crocodilians. *Geological Magazine*, *4*, 307–312.

Lydekker, R. (1888). *Catalogue of the fossil Reptilia and Amphibia in the British Museum (Natural History). Part I*. British Museum (Natural History).

Macaluso, L., Martin, J. E., Del Favero, L., & Delfino, M. (2019). Revision of the crocodilians from the Oligocene of Monteviale, Italy, and the diversity of European eusuchians across the Eocene-Oligocene boundary. *Journal of Vertebrate Paleontology*, *39*(2), e1601098.

Maccagno, A. M. (1947). Descrizione di una nuova specie di "*Crocodilus*" del giacimento di Sahabi (Sirtica). *Atti della Reale Accademia Nazionale dei Lincei: Memorie della Classe di Scienze fisiche, Mathematiche e Naturale, Serie 8*, *1*(2), 61–96.

MacFadden, B. J., Bloch, J. I., Evans, H., Foster, D. A., Morgan, G. S., Rincon, A., & Wood, A. R. (2014). Temporal calibration and biochronology of the Centenario Fauna, early Miocene of Panama. *The Journal of Geology*, *122*(2), 113–135.

Maddison, W. P. (1993). Missing data versus missing characters in phylogenetic analysis. *Systematic Biology*, *42*(4), 576–581.

Man, Z., Yishu, W., Peng, Y., & Xiaobing, W. (2011). Crocodilian phylogeny inferred from twelve mitochondrial protein-coding genes, with new complete mitochondrial genomic sequences for *Crocodylus acutus* and *Crocodylus novaeguineae*. *Molecular Phylogenetics and Evolution*, *60*(1), 62–67.

Mannion, P. D., Benson, R. B. J., Carrano, M. T., Tennant, J. P., Judd, J., & Butler, R. J. (2015). Climate constrains the evolutionary history and biodiversity of crocodylians. *Nature Communications*, *6*(1), 1–9.

Mannion, P. D., Chiarenza, A. A., Godoy, P. L., & Cheah, Y. N. (2019). Spatiotemporal sampling patterns in the 230 million year fossil record of terrestrial crocodylomorphs and their impact on diversity. *Palaeontology*, *62*(4), 615–637.

Mannion, P. D., & Upchurch, P. (2011). A re-evaluation of the 'mid-Cretaceous sauropod hiatus' and the impact of uneven sampling of the fossil record on patterns of regional dinosaur extinction. *Palaeogeography, Palaeoclimatology, Palaeoecology*, *299*(3-4), 529–540.

Mannion, P. D., Upchurch, P., Barnes, R. N., & Mateus, O. (2013). Osteology of the Late Jurassic Portuguese sauropod dinosaur *Lusotitan atalaiensis* (Macronaria) and the evolutionary history of basal titanosauriforms. *Zoological Journal of the Linnean Society*, *168*(1), 98–206.

Markwick, P. J. (1998). Crocodilian diversity in space and time: the role of climate in paleoecology and its implication for understanding K/T extinctions. *Paleobiology*, *24*(4), 470–497.

Marsh, O. C. (1870). Notice of a new species of gavial from the Eocene of New Jersey. *American Journal of Science*, *50*, 2–3.

Marsh, O. C. (1871). Notice of some new Fossil Reptiles from the Cretaceous and Tertiary Formations. *American Journal of Science and Arts*, *1*(6), 447–459.

Marsh, O. C. (1872). Preliminary Description of New Tertiary Reptiles. *American Journal of Science*, *4*(22), 298–309.

Martin, B. G. H., & Bellairs, A. d. (1977). The narial excrescence and pterygoid bulla of the gharial, *Gavialis gangeticus* (Crocodilia). *Journal of Zoology*, *182*(4), 541–558.

Martin, H. A. (2006). Cenozoic climatic change and the development of the arid vegetation in Australia. *Journal of Arid Environments*, *66*(3), 533–563.

Martin, J. E. (2007). New material of the Late Cretaceous globidontan *Acynodon iberoccitanus* (Crocodylia) from southern France. *Journal of Vertebrate Paleontology*, *27*(2), 362–372.

Martin, J. E. (2010a). A new species of *Diplocynodon* (Crocodylia, Alligatoroidea) from the Late Eocene of the Massif Central, France, and the evolution of the genus in the climatic context of the Late Palaeogene. *Geological Magazine*, *147*(4), 596–610.

Martin, J. E. (2010b). *Allodaposuchus* Nopsca, 1928 (Crocodylia, Eusuchia), from the Late Cretaceous of southern France and its relationships to Alligatoroidea. *Journal of Vertebrate Paleontology*, *30*(3), 756–767.

Martin, J. E. (2019). The taxonomic content of the genus *Gavialis* from the Siwalik Hills of India and Pakistan. *Papers in Palaeontology*, *5*(3), 483–497.

Martin, J. E., Antoine, P.-O., Perrier, V., Welcomme, J.-L., Metais, G., & Marivaux, L. (2019a). A large crocodyloid from the Oligocene of the Bugti Hills, Pakistan. *Journal of Vertebrate Paleontology*, *39*(4), e1671427.

Martin, J. E., Buffetaut, E., Naksri, W., Lauprasert, K., & Claude, J. (2012). *Gavialis* from the Pleistocene of Thailand and its relevance for drainage connections from India to Java. *PloS one*, *7*(9), e44541.

Martin, J. E., & Delfino, M. (2010). Recent advances in the comprehension of the biogeography of Cretaceous European eusuchians. *Palaeogeography, Palaeoclimatology, Palaeoecology*, *293*(3-4), 406–418.

Martin, J. E., Delfino, M., Garcia, G., Godefroit, P., Berton, S., & Valentin, X. (2016a). New specimens of *Allodaposuchus precedens* from France: intraspecific variability and the diversity of European Late Cretaceous eusuchians. *Zoological Journal of the Linnean Society*, *176*(3), 607–631.

Martin, J. E., Delfino, M., & Smith, T. (2016b). Osteology and affinities of Dollo's goniopholidid (Mesoeucrocodylia) from the Early Cretaceous of Bernissart, Belgium. *Journal of Vertebrate Paleontology*, *36*(6), e1222534.

Martin, J. E., & Gross, M. (2011). Taxonomic clarification of *Diplocynodon* Pomel, 1847 (Crocodilia) from the Miocene of Styria, Austria. *Neues Jahrbuch für Geologie und Paläontologie-Abhandlungen*, *261*(2), 177–193.

Martin, J. E., & Lauprasert, K. (2010). A new primitive alligatorine from the Eocene of Thailand: relevance of Asiatic members to the radiation of the group. *Zoological Journal of the Linnean Society*, *158*(3), 608–628.

Martin, J. E., Lauprasert, K., Tong, H., Suteethorn, V., & Buffetaut, E. (2019b). An Eocene tomistomine from peninsular Thailand. *Annales de Paléontologie*, *105*(3), 245–253.

Martin, J. E., Smith, T., de Lapparent de Broin, F., Escuillié, F., & Delfino, M. (2014). Late Palaeocene eusuchian remains from Mont de Berru, France, and the origin of the alligatoroid *Diplocynodon*. *Zoological Journal of the Linnean Society*, *172*(4), 867–891.

Martin, J. E., Smith, T., Salaviale, C., Adrien, J., & Delfino, M. (2020). Virtual reconstruction of the skull of *Bernissartia fagesii* and current understanding of the neosuchian–eusuchian transition. *Journal of Systematic Palaeontology*, 1–23.

Massonne, T., Vasilyan, D., Rabi, M., & Böhme, M. (2019). A new alligatoroid from the Eocene of Vietnam highlights an extinct Asian clade independent from extant *Alligator sinensis*. *PeerJ*, *7*, e7562.

Mateus, O., Puértolas-Pascual, E., & Callapez, P. M. (2019). A new eusuchian crocodylomorph from the Cenomanian (Late Cretaceous) of Portugal reveals novel implications on the origin of Crocodylia. *Zoological Journal of the Linnean Society*, *186*(2), 501–528.

McAliley, L. R., Willis, R. E., Ray, D. A., White, P. S., Brochu, C. A., & Densmore III, L. D. (2006). Are crocodiles really monophyletic?–Evidence for subdivisions from sequence and morphological data. *Molecular Phylogenetics and Evolution*, *39*(1), 16–32.

Mead, J. I., Steadman, D. W., Bedford, S. H., Bell, C. J., & Spriggs, M. (2002). New extinct mekosuchine crocodile from Vanuatu, South Pacific. *Copeia*, *2002*(3), 632–641.

Medem, F. (1958). The crocodilian genus *Paleosuchus*. *Fieldiana Zoology*, *39*.

Medem, F. (1960). Notes on the Paraguay caiman, *Caiman yacare* Daudin. *Mitteilungen aus dem Museum für Naturkunde in Berlin. Zoologisches Museum und Institut für Spezielle Zoologie (Berlin)*, *36*, 129–142.

Meers, M. B. (2003). Crocodylian forelimb musculature and its relevance to Archosauria. *The Anatomical Record Part A: Discoveries in Molecular, Cellular, and Evolutionary Biology: An Official Publication of the American Association of Anatomists*, *274*(2), 891–916.

Meganathan, P. R., Dubey, B., Batzer, M. A., Ray, D. A., & Haque, I. (2010). Molecular phylogenetic analyses of genus *Crocodylus* (Eusuchia, Crocodylia, Crocodylidae) and the taxonomic position of *Crocodylus porosus*. *Molecular Phylogenetics and Evolution*, *57*(1), 393–402.

Megirian, D. (1994). A new species of *Quinkana* (Molnar) (Eusuchia: Crocodylidae) from the Miocene Camfield beds of Northern Australia. *The Beagle: Records of the Museums and Art Galleries of the Northern Territory*, *11*, 145–166.

Megirian, D., Murray, P. F., & Willis, P. (1991). A new crocodile of the gavial ecomorph morphology from the Miocene of northern Australia. *The Beagle: Records of the Museums and Art Galleries of the Northern Territory*, *8*, 135.

Melstrom, K. M., & Irmis, R. B. (2019). Repeated evolution of herbivorous crocodyliforms during the age of dinosaurs. *Current Biology*, *29*(14), 2389–2395.

Meredith, R. W., Hekkala, E. R., Amato, G., & Gatesy, J. (2011). A phylogenetic hypothesis for *Crocodylus* (Crocodylia) based on mitochondrial DNA: evidence for a trans-Atlantic voyage from Africa to the New World. *Molecular Phylogenetics and Evolution*, *60*(1), 183–191.

Meyer, E. R. (1984). Crocodilians as living fossils. *Living fossils* (pp. 105–131). Springer.

Mickevich, M. F., & Johnson, M. S. (1976). Congruence between morphological and allozyme data in evolutionary inference and character evolution. *Systematic Zoology*, *25*(3), 260–270.

Miller, W. E. (1980). The late Pliocene Las Tunas local fauna from southernmost Baja California, Mexico. *Journal of Paleontology*, 762–805.

Molnar, R. E. (1981). Pleistocene ziphodont crocodilians of Queensland. *Records of the Australian Museum*, *33*(19), 803–834.

Molnar, R. E. (1982a). A longirostrine crocodilian from Murua (Woodlark), Solomon Sea. *Memoirs of the Queensland Museum*, *20*, 675–685.

Molnar, R. E. (1982b). Cenozoic fossil reptiles in Australia. In P. V. Rich & E. M. Thompson (Eds.), *The fossil vertebrate record of australia* (pp. 227–234). Monash University, Melbourne.

Molnar, R. E. (1982c). *Pallimnarchus* and other Cenozoic crocodiles of Queensland. *Memoirs of the Queensland Museum*, *20*(3), 657–673.

Molnar, R. E. (1982d). Pleistocene ziphodont crocodilians of Queensland. *Records of the Australian Museum*, *33*(19), 803–834.

Molnar, R. E., Worthy, T., & Willis, P. M. A. (2002). An extinct Pleistocene endemic mekosuchine crocodylian from Fiji. *Journal of Vertebrate Paleontology*, *22*(3), 612–628.

Molnar, R. E., & Pole, M. (1997). A Miocene crocodilian from New Zealand. *Alcheringa*, *21*(1), 65–70.

Montefeltro, F. C., Larsson, H. C. E., de França, M. A. G., & Langer, M. C. (2013). A new neosuchian with Asian affinities from the Jurassic of northeastern Brazil. *Naturwissenschaften*, *100*(9), 835–841.

Montes, C., Cardona, A., Jaramillo, C., Pardo, A., Silva, J. C., Valencia, V., Ayala, C., Pérez-Angel, L. C., Rodriguez-Parra, L., Ramirez, V., & Niño, H. (2015). Middle Miocene closure of the Central American Seaway. *Science*, *348*(6231), 226–229.

Montes, C., Cardona, A., McFadden, R., Morón, S. E., Silva, C. A., Restrepo-Moreno, S., Ramírez, D. A., Hoyos, N., Wilson, J., Farris, D., & Bayona, G. A. (2012). Evidence for middle Eocene and younger land emergence in Central Panama: Implications for Isthmus closure. *Geological Society of America Bulletin*, *124*, 780–799.

Mook, C. C. (1921a). *Allognathosuchus*, a new genus of Eocene crocodilians. *Bulletin of the American Museum on Natural History*, *44*, 105–110.

Mook, C. C. (1921b). Description of a skull of a Bridger crocodilian. *Bulletin of the American Museum on Natural History*, *44*, 111–116.

Mook, C. C. (1921c). Notes on the postcranial skeleton in the Crocodilia. *Bulletin of American Museum of Natural History*, *44*, 67–100.

Mook, C. C. (1921d). The skull of *Crocodilus acer* Cope. *Bulletin of the American Museum on Natural History*, *44*, 117–121.

Mook, C. C. (1923). A new species of *Alligator* from the Snake Creek beds. *American Museum Novitates*, *73*, 1–13.

Mook, C. C. (1924). A new crocodilian from the Wasatch beds. *American Museum Novitates*, *137*, 1–4.

Mook, C. C. (1927). The skull characters of *Crocodilus megarhinus* Andrews. *American Museum Novitates*, *289*, 1–8.

Mook, C. C. (1930). A new species of crocodilian from the Torrejon Beds. *American Museum Novitates*, *447*, 1–11.

Mook, C. C. (1932). A new species of fossil gavial from the Siwalik beds. *American Museum Novitates*, *514*, 1–5.

Mook, C. C. (1933). A skull with jaws of *Crocodilus sivalensis* Lydekker. *American Museum Novitates*, *670*, 1–10.

Mook, C. C. (1934). The evolution and classification of the Crocodilia. *The Journal of Geology*, *42*(3), 295–304.

Mook, C. C. (1941a). A new crocodilian from the Lance Formation. *American Museum Novitates*, *1128*, 1–5.

Mook, C. C. (1941b). A new crocodilian, *Hassiacosuchus kayi*, from the Bridger Eocene beds of Wyoming. *Annals of the Carnegie Museum*, *28*(12), 207–220.

Mook, C. C. (1942). A new fossil crocodilian from the Paleocene of New Mexico. *American Museum Novitates*, *1189*, 1–4.

Mook, C. C. (1946). A new Pliocene alligator from Nebraska. *American Museum Novitates*, *1311*, 1–12.

Mook, C. C. (1959a). A new Pleistocene crocodilian from Guatemala. *American Museum Novitates*, *1975*, 1–6.

Mook, C. C. (1959b). A new species of fossil crocodile of the genus *Leidyosuchus* from the Green River beds. *American Museum Novitates*, *1933*, 1–6.

Mook, C. C. (1960). *Diplocynodon* remains from the Bridger beds of Wyoming. *American Museum Novitates*, *2007*, 1–4.

Mook, C. C. (1961). Notes on the skull characters of *Allognathosuchus polyodon*. *American Museum Novitates*, *2072*, 1–5.

Moreno-Bernal, J. W., Head, J., & Jaramillo, C. A. (2016). Fossil crocodilians from the High Guajira Peninsula of Colombia: Neogene faunal change in northernmost South America. *Journal of Vertebrate Paleontology*, *36*(3), e1110586.

Morgan, G. S., & Albury, N. A. (2013). The Cuban crocodile (*Crocodylus rhombifer*) from late Quaternary fossil deposits in the Bahamas and Cayman Islands. *Bulletin of the Florida Museum of Natural History*, *52*(3), 162–236.

Morgan, G. S., Franz, R., & Crombie, R. I. (1993). The Cuban crocodile, *Crocodylus rhombifer*, from late Quaternary fossil deposits on Grand Cayman. *Caribbean Journal of Science*, *29*(3-4), 153–164.

Mortimer, N., Campbell, H. J., Tulloch, A. J., King, P. R., Stagpoole, V. M., Wood, R. A., Rattenbury, M. S., Sutherland, R., Adams, C. J., Collot, J., & Seton, M. (2017). Zealandia: Earth's hidden continent. *GSA today*, *27*(3), 27–35.

Müller, L. (1927). Ergebnisse der Forschungsreisen Prof. E. Stromers in den Wüsten Ägypteus. Abhandlungen Bayerisch Akademie der Wissenschaften. *Mathematisch-Naturwissenschaftelischt abtelund*, *31*, 1–97.

Myrick, A. C. (2001). *Thecachampsa antiqua* (Leidy, 1852) (Crocodylidae, Thoracosaurinae) from fossil marine deposits at Lee Creek Mine, Aurora, North Carolina, USA. *Smithsonian Contributions to Paleobiology*, *90*, 219–225.

Narváez, I., Brochu, C. A., Escaso, F., Pérez-García, A., & Ortega, F. (2016). New Spanish Late Cretaceous eusuchian reveals the synchronic and sympatric presence of two allodaposuchids. *Cretaceous Research*, *65*, 112–125.

Narváez, I., Brochu, C. A., De Celis, A., Codrea, V., Escaso, F., Pérez-García, A., & Ortega, F. (2019). New diagnosis for *Allodaposuchus precedens*, the type species of the European Upper Cretaceous clade Allodaposuchidae. *Zoological Journal of the Linnean Society*, *189*(2), 618–634.

Narváez, I., Brochu, C. A., Escaso, F., Pérez-García, A., & Ortega, F. (2015). New crocodyliforms from southwestern Europe and definition of a diverse clade of European Late Cretaceous basal eusuchians. *PLoS One*, *10*(11), e0140679.

Neall, V. E., & Trewick, S. A. (2008). The age and origin of the Pacific islands: a geological overview. *Philosophical Transactions of the Royal Society B: Biological Sciences*, *363*(1508), 3293–3308.

Nesbitt, S. J. (2011). The early evolution of archosaurs: relationships and the origin of major clades. *Bulletin of the American Museum of Natural History*, *2011*(352), 1–292.

Nesbitt, S. J., Turner, A. H., & Weinbaum, J. C. (2012). A survey of skeletal elements in the orbit of Pseudosuchia and the origin of the crocodylian palpebral. *Earth and Environmental Science Transactions of the Royal Society of Edinburgh*, *103*(3–4), 365–381.

Nicholl, C., Rio, J. P., & Mannion, P. D. (In prep.). The early Miocene Maltese crocodile *Melitosaurus champsoides* and a re-examination of the phylogenetic and biogeographical relationships of Tomistominae.

Nicolaï, M. P. J., & Matzke, N. J. (2019). Trait-based range expansion aided in the global radiation of Crocodylidae. *Global Ecology and Biogeography*, *28*(9), 1244–1258.

Nopcsa, F. (1923). Die Familien der Reptilien. *Fortschritte der Geologie und Palaeontologie*, *2*, 1–210.

Norell, M. A., & Clark, J. M. (1990). A reanalysis of *Bernissartia fagesii*, with comments on its phylogenetic position and its bearing on the origin and diagnosis of the Eusuchia. *Bulletin de l'Institut Royal des Sciences Naturelles de Belgique*, *60*, 115–128.

Norell, M. A. (1988). *Cladistic approaches to paleobiology as applied to the phylogeny of alligatorids* (Thesis).

Norell, M. A. (1989). The higher level relationships of the extant Crocodylia. *Journal of Herpetology*, *23*(4), 325–335.

Norell, M. A., Clark, J. M., & Hutchison, J. H. (1994). The Late Cretaceous alligatoroid *Brachychampsa montana* (Crocodylia): new material and putative relationships. *American Museum Novitates*, *3116*, 1–26.

Oaks, J. R. (2011). A time-calibrated species tree of Crocodylia reveals a recent radiation of the true crocodiles. *Evolution: International Journal of Organic Evolution*, *65*(11), 3285–3297.

O'Dea, A., Lessios, H. A., Coates, A. G., Eytan, R. I., Restrepo-Moreno, S. A., Cione, A. L., Collins, L. S., De Queiroz, A., Farris, D. W., Norris, R. D., & Stallard, R. F. (2016). Formation of the Isthmus of Panama. *Science advances*, *2*(8), e1600883.

O'Reilly, J. E., Puttick, M. N., Parry, L., Tanner, A. R., Tarver, J. E., Fleming, J., Pisani, D., & Donoghue, P. C. J. (2016). Bayesian methods outperform parsimony but at the expense of precision in the estimation of phylogeny from discrete morphological data. *Biology letters*, *12*(4), 20160081.

Ortega, F., Gasparini, Z., Buscalioni, A. D., & Calvo, J. O. (2000). A new species of *Araripesuchus* (Crocodylomorpha, Mesoeucrocodylia) from the lower Cretaceous of Patagonia (Argentina). *Journal of Vertebrate Paleontology*, *20*(1), 57–76.

Ősi, A. (2008). Cranial osteology of *Iharkutosuchus makadii*, a Late Cretaceous basal eusuchian crocodyliform from Hungary. *Neues Jahrbuch für Geologie und Paläontologie-Abhandlungen*, *248*(3), 279–299.

Ősi, A., Bodor, E. R., Makádi, L., & Rabi, M. (2016). Vertebrate remains from the Upper Cretaceous (Santonian) Ajka Coal formation, western Hungary. *Cretaceous Research*, *57*, 228–238.

Ősi, A., Clark, J. M., & Weishampel, D. B. (2007). First report on a new basal eusuchian crocodyliform with multicusped teeth from the Upper Cretaceous (Santonian) of Hungary. *Neues Jahrbuch für Geologie und Paläontologie-Abhandlungen*, *243*(2), 169–177.

Ősi, A., & Weishampel, D. B. (2009). Jaw mechanism and dental function in the Late Cretaceous basal eusuchian *Iharkutosuchus*. *Journal of Morphology*, *270*(8), 903–920.

Owen, R. (1848). On the fossils obtained by the Marchioness of Hastings from the freshwater Eocene beds of the Hordle Cliffs. *Report of the British Association for the Advancement of Science*, *17*, 65–66.

Owen, R. (1850). Monograph on the fossil Reptilia of the London Clay, and of the Bracklesham and other Tertiary Beds. *Monograph of the Palaeontographical Society London*, *3*, 1–50.

Pan, T., Miao, J.-S., Zhang, H.-B., Yan, P., Lee, P.-S., Jiang, X.-Y., Ouyang, J.-H., Deng, Y.-P., Zhang, B.-W., & Wu, X.-B. (2020). Near-complete phylogeny of extant Crocodylia (Reptilia) using mitogenome-based data. *Zoological Journal of the Linnean Society*.

Parins-Fukuchi, C. (2017). Use of continuous traits can improve morphological phylogenetics. *Systematic biology*, *67*(2), 328–339.

Pickford, M. (1994). Late Cenozoic crocodiles (Reptilia: Crocodylidae) from the Western Rift, Uganda. *Geology and palaeobiology of the Albertine rift valley, Uganda-Zaire*, *2*, 137–155.

Pickford, M. (2003). A new species of crocodile from Early and Middle Miocene deposits of the Lower Orange River Valley, Namibia, and the origins of the Nile crocodile (*Crocodylus niloticus*). *Geological Survey of Namibia Memoir*, *19*, 51–65.

Pictet, F. J., Gaudin, C., & de La Harpe, P. (1857). Mémoire sur les animaux vertébrés trouvés dans le terrain sidérolitique du Canton de Vaud et appartenant á la faune Eocéne. *Matériaux pour la Paléontologie Suisse, Ser. 1*, (2), 1–20.

Pinheiro, A. E. P., Fortier, D. C., Pol, D., Campos, D. A., & Bergqvist, L. P. (2013). A new *Eocaiman* (Alligatoridae, Crocodylia) from the Itaboraí Basin, Paleogene of Rio de Janeiro, Brazil. *Historical Biology*, *25*(3), 327–337.

Piras, P., & Buscalioni, A. D. (2006). *Diplocynodon muelleri* comb. nov., an Oligocene diplocynodontine alligatoroid from Catalonia (Ebro Basin, Lleida province, Spain). *Journal of Vertebrate Paleontology*, *26*(3), 608–620.

Piras, P., Delfino, M., Del Favero, L., & Kotsakis, T. (2007). Phylogenetic position of the crocodylian *Megadontosuchus arduini* and tomistomine palaeobiogeography. *Acta Palaeontologica Polonica*, *52*(2), 315–328.

Piveteau, J. (1927). *Études sur quelques amphibiens et reptiles fossiles, II: Reptile du Montien* (Vol. 16). Annales de Paléontologie.

Poe, S. (1997). Data set incongruence and the phylogeny of crocodilians. *Systematic Biology*, *45*(4), 393–414.

Pol, D., Leardi, J. M., Lecuona, A., & Krause, M. (2012). Postcranial anatomy of *Sebecus icaeorhinus* (Crocodyliformes, Sebecidae) from the Eocene of Patagonia. *Journal of Vertebrate Paleontology*, *32*(2), 328–354.

Pol, D., & Norell, M. A. (2001). Comments on the Manhattan stratigraphic measure. *Cladistics*, *17*(3), 285–289.

Pol, D., & Norell, M. A. (2004). A new crocodyliform from Zos Canyon, Mongolia. *American Museum Novitates*, *3445*, 1–36.

Pol, D., Turner, A. H., & Norell, M. A. (2009). Morphology of the Late Cretaceous crocodylomorph *Shamosuchus djadochtaensis* and a discussion of neosuchian phylogeny as related to the origin of Eusuchia. *Bulletin of the American Museum of Natural History*, *324*, 1–104.

Pomel, A. (1847). Note sur les animaux fossiles découverts dans le département de l'Allier. *Bulletin de la Société Géologique de France*, *4*, 378–385.

Pomel, A. (1853). *Catalogue méthodique et descriptif des vértébres fossiles découverts dans le bassin hydrographique supérieur de la Loire et surtout dans la vallée de son affluent principal l'Allier*. J.-B. Bailliére.

Pragner, E. (1845). Über *Enneodon ungeri*, ein neues Genus fossiler Saurieraus den Tertiär Gebilden zu Wies im Marburger Kreise Steiermark's. *Steiermärkische Zeitschrift, Neue Folge*, *8*, 114–139.

Price, L. I. (1964). Sôbre o crânio de um grande crocodilídeo extinto do Alto Rio Juruá, Estado do Acre. *Anais da Academia Brasileira de Ciências*, *56*, 59–66.

Puértolas-Pascual, E., Blanco, A., Brochu, C. A., & Canudo, J. I. (2016). Review of the Late Cretaceous-early Paleogene crocodylomorphs of Europe: Extinction patterns across the K-Pg boundary. *Cretaceous Research*, *57*, 565–590.

Puértolas-Pascual, E., Canudo, J. I., & Cruzado-Caballero, P. (2011). A new crocodylian from the Late Maastrichtian of Spain: implications for the initial radiation of crocodyloids. *PloS one*, *6*(6), e20011.

R Core Team. (2018). R: A language and environment for statistical computing. R Foundation for Statistical Computing, Vienna, Austria (https://www.R-project.org/).

Rae, T. C. (1998). The logical basis for the use of continuous characters in phylogenetic systematics. *Cladistics*, *14*(3), 221–228.

Rana, R. S., & Sati, K. K. (2000). Late Cretaceous-Palaeocene crocodilians from the Deccan Trap associated sedimentary sequences of peninsular India. *Journal of the Palaeontological Society of India*, *45*, 123–136.

Randle, E., & Sansom, R. S. (2017). Exploring phylogenetic relationships of Pteraspidiformes heterostracans (stem-gnathostomes) using continuous and discrete characters. *Journal of Systematic Palaeontology*, *15*(7), 583–599.

Rauhe, M., Frey, E., Pemberton, D. S., & Rossmann, T. (1999). Fossil crocodilians from the late Miocene Baynunah Formation of the Emirate of Abu Dhabi, United Arab Emirates: osteology and palaeoecology. In P. J. Whybrow & A. Hill (Eds.), *Fossil vertebrates of arabia* (pp. 163–185). Yale University Press, New Haven.

Riff, D., & Aguilera, O. A. (2008). The world's largest gharials *Gryposuchus*: description of *G. croizati* n. sp. (Crocodylia, Gavialidae) from the Upper Miocene Urumaco Formation, Venezuela. *Paläontologische Zeitschrift*, *82*(2), 178–195.

Rio, J. P., Mannion, P. D., Tschopp, E., Martin, J. E., & Delfino, M. (2020). Reappraisal of the morphology and phylogenetic relationships of the alligatoroid crocodylian *Diplocynodon hantoniensis* from the late Eocene of the United Kingdom. *Zoological Journal of the Linnean Society*, *188*(2), 579–629.

Rogers, J. V. (2003). *Pachycheilosuchus trinquei*, a new procoelous crocodyliform from the Lower Cretaceous (Albian) Glen Rose Formation of Texas. *Journal of Vertebrate Paleontology*, *23*(1), 128–145.

Rohrmann, A., Sachse, D., Mulch, A., Pingel, H., Tofelde, S., Alonso, R. N., & Strecker, M. R. (2016). Miocene orographic uplift forces rapid hydrological change in the southern central Andes. *Scientific reports*, *6*, 35678.

Romer, A. S. (1956). *Osteology of the Reptiles*. University of Chicago Press.

Roos, J., Aggarwal, R. K., & Janke, A. (2007). Extended mitogenomic phylogenetic analyses yield new insight into crocodylian evolution and their survival of the Cretaceous–Tertiary boundary. *Molecular Phylogenetics and Evolution*, *45*(2), 663–673.

Ross, F. D., & Mayer, G. C. (1983). On the dorsal armor of the Crocodilia. In A. G. Rhodin & K. Miyata (Eds.), *Advances in herpetology and evolutionary biology* (pp. 305–331). Harvard University Press.

Rossmann, T. (1998). Studien an känozoischen Krokodilen: 2. Taxonomische Revision der Familie Pristichampsidae Efimov (Crocodilia: Eusuchia). *Neues Jahrbuch für Geologie und Paläontologie Abhandlungen*, *210*(1), 85–128.

Rossmann, T. (2000). Skelettanatomische Beschreibung von *Pristichampus rollinatii* (Gray) (Crocodilia, Eusuchia) aus dem Paläogen von Europa, Nordamerika und Ostasien. *Courier Forschungsinstitut Senckenberg*, *221*, 1–107.

Rovereto, C. (1912). Los crocodilos fósiles en las capas de Paraná. *Anales de Museo Nacional de Buenos Aires*, *22*.

Rusconi, C. (1937). Nuevo aligatorino del Paleoceno Argentino. *Boletin Paleontológico de Buenos Aires*, *8*, 1–5.

Salas-Gismondi, R., Antoine, P. O., Baby, P., Brusset, S., Benammi, M., Espurt, N., De Franceschi, D., Pujos, F., Tejada, J., & Urbina, M. (2007). Middle Miocene crocodiles from the Fitzcarrald Arch, Amazonian Peru. *Cuadernos del Museo Geominero*, *8*, 355–360.

Salas-Gismondi, R., Flynn, J. J., Baby, P., Tejada-Lara, J. V., Claude, J., & Antoine, P.-O. (2016). A new 13 million year old gavialoid crocodylian from proto-Amazonian mega-wetlands reveals parallel evolutionary trends in skull shape linked to longirostry. *PloS one*, *11*(4), e0152453.

Salas-Gismondi, R., Flynn, J. J., Baby, P., Tejada-Lara, J. V., Wesselingh, F. P., & Antoine, P.-O. (2015). A Miocene hyperdiverse crocodylian community reveals peculiar trophic dynamics in proto-Amazonian mega-wetlands. *Proceedings of the Royal Society B: Biological Sciences*, *282*(1804), 20142490.

Salas-Gismondi, R., Moreno-Bernal, J. W., Scheyer, T. M., Sánchez-Villagra, M. R., & Jaramillo, C. (2019). New Miocene Caribbean gavialoids and patterns of longirostry in crocodylians. *Journal of Systematic Palaeontology*, *17*(12), 1049–1075.

Salisbury, S. W., & Willis, P. M. A. (1996). A new crocodylian from the early Eocene of south-eastern Queensland and a preliminary investigation of the phylogenetic relationships of crocodyloids. *Alcheringa*, *20*(3), 179–226.

Salisbury, S. W., Molnar, R. E., Frey, E., & Willis, P. M. A. (2006). The origin of modern crocodyliforms: new evidence from the Cretaceous of Australia. *Proceedings of the Royal Society B: Biological Sciences*, *273*(1600), 2439–2448.

Schellart, W. P., Lister, G. S., & Toy, V. G. (2006). A Late Cretaceous and Cenozoic reconstruction of the Southwest Pacific region: tectonics controlled by subduction and slab rollback processes. *Earth-Science Reviews*, *76*(3-4), 191–233.

Scheyer, T. M., Aguilera, O. A., Delfino, M., Fortier, D. C., Carlini, A. A., Sánchez, R., Carrillo-Briceño, J. D., Quiroz, L., & Sánchez-Villagra, M. R. (2013). Crocodylian diversity peak and extinction in the late Cenozoic of the northern Neotropics. *Nature Communications*, *4*(1907), 1–9.

Scheyer, T. M., & Delfino, M. (2016). The late Miocene caimanine fauna (Crocodylia: Alligatoroidea) of the Urumaco Formation, Venezuela. *Palaeontologia Electronica*, *19*(3), 1–57.

Scheyer, T. M., Hutchinson, J. R., Strauss, O., Delfino, M., Carrillo-Briceño, J. D., Sánchez, R., & Sánchez-Villagra, M. R. (2019). Giant extinct caiman breaks constraint on the axial skeleton of extant crocodylians. *eLife*, *8*, e49972.

Schmidt, K. P. (1938). New crocodilians from the upper Paleocene of western Colorado. *Geological Series of the Field Museum of Natural History*, *6*, 315–321.

Schmidt, K. P. (1941). A new fossil alligator from Nebraska. *Fieldiana*, *8*, 27–32.

Schmitz, A., Mansfeld, P., Hekkala, E., Shine, T., Nickel, H., Amato, G., & Böhme, W. (2003). Molecular evidence for species level divergence in African Nile crocodiles *Crocodylus niloticus* (Laurenti, 1786). *Comptes Rendus Palevol*, *2*(8), 703–712.

Schumacher, G.-H. (1973). The head muscles and hyolaryngeal skeleton of turtles and crocodilians. In C. Gans & T. S. Parsons (Eds.), *Biology of the reptilia* (pp. 101–199).

Schwarz, D., Raddatz, M., & Wings, O. (2017). *Knoetschkesuchus langenbergensis* gen. nov. sp. nov., a new atoposaurid crocodyliform from the Upper Jurassic Langenberg Quarry (Lower Saxony, northwestern Germany), and its relationships to *Theriosuchus*. *PloS one*, *12*(2).

Schwimmer, D. R. (2002). *King of the crocodylians: The Paleobiology of Deinosuchus*. Indiana University Press.

Sellards, E. H. (1915). A new gavial from the late Tertiary of Florida. *American Journal of Science*, (236), 135–138.

Sereno, P. C. (2007). Logical basis for morphological characters in phylogenetics. *Cladistics*, *23*(6), 565–587.

Sereno, P. C., Larsson, H. C. E., Sidor, C. A., & Gado, B. (2001). The giant crocodyliform *Sarcosuchus* from the Cretaceous of Africa. *Science*, *294*(5546), 1516–1519.

Serrano-Martínez, A., Knoll, F., Narváez, I., Lautenschlager, S., & Ortega, F. (2019a). Inner skull cavities of the basal eusuchian *Lohuecosuchus megadontos* (Upper Cretaceous, Spain) and neurosensorial implications. *Cretaceous Research*, *93*, 66–77.

Serrano-Martínez, A., Knoll, F., Narváez, I., & Ortega, F. (2019b). Brain and pneumatic cavities of the braincase of the basal alligatoroid *Diplocynodon tormis* (Eocene, Spain). *Journal of Vertebrate Paleontology*, *39*(1), e1572612.

Shan, H.-Y., Cheng, Y.-N., & Wu, X.-C. (2013). The first fossil skull of *Alligator sinensis* from the Pleistocene, Taiwan, with a paleogeographic implication of the species. *Journal of Asian Earth Sciences*, *69*, 17–25.

Shan, H.-Y., Wu, X.-C., Cheng, Y.-N., & Sato, T. (2009). A new tomistomine (Crocodylia) from the Miocene of Taiwan. *Canadian Journal of Earth Sciences*, *46*(7), 529–555.

Shan, H.-Y., Wu, X.-C., Cheng, Y.-N., & Sato, T. (2017). *Maomingosuchus petrolica*, a restudy of '*Tomistoma*' *petrolica* Yeh, 1958. *Palaeoworld*, *26*(4), 672–690.

Shankar, K., & Rao, C. V. N. K. (1994). First report of a fossil marsh crocodile *Crocodylus palustris* from the Manneru Valley, Andhra Pradesh. *Current Science*, *67*(9-10), 687–689.

Shirley, M. H., Villanova, V. L., Vliet, K. A., & Austin, J. D. (2015). Genetic barcoding facilitates captive and wild management of three cryptic African crocodile species complexes. *Animal Conservation*, *18*(4), 322–330.

Shirley, M. H., Carr, A. N., Nestler, J. H., Vliet, K. A., & Brochu, C. A. (2018). Systematic revision of the living African slender-snouted crocodiles (*Mecistops* Gray, 1844). *Zootaxa*, *4504*(2), 151–193.

Shirley, M. H., Vliet, K. A., Carr, A. N., & Austin, J. D. (2014). Rigorous approaches to species delimitation have significant implications for African crocodilian systematics and conservation. *Proceedings of the Royal Society B: Biological Sciences*, *281*(1776), 20132483.

Siddall, M. E. (1998). Stratigraphic fit to phylogenies: a proposed solution. *Cladistics*, *14*(2), 201–208.

Sill, W. D. (1968). The zoogeography of the Crocodilia. *Copeia*, 76–88.

Sill, W. D. (1970). Nota preliminar sobre un nuevo Gavial del Plioceno de Venezuela y una discusion de los gaviales Sudamericanos. *Ameghiniana*, *7*(2), 151–159.

Simpson, G. G. (1930). *Allognathosuchus mooki*, a new crocodile from the Puerco Formation. *American Museum Novitates*, *445*, 1–16.

Simpson, G. G. (1933). A new crocodilian from the Notostylops beds of Patagonia. *American Museum Novitates*, *623*, 1–9.

Simpson, G. G. (1937). An ancient eusuchian crocodile from Patagonia. *American Museum Novitates*, *965*, 1–20.

Skutschas, P. P., Danilov, I. G., Kodrul, T. M., & Jin, J. (2014). The first discovery of an alligatorid (Crocodylia, Alligatoroidea, Alligatoridae) in the Eocene of China. *Journal of Vertebrate Paleontology*, *34*(2), 471–476.

Smith, A. B. (2000). Stratigraphy in phylogeny reconstruction. *Journal of Paleontology*, *74*(5), 763–766.

Smith, T., Quesnel, F., De Plöeg, G., De Franceschi, D., Metais, G., De Bast, E., Solé, F., Folie, A., Boura, A., Claude, J., Dupuis, C., Ggnaisaon, C., Iakovleva, A., Martin, J., Maubert, F., Prieur, J., Roche, E., Storme, J.-Y., Thomas, R., … Buffetaut, E. (2014). First Clarkforkian Equivalent Land Mammal Age in the latest Paleocene Basal Sparnacian Facies of Europe: Fauna, Flora, Paleoenvironment and (Bio)stratigraphy. *PLoS One*, *9*(1).

Snyder, D. (2007). Morphology and systematics of two Miocene alligators from Florida, with a discussion of *Alligator* biogeography. *Journal of Paleontology*, *81*(5), 917–928.

Solórzano, A., Núñez-Flores, M., Inostroza-Michael, O., & Hernández, C. E. (2020). Biotic and abiotic factors driving the diversification dynamics of Crocodylia. *Palaeontology*, *63*(3).

Solórzano, A., Núñez-Flores, M., & Rincón, A. D. (2018). *Gryposuchus* (Crocodylia, Gavialoidea) from the early Miocene of Venezuela. *Palaontologische Zeitschrift*, *92*(1), 121–129.

Solórzano, A., Rincón, A. D., Cidade, G. M., Núñez-Flores, M., & Sánchez, L. (2019). Lower Miocene alligatoroids (Crocodylia) from the Castillo Formation, northwest of Venezuela. *Palaeobiodiversity and Palaeoenvironments*, *99*(2), 241–259.

Sookias, R. B. (2020). Exploring the effects of character construction and choice, outgroups and analytical method on phylogenetic inference from discrete characters in extant crocodilians. *Zoological Journal of the Linnean Society*, *189*(2), 670–699.

Souza-Filho, J. P. (1991). *Charactosuchus sansaoi*, uma nova espécie de Crocodilidae (Crocodylia) do Neógeno do Estado o Acre, Brasil. *Actas do XII Congreso Brasileiro de Paleontologia*, *36*, S50.

Souza-Filho, J. P., & Bocquentin, J. (1989). *Brasilosuchus mendensi* n. g., n. sp., um novo representante da familia Gavialidae do Neógeno do Estado do Acre, Brasil. *Anais do XI Congreso Brasiliero de Paleontologia*, *1*, 457–463.

Souza-Filho, J. P., & Maciente, A. (2009). Estudos complementares sobre *Brasilosuchus mendesi* (Crocodylia, Crocodilidae) do Neógeno da Formação Solimões, Estado do acre, Brasil. *XXI Congresso Brasileiro de Paleontologia*.

Souza-Filho, J. P., Souza, R. G., Hsiou, A. S., Riff, D., Guilherme, E., Negri, F. R., & Cidade, G. M. (2019). A new caimanine (Crocodylia, Alligatoroidea) species from the Solimões Formation of Brazil and the phylogeny of Caimaninae. *Journal of Vertebrate Paleontology*, *38*(5), e1528450.

Steel, R. (1973). Crocodylia. *Handbuch der Palaeontologie*, *16*, 1–116.

Stein, M., Hand, S. J., & Archer, M. (2016). A new crocodile displaying extreme constriction of the mandible, from the late Oligocene of Riversleigh, Australia. *Journal of Vertebrate Paleontology*, *36*(5), e1179041.

Stein, M., Salisbury, S. W., Hand, S. J., Archer, M., & Godthelp, H. (2012). Humeral morphology of the early Eocene mekosuchine crocodylian *Kambara* from the Tingamarra Local Fauna southeastern Queensland, Australia. *Alcheringa: an Australasian Journal of Palaeontology*, *36*(4), 473–486.

Sternberg, C. M. (1932). A new fossil crocodile from Saskatchewan. *The Canadian Field-Naturalist*, *44*, 128–133.

Stevens, P. F. (1991). Character states, morphological variation, and phylogenetic analysis: a review. *Systematic botany*, *16*(3), 553–583.

Storrs, G. W. (2003). Late Miocene-Early Pliocene crocodilian fauna of Lothagam, southwest Turkana Basin, Kenya. In H. J. M. Leakey M G (Ed.), *Lothagam: The dawn of humanity in eastern africa* (pp. 137–159). Colombia Univeristy Press.

Storrs, G. W., Lucas, S. G., & Schoch, R. M. (1983). Endocranial cast of an early Paleocene crocodilian from the San Juan basin, New Mexico. *Copeia*, *1983*(3), 842–845.

Taplin, L. E., & Grigg, G. C. (1989). Historical zoogeography of the eusuchian crocodilians: a physiological perspective. *American Zoologist*, *29*(3), 885–901.

Taplin, L. E., Grigg, G. C., & Beard, L. (1985). Salt gland function in fresh water crocodiles: evidence for a marine phase in eusuchian evolution. In G. Grgg, R. Shine, & H. Ehmann (Eds.), *Biology of australasian frogs and reptiles* (pp. 403–410). Surrey Beatty; Sons.

Taplin, L. E., Grigg, G. C., Harlow, P., Ellis, T. M., & Dunson, W. A. (1982). Lingual salt glands in *Crocodylus acutus* and *C. johnstoni* and their absence from *Alligator mississipiensis* and *Caiman crocodilus*. *Journal of Comparative Physiology B: Biochemical, Systemic, and Environmental Physiology*, *149*(1), 43–47.

Tarsitano, S. F. (1985). Cranial metamorphosis and the origin of the Eusuchia. *Neues Jahrbuch für Geologie und Paläontologie. Abhandlungen*, *170*(1), 27–44.

Tarsitano, S. F., Frey, E., & Riess, J. (1989). The evolution of the Crocodilia: a conflict between morphological and biochemical data. *American Zoologist*, *29*(3), 843–856.

Tchernov, E. (1986). Évolution des Crocodiles en Afrique du Nord et de l'Est. *Éditions du Centre National de la Recherche Scientifique*.

Tchernov, E., & Van Couvering, J. (1978). New crocodiles from the Early Miocene of Kenya. *Palaeontology*, *21*(4), 857–867.

Tennant, J. P., Mannion, P. D., & Upchurch, P. (2016). Evolutionary relationships and systematics of Atoposauridae (Crocodylomorpha: Neosuchia): implications for the rise of Eusuchia. *Zoological Journal of the Linnean Society*, *177*(4), 854–936.

Thiele, K. (1993). The holy grail of the perfect character: the cladistic treatment of morphometric data. *Cladistics*, *9*(3), 275–304.

Toula, F., & Kail, J. A. (1885). Über einen Krokodil-Schädel aus den Tertiärablagerungen von Eggenburg in Niederösterreich: eine paläontologische Studie. *Denkschriften der Keiserlichen Akademie der Wissenschaften, Mathematisch-Naturwissenschatflliche Klasse*, *50*.

Trueman, J. W. H. (1998). Reverse successive weighting. *Systematic Biology*, *47*(4), 733–737.

Tschopp, E., Mateus, O., & Benson, R. B. J. (2015). A specimen-level phylogenetic analysis and taxonomic revision of Diplodocidae (Dinosauria, Sauropoda). *PeerJ*, *3*, e857.

Tschopp, E., & Upchurch, P. (2019). The challenges and potential utility of phenotypic specimen-level phylogeny based on maximum parsimony. *Earth and Environmental Science Transactions of the Royal Society of Edinburgh*, *109*(1-2), 301–323.

Tumarkin-Deratzian, A. R., Vann, D. R., & Dodson, P. (2007). Growth and textural ageing in long bones of the American alligator *Alligator mississippiensis* (Crocodylia: Alligatoridae). *Zoological Journal of the Linnean Society*, *150*(1), 1–39.

Turner, A. H. (2015). A review of *Shamosuchus* and *Paralligator* (Crocodyliformes, Neosuchia) from the Cretaceous of Asia. *PLoS One*, *10*(2), e0118116.

Turner, A. H., & Pritchard, A. C. (2015). The monophyly of Susisuchidae (Crocodyliformes) and its phylogenetic placement in Neosuchia. *PeerJ*, *3*, e759.

Vaillant, L. (1872). Étude zoologique sur les crocodiliens fossiles tertiaires de Saint-Gérand le Puy. *Annales des Sciences Géologiques*, *3*(1), 1–57.

van Tuinen, M., & Torres, C. R. (2015). Potential for bias and low precision in molecular divergence time estimation of the Canopy of Life: an example from aquatic bird families. *Frontiers in genetics*, *6*, 203.

Varona, L. S. (1984). Los cocodrilos fosiles De Cuba (Reptilia: Crocodylidae). *Caribbean Journal of Science*, *20*(1-2), 13–18.

Vasse, D. (1992). Un crâne d'*Asiatosuchus germanicus* du Lutétien d'Issel (Aude). Bilan sur le genre *Asiatosuchus* en Europe. *Geobios*, *25*(2), 293–304.

Vélez-Juarbe, J., Brochu, C. A., & Santos, H. (2007). A gharial from the Oligocene of Puerto Rico: transoceanic dispersal in the history of a non-marine reptile. *Proceedings of the Royal Society B: Biological Sciences*, *274*(1615), 1245–1254.

Venegas-Anaya, M., Crawford, A. J., Escobedo Galván, A. H., Sanjur, O. I., Densmore III, L. D., & Bermingham, E. (2008). Mitochondrial DNA phylogeography of *Caiman crocodilus* in Mesoamerica and South America. *Journal of Experimental Zoology Part A: Ecological Genetics and Physiology*, *309*(10), 614–627.

Vianna, A., & Moraes, A. (1945). Sur un crâne de crocodile fossile decouvert dans le Miocène de Lisbonne. *Boletim de la Sociedade Geológica de Portugal*, *4*, 161–170.

Vickaryous, M. K., & Hall, B. K. (2008). Development of the dermal skeleton in *Alligator mississippiensis* (Archosauria, Crocodylia) with comments on the homology of osteoderms. *Journal of morphology*, *269*(4), 398–422.

Vignaud, P., Brunet, M., Guevel, B., & Jehenne, Y. (1996). Un crâne de *Diplocynodon* (Crocodylomorpha, Alligatoridae) de l'Oligocène inférieur de Dordogne (France). *Comptes rendus de l'Académie des sciences. Série 2. Sciences de la terre et des planètes*, *322*(7), 595–601.

von Meyer, H. (1857). Beiträge zur näheren Kenntniss fossiler Reptilien. *Neues Jahrbuch für Geologie und Paläontologie Abhandlungen*, 532–543.

Wang, Y.-Y., Sullivan, C., & Liu, J. (2016). Taxonomic revision of *Eoalligator* (Crocodylia, Brevirostres) and the paleogeographic origins of the Chinese alligatoroids. *PeerJ*, *4*, e2356.

Wassersug, R. J., & Hecht, M. K. (1985). The status of the crocodylid genera *Procaimanoidea* and *Hassiacosuchus* in the New World. *Herpetologica*, *23*, 30–34.

Webb, G. J. W., Manolis, S. C., & Brien, M. L. (2010). Saltwater crocodile *Crocodylus porosus*. In S. C. Manolis & C. Stevenson (Eds.), *Crocodiles. Status Survey and Conservation Action Plan. Third Edition* (pp. 99–113). Crocodile Specialist Group.

Weems, R. E. (2018). Crocodilians of the Calvert Cliffs. In S. J. Godfrey (Ed.), *The Geology and Vertebrate Paleontology of Calvert Cliffs, Maryland, USA* (pp. 213–240). Smithsonian Institution Scholarly Press.

Weems, R. E., & Grimsley, G. J. (1999). *Early Eocene vertebrates and plants from the Fisher/Sullivan site (Nanjemoy Formation) Stafford County, Virginia* (Vol. 152). Commonwealth of Virginia, Department of Mines, Minerals; Energy, Division of Mineral Resources.

Weitzel, K. (1935). *Hassiacosuchus haupti* n. gn. sp., ein durophages Krokodil aus dem Mitteleozän von Messel. *Notizblatt des Vereins für Erdkunde und der hessischen geologischen Landesantalt zu Darmstadt*, *16*.

Wermuth, H. (1953). Systematik der rezenten Krokodile. *Mitteilungen der Zoologisches Museum Berlin*, *29*, 375–511.

White, T. E. (1942). A new alligator from the Miocene of Florida. *Copeia*, *1942*(1), 3–7.

Whiting, E. T., & Hastings, A. K. (2015). First fossil *Alligator* from the late Eocene of Nebraska and the Late Paleogene record of alligators in the Great Plains. *Journal of Herpetology*, *49*(4), 560–569.

Whiting, E. T., & Head, J. J. (2020). Neogene crocodylians from the Central Great Plains: spatiotemporal histories and relationships with regional climatic and environmental changes. *Journal of Vertebrate Paleontology*, e1764007.

Whiting, E. T., Steadman, D. W., & Krigbaum, J. (2016a). Paleoecology of Miocene crocodylians in Florida: insights from stable isotope analysis. *Palaeogeography, Palaeoclimatology, Palaeoecology*, *451*, 23–34.

Whiting, E. T., Steadman, D. W., & Vliet, K. A. (2016b). Cranial polymorphism and systematics of Miocene and living alligator in North America. *Journal of Herpetology*, *50*(2), 306–315.

Wiens, J. J. (2001). Character analysis in morphological phylogenetics: problems and solutions. *Systematic Biology*, *50*(5), 689–699.

Wilberg, E. W. (2015). What's in an outgroup? The impact of outgroup choice on the phylogenetic position of Thalattosuchia (Crocodylomorpha) and the origin of Crocodyliformes. *Systematic Biology*, *64*(4), 621–637.

Wilberg, E. W. (2017). Investigating patterns of crocodyliform cranial disparity through the Mesozoic and Cenozoic. *Zoological Journal of the Linnean Society*, *181*(1), 189–208.

Wilberg, E. W., Turner, A. H., & Brochu, C. A. (2019). Evolutionary structure and timing of major habitat shifts in Crocodylomorpha. *Scientific Reports*, *9*(1), 1–10.

Wilf, P., Cúneo, N. R., Escapa, I. H., Pol, D., & Woodburne, M. O. (2013). Splendid and seldom isolated: the paleobiogeography of Patagonia. *Annual Review of Earth and Planetary Sciences*, *41*.

Wilkinson, M. (1995). A comparison of two methods of character construction. *Cladistics*, *11*(3), 297–308.

Willerslev, E., & Cooper, A. (2005). Ancient DNA. *Proceedings of the Royal Society B: Biological Sciences*, *272*(1558), 3–16.

Willis, P. M. A. (1997a). New crocodilians from the Late Oligocene White Hunter Site, Riversleigh, northwestern Queensland. *Memoirs of the Queensland Museum*, *41*, 423–438.

Willis, P. M. A. (1997b). Review of fossil crocodilians from Australasia. *Australian Zoologist*, *30*(3), 287–298.

Willis, P. M. A. (2001). New crocodilian material from the Miocene of Riversleigh (northwestern Queensland, Australia). *Crocodilian biology and evolution*, 64–74.

Willis, P. M. A., & Archer, M. (1990). A Pleistocene longirostrine crocodilian from Riversleigh: first fossil occurrence of *Crocodylus johnstoni* Krefft. *Memoirs of the Queensland Museum*, *28*(1), 159–163.

Willis, P. M. A., & Mackness, B. S. (1996). *Ouinkana babarra*, a new species of ziphodont mekosuchine crocodile from the early Pliocene Bluff Downs local fauna, northern Australia with a revision of the genus. *Proceedings of the Linnean Society of New South Wales*, *116*, 143–151.

Willis, P. M. A., Murray, P. F., & Megirian, D. (1990). *Baru darrowi* gen. et sp. nov., a large broad-snouted crocodyline (Eusuchia: Crocodylidae) from mid-Tertiary freshwater limestones in northern Australia. *Memoirs of the Queensland Museum*, *29*(2), 521–540.

Willis, P. M. A. (1993). *Trilophosuchus rackhami* gen. et sp. nov., a new crocodilian from the early Miocene limestones of Riversleigh, northwestern Queensland. *Journal of Vertebrate Paleontology*, *13*(1), 90–98.

Willis, P. M. A., & Molnar, R. E. (1991a). A longirostrine crocodile from the Early Tertiary of southeastern Queensland. *Alcheringa*, *15*(3), 229–233.

Willis, P. M. A., & Molnar, R. E. (1991b). A new middle Tertiary crocodile from Lake Palankarinna, South Australia. *Records of the South Australian Museum*, *25*(1), 39–55.

Willis, P. M. A., & Molnar, R. E. (1997). A review of the Plio-Pleistocene crocodilian genus *Pallimnarchus*. *Proceedings of the Linnean Society of New South Wales*, *117*, 223–242.

Willis, P. M. A., Molnar, R. E., & Scanlon, J. D. (1993). An early Eocene crocodilian from Murgon, southeastern Queensland. *Kaupia*, *3*, 27–33.

Willis, P. M. A., & Stilwell, J. D. (2000). A probable piscivorous crocodile from Eocene deposits of McMurdo Sound, East Antarctica. *Paleobiology and Paleoenvironments of Eocene Rocks: McMurdo Sound, East Antarctica*, *76*, 355–358.

Willis, R. E. (2009). Transthyretin gene (TTR) intron 1 elucidates crocodylian phylogenetic relationships. *Molecular Phylogenetics and Evolution*, *53*(3), 1049–1054.

Willis, R. E., McAliley, L. R., Neeley, E. D., & Densmore III, L. D. (2007). Evidence for placing the false gharial (*Tomistoma schlegelii*) into the family Gavialidae: inferences from nuclear gene sequences. *Molecular Phylogenetics and Evolution*, *43*(3), 787–794.

Wills, M. A. (1999). Congruence between phylogeny and stratigraphy: randomization tests and the gap excess ratio. *Systematic Biology*, *48*(3), 559–580.

Witmer, L. M. (1997). The evolution of the antorbital cavity of archosaurs: a study in soft-tissue reconstruction in the fossil record with an analysis of the function of pneumaticity. *Journal of Vertebrate Paleontology*, *17*(S1), 1–76.

Wood, S. (1844). Record of the discovery of an alligator with several new Mammalia in the freshwater strata at Hordwell. *Annals and Magazine of Natural History*, *14*(92), 349–351.

Wood, S. (1846). On the discovery of an alligator and of several new Mammalia in the Hordwell Cliff; with observations upon the geological phenomena of that locality. *The London Geological Journal, and Record of Discoveries in British and Foreign Paleontology*, *1*, 1–7.

Woodburne, M. O. (2010). The Great American Biotic Interchange: dispersals, tectonics, climate, sea level and holding pens. *Journal of mammalian evolution*, *17*(4), 245–264.

Woodward, A. S. (1885). On the literature and nomenclature of British fossil Crocodilia. *Geological Magazine*, *2*, 496–510.

Worthy, T. H., De Pietri, V. L., & Scofield, R. P. (2017). Recent advances in avian palaeobiology in New Zealand with implications for understanding New Zealand's geological, climatic and evolutionary histories. *New Zealand Journal of Zoology*, *44*(3), 177–211.

Wright, A. M., & Hillis, D. M. (2014). Bayesian analysis using a simple likelihood model outperforms parsimony for estimation of phylogeny from discrete morphological data. *PLoS One*, *9*(10), e109210.

Wright, T. (1851). A stratigraphical account of the section at Hordwell, Beacon and Barton Cliffs, on the coast of Hampshire. *Annals and Magazine of Natural History (Series 2)*, *7*, 433–446.

Wu, X. C., Li, C., & Wang, Y. Y. (2018). Taxonomic reassessment and phylogenetic test of *Asiatosuchus nanlingensis* Young, 1964 and *Eoalligator chunyii* Young, 1964. *Vertebrata PalAsiatica*, *56*(2), 137–146.

Wu, X.-C., & Brinkman, D. B. (1993). A new crocodylomorph of "mesosuchian" grade from the Upper Cretaceous Upper Milk River Formation, southern Alberta. *Journal of Vertebrate Paleontology*, *13*(2), 153–160.

Wu, X.-C., & Brinkman, D. B. (2015). A new crocodylian (Eusuchia) from the uppermost Cretaceous of Alberta, Canada. *Canadian Journal of Earth Sciences*, *52*(8), 590–607.

Wu, X.-C., Brinkman, D. B., & Russell, A. P. (1996). A new alligator from the Upper Cretaceaous of Canada and the relationship of early eusuchians. *Palaeontology*, *39*, 351–376.

Wu, X.-C., Russell, A. P., & Brinkman, D. B. (2001a). A review of *Leidyosuchus canadensis* Lambe, 1907 (Archosauria: Crocodylia) and an assessment of cranial variation based upon new material. *Canadian Journal of Earth Sciences*, *38*(12), 1665–1687.

Wu, X.-C., Russell, A. P., & Cumbaa, S. L. (2001b). *Terminonaris* (Archosauria: Crocodyliformes): New material from Saskatchewan, Canada, and comments on its phylogenetic relationships. *Journal of Vertebrate Paleontology*, *21*(3), 492–514.

Wu, X.-C., & Sues, H.-D. (1996). Anatomy and phylogenetic relationships of *Chimaerasuchus paradoxus*, an unusual crocodyliform reptile from the Lower Cretaceous of Hubei, China. *Journal of Vertebrate Paleontology*, *16*(4), 688–702.

Wu, X.-C., Sues, H.-D., & Dong, Z.-M. (1997). *Sichuanosuchus shuhanensis*, a new? Early Cretaceous protosuchian (Archosauria: Crocodyliformes) from Sichuan (China), and the monophyly of Protosuchia. *Journal of Vertebrate Paleontology*, *17*(1), 89–103.

Yan, P., Feng, G., Li, X., & Wu, X. (2010). Two complete mitochondrial genomes of *Crocodylus* and implications for crocodilians phylogeny. *Amphibia-reptilia*, *31*(3), 299–309.

Yang, Z., & Rannala, B. (2012). Molecular phylogenetics: principles and practice. *Nature reviews genetics*, *13*(5), 303–314.

Yates, A. M. (2017). The biochronology and palaeobiogeography of *Baru* (Crocodylia: Mekosuchinae) based on new specimens from the Northern Territory and Queensland, Australia. *PeerJ*, *5*, e3458.

Yates, A. M., & Pledge, N. S. (2017). A Pliocene mekosuchine (Eusuchia: Crocodilia) from the Lake Eyre Basin of South Australia. *Journal of Vertebrate Paleontology*, *37*(1), e1244540.

Yeh, H. K. (1958). A new crocodile from Maoming, Kwangtung. *Vertebrata PalAsiatica*, *2*(4), 237–242.

Yi, H., Tennant, J. P., Young, M. T., Challands, T. J., Foffa, D., Hudson, J. D., Ross, D. A., & Brusatte, S. L. (2017). An unusual small-bodied crocodyliform from the Middle Jurassic of Scotland, UK, and potential evidence for an early diversification of advanced neosuchians. *Earth and Environmental Science Transactions of the Royal Society of Edinburgh*, *107*(1), 1–12.

Young, C. C. (1964). New fossil crocodiles from China. *Vertebrata Palasiatica*, *8*(2), 189–208.

Zachos, J., Pagani, M., Sloan, L., Thomas, E., & Billups, K. (2001). Trends, rhythms, and aberrations in global climate 65 Ma to present. *Science*, *292*(5517), 686–693.

Zanazzi, A., Kohn, M. J., MacFadden, B. J., & Terry, D. O. (2007). Large temperature drop across the Eocene–Oligocene transition in central North America. *Nature*, *445*(7128), 639–642.

Zangerl, R. (1944). *Brachyuranochampsa eversolei*, gen. et sp. nov., a new crocodilian from the Washakie Eocene of Wyoming. *Annals of the Carnegie Museum*, *30*, 77–84.

Zigno, A. (1880). Sopra un cranio di coccodrillo scoperto nel terreno eoceno del Veronese. *Atti della Reale Accademia Nazionale dei Lincei: Memorie della Classe di Scienze fisiche, Mathematiche e Naturale, Serie 3*, *5*, 65–72.

Zittel, K. A. (1890). *Handbuch der Palaeontologie. I. Abtheilung Palaeozoologie. III Band. Pisces, Amphibia, Reptilia, Aves* (Vol. 3). R. Oldenbourg.

# Appendix A

# Referred material of *Diplocynodon hantoniensis*

---

**NHMUK**: skulls (R 1041, R 1042, OR 25167, OR 25170.a, OR 29694, OR 30287 partim, OR 30392 OR 30393 [type of '*Crocodilus hastingsiae*'], OR 30414 partim); rostrum fragment (OR 30381 partim); premaxillae (OR 30289 partim, OR 30369, OR 30370, OR 30414 partim); maxilla (R 5010 partim, OR 25168, OR 25169, OR 25170, OR 30289 partim); nasal (OR 30289 partim); jugals (OR 25188 [with partial quadratojugal], OR 25219, OR 30289 partim); quadrates (OR 25187, OR 25193. OR 30372, OR 30382, OR 30414 partim); pterygoid (OR 30251 [with fragmentary ectopterygoids and palatine]); ectopterygoids (OR 25216 [with pterygoid fragment], OR 25217); basioccipital (OR 36812); lower jaws (R 1043, R 1045 partim, R 5267 partim, OR 25178, OR 30274, OR 30381 partim, OR 30394, OR 30396 [two rami in connection], OR 30397); dentaries (R 1044, R 5010 partim, R 5121, R 5212, R 5216, R 5217, OR 30318 partim, OR 30321, OR 30287 partim, OR 30289 partim, OR 30338, OR 30365, OR 30378, OR 30383); angulars (R 5217 partim, OR 30285, OR 30289 partim, OR 30307, OR 30308, OR 30318 partim, OR 30414 partim); articulars (OR 25192, OR 30282, OR 30283, OR 30284, OR 30388 partim, OR 30289 partim, OR 30363, OR 30363.a, OR 30388 partim [joined with 30289], OR 30414 partim); surangular (OR 30414 partim); tooth bearing bone (OR 25260); isolated teeth (R 1043, R 5009, R.6323, R 6852, OR 25165, OR 25598, OR 30317 partim); proatlas (OR 30289 partim); odontoid process (OR 25186); axes (two unnumbered specimens); vertebrae (R 1041, R 1045 partim, R 1046, R 1047, R 1048, R 1049, R 1050, R 1051, R 1052, R.1068 partim, R 5213, R 5267 partim, OR 25175, OR 25177, OR 25176, OR 25179, OR 25180, OR 25181, OR 25182, OR 25195, OR 25199, OR 25201, OR 25207, OR 25208, OR 25209, OR 25210, OR 25213, OR 25214, OR 25215, OR 25222, OR 25223, OR 25224, OR 30289 partim, OR 30402 partim, plus unnumbered specimens); ribs (R.1068 partim, OR 25191, OR 25248, OR 30402 partim, OR 30414 partim); osteoderms (R 1043,

R 1045 partim, R 1068 partim, R 5214, R 5267 partim, OR 25174, OR 30318 partim, OR 30366, OR 30367, OR 30368, OR 30388 partim, OR 30414 partim, plus one unnumbered specimen); scapulae (OR 30247 partim, OR 30414 partim); coracoids (OR 25245, OR 30359); humeri (OR 25237, OR 30206, OR 30206.a, OR 30219, OR 30247 partim); radii (OR 25244 partim, OR 30401); ulnae (OR 25239, OR 30236, OR 30237, OR 30247 partim, OR 30389); radiale (R.1054); ilia (OR 25252, OR 25253, OR 30362, OR 30414 partim); ischia (OR 30354 partim); femora (R 5215, R 5267 partim, OR 25231, OR 25232, OR 25238, OR 25244 partim, OR 30210, OR 30211, OR 30213, OR 30214, OR 30222, OR 30223, OR 30228, OR 30247 partim, OR 30399, OR 30414 partim); tibiae (R 5267 partim, OR 25236, OR 30215, OR 30216, OR 30217, OR 30242, partim, OR 30414 partim); fibulae (OR 30233, OR 30234, OR 30235, OR 30241); metapodials (R 1053 partim, R 5267 partim, OR 25244 partim, OR 25254, OR 30240, OR 30242 partim, OR 30243, OR 30246, OR 30247 partim, OR 30336); phalanges (R 1053 partim, R.1054 partim, R 5267 partim, OR 25243). **CAMSM**: skulls (TN 907 partim, TN 917, TN 918 partim); lower jaws (TN 904; TN 907 partim); dentaries (C31041, C31042, C31043, plus 8 unnumbered specimens); angulars (C31044, 31045); cervical vertebrae (C31026–40); dorsal vertebrae (C31012–25); caudal vertebrae (C30999–31011); osteoderms (C31046–95; C31352–87).

# Appendix B

# List of Specimens Examined

Table B.1: Sources of data for specimens included in the phylogenetic analysis.

| Taxon | Specimens Examined | Literature Used |
|---|---|---|
| *Acresuchus pachytemporalis* | UFAC 2507 (holotype), UFAC 1187, UFAC 1379, UFAC 1486, UFAC 3142, UFAC 4153, UFAC 4154, UFAC 4183, UFAC 4678, UFAC 5256, UFAC 6384 | Souza-Filho et al. (2019) |
| *Acynodon iberoccitanus* | – | Buscalioni et al. (1997); Martin (2007) |
| *Agaresuchus fontisensis* | – | Narváez et al. (2016) |
| *Aktiogavialis caribesi* | – | Salas-Gismondi et al. (2019) |
| *Alligator mcgrewi* | FMNH 26242 (holotype), AMNH FAM 7905, AMNH FAM 8700, AMNH 17090 | Schmidt (1941) |
| *Alligator mefferdi* | AMNH 7016 (holotype) | Mook (1941a) |
| *Alligator mississippiensis* | AMNH 71621, FMNH 8202, NHMUK 1873.2.21.1, NHMUK 68.2.12.6, USNM 25148, USNM 30691 | – |
| *Alligator olseni* | MCZ 1887 (holotype), MCZ 1888, MCZ 1889, MCZ 4698, MCZ 4702, MCZ 1899, MCZ 4719, MCZ 4736, MCZ 4716, MCZ 4717, MCZ 4730, MCZ 4732, MCZ 4723, MCZ uncat. | White (1942) |

| Taxon | Specimens Examined | Literature Used |
|---|---|---|
| *Alligator prenasalis* | AMNH 4994, FMNH 12141 (holotype of *Allognathosuchus riggsi*), YPM PU 13799, YPM PU 16273, YPM PU 14063 | Loomis (1904) |
| *Alligator sinensis* | AMNH 23907, USNM 292078, USNM 67712, USNM 52558, USNM 52557, NHMUK X184 | Cong et al. (1998) |
| *Allodaposuchus precedens* | MMS/VBN-12-10A, MMS/VBN-12-42 (Photographs by Jeremy Martin) | Buscalioni et al. (2001); Martin (2010b); Delfino et al. (2008a);Martin et al. (2016a); Narváez et al. (2019) |
| *Allognathosuchus polyodon* | USNM 4112 | Mook (1921a, 1961); Brochu (2004b) |
| *Allognathosuchus wartheni* | YPM PU 16989 | Case (1925); Brochu (2004b) |
| *Arambourgia gaudryi* | MNHN QU17155 | Kälin (1939) |
| *Argochampsa krebsi* | NHMUK R 36872 | Hua and Jouve (2004); Jouve et al. (2006b) |
| *Asiatosuchus depressifrons* | MNHN G 159, IRScNB IG 9912, IRScNB R 251, IRScNB R 253, IRScNB R 254 | Delfino and Smith (2009) |
| *Asiatosuchus germanicus* | SMF Me 1801, HLMD-Me-1352, HLMD-Me-5344, HLMD-Me-5640, HLMD-Me-5649, HLMD-Me-5652, HLMD-Me-5669, HLMD-Me-5670, HLMD-Me-6020, HLMD-Me-7499, HLMD-Me-3092 | Berg (1966) |
| *Asiatosuchus nanlingensis* | IVPP V 2772, IVPP V 2773 | Wang et al. (2016) |
| *Australosuchus clarkae* | QM F18151, QM F16788 (holotype), QM F18102, QM uncat. (maxilla), AMNH 12177, AMNH 12200, AMNH 23049, AMNH 23050, AMNH 23051, UCMP 71396, UCMP 100028, UCMP 88192, UCMP 6213, UCMP 100027, UCMP 154338 | Willis and Molnar (1991b) |

| Taxon | Specimens Examined | Literature Used |
|---|---|---|
| *Baru darrowi* | – | Willis et al. (1990) |
| *Baru huberi* | QM F31060 (holotype), QM F31061, QM F31062, QM F31063, QM F31064, QM F31065, QM F31066, QM F31067, QM F31069 (paratype) | Willis (1997a) |
| *Baru wickeni* | QM F16822 (holotype), QM F16823, QM F31070, QM F31071, QM F31072, QM F31073, QM F31074 | Willis (1997a); Yates (2017) |
| *Bernissartia fagesii* | IRScNB 1538 | Buffetaut and Ford (1979); Norell and Clark (1990) |
| *Borealosuchus acutidentatus* | NMC 8544 (Photographs provided by Jordon Mallon) | Sternberg (1932); Brochu (1997a) |
| *Borealosuchus formidabilis* | YPM 16242, YPM 16241, YPM 6512 | Erickson (1976); Brochu (1997a) |
| *Borealosuchus sternbergii* | USNM V 6533 (holotype), UCMP 284939, UCMP 173976, UCMP 154335, UCMP 137144, UCMP 134470, UCMP 133930, UCMP 133903, UCMP 130469, UCMP 130435, UCMP 130434, UCMP 129345, UCMP 129206, UCMP 126099, UCMP 119282, UCMP 77111 | Gilmore (1910); Brochu (1997a) |
| *Borealosuchus threensis* | – | Brochu et al. (2012) |
| *Borealosuchus wilsoni* | AMNH 6050 (holotype *Diplocynodon stuckeri*), AMNH 7637 (holotype of *Leidyosuchus wilsoni*), FMNH PR 1674 | Mook (1959b) |
| *Bottosaurus harlani* | – | Cossette and Brochu (2018) |
| *Boverisuchus magnifrons* | – | Rossmann (1998); Brochu (2012) |
| *Boverisuchus vorax* | YPM 249 (holotype), FMNH PR 399, UCMP 170767 | Rossmann (2000); Brochu (2012) |
| *Brachychampsa montana* | AMNH 5032 (holotype), UCMP 133901 | Norell et al. (1994) |
| *Brochuchus pigotti* | NHMUK PV R 7729 | Conrad et al. (2013) |
| *Caiman brevirostris* | UFAC 196 (holotype), UFAC 5388 | Fortier et al. (2014) |

| Taxon | Specimens Examined | Literature Used |
|---|---|---|
| *Caiman crocodilus* | *Caiman crocodilus apaporiensis*: FMNH 69812 (holotype), UCMP 42844, UCMP 42843, USNM 69822 (paratype); *Caiman crocodilus chiapasius*: FMNH 73694, FMNH 73701, FMNH 73712, FMNH 73721, FMNH 73724; *Caiman crocodilus fuscus*: FMNH 69835, FMNH 69837, FMNH 69844, FMNH 69848, FMNH 69849, FMNH 69859; *Caiman crocodilus* (subspecies indet): USNM 142089, USNM 217264, USNM 54094, USNM 306645, USNM 134499, | – |
| *Caiman gasparinae* | MLP-IV-15-1, MLP-IV-15-2, MLP-IV-15-4 | Bona and Carabajal (2013) |
| *Caiman latirostris* | AMNH 143183, FMNH 9713, MACN-PV 1420, NHMUK 86.10.4.2, USNM 98780 | Bona and Desojo (2011) |
| *Caiman lutescens* | MACN-PV 13551 | Rovereto (1912) |
| '*Caiman* cf. *lutescens*', ('La Venta Caiman') | UCMP 39978 | Langston (1965) |
| *Caiman wannlangstoni* | – | Salas-Gismondi et al. (2015) |
| *Caiman yacare* | AMNH 97300, FMNH 9141, MLP uncat. | Medem (1960) |
| *Ceratosuchus burdoschi* | FMNH P 15576 (holotype), FMNH PR 208 | Schmidt (1938) |
| *Crocodylus acutus* | AMNH 7121, FMNH 69884, FMNH 59070, NHMUK 1975.997, USNM 243433, USNM 52491 | Mook (1921c) |
| '*Crocodylus*' *affinis* | AMNH 1213, AMNH 1719, AMNH 6166, AMNH 16609, AMNH 16622, AMNH 6176, FMNH 12202, UCMP 131090, UCMP 81325, UCMP 154341, YPM 1352, YPM 265, YPM 266, YPM 246, USNM 18171 (originally referred to *Crocodylus acer*) | Mook (1921b) |

| Taxon | Specimens Examined | Literature Used |
|---|---|---|
| *Crocodylus anthropophagus* | NHMUK R5893 | Brochu et al. (2010) |
| *Crocodylus intermedius* | FMNH 75659, FMNH 75662, FMNH 75658, NHMUK 1851.8.25.29, NHMUK 62.10.19.1 | – |
| *Crocodylus johnstoni* | QM J4280, QM J4281, QM F39230, QM J45309, QM J58446, USNM 299810, USNM 64091 | – |
| '*Crocodylus*' *megarhinus* | AMNH 5061, AMNH 5062, SMNS 2650, YPM 058532, NHMUK PV R 3327 | Adams (2016) |
| *Crocodylus mindorensis* | FMNH 1135 (holotype), FMNH 19891 (paratype), USNM 228407, USNM 37435 | – |
| *Crocodylus moreletii* | NHMUK 1861.4.1.4, USNM 71954, USNM 71959 | – |
| *Crocodylus niloticus* | AMNH 88634, AMNH 137163, AMNH 137180, NHMUK 1934.6.3.1, NHMUK 64.1.25.4, NHMUK 1904.10.10.1, USNM 233977, USNM 63592, USNM 195448 | – |
| *Crocodylus novaeguineae* | NHMUK 1886.5.20.1 | – |
| *Crocodylus palaeindicus* | AMNH 1915, NHMUK 39795 ('C. sivalensis'), NHMUK 39799, NHMUK 39797, NHMUK 39801 | Lydekker (1886) |
| *Crocodylus palustris* | NHMUK 97.12.31.1 (*C. palustris kimbula*), NHMUK 1845.1.8.204, NHMUK 1861.4.1.5, NHMUK 1868.4.9.11, AMNH 77632 | – |

| Taxon | Specimens Examined | Literature Used |
|---|---|---|
| *Crocodylus porosus* | AMNH 7115, FMNH 22026, FMNH 15226, FMNH 15229, NHMUK 1886.5.20.3, NHMUK 1864.9.11.1, NHMUK 1852.12.9.2, QM J93350, QM J5005, QM J39283, QM J47446, QM J47447, QM J47448, QM J48127, USNM 72730, USNM 61206 | – |
| *Crocodylus rhombifer* | AMNH 77595, AMNH 141073, AMNH R154087 (Fidel), USNM 544377 | – |
| *Crocodylus siamensis* | AMNH 118712, NHMUK 1921.4.1.171, NHMUK 1921.4.1.168, NHMUK 1921.4.1.172, NHMUK 1931.12.6.6, USNM 8893 | – |
| *Crocodylus thorbjarnarsoni* | – | Brochu and Storrs (2012) |
| *Diplocynodon darwini* | SMF Me 896, SMF Me 898, SMF Me 900, SMF Me 1137, SMF Me 1289, SMF Me 2748, HLMD-Me-233, HLMD-Me-236, HLMD-Me-5317, HLMD-Me-5349, HLMD-Me-5485, HLMD-Me-5650, HLMD-Me-7492, HLMD-Me-7500, HLMD-Me-10262, HLMD-Me-10496, HLMD-Me-14600a | Ludwig (1877) |
| *Diplocynodon deponiae* | SMF Me 899 (holotype), SMF Me 1114a, SMF Me 1348a, SMF Me 2609, SMF Me 11053b, HLMD-Be-147, HLMD-Me-8080, IRScNB R 261 | Frey et al. (1987); Delfino and Smith (2012) |
| *Diplocynodon hantoniensis* | Specimens too numerous to list, see Rio et al. (2020). | Rio et al. (2020) |
| *Diplocynodon muelleri* | – | Piras and Buscalioni (2006) |

| Taxon | Specimens Examined | Literature Used |
|---|---|---|
| *Diplocynodon ratelii* | MNHN SG13736, MNHN SG 539, MNHN SG 557, MNHN uncat. (exposing braincase), MNHN G 660, MNHN SG 623, MNHN SG 624, MNH SG 625, MNHN SG 523, MNHN SG 631, MNHN SG 632, MNHN SG 12985, MNHN SG 635, MNHN SG 678, MNHN SG 614, MNHN SG 493, MNHN SG 643, MNHN SG 648, Catalogued as '*Diplocynodon gracilis*': NHMUK 26841, NHMUK 30945, NHMUK 27751, NHMUK 26846a, NHMUK R.789, NHMUK 26842. | Aráez et al. (2017) |
| *Diplocynodon remensis* | MNHN F BR 4020 | Martin et al. (2014) |
| *Diplocynodon tormis* | – | Buscalioni et al. (1992); Serrano-Martínez et al. (2019b) |
| *Dollosuchoides densmorei* | | Brochu (2007b) |
| *Eocaiman cavernensis* | AMNH 3158 (holotype), AMNH 19170 (*Eocaiman* sp. consulted but not scored) | Simpson (1933); Godoy (2014) |
| *Eocaiman palaeocenicus* | MPEF PV 1933a, MACN-PV CH1914, MACN-PV CH 1915, MACN-PV CH 1916, MACN-PV CH 1627 | Bona (2007) |
| *Eogavialis africanum* | NHMUK PV R 3329 (cast of holotype), NHMUK PV R3108, NHMUK PV R 3430, NHMUK PV R 3325, SMNS 11224-1, SMNS 11224-3, SMNS 11225, SMNS 11785, YPM 6263; Catalogued as '*Tomistoma*' *gavialoides* (= *E. africanum*): AMNH FR 5066, AMNH 5068, AMNH 5069, AMNH 5070, AMNH 5071, AMNH 5073, AMNH 5074 , AMNH 5075 | Andrews (1906) |
| *Eosuchus lerichei* | IRScNB R 49 | Delfino et al. (2005) |

| Taxon | Specimens Examined | Literature Used |
|---|---|---|
| *Eosuchus minor* | USNM 321932, USNM 321933, USNM 299730, YPM 282 | Brochu (2006b) |
| *Eothoracosaurus mississippiensis* | AMNH 3841 | Brochu (2004a) |
| *Euthecodon arambourgi* | MNHN ZEL 001 | Ginsburg and Buffetaut (1978) |
| *Gavialis browni* | AMNH 6279 | Mook (1932) |
| *Gavialis gangeticus* | AMNH 110145, FMNH 98864, NHMUK uncat., NHMUK 1846.1.7.3, NHMUK 1935.6.4.1, NHMUK 1974.3009, NHMUK 704, NHMUK 96.7.7.4, UMZC R 5783, USNM 576261 | – |
| *Gavialis lewisi* | YPM VP 3226 | Lull (1944) |
| *Gavialosuchus eggenburgensis* | NHMUK PV R 797 (cast of holotype) | Toula and Kail (1885) |
| Glen Rose form | MCZ 4384, USNM 22039 | |
| *Globidentosuchus brachyrostris* | MCZ 4336, AMU-CURS-222 (Photographs provided by Torsten Scheyer) | Scheyer and Delfino (2016); Hastings et al. (2016) |
| *Gnatusuchus pebasensis* | – | Salas-Gismondi et al. (2015) |
| *Gryposuchus colombianus* | UCMP 41136 (holotype), UCMP 40293, UCMP 40062, UCMP 38358 | Langston (1965); Langston and Gasparini (1997) |
| *Gryposuchus croizati* | – | Riff and Aguilera (2008) |
| *Gryposuchus neogaeus* | MACN-PV 6218, MLP 26-413, MLP 68-18-5-1 | Gasparini (1968) |
| *Gryposuchus pachakamue* | – | Salas-Gismondi et al. (2016) |
| *Hassiacosuchus haupti* | HLMD-Be-137, HLMD-Me-1435, HLMD-Me-4415, HLMD-Me-5261, HLMD-Me-6117, HLMD-Me-9119 | Weitzel (1935); Berg (1966); Brochu (2004b) |
| *Hylaeochampsa vectiana* | NHMUK R177 | Clark and Norell (1992) |
| *Iharkutosuchus makadii* | – | Ősi et al. (2007); Ősi (2008); Ősi and Weishampel (2009); Mateus et al. (2019, Supporting Information) |

| Taxon | Specimens Examined | Literature Used |
|---|---|---|
| *Ikanogavialis gameroi* | | Sill (1970) |
| *Isisfordia duncani* | QM F36211 (holotype), QM F44320 (paratype) | Salisbury et al. (2006) |
| *Jiangxisuchus nankangensis* | | Li et al. (2019) |
| *Kambara implexidens* | QM F29662 (holotype), QM F29663, QM F29680, QM F30077, QM F21116, QM F21118, QM F21131, QM F29664, QM F29678 | Salisbury and Willis (1996) |
| *Kambara murgonensis* | QM F11625, QM F21125, QM F21134, QM F29667, QM F29669, QM F29683, QM F29691, QM F21117, QM F29665, QM F29666, QM F31234, QM F31284 | Willis et al. (1993) |
| *Kambara taraina* | – | Buchanan (2009) |
| *Kentisuchus spenceri* | NHMUK 19633 (holotype), NHMUK 38974, NHMUK 37717 ('*Crocodilus spenceri*') | Brochu (2007b) |
| *Kuttanacaiman iquitosensis* | – | Salas-Gismondi et al. (2015) |
| *Leidyosuchus canadensis* | AMNH 5352, NHMUK R10904 (cast of RTMP 29.28.1), UCMP 131696 | Wu et al. (2001a) |
| *Lohuecosuchus megadontos* | – | Narváez et al. (2015); Serrano-Martínez et al. (2019a) |
| *Maomingosuchus petrolica* | IVPP V.2303, IVPP V.5015, IVPP (unnumbered skull), ZMNH M1201, ZMNH S1 | Yeh (1958); Shan et al. (2017) |
| *Maroccosuchus zennaroi* | MNHN APH 18, IRScNB R408 | Jouve et al. (2015) |
| *Mecistops cataphractus* | AMNH 73803, NHMUK 62.6.30.8, NHMUK 1865.4.6.1, NHMUK 1900.2.27.1, 1924.5.10.1, USNM 60578 | |
| *Mekosuchus inexpectatus* | MNHN NCP 06, MNHN NCP 07 | Balouet and Buffetaut (1987) |
| *Mekosuchus sanderi* | QM F31188 (holotype), QM F31186, QM F31187, QM F31166 | Willis (2001) |
| *Mekosuchus whitehunterensis* | QM F31051 (holotype), QM F31052, QM F31053, QM F31054 | Willis (1997a) |

| Taxon | Specimens Examined | Literature Used |
|---|---|---|
| *Melanosuchus niger* | AMNH 97325, FMNH 45653, NHMUK 1872.6.4.1, NHMUK 45.8.25.125 | |
| *Mourasuchus amazonensis* | UFAC 1424 | Langston (1966); Cidade et al. (2019c) |
| *Mourasuchus arendsi* | MLP 73-IV-15-8 (holotype of *Mourasuchus nativus*), MLP 73-IV-15-9, UFAC 1431, UFAC 1477, UFAC 1666, UFAC 2515, UFAC 3717, UFAC 4259, UFAC 5716, UFAC 5883, UFAC 1484, UFAC 1485 | Gasparini (1985); Bona et al. (2013a); Cidade et al. (2019e) |
| *Mourasuchus atopus* | UCMP 38012 (holotype) | Langston (1965) |
| *Navajosuchus mooki* | AMNH 6780, AMNH 5186, MCZ 8381 | Simpson (1930); Mook (1942); Brochu (2004b) |
| *Necrosuchus ionensis* | AMNH 3219 (holotype) | Brochu (2011); Cidade et al. (2020a) |
| *Osteolaemus tetraspis* | AMNH 69057, AMNH 117801, FMNH 229974, NHMUK 1862.6.30.5, USNM 233978, USNM 285136 | – |
| *Paleosuchus palpebrosus* | AMNH 93812, AMNH 97326 | Medem (1958) |
| *Paleosuchus trigonatus* | AMNH 66391, NHMUK 1868.10.8.1, USNM 302052 | Medem (1958) |
| *Paratomistoma courti* | – | Brochu and Gingerich (2000) |
| *Penghusuchus pani* | – | Shan et al. (2009); Iijima and Kobayashi (2019) |
| *Piscogavialis jugaliperforatus* | SMNK 1282 PAL | Kraus (1998) |
| *Planocrania datangensis* | IVPP V5016 | Brochu (2012) |
| *Planocrania hengdongensis* | IVPP V6074 | Brochu (2012) |
| *Portugalosuchus azenhae* | – | Mateus et al. (2019) |
| *Procaimanoidea utahensis* | USNM 15996 (holotype) | Gilmore (1946) |
| *Protocaiman peligrensis* | MLP 80X-10-1 (holotype) | Bona et al. (2018) |

| Taxon | Specimens Examined | Literature Used |
|---|---|---|
| *Purussaurus brasiliensis* | UFAC 1118, UFAC 1403, UFAC 1773, UFAC 2505, UFAC 4249, UFAC 4770, UFAC 5299, UFAC 5300, UFAC 5507, UFAC 5862, UFAC 1709, UFAC 3520, UFAC 4686 | Bocquentin-Villanueva et al. (1989) |
| *Purussaurus mirandai* | – | Aguilera et al. (2006) |
| *Purussaurus neivensis* | USNM 10889 (holotype), UCMP 38108, UCMP 38932, UCMP 39657, UCMP 39704, UCMP 41101, UCMP 45719 | Langston (1965) |
| *Quinkana* | *Quinkana barbarra*: QM F23220 (holotype), QM F23223, QM F23222, QM F23221; *Quinkana meboldi*: QM F31056 (holotype), QM F31059 (paratype), QM F31057 (paratype), QM F31058 | Molnar (1981); Megirian (1994); Willis and Mackness (1996) |
| *Shamosuchus djadochtaensis* | – | Pol et al. (2009); Turner (2015) |
| *Siquisiquesuchus venezuelensis* | – | Brochu and Rincón (2004) |
| *Stangerochampsa mccabei* | – | Wu et al. (1996) |
| *Thecachampsa antiquus* | Catalogued as '*Gavialosuchus americanus*': AMNH 1651 , AMNH FR 5662, AMNH FR 5663, AMNH 6160 (holotype) | Weems (2018) |
| *Thecachampsa sericodon* | USNM 24938 | Weems (2018) |
| *Theriosuchus pusillus* | NHMUK 48328, NHMUK 48240, NHMUK 48282, NHMUK 48228, NHMUK 48329A, NHMUK 48279, NHMUK 48218, NHMUK 48216, NHMUK 48330 | Turner (2015); Tennant et al. (2016) |
| *Thoracosaurus isorhynchus* | MNHN 1902-22 (holotype), MNHN.F.MTA 61 | Piveteau (1927) |

| Taxon | Specimens Examined | Literature Used |
|---|---|---|
| *Thoracosaurus neocesariensis* | AMNH 3841, AMNH 2542, AMNH 2200, AMNH 2199, AMNH 2209, AMNH 2388, AMNH 1429, YPM 404 | Brochu (2004a) |
| *Tomistoma cairense* | SMNS 10575, SMNS 50739, SMNS 50739a, SMNS 50740, SMNS 50741, SMNS 50742, SMNS 50745 | Müller (1927) |
| *Tomistoma dowsoni* | NHMUK PV R 4769 | Fourtau (1920) |
| *Tomistoma lusitanica* | – | Antunes (1961) |
| *Tomistoma schlegelii* | AMNH 113078, NHMUK 1886.5.20.3, NHMUK 1894.2.21.1, NHMUK 1899.1.31.1, NHMUK 1848.10.31.19, USNM 52972, USNM 211323 | – |
| *Toyotamaphimeia machikanensis* | – | Kobayashi et al. (2006); Iijima and Kobayashi (2019) |
| *Trilophosuchus rackhami* | QM F16856 (holotype), QM F31185 | Willis (1993) |
| *Tsoabichi greenriverensis* | AMNH 3666, FMNH 1793 | Brochu (2010) |
| *Ultrastenos willisi* | QM 31075, QM 31076, QM 31077, QM31078 | Stein et al. (2016) |
| *Voay robustus* | NHMUK R 36666, NHMUK R36659, NHMUK R 36661, NHMUK R 36685, NHMUK R 36686, NHMUK R 220, NHMUK R 36653, NHMUK R 36685 | Brochu (2007a) |
| *Wannaganosuchus brachymanus* | – | Erickson (1982) |
| *Wannchampsus kirpachi* | – | Adams (2014) |

# Appendix C

# Rejected Characters

Table C.1: Rejected characters.

| Study | Character | Reason for rejection |
|---|---|---|
| Groh et al. (2020) | 2 | not applicable to this dataset |
| Groh et al. (2020) | 6 | not applicable to this dataset |
| Groh et al. (2020) | 7 | not applicable to this dataset |
| Groh et al. (2020) | 8 | similar to character 5 in this dataset |
| Groh et al. (2020) | 9 | not applicable to this dataset |
| Groh et al. (2020) | 10 | similar to character 141 in this dataset |
| Groh et al. (2020) | 11 | not applicable to this dataset |
| Groh et al. (2020) | 14 | continuous character not measured |
| Groh et al. (2020) | 15 | not applicable to this dataset |
| Groh et al. (2020) | 17 | similar to character 53 in this dataset |
| Groh et al. (2020) | 18 | similar to character 58 in this dataset |
| Groh et al. (2020) | 19 | not applicable to this dataset |
| Groh et al. (2020) | 20 | not applicable to this dataset |
| Groh et al. (2020) | 21 | similar to character 6 in this dataset |
| Groh et al. (2020) | 22 | similar to character 61 in this dataset |
| Groh et al. (2020) | 23 | similar to character 62 in this dataset |
| Groh et al. (2020) | 24 | similar to character 6 in this dataset |
| Groh et al. (2020) | 25 | similar to character 6 in this dataset |
| Groh et al. (2020) | 29 | not applicable to this dataset |
| Groh et al. (2020) | 32 | similar to character 6 in this dataset |
| Groh et al. (2020) | 36 | similar to character 183 in this dataset |

| Study | Character | Reason for rejection |
|---|---|---|
| Groh et al. (2020) | 37 | similar to character 1 in this dataset |
| Groh et al. (2020) | 40 | similar to character 10 in this dataset |
| Groh et al. (2020) | 43 | similar to character 2 in this dataset |
| Groh et al. (2020) | 44 | similar to character 8 in this dataset |
| Groh et al. (2020) | 45 | similar to character 8 in this dataset |
| Groh et al. (2020) | 48 | similar to character 14 in this dataset |
| Groh et al. (2020) | 49 | not applicable to this dataset |
| Groh et al. (2020) | 50 | not applicable to this dataset |
| Groh et al. (2020) | 51 | not applicable to this dataset |
| Groh et al. (2020) | 53 | similar to character 218 in this dataset |
| Groh et al. (2020) | 54 | similar to character 220 in this dataset |
| Groh et al. (2020) | 57 | similar to character 262 in this dataset |
| Groh et al. (2020) | 58 | not applicable to this dataset |
| Groh et al. (2020) | 59 | similar to character 266 in this dataset |
| Groh et al. (2020) | 60 | similar to character 277 in this dataset |
| Groh et al. (2020) | 62 | similar to character 275 in this dataset |
| Groh et al. (2020) | 63 | not applicable to this dataset |
| Groh et al. (2020) | 64 | similar to character 280 in this dataset |
| Groh et al. (2020) | 65 | not applicable to this dataset |
| Groh et al. (2020) | 66 | not applicable to this dataset |
| Groh et al. (2020) | 67 | similar to character 301 in this dataset |
| Groh et al. (2020) | 70 | not applicable to this dataset |
| Groh et al. (2020) | 71 | continuous character not measured |
| Groh et al. (2020) | 72 | continuous character not measured |
| Groh et al. (2020) | 73 | continuous character not measured |
| Groh et al. (2020) | 74 | continuous character not measured |
| Groh et al. (2020) | 75 | continuous character not measured |
| Groh et al. (2020) | 76 | considered impractical to measure |
| Groh et al. (2020) | 77 | not applicable to this dataset |
| Groh et al. (2020) | 78 | considered impractical to measure |
| Groh et al. (2020) | 79 | continuous character not measured |
| Groh et al. (2020) | 81 | continuous character not measured |
| Groh et al. (2020) | 107 | invalid character considered artefact of preservation |

| Study | Character | Reason for rejection |
|---|---|---|
| Groh et al. (2020) | 116 | not applicable to this dataset |
| Groh et al. (2020) | 123 | considerable ontogenetic and intraspecific variation in character |
| Groh et al. (2020) | 130 | not applicable to this dataset |
| Groh et al. (2020) | 138 | similar to character 159 in this dataset |
| Groh et al. (2020) | 143 | similar to character 179 in this dataset |
| Groh et al. (2020) | 158 | similar to character 60 in this dataset |
| Groh et al. (2020) | 163 | anatomically invalid character |
| Groh et al. (2020) | 261 | anatomically invalid character |
| Groh et al. (2020) | 291 | not applicable to this dataset |
| Groh et al. (2020) | 295 | not applicable to this dataset |
| Groh et al. (2020) | 362 | not applicable to this dataset |
| Groh et al. (2020) | 381 | ontogenetically variable |
| Groh et al. (2020) | 384 | all taxa scored the same in this dataset |
| Groh et al. (2020) | 414 | character 155 in this dataset |
| Groh et al. (2020) | 423 | not applicable to this dataset |
| Iijima and Kobayashi (2019) | 245 | no variation in taxa |
| Salas-Gismondi et al. (2019) | 207 | similar to character 14 in this dataset |
| Salas-Gismondi et al. (2019) | 208 | similar to character 11 in this dataset |
| Salas-Gismondi et al. (2019) | 209 | similar to character 9 in this dataset |
| Lee and Yates (2018) | 1 | anatomically invalid character |
| Lee and Yates (2018) | 6 | no variation in taxa |
| Lee and Yates (2018) | 13 | redundant with character 143 in this dataset |
| Lee and Yates (2018) | 15 | scores do not match observations |
| Lee and Yates (2018) | 17 | scores do not match observations |
| Lee and Yates (2018) | 32 | no variation in taxa |
| Lee and Yates (2018) | 35 | anatomically invalid character |
| Lee and Yates (2018) | 47 | anatomically invalid character |
| Lee and Yates (2018) | 54 | no variation in taxa |
| Lee and Yates (2018) | 62 | no variation in taxa |
| Lee and Yates (2018) | 73 | redundant with character 84 in this dataset |
| Lee and Yates (2018) | 82 | varies intraspecifically |

| Study | Character | Reason for rejection |
|---|---|---|
| Lee and Yates (2018) | 83 | similar to character 84 in this dataset |
| Lee and Yates (2018) | 84 | no variation in taxa |
| Lee and Yates (2018) | 85 | no variation in taxa |
| Lee and Yates (2018) | 86 | no variation in taxa |
| Lee and Yates (2018) | 89 | no variation in taxa |
| Lee and Yates (2018) | 93 | no variation in taxa |
| Lee and Yates (2018) | 94 | redundant with character 8 in this dataset |
| Lee and Yates (2018) | 102 | no variation in taxa |
| Lee and Yates (2018) | 113 | variable within species ontogenetically |
| Lee and Yates (2018) | 114 | variable within species ontogenetically |
| Lee and Yates (2018) | 116 | no variation in taxa |
| Lee and Yates (2018) | 141 | varies intraspecifically |
| Lee and Yates (2018) | 148 | similar to character 171 in this dataset |
| Lee and Yates (2018) | 149 | similar to character 172 in this dataset |
| Lee and Yates (2018) | 153 | no variation in taxa |
| Lee and Yates (2018) | 170 | autapomorphy of *Crocodylus johnstoni* in this dataset |
| Lee and Yates (2018) | 172 | no variation in taxa |
| Lee and Yates (2018) | 177 | no variation in taxa |
| Lee and Yates (2018) | 178 | similar to character 151 in this dataset |
| Lee and Yates (2018) | 179 | no variation in taxa |
| Lee and Yates (2018) | 181 | no variation in taxa |
| Lee and Yates (2018) | 183 | varies intraspecifically |
| Lee and Yates (2018) | 189 | no variation in taxa |
| Lee and Yates (2018) | 193 | no variation in taxa |
| Lee and Yates (2018) | 200 | no variation in taxa |
| Lee and Yates (2018) | 218 | no variation in taxa |
| Lee and Yates (2018) | 219 | not practical to score |
| Lee and Yates (2018) | 237 | no variation in taxa |
| Lee and Yates (2018) | 262 | character 321 in this dataset |
| Lee and Yates (2018) | 277 | character 317 in this dataset |
| Cidade et al. (2017) | 187 | no variation in taxa |
| Jouve (2016) | 140 | similar to character 9 in this dataset |
| Jouve (2016) | 211 | no variation in taxa |

| Study | Character | Reason for rejection |
|---|---|---|
| Jouve (2016) | 241 | similar to character 126 in this dataset |
| Salas-Gismondi et al. (2016) | 202 | no variation in taxa |
| Salas-Gismondi et al. (2016) | 206 | similar to character 72 in this dataset |
| Jouve et al. (2015) | 203 | similar to character 147 in this dataset |
| Jouve et al. (2015) | 205 | similar to character 46 in this dataset |
| Jouve et al. (2015) | 226 | varies intraspecifically |
| Jouve et al. (2015) | 227 | similar to character 147 in this dataset |
| Jouve et al. (2015) | 238 | similar to character 13 in this dataset |
| Salas-Gismondi et al. (2015) | 199 | no variation in taxa |
| Brochu and Storrs (2012) | 189 | no variation in taxa |
| Brochu and Storrs (2012) | 182 | all taxa scored as "?" |
| Brochu (2011) | 106 | similar to character 147 here |
| Brochu (2011) | 20 | no variation in taxa |
| Brochu (2011) | 179 | no variation in taxa |
| Buscalioni et al. (2011) | 181 | no variation in taxa |
| Buscalioni et al. (2011) | 182 | no variation in taxa |
| Buscalioni et al. (2011) | 183 | similar to character 13 in this dataset |
| Jouve et al. (2008) | 170 | similar to character 2 in this dataset |
| Jouve et al. (2008) | 185 | no variation in taxa |
| Jouve et al. (2008) | 187 | similar to character 16 in this dataset |
| Jouve et al. (2008) | 192 | similar to character 50 in this dataset |
| Jouve et al. (2008) | 193 | similar to character 50 in this dataset |
| Jouve et al. (2008) | 194 | considered impractical to score |
| Ősi et al. (2007) | 166 | autapomorphy of *Iharkutosuchus* makadii |
| Ősi et al. (2007) | 167 | no variation in taxa |
| Ősi et al. (2007) | 169 | no variation in taxa |
| Salisbury et al. (2006) | 169 | no variation in taxa |
| Salisbury et al. (2006) | 172 | similar to characters 188 and 189 here |
| Salisbury et al. (2006) | 173 | autapomorphy of *Isisfordia duncani* in this dataset |
| Ortega et al. (2000) | 115 | no variation in taxa |
| Ortega et al. (2000) | 161 | no variation in taxa |
| Brochu (1999) | 1 | no variation in taxa |

| Study | Character | Reason for rejection |
|---|---|---|
| Brochu (1999) | 2 | no variation in taxa |
| Brochu (1999) | 56 | anatomically invalid character (see character list) |
| Brochu (1999) | 60 | no variation in taxa |
| Brochu (1999) | 125 | uninformative as state 1 is autapomorphy of *Melanosuchus niger* |
| Brochu (1999) | 160 | uninformative state 1 is autapomorphy of *Gavialis gangeticus* |
| Brochu (1999) | 161 | similar to character 3 here |
| Brochu (1999) | 163 | no variation in taxa |
| Brochu (1999) | 164 | no variation in taxa |
| Norell and Clark (1990) | 2 | no variation in taxa |
| Norell and Clark (1990) | 3 | no variation in taxa |

# Appendix D

# Measurements for Continuous Characters 1–26

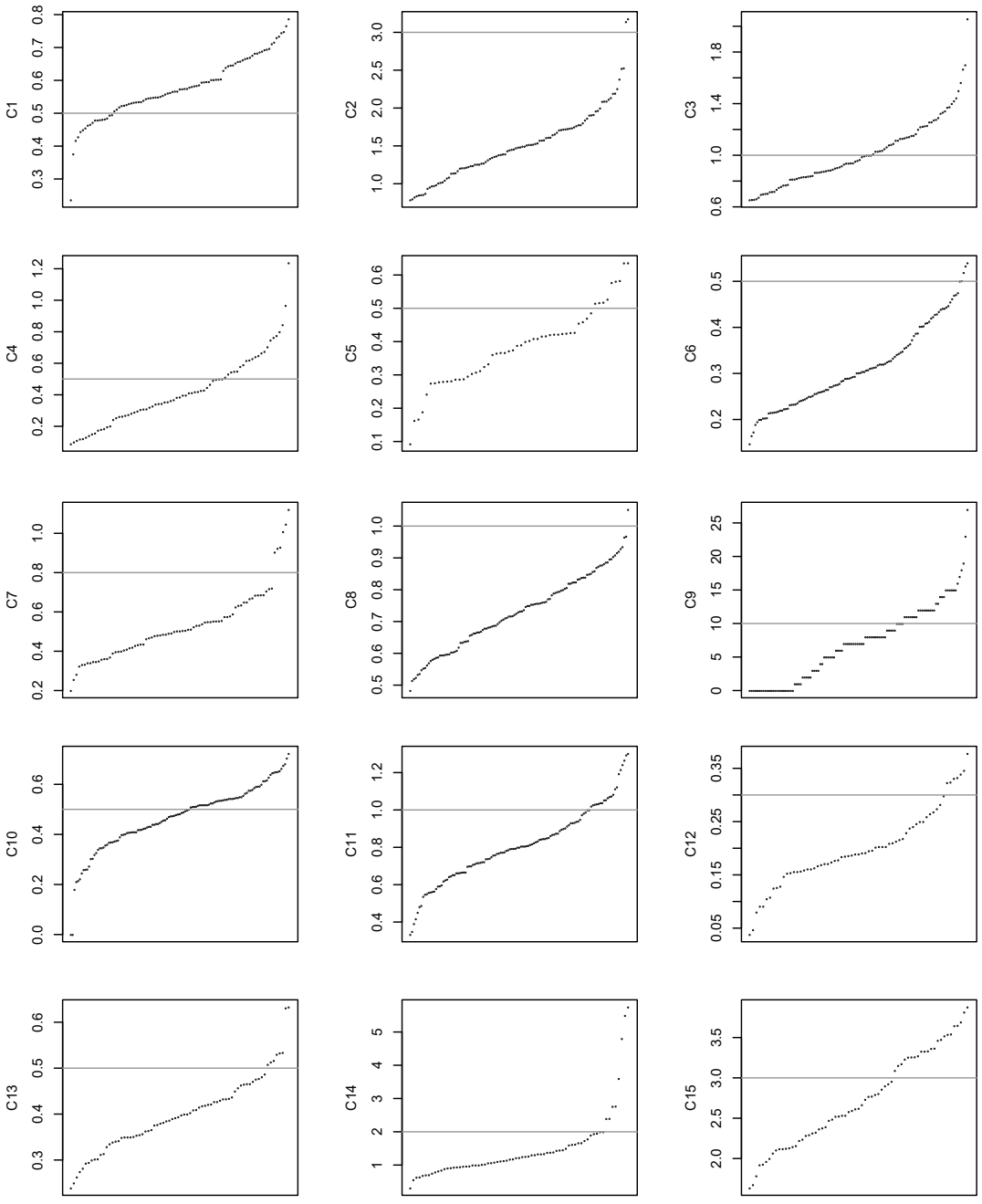



Figure D.1: Measured values for continuous characters 1–15. Points represent the ratios of measured values for taxa in this analysis ordered from smallest to largest. Horizontal grey lines indicate the threshold value delimiting character states. See Section 3.2.1.

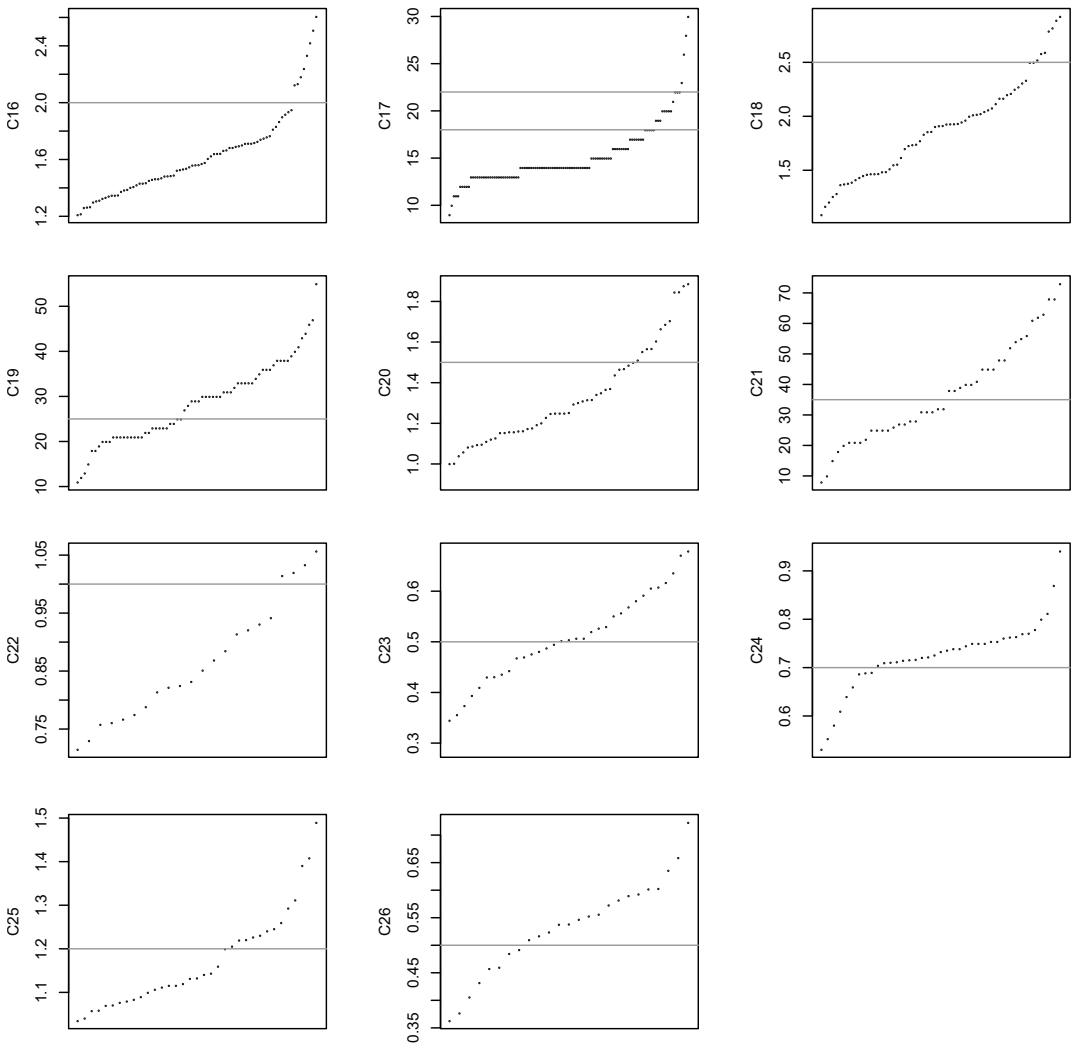



Figure D.2: Measured values for for continuous characters 16–26. Points represent the ratios of measured values for taxa in this analysis ordered from smallest to largest. Horizontal grey lines indicate the threshold value delimiting character states. See Section 3.2.2.

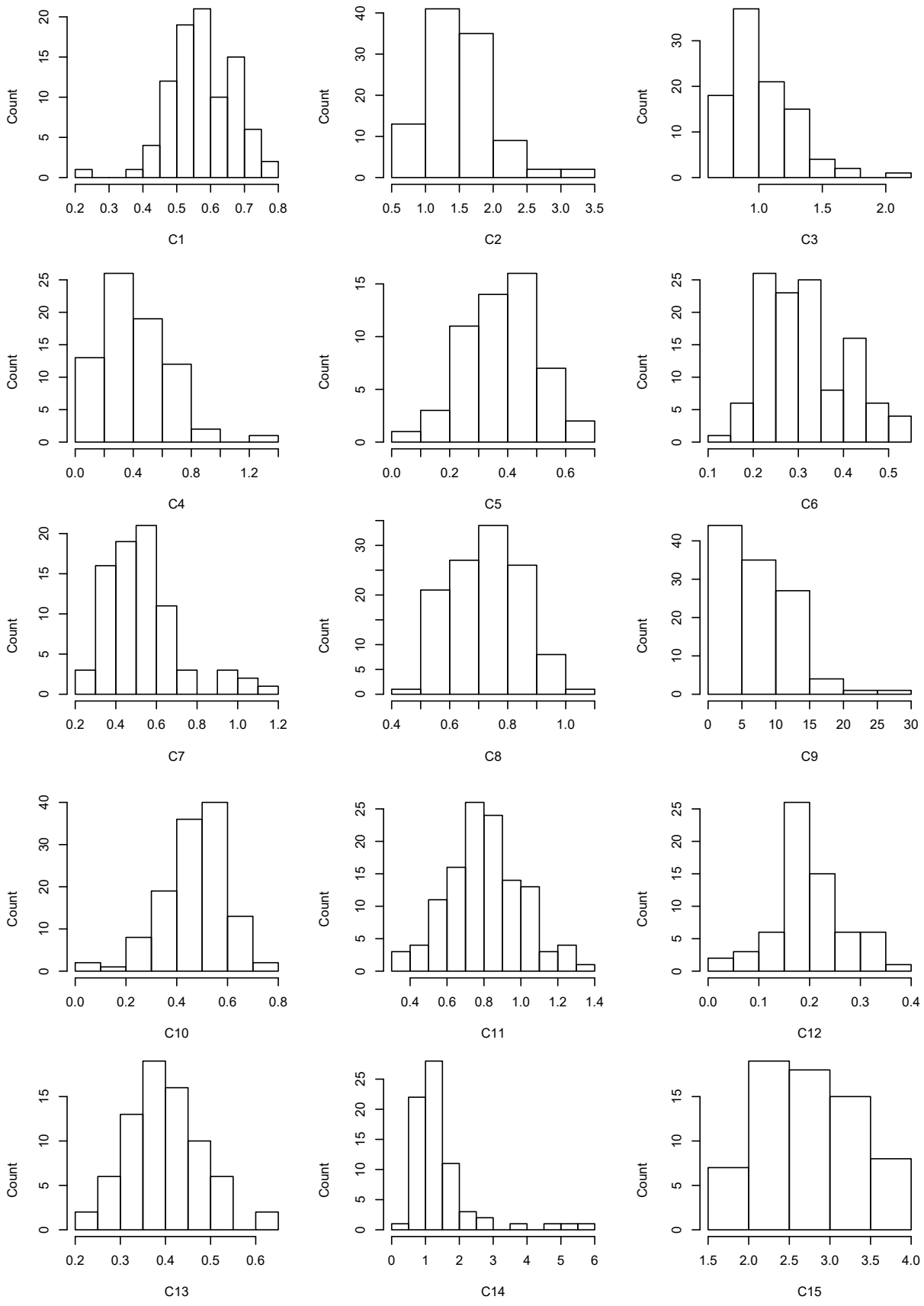



Figure D.3: Histograms of measurements for characters 1–15.

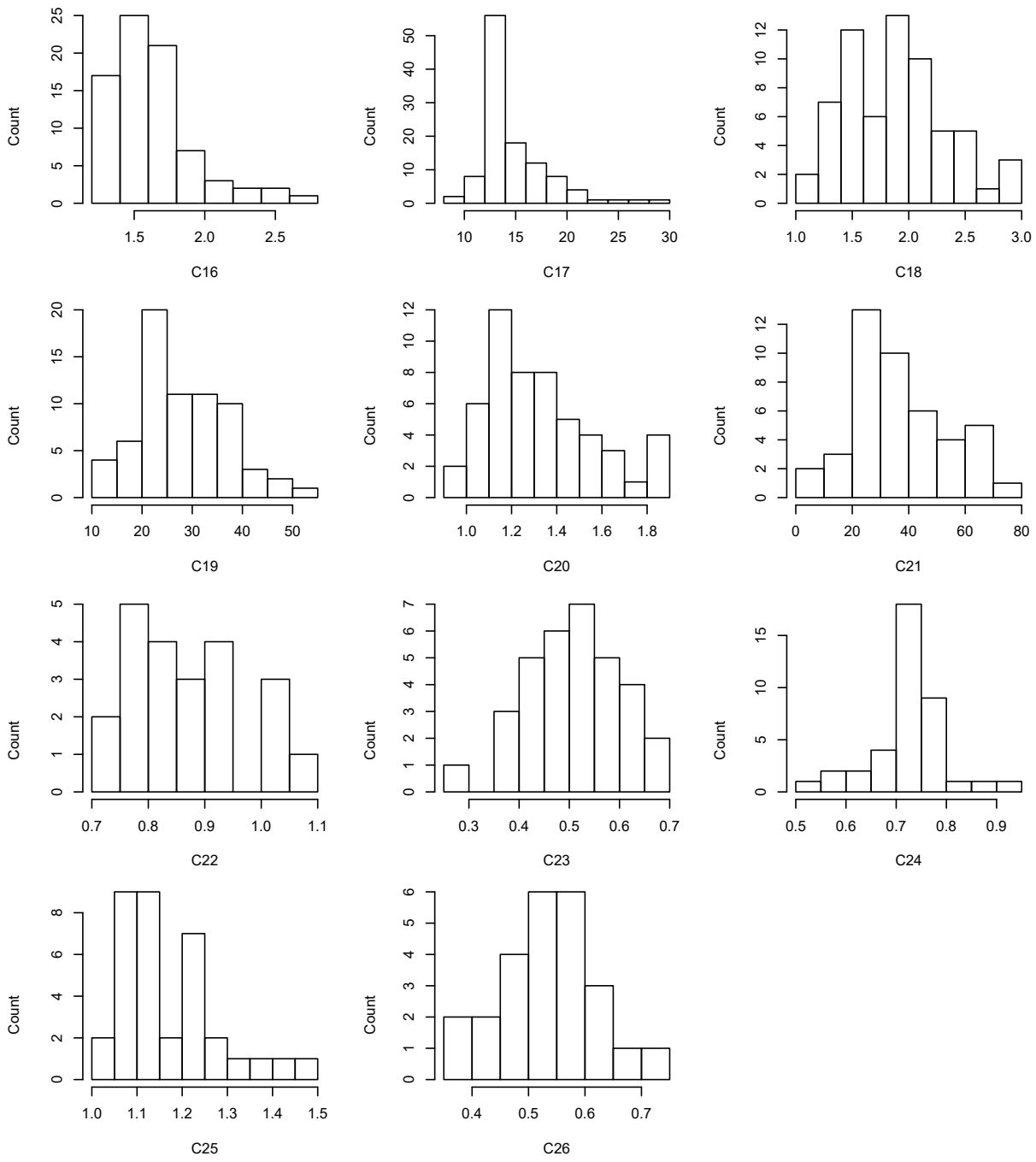



Figure D.4: Histograms of measurements for characters 16–26.

Table D.1: Results of the Shapiro-Wilk test.

| Character | W | *p* | Distribution |
|---|---|---|---|
| 1 | 0.97851 | 0.1373 | Normal |
| 2 | 0.94153 | 0.0003472 | – |
| 3 | 0.93183 | 0.00007489 | – |
| 4 | 0.94629 | 0.003671 | – |
| 5 | 0.98004 | 0.5019 | Normal |
| 6 | 0.95728 | 0.001036 | – |
| 7 | 0.91432 | 0.00005745 | – |
| 8 | 0.98562 | 0.2585 | Normal |
| 9 | 0.93213 | 0.00002467 | – |
| 10 | 0.95724 | 0.0007199 | – |
| 11 | 0.99108 | 0.64 | Normal |
| 12 | 0.97204 | 0.1479 | Normal |
| 13 | 0.97869 | 0.2449 | Normal |
| 14 | 0.68975 | 5.807E-11 | – |
| 15 | 0.96427 | 0.05131 | Normal |
| 16 | 0.89628 | 0.00001073 | – |
| 17 | 0.83056 | 5.271E-10 | – |
| 18 | 0.96658 | 0.08019 | Normal |
| 19 | 0.97372 | 0.1604 | Normal |
| 20 | 0.93286 | 0.005251 | – |
| 21 | 0.95903 | 0.1197 | Normal |
| 22 | 0.94229 | 0.2206 | Normal |
| 23 | 0.98978 | 0.9857 | Normal |
| 24 | 0.91901 | 0.008111 | – |
| 25 | 0.89722 | 0.003332 | – |
| 26 | 0.9851 | 0.9643 | Normal |

# Appendix E

# Taxon Stratigraphic Ranges

Table E.1: First and last appearance dates used in measures of stratigraphic congruence.

| Taxon | FAD | LAD |
|---|---|---|
| *Acresuchus pachytemporalis* | 11.62 | 5.333 |
| *Acynodon iberoccitanus* | 77.9 | 66 |
| *Agaresuchus fontisensis* | 77.9 | 69 |
| *Aktiogavialis caribesi* | 11.6 | 7.2 |
| *Alligator mcgrewi* | 20.43 | 15.97 |
| *Alligator mefferdi* | 13.8 | 10.3 |
| *Alligator mississippiensis* | 10.3 | 0 |
| *Alligator olseni* | 20.4 | 16 |
| *Alligator prenasalis* | 37.2 | 33.9 |
| *Alligator sinensis* | 3.6 | 0 |
| *Allodaposuchus precedens* | 77.9 | 66 |
| *Allognathosuchus polyodon* | 50.3 | 47.8 |
| *Allognathosuchus wartheni* | 56 | 50.3 |
| *Arambourgia gaudryi* | 37.8 | 33.9 |
| *Argochampsa krebsi* | 66 | 56 |
| *Asiatosuchus depressifrons* | 56 | 47.8 |
| *Asiatosuchus germanicus* | 47.8 | 41.2 |
| *Asiatosuchus nanlingensis* | 61.6 | 59.2 |
| *Australosuchus clarkae* | 28.1 | 16 |
| *Baru darrowi* | 16 | 11.6 |

| Taxon | FAD | LAD |
|---|---|---|
| *Baru huberi* | 28.1 | 23 |
| *Baru wickeni* | 28.1 | 23 |
| *Bernissartia fagesii* | 129.4 | 125 |
| *Borealosuchus acutidentatus* | 66 | 63.3 |
| *Borealosuchus formidabilis* | 61.6 | 59.2 |
| *Borealosuchus sternbergii* | 70.6 | 63.3 |
| *Borealosuchus threensis* | 70.6 | 61.7 |
| *Borealosuchus wilsoni* | 56 | 47.8 |
| *Bottosaurus harlani* | 70.6 | 66 |
| *Boverisuchus magnifrons* | 47.8 | 41.2 |
| *Boverisuchus vorax* | 50.3 | 47.8 |
| *Brachychampsa montana* | 72.1 | 66 |
| *Brochuchus pigotti* | 20.4 | 16 |
| *Caiman brevirostris* | 11.6 | 5.3 |
| *Caiman crocodilus* | 2.58 | 0 |
| *Caiman gasparinae* | 11.6 | 7.2 |
| *Caiman latirostris* | 9 | 0 |
| *Caiman lutescens* | 11.6 | 7.2 |
| *Caiman wannlangstoni* | 16 | 5.3 |
| *Caiman yacare* | 11.6 | 0 |
| *Ceratosuchus burdoschi* | 56.8 | 56 |
| *Crocodylus acutus* | 2.6 | 0.1 |
| ’*Crocodylus*’ *affinis* | 50.3 | 47.8 |
| *Crocodylus anthropophagus* | 1.8 | 0.01 |
| *Crocodylus intermedius* | 0.1 | 0 |
| *Crocodylus johnstoni* | 2.6 | 0 |
| ’*Crocodylus*’ *megarhinus* | 33.9 | 28.1 |
| *Crocodylus mindorensis* | 0.1 | 0 |
| *Crocodylus moreletii* | 0.1 | 0 |
| *Crocodylus niloticus* | 11.6 | 0 |
| *Crocodylus novaeguineae* | 0.1 | 0 |
| *Crocodylus palaeindicus* | 11.6 | 2.6 |
| *Crocodylus palustris* | 0.1 | 0.01 |
| *Crocodylus porosus* | 5.3 | 0 |

| Taxon | FAD | LAD |
|---|---|---|
| *Crocodylus rhombifer* | 2.6 | 0 |
| *Crocodylus siamensis* | 2.6 | 0.8 |
| *Crocodylus thorbjarnarsoni* | 5.3 | 1.8 |
| *Caiman* cf. *lutescens*, ('La Venta *Caiman*') | 11.6 | 7.2 |
| *Dadagavialis gunai* | 23.03 | 15.97 |
| *Diplocynodon darwini* | 47.8 | 41.2 |
| *Diplocynodon deponiae* | 47.8 | 41.2 |
| *Diplocynodon hantoniensis* | 37.8 | 33.9 |
| *Diplocynodon muelleri* | 33.9 | 28.1 |
| *Diplocynodon ratelii* | 23 | 13.8 |
| *Diplocynodon remensis* | 59.2 | 56 |
| *Diplocynodon tormis* | 41.2 | 37.8 |
| *Dollosuchoides densmorei* | 47.8 | 41.2 |
| *Eocaiman cavernensis* | 47.8 | 37.8 |
| *Eocaiman palaeocenicus* | 66 | 61.6 |
| *Eogavialis africanum* | 38 | 28.4 |
| *Eosuchus lerichei* | 58.7 | 55.8 |
| *Eosuchus minor* | 59.2 | 47.8 |
| *Eothoracosaurus mississippiensis* | 72.6 | 66 |
| *Euthecodon arambourgi* | 23 | 16 |
| *Gavialis browni* | 11.6 | 5.3 |
| *Gavialis gangeticus* | 2.6 | 0 |
| *Gavialis lewisi* | 5.3 | 2.6 |
| *Gavialosuchus eggenburgensis* | 20.4 | 16 |
| Glen Rose form | 125 | 100.5 |
| *Globidentosuchus brachyrostris* | 11.6 | 5.3 |
| *Gnatusuchus pebasensis* | 16 | 11.6 |
| *Gryposuchus colombianus* | 16 | 11.6 |
| *Gryposuchus croizati* | 11.6 | 5.3 |
| *Gryposuchus neogaeus* | 11.6 | 7.2 |
| *Gryposuchus pachakamue* | 16 | 11.6 |
| *Hassiacosuchus haupti* | 47.8 | 41.2 |
| *Hylaeochampsa vectiana* | 127.2 | 125 |
| *Iharkutosuchus makadii* | 86.3 | 83.6 |

| Taxon | FAD | LAD |
|---|---|---|
| *Ikanogavialis gameroi* | 11.6 | 6.8 |
| *Isisfordia duncani* | 106.8 | 97.2 |
| *Jiangxisuchus nankangensis* | 70.6 | 66 |
| *Kambara implexidens* | 56 | 47.8 |
| *Kambara murgonensis* | 56 | 47.8 |
| *Kambara taraina* | 47.8 | 33.9 |
| *Kentisuchus spenceri* | 55.8 | 48.6 |
| *Kuttanacaiman iquitosensis* | 16 | 11.6 |
| *Leidyosuchus canadensis* | 77.9 | 72.1 |
| *Lohuecosuchus megadontos* | 77.9 | 69 |
| *Maomingosuchus petrolica* | 37.8 | 33.9 |
| *Maroccosuchus zennaroi* | 55.8 | 48.6 |
| *Mecistops cataphractus* | 11.6 | 0 |
| *Mekosuchus inexpectatus* | 0.01 | 0 |
| *Mekosuchus sanderi* | 16 | 11.6 |
| *Mekosuchus whitehunterensis* | 28.1 | 23 |
| *Melanosuchus niger* | 0.1 | 0 |
| *Mourasuchus amazonensis* | 11.6 | 7.2 |
| *Mourasuchus arendsi* | 11.6 | 5.3 |
| *Mourasuchus atopus* | 16 | 5.3 |
| *Navajosuchus mooki* | 66 | 61.6 |
| *Necrosuchus ionensis* | 61.6 | 59.2 |
| *Osteolaemus tetraspis* | 11.6 | 0 |
| *Paleosuchus palpebrosus* | 0.1 | 0 |
| *Paleosuchus trigonatus* | 0.1 | 0 |
| *Paratomistoma courti* | 41.3 | 38 |
| *Penghusuchus pani* | 11.5 | 5.3 |
| *Piscogavialis jugaliperforatus* | 11.6 | 5.3 |
| *Planocrania datangensis* | 61.6 | 59.2 |
| *Planocrania hengdongensis* | 59.2 | 56 |
| *Portugalosuchus azenhae* | 99.7 | 94.3 |
| *Procaimanoidea utahensis* | 46.2 | 41.2 |
| *Protocaiman peligrensis* | 66 | 61.6 |
| *Purussaurus barasiliensis* | 11.6 | 7.2 |

| Taxon | FAD | LAD |
|---|---|---|
| *Purussaurus mirandai* | 11.6 | 5.3 |
| *Purussaurus neivensis* | 16 | 5.3 |
| *Quinkana* | 28.1 | 0.01 |
| *Shamosuchus djadochtaensis* | 83.6 | 72.1 |
| *Siquisiquesuchus venezuelensis* | 20.4 | 16 |
| *Stangerochampsa mccabei* | 70.6 | 66 |
| *Thecachampsa antiquus* | 13.8 | 5.3 |
| *Thecachampsa sericodon* | 15.97 | 11.6 |
| *Theriosuchus pusillus* | 145.5 | 140.2 |
| *Thoracosaurus isorhynchus* | 70.6 | 61.6 |
| *Thoracosaurus neocesariensis* | 70.6 | 61.7 |
| *Tomistoma cairense* | 47.8 | 41.2 |
| *Tomistoma dowsoni* | 23 | 16 |
| *Tomistoma lusitanica* | 20.4 | 7.2 |
| *Tomistoma schlegelii* | 0.1 | 0 |
| *Toyotamaphimeia machikanensis* | 0.8 | 0.1 |
| *Trilophosuchus rackhami* | 16 | 11.6 |
| *Tsoabichi greenriverensis* | 56 | 47.8 |
| *Ultrastenos willisi* | 28.1 | 23 |
| *Voay robustus* | 0.1 | 0.01 |
| *Wannaganosuchus brachymanus* | 61.6 | 56 |
| *Wannchampsus kirpachi* | 119 | 113 |

# Appendix F

# Constrained Analyses

Table F.1: Summary of constrained analyses.

| Constraint | MPTs | Tree length | Tree length increase | Templeton test |
|---|---|---|---|---|
| (1) *Diplocynodon* monophyletic | 3 | 8282.499 | 100.643 | insignificant |
| (2) *Eocaiman* forced into Caimaninae | 3 | 8190.625 | 8.769 | insignificant |
| (3) *Eocaiman* forced into clade of South American caimanines | 3 | 8254.124 | 72.269 | insignificant |
| (4) Extant Jacareans (sensu Norell, 1988) monophyletic, with the following floating taxa: *Caiman wannlangstoni*, *Caiman brevirostris*, UCMP 39978, *Acresuchus pachytemporalis*, *Purussaurus*, and *Necrosuchus* | 3 | 8182.617 | 0.761 | insignificant |
| (5) Force *Portugalosuchus* out of Crocodylia, 'thoracosaurs' float | 9 | 8829.43595 | 47.58 | insignificant |
| (6) Force "Brevirostres", i.e. Alligatoroidea + "Crocodyloidea" | 3 | 8187.359 | 5.503 | significant |
| (7) 'Thoracosaurs' forced out of Crocodylia. *Portugalosuchus*, planocraniids, and *Borealosuchus* float | 3 | 8373.965 | 192.110 | significant |
| (8) 'Thoracosaurs' forced out of Gavialidae (*Gavialis*+*Tomistoma*), all non-thoracosaurine gavialoids float | 3 | 8184.082 | 2.226 | insignificant |
| (9) 'Thoracosaurs' forced out of Crocodylia (*Argochampsa*, *Eogavialis*, *Portugalosuchus*, planocraniids, *Borealosuchus* float) | 9 | 8286.94 | 105.085 | significant |
| (10) *Asiatosuchus germanicus*, *Asiatosuchus depressifrons*, and '*Crocodylus*' *affinis* forced out of Longirostres, *Jiangxisuchus* floats | 3 | 8188.548 | 6.692 | insignificant |
| (11) Monophyletic mekosuchinae forced outside of Longirostres, *Quinkana*, *Australosuchus* and *Asiatosuchus nanlingensis* float in Mekosuchinae and Crocodyloidea | 3 | 8198.052 | 16.196 | insignificant |
| (12) Force *Asiatosuchus nanlingensis* forced out of Mekosuchinae. *Australosuchus* and *Quinkana* float | 3 | 8202.683 | 20.827 | insignificant |
| (13) *Quinkana* and *Australosuchus* forced in Mekosuchinae, *Asiatosuchus nanlingensis* floats | 3 | 8204.086 | 22.230 | significant |
| (14) *Mecistops* forced into monophyletic Osteolaeminae | 3 | 8201.109 | 19.254 | insignificant |

1. *Diplocynodon* monophyletic.

   force + [69 70 71 72 73 74 75];

2. *Eocaiman* in Caimaninae.

   force + [12 37 40 42 43 44 45 46 47 48 49 50 77 78 88 89 100 106 108 109 110 111 113 114 121 122 123 124 127 139 142];

3. *Eocaiman* in Caimaninae (excluding clade of basal North American taxa).

   force + [12 37 42 43 44 45 46 47 48 49 77 78 88 89 100 106 108 109 110 111 113 114 121 122 123 124 139];

4. Jacarea sensu Norell (1988), putative jacareans set to float (see main text).

   force + [43 45 49 106 (42 47 48 12 122 123 124)];

5. Traditional morphological topology, i.e. (Crocodylinae + Tomistominae) + Alligatoroidea.

   force + [12 14 15 16 17 18 19 20 21 22 23 24 26 27 28 29 30 31 37 40 41 42 43 44 45 46 47 48 49 50 51 52 53 54 55 56 57 58 59 60 61 62 63 64 65 66 67 69 70 71 72 73 74 75 76 77 78 83 87 88 89 95 96 97 98 99 100 101 102 103 104 105 106 107 108 109 110 111 112 113 114 115 116 120 121 122 123 124 125 127 128 129 132 133 134 135 136 137 138 139 140 141 142];

6. *Portugalosuchus* excluded from Crocodylia.

   force + [12 13 14 15 16 17 18 19 20 21 22 23 24 26 27 28 29 30 31 37 40 41 42 43 44 45 46 47 48 49 50 51 52 53 54 55 56 57 58 59 60 61 62 63 64 65 66 67 68 69 70 71 72 73 74 75 76 77 78 83 84 85 86 87 88 89 90 91 92 93 94 95 96 97 98 99 100 101 102 103 104 105 106 107 108 109 110 111 112 113 114 115 116 117 120 121 122 123 124 125 126 127 128 129 132 133 134 135 136 137 138 139 140 141 142 (32 33 34 35 36 38 39 118 119 25 79 80 81 82 130 131)];

7. 'Thoracosaurs' forced out of Crocodylia, *Portugalosuchus*, Planocraniidae, *Borealosuchus* float.

   force + [12 13 14 15 16 17 18 19 20 21 22 23 24 26 27 28 29 30 31 37 40 41 42 43 44 45 46 47 48 49 50 51 52 53 54 55 56 57 58 59 60 61 62 63 64 65 66 67 68 69 70 71 72 73 74 75 76 77 78 83 84 85 86 87 88 89 90 91 92 93 94 95 96 97 98 99 100 101 102 103 104 105 106 107 108 109 110 111 112 113 114 115 116 117 120 121 122 123 124 125 126 127 128 129 132 133 134 135 136 137 138 139 140 141 142 (9 32 33 34 35 36 38 39 118 119)];

8. 'Thoracosaurs' forced out of Gavialidae, all non-thoracosaurine gavialoids float.

   force + [85 136 (9 13 68 76 84 86 87 90 91 92 93 94 99 107 115 116 117 126 128 129 132 133 134 135 137)];

9. 'Thoracosaurs' forced out of Crocodylia, *Portugalosuchus*, *Eogavialis*, *Argochampsa*, Planocraniidae, *Borealosuchus* float.

   force + [12 13 14 15 16 17 18 19 20 21 22 23 24 26 27 28 29 30 31 37 40 41 42 43 44 45 46 47 48 49 50 51 52 53 54 55 56 57 58 59 60 61 62 63 64 65 66 67 68 69 70 71 72 73 74 75 76 77 78 83 84 85 86 87 88 89 90 91 92 93 94 95 96 97 98 99 100 101 102 103 104 105 106 107 108 109 110 111 112 113 114 115 116 117 120 121 122 123 124 125 126 127 128 129 132 133 134 135 136 137 138 139 140 141 142 (9 25 32 33 34 35 36 38 39 79 118 119)];

10. *Asiatosuchus germanicus*, *Asiatosuchus depressifrons*, *Crocodylus affinis* on stem of Longirostres, *Jiangxisuchus* floats.

    force + [9 13 25 26 27 28 29 30 31 41 51 52 53 54 55 56 57 58 59 60 61 62 63 64 65 66 67 68 76 79 80 81 82 83 84 85 86 87 90 91 92 93 94 95 96 97 98 99 102 103 104 105 107 112 115 116 117 125 126 128 129 130 131 132 133 134 135 136 137 138 140 141];
    force + [9 13 25 27 28 29 30 31 41 51 53 55 56 57 58 59 60 61 62 63 64 65 66 67 68 76 79 80 81 82 83 84 85 86 87 90 91 92 93 94 96 97 98 99 102 103 104 105 107 112 115 116 117 125 126 128 129 130 131 132 133 134 135 136 137 138 140 141 (95)];

11. Monophyletic Mekosuchinae to stem longirostres.

    force + [29 30 31 103 104 105 138 140 96 97 98 (27 28 125)];
    force + [9 13 25 26 27 28 29 30 31 41 51 52 53 54 55 56 57 58 59 60 61 62 63 64 65 66 67 68 76 79 80 81 82 83 84 85 86 87 90 91 92 93 94 95 96 97 98 99 102 103 104 105 107 112 115 116 117 125 126 128 129 130 131 132 133 134 135 136 137 138 140 141];
    force + [9 13 25 41 51 53 55 56 57 58 59 60 61 62 63 64 65 66 67 68 76 79 80 81 82 83 84 85 86 87 90 91 92 93 94 95 99 102 107 112 115 116 117 126 128 129 130 131 132 133 134 135 136 137 141 (26 27 28 52 54 125)]

12. *Asiatosuchus nanlingensis* excluded from Mekosuchinae, *Australosuchus* and *Quinkana* float in Mekosuchinae.

    force + [29 30 31 103 104 105 138 140 96 97 98 (28 125)];

13. *Quinkana* and *Australosuchus* in Mekosuchinae, *Asiatosuchus nanlingensis* floats.

    force + [29 30 31 103 104 105 138 140 96 97 98 28 125 (27)];

14. *Mecistops* in Osteolaeminae

    force + [41 83 102 112 141];




Figure F.1: Strict consensus of 3 MPTs when *Diplocynodon* is constrained as being monophyletic.

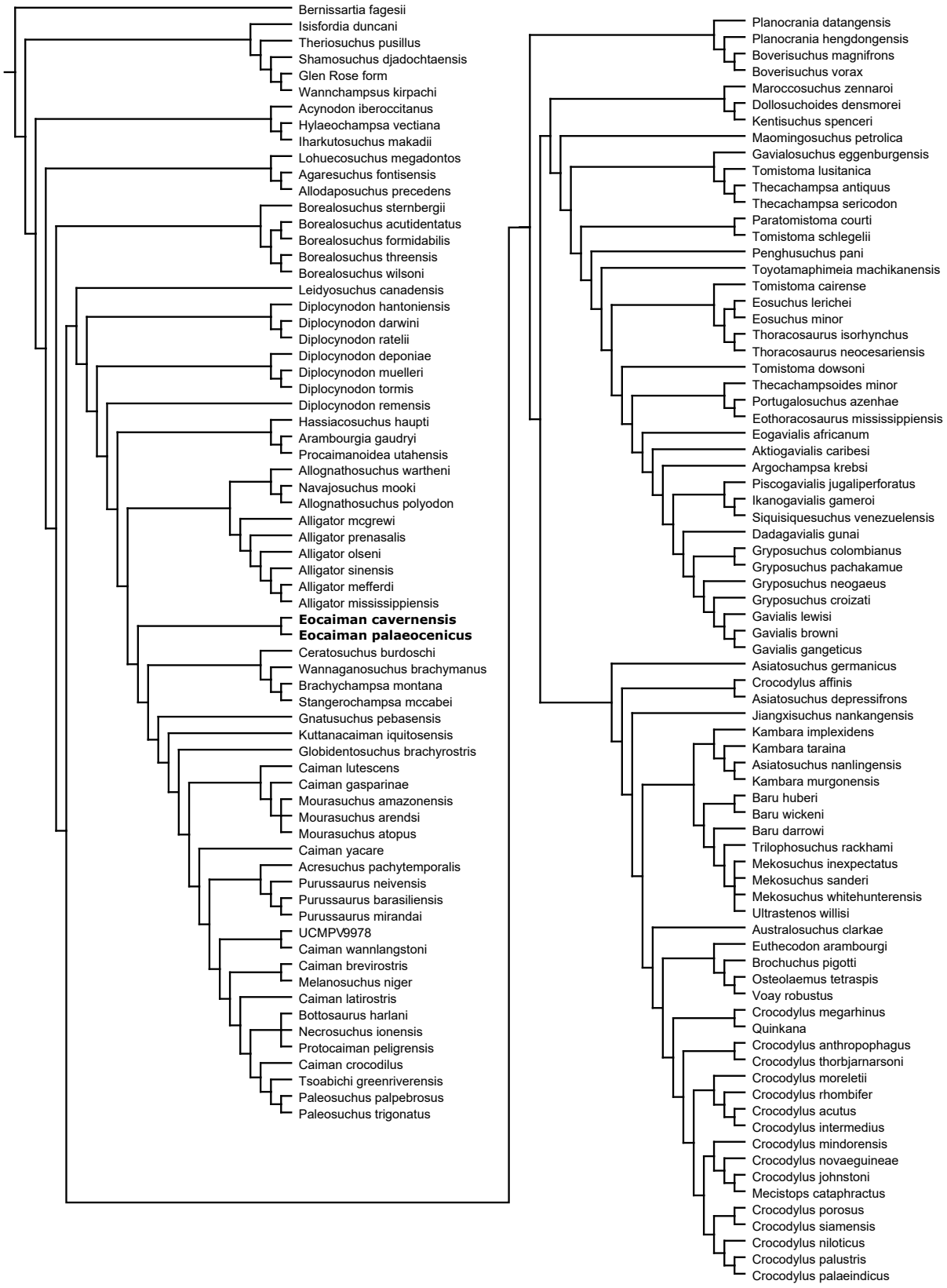



Figure F.2: Strict consensus of 3 MPTs when *Eocaiman* is constrained to be recovered within Caimaninae.

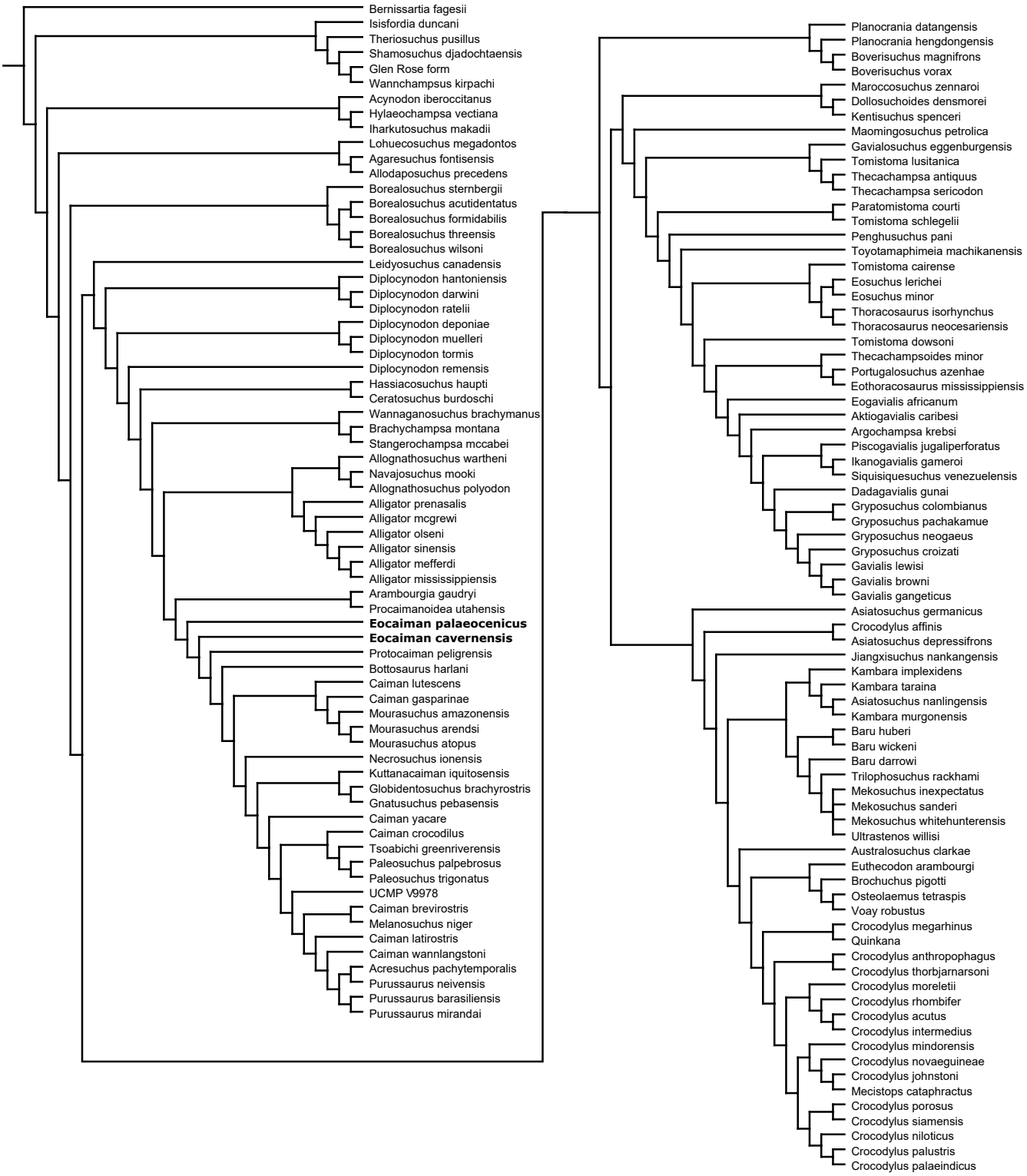



Figure F.3: Strict consensus of 3 MPTs when *Eocaiman* is constained to be recovered in Caimaninae, excluding the North American clade.

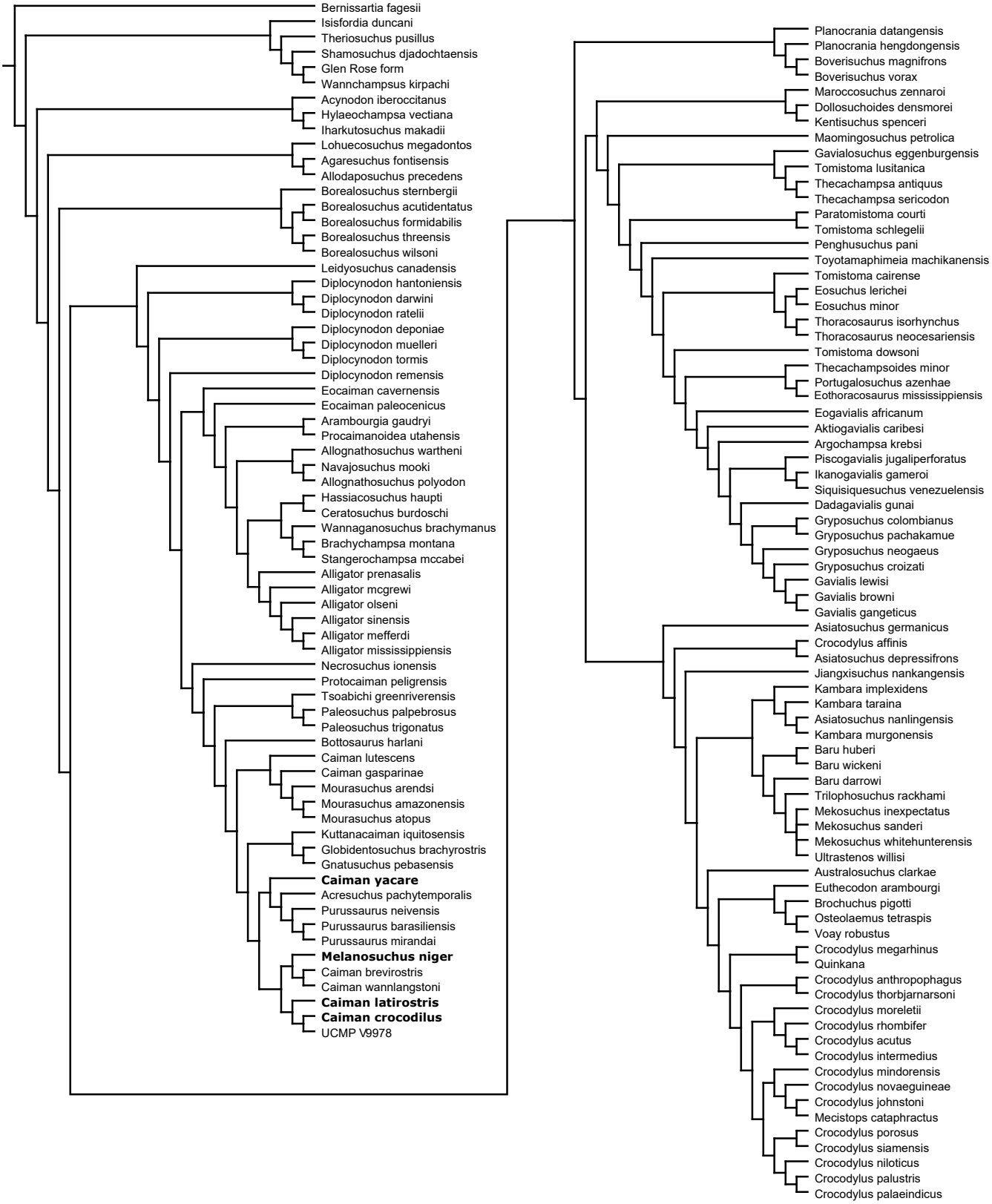



Figure F.4: Strict consensus of 3 MPTs when extant jacareans i.e. *Caiman* and *Melanosuchus* are constrained as a monophyletic group.




Figure F.5: Strict consensus of 3 MPTs when the traditional morphological topology is constrained, i.e. Alligatoroidea + "Crocodyloidea".




Figure F.6: Strict consensus of 3 MPTs when *Portugalosuchus* is excluded from Crocodylia




Figure F.7: Strict consensus of 3 MPTs when *Asiatosuchus germanicus*, *Asiatosuchus depressifrons*, and '*Crocodylus*' *affinis* are forced to be exlcuded from Longirostres

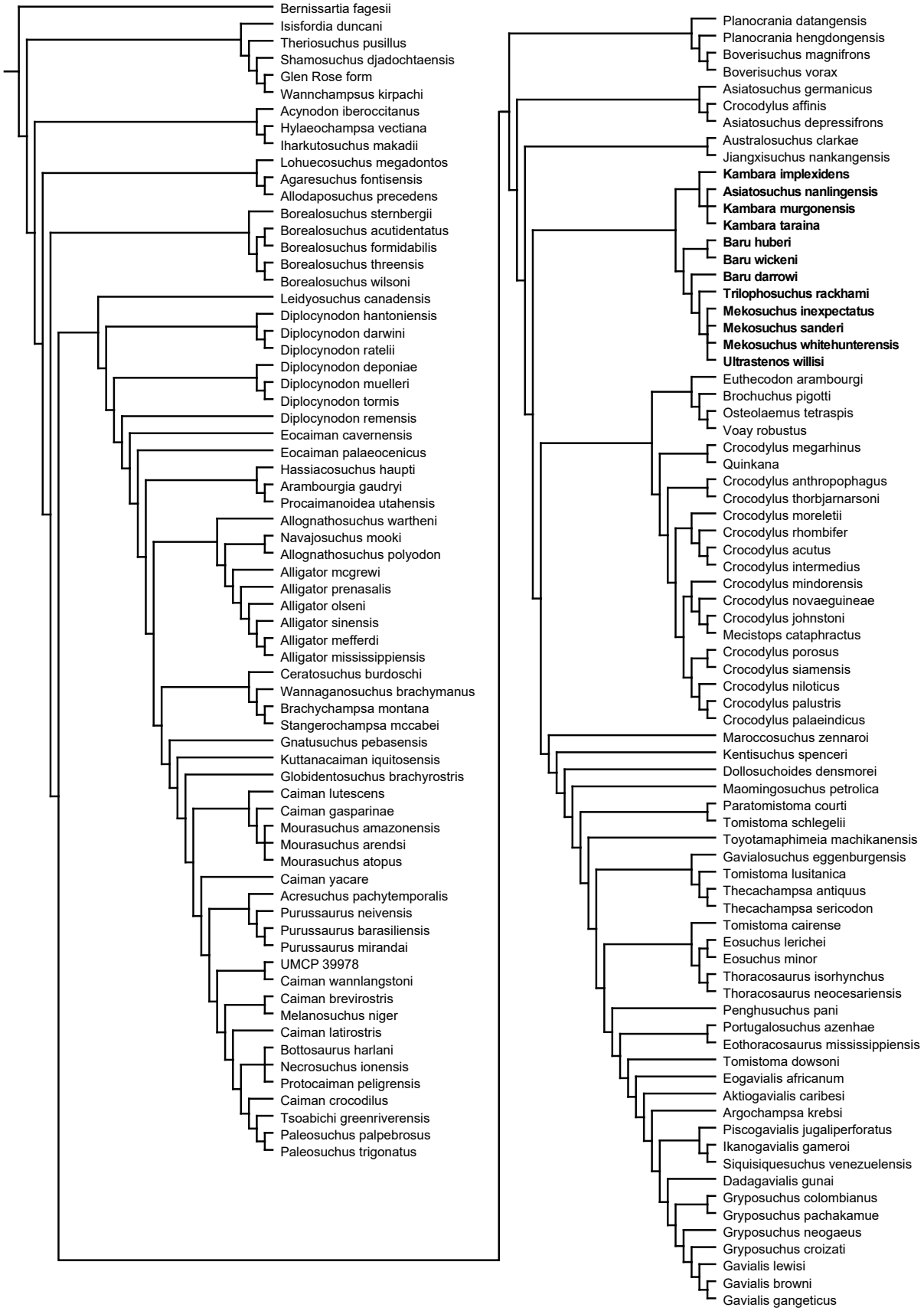



Figure F.8: Strict consensus of 3 MPTs when Mekosuchinae is forced to be recovered outside of Longirostres.

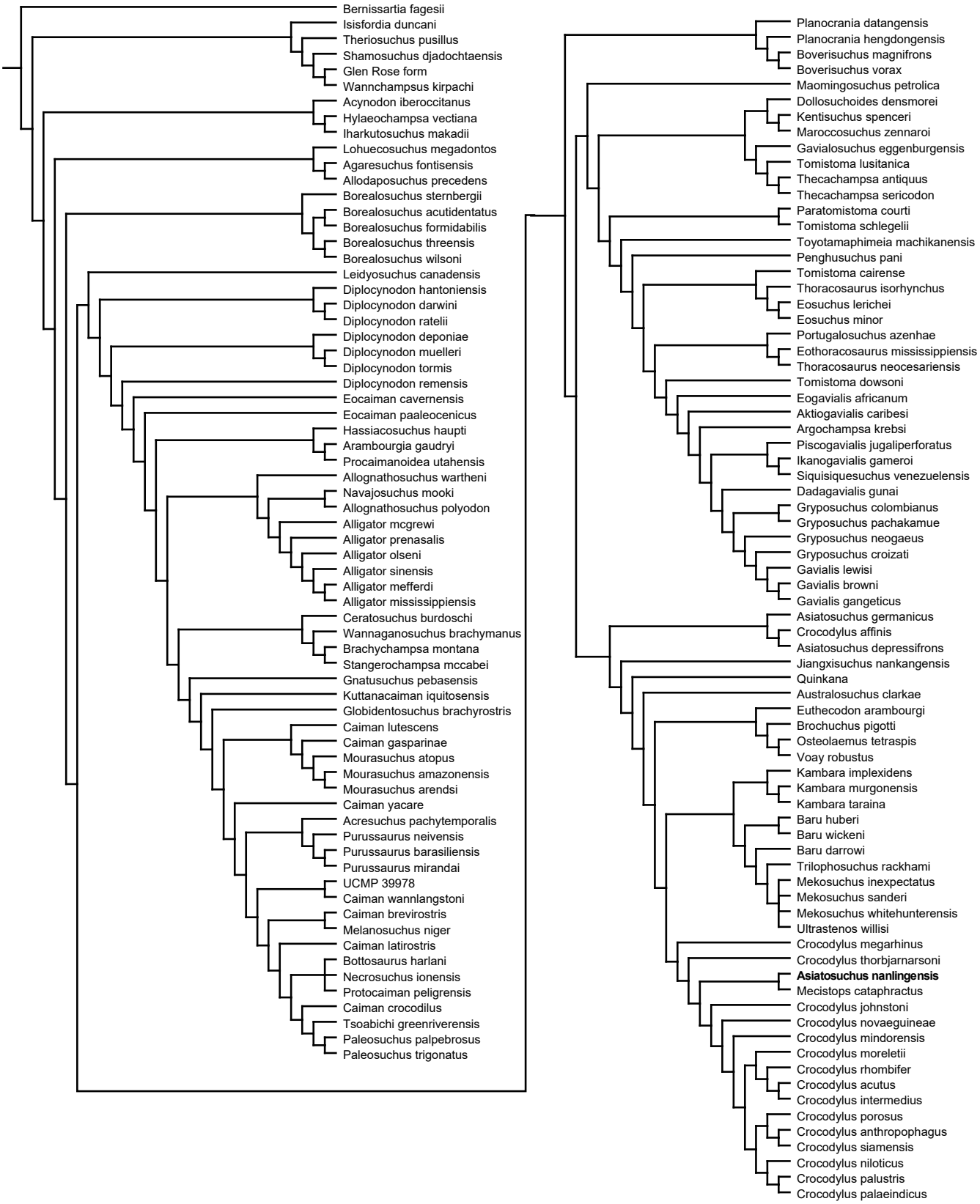



Figure F.9: Strict consensus of 3 MPTs when *Asiatosuchus nanlingensis* is forced outside of Mekosuchinae

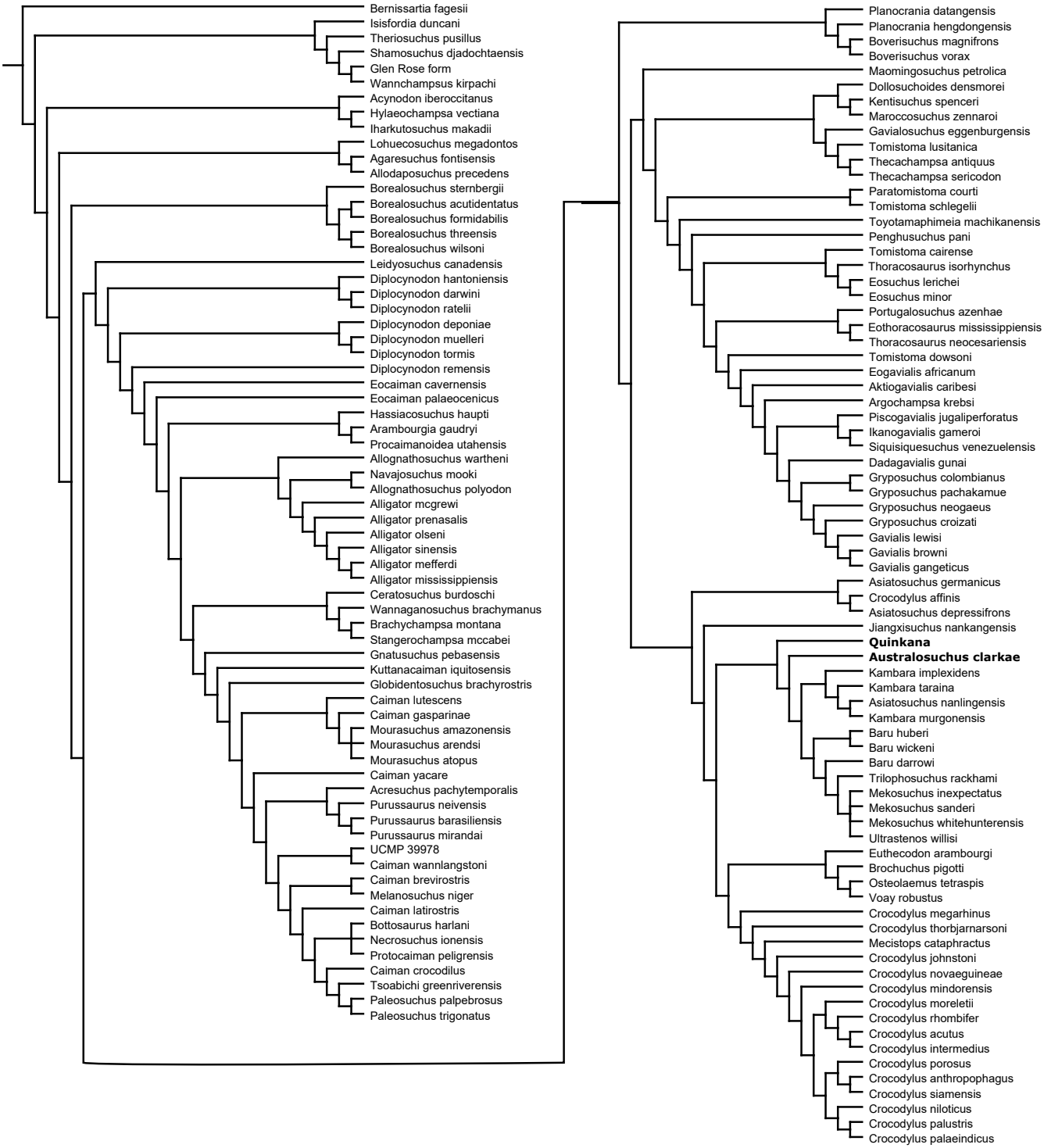



Figure F.10: Strict consensus of 3 MPTs when *Australosuchus* and *Quinkana* are forced to be recovered in Mekosuchinae.




Figure F.11: Strict consensus of 3 MPTs when *Mecistops* is constrained to be recovered in Osteolaeminae

# Appendix G

# Strict Consensus Trees from All Analyses




Figure G.1: Strict consensus of 6 MPTs from Analysis 1.1




Figure G.2: Strict consensus of 9 MPTs from Analysis 1.2

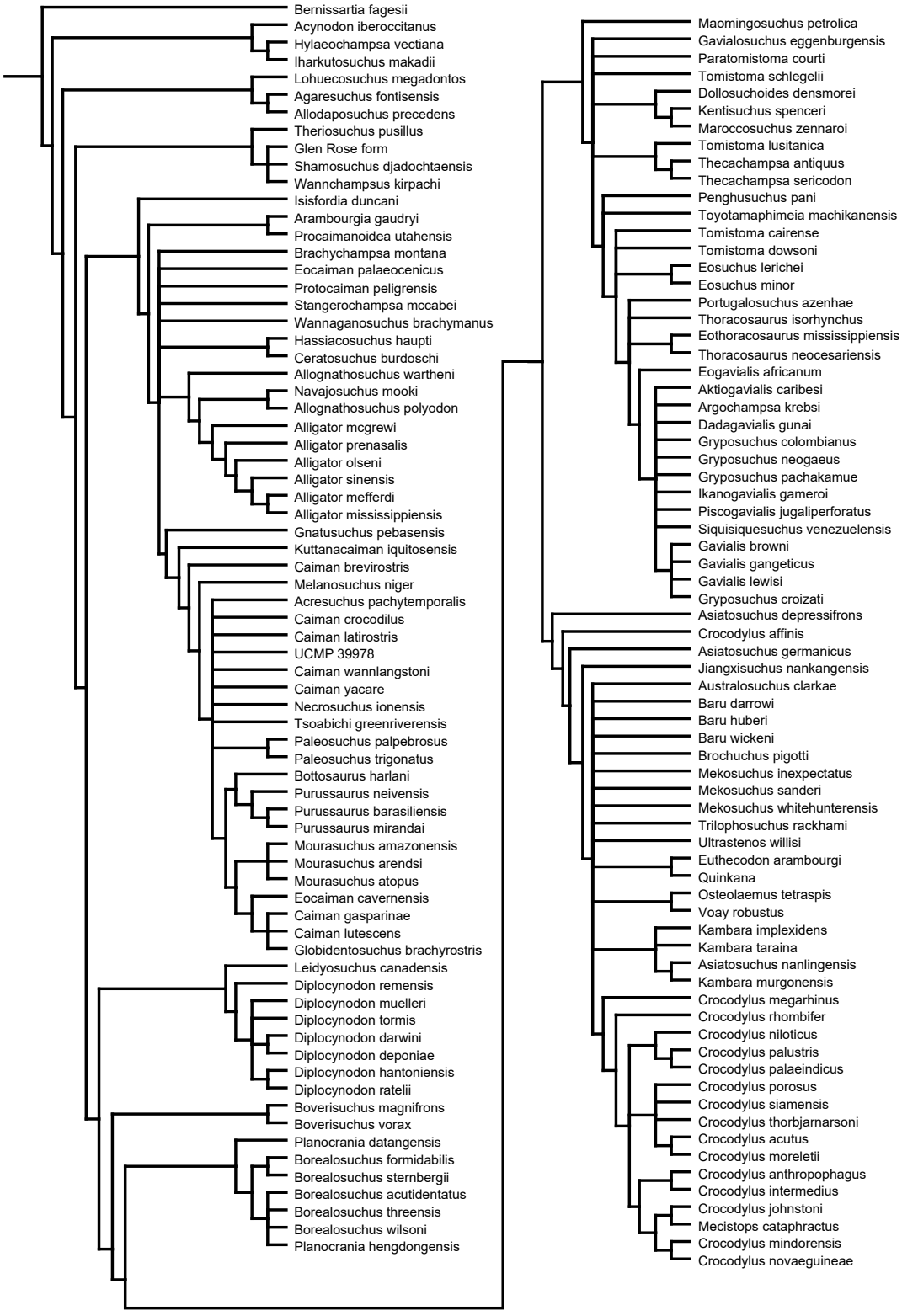



Figure G.3: Strict consensus of 400,000 MPTs from Analysis 2.1

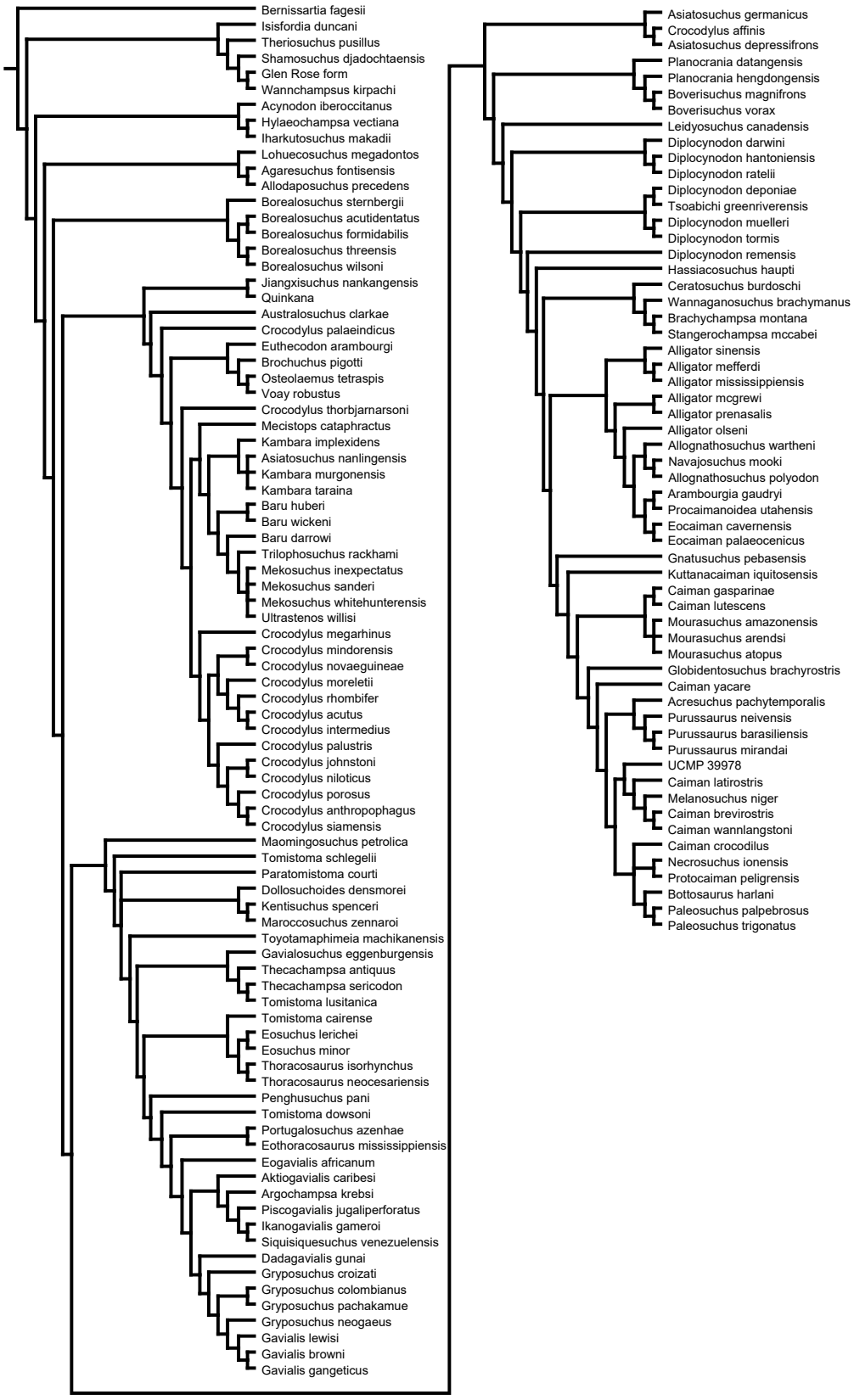



Figure G.4: Strict consensus of 3 MPTs from Analysis 2.2

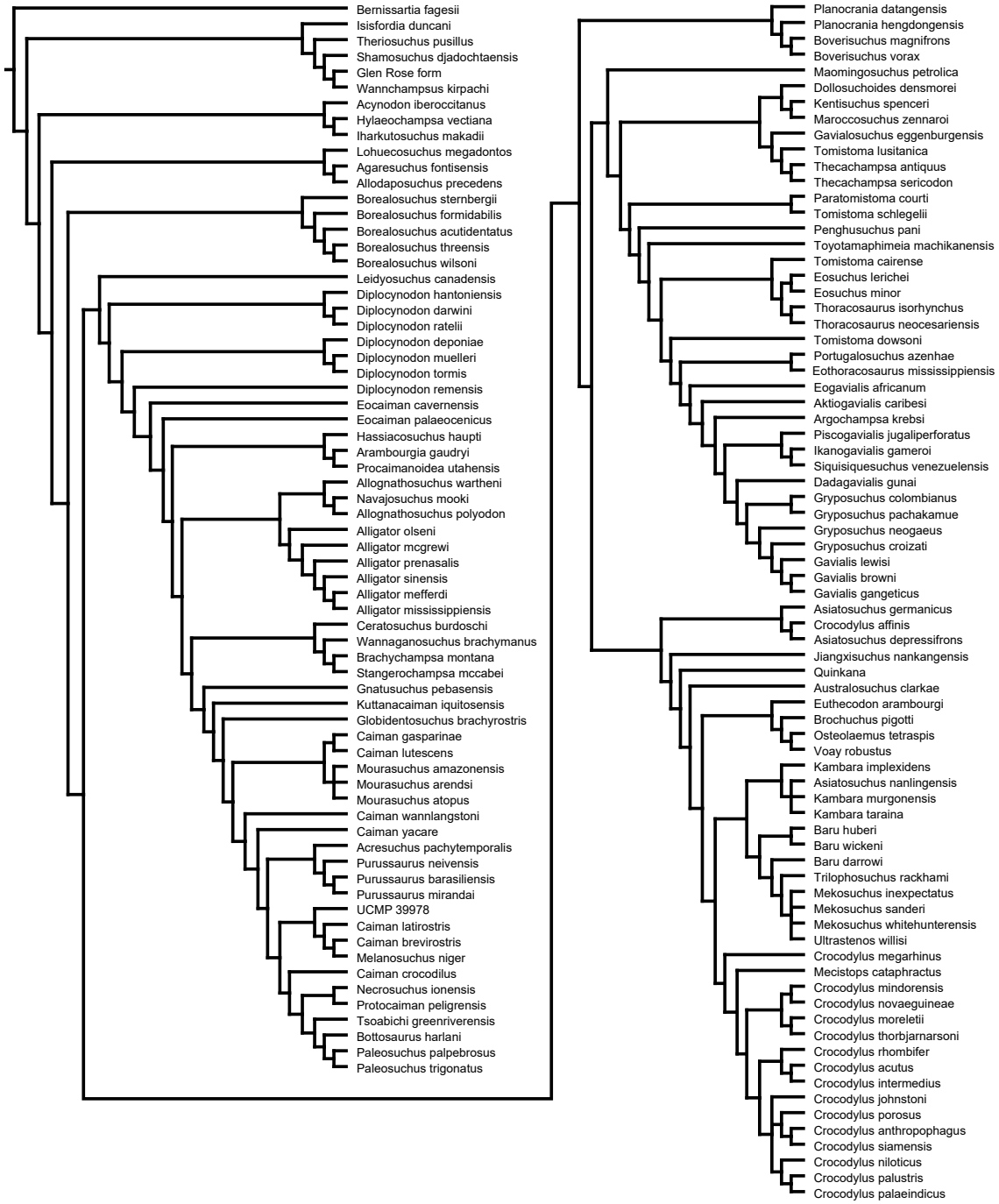



Figure G.5: Strict consensus of 3 MPTs from Analysis 2.3

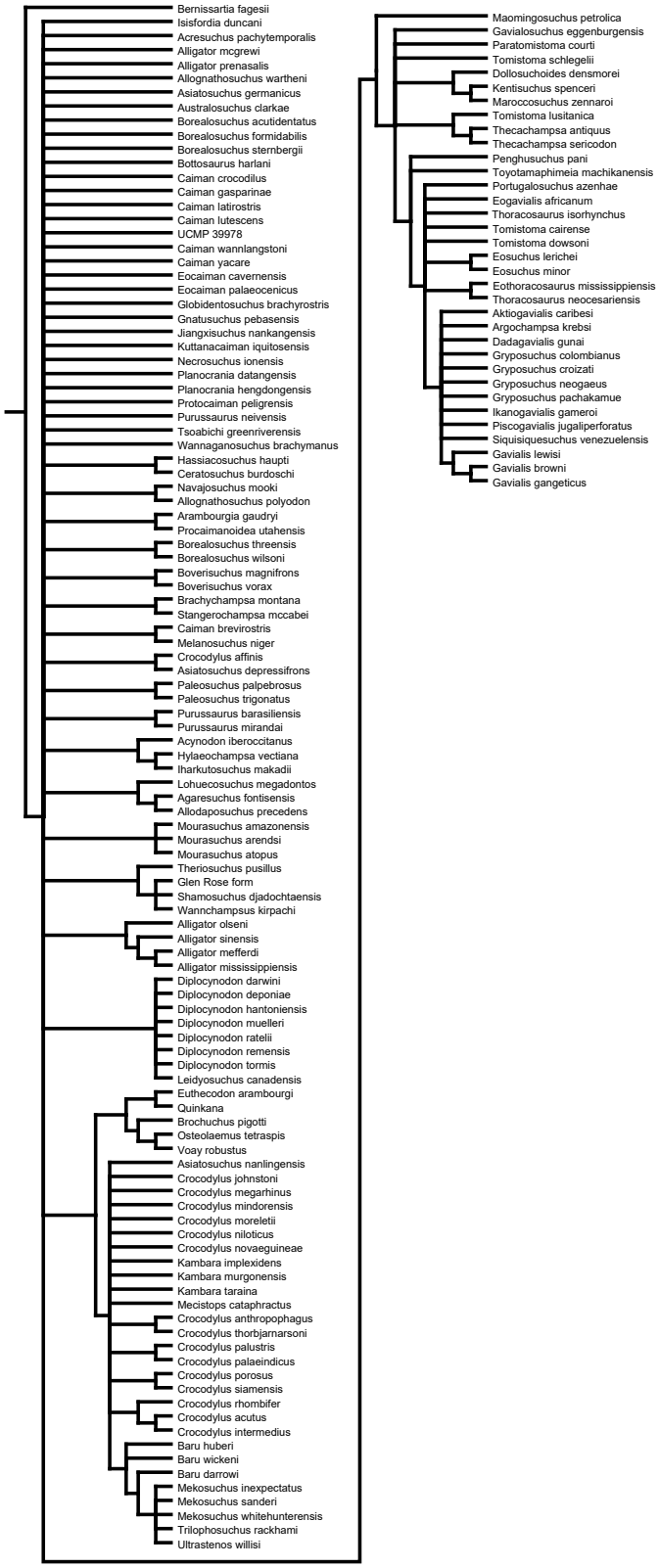



Figure G.6: Strict consensus of 400,000 MPTs from Analysis 3.1




Figure G.7: Strict consensus of 69 MPTs from Analysis 3.2

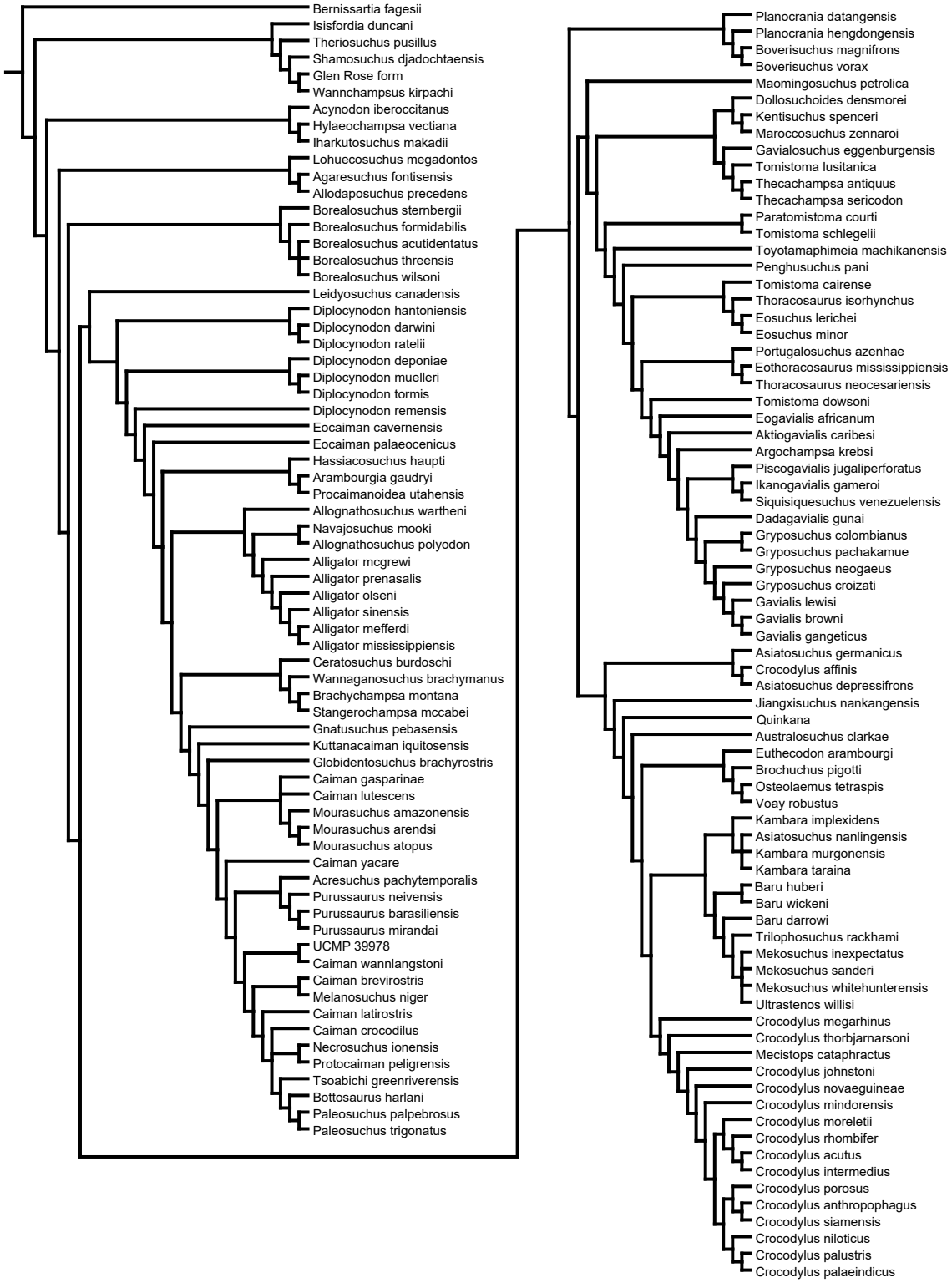



Figure G.8: Strict consensus of 3 MPTs from Analysis 3.3

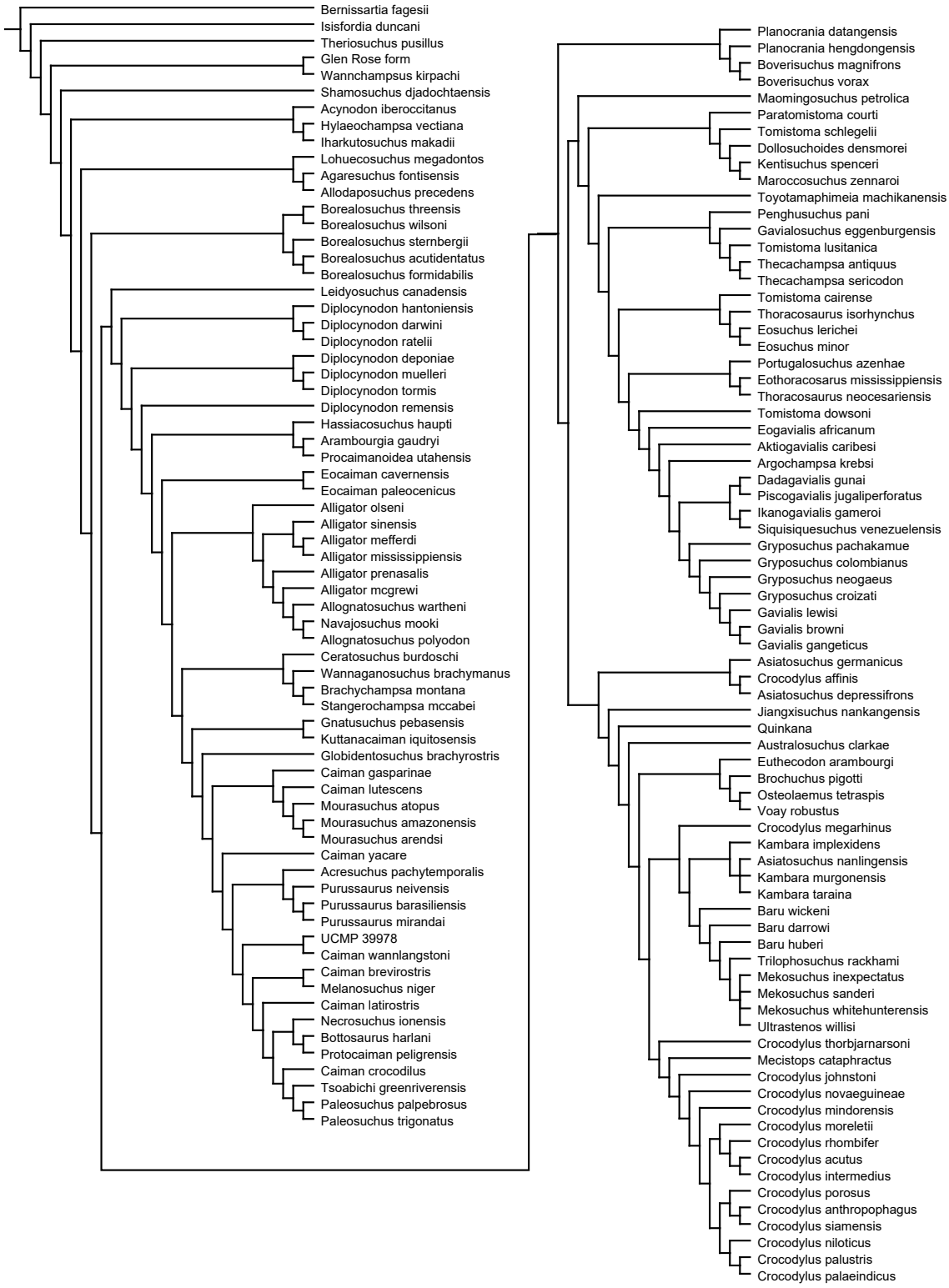



Figure G.9: Strict consensus of 3 MPTs from Analysis 1.3 when longirostrine characters are inactive

# Appendix H

# Comparisons between Strict Consensus Trees

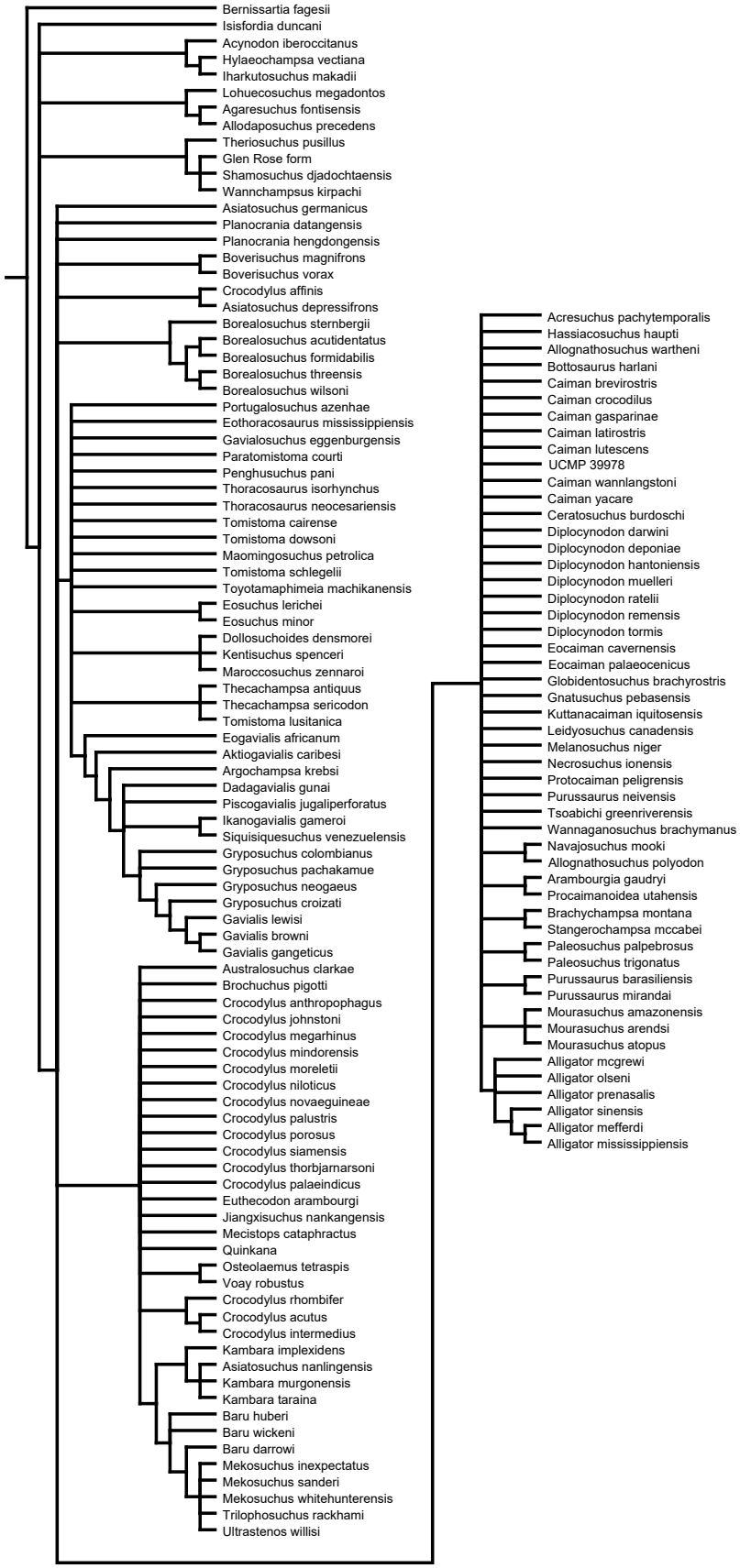



Figure H.1: Strict consensus of most parsimonious trees from analyses 1.1, 1.2, and 1.3




Figure H.2: Strict consensus of most parsimonious trees from analyses 1.3, 2.3, and 3.3

# Appendix I

# Character Consistency Index (CI) Values from Analysis 1.3

1. 0.0979
2. 0.3422
3. 0.1562
4. 0.1645
5. 0.0874
6. 0.0425
7. 0.1374
8. 0.0438
9. 0.0236
10. 0.0824
11. 0.0909
12. 0.0578
13. 0.0498
14. 0.0116
15. 0.2266
16. 0.1544
17. 0.0404
18. 0.3049
19. 0.0649
20. 0.1693
21. 0.0976
22. 0.0889
23. 0.0947
24. 0.2022
25. 0.1237
26. 0.1212
27. 0.3333
28. 0.3333
29. 1
30. 0.0833
31. 0.0769
32. 0.1667
33. 0.1429
34. 0.5
35. 1
36. 1
37. 0.1429
38. 0.1667
39. 1
40. 1
41. 0.0588
42. 0.5
43. 0.5
44. 0.1429
45. 1
46. 0.0909
47. 0.25
48. 0.3333
49. 0.0909
50. 0.0833
51. 0.5
52. 0.1667
53. 0.1
54. 0.0476
55. 0.1429
56. 0.1667
57. 0.0833
58. 0.0571
59. 0.3333
60. 0.0909
61. 0.1111
62. 0.1429
63. 0.05
64. 0.5
65. 1
66. 1
67. 0.25
68. 1
69. 0.3333
70. 0.1
71. 0.5
72. 0.087
73. 0.0667
74. 0.0455
75. 0.0625
76. 0.0345
77. 0.1111
78. 0.1333
79. 0.0588
80. 0.3333
81. 0.3333
82. 0.1667
83. 0.2
84. 0.3333

85. 0.5
86. 1
87. 0.2
88. 0.4
89. 0.1429
90. 0.1667
91. 0.3333
92. 0.1667
93. 0.1111
94. 0.15
95. 0.25
96. 0.0769
97. 0.25
98. 0.1667
99. 0.1
100. 0.2
101. 1
102. 0.1667
103. 0.25
104. 0.5
105. 0.1429
106. 0.1667
107. 0.1667
108. 0.1
109. 0.1538
110. 0.2222
111. 1
112. 0.3333
113. 0.5
114. 0.125
115. 0.0714
116. 1
117. 0.3333
118. 0.1667
119. 0.1765
120. 1
121. 0.125
122. 1
123. 0.2
124. 0.1
125. 1
126. 0.2
127. 0.25
128. 0.3333
129. 0.25
130. 0.0909
131. 0.25
132. 0.2
133. 0.5
134. 0.1667
135. 0.1429
136. 0.1667
137. 0.3333
138. 0.1111
139. 0.0714
140. 0.5
141. 0.1304
142. 0.1316
143. 0.3333
144. 0.1667
145. 0.05
146. 0.1
147. 0.5833
148. 0.1111
149. 0.2
150. 0.125
151. 0.1667
152. 0.1667
153. 0.5
154. 0.0556
155. 0.3333
156. 0.2
157. 1
158. 0.3333
159. 0.3333
160. 0.1
161. 0.125
162. 0.1
163. 0.0667
164. 0.1667
165. 0.5
166. 0.125
167. 0.0833
168. 0.1429
169. 0.125
170. 1
171. 0.1111
172. 0.2
173. 0.0588
174. 0.0667
175. 0.0769
176. 0.3333
177. 0.3333
178. 1
179. 0.3333
180. 0.2
181. 0.1
182. 1
183. 0.125
184. 0.0833
185. 0.25
186. 0.5
187. 1
188. 0.6667
189. 0.2
190. 0.2727
191. 0.0833
192. 0.1667
193. 0.0833
194. 0.2
195. 0.375
196. 0.2
197. 0.0667
198. 1
199. 1
200. 0.5
201. 0.25
202. 0.25
203. 0.25
204. 0.3333
205. 0.25
206. 0.25
207. 0.3333
208. 0.5
209. 0.3
210. 0.5
211. 0.2
212. 0.25
213. 1
214. 0.1333
215. 0.1429
216. 0.2
217. 0.2
218. 0.3333
219. 0.3077
220. 0.2222
221. 0.1379
222. 0.0909
223. 1
224. 0.3

225. 0.3333
226. 0.0909
227. 0.25
228. 1
229. 0.0769
230. 0.6667
231. 1
232. 1
233. 1
234. 0.5
235. 0.1818
236. 0.1429
237. 0.1
238. 0.3333
239. 0.1429
240. 0.0909
241. 0.1429
242. 0.125
243. 0.125
244. 0.0909
245. 0.1
246. 0.1429
247. 0.1111
248. 0.25
249. 0.125
250. 0.5
251. 0.0769
252. 0.25
253. 0.0833
254. 0.2
255. 0.5
256. 0.3333
257. 0.25
258. 0.1429
259. 0.5
260. 1
261. 0.1667
262. 0.3333
263. 0.5
264. 0.2
265. 0.25
266. 0.5
267. 0.2
268. 0.5
269. 1
270. 0.5
271. 0.5
272. 0.5
273. 0.0714
274. 0.0909
275. 0.1667
276. 0.3333
277. 0.1429
278. 0.5
279. 0.5
280. 0.1667
281. 100
282. 0.3333
283. 1
284. 0.2857
285. 0.5
286. 1
287. 1
288. 1
289. 0.1667
290. 1
291. 1
292. 1
293. 0.6667
294. 0.5
295. 1
296. 0.3333
297. 0.2857
298. 1
299. 0.2
300. 0.5
301. 0.1667
302. 0.1429
303. 0.5
304. 0.5
305. 0.5
306. 0.3333
307. 0.0909
308. 0.1538
309. 0.1
310. 1
311. 0.25
312. 0.5
313. 1
314. 1
315. 1
316. 0.2
317. 1
318. 0.3333
319. 0.5
320. 1
321. 0.2
322. 0.25
323. 0.4
324. 0.3636
325. 0.25
326. 0.1
327. 0.1111
328. 0.25
329. 0.3333
330. 0.5

# Appendix J

# Character score changes

Table J.1: Score changes in gavialoid taxa for characters recovered as synapomorphies of Gavialoidea and less inclusive clades that unite "tomistomines" and "gavialoids" (see Section 4.4.7). Comparisons are made relative to three data-sets to account for differences in taxon sampling between studies.

| Character | Node | Jouve (2016) | Narvaéz et al. (2016) | Salas-Gismondi et al. (2019) |
|---|---|---|---|---|
| 41-1 | Gavialoidea | *Tomistoma cairense*: ? → 1 | *Maomingosuchus petrolica*: ? → 1; *Tomistoma cairense*: ? → 1 | *Aktiogavialis caribesi*: ? → 1; *Dadagavialis gunai*: ? → ?; *Ikanogavialis gameroi*: ? → 1; *Tomistoma cairense*: ? → 1 |
| 50-1 | Gavialoidea | *Penghusuchus pani*: ? → 1 | *Maomingosuchus petrolica*: ? → 1 | NA |
| 75-2 | Gavialoidea | *Eogavialis africanum*: 1 → 2; *Eosuchus lerichei*: 2 → 0; *Eosuchus minor*: 2 → 1; *Ikanogavialis gameroi*: 2 → 1 | *Eogavialis africanum*: 1 → 2; *Eosuchus lerichei*: 2 → 0 | *Eogavialis africanum*: 1 → 2; *Eosuchus lerichei*: 2 → 0; Gryposuchus croizati: ? → 0; *Ikanogavialis gameroi*: 2 → 1 |
| 107-1 | Gavialoidea | *Dollosuchoides densmorei*: 1 → ?; *Eosuchus lerichei*: 1 → 0; *Ikanogavialis gameroi*: ? → 1; *Kentisuchus spenceri*: 0 → 1; *Moroccosuchus zennaroi*: 0 → 1; *Penghusuchus pani*: ? → 1; *Siquisiquesuchus venezuelensis*: 1 → ?; *Tomistoma cairense*: 1 → 0; *Toyotamaphimeia machikanensis*: ? → 1 | *Dollosuchoides densmorei*: 1 → ?; *Eosuchus lerichei*: 1 → 0; *Kentisuchus spenceri*: 0 → 1; *Tomistoma cairense*: 1 → 0 | *Aktiogavialis caribesi*: 1 → ?; *Eosuchus lerichei*: 1 → 0; Gryposuchus croizati: 1 → ?; *Kentisuchus spenceri*: 0 → 1; *Siquisiquesuchus venezuelensis*: 1 → ? |

| Character | Node | Jouve (2016) | Narvaéz et al. (2016) | Salas-Gismondi et al. (2019) |
|---|---|---|---|---|
| 136-1 | Gavialoidea | *Argochampsa krebsi*: ? → 1; *Dollosuchoides densmorei*: 1 → ?; *Eogavialis africanum*: 2 → 1; *Gavialis gangeticus*: 2 → 1; *Gryposuchus colombianus*: 2 → 1; *Ikanogavialis gameroi*: 2 → ?; *Piscogavialis jugaliperforatus*: 2 → 1; *Siquisiquesuchus venezuelensis*: 2 → ?; *Thecachampsa antiquus*: 1 → ?; *Thoracosaurus neocesariensis*: 0 → ?; *Tomistoma cairense*: ? → 1 | *Dollosuchoides densmorei*: 0 → ?; *Eogavialis africanum*: 0 → 1; *Gavialis gangeticus*: 2 → 1; Gavialis lewisi: 2 → 1; *Gryposuchus colombianus*: 2 → 1; *Maomingosuchus petrolica*: ? → 1; *Piscogavialis jugaliperforatus*: 2 → 1; *Thecachampsa antiquus*: 1 → ?; *Thoracosaurus neocesariensis*: 0 → ?; *Tomistoma cairense*: ? → 1 | *Aktiogavialis caribesi*: ? → 1; *Argochampsa krebsi*: ? → 1; *Eogavialis africanum*: 0 → 1; Gryposuchus croizati: 1 → ?; *Gryposuchus neogaeus*: ? → 1; *Ikanogavialis gameroi*: 1 → ?; *Siquisiquesuchus venezuelensis*: 1 → ?; *Thecachampsa antiquus*: 1 → ?; *Thoracosaurus neocesariensis*: 0 → ? |
| 144-1 | Gavialoidea | *Eosuchus lerichei*: 1 → 0; *Eosuchus minor*: ? → 0; *Eothoracosaurus mississippiensis*: 1 → 0 | NA Character not employed | NA Character not employed |
| 151-2 | Gavialoidea | *Thoracosaurus neocesariensis*: 2 → ?; *Toyotamaphimeia machikanensis*: 0 → 2 | *Thoracosaurus neocesariensis*: 2 → ?; *Toyotamaphimeia machikanensis*: 0 → 2 | *Thoracosaurus neocesariensis*: 2 → ? |
| 154-0 | Gavialoidea | NA New character | NA New character | NA New character |

| Character | Node | Jouve (2016) | Narvaéz et al. (2016) | Salas-Gismondi et al. (2019) |
|---|---|---|---|---|
| 183-1 | Gavialoidea | *Argochampsa krebsi*: 0 → ?; *Gavialosuchus eggenburgensis*: ? → 0; *Thecachampsa antiquus*: 1 → 0; *Thoracosaurus isorhynchus*: 0 → ?; *Thoracosaurus neocesariensis*: 0 → ? | Gavialis lewisi: 0 → ?; *Gavialosuchus eggenburgensis*: ? → 0; *Maomingosuchus petrolica*: 0 → 1; *Thecachampsa antiquus*: 1 → 0; *Thoracosaurus isorhynchus*: 0 → ?; *Thoracosaurus neocesariensis*: 0 → ? | *Argochampsa krebsi*: 0 → ?; *Thecachampsa antiquus*: 1 → 0; *Thoracosaurus neocesariensis*: 0 → ? |
| 191-0 | Gavialoidea | NA New character | NA New character | NA New character |
| 206-0 | Gavialoidea | *Eosuchus lerichei*: ? → 0; *Eothoracosaurus mississippiensis*: ? → 0; *Gavialosuchus eggenburgensis*: 1 → ?; *Thecachampsa antiquus*: 0 → ?; *Thoracosaurus isorhynchus*: 0 → ?; *Tomistoma cairense*: ? → 0; *Tomistoma lusitanica*: 1 → ?; *Toyotamaphimeia machikanensis*: 0 → ? | *Eosuchus lerichei*: ? → 0; *Eothoracosaurus mississippiensis*: ? → 0; *Maomingosuchus petrolica*: ? → 1; *Thoracosaurus isorhynchus*: 0 → ?; *Tomistoma cairense*: ? → 0; *Tomistoma lusitanica*: 1 → ? | *Eosuchus lerichei*: ? → 0; *Eothoracosaurus mississippiensis*: ? → 0; *Ikanogavialis gameroi*: 0 → ? |
| 221-2 | Gavialoidea | NA Modified | NA Modified | NA Modified |
| 46-1 | Unnamed clade 1 | NA modified | NA modified | NA modified |

| Character | Node | Jouve (2016) | Narvaéz et al. (2016) | Salas-Gismondi et al. (2019) |
|---|---|---|---|---|
| 98-1 | Unnamed clade 1 | NA character not present | NA character not present | *Eosuchus lerichei*: 1 → 0; *Eosuchus minor*: 1 → ?; *Gavialis gangeticus*: 0 → 1; *Thecachampsa antiquus*: 1 → ?; *Tomistoma schlegelii*: 0 → 1 |
| 220-0 | Unnamed clade 1 | *Dollosuchoides densmorei*: 0 → ?; *Eosuchus minor*: 0 → 1; *Penghusuchus pani*: 0 → 1; *Thoracosaurus isorhynchus*: 0 → ?; *Thoracosaurus neocesariensis*: 0 → ?; *Toyotamaphimeia machikanensis*: 0 → ? | *Dollosuchoides densmorei*: 1 → ?; *Eosuchus minor*: 0 → 1; Gavialis lewisi: 0 → ?; *Maomingosuchus petrolica*: ? → 0; *Thoracosaurus isorhynchus*: 0 → ?; *Thoracosaurus neocesariensis*: 0 → ?; *Toyotamaphimeia machikanensis*: 0 → ? | *Aktiogavialis caribesi*: 0 → ?; *Eosuchus minor*: 0 → 1; *Kentisuchus spenceri*: 1 → ?; *Thoracosaurus neocesariensis*: 0 → ? |
| 224-2 | Unnamed clade 1 | NA modified | NA modified | NA modified |
| 219-3 | Gavialidae | *Argochampsa krebsi*: 3 → ?; *Dollosuchoides densmorei*: 2 → 3; *Thoracosaurus isorhynchus*: 3 → ?; *Thoracosaurus neocesariensis*: 3 → ?; *Tomistoma cairense*: ? → 3; *Tomistoma schlegelii*: 0 → 3; *Toyotamaphimeia machikanensis*: 2 → ? | *Dollosuchoides densmorei*: ? → 3; *Eogavialis africanum*: ? → 3; *Eosuchus lerichei*: ? → 3; *Eosuchus minor*: ? → 3; *Eothoracosaurus mississippiensis*: ? → 3 | NA modified |

| Character | Node | Jouve (2016) | Narvaéz et al. (2016) | Salas-Gismondi et al. (2019) |
|---|---|---|---|---|
| 280-1 | Gavialidae | *Dollosuchoides densmorei*: 0 → ?; *Thecachampsa antiquus*: 0 → ? | *Dollosuchoides densmorei*: 0 → ?; *Maomingosuchus petrolica*: ? → 0; *Thecachampsa antiquus*: 0 → ? | No changes |
| 328-0 | Gavialidae | NA modified | *Maomingosuchus petrolica*: ? → 1 | No changes |
| 89-0 | Unnamed clade 2 | *Argochampsa krebsi*: 1 → 0; *Dollosuchoides densmorei*: 0 → ?; *Eosuchus lerichei*: 1 → 0; *Eosuchus minor*: 1 → 0; *Eothoracosaurus mississippiensis*: 1 → 0; *Ikanogavialis gameroi*: 1 → 0; *Kentisuchus spenceri*: 0 → 1; *Moroccosuchus zennaroi*: 0 → 1; *Piscogavialis jugaliperforatus*: 1 → 0; *Thoracosaurus isorhynchus*: 1 → 0; *Thoracosaurus neocesariensis*: 1 → ?; *Tomistoma cairense*: 1 → 0; *Tomistoma lusitanica*: 1 → 0 | *Dollosuchoides densmorei*: 0 → ?; *Gavialosuchus eggenburgensis*: 0 → 1; *Maomingosuchus petrolica*: 0 → 1; *Thoracosaurus neocesariensis*: 0 → ?; *Tomistoma lusitanica*: 1 → 0 | *Argochampsa krebsi*: 1 → 0; *Dadagavialis gunai*: 0 → ?; *Eosuchus lerichei*: ? → 0; *Siquisiquesuchus venezuelensis*: 0 → ?; *Thecachampsa antiquus*: 1 → 0; *Thoracosaurus neocesariensis*: 0 → ? |
| 147-5 | Unnamed clade 2 | NA character modified | NA character modified | NA character modified |

| Character | Node | Jouve (2016) | Narvaéz et al. (2016) | Salas-Gismondi et al. (2019) |
|---|---|---|---|---|
| 193-1 | Unnamed clade 2 | *Argochampsa krebsi*: ? → 1; *Eogavialis africanum*: 1 → 0; *Gryposuchus colombianus*: 1 → ?; *Ikanogavialis gameroi*: ? → 1; *Kentisuchus spenceri*: 1 → ? | *Dollosuchoides densmorei*: 0 → ?; *Eogavialis africanum*: 1 → 0; *Eosuchus lerichei*: 1 → 0; *Eosuchus minor*: 1 → ?; *Eothoracosaurus mississippiensis*: ? → 1 | *Aktiogavialis caribesi*: ? → 1; *Argochampsa krebsi*: ? → 1; *Eogavialis africanum*: 1 → 0; *Eosuchus lerichei*: ? → 0; *Eosuchus minor*: 1 → ?; *Eothoracosaurus mississippiensis*: ? → 1; *Gryposuchus colombianus*: 1 → ? |
| 247-0 | Unnamed clade 2 | *Argochampsa krebsi*: ? → 1; *Eosuchus lerichei*: 0 → ?; *Ikanogavialis gameroi*: 0 → ?; *Kentisuchus spenceri*: ? → 1; *Moroccosuchus zennaroi*: 1 → ?; *Siquisiquesuchus venezuelensis*: 0 → ?; *Thecachampsa antiquus*: 1 → ?; *Thoracosaurus isorhynchus*: 0 → ?; *Thoracosaurus neocesariensis*: 0 → ?; *Tomistoma lusitanica*: ? → 0 | *Eosuchus lerichei*: 0 → ?; *Eothoracosaurus mississippiensis*: ? → 0; *Thecachampsa antiquus*: 1 → ?; *Theriosuchus pusillus*: 0 → ?; *Thoracosaurus isorhynchus*: 0 → ?; *Thoracosaurus neocesariensis*: 0 → ?; *Tomistoma lusitanica*: 1 → 0; *Toyotamaphimeia machikanensis*: 1 → 0 | *Argochampsa krebsi*: ? → 1; *Eothoracosaurus mississippiensis*: ? → 0; *Ikanogavialis gameroi*: 0 → ?; *Piscogavialis jugaliperforatus*: 0 → ?; *Thecachampsa antiquus*: 1 → ?; *Thoracosaurus neocesariensis*: 0 → ? |

| Character | Node | Jouve (2016) | Narvaéz et al. (2016) | Salas-Gismondi et al. (2019) |
|---|---|---|---|---|
| 278-1 | Unnamed clade 2 | *Argochampsa krebsi*: 1 → ?; *Eosuchus lerichei*: ? → 0; *Penghusuchus pani*: ? → 1; *Thecachampsa antiquus*: 0 → ?; *Toyotamaphimeia machikanensis*: 0 → 1 | *Dollosuchoides densmorei*: 0 → ?; *Eosuchus lerichei*: ? → 0; *Maomingosuchus petrolica*: ? → 0; *Thecachampsa antiquus*: 0 → ? | *Argochampsa krebsi*: 1 → ?; *Eosuchus lerichei*: 1 → 0 |
| 288-0 | Unnamed clade 2 | Character not used | Character not used | Character not used |
| 149-1 | Unnamed clade 3 | NA New character | NA New character | NA New character |
| 253-1 | Unnamed clade 3 | *Eosuchus minor*: 0 → 1; *Eothoracosaurus mississippiensis*: ? → 1; *Gryposuchus colombianus*: 0 → ?; *Kentisuchus spenceri*: 1 → 0; *Moroccosuchus zennaroi*: 1 → 0; *Thecachampsa antiquus*: 1 → ?; *Thoracosaurus isorhynchus*: 0 → ?; *Tomistoma lusitanica*: 0 → ? | *Eosuchus minor*: 0 → 1; *Eothoracosaurus mississippiensis*: ? → 1; *Gryposuchus colombianus*: 0 → ?; *Kentisuchus spenceri*: 1 → 0; *Maomingosuchus petrolica*: 1 → ?; *Thecachampsa antiquus*: 1 → ?; *Thoracosaurus isorhynchus*: 0 → ? | *Eosuchus minor*: 0 → 1; *Eothoracosaurus mississippiensis*: ? → 1; *Kentisuchus spenceri*: 1 → 0; *Piscogavialis jugaliperforatus*: 1 → ?; *Thecachampsa antiquus*: 1 → ? |
| 147-7 | Unnamed clade 4 | NA modified | NA modified | NA modified |